THE PHYSICAL REVIEW

VOLUME 96 *Second Series* NUMBER 6

DECEMBER 15, 1954

Published for the

AMERICAN PHYSICAL SOCIETY

by the

AMERICAN INSTITUTE OF PHYSICS

Incorporated

LANCASTER, PA., AND NEW YORK, N. Y.

THE
PHYSICAL REVIEW

A journal of experimental and theoretical physics established by E. L. Nichols in 1893

SECOND SERIEL, VOL. 96, NO. 6 DECEMBER 15, 1954

On the Theory of Liquid He^3

LOUIS GOLDSTEIN
University of California, Los Alamos Scientific Laboratory, Los Alamos, New Mexico
(Received July 29, 1954)

The difficulties raised by the elementary interpretation of the recently observed temperature variation of the nuclear paramagnetic susceptibility of liquid He^3 as an ideal antisymmetric fluid type of degeneration phenomenon are discussed. The susceptibility data are then shown to lead to a direct and rigorous evaluation of the entropy of spin disorder and the associated heat capacity. The observed enormous total entropy of liquid He^3 at low temperatures is thus explained to be overwhelmingly entropy of spin disorder. The spin heat capacity is about half of the observed total heat capacity at the lowest temperature of observations. It should tend to become the dominant part of the total liquid heat capacity below this temperature. The maximum of the spin heat capacity at low enough temperatures may become observable indirectly through the total heat capacity of the liquid.

1. INTRODUCTION

THE experimental results obtained recently on a number of fundamental properties of liquid He^3 appear to justify their discussion within the framework of the still fragmentary theory of this liquid. The present paper will be concerned mainly with the exploitation of the measurements[1,2] of the nuclear paramagnetic susceptibility of liquid He^3. It will thus be shown, seemingly on quite general grounds, that the susceptibility data supply, over the whole experimentally explored temperature interval, the number of He^3 atoms which are in doubly spin-degenerate levels and their complement, or the number of those which are aligned with their spin momenta antiparallel. These are thus in nondegenerate levels as a result of the effect of a spin ordering internal field, as intimated by the experimental workers.[2] On the basis of this result, the susceptibility data appear directly to determine the entropy of spin disorder and, through its temperature variation, the associated spin heat capacity of the liquid. The knowledge of these partial spin properties of the fluid could be evidently of importance insofar as their subtraction from the calorimetrically measured total entropy and heat capacity yields the "lattice" or "non-spin" entropy and heat capacity. The separate availability of these partial properties could be helpful in the investigations of the foundations of the theory of liquid He^3.

Before entering, however, into the main topic of this paper which we have just outlined, it seems necessary to discuss first the possible theoretical meanings of the susceptibility data, using here some of the results obtained previously by us[3] in the investigations of the magnetic properties of liquid He^3.

2. EXCHANGE ENERGY AND CHARACTERISTIC SPIN ORDERING TEMPERATURE IN LIQUID He^3

In our previous work[3] the exchange energy per liquid He^3 atom has been computed at the temperature of absolute zero and in the two limiting spin or magnetic configurations,

$$\mu_{tot} = \begin{cases} N\mu, (f) \\ 0, (a) \end{cases}$$

of total magnetic moment $N\mu$, N being the total number of atoms of the system and μ the measured He^3 nuclear magnetic moment, or vanishing moment. The former was called the ferromagnetic (f), the latter the antiferromagnetic configuration (a). The total energy of the latter configuration was proved to be lower than that of the former. This total energy was written to be

[1] Fairbank, Ard, Dehmelt, Gordy, and Williams, Phys. Rev. 92, 208 (1953).
[2] Fairbank, Ard, and Walters, Post-deadline paper, Washington D. C. meeting of American Physical Society, April 29–May 1, 1954.
[3] L. Goldstein and M. Goldstein, Phys. Rev. 76, 464(A) (1949); J. Chem. Phys. 18, 538 (1950).

the algebraic sum of the kinetic, potential, and exchange energies, the latter being positive here for all physically plausible closest distances of approach of two He^3 atoms. The following admittedly crude approximations were involved in these calculations. The kinetic energy was taken to be that of a completely degenerate ideal antisymmetric fluid formed by the He^3 atoms with the known mass per atom and the extrapolated density of the liquid. In the calculation of the mean potential energy the ever-present spatial correlations between the liquid atoms have been neglected. This was equivalent to using the limiting large separation expression $n_0 dv(r)$ for the probability of finding an atom in the volume element dv, whose center is at a distance r from the origin atom, n_0 being the mean atomic concentration at the absolute zero. Finally, in the evaluation of the exchange energies, the close packing of the ideal antisymmetric collection of atoms in momentum space and the asymptotic free particle level density in this space proportional to the square of their linear momentum were used in conformity with the formalism of the ideal antisymmetric fluid model. It was thus proved that, within these limitations, the exchange energy per liquid He^3 atom in the antiferromagnetic configuration, the only one of interest to us here, was given by

$$E_{x,0} = -\tfrac{3}{2}\int_a^\infty \Phi(r) J_{\frac{1}{2}}^2(k_0 r)\frac{dr}{r}, \qquad (1)$$

where k_0, the length of the wave vector at the surface of the closely packed momentum sphere of radius p_0 associated with the antiferromagnetic configuration, is p_0/h, h being Planck's constant divided by 2π; $\Phi(r)$ is the mutual potential energy of two stationary He atoms separated by a distance r; $J_{\frac{1}{2}}(y)$ is the Bessel function of order $\frac{1}{2}$; and a, a cutoff length which had to be introduced because of the diverging character of the integrand at close separations. Physically the cutoff length a is equivalent to the assumption that the probability of finding two He atoms at distances $r \leqslant a$ vanishes identically. The exchange energy (1) was evaluated numerically with both the so-called Slater-Kirkwood (S-K) and Margenau[4] (M) approximate potential energy expressions, $\phi_{S\text{-}K}$ and ϕ_M, for various values of the distance of closest approach a. The results appear in Figs. 1 and 2 of our previous work.[3] It seems of interest to give here a few E_x values of physical interest. These are included in Table I, in temperature units $E_x(a)/k$, k being Boltzmann's constant.

A glance at Table I shows that for the physically plausible cut-off distances $a \sim 2.5$–2.6A, where the mutual potential energies become negative, or binding, the approximate antiparallel spin ordering energies or characteristic temperatures are of the order of magnitude of one °K. At the present time, one is apparently

[4] J. C. Slater and J. G. Kirkwood, Phys. Rev. 37, 682 (1931); H. Margenau, Phys. Rev. 56, 1000 (1939).

TABLE I. Approximate exchange energies per liquid He^3 atom, °K units, for two types of potential energies and various cutoff distances a, (A). The liquid is at the absolute zero temperature.

a A	$E_{x,S\text{-}K}(a)/k$ °K/atom	$E_{x,M}(a)/k$ °K/atom
2.4	0.72	1.62
2.5	1.03	1.68
2.6	1.12	1.59
2.7	1.07	1.42
2.8	0.98	1.23

inclined to consider $\phi_{S-K}(r)$ as a closer approximation to the correct potential energy function than $\phi_M(r)$. At any rate, keeping in mind the approximations involved in the derivation of the spin orientation energy or characteristic temperature of about one °K, the latter cannot be interpreted in any other way than by associating it with an "antiferromagnetic" internal field energy per atom. In the present system of the coupled He^3 atoms this approximate spin ordering energy, resulting from the interaction of two atoms and the antisymmetric character of their wave function, might be envisaged as a quantity more closely connected to the fundamental properties of liquid He^3 than the degeneration temperature

$$T_0 = (h^2/2mk)(3n_0/8\pi)^{\frac{2}{3}}, \qquad (2)$$

associated with a system of ideal antisymmetric He^3 atoms of actual or effective mass m and concentration n_0. The effective mass concept would, of course, be helpful for taking into account, in a rather indirect way, the atomic interactions.

In the evaluation of the energies of Table I, the limitations resulting from the plane wave character of the individual atomic wave functions should lead to an overestimation of these exchange energies. More localized wave functions which could be associated with liquid atoms are expected to yield lower exchange energies. It is unlikely that the assumption of the close packing of a momentum sphere, even though centered at the origin of the momentum space, is too far from the actual state of affairs in the liquid at the absolute zero and vanishing total spin momentum, particularly as far as the calculation of the exchange energy is concerned. The latter depends, indeed, only on the distance of two atoms in momentum space and not on their individual momenta. In estimating the effect of using the free particle level density in these calculations, one might be inclined to say that this results in overestimating the exchange energy at least in parts of the spectrum. This could, however, be compensated for by the contributions from other portions of the energy spectrum.

Even though the directly evaluated exchange energies are relatively close to the experimentally found ordering energy[2] of about 0.45°K, the preceding studies do not explain why the experimentally established liquid He^3 paramagnetic susceptibility law should be so closely

approximated by the Pauli susceptibility formula[5]

$$\chi_P(T)=(n\mu^2/kT)[-F'(\alpha)/F(\alpha)], \tag{3}$$

valid for an ideal antisymmetric gas of particles with spin $\hbar/2$, magnetic moment μ, concentration n, and degeneration temperature $T_0=0.45°K$. Here, for $\alpha>1$,

$$F(\alpha)=\sum_1^\infty(-)^{n-1}n^{-\frac{3}{2}}\exp(-n\alpha)=\tfrac{2}{3}(T_0/T);$$
$$F'(\alpha)=dF/d\alpha, \tag{4}$$

α being the negative Gibbs free energy per atom in units of kT. Clearly, it has not as yet been proved that the analytic form of the liquid He³ susceptibility law is necessarily given by (3). The use of the "apparent" degeneration temperature of 0.45°K in connection with (3) tends to imply that this same temperature should appear in the expressions of the different thermal properties of the system, in accordance with its description as an ideal antisymmetric fluid of atoms of mass about ten times the atomic mass of He³ and the actual density[6] of the liquid. These indeed yield with (2) a degeneration temperature of about 0.45°K. However, in the temperature interval explored so far, where $T\gtrsim 0.4$–$0.5°K$, the entropy and heat capacity data[7] in liquid He³ rule out completely the possibility of accounting for them in terms of the ideal fluid formalism with a degeneration temperature of about 0.45°K.

It may be noted here that the degeneration temperature of about 5°K resulting from (2) where the liquid is pictured as a limiting ideal fluid leads to entropy values which appear to approximate crudely the measured entropies. This is however not the case with the heat capacities and the paramagnetic nuclear susceptibility.

We may thus conclude this section by saying that, at the present time, there is no unique and simple theoretical approach which accounts simultaneously for both the measured susceptibilities[1,2] and the entropies and heat capacities[7] of liquid He³. However, the previously estimated[3] antiferromagnetic spin ordering energy of about 1.0°K, Table I, appears to be a fair approximation of the empirically obtained value of this energy derived from the susceptibility values.[2]

3. ENTROPY AND HEAT CAPACITY OF SPIN DISORDER IN LIQUID He³

We shall now derive an entropy of spin disorder and the associated heat capacity which should be closely connected with the rigorous formulation of these thermal properties resulting from first principles within the framework of the correct theory of liquid He³.

The liquid He³ nuclear paramagnetic susceptibility measurements[1,2] over a wide temperature interval prove that at high temperatures the liquid tends to behave as an ideal paramagnetic system whose susceptibility obeys the Curie-Langevin law,[8] and at low temperatures its susceptibility is continuously reduced below the values predicted by the ideal limiting Langevin formula. The liquid ceases to be an ideal paramagnet as the temperature decreases and increasingly deviates from the ideal behavior as the low-temperature region is approached. An important feature of the empirical susceptibility law, over the temperature range explored so far, is its monotonic increase with decreasing temperatures.

In the present case of pure spin paramagnetism, the empirical susceptibility law can be explained on quite general grounds. Its results from the interplay of the disordering effects of thermal origin and the ordering effects due to both the application of a constant and uniform external magnetic field and the existence of an internal field, the latter tending to achieve antiparallel orientation of the nuclear spins.[3] Actually we are in presence of a "three-way" competition, insofar as the internal spin ordering phenomenon tends to oppose also the magnetization effect of the applied field. The existence of the internal field is of course a permanent and fundamental characteristic of the system. Let, then, $\nu(T)$ be the number, per unit volume, of those atoms or spin moments of the system at the finite temperature T which, as a result of thermal disorder, have escaped the orienting effect of the internal field. The magnetic moment $M(H,T)$ per unit volume induced in the system at temperature T, by application of the external uniform field of strength H, is given by the quantum-mechanical formula of Brillouin[9] for independent spins, or

$$M(H,T)=\nu(T)\mu B_{\frac{1}{2}}(\mu H/kT)$$
$$=\nu(T)\mu\tanh(\mu H/kT), \tag{5}$$

for spin moments $\hbar/2$ and actual magnetic moments μ. In the paramagnetic range $\mu H\ll kT$ this yields the susceptibility

$$\chi(T)=\lim_{\mu H\ll kT} M/H$$
$$=\nu(T)\mu^2/kT. \tag{6}$$

Hence, on the basis of the above reasoning,

$$\chi(T)/\chi_0(T)=\nu(T)/n, \tag{7}$$

where

$$\chi_0(T)=n\mu^2/kT \tag{8}$$

is the limiting Curie-Langevin susceptibility law, n being the atomic concentration in the system at temperature T. The ratio of the measured and ideal limiting susceptibilities, at the same temperature, is thus equal to the fraction of those atoms which, in absence of the external field, are in the double spin-degenerate levels

[5] W. Pauli, Jr., Z. Physik. **41**, 81 (1927).
[6] Grilly, Hammel, and Sydoriak, Phys. Rev. **75**, 1103 (1949); E. C. Kerr, Phys. Rev. **96**, (1954).
[7] G. deVries and J. G. Daunt, Phys. Rev. **92**, 1572 (1953); **93**, 631 (1954). T. R. Roberts and S. G. Sydoriak, Phys. Rev. **93**, 1418 (1954). Osborne, Abraham, and Weinstock, Phys. Rev. **94**, 202 (1954).
[8] P. Langevin, Ann. chim. et phys. **5**, 70 (1905).
[9] L. Brillouin, J. phys. et radium **8**, 74 (1927).

as stated by Fairbank and his collaborators on the basis of the ideal antisymmetric Fermi fluid type of degeneration mechanism. The preceding derivation of the ratio (7) is however quite general and independent of the particular mechanism responsible for the antiparallel alignment of the spins of the system.

It appears interesting to recall here the rigorous proof of the ratio (7) in the formalism of ideal antisymmetric fluids of atoms with spin sh. Here one can start from first principles, as was first shown by Bloch[10] in the course of his discussion of the Pauli-formula (3). Let n_i be, at temperature T, the mean number of atoms in the state of kinetic energy ϵ_i, of spin degeneracy g, or $(2s+1)$. By definition,

$$n_i(T)=g[\exp(\alpha+\epsilon_i/kT)+1]^{-1}. \tag{9}$$

The probability of finding only one single atom in the group of g levels, or the g-fold level, is $n_i(T)$ times the probability that in this level group is empty. This latter probability is, by definition, $(1-n_i/g)$. Hence, the probability for having only a single atom of energy ϵ_i is

$$\sigma_i(T)=n_i(T)(1-n_i/g). \tag{10}$$

The total number of atoms in the system occupying singly the g-fold levels is thus

$$N_\sigma(T)=\sum_i \sigma_i(T), \tag{11}$$

the summation extending over the whole spectrum of the system. With the free particle continuous spectrum approximation $\epsilon(p)=p^2/2m$, p being their linear momentum and m their mass, and the associated level density $4\pi(V/h^3)p^2dp$ one finds in the whole system occupying volume V, using (9), (10), and (11),

$$N_\sigma(T)=4\pi g(V/h^3)\int_0^\infty \left\{p^2\left[\exp\left(\alpha+\frac{p^2}{2mkT}\right)\right]\Big/ \left[1+\exp\left(\alpha+\frac{p^2}{2mkT}\right)\right]^2\right\}dp, \tag{12}$$

which yields easily, when the denominator,

$$N_\sigma(T)=gV(2\pi mkT/h^2)^{\frac{3}{2}}\sum_{\lambda=1}^{\infty}(-)^{\lambda-1}\lambda^{-\frac{3}{2}}\exp(-\lambda\alpha), \tag{13}$$

is expanded. But from the definition of the parameter α, N being the total number of atoms of the system at temperature T, one has

$$\begin{aligned} N/V&=n\\ &=g(2\pi mkT/h^2)^{\frac{3}{2}}\sum_{\lambda=1}^{\infty}(-)^{\lambda-1}\lambda^{-\frac{3}{2}}\exp(-\lambda\alpha)\\ &=g(2\pi mkT/h^2)^{\frac{3}{2}}F(\alpha). \end{aligned} \tag{14}$$

[10] F. Bloch, Z. Physik 53, 216 (1929).

And finally, dividing (13) by (14), one obtains

$$\begin{aligned} \nu(T)/n&=\left[-\frac{1}{F(\alpha)}(dF/d\alpha)\right]\\ &=\chi_P(T)/\chi_0(T), \end{aligned} \tag{15}$$

using (3) and (8) for χ_P and $\chi_0(T)$, respectively. The general relation (7) is thus proved rigorously for ideal antisymmetric fluids.

The susceptibility measurements define through (7) the number of liquid He^3 atoms which have "freed" themselves from the spin orienting internal field and became thus, as far as their spins are concerned, independent. If the volume of the liquid is V, the total number of these spin-free or spin-disordered atoms is

$$N_\sigma(T)=\nu(T)V, \tag{16}$$

and the total number of their spin configurations is, g or $(2s+1)$ being equal to 2 for spins $\frac{1}{2}$,

$$P_\sigma(T)=2^{N\sigma(T)}. \tag{17}$$

By Boltzmann's theorem, they contribute to the total entropy of the liquid the entropy of spin disorder

$$S_\sigma(T)=N_\sigma(T)k\ln 2, \tag{18}$$

or, per mole of the liquid, N being Avogadro's number,

$$\begin{aligned} S_\sigma(T)&=(N_\sigma/N)R\ln 2\\ &=[\chi(T)/\chi_0(T)]R\ln 2, \end{aligned} \tag{19}$$

R being the gas constant, and where use has been made of (7). For our evaluation of the entropy of spin-disorder only the experimental values of $\chi(T)/\chi_0(T)$ are needed. The analytical form of the latter ratio and the knowledge of the detailed mechanism explaining the empirical susceptibility law are not needed at all, provided, of course, that this empirical susceptibility law belongs to that very wide class of susceptibilities for which the reasoning leading to (7) is valid.[11]

To the spin entropy (19) there is associated a heat capacity of spin disorder

$$\begin{aligned} C_\sigma(T)&=T(dS_\sigma/dT)\\ &=RT(\ln 2)(d/dT)[\chi(T)/\chi_0(T)], \end{aligned} \tag{20}$$

where, of course, the temperature derivative can be evaluated directly with the empirical ratio $\chi(T)/\chi_0(T)$. The knowledge of the latter determines thus also the heat capacity of spin disorder in liquid He^3 in as absolute a way as it determines the spin entropy.

At the present time, and for reasons of simplifying the above calculations of entropy and heat capacity of spin disorder, it is convenient to adopt for $\chi(T)/\chi_0(T)$ the expression resulting from (3), that is Eq. (15),

[11] That the susceptibility measurements should lead to the entropy of spin disorder in liquid He^3 has been suggested independently by Drs. T. R. Roberts and S. G. Sydoriak of this laboratory before the recent results of Fairbank and his group (reference 2) became available.

which is claimed[2] by the experimental workers to constitute a fair analytical approximation to the measured values of this ratio, with an "apparent" degeneration temperature T_0 of 0.45°K. Hence, the spin entropy (19) becomes with (15),

$$S_\sigma(T)/R=[-F'(\alpha)/F(\alpha)](\ln 2). \quad (21)$$

We want to emphasize, however, that the use of the preceding analytical approximation of the spin entropy in liquid He³ cannot and need not be, at the present time, interpreted as being equivalent to an acceptance of the elementary statistical gas degeneration mechanism on which it is based. The various difficulties raised by such an interpretation have been discussed in the preceding section.

The limiting values of S_σ, at both ends of the temperature interval, are:

$$\lim_{T \text{ large}} S_\sigma/R=(\ln 2)\lim_{\alpha\gg 1}[-F'(\alpha)/F(\alpha)]=\ln 2, \quad (22)$$

if the definition (4) of $F(\alpha)$ is used. Up to terms in $(1/\alpha^2)$, or $(T/T_0)^2$, one has

$$\lim_{T \text{ small}} S_\sigma/R=(\ln 2)\lim_{\alpha\ll 0}[-F'(\alpha)/F(\alpha)]$$
$$=(\tfrac{3}{2}\ln 2)\frac{1}{(-\alpha)}\left[1-\frac{\pi^2}{6\alpha^2}\right]$$
$$=(\tfrac{3}{2}\ln 2)(T/T_0)\left[1-\frac{\pi^2}{12}(T/T_0)^2\right]. \quad (23)$$

The low-temperature expansion of $F(\alpha)$,

$$F(\alpha)\underset{\alpha\ll 0}{=}\frac{1}{\Gamma(5/2)}(-\alpha)^{\frac{1}{2}}\left[1+\frac{\pi^2}{8\alpha^2}\right], \quad (24)$$

has been used in deriving (23). The analytical approximation (21) of S_σ predicts thus the linear vanishing of the spin entropy with temperature.

The spin heat capacity $C_\sigma(T)$, Eq. (20), becomes, within the same formalism,

$$C_\sigma(T)/R=(\ln 2)T\left[\left(\frac{F'(\alpha)}{F(\alpha)}\right)^2-\frac{F''(\alpha)}{F(\alpha)}\right]\left(\frac{d\alpha}{dT}\right)$$
$$=(\tfrac{3}{2}\ln 2)\left[\frac{F''(\alpha)}{F'(\alpha)}-\frac{F'(\alpha)}{F(\alpha)}\right], \quad (25)$$

since from (4),

$$T(d\alpha/dT)=-\tfrac{3}{2}(F(\alpha)/F'(\alpha)). \quad (26)$$

In the high and low temperature limits, one obtains

$$\lim_{T \text{ large}} C_\sigma/R=0, \quad (27)$$

since

$$\lim_{\alpha\gg 1}[F''(\alpha)/F'(\alpha)]\to -1, \quad \lim_{\alpha\gg 1}[-F'(\alpha)/F(\alpha)]\to 1.$$

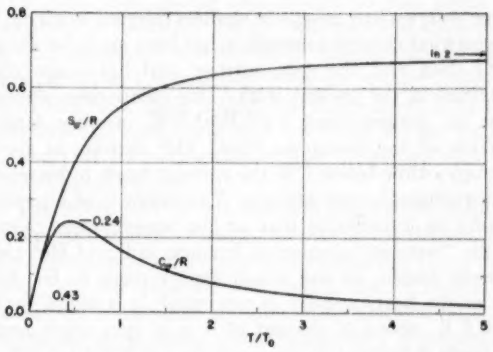

FIG. 1. Molar spin entropy S_σ/R and spin heat capacity C_σ/R in liquid He³ as a function of the temperature ratio T/T_0, T_0 being a characteristic temperature of spin orientation of about 0.45°K, according to the nuclear paramagnetic susceptibility data (reference 2).

Also, up to terms in $(1/\alpha^2)$, or $(T/T_0)^2$,

$$\lim_{T \text{ small}} C_\sigma/R=(\tfrac{3}{2}\ln 2)\frac{1}{(-\alpha)}\left(1-\frac{\pi^2}{3\alpha^2}\right)$$
$$=(\tfrac{3}{2}\ln 2)(T/T_0)[1-\tfrac{1}{4}\pi^2(T/T_0)^2]. \quad (28)$$

C_σ vanishes thus at both ends of the temperature interval. Since it is always positive, $S_\sigma(T)$ being a monotonically increasing function of T, it has at least one maximum. The position of this maximum is at $\alpha=-1.90$, $T/T_0=0.43$, and the peak value of C_σ/R is 0.24.

It is interesting to note here, in passing, that the very low-temperature spin entropy and spin heat capacity of the ideal antisymmetric fluid, up to terms linear in T, are only relatively small fractions of the total entropy and heat capacity. The ratios S_σ/S_{tot} and C_σ/C_{tot} equal $3\ln 2/\pi^2$ or 0.21. The spin portions of these quantities amount only to 21 percent of the totals at these low temperatures.

By using the Tables[12] of the function $F(\alpha)$ and its derivatives at $T/T_0\leqslant 2$, $\alpha\leqslant 1.23$, and the expansion (4) at $T/T_0>2$, the analytical approximations (21) and (25) of the spin entropy S_σ/R and spin heat capacity C_σ/R have been evaluated[13] in the range $0\leqslant T/T_0\leqslant 5$, $-20\leqslant\alpha\leqslant 2.7$. They are given in Fig. 1.

As mentioned in the Introduction, the knowledge of the spin entropy and the associated heat capacity allows one, after subtracting them from the measured total liquid He³ entropy and heat capacity, to obtain the nonspin or lattice portions of these thermal properties. Using the entropy and heat capacity data of the

[12] J. McDougall and E. C. Stoner, Trans. Roy. Soc. (London) **A237**, 67 (1938).

[13] I wish to thank here Mr. Max Goldstein and Miss M. L. Johnson for these calculations, and Mrs. L. E. Moss for the preparation of the graph. The low-temperature, $T/T_0\leqslant 2$, susceptibilities have been used already in Table I of our previous work, reference 3.

three independent groups of workers referred to above,[7] a somewhat cursory comparison has been made between their data and the spin entropy and heat capacity obtained in the present work. This comparison shows that at temperatures $1.0 \leqslant T \leqslant 1.5°K$, a very large portion of the enormous liquid He^3 entropy is spin entropy, while below 1°K the entropy tends to become overwhelmingly spin entropy. This result is of interest insofar as it indicates that at low temperatures most of the "nonspin" degrees of freedom of liquid He^3 are already frozen, as one would expect them to be. As far as the heat capacity is concerned, it is found that at 0.4°K, about 40 percent of it is of spin origin and C_σ tends to become its dominant part at $T \leqslant 0.4$–$0.3°K$. The characteristic peak of the spin heat capacity might be detectable in its effect on the total heat capacity at temperatures lower than those reached so far. The qualitative shape of the spin heat capacity curve is, of course, of permanent significance and is not connected with the analytical approximations used in the computation of the C_σ curve of Fig. 1.

It is expected that the experimental workers in the field of entropy and heat capacity investigations of liquid He^3 might analyze, in greater detail, their own respective data with the help of the practically absolute spin entropies and spin heat capacities obtained above. These experimental data appear, at the present time, to be still somewhat of preliminary character.

In conclusion we may thus say that a rigorous explanation has been given here for the origin of the very large liquid He^3 entropy at low temperatures. This is based on a rigorous evaluation of the partial entropy and heat capacity of spin disorder using the experimentally measured nuclear paramagnetic susceptibilities. It may be expected that the peculiar maximum of the spin heat capacity becomes observable indirectly on the total liquid heat capacity at low enough temperatures.

PHYSICAL REVIEW VOLUME 96, NUMBER 6 DECEMBER 15, 1954

Statistical Mechanics of Helium II near 1°K*

O. K. Rice
Department of Chemistry, University of North Carolina, Chapel Hill, North Carolina
(Received August 30, 1954)

It now seems probable that the roton excitations in helium II can be considered to be cooperative motions of small groups of atoms, the group as a whole being in an excited quantum state. This leads to a very literal interpretation of the two-fluid hypothesis, and suggests that the entropy of mixing of rotons and the unexcited atoms be calculated on the basis of the lattice theory of liquids. From this the thermodynamic properties of liquid helium are deduced, and the degeneracy of the roton energy level (giving the intrinsic entropy of the rotons) is obtained from the observed specific heat. The change in the thermodynamic properties of normal fluid (rotons) between 0°K and the λ point is discussed. Finally the peculiar properties of the coefficient of thermal expansion are considered in the light of the two-fluid hypothesis.

THE nature of the roton excitations in liquid helium II has recently been discussed by Feynman[1] who concluded that they involve cooperative motions, perhaps rotations, of a small number of atoms. Somewhat similar ideas, though differing in detail, had previously been advanced by Toda[2] and Matsubara.[3]

In considering the statistical behavior of the rotons it has generally been assumed that they can be treated as though they were a Bose-Einstein gas of particles of some particular effective mass. This was done originally by Landau,[4] and the thermodynamics of such a system has recently been considered in some detail by Goldstein[5] who has discussed some of the difficulties which arise. Landau's treatment is based upon the idea that the excitations arise from interactions of waves, which can be represented as excitons or considered as wave packets. The excitons are assumed to have a certain effective mass and to obey Bose-Einstein statistics. These assumptions serve to determine the entropy contributed by the excitons, but the effective mass must be taken as a parameter, and it is difficult to interpret.

Since the roton interactions are apparently localized over a region containing only a few atoms, it would seem reasonable to explore some other type of approximation, such as the lattice theory of liquids. Indeed, the lattice theory of liquids would seem to be peculiarly adapted to treatment of the rotons in the region around 1°K where the rotons are few in number. For in this temperature region the roton, according to the picture which has been developing, represents a small group of atoms in a single quantum state (though the energy may be broadened by interaction with the neighboring

* Work supported by the U. S. Office of Naval Research.
[1] R. P. Feynman, Phys. Rev. **94**, 262 (1954).
[2] M. Toda, Progr. Theoret. Phys. (Japan) **6**, 458 (1951).
[3] T. Matsubara, Progr. Theoret. Phys. (Japan) **6**, 714 (1951).
[4] L. D. Landau, J. Phys. (U.S.S.R.) **5**, 71 (1941); **8**, 1 (1944); **11**, 91 (1947); see R. B. Dingle, Advances in Phys. **1**, 111 (1952).
[5] L. Goldstein, Phys. Rev. **89**, 597 (1953).

molecules) and the state of the superfluid substrate does not depend on the position of the roton. At a sufficiently low temperature no account need be taken of more highly excited roton states of the same group of atoms; probably the only distinction between quantum states that needs to be considered resides in their nature and in the number of atoms involved. Thus there will be some multiplicity of the quantum state, and we shall as a first approximation consider it as a degenerate state of energy ϵ and multiplicity m. Furthermore, at the low temperatures considered, the rotons are independent of each other. We thus have two kinds of entities involved, namely, unexcited atoms and rotons, or groups of atoms in an excited energy level. It is seen that this enables us to give quite a literal interpretation of the two-fluid hypothesis if we say that the unexcited portion forms the superfluid, while the atoms in the rotons constitute the normal fluid. We consider helium II as a mixture of the two, and the number of different configurations of the system will depend upon the number of ways in which rotons and atoms can be arranged in order, provided that the density of rotons is small enough so that the question of overlapping does not arise. This results in an entropy of mixing given by

$$S_m = k \ln\left(\frac{(N-nq+n)!}{(N-nq)!n!}\right), \tag{1}$$

where N is the total number of atoms, including those in the rotons, n is the total number of rotons, and q is the average number of atoms in a roton. Since a roton has a degeneracy of m, the entropy of a roton is

$$S_r = k \ln m, \tag{2}$$

and its free energy (which can be taken as essentially the Gibbs free energy) is

$$G_r = \epsilon - kT \ln m. \tag{3}$$

If the free energy of the superfluid is taken as zero, the total free energy of the whole system is

$$G = nG_r - TS_m. \tag{4}$$

The equilibrium value of n is found by making G a minimum. Differentiating Eq. (4) with respect to n, using Eqs. (1) and (3), with the Stirling approximation, and setting the result equal to zero, we find

$$\epsilon - kT \ln m + (q-1)kT \ln(N-nq+n) - qkT \ln(N-nq) + kT \ln n = 0. \tag{5}$$

If the roton concentration is small, i.e., if n is very small compared to N, we obtain

$$n = Nme^{-\epsilon/kT}. \tag{6}$$

The roton part of the specific heat is given roughly (assuming ϵ is constant) by $\epsilon dn/dT$, hence we write

$$C = (Nm\epsilon^2/kT^2)e^{-\epsilon/kT}. \tag{7}$$

This form is of course very similar to that which is obtained in Landau's theory; the principal difference is that the factor in front of the exponential depends directly on m the multiplicity of the energy states of the roton, and there is no term which arises from the translational energy states of the roton, for the simple reason that we have assumed that the rotons have no translational energy.

The latter point is one that will stand some amplification. In Landau's theory, the velocity of the roton is not the material velocity of atoms exhibiting the excitation, but the velocity with which the excitation is passed on from point to point. The effective mass is, therefore, as we have noted, essentially a parameter which has to be chosen to give the proper entropy of the rotons, so that we have a factor of the right size to replace $Nm\epsilon^2/kT^2$ in Eq. (7) (or it may possibly be deduced from Feynman's theory). At least in the range of small density of rotons it is possible to make the thermodynamic consequences of the two theories coincide by the proper choice of the effective mass, on the one hand, or the multiplicity factor m, on the other. If the two theories turn out to be equivalent it will nevertheless be advantageous to have the value of m, which is more readily interpreted.

However, it is one of the properties of superfluid that it can flow freely around obstacles, and such obstacles should include particles of normal fluid. Thus there is certainly the possibility of bodily relative motion between the rotons and the superfluid. In this case, the total energy of the rotons would have the form $\epsilon + p^2/2\mu$, where p is the momentum and μ the effective mass. This is the same in form as the expression for the energy of rotons *first* suggested by Landau in 1941, though the significance of p is different. If this form of energy is used, and the rotons are assumed to be freely moving particles the value of μ required to give the proper entropy so as to obtain the observed specific heat of liquid helium is just of the order of magnitude expected for rotons of the size we have assumed. However, it is known that there is a critical velocity for thin films, in which the superfluid is moving and the normal fluid is stationary. This is[6] about 50 cm sec^{-1}, while the average thermal velocity of rotons consisting of 8 to 10 helium atoms, if behaving like an ideal gas at 1°K, would be at least 1000 cm sec^{-1}. Therefore it seems improbable that there can be development of an entropy of translation of the ideal gas type, and I believe that it is preferable to set up the expression for S_m in the form of Eq. (1). The actual bodily motion of rotons with respect to superfluid, though limited by the critical velocity, should be quite ample to account for second sound and the peculiar flow properties of liquid helium in the roton region. The whole development sug-

[6] K. R. Atkins, Advances in Phys. **1**, 169 (1952), see p. 189. It is true that the critical velocity increases as the film becomes thinner, so some question may exist regarding the upper limit.

gests that quite a literal interpretation of the two-fluid hypothesis may have considerable validity.

We shall now use Eq. (7) to determine ϵ/k and m. Using the specific heat data of Kramers, Wasscher, and Gorter[7] between 1.0° and 1.5°K and allowing for the phonon contribution by subtracting $0.0235\ T^3$ joule g^{-1} deg^{-1}, we obtain

$$\epsilon/k = 10.1°\text{K}, \quad m = 9.3.$$

The value of ϵ is of course approximately the same as the value of the energy increment obtained in Landau's theory. The value of m is rough since it depends fairly strongly on ϵ/k. Feynman[1] has suggested that the average roton might consist of six helium atoms involved in some kind of cooperative motion. If there were a range of about nine or ten in the number of helium atoms involved, this would account for the value of m. This might indicate that actually, on the average, eight or ten helium atoms are involved in a roton.

In making these calculations we have assumed that the roton concentration is small. It is somewhat tempting to suppose, however, that Eqs. (1) through (5) could be used at much higher concentrations (i.e., higher temperatures) provided ϵ and m could be evaluated as functions of T. As T increases, higher-energy levels must become accessible, so the value of ϵ (which is essentially an average value) and m must both increase. It may be possible to make a rough interpolation, since the values are known at the λ point, where the liquid is almost pure normal fluid. If there is actually an average of eight atoms per roton, the value of ϵ/k corresponds to an energy of about 2.5 calories per mole of helium in rotons, which is not far from the energy of liquid helium at the λ point, namely, 3.0 calories per mole, so that relatively little change is found in the average energy of superfluid over this range of temperatures. Still using eight atoms per roton, we find a change in entropy from about $(R/8)\ \ln 9.3 = 0.55$ to about 1.6 eu (entropy units) per gram atom, corresponding to about a 1.7-fold increase in the number of available energy levels for each atom, or about a 70-fold increase per roton of eight atoms. This seems to be a rather large change and means that as the roton concentration increases and some of them coalesce, there is a disproportionate increase in the number of energy levels, which certainly in large measure compensates for the decrease in entropy of mixing which occurs when concentration of rotons increases. This is, presumably, what causes the continued increase in specific heat up to the λ point. Looked at from the point of view of the energy levels of the whole system, we may say that there are many low-energy levels (case of few rotons) because these are localized and can be located in different regions of the fluid (entropy of mixing); on the other hand, the density of high-energy levels (case of many rotons) receives a contribution because the presence of some freely moving atoms makes it easier for other atoms to move freely also, when the rotons coalesce, and there may be highly excited energy levels in which the energy *per atom* is even lower than it is in isolated rotons.

The value of ϵ is comparable to the heat of vaporization of liquid helium, and one might intuitively expect that a single atom could be excited to a number of energy levels with energy appreciably less than the energy necessary to separate it from the liquid altogether. However, the result seems to be that this cannot occur in the case of helium. By the time the liquid gets to the λ point, it may be that individual atoms can move through the liquid fairly readily without each one having enough energy to evaporate, as we suggested in a previous paper.[8]

If this picture of liquid helium has any element of truth, it will be clear that entropy of mixing of superfluid and normal fluid must play an important role in determining the properties of the liquid, and that we were, therefore, correct in taking it into account in our discussion of the thermodynamics of liquid helium,[9] though some of the details may need to be changed (see Appendix). The present picture also is in accord with the ideas which we have discussed recently in considering the λ transition,[8] in that a separation of superfluid and normal fluid is visualized. The point of view taken here is that which is appropriate for a dilute solution of normal fluid in superfluid, whereas in discussing the λ point it is necessary to consider the reverse case.

Finally, as a sort of addendum, we should like to make a few remarks concerning the peculiar behavior of the coefficient of expansion of helium II. Atkins and Edwards[10] have recently found that there is a slight expansion with increasing temperature in the phonon range, as might be expected, followed by the well-known rather considerable contraction between 1°K and the λ point. On the basis of the two-fluid hypothesis this is formally accounted for by saying that normal fluid has a slightly smaller volume than superfluid.[11] In order to understand this further we have to inquire why the thermal plus zero-point energy of normal fluid changes less rapidly with the density than is the case with

[7] Kramers, Wasscher, and Gorter, Physica **18**, 329 (1952).

[8] O. K. Rice, Phys. Rev. **93**, 1161 (1954). The results of this paper, however, do not depend upon the detailed nature of the excitations.

[9] O. K. Rice, Phys. Rev. **76**, 1701 (1949). Indeed the existence of entropy of mixing was already implicit in Landau's original treatment, and Landau noted [L. D. Landau, Phys. Rev. **75**, 884 (1949)] that his theory was different from that of L. Tisza [Phys. Rev. **72**, 838 (1947)] in that it did not make the entropy proportional to the density of normal fluid.

[10] K. R. Atkins and M. H. Edwards, Phys. Rev. **93**, 1416 (1954).

[11] We have already (reference 9) treated the dependence of the λ temperature on pressure from this point of view. This calculation indicates that the partial volume of each of the two fluids may itself vary somewhat with circumstances.

superfluid.[12] The ground state energy (aside from the background of potential energy) is zero-point energy only, which depends upon the free range of motion of an atom hemmed in between other atoms. But a free range of motion, depending on the space between atoms, is very strongly dependent on density. An excited energy level probably involves motions of atoms through larger distances, and these distances will probably depend less strongly on density. Thus such an energy level itself does not depend so strongly on density, and that part of the helium where such an energy is excited settles down to a smaller interatomic distance, since this results, especially in liquid helium, in a lowering of the potential energy. Thus the negative coefficient of thermal expansion seems reasonable enough.

APPENDIX

It seems desirable to set forth the expressions for the partial molecular entropies, $\bar{s}_n$ and $\bar{s}_s$, for normal and superfluid, respectively, which are obtained from the theory here developed for the dilute roton region. $\bar{s}_n$ can be obtained by differentiating the entropy $S=S_m+nS_r$ with respect to n, holding $N-nq$, the number of superfluid atoms, constant, and then dividing by q, the number of atoms in a roton. This gives, if $n/N \ll 1$,

$$\bar{s}_n=(k/q)[\ln(N/n)+\ln m]. \tag{8}$$

The molecular entropy is given, at mole fractions x_n and x_s by

$$s=x_n\bar{s}_n+x_s\bar{s}_s=(qn/N)\bar{s}_n+[(N-qn)/N]\bar{s}_s. \tag{9}$$

Using Eq. (7), and neglecting the phonon contribution, we also have

$$\begin{aligned} s&=\int_0^T (C/NT)dT \\ &=\int_0^T (m\epsilon^2/kT^3)e^{-\epsilon/kT}dT \\ &=mke^{-\epsilon/kT}(1+\epsilon/kT). \end{aligned} \tag{10}$$

From Eqs. (6), (8), (9), and (10), and noting that qn/N is small, we obtain

$$\begin{aligned} \bar{s}_s&=mke^{-\epsilon/kT} \\ &=s/(1+\epsilon/kT). \end{aligned} \tag{11}$$

When it was assumed that s had the form,

$$s=s_\lambda(T/T_\lambda)^r,$$

where s_λ and T_λ denote values at the λ point and r is a constant, we found,[13] under the further assumption that there is no *enthalpy* of mixing of normal and superfluid but only *entropy* of mixing, that

$$\bar{s}_s=s/(1+r);$$

this is quite analogous to Eq. (11), only the dimensionless quantity ϵ/kT being replaced by its near equivalent, r.

[12] The rate of increase of this energy with decreasing volume represents a pressure which pushes outward, and which is balanced by the pressure due to the potential energy.

[13] O. K. Rice, Phys. Rev. **78**, 182 (1950).

Heat and Entropy of Mixing of He^3 and He^4 on the Basis of the Two-Fluid Theory of He^4†

O. K. Rice
Department of Chemistry, University of North Carolina, Chapel Hill, North Carolina
(Received September 3, 1954)

Recent data on the heat and entropy of mixing of He^3 and He^4 are treated by use of the two-fluid theory of He^4 together with Taconis' hypothesis that the He^3 dissolves only in normal fluid. Solution of He^3 causes normal fluid to be formed due to osmotic effects. It is assumed that the heat of mixing is a measure of the amount of normal fluid formed. It is then possible roughly to calculate the entropy of mixing of He^3 and He^4, taking into account entropy of mixing of He^3 and normal He^4, intrinsic entropy of the normal He^4 formed, and the entropy of mixing of normal and superfluid. This gives reasonable agreement with experiment. It is also shown that the theory indicates reasonably good fulfillment of the condition for internal equilibrium between normal and superfluid.

RECENTLY Sommers, Keller, and Dash[1] have measured the heat of mixing of He^3 with He^4 to form an 8.6 percent solution of He^3 in He^4 at 1.02°K. The integral heat of mixing was found to be about 0.17 cal absorbed per mole of solution, and the entropy of mixing times the temperature was 0.06 cal per mole less than would be expected from an ideal classical solution. Heats of mixing can of course be calculated from any well defined theory of mixing of He^3 and He^4, and Nanda[2] has recently given a tabulation of results obtained from several such theories. He has pointed out that valuable information on the mechanism of mixing might be obtained from data over a range of temperatures. Though such data are not at present available, it is to be noted that Sommers, Keller, and Dash actually provided two items, the heat and entropy of mixing, and together they can give more information than the heat of mixing alone at a single temperature.

We should like to consider these data from a rough mechanistic point of view, based upon a theory of helium II around 1°K which we have recently developed.[3] This theory involves a rather literal interpretation of the two-fluid hypothesis, the superfluid and the normal fluid (the latter being in the form of rotons when the temperature is near 1°K) being separated in ordinary space and having an entropy of mixing. This lends itself very readily, as may be seen, to the application of the Taconis[4] hypothesis which states that He^3 dissolves only in the normal-fluid part of He^4. This hypothesis we shall assume to be true, and from it the positive heat of mixing can be understood in a qualitative way. Addition of He^3 to He^4 produces osmotic forces which cause more normal fluid to be formed,[5] thus requiring absorption of heat.[6] We shall, in fact, try the very rough assumption that *all* the heat absorbed is due to the formation of more normal fluid, and that this normal fluid requires the same amount of energy (which we take from reference 3 to be 2.5 cal per mole of normal fluid around 1°K) as when it is formed in pure He^4. This may seem especially questionable when the normal fluid is in the form of rotons, and when the total amount of normal fluid does not exceed the amount of He^3; nevertheless it seems to be the most sensible first approximation. On this basis, the heat of mixing found by Sommers, Keller, and Dash means that the presence of 0.086 mole of He^3 in a solution containing a total of 1 mole induces the formation of $0.17/2.5=0.068$ mole of normal fluid at 1.02°K. The original amount of normal fluid at this temperature is negligible. Thus, by the Taconis hypothesis, the mole fractions within the rotons are $x_{3r}=0.56$ and $x_{4r}=0.44$.

Actually the amount of normal fluid formed should be calculated on the basis of a definite theory of mixing by setting the chemical potential of normal fluid in a mixture equal to that of superfluid. This requires somewhat involved considerations, however, and we shall first proceed to estimate the entropy of mixture based on the above estimate of the amount of normal fluid formed, and shall later attempt to check the equality of the chemical potentials.

In reference 3 we supposed that the normal fluid consisted of rotons containing about 8 atoms each. We shall continue to make the rough assumption that normal fluid consists of rotons of 8 atoms each, but will suppose that these may be partly He^4 and partly He^3. The entropy of mixing S_{mr} of He^4 and He^3 within the rotons times the temperature will be

$$TS_{mr}=-RTx_{3r}\ln x_{3r}-RTx_{4r}\ln x_{4r} \qquad (1)$$

per mole of rotons. Within the rotons there will be $x_r=0.154$ moles of material per mole of total fluid.

† Work supported by U. S. Office of Naval Research.
[1] Sommers, Keller, and Dash, Phys. Rev. **92**, 1345 (1953).
[2] V. S. Nanda, Phys. Rev. **94**, 241 (1954).
[3] O. K. Rice, preceding paper [Phys. Rev. **96**, 1460 (1954)].
[4] Taconis, Beenakker, Nier, and Aldrich, Phys. Rev. **75**, 1966 (1949).
[5] O. K. Rice, Phys. Rev. **77**, 142 (1950).
[6] L. Goldstein, Phys. Rev. **95**, 869 (1954), has just published results for the heat and entropy of mixing of ideal Bose and Fermi gases. For thermodynamic variables corresponding to the experiment of Sommers, Keller, and Dash the heat of mixing thus obtained is 0.1 cal absorbed per mole of mixture, and the entropy times the temperature is 0.11 cal per mole less than that for ideal classical gases. Since the total volume is assumed to remain constant in the mixing process, the effect of the mixing in this ideal gas theory is a mutual dilution, which pulls the Bose gas molecules into higher-energy levels (i.e., changes superfluid to normal fluid, wherein the ideal gas theory resembles the one we are considering here) and allows the Fermi gas molecules to sink into lower levels, a partially but not completely compensating effect.

We thus have for the entropy of mixing within rotons

$$x_r TS_{mr} = 0.214 \text{ cal/mole.}$$

We next consider the entropy of mixing of rotons and superfluid. This is given by Eq. (1) of the cited paper,[3] and we assume this is unchanged. We shall use this equation in the form it takes when the number of rotons is small compared to the number of superfluid atoms, namely,

$$S_{mrs} = nk + nk \ln(N'/n). \tag{2}$$

Here k is the Boltzmann constant, n is the number of rotons, and N' is the total of atoms not in rotons. In this case $N = N' + nq$ (where q is the number of atoms per roton, taken here as 8) is equal to Avogadro's number. Actually, it is hardly justified in the case under consideration to suppose that the roton concentration is small, and there are even likely to be some complications arising from coalescence of rotons. We know so little about how to handle this situation, however, that it seems just as well to get a rough estimate by the use of Eq. (2).

Assuming $q=8$, and recalling that in the case considered there are 0.154 mole in the rotons per mole of material, we see that $n = (0.154/8)N$ and $N'/n = 8(0.846/0.154)$. Hence for one mole of solution,

$$TS_{mrs} = 0.186 \text{ cal/mole.}$$

Finally we have to consider the entropy S_{4r} of the He^4 in the rotons formed on solution of He^3. By Eq. (2) of reference 3 this was $k \ln m$ in pure He^4, m being the degeneracy of the roton excitation. This means an entropy of $(k/q) \ln m$ per atom. The number of He^4 atoms per roton in the present case is $x_{4r}q$ and the total number of rotons is n. We therefore have

$$S_{4r} = n x_{4r} k \ln m, \tag{3}$$

and using $n = (0.154/8)N$, recalling that $x_{4r} = 0.44$, and taking $m = 9.3$ from reference 3, we have

$$TS_{4r} = 0.038 \text{ cal/mole.}$$

Adding together the contributions we obtain for the total entropy of mixing per mole of solution,

$$TS_m = x_r TS_{mr} + TS_{mrs} + TS_{4r} = 0.44 \text{ cal/mole.}$$

For a classical ideal fluid we would have

$$TS_m = -RTx_3 \ln x_3 - RTx_4 \ln x_4,$$

where, in this case, $x_3 = 0.086$ and $x_4 = 0.914$. This is equal to 0.60. It is seen that our calculated value is 0.16 cal/mole less than the ideal energy of mixing times the temperature, while according the Sommers, Keller, and Dash the observed entropy of mixing times T is 0.06 less than the ideal entropy. In view of the rather rough approximations made, it appears that we have achieved a reasonably good correlation of the entropy of mixing with the heat of mixing. It should be noted that the experimental data were also rough.

We now turn to the question of the equality of the chemical potential of the superfluid with that of the normal part of He^4, namely the part in the rotons. The chemical potential of the superfluid is equal to $-T\bar{S}_s$, where $\bar{S}_s$ is the partial molal entropy of superfluid, the enthalpy of superfluid being taken as zero. By Eqs. (11) and (6) of reference 3, we see that $\bar{S}_s$ is roughly equal to $(n/N)R$, which is very small. Hence, we must essentially have

$$\bar{H}_n = T\bar{S}_n, \tag{4}$$

for the normal fluid. $\bar{H}_n$ is approximately 2.5 cal per mole. In calculating $\bar{S}_n$ we consider what happens when a small amount of normal fluid, say, dn_r atoms, is added to the rotons. In the first place we note that it mixes with the He^3 and the partial molal entropy of mixing is $-R \ln x_{4r}$. Secondly, the partial molal entropy arising from intrinsic entropy is $(R/q) \ln m$. Finally, there is a change in the number of rotons given by $dn = dn_r/q$, and there will be a contribution from the entropy of mixing equal to $q^{-1}\partial S_{mrs}/\partial n$ per molecule. Thus this contribution to the partial molal entropy is $(R/q) \ln(N'/n)$, and we may write

$$T\bar{S}_n = -RT \ln x_{4r} + (RT/q) \ln m + (RT/q) \ln(N'/n) = 3.2.$$

Again, considering the roughness of the calculation, this would seem to balance $\bar{H}_n$ fairly well. Within the limits of the approximations involved, we may be said, then, to have a reasonable explanation for the heat mixing of He^3 and He^4 at 1.02°K, and the attendant change of entropy.

Secondary Emission by Positive Ion Bombardment

MANUEL SCHWARTZ AND PAUL L. COPELAND
Department of Physics, Illinois Institute of Technology, Chicago, Illinois
(Received August 6, 1954)

The investigation was undertaken primarily to determine the ratio of the secondary electron current to the primary ion current, i_s/i_p, for mercury ions bombarding a mercury target. The beam constituted a source of continually renewed surface of the target material. By varying the electron accelerating potential in the ion source, the proportions of the various types of ions present in the beam were altered. Thus the influence of mercury ions having different charges upon the secondary electron yield was determined. Some work was also done with cadmium ions bombarding a cadmium target.

Singly charged mercury ions formed by electrons of up to 27 v in the ion source gave a secondary emission coefficient, γ, ranging from 1.2 percent at 4.2 kev to 4.8 percent at 9.2 kev. For electron accelerating potentials of 73 v, 110 v, and 430 v, ratios i_s/i_p were determined. At 430 v, i_s/i_p varied from 3.2 percent at 1.2 kv to 11 percent at 9.2 kv. Estimates were made of γ for Hg^{2+} and Hg^{3+} ions.

In the case of cadmium, the electron accelerating potential was maintained at 450 v. Here i_s/i_p was exceedingly high for an untreated target, varying from 35 percent at 1.5 kv to 190 percent at 7.3 kv. Renewing the surface of the cadmium target by an additional source of cadmium vapor resulted in some reduction of i_s/i_p.

INTRODUCTION

THE summary of earlier studies by Massey and Burhop[1] indicates that the secondary electron coefficient has been determined for light, slow-moving ions bombarding a variety of targets. More recently Hagstrum[2] has discussed certain discrepancies in some of the previous work. However, in contrast to light ions. there have been few attempts to use heavy, slow-moving ions. Linford[3] has bombarded many targets with high-speed mercury ions; however, no systematic study has been made hitherto with slow-moving mercury ions.

Although Bruining and deBoer[4] measured the secondary emission due to primary electrons for alkali metal surfaces on which new material was constantly condensed from the vapor phase, there appears to be little evidence in the literature of attempts to use ions and target materials of the same element.[5] This affords a means of reducing the influence of contamination of the target material. As a consequence, this investigation was undertaken with mercury ions bombarding a mercury target and with cadmium ions bombarding a cadmium target.

APPARATUS

The experimental tube is shown in Fig. 1. At *A*, a sample of especially pure mercury metal of instrument grade was introduced. After the tube was evacuated, the mercury served as a source of mercury vapor. The filament *B*, a thin tungsten spiral, was supplied with current by several storage batteries, controlled by a rheostat and indicated on an ammeter. All the electrodes were made of nickel. Electrode *C*, a disk of large aperture, was approximately 110 volts positive with respect to the filament *B*. This voltage was maintained by using a selenium rectifier and filter. By means of this arrangement, the electrons thermionically emitted by the filament were accelerated toward electrode *C*. The electrons, colliding with the mercury vapor in the evacuated tube, ionized some of the mercury. The ion and electron beams were separated by the presence of electrode *D*, a disk with a central aperture approximately 5 mm in diameter. Electrode *D* was made about 200 volts negative with respect to electrode *C*.

The main accelerating voltage was controlled by using a high-tension power supply of conventional design, filtered by a condenser of large capacity. By means of this supply, a range of voltages extending to 10 kilovolts was readily obtained. This voltage appeared across a system of two electrodes, the upper one being electrode *D* and the lower one, electrode *E*. No attempt was made to produce a sharply focused beam. However, the presence of the cup *J* filled with dry ice and acetone assisted the formation of an ion beam and prevented the mercury discharge from penetrating into the lower parts of the tube.

The electrodes *F*, *G*, and *H* and the mercury pool *I* constituted the collecting system. The uppermost electrode *F* had an aperture approximately 5 mm in diameter. Immediately below it was electrode *G* with an aperture roughly 12 mm in diameter. This electrode shielded the collecting cylinder *H* from the direct effects of the positive ion beam. The cylinder was about 2.5 cm long and 5 cm in diameter.

To maintain the voltages on the electrodes comprising the collecting system, dry cells of 22.5 and 45 volts mounted on insulating bases, were used. Relative to ground, electrode *E* was 45 volts positive, electrode *F* was at zero potential, electrode *G* was 45 volts negative, the collecting cylinder *H* was at zero potential, and the mercury pool was 22.5 volts negative. It had pre-

[1] H. S. W. Massey, and E. H. S. Burhop, *Electronic and Ionic Impact Phenomena* (Clarendon Press, Oxford, 1952).
[2] H. D. Hagstrum, Phys. Rev. **89**, 244 (1953).
[3] L. H. Linford, Phys. Rev. **47**, 279 (1935).
[4] H. Bruining, and J. H. deBoer, Physica **5**, 17 (1938).
[5] Y. A. Dunaer, and I. P. Flaks, Compt. rend. acad. sci. (U.R.S.S.) **91**, 43 (1953).

viously been found by using variable power supplies that a wide range of voltages could be employed without influencing the measurements. The only precaution necessary was the maintenance of the correct relative polarity between adjacent electrodes.

The following precautions were taken. The lower part of the tube was surrounded with a Faraday cage to reduce induced currents which might have been detected with the sensitive dc microammeters used for the measurement of both the target and collector currents. In order to obtain reproducible readings, it was found necessary to freeze the mercury target. Otherwise, the ion beam colliding with the mercury vapor in the vicinity of the target caused ionization which vitiated the results.

The tube was aligned so that light from the filament illuminated an area of the target. An Alnico magnet was used to neutralize the results of stray fields so that the ion beam passed through the aperture in E.

The vacuum system was of a simple and conventional design. The apparatus was exhausted to a pressure below 10^{-6} mm Hg by a two-stage mercury diffusion pump backed by a Cenco Presso-Vac pump. The vacuum system was provided with the usual liquid air cold traps. In addition, a large U-shaped cold trap could be maintained throughout the night by filling a large vacuum flask with dry ice and acetone. The gas pressure was read by an RCA type 1949 hot-cathode ionization gauge. The entire system had only one stopcock and this was placed on the high-pressure side of the diffusion pump.

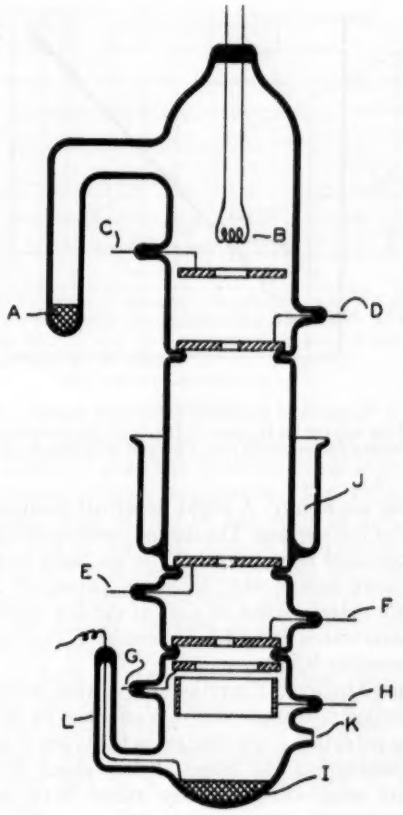

FIG. 1. Electronic tube.

MERCURY EXPERIMENT

Clean instrument mercury was put into the target receptacle I and into the reservoir A of the ion source. The system was evacuated to a pressure in the order of 10^{-6} mm Hg of permanent gas pressure as indicated by the ionization gauge. The filament in the ion source was then heated. This resulted in a sudden increase in the permanent gas pressure. However, within an hour the vacuum returned to about 10^{-6} mm Hg. The switches between the filament and the electrode C and that between C and D were then closed. The resulting electron and ion bombardment again resulted in an increase in pressure. After several hours, however, the pressure was restored. It was possible by continuous pumping over a period of several days to obtain readings with a permanent gas pressure of less than 10^{-6} mm Hg. The readings reported were obtained under these conditions.

The accelerating potential was initially set at 4 kv, and within 10 minutes or so the meters attained stable readings. Prior to this period, the readings were somewhat higher than the final values. Examination of the target revealed that a fresh clean spot of mercury, located in an essentially central position, appeared on the surface of the frozen target. From this fact, it might be inferred that the mercury ions were constantly being deposited in sufficient amount to keep the bombarded portion of the surface relatively fresh and free from adsorbed gas.

In view of the positive ion analysis of mercury by Bleakney,[6] it was decided to determine i_s/i_p for electron accelerating potentials other than 110 ev. In order to insure that the changes in the ratio constituted a real effect, it was usually customary to take alternate readings at two different electron accelerating potentials throughout the energy range. This was not done for the 27-ev case. However, each set of readings in this case was immediately followed by a set of readings of the 110-v case. Finally it is to be noted that for the two lower electron accelerating potentials, the voltage on electrode D was made only 30 to 90 volts negative with respect to the voltage on electrode C.

RESULTS AND CONCLUSIONS

Figure 2 indicates the ratios of i_s/i_p for mercury ions bombarding a mercury target. The mercury ions were produced by electrons with maximum energy of 110 ev. The trend of the curve is essentially linear with in-

[6] W. Bleakney, Phys. Rev. **35**, 139 (1930).

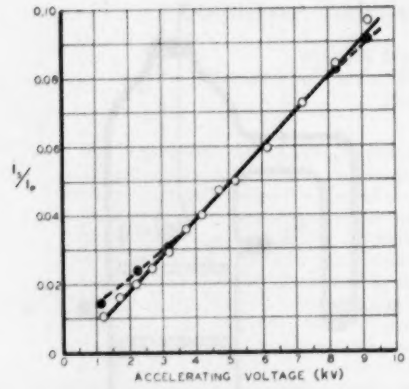

FIG. 2. Variation of secondary to primary current, i_s/i_p, with applied ion voltage for Hg ions on Hg. Solid line indicates original data. Dashed line indicates recent data with increased ion current.

creasing ion energy. A slight departure from linearity occurs at low energies. The dashed portions of the curve were obtained most recently. The ion beam was somewhat more intense and, therefore, permitted a more accurate determination of i_s/i_p at the low-energy end. The ratio varies from 1.5 percent at 1.2 kv to about 9.2 percent at 9.2 kv.

Figure 3 indicates the ratios of i_s/i_p when the electron accelerating potentials varied. Variations in the accelerating potentials cause changes in the types of mercury ions bombarding the target. Below about 30 ev the ions are singly-charged. From about 30 ev to 71 ev doubly-charged ions occur as well as singly-charged ions. At 110 ev a small percentage of triply-charged ions appear in the beam. Electron energies of 430 ev give rise to ions of four or five charges. The curves indicate the changes in the ratio for electron accelerating potentials of approximately 27, 73, 110, and 430 v, respectively. With increasing electron accelerating potential, i_s/i_p increases. Thus, at 4.2 kv, the value of i_s/i_p changes from 1.2 percent at 27 v to 5.8 percent at 430 v. At 9.2 kv, the effect is somewhat less pronounced, changing from 4.8 percent at 27 v to 11 percent at 430 v. It is to be noted, further, that at 27 v i_s/i_p is identical with γ for singly-charged mercury ions.

From the data indicated in Fig. 3, it is possible to estimate γ for Hg^{2+} and Hg^{3+} ions. The estimates, while admittedly rough, are significant in that they indicate a trend. The following consideration shows the procedure for obtaining γ for Hg^{2+} ions. A similar procedure determines γ for Hg^{3+} ions.

Let N = the number of electrons ejected by one singly-charged ion at a specified voltage, x = the number of electrons ejected by one doubly-charged ion at the same voltage, a = the fraction of singly-charged ions in the primary beam, b = the fraction of doubly-charged ions in the primary beam, and i_s/i_p = the measured ratio of the secondary electron current to the primary ion beam. Then, it follows that

$$\frac{i_s}{i_p}=\frac{aN+bx}{a+2b}.$$

From the results of Bleakney, a and b are known for each specified electron voltage. The experimental results for singly-charged ions indicated by the 27-v curve in Fig. 3 determines N. Further, i_s/i_p is given by the 73-v curve. Therefore, x can be evaluated.

The results of the analysis are shown in Table I, and the meaning of the entries can be explained as follows. Column I gives the applied voltage used for ion acceleration. For doubly-charged and triply-charged ions, the kinetic energy in kev is obtained by multiplying the applied voltage by a factor of two and three respectively. Column II gives the experimental results for Hg ions. Column III gives the calculated results for Hg^{2+} ions. A significant defect in the analysis is the fact that we have applied Bleakney's results for the efficiency of production of ions by electrons of a single energy to the electrons in the present experiment having all values up to the specified voltage. As a consequence, we somewhat underestimate the fraction of singly-charged ions. The importance of this consideration is reduced by the fact that electrons of higher energies are more effective in the production of ions and at 73 volts it is somewhat compensated by the fact that there will be a small trace of triply-charged ions and these ions have been excluded from the calculation of γ for Hg^{2+} ions. Also the fractions corresponding to 70 ev were read from Bleakney's data, tending to correct further for the above.

Column IV gives the value of γ for Hg^{3+} ions under the assumption that the composition of the beam is determined by electrons of 110 ev. However, since the range of voltages is greater in this case, there will be a more serious underestimation of the percentage of singly charged ions in the primary beam. Column V gives the values of γ for Hg^{3+} ions, if the effective electron potential is assumed to be 100 ev. While this

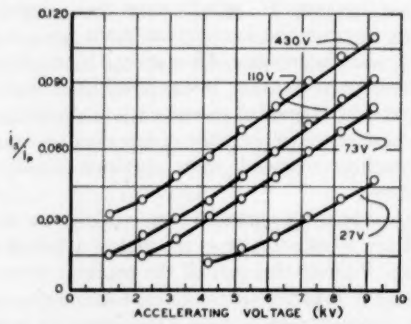

FIG. 3. Variation of secondary to primary current, i_s/i_p, with applied ion voltage for Hg ions on Hg for different electron accelerating potentials.

choice is arbitrary, it should be somewhat closer to the actual state of affairs in view of the above discussion. Further, the estimate of γ for Hg^{3+} ions is least accurate in view of the very small percentage of triply charged ions in the beam. The decrease from 1.2 to 0.96 when the energy is raised by increasing the potential difference from 8.2 to 9.2 kv is believed to represent experimental error rather than an actual decrease in the secondary emission coefficient.

According to Bleakney's results, the ionization potentials of Hg^{+}, Hg^{2+} and Hg^{3+} ions are approximately 10.4, 30, and 71 v. Columns II, III, and V show roughly that the values of γ increase with increasing ionization potential. This inference is born out by other experiments[2,7,8] in the low-energy range, and it has a theoretical interpretation since it implies that more potential energy from ions of higher charge is available to electrons of the metal for surmounting the potential barrier at the surface.

CADMIUM EXPERIMENT

Identical apparatus and similar procedures were adopted in the cadmium experiment. The sidearm A was filled with bits of cadmium metal. The target was composed of three thin cadmium disks backed by nickel for rigidity. It was found necessary to bring the filament closer to electrode C and to apply an electron accelerating potential of 450 v in order to generate ions.

In view of the high ratios in the case of cadmium, it was decided to study the nature of the surface before and after cadmium had been evaporated onto the target. Continued evaporation and pumping gradually brought the values down and these were remaining essentially constant by the fourth day. Finally, readings were also taken when mercury vapor diffused into the electronic tube from the mercury diffusion pump, after the removal of the cold trap.

TABLE I. Variations of γ with ionic charge for different applied ion voltages.

Applied ion voltage (kv)	Hg (experimental)	Hg^{2+} (corrected)	Hg^{3+} (uncorrected)	Hg^{3+} (corrected)
4.2	0.012	0.22	0.14	0.71
5.2	0.018	0.26	0.18	0.82
6.2	0.023	0.30	0.27	1.0
7.2	0.032	0.34	0.30	1.1
8.2	0.040	0.38	0.30	1.2
9.2	0.048	0.42	0.12	0.96

[7] M. L. E. Oliphant, and P. B. Moon, Proc. Roy. Soc. (London) **127**, 388 (1930).
[8] R. C. Bradley, Phys. Rev. **93**, 719 (1954).

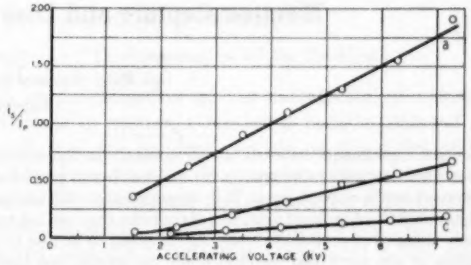

FIG. 4. Variation of secondary to primary current, i_s/i_p, with applied ion voltage for (a) untreated Cd ions on Cd, (b) Cd ions on evaporated Cd, and (c) a mixture of Hg and Cd ions on Cd with Hg present on Cd surface.

RESULTS

Figure 4 compares three different sets of data. The upper curve (a) gives the yield for an untreated cadmium target without evaporation. The yields were surprisingly high. At 1.5 kv the value of i_s/i_p is 35 percent, and at 7.3 kv it rises to 190 percent. The middle curve (b) shows the much lower ratio obtained for cadmium after evaporation. The lower curve (c) shows the further decrease in i_s/i_p when mercury diffused into the tube.

On the basis of energy and ionization potential or velocity[9] and ionization potential the results of cadmium and those of mercury should not differ to any considerable extent. It would appear that the difference must arise due to a marked difference in surface conditions.

SUMMARY OF RESULTS

The results may be summed up as follows. For a specific source of ions bombarding a specific target, the results can be understood in terms of the influence of velocity and the ionization potential of the incident ions. For ions of low energy, the ionization potential would appear to predominate in determining the secondary yield. As the energy of the ions increases, the influence of the ionization potential continues to manifest itself, although to lesser extent. The velocity factor eventually should mask the ionization potential.

In comparing two different targets, the nature of the surface of each has to be considered. Our results confirm the fact that in positive ion work, the secondary electron yields are extremely sensitive to the presence of traces of impurities adsorbed on the surface. In this work it is especially important to find a means of renewing the surface, and, thereby, of obtaining yields approaching those characteristic of the target material.

[9] W. Ploch, Z. Physik. **130**, 174 (1951).

Electron Capture and Loss by Moving Ions in Dense Media

JACOB NEUFELD
Oak Ridge National Laboratory, Oak Ridge, Tennessee
(Received May 26, 1954)

Several experiments have shown an anomaly in the stopping power which appears to be greater for incident heavy particles in condensed media than in gases. It is suggested that this anomaly is characteristic of incident ions, i.e., of particles that are not completely stripped of orbital electrons, and it seems to be due to the reaction of the perturbed medium upon the moving ion having charge Ze, which reaction results in a field $F=(1/Ze)(dW/dz)$ acting against the motion of the ion (dW/dz is the energy loss per cm). Although F is relatively weak in gases, it is substantial in condensed media and may cause the spontaneous emission of electrons carried by the ion (autoionization), thus increasing the ions' effective charge. The higher effective charge accounts for the higher stopping power in condensed media. It has been determined that when an incident helium atom passing through a liquid undergoes a collision, thus emerging in a singly ionized and excited state, it cannot exist in such a state since it becomes instantly doubly ionized. However, the same type of collision occurring in a gas leaves the atom singly ionized. The effective charge of the incident particle depends upon the values ϕ_0, ϕ_1, and ϕ_2, representing the probability of the particle's being neutral, singly ionized, and doubly ionized, respectively, where $\phi_0:\phi_1:\phi_2=\sigma_{10}\sigma_{21}:\sigma_{01}\sigma_{21}:\sigma_{01}\sigma_{12}$ (σ_{if} represents the cross section for electron loss or capture; i and f represent the charge before and after the event, respectively). It is shown that σ_{if} is higher for a condensed medium than for a gas when $i<f$ and lower when $i>f$. σ_{if} has been calculated for He passing through argon gas at 400 kev, and gives roughly $\phi_0:\phi_1:\phi_2=0.05:0.75:0.20$; thus, an average square charge is $\langle e^2\rangle_{Av}=1.55e^2$. If autoionization is taken into account, σ_{if} for He in liquid argon gives roughly $\phi_0:\phi_1:\phi_2=0.04:0.70:0.26$, and thus $\langle e^2\rangle_{Av}=1.74e^2$.

I. INTRODUCTION

IN the past several years attention has been called to an apparent anomaly in the behavior of an alpha particle passing through water. Early experiments performed by Michl[1] and Philipp[2] and confirmed more recently by Appleyard[3] have established that water in the liquid state has a stopping power for alpha particles higher by 10–20 percent than that of water vapor. Consequently, the Bragg rule which claims additivity of atomic stopping power for all media is questioned.

In contrast to the aforementioned work, two experiments appear to throw a cloud of uncertainty on the situation. For example, de Carvalho[4] reaches the conclusion that the stopping power for alpha particles is the same for vapors and condensed media, and similar results have been obtained by Ellis, Rossi, and Failla.[5,6] Platzman[7] has given a critical review of the experiments and discussed the influence of electronic binding on the stopping power.

It is difficult on the basis of the few and discordant experimental studies that have been made to reach a conclusion about the existence and the possible extent of the anomaly. The purpose of this paper is to point out a factor that may account in part for the larger stopping power for ions moving in condensed media.

II. EFFECT OF THE MEDIUM

A. General

It is suggested that the anomaly in the stopping power is due to a "density effect" of the surrounding medium upon a moving particle. The "density effect" referred to here is of an entirely different nature than the "density effect" suggested by Swann,[8] the theory of which has been given by Fermi.[9] The latter density effect accounts for a decreased stopping power in condensed media, while we are concerned with an increased stopping power. Furthermore, the Swann-Fermi density effect is characteristic of particles having relativistic velocities, while we are interested in particles moving rather slowly.

We are concerned here with particles that are not completely stripped of orbital electrons and which successively lose and capture electrons while colliding with the surrounding atoms. Because of the "density effect," an ion of a given velocity has a higher effective charge when traversing a medium in a condensed state (solid or liquid) than when traversing a medium of the same composition but in the gaseous state. The higher effective charge may account for the higher stopping power of ions traversing condensed media and thus give a plausible explanation of the anomaly.

The dependence of the charge of a moving ion upon the character of the surrounding medium has been studied experimentally by Lassen,[10] who has shown that a fission fragment in various gases has a much lower average charge than a fission fragment of the same velocity passing through a solid. The results of Lassen are significant because they confirm the effect of the density of the medium on the charge of the particle. Furthermore, they corroborate the existence of the anomaly in the stopping power, at least insofar as they relate to fission fragments.

Further confirmation of the effect of the density of the medium on a moving ion may be obtained from the

[1] W. Michl, Sitzber. Akad. Wiss. Wien, Math.-naturw. Kl. **123**, 1965 (1914).
[2] K. Philipp, Z. Physik **17**, 23 (1923).
[3] R. K. Appleyard, Proc. Cambridge Phil. Soc. **47**, 443 (1950).
[4] H. G. de Carvalho, Phys. Rev. **78**, 330 (1950).
[5] Ellis, Rossi, and Failla, Phys. Rev. **86**, 562 (1952).
[6] R. H. Ellis, Jr., Rev. Sci. Instr. **25**, 336 (1954).
[7] R. L. Platzman, *Symposium on Radiobiology*, edited by J. J. Nickson (John Wiley & Sons, New York, 1952), p. 139.
[8] W. F. G. Swann, J. Franklin Inst. **226**, 598 (1938).
[9] E. Fermi, Phys. Rev. **57**, 485 (1940).
[10] N. O. Lassen, Kgl. Danske Videnskab. Selskab, mat.-fys. Medd. **26**, 5 (1951).

experiments of Allison, Casson, and Weyl[11] on helium particles that attained charge equilibrium in metal foils and from the experiments of Snitzer[12] on helium particles passing through gases. Allison and Warshaw[13] have compared the results of these experiments and have shown that the ratio He^{++}/He^{+} in ions which have been equilibrated by scattering from a metal surface is considerably greater than in those in which equilibrium has been produced by passage through air. These experiments cover an energy range 175 kev–400 kev for the incident helium ion, and they appear to indicate that the effective charge, and consequently the stopping power of alpha particles, is higher in metal foils than in air.

A quantitative study of the density effect is difficult, since there is no exact method for calculating the effective charge of ions moving in various media. Some estimates have been made by Bohr,[14–16] Lamb,[17] Knipp and Teller,[18] and Brunings, Knipp, and Teller,[19] who assumed that the effective charge of an ion is a unique function of its velocity. They considered a relationship between the orbital velocity of the most easily removed electron and the velocity of the ion and assumed that this relationship is independent of the surrounding medium. They have neglected, therefore, the effect of the medium upon the moving ion, and such an effect is the subject of our discussion.

We take the specific case of an incident particle having atomic number $Z_1=2$ (helium), velocity $v=2v_0(v_0=e^2/\hbar)$, and surrounded by a medium having atomic number $Z_2=18$ (argon). Because of the density effect, the effective charge of the particle is higher in liquid argon than in argon gas. The effective charge is expressed in terms of cross sections (σ_{if}) for electron capture and loss; i and f represent the charge of the moving particle before the event and after the event, respectively. It will be shown that for electron loss, i.e., when $i<f$,

$$\sigma_{if}^{(d)} \geqslant \sigma_{if}^{(g)}; \tag{1}$$

and conversely, for electron capture, i.e., when $i>f$,

$$\sigma_{if}^{(d)} \leqslant \sigma_{if}^{(g)}. \tag{2}$$

In the above inequalities, $\sigma_{if}^{(d)}$ and $\sigma_{if}^{(g)}$ refer to condensed media and to gases, respectively. We shall use the superscripts (d) and (g) to designate quantities that relate to condensed media and gases, respectively.

[11] Allison, Casson, and Weyl (to be published). Some of the results of these experiments are briefly stated in reference 13.
[12] E. Snitzer, Phys. Rev. **89**, 1237 (1953).
[13] S. K. Allison and S. D. Warshaw, Revs. Modern Phys. **25**, 779 (1953).
[14] N. Bohr, Rev. **58**, 654 (1940).
[15] N. Bohr, Phys. Rev. **59**, 270 (1941).
[16] N. Bohr, Kgl. Danske Videnskab. Selskab, mat.-fys. Medd. **18**, 8 (1948).
[17] W. E. Lamb, Phys. Rev. **58**, 696 (1940).
[18] J. K. Knipp and E. Teller, Phys. Rev. **59**, 659 (1941).
[19] Bruning, Knipp, and Teller, Phys. Rev. **60**, 657 (1941).

B. Autoionization

(1) *Formulation of the Problem*

In an investigation of the interaction of charged particles with matter, attention is usually centered on the effect of the incident particle on the surrounding medium. Here we take the opposite point of view and consider the reaction of the perturbed medium on the particle. As shown by Bohr,[16] the perturbed medium is polarized and the polarization is localized in the wake of the incident particle. Since the polarization is not uniformly distributed, we obtain an electric field which is directed against the motion of the particle. The magnitude of this field at the position of the particle is

$$F=(1/Ze)(dW/dz), \tag{3}$$

where dW/dz is the energy loss per unit of length of the particle track (aligned along z axis), and Ze is the charge of the incident particle.

The value dW/dz depends on the number of atoms per unit volume in the stopping medium and if the medium is condensed the values dW/dz and F are relatively large. If, however, the medium is a gas, both dW/dz and F are relatively small.

The field F acts as a brake on the incident particle, and if the particle is an ion, its structure is distorted by polarization along the direction of motion. In a gas, F is small, and the resulting polarization is weak, having negligible effect on the structure of the moving ion. However, in the case of a solid or liquid, we have a strong polarizing field which may cause emission of electrons carried by the ion (autoionization). This process would increase the effective charge on the ion, and the higher effective charge would account, at least in part, for the higher energy loss due to ionization and excitation of the medium.

Autoionization under the effect of a strong electric field has been discussed by Oppenheimer[20] and more in detail by Lanczos[21] and by Bethe[22] in connection with the Stark effect in hydrogen. We shall consider this effect as applied to a nucleus of charge number Z_1 carrying a single bound electron.

The wave function of an electron in the Coulomb field due to the nucleus and in the potential field eFz due to the surrounding medium can be expressed as follows:

$$\frac{\chi_1(\xi)\chi_2(\eta)}{\xi^{\frac{1}{2}}\eta^{\frac{1}{2}}}e^{im\varphi}, \tag{4}$$

where ξ, η, φ are parabolic coordinates, m is the magnetic quantum number, and $\chi_1(\xi)$, $\chi_2(\eta)$ satisfy the

[20] J. R. Oppenheimer, Phys. Rev. **31**, 66 (1928).
[21] C. Lanczos, Z. Physik **62**, 518 (1930); **65**, 431 (1930); **68**, 204 (1931).
[22] H. A. Bethe, *Handbuch der Physik* (Springer, Berlin, 1933), Vol. 24, No. 1, p. 410.

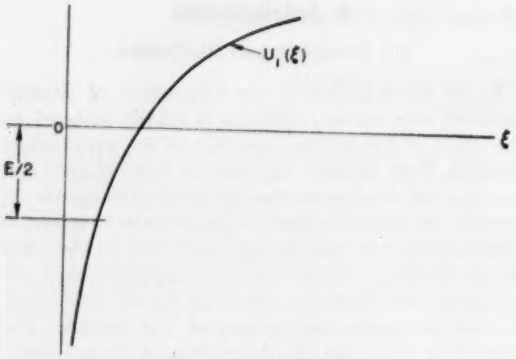

FIG. 1. Plot of $U_1(\xi)$.

following equations:

$$\frac{d^2\chi_1}{d\xi^2}+\left[\frac{E}{2}+\frac{(2n_1+m+1)Z_1}{2n\xi}-\frac{m^2-1}{4\xi^2}-\frac{F\xi}{4}\right]=0, \quad (5)$$

$$\frac{d^2\chi_2}{d\eta^2}+\left[\frac{E}{2}+\frac{(2n_2+m+1)Z_1}{2n\eta}-\frac{m^2-1}{4\eta^2}+\frac{F\eta}{4}\right]=0. \quad (6)$$

Here n is the "effective" principal quantum number, and n_1, n_2 are the "effective" parabolic quantum numbers; the electron energy E is expressed in atomic units of $me^4/\hbar^2$, and the field F is expressed in atomic units of $m^2e^5/\hbar^4$.

Each of the Eqs. (5) and (6) represents formally the one-dimensional Schrödinger equation of a particle having energy $E/2$ moving in potential fields $U_1(\xi)$, $U_2(\eta)$, where

$$U_1(\xi)=-\frac{(2n_1+m+1)Z_1}{2n\xi}+\frac{m^2-1}{4\xi^2}+\frac{F\xi}{4}, \quad (7)$$

$$U_2(\eta)=-\frac{(2n_2+m+1)Z_1}{2n\eta}+\frac{m^2-1}{4\eta^2}-\frac{F\eta}{4}. \quad (8)$$

Following Lanczos, we neglect the terms $(m^2-1)/4\xi^2$ and $(m^2-1)/4\eta^2$, and we take $m=0$. Then,

$$U_1(\xi)=-\frac{(2n_1+1)Z_1}{2n\xi}+\frac{F\xi}{4}, \quad (9)$$

$$U_2(\eta)=-\frac{(2n_2+1)Z_1}{2n\eta}-\frac{F\eta}{4}. \quad (10)$$

(2) *Delayed Ionization*

The potentials $U_1(\xi)$ and $U_2(\eta)$ are of the form illustrated in Figs. 1 and 2. The form of $U_1(\xi)$ gives discrete energy levels. The form of $U_2(\eta)$ exhibits a potential barrier separating two regions within which the electron motion is classically possible for any negative energy E: region I in the immediate neighborhood of the nucleus and region II at sufficiently large distances from the nucleus. Consequently, a bound electron has a finite probability of penetrating through the barrier and escaping from the neighborhood of the nucleus into the distant region. The probability[21] of such an escape per unit of time is

$$S=e^{-2I_2}/4I_1, \text{ atomic units of } (me^4/\hbar^3), \quad (11)$$

where

$$\alpha=F/Z_1^3, \quad (12)$$

$$I_1=\frac{\cos(\varphi_2/2)}{\alpha n}[K(k_2)-E(k_2)], \quad (13)$$

$$I_2=\frac{\sin\varphi_2\sin(\varphi_2/2)}{6\alpha n^3}\left[\frac{E'(k_2)}{\sin^2(\varphi_2/2)}-2K'(k_2)\right], \quad (14)$$

$$\sin^2\varphi_2=16n^3(n_2+\tfrac{1}{2})\alpha, \quad (15)$$

$$k_2=\tan(\varphi_2/2). \quad (16)$$

In the above formulas, K, K', E, and E' are complete elliptic integrals of the parameter k_2.[22]

The "effective" parabolic quantum numbers that appear above vary with F and are not integers. For $F=0$, they become integers and identical with the parabolic quantum numbers; i.e., $n_1=\nu_1$, $n_2=\nu_2$. The principal quantum number $\nu=\nu_1+\nu_2+1$.

For a given applied field F, the effective quantum numbers n, n_1, and n_2 may be determined from (15) and (16) given above and (17), (18), (19), (20), and (21) which follow[22]:

$$n=n_1+n_2+1, \quad (17)$$

$$\frac{n_1+\frac{1}{2}}{\nu_1+\frac{1}{2}}=\frac{3\pi}{8}\frac{\sin^2\varphi_1}{(\cos\varphi_1)^{\frac{1}{2}}[(1+\cos\varphi_1)K(k_1)-2\cos\varphi_1E(k_1)]}\equiv F_1(\varphi_1), \quad (18)$$

$$\frac{n_2+\frac{1}{2}}{\nu_2+\frac{1}{2}}=\frac{3\pi}{8}\frac{\sin^2\varphi_2}{2\cos(\varphi_2/2)[E(k_2)-\cos\varphi_2K(k_2)]}\equiv F_2(\varphi_2), \quad (19)$$

$$\tan^2\varphi_1=16n^3(n_1+\tfrac{1}{2}), \quad (20)$$

$$k_1=\sin(\varphi_1/2). \quad (21)$$

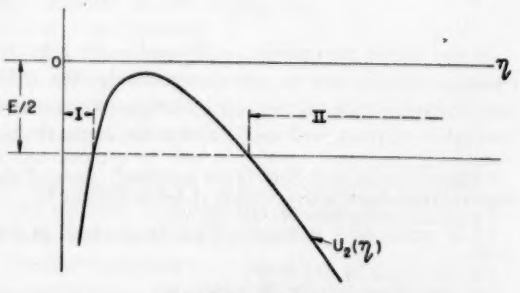

FIG. 2. Plot of $U_2(\eta)$.

[22] For a table of functions K, K', E, and E', see for instance L. M. Milne-Thomson, *Jacobian Elliptic Function Tables* (Dover Publications, Inc., New York, 1950), p. 106. In these tables, the parameter $m=k_2^2$.

We shall now determine the effective parabolic quantum numbers corresponding to $\nu=1$.

We put $\nu_1=0$ and $\nu_2=0$ in (18) and (19), respectively. Then, taking into account (18), (19), (15), and (20), we obtain

$$\sin^2\varphi_2/F_2(\varphi_2)=\tan^2\varphi_1/F_1(\varphi_1). \tag{22}$$

This yields a relation between φ_1 and φ_2 which is shown graphically in Fig. 3. Taking into account (18), (19), and (17), we obtain for $\nu_1=\nu_2=0$:

$$n=[F_1(\varphi_1)+F_2(\varphi_2)]/2. \tag{23}$$

By means of the graph of Fig. 3, we replace φ_1 by φ_2 in (23). This gives n as a function of φ_2, which is represented in Fig. 4 by curve A.

By means of (15) and (19), we represent n as a function of φ_2 and obtain

$$n^3=\sin^2\varphi_2/8\alpha F_2(\varphi_2). \tag{24}$$

In accordance with (24), n has been plotted as a function of φ_2 for various values of α. (See curves B). The intersection of each of the curves B with the curve A gives n and φ_2 corresponding to a given α. By means of (15), (20), and Fig. 3, the values n and φ_2 determine the corresponding values of n_1 and n_2. Figure 4 shows n_1 and n_2 as functions of α for $\nu_1=\nu_2=0$.

(3) *Instantaneous Ionization*

The width of the barrier separating the region I from the region II decreases with increase in F, and for sufficiently large values of F, the barrier disappears entirely, causing instantaneous ionization.

The quantity α expresses the effectiveness of the medium in producing ionization, and we shall determine for what values of α the potential barrier disappears, i.e., the instantaneous ionization takes place. We shall assume that the bound electron was initially in one of the following orbits: (1) $\nu_1=0$, $\nu_2=0$; (2) $\nu_1=1$, $\nu_2=0$; and (3) $\nu_1=0$, $\nu_2=1$.

The potential barrier disappears for $\varphi_2=90°$. Inserting this value in Eqs. (15) (16), (17), and (19), we obtain

$$n=[6.664(2\nu_2+1)\alpha]^{-\frac{1}{3}}, \tag{25}$$

$$n_1=[6.664(2\nu_2+1)\alpha]^{-\frac{1}{3}}-0.833\nu_2-1.0835. \tag{26}$$

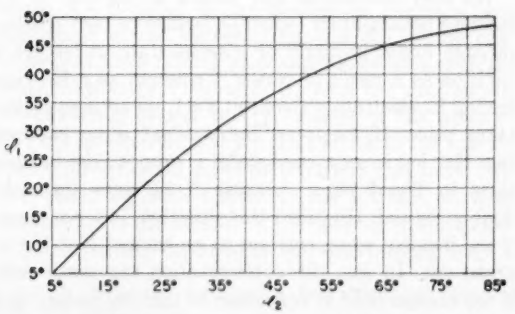

FIG. 3. Plot of φ_2 as a function of φ_1.

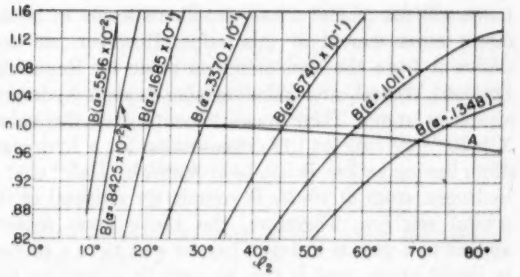

FIG. 4. Plot of n as a function of φ_2.

We have thus determined n and n_1 corresponding to a given α and ν_2. By means of (20) we determine φ_1 from n, n_1, and by means of (21) we determine k_1 from φ_1. The values φ_1 and k_1 are thus functions of α and ν_2. Substituting these values in (18), we obtain a relationship between ν_1, ν_2, and α. If this relationship is satisfied, the potential barrier disappears and instantaneous ionization takes place. The results can be stated as follows:

For $\nu_1=0$, $\nu_2=0$, the instantaneous ionization takes place if

$$\alpha>0.1666 \text{ atomic unit.} \tag{27}$$

For $\nu_1=1$, $\nu_2=0$, the instantaneous ionization takes place if

$$\alpha>0.0138 \text{ atomic unit,} \tag{28}$$

and for $\nu_1=0$, $\nu_2=1$, we have instantaneous ionization if

$$\alpha>0.0088 \text{ atomic unit.} \tag{29}$$

C. Numerical Example

(1) *Magnitude of the Applied Field*

We shall now apply our results to a helium particle moving with the velocity $v=2v_0$ in argon which may be either in the gaseous or the liquid state. The incident particle has three possible charge states, and we designate by ϕ_0, ϕ_1, ϕ_2 the probability of the particle's being neutral, singly ionized, and doubly ionized, respectively.

A doubly ionized helium atom (He^{++}) has no bound electrons; thus, even though the surrounding medium exerts on it a field F, its structure does not change whatever the magnitude of the field may be. Consequently, the stopping power of He^{++} is substantially independent of the state of condensation of the medium.

The energy loss of a neutral helium atom (He^0) is due entirely to close collisions with the surrounding atoms. Therefore, we shall neglect the effect of the medium and assume that $F=0$, both for condensed media and gases. Thus, the stopping power of He^0 is substantially independent of the state of condensation of the medium.

We shall consider now the reaction of the medium on a singly ionized helium atom (He^+). In accordance with (3), the value F is determined by the stopping

power dW/dz of He^+ in argon. There seems to be no direct measurement of this value. However, we can derive it from the measurements made by Reynolds, Dunbar, Wenzel, and Whaling[24] on incident hydrogen atoms in argon. These measurements gave the value 32×10^{-15} ev cm^2 for the cross section for a hydrogen atom having $v=2v_0$. It has been shown by Hall[25] that a hydrogen atom at $v=2v_0$ is completely stripped of its orbital electron. Therefore, the above cross section applies to a proton in argon gas, as well as to a proton in liquid argon, and it can be used to determine the corresponding values of dW/dz for both media. We obtain for an incident proton in liquid and gas, respectively,

$$(dW/dz)^{(d)}=6.92\times10^8 \text{ ev/cm},$$
$$(dW/dz)^{(g)}=8.75\times10^5 \text{ ev/cm}. \quad (30)$$

The values (30) should closely approximate $(dW/dz)^{(d)}$ and $(dW/dz)^{(g)}$ for He^+ ions having the same velocity as protons. Therefore, substituting these values in (3), the field exerted by the surrounding liquid argon on an incident He^+ ion is

$$F^{(d)}=0.1348 \text{ atomic unit}, \quad (31a)$$

and the corresponding field exerted by argon gas is

$$F^{(g)}=1.7\times10^{-4} \text{ atomic unit}. \quad (31b)$$

(2) *Autoionization*

From (12) and (31a,b), we obtain for an incident He^+ ion

$$\alpha^{(d)}=0.0168 \text{ atomic unit}, \quad (32a)$$

$$\alpha^{(g)}=0.21\times10^{-4} \text{ atomic unit}. \quad (32b)$$

Comparison of the values (32a,b) with inequalities (27), (28), (29) leads to the following conclusions: (a) He^+ cannot be brought into an excited state in liquid argon since such a state would lead to an instantaneous ionization. (b) The instantaneous ionization does not occur in argon gas or liquid if He^+ is in the ground state, and it does not occur in argon gas if He^+ is in its first excited state.

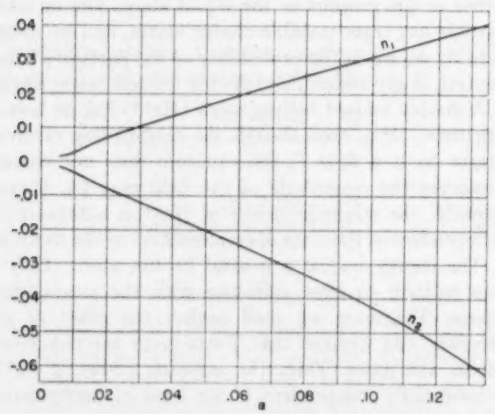

FIG. 5. Plot of n_1 and n_2 as a function of α.

[24] Reynolds, Dunbar, Wenzel, and Whaling, Phys. Rev. **92**, 742 (1953).
[25] T. Hall, Phys. Rev. **79**, 504 (1950).

We shall now determine the probability of autoionization per unit of time for He^+ in the ground state, both in argon gas and liquid.

It is apparent from Fig. 5 that for $\nu_1=\nu_2=0$ the effective quantum numbers do not vary significantly with F. For the value (32a), we have $n_1=0.0058$, $n_2=-0.0066$, and for the value (32b), we may assume both n_1 and n_2 equal to zero. These values when substituted in (11) give the following:

$$S^{(d)}\sim0.41\times10^8 \text{ sec}^{-1}, \quad (33a)$$

$$S^{(g)}\ll0.01 \text{ sec}^{-1}. \quad (33b)$$

Designating by $\Sigma_a^{(d)}$ and $\Sigma_a^{(g)}$ the probability of autoionization per cm of the particle track in liquid and gas, respectively, we obtain

$$\Sigma_a^{(d)}=S^{(d)}/v=9.56\times10^{-7} \text{ cm}^{-1}, \quad (34a)$$

$$\Sigma_a^{(g)}=S^{(g)}/v=0.25\times10^{-11} \text{ cm}^{-1}. \quad (34b)$$

In order to determine the effectiveness of autoionization, we shall compare the values (34a,b) with the probability of ionization $\Sigma_c^{(d)}$ and $\Sigma_c^{(g)}$ per cm of the particle track due to the collision of the particle with the surrounding atoms. Taking into account that the cross section for electron loss is of the order of magnitude of πa_0^2 (where $a_0=\hbar^2/me^2$), we obtain the following for the liquids and the gas, respectively:

$$\Sigma_c^{(d)}\sim N^{(d)}\pi a_0^2=1.86\times10^6 \text{ cm}^{-1}, \quad (35a)$$

$$\Sigma_c^{(g)}\sim N^{(g)}\pi a_0^2=2.36\times10^3 \text{ cm}^{-1}, \quad (35b)$$

where $N^{(d)}$ and $N^{(g)}$ designate the number of atoms per cm^3 in liquid argon and argon gas, respectively.

The values (34*a*,*b*) are very small when compared with (35*a*,*b*) and, therefore, the autoionization of He^+ in the ground state may be neglected.

We may summarize our results as follows: If an incident helium atom (whether ionized or not) passing through argon in liquid or gaseous state undergoes a collision as a result of which it emerges as a He^+ ion having its electron in the orbit $\nu=1$, no autoionization takes place. If, however, the incident atom emerges as a He^+ ion in an excited state, it cannot exist in such state in liquid argon because it becomes instantly doubly ionized. However, this situation does not occur if the incident atom emerges as an excited He^+ ion in argon gas. In gas, the autoionization can occur only if the excited level is very close to the continuum, and this case can be, for our purposes, ignored.

III. ELECTRON LOSS AND CAPTURE

A. General

So far the results obtained are based on a relatively exact theory and an effect of the medium on the autoionization of an incident particle has been established. The particle while passing through the medium undergoes continual collisions during which it captures and loses orbital electrons. We shall now investigate the effect of the medium on the cross section for the electron loss and capture. In that connection, we shall take into account only those events that result in a loss or capture of a single electron and neglect the cross section involving double electron transfers.

The problem is difficult since there is no exact method for computing the cross section for helium ions moving in argon. Some investigations[26,27] dealing with the problem were concerned with the passage of hydrogen ions through hydrogen gas and, therefore, are of little interest for our purposes.

Therefore, we shall rely on the methods established by Bohr[16] which, in order of magnitude, agree with the experiments. Our purpose is not to calculate exactly the cross section for electron loss and capture, but rather to give a general discussion of various factors that influence the magnitude of these cross sections in gases and condensed media. By applying uniformly the same general considerations to all media and by taking into account the characteristic effects caused by the condensed media, we can make some estimates as to the extent to which the cross sections in condensed media depart from the corresponding cross sections in gases. In view of the cursory nature of Bohr's theory, our results should be interpreted as merely indicating orders of magnitude.

B. Electron Capture

We consider a particle of charge Z_1e penetrating with velocity v into the electron cloud surrounding a nucleus of charge Z_2e and subsequently capturing an electron into its orbit ν. By means of statistical arguments, Bohr expressed the cross section for capture as follows:

$$\sigma_c = \sigma f N, \tag{36}$$

where $N \sim Z_2^{\frac{1}{2}}(v/v_0)$ is the number of electrons that participate in the capturing process (i.e., those electrons that have orbital velocities comparable with the particle velocity). $\sigma \sim 4\pi a_0^2 Z_1^2 (v_0/v)^4$ is the cross section corresponding to the energy transfer of the order of $mv^2/2$ to an electron, and f is the fraction of the velocity space corresponding to those electrons that have relative velocities, with respect to the incident particle, comparable to the velocity of the electron after capture.

If the particle captures an electron into an orbit ν, then the electron velocity is $Z_1 v/\nu$, and, therefore,

$$f \sim (Z_1 v_0^3/\nu v)^2. \tag{37}$$

Substituting the above values of N, σ, and f in (36), we obtain:

$$\sigma_c^{(\nu)} \sim \frac{4\pi a_0^2 Z_1^5 Z_2^{\frac{1}{2}}}{\nu^3}\left(\frac{v_0}{v}\right)^6. \tag{38}$$

Bohr's formula has been derived under the assumption that $\nu = 1$, i.e.,

$$\sigma_c^{(1)} \sim 4\pi a_0^2 Z_1^5 Z_2^{\frac{1}{2}} (v_0/v)^6. \tag{39}$$

The total capture cross section can be expressed as

$$\sigma_c = \sum_1^\infty \sigma_c^{(\nu)} \sim 4.8\pi a_0^2 Z_1^5. \tag{40}$$

C. Electron Loss and Excitation

Bohr considered this problem in the system of coordinates moving with the particle and neglected the binding energy of the orbital electron attached to the incident particle. He dealt, therefore, with a stationary electron perturbed by a screened Coulomb field moving with a velocity v. The character of the perturbation depends upon the screening parameter defined by Bohr as

$$\zeta = b/a, \tag{41}$$

where b is the collision diameter, i.e.,

$$b = 2Z_2 e^2/mv^2, \tag{42}$$

and a is the radius of the deflecting atom, i.e.,

$$a = a_0/Z_2^{\frac{1}{2}}. \tag{43}$$

Substituting (42) and (43) in (41), we obtain

$$\zeta = 2Z_2^{4/3}(v_0/v)^2. \tag{44}$$

Bohr took as an example an alpha particle moving in air with a velocity $v = 6v_0$, for which (44) gives $\zeta \sim 1$. He dealt, therefore, with the case of "intermediate screening" for which the deflecting field may be approximated by a potential of the type k/r^2 (k is a suitable constant). By assuming such a potential, Bohr obtained for the cross section for electron loss

$$\sigma_l \sim \pi a_0^2 Z_2^{\frac{1}{2}} Z_1^{-1} (v_0/v). \tag{45}$$

In our case, however, the surrounding medium is argon, and the velocity of the particle is $v = 2v_0$. Consequently, $\zeta \sim 20$, and the problem arises whether we have "intermediate screening" or "excessive screening."

In the case of "excessive screening," the scattering of the electron by the screened Coulomb field is substantially isotropic, and the cross section for ionization is

$$\sigma_l \sim \sigma_0 (T_m - I)/T_m, \tag{46}$$

where $\sigma_0 = \pi a_0^2/Z_2^{\frac{1}{2}}$ is the geometrical cross section, $T_m = 2mv^2$ is the maximum energy transferred, and

[26] D. R. Bates and A. Dalgarno, Proc. Phys. Soc. (London) **A55**, 919 (1952).
[27] J. D. Jackson and H. Schiff, Phys. Rev. **89**, 359 (1953).

$I=mZ_1^2v_0^2/2$ is the ionization energy. Consequently,

$$\sigma_I\sim\frac{\pi a_0^2}{Z_2^{\frac{1}{2}}}\left[1-\frac{Z_1^2}{4}\left(\frac{v_0}{v}\right)^2\right]. \tag{47}$$

In order to determine whether the case of $\zeta\sim 20$ is better approximated by "intermediate screening" or "excessive screening," we have applied both (45) and (47) to two cases for which experimental data are available, i.e., the measurement of the charge distribution of incident hydrogen atoms in air[28] for $v=1.26v_0$ and in neon[29] for $v=1.46v_0$. The expression (45) gives values that differ from the measured values by less than 15 percent, while expression (47) gives values about 40 times too small. We shall, therefore, use (45) and base our considerations on "intermediate screening."

According to Bohr, $\sigma_I\sim\pi i^2$, where i is the impact parameter corresponding to the angular deflection $\vartheta=\vartheta_I$, for which the energy transfer is equal to the ionization energy I. Consequently, the expression (45) represents the cross section for processes for which the energy transfer to the electron $T>I$.

We shall determine the cross section σ_{exc} for processes for which the energy transfer to the electron is $T>T_{exc}$, where T_{exc} is the energy required to raise an electron from the ground state to an excited state characterized by the quantum number ν:

$$T_{exc}=\tfrac{1}{2}mZ_1^2v_0^2\left(1-\frac{1}{\nu^2}\right). \tag{48}$$

Consequently, the angular deflection is $\vartheta>\vartheta_{exc}$, where

$$\vartheta_{exc}=\frac{Z_1v_0}{v}\left(1-\frac{1}{\nu^2}\right)^{\frac{1}{2}}, \tag{49}$$

and

$$\sigma_{exc}\sim\frac{\pi a_0^2Z_2^{\frac{1}{2}}}{Z_1(1-\nu^{-2})^{\frac{1}{2}}}. \tag{50}$$

D. Charge Exchange in Argon Gas

Previously, we have found that in argon gas F is negligibly small. Therefore, the incident particle is undisturbed by the surrounding medium before and after the collision, and no autoionization takes place. We shall calculate the cross section for electron capture and loss for an incident helium particle having $v=2v_0$.

Any collision resulting from an electron capture into an orbit $\nu\geqslant 2$ is followed by the emission of a photon as a result of which the electron falls into the ground state. Therefore, the capture cross section is determined by (40), and we obtain

$$\sigma_{10}^{(g)}\sim 0.19\pi a_0^2, \tag{51}$$

$$\sigma_{21}^{(g)}\sim 6.28\pi a_0^2. \tag{52}$$

[28] H. Kanner, Phys. Rev. 84, 1211 (1951).
[29] P. M. Stier (private communication).

For the electron loss cross section, we obtain by means of (45)

$$\sigma_{01}^{(g)}\sim 3.43\pi a_0^2, \tag{53}$$

$$\sigma_{12}^{(g)}\sim 1.71\pi a_0^2. \tag{54}$$

E. Charge Exchange in Liquid Argon

The mechanism of collisions of helium particles with the surrounding atoms depends on the applied field F. Bohr's theory of electron capture and loss is applicable when $F=0$, but in view of the cursory nature of Bohr's arguments, we shall apply them also when $F\neq 0$. However, account will be taken of the effect of the field F on the incident particle prior to and after the collision. Collisions leading to the following transitions will be considered: $He^+\rightarrow He^0$; $He^0\rightarrow He^+$; $He^{++}\rightarrow He^+$; and $He^+\rightarrow He^{++}$.

(1) *Transition $He^+\rightarrow He^0$*

Prior to this transition, the incident particle was a singly ionized helium atom having its bound electron in the orbit $\nu=1$. It has been shown previously that such a particle is "stable," i.e., its autoionization is negligible both in liquids and gases. As a result of a collision with an argon atom, the incident particle emerged as a neutral helium atom, and as such, it remained stable since the reaction of the medium to a neutral particle may be neglected ($F\sim 0$). Therefore, the state of condensation of the medium does not affect the charge of the particle before or after the transition. However, the collision process is different in gases and in liquids because of a polarizing field in liquids. On the other hand, the general assumptions underlying Bohr's theory are not substantially modified by the presence of a polarizing force. Therefore, we obtain

$$\sigma_{10}^{(d)}=\sigma_{10}^{(g)}. \tag{55}$$

(2) *Transition $He^0\rightarrow He^+$*

We assume that the process is the same in gases and liquids since, as indicated above, He^0 and He^+ are stable in both media. Thus,

$$\sigma_{01}^{(d)}=\sigma_{01}^{(g)}. \tag{56}$$

(3) *Transition $He^{++}\rightarrow He^+$*

In gases an incident He^{++} particle may capture an electron either into its lowest orbit or into an excited state. In the latter case, the electron capture is followed by the emission of a photon and thus does not change the character of the transition. In liquid, however, the electron can be captured only into its lowest orbit. A capture into an orbit $\nu\geqslant 2$ is not possible since an excited He^+ ion becomes instantly ionized. We shall apply, therefore, the formula (50) and obtain

$$\sigma_{21}^{(d)}\sim 5.24\pi a_0^2. \tag{57}$$

(4) *Transition $He^+ \rightarrow He^{++}$*

In gases, this transition occurs only if He^+ receives energy at least equal to its ionization energy. In liquids, however, a smaller energy transfer is required to produce this transition since any collision that would excite He^+ will be followed by an immediate ionization.

Therefore, we apply the formula (50) by taking $\nu=2$ and obtain

$$\sigma_{12}^{(d)} \sim 1.98\pi a_0^2. \tag{58}$$

IV. EFFECTIVE CHARGE

A. Charge Equilibrium

If an incident helium particle undergoes many charge exchange collisions without substantially altering its velocity, a state of equilibrium is reached in which the charge composition of the particle remains constant as long as its velocity does not substantially change.

We shall determine now whether there is a state of equilibrium for a helium particle moving through argon with velocity $v=2v_0$. In that connection, we shall consider a charge exchange cycle, the cross section for which can be either $\sigma_i^{(1)}$ or $\sigma_i^{(2)}$, where

$$\sigma_i^{(1)} = \sigma_{if} + \sigma_{fi}, \tag{59}$$

$$\sigma_i^{(2)} = \sigma_{ik} + \sigma_{kl} + \sigma_{lk} + \sigma_{ki}. \tag{60}$$

In the first case, the particle undergoes transition of the type $i \rightarrow f \rightarrow i$, involving one intermediate state, and in the second case, the transition is of the type $i \rightarrow k \rightarrow l \rightarrow k \rightarrow i$, involving two intermediate states. We obtain from (51), (52), (53), and (54)

$$\sigma_0^{(1)} = \sigma_1^{(1)} \sim 3.6\pi a_0^2; \quad \sigma_2^{(1)} \sim 8\pi a_0^2,$$

and $\sigma_0^{(2)} = \sigma_2^{(2)} \sim 11.6\pi a_0^2$. Consequently, the mean free path for the charge exchange cycle satisfies the following inequality:

$$\lambda \leqslant (N\sigma_0^{(1)})^{-1} \text{ cm}, \tag{61}$$

where N is the number of argon atoms per cm^3. The atomic stopping power of an incident helium particle having $v=2v_0$ measured by Weyl[30] is 79×10^{-15} ev cm^2. Consequently, the energy loss per cm of path due to ionization, excitation, and charge exchange collision is

$$dW/dz \sim N\times 79\times 10^{-15} \text{ ev/cm}, \tag{62}$$

and the maximum value of the energy loss over the distance λ is

$$\Delta W_{\max} = 79/\sigma_0^{(1)} \sim 250 \text{ ev}. \tag{63}$$

It is apparent from (63) that it should take many mean free paths to change substantially the velocity of the particle, and, therefore, we are justified in considering the particle in the state of charge equilibrium.

[30] P. K. Weyl, Phys. Rev. **91**, 289 (1953).

B. Charge Composition in Liquid Argon and Argon Gas

Under these conditions, the distribution of charges of the particle is described by

$$\phi_0 : \phi_1 : \phi_2 = \sigma_{10}\sigma_{21} : \sigma_{01}\sigma_{21} : \sigma_{01}\sigma_{12}, \tag{64}$$

where ϕ_0, ϕ_1, and ϕ_2 represent the probability of the particle's being neutral, singly ionized, and doubly ionized, respectively.[12]

We shall now proceed to determine the distribution of charges of the particle in argon gas and in liquid argon. Substituting (51), (52), (53), and (54) in (64), we obtain for the incident particle having $v=2v_0$ in the gas

$$\phi_0^{(g)} : \phi_1^{(g)} : \phi_2^{(g)} = 0.05 : 0.75 : 0.20, \tag{65}$$

and, consequently, the effective charge of the alpha particle is

$$\langle \epsilon^2 \rangle_{Ar}^{(g)} = \phi_1^{(g)} e^2 + 4\phi_2^{(g)} e^2 = 1.55 e^2. \tag{66}$$

Similarly, substituting (55), (56), (57), and (58) in (64), we obtain for the liquid

$$\phi_0^{(d)} : \phi_1^{(d)} : \phi_2^{(d)} = 0.04 : 0.70 : 0.26, \tag{67}$$

and the effective charge is

$$\langle \epsilon^2 \rangle_{Ar}^{(d)} = 1.74 e^2. \tag{68}$$

It may be of interest to note that the measured values for the alpha particle in argon gas are as follows[12]:

$$\phi_0^{(g)} : \phi_1^{(g)} : \phi_2^{(g)} = 0.07 : 0.71 : 0.22, \tag{69}$$

and

$$\langle \epsilon^2 \rangle_{Ar}^{(g)} = 1.59 e^2. \tag{70}$$

By comparison of (66) and (68), it is apparent that the average square charge of the alpha particle in liquid exceeds the one in gas by about 13 percent.

V. CONCLUSION

Our results may be summarized as follows:

1. An ion moving in a condensed medium is subjected to a polarizing force that causes autoionization. Therefore, the effect of the medium should account for a higher effective charge of the ion. This effect, insofar as it relates to fission fragments, is supported by experiments of Lassen,[10] who reported a large difference between the charges of fission fragments in gaseous and solid stopping media. Furthermore, experiments of Allison, Casson, and Weyl[11] and of Snitzer[12] support the existence of this effect for alpha particles in the energy range 175 kev–400 kev.

2. An alpha particle having velocity $v=2v_0$ has a larger effective charge in liquid argon than in argon gas, since it has been established that any collision in the liquid leading to an excited He^+ is followed by instantaneous ionization, and such a collision, when occurring in gas, does not cause ionization.

3. An alpha particle having velocity $v=2v_0$ has an effective charge higher by 13 percent in liquid argon than in argon gas. To derive this value, we used an approximate theory of electron capture and loss, and, therefore, our result indicates merely an order of magnitude. It is not possible to evaluate this since the reliability of the experimental data is questioned. The fact that only five experiments have been reported and results are contradictory indicates the formidable difficulties in obtaining exact data. By assuming that the anomaly in the stopping power exists, it is questioned whether those measurements that reported the anomaly are sufficiently precise. According to Appleyard,[3] the average stopping power of an alpha particle in the energy range from zero to 4.5 Mev is 15 percent higher in water than the theoretical one for water vapor. Qualitatively, this agrees with out results. However, according to our interpretation, the anomaly exists only for alpha particles in the energy range below 2 Mev. For energies above this range, the alpha particle is completely stripped of its orbital electrons, and, therefore, its stopping power should be the same for liquid media and gases. However, Appleyard found that the stopping power at 4.5 Mev is higher in water than in water vapor, and these results cannot be explained on the basis of our assumptions.

4. According to Michl,[1] the range of a Po alpha particle (5.298 Mev) is 20 percent smaller than that calculated for water vapor and according to Philipp,[2] the range of RaC alpha particles (7.680 Mev) is 16 percent smaller. If Michl's and Philipp's measurements are exact, then our approximate values of $\langle\epsilon^2\rangle_N$ in liquid argon and gas represent an underestimate. Also, this appears from the experimental data of Snitzer[12] and of Allison, Casson, and Weyl[11] shown in Table I. The density effect measured as P designates the increase in percent in the value ϕ_2/ϕ_1 due to the state of condensation of the medium. We obtain from (65) and (67) $P=37$ percent. However, the experiments give $P=61$ percent, which indicates a higher effective charge than the one calculated.

TABLE I. Comparison of experimental data with calculated values.

	Calculated	Experimental
$(\phi_2/\phi_1)^{(a)}$	0.27 (argon gas)	0.31 (argon gas) Snitzer[a]
$(\phi_2/\phi_1)^{d}$	0.37 (liquid argon)	0.50 (gold) Allison, Casson, Weyl[b]
Density effect P	37%	61%

[a] See reference 12.
[b] See reference 11.

As stated above, the scarcity of data is partly caused by experimental difficulties. Possibly, as suggested by Platzman,[7] this energy region was considered of minor importance in experiments of nuclear physics. However, if such a situation existed in the past, it certainly has undergone a fundamental change in the last several years. The density effect in low-energy regions has become of definite practical interest in problems dealing with the interaction of charged particles and living tissue and in any processes involving charge exchange between the incident ions and the surrounding medium.

The computations have been carried out by Mary Todd of the ORNL Mathematics Panel.

Measurement and Theoretical Study of Electrical Conductivity and Hall Effect in Oxide Cathodes*

R. FORMAN
National Bureau of Standards, Washington, D. C., and University of Maryland, College Park, Maryland
(Received August 23, 1954)

Hall effect and electrical conductivity measurements have been made on the oxide cathode over the temperature range 500° to 1000°K. The Hall coefficient of the oxide cathode is negative and the Hall coefficient has a maximum value in the range 600° to 800°K. Above 700°K the values for electron mobility are very large, and below 700°K the mobility decreases rapidly with decreasing temperature. Large magnetoresistive effects were observed, and these were found to be dependent on the temperature and the degree of porosity of the cathode. These results are consistent with the porous semiconductor model for the oxide cathode as originally suggested by Loosjes and Vink. A mathematical theory, based on the high-temperature pore conductivity model, is developed which is in qualitative agreement with the data.

I. INTRODUCTION

IN recent years two theories have been proposed to explain the physical properties of the oxide cathode. The semiconductor model has been proposed by numerous investigators.[1,2] The other theory, suggested by Loosjes and Vink,[3] states that the oxide cathode is a porous semiconductor in which the following two distinct conduction mechanisms operate in parallel. In the low-temperature regions (below 700°K) the conductivity is predominantly due to semiconduction through the crystals of the coating. In the high-temperature range the conductivity is attributed to an electron gas in the pores of the cathode coating. Recently additional evidence has been reported indicating that the Loosjes and Vink theory may be valid,[4–6] but the evidence is far from conclusive.[2,7]

Hall and conductivity measurements offer a means for differentiating between the two physical models. Such measurements,[7–9] at temperatures above 700°K, have been reported in the literature. The results have been interpreted, by using a semiconductor model, but a number of anomalous observations were reported which seem inconsistent with this model, such as (1) large Hall coefficients, (2) high values for the mobility, and (3) large magnetoresistive effects.

In the following sections, measurements of conductivity and Hall effect of oxide cathodes over the temperature range 500° to 1000°K are described. A mathematical theory is then developed, based on the model suggested by Loosjes and Vink, which explains the experimental data at elevated temperatures and is consistent with data obtained by previous investigators. The theory is then compared with the experimental data, and the results are interpreted.

II. EXPERIMENTAL PROCEDURE

A magnesium oxide crucible, shown in Fig. 1, was used as the sample holder. The crucibles were prepared from MgO of 99.8 percent purity, shown as *C*, and a description of their preparation is given elsewhere.[10]

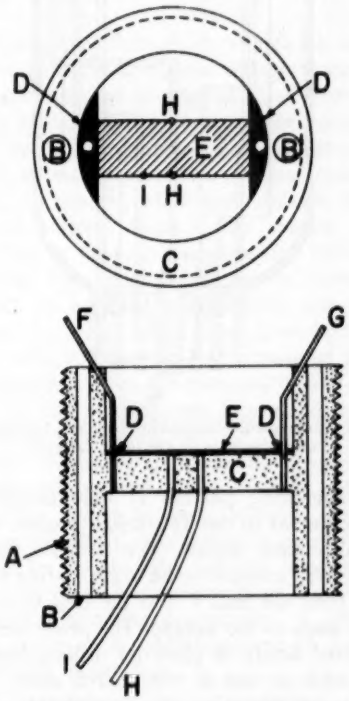

FIG. 1. MgO base used as a sample holder for the deposited oxide cathode. *A* designates a bifilar winding on the MgO base and *B* denotes the support holes. The lead *G* is also the platinum part of a Pt-Pt (13 percent Rh) thermocouple.

* This paper is a portion of a dissertation presented by the author in partial fulfillment of the requirements for the degree of Doctor of Philosophy at the University of Maryland.

[1] Hannay, McNair, and White, J. Appl. Phys. **20**, 669 (1949).
[2] L. S. Nergaard, R.C.A. Rev. **13**, 464 (1952).
[3] R. Loosjes and H. J. Vink, Philips Research Repts. **4**, 449 (1949).
[4] R. C. Hughes and P. P. Coppola, Phys. Rev. **88**, 364 (1952).
[5] E. B. Hensley, J. Appl. Phys. **23**, 1122 (1952).
[6] J. R. Young, J. Appl. Phys. **23**, 1129 (1952).
[7] D. A. Wright and J. Wood, Proc. Roy. Soc. (London) **65B**, 134 (1952).
[8] D. A. Wright, Brit. J. Appl. Phys. **1**, 150 (1950).
[9] Ishikawa, Sato, Okumura, and Sasaki, Phys. Rev. **84**, 371 (1951).
[10] W. B. Haliday and J. R. Nall, Rev. Sci. Instr. **25**, 1225 (1954).

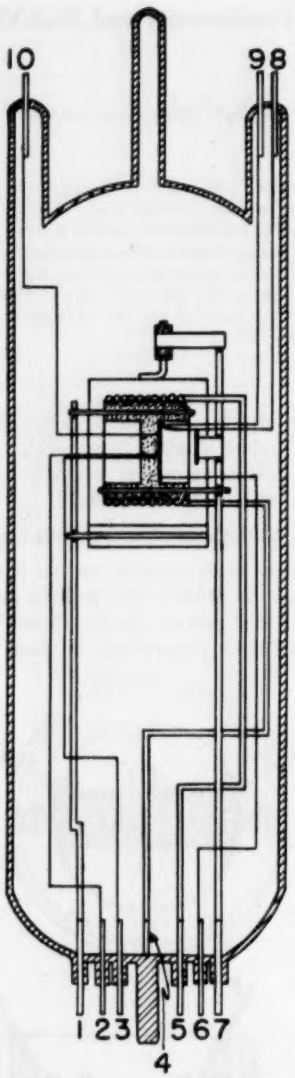

FIG. 2. Vacuum tube for making Hall and conductivity measurements on the oxide cathode.

The metal-ceramic patches *D* were prepared by a technique similar to the Telefunken process developed for metal-ceramic brazes. The metallic contacts *D* make electrical contact to the oxide coating *E* and also serve to bind the lead *F* and the lead *G* in place as electrical leads to the sample. The probe wires *H* and *I* were fixed firmly in place by drilling holes in the crucible while it was in the unfired state. Platinum probes having the same diameter (0.015 in.) as the holes were then inserted, and the crucible was fired to 1650°C in air. During the firing the ceramic shrank 9 to 12 percent, and the platinum leads became firmly imbedded. The cathode coating is a double carbonate known commercially as C51-2 and is prepared from an equimolecular mixture of barium and strontium carbonates. The cathodes were sprayed with a type CV-DeVilbiss spray gun. Each of the various coatings was approximately one cm in length, 0.25 cm wide and 0.01 cm thick.

A platinum heater wire was wound over the bifilar threaded portion of the crucible which was then mounted in a tube sketched in Fig. 2. A molybdenum anode for collecting emission current and a molybdenum heat shield are incorporated in the tube. The anode lead also supports the heat shield but is insulated from it by an alundum sleeve. The tube contained a batalum getter which was welded to one of the leads in the tube.

The tube was processed on a vacuum system which included an oil diffusion pump, two Westinghouse metal valves, thermocouple and ionization gauges, and an ethane gas bottle. The high-vacuum end of the system was baked out at 400°C for 14 hours, and the metal parts in the tube were outgassed by inductive heating before the cathodes were processed. Activation consisted of treating the cathodes in ethane using a procedure similar to that described by Wright.[8] In general, as a result of activation, both emission and conductivity increased by a factor of 10–20. The pressure in the tubes, before they were sealed off the vacuum system, was better than 10^{-6} mm of Hg.

Five tubes were prepared and tested, and they are designated in the text as CH3 to CH7 inclusively. The density[11] or porosity of the cathodes in these five tubes were varied. Table I describes the properties of the different cathodes.

Measurement difficulties were experienced with tube CH3. The Hall and conductivity probes in this tube extended above the sample, making very poor contact with the oxide coating, and this was responsible for generating noise voltages at low temperatures. This difficulty was eliminated in all of the other tubes by cutting the probes down flush with the MgO base and then depositing the coating over the probes so that they were completely covered by the sample.

Preliminary experiments on the conductivity of the oxide cathode indicated that the resistance of some samples was as high as 10^{10} ohms at low temperatures (500°K). Such high-resistance samples required the use of a vibrating reed electrometer, such as that of the Applied Physics Laboratory of Pasadena, California,

TABLE I. Properties of the different cathodes.

Tube	Density of coating g/cm³	Method of depositing coating	Activated with ethane
CH3	0.3–0.4	Sprayed	No
CH4	0.7–0.8	Sprayed	Yes
CH5	0.9–1.0	Sprayed	No
CH6	0.4–0.5	Sprayed	Yes
CH7	1.3–1.4	Brushed on	Yes

[11] The density was measured by depositing the oxide alternately on the magnesia base and on a nickel strip in an identical manner. The weight and dimensions of the coating were then measured on the nickel strip.

as a voltage-indicating device. The electrometer has an input resistance greater than 10^{15} ohms and will not affect the electrical properties of the sample when placed across the Hall or conductivity probes.

The electrical circuit for making these measurements is illustrated in Fig. 3. The switch in the electrometer circuit is a Teflon selector switch. The resistance selector switch is a Centralab ceramic series switch which was coated with polystyrene to reduce leakage as described by Glass.[12] The reversing switches and batteries, which supply the conduction current through the sample, are encased in a polystyrene box to insulate them from the shielded box enclosing the electrical circuit. The 1.5-volt cell in the Hall circuit is used to eliminate the IR drop across the Hall probes. The current through the sample is determined by the voltage drop across the fixed resistors R_1, R_2, R_3, and R_4. Their respective values are 10^5, 10^6, 10^7, and 10^9 ohms. To minimize thermionic electron currents when Hall and conductivity measurements were made, it was necessary to bias the heater positive with respect to the heat shield and the sample positive with respect to the molybdenum anode. Extreme shielding precautions had to be taken in these measurements in order to obtain reliable results.

The conductivity and Hall measurements were made by the following procedure. After the tube was placed between the magnet pole faces, with the magnetic field direction perpendicular to the sample face, the temperature of the sample was raised to the highest value it attained in the measurements. The temperature of the cathode was recorded after it reached thermal equilibrium. The current through the sample was regulated to give the most advantageous voltage reading. This could be accomplished in practically all cases by the use of the 1.5-volt battery source. The voltage drop across the conductivity probes and the current through the sample were then measured with no applied magnetic field. In general, when the magnetic field was applied, the current through the sample changed markedly due to the high magnetization resistance of the material. The value of the current through the sample with an applied magnetic field was recorded and checked by reversing the polarity of the magnetic field. The Hall voltage was then measured with the magnetic field in a given direction and then of opposite polarity. The field strength used in practically all Hall measurements was either 500 or 1000 gauss. The temperature of the sample was then progressively lowered approximately 50°C at a time, and similar electrical data taken at each setting. The lowest temperature at which measurements could be taken was limited by (a) the Hall voltages becoming indetectable or (b) noise fluctuations across the high-resistivity samples becoming appreciable. A few points were also taken on a reheating cycle to insure the reproduceability of the data.

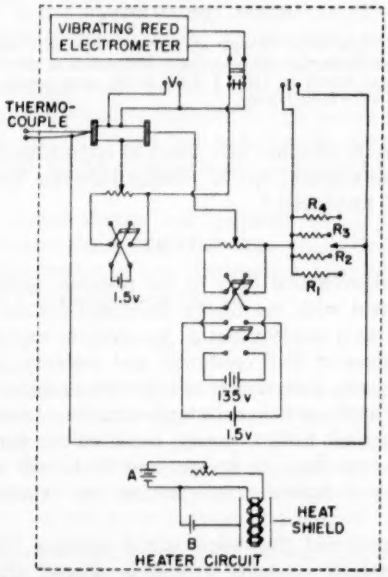

FIG. 3. Circuit diagram of electrical equipment for measuring the conductivity and the Hall coefficient at different temperatures.

[12] F. M. Glass, Rev. Sci. Instr. **20**, 239 (1949).

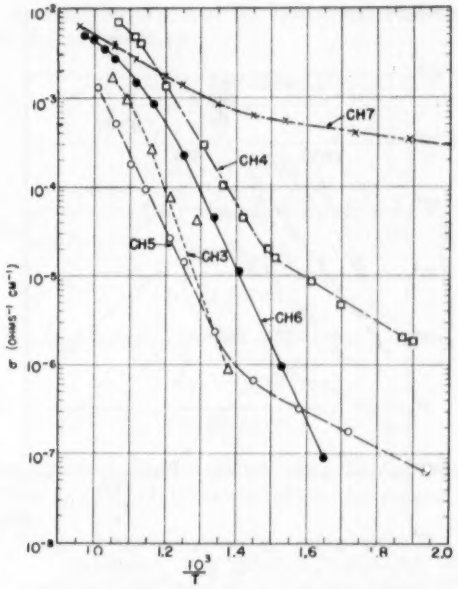

FIG. 4. Conductivity of the oxide cathode as a function of the inverse absolute temperature. Properties of the different cathodes are shown in Table I.

III. EXPERIMENTAL RESULTS

Conductivity and Hall data for the five tubes tested are shown in Figs. 4 and 5. The relative porosities of the different cathodes are shown in Table I.

The denser cathodes illustrate the break in the slope of the conductivity curve at about 700°K as described

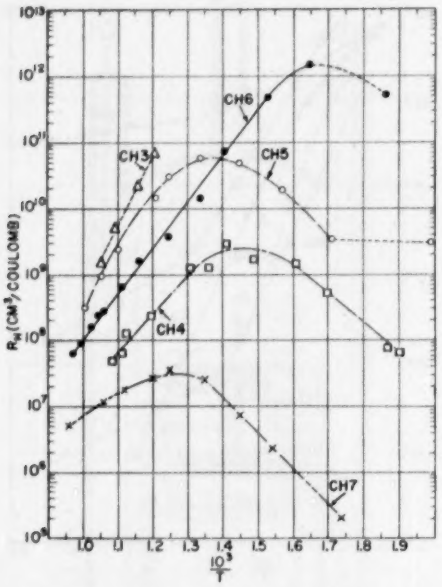

FIG. 5. Hall coefficient of the oxide cathode as a function of the inverse absolute temperature. Properties of the different cathodes are shown in Table I. The last point in the Hall curves for CH5 and CH6 are upper limits for the Hall coefficient. The accuracy of the measurements in these two tubes was limited by noise and is indicated in both curves by the dashed portion.

by Loosjes and Vink.[3] This is seen to be independent of activation. In the temperature range covered by these measurements, the most porous cathodes do not show any break in the slope of the conductivity curve. The magnitude of the Hall coefficient was relatively large and the sign of the Hall coefficient was negative on all samples. Figure 5 shows that all the Hall curves, except that for CH3, have a maximum. Data on CH3 at lower temperatures were not taken because of the higher noise level in the tube. Experimental evidence was obtained which showed that the Hall coefficient was independent of magnetic field at high temperatures and dependent on magnetic field at lower temperatures, corresponding to the transition temperature range discussed later, but this was not investigated in great detail.

If the Hall coefficient or conductivity curves are considered as exponential functions of T for all samples, one finds that the activation energies, as determined from the slopes of the linear portions of the curves at high temperatures, fall within the range of 0.5 to 2.2 ev. For a given sample the values of the activation energy in the high temperature range, obtained from the conductivity and Hall curves respectively, differ by not more than 0.25 ev.

TABLE II. Apparent mobility of different cathodes at 1000°K.

Tube No.	CH3	CH4	CH5	CH6	CH7
Mobility (cm²/volt sec)	4×10^{4}	3×10^{5}	4×10^{5}	4×10^{5}	3×10

An "apparent" mobility of the carriers, μ, in all these samples is defined by the usual relation, $\mu=\sigma_0 R_H$, where σ_0 is the conductivity with no applied magnetic field and R_H is the Hall coefficient.[13] The mobility at high temperatures, 800° to 1000°K, was found to be large for all samples. As the temperature was progressively lowered, the "apparent" mobility decreased with decreasing temperature. The values for mobility of the different samples at approximately 1000°K are tabulated in Table II. The data on tubes CH4, CH5, CH6, and CH7 are considered to be more reliable than those for CH3, because of the difficulty with the probe wires of the latter tube mentioned earlier.

The oxide cathode also exhibits very unusual conductivity properties in the presence of a magnetic field. The resistivity of some of the samples could be increased by a factor of ten by applying a transverse magnetic field of 500 gauss. The marked change in conductivity is illustrated in Fig. 6 which is a plot of the fractional change in conductivity with applied magnetic field for the tubes CH4, CH5, CH6, and CH7.

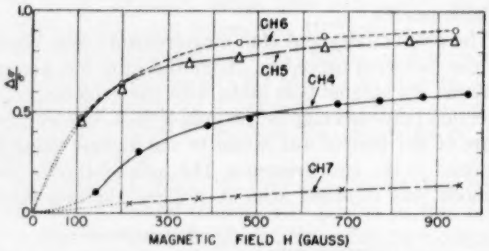

FIG. 6. Fractional change in conductivity with increasing magnetic field for the oxide cathode. Properties of the different cathodes are shown in Table I. CH6 is the most porous sample and CH7 is the least porous.

The data on all tubes were taken at approximately the same temperature, 950°K. Similar behavior has been observed previously.[9]

IV. THEORY

The experimental data of the previous section are inconsistent with the theory developed for the oxide cathode as a semiconductor. In order to explain the large values of Hall coefficient and mobility at high temperatures, a maximum at high temperatures in the curve of $\log R_H$ *vs* T^{-1}, and a large variation of resistance with magnetic field, a theory, based on the pore conduction hypothesis of Loosjes and Vink, will be proposed as a basis for interpreting the experimental results.

The proposed theoretical model assumes that the oxide cathode contains irregularly shaped channels, composed of irregularly shaped pores or cavities, whose

[13] This definition loses its significance when several mechanisms of conduction arise. Such a situation will be discussed later.

walls are thermionic emitters. The mean free path in this channel is assumed to be dependent only on the geometry and linear dimensions of the pores. At high temperatures, an electron gas, in thermodynamic equilibrium, will then exist in the channel, and the electric and magnetic properties of this gas will be studied. The model assumes that the conduction mechanism in the oxide cathode at high temperatures is predominantly due to a flow of electrons through the pores and that conduction current through the pore walls is negligible.

A simple kinetic theory treatment of the electron gas indicates that the mobility, μ, is given by the expression[14]

$$\mu=\frac{el}{2(3km)^{\frac{1}{2}}}T^{-\frac{1}{2}}, \tag{1}$$

where l is the mean free path or linear dimension of the pore, and e, m, k, and T are the electronic charge, electronic mass, Boltzmann's constant, and the temperature, respectively. A more general treatment, however, is desirable. This treatment is similar to that developed by Gans[15] for the free electron theory of metals and is in Seitz.[16]

The electron gas is assumed to obey Maxwell-Boltzmann statistics and the distribution function, f_0, giving the number of particles in a volume element $dxdydzdv_xdv_ydv_z$ in phase space, is given by

$$f_0=\frac{2m^3}{h^3}\exp\left\{-\frac{e\phi}{kT}\right\}\exp\left\{-\frac{\epsilon-eV_p(x,y,z)}{kT}\right\}. \tag{2}$$

ϕ is the work function for the material in the emitting walls, ϵ is the kinetic energy, and $V_p(x,y,z)$ is the electrostatic potential energy for the electrons in the volume element in phase space. The quantities m, k, and h are respectively the electronic mass, Boltzmann's constant, and Planck's constant. In this treatment it is assumed that the mean free path for the electrons is determined by the average linear dimensions l of the pores.

If a crossed electric and magnetic field is applied (i.e., electric field in the x direction, magnetic field in the z direction), the new distribution function, f, is given to a first approximation by

$$f=f_0+v_x\chi_1(v)+v_y\chi_2(v), \tag{3}$$

where χ_1 and χ_2 are functions of the scalar magnitude of $\mathbf{v}$; v_x and v_y are the respective electron velocities in the x and y directions. Assuming that the collisions between the electron gas and cavity walls are elastic[17] and isotropic and that no temperature gradient exists, one finds, following the method of reference 15, that the conductivity, σ_H, and the isothermal Hall coefficient, R_H, are given by

$$\sigma_H=\frac{I_x}{E_x}=-\frac{4\pi e^2}{3}\frac{L_1^2+L_2^2}{L_1}, \tag{4}$$

$$R_H=\frac{E_yc}{I_xH_z}=\frac{3}{4\pi e^2}\frac{L_2}{L_1^2+L_2^2}\frac{c}{H_z}, \tag{5}$$

where

$$L_1=\int_0^\infty\frac{lv^2}{1+s^2}\frac{\partial f_0}{\partial\epsilon}vdv, \tag{6}$$

$$L_2=\int_0^\infty\frac{lsv^2}{1+s^2}\frac{\partial f_0}{\partial\epsilon}vdv, \tag{7}$$

and

$$s=elH_z/mcv. \tag{8}$$

When L_1 and L_2 are evaluated, using the distribution function f_0 [Eq. (2)], the expressions for σ_H and R_H become

$$\sigma_H=\frac{16\pi e^2ml}{3h^3}kT\exp\left\{-\frac{e(\phi-\bar{V}_p)}{kT}\right\}\frac{F_1^2+F_2^2}{F_1}, \tag{9}$$

and

$$R_H=-\frac{3ch^3}{16\pi e^2mlkTH_z}\exp\left\{\frac{e(\phi-\bar{V}_p)}{kT}\right\}\frac{F_2}{F_1^2+F_2^2}; \tag{10}$$

where

$$F_1\left(\frac{a}{kT}\right)=1-\left(\frac{a}{kT}\right)+\left(\frac{a}{kT}\right)^2\times\exp\left\{\frac{a}{kT}\right\}\left[-\mathrm{Ei}\left(-\frac{a}{kT}\right)\right], \tag{11}$$

$$F_2\left(\frac{a}{kT}\right)=\left(\frac{a}{kT}\right)^{\frac{1}{2}}\left[\frac{\pi^{\frac{1}{2}}}{2}-\pi^{\frac{1}{2}}\left(\frac{a}{kT}\right)+\pi\left(\frac{a}{kT}\right)^{\frac{1}{2}}\times\exp\left(\frac{a}{kT}\right)\mathrm{erfc}\left\{\left(\frac{a}{kT}\right)^{\frac{1}{2}}\right\}\right], \tag{12}$$

$$a=e^2l^2H_z^2/2mc^2, \tag{13}$$

and $\bar{V}_p$ is the average electrostatic potential energy in the cavity. The functions F_1, F_2, and $F_1^2+F_2^2$ are plotted graphically in Fig. 7.

The conductivity, σ_0, of the electron gas model, with no applied magnetic field, is given by setting $F_1=1$ and $F_2=0$ in Eqs. (11) and (12). The result is

$$\sigma_0=\frac{16\pi e^2ml}{3h^3}kT\exp\left\{-\frac{e(\phi-\bar{V}_p)}{kT}\right\} \tag{14}$$

which is very similar to the expression derived by Hensley[5] by a different approach using a similar model.

The mobility obtained from the experimental data by the usual relationship, $\mu=\sigma_0R_H$, can be theoretically

[14] All derivations in this paper are in Gaussian units.
[15] R. Gans, Ann. Physik **20**, 293 (1906).
[16] F. Seitz, *The Modern Theory of Solids* (McGraw-Hill Book Company, Inc., New York and London, 1940), pp. 168–194.
[17] This simple assumption may be too idealized, but it leads to results which are of the correct order of magnitude.

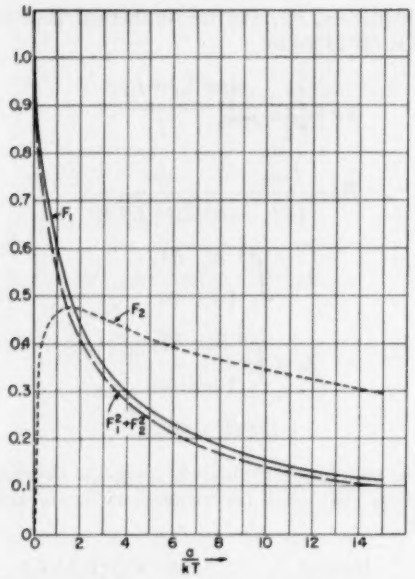

FIG. 7. The numerical values of the functions F_1, F_2 [Eqs. (11) and (12)] and $F_1^2+F_2^2$ plotted as a function of the parameter a/kT. The abscissa a/kT is equal to $e^2p^2H_z^2/2mc^2kT$. For a given mean free path and temperature the abscissa is proportional to the value of the magnetic field squared.

determined from Eqs. (10) and (14). This is given by

$$\sigma_0 R_H=\frac{el}{(2mk)^{\frac{1}{2}}}T^{-\frac{1}{2}}\left(\frac{a}{kT}\right)^{-\frac{1}{2}}\frac{F_2}{F_1^2+F_2^2}. \tag{15}$$

It can be shown that the order of magnitude of $\{(a/kT)^{-\frac{1}{2}}F_2/F_1^2+F_2^2\}$ is approximately unity for all values of a/kT, and this leads to the expression

$$\mu=\sigma_0 R_H\cong\frac{el}{(2mk)^{\frac{1}{2}}}T^{-\frac{1}{2}}. \tag{16}$$

If the theoretical expression for the density of electrons is computed, the result is given by

$$n=\int_{-\infty}^{\infty}\int_{-\infty}^{\infty}\int_{-\infty}^{\infty}f_0 dv_x dv_y dv_z$$
$$=\frac{2}{h^3}(2\pi mkT)^{\frac{3}{2}}\exp\left\{-\frac{e(\phi-\bar{V}_p)}{kT}\right\}. \tag{17}$$

From Eqs. (10) and (17) and the same approximation as above for $\{(a/kT)^{-\frac{1}{2}}F_2/F_1^2+F_2^2\}$, an expression can be derived relating the Hall coefficient to the density of carriers, namely,

$$R_H\cong-1/en, \tag{18}$$

which is very similar to the functional relationship of these quantities in semiconductor theory.

Another quantity which is of considerable interest, theoretically and experimentally, is that of the fractional change of conductivity with applied magnetic field. From Eqs. (9) and (14) this is given by

$$\Delta\sigma/\sigma_0=1-(\sigma_H/\sigma_0)=1-F_1-F_2^2/F_1. \tag{19}$$

If $\Delta\sigma/\sigma_0$ is plotted as a function of a/kT (H_z is the variable parameter in a/kT), the maximum fractional change in conductivity is given by

$$\lim_{a/kT\to\infty}\frac{\Delta\sigma}{\sigma_0}\to 0.116. \tag{20}$$

This value is low compared to what one observes in the experimental data. The above theory gives order-of-magnitude agreement with the experimental mobility data, but Eq. (20) shows that the theory does not give satisfactory results if effects smaller than an order of magnitude are considered.

An expression, which is consistent with the experimental data for magnetoresistive effects, can be obtained by a modification of the previous treatment. If an electron follows a cyclic or trochoidal path in a crossed electric and magnetic field, it obtains a steady drift velocity in a direction perpendicular to both the electric and magnetic fields. Since the drift is at right angles to the electric field, the cyclic electrons on the average do not contribute to the conduction current. This leads to the hypothesis that only those electrons which suffer collisions in a time short compared to the period of the cycloidal motion contribute to the conduction current. This hypothesis can be incorporated into the theory if it is assumed that only those electrons whose x component of velocity is greater than $v_{0x}=elH_z/mc$, where eH_z/mc is the cyclotron frequency, contribute to the conduction current. One then obtains for the current in the x direction

$$I_x=-2\int_{v_{0x}}^{\infty}\int_{-\infty}^{\infty}\int_{-\infty}^{\infty}ev_x^2\chi_1(v)dv_x dv_y dv_z, \tag{21}$$

where χ_1 is defined in Eq. (3) and can be evaluated to give

$$\chi_1=\frac{el}{v}\frac{\partial f_0}{\partial\epsilon}\left[\frac{E_x-sE_y}{1+s^2}\right], \tag{22}$$

where s is given by Eq. (8).

Since the Hall voltage is always smaller than the conduction voltage ($E_x>E_y$) and, in the range of the integration variable, $s<1$, the bracketed term in Eq. (22) becomes E_x. If this simplified expression for χ_1 is inserted in Eq. (21) and the integrand is evaluated, one obtains for the conductivity

$$\sigma_H=A\left[\frac{a}{kT}\left\{i\,\mathrm{erfc}\left(\frac{a}{kT}\right)^{\frac{1}{2}}\right\}+\frac{2a}{kT}\left\{i^2\,\mathrm{erfc}\left(\frac{a}{kT}\right)^{\frac{1}{2}}\right\}\right.$$
$$\left.+2\left\{i^3\,\mathrm{erfc}\left(\frac{a}{kT}\right)^{\frac{1}{2}}\right\}\right], \tag{23}$$

where

$$A=\frac{2^7\pi^4e^2mlkT}{h^3}\exp\left\{-\frac{e(\phi-\bar{V}_p)}{kT}\right\}, \quad (24)$$

where a is defined in Eq. (13) and

$$\left\{i^n\operatorname{erfc}\left(\frac{a}{kT}\right)^{\frac{1}{2}}\right\}=\int_{(a/kT)^{\frac{1}{2}}}^{\infty}\{i^{n-1}\operatorname{erfc}\xi\}d\xi, \quad n=1, 2\cdots. \quad (25)$$

The notation of Eq. (25) is adopted from Carslaw and Jaeger.[18]

To obtain σ_0 set $H_z=0$ (or $a/kT=0$). The resulting expression is

$$\sigma_0=\frac{2^7\pi^4e^2mlkT}{h^3}\exp\left\{-\frac{e(\phi-\bar{V}_p)}{kT}\right\}[2\{i^3\operatorname{erfc}(0)\}]. \quad (26)$$

The quantity of particular interest is the fractional change of conductivity with applied magnetic field or the expression $\Delta\sigma/\sigma_0$. This expression has been evaluated numerically from Eqs. (23) and (26) and is shown graphically in Fig. 8. The curve in Fig. 8 is similar to the experimental curves of magnetization conductivity. A comparison of the theory and the experimental data will be made in Sec. V.

V. COMPARISON OF THEORY WITH EXPERIMENT AND CONCLUSIONS

The large values of "apparent" mobility, obtained experimentally, are consistent with the theoretical values for mobility as given by Eqs. (1) and (16). If the mobility is expressed in conventional units, cm²/volt sec, and evaluated at 1000°K, both equations yield a value for mobility given by

$$\mu\cong 10^3 l, \quad (27)$$

where l, the mean free path, is expressed in cm. For a mean free path between 10^{-4} and 10^{-3} cm, this value for mobility is in the same order of magnitude as the experimental values for tubes CH4, CH5, CH6, and CH7 (Table II). This range of values for the mean free path is consistent with the range of values one encounters for the linear dimensions of the pores in an oxide cathode.

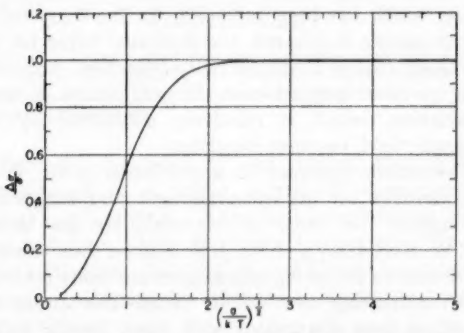

FIG. 8. Theoretical curve of fractional change in conductivity with magnetic field for a constant value of the mean free path and temperature. The abscissa $(a/kT)^{\frac{1}{2}}$ is equal to $elH_z/(2mc^2kT)^{\frac{1}{2}}$ and is proportional to the magnetic field for a given value of l and T.

[18] H. S. Carslaw and J. C. Jaeger, *Conduction of Heat in Solids* (Oxford University Press, London, 1950), p. 371.

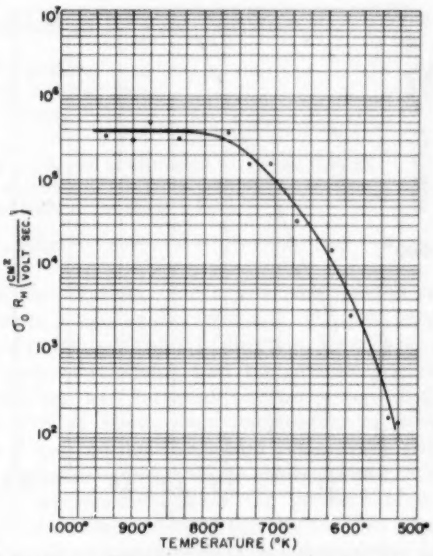

FIG. 9. "Apparent" mobility of sample CH4 *versus* temperature.

Figure 9 illustrates a typical plot of "apparent" mobility, $\mu=\sigma_0R_H$, *vs* temperature. This curve was obtained from sample CH4. These data strongly suggest the validity of the hypothesis originally proposed by Loosjes and Vink. Above 750°K the mobility is high and is consistent with the theoretical value for mobility obtained from the electron gas model. Below 750°K the "apparent" mobility drops rapidly and is approximately 100 cm²/volt sec at 525°K. This low value for mobility is approaching the value one would expect for a semiconductor model. Pell's[19] data on single crystals of barium oxide showed a mobility in the range of 1–10 cm²/volt sec at 500°–800°K. It should be noted that there is theoretical justification for considering σ_0R_H as a mobility at low temperatures (semiconductor) and at high temperatures (electron-gas model), but there is no such justification in the transition region where σ_0R_H is rapidly decreasing and two parallel conduction mechanisms exist.

This leads to the following proposed model for an oxide cathode over the temperature range 500° to 1000°K. At high temperatures (above 700° to 800°K) the mechanism for electrical conduction is predominantly pore conduction. At low temperatures (500°–700°K) there is a transition range where two equivalent parallel mechanisms exist, namely that of pore conduc-

[19] E. M. Pell, Phys. Rev. **87**, 457 (1952).

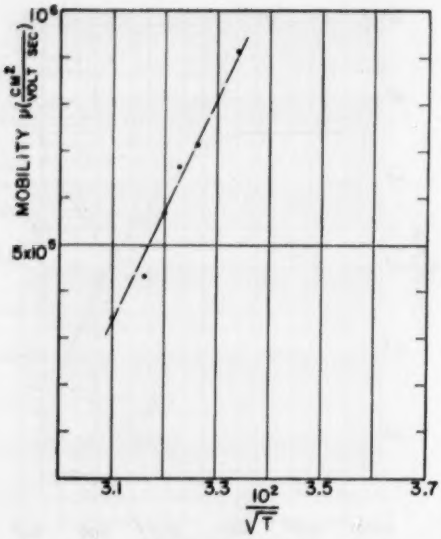

FIG. 10. Plot of mobility of sample CH6 *versus* the inverse of the square root of the absolute temperature.

tion and semiconduction. At the lowest temperature (500°K), semiconduction predominates.

The hypothetical model for the oxide cathode also indicates an explanation for the maximum in the Hall curves of Fig. 5. In the high-temperature range the Hall coefficient increases with decreasing temperature because the density of the electron gas in the pores decreases [Eq. (18)]. As the transition region is reached, the mechanism for semiconduction becomes more important. The density of carriers in the semiconductor is high, and as the temperature is progressively lowered the Hall coefficient decreases, indicating that the density of carriers is increasing as the mechanism of semiconduction takes over.

A break in the conductivity curve like that shown by samples CH4, CH5, and CH7 has been observed previously by other investigators,[3–5] and has been explained by a model similar to that proposed in this paper. The absence of a break in the conductivity curve for CH6 can be attributed to the fact that the area of contact between crystalline particles is probably small because CH6 had a high degree of porosity. This is also consistent with the Hall data for CH6, which has a maximum below the temperature range in which the conductivity was measured.

Another interesting comparison can be made between the experimental data and the theory if one considers the variation of mobility with temperature in the high-temperature region. Equation (16) predicts the mobility is proportional to $T^{-\frac{1}{2}}$. This relationship has been found in samples CH3 and CH6. The data for CH6 is plotted in Fig. 10 and is seen to be in agreement with the theory. The denser samples CH4, CH5, and CH7 did not illustrate this behavior. The mobility data at high temperatures for these samples were scattered as illustrated in Fig. 9 for CH4.

A comparison between the theory and experiment can also be made on the fractional change of conductivity with magnetic field. The abscissa coordinate in Fig. 8 is given as

$$\left(\frac{a}{kT}\right)^{\frac{1}{2}}=\frac{el}{(2mc^2kT)^{\frac{1}{2}}}H_z. \tag{28}$$

If one assumes $l\cong 10^{-3}$ cm and $T=950°$K, then $(a/kT)^{\frac{1}{2}}\cong 10^{-3}H_z$. This theoretically predicts a saturation effect in the magnetization conductivity at about 2000 gauss. This differs by a factor of 2 or 3 with the data from the experimental curves for CH4, CH5, and CH6, shown in Fig. 6, but it is in reasonable agreement considering the approximations used.

An examination is also made of another interesting phenomenon, *viz.*, variation of magnetization conductivity with temperature. This is illustrated in Fig. 11

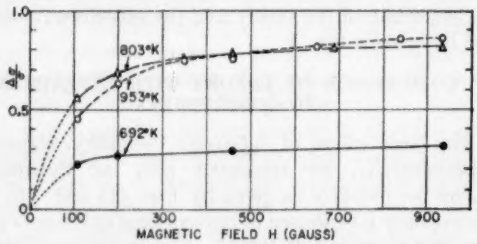

FIG. 11. Fractional change in conductivity for sample CH5 *versus* the magnetic field with temperature as a variable parameter. At 500°K no measurable change of conductivity with magnetic field (up to 1000 gauss) was observed.

for the case of CH5. The data are consistent with the model which has been proposed. As the temperature of the sample is lowered, the saturated value for the fractional change in conductivity decreases, indicating that at lower temperatures the mechanism of semiconduction, which is relatively unaffected by the magnetic field, becomes important.

The author expresses his appreciation to Dr. R. G. Breckenridge for his encouragement and suggestions throughout the course of this work. He also thanks Mr. W. B. Haliday and Mr. J. R. Nall for their valuable assistance in preparing the magnesium oxide crucibles and constructing most of the tubes. The author has benefited from discussions with many people and is especially indebted to Dr. C. H. Page, Dr. W. Gruner, Dr. M. Abramowitz, Dr. G. F. Rouse, and Dr. F. G. Brickwedde.

Low-Temperature Acoustic Relaxation in Ni–Fe Ferrites

M. E. FINE* AND N. T. KENNEY
Bell Telephone Laboratories, Murray Hill, New Jersey
(Received September 2, 1954)

An acoustic relaxation effect occurs near 40°K in $Ni_{0.75}Fe_{2.25}O_4$ and is attributed to a stress-induced change in distribution of Fe^{++} and Fe^{+++} similar to that occurring in magnetite. The process involves electron diffusion. The activation energy is between 0.026 and 0.055 ev per electron jump.

IN magnetite[1] a low-temperature ordering transformation ($T_c \cong 115$°K) occurs which involves the distribution of Fe^{++} and Fe^{+++} among the available octahedral sites in the structure. Only electron diffusion is involved since $Fe^{+++} + e \rightleftarrows Fe^{++}$. An applied stress[2,3] changes the local distribution of Fe^{++} and Fe^{+++}. For example, a tensile stress would induce more of the larger Fe^{++} ions to be distributed in the stress direction. This additional strain lowers Young's modulus for the ⟨111⟩ direction in magnetite[3] at temperatures as high as 600°K. Considering the stress constant, the induced strain from change in distribution of Fe^{++} and Fe^{+++} and the decrease in modulus therefrom reach their maximum at the critical ordering temperature, 110°K in the sample of magnetite studied.[3] The internal friction peaks at 95°K where the relaxation time for the electron diffusion process and the period of the impressed vibrations are approximately equal.

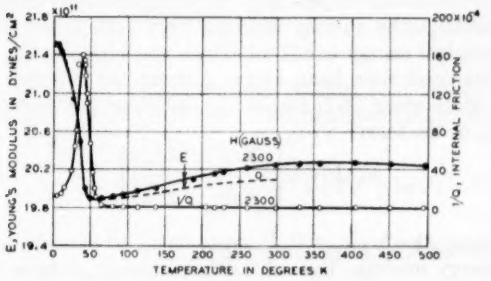

FIG. 1. Young's modulus and logitudinal internal friction of ⟨111⟩ in $Ni_{0.75}Fe_{2.25}O_4$. The frequency of measurement was approximately 83 kc/sec. The external magnetic field was applied in the ⟨111⟩ direction.

Recently, the elasticity and internal friction were investigated in a single crystal of approximately $Ni_{0.75}Fe_{2.25}O_4$ (that is, $\frac{3}{4}$ of the Fe^{++} is replaced by Ni^{++}) obtained from Linde Air Products Company through Dr. G. W. Clark. Galt, Yager, and Merritt have studied domain wall velocities[4] and ferromagnetic resonance[5] in similar crystals. The crystal was ground into a cylinder, 5 mm in diameter and 38.3 mm long, accurately oriented in a [111] direction. Young's modulus, the torsional modulus, and the internal friction for longitudinal and torsional vibrations were measured from 2°K to above room temperature as shown in Figs. 1 and 2 using a resonant piezoelectric method. The equipment and procedure are described elsewhere.[6]

The measurements show the presence of a low-temperature relaxation effect in the $Ni_{0.75}Fe_{2.25}O_4$ crystal. The relaxation effect is presumably a stress-induced change in distribution of Fe^{++} and Fe^{+++}, that is a remnant of the magnetite effect is present. The internal friction peak occurs near 38°K as shown in Figs. 1 and 2. Near this temperature the observed Young's modulus, Fig. 1, abruptly increases, approaching the value for the unrelaxed modulus at very low temperatures, but there is no sharp minimum as in magnetite. If the difference between the relaxed and unrelaxed moduli were constant, the relaxed modulus would increase on cooling; however, the relaxed modulus decreases on cooling until near the temperature of the internal friction peak. Thus a given applied stress induces more configurational strain at low temperatures, but the effect is present at 500°K since even here the temperature coefficient of modulus is abnormally low. If vibrations of much lower frequency are used, the relaxed modulus can be observed below 50°K. There is a possibility that the relaxed modulus might have a sharp minimum below 50°K, but nothing

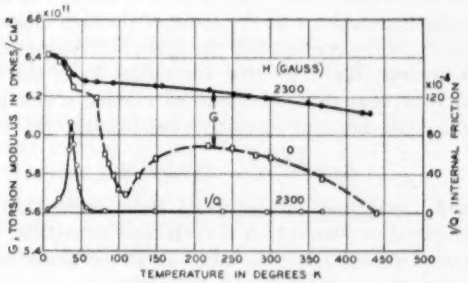

FIG. 2. Torsional modulus and torsional internal friction of ⟨111⟩ in $Ni_{0.75}Fe_{2.25}O_4$. Torsional waves were propagated in a ⟨111⟩ direction. The frequency was approximately 50 kc/sec. The external magnetic field was applied in the ⟨111⟩ that was the direction of wave propagation.

* Present address: Department of Metallurgy, Technological Institute, Northwestern University, Evanston, Illinois.
[1] Verwey, Haayman, and Romeijn, J. Chem. Phys. **15**, 181 (1947).
[2] L. R. Bickford, Revs. Modern Phys. **25**, 75 (1953).
[3] M. E. Fine and Nancy T. Kenney, Phys. Rev. **94**, 1573 (1954).
[4] J. K. Galt, Bell System Tech. J. **33**, 1023 (1954).
[5] Galt, Yager, and Merritt, Phys. Rev. **93**, 1119 (1954).
[6] M. E. Fine (to be published).

indicative of a critical ordering temperature is observed above 50°K.

When no external magnetic field is present, the torsion modulus has a minimum near 105°K, Fig. 2, but this disappears when the sample is saturated. It is thus a domain wall motion effect and is associated with changes in magnetostriction and permeability.

The longitudinal internal friction was also measured near 275 kc/sec. The measurements, not shown, are less reliable than those for the lower frequency since the experimental conditions were not as satisfactory, but the internal friction appeared to peak at a temperature 3 to 7° higher than the 83-kc/sec measurements. This corresponds to an activation energy of between 0.055 and 0.026 ev per electron jump. The value obtained from ferromagnetic resonance line widths[5] is within this range.

The authors are indebted to W. C. Ellis, J. K. Galt, and E. E. Schumacher for helpful discussions and encouragement.

PHYSICAL REVIEW VOLUME 96, NUMBER 6 DECEMBER 15, 1954

Theory of Donor and Acceptor States in Silicon and Germanium

C. KITTEL AND A. H. MITCHELL
Department of Physics, University of California, Berkeley, California
(Received September 7, 1954)

An exact theory of impurity states in crystals is developed, and an evaluation is given of the applicability of the Wannier equation to the donor states in Si and Ge in view of the multiple energy minima in the conduction band. The theory is extended to include degenerate bands, and it is shown by two different methods that the Wannier equation is to be replaced by a set of coupled wave equations. The theory is applied to acceptor states in Si and Ge. The agreement with experiment is fairly good for both donors and acceptors.

WE are concerned here with the calculation of the ionization energies of the shallow donor and acceptor impurity states in silicon and germanium. The ionization of these levels is largely responsible for the charge carrier concentrations observed at room temperature and below. The central experimental facts[1] are that the approximate ionization energies of electrons associated with pentavalent substitutional impurities are 0.04 ev in Si and 0.01 ev in Ge, and the ionization energies of holes associated with trivalent substitutional impurities are about 0.05 ev in Si and 0.01 ev in Ge. The general picture which one has of the donor and acceptor ground states is that their wave functions are spread out over a hydrogenic $1s$ orbital with a large effective radius, of the order of 20 A or more. The loose binding is thought to be the result of the high dielectric constant of the crystals and the light effective masses of the carriers. We recall that the radius R_0 of the first Bohr orbit of an electron of mass m^* moving in a medium of dielectric constant ϵ around a fixed charge $|e|$ is

$$R_0=\epsilon\hbar^2/m^*e^2=(\epsilon m/m^*)a_{\mathrm{H}}, \tag{1}$$

where $a_{\mathrm{H}}=\hbar^2/me^2$ is the usual Bohr radius. As an example, $R_0\approx 50a_{\mathrm{H}}\approx 25$ A if $\epsilon=16$ and $m^*=0.3m$. The effective nuclear charge is taken as $\pm e$ for pentavalent or trivalent substitutional impurities in silicon or germanium.

Our interest in the problem was heightened by the striking circumstance that in both Si and Ge the ionization energies of donors are approximately equal to the ionization energies of acceptors. This is the more remarkable because the forms of the conduction and valence bands are known from cyclotron resonance experiments[2] to be entirely different from each other. The principal energy bands for silicon are shown in Fig. 1. The conduction band energy surfaces are spheroids in k space along ⟨111⟩ axes in Ge and along ⟨100⟩ axes in Si, of the form

$$E(\Delta\mathbf{k})=\hbar^2\left[\frac{(\Delta k_{\parallel})^2}{2m_1}+\frac{(\Delta k_{\perp})^2}{2m_2}\right], \tag{1}$$

where $\Delta\mathbf{k}=\mathbf{k}-\mathbf{k}_i$, with $\mathbf{k}_i$ at one of the set of equivalent energy minima. The valence band energy surfaces for both crystals consist of two fluted or warped spheres[3] degenerate at $k=0$:

$$E(\mathbf{k})=Ak^2\pm[B^2k^4+C^2(k_x^2k_y^2+k_y^2k_z^2+k_z^2k_x^2)]^{\frac{1}{2}}. \tag{2}$$

The numerical calculations given below suggest that the apparent equality of donor and acceptor energies is only accidental, without fundamental significance.

IMPURITY STATE THEORY

The unusual character of the energy surfaces in Si and Ge makes one hesitant about applying the Wannier theorem[4] without further examination. We have

[1] See, for example, J. A. Burton, Physica (to be published).

[2] For a review of this work, see papers by Kip, Lax, and Kittel, Physica (to be published).

[3] Dresselhaus, Kip, and Kittel, Phys. Rev. **95**, 568 (1954).

[4] G. H. Wannier, Phys. Rev. **52**, 191 (1937); J. C. Slater, Phys. Rev. **76**, 1592 (1949); G. F. Koster and J. C. Slater, Phys. Rev. **95**, 1167 (1954); for further references, see J. Friedel, J. phys. et radium **15**, 28 (1954).

developed a method for determining the applicability of the Wannier theorem and for estimating the importance of the corrections associated with the multiplicity of the conduction band energy minima and the approximate degeneracy of the valence band energy surfaces. Our general method is exact in principle and leads to an enhanced understanding of the Wannier theorem. After completing our development we found that the basic idea had been anticipated in one of the methods given by Adams.[5] Our development is more revealing for the present applications, which have not been considered previously.

The line of attack is to compare the Wannier effective Hamiltonian in a plane wave representation with the exact Hamiltonian in a Bloch function representation. The Schrödinger equation of one electron in the perturbed periodic lattice is

$$(\mathcal{H}_0+\delta V)\Psi=W\Psi, \tag{3}$$

where $\mathcal{H}_0$ refers to the unperturbed lattice and δV is the perturbation. The equation of the unperturbed problem is

$$\mathcal{H}_0\psi_{\mathbf{k}}{}^l=E^l(\mathbf{k})\psi_{\mathbf{k}}{}^l, \tag{4}$$

where

$$\psi_{\mathbf{k}}{}^l=u_{\mathbf{k}}{}^l(\mathbf{r})e^{i\mathbf{k}\cdot\mathbf{r}} \tag{5}$$

is the Bloch function with wave vector $\mathbf{k}$ and belonging to the lth energy band. The solutions Ψ of the perturbed problem may be expressed as sums over the complete set of $\psi_{\mathbf{k}}{}^l$:

$$\Psi=\sum_{l,\mathbf{k}} a_{\mathbf{k}}{}^l\psi_{\mathbf{k}}{}^l. \tag{6}$$

We substitute this expansion in Eq. (3), multiply through by Ψ^* and integrate over coordinate space. We find directly

$$W=\sum_{l,\mathbf{k}} |a_{\mathbf{k}}{}^l|^2E^l(\mathbf{k})+\sum_{l',\mathbf{k}'l,\mathbf{k}} a_{\mathbf{k}'}{}^{l'*}a_{\mathbf{k}}{}^l(\psi_{\mathbf{k}'}{}^{l'},\delta V\psi_{\mathbf{k}}{}^l). \tag{7}$$

It is useful to expand the perturbation in a Fourier series:

$$\delta V=\sum_{\mathbf{K}} b_{\mathbf{K}}e^{i\mathbf{K}\cdot\mathbf{r}}. \tag{8}$$

The matrix element in Eq. (7) may now be written

$$(\psi_{\mathbf{k}'}{}^{l'},\delta V\psi_{\mathbf{k}}{}^l)=\sum_{\mathbf{K}} b_{\mathbf{K}}\int u_{\mathbf{k}'}{}^{l'*}u_{\mathbf{k}}{}^l e^{i(-\mathbf{k}'+\mathbf{K}+\mathbf{k})\cdot\mathbf{r}}d\mathbf{r}. \tag{9}$$

It is the well-known property of periodic functions that the integral cannot be different from zero unless

$$\mathbf{k}'=\mathbf{k}+\mathbf{K}. \tag{10}$$

We use the reduced zone convention, according to which all wave vectors $\mathbf{k}$ and $\mathbf{k}'$ lie in the central Brillouin zone. If the sum $\mathbf{k}+\mathbf{K}$ would lie otherwise outside the central zone, we may subtract 2π times the appropriate reciprocal lattice vector to bring it into the central zone.

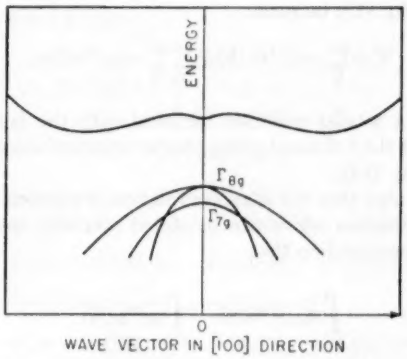

FIG. 1. Energy band scheme for silicon as determined by cyclotron resonance. The bands will not really cross.

We have now the result

$$W=\sum_{l,\mathbf{k}} |a_{\mathbf{k}}{}^l|^2E^l(\mathbf{k})+\sum_{l'}\sum_{l,\mathbf{k}}\sum_{\mathbf{K}} a_{\mathbf{k}+\mathbf{K}}{}^{l'*}a_{\mathbf{k}}{}^l b_{\mathbf{K}}\Delta_{\mathbf{k}+\mathbf{K},\mathbf{k}}{}^{l'l}, \tag{11}$$

where

$$\Delta_{\mathbf{k}+\mathbf{K},\mathbf{k}}{}^{l'l}=\int u_{\mathbf{k}+\mathbf{K}}{}^{l'*}u_{\mathbf{k}}{}^l d\mathbf{r}. \tag{12}$$

It is to be emphasized that Eq. (11) is an exact result. The energy eigenvalues may be found as the roots of the secular equation associated with the diagonalization of Eq. (11).

The Wannier equation follows when a simple and revealing assumption is made. We know that, by the orthogonality property of the Bloch functions,

$$\Delta_{\mathbf{k},\mathbf{k}}{}^{l'l}=\delta_{l'l}. \tag{13}$$

Thus, if we may neglect $\mathbf{K}$ in Eq. (12), the fundamental equation (8) becomes

$$W=\sum_{l}\{\sum_{\mathbf{k}} |a_{\mathbf{k}}{}^l|^2E^l(\mathbf{k})+\sum_{\mathbf{k}}\sum_{\mathbf{K}} a_{\mathbf{k}+\mathbf{K}}{}^{l*}a_{\mathbf{k}}{}^l b_{\mathbf{K}}\}. \tag{14}$$

In this approximation different bands l are entirely independent. We now show that this equation is equivalent to the Wannier equation.

We consider the problem of a free particle (not in the crystal) moving in the potential δV. We take the effective kinetic energy operator to be $E^l(-i\nabla)$, understood to be the same function of $-i\nabla$ as the energy eigenvalue $E^l(\mathbf{k})$ in Eq. (4) is of $\mathbf{k}$. The Wannier equation in the usual form is

$$[E^l(-i\nabla)+\delta V]\phi=W\phi. \tag{15}$$

We can transform this to look like Eq. (14). We consider ϕ in the plane wave representation:

$$\phi=\sum_{\mathbf{k}} a_{\mathbf{k}}{}^l e^{i\mathbf{k}\cdot\mathbf{r}}. \tag{16}$$

[5] E. N. Adams II, J. Chem. Phys. 2013 (1953); see also S. Pekar, J. Phys. (U.S.S.R.) **10**, 431 (1946).

Then Eq. (15) becomes

$$W=\sum_{\mathbf{k}}|a_{\mathbf{k}}{}^{l}|^{2}E_{l}(\mathbf{k})+\sum_{\mathbf{k}}\sum_{\mathbf{K}}a_{\mathbf{k}+\mathbf{K}}{}^{l*}a_{\mathbf{k}}{}^{l}b_{\mathbf{K}}, \quad (17)$$

giving a secular equation identical with the factored part for the l th band of the secular equation associated with Eq. (14).

It is seen that the Wannier theorem is rigorous in an approximation which can be stated precisely, namely, the approximation that

$$\int u_{\mathbf{k}+\mathbf{K}}{}^{l'*}u_{\mathbf{k}}{}^{l}d\tau=\int u_{\mathbf{k}}{}^{l'*}u_{\mathbf{k}}{}^{l}d\tau. \quad (18)$$

The following two sections of this paper consider the applicability of this approximation to our semiconductor problems.

DONOR STATES

The conduction band edge of silicon consists of six equivalent spheroids oriented along the set of six equivalent ⟨100⟩ directions in $\mathbf{k}$ space. The conduction band edge of germanium consists of eight (or four, if centered at the zone boundary) equivalent spheriods oriented along the set of eight equivalent ⟨111⟩ axes in $\mathbf{k}$ space.

The first question to investigate is the effect of multiple minima in $E^{l}(\mathbf{k})$ on the solutions of the Wannier equation. The forms (14) or (17) show that the impurity state problem may be factored into separate problems relating to each energy spheroid separately if the condition is satisfied that the important $a_{\mathbf{k}+\mathbf{K}}$ all lie comfortably within the same region of $\mathbf{k}$ space as the $a_{\mathbf{k}}$ from which they originate. In other words, we require that the sum

$$\sum_{\mathbf{k}}\sum_{\mathbf{K}}a_{\mathbf{k}+\mathbf{K}}{}^{l*}a_{\mathbf{k}}{}^{l}b_{\mathbf{K}} \quad (19)$$

should group into the appropriate number of separate parts, each part clustered about a different band edge point $\mathbf{k}_i$, with only insignificant cross terms between the different parts. When this condition is met we can confidently calculate the donor energy by taking one energy spheroid by itself and know that the resulting value will not be affected by including states from the other equivalent spheroids. The actual eigenstates will involve all spheroids, but the energy can be calculated from one spheroid. The eigenstates must transform as irreducible representations of the symmetry group of the Wannier Hamiltonian.

We now look into the Fourier coefficients $a_{\mathbf{k}}$, $b_{\mathbf{K}}$. For an order-of-magnitude estimate we consider the analysis of the function

$$\phi=e^{-r/R_0}, \quad (20)$$

as for the ground state of hydrogen. For this function the k dependence is given by

$$a_{\mathbf{k}}\sim 1/(1+k^{2}R_{0}^{2})^{2}, \quad (21)$$

and for a Coulomb potential $\delta V\sim 1/r$ we have

$$b_{\mathbf{K}}\sim 1/K^{2}. \quad (22)$$

We note that $b_{\mathbf{K}}K^{2}dK$ is constant. It is now obvious that the convergence of the sum (19) is excellent when $kR_0\gg 1$. From Eq. (1) we know that R_0 is of the order of $50a_{\mathrm{H}}$, while the values of $(\Delta k)_0$ connecting separate energy minima of the conduction band are presumably of the order of 2π times the reciprocal lattice parameter, or $(\Delta k)_0\approx 0.5/a_{\mathrm{H}}$. Therefore $(\Delta k)_0R_0\approx 25$, assuring good convergence for the donor ground state problem when solved around a single energy minimum with a surface of the form (1).

Having disposed of the problem of the multiple minima, we must now consider the applicability of the approximation

$$\Delta_{\mathbf{k}+\mathbf{K},\mathbf{k}}{}^{l'l}\cong\delta_{l'l}, \quad (23)$$

which led to the Wannier equation. This question arises, of course, in any application of the Wannier equation. We restrict ourselves in this section to a study of the situation in the neighborhood of one spheroidal energy minimum of the conduction band.

We use the property that it is possible to obtain $u_{\mathbf{k}+\mathbf{K}}$ from $u_{\mathbf{k}}$ to the first order in $\mathbf{K}$ by the equation

$$u_{\mathbf{k}+\mathbf{K}}{}^{l}=u_{\mathbf{k}}{}^{l}-(i\hbar^{2}/m)\sum_{l'}\frac{\mathbf{K}\cdot\int u_{\mathbf{k}}{}^{l'*}\nabla u_{\mathbf{k}}{}^{l}d\tau}{E^{l}(\mathbf{k})-E^{l'}(\mathbf{k})}u_{\mathbf{k}}{}^{l'}. \quad (24)$$

The normalization is not affected to first order in K, so that

$$\Delta_{\mathbf{k}+\mathbf{K},\mathbf{k}}{}^{ll}=1+O(K^{2}). \quad (25)$$

However,

$$\Delta_{\mathbf{k}+\mathbf{K},\mathbf{k}}{}^{l'l}=\delta_{l'l}+\frac{i\hbar^{2}}{m}\frac{\mathbf{K}\cdot\int u_{\mathbf{k}}{}^{l}\nabla u_{\mathbf{k}}{}^{l'*}d\tau}{E^{l'}(\mathbf{k})-E^{l}(\mathbf{k})}+O(K^{2}), \quad (26)$$

while in this approximation the effective mass tensor is given by

$$\left(\frac{1}{m^{*}}\right)_{ij}=\frac{\delta_{ij}}{m}+\left(\frac{\hbar^{2}}{m^{2}}\right)\frac{\partial^{2}}{\partial K_{i}\partial K_{j}}\times\sum_{l'}\frac{|\mathbf{K}\cdot\int u_{\mathbf{k}}{}^{l'*}\nabla u_{\mathbf{k}}{}^{l}d\tau|^{2}}{E^{l}(\mathbf{k})-E^{l'}(\mathbf{k})}. \quad (27)$$

We can make an estimate of the right-hand side of Eq. (26), along a principal axis of the energy surface, if we make the assumption that perturbations by a single band l' determine the effective mass in the band l; we also assume for convenience that $(1/m^{*})\ll(1/m)$. Then, in the principal direction,

$$\frac{1}{m^{*}}\approx\frac{2\hbar^{2}}{m^{2}}\frac{|\int u_{\mathbf{k}}{}^{l'*}\nabla u_{\mathbf{k}}{}^{l}d\tau|^{2}}{E^{l}(\mathbf{k})-E^{l'}(\mathbf{k})}. \quad (28)$$

Using Eq. (26),

$$\frac{1}{m^{*}}\approx\frac{2}{\hbar^{2}K^{2}}[E^{l}(\mathbf{k})-E^{l'}(\mathbf{k})]|\Delta_{\mathbf{k}+\mathbf{K},\mathbf{k}}{}^{l'l}|^{2}, \quad (29)$$

so that

$$\Delta_{\mathbf{k}+\mathbf{K},\mathbf{k}}{}^{l'l}\approx\left[\frac{\hbar^2K^2/2m^*}{E^l(\mathbf{k})-E^{l'}(\mathbf{k})}\right]^{\frac{1}{2}}. \quad (30)$$

The range of $\mathbf{K}$ of importance is of the order of $1/R_0$, where R_0 is the orbital radius. We can expect therefore for the important terms,

$$\Delta^{l'l}\approx\left[\frac{\text{impurity ionization energy}}{\text{band gap, taken at } k}\right]^{\frac{1}{2}}, \quad (31)$$

so that $\Delta^{l'l}$ may be of the order of 0.1 for Si and Ge. We are going to neglect it in the calculations reported directly below, but it is useful to realize that the error introduced by the neglect may be of the order of 10 percent of the effective potential δV.

The next question to consider is that of the effective potential energy. We shall use as the potential energy of an electron in the field of a donor atom

$$\delta V=-e^2/\epsilon r, \quad (32)$$

where ϵ is the dielectric constant. At the relevant energies ($W_{\text{ionization}}\ll W_{\text{gap}}$) the static dielectric constant may be used. We are not aware that a careful analysis has ever been carried out of the applicability of Eq. (32) to the circumstances of the present problem. It is tempting to let $\epsilon\rightarrow 1$ for small r well within the outer shells of the donor atom. We are not entirely certain, however, that the Wannier equation can be used to describe effects so restricted in range. Pauling gives the ionic radius of P^{5+} as 0.34A, so that at this point e^2/r is much greater than the important interband energies. There is undoubtedly some increase in binding and a pileup of charge near the donor nucleus, but we will have to omit these effects because we do not yet know how to treat them with a rigor comparable to that of the rest of the present calculation. The eigenvalue equation is

$$-\frac{\hbar^2}{2m}\left[\frac{1}{\alpha_1}\frac{\partial^2}{\partial x^2}+\frac{1}{\alpha_2}\left(\frac{\partial^2}{\partial y^2}+\frac{\partial^2}{\partial z^2}\right)\right]\phi-\frac{e^2}{\epsilon r}\phi=W\phi, \quad (33)$$

where $m_i^*=\alpha_i m$. This equation is not separable completely for $\alpha_1\neq\alpha_2$. We determine an upper bound to the ground-state energy W_0, relative to the bottom of the conduction band continuum, by a variational calculation. The variational function was of the form

$$\phi=\left[\frac{ab^2}{\pi r_0{}^3}\right]^{\frac{1}{2}}\exp\{-[a^2x^2+b^2(y^2+z^2)]^{\frac{1}{2}}/r_0\}, \quad (34)$$

where $r_0=\epsilon\hbar^2/me^2$. We obtain

$$W_0=-3\left(\frac{me^4}{2\epsilon^2\hbar^2}\right)(\rho^2+1)\left[\frac{\rho^2+1}{\alpha_1}+\frac{2}{\alpha_2}\right]^{-1}\left(\frac{\tan^{-1}\rho}{\rho}\right)^2, \quad (35)$$

where ρ is to be chosen to minimize W_0. We then determine a and b from

$$b=3(\rho^2+1)^{\frac{1}{2}}\left[\frac{\rho^2+1}{\alpha_1}+\frac{2}{\alpha_2}\right]^{-1}\frac{\tan^{-1}\rho}{\rho}$$

and

$$a=(\rho^2+1)^{\frac{1}{2}}b.$$

The results were as follows:

For n−Ge with $\alpha_1=1.58$, $\alpha_2=0.082$, $\epsilon=16$:

$$W_0=-0.00905 \text{ ev}, \quad a^2=0.135, \quad b^2=0.0174.$$

For n−Si with $\alpha_1=1$, $\alpha_2=0.2$, $\epsilon=12$:

$$W_0=-0.0298 \text{ ev}, \quad a^2=0.216, \quad b^2=0.0729.$$

Using the four-parameter variation function,

$$\psi=N[a+bx^2+c(y^2+z^2)]\exp\{-[dx^2+e(y^2+z^2)]^{\frac{1}{2}}\},$$

the energy was not lowered by as much as one percent. It may be noted that the extent of the Ge ground state in the yz plane is of the order of 60 A.

DISCUSSION OF RESULTS

Burstein, Oberly, and Davisson[6] report that the donor ionization energy in silicon is 0.04 ev, based on measurements of the infrared photoconductive response. Morin, Maita, Shulman, and Hannay[7] report for Si the values 0.039 ev for P donor atoms; 0.049 ev for As; 0.039 ev for Sb. Their values are derived from Hall coefficient data. A representative experimental value may be taken to be 0.04 ev, although it is not clear why the arsenic donors give 0.049 ev. Our calculated lower bound to the numerical value of the ionization energy is 0.030 ev and is in fair agreement therefore with the observations. There is some uncertainty in principle in the interpretation of all the observations.

Burton [8] reported at the 1954 Amsterdam conference on semiconductors the following ionization energies for donor atoms in Ge, based on Hall effect measurements:

P, 0.0120 ev; As, 0.0127 ev; Sb, 0.0096 ev.

The calculated lower limit to the ionization energy is 0.0090 ev. This is also somewhat lower than the experimental values.

ACCEPTOR STATES

As shown in Fig. 1, the valence band actually consists of two bands which are degenerate at the center of the Brillouin zone; there is also a third band which at the center of the zone is lower in energy by the amount of the spin-orbit coupling energy. To terms in k^2, the energy surfaces are described by

$$E_{1,2}(\mathbf{k})=Ak^2\pm[B^2k^4+C^2(k_x{}^2k_y{}^2+k_y{}^2k_z{}^2+k_z{}^2k_x{}^2)]^{\frac{1}{2}}, \quad (36)$$

[6] Burstein, Oberly, and Davisson, Phys. Rev. **89**, 331 (1953).
[7] Morin, Maita, Shulman, and Hannay, Phys. Rev. **96**, 833(A) (1954).
[8] J. A. Burton, reference 1; T. H. Geballe and F. J. Morin, Phys. Rev. **95**, 1085 (1954).

and

$$E_2(\mathbf{k}) = -\Delta + Ak^2, \tag{37}$$

where Δ is the separation between bands at $\mathbf{k}=0$.

When the energy minimum of a band is at or close to a point in k space at which several bands are degenerate, the theory of impurity states has to be revised and the Wannier equation replaced by a set of coupled differential equations. The unperturbed Hamiltonian and the impurity perturbation should be in effect diagonalized simultaneously. We develop the necessary theory below.

We suppose that we have n orthogonal states $\phi_0{}^i$ degenerate at $\mathbf{k}=0$. We make an arbitrary choice of the $\phi_0{}^i$ once and for all. By perturbation theory we obtain a set of functions $\phi_\mathbf{k}{}^i$. To first order in $\mathbf{k}$,

$$\phi_\mathbf{k}{}^j = \left\{ \phi_0{}^j - (i\hbar^2/m) \sum_l \frac{\mathbf{k}\cdot \int \psi_0{}^{l*} \nabla \phi_0{}^j d\tau}{E^l(0) - E^j(0)} \psi_0{}^l \right\} e^{i\mathbf{k}\cdot\mathbf{r}}. \tag{38}$$

The sum is over all bands l, but in our applications the matrix elements connecting the degenerate functions $\phi_0{}^i$ will vanish. It is important to recognize that the $\phi_\mathbf{k}{}^i$ defined by (38) are eigenfunctions of the crystal translation operator and have the eigenvalue $e^{i\mathbf{k}\cdot\mathbf{r}}$. The $\phi_\mathbf{k}{}^i$ are *not*, in general, eigenfunctions of the crystal Hamiltonian $\mathcal{H}_0$. The eigenfunctions $\psi_\mathbf{k}{}^j$ of $\mathcal{H}_0$ are linear combinations of the $\phi_\mathbf{k}{}^i$:

$$\psi_\mathbf{k}{}^j = \sum_i c_\mathbf{k}{}^{ji} \phi_\mathbf{k}{}^i. \tag{39}$$

The coefficients $c_\mathbf{k}{}^{ji}$ may be fairly complicated functions of $\mathbf{k}$; for this reason our theory is simpler when set up first in terms of the $\phi_\mathbf{k}{}^i$.

We call the $\phi_\mathbf{k}{}^i$ *pseudo-Bloch* functions, as they obviously share some of the properties of Bloch functions. The functions given by Eq. (38) are approximately orthogonal, and we may treat them as orthogonal for our purposes. The pseudo-Bloch functions are of value even in the unperturbed problem, as the secular equation in the pseudo-Bloch representation is identical with that obtained less directly with the usual method of Van Vleck and Shockley.

We now look for a solution to the perturbed problem in the form

$$\Psi = \sum_{i,\mathbf{k}} a_\mathbf{k}{}^i \phi_\mathbf{k}{}^i. \tag{40}$$

We neglect other bands l except as they are already mixed in the $\phi_\mathbf{k}{}^i$ by Eq. (38). We are trying to establish a modified Wannier equation. Taking matrix elements of $\mathcal{H}_0+\delta V$, we have

$$(\phi_\mathbf{k}{}^j|\mathcal{H}_0+\delta V|\Psi) = a_\mathbf{k}{}^j W = \sum_i a_\mathbf{k}{}^i (\phi_\mathbf{k}{}^j|\mathcal{H}_0|\phi_\mathbf{k}{}^i) + \sum_{i,\mathbf{k}'} a_{\mathbf{k}'}{}^i (\phi_\mathbf{k}{}^j|\delta V|\phi_{\mathbf{k}'}{}^i). \tag{41}$$

Writing $\delta V = \sum b_\mathbf{K} e^{i\mathbf{K}\cdot\mathbf{r}}$,

$$(\phi_\mathbf{k}{}^j|\delta V|\phi_{\mathbf{k}'}{}^i) = b_\mathbf{K} \Delta_{\mathbf{k},\mathbf{k}-\mathbf{K}}{}^{ji}, \tag{42}$$

where Δ is defined by Eq. (12). To a good approximation for our n bands,

$$\Delta_{\mathbf{k},\mathbf{k}-\mathbf{K}}{}^{ji} \cong \delta_{ji}; \tag{43}$$

this approximation is better than the earlier one of neglecting mixing of higher bands. The secular equation takes the form

$$W a_\mathbf{k}{}^j = \sum_i a_\mathbf{k}{}^i \mathcal{H}^{ji}(\mathbf{k}) + a_{\mathbf{k}-\mathbf{K}}{}^j b_\mathbf{K}, \tag{44}$$

where

$$\mathcal{H}^{ji}(\mathbf{k}) = (\phi_\mathbf{k}{}^j|\mathcal{H}_0|\phi_\mathbf{k}{}^i);$$

to the second order in $\mathbf{k}$,

$$\mathcal{H}^{ji}(\mathbf{k}) = A^{ji}\delta_{ji} + \sum_{p,q} B_{pq}{}^{ji} k_p k_q, \tag{45}$$

where p,q run over x, y, z.

We now propose that for degenerate situations the Wannier equation should be replaced by the following set of coupled wave equations:

$$\sum_i \mathcal{H}^{ji}(-i\nabla) U^i(\mathbf{r}) + \delta V U^j(\mathbf{r}) = W U^j(\mathbf{r}), \tag{46}$$

where $\mathcal{H}^{ji}(-i\nabla)$ is a differential operator derived from $\mathcal{H}^{ji}(\mathbf{k})$ by replacing $\mathbf{k}$ by $-i\nabla$. We note that $\mathcal{H}^{ji}$ is a much simpler operator in the pseudo-Bloch representation $\phi_\mathbf{k}{}^i$ than in the diagonalized Bloch representation $\psi_\mathbf{k}{}^i$. The proof of Eq. (46) follows readily from the secular equation (44). We suppose that the U^i may be expanded in plane waves,

$$U^i(\mathbf{r}) = \sum_\mathbf{k} a_\mathbf{k}{}^i e^{i\mathbf{k}\cdot\mathbf{r}}. \tag{47}$$

The secular equation which results from Eq. (46) is identical with Eq. (44). This completes the proof.

It is now desirable to establish a physical interpretation of the functions $U^i(\mathbf{r})$. To do this we must start out with a new derivation of our modified Wannier equation Eq. (46). We follow the lines of the usual proof of the Wannier theorem for a single band, generalizing as required. We define a set w^i of pseudo-Wannier functions for the bands degenerate at $\mathbf{k}=0$:

$$w_n{}^i = w^i(x-x_n) = N^{-\frac{1}{2}} \sum_k e^{-ikx_n} \phi_k{}^i(x); \tag{48}$$

$$\phi_k{}^i(x) = N^{-\frac{1}{2}} \sum_n e^{ikx_n} w^i(x-x_n). \tag{49}$$

We look for a solution of the perturbed problem in the form

$$\Psi = \sum_{i,n} U^i(x_n) w^i(x-x_n). \tag{50}$$

We treat this function exactly as in the standard derivation for the nondegenerate problem, using the approximation (for δV slowly varying)

$$\int w_m{}^* \delta V \sum_{i,n} U^i(x_n) w_n{}^i dx \cong \delta V(x_m) U^i(x_m), \tag{51}$$

and at the appropriate stage making use of the fact that $\mathcal{H}^{ji}(\mathbf{k})$ is periodic in the reduced zone scheme:

$$\mathcal{H}^{ji}(k) = \sum_s A^{ji}(x_s) e^{-ikx_s}, \tag{52}$$

so that

$$\mathcal{H}^{ji}(-id/dx)=\sum_s A^{ji}(x_s)e^{(-x_s d/dx)}. \quad (53)$$

We are led to the set of coupled wave equations

$$\sum_i \mathcal{H}^{ji}(-i\nabla)U^i(\mathbf{r})+\delta V U^j(\mathbf{r})=WU^j(\mathbf{r}), \quad (54)$$

identical with Eq. (46). We now have, however, the interpretation in Eq. (50) of the U^i as envelope functions of the pseudo-Wannier functions $w^i(x-x_n)$.

We have established above the important result that for degenerate bands the ordinary Wannier equation is replaced by the set of coupled differential equations[9] (54). We now consider the application to the valence band edge in germanium and silicon. It is known from cyclotron resonance that the highest state in the valence band is 4-fold degenerate and transforms as the irreducible representation Γ_{8g} of the cubic group. We have then to deal with a set of four coupled wave equations, analogous to the Dirac equations. The band associated with $\Gamma_{7g}(J=\frac{1}{2})$ does not mix in.

We choose a system of representation in which the ϕ_0^i transform as $m_J=\frac{3}{2}, \frac{1}{2}, -\frac{1}{2}, -\frac{3}{2}$. The matrix operator becomes, symbolically,

$$\begin{bmatrix} Ak^2+Bk_z^2+\delta V-W & -Dik_zk_+ & Ek_+^2+Jk_-^2 & 0 \\ Dik_zk_- & Ck^2-Bk_z^2+\delta V-W & 0 & Ek_+^2+Jk_-^2 \\ Ek_-^2+Jk_+^2 & 0 & Ck^2-Bk_z^2+\delta V-W & Dik_zk_+ \\ 0 & Ek_-^2+Jk_+^2 & -Dik_zk_- & Ak^2+Bk_z^2+\delta V-W \end{bmatrix} U=0. \quad (55)$$

The constants A, B, C, D, E, J can be expressed in terms of three constants F, G, H related to sums of matrix elements squared over energy denominators. The relations are known from unpublished work by Dresselhaus. The constants can be determined from cyclotron resonance results.

The perturbation $\delta V=-e^2/\epsilon r$ is invariant under time reversal, so that by the Kramers theorem the eigenvalues of (54) must occur in pairs. This means that for real trial functions it is reasonable to take $U_1=U_4$; $U_2=U_3$. In a magnetic field the Kramers degeneracy is lifted, and four different functions are required in principle.

Consideration of the expression (2) for the unperturbed energy shows[10] that the 4×4 matrix operator may be factored into two identical 2×2 non-Hermitian matrices which do not contain square roots of differential operators. The elements of these matrices are

$$\mathcal{H}_{11}=-\left[A+\left(B^2+\frac{1}{3}C^2\right)^{\frac{1}{2}}\right]\nabla^2-\frac{e^2}{\epsilon r}-W,$$

$$\mathcal{H}_{22}=-\left[A-\left(B^2+\frac{1}{3}C^2\right)^{\frac{1}{2}}\right]\nabla^2-\frac{e^2}{\epsilon r}-W,$$

$$\mathcal{H}_{12}=-\mathcal{H}_{21}^*=\frac{C}{3^{\frac{1}{2}}}\left(\frac{\partial^2}{\partial x^2}+\omega\frac{\partial^2}{\partial y^2}+\omega^2\frac{\partial^2}{\partial z^2}\right),$$

where $\omega^3=1$ and A, B, and C are defined by Eq. (2). If we treat the off-diagonal elements as perturbations, we obtain in the zeroth-order approximation two hydrogen-like equations with different effective masses. The larger effective mass and ionization energy that we obtain are $m^*=0.58m$, $W_0=0.055$ ev for Si, and $m^*=0.42m$, $W_0=0.022$ ev for Ge. A second-order perturbation calculation lowered the energy by less than one percent in both cases.

The result is not reliable, however, as noncommutability was neglected in the transformation.

ACKNOWLEDGMENTS

We are indebted to Mr. G. Dresselhaus for helpful discussions and for making available his calculations on the valence band energy surfaces. We profited from a conversation with Professor J. M. Luttinger and from correspondence with Professor J. Bardeen. This research has been supported in part by the U. S. Office of Naval Research and the U. S. Signal Corps.

[9] J. M. Luttinger and W. Kohn (private communication) have found independently a result of this type.

[10] This factorization was performed by G. Dresselhaus.

Large Magnetic Kerr Rotation in BiMn Alloy

B. W. Roberts and C. P. Bean
General Electric Research Laboratory, Schenectady, New York
(Received September 1, 1954)

Ferromagnetic domains in BiMn crystallites are found to be easily observed by utilizing plane polarized light in reflection. A crystallite viewed parallel to the c_0 axis shows a characteristic "rick rack" or zigzag pattern of domains as a stable configuration in zero field. Magnetic domain patterns reminiscent of spiral surface growth are observed. The large magneto-optic rotation is thought to be due to the high resistivity of BiMn alloy.

MAGNETIC domain patterns[1,2] have been observed optically in some large grains of ferromagnetic BiMn alloy prepared at temperatures below the magnetic transformation (360°C). The patterns are easily observed and often appear nearly black-and-white when viewed through the polarizing arrangement of a Bausch and Lomb research metallograph which utilizes the Foster type vertical illuminating prism. The surface need only be smoothly polished with alcohol as a lubricant.

The surface of the grain in Fig. 1 which has its c_0 axis perpendicular to the paper has not been touched between successive frames. Figure 1(b) is the area of Fig. 1(a) after a field of 15 000 oersted has been applied parallel with the surface. Small pattern movements are observable. When the same field is applied perpendicular to the surface the "rick-rack" or zig-zag pattern is seen to break up into separate domain regions and some of these are rough six-sided rings as in Fig. 1(c). BiMn has the hexagonal (NiAs) crystal

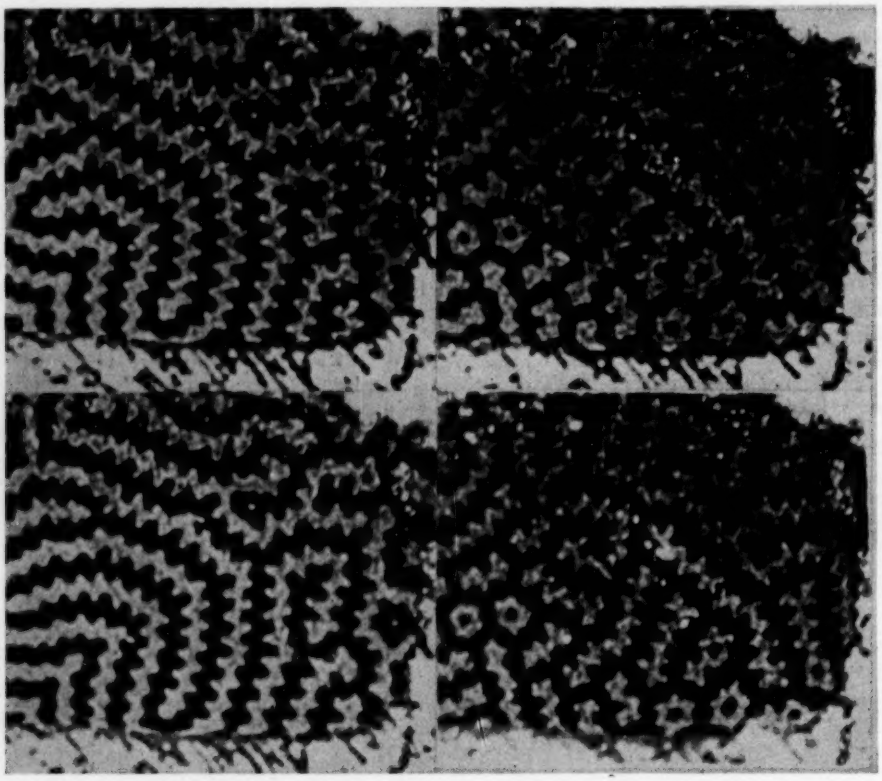

FIG. 1. (a) Original domain pattern on BiMn grain. (b) Same area after 15 000-oe field applied parallel with the surface. (c) Same field applied perpendicular to surface and (d) after cooling to 77.3°K for one minute. 2500×.

[1] In cobalt. Williams, Foster, and Wood, Phys. Rev. **82**, 119 (1951); C. A. Fowler and E. M. Fryer, Phys. Rev. **95**, 564 (1954).
[2] In silicon iron. C. A. Fowler and E. M. Fryer, Phys. Rev. **86**, 426 (1952); Phys. Rev. **94**, 52 (1954).

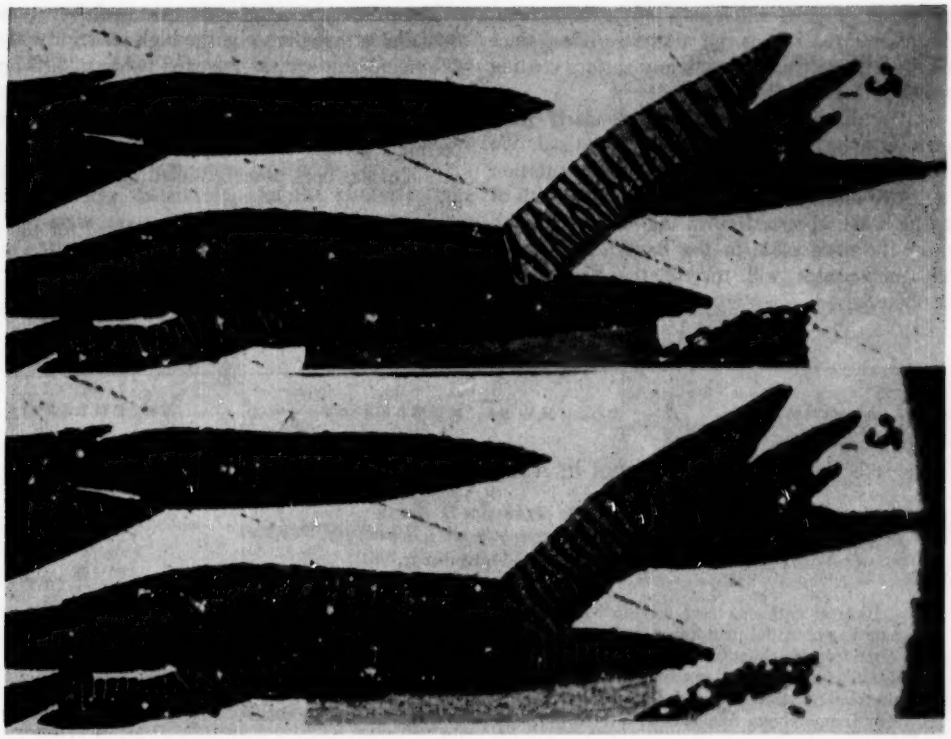

FIG. 2. (a) BiMn domain pattern when observed roughly perpendicular to c_0 axis. (b) Same area after 10 000-oe field was applied in random directions. 700×.

structure which may relate to the rings. The last frame shows the effect of holding the sample in liquid nitrogen for one minute and quickly warming to room temperature. Again small movements are observable which may result from a reorganization of the domains at low temperature due to the marked change in the magnetocrystalline anisotropy energy.[3] There is also the possibility of strain-induced domain motion due to the grain being enclosed in a Bi matrix.

When a group of grains is observed roughly perpendicular to the c_0 axis, the patterns in Fig. 2 are found to be typical. The light grey area is the Bi matrix and the darker BiMn particles have nearly parallel domain patterns which vary in width as they move across the grain. Figure 2(b) shows the area of 2(a) after a 10 000-oersted field has been applied in random directions with respect to the sample. Almost all configurations have obvious domain movement present. The domains are continuous at the crystal-grain boundaries and this was found to hold true regardless of the relative orientations of adjacent grains even up to 90°. Clear Bitter patterns were found to form at the boundaries of the domains.

Figure 3 shows a magnetic domain pattern reminiscent of the many spiral growth patterns being found on crystal surfaces due to growth steps. Seven segments

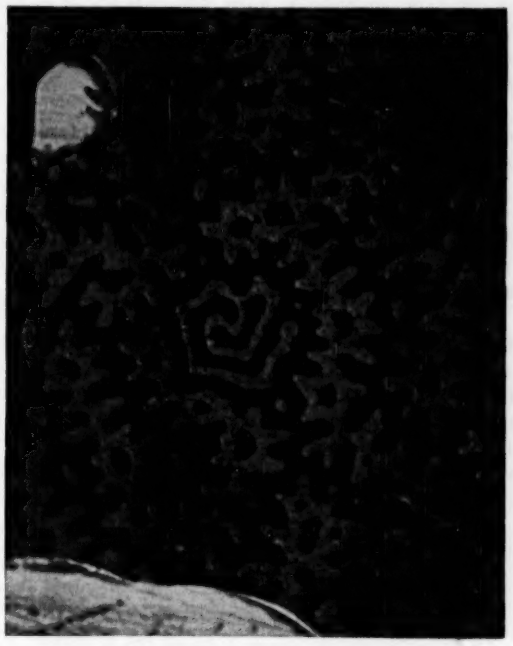

FIG. 3. Spiral-shaped domain pattern observed on BiMn grain. 4000×.

[3] C. Guillaud, J. phys. et radium **12**, 492 (1951).

occur on the outer spiral which may reflect the hexagonal BiMn structure. This is not a surface effect since the light is scattered from beneath any surface coating or disturbance due to polishing.

The light which is scattered perpendicularly from these surfaces appears to be elliptically polarized. We have had difficulty in measuring the amount of rotation and the degree of ellipticity due to the small width of the domains when observed down the c_0 axis. A small rotation of the mica plate in the Bausch and Lomb elliptical compensator will reverse the domain intensities observed.

The primary reason for the ease in observation of the domains is thought to be the high resistivity of BiMn, 424 micro-ohm cm, as reported by Kondo.[4] The lower number of conduction electrons would permit deeper penetration into the region of magnetization and thus permit a greater total rotation of the plane of polarization as has been observed in studies of thin-magnetic films.

We are indebted to Miss Jean Hurd for the metallographic preparation and pictures shown here.

[4] K. Kondo, J. Phys. Soc. Japan **5**, 307 (1950).

PHYSICAL REVIEW VOLUME 96, NUMBER 6 DECEMBER 15, 1954

Fermi Level in Amorphous Antimony Films

E. Taft and L. Apker
General Electric Research Laboratory, Schenectady, New York
(Received September 2, 1954)

Films of antimony were deposited by evaporation on interchangeable emitters in concentric-sphere, retarding-potential phototubes. Below thicknesses of about 300 A, they behaved as semiconductors. The Fermi level lay about 0.1 ev above the occupied band. They converted irreversibly to the normal crystalline metallic form at 200°C or somewhat higher. The results are consistent with previous measurements on the electrical resistance and optical transmission of thin antimony films; they indicate that the semiconducting form is amorphous. Analogies with the behavior of arsenic are mentioned.

An amorphous form of antimony has been recognized for many years.[1] It is especially common in very thin evaporated films, and it is stable in this form considerably above room temperature. The electrical resistivity[2] and optical absorption[1] of this material indicate that it is a semiconductor.

The present paper supports this view and discusses a direct photoelectric determination of the Fermi level relative to the occupied band of electron energy states. The approach was identical with that used in previous work on amorphous arsenic.[3] Two separate concentric sphere phototubes were used. Results were duplicated with antimony films deposited on substrates of nickel and of crystalline Ge.

Figure 1 shows the current-voltage characteristics for the photoemission from films of antimony deposited on substrates held near room temperature. If the films were below about 300A in thickness, they showed a behavior quite typical of a semiconductor (curve 2). Above this thickness, they were clearly normal crystalline antimony, and showed the photoelectric behavior typical of this poor metal (curve 1).[4] Further, films about 50 a.u. in thickness underwent a transition from semiconducting to metallic behavior upon heating to 200°C or thereabouts for a few minutes.

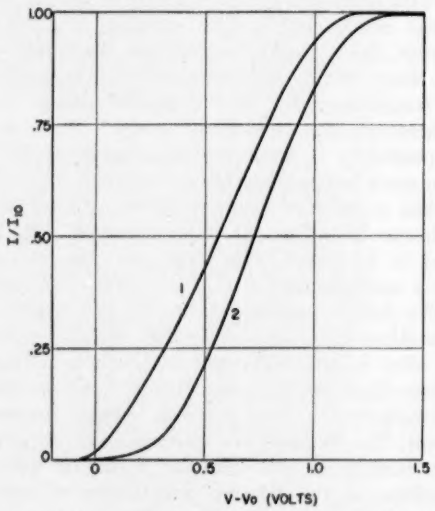

Fig. 1. Current-voltage characteristics for photoemission from antimony films in concentric-sphere phototube at $h\nu = 5.80$ ev. Currents are normalized at a collector potential $V = 10$ v. Abscissas are given relative to the 0°K stopping potential V_0 of an ideal metal, a voltage corresponding to the common Fermi level of all the interchangeable emitters. Curve 1 is for crystalline antimony; curve 2 is for the semiconducting amorphous variety.

[1] Hans Murman, Z. Physik **54**, 741 (1929); for discussions, see H. Krebs, *Semiconducting Materials*, H. K. Henisch, editor (Butterworths Scientific Publications, Ltd., London, 1950); F. S. Moss, *Photoconductivity in the Elements* (Academic Press, Inc., New York, 1952); an example of recent work is Julius Cohn, J. Appl. Phys. **25**, 798 (1954).
[2] R. Suhrmann and W. Berndt, Z. Physik **115**, 17 (1940).
[3] E. Taft and L. Apker, Phys. Rev. **75**, 1181 (1949).
[4] Apker, Taft, and Dickey, Phys. Rev. **76**, 270 (1949).

One concludes that the thin, semiconducting antimony films were behaving quite like the genuinely amorphous form of the element recognized by previous workers.[5] The data in Fig. 1 indicate that the Fermi level in this semiconductor lies above the occupied band of electron energy states by an amount of order 0.1 ev. This may be seen more clearly in Fig. 2, which shows the energy distributions of the photoelectrons from the amorphous as well as from the crystalline form of antimony. The amorphous variety displays the

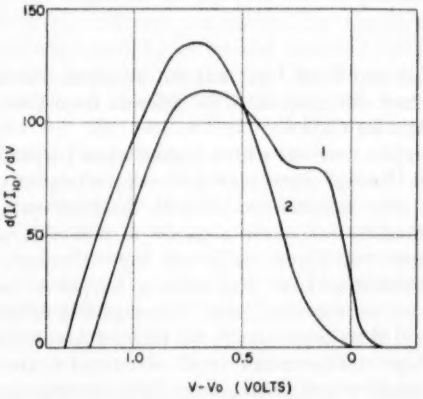

FIG. 2. Normalized energy distributions obtained by differentiation of curves in Fig. 1. Abscissa is reversed from Fig. 1 in order that energies increase toward the right. Note the sparsity of electrons originating just below the Fermi level in amorphous films (curve 2) and the plateau which appears in this region when the material is crystallized (curve 1).

pronounced sparsity of high-energy electrons expected from the energy structure mentioned above.

The Fermi level determination given here is consistent with observations in the literature on resistivity and optical properties.

Independent evidence for these views appears in the spectral distributions of the photoelectric yield as shown in Fig. 3. Although the saturation points on the current-voltage characteristics of Fig. 1 show that the work

[5] J. A. Prins, Nature **131**, 760 (1933).

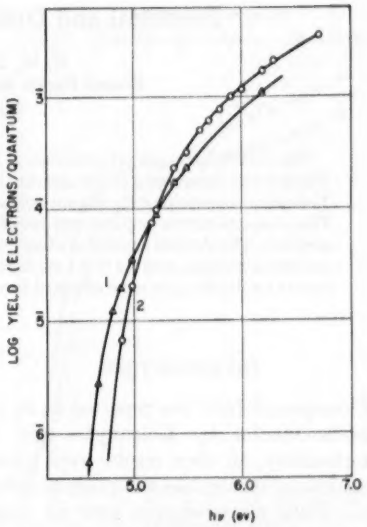

FIG. 3. Spectral distribution of the photoelectric yield from antimony films. Note higher threshold for amorphous material even though the work function determined from saturation point in Fig. 1 is lower than for crystalline film.

function of amorphous antimony is lower than that of the crystalline material (4.49 ev *vs* 4.60), the photoelectric threshold of the amorphous form is higher—a behavior consistent with a scarcity of occupied energy states just below the Fermi level.

Amorphous antimony is similar to amorphous arsenic, except that the forbidden energy zone is smaller in the former, as one would expect. Crystallization of these materials gives rise to a characteristic structure in the energy distribution of the photoelectrons and in the deduced energy level spectrum of the solid.[3,4] Levels lying 1 ev or thereabouts below the Fermi level are not much affected in density. Between the edge of the occupied band of the semiconductor and the Fermi level, however, a relatively low but clearly discernable group of occupied energy levels appears on crystallization. It is this group, of course, which is responsible for the characteristic poorly metallic behavior of these crystals.

Electrical and Optical Properties of Indium Selenide

R. W. DAMON AND R. W. REDINGTON
General Electric Research Laboratory, Schenectady, New York
(Received September 1, 1954)

The electrical and optical properties of InSe have been investigated with single crystals of the compound. The spectral dependence of the optical absorption coefficient and of the photoconductivity was measured. The optical absorption edge was not sufficiently well defined for the band gap to be estimated unambiguously. The photoconductive response was mostly in the visible, and its sensitivity comparable with that of gray selenium. The thermal activation energy of the electrical conductivity was about 1 ev in what is presumably the intrinsic region; and 0.2 to 0.4 ev, depending on the particular sample, at lower temperatures. Conflicting results for carrier type were obtained from several different experiments.

INTRODUCTION

THE compound InSe was reported to be a "good" photoconductor by Kolomiyets and Ryvkin,[1] but, unfortunately, all their results were presented on relative scales and no mention was made of the electrical properties. Their measurements were all made either on ground and polished polycrystalline plates or on evaporated layers with various heat treatments in selenium vapor. Recently, measurements in this country on evaporated layers of InSe have been reported.[2] Single crystals of InSe were used for most of the work described in the present report.

SAMPLE PREPARATION

The samples of InSe were prepared by reaction in vacuum of stoichiometric amounts of indium and selenium.[3] Most of the samples were prepared with 99.97+ percent indium from the Indium Corporation of America and with high-purity selenium from the American Selenium Company. One sample, designated "zone-refined" in later sections, was prepared with 99.999 percent selenium from Canadian Copper Refining and Smelting Company and with zone-melted indium. The compound prepared from these materials was also zone-melted in a dry hydrogen atmosphere.

The samples of InSe were crystallized in a small Stockbarger-type furnace. The ingots were approximately 1 cm in diameter and 2 cm long. The melting point of InSe is 660°C, and it was comparatively easy to grow large single-crystal regions in the samples. However, it was quite difficult to convert the entire sample into a single crystal. One early sample consisted of a number of needle-like crystals with a complicated monoclinic structure. Most of our samples, however, have had a mica-like structure, with one very easy cleavage plane. The structure of the mica-like material has not been determined, but a Laue photograph showed trigonal symmetry. A powder photograph had some lines in common with the pattern published by Klemm and Vogel,[4] but was not identical. The crystal structure also appears to be different from that found recently for GaSe.[5]

Samples were cut with a jeweler's saw perpendicular to the cleavage plane, and by cleavage along the planes. The thin samples for optical measurements were prepared by successive cleavage of a sample pressed between two layers of Scotch tape. Contacts could be soldered to InSe with indium, but these contacts were not consistently ohmic. No completely satisfactory method of making contacts was found. Pressure contacts for high temperatures, and silver paste for room temperature and below, were fairly satisfactory and were used in most of the work.

OPTICAL ABSORPTION

The optical absorption of indium selenide was measured on a series of layers cleaved from a single crystal, ranging in thickness from about 0.5 to 80 microns. The absorption coefficient calculated from optical transmission data is shown as a function of photon energy in Fig. 1. The optical thickness of the samples was determined from interference effects in the transmission region, and the refractive index from the reflection coefficient. The refractive index is about 3 in this region. The thickness measurements were verified with a micrometer on the thicker samples. The transmission was measured with a PbS detector and a 931-A photocell, with corrections for absorption of the sample support (Scotch tape), and for long-wavelength reflection. Only those data were used for which optical transmission was less than 10 percent, to eliminate interference effects. A rough check on these results was obtained by plotting transmission *vs* thickness at several wavelengths; this indicated that reflection effects were satisfactorily eliminated.

The absorption edge is not clearly defined, and there is the possibility that the absorption at low photon energy might be attributed to impurities. Data taken on "zone-refined" samples, however, showed no difference in the absorption constant at photon energies up

[1] B. T. Kolomiyets and S. M. Ryvkin, Zhur. Tekh. Fiz. **9**, 987 (1947).
[2] Donald E. Bode and Henry Levinstein, J. Opt. Soc. Am. **43**, 1209 (1953).
[3] W. D. Lawson, J. Appl. Phys. **23**, 495 (1952).
[4] W. Klemm and H. U. v. Vogel, Z. anorg. u. allgem. Chem. **219**, 45 (1934).
[5] K. Schubert and E. Doore, Naturwiss. **40**, 604 (1953).

to 2.2 ev, so we conclude that this absorption is a property of the InSe crystals grown from the melt; this does not exclude the possibility of a nonstoichometric equilibrium under our conditions of preparation

PHOTOCONDUCTIVITY

The photoconductive spectral response was also measured in cleaved layers, with the results shown in Fig. 2. These data were taken on samples of different thickness, and at different field strengths. The difference in spectral response at low energies is presumably caused by the different absorption. For the range of field strengths used, up to several thousand volts/cm, the photocurrent was proportional to the voltage in each sample. A similar spectral response was also observed for the photovoltaic effect, obtained by illuminating the sample asymmetrically.

We do not find the long-wavelength band of sensitivity observed by Bode and Levinstein,[2] but the main band of photoconductivity extends to longer wavelength in our cleaved layer than in their evaporated layers. We have also measured the photoconductive time constant, and find a value about one millisecond, essentially independent of wavelength from 0.6 to 1.2 microns. There was no evidence of the short time constant observed at long wavelength by Bode and Levinstein, which further indicates that the sensitivity in this region is probably due to imperfections in their films.

Kolomiyets and Ryvkin[1] have measured optical absorption and photoconductive response in both ground plates and evaporated layers of InSe. We cannot compare our data, however, since they specified neither the sample thickness nor the units in which incident light was measured.

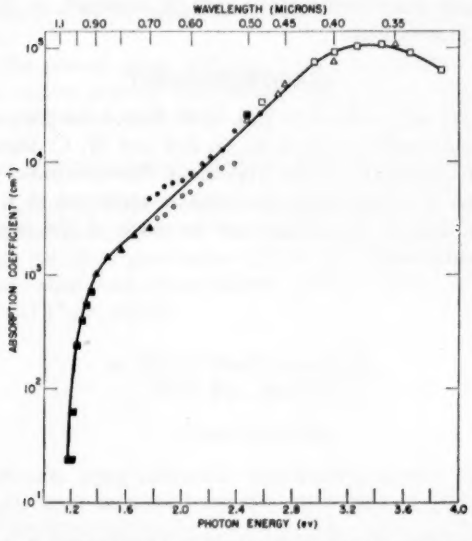

FIG. 1. Optical absorption coefficient of InSe. The different symbols refer to samples of various thickness, except that ▲ and ○ refer to the same sample with different detectors.

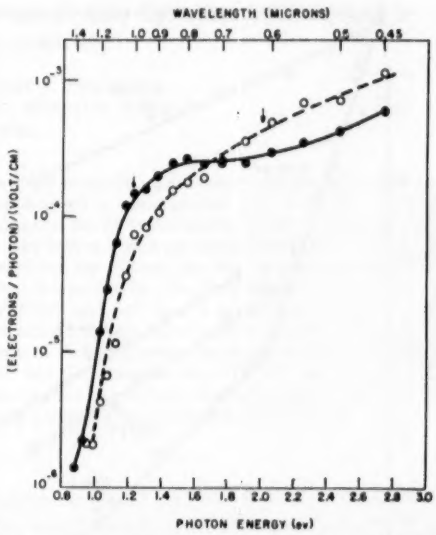

FIG. 2. Spectral dependence of the photoconductivity in InSe. The conductivity was measured parallel to the cleavage plane. The arrows indicate photon energy for 90 percent absorption in each sample. ○—3 microns thick, 30 v/cm; ●—50 microns thick, 3000 v/cm.

ELECTRICAL CONDUCTIVITY

The electrical conductivity of InSe was measured in a vacuum oven at pressures of about 10^{-6} mm of Hg. The temperatures were measured with a platinum-platinum+10 percent rhodium thermocouple in metallic contact with the oven block. Some measurements were made using separate current and potential electrodes. However, these gave results identical with the simpler two-electrode system which was used for the results reported here.

Figure 3 shows the temperature dependence of the conductivity in several samples. The conductivity measurements were reproducible with increasing or decreasing temperature. The conductivity of the "zone-refined" sample was not measured as a function of temperature. The room temperature conductivity of this sample was 5.3×10^{-3} (ohm-cm)$^{-1}$ parallel to the cleavage plane, and 8×10^{-5} (ohm-cm)$^{-1}$ perpendicular to the cleavage plane. The line with slope 0.96 ev was common to all these samples in the higher temperature range. As the optical absorption data do not indicate an unambiguous "absorption edge," a comparison of this presumably "intrinsic" activation energy with the optical data does not seem fruitful.

CARRIER TYPE

Several experiments were performed to determine the carrier type in single-crystal samples of InSe. An attempt to measure the Hall effect in two different

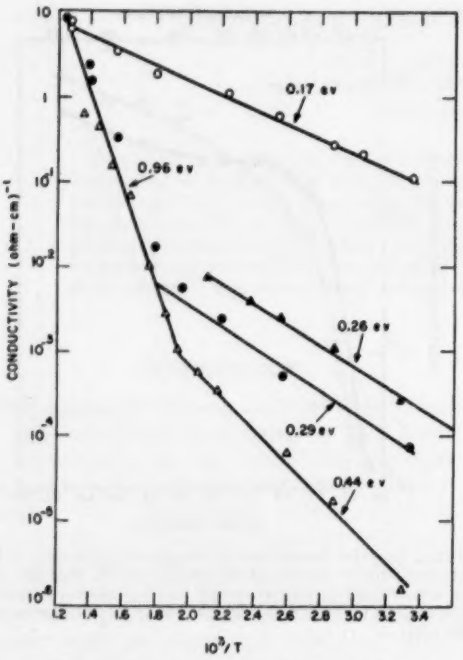

FIG. 3. Temperature dependence of the electrical conductivity of InSe. Activation energies are given for each sample. ○ polycrystalline; ▲, ● single crystals, conductivity parallel to cleavage plane, △ single crystal, conductivity perpendicular to cleavage plane.

ingots was unsuccessful, although the sensitivity was sufficient to measure a mobility greater than 0.1 cm²/volt-sec for a single-carrier type of semiconductor. With an etched tungsten point, rectification was observed corresponding to *p*-type conductivity. This was verified by the photovoltaic effect at the same point contact. However, thermoelectric power measurements, made without moving the tungsten point, indicated *n*-type conductivity. Further measurements of thermoelectric power on another sample from the same ingot showed *p*-type conductivity. These latter measurements were made with platinum-disk electrodes, and the thermoelectric power was essentially constant, at about 200 μvolt/°C, from liquid nitrogen to room temperature. This uncertainty in the sign of the thermoelectric power may be the result of a surface oxidation, since the last sample had been exposed to the air for several weeks, while the first had a freshly cleaved surface. The different sign of the carriers obtained from different experiments with the point contact can apparently be explained by assuming that InSe is not a single-carrier type of semiconductor, at least within the surface region.

These experiments were repeated on a sample cleaved from the "zone-refined" ingot. In this material, a Hall effect was measured corresponding to a mobility of 5 cm²/volt-sec, with hole carriers. Measurements of the photovoltaic effect indicated *n*-type conductivity, however, as did the thermoelectric effect. The thermoelectric power in this sample was 525 μvolt/°C at room temperature.

DISCUSSION

If one considers only the resistivity and Hall-effect data as being significant in indicating the properties of the bulk material, attributing the difficulties with rectification, photovoltaic, and thermoelectric effects to a surface layer, then from the mobility of 5 cm²/volt-sec and resistivity of 5.3×10^{-3} (ohm-cm)$^{-1}$ for the "zone-refined" material, we can calculate a room-temperature carrier density of about 6×10^{15} cm^{-3}. With no information on the mobility in the unzoned material, a carrier density cannot be calculated, but it appears from the resistivity change and from the optical absorption data that the principal effect of the zone refining has been to increase the carrier mobility. Since consistent results for carrier type, mobility, and carrier density cannot be obtained from our data on resistivity, Hall effect, and thermoelectric power, not much quantitative value can be attached to these interpretations.

ACKNOWLEDGMENT

We are indebted to Mrs. B. F. Decker for the x-ray measurements, and to E. M. Pell and W. C. Dunlap for assistance in the Hall-effect measurements. We wish to acknowledge the valuable assistance of J. R. Eshbach in discussions and in much of the experimental work.

Magnetic and Crystalline Behavior of Certain Oxide Systems with Spinel and Perovskite Structures

LOUIS R. MAXWELL AND STANLEY J. PICKART
United States Naval Ordnance Laboratory, White Oak, Maryland
(Received July 21, 1954)

A series of substitutions have been performed on nickel ferrite where the Fe^{3+} is replaced, by varying amounts, with In^{3+}, Sc^{3+}, Y^{3+}, Gd^{3+}, and La^{3+}. In^{3+} went into solid solution with the nickel ferrite to form a spinel structure whose lattice constant a_0 increased linearly with increasing amounts of In^{3+} to a maximum value of 8.708A for 1.5 In^{3+} ions per molecule. At greater concentration of In^{3+}, the starting materials appeared as a mixed phase with $NiO \cdot Fe_{0.5}In_{1.5}O_3$. The saturation magnetization (μ_0), obtained by extrapolation to absolute zero, increased with increasing amounts of In^{3+}, in a manner indicating that the In^{3+} ions preferred the A sites. In the case of Sc^{3+}, an increased cell size was found which "leveled off" at $a_0=8.41$A for 0.75 Sc^{3+} ions per molecule. μ_0 decreased with increasing Sc^{3+} content and approached a compensation point similar to that found previously for the Al^{3+} substitution. It is concluded that trivalent metal ions having a rare gas electronic structure, by showing a preference for the *B* sites, give rise to compensation points and the Néel *P*-type curves. The Curie temperatures for the substitution of In^{3+} and Sc^{3+} show a nearly linear decrease with conconcentration but with slopes greater and less, respectively, than the slope of the single curve found previously to represent both the Al^{3+} and Ga^{3+} substitutions. The Y^{3+}, Gd^{3+}, and La^{3+} substitutions resulted in a mixed solution of nickel ferrite and corresponding perovskite structures formed with Fe^{3+}.

I. INTRODUCTION

WHEN trivalent aluminum is substituted in nickel ferrite, the Al^{3+} ions move into the *B* sites in such a manner as to produce a compensation point[1,2] at a composition of approximately 0.7 of an aluminum ion per molecule; the Néel *P*-type curve [Fig. 5(a) of reference 1, curve for $t=0.63$] occurs when the concentration of Al^{3+} is slightly less than 0.7. In the case of the nickel ferrite-gallates, no compensation point was found;[1] the preference of Ga^{3+} for the *A* sites results in a maximum in the saturation magnetization near the compensation point found for the nickel ferrite-aluminates. Maxwell and Pickart[1] found that the nickel ferrite-aluminates and nickel ferrite-gallates have a common Curie temperature, for equal numbers of nonmagnetic ions per molecule, that decreases nearly linearly with increasing amounts of the nonmagnetic ion.

The present paper will report on a continuation of the above type of substitution experiments to ions having greater ionic radii.

II. EXPERIMENTAL RESULTS AND DISCUSSION

The method used for the preparation of the materials and the measurement of their magnetic properties has been described previously.[1] All of the materials were slow-cooled from approximately 1400°C at an average rate of 1° per minute.

A. Nickel Ferrite-Indates ($NiO \cdot Fe_{2-t}In_tO_3$)

1. Crystal Structure

Powder x-ray diffraction examination showed that In_2O_3 went into solid solution with NiO to form a homogeneous spinel whose length of edge of unit cell (a_0) increased linearly with t up to $t=1.5$, as illustrated by Fig. 1. Chemical analysis made of the material formed for the substitution at $t=1.5$ showed that Ni^{2+}, In^{3+}, Fe^{3+}, and O^{2-} were present in the proper amounts to give the spinel $NiO \cdot Fe_{0.5}In_{1.5}O_3$. For values of t between 1.5 and 1.875, a_0 remained constant at a value of 8.71A; within this region there appeared diffraction lines from NiO and In_2O_3, which showed that there existed a mixture of $NiO \cdot Fe_{0.5}In_{1.5}O_3$ and the starting materials. At $t=2.0$, we found diffraction patterns from only NiO and In_2O_3 even when the sample was quenched after prolonged heating.

2. Magnetic Properties

The variation of saturation magnetization (μ) normalized with respect to the saturation magnetization at absolute zero (μ_0)—obtained by extrapolation—is shown as a function of the normalized temperature in Fig. 2(a) for values of t from 0 to 1.0. The curves are similar to those found for the gallium substitution[1] and appear to be characteristic of the magnetic behavior of those trivalent ions that prefer the four coordination positions. The μ *vs* temperature relationship for $t=1.5$ did not show a constant slope over a

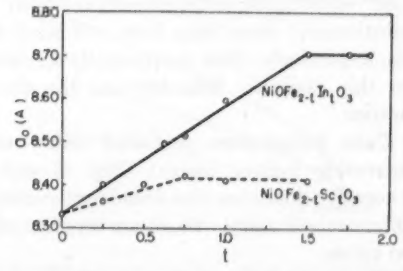

FIG. 1. Variation of unit cell size (a_0) with composition for nickel ferrite-indates and nickel ferrite-scandates.

[1] L. R. Maxwell and S. J. Pickart, Phys. Rev. **92**, 1120 (1953).
[2] E. W. Gorter, Ph.D. Thesis, University of Leyden, 9 June 1954 (to appear in Phillips Research Reports).

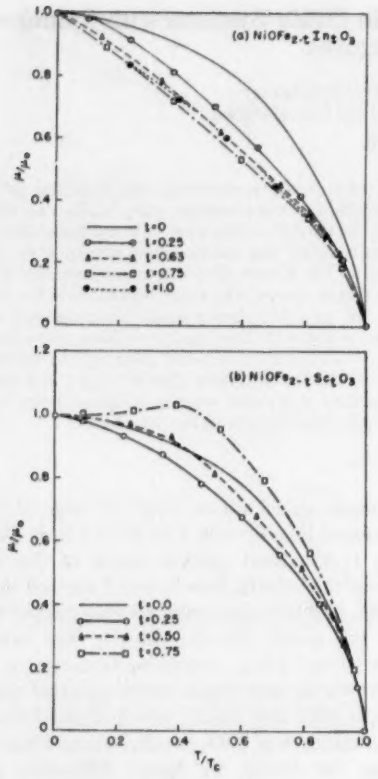

FIG. 2. Normalized thermomagnetization curves for (a) nickel ferrite-indates and (b) nickel ferrite-scandates.

sufficient range to warrant the development of a normalized curve.

μ_0 was found to increase with t starting at $t=0$ (Fig. 3) with an initial slope calculated for all of the In^{3+} ions going preferentially into the A sites, an action that is expected in view of the fact[3] that In^{3+} is known to prefer the A sites. The departure of μ_0 from this linear increase, which results in a maximum occurring at about $t=0.5$, is attributed to a certain fraction of the In^{3+} ions going into the B sites or to the predominance of the negative B-B interaction.

The In^{3+} substitution in this respect is similar to the Ga^{3+} substitution;[1] since these ions have filled $4d$ and $3d$ shells, respectively, there is apparently a correlation between this magnetic behavior and the electronic configuration.

The Curie temperature decreased nearly linearly with increasing indium content (Fig. 4) and at a greater negative slope than that found for the aluminum and gallium substitutions,[1] which are represented by a common curve.

[3] E. J. W. Verwey and E. L. Heilmann, J. Chem. Phys. 15, 174 (1947).

B. Nickel Ferrite-Scandates ($NiO \cdot Fe_{2-t}Sc_tO_3$)

1. Crystal Structure

In the case of the scandates, the initial increase of a_0 (Fig. 1) was less than that observed for the indates yet it flattened off earlier, at $t=0.75$, where $a_0=8.41$A. For values of t greater than 0.75, the diffraction lines of the starting oxides begin to appear, and for $t=2.0$ we find only lines from NiO and Sc_2O_3 that again persisted when the material was quenched after prolonged heating.

2. Magnetic Properties

The thermomagnetic properties of the scandates are shown in the normalized form in Fig. 2(b). For $t=0.75$, we find an increase in the normalized magnetization similar to the P-type curve predicted by Néel[4] and similar to the one observed[1,2] for the aluminum substitution at a value ($t=0.63$) slightly less than that corresponding to the compensation point.

μ_0 decreased with increasing t (Fig. 3) with an initial negative slope indicating that all of the Sc^{3+} is going preferentially to the B sites. The decrease in μ_0 continues at a lesser rate but approaches a compensation point in a manner similar to that[1,2] for the substitution of Al^{3+}. However, the crossover is not reached because, for values of t greater than 0.75, the spinels would not form under conditions of preparation used.

It becomes apparent from both the scandium and aluminum substitutions that there is a definite correlation between the Néel P-type curves and the existence of a compensation point. In both instances, the P-type curves appeared for a t value slightly less than that which corresponds to the compensation point. The

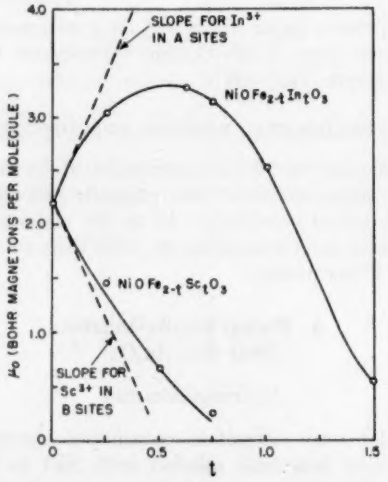

FIG. 3. Variation of μ_0 with composition for nickel ferrite-indates and nickel ferrite-scandates.

[4] L. Néel, Ann. phys. 3, 137 (1948).

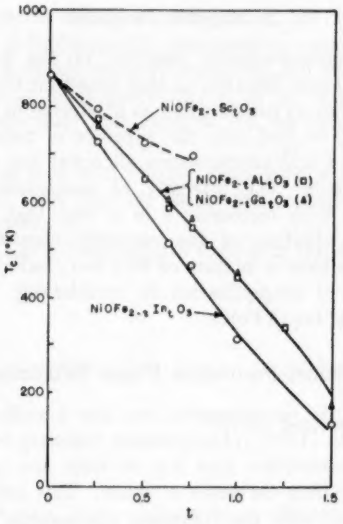

FIG. 4. Variation of Curie temperature (T_c) with composition for nickel ferrite-indates and nickel ferrite-scandates, including previous data (see reference 1) for nickel ferrite-aluminates and gallates.

fact that the *P*-type curve should occur in the vicinity of the compensation point has been explained by Gorter[2] by the Néel theory as formulated for one type of magnetic ion (Fe^{3+}).

It was found that the Curie temperature decreased with t (Fig. 4) at a slower rate than for all of the previous substitutions.

C. Nickel Ferrite-Yttrates (Spinel-Perovskite Phases)

1. Crystal Structure

Another type of reaction appeared when an attempt was made to replace trivalent iron by Y^{3+}. As Y^{3+} was added, it combined with an equal amount of Fe^{3+} to form $(YFe)O_3$,[5] which has a distorted perovskite structure classified by Keith and Roy as the $(YCr)O_3$ structure. At $t=0.25$ there appears the prominent perovskite reflection at a spacing of 2.69A. For increasing values of t, this reflection increases in intensity and NiO appears. At $t=1.0$, all of the iron has combined with all of the yttrium to yield the deformed perovskite structure; the reflections due to NiO are prominent, indicating that it exists as a separate phase. When more yttrium is added, the excess Y_2O_3 begins to show and at $t=2.0$, we end up with only the starting materials, i.e., NiO and Y_2O_3.

2. Magnetic Properties

The thermomagnetic data indicate that the only magnetic phase present is the nickel ferrite. This can be seen from Fig. 5(a) where we plot the intensity of magnetization (I) per gram as a function of temperature. There is a continuous decrease in I with increasing t roughly proportional to the amount of nickel ferrite remaining as a separate phase, in a manner expected on the basis of the x-ray diffraction results. Furthermore, all of the curves give approximately the same Curie temperature (about 600°C).

At $t=1.0$, we find [Fig. 5(a)] essentially a paramagnetic material, $(YFe)O_3$, whose susceptibility is decreasing gradually with increasing temperature without a break at the Curie temperature for nickel ferrite.

D. Nickel Ferrite-Gadolinates (Spinel-Perovskite Phases)

1. Crystal Structure

Substitution of trivalent gadolinium through $t=1.0$ showed that, as in the case of the substitution of Y^{3+}, the Gd^{3+} prefers to combine with Fe^{3+} to form a distorted perovskite structure whose lattice parameter a^* is 3.45A. The diffraction pattern of NiO appeared with increasing intensity as t increased while the intensity of the lines due to the nickel ferrite decreased correspondingly.

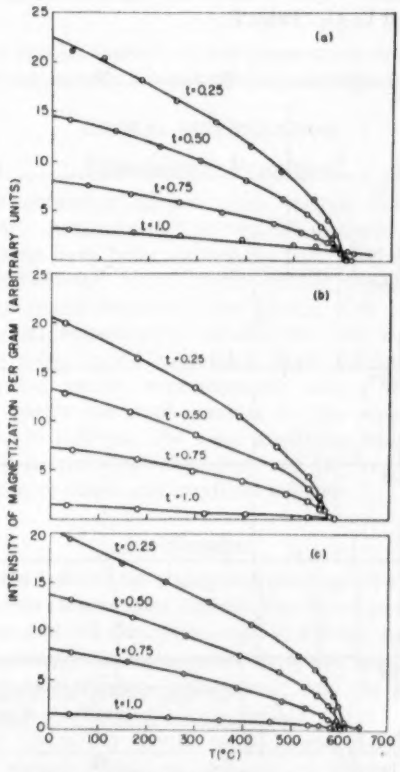

FIG. 5. Thermomagnetization curves for (a) nickel ferrite-yttrates, (b) nickel ferrite-gadolinates and (c) nickel ferrite-lanthanates.

[5] M. L. Keith and R. Roy, Am. Mineralogist 39, 1 (1954).

2. Magnetic Properties

The thermomagnetic data [Fig. 5(b)] show a variation of the intensity of magnetization with temperature characteristic of nickel ferrite. There is a continual decrease of I with increasing t roughly proportional to the amount of nickel ferrite present.

At $t=1.0$, where we have only $(GdFe)O_3$ and NiO, the combined material has only a trace of a paramagnetic response.

E. Nickel Ferrite-Lanthanates (Spinel-Perovskite Phases)

1. Crystal Structure

For the lanthanum substitution, the phase relationships follow a behavior (Fig. 6) similar in part to that observed for the yttrium substitution; for values of t up to and including $t=1.0$ the La^{3+} combines with Fe^{3+} to form a very nearly cubic perovskite structure.[5] At $t=1.5$, there appears to be a shift in the reflections of the perovskite structure to slightly smaller Bragg spacings with the appearance of a new phase. At $t=2.0$, the former perovskite structure is gone—since there is no more iron present—and an apparently homogeneous system exists through a combination of NiO and La_2O_3 (Table I).

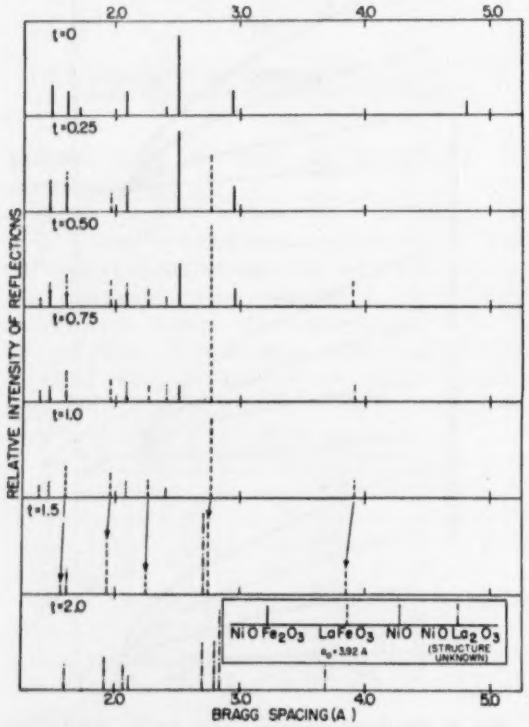

FIG. 6. Relative intensities of x-ray diffraction patterns of the system $NiO \cdot Fe_{2-t}La_tO_3$ for various values of t.

2. Magnetic Properties

The thermomagnetic behavior of the lanthanate series is almost identical to that found for the yttrium and gadolinium substitutions as illustrated in Fig. 5(c). Similarly, we find only the presence of nickel ferrite since the Curie temperatures all equal the value for nickel ferrite. The intensity of magnetization also decreases with increasing t in a way that indicates simply a dilution of the magnetic constituent. At $t=1.0$, we have a mixture of NiO and $(LaFe)O_3$ whose intensity of magnetization is considerably less than that found for $(YFe)O_3$.

F. Spinel-Perovskite Phase Relationships

When the nonmagnetic ion has a radius greater than 0.92A (In^{3+}), it has a greater tendency to combine with the trivalent iron ion to form the perovskite structure than to make a spinel. This action is in agreement with the following relationship[6] required for the formation of the perovskite structure:

$$r_A + r_O = \tau\sqrt{2}(r_B + r_O),$$

where r_A, r_B, and r_O are the ionic radii for the two metallic ions in order of decreasing radii and the radius of the oxygen ion, respectively. τ is a parameter that varies between approximately 0.8 and 1.0 and permits a certain amount of deformation of the cubic structure. In the present case, $\tau=0.85$, 0.86 and 0.90 for $(YFe)O_3$, $(GdFe)O_3$, and $(LaFe)O_3$, respectively.

III. CONCLUSIONS

The behavior of nonmagnetic trivalent ions as replacements for Fe^{3+} in nickel ferrite can be adequately described as follows:

a. Those ions whose radii are less than *ca* 0.9A, (except B^{3+}), form a homogeneous spinel, with certain limitations upon the maximum number of ions that can be substituted per molecule.

b. Trivalent ions having radii greater than *ca* 0.9A combine with Fe^{3+} to form a perovskite structure existing as a separate phase. The ferrimagnetic properties in these instances are those of the remaining nickel ferrite.

TABLE I. X-ray diffraction pattern of $NiOLa_2O_3$.

Bragg spacing d (A)	Relative intensity
3.68	40
2.85	100
2.81	50
2.73	90
2.11	20
2.07	20
1.93	20
1.60	30

[6] A. F. Wells, *Structural Inorganic Chemistry* (Clarendon Press, Oxford. 1950), p. 376.

c. When the electronic configuration has the rare gas structure a ferrimagnetic compensation point is either reached or closely approximated, and the Néel *P*-type curves occur for a concentration of the trivalent ion slightly less than that required for the compensation point.

d. Those ions with filled *d* shells yield a maximum μ_0 greater than that for nickel ferrite and show no *P*-type curves.

e. The Curie temperatures vary with the number of nonmagnetic trivalent ions per molecule in a manner that bears no simple relationship with the distance between magnetic ions.

IV. ACKNOWLEDGMENTS

We are indebted to Professor J. Shereshefsky of Howard University and Dr. T. P. Perros of George Washington University for assistance in the preparation of the materials studied, and to Dr. J. Samuel Smart and Dr. Roald K. Wangsness for helpful discussions.

PHYSICAL REVIEW VOLUME 96, NUMBER 6 DECEMBER 15, 1954

Color Centers in Chrome Alum Crystals

E. A. Braun, A. Many, and A. E. Simchen*
Department of Physics, The Hebrew University, Jerusalem, Israel
(Received June 25, 1954; revised manuscript received September 7, 1954)

Color centers have been observed in chrome alum crystals following their irradiation by x-rays. The absorption band thus produced has an apparent peak at 228 mμ, and its intensity increases with the time of irradiation, tending to saturation. The color band decays spontaneously with time, the half-life time at room temperature being several weeks. The band can be bleached by exposure to light of any wavelength within the band (215 to 400 mμ). The crystals do not exhibit photoconductivity either before or after x-ray irradiation.

INTRODUCTION

COLOR centers have been extensively studied in alkali halides.[1] Recently they have been reported to exist in several other simple crystals, such as fluorspar,[2] ammonium halides,[3] and quartz.[4]

In this paper, results are described which indicate that color centers can be produced in potassium chrome alum single crystals [$KCr(SO_4)_2 \cdot 12H_2O$].

The general chemical formula of the alums is $M^+M^{3+} \times (SO_4)_2 \cdot 12H_2O$, where M^+ is any alkali metal ion or a radical like NH_4^+; M^{3+} is a trivalent cation such as Cr^{3+}, Fe^{3+}, Co^{3+}, or V^{3+}. The chemical bonds in the alums are of a mixed nature, some being ionic while others are covalent. The water molecules serve as packing water.[5]

The alum crystals belong to the cubic system and are usually easily crystallized from aqueous solution in the form of octahedra. The common alums melt at low temperatures (usually below 100°C) and decompose easily at even lower temperatures by losing part of their water. It should be mentioned that alum crystals are of special interest in low-temperature technique, where use is made of their adiabatic demagnetization.[6]

OPTICAL INVESTIGATION

Experimental Procedure

The potassium chrome alum crystals used were "Baker's chemical pure" or "Baker's analyzed;" some specimens have been additionally recrystallized from aqueous solution. As the crystals exhibit poor cleavage, the specimens measured were ground with fine carborundum suspended in alcohol. In this way, flat pieces down to 0.4 mm thick were obtained. The absorption spectra were measured with a Beckman D.U. quartz spectrophotometer in the range from 210 mμ to 1200 mμ. The x-ray irradiation was carried out on a crystallographic x-ray set (45 kv, 15 ma) with copper target and beryllium window.

Results

Figure 1 shows the absorption spectrum of a typical potassium chrome alum crystal. The bands at 410 and 560 mμ and the absorption edge at 215 mμ appear in approximately the same positions in the spectrum of the aqueous solution (not shown); only the band at 260 mμ is characteristic of the crystal.

The absorption spectra of a chrome alum crystal after various times of exposure to filtered x-rays

* Scientific Department, Ministry of Defense, Israel.

[1] See for example F. Seitz, Revs. Modern Phys. **26**, 7 (1954); N. F. Mott and R. W. Gurney, *Electronic Processes In Ionic Crystals* (Claredon Press, Oxford, 1950), second edition.

[2] F. Lüty, Z. Physik **134**, 596 (1953); A. Smakula, Phys. Rev. **91**, 1570 (1953).

[3] H. Rüchardt, Z. Physik **134**, 554 (1953).

[4] E. W. J. Mitchell and E. G. S. Paige, Proc. Phys. Soc. (London) **67**, 262 (1954).

[5] F. Ephraim, *Inorganic Chemistry* (Gurney and Jackson, London, 1943), fourth English edition.

[6] C. Kittel, *Introduction To Solid State Physics* (John Wiley and Sons, Inc., New York, 1953).

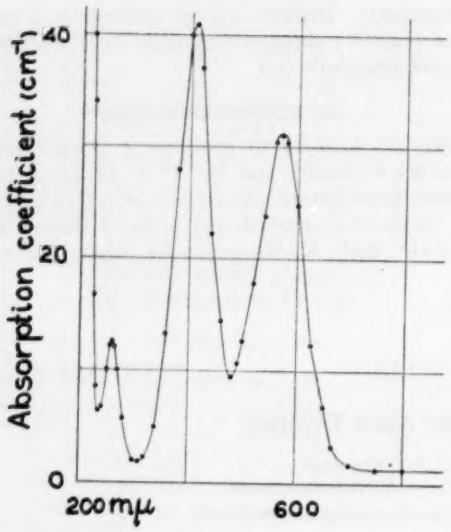

FIG. 1. Absorption spectrum of a potassium chrome alum crystal.

(CuK_α) are given in Fig. 2. The changes in ultraviolet absorption are produced by the introduction of color centers. This may be more clearly seen by plotting the difference of absorption before and after x-ray irradiation against wavelength (Fig. 3). It should be noted that this band is rather wide. The apparent peak at 228 mμ may be erroneous, as it falls near the U.V. limit of sensitivity of the Beckman spectrophotometer.

The growth of the color band with x-ray irradiation (CuK_α) is shown in Fig. 4, where the increase of optical density is plotted against time of irradiation for three wavelengths inside the color band. (With "white" x-rays this buildup proceeds much more rapidly.) It will be observed that the curves tend to saturation values, indicating an upper limit to the number of color centers attainable by the method employed.

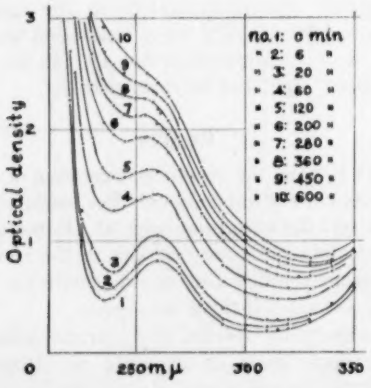

FIG. 2. Absorption spectra of a chrome alum crystal after various times of x-ray irradiation (CuK_α).

The apparently discontinuous drops in the curves of Fig. 4 are caused by the spontaneous decay of the color band during the interruptions of a few days between two successive x-ray irradiations. When the irradiated crystal is left at room temperature, the color band decays slowly with time, the half-life being of the order of a few weeks. At liquid air temperature no such decay occurs, which shows it to be of thermal origin. In Fig. 5, the color band absorption is plotted against time on a log-log scale for various wavelengths within the band. No reasonable decay law could be deduced from these experimental values.

The color band can be bleached by exposing the colored crystal to ultraviolet light. The bleaching was carried out both with filtered and unfiltered light and it was found that it may be obtained by light of any wavelength within the color band.

The ultraviolet light source was a 250-watt Hanovia high-pressure mercury arc lamp focused on the crystal

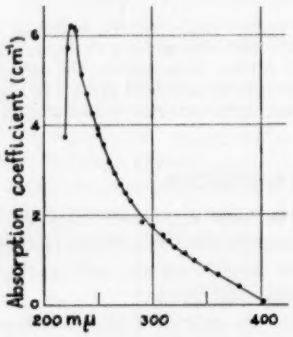

FIG. 3. Color band in chrome alum as obtained from the difference of absorption before and after x-ray irradiation.

from a distance of about 20 cm. Under these conditions, 45 minutes of irradiation with 360 mμ light reduced the intensity of the color band by about 10 percent. The whole band is bleached at approximately the same rate and no new absorption bands appear after bleaching.

PHOTOCONDUCTIVITY

The crystals were prepared for electrical measurements in the same manner as above. The usual method of evaporating contacts on the crystal for conduction measurements could not be employed, as the crystals are unstable in vacuum, and lose their waters of crystallization, and crumble to powder. Therefore, two thin metal strips were pasted on the crystal ends with conducting paint.

The conductivity was measured by a bridge method in which the null indicator employed a low grid-current electrometer tube.

The resistivity of the potassium chrome alum crystals thus obtained was of the order of 5×10^{10} ohm-cm, but decreased with the time of application of the voltage, although the latter did not exceed 100 v.

No photoconductivity was observed either before or after x-ray irradiation. The sensitivity of the measurement was such as to allow the detection of a change in resistivity of less than 1 percent.

DISCUSSION

It is very difficult to reach any definite conclusion about the nature of the color centers described. First, alum crystals are much more complex than those treated hitherto, and, secondly, the experimental material is in sufficient. However, our results may be summed up and from this a few tentative suggestions may be given.

(a) In addition to the chrome alum crystals, the other alums at our disposal [$KAl(SO_4)_2 \cdot 12H_2O$; $NH_4Al(SO_4)_2 \cdot 12H_2O$; $NH_4Fe(SO_4)_2 \cdot 12H_2O$] were examined. The first two show no color centers, while the third is too unstable to give definite results.

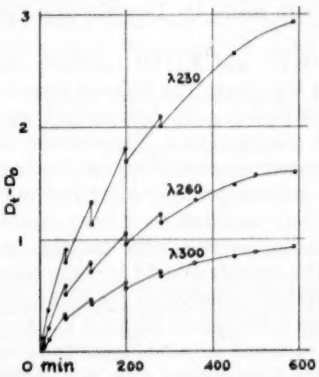

FIG. 4. Growth of color center absorption with time of x-ray irradiation, for three wavelengths within the band.

(b) The number of color centers obtainable by x-ray irradiation seems to have an upper limit (Fig. 4).

(c) The bleaching efficiency is low, and no photoconductivity was observed although the color band absorption is fairly high and comparable to that in the alkali halides.

(d) The color band has the same form and position in all the samples of chrome alum studied, although they come from different batches of material.

Impurities may play a role in the production of the color centers. This is unlikely in view of point (d) but not impossible, as all the batches examined may contain certain impurities which are unaffected by the standard purification procedures.

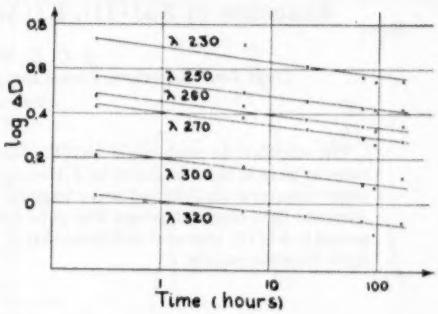

FIG. 5. Thermal decay of color centers at room temperature.

Another possibility is that the chrome ion is directly or indirectly involved in producing the centers. This follows from the fact that only the alum containing chrome ions showed color centers [point (a)]. In analogy with alkali halides, one can assume that the coloring can arise from ion vacancies, and only in the chrome containing alum are conditions correct for color centers to be stable enough to be observed at room temperature. Alternatively, one can assume that the chrome ion is more directly involved in the coloring through such a mechanism as the following: The x rays free an electron from the valence band and this becomes captured at a Cr^{3+} ion, thus changing it into a Cr^{2+} ion. The color absorption band would then correspond to transitions characteristic of Cr^{2+}. This assumption is supported by the fact that in the emission spectrum of Cr III many strong lines exist in the wavelength region of the color band. From the saturation of the coloring [point (b)] it follows that not all the chrome ions are able to become centers, but only a small proportion of them. This may be due to interaction among them as suggested by Rüchardt for ammonium halides,[3] or due to impurities or vacancies playing a role.

A possible explanation of point (c) is that by the absorption of light quanta, the electrons in the centers are raised to an excited level, and from there most of them return to the ground level; only a small fraction of them reach the conduction band and subsequently drop to the valence band.

It is hoped that more definite conclusions will be reached by extending the measurements to low temperatures and by studying other alums, especially those containing chrome and other transition metals.

Response of NaI(Tl), KI(Tl), and Stilbene to Fission Fragments

J. C. D. MILTON AND J. S. FRASER
Chalk River Laboratory, Atomic Energy of Canada Limited, Chalk River, Ontario, Canada
(Received August 30, 1954)

The scintillations produced in NaI(Tl), KI(Tl), and stilbene by fission fragments are found to be about twice as large as those produced by 5-Mev alpha particles. The superior resolution of the inorganic crystals clearly separates the light and heavy fragment groups. The larger scintillations are associated with the more energetic light-fragment group. The pulse height as a function of residual range was measured for both groups in KI(Tl), whence it was found that at large values of the specific energy loss the specific fluorescence again increases rapidly.

I. INTRODUCTION

ALTHOUGH a great deal has been done on the scintillation response of both inorganic and organic phosphors to light particles[1] and light nuclei[2] such as H, D, He, and Ne, nothing is known about the response to energetic, heavy, multiply ionized particles such as fission fragments. Since most phosphors, particularly the organic ones, are showing signs of saturation[3] for α particles with energies of a few Mev, and since the mean range of the more energetic light fragment group is about $\frac{3}{4}$ that of a 5-Mev α particle, it might be thought that fission fragment scintillations would be smaller than those of α particles. However, in all 3 phosphors investigated, the fission fragment pulses were larger. Apart from its intrinsic interest, knowledge of the scintillation response is critical in all experiments involving fission fragments and fast coincidence techniques, where scintillation counters are desirable.

II. EXPERIMENTAL PROCEDURE

The apparatus used in comparing the crystals is shown in Fig. 1. It consists of a small vacuum chamber made of aluminum tubing (0.050-in. wall) with a 5819 photomultiplier inserted at one end. The source of fissionable material used was U^{233}, 180 $\mu g/cm^2$ thick, electroplated on a 1-in. diameter nickel disk placed in a beam of slow neutrons from the thermal column of the NRX reactor at the Chalk River Laboratory. The source was mounted on a long thin aluminum stand-off to reduce the amount of material in the beam. The crystals were mounted on a thin Lucite light pipe, about 3 mm thick at the center. All optical contacts were made by Dow-Corning "200" silicone fluid.

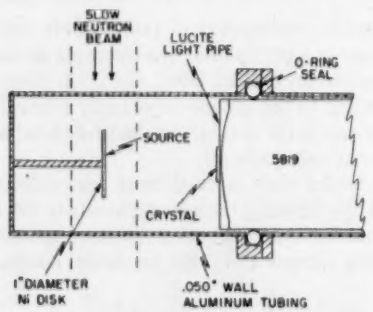

FIG. 1. Schematic drawing of vacuum chamber used in the comparison of phosphors.

The NaI(Tl) and KI(Tl) crystals[4] were 1 cm on edge and $\frac{1}{2}$ mm thick. The NaI was cleaved and placed on the light pipe in a dry box through which moisture free argon was circulated. The vacuum chamber was then assembled, removed from the dry box and evacuated. The stilbene crystal,[5] 5 mg/cm² thick, $1\frac{1}{4}$ in. in diameter, was mounted on a light pipe of the same dimensions as the one used for the two inorganic crystals. The crystals were $1\frac{3}{4}$ in. away from the source.

The amplified pulses from the photomultiplier were analyzed by a 30-channel Marconi kicksorter. As there is a large variation in pulse height from one crystal to another, the pulse height scale was calibrated in the units of a standard pulser which fed pulses through a small condenser permanently attached to the input of the amplifier system. After crystals were changed,

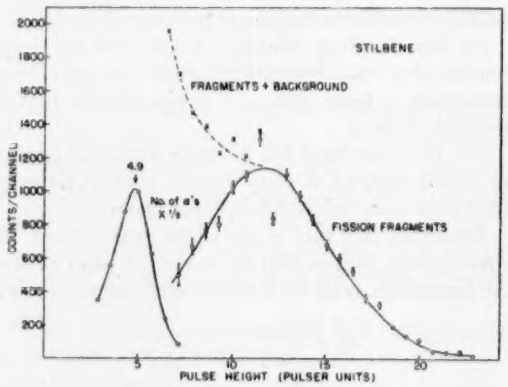

FIG. 2. Pulse height spectrum of fission fragments on stilbene.

[1] See, e.g., Taylor, Jentschke, Remley, Eby, and Kruger, Phys. Rev. 84, 1034 (1951).
[2] S. K. Allison and H. Casson, Phys. Rev. 90, 880 (1953).
[3] J. B. Birks, Phys. Rev. 84, 364 (1951); Phys. Rev. 86, 568 (1952).
[4] Supplied by Harshaw Chemical Company, Cleveland, Ohio.
[5] Supplied by Larco Nuclear Instrument Company, Palisades Park, New Jersey.

the voltage on the photomultiplier was returned to its previous value to within 0.1 percent. The data were taken in a single morning so that errors due to slow drifts were minimized.

III. RESULTS

The results are shown in Figs. 2–4. For comparison the 4.82-Mev U^{233} α particles are shown. The counting times for the fission fragments and α particles were not the same so that the relative number of counts is not significant. Only the position of the peak is important. The two fission fragment groups are well resolved by the inorganic crystals, but not by the stilbene. In all three cases, however, the fission fragment pulses are larger than the α pulses. The relative pulse heights are summarized in Table I. The relative α pulse heights agree well with the results of previous workers.[6]

If the width of the α peak in KI is assumed to be due solely to the statistical fluctuations of photoelectron production in the photomultiplier, then a width for the NaI α peak may be computed from the relative pulse heights. The observed width is greater than the calculated one. If then we use the fission fragment distribution observed in KI and from it compute the distribution in NaI, taking into account the poorer resolution necessary to give the observed α-peak width in NaI, we obtain a curve in good agreement with the experimentally observed fragment distribution. This suggests that the poorer fission fragment resolution of NaI is not something intrinsic, but is connected with the particular crystal used,—is perhaps caused by non-uniformity, or slight surface deterioration. Similarly in stilbene the observed α-peak width is again wider than the one computed from the KI results. In this case the thickness of the crystal is comparable to the range of the α particles so that thin spots in the crystal may contribute a low-energy tail. The width of the α peak is such that one would not expect to resolve the two fission-fragment groups.

TABLE I. Relative pulse heights.

	Light/α	Heavy/α	Alpha
NaI	2.1	1.6	17.8
KI	3.5	2.3	3.8
Stilbene	2		1

TABLE II. Fast coincidence figure of merit for three phosphors.

Phosphor	KI	NaI	Stilbene
$\bar{t}$(mμsec)	3	0.2	0.1

For fast-coincidence work a figure of merit may be defined as a number proportional to the average time $\bar{t}$ taken for the first photoelectron to leave the photocathode;[7] $\bar{t}=\tau/\bar{R}$, where τ is the mean life of the scintillations (the decay time) and $\bar{R}$ is the average number of photoelectrons emitted per pulse. The value of $\bar{t}$ depends on the photomultiplier and light collecting system used. The numbers shown in Table II are for the 5819 used in this experiment, an average tube. The values shown in the table were computed for the most probable light-fragment pulse height in the cases of NaI and KI, and for the most probable pulse height in the case of stilbene. Where the added energy resolution is important, use of NaI is indicated despite the slight decrease in speed.

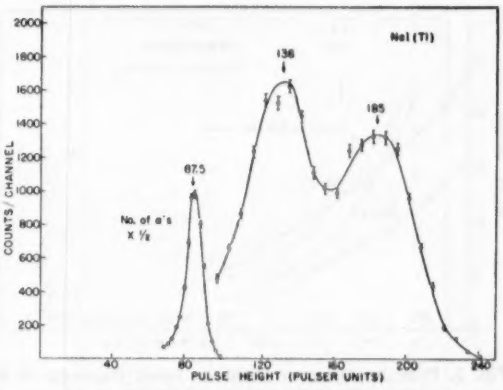

FIG. 3. Pulse height spectrum of fission fragments on NaI(Tl).

IV. FURTHER EXPERIMENTS WITH KI

In order to gain more information on the scintillation response to fission fragments, two further experiments with KI were performed. The first established that the larger scintillations were produced by the more energetic light-fragment group.

Identification of Fragment Group with Pulse Size

A thin source, a few μg of U^{233} in a collodion foil, was mounted in an ionization chamber filled to a pressure of

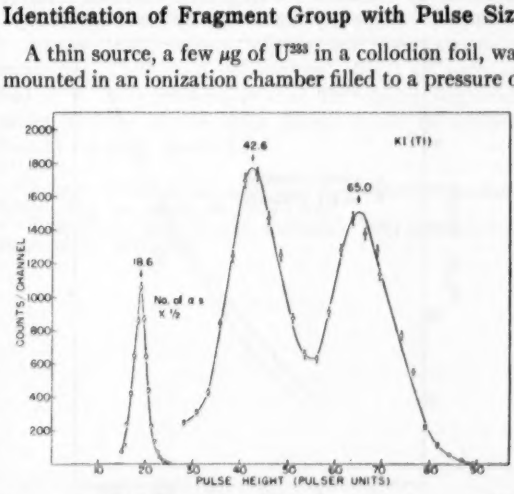

FIG. 4. Pulse height spectrum of fission fragments on KI(Tl).

[6] E.g., R. Hofstadter, Nucleonics **6**, No. 5, p. 70 (1950).

[7] R. F. Post and L. I. Schiff, Phys. Rev. **80**, 1113 (1950).

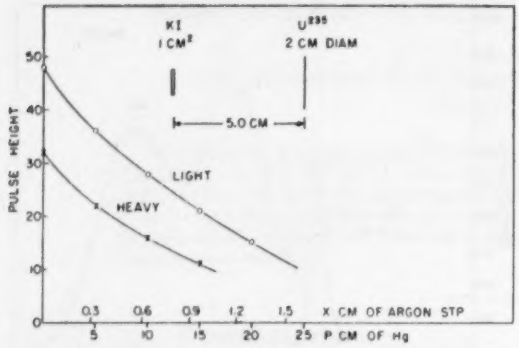

FIG. 5. Pulse height *versus* range for fission fragments in KI showing the source and crystal geometry used.

20 cm of Hg with argon plus CO_2. One fragment entered the ion chamber while the paired fragment entered a KI crystal 1 cm from the source. A single channel analyzer was set on one of the groups of pulses from the scintillation counter and the output used to gate the 30-channel kicksorter recording the ionization chamber pulses. In this way it was found that large scintillation pulses were paired with small ionization pulses and *vice versa*.

Specific Fluorescence of KI

The final experiment was designed to measure the specific fluorescence dL/dx as a function of the residual range of the fragment. To avoid confusion of the fragment pulses with α-particle pulses, the source used was of uranium enriched to 14 percent U^{235} and electroplated on a nickel disk to a thickness of 180 $\mu g/cm^2$. The arrangement of source and crystal is shown schematically in Fig. 5. By varying the pressure of argon in the chamber the fragments could be suitably slowed down before entering the crystal. The scintillation pulses were recorded on a 30-channel kicksorter. The peaks of the light- and heavy-fragment groups are plotted as a function of pressure in Fig. 5. Knowing the pressure and the distance, the equivalent distance travelled in argon at STP can be calculated and is also shown in Fig. 5.

From these data we calculated the scintillation response as a function of residual range and of energy using the range-energy relations given by Lassen.[8] The results are shown in Figs. 6 and 7. These curves should be considered only as illustrative of general trends because of the numerous uncertainties involved. For instance, the relative position of the light- and heavy-fragment points on the pulse height-range curve depends on the assumed maximum range. A shift of

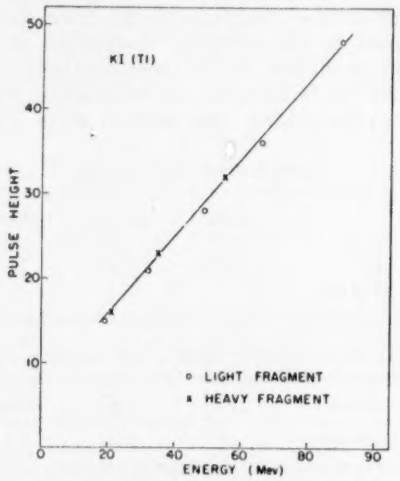

FIG. 7. Pulse height *versus* energy for fission fragments in KI (see text).

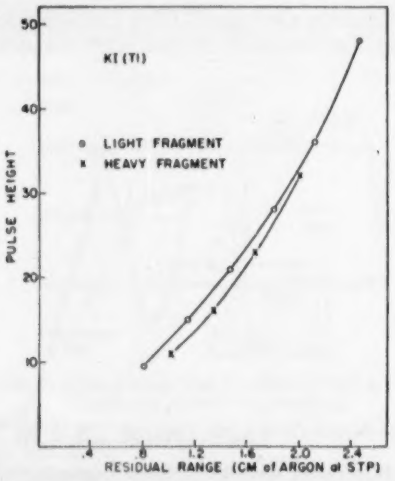

FIG. 6. Pulse height *versus* residual range for fission fragments in KI (see text).

0.08 cm in the maximum range of one of the fragments would put the two curves into apparent coincidence. There is some doubt as to the correct range to use, and such a shift is entirely possible. A second instance is the apparent positive intercept on the pulse height axis of the extrapolated pulse height-energy curve. In this case the range-energy curves of Lassen were based on an energy of 86 Mev for the most probable light fragment energy whereas a better value now is 98.4 Mev.[9] We have not attempted to correct Lassen's data because of the unknown variation of the ionization defect[9] with energy.

The data can be treated in one further way, by plotting specific fluorescence dL/dx as a function of the specific energy loss dE/dx. This has been done in Fig. 8. In the derivation of the values of dE/dx, KI was

[8] N. O. Lassen, Kgl. Danske Videnskab. Selskabs, Mat.-fys. Medd. **25**, No. 11 (1949).
[9] R. B. Leachman, Phys. Rev. **87**, 444 (1952).

considered as equivalent to an equal, condensed mass of 50 percent argon plus 50 percent xenon so that Lassen's[8] results for these two gases could be used. The specific fluorescence was obtained by differentiating the curves of Fig. 6. The uncertainties shown in Fig. 8 are the estimated errors in determining the derivative. Despite these uncertainties there is definite evidence for an increase of the slope at the higher energy losses, but no real difference between the light and heavy fragments. The rapid increase of dL/dx at high dE/dx is quite different from the behavior of NaI under α bombardment at $dE/dx \sim 1$ Mev/cm as observed by Taylor *et al.*[1]

Such a curve may be fitted by a formula of the type suggested by Chou:[10]

$$\frac{dL}{dx}=\frac{AdE/dx}{a+bdE/dx+c(dE/dx)^2}, \tag{1}$$

for organic scintillators, but not by the simpler formula suggested earlier by Birks[11] in which $c=0$. The solid line shown in Fig. 8 has been computed from Eq. (1) by putting $a=0$, $b=0.0634$, $c=-4.73\times10^{-4}$. The zero value for a is not significant as the results in the region of large dE/dx are insensitive to this parameter. The previously published results for KI(Tl) in the region of small energy loss are contradictory: using α particles of energies up to 17 Mev, Franzen[12] found a linear relation between L and E; Link and Walker[13] (40-Mev maximum) obtained a plot of L *vs* E which was concave towards the energy axis, while Raffle and Robbins[14] (8.8-Mev maximum) and Almqvist[15] (7-Mev maximum) found one which was convex. If we assume, as found by Raffle and Robbins, and Almqvist, that the behavior of KI(Tl) is similar to that of NaI(Tl),[1,16] then b and a in Eq. (1) would be approximately equal. If a were made equal to 0.06, the resulting curve in Fig. 8 would be indistinguishable from that shown. Before any great validity is ascribed to Eq. (1), it would be necessary to have better data on the scintillation response to α particles up to 30 Mev and a more exact knowledge of the range-energy relation for fission fragments.

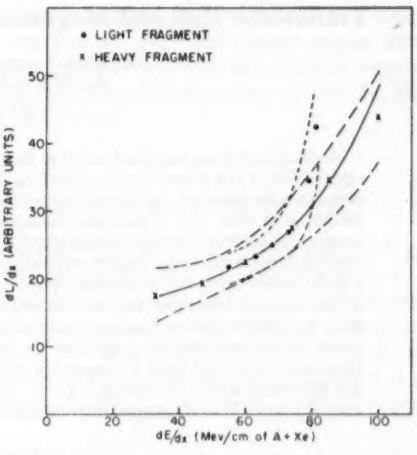

FIG. 8. Specific fluorescence as a function of the specific energy loss for fission fragments in KI (see text). dE/dx calculated from the data of Lassen assuming KI is equivalent to an equal mixture of argon plus xenon. The dotted and dashed lines are estimated limits of error in dL/dx. The solid line is computed from Eq. (1) with $a=0$, $b=0.063$, $c=-4.73\times10^{-4}$.

Some general conclusions may be derived from the curves of Figs. 5 and 8. It will be seen that most of the light is produced near the beginning of the fission fragment track where the rate of energy loss is high. This means, first of all, that there can be no large contribution to the light output made by the nuclear recoils[17,18] since these all occur near the end of the track where the fragment is moving slowly. Secondly, it means that surface effects will be extremely important. Thus, in a deliquescent substance such as NaI it is quite reasonable that the fission fragment pulses, relative to the alpha pulses, would be smaller than in the more stable KI.

[10] C. N. Chou, Phys. Rev. **87**, 904 (1952).
[11] J. B. Birks, Phys. Rev. **84**, 364 (1951); *Scintillation Counters* (Pergamon Press, London, 1953).
[12] Franzen, Peelle, and Sherr, Phys. Rev. **79**, 742 (1950).
[13] W. T. Link and D. Walker, Proc. Phys. Soc. (London) **A66**, 767 (1953).
[14] J. E. Raffle and E. J. Robbins, Proc. Phys. Soc. (London) **B65**, 320 (1952).
[15] E. Almqvist, Thesis, University of Liverpool, 1954 (unpublished).
[16] R. H. Lovberg, Phys. Rev. **84**, 852 (1952).
[17] Boggild, Brostrom, and Lauritsen, Kgl. Danske Videnskab. Selskab, Mat.-fys. Medd. **18**, No. 4 (1940).
[18] Niels Bohr, Kgl. Danske Videnskab. Selskab, Mat.-fys. Medd. **18**, No. 8 (1948).

Transverse Hall and Magnetoresistance Effects in p-Type Germanium

R. K. WILLARDSON, T. C. HARMAN, AND A. C. BEER
Battelle Memorial Institute, Columbus, Ohio

(Received July 23, 1954)

Modification of the two-band model to include existence of a small number of high-mobility holes permits calculations of the magnitude, temperature dependence, and magnetic-field dependence of Hall and magnetoresistance effects in high-purity p-type germanium, which are in excellent quantitative agreement with experimental data. For a specimen containing 4.3×10^{13} acceptors/cm^3, the data indicate at 300°K the presence of 1.1×10^{13} positive carriers/cm^3 with a mobility of 15 000 cm^2/volt-sec. At 205°K these high-mobility holes increase the magnetoresistance at weak fields by a factor of 25 and the Hall coefficient by 1.6. Results indicate that Hall mobilities computed by taking the product $R\sigma$ must be interpreted with caution, or unwarranted inferences may be drawn. For the specimens studied, mobilities computed from the Hall data, by using equations based on spherical energy surfaces but taking into account the fast holes and the values of the magnetic fields, agree within experimental error with the values obtained by other methods. Discussion of the fast holes in connection with valence band degeneracy, cyclotron resonance observations, and interband optical transitions is given. The desirability of using data taken at large and at very small magnetic fields in analyzing galvanomagnetic phenomena is emphasized.

INTRODUCTION

IN the customary development of Hall coefficient equations for calculations of charge-carrier densities, a weak magnetic field approximation is used, since the integration over the distribution of electron velocities is comparatively simple for this limiting case.[1] In order for this approximation to be valid, the Hall coefficient must be independent of magnetic field. Ordinarily, it is assumed that fields of from one to six kilogauss satisfy these restrictions. However, measurements of Hall coefficients as a function of magnetic field in p-type germanium have shown significantly large variations in this range of field strengths.[2,3] More recently, data at 77°K on p-type high-purity germanium specimens show increases of over 50 percent for the Hall coefficient as the magnetic field is decreased from 1000 to 100 gauss.[4] It is thus apparent that the use of the weak-field expressions for the Hall effect is not justified in this case. An obvious alternative is the employment of the exact relationships valid for arbitrary values of magnetic field.[5] It has been established, however, that such a treatment does not predict the behavior in p-type germanium, although it does explain the Hall and magnetoresistance effects in indium antimonide.[6] The disagreement appears quite fundamental and cannot be accounted for by such considerations as impurity, or other types of scattering mechanisms having a power-law dependency of mean-free path on energy.

MAJOR FACTORS TO BE CONSIDERED

In obtaining an explanation of the behavior of Hall and magnetoresistance effects in p-type germanium, the following previously established considerations are significant, namely:

(1) For ordinary magnetic fields the temperature at which the Hall coefficient becomes zero decreases with increasing magnetic field, and in this temperature region, the effect of an increased magnetic field is to make the Hall coefficient less positive (or more negative).

(2) In the extrinsic region there occur large decreases in Hall coefficient with increasing magnetic field. At lower temperatures the rate becomes more rapid, so that a limiting value is approached for moderate fields.

(3) Measurements at a fixed, weak magnetic field in the extrinsic region give a Hall coefficient which decreases as the temperature is lowered.

As a result of this behavior, the use of weak-field Hall measurements to determine extrinsic carrier concentrations, using the conventional equations, gives results of dubious validity. For example, the decrease of Hall coefficient in the extrinsic region as the temperature is lowered would be interpreted as an increase in carrier concentration. Furthermore, calculations of hole mobilities yield results which are in serious disagreement with those determined by drift techniques.[7] It is significant to note, however, that if extrinsic carrier concentrations are determined using the limiting values of Hall coefficients for strong magnetic fields, neither of these inconsistencies is present.[4]

The magnetic-field dependence of the Hall coefficient in the extrinsic region is indicative of unusually high mobility carriers. On the other hand, drift-mobility measurements and calculations from conductivity data indicate that most of the p-type conductivity results from carriers with room-temperature mobility of approximately 1900 cm^2/volt-sec.[7,8]

It is possible to reconcile these apparently conflicting observations by assuming that there exist a relatively

[1] See, for example, F. Seitz, *The Modern Theory of Solids* (McGraw-Hill Book Company, New York, 1940), p. 192.
[2] W. C. Dunlap, Phys. Rev. **71**, 471 (1947); **79**, 286 (1950); **82**, 329 (1951).
[3] Purdue University Theses; W. M. Scanlon, 1948 (unpublished); J. W. Cleland, 1949 (unpublished).
[4] Harman, Willardson, and Beer, Phys. Rev. **94**, 1065 (1954).
[5] See J. W. Harding, Proc. Roy. Soc. (London) **A140**, 205 (1933).
[6] Harman, Willardson, and Beer, Phys. Rev. **95**, 699 (1954).
[7] M. B. Prince, Phys. Rev. **92**, 681 (1953).
[8] L. P. Hunter, Phys. Rev. **91**, 579 (1953).

small number of holes with a mobility considerably higher than those either of the majority holes or of the electrons. As will be shown subsequently, such a model can explain quite effectively the behavior enumerated above. Such a high-mobility carrier would be expected to possess an effective mass significantly less even than that of the electrons in germanium. That this state of affairs might exist has recently been given support by a number of investigations on germanium. For example, calculations by Herman and Callaway[9] indicate a triple degeneracy in the valence band. Such a structure was also discussed by Briggs and Fletcher[10] in connection with their data on the infrared absorption by free holes. A requirement was stated that holes from one set of these states have a rather small effective mass, perhaps $\frac{1}{10}$ that of the free electron mass. This scheme has also been discussed by Burstein[11] in connection with observations on zinc- and indium-doped germanium.

The most substantial support, however, comes from recent experiments on cyclotron resonance.[12] The data indicate the existence of two discrete effective mass values ($m^*=0.04m$ and $m^*=0.30m$) in p-type germanium.

DEVELOPMENT OF EQUATIONS

The well-known expressions for the current densities j_x and j_y with an electric field E_x and E_y, and magnetic field H_z may, in the absence of temperature gradients, be written in the form:

$$j_x=|e|\sum_k A_kE_x+\sum_k e_kB_kE_y, \tag{1}$$

$$j_y=-\sum_k e_kB_kE_x+|e|\sum_k A_kE_y, \tag{2}$$

where the summations are over each charge carrier having a specific mobility, and where the electronic charge e_k is negative for electrons and positive for holes.

For a mean-free path independent of energy, classical statistics, and spherical energy surfaces, the coefficients A_k and B_k can be expressed in terms of carrier densities n_k and zero magnetic-field mobilities μ_k^0 as follows:[13]

$$A_k=n_k\mu_k^0\int_0^\infty x^3e^{-x}(x+\gamma_k)^{-1}dx\equiv n_k\mu_k^0K_k, \tag{3}$$

$$B_k=n_k\mu_k^0\gamma_k^{\frac{1}{2}}\int_0^\infty x^{3/2}e^{-x}(x+\gamma_k)^{-1}dx\equiv\tfrac{1}{2}\pi^{\frac{1}{2}}n_k\mu_k^0\gamma_k^{\frac{1}{2}}L_k, \tag{4}$$

where

$$\gamma_k\equiv(9\pi/16)(\mu_k^0H_z)^2. \tag{5}$$

The magnetic field parameter γ is dimensionless, and if H is given in gauss, then μ^0 must also be expressed in electromagnetic units.

[9] F. Herman and J. Callaway, Phys. Rev. **89**, 518 (1953).
[10] H. B. Briggs and R. C. Fletcher, Phys. Rev. **91**, 1342 (1953).
[11] Burstein, Henvis, and Sclar, Phys. Rev. **94**, 750 (1954).
[12] Dresselhaus, Kip, and Kittel, Phys. Rev. **92**, 827 (1953).
[13] V. A. Johnson and W. J. Whitesell, Phys. Rev. **89**, 941 (1953).

The dimensionless integrals K and L, which arise from integrations over the charge-carrier energies, may be expressed in terms of standard exponential integrals and error functions, as defined in Jahnke-Emde, as follows:[5]

$$\begin{aligned}K(\gamma)&=1-\gamma-\gamma^2e^\gamma\,\mathrm{Ei}(-\gamma),\\ L(\gamma)&=1-2\gamma+2\pi^{\frac{1}{2}}\gamma^{\frac{1}{2}}e^\gamma[1-\Phi(\gamma^{\frac{1}{2}})].\end{aligned} \tag{6}$$

The usual weak-field approximations to Eqs. (6) neglect terms higher than the first degree in γ. Since magnetoresistance calculations involve differences, adequate accuracy is realized in this approximation only when $\gamma<0.001$. It is therefore of very limited validity in cases where high mobilities are encountered. A somewhat better approximation, involving Euler's constant, is

$$\begin{aligned}K(\gamma)&\cong1-\gamma-\gamma^2(0.577+\log_e\gamma), &&\gamma<0.025;\\ L(\gamma)&\cong1-2\gamma+2\pi^{\frac{1}{2}}\gamma^{\frac{1}{2}}, &&\gamma<0.01.\end{aligned} \tag{7}$$

For strong magnetic fields, say $\gamma>25$, the following asymptotic expansions can be used:

$$\begin{aligned}K(\gamma)&\simeq2!/\gamma-3!/\gamma^2+\cdots,\\ L(\gamma)&\simeq1\cdot3/2\gamma-1\cdot3\cdot5/2^2\gamma^2+\cdots,\end{aligned}\qquad(\gamma>25). \tag{8}$$

The Hall coefficient and magnetoresistance are defined for $j_y=0$ as follows:

$$R\equiv E_y/j_xH_z,\quad \Delta\rho/\rho_H\equiv1-(\sigma/\sigma_0)\equiv1-(j_x/j_x^0). \tag{9}$$

For the case of p-type germanium, let us denote the electrons by subscript 1, the ordinary holes by 2, and the high-mobility holes by 3. Then, the preceding equations can be shown to yield:

$$R=-\frac{3\pi}{8|e|n_2}\times\frac{abL_1-L_2-cdL_3}{[aK_1+K_2+cK_3]^2+\frac{1}{4}\pi\gamma_2[abL_1-L_2-cdL_3]^2}, \tag{10}$$

$$\Delta\rho/\rho_H=1-\frac{[aK_1+K_2+cK_3]^2+\frac{1}{4}\pi\gamma_2(abL_1-L_2-cdL_3)^2}{[a+1+c][aK_1+K_2+cK_3]}, \tag{11}$$

where

$$a=\sigma_1^0/\sigma_2^0,\quad b=\mu_1^0/\mu_2^0,\quad c=\sigma_3^0/\sigma_2^0,\quad d=\mu_3^0/\mu_2^0. \tag{12}$$

In the numerator of the expression for the Hall coefficient, the contribution of the term involving the high-mobility holes in the case of weak fields varies linearly with concentration, but as the square of the mobility. Thus, in the extrinsic region ($a=0$), we see that a very small percentage of high-mobility carriers can influence strongly the magnitude of the weak-field Hall coefficient. For example, in the extrinsic region for

sufficiently weak fields, Eq. (10) reduces to

$$R_{H\to 0}=\frac{3\pi}{8|e|n_2}\frac{1+(n_3/n_2)(\mu_3^0/\mu_2^0)^2}{[1+(n_3/n_2)(\mu_3^0/\mu_2^0)]^2}. \quad (13)$$

Thus, if the density of the high mobility holes is only 2 percent that of the others, and their mobility is 8 times as large,[14] then they will increase the Hall coefficient by a factor of 1.7. If, however, data are taken for the limit of strong magnetic fields, then it can be seen from Eqs. (8) and (10) that

$$R_{H\to\infty}=1/|e|(n_2+n_3). \quad (14)$$

In this case, the extrinsic Hall coefficient is related only to the total extrinsic carrier concentration and involves no weighting factors containing mobilities.

A region of special interest is where the Hall coefficient is zero. The relationship valid in these regions for the limiting case of very weak magnetic fields is:

$$R_{H\to 0}=0, \quad (n_1/n_2)(\mu_1^0/\mu_2^0)^2=1+(n_3/n_2)(\mu_3^0/\mu_2^0)^2. \quad (15)$$

For the ordinary two-band model ($n_i=0$), the above equation reduces to the familiar expression used to determine the electron-hole mobility ratios from data on p-type specimens. If the fast holes are neglected in a germanium specimen where 2 percent of the holes have a mobility of 8 times as large, the value obtained for μ_1^0/μ_2^0 is 1.3.[15] If, however, use is made of the complete expression in Eq. (15), which takes the fast holes into account, then one obtains a value of μ_1^0/μ_2^0 equal to 2.0, a result in agreement with that obtained from analysis of conductivity data alone.[8] The above values are intended merely to be illustrative, since Eq. (15) applies only in the limit of zero magnetic field. In analyzing actual data, the magnetic-field parameters must be considered. Also, the analysis of the conductivity data should be modified to distinguish the contributions due to the fast holes. This would lower the value attributed to μ_2^0 and, hence, increase μ_1^0/μ_2^0 slightly.

In the limit of very strong fields, one obtains:

$$R_{H\to\infty}=0, \quad n_1=n_2+n_3. \quad (16)$$

Here, the μ^0 factors are absent and, hence, the effect of the small number of fast holes is of much less significance.

Another interesting consequence of the additional high-mobility hole is its effect on the temperature dependence of the magnetoresistance. It has previously been pointed out how the two-carrier model predicts a maximum in the neighborhood of the Hall coefficient maximum, which is apparently absent in p-type germanium, but which is observed in indium antimonide.[6] A study of Eq. (11) shows how this can occur. If the magnetic field is not too large, it is the first term of the numerator which is significant in the region near the Hall coefficient maximum. As the temperature is lowered, from, say intrinsic, $\Delta\rho/\rho_H$ increases due to the increasing mobilities and the resulting decrease in the values of the functions represented by the K's. In the two-carrier example, in which the electrons have a greater mobility than the holes, as the temperature is further lowered, the diminishing contribution of the electrons gradually causes the denominator to offset the previous trend, and $\Delta\rho/\rho_H$ starts to decrease. At still lower temperatures, the electronic contributions are no longer significant in either member of the fraction. Then, the magnetoresistance rises again, to increase monotonically to the saturation value of 0.116. In the three-carrier case, however, the pertinent fact to note is that, unlike the electron density, the high-mobility hole density varies only slowly with temperature. The result is that the inclusion of the high-mobility holes can prevent the intermediate decrease in $\Delta\rho/\rho_H$ with decreasing temperature and preclude the occurrence of a maximum. It is to be noted, however, that the relative importance of the various terms in Eq. (11) changes with increasing magnetic field. Hence, by appropriate choice of carrier-density and mobility ratios, a maximum may be obtained in p-type germanium for certain magnetic-field strengths.

Since the general magnetoresistance equation is complicated, it is informative to examine the two limiting cases, as was done for the Hall coefficient. For weak magnetic fields, it is readily established that Eq. (11) in the extrinsic region reduces to

$$\lim_{H\to 0}\left(\frac{\Delta\rho}{\rho_H}\right)=\frac{9\pi}{16}(\mu_2^0)^2H^2\left[\frac{1+(n_3/n_2)(\mu_3^0/\mu_2^0)^3}{1+(n_3/n_2)(\mu_3^0/\mu_2^0)}-\frac{\pi}{4}\left(\frac{1+(n_3/n_2)(\mu_3^0/\mu_2^0)^2}{1+(n_3/n_2)(\mu_3^0/\mu_2^0)}\right)^2\right]. \quad (17)$$

The above relationship is a good approximation if $\gamma<0.001$. In such case the effect of the presence of high-mobility holes is quite striking. For example, if only ordinary holes of mobility μ_2^0 are present ($n_3=0$),[16] the factor in brackets has the value 0.21. If, however, 2 percent of the holes have mobilities 8 times that of the others, then the value of the factor increases to 6.7, giving an increase in magnetoresistance of over 30 times.

For the strong field limit in the extrinsic region, Eq. (11) becomes:

$$\lim_{H\to\infty}\left(\frac{\Delta\rho}{\rho_H}\right)=1-\left(\frac{9\pi}{32}\right)\times\frac{(1+n_3/n_2)^2}{[1+(n_3/n_2)(\mu_3^0/\mu_2^0)][1+(n_3/n_2)(\mu_2^0/\mu_3^0)]}. \quad (18)$$

[14] The values $n_3/n_2=0.02$ and $\mu_3^0/\mu_2^0=8$ follow from an analysis of the experimental data on p-type germanium (see following section).

[15] See, for example, Hunter, Huibregtse, and Anderson, Phys. Rev. **91**, 1315 (1953).

[16] This gives the familiar magnetoresistance equation. See, for example, Eq. (7) in G. L. Pearson and H. Suhl, Phys. Rev. **83**, 768 (1951).

A good approximation to this limit is reached when $\gamma > 100$. If one carrier only is present ($n_3 = 0$), the expression reduces to the asymptotic limit of 0.116 given by Harding[5] and others. For the special case where $n_3/n_2 = 0.02$ and $\mu_3^0/\mu_2^0 = 8$, the limit becomes 0.21, an increase of almost a factor of two.

EXPERIMENTAL PROCEDURE

The fundamental experimental data obtained to test the theoretical predictions were resistivity and Hall voltage as functions of magnetic field at several fixed temperatures, and the temperature at which the Hall voltage was zero as a function of magnetic field. Resistances were determined by the potential probe method, Hall effects from the transverse voltages in a magnetic field, and temperatures from the thermoelectric voltages of copper-constantan thermocouples attached at both ends of the specimen.

A Leeds and Northrup Type K-2 potentiometer was used to measure all of the above dc voltages. A rotating coil driven by a synchronous motor was used for measuring the magnetic field. The indicating instrument for the ac voltage was a Ballantine Model 310A Electronic Voltmeter, and the system was calibrated by means of a large, standard permanent magnet which is used for nuclear resonance studies at The Ohio State University. The specimen and its holder were enclosed in an evacuated Pyrex tube, maintained at the desired temperature by the use of a small heating coil and a thermos flask containing either liquid nitrogen or an acetone-dry ice mixture. Effects of temperature gradients (actually negligible) were eliminated by averaging the voltages obtained for sample currents in opposite directions. The small IR drop between the Hall probes was eliminated by measurements for both magnetic-field polarities. The current density through the sample, determined from the voltage drop across a precision resistor, was held constant at 6.0 milliamperes/cm². The crystal orientation, determined by A. E. Austin of the Structural Chemistry Division of Battelle Memorial Institute, was obtained from a back-reflection Laue pattern.

COMPARISON OF THEORETICAL PREDICTIONS WITH EXPERIMENT

(a) Hall Coefficient, Extrinsic Region

Measurements were made on a specimen cut from a single crystal of p-type germanium, intrinsic at room temperature. Surfaces of the sample were carefully ground in order to maximize the surface recombination velocity and minimize the effects of diffusion currents. The Hall coefficients are shown in Fig. 1. One region of primary interest is that in which the temperature is low enough that the contribution of the electrons is negligible, yet high enough that only lattice scattering need be considered. These conditions are realized at 205°K. Accordingly, the parameters in the equations

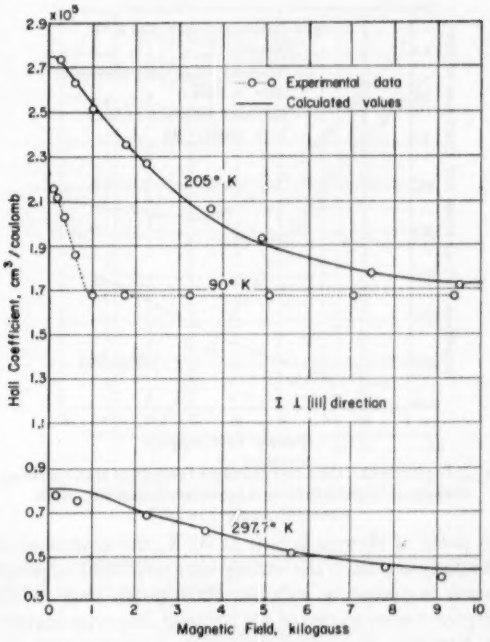

FIG. 1. Hall coefficient as a function of magnetic field for a p-type germanium specimen.

developed in the preceding section were evaluated at this temperature. In a particular calculation, the density of the slow holes is obtained in first approximation from Hall measurements taken at strong magnetic fields. An approximate mobility then follows from the conductivity data. These results, combined with the data taken at very weak fields, then give in first approximation the mobilities and densities of the fast holes. Another important consideration in determining the mobility of the fast holes is the rate of decrease of the Hall coefficient with increasing field. The values obtained by successive approximations are given in Table I for 205°K. It is seen that these values provide an excellent fit to the experimental points.

TABLE I. Tabulated values of basic parameters.

Temperature, °K	n_2,[a] cm^{-3}	n_1/n_2,[b]	n_3/n_2,[a]	μ_2^0,[c] cm²/volt-sec	μ_1^0/μ_2^0,[d]	μ_3^0/μ_2^0,[a]
205.	4.23×10^{13}	0	0.0187	4500	...	7.5
296.7	5.08×10^{13}	0.170	0.02	1900	2.2	8.0
297.7	5.16×10^{13}	0.184	0.02	1895	2.2	8.0
307.2	6.30×10^{13}	0.335	0.0200	1755	2.25	8.0
310.1	6.80×10^{13}	0.386	0.0208	1710	2.25	8.0
312.5	7.29×10^{13}	0.427	0.0206	1685	2.25	8.0
314.8	7.81×10^{13}	0.468	0.0214	1655	2.25	8.0

[a] Determined from Hall coefficients as functions of temperature and magnetic field, using other parameters as listed above, except at 296.7°K, where magnetoresistance data were used.
[b] Calculated with $n_1 n_2 = 6.25\times10^{26}$ cm^{-6} at $T = 300$°K; $E(0) = 0.75$ ev; see E. M. Conwell, Proc. Inst. Radio Engrs. **40**, 1327 (1952).
[c] Determined at low temperatures from extrinsic data; higher temperature values computed by using $T^{-2.33}$ temperature dependence (values so obtained are within probable error of drift data (see reference 7).
[d] Drift data indicate values from 2.0 to 2.25, using limits of probable error and temperature dependences given in reference 7 over the interval from 296°K to 315°K. Our Hall data favor the higher values.

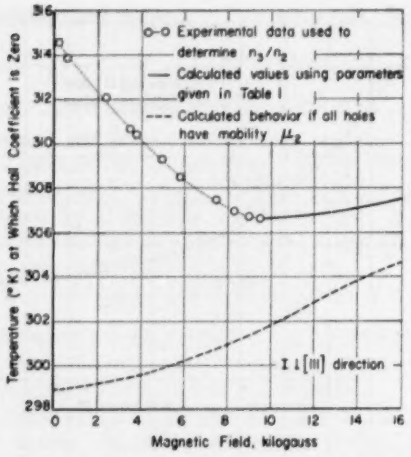
o-o Experimental data used to determine n_3/n_2
— Calculated values using parameters given in Table I
--- Calculated behavior if all holes have mobility μ_2
I ⊥ [111] direction
Temperature (°K) at Which Hall Coefficient is Zero
Magnetic Field, kilogauss

FIG. 2. Experimental data and calculated results of Hall coefficient crossover temperatures as a function of magnetic field.

A point of interest is that at 90°K, the experimental data indicate that the strong magnetic-field approximation is probably valid at 1000 gauss. Due to the acceptor concentration of $4\times10^{13}/cm^3$, impurity scattering becomes significant and thus complicates[17] the analysis of the 90°K curve. Quantitative calculations were therefore not carried out. However, it is readily seen that the preceding equations predict a large slope at weak fields and the asymptotic behavior above 1000 gauss.

(b) Hall Coefficient, Transition Region

The data near room temperature (297.7°K) also are shown in Fig. 1. At this temperature, all three types of carriers must be considered. The number of parameters is therefore too large to be satisfactorily determined from observations taken at a single temperature. However, the electron concentration at a given temperature can be obtained from the extrinsic carrier density and the intrinsic carrier concentration product. The contributions of the fast holes are then obtained from measurements in the neighborhood of the Hall coefficient crossover.

Data taken in the neighborhood of the Hall coefficient zeros are especially desirable for computational purposes due to the simplification in the equations. The temperatures of the Hall coefficient zeros as a function of magnetic field are shown by the experimental points in Fig. 2. In practice, the magnetic-field parameters were computed for the points at 0, 2, 4, and 8 kilogauss. The electron-current parameters were evaluated for the corresponding temperatures of 314.8, 312.5, 310.1, and 307.2°K in the manner previously described. These data must satisfy the equation

$$(n_1/n_2)(\mu_1^0/\mu_2^0)^2L_1=L_2+(n_3/n_2)(\mu_3^0/\mu_2^0)^2L_3. \quad (19)$$

[17] For a treatment of the types of integrals involved, see reference 13.

The magnitude of $(n_3/n_2)(\mu_3^0/\mu_2^0)^2$ which satisfies the above equation is strongly dependent on the value of μ_1^0/μ_2^0. The requirement that the fast-hole parameters be relatively independent of temperature in the region from 297 to 315°K allows μ_1^0/μ_2^0 to be evaluated. The additional constraints on the fast-hole parameters given by the dependence of Hall coefficient on magnetic field at any given temperature permits a determination of μ_3^0/μ_2^0. The results of such calculations are summarized in Table I.

An extremely interesting calculation which can now be made by use of the results in Table I is the determination of the magnetic-field dependence of the temperature at which the Hall coefficient is zero for larger fields. The results of such calculations are shown in Fig. 2. It will be noted that a minimum is predicted for the temperature at which the Hall coefficient is zero. For comparison purposes, the results of similar calculations for a two-carrier model (electrons and slow holes only) are indicated by the dashed curve. The difference in slope between the two curves, which is so conspicuous at low fields, is seen to disappear as higher field strengths are reached.

Using the values of the parameters tabulated in Table I, the magnetic-field dependence of the Hall coefficient has been calculated at four different temperatures for which experimental data were available. Results are presented in Fig. 3.

(c) Transverse Magnetoresistance Effects

Results of previous calculations of magnetoresistance effects have left much to be desired.[18] In many cases, the magnitudes have been too low by a factor of ten or more. Logical improvements have been suggested

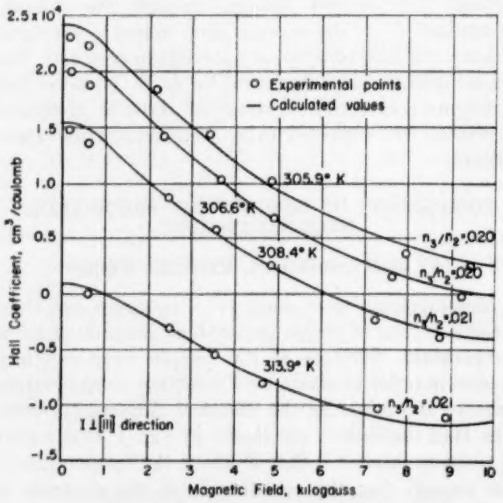

FIG. 3. Dependence of Hall coefficient on magnetic field for a p-type germanium specimen.

[18] See discussion in references 13 and 16.

by several investigators, but these have involved the introduction of anisotropies (e.g., nonspherical energy surfaces or anisotropic mean-free paths) with the result that the exact formulations had to be restricted to very general relationships. Due to mathematical difficulties exact solutions in most cases were not possible.

It was shown in a preceding section how the presence of a small number of fast holes could increase the magnetoresistance by an order of magnitude. It is therefore of great interest to calculate the magnetoresistance effect as a function of magnetic field from Eq. (11), using the values of the parameters previously determined from the Hall coefficient measurements (see Table I), and then to compare these results with experiment. This has been done in Fig. 4 for the extrinsic region (205°K). The agreement is good throughout the whole range. We have chosen to plot the quantity $\Delta\rho/\rho_H H^2$, a representation which emphasizes the behavior at weak fields. It is seen that quadratic dependence of $\Delta\rho/\rho_H$ on H is valid only below, say, 100 gauss. In order to emphasize the extreme influence of the fast holes on magnetoresistance effects, especially at weak fields, Eq. (11) was also evaluated for the case where no fast holes were present. Results are shown by the dashed curve in Fig. 4.

Another determination of magnetoresistance has been carried out in the transition region where all three types of carriers are important. The results of the calculations using the parameters listed in Table I, along with the experimental points, are shown in Fig. 5.

The possibility that transverse magnetoresistance effects in p-type germanium can be accurately predicted without introducing the severe complications of anisotropy raises the question as to whether undue emphasis has not been placed on the importance of nonspherical

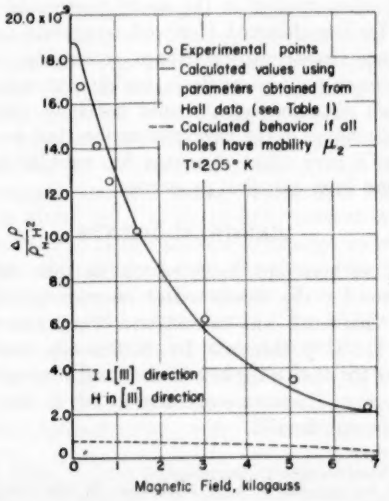

FIG. 4. $\Delta\rho/\rho_H H^2$ *versus* H for a p-type germanium specimen.

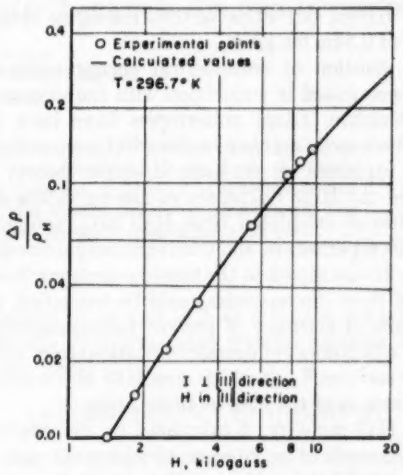

FIG. 5. Magnetoresistance as a function of magnetic field in p-type germanium.

energy surfaces in connection with galvanomagnetic effects in p-type germanium.

DISCUSSION

A question of great interest is the temperature dependency of n_3/n_2. Unfortunately, the precision of determination of this quantity is hardly adequate unless the other parameters are known quite accurately. Improved results might also be obtained by extending measurements to include much larger magnetic-field strengths. In addition, very precise temperature measurements are desirable, especially in the neighborhood of the Hall coefficient zeros. However, if more precise quantitative interpretations are to be made of calculations in the region where electron currents are significant, it will probably be necessary to take into account the pronounced anisotropy of the conduction band.[19]

Another point of interest is the magnitude of n_3/n_2, inasmuch as it gives information on the relative densities of states and hence, on the effective mass ratios of the two types of holes. In the approximation of spherical energy surfaces, density of states ratios give the following relationship:

$$n_3/n_2=(g_3/g_2)(m_3/m_2)^{\frac{1}{2}}, \tag{20}$$

where g_3 and g_2 are weighting factors dependent on the multiplicity of sources of carriers associated with masses m_3 and m_2 respectively. If significant splitting occurs, due to spin-orbit coupling, for example, then the weighting factor will be temperature dependent in those regions where the energy difference is not negligible compared with kT. With g_3 taken as unity and

[19] See, for example, Lax, Zeiger, Dexter, and Rosenblum, Phys. Rev. **93**, 1418 (1954); B. Abeles and S. Meiboom, Phys. Rev. **95**, 31 (1954); M. Shibuya, J. Phys. Soc. Japan **9**, 134 (1954).

m_3 as[20] $0.04m$, our value of 0.02 for n_3/n_2 leads to a value[21] of $0.54m$ for $g_2^{\frac{1}{2}} m_2$.

The question of nonspherical energy surfaces has often been raised in connection with the valence band of germanium. Large anisotropies have been postulated, because a number of electrical properties could not be explained on the basis of simple theory. These included the large discrepancies among values of hole mobilities as calculated from Hall data, conductivity and drift experiments, and transverse magnetoresistance effects. It was shown in the previous sections, however, that all these discrepancies could be reconciled, within the limits of accuracy of present measurements, by a theory which does not consider deviations from spherical energy surfaces,[22] but which does take into account the contributions of the high-mobility holes.

The Hall mobility, if calculated by the relationship $\mu_H = R\sigma$, needs to be interpreted with great care. With the above definition it is readily seen that in the case of spherical energy surfaces the ratio μ_H/μ is $3\pi/8$ for zero magnetic field, classical statistics, and negligible impurity scattering; is unity for zero-magnetic field and degenerate statistics; and in practice, is magnetic-field dependent for high-mobility materials. Furthermore, where more than one carrier is significant, the quantity $R\sigma$ has no obvious interpretation. For example, in extrinsic p-type germanium, values of μ_H/μ (i.e., $R\sigma/\mu$) of 1.17 at 90°K, 1.47 at 205°K, and 1.8 at 300°K are reported.[23] The magnitude and temperature dependence of this ratio has been interpreted as having significance with regard to the shape and number of surfaces of minimum energy in the Brillouin zone. However, analysis of these values by the methods developed in this paper shows that they can be accounted for by simple theory, assuming spherical energy surfaces but taking into account the fast holes and the value of the magnetic fields. Let us assume that a constant field of 4000 gauss was used in the measurements. At 90°K, the magnetic-field parameter γ is greater than four, even for the slow holes, so that the large magnetic-field approximation is fairly good. The factor $3\pi/8$ should, therefore, be replaced by approximately unity. The additional 17 percent results from the increase in σ due to the contributions of the fast holes. At 205°K, the Hall coefficient has been increased by 25 percent, due to the influence of the fast holes at the lower values of γ. Hence, $R\sigma/\mu$ becomes 1.47. At 300°K, γ is still smaller, so that R has been increased by 55 percent and $R\sigma/\mu$ is now 1.8.

A practical consequence of the developments presented in this paper is the emphasis placed on the value of extending experimental data to include measurements below 1000 gauss and above 10 000 gauss. The importance of specifying actual magnetic-field strengths used in obtaining galvanomagnetic data is obvious.

A pertinent consideration is the possibility of measuring the mobility of the fast holes by drift techniques. In addition to the obvious problem arising from their small numbers, the lifetimes of injected high-mobility holes may be so small as to cause difficulty. It has been pointed out by Burstein[24] that interband transitions could greatly reduce the times the fast holes remain in such states and thus make their direct observation virtually impossible.

In order for the mathematics to remain tractable and allow calculations to be readily performed, simplified equations have been applied in this initial treatment of our proposed model. Probably the point most deserving of immediate attention is the effect of interband transitions. The fact that the temperature variation of hole mobilities is significantly different from $T^{-1.5}$ certainly suggests that the scattering processes need to be re-examined, inasmuch as recent evidence on the valence-band structure in germanium renders it difficult to attribute these deviations to non-spherical or non-centrally located energy surfaces. Another argument for re-examination of the scattering processes is the inapplicability of the relationship[25] $\mu_2/\mu_2 \sim (m_2/m_3)^{5/2}$, since it would predict too large a value for the mobility ratio. In view of these considerations it is quite remarkable how consistently well the elementary theory when applied to the model postulated can account for the observed Hall and transverse magnetoresistance characteristics. Hence, it may be expected that a more rigorous analysis, taking into account the concepts discussed here, should not only yield more accurate values of the basic parameters, but would also provide a very effective means for establishing band structure from electrical properties.

ACKNOWLEDGMENTS

The authors are indebted to Battelle Memorial Institute for the fundamental research grant under which this work was carried out. They also wish to thank Dr. R. J. Harrison, Dr. E. Baroody, and Dr. T. Krieger for their suggestions and critical review of the manuscript. Thanks are also due to Dr. C. Herring for helpful comments.

[20] In this calculation, we assume in going from 4°K to room temperature that the variation in m_3 is small compared to that in m_2, due to the greater isotropy of the surfaces corresponding to mass m_3. See Dexter, Zeiger, and Lax, Phys. Rev. **95**, 557 (1954); Dresselhaus, Kip, and Kittel, Phys. Rev. **95**, 568 (1954).

[21] From their thermoelectric power data, T. H. Geballe and G. W. Hull [Phys. Rev. **94**, 1134 (1954)] obtain a value of $0.75 \pm 0.2m$ for the "density of states" effective mass parameter for holes.

[22] We do not mean to imply that slight anisotropies do not exist in the valence band of germanium, but, rather, to suggest that their effect on Hall coefficient and transverse magnetoresistance is small. In this connection, the papers referenced in footnote 20 are of interest.

[23] F. J. Morin, Phys. Rev. **93**, 62 (1954), and F. J. Morin and J. P. Maita, Phys. Rev. **94**, 1525 (1954).

[24] E. Burstein (private discussion).

[25] See, for example, F. Seitz, Phys. Rev. **73**, 549 (1948).

Equivalence of X-Ray Lattice Parameter and Density Changes in Neutron-Irradiated LiF

D. Binder and W. J. Sturm
Oak Ridge National Laboratory, Oak Ridge, Tennessee
(Received September 13, 1954)

The lattice expansion in neutron-irradiated LiF was investigated in order to establish either Frenkel or Schottky defects as the cause of the expansion. For uniformly irradiated crystals, it was shown that x-ray lattice parameter and density changes are equivalent to within 6 percent. It follows that Schottky defects cannot account for more than 6 percent of the expansion and that Frenkel defects are predominant. The annealing of a nonuniformly irradiated crystal indicates a recovery process of order higher than one.

INTRODUCTION

THE lattice expansion of LiF single crystals irradiated with pile neutrons was observed by x-ray lattice parameter and density changes. It is reasonable to assume that the expansion was caused by irradiation induced atomic displacements. If these displacements lead to Frenkel defects, or equal numbers of vacancies and interstitial atoms, then recent theoretical work[1,2] has shown that the x-ray and density changes would be equivalent. On the other hand, if the displacements lead to Schottky defects, or pure vacancies with the extra atoms going to the surface, the density change would be larger. The LiF measurements were used to decide between Frenkel and Schottky defects for an irradiation-induced lattice expansion. The choice of LiF is a convenient one; large lattice expansions may be observed for short irradiations because of the large $Li^6(n,\alpha)H^3$ cross section. This reaction converts the slow-neutron flux of the pile into energetic alphas and tritons, which are the major cause of displacements in the lattice.

X-RAY AND DENSITY MEASUREMENTS

X-ray lattice parameter measurements of the crystals (obtained from the Harshaw Chemical Company) were made with a North American Phillips Company x-ray spectrometer, using the 200 and 400 reflections of the Cu $K\alpha$ doublet. The zero for the Bragg angles was established in each measurement by making the two reflections consistent with Bragg's law, or the ratio of the sines of the 200 and 400 Bragg angles equal to one-half. For 10 unirradiated crystals used in these measurements, the 400 Bragg angles thus corrected agreed to within $\pm 0.3'$ of arc (± 0.007 percent in lattice parameter). The lattice parameter change induced by irradiation was obtained from the change in the corrected 400 angles of each crystal. (For the relative measurements used here, refractive index effects cancel out.) Some line broadening was observed in the irradiated crystals, but this did not contribute appreciably to the error in the x-ray measurement.

Density measurements were effected by weighing each crystal in air and CCl_4 at a known temperature. The density of unirradiated crystals between 20 and 26°C was found to be

$$\rho = (2.64639 - 2.916 \times 10^{-4} t) \pm 0.00022, \quad (1)$$

where t is the temperature in °C. This agrees within experimental error with the value of 2.63905 ± 0.0001 at 25°C[3] and 2.64030 ± 0.00014 at 20°C[4] given by independent measurements. A density *versus* temperature curve was plotted for one irradiated crystal, and the slope was in good agreement with Eq. (1). Further measurements on irradiated crystals were made at one temperature, and the density change was obtained using Eq. (1).

EQUIVALENCE OF X-RAY AND DENSITY CHANGES

a. Pile Neutron Experiment

Since the x-ray measurement, involving a relatively small penetration, will detect changes at the surface of a crystal, and the density measurement changes throughout the volume, care must be taken to irradiate the crystal uniformly. The $Li^6(n,\alpha)H^3$ reaction absorbs the thermal neutrons, and their "e thickness" in LiF is 0.3 cm. In order to use thermal neutrons, a crystal was chosen whose thickness was small compared to 0.3 cm and which was large enough for accurate density measurements.

The crystal was 0.075 cm thick by 2.6 cm square and was given an irradiation of 6×10^{16} neutrons per cm^2 in the ORNL graphite reactor. This resulted in a lattice expansion as shown by the uppermost point in Fig. 1, where the change in lattice parameter derived from x-ray measurements, $(\Delta a/a)_x$, is plotted against that derived from density measurements, $(\Delta a/a)_\rho$. The lower points represent the results of thermal anneals at successively higher temperatures from 315°C to 550°C, gradually bringing the lattice back to its original state. The points lie along a straight line of slope 1.05 ± 0.02. The straightness of the line indicates that the slope is a valid parameter for comparing x-ray and density changes.

[1] P. H. Miller, Jr., and B. R. Russell, J. Appl. Phys. **24**, 1248 (1953).
[2] J. D. Eshelby, J. Appl. Phys. **24**, 1249 (1953); **25**, 255 (1954).
[3] C. A. Hutchison and H. L. Johnston, J. Am. Chem. Soc. **62**, 3167 (1940).
[4] D. A. Hutchison, J. Chem. Phys. **13**, 383 (1945).

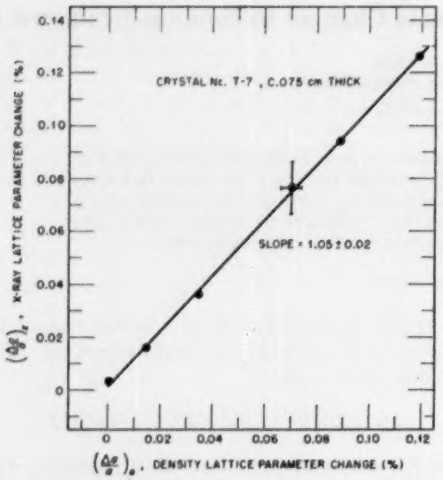

FIG. 1. Lattice expansion for a thin crystal as derived from x-ray and density measurements.

The crystal thickness was not entirely negligible compared with the e thickness for thermal neutrons, and the small deviation from unity in the slope is caused by neutron attenuation, resulting in a nonuniformity in atomic displacements throughout the crystal. The expansion cannot be explained by helium and tritium impurities since 6×10^{16} neutrons per cm^2 produce a concentration of 3×10^{-6} for each impurity, which would account for less than 0.2 percent of the lattice expansion.

To calculate the slope including neutron attenuation, we note that, disregarding saturation and elastic effects, $(\Delta a/a)_x$ is proportional to the surface yield of the $Li^6(n,\alpha)H^3$ reaction and $(\Delta a/a)_\rho$ is proportional to the volume yield. Since the plot of $(\Delta a/a)_x$ *versus* $(\Delta a/a)_\rho$ is a straight line with slope near unity, saturation affects both these quantities in the same way. Thus we can ignore saturation, and the slope of the line is related to the ratio of the aforementioned surface-to-volume yields. It is not equal to this ratio because there is an anisotropic expansion of the crystal which will be taken into consideration as a final step in the calculation.

The crystal's dimensions are such that it approximates an infinite slab for which the yields may be calculated analytically. Consider an isotropic flux of uniform energy, nv per unit solid angle, incident upon an infinite slab of thickness x_0. The number of neutrons per cm^2 per sec incident on both surfaces, n_0, is $nv/2$, and the number absorbed is

$$n_a=\int_0^{\pi/2} nv\cos\theta[1-\exp(-N\sigma_a x_0/\cos\theta)]\sin\theta d\theta, \quad (2)$$

where θ is the incident angle, N the number of Li atoms per cm^3, and σ_a is the $Li(n,\alpha)H^3$ reaction cross section for thermal neutrons. Assuming, for the moment, a Maxwellian distribution of neutrons and noting that we have a "1/v" reaction,

$$\sigma_a=1.128\sigma_0(T/293)^{\frac{1}{2}},$$

where σ_0 is the absorption cross section for monoenergetic neutrons at 0.025 ev, and T is the neutron temperature in °K.[5] The neutron cross-section tables[6] give 70 barns for σ_0, and T may be estimated by adding 140°C[7] to the moderator temperature of about 140°C. This gives 57.4 barns for σ_a. An error of 5 percent in σ_a will result in an error of less than 1 percent in slope. Integrating Eq. (2) and dividing by n_0x_0, we obtain the fraction of neutrons absorbed per unit thickness,

$$\frac{n_a}{n_0x_0}=\frac{1}{x_0}\left\{1+(\alpha_ax_0-1)e^{-\alpha_ax_0}-\alpha_a^2x_0^2\int_{\alpha_ax_0}^{\infty}\frac{e^{-y}}{y}dy\right\}, \quad (3)$$

where $\alpha_a=N\sigma_a$ and the integral is tabulated.[8] This result has been obtained by many investigators.[9]

The rate of neutron absorption per cm^3 in a surface layer, normalized to unit thickness, is

$$n_{as}=\frac{1}{2}\int_0^{\pi/2}(nv\cos\theta)\left(\frac{\alpha_a}{\cos\theta}\right)\left[1+\exp\left(-\frac{\alpha_tx_0}{\cos\theta}\right)\right]\sin\theta d\theta$$

$$=\frac{nv}{2}\alpha_a\left(1+e^{-\alpha_tx_0}-\alpha_tx_0\int_{\alpha_tx_0}^{\infty}\frac{e^{-y}}{y}dy\right), \quad (4)$$

where $\alpha_t=N(\sigma_a+\sigma_s)$, and σ_s is the sum of the scattering cross sections for Li and F (5.5 barns).

The ratio of the surface-to-volume yields for thermal neutrons is

$$R=\frac{n_{as}/n_0}{n_a/n_0x_0}$$

$$=\alpha_ax_0\frac{1+e^{-\alpha_tx_0}-\alpha_tx_0\int_{\alpha_tx_0}^{\infty}\frac{e^{-y}}{y}dy}{1+(\alpha_ax_0-1)e^{-\alpha_ax_0}-\alpha_a^2x_0^2\int_{\alpha_ax_0}^{\infty}\frac{e^{-y}}{y}dy}. \quad (5)$$

Substituting the values for the crystal in Fig. 1, 3.52 cm^{-1} for α_a, 3.86 cm^{-1} for α_t, and 0.075 cm for x_0, we obtain 1.07 for R.

To correct for epithermal neutrons assume a "cadmium ratio" of 20, or that 5 percent of the yield is due

---

[5] D. J. Hughes, *Pile Neutron Research* (Addison-Wesley Press, Inc., Cambridge, 1953), p. 90.

[6] *Neutron Cross Sections*, Atomic Energy Commission Report AECU 2040 (Office of Technical Services, Department of Commerce, Washington 25, D. C., 1952).

[7] G. M. Branch, Manhattan District Declassified Document MDDC-747, 1946 (unpublished).

[8] E. Jahnke and F. Emde, *Tables of Functions with Formulae and Curves* (Dover, New York, 1945).

[9] See the references in R. Keyes, Atomic Energy Commission Report AECD-3000, 1950 (unpublished).

to epithermals, neglecting attenuation. The epithermal yield is comparatively uniform throughout the crystal and is introduced by adding $0.1\alpha_a$ to n_{as}/n_0 and n_a/n_0x_0 in the first part of Eq. (5). The result is a corrected ratio of 1.06.

Since there is a nonuniform distribution of defects, the calculation of the experimental slope becomes a problem of a self-strained system with cubic anisotropy. In order to evaluate the lattice expansion in the direction of the crystal thickness (z axis), we assume Hooke's law, net zero tensile stresses in the x and y directions, and zero stress at the surface. The resultant strain on the surface in the z direction will be given by

$$e_z=\frac{\beta}{1-\nu}\left\{\frac{n_{as}}{n_0}(1+\nu)-2\nu\frac{n_a}{n_0x_0}\right\},$$

where β is the constant of proportionality in a non-constrained system between e_z and the fraction of neutrons absorbed, and ν is Poisson's ratio. The average strain in the z direction is $\beta n_a/n_0x_0$, and the experimental slope S is the ratio of the two, or

$$S=\frac{1+\nu}{1-\nu}R-\frac{2\nu}{1-\nu}.$$

Taking 0.278 as a value of ν, for Harshaw crystals,[10] we obtain 1.11 ± 0.05 for S. Comparing with the experimental slope of 1.05 ± 0.02, the deviation from unity not caused by neutron attenuation is 6 ± 5 percent. Thus we have established the equivalence of x-ray and density changes caused by lattice defects within 11 percent.

b. Epithermal Neutron Experiment

Neutron attenuation may be reduced by shielding the crystal with cadmium, leaving only the epicadmium flux effective for the (n,α) reaction and for any direct atomic displacements. The appropriate cross sections for these processes are much smaller, and an irradiation 17 times as long was required for comparable results. Two crystals, one twice as thick as the other, were shielded with 0.030″ of cadmium, and the results of the irradiation and successive anneals from 315°C to 550°C are shown in Fig. 2. Since the data scatter about the same straight line, within error, there is no detectable effect caused by thickness or attenuation, and $(\Delta a/a)_x$ may be compared with $(\Delta a/a)_\rho$ directly, yielding the fact that x-ray and density changes are equivalent within 6 percent. The fact that these data require no correction for neutron attenuation makes the result more reliable, and we conclude that x-ray and density changes in neutron-irradiated LiF are equivalent to within 6 percent.

[10] S. Rao, Curr. Sci. 18, 336 (1949).

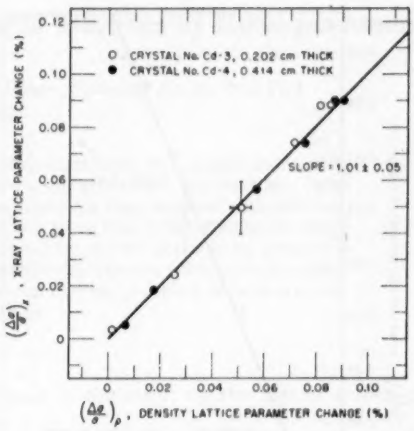

FIG. 2. Lattice expansion for cadmium shielded crystals as derived from x-ray and density measurements.

FRENKEL *VERSUS* SCHOTTKY DEFECTS

The displaced atoms causing the expansion may lead to either Schottky or Frenkel defects. A Schottky defect is produced when an atom at a normal lattice site comes to the surface leaving a vacancy behind. The additional atomic volume on the surface is seen by the density, but not the x-ray, measurement. This was pointed out by Seitz[11] in connection with experiments determining Avogadro's number. For Schottky defects, Seitz showed in effect that[12]

$$n_s=-\Delta(\rho v_c)/\rho v_c, \tag{6}$$

where ρ is the density, v_c is the volume of a unit cell, as seen by x-rays, and n_s is the concentration of Schottky defects. In our notation,

$$n_s=3[(\Delta a/a)_\rho-(\Delta a/a)_x]. \tag{7}$$

From the previous section, the quantity in square brackets is zero to within 6 percent of the lattice expansion, or n_s is at most equal to 6 percent of the volume expansion. Since Schottky defects cause a volume expansion about equal to their concentration, this mechanism cannot account for more than 6 percent of the observed expansion.

The above restriction does not apply to Frenkel defects, or vacancy interstitial pairs. Recent theoretical work[1,2] has shown that these defects are characterized by an exact equivalence of $(\Delta a/a)_x$ and $(\Delta a/a)_\rho$. We therefore conclude that the lattice expansion in neutron-irradiated LiF is predominantly due to Frenkel defects.

THE ANNEALING PROCESS

In order to study the annealing process, several non-uniform irradiations were made on thick crystals.

[11] F. Seitz, Revs. Modern Phys. 18, 384 (1946).

[12] See reference 11. Equation (6) shows a minus sign not shown in Seitz's article, where he was concerned only with absolute magnitudes.

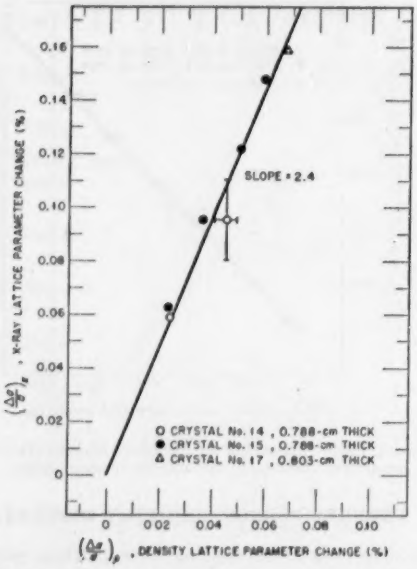
SLOPE = 2.4
O CRYSTAL No. 14 , 0.788-cm THICK
● CRYSTAL No. 15 , 0.788-cm THICK
△ CRYSTAL No. 17 , 0.803-cm THICK
X-RAY LATTICE PARAMETER CHANGE (%)
DENSITY LATTICE PARAMETER CHANGE (%)

FIG. 3. Lattice expansion for thick crystals as derived from x-ray and density measurements.

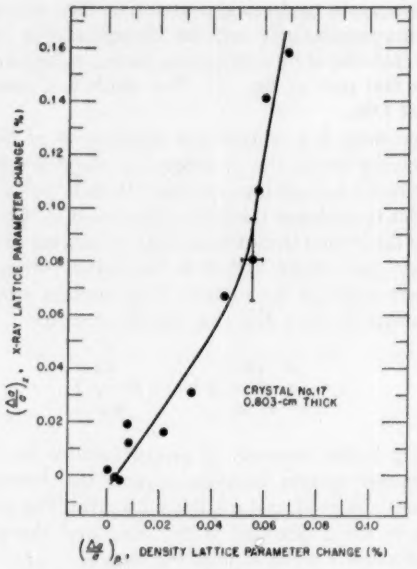

FIG. 4. Annealing data for a thick crystal as derived from x-ray and density measurements.

Three crystals 2.6 cm square by 0.8 cm thick were subjected to single or successive irradiations that totaled up to 6×10^{16} neutrons per cm^2, and the results are shown in Fig. 3. X-ray measurements were taken on the 2.6-cm square surfaces. Crystal No. 17 was then annealed at successively higher temperatures from 275°C to 560°C, with the results shown in Fig. 4. The original slope of 2.4 in Fig. 3 indicates a nonuniform distribution of defects, as expected, while the annealing points in Fig. 4 approach a line of smaller slope, indicating a change toward a more uniform defect distribution.

To explain the annealing process, we need a rough approximation to the original defect distribution. Taking the e thickness for thermal neutrons as 0.3 cm and the average path for a neutron as twice the perpendicular distance from the largest surface, the neutrons from one large face of the crystal are attenuated to about $e^{-8/3}$ on reaching the center and $e^{-16/3}$ on reaching the opposite face. Adding the contributions from both sides, the ratio of neutrons reaching the surface to those reaching the center is about 1.00 to 0.14. Since the x-ray measurement will detect changes at the surface and the density measurement changes throughout the volume, any change in defect distribution will show up easily starting with the above ratio.

There are two processes which might change the distribution, diffusion and recombination of vacancies and interstitials. The two compete since, if recombination occurs over a short diffusion path, diffusion will not change the defect distribution. In fact, an order of magnitude argument shows that this is the case. In the least favorable region for recombination, the center of the crystal, there was originally a lattice expansion of 14 percent that on the surface, or a $(\Delta a/a)_x$ of 2.2×10^{-4}. If we assume that a vacancy interstitial pair is equivalent at most to an extra average atomic volume, the minimum concentrations of pairs in the interior is 6.6×10^{-4}. Then a vacancy or interstitial will have to take only 1.5×10^3 interatomic steps before recombination. Assuming a random-walk process, the average distance travelled in any one direction is a factor of 10^6 smaller than the crystal thickness, too small to change the macroscopic defect distribution. The argument is even stronger in the higher defect concentration near the surface.

Having eliminated diffusion, consider the recombination processes. In a process of order one, such as the recombination of neighboring vacancies and interstitials, there would be no change in the defect distribution. In a process of order higher than one, the high concentration of defects near the surface decreases proportionately faster than the low concentration in the interior, tending toward a more uniform defect distribution. This explains the curvature of the line in Fig. 4 and establishes the annealing process as of order higher than one.

The authors would like to acknowledge the help of Mr. G. E. Klein and Mr. F. A. Sherrill in the x-ray measurements, and thank Mr. J. D. Eshelby for his suggestions on the elastic behavior of the crystal.

Perturbation Calculation of the Elastic Scattering of Electrons by Hydrogen Atoms*

SIDNEY BOROWITZ
Physics Department, College of Engineering, New York University, University Heights, New York
(Received July 12, 1954)

A perturbation calculation has been carried out for the scattering of electrons by hydrogen atoms, using as the perturbation only the interaction between the two electrons, and retaining in the result only terms of the highest power in the incident energy of the electron. The results are then compared with more conventional first-order perturbation calculations for this problem. It is found that to the order in the energy that we retain, the results for direct-scattered amplitudes obtained by the two perturbation procedures are the same, whereas in the results for the exchange-scattered amplitudes there is a difference in the energy dependence. While no conclusions can be drawn as to which perturbation procedure is more accurate, some reasons are given for preferring the calculation performed here.

1. INTRODUCTION

THE customary method[1] for treating the scattering of electrons by hydrogen atoms in the Born approximation is to take as the perturbation the interaction of the incoming electron with both particles of the atom, and to take matrix elements of this perturbation between initial and final states of the system. We shall call this the method of the "asymmetric perturbation," since it is not symmetric in the two electrons.

If the mass of the proton is taken to be infinite, one can, as an alternative, take as the perturbation simply the interaction between the two electrons. (This we call the "symmetric perturbation.") In this case the unperturbed Hamiltonian is separable, and the initial and final state wave functions corresponding to it can be exhibited in closed form.

This latter procedure is likely to lead to more accurate results than the former, since we include more of the interaction in our unperturbed problem. This advantage will be most pronounced in the calculation of exchange scattering. In this case the approximation with the asymmetric perturbation seems to be particularly poor since it leads to the physically absurd result that exchange scattering will occur even when the interaction between the two electrons vanishes.

In this paper we shall calculate separately the direct and the elastic exchange-scattered amplitude in the first Born approximation, taking as the perturbation the interaction between the two electrons. These two amplitudes can then be combined[1] to give the total differential cross section. We will consider energies high enough so that the term we calculate is likely to be the first of a convergent series, yet not so large that we need include relativistic effects. Since the energies we consider will be high, we will compute only the dependence of the result on the highest power of the energy.

As our results will show, the direct-scattered amplitude is the same, to the highest power in the energy, whether one uses the symmetric or asymmetric perturbation. For the exchange-scattered amplitude, on the other hand. the energy dependence at high energies in our results differs from that obtained by the method of asymmetric perturbation. Recalling the unphysical nature of the expression for the exchange-scattered amplitude when the asymmetric perturbation is used, we may presume that this amplitude is given more correctly by our calculation.

After some preliminary remarks in Sec. 2 which establish the integrals which must be evaluated, we calculate, in Sec. 3, the elastic direct-scattered amplitude and the elastic exchange-scattered amplitude. In Sec. 4 we discuss the results and compare them with the results of a similar calculation done with the asymmetric perturbation. The Appendix is devoted to a detailed evaluation of a typical integral occurring in Sec. 3.

2. PRELIMINARY CONSIDERATIONS

In order to calculate the elastic-scattered amplitudes, we take the mass of the proton to be infinite and seek a solution of the Schrödinger equation for the system

$$\left\{\Delta_1+\Delta_2+2\left(E+\frac{1}{r_1}+\frac{1}{r_2}-\frac{1}{r_{12}}\right)\right\}\Psi=0, \qquad (2.1)$$

which represents an incoming plane wave in electron 1 and outgoing spherical waves in particles 1 or 2 as r_1 or $r_2\to\infty$. We are using a system of units in which $m=\hbar=e=1$. The unit of length is thus the Bohr radius, and the unit of energy is 27.06 ev, that is, twice the ionization energy of hydrogen. The outgoing spherical waves each correspond to one of the energies allowed by the conservation of energy. When we confine ourselves to elastic scattering, as we do in this paper, we seek the coefficients f_0 and g_0 of the outgoing spherical waves as r_1 and r_2, respectively, approach infinity. These are the coefficients of the spherical waves having the same energy as the incoming particle.

* The research reported in this article was done in part at the Institute of Mathematical Sciences, New York University under sponsorship of the Geophysics Research Directorate, Air Force Cambridge Research Center, and in part at the Physics Department, College of Engineering, New York University, under sponsorship of the Office of Naval Research.

[1] N. F. Mott and H. S. W. Massey, *Theory of Atomic Collisions* (Clarendon Press, Oxford, 1949), second edition, Chap. VIII.

The expression for the exchange-scattered amplitude in first-order perturbation is given by

$$g_0=-\frac{1}{2\pi}\int\Psi_f^*V\Psi_i d\tau_1 d\tau_2, \tag{2.2}$$

where V is the perturbation. When we choose the asymmetric perturbation

$$V=2(1/r_1-1/r_{12}), \tag{2.3}$$

then the exchange-scattered amplitude is

$$g_{0a}=-\frac{1}{\pi^2}\int\exp(-r_1-i\mathbf{k}_n\cdot\mathbf{r}_2+i\mathbf{k}_0\cdot\mathbf{r}_1)\times\left[\frac{1}{r_1}-\frac{1}{r_{12}}\right]d\tau_1 d\tau_2, \tag{2.4}$$

where $\mathbf{k}_0$, $\mathbf{k}_n$ are the propagation vectors of the electrons in the initial and final states.

In the case of the exchange-scattered amplitude in Eq. (2.4), there is some question as to whether the perturbation V should be $2(1/r_1-1/r_{12})$ or $2(1/r_2-1/r_{12})$. If, as in this case, one knows the bound-state wave functions exactly, either perturbation yields the same result;[2] however, in problems involving more complicated atoms whose wave functions are not known precisely, this freedom of choice is the origin of the post-prior discrepancy.[3]

If one chooses the symmetric perturbation

$$V=2/r_{12}, \tag{2.5}$$

then the exchange-scattered amplitude is given by

$$g_{0s}=\frac{N^2}{\pi^2}\int\exp(-r_1+i\mathbf{k}_0\cdot\mathbf{r}_1-r_2-i\mathbf{k}_n\cdot\mathbf{r}_2)\frac{1}{r_{12}}\times{}_1F_1(-i/k,1,i(kr_2+\mathbf{k}_n\cdot\mathbf{r}_2))\times{}_1F_1(-i/k,1,i(kr_1-\mathbf{k}_0\cdot\mathbf{r}_1))d\tau_1 d\tau_2, \tag{2.6}$$

where $k=|\mathbf{k}_0|=|\mathbf{k}_n|$, and $k^2=2(E+\frac{1}{2})$; furthermore,

$$N^2=\frac{(\pi/k)\exp(-\pi/k)}{\sinh(\pi/k)} \tag{2.7}$$

is the normalization constant for the continuum hydrogen functions corresponding to incident waves of unit amplitude. The ${}_1F_1$ are confluent hypergeometric functions.

The direct-scattered amplitude when the asymmetric perturbation in Eq. (2.3) is used can also be obtained from Eq. (2.2); we have

$$f_{0a}=-\frac{1}{\pi^2}\int\exp[-2r_2+i(\mathbf{k}_0-\mathbf{k}_n)\cdot\mathbf{r}_1]\times\left(\frac{1}{r_1}-\frac{1}{r_{12}}\right)d\tau_1 d\tau_2. \tag{2.8}$$

If, however, we use the symmetric perturbation of Eq. (2.5), we must add the Rutherford scattering amplitude to the amplitude corresponding to Eq. (2.2). This additional term arises from the circumstance that our unperturbed problem contains an outgoing wave as $r_1\to\infty$.[4] For the symmetric perturbation we have, then,[5]

$$f_{0s}=\frac{N^2}{\pi^2}\int\exp[-2r_2+i(\mathbf{k}_0-\mathbf{k}_n)\cdot\mathbf{r}_1]\times{}_1F_1(-i/k,1,i(kr_1+\mathbf{k}_n\cdot\mathbf{r}_1))\frac{1}{r_{12}}\times{}_1F_1(-i/k,1,i(kr_1-\mathbf{k}_0\cdot\mathbf{r}_1))d\tau_1 d\tau_2+R, \tag{2.9}$$

where

$$R=\frac{[2ikr\sin^2(\theta/2)]^{i/k}}{[-2ikr\sin^2(\theta/2)]^{-i/k}}\frac{\Gamma(1-i/k)}{\Gamma(1+i/k)}\frac{1}{k^2}\frac{1}{\sin^2(\theta/2)}; \tag{2.10}$$

here Γ is the gamma function of its argument.

The calculation of Eqs. (2.9) and (2.6) will give respectively the direct- and exchange-scattered amplitudes in our approximation. These will be compared with the results obtained from Eqs. (2.8) and (2.4) which have been computed by Corinaldesi and Trainor.[6]

3. DIRECT SCATTERING

The integration of (2.9) with respect to the $\mathbf{r}_2$ coordinate can be done immediately, and yields

$$f_{0s}=\frac{N^2}{\pi}\int\left\{\exp[-2r_1+i(\mathbf{k}_0-\mathbf{k}_n)\cdot\mathbf{r}_1]\times{}_1F_1(-i/k,1,i(kr_1+\mathbf{k}_n\cdot\mathbf{r}_1))\times\left[1+\frac{1}{r_1}\right]{}_1F_1(-i/k,1,i(kr_1-\mathbf{k}_0\cdot\mathbf{r}_1))\right\}d\tau_1+\frac{N^2}{\pi}\int\left\{\exp[i(\mathbf{k}_0-\mathbf{k}_n)\cdot\mathbf{r}_1]\times{}_1F_1(-i/k,1,i(kr_1+\mathbf{k}_n\cdot\mathbf{r}_1))\frac{1}{r_1}\times{}_1F_1(-i/k,1,i(kr_1-\mathbf{k}_0\cdot\mathbf{r}_1))\right\}d\tau_1+R. \tag{3.1}$$

The second and third terms of Eq. (3.1) may be considered in a different context. Suppose one considered the scattering of an electron by a positive and negative charge of the same magnitude situated at the same point in space. If now one evaluates the scattered amplitude in first Born approximation, using as the unperturbed problem the potential due to the positive charge alone, then the result is just the sum of the

[2] S. Altshuler, Phys. Rev. **91**, 1167 (1953).
[3] D. R. Bates *et al.*, Trans. Roy. Soc. (London) **A243**, 93 (1950).
[4] S. Borowitz and B. Friedman, Phys. Rev. **89**, 441 (1953).
[5] A. Sommerfeld, *Wellenmechanik* (Frederich Ungar Publishing Company, New York, 1939), p. 502; H. A. Bethe and G. Breit, Phys. Rev. **93**, 888 (1954).
[6] A. Corinaldesi and P. Trainor, Nuovo cimento **2**, 940 (1952).

second and third terms of Eq. (3.1). This sum is not zero, due to the crudity of the first Born approximation.[7] Obviously, however, the scattering due to this configuration, if calculated exactly, would vanish. Therefore we feel justified in considering the second term in Eq. (3.1) as cancelled by the third.

The first term of Eq. (3.1) then gives us the symmetric-scattered amplitude. We write this as

$$f_{0s}=-(N^2/\pi)(I_0+I_1), \tag{3.2}$$

where

$$I_0=\int \exp[-\lambda r+i(\mathbf{k}_0-\mathbf{k}_n)\cdot\mathbf{r}] \times {}_1F_1(-i/k,\,1,\,i(kr+\mathbf{k}_n\cdot\mathbf{r})) \times {}_1F_1(-i/k,\,1,\,i(kr-\mathbf{k}_0\cdot\mathbf{r}))\frac{d\tau}{r}\Big|_{\lambda=2}, \tag{3.3}$$

and

$$I_1=-\partial I_0/\partial\lambda\,|_{\lambda=2}. \tag{3.4}$$

Using a method introduced by Sommerfeld,[8] we have computed the integral I_0; the result is

$$I_0=\frac{4\pi}{4k^2\sin^2(\theta/2)+\lambda^2}e^{\pi/k}\left[\frac{4(k+\frac{1}{2}i\lambda)^2}{4k^2\sin^2(\theta/2)+\lambda^2}\right]^{i/k} \times {}_2F_1\left(1+i/k,\,-i/k,\,1,\,1-\frac{\lambda^2}{4k^2\sin^2(\theta/2)+\lambda^2}\right)\Big|_{\lambda=2}, \tag{3.5}$$

where ${}_2F_1$ is the hypergeometric function of its argument.

From Eqs. (3.4) and (3.5) one could calculate f_{0s} exactly; but we are interested only in the highest power of k in f_{0s}. To find this we first investigate the highest power of k in I_0. This involves the reduction of the hypergeometric function ${}_2F_1$. We set

$$\frac{\lambda^2}{4k^2\sin^2(\theta/2)+\lambda^2}=\epsilon; \tag{3.6}$$

then we have

$${}_2F_1(1+i/k,\,-i/k,\,1,\,1-\epsilon) =\frac{1}{\Gamma(1+i/k)\Gamma(-i/k)}\sum_{n=0}^{\infty}\frac{(1+i/k)_n(-i/k)_n}{n!n!} \times[2\Psi(1+n)-\Psi(1+i/k+n) +\Psi(-i/k+n)-\log\epsilon]\epsilon^n, \tag{3.7}$$

(Erdelyi,[9] p. 112, formula 14 with $m=0$). Here $\Psi(x)=\Gamma'(x)/\Gamma(x)$. To the highest power of k,

$${}_2F_1(1+i/k,\,-i/k,\,1,\,1-\epsilon)\cong\frac{1}{\Gamma(1+i/k)\Gamma(-i/k)} \times[-2\gamma+\Psi(-i/k)\Psi(1+i/k)], \tag{3.8}$$

where $\gamma=$ Euler's constant $=0.577215\cdots$. But

$$\Gamma(1+i/k)\Gamma(-i/k)=\frac{\pi i}{\sinh(\pi/k)} \tag{3.9}$$

(Erdelyi,[9] p. 3), and

$$\Psi(-i/k)-\Psi(1+i/k)=(\pi/i)\coth(\pi/k) \tag{3.10}$$

(Erdelyi,[9] p. 15). Consequently,

$${}_2F_1(1+i/k,\,1,\,1-\epsilon) \cong\frac{\sinh(\pi/k)}{\pi i}\left[-\gamma+\frac{\pi}{i}\coth(\pi/k)-\log\epsilon\right] \cong-\cosh(\pi/k)\cong-1 \tag{3.11}$$

to the highest power of k.

The contribution of I_1 can be evaluated from Eq. (3.4). Differentiating the coefficient of the hypergeometric function gives terms of lower order in k than those we have considered. Hence we must differentiate the hypergeometric function. We obtain

$$I_1\cong-\frac{4\pi}{4k^2\sin^2(\theta/2)+\lambda^2}e^{\pi/k}\left[\frac{4(k+\frac{1}{2}i\lambda)^2}{4k^2\sin^2(\theta/2)+\lambda^2}\right]^{i/k} \times\frac{d}{d\lambda}\left[{}_2F_1\left(1+\frac{i}{k},\,-\frac{i}{k},\,1,\,1-\frac{\lambda^2}{4k^2\sin^2(\theta/2)+\lambda^2}\right)\right]\Big|_{\lambda=2} =-\frac{4\pi}{4k^2\sin^2(\theta/2)+\lambda^2}e^{\pi/k}\left[\frac{4(k+\frac{1}{2}i\lambda)^2}{4k^2\sin^2(\theta/2)+\lambda^2}\right]^{i/k} \times\left(1+\frac{i}{k}\right)\left(-\frac{i}{k}\right){}_2F_1\left(2+\frac{i}{k},\,1-\frac{i}{k},\,2,\,1-\frac{\lambda^2}{4k^2\sin^2(\theta/2)+\lambda^2}\right)-\frac{8\lambda k^2\sin^2(\theta/2)}{[4k^2\sin^2(\theta/2)+\lambda^2]^2} \tag{3.12}$$

(Erdelyi,[9] p. 102). But

$${}_2F_1(2+i/k,\,1-i/k,\,2,\,1-\epsilon) =\frac{1}{\epsilon\Gamma(2+i/k)\Gamma(1-i/k)}+\frac{(-1)^n}{(1+i/k)(-i/k)} \times\sum_{n=0}^{\infty}\frac{(2+i/k)_n(1-i/k)_n}{(n+1)!n!}[\Psi(1+n)+\Psi(2+n) -\Psi(2+i/k+n)+\Psi(1-i/k+n)-\log\epsilon]\epsilon^n \tag{3.13}$$

[7] I am indebted to Professor Zumino for this remark. A direct calculation of the second term of Eq. (3.1) gives an infinite result when $|k_0|=|k_n|$. This is related to the fact that plane waves cannot be generated by iterating with hydrogenic wave functions.

[8] A. Sommerfeld, reference 5, pp. 503–506. A. Nordsieck [Phys. Rev. **93**, 785 (1954)] has also computed the integral I_0 and obtained the same result as we did. Nordsieck has confined himself to the case where λ is small. However, his result can be shown to be valid for all positive λ.

[9] Erdelyi, Magnus, Oberhettinger, and Tricomi, *Higher Transcendental Functions* (McGraw-Hill Book Company, New York, 1953), Vol. 1.

(Erdelyi,[9] p. 110). Now we restrict ourselves to the highest power of k, and use Eq. (3.9) and the fact that

$$\Psi(1-i/k)-\Psi(1+i/k)=-\frac{1}{i/k}+\pi\cot(\pi i/k) \quad (3.14)$$

(Erdelyi,[9] p. 16) to obtain

$${}_2F_1(2+i/k, 1-i/k, 2, 1-\epsilon)\cong 2. \quad (3.15)$$

Thus the contribution of I_1 to f_0 is of the order of $1/k^3$ with respect to the I_0. To find the contribution of I_0 to f_0, we substitute Eq. (3.11) into Eq. (3.5), and substitute the result into Eq. (3.2); using Eq. (2.7) we obtain

$$f_0=-\frac{1}{k^2\sin^2(\theta/2)+1}, \quad (3.16)$$

to the highest power in k. This is precisely the result to the highest power in k which is obtained when one uses the asymmetric perturbation.[6]

4. EXCHANGE SCATTERING

The exchange-scattered amplitude in first-order perturbation theory, with $1/r_{12}$ as the perturbation, is given by Eq. (2.6). In order to evaluate this integral we first introduce the Fourier transform,

$$\frac{1}{r_{12}}=\frac{1}{2\pi^2}\int\frac{\exp[i\mathbf{K}\cdot(\mathbf{r}_1-\mathbf{r}_2)]}{K^2-i\epsilon}d\mathbf{K}. \quad (4.1)$$

[In what follows we will omit explicit mention of the ϵ in Eq. (4.1).] Equation (2.6), then, becomes

$$g_0=-\frac{N^2}{2\pi^4}\int\exp[-r_1+i(\mathbf{K}-\mathbf{k}_n)\cdot\mathbf{r}_1-r_2-i(\mathbf{K}-\mathbf{k}_0)\cdot\mathbf{r}_2]\times{}_1F_1(-i/k, 1, i(kr_2-\mathbf{k}_0\cdot\mathbf{r}_2))\times{}_1F_1(-i/k, 1, i(kr_1+\mathbf{k}_n\cdot\mathbf{r}_1))\frac{d\mathbf{K}}{K^2}d\tau_1 d\tau_2. \quad (4.2)$$

Equation (4.2) can now be separated into a product of functions of r_1 and r_2:

$$g_0=-\frac{N^2}{2\pi^4}\int J_1'(\mathbf{K})J_2'(\mathbf{K})\frac{d\mathbf{K}}{K^2}, \quad (4.3)$$

where

$$J_1'(\mathbf{K})=\int\exp[-r_1+i(\mathbf{K}-\mathbf{k}_n)\cdot\mathbf{r}_1]\times{}_1F_1(-i/k, 1, i(kr_1+\mathbf{k}_n\cdot\mathbf{r}_1))d\tau_1, \quad (4.4)$$

$$J_2'(\mathbf{K})=\int\exp[-r_2-i(\mathbf{K}-\mathbf{k}_0)\cdot\mathbf{r}_2]\times{}_1F_1(-i/k, 1, i(kr-\mathbf{k}_0\cdot\mathbf{r}_2))d\tau_2. \quad (4.5)$$

Instead of evaluating Eq. (4.4) directly, it is simpler to evaluate the integral

$$J_1(\alpha,\mathbf{K})=\int\exp[-\alpha r_1+i(\mathbf{K}-\mathbf{k}_n)\cdot\mathbf{r}_1]\times{}_1F_1(-i/k, 1, i(kr_1+\mathbf{k}_n\cdot\mathbf{r}_1))r_1dr_1d\Omega_1d\phi, \quad (4.6)$$

which is related to J_1' by

$$J_1'=-\partial J_1/\partial\alpha|_{\alpha=1}. \quad (4.7)$$

We may proceed similarly for Eq. (4.5). Then we obtain

$$g_{0s}=-\frac{N^2}{2\pi^4}\int\frac{\partial^2}{\partial\alpha\partial\beta}J_1(\alpha,\mathbf{K})J_2(\beta,\mathbf{K})\frac{d\mathbf{K}}{K^2}. \quad (4.8)$$

The difficulty in evaluating the integrals corresponding to J_1 and J_2 lies in the fact that two distinct and variable angles are involved, namely the angles between $(\mathbf{K}-\mathbf{k}_n)$ and $\mathbf{r}$ and between $\mathbf{k}_n$ and $\mathbf{r}$. We can circumvent this difficulty by using an integral representation[10] for the confluent hypergeometric function. This yields

$$J_1=\frac{1}{2\pi i}\oint\left(\frac{u}{u+1}\right)^{i/k}\frac{1}{u}\exp\{-r(\alpha+iku)+i[\mathbf{K}-\mathbf{k}_n(1+u)]\cdot\mathbf{r}\}rdrd\Omega du, \quad (4.9)$$

where the integration in u space is a path surrounding the points 0 and -1. The space integrals of Eq. (3.1) are now readily evaluated to give

$$J_1=\frac{1}{2\pi i}\oint\left(\frac{u}{u+1}\right)^{i/k}\frac{1}{u}\frac{4\pi}{(\alpha+iku)^2+[\mathbf{K}-\mathbf{k}_n(1+u)]^2}du,$$

$$=\frac{1}{2\pi i}\oint\left(\frac{u}{u+1}\right)^{i/k}\frac{1}{u}\frac{4\pi}{\xi-\zeta u}du, \quad (4.10)$$

where

$$\xi=(\alpha^2+|\mathbf{K}-\mathbf{k}_n|^2),$$
$$\zeta=[2(\mathbf{K},\mathbf{k}_n)-k^2-i\alpha k]. \quad (4.11)$$

Now as $u\to\infty$ the integrand of Eq. (3.2) tends to zero as $1/u^2$. Since ξ/ζ does not lie on the real axis between -1 and 0, we may evaluate Eq. (4.10) by the residue theorem; we get

$$J_1=\frac{4\pi}{\xi}\left(\frac{\xi}{\xi+\zeta}\right)^{i/k}. \quad (4.12)$$

Since we wish to find $\partial J_1/\partial\alpha|_{\alpha=1}$ rather than J, we differentiate Eq. (4.12) with respect to α and set the derivative equal to 1. The result is

$$\left.\frac{\partial J_1}{\partial\alpha}\right|_{\alpha=1}=-\frac{16\pi}{(1+|\mathbf{K}-\mathbf{k}_n|^2)^2}\times\left(\frac{K^2-(\mathbf{n},\mathbf{K})(k+i)}{K^2-(k+i)^2}\right)\left(\frac{\xi}{\xi+\zeta}\right)^{i/k}. \quad (4.13)$$

Here $\mathbf{n}$ is a unit vector in the direction of k_n. By a

[10] See A. Sommerfeld, reference 5, p. 461.

similar procedure we obtain

$$\left.\frac{\partial J_2}{\partial\beta}\right|_{\beta=1}=-\frac{16\pi}{(1+|\mathbf{K}-\mathbf{k}_0|^2)^2}\left(\frac{K^2-(\mathbf{n}_0,\mathbf{K})(k+i)}{[K^2-(k+i)^2]}\right)\left(\frac{\xi_0}{\xi_0+\zeta_0}\right)^{i/k}, \tag{4.14}$$

where ξ_0 and ζ_0 are related to $\mathbf{k}_0$ as ξ and ζ to $\mathbf{k}_n$.

Now using Eqs. (4.8), (4.13), and (4.14), we obtain

$$g_{0s}=-\frac{128N^2}{\pi^2}\cdot\int\frac{d\mathbf{K}}{K^2}\frac{K^4-K^2(k+i)[(\mathbf{n}_0,\mathbf{K})+(\mathbf{n},\mathbf{K})]+(k+i)^2[(\mathbf{n}_0,\mathbf{K})(\mathbf{n},\mathbf{K})]}{(1+|\mathbf{K}-\mathbf{k}_0|^2)^2(1+|\mathbf{K}-\mathbf{k}_n|^2)^2[K^2-(k+i)^2]^2}\left(\frac{\xi}{\xi+\zeta}\right)^{i/k}\left(\frac{\xi_0}{\xi_0+\zeta_0}\right)^{i/k}. \tag{4.15}$$

It is interesting to compare Eq. (4.15) with the corresponding term that would arise if one were to compute the matrix elements of $1/r_{12}$ using plane waves instead of hydrogenic continuum functions; this term is

$$g_{0p}=-\frac{32}{\pi^2}\int\frac{d\mathbf{K}}{K^2}\frac{1}{(1+|\mathbf{K}-\mathbf{k}_0|^2)^2}\frac{1}{(1+|\mathbf{K}-\mathbf{k}_n|^2)^2}. \tag{4.16}$$

The differences between Eqs. (4.16) and (4.15) which can be identified are: (i)—that Eq. (4.16) contains a normalization constant N^2, which tends to 1 as $k\to\infty$; (ii)—Eq. (4.15) contains an extra term $[K^2-(k+i)^2]^2$ in the denominator; this is the sort of term that would arise from the matrix element of $1/r_{12}$ between outgoing spherical waves of the form e^{ikr}/r; and (iii)—Eq. (4.15) contains the factors $[\xi/(\xi+\zeta)]^{i/k}$ and $[\xi_0/(\xi_0+\zeta_0)]^{i/k}$, which resemble terms that might come from a logarithmic phase factor at infinity in the asymptotic form of the continuum hydrogenic wave functions. We shall now show that if, as in the present study, we consider only the highest power in k in g_{0s}, we may replace the last two factors in Eq. (4.15) by unity. First we note that since the integral is absolutely convergent we may expand $[\xi/(\xi+\zeta)]^{i/k}$ and $[\xi_0/(\xi_0+\zeta_0)]^{i/k}$. The result of this expansion is $1+S$, where S is a complex number whose real part is $\leq\pi/k$ and whose imaginary part is $\leq(p/k)\log k$, with p finite. Since both these terms approach 0 as $k\to\infty$, we may neglect S in investigating the k-dependence of g_{0s} as $k\to\infty$.

Now, replacing $[\xi/(\xi+\zeta)]^{i/k}$ and $[\xi_0/(\xi_0+\zeta_0)]^{i/k}$ by 1 in Eq. (4.15), we have the approximate expression:

$$g_{0s}\cong-\frac{128N^2}{\pi^2}\int\frac{d\mathbf{K}}{K^2}\left(\frac{K^4-K^2(k+i)[(\mathbf{n}_0,\mathbf{K})+(\mathbf{n},\mathbf{K})]+(k+i)^2[(\mathbf{n}_0,\mathbf{K})(\mathbf{n},\mathbf{K})]}{(1+|\mathbf{K}-\mathbf{k}_0|^2)^2[K^2-(k+i)^2]^2(1+|\mathbf{K}-\mathbf{k}_n|^2)^2}\right), \tag{4.17}$$

which we shall now proceed to evaluate exactly. Equation (4.17) may be simplified somewhat and then written in the more tractable form

$$\begin{aligned}g_{0s}\cong-\frac{128N^2}{\pi^2}\int d\mathbf{K}&\frac{1}{[K^2-(k+i)^2](1+|\mathbf{K}-\mathbf{k}_0|^2)^2(1+|\mathbf{K}-\mathbf{k}_n|^2)^2}+\frac{(k+i)^2}{[K^2-(k+i)^2]^2(1+|\mathbf{K}-\mathbf{k}_0|^2)^2(1+|\mathbf{K}-\mathbf{k}_n|^2)^2}\\&-\frac{(k+i)[(\mathbf{n}_0,\mathbf{K})+(\mathbf{n},\mathbf{K})]}{[K^2-(k+i)^2]^2(1+|\mathbf{K}-\mathbf{k}_0|^2)^2(1+|\mathbf{K}-\mathbf{k}_n|^2)^2}+\frac{(k+i)^2(\mathbf{k}_0,\mathbf{K})(\mathbf{k},\mathbf{K})}{K^2[K^2-(k+i)^2]^2(1+|\mathbf{K}-\mathbf{k}_0|^2)^2(1+|\mathbf{K}-\mathbf{k}_n|^2)^2}.\end{aligned} \tag{4.18}$$

The four terms of Eq. (4.18) will henceforth be designated as integrals I, II, III, IV respectively. These integrals can be evaluated by the method developed by Feynman.[11] In this technique terms of the form $1/A_1\cdots A_n$ are replaced by integrals, as follows:

$$\frac{1}{A_1\cdots A_n}=(n-1)!\int\frac{\delta(x_1+x_2+\cdots x_{n-1})dx_1\cdots dx_n}{[Ax_1\cdots+A_nx_n]^n},\quad x_i\geq0. \tag{4.19}$$

Our denominators in Eq. (4.18) do not occur to the first power, but can be put in the form (4.19) since

$$\frac{1}{A_1^s\cdots A_2\cdots A_n}=(-1)^{s-1}(n+s-1)!\int\frac{x_1^s\delta(x_1+x_2\cdots+x_n-1)dx_1\cdots dx_n}{[Ax_1+\cdots+A_nx_n]^{n+s}},\quad x_i\geq0,\quad i=1,2,\cdots n. \tag{4.20}$$

Also, the terms in Eq. (4.18) containing $(\mathbf{n}_0,\mathbf{K})$ in the numerator can be put in the form (4.19) using the identity

$$\frac{(\mathbf{n}_0,\mathbf{K})}{[1+K^2-2(\mathbf{K},\mathbf{k}_0)+k^2]^2}=\frac{1}{2}\frac{\partial}{\partial k_0}\frac{1}{[1+K^2-2(\mathbf{K},\mathbf{k}_0)+k^2]}. \tag{4.21}$$

[11] R. P. Feynman, Phys. Rev. **76**, 769 (1949); R. Jost and A. Pais, Phys. Rev. **82**, 840 (1951).

Using Eqs. (4.20), (4.21), and (4.19), Eq. (4.18) becomes

$$\mathrm{I}=4!\int\frac{x_2x_3\delta(x_1+x_2+x_3-1)dx_1dx_2dx_3d\mathbf{K}}{\{[K^2-(k+i)^2]x_1+(|\mathbf{K}-\mathbf{k}_0|^2+1)x_2+(|\mathbf{K}-\mathbf{k}_n|^2+1)x_3\}^5}, \tag{4.22}$$

$$\frac{\mathrm{II}}{(k+i)^2}=-5!\int\frac{x_1x_2x_3\delta(x_1+x_2+x_3-1)dx_1dx_2dx_3d\mathbf{K}}{\{[K^2-(k+i)^2]x_1+(|\mathbf{K}-\mathbf{k}_0|^2+1)x_2+(|\mathbf{K}-\mathbf{k}_n|^2+1)x_3\}^6}, \tag{4.23}$$

$$\begin{aligned}\frac{\mathrm{III}}{(k+i)}=&-\frac{1}{2}\frac{\partial}{\partial k_0}4!\int\frac{x_1x_2\delta(x_1+x_2+x_3-1)dx_1dx_2dx_3d\mathbf{K}}{\{[K^2-(k+i)^2]x_1+(1+K^2+k^2-2(\mathbf{K},\mathbf{k}_0))x_2+(1+|\mathbf{K}-\mathbf{k}_n|^2)x_3\}^5}\\&-\frac{1}{2}\frac{\partial}{\partial k_n}4!\int\frac{x_1x_2\delta(x_1+x_2+x_3-1)dx_1dx_2dx_3d\mathbf{K}}{\{[K^2-(k+i)^2]x_1+(1+|\mathbf{K}-\mathbf{k}_0|^2)x_2+[1+K^2+k^2-2(\mathbf{K},\mathbf{k}_n)]x_3\}^5},\end{aligned} \tag{4.24}$$

$$\frac{\mathrm{IV}}{(k+i)^2}=-\frac{1}{4}\frac{\partial}{\partial k_0}\frac{\partial}{\partial k_n}4!\int\frac{x_4\delta(x_1+x_2+x_3+x_4-1)dx_1dx_2dx_3d\mathbf{K}}{\{K^2x_1+[1+K^2+k^2-2(\mathbf{K},\mathbf{k}_0)]x_2+[1+K^2+k^2-2(\mathbf{K},\mathbf{k}_n)]x_3+[K^2-(k+i)^2]x_4\}^5},$$

$$x_i\geq 0. \tag{4.25}$$

We now follow the Feynman technique exactly in evaluating Eqs. (4.22)–(4.25). As an example of the use of this method we have computed Eq. (4.24) in detail in Appendix I. The others are computed by a straightforward use of the same method. We obtain

$$\mathrm{I}=\frac{15\pi^2}{64}\frac{1}{(k^2\mu)^{7/2}}\int_0^1du\int_{-u}^{u}dv\left[\frac{u^3-v^2}{(\omega-v^2)^{7/2}}\right], \tag{4.26}$$

$$\mathrm{II}=\frac{-105\pi^2}{128}\frac{\rho^2}{k^7\mu^{9/2}}\int_0^1du\int_{-u}^{u}dv\left[\frac{(u^2-v^2)(1-u)}{(\omega-v^2)^{9/2}}\right], \tag{4.27}$$

$$\mathrm{III}=-\frac{105\pi^2}{64}\frac{\rho}{k^7\mu^{9/2}}(1-\mu)\int_0^1du\int_{-u}^{u}dv\left[\frac{(u^2-v^2)(1-u)u}{(\omega-v^2)^{9/2}}\right], \tag{4.28}$$

$$\begin{aligned}\mathrm{IV}=&+\frac{3\pi^2}{64}\frac{1}{(k+i)^2}\frac{1}{(k^2\mu)^{5/2}}(1-2\mu)\int_0^1du\int_{-u}^{u}dv(u^2-v^2)\left[\frac{1}{(\omega-v^2)^{5/2}}-\frac{1}{(\gamma-v^2)^{5/2}}\right]\\&+\frac{15\pi^2}{128}\frac{1-2\mu}{(k^2\mu)^{7/2}}\int_0^1du\int_{-u}^{u}dv\left[\frac{(u^2-v^2)(1-u)}{(\omega-v^2)^{7/2}}\right]+\frac{15\pi^2}{64}\frac{1}{\rho^2}\frac{1}{(k^2\mu)^{7/2}}\int_0^1du\int_{-u}^{u}dv(u^2-v^2)[u^2(1-\mu)^2-\mu^2v^2]\\&\times\left[\frac{1}{(\omega-v^2)^{7/2}}-\frac{1}{(\gamma-v^2)^{7/2}}\right]+\frac{105\pi^2}{128}\frac{1}{k^7}\frac{1}{\mu^{9/2}}\int_0^1du\int_{-u}^{u}dv\left[\frac{(u^2-v^2)[u^2(1-\mu)^2-\mu^2v^2](1-u)}{(\omega-v^2)^{9/2}}\right].\end{aligned} \tag{4.29}$$

In Eqs. (4.26)–(4.29) the following symbols have been used:

$$\begin{aligned}&\mu=(1-\cos\theta)/2=\sin^2(\theta/2),\\&\qquad\text{where }\theta\text{ is the angle between }\mathbf{k}_0\text{ and }\mathbf{k}_n;\\&\rho=1+i/k;\\&\omega=u^2-(1/\mu)(u-\rho)^2;\\&\gamma=(u/\mu)[u(\mu-1)+(1+1/k^2)].\end{aligned} \tag{4.30}$$

The integrals (4.26)–(4.29), while elementary, are extremely laborious to compute. We shall restrict ourselves in what follows to computing the terms corresponding to the highest power of k in the result. Superficially, one might draw the conclusion that g_{0s} behaves like $1/k^7$ as $k\to\infty$, since the only dependence of k in the integrands arises from terms which go to zero as $k\to\infty$. However, more careful examination shows that the integrals have a singularity at $u=1$ when $k\to\infty$ and thus depend strongly on k.

The terms containing the highest powers of k in Eqs. (4.26)–(4.29) are those which have the highest powers of $(\omega-u^2)$ in the denominator. Accordingly, we will examine the k-dependence of Eqs. (4.21), (4.27), and the last line of (4.29). When we do this the validity of the above statement will become obvious.

First we carry out the v integrations and retain

terms only to $1/(\omega-u^2)^{5/2}$; we get

$$\mathrm{II}=-\frac{105\pi^2}{128}\frac{\rho^2}{k^7}\frac{1}{\mu^{9/2}}\int_0^1 du u^2(1-u)\left\{\frac{2}{7}\frac{u}{\omega(\omega-u^2)^{7/2}}+\frac{12}{35}\frac{u}{\omega^2(\omega-u^2)^{5/2}}+\cdots\right\}$$
$$-u(1-u)\left\{\frac{2}{7}\frac{1}{(\omega-u^2)^{7/2}}+\frac{2}{35}\frac{1}{\omega(\omega-u^2)^{5/2}}+\cdots\right\}$$
$$=-\frac{105\pi^2}{128}\frac{\rho^2}{k^7}\frac{1}{\mu^{9/2}}\left[\int_0^1\frac{4}{35}\frac{(u^3-u^4)du}{\omega^2(\omega-u^2)^{5/2}}+\text{terms } O((\omega-u^2)^{-3/2})\right]. \tag{4.31}$$

Similarly,

$$\mathrm{III}=-\frac{105\pi^2}{64}\frac{\rho}{k^7}\frac{1}{\mu^{9/2}}(1-\mu)\left[\int_0^1\frac{4}{35}\frac{(u^4-u^5)du}{\omega^2(\omega-u^2)^{5/2}}+\text{terms } O((\omega-u^2)^{-3/2})\right] \tag{4.32}$$

and

$$\mathrm{IV}=-\frac{105\pi^2}{128}\frac{1}{k^7}\frac{1}{\mu^{9/2}}(1-\mu)^2\left[\int_0^1\frac{4}{35}\frac{(u^5-u^6)du}{\omega^2(\omega-u^2)^{5/2}}+\int_0^1\frac{u-u^2}{(\omega-u^2)^{5/2}}du+\text{terms } O((\omega-u^2)^{-3/2})\right]. \tag{4.33}$$

If one now substitutes the value of ω from Eq. (4.30) into Eqs. (4.31)–(4.32) one obtains integrals of the form

$$\int_0^1\frac{du(u^n-u^{n+1})}{(u-u_1)^2(u-u_2)^2(u-\rho)^5}, \tag{4.34}$$

where

$$u_1=\frac{\rho}{1-\mu}(1-\sqrt{\mu}),\quad u_2=\frac{\rho}{1-\mu}(1+\sqrt{\mu}).$$

If $k^2\mu\gg1$, then the highest power of k arising from terms of the form (4.34) comes from the upper limit when $(u-\rho)^{-n}$ is integrated after Eq. (4.34) is decomposed into partial fractions. In this case, the k-dependence of the other factors can be neglected. However, if $k^2\mu\gtrsim1$, then there will be a strong k-dependence arising from terms of the form $(u-u_1)^{-m}$ or $(u-u_2)^{-m}$. Instead of investigating this explicitly, we will determine the k-dependence of g_0 in this range by evaluating Eqs. (4.26)–(4.29) for $\mu=0$.

After decomposing Eqs. (4.31) to (4.33) into partial fractions, we consider only terms of the form $(u-\rho)^{-5}$ and $(u-\rho)^{-4}$. If these are integrated we get

$$\mathrm{II}+\mathrm{III}+\mathrm{IV}_4=\frac{\pi^2}{128}\frac{1}{k^4}\frac{1}{\mu^2}[3-\mu^2],\quad k^2\mu\gg1. \tag{4.35}$$

To find the highest power of k when $\mu=0$, it is most convenient to return to Eqs. (4.26)–(4.29) and to set $\mu=0$ there. Again we find that II, III, IV_4 contribute to the highest power of k; the result is

$$\mathrm{II}+\mathrm{III}+\mathrm{IV}_4=5\pi^2/128;\quad \mu=0. \tag{4.36}$$

Inserting Eqs. (4.20) and (4.21) into the expression for g_{0s}, we have

$$g_{0s}=\frac{1}{k^4}\left[\frac{3}{\mu^2}-1\right],\quad k^2\mu\gg1; \tag{4.37}$$

and

$$g_{0s}=-5,\quad \mu=0. \tag{4.38}$$

Corinaldesi and Trainor[6] have computed the elastic exchange scattered cross section, with $2(1/r_1-1/r_{12})$ as the perturbation using Eq. (2.4). Their result, to first approximation, is

$$g_{0s}=\frac{16}{(1+k^2)^3}-\frac{1}{(1+k^2)^3}\left[\frac{k^4}{(1+k^2\mu)^2}+2k^2\left[\frac{\tan^{-1}(k^2\mu)^{1/2}}{(k^2\mu)^{3/2}}-\frac{1}{[k^2\mu(1+k^2\mu)]^2}\right]-\frac{3+2k^2\mu}{(1+k^2\mu)^2}+\frac{2}{(k^2\mu)^{1/2}}\tan^{-1}(k^2\mu)^{1/2}\right]. \tag{4.39}$$

In order to compare this with our result [Eqs. (4.37) and (4.38)], we select the highest power of k from Eq. (4.39), and this gives

$$g_{0a}\cong\frac{1}{k^6}\left(16-\frac{1}{\mu^2}\right),\quad k^2\mu\gg1; \tag{4.40}$$

and

$$g_{0a}=-1/k^2,\quad \mu=0. \tag{4.41}$$

5. DISCUSSION

If we were to compare the symmetric and the asymmetric perturbation procedures, we would expect that the former would give results closer to the exact solution than those obtained by the asymmetric method. There are two reasons for this. First, the symmetric perturbation method includes more of the interaction in the unperturbed Hamiltonian. Second, the formula given for the exchange scattered amplitude, using the asymmetric perturbation procedure, gives a result different from zero even when the interaction between the two electrons vanishes, whereas the symmetric perturbation does give a zero result under these circumstances. This would indicate that the first-order approximation is much poorer in the asymmetric method in the symmetric one.

The results for the two different approximations can be compared by considering Eqs. (4.37), (4.38), (4.40), (4.41), and (3.16). The meaning of these equations can be stated as follows: The direct-scattered amplitude is the same to the highest power of the energy when one uses either perturbation scheme. The fact that more of the interaction is included in the unperturbed Hamiltonian results in some additional terms, but they vanish as $k\to\infty$. The results for exchange scattering, however, exhibit quite different energy dependences in the limit of infinite k in the two different procedures. Since, as has been indicated above, the results using the asymmetric perturbation procedure are obviously incorrect, we feel that the results for exchange scattering that we have obtained must be more accurate.

In three-body scattering problems such as the scattering of neutrons by deuterons, where the masses of all three bodies are comparable, one cannot employ the symmetric perturbation procedure, and whatever calculations have been made in the Born approximation have used the asymmetric scheme. If the conclusions arrived at here could be extrapolated to these problems, there must be some doubt as to the validity of the results already obtained for those cases where exchange scattering plays a significant role. For such problems, other approximation methods should be investigated.

The direct-scattered amplitude in the case of elastic scattering by hydrogen atoms is so much larger than the exchange-scattered amplitude, that there is no possibility of verifying experimentally the theoretical difference between the results of the symmetric and the asymmetric methods.

There is a possibility, however, of checking experimentally the effectiveness of the type of perturbation method presented here. Corinaldesi and Trainor[6] have shown that some inelastic scattering processes have approximately the same energy dependence for the direct- and exchange-scattered amplitude. If the symmetric perturbation theory will alter substantially the exchange-scattered term for this process, then an experiment measuring the cross section for this process will enable us to choose between the two formulations. This investigation is being undertaken.

6. ACKNOWLEDGMENTS

This research was undertaken as a result of a conversation with Professor Walter Kohn. Professor Wilhelm Magnus has helped with the hypergeometric functions and with some other mathematical questions.

APPENDIX

We carry out here the detailed evaluation of the integral (4.24) because it exhibits not only the method of Feynman,[11] but also illustrates how we handle the additional complication of differentiating with respect to k_0 and k_n. We repeat Eq. (4.24) here:

$$\frac{\text{III}}{k+i}=-\frac{1}{2}\frac{\partial}{\partial k_0}4!\int\frac{x_1x_3\delta(x_1+x_2+x_3-1)dx_1dx_2dx_3d\mathbf{K}}{\{[K^2-(k+i)^2]x_1+[1+K^2+k^2-2(\mathbf{K},\mathbf{k}_0)]x_2+[1+|\mathbf{K}-\mathbf{k}_n|^2]x_3\}^5}$$

$$-\frac{1}{2}\frac{\partial}{\partial k_n}4!\int\frac{x_1x_2\delta(x_1+x_2+x_3-1)dx_1dx_2dx_3d\mathbf{K}}{\{[K^2-(k+i)^2]x_1+(1+|\mathbf{K}-\mathbf{k}_0|^2)x_2+[1+K^2-2(\mathbf{K},\mathbf{k}_n)+k^2]x_3\}^5}. \tag{A.1}$$

Now we let $\mathbf{P}=\mathbf{K}-\mathbf{k}_0x_2-\mathbf{k}_nx_3$ and carry out the integration with respect to x_1. Then we differentiate with respect to k_0 and k_n to obtain

$$\frac{\text{III}}{(k+i)}=-5!k\int\frac{(1-(x_2+x_3))x_2x_3(x_2+x_3)(1+\xi)dx_2dx_3d\mathbf{P}}{(P^2+\Theta^2)^6} \tag{A.2}$$

where $\xi=\cos\theta$

$$\Theta^2=4k^2x_2x_3\mu-[k(x_2+x_3)-(k+i)]^2.$$

We now can carry out the integrations with respect to $\mathbf{P}$ immediately, to obtain

$$\text{III}=-\frac{105\pi^2}{8}k(k+i)(1-\mu)\int_0^1dx_2\int_0^{1-x_2}dx_3\frac{(x_2+x_3)(1-(x_2+x_3))x_2x_3}{[4k^2x_2x_3\mu-(k(x_2+x_3)-(k+i))^2]^{9/2}}. \tag{A.3}$$

Now let $x_2+x_3=u$, $x_2-x_3=v$. Then

$$\text{III}=-\frac{105\pi^2}{64}\frac{\rho}{k^7\mu^{9/2}}(1-\mu)\int_0^1du\int_{-u}^{u}dv\frac{(u^2-v^2)(1-u)u}{(\omega-v^2)^{9/2}}. \tag{A.4}$$

This is the result given in the text.

Optical Studies of Radioactive Mercury*

F. BITTER, S. P. DAVIS, B. RICHTER,† AND J. E. R. YOUNG
Department of Physics, Research Laboratory of Electronics and Spectroscopy Laboratory, Massachusetts Institute of Technology, Cambridge, Massachusetts

(Received July 6, 1954)

A technique has been developed for studying the hyperfine structure of the resonance radiation of mercury. A single Zeeman component of the 2536 A line of Hg^{198} is used as a variable-frequency monochromatic light source, and the field strength applied to the arc lamp to produce resonance absorption in a resonance lamp is a measure of the resonance frequency. Natural mercury, and radioactive mercury produced by bombarding gold with 15-Mev deuterons were investigated in this way and also (by means of an echelle spectrograph) in the emission spectrum of an electrodeless discharge. Several observed lines have not been conclusively identified.

The magnetic moment of Hg^{197} is 4 percent greater than that of Hg^{199}. The isotope shift of isotopes with even mass number decreases with decreasing mass number. This effect may be due in part to the increasing quadrupole moment with neutron deficiency in these isotopes.

THE work reported below is part of a general program of exploration of atomic energy levels in search of information about nuclear structure that is revealed by the interaction of the nucleus with the atomic electrons. For the past year and a half we have been developing methods and techniques applicable to mercury because of the ease with which the famous ultraviolet resonance line at 2537 A and other lines originating on various metastable levels may be excited, because hyperfine structure and isotope shift are readily measurable, and because a whole series of radioactive isotopes having half-lives of the order of hours are available for investigation. We had hoped, by this time, to have obtained more data, and more accurate data, than is reported in this paper. It has now become quite clear that to reach many of our objectives we shall have to construct new apparatus, which will incidentally facilitate the observations in which we have been engaged. It was therefore decided to report our progress and to summarize our experiences and results at this stage.

As a first project, we set ourselves the task of investigating the hyperfine structure of the resonance radiation of radioactive isotopes of mercury. Resonance radiation was chosen because, in principle at least, it could be investigated with only enough atoms to fill a small cell at some very low pressure, whereas other spectral lines would require an emission spectrum produced in an electrical discharge that might drive the mercury into the cell walls, and thus require more atoms to produce observable effects for many hours of observation. Moreover, a "magnetic scanning" technique (described below), ideally suited to the investigation of the hyperfine structure of very small quantities of mercury, was being developed in our laboratory.[1] We therefore set out, first of all, to establish our requirements by studying the hyperfine structure of the resonance radiation of natural mercury.

HYPERFINE STRUCTURE OF RESONANCE RADIATION OF NATURAL MERCURY

A summary of experimental data on hyperfine structure and isotope shift, compiled by Brix and Kopfermann, is contained in a section of the 1952 edition of the Landolt-Börnstein tables in the volume dealing with nuclear data. This is an excellent guide to the abundant literature on the subject. The material dealing with the resonance radiation of mercury may be divided into two main categories. The first relates to emission spectra analyzed by conventional optical equipment. The outstanding reference to work of this kind dealing with the resonance line of mercury is by Schüler and Keyston.[2] The second category is concerned with absorption spectra. Mrozowski[3] showed that if resonance radiation from a natural mercury lamp is passed through a mercury absorption filter in a strong magnetic field, all but one of the hyperfine structure components are removed from the beam. A variety of investigators, particularly Buhl,[4] used this single line to investigate the hyperfine structure of mercury in a very ingenious way. It was allowed to fall on a resonance lamp containing natural mercury in a magnetic field. As the field was varied, the frequencies of various Zeeman components of different hyperfine structure lines successively reached the frequency of the single incident line. Whenever this condition was obtained, resonance radiation was removed from the incident beam and was reradiated in all directions. From a knowledge of the fields for which this occurred, the zero field pattern could be reconstructed by using the available auxiliary data about the approximate locations and g factors of the various lines and levels.

* This work was supported in part by the Signal Corps; the Office of Scientific Research, Air Research, and Development Command; and the Office of Naval Research; in part by a U. S. Atomic Energy Commission Contract.

† Work performed while a National Science Foundation fellow.

[1] Bitter, Plotkin, Richter, Teviotdale, and Young, Phys. Rev. **91**, 421 (1953).

[2] H. Schüler and J. E. Keyston, Z. Physik **72**, 423 (1931).

[3] S. Mrozowski, Acad. Polonaise Sci. et Lettres Bull. No. 9–10A, pp. 464, 1930, Bull. No. 6A, pp. 489, 1931.

[4] O. Buhl, Z. Physik **109**, 180 (1938); and **110**, 395 (1938).

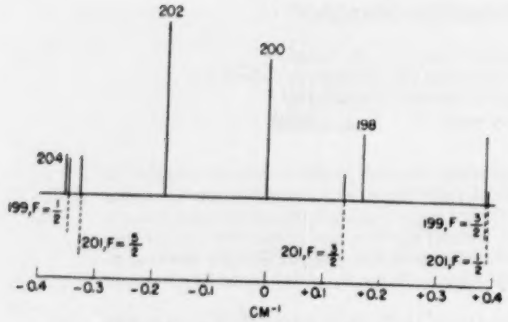

FIG. 1. The hyperfine structure of $\lambda = 2537$ A of mercury.

Brix and Kopfermann conclude from a review of all available experimental data that the best present estimate for the structure of the 2537 A line of mercury is that shown in Fig. 1. We shall return to a comparison of these results with our own in the last section of this paper, and content ourselves at this point with a qualitative review of the main features.

The levels involved in the emission of the resonance line are the $^3P_1$ excited state and the $^1S_0$ ground state. The ground state has no electronic magnetic moment and is therefore always single, regardless of the nuclear angular momentum. Since mercury nuclei contain an even number of protons, nuclei with an even mass number will contain an even number of neutrons and may be expected to have $I = 0$. The resonance lines from these even isotopes will therefore be single lines. The positions of these lines for mass numbers 198, 200, 202, and 204 are shown in Fig. 1. Hg^{196} is present to only 0.15 percent and had not been observed in natural mercury. The height of the vertical lines for the even-even isotopes is proportional to the abundance of the isotope. Hg^{199} has a spin $I = 1/2$, and the excited state splits into two, with $F = 1/2$ and $3/2$. The resulting two lines are shown, one near each end of the pattern, in Fig. 1. Hg^{201} has a nuclear spin of $3/2$, and the hyperfine structure pattern contains the three lines shown. The typical observed structure consists of five lines of comparable intensity four of which are approximately equally spaced, the fifth on the short wavelength side being somewhat more separated from its neighbor. The structure of the unresolved lines is inferred from data on other lines, and from Zeeman effect investigations.

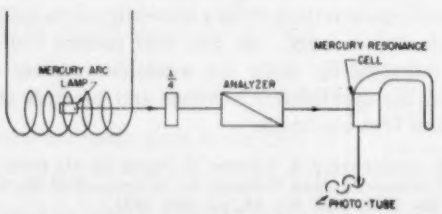

FIG. 2. Diagram of the apparatus used for magnetic scanning.

DESCRIPTION OF APPARATUS USED IN MAGNETIC SCANNING EXPERIMENTS

The main features of our apparatus are shown schematically in Fig. 2. A mercury arc lamp containing only the 198 isotope is placed in a magnetic field, and a beam is formed in the direction of the field. The Zeeman effect for an even isotope consists of a classical triplet with only the two outer circularly polarized components radiated in the direction of the beam. By means of a quarter-wave plate and a suitably oriented analyzing prism, either one of the two frequencies present may be suppressed. The apparatus provides a single line of variable frequency, the frequency being determined by the orientation of the prism and the magnitude and sense of the magnetic field applied to the arc, or scanning field, as we shall call it. This light is allowed to fall on a resonance lamp containing the sample to be investigated, and the emission of resonance radiation is detected with a galvanometer and photomultiplier. The frequency at which resonance is observed may then be calculated from the strength of the scanning field and the known g factor of the even isotopes of mercury.

The arc consisted of a vycor tube, approximately 5 mm in diameter, containing argon at a pressure of a few millimeters and the Hg^{198}, and was excited by means of a 200-Mc/sec oscillator to give an electrodeless discharge. Filled tubes approximately 6 inches long were supplied by Baird Associates. They were cut with a torch into two or three pieces in order to fit into the magnet used; it was found that all the pieces could be used as light sources. Since some of these pieces must have contained mostly vapor, and little if any condensed mercury, this was an indication that an electrodeless discharge of the kind used requires very little excess mercury. Abnormal line shapes were occasionally encountered. These were presumably due to the self-reversal of the resonance line. They were completely eliminated by water-cooling the arc.

The scanning magnet was an air-core solenoid having an inside diameter of 4.5 inches and being capable of producing fields up to 50 kilogauss.[5] Since the field in this magnet is not exactly proportional to the magnet current, and depends on the temperature distribution in the magnet, it was monitored by a Laboratory for Electronics nuclear resonance magnetometer. Although this magnet was far from ideal for our purpose, it was used for this preliminary work. The field fluctuated irregularly, sometimes by as much as 50 gauss. It was sufficiently uniform to see resonances on an oscilloscope only when the probe was within an inch of the center. For the most precise measurements the probe was kept at the center, and the arc lamp was placed $1\frac{1}{8}$ inches above the probe. In this way the relative magnitudes of the fields used could be accurately determined. The absolute magnitude at the lamp was estimated to be

[5] F. Bitter, Rev. Sci. Instr. **10**, 373 (1939).

2.5 percent lower than the field at the magnetometer probe.

The light from the lamp was focused into a parallel beam by means of a quartz lens, and then passed through a crystalline quartz quarter-wave plate, and a Glazebrook prism cemented with glycerine. A small brass rod, not shown in Fig. 2, could be inserted into this beam to scatter light into an auxiliary photo tube to monitor the lamp intensity.

The plane-polarized monochromatic beam illuminated a quartz cell placed between the poles of a small iron core magnet capable of producing fields up to 10 kilogauss. This made possible the investigation of the Zeeman effect of the resonance radiation. The resonance lamp cells were made for us by the Neider Fuzed Quartz Company. They were in the shape of small cubes having edge lengths ranging from 0.5 inch to 1 inch. One face was drawn out into a tail and could be immersed in a low-temperature bath. Although these lamps usually behaved satisfactorily, anomalous line shapes attributable to causes that we have not investigated in detail were occasionally observed. They may have been associated with the presence of condensed mercury at the lamp faces, since the procedure of flaming the faces of the lamp and insuring that condensed mercury remains in the tail seems to have cured these difficulties.

In some of the first lamps that we filled with radioactive mercury, the resonance radiation disappeared even though they had appeared to be quite satisfactory immediately after filling. Flaming sometimes made the resonance radiation disappear completely. This effect was unquestionably the result of some kind of chemical cleanup associated with impurities retained in the liquid air traps used to hold the mercury during the filling process while the cells were being evacuated. It was found that the mercury could be selectively held on clean gold foil at room temperature during the pumping process. Then, after the cell was sealed off, the mercury could be removed from the gold by gentle heating. The cell was, of course, carefully baked out before filling. These precautions sufficed to remove the troubles with chemical cleanup of the resonance cells.

The resonance radiation from these cells was either focused on an IP28 photomultiplier by means of another quartz lens, or was "conducted" to it by means of a glass tube, 0.5 inch in diameter, silvered on the inside. The photomultiplier current could be either measured directly with a galvanometer, or balanced by the current from the auxiliary photomultiplier, mentioned before, in an optical bridge.[6] For quick but less accurate observations the potential across a shunt carrying the scanning magnet current was applied to the horizontal plates of an oscilloscope with a dc amplifier and the vertical plates to a resistor carrying the photomultiplier current. This could be done, since the magnet power supply was not grounded. The field could then be varied from +10 kilogauss to −10 kilogauss in a half-minute or so, and the oscilloscope trace photographed with a Land camera, yielding pictures of the hyperfine structure of the resonance radiation like that shown in Fig. 3. This was an extremely useful technique in establishing interesting conditions for more detailed study with the galvanometer.

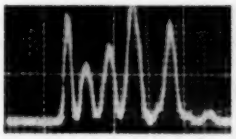

FIG. 3. Oscilloscope trace of the hyperfine structure of the resonance radiation of natural mercury.

In some of our experiments it was found helpful to eliminate the light caused by fluorescence of the quartz cell by placing a Corning 9863 filter in front of the photomultiplier.

TYPICAL RESULTS

Typical results obtained with the apparatus described above are shown in Fig. 4. The upper curve is for natural mercury, and was obtained with the resonance cell at room temperature. The five main peaks expected

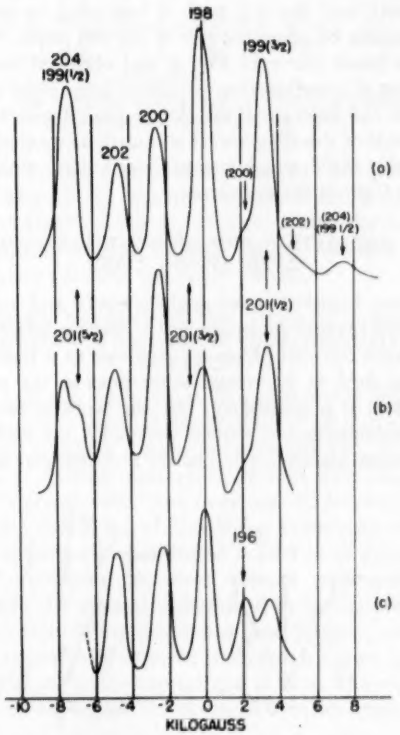

FIG. 4. The hyperfine structure of the resonance radiation from three samples of mercury having different isotopic compositions.

[6] O. Oldenburg and H. P. Broida, J. Opt. Soc. Am. **40**, 381 (1950).

are clearly shown. In addition, there are three small partly resolved peaks on the right side of the figure. These are also visible in the oscilloscope trace in Fig. 3. They are attributable to the fact that the light transmitted by the quarter-wave plate is not completely plane-polarized, and the Glazebrook prism, consequently, does not quite completely eliminate one of the two radiated frequencies. They are reflections of the peaks to the left of the central 198 peak.

The maximum of the 198 peak is slightly to the left of the zero field line. This is presumably caused by the presence of the small unresolved 201(3/2) peak.

The positions of these peaks will be discussed in the last section of this paper, their magnitude in the next section, in which we take up the separation and identification of overlapping peaks. The width of these lines at half maximum is about 1 kilogauss or, using a conversion factor derived further on, 0.063 cm^{-1}. Their Doppler width at room temperature would be 0.035 cm^{-1}.

The middle curve in Fig. 4 was obtained with a sample of mercury enriched in the 201 isotope, furnished by the Atomic Energy Commission. Its composition was 37.3 percent even isotopes, 4.76 percent Hg^{199}, and 57 percent Hg^{201}. The corresponding percentages for natural mercury are 69.8 percent, 17.0 percent, and 13.2 percent. The 5/2 peak of 201 on the left is quite apparent, and the 3/2 peak is beginning to make an appreciable bulge on the side of the 198 peak.

The lower curve in Fig. 4 was obtained from the residues of a radioactive resonance lamp some months after it had been prepared. A new peak appears on the right side of this diagram. It is caused, as we shall show, by stable Hg^{196}, which was produced along with radioactive Hg^{197} in the cyclotron.

SEPARATION AND IDENTIFICATION OF OVERLAPPING LINES

It was hoped that we might identify and locate all the lines present by producing a Zeeman effect in the resonance cell and following each line as a function of applied field as it crossed other lines in the pattern. This still is a possibility, but the work is extremely time-consuming and tedious except for the isotopes of even mass number. The central π-component of these lines is undisplaced by a magnetic field, whereas the π-components of the lines resulting from the odd isotopes are not independent of field strength. By using incident radiation polarized with its electric vector parallel to the auxiliary Zeeman field, it is possible to be certain that a line comes from an isotope of even mass number, and second, to remove any overlying lines by a suitable choice of field strength. This was done in identifying and measuring the position of the line due to the even isotopes.

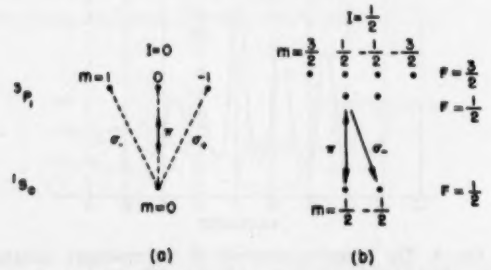

FIG. 5. Transition diagram for the even isotopes and Hg^{199}.

The lines from isotopes of odd mass number are more difficult to handle. If the lines to be measured are well separated from their neighbors, it is, of course, possible to split them, count the number of components, and measure their g factor. But when the lines are faint and are covered by other lines, it was found difficult to carry out such a procedure with certainty. At one point we hoped to simplify the patterns to be studied by excluding some lines on the basis of their polarization. Thus, for example, if we excite one of the even isotopes with light polarized parallel to the splitting field, this will necessarily put the atom in an excited state with $m=0$, and the only possible radiative transition back to the ground state is the correspond-transition shown in Fig. 5(a). If we exclude the π component in the resonance radiation either by means of an analyzing prism, or by observing in the direction of the field, we should expect to find the resonance radiation suppressed, particularly if we use sufficiently low vapor pressures so that depolarizing collisions are avoided. For the isotopes of odd mass number, on the other hand, exciting with π radiation should not eliminate σ_- resonance radiation, since there are two possible transitions to the ground state, one π and one σ_- as shown in Fig. 5(b). The expected effect was in fact not realized to a sufficient extent to make this scheme practically useful for selectively suppressing the lines caused by the even isotopes.

An aspect of our results not yet brought out is that the relative intensities of the various peaks are a function of the vapor pressure determined by the temperature of the tail of the lamp. Each peak has its maximum height at some temperature which is different for the various peaks. As pointed out by Mrozowski,[7] geometrical factors may be very important in determining the temperature at which the maximum is obtained. We have made no investigation of this point.

A particularly marked instance of effects resulting from this maximum in the intensity of the resonance radiation was observed in a cell containing 90 percent Hg^{204}. This sample was also supplied to us by the U. S. Atomic Energy Commission. At room temperature there was no 204 peak at all, but all of the other peaks, caused by minor amounts of the other isotopes present, showed up clearly. When the tail of the lamp was cooled to −30°C, the 204 peak alone was present, and the

[7] S. Mrozowski, Phys. Rev. 93, 641 (1954).

others were too faint to observe. Unfortunately, this selective suppression of peaks is effective only when concentration differences approach 100 percent.

The problem of isolating and identifying overlapping peaks resulting from isotopes of odd mass number is now being worked on, and we hope to report on practical usable methods in the not too distant future.

PREPARATION OF RADIOACTIVE MERCURY

The mercury isotopes were prepared by bombarding a 4 mil thick gold foil with 15-Mev deuterons in the M.I.T. cyclotron. The thickness of the gold foil was such that the energy of the deuterons after traversing the foil would be reduced to near the threshold of the reaction $Au^{197}(d,2n)Hg^{197}$. This energy-loss requirement on the gold thickness was set to reduce Hg^{198} contamination produced in the reaction

$$Au^{197}(d,p)Au^{198}\rightarrow\beta^{-}+Hg^{198}$$

for the cross section for this reaction is well below its maximum value at the threshold of the $(d,2n)$ reaction, and decreases with increasing energy.

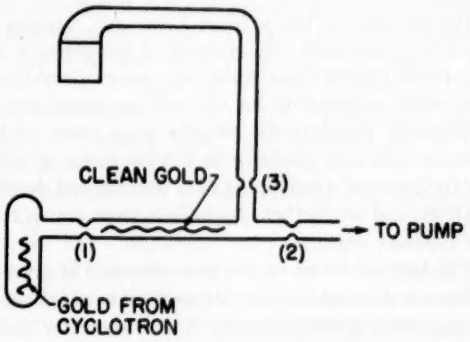

FIG. 6. The distillation apparatus used to separate radioactive mercury from gold.

Before irradiation, mercury surface contamination was removed from the gold by heating in a hydrogen atmosphere for one and a half hours at a temperature of 900°C. As soon as the gold had cooled, it was placed in the cyclotron.

The gold was bombarded with deuterons at a beam current of 40 μa for a period of 12 hours. An additional period of four hours was allowed for the very intense, short-lived activity in the aluminum target-backing to die out. The gold was then cut from the target and placed in the quartz vacuum system illustrated in Fig. 6. After the vacuum system had been pumped down, the target gold was heated to just above its melting point with an induction heater, and the mercury distilled off. The mercury was then caught on the surface of another piece of clean gold which had been previously heated to drive out occluded gases and placed in the vacuum system. The system was then sealed off at point (1),

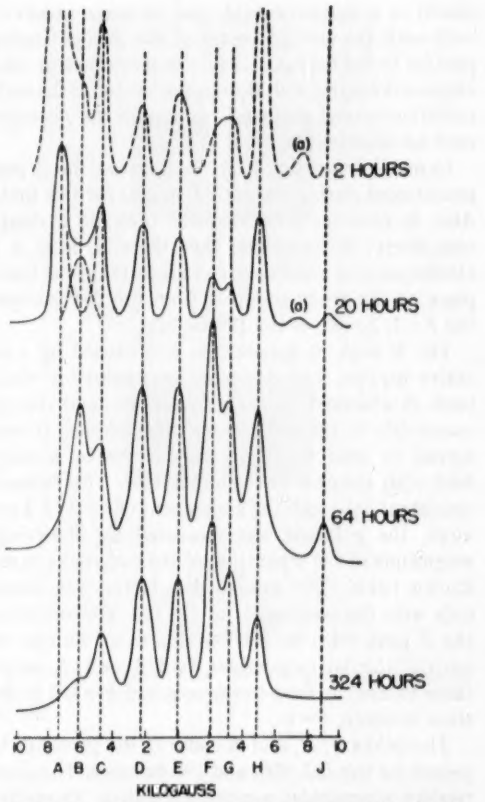

FIG. 7. The hyperfine structure of the resonance radiation of radioactive mercury at various times.

allowed to pump down, and then sealed off at point (2). The resonance cell was then placed in liquid air, and the "catching" gold gently heated to drive the mercury off its surface and into the cell. The cell was then sealed off at point (3), and was ready for use.

HYPERFINE STRUCTURE AND ZEEMAN EFFECT OF RESONANCE RADIATION OF RADIOACTIVE SAMPLES

The first run with radioactive mercury in February 1953 was successful. A large number of curves were recorded, of which a representative selection is shown in Fig. 7. At least nine resolved lines were observed. About a dozen runs have been undertaken since that time with the object of identifying these various lines. Many of these runs yielded no results at all because of faulty techniques. However, enough work has been done with the apparatus described to indicate that the point of diminishing return has been reached, and that a new approach is required if further progress is to be made without undue expenditure of time. The results of our efforts to identify the observed lines are summarized below.

The procedure used to identify the peaks was to observe the splitting when the resonance lamp was

placed in a magnetic field, and to make observations both with the electric vector of the incident radiation parallel to the field (i.e., with the π component used for illumination) and with the electric vector of the incident radiation normal to the field (i.e., with the σ component used for illumination).

In none of the runs after the first was the A peak as pronounced during the early hours as for this first run. Also, in none of the subsequent runs did it disappear completely. We conclude that there is, here, a peak attributable to a radioactive isotope falling at the same place as the peaks resulting from the 204 isotope and the $F=1/2$ peak of the 199 isotope.

The B peak is, apparently, also caused by a radioactive isotope, since it comes at a point for which no peak is observed in natural mercury and disappears completely in the spectrum of the residues. It was observed to split into two components in a magnetic field with either π or σ illumination. This behavior is consistent only with the assignment of $F=1/2$. Furthermore, the g factor was measured by observing the magnitude of the separation of the two peaks in several known fields. The measured g factor was consistent only with the assignment of $F=1/2$. We conclude that the B peak must be attributable to an isotope with a nuclear angular momentum $I=3/2$, or $1/2$, since only these values can lead to the required $F=1/2$ in the $^3P_1$ state in which $J=1$.

The peaks C, D, and E come at the places to be expected for the 202, 200, and 198 isotopes. The changing relative magnitudes are not enough in themselves to justify assigning any of these peaks to a radioactive isotope. The G peak comes at the point where the 199 $F=3/2$ peak is to be expected. If the G peak is from 199, it is difficult to understand the absence of the corresponding $F=1/2$ peak at A in the 324-hour curve of Fig. 7. If it is not from the 199 isotope, then it is hard to understand the presence of the 202 and 200 peaks, which could not possibly have been made by bombarding Au^{197} with deuterons and must therefore be caused by contamination. We must be satisfied for the present with the negative statement that there is no conclusive evidence for the presence of radioactive peaks at C, D, E, and G, although it is perfectly possible that these peaks may completely or partly overlap peaks due to radioactive isotopes.

Peak F is surely attributable, at least in part, to the stable isotope 196. It is unchanged in strong fields when π illumination is used and is split into two components when σ illumination is used. It is found in the spectra of the residual vapor after radioactivity has decayed, as shown in Fig. 4(c). It must therefore come from a stable isotope with $I=0$, and this can only be the isotope 196.

The peak at H is caused by a radioactive isotope. It is split into two components by a magnetic field when π illumination is used, but when σ illumination is used two additional components appear. This is consistent with the assignment of $F=3/2$, as is the measured value of the g factor. We conclude that this line must be due to a nucleus with $I=5/2$, $3/2$, or $1/2$.

The splitting of the peak at J was too complex to make an assignment. The number of components was apparently greater than two or four, which should have been easily recognizable for this well-separated line.

Although photographic records were made of the Zeeman splittings produced in a wide range of fields, the confusion of overlapping lines discouraged detailed analysis, and no further conclusions were drawn from the available data.

The location of all of the lines observed is given in Table I in the next section. Although most of the observations were recorded simply as galvanometer deflections for a given magnet current, a series of measurements, particularly for the even isotopes, was made in which the deflection was observed as a function of the proton resonance frequency near the intensity maxima. The optical frequency difference Δf in cm^{-1} is then given in terms of the observed proton resonance frequency f_p measured in cycles per second by the relation

$$\Delta f=\frac{g_{Hg}}{g_p}\frac{M_p}{m}\frac{f_p}{c}.$$

The values of the constants used in applying this relation were 1836 for the ratio of the mass of the proton to that of the electron, 5.585 for the gyromagnetic ratio of the proton,[8] 3.00×10^{10} cm/sec for the velocity of light, and 1.484 for the g factor of the $^3P_1$ state of the even isotopes of mercury.[9] Our results are probably correct to within approximately ±3 percent.

TABLE I. Summary of results. The numbers listed are the displacements of the various lines observed from the Hg^{200} line in cm^{-1}. The numbers given are estimated to be reliable to ±3 percent.

Line	Position according to Brix and Kopfermann	Present investigation
A		−0.343
204	−0.354	−0.343
199(1/2)	−0.350	−0.343
201(5/2)	−0.329	−0.294
197(1/2)		−0.254
202	−0.179	−0.171
201 c.g.	−0.054	
200	0	0
201(3/2)	+0.136	
199 c.g.	0.143	0.136
198	0.168	0.157
197 c.g.		0.245
196		0.293
199(3/2)	0.389	0.376
201(1/2)	0.390	
197(3/2)		0.495
J		0.788

[8] Sommer, Thomas, and Hipple, Phys. Rev. 82, 697 (1951).
[9] J. Brossel and F. Bitter, Phys. Rev. 86, 308 (1952).

SPECTROGRAPHIC STUDY OF LINE 4047 OF RADIOACTIVE SAMPLES

In connection with the work on radioactive mercury 197, it was thought worth while to examine other levels than those connected with the 2537 A line in order to confirm the values of nuclear spin and magnetic moment as determined from magneto-optic measurements on this line. Since the emission spectrum of mercury was easily obtainable in an electrodeless discharge, and a spectrograph of fairly high resolution was available, this method of attack was tried. The line at 4047 A was chosen because it was due to the relatively simple transition $^3P_0-^3S_1$ giving one line for the even isotopes, two lines ($F=1/2$ and $3/2$) for 199, and three lines ($F=1/2$, $3/2$, $5/2$) for 201. The hfs of the line, as given by Schüler and Keyston.[2]

The source was a sealed quartz tube 3 mm by 30 mm, containing the radioactive mercury and argon gas at approximately 7 mm Hg pressure. As determined from the counting rate, there were initially about 2×10^{15} atoms, or 0.5 μg, of radioactive mercury present. Excitation was provided by a 10-cm wavelength magnetron. The tube was placed inside the center conductor at the open end of a coaxial pipe and was cooled with air.

The spectrograph used was a 200 groove/inch Bausch and Lomb echelle, in a Wadsworth mounting.[10] At 4047 A, it has a theoretical resolving power of 330 000 and a plate factor of 0.4 A/mm. All exposures were taken on Eastman type IV-0 spectroscopic plates. Times varied from one to 30 minutes.

Spectrograms were taken beginning about 12 hours after cyclotron bombardment of the gold foil had stopped. For comparison purposes, the spectra of mercury 198 and ordinary mercury were placed on opposite sides of the spectrum of the radioactive sample, overlapping slightly. When first excited, the tube showed the mercury spectrum as well as C_2 and CN bands, as observed in a visual spectroscope. The intensity of the mercury lines increased and that of the impurities decreased as the temperature became higher. The discharge did not fill the tube, unlike all of the previous ones containing ordinary mercury. One attempt was made to apply a magnetic field, but it was unsuccessful because the field extinguished the discharge.

Two spectrograms of the line at 4047 A are shown in Fig. 8. One was taken within one half-life of mercury 197 after bombardment had stopped, and the other at about six half-lives. The upper line in each case is due to the radioactive sample, and the lower to ordinary mercury. Figure 8(b) clearly shows no appreciable difference in the two lines, indicating that the residue from the radioactive sample is ordinary mercury. Figure 8(a), however, shows two important differences

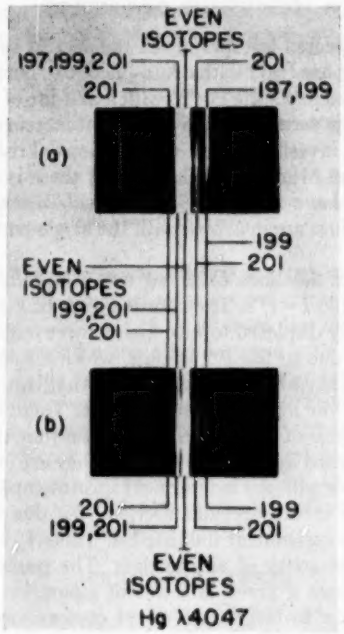

FIG. 8. Photograph of the hyperfine structure of the resonance radiation of two samples of mercury having different isotopic compositions.

in the lines. The relative intensities of the hfs components are not the same, and one component is shifted away from the center, toward longer wavelengths. These spectrograms are consistent with the assumption that the radioactive sample contains some ordinary mercury as a contaminant, and that 197 has a spin of 1/2 (the same as 199) and a magnetic moment slightly greater than 199. The hfs components belonging to 201 and the even isotopes coincide in each photograph, as they should. Only one of the components of 197 is more intense than, and appears to be shifted relative to, those of 199, because the other is overexposed and is not resolved from a component of 201.

Since 199 is still present in the radioactive sample, the center of gravity of the components (slightly different if 197 alone were present) is shifted in the direction of smaller over-all splitting. The measured ratio μ_{197}/μ_{199} is therefore smaller than the true ratio. Measurement and comparison of the relative spacings of the hfs components of 197 and 199, on two different plates, give the ratio $\mu_{197}/\mu_{199}=1.033\pm0.016$.

Spectrograms of other strong lines in the mercury emission spectrum were taken at the same time. They were not used for measurement because of the complexity of their hfs components. The 2537 A line was heavily over-exposed on most plates, and in addition did not have narrow lines, probably because of the high temperature at which the tube was operated.

[10] Harrison, Archer, and Camus, J. Opt. Soc. Am. **42**, 706 (1952). Harrison, Davis, and Robertson, J. Opt. Soc. Am. **43**, 853 (1953).

DISCUSSION OF RESULTS

The expected isotopes in the radioactive samples investigated are Hg^{197} with a half-life of 64 hours, and the isomeric excited state Hg^{197*} with a half-life of 23 hours. (The entire series of neutron deficient mercury isotopes has been investigated by Gillon, Gopalakrishnan, de-Shalit, and Mihelich.[11]) The spins of these isotopes are found to have the values 1/2 and 13/2, respectively. These values are in accord with the single-particle shell model.

Two of the lines observed are compatible with a nuclear spin $I=1/2$. They are B and H of Fig. 7. They are slightly displaced toward higher wave numbers from the lines due to the 199 isotope, which also has a spin $I=1/2$. They are in the same order, that is, the $F=3/2$ line is on the high wave number side. There is nothing in the decay of these lines to indicate that they could not be caused by the same isotope. They are in positions compatible with the independent spectroscopic evidence discussed in the previous section. We therefore have made the assignment indicated in Table I, which contains a summary of all our data. The position of the various lines is given in terms of separation from the 200 isotope to facilitate a direct comparison with the results listed by Brix and Kopfermann in the Landolt-Bornstein Tables.

For natural mercury, the agreement between our results and the summary of previous results is within the experimental error except for the 201 $F=5/2$ line. We consider our result the more reliable since we had, for the first time, an enriched isotope in which this line was partly resolved. We did not attempt a recalculation of the magnetic moment or quadrupole moment of the 201 isotope, since the remaining lines were not resolved by the methods used, but we hope to return to this point in a later communication.

The magnetic moment of the 197 isotope may be computed from the observed hyperfine structure of this and the very similar 199 isotope, and the observed moment[12] of Hg^{199}, which for our purposes may be taken as 0.50 nuclear magnetons. The result is

$$\mu_{Hg^{197}}=0.50\times0.749/0.719=0.50\times1.04$$
$$=0.52 \text{ nuclear magnetons.}$$

The results for the isotope shift of the even isotopes is shown in Fig. 9, where the results of other observers are also plotted. We believe the smooth trend shown by our data to be substantially correct. It is in agreement with the results obtained by various observers using other spectral lines. Of these we quote only Murakawa,[13] who recently published an estimate of the isotope shift for Hg^{196} in a sample in which the natural abundance of 0.15 percent was boosted to 1.46 percent. The observations on the line Hg II λ6150 are tabulated below, together with our own results on isotope shift, using a scale in which the 204–202 displacement is unity.

	204–202	202–200	200–198	198–196
Murakawa	1.0	1.0	0.85	0.60
Present study	1.0	1.0	0.91	0.79

Considering the difficulty of Murakawa's estimate of 0.019 cm^{-1} for the 198–196 displacement in which the 196 line was unresolved but appeared only as a somewhat diffuse edge on the 198 line, the agreement must be considered excellent.

We can hardly hope to discover the meaning of this trend in isotope shift for the theory of nuclear structure without a good deal more evidence. There are undoubtedly departures from the $A^{1/3}$ law for the nuclear radius for various different reasons in different parts of the nuclear "periodic table."

Wilets, Hill, and Ford[14] discuss a variety of reasons for anomalous isotope shifts, of which we shall take up only that due to nuclear electric quadrupole moments, first suggested by Brix and Kopfermann.[15] Mercury, with $Z=80$, lacks two protons of having a closed shell with 82, and the isotope Hg^{204} lacks two neutrons of having a closed shell with 126.

As more and more neutrons are taken out of the closed shell, progressively larger quadrupole moments are to be expected. Exceptionally large quadrupole moments are found in nuclei in which 10 or more nucleons are lacking from closed shells. In this group,

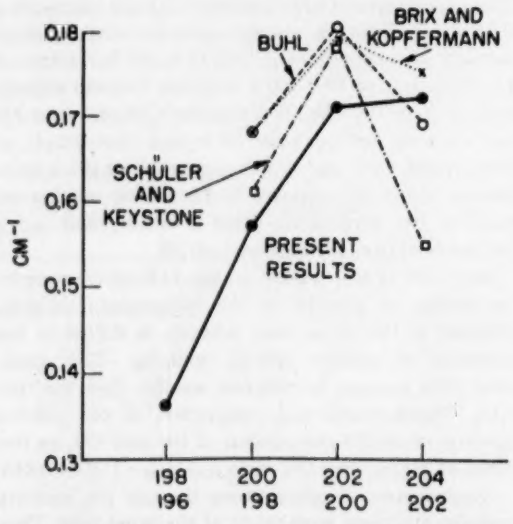

FIG. 9. Isotope shift of the resonance radiation of the even isotopes of mercury. The position of the Hg^{204} peak was obtained with a sample, previously mentioned, markedly enriched in this isotope.

[11] Gillon, Gopalakrishnan, de-Shalit, and Mihelich, Phys. Rev. 93, 124 (1954).

[12] W. G. Proctor and F. C. Yu, Phys. Rev. 81, 20 (1951).

[13] K. Murakawa, Phys. Rev. 93, 1232 (1954).

[14] Wilets, Hill, and Ford, Phys. Rev. 91, 1488 (1953).

[15] P. Brix and H. Kopfermann, Physik 126, 344 (1949). For a further discussion of intrinsic quadrupole moments of nuclei with spin 0 or ½, see also A. Bohr and B. Mottleson, Kgl. Danske Videnskab. Selskab, Mat.-fys. Medd. 27, No. 16 (1953).

values of Q/R^2 in the range of 5–10 are observed. Since Hg^{196} lacks 10 neutrons from a closed shell, it is interesting to consider whether the observed trend in the isotope shift might be related to the intrinsic quadrupole moments.

Electronic energy levels are raised due to the finite size of a nucleus by an amount proportional to the mean value of ρr^2 averaged over the nucleus. For a nucleus with quadrupole moment Q and a volume equal to that of a sphere of radius R, the mean value of ρr^2 is proportional to

$$ZR^2[1+(\tfrac{5}{6}Q/ZR^2)^2].$$

The change in an energy level δ resulting from a change in neutron number δN, assuming $R=R_0A^{1/3}$, is

$$\delta=\text{const}\left[\frac{2}{3}\frac{1+(\tfrac{5}{6}Q/ZR^2)^2}{A}+\frac{d(\tfrac{5}{6}Q/ZR^2)^2}{dN}\right]\delta N.$$

If we call the first term δ_R the isotope shift caused by the change in volume, and the second term δ_Q the isotope shift caused by the change in shape, the above expression may be put into the form

$$\frac{\delta_Q}{\delta_R}=\frac{25A}{48Z^2}\delta\left(\frac{Q}{R^2}\right)^2.$$

If we assume the normal volume effect for all the isotope shifts shown in Fig. 9 to be approximately 0.172 cm^{-1}, and the departures from this value to be the decrease δ_Q due to the change in quadrupole moment, we can compute the changes in Q/R^2 from one isotope to another. The effects for 204–202 are too small for us to estimate. However, if we assume a value of Q/R^2 for Hg^{202}, the calculation of Q/R^2 from the data can be carried through for the other isotopes with the results given in Table II. These values appear to be of the correct order of magnitude, and it would therefore seem reasonable to assume that, pending the accumulation of further evidence, the anomalous isotope shift for the even-even mercury nuclei is, at least in part, attributable to the variation of the intrinsic quadrupole moment from one isotope to another.

TABLE II. Assumed and calculated values of Q/R^2.

Assumed value[a] of Q/R^2 Hg^{202}	Calculated value of Q/R^2 from observed isotope shift Hg^{200}	Hg^{198}	Hg^{196}
0.2	0.63	2.41	4.35
0.4	0.72	2.44	4.37
1.0	1.16	2.61	4.46

[a] The experimental value of Q/R^2 for Hg^{204} is 0.6.

ACKNOWLEDGMENTS

We are indebted to Henry Plotkin, who took part in the original experiments leading to the establishment of the magnetic-scanning technique, and who helped us throughout in making observations, and particularly to Alan Teviotdale whose participation in our endeavors was terminated by a fatal accident last summer. His patience and devotion were perhaps the most important factors in overcoming the discouraging difficulties which delayed us for almost a year.

Dissociation Energy of NO and N_2*

M. Brook† and J. Kaplan
Institute of Geophysics,‡ University of California, Los Angeles, California
(Received September 1, 1954)

The vibrational levels of the $X^2\pi$ ground state of NO have been observed up to $v=23$, or an energy of 4.46 ev. In order that D_0(NO) be 5.29 ev, a very sharp and sudden drop in the $\Delta G(v)$ values is necessary. No such tendency is observed, and therefore the higher value of D_0(NO) = 6.48 ev appears most probable. This value then fixes $D_0(N_2)=9.76$ ev. A new system of NO bands in the near infrared is reported. These are probably due to a $^4\pi \rightarrow {}^4\pi$ transition.

INTRODUCTION

THE emission spectrum of NO has been studied extensively in the past.[1,2] In an attempt to establish the dissociation energy of N_2, the β bands ($B^2\pi \rightarrow X^2\pi$) of NO have been re-examined. The dissociation energy of NO is related to the dissociation energy of N_2 by[3] $N_2+O_2+1.87$ ev $\rightarrow 2NO$. From spectroscopic studies, the value of $D_0(N_2)$ has been found to be either 7.37 ev or 9.76 ev; similarly, for the NO molecule, D_0(NO) is either 5.29 ev or 6.48 ev.

The highest observed vibrational level of the ground state $X^1\Sigma$ of N_2 is $v=27$, corresponding to an energy of 6.6 ev. For NO, prior to this investigation, the highest observed vibrational level of the ground state $X^2\pi$ was $v=18$, corresponding to 3.65-ev energy. The present investigation was undertaken in the hope that the vibrational levels of the ground state of NO could be extended up to or beyond the energy of 5.29 ev. Although this extension has not been completely realized, the results are considered of sufficient interest to warrant a brief description.

EXPERIMENTAL PROCEDURE

The β bands of NO were excited by introducing a small amount of oxygen into active nitrogen. A continuous flow system was used in which the oxygen and nitrogen were mixed in the proper ratio prior to the discharge. The amount of oxygen was adjusted to just below the point at which the air afterglow (white continuum) appeared. At this stage, the nitrogen bands were very weak, and the β bands of NO very strong.

The gas was excited in a quartz tube using a vacuum tube oscillator of 1.5-kw input power operating in the frequency range 50–70 Mc/sec. The quartz discharge tube was located between the inner and outer conductor at the end of a quarter wave concentric line. The line was tuned to produce gas breakdown at the high pressures used, i.e., 15–30 mm Hg, by a variable vacuum capacitor. After passing through the discharge region the gas was drawn through a Pyrex tube 2.5 in. in diameter and 24 in. long into the vacuum pump.

Spectrograms were taken through a quartz window on one end of the Pyrex tube. The spectrograph was constructed in this laboratory by Mr. C. J. Silvernail, and consists of a 5 in.×6 in. 15 000-line/in. plane grating used in conjunction with an $f1:2$ Maksutov type camera. The camera has a 5-in. calcium fluoride corrector lens and an 8-in. diameter spherical mirror. For the present work the grating was used in the first order and gave a linear dispersion of 58 A/mm at the plate.

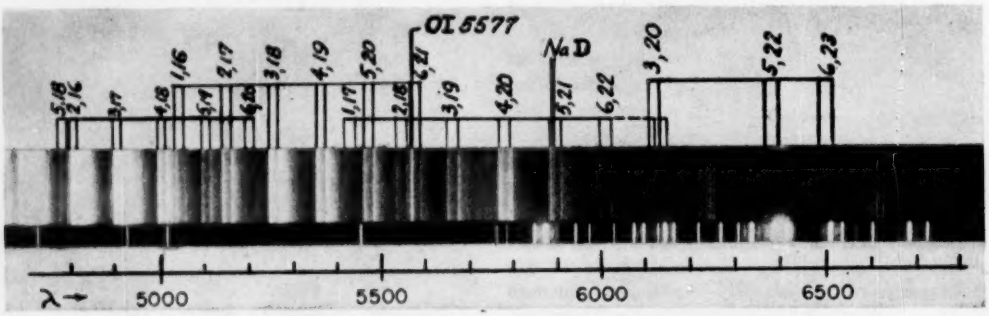

FIG. 1. New NO β bands excited in active nitrogen. Eastman 103aF plate.

* This work was supported in part by the Geophysics Research Division of the Air Force Cambridge Research Center.
† Now at New Mexico Institute of Mining and Technology, Socorro, New Mexico.
‡ Publication No. 48.
[1] Jenkins, Barten, and Mulliken, Phys. Rev. **30**, 150 (1927).
[2] A. G. Gaydon, Proc. Phys. Soc. (London) **56**, 95, 160 (1944).
[3] F. R. Bichowsky and F. D. Rossini, *Thermochemistry of Chemical Substances* (Reinhold Publishing Company, New York, 1936).

TABLE I. Deslandres table of new NO β bands.

v' \ v''	16	17	18	19	20	21	22	23
1	19 773 (5056.0) 19 850 (5036.3)	18 346 (5449.2) 18 431 (5424.1)						
2	20 785 (4809.9) 20 871 (4790.1)	19 360 (5163.8) 19 442 (5142.2)	17 961 (5566.1) 18 040 (5541.7)					
3		20 354 (4911.8) 20 436 (4892.1)	18 966 (5271.2) 19 038 (5250.1)	17 594 (5682.2) 17 674 (5656.5)	16 261 (6148.0) 16 338 (6118.9)			
4			19 939 (5013.8) 20 016 (4994.5)	18 577 (5381.4) 18 653 (5359.5)	17 247 (5796.4) 17 318 (5772.7)			
5			20 912 (4780.5) 20 991 (4762.7)	19 545 (5114.9) 19 620 (5095.3)	18 211 (5489.8) 18 284 (5467.6)	16 911 (5911.8) 16 982 (5887.1)	15 640 (6392.3) 15 711 (6363.4)	
6					19 169 (5215.2) 19 241 (5195.9)	17 865 (5595.9) 17 932 (5575.0)	16 597 (6023.7) 16 665 (5998.8)	15 354 (6510.9) 15 426 (6480.7)

RESULTS AND CONCLUSIONS

Figure 1 is a reproduction of the afterglow spectrum covering the region 4700–6800A taken on an Eastman 103aF plate. A total of 18 new β bands have been identified, raising the highest observed vibrational level of the ground state of NO to $v=23$. This corresponds to an energy of 4.46 ev, or 35 988 cm^{-1}. Also present on the plate are a number of weak first positive nitrogen bands as well as the forbidden atomic oxygen line λ5577. A Deslandres table of the new β bands is shown in Table I.

Figure 2 is a plot of the $\Delta G(v)$ values against the term values $G(v)$ for all the observed levels of the ground state of NO. The $\Delta G(v)$ and $G(v)$ values were computed from the present measurements and from the list of band heads given by Pearse and Gaydon.[4] As is evident from Fig. 2, the curve shows little tendency to cross the $G(v)$ axis for the value $D_0=5.29$ ev. For this lower value of D_0(NO), a very sharp and sudden drop in the $\Delta G(v)$ values is necessary. For this reason

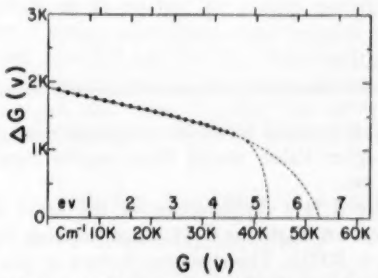

FIG. 2. Plot of $\Delta G(v)$ *vs* $G(v)$ for the observed levels of the $X^2\pi$ ground state of NO. The dashed portions of the curve represent extrapolations to the two possible values of D_0(NO).

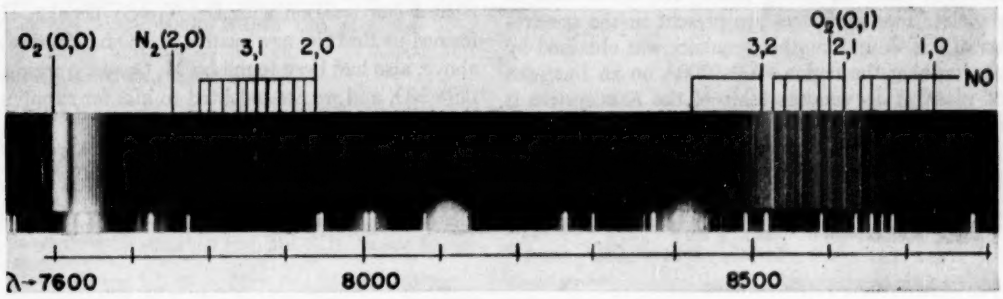

FIG. 3. Spectrogram of a new system of NO bands in the near infrared. Eastman 1−*N* plate.

[4] R. W. B. Pearse and A. G. Gaydon, *The Identification of Molecular Spectra* (John Wiley and Sons, Inc., New York, 1950).

TABLE II. Deslandre table of new NO β bands in the near infrared.

v'' \ v'	0 ν	0 λ		1 ν	1 λ		2 ν	2 λ
0	10 272	(9732.5)						
	10 300	(9706.0)						
	10 323	(9684.4)						
	10 350	(9659.0)						
	10 375	(9636.0)						
	10 395	(9617.3)						
	1175							
	1176							
1	11 447	(8733.3)	993	10454	(9563.1)			
	11 472	(8714.4)		10 477	(9542.1)			
	11 489	(8701.8)		10 496	(9525.0)			
	11 522	(8676.5)		10 527	(9497.0)			
	11 549	(8656.1)		10 555	(9471.8)			
	11 571	(8640.3)	996	10 575	(9453.5)			
	1145			1144				
	1145			1145				
2	12 592	(7939.1)	994	11 598	(8619.8)			
	12 614	(7925.6)		...	...			
	12 636	(7912.0)		11 640	(8588.8)			
	12 667	(7892.4)		11 673	(8565.2)			
	12 693	(7876.1)		11 701	(8544.6)			
	12 716	(7861.9)	996	11 720	(8529.9)			
				1118				
				1117				
3				12 716	(7861.9)	974	11 742	(8514.2)
				...	...		...	...
				12 756	(7837.1)		...	...
				12 787	(7818.3)		...	...
				12 814	(7801.8)		...	...
				12 837	(7787.6)	972	11 865	(8425.65)

the higher value of $D_0=6.48$ ev appears more probable. This higher value would then require that $D_0(N_2)=9.76$ ev.

Figure 3 is a reproduction of the same afterglow taken on an Eastman $1-N$ plate covering the region 7500A to 9000A. The strongest feature of this spectrogram is the atmospheric O_2 (0,0) band at 7594A. The (0,1) O_2 band at 8597A is also present. The occurrence of these bands with such great intensity under conditions in which the oxygen is present only as an impurity (~3–5 percent) is rather surprising. The other prominent feature is a new system of bands belonging to the molecule NO, and probably due to a $^4\pi \rightarrow {}^4\pi$ transition. The bands show six strong heads, and are shaded to the violet. Two sequences are present in the spectrogram of Fig. 3, and another sequence was obtained by photographing the region 8500–9700A on an Eastman 1-M plate. A Deslandres table of the new system is given in Table II.

It is tempting to identify the lower state of these new bands with the upper state $B^2\pi$ of the β bands. The observed wave number differences of 994 cm^{-1} and 973 cm^{-1} agree reasonably well with the wave number differences of 996 cm^{-1} and 974 cm^{-1} between the $v=2, 3$, and 4 levels, respectively, of the $B^2\pi$ state. The presence of six strong heads, however, makes this identification improbable. A $^4\pi \rightarrow {}^4\pi$ transition would account for the six strong heads.

ACKNOWLEDGMENTS

During the course of this work we benefited greatly from a conversation with Dr. Yoshio Tanaka. He informed us that the new system of NO bands, described above, also had been found by M. Ogawa working with pure NO, and we are indebted to him for supplying us with a photograph of these bands.

Hyperfine Structure of the Spectra of Nd and Gd†

KIYOSHI MURAKAWA
Institute of Science and Technology, Komaba-machi, Meguro-ku, Tokyo, Japan
(Received September 1, 1954)

Study of the hyperfine structure of the spectrum of Nd II with separated isotopes yielded the result that the nuclear magnetic moments of the odd isotopes are $\mu(Nd^{143})=-1.1\pm0.1$ nm and $\mu(Nd^{145})=-0.69\pm0.10$ nm. The isotope shift in Nd I λ4924 was measured and the ratio of the distances of the neighboring isotopes was found to be $\Delta\nu(142-143):\Delta\nu(143-144):\Delta\nu(144-145):\Delta\nu(145-146):\Delta\nu(146-148):\Delta\nu(148-150)=0.4_0:0.5_7:0.2_0:0.7_3:1:1.5$. From the hyperfine structure of the spectrum of Gd I the nuclear spins of the odd isotopes Gd^{155} and Gd^{157} were found to be equal to or larger than 5/2, the magnetic moments being negative. Under the assumption that the spins are equal to the values predicted by the nuclear shell structure theory, namely 7/2, the magnetic moments were calculated to be $\mu(Gd^{155})=-0.19\pm0.05$ nm and $\mu(Gd^{157})=-0.33\pm0.06$ nm. An anomalous isotope shift of the even isotopes of Gd was found: $\Delta\nu(160-158):\Delta\nu(158-156):\Delta\nu(156-154):\Delta\nu(154-152)=1:0.97\pm0.02:1.21\pm0.05:2.2\pm0.1$.

I. HYPERFINE STRUCTURE OF THE SPECTRUM OF Nd

USING a liquid-air cooled or water cooled hollow cathode discharge tube, a Febry-Pérot etalon and enriched isotopes of Nd^{143} and Nd^{145} whose isotopic constitutions are shown in Table I, Ross and the author studied the hyperfine structure (hfs) of the spectrum of Nd. A short summary of the result of the investigation was published,[1] it being found that the spins of Nd^{143} and Nd^{145} are both 7/2 and the ratio of the magnetic moments is

$$\mu(Nd^{143})/\mu(Nd^{145})=1.60\pm0.06. \quad (1)$$

In a somewhat earlier work, Bleaney and Scovil[2] deduced the same nuclear spins, using paramagnetic resonance technique, and got a more precise value of the ratio of the magnetic moments (1.6083±0.0012).

One of the purposes of the present paper is to deduce the magnetic moments of Nd^{143} and Nd^{145} by a calculation that is more rigorous than that given in reference 1.

In the previous work[1] the line Nd II λ4303 ($4f^36s\ ^6I_{7/2}-{}^6K_{9/2}{}^0$)[3] was studied in detail and it was found that Nd^{143} has the total splitting of 0.260 cm^{-1}, the component of the lowest frequency side being the strongest. The line Nd II λ4401 ($4f^36s\ ^6I_{9/2}-{}^6K_{9/2}{}^0$) was found to be single in both the 143 and 145 samples, as far as the diagonal components are concerned. We may assume that the interval factors of the initial and the final levels of λ4401 are equal within the accuracy of 5 percent. These findings about the hfs of λ4303 and λ4401 lead, therefore, to the relation

$$28A^{143}(4f^46s\ ^6I_{7/2})-35A^{143}(4f^46s\ ^6I_{9/2}')=0.260\ cm^{-1}. \quad (2)$$

The complex $4f^4$ will be assumed to form an ion ^5I via an *LS* coupling, the 6*s*-electron being combined to ^5I by an intermediate coupling. The wave function that depends upon the coupling will be suffixed by ′. In order to solve Eq. (1) we have to determine the coefficients of coupling by solving the energy matrix[4] which is given in Table II. The levels $^{4,6}I$ from the configuration $4f^46s$ with higher *J* values are near to levels from the configuration $4f^36s5d$ and are likely to be perturbed, so in solving the energy matrix levels with lower *J* values were given larger weights. In this way we get $\zeta_{4f}=870$ and $G=216$. Substituting these values in the energy matrix and using the usual procedure, we get the wave function for $4f^4(^5I)6s$ in intermediate coupling in terms of wave functions in *LS* coupling:

$$^6I_{9/2}'=K_1\,{}^6I_{9/2}+K_2\,{}^4I_{9/2},\ K_1=0.9885,\ K_2=0.1511. \quad (3)$$

Then the interval factor is calculated to be

$$\begin{aligned}A(^6I_{9/2}')=&K_1^2[-(17/495)a(s)+(18632/16335)a_f]\\&+K_2^2[(3/55)a(s)+(749/605)a_f]\\&+2K_1K_2[\{4(14)^{\frac{1}{2}}/165\}a(s)\\&-\{13(14)^{\frac{1}{2}}/10890\}a_f],\end{aligned} \quad (4)$$

in which we have neglected the relativity correction for the *f* electrons and have put

$$a_f=\frac{\zeta_f}{Z_f{}^*1836}\frac{\mu}{I}. \quad (5)$$

TABLE I. Isotopic constitution (percent) of the samples of neodymium.

Sample label	Isotope 142	143	144	145	146	148	150
143	4.04	83.93	8.83	1.78	1.16	0.15	0.11
145	1.18	0.84	4.83	78.60	13.71	0.63	0.21
Natural	27.13	12.20	23.87	8.30	17.18	5.72	5.60

† The work with enriched isotopes was performed at the University of Wisconsin in 1950–1951 and was supported by the U. S. Office of Naval Research. The work with natural samples was performed in Tokyo. The enriched isotopes were produced by the Y-12 plant, Carbide and Chemical Division, Oak Ridge, and were obtained by allocation from the U. S. Atomic Energy Commission.

[1] K. Murakawa and J. S. Ross, Phys. Rev. **82**, 967 (1951).

[2] B. Bleaney and H. E. D. Scovil, Proc. Phys. Soc. (London) **63**, 1369 (1950).

[3] The Nd II spectrum was classified by Albertson, Harrison and McNally, Phys. Rev. **61**, 167 (1942).

[4] The notations are the same as those in the book of E. U. Condon and G. H. Shortley, *The Theory of Atomic Spectra* (Cambridge University Press, London, 1935).

TABLE II. Energy matrix of $4f^4(^5I)6s$ in LS coupling.

	$J=17/2$	
^6I	$3\zeta-(7/2)G$	
	$J=13/2$	
^6I	$-(1/5)\zeta-(7/2)G$	$-(1/10)66^{\frac{1}{2}}\zeta$
^4I	$-(1/10)66^{\frac{1}{2}}\zeta$	$(9/20)\zeta+(3/2)G$
	$J=9/2$	
^6I	$-(13/5)\zeta-(7/2)G$	$-(3/20)14^{\frac{1}{2}}\zeta$
^4I	$-(3/20)14^{\frac{1}{2}}\zeta$	$-(63/20)\zeta+(3/2)G$

	$J=15/2$	
^6I	$(13/10)\zeta-(7/2)G$	$-(1/10)51^{\frac{1}{2}}\zeta$
^4I	$-(1/10)51^{\frac{1}{2}}\zeta$	$(27/10)\zeta+(3/2)G$
	$J=11/2$	
^6I	$-(3/2)\zeta-(7/2)G$	$-(3/4)\zeta$
^4I	$-(3/4)\zeta$	$-(3/2)\zeta+(3/2)G$
	$J=7/2$	
^6I	$-(7/2)\zeta-(7/2)G$	

The level $^6I_{7/2}$ is independent of coupling, and we have

$$A(^6I_{7/2})=-(1/9)a(s)+(448/297)a_f^*. \quad (6)$$

Substituting the Goudsmit-Fermi-Segrè formula with the finite nuclear volume correction and Eq. (5) in Eqs. (3), (4), and (6), we get

$$A(^6I_{9/2}')=0.005298\mu, \quad A(^6I_{7/2})=-0.001508\mu. \quad (7)$$

Putting Eq. (7) in Eq. (2), we get finally

$$\mu(\mathrm{Nd}^{143})=-1.1\pm0.1 \text{ nm},$$

and by the aid of the relation (1), we get

$$\mu(\mathrm{Nd}^{145})=-0.69\pm0.10 \text{ nm}.$$

In a recent work Bleaney *et al.*[5] quote the calculation of Elliott and Stevens: $|\mu(\mathrm{Nd}^{143})|=1.0\pm25$ percent, $|\mu(\mathrm{Nd}^{145})|=0.62\pm25$ percent.

The shift of the even isotopes in the spectrum of Nd I was studied by Klinkenberg,[6] and he found an anomalously large isotope shift of $\mathrm{Nd}^{148}-\mathrm{Nd}^{150}$. In the present work, using natural neodymium also, Klinkenberg's lines were measured with an accuracy better than that of Klinkenberg. None of them was found among the classified lines of Schuurmans[7] and Klinkenberg.[8] Of the classified lines, the line λ4924 ($4f^46s^2\,{}^5I_4-20_5$) [the level 20300.86 ($J=5$) found by Klinkenberg[8] is here denoted as 20_5 for brevity] was found to have the largest shift. The measured hfs for this line is given in Fig. 1. The hfs of the same line for the enriched isotopes was not resolved, but from the measured intensity distribution the centers of gravity of Nd^{143} and Nd^{145} could be determined, and are given at the bottom of Fig. 1. The shift in the even isotopes will be discussed in Sec. III.

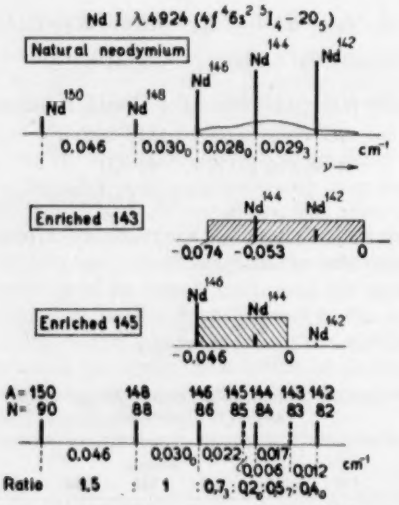

FIG. 1. Hfs of Nd I λ4924 and the isotope shift. A and N are atomic number and neutron number respectively.

II. HYPERFINE STRUCTURE OF THE SPECTRUM OF Gd

The shift of even isotopes in the spectrum of Gd was first measured by Klinkenberg.[8] Suwa[9] and Brix and Engler[10] measured more accurately the hfs of the Gd lines, but none of them detected components due to Gd^{154} and Gd^{152}.

Natural gadolinium is known to consist of seven isotopes:[11] 160 (21.79), 158 (24.78), 157 (15.71), 156 (20.59), 155 (14.78), 154 (2.15), and 152 (0.20). A number in parentheses represents the abundance in percent. The purpose of the present work is to detect the components due to the rarer isotopes Gd^{154} and Gd^{152} and to measure the magnetic moments of the odd isotopes. A liquid-air cooled hollow-cathode discharge tube which has been improved since 1951 was used.[12] In lines in which the splittings of Gd^{155} and Gd^{157} respectively are negligibly small, the component due to Gd^{154} could be clearly observed. In several lines the component due to Gd^{152} could be recognized on heavily exposed plates. A typical example is the line λ4092.7,[13] and the result of measurement is shown in Fig. 2. Some of the interference patterns of λ4092.7 are repro-

[5] Bleaney, Scovil, and Trenam, Proc. Roy. Soc. (London) **223**, 1 (1954).

[6] P. F. A. Klinkenberg, Physica **11**, 327 (1945). Quite recently G. Nöldeke and A. Steudel [Z. Physik **137**, 632 (1954)] have studied the same subject as Klinkenberg more accurately.

[7] P. Schuurmans, Physica **11**, 419 (1946).

[8] P. F. A. Klinkenberg, Physica **12**, 33 (1946).

[9] S. Suwa, Phys. Rev. **86**, 247 (1952); J. Phys. Soc. (Japan) **8**, 377 (1953).

[10] P. Brix and H. D. Engler, Z. Physik **133**, 362 (1952).

[11] D. C. Hess, Phys. Rev. **74**, 773 (1948).

[12] K. Murakawa, J. Phys. Soc. Japan **9**, 391 (1954).

[13] The Ge I and Gd II spectra were classified extensively by H. N. Russell, J. Opt. Soc. Am. **40**, 550 (1950).

duced in Fig. 3. The position of the Gd^{152} component relative to the Gd^{160} component is somewhat difficult to measure, and an error of ± 0.006 cm^{-1} must be admitted.

In the unclassified line λ4436.1 (see Fig. 2) the positions of the components due to Gd^{160}, Gd^{158}, and Gd^{156} are least disturbed by the odd isotopes. From the hfs of λ4436.1 and λ4092.7 the ratio of the distances of the neighboring isotopes is observed to be $\Delta\nu$ (160−158) : $\Delta\nu$ (158−156) : $\Delta\nu$ (156−154) : $\Delta\nu$ (154−152) = 1 : 0.97 ±0.02 : 1.21±0.05 : 2.2±0.1. With respect to the odd isotopes we get $\Delta\nu$ (160−158) : $\Delta\nu$ (158−157) : $\Delta\nu$ (156−155) = 1 : 0.92±0.02 : 0.74±0.02. Suwa[9] obtained $\Delta\nu$ (160−158) : $\Delta\nu$ (158−156) = 1 : 0.97±0.06. Brix and Engler[10] found 160−158−156 to be equidistant within the accuracy of their measurements.

The line λ4436 has large splittings of the odd isotopes (see Fig. 2). The intensity distribution shows that the

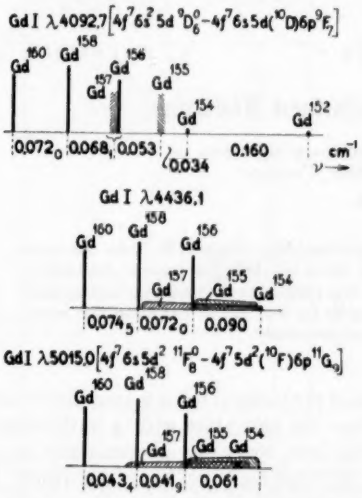

FIG. 2. Hfs of Gd I λ4092.7, λ4436.1 and λ5015.0.

spins of Gd^{157} and Gd^{155} are at least 2, so that they must be 5/2, 7/2, or 9/2. With respect to the signs of the magnetic moments of the odd isotopes, the hfs of λ5015.0 (see Fig. 2) is more favorable for negative than for positive moments, although a slight amount of room is left for positive moments. The single-particle model of the nuclear shell structure predicts the state $f_{7/2}$ for Gd^{157} and Gd^{155}, so we shall assume that the spins of Gd^{157} and Gd^{155} are 7/2 and calculate the magnetic moments.

The total width of the Gd^{155} structure in λ5015 (see Fig. 2) was found to be approximately 0.061 cm^{-1}. Thus we have

$$(119/2)A(4f^7 6s5d^2\ {}^{11}F_8^0) - (133/2)A(4f^7 5d^2 6p\ {}^{11}G_9) = -0.061\ \text{cm}^{-1}.$$

Assuming that the complex $4f^7\ {}^8S_{7/2}$ is of LS coupling and therefore contributes nothing to the hfs splitting,

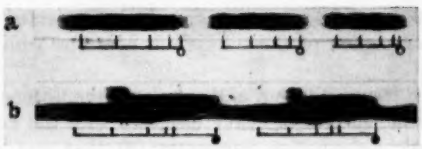

FIG. 3. Enlargement of interference patterns of Gd I λ4092.7. (a) 15-mm etalon. (b) 8-mm etalon. The components due to Gd^{154} and Gd^{152} are marked with ○ and ● respectively.

and using the relations

$$A(4f^7 5d^2 6s\ {}^{11}F_8) = (37/80)a_d' + (3/80)a_d'' + (1/5)a_d''' + (1/16)a(s),$$

$$A(4f^7 5d^2 6p\ {}^{11}G_9) = (37/90)a_d' + (1/30)a_d'' + (8/45)a_d''' + (1/6)a_p',$$

we get

$$\mu(Gd^{155}) = -0.19\pm 0.05\ \text{nm},$$

where we have assumed that $\zeta_{5d} = 864$ cm^{-1} and $\zeta_{6p} \approx 1250$ cm^{-1} for Gd I. Similarly we get

$$\mu(Gd^{157}) = -0.33\pm 0.06\ \text{nm}.$$

Suwa[9] deduced $|\mu(Gd^{155})| = 0.2_5\pm 0.15$ nm and $|\mu(Gd^{157})| = 0.3\pm 0.2$ nm from the measurement of the same spectrum.

III. DISCUSSION OF THE ISOTOPE SHIFT

The large isotope shifts between the neutron numbers (N) 90 and 88 in Nd and Sm are now well known. A third example has been found in Gd in the present work. The ratio of the distances between neighboring isotopes in these elements is summarized in Table III, and it is seen that the trend is the same in all of the three elements listed.

The subshell of $h_{9/2}$ neutrons is completed at $N = 92$. The above-mentioned anomaly can be phenomenologically described by the apparent attraction of the $N90 (= 92-2)$ component to the $N92$ component and the resultant large shift between the $N90$ and $N88$ components. Exactly the same phenomenon is observed at the completion of the subshell of $h_{11/2}$ neutrons which occurs at $N = 76$: Ross and the author[14] detected in the spectrum of Te II an anomalously large shift between the $N74 (= 76-2)$ and $N72$ components and a relatively small shift between the $N76$ and $N74$ components. The observed facts seem to show that the

TABLE III. Isotope shift in Gd, Nd, and Sm.

Element	N 96	94	92	90	88	86	84	82
Gd		0.83 :	0.80 : 1 :	1.9				
Nd				2 :	1.30 :	1.22 :	1.27	
Sm[a]			1 :	1.85 :	1.26 :	1.105×2		

[a] Data were taken from P. Brix and H. Kopfermann, Z. Physik **126**, 344 (1949). Sm isotope for $N = 84$ does not exist, so the shift for 86 −82 is given.

[14] J. S. Ross and K. Murakawa, Phys. Rev. **85**, 559 (1952).

conspicuous isotope shift anomaly is connected with the completion of the subshell of neutrons with high l value.

Ford [15] and Wilets *et al.*[16] correlated the isotope shift in atomic spectra of heavy elements with the nuclear intrinsic deformation parameter (β) that was introduced by Bohr,[17] in such a way that the actual shift minus the shift predicted by the finite volume theory determines $d\beta/dN$ but not β itself. The above-mentioned shift anomaly would enter as anomalous slope in the β *versus* N curve in even-even nuclei (Fig. 4 of the article of Ford[15]). In this connection it may be remarked that in even-even nuclei the β *versus* N curve is relatively simple, β vanishing only at magic numbers, and the completion of subshell has a minor effect on the general trend of β, according to Ford's Fig. 4. In contrast to this, in even-odd nuclei the completion of subshell has often a marked influence on the form of the β *versus* Z curve (Z=proton number).[18] These facts will probably be connected with the more pronounced importance of the rôle which the alpha-particle model plays in even-even nuclei.

I should like to thank Dr. Ross for his kind cooperation in the work with enriched isotopes. The very pure sample of gadolinium which was used in the present experiment was kindly given to me by Professor Mack to whom my thanks are due.

[15] K. W. Ford, Phys. Rev. **90**, 29 (1953).
[16] Wilets, Hill, and Ford, Phys. Rev. **91**, 1488 (1953).
[17] A. Bohr, Kgl. Danske Videnskab. Selskab, Mat.-fys. Medd. **26**, No. 14 (1952).
[18] See, for example, K. Murakawa and T. Kamei, Phys. Rev. **92**, 325 (1935).

PHYSICAL REVIEW VOLUME 96, NUMBER 6 DECEMBER 15, 1954

Stern-Gerlach Experiment on Polarized Neutrons

J. E. Sherwood, T. E. Stephenson, and Seymour Bernstein
Oak Ridge National Laboratory, Oak Ridge, Tennessee

(Received July 29, 1954)

A neutron beam was polarized by total reflection from a magnetized iron mirror. The beam was then analyzed by passing it through an inhomogeneous magnetic field. From the deflection pattern obtained, it is inferred that the resultant neutron spin in the polarized beam was parallel to the magnetic field applied to the mirror. Thus the nuclear and magnetic scattering amplitudes for iron are of the same sign when the neutron spin and electronic spin are oppositely directed, and conversely.

INTRODUCTION

When a beam of neutrons passes through a material body the process may be considered analogous to the passage of light through a refractive medium. Thus we may define an index of refraction $n=[(E-V)/E]^{\frac{1}{2}}$, where E is the energy of a neutron, and V is the average potential energy of the neutron while in the body. If θ is the glancing angle of incidence, it follows that total reflection will occur for $\theta=(V/E)^{\frac{1}{2}}$. In other words, all wavelengths greater than the critical wavelength,

$$\lambda_c=\theta(h^2/2mV)^{\frac{1}{2}},$$

will be totally reflected.

In the case of a magnetized iron mirror, the potential energy is $V=V_n+V_m$, where V_n is that due to the nuclei and $V_m=-\boldsymbol{\mu}\cdot\mathbf{B}$ is the potential energy of the neutron's magnetic moment $\boldsymbol{\mu}$ in the average net field $\mathbf{B}$. Thus, if λ_c^+ and λ_c^- are the critical wavelengths for $\boldsymbol{\mu}$ parallel to $\mathbf{B}$ and $\boldsymbol{\mu}$ antiparallel to $\mathbf{B}$, respectively, we have

$$\lambda_c^+>\lambda_c^- \quad (B\neq 0).$$

The spectrum of reflected neutrons will therefore have the general appearance shown in Fig. 1 (if the spectrum of the incident beam is assumed to be Maxwellian). Thus the spin state with $\boldsymbol{\mu}$ antiparallel to $\mathbf{B}$ is more abundant. Since the gyromagnetic ratio of the neutron is negative,[1] we have the result that the resultant spin of the neutrons in the totally reflected

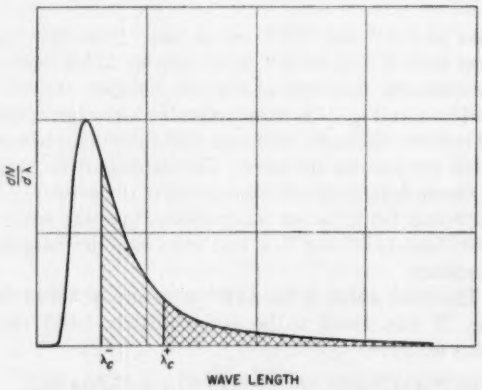

Fig. 1. Intensity distribution of neutrons reflected from magnetized iron mirror. For $\boldsymbol{\mu}$ parallel to $\mathbf{B}$, $\lambda>\lambda_c^+$. For $\boldsymbol{\mu}$ antiparallel to $\mathbf{B}$, $\lambda>\lambda_c^-$.

[1] P. N. Powers, Phys. Rev. **54**, 827 (1938).

beam is parallel to the applied magnetic field. It may be noted that the direction of the dominant neutron spin in a beam of polarized neutrons is significant in the interpretation of experiments on the interaction of polarized neutron beams with polarized target nuclei.[2,3] However, in no other experiments with polarized neutrons has the direction of the neutron spin been of consequence. Only neutron intensities were involved.

In order to check the results of the above argument in a very direct manner, we have carried out a Stern-Gerlach type of experiment in which a beam of polarized neutrons is deflected magnetically. This experiment is described below.

DESCRIPTION OF THE APPARATUS

The mirror was of soft iron, about $1\frac{3}{4}$ in.$\times$6 in. long, and was magnetized parallel to the face in a direction perpendicular to the length and to the neutron beam. The exit edge of the mirror was rounded off so that the magnetic field in this region would change less abruptly. It was felt that this procedure would partially alleviate the depolarization effects found by early experimenters. The glancing angle of the neutron beam upon the mirror was approximately 3×10^{-3} radian (10 minutes).

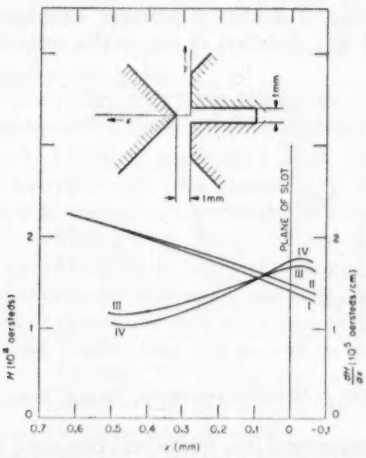

FIG. 2. Field strength and inhomogeneity of magnetic field in gap (reference 5): Curve I: Field strength in the plane of symmetry. Curve II: Field strength 0.2 mm outside plane of symmetry. Curve III: Inhomogeneity in the plane of symmetry. Curve IV: Inhomogeneity 0.2 mm outside plane of symmetry.

The slot-wedge type of deflecting field was felt to give the highest gradient consistent with reasonable cost. Since this arrangement had been thoroughly investigated by the early molecular beam experimenters,[4] the cross section of their magnet gap was copied. Figure 2[5] describes the cross section and magnetic characteristics of the gap; the length chosen was 1 meter. The average field in our magnet gap was found to be about 20 000 oersteds by means of a bismuth wire measurement. The field was maintained by four large solenoids of about 13 000 ampere-turns each.

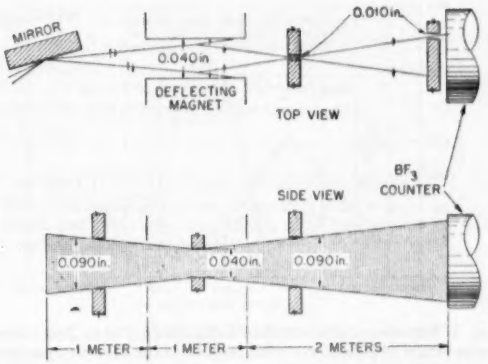

FIG. 3. Schematic diagram of beam collimation system showing typical trajectories and vertical slits (top view) and horizontal slits (side view).

The detector was a conventional arrangement consisting of a well-shielded BF_3 counter about 1 in. in diameter and 8 in. long. Its efficiency was about 90 percent for the reflected neutrons. Standard amplifiers and scale-of-64 registers were used. Background was 1.6 counts/min.

Even with a gradient of the order of 10^5 oersteds/cm extended over a length of a meter, the deflections produced are inconveniently small. This, together with the difficulty of producing such a gradient over a large space, requires a very high degree of collimation, in order to ensure that only those neutrons which spend an appreciable length of time in the region of high gradient will be counted. This was achieved, as shown in Fig. 3, by a combination of cadmium slits and holes. The main collimation was provided by the 0.010-in. vertical slit at the exit end of the deflecting

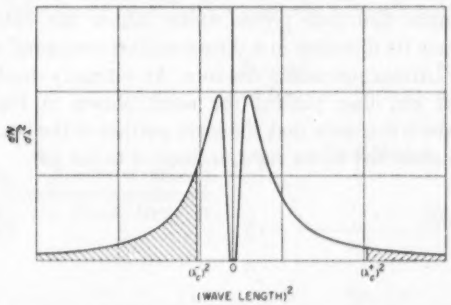

FIG. 4. Expected deflection pattern for infinite resolving power and perfect collimation. Shaded areas are derived from Fig. 1.

[2] Bernstein, Roberts, Stanford, Dabbs, and Stephenson, Phys. Rev. **94**, 1243 (1954).

[3] Roberts, Bernstein, Dabbs, and Stanford, Phys. Rev. **95**, 105 (1954).

[4] I. Estermann and O. Stern, Z. Physik **85**, 17 (1933).

[5] Reference 4, p. 18.

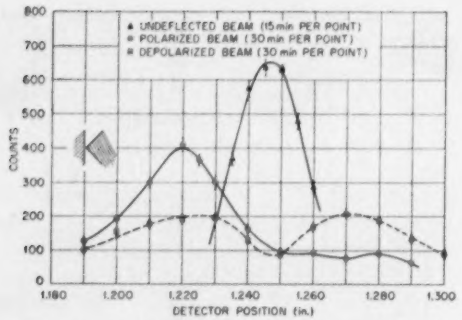
▲ UNDEFLECTED BEAM (15 min PER POINT)
● POLARIZED BEAM (30 min PER POINT)
■ DEPOLARIZED BEAM (30 min PER POINT)
COUNTS
DETECTOR POSITION (in.)

FIG. 5. Experimentally observed deflection patterns. Inset shows orientation of pole pieces with respect to the intensity pattern.

magnet. It is easily seen that this location of the slit does not complicate the interpretation of the results and leads to much better collimation than is obtained with the slit preceding the deflecting magnet.

PROCEDURE

Neutrons in the two spin states will suffer opposite forces in the deflecting magnet so that, with perfect collimation and infinitely good resolution, one should obtain an intensity distribution in the beam as shown in Fig. 4. (Displacement is proportional to λ^2.)

In practice, however, a 0.010-in. slit is translated across the face of the detector and yields the result shown in Fig. 5. For comparative purposes, undeflected and deflected-depolarized beams are shown there also. The depolarization was accomplished by interposing a soft iron shim in the beam between the mirror and the deflecting magnet, at a place where the magnetic field was small. For these data, the field between mirror and deflecting magnet was such as to permit only adiabatic transitions.

The experiment was repeated under conditions in which the neutron spins were "flipped" relative to the magnetic field, during their passage from the mirror to the deflecting magnet. This spin reversal was brought about by means of an arrangement of permanent magnets and pole pieces which caused the field to reverse its direction in a distance short compared with the Larmor precession distance. An intensity-displacement run then yielded the result shown in Fig. 6, in which it is seen that the main portion of the beam is now deflected to the right, instead of to the left.

INTERPRETATION OF RESULTS

If we consider only the normal pattern, Fig. 5, and agree to take the positive x axis to the right, the following argument applies: The energy of the dipole is $W=-\boldsymbol{\mu}\cdot\mathbf{H}=-(\boldsymbol{\mu}\cdot\mathbf{h})H$, where $\mathbf{h}$ is a unit vector in the direction of the magnetic field $\mathbf{H}$, and H is the magnitude of the field. Then, along the x axis, $F_x=-\partial W/\partial x=(\boldsymbol{\mu}\cdot\mathbf{h})\partial H/\partial x$. By inspection of Fig. 5, it is seen that $F_x<0$ and $\partial H/\partial x>0$. It follows that $\boldsymbol{\mu}\cdot\mathbf{h}<0$. Thus, since the gyromagnetic ratio of the neutron is negative, the experiment shows directly that the resultant spin in a neutron beam polarized by reflection from magnetized iron is parallel to the magnetic field applied to the mirror.

From this it can be shown that the nuclear and magnetic scattering amplitudes (for iron) are of the same sign when the neutron spin and electronic spin are oppositely directed, and conversely.

By means of double-transmission experiments, the resultant spin direction in the totally reflected beam

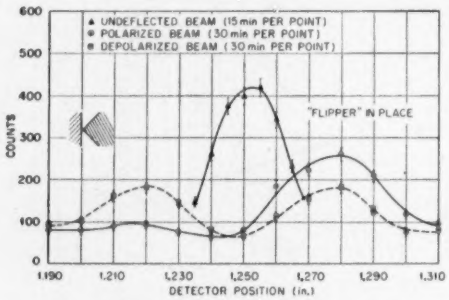
▲ UNDEFLECTED BEAM (15 min PER POINT)
● POLARIZED BEAM (30 min PER POINT)
■ DEPOLARIZED BEAM (30 min PER POINT)
"FLIPPER" IN PLACE
COUNTS
DETECTOR POSITION (in.)

FIG. 6. Deflection pattern for "flipped" beam.

from a magnetized iron mirror was compared with the resultant spin direction produced by transmission through magnetized polycrystalline iron. We find that for a sample magnetized perpendicular to the neutron velocity, the resultant neutron spins in the transmitted beam are directed opposite to the applied magnetic field. In the case of a single crystal of magnetite, in which the magnetic field was applied perpendicular to the scattering plane, the resultant spin in a beam reflected from the 220 planes is opposite to the applied magnetic field also.

ACKNOWLEDGMENT

We are very grateful to Professor J. M. Jauch for numerous helpful discussions.

Decay of Pm^{150}†*

VERA KISTIAKOWSKY FISCHER‡
Radiation Laboratory, Department of Physics, University of California, Berkeley, California, and United States Naval Radiological Defense Laboratory, San Francisco, California

(Received August 3, 1954)

A grey wedge pulse height analyzer was used to study the decay of Pm^{150} with and without coincidence arrangements. Gamma rays 3.0, 2.6, 2.0, 1.67, 1.32, 1.17, 0.82, 0.43, and 0.34 Mev in energy were observed, some in coincidence with 2.01- and 3.00-Mev negatrons which had previously been shown to be emitted. A decay scheme is suggested and some remarks on the beta stability of Nd^{150} are made.

INTRODUCTION

It has been shown by Long and Pool[1] and this author[2] that Pm^{150} decays to Sm^{150} by negatron emission with a 161-minute half-life. Hibdon and Muehlhause[3] have studied the conversion electrons of gamma rays from excited states of Sm^{150} produced by neutron capture by Sm^{149}. They found that 336.7- and 440.2-kev gamma rays were emitted, and proposed the level assignments shown in Fig. 1.

Previous studies with a double-focusing beta-ray spectrometer indicated that Pm^{150} decays by emitting 2.01- and 3.00-Mev negatrons.[2] Lead absorption studies showed at least two gamma rays, ~1.4 and ~0.3 Mev in energy, to be present. In the course of the present work Dr. T. Passell of this laboratory (University of California) examined a sample with the same instrument for conversion electrons. Peaks due to a 336-kev gamma ray were seen, in agreement with Hibdon and Muehlhause, but none from a 440-kev gamma ray. However, the sample was so weak that peaks less than one-third as abundant as those observed would not have been detected.

Two considerations prompted a further study of the decay of Pm^{150}. First, the Bohr-Mottelson[4] collective model of the nucleus which successfully treats excited states in even-even nuclei as rotational states, uses Sm^{150} as one example. This makes further knowledge of its levels seem desirable. Second, a knowledge of the Pm^{150}-Sm^{150} ground-state energy difference, in conjunction with the known Nd^{150}-Sm^{150} mass difference, might permit a verification of the suggestion by Kohman[5] that Nd^{150}, which occurs in nature, is probably beta unstable.

Sample Preparation

The samples studied were prepared by bombarding Nd_2O_3 enriched with Nd^{150} with ~9-Mev protons from the 60-inch cyclotron at Crocker Radiation Laboratory for one hour at an average external beam current of one microampere. The (p,n) and $(p,2n)$ reactions occur with comparable cross sections (~2 millibarns), and at the end of bombardment ~5 percent of the disintegrations are those of Pm^{149}, a negatron emitter with a 54-hour half-life.

The samples were purified from non-rare-earth activities by dissolving them in dilute nitric acid from which the rare earth fluoride was precipitated. This was dissolved in concentrated boric and nitric acids and the hydroxide was precipitated. The sample was then mounted on a platinum disk for study.

Apparatus

Grey Wedge Analyzer

The reader is referred to Bernstein, Chase, and Schardt[6] for a discussion of the principles and problems of grey wedge pulse-height analysis. However, since the arrangement used was developed at this laboratory (University of California) and differs from that published in the reference given above, it is discussed briefly here.

A block diagram is given in Fig. 2. The first unit is a conventional NaI(Tl)-DuMont 6292 phototube package incorporating 1-μsec delay-line clipping necessary for the coincidence work and a cathode follower output.

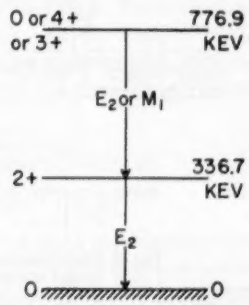

Fig. 1. Results of Hibdon and Muehlhause (see reference 4) for the lowest levels of $_{62}Sm^{150}$.

* This work was sponsored in part by the U. S. Atomic Energy Commission.

† The completion of this study was made possible by the Sarah Berliner fellowship (1953–1954) of the American Association of University Women.

‡ Now at Columbia University, New York, New York.

[1] J. K. Long and M. L. Pool, Phys. Rev. **85**, 137 (1952).

[2] Vera Kistiakowsky, Phys. Rev. **87**, 859 (1952).

[3] C. T. Hibdon and C. O. Muehlhause, Phys. Rev. **88**, 943 (1952).

[4] A. Bohr and B. R. Mottelson, Kgl. Danske Videnskab. Selskab, Mat.-fys. Medd. **27**, No. 16 (1953).

[5] T. P. Kohman, Phys. Rev. **73**, 16 (1948); (private communication, 1954).

[6] Bernstein, Chase, and Schardt, Rev. Sci. Instr. **24**, 437 (1953).

The pulses are amplified by a standard nonoverloading UCRL linear amplifier. They then trigger the sweep of a Textronics 512AD oscilloscope, the output 16-μsec gate pulse of which is sent to the pulse stretcher unit. This consists basically of a normally conducting diode which is clamped for the duration of the gate pulse. The linear amplifier pulses going into this unit are delayed 1.25 μsec and then charge a condenser which discharges only when the diode again becomes conducting. The stretched pulse which goes to the oscilloscope signal input is constant in amplitude to $\sim$2 percent and the device is linear to $\sim$2 percent in the operating range of 5–95 volts.

A third output of the linear amplifier is used to trigger a standard UCRL variable delay and gate unit. A suitably delayed 12-μsec positive gate pulse from this unit is amplified, inverted, and clipped to a constant amplitude of -40 volts by the intensifier pulse shaper, and is then used to intensify the oscilloscope trace.

The 512AD Textronics oscilloscope is equipped with a 5*XP*11-*M* tube and modified to be used with an external high-voltage supply. The traces were photographed by a 4-by-5-inch view camera with a 127-mm *f*4.5 lens. A 4-by-5-inch grey wedge was mounted in the back of the camera directly in front of the film. After experiments with several types of film, Kodak Super Ortho Press was settled upon, because it combines workable film-speed and contrast qualities. The latter were emphasized by overdeveloping in Kodak D-19.

The NaI(Tl) crystals[7] used were packaged with a MgO diffuse reflector. A crystal 1.5 inches in diameter by 2 inches long was used for high energy gamma-ray studies, while another, 1.5 inches in diameter by $\frac{1}{2}$ inch long, was used for lower energy portions of the spectrum. Beryllium absorbers of 1500 mg/cm^2 were used to remove the negatron spectra.

Pictures were enlarged, and corrected for a slight barrel distortion of the pulses on the oscilloscope face by reading them from a grid. A relative calibration of exposure amplitude *versus* counting rate was made and

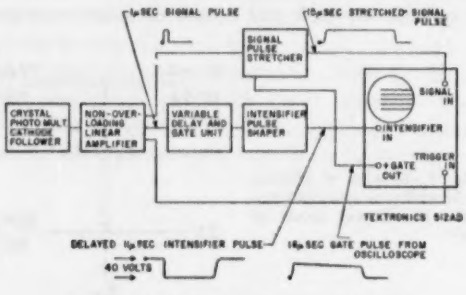

FIG. 2. Block diagram of grey wedge pulse height analyzer electronics.

[7] Obtained from the Harshaw Chemical Company, Cleveland 6, Ohio.

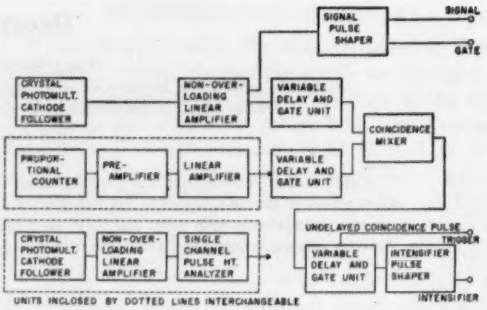

FIG. 3. Block diagram of coincidence experiment electronics.

checked roughly before each series of pictures for the given experimental conditions. Energy calibration was made before each experiment by using samples of Co^{56}, Co^{60}, Na^{22}, Cs^{137}, Cd^{109}, and Am^{241}, and some points were retaken at intervals to check for drifts. The distributions of the peaks in such pictures were also used in interpreting the unknown spectra.

The limits of error quoted on the gamma-ray energies include small uncertainties in the energy calibration as well as the uncertainties of reading the pictures.

Coincidence Experiments

Figure 3 is a block diagram of the coincidence experiment electronics. Pulses from the scintillation counter are coincidized either with those from a proportional counter or with those from a single-channel pulse height analyzer which examines the pulse distribution from a second scintillation counter. The resolving time of the arrangement is $\sim$3 μsec, placing a severe limitation on the count rate allowable. In all cases experiments were performed with maximum possible grometry: 16 percent for each of the scintillation counters and 25 percent for the proportional counter. Samples of various strengths were used to adjust the count rate to an optimum value with respect to both chance coincidence and statistics.

The coincidence signal is fed into a variable delay and gate unit. An undelayed pulse from the discriminator in the gate input is used to trigger the grey wedge analyzer oscilloscope, while the delayed gate pulse is used for intensification as before.

No attempt is made to achieve actual pulse height-to-energy correspondence for beta particles in the gas counter. It is operated in the proportional region rather than the Geiger region for the sake of resolution time, and its pulses are *RC*-clipped to 1 μsec (decay from 90 percent to 10 percent maximum). Decisions as to beta-gamma coincidences were made by quantitatively comparing spectra in coincidence with the proportional counter with various thicknesses of absorber in front of it.

RESULTS

The first noncoincidence experiments and all the coincidence experiments indicated the presence of gamma rays up to ~2.5 Mev in the decay of Pm^{150}. Later experiments, in which several long exposures of the high-energy spectrum were taken, showed another peak at 3.0 Mev and were better in high-energy calibration. Figure 4 shows one of these pictures, and Fig. 5 contains the spectrum obtained with twice the linear amplifier gain of Fig. 4.

The results are summarized in Table I. Three dots represent those points on which no conclusions could be drawn, owing to insufficient data. "*O*" stands for observed, "*N*" stands for observed to be absent, and "?" for uncertainty. The approximate relative abundances were calculated by comparison with the spectra obtained for samples having known relative abundances. Owing to uncertainties involved in this method the numbers given are good only to an order of magnitude.

All the gamma-ray peaks observed in the noncoincidence experiments stay in the same ratios to one another during the first nine hours of decay, and during this period the gross decay has a half life of 161 minutes. After that the decay rate decreases and peaks belonging to the 285-kev and 1-Mev gamma rays of Pm^{149} change the spectrum. It was found that the number of gamma rays in the energy interval 3.0±0.25 Mev decreases with a half-life of (160_{-60}^{+160}) minutes. Unfortunately it was impossible to make a sufficiently active sample to permit a more accurate determination.

Before the 3.0-Mev gamma ray had been discovered,

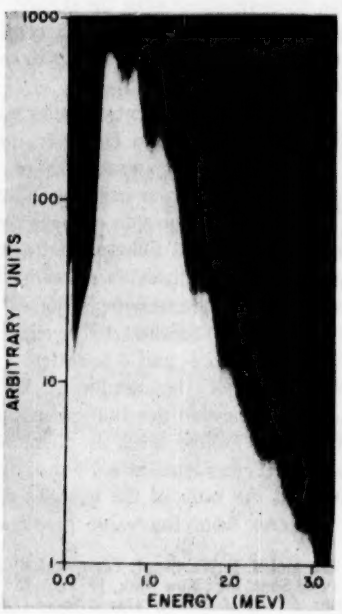

FIG. 4. Gamma-ray spectrum of Pm^{150}; higher energies.

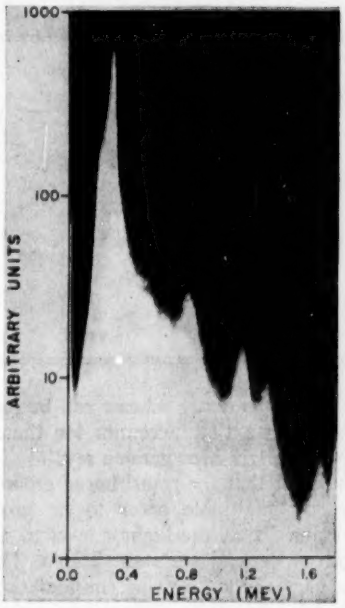

FIG. 5. Gamma-ray spectrum of Pm^{150}; intermediate energies.

no decay scheme agreeing with all the experimental results could be formulated. Therefore the old beta-ray spectroscopy results were re-examined to determine if they could be in error. Four independent sets of data give Fermi-Kurie plots which resolve to give 2.01- and 3.00-Mev components. One, shown in Fig. 6, also exhibits a 0.97-Mev negatron due to Pm^{149}. However, the author would like to revise her earlier calculation of the relative intensities to (20±10 percent) and (80±10 percent) respectively for the 3.00- and 2.01-Mev components.

CONCLUSIONS

Figure 7 shows the simplest decay scheme in agreement with all the results of these and previous experiments. It is not thought that all the transitions indicated occur. They are just listed to show how they could be explained by the observed energy spectrum.

At first it was postulated that the 3.0-Mev gamma ray arises from a transition to ground state. There are three objections to this. First, although the energies of the highest energy gamma rays are uncertain by 0.1 Mev, their differences are certain to the accuracy of reading the pictures. Thus

$$E_{(3.0\ \mathrm{Mev})} - E_{(2.6\ \mathrm{Mev})} = 0.40 \pm 0.05,$$
$$E_{(2.6\ \mathrm{Mev})} - E_{(2.0\ \mathrm{Mev})} = 0.57 \pm 0.05.$$

If the 3.0-, 2.6-, and 2.0-Mev gamma rays corresponded to transitions to the ground state and first and second excited states, one would expect differences of 0.34 and 0.44 Mev, respectively.

TABLE I. Energies of observed gamma rays.

Energy (Mev)	Approximate relative abundance	Occurrence in decay scheme	Observations: No coincidence	Coincidence 2-Mev $\beta-$	Coincidence 3-Mev $\beta-$	Coincidence 0.34-Mev γ
3.0 ±0.1	0.004	γ_1	0	Distribution of pulses up to ~ 2.5 Mev	...	Distribution of pulses up to ~2.0 Mev
2.6 ±0.1	0.008	γ_2	0		...	
2.0 ±0.1	0.004	γ_3, γ_6, γ_{10}	0		...	
1.67±0.05	0.008	γ_7, γ_{11}	0	0	...	0
1.32±0.05	0.04	γ_4	0	0	0	0
?1.24	...	γ_{12}	...	...	0?	...
1.17±0.05	0.04	γ_5, γ_{12}, γ_{14}	0	0	...	N
?0.96	...	γ_5	0?	...	...	...
0.82±0.02	0.4	γ_{13}, γ_{15}	0	0	0	0
0.43±0.02	0.2	γ_{17}	0	0	...	0
?0.39	...	γ_9, γ_{16}	...	...	0?	0?
0.34±0.01	1.0	γ_8, γ_{18}	0	0	...	N

Second, no simple decay scheme can be formulated from this postulate that accounts for the observed abundance of the 1.17-Mev gamma ray.

Third, in order that the transition of ground have a sufficiently low multipole order to be probable, it must be assumed that the highest level to which the Pm^{150} negatron decays has a small spin. This seems unlikely in view of the following considerations. From Klinkenberg's[8] tables the 61st proton of Pm^{150} is assigned to a $d_{5/2}$ state, and the 89th neutron to a $f_{7/2}$ state. If Nordheim's[9] rules for odd-odd isotopes are used in conjunction with Schwartz's[10] remarks, the ground state of Pm^{150} is expected to have odd parity and spin, J; $1<J\leq 6$. The $\log(ft)$ values indicate that the negatron transitions are first-forbidden, and thus the levels in Sm^{150} to which the decay leads should have even parity and spin differing by zero or one unit from that of the ground state of Pm^{150}. Thus if the highest levels in Sm^{150} have spin less than 4 and Pm^{150} has spin less than 5, negatron transitions to intermediate levels of spin of at least 3 would be expected to occur.

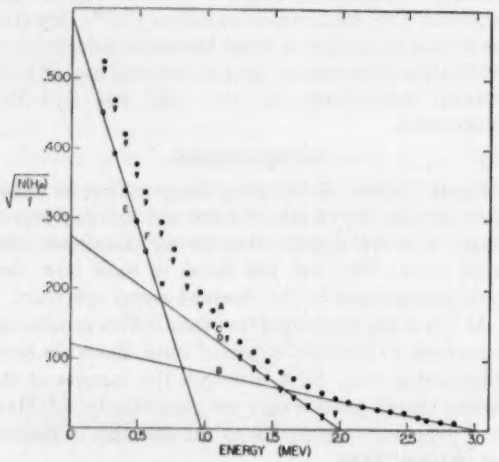

FIG. 6. Fermi-Kurie plot of beta-ray spectrometer data for the 161-minute and 54-hour half-life activities from $Nd^{150}+p$ bombardments: (a), from gross data corrected for 161-minute half-life decay; (b), 3-Mev component; (c), from gross data with 3-Mev component subtracted; (d), 2-Mev component; (e), from gross data with 2-Mev and 3-Mev components subtracted and corrected for 54-hour half-life decay; (f), 0.97-Mev component.

These three arguments are satisfied if it is assumed that the 3.0-Mev gamma ray arises from a transition to the first excited state. The energies of this and the second level are taken from the work previously mentioned. The remaining levels represent the most obvious choices satisfying the experimental results. The three most important justifications should by mentioned, however, although a detailed discussion would take too long. First, if the highest level is at 3.3±0.1 Mev, there must be another, 1 Mev below, to account for the negatron decay. Second, the level at 1.17±0.05 Mev accounts for the 1.17-Mev gamma ray, which is not in coincidence with the 0.34-Mev gamma ray. Third, the level at 2.0±0.1 Mev accounts for the abundance of the 1.67-Mev gamma ray in coincidence with the 2-Mev negatron.

On the basis of the experimental results no spin and parity assignments can be made. However, the observation that γ_1 and γ_2 have abundances of the same order of magnitude is not compatible with a difference of two or more between the spin changes occurring in these two transitions. This follows from a calculation of the transition probabilities as given in Blatt and Weisskopf.[11] In several recent compilations[4,12,13] of data on even-even isotopes, the first two excited levels of Sm^{150} are assigned to 2+ and 4+ states. This is the best interpretation of the results of Hibdon and Muehlhause,[3] but they do not rule out assignment of 3+ to the second excited level. In these papers[4,12,13] where this level is considered as a 4+ rotational state, the deviation of the ratio of the energies of the first two excited states from the value predicted by the

[8] P. F. A. Klinkenberg, Revs. Modern Phys. 24, 63 (1952).
[9] L. Nordheim, Phys. Rev. 78, 294 (1950).
[10] C. Schwartz, Phys. Rev. 94, 95 (1954).
[11] J. M. Blatt and V. F. Weisskopf, *Theoretical Nuclear Physics* (John Wiley and Sons, Inc., New York, 1952), p. 627
[12] Aage Bohr, *Rotational States of Atomic Nuclei* (Ejnar Munksgaards Forlag, Køpenhavn, 1954).
[13] E. L. Church and M. Goldhaber (to be published, 1954).

formula for rotational levels,[12]

$$E_I=\frac{\hbar^2}{2\Im}I(I+1),$$

is accounted for by an increase in nuclear deformation due to a vibration-rotation type of interaction. The correction term[12] is

$$\Delta E_I\approx-2\left(\frac{1}{\hbar\omega_{\text{vib}}}\right)^2\left(\frac{\hbar^2}{\Im}\right)^3 I^2(I+1)^2.$$

By calculating on the assumption that $E_2=337$ kev and $E_4=777$ kev, it is found that ΔE_I is 1.2 percent and 39 percent of E_I for E_2 and E_4 respectively. Thus the criterion for the existence of a rotational spectrum,[12] that ΔE_I be small compared to E_I, is not fulfilled for $I\geq 4$. It is not unreasonable, therefore, to suggest that the second excited state of Sm^{150} is a 3+ rather than a 4+ state. Since the first excited state is 2+, the relative abundance of γ_1 and γ_2 is then much more easily explained.

There are other indications that Sm^{150} is not a strong-coupling case. The large isotope shifts observed between spectra of isotopes with 82+6 neutrons and those with 82+8 neutrons, e.g., $_{62}Sm^{150}-{}_{62}Sm^{152}$ and $_{63}Eu^{151}-{}_{63}Eu^{153}$,[14] and $_{60}Nd^{148}-{}_{60}Nd^{150}$,[15] suggest that some change in nuclear structure takes place between these neutron numbers. Rasmussen[16] has pointed out that the large quadrupole moment of $_{63}Eu^{153}$ indicating a large spheroidal distortion of the nucleus suggests applicability of the strong-coupling model. It seems reasonable, therefore, to suppose that the change that occurs is from intermediate to strong coupling.

Stability of Nd^{150}

Kohman[5] has pointed out that Nd^{150} would be expected to be unstable with respect to negatron decay to Pm^{150}. However, Mulholland and Kohman[17] did not observe any appreciable activity in neodymium, and placed a lower limit of 2×10^{15} years on the possible half-life of such decay.

Hoagg and Duckworth[18] have obtained a Nd^{150}-Sm^{150} mass difference of 4.6±0.8 Mev. Since the proposed Pm^{150}-Sm^{150} ground-state energy difference is 5.3±0.15 Mev, the Nd^{150}-Pm^{150} difference is −0.7±1.0 Mev and Nd^{150} may or may not be stable. If it is not, then it is unstable by at most 0.3 Mev. If one accepts the previous arguments for an assignment of negative parity and spin 5 or 6 to be the ground state of Pm^{150}, the negatron decay would be at least fifth-forbidden. A reasonable choice of log(ft) would be 26, and from this a lower limit of 10^{18} years can be set on the half-life.

If, on the other hand, Pm^{150} is unstable with respect to Nd^{150}, this mode of decay would not be detected. If one assumes the 4+ level of $_{60}Nd^{150}{}_{90}$ to be analogous to that of $_{62}Sm^{152}{}_{90}$, it would be at 0.37 Mev.[13] Assuming first-forbidden electron capture to such a level, a minimum half-life for decay of Pm^{150} to Sm^{150} is found to be twenty times greater than that known for the negatron decay to Nd^{150}.

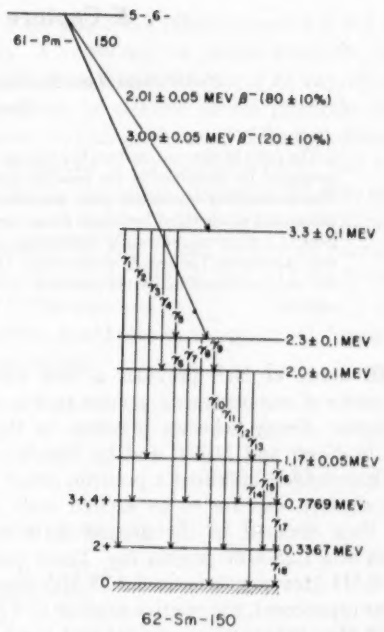

FIG. 7. Decay scheme proposed for Pm^{150}.

ACKNOWLEDGMENTS

It is a pleasure to acknowledge some valuable discussions with Professor J. O. Rasmussen, Jr., and a fruitful correspondence with Professor T. P. Kohman. I also wish to thank Dr. B. T. Youtz and Mr. L. T. Kerth for the grey wedge analyzer design and the Isotope Research and Development Division, Oak Ridge, Tennessee, for making available to me the enriched isotope that made this work possible.

[14] P. Brix and H. Kopferman, Phys. Rev. **85**, 1050 (1952).
[15] P. F. A. Klinkenberg, Physica **11**, 327 (1945).
[16] J. O. Rasmussen, Jr., Arkiv Fysik **7**, 185 (1953).
[17] G. I. Mulholland and T. P. Kohman, Phys. Rev. **85**, 144 (1952).
[18] B. G. Hoagg and H. E. Duckworth, Can. J. Phys. **32**, 65 (1954).

K Capture to Positron Ratio for Na^{22}

W. E. KREGER
United States Naval Radiological Defense Laboratory, San Francisco, California
(Received September 13, 1954)

The ratio of electron capture to positron emission from Na^{22} to the 1.28-Mev excited state of Ne^{22} has been measured by determining the relative number of 1.28-Mev and 0.511-Mev gamma rays from this decay. The gamma-ray intensities were measured with a 4-in. by 4-in. NaI(Tl) scintillation spectrometer and a collimated geometry. Photopeak areas were determined for the two gamma-ray energies, and using photopeak to total areas previously determined and NaI absorption coefficients, the ratio of gamma-ray intensities was calculated. The results showed that 11.0±0.9 percent of the disintegrations to the excited state of Ne^{22} are not accompanied by the emission of two 0.511-Mev quanta, and therefore decay by orbital electron capture.

THE decay of Na^{22} provides a very convenient source of monoenergetic gamma rays in the one-Mev region. Decay schemes previous to the recent papers by Sherr and Miller[1] and by Maeder, Müller, and Wintersteiger[2] indicated a positron decay without orbital electron capture to an excited state of Ne^{22}, which then decayed to the ground state with the emission of a 1.28-Mev gamma ray. There would thus be two 0.511-Mev quanta for each 1.28-Mev gamma ray.

In our experiment, the relative number of 0.511-Mev and 1.28-Mev quanta was measured with a scintillation spectrometer. By this means, it was possible to determine how many of the decays from the excited state to the ground state with the emission of 1.28-Mev gamma rays were not accompanied by the emission of two 0.511-Mev gamma rays. This would indicate the number of disintegrations to the excited state of Ne^{22} which went by *K* capture rather than positron emission.

A 4-in. diameter by 4-in. long NaI crystal with a lead shield and collimating hole was used as the gamma detector. The crystal was optically coupled to a 2-in. Dumont 6292 photomultiplier tube. The collimator was six inches of lead with a hole having a $1\frac{1}{4}$-in. diameter at the crystal end and a 1-in. diameter at the source end. The pulse spectrum was analyzed by an automatic recording single-channel pulse-height analyzer.

The source used was $Na^{22}Cl$ deposited on a quarter-centimeter diameter thin disk of aluminum. This source was surrounded with 0.9 mm of Al which served to stop all the positrons. The source was placed at the apex of the cone formed by the collimator walls. The pulse spectrum taken with the Na^{22} source and the detector described is shown in Fig. 1. In order to determine relative strengths of the two monoenergetic gamma rays emitted, the photopeak areas were measured.

In the crystal of this size, the photoelectric peak response is considerably enhanced by the addition of pulses occurring when an incident gamma-ray Compton scatters and then has its scattered gamma-photon photoelectrically absorbed within the crystal. While the absolute detection efficiency in the whole pulse spectrum for such a crystal and geometry can be calculated from the NaI absorption coefficients, it is necessary to determine the photopeak efficiency at a

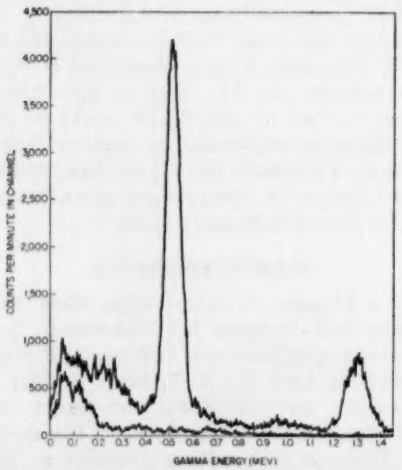

FIG. 1. Scintillation spectrometer pulse spectrum for gamma rays from Na^{22} decay. Detector: 4-in. diameter×4-in. NaI crystal; collimated geometry; single-channel analyzer; and automatic recording.

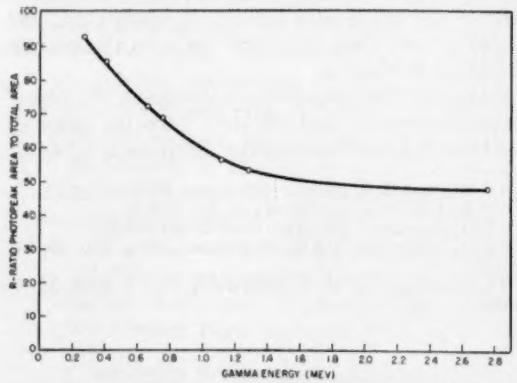

FIG. 2. Ratio of photopeak area to total area for a NaI scintillation spectrometer 4 in. in diameter and 4 in. long with collimated geometry. The source is on the axis of the crystal.

[1] R. Sherr and R. H. Miller, Phys. Rev. **93**, 1076 (1954).
[2] Maeder, Müller, and Wintersteiger, Helv. Phys. Acta **27**, 3 (1954).

given energy, either experimentally or by a rather involved calculation.

We have measured the relative photopeak efficiencies for the geometrical spectrometer arrangement discussed above for six monoenergetic gamma rays. This photopeak efficiency is shown in Fig. 2. From the results of this experiment, it was possible to calculate relative strengths of the two gamma rays present from the decay of Na^{22}. With the source solid angle the same for both gammas, the ratio of strengths of the two gammas is given by

$$\frac{\gamma_1}{\gamma_2}=\frac{\{1-\exp[-\mu(E_1)x]\}\{F(E_1)\}\{A(E_1)\}}{\{1-\exp[-\mu(E_2)x]\}\{F(E_2)\}\{A(E_2)\}},$$

where F is the photopeak efficiency and A is the photopeak area. A correction to source strengths for the difference in absorption in 0.9 mm of Al was calculated. The calculation of relative source strengths for the two gamma rays showed that (11.0±0.9) percent of the disintegrations to the excited state of Ne^{22} are not accompanied by the emission of two 0.511-Mev quanta, and therefore decay by orbital electron capture. This result agrees with the values (9.9±0.6) percent obtained by Sherr and Miller[1] and (11.5±5) percent obtained by Maeder *et al.*[2]

The author would like to thank Dr. C. Sharp Cook for his suggestions.

PHYSICAL REVIEW VOLUME 96, NUMBER 6 DECEMBER 15, 1954

Decay of $_{32}Ge^{75m}$ (49 sec), $_{32}Ge^{77m}$ (52 sec), and $_{32}Ge^{77}$ (12 hr)

S. B. Burson, W. C. Jordon, and J. M. LeBlanc
Argonne National Laboratory, Lemont, Illinois

(Received August 18, 1954)

The investigations herein described have been carried out by using a scintillation coincidence spectrometer and 180° focusing magnetic spectrographs. Sources are prepared by the activation of both normal germanium and the enriched isotopes thereof in the Argonne reactor (CP-3'). Three of the neutron-induced activities of germanium are studied.

$_{32}Ge^{75m}$ *(49 sec):* The half-life and isotopic assignment of the activity are confirmed. From internal-conversion measurements, the energy of the isomeric transition is found to be 138.5±1.0 kev, and the K/L ratio estimated to be ~3.

$_{32}Ge^{77m}$ *(52 sec):* The isotopic assignment of the activity is confirmed and the half-life measured to be 52±2 seconds. The isomeric state of Ge^{77} decays by three branches: an isomeric transition of 159±3 kev to the ground state of Ge^{77}, an ~2.7-Mev beta ray to a 215±3-kev excited state of As^{77}, and an ~2.9-Mev beta ray to the ground state.

$_{32}Ge^{77}$ *(12 hr):* From the scintillation spectrometer measurements, the presence of eighteen gamma rays is deduced. Though beta-gamma and gamma-gamma coincidence experiments these are incorporated into a decay scheme which includes the 52-second isomeric state of Ge^{77} and nine excited states of As^{77}.

APPARATUS AND METHODS

NORMAL germanium has been found to consist of five stable isotopes. Neutron capture in three of these results in the formation of Ge^{71} (11 day), Ge^{75m} (49 sec), Ge^{75} (80 min), Ge^{77m} (52 sec), and Ge^{77} (12 hr). Previous studies of these activities have not been exhaustive. We have undertaken to investigate the two metastable states, Ge^{75m} and Ge^{77m}, and the 12 hour activity of the ground state of Ge^{77}.

The scintillation coincidence spectrometer[1] employed in this study is composed of two independent spectrometers, one incorporating a ten-channel pulse-height analyzer, and the other a single-channel analyzer. The ten-channel analyzer is used independently to examine the "normal" pulse-height distribution associated with the source, while both analyzers are employed to search for various coincidence combinations of the peaks found in the normal spectrum. In examining a normal gamma-ray spectrum, the sources are placed approximately six inches from the detecting crystal, and a collimator is interposed. (The collimator consists of a 2-in. lead block through which a ¾-in.-diameter hole is bored.) These arrangements serve two purposes: to increase the amplitude of the "photopeak" relative to the Compton distribution and to eliminate the possibility of "sum" peaks caused by the simultaneous detection of two coincident radiations. Many operational details of this instrument have been previously discussed.[2]

The efficiency and resolution of the scintillation coincidence spectrometer have been improved by the installation of larger NaI(Tl) crystals than those previously used and by replacing the R.C.A. type 5819 photomultipliers with Dumont type 6292 tubes. (The resolution is now about 8 percent for the 662-kev gamma ray of Cs^{137}.) The new crystals are nearly cubic,

[1] S. Burson and W. Jordon, Phys. Rev. **91**, 498 (1953).

[2] Burson, Jordon, and LeBlanc, Phys. Rev. **94**, 103 (1954).

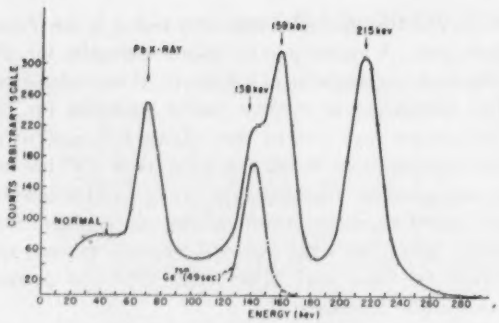

FIG. 1. The pulse-height distribution of $_{32}Ge^{77m}$ (52 sec) and $_{32}Ge^{75m}$ (49 sec).

measuring $2\frac{1}{4}$ in.$\times 2\frac{1}{4}$ in.$\times 2\frac{1}{8}$ in. For beta-ray detection, the NaI crystal in the single-channel arm of the circuit is replaced by an anthracene crystal. This instrument is supplemented by internal-conversion-electron spectrographs[3] which are used, where possible, to ascertain more accurate transition energies. Coincidence measurements yield information relating the various transitions, which, together with the energies, permit a decay scheme to be constructed.

Ge^{75m} (49 sec)

In 1952, Flammersfeld[4] reported an activity with a half-life of 42 seconds which he assigned to a metastable state of Ge^{75}. By means of absorption measurements, he determined the energy of the conversion electrons associated with the activity to be 140 kev. Subsequently, Smith *et al.*[5] reported having independently observed and studied this activity. They assign an energy of about 175 kev to the isomeric transition from scintillation-spectrometer measurements and assign a value of 48±2 seconds for the half-life. From energy-lifetime considerations, they conclude the character of the radiation to be E3. Campbell[6] reports the energy of the isomeric transition to be about 150 kev.

Our measurement of the half-life yielded a value of 49±2 seconds in good agreement with that of Smith *et al.* We have determined the transition energy both by scintillation spectrometer and by internal-conversion-electron measurements. The scintillation spectrometer was calibrated for this measurement with the 159-kev gamma ray of Te^{123}, and the energy of the gamma ray was measured to be 142±3 kev (Fig. 1). A more accurate measurement was made using a magnetic electron spectrograph. Fifty irradiations of a source brought out K and L lines on the photographic plates from which the energy is found to be 138.5±1.0 kev. From visual examination of the plate, the K/L ratio is estimated to be greater than 3.

A search was made for other radiations which might be associated with this activity, but none were found. It is thus concluded that Ge^{75m} decays to the ground state of Ge^{75} by means of either the emission of a 138.5-kev gamma ray or of internal-conversion electrons.

Ge^{77m} (52 sec)

Arnold and Sugarman[7] reported an activity of 59±2 seconds which they assigned to an isomeric state in Ge^{77}. They measured the energy of the beta ray to be 2.8 Mev by absorption in aluminum and observed no gamma rays. By means of a scintillation spectrograph, Mitchell and Smith[8] reported the energy of the isomeric transition to be 380 kev.

Our examination of the normal scintillation spectrum shows the presence of two photopeaks associated with this activity. These represent gamma rays with energies of 159±3 and 215±3 kev (Fig. 1). The 159-kev gamma ray of Te^{123} was used for calibration. Although the source was produced by neutron irradiation of enriched Ge^{76}, the 138.5-kev gamma ray still appears to be due to incomplete isotopic separation.

By following the decay of the 215-kev peak, the lifetime of the metastable state was found to be 52±2 seconds.

A search for gamma-gamma coincidences showed the two radiations not to be in coincidence. The 215-kev gamma ray was found to be in coincidence with beta rays, while the 159-kev radiation was not (Fig. 2). Absorption measurements in aluminum show the beta ray in coincidence with the 215-kev gamma ray to have a half-thickness of approximately 170 mg/cm², corresponding to an end-point energy of about 2.7 Mev. From the beta-gamma coincidence measurements we estimate the beta branching to the excited state of As^{77} to be approximately one-tenth of that to the ground state. Thus, it is concluded that the isomeric state of Ge^{77} decays by three branches: an isomeric transition of 159 kev to the ground state of Ge^{77}, an

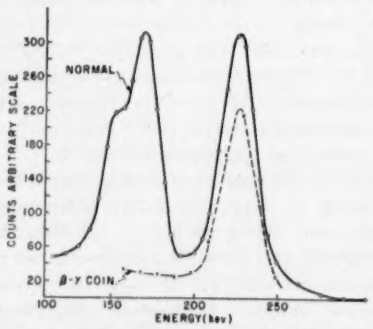

FIG. 2. Beta-gamma coincidence pulse-height distribution of $_{32}Ge^{77m}$ (52 sec).

[3] Rutledge, Cork, and Burson, Phys. Rev. **86**, 775 (1952).
[4] A. Flammersfeld, Z. Naturforsch. **7a**, 295 (1952).
[5] Smith, Caird, and Mitchell, Phys. Rev. **88**, 150 (1952).
[6] E. C. Campbell, private communication to Hollander, Perlman, and Seaborg, Revs. Modern Phys. **25**, 504 (1953).
[7] J. Arnold and N. Sugarman, J. Chem. Phys. **15**, 703 (1947).
[8] A. Mitchell and A. Smith, Phys. Rev. **85**, 153 (1952).

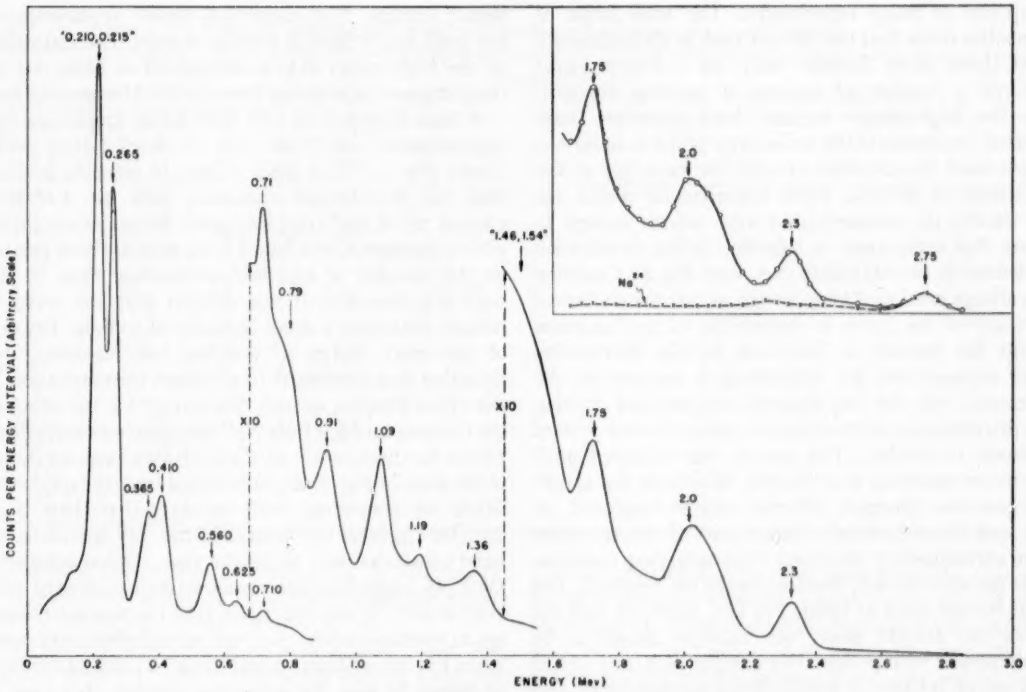

FIG. 3. Normal pulse-height distribution of $_{32}Ge^{77}$ (12 hr).

~2.7-Mev beta ray to a 215-kev excited state of As^{77}, and an ~2.9-Mev beta ray to the ground state.

Ge^{77} (12 hour)

Sagane[9] produced an activity with a half-life of about eight hours by irradiating germanium with neutrons and deuterons and assigned it to Ge^{77}. Seaborg *et al.*[10] confirmed the assignment and measured the half-life to be 12 hours. Sagane *et al.*[11] measured the maximum beta-ray energy to be 1.9 Mev. Steinberg and Engelkemeir[12] measured the beta energy to be 2.0 Mev and also detected gamma radiation. To the beta ray, Mandeville *et al.*[13] assigned a value of 1.74 Mev, verified the generic relationship, showing the 12-hour germanium to be the parent of the 40-hour As^{77}, and observed coincidences between the beta rays and gamma rays with a nominal energy of about 0.5 Mev (by absorption methods). Reynolds[14] (also by absorption methods) found an energy value of 1.8 Mev for the beta ray and analyzed the gamma radiation into two components of about 0.3 and 0.6 Mev. He observed coincidences between beta rays and each of the gamma-ray components, and also between two gamma rays, both of about 0.3 Mev, but no coincidences between the 0.3-Mev radiations and those of about 0.6 Mev. Using a lens spectrometer, Smith[15] resolved the beta spectrum into three components, 2.196, 1.379, and 0.710 Mev. From internal conversion and the photo electrons from secondary radiators, he reports thirteen gamma rays. These measurements, together with the results of some coincidence experiments, were used to present a decay scheme. Two more gamma rays of 2.3 and 2.7 Mev were observed by Saraf *et al.*[16] and attributed to the 12-hour Ge^{77}.

Our efforts have been directed toward a detailed study of the gamma-ray spectrum and in particular, through extensive coincidence measurements, the construction of a decay scheme. Our result differs markedly from that of Smith, which is not surprising since, in addition to other discrepancies, our scintillation spectrometer revealed the presence of at least eight gamma rays not detected by his apparatus.

THE GAMMA-RAY SPECTRUM

The normal scintillation pulse-height distribution is shown in Fig. 3. The curve presented represents a

[9] R. Sagane, Phys. Rev. **53**, 212 (1938); Phys. Rev. **55**, 31 (1939).
[10] Seaborg, Livingood, and Friedlander, Phys. Rev. **59**, 320 (1941).
[11] Sagane, Miyamoto, and Ikawa, Phys. Rev. **59**, 904 (1941).
[12] E. Steinberg and D. Engelkemeir, *Radiochemical Studies: The Fission Products* (McGraw-Hill Book Company, Inc., New York, 1951), Paper No. 54, National Nuclear Energy Series, Plutonium Project Record, Vol. 9, Div. IV.
[13] Woo, Mandeville, Scherb, and Keighton, Phys. Rev. **75**, 1286 (1949); Mandeville, Woo, Scherb, Keighton, and Shapiro, Phys. Rev. **75**, 1528 (1949).
[14] S. A. Reynolds, Oak Ridge National Laboratory Report ORNL-867, 24 (unpublished).
[15] A. B. Smith, Phys. Rev. **86**, 98 (1952); A. Smith and A. Mitchell, Phys. Rev. **85**, 153 (1952).
[16] Saraf, Varma, and Mandeville, Phys. Rev. **91**, 1216 (1953).

composite of many experiments. The wide range of intensities (note that the 210-kev peak is approximately 1000 times more intense than the 2.3-Mev peak) required a number of sources of varying strength. For the high-energy regions, lead absorbers were inserted to attenuate the low-energy peaks in order not to overload the amplifier or shift the base line of the discriminator circuits. While experimental points are not shown, the channels used were narrow enough to insure that every peak or inflection in the distribution be defined by several points (e.g., inset Fig. 3). Counting was always continued long enough so that the statistical accuracy of the curve is comparable to the thickness of the line defining it. The data for the distribution were accumulated by bracketing a portion of the spectrum with the ten-channel analyzer and moving the discriminator to an adjacent region to allow several channels to overlap. This process was repeated until the entire spectrum was covered. Whenever the amplifier gain was changed, different sources employed, or the lead filters inserted, the sections of the spectrum were normalized by matching the overlapping portions.

In the distribution, fourteen peaks are resolved. The most intense peak at about 210 kev, hereafter referred to as the 210,215 peak, will later be shown to be complex and to represent two gamma rays, one of 210 and one of 215 kev. The coincidence measurements also show that the shoulder on the high-energy side of the 710-kev peak represents the photopeak of a gamma ray of about 790 kev. While no other experiments explain the significance of the shoulder at about 1.5 Mev, the decay scheme proposed does provide for transitions of about this energy. The shoulder is too intense to be accounted for by attributing it to Compton distributions or other secondary effects of the gamma rays of higher energy. The somewhat broad appearance of the peak at 2.0 Mev is worthy of note. The distortion on the high-energy side is interpreted as being due to the Compton distribution from the 2.3-Mev gamma ray.

A peak appeared at 2.75 Mev whose amplitude was approximately one-third that of the 2.3-Mev peak. (Inset Fig. 3.) This peak is seen to coincide exactly with the distribution associated with the 2.75-Mev gamma ray of Na^{24} (dashed curve). Since the amplitude of this photopeak was found to be several times greater in the samples of enriched germanium than in the normal germanium, it was evident that the enriched isotope contained a small impurity of sodium. Because of the exact energy fit and the low intensity, this radiation was attributed to a sodium contamination in the other samples as well. To correct for the effect of the contamination, a pure Na^{24} spectrum was normalized to the Ge distribution at the 2.75-Mev peak as shown in the inset in Fig. 3, and subtracted from the spectrum. While we cannot say with certainty that there is no 2.75-Mev gamma ray present in the Ge^{77} spectrum, we have concluded this to be the case. The spectrum of Ga^{72} (14 hour) was also examined and compared with that of Ge^{77}. It was concluded that Ga was not present as a contamination. In our scintillation spectrum, when the lead collimator was in use, a peak was present at about 73 kev. To determine whether this peak in part represented a gamma ray or was entirely due to secondary radiation, the lead shielding was replaced by concrete blocks. It was then found that the 73-kev peak had vanished and the only rise in the distribution between about 20 and 200 kev could be attributed to the Compton electrons from the higher energy gamma rays. We also found no evidence for the gamma rays of 300, 327, 425, or 466 kev.

Only two of the gamma rays were measured by internal conversion, the 210- and the 265-kev radiations. While a faint K line for the 215-kev gamma ray was visible, it was not well enough defined to be considered as a reliable datum.

Table I lists all of the gamma rays observed by us, including those detected only through coincidence measurements. For purposes of convenient comparison, the gamma rays reported by Smith and by Saraf *et al.* are also listed.

TABLE I. Gamma rays associated with $_{32}Ge^{77}$(12 hr).

Present investigation	Smith	Saraf *et al.*
	0.042	
	0.073	
0.210±0.001		
0.215±0.003	0.213	
0.265±0.001	0.264	
	0.300	
	0.327	
0.365±0.007	0.368	
0.410±0.008	0.408	
	0.418	
	0.466	
0.560±0.010	0.564	
0.625±0.015		
0.710±0.015		
0.79 ±0.02		
0.91 ±0.02		
1.09 ±0.02	1.105	
1.19 ±0.02		
1.36 ±0.03		
1.46 } Unresolved		
1.54 }		
1.75 ±0.03	1.75	
2.00 ±0.05		
2.30 ±0.05		2.3
		2.7

COINCIDENCE MEASUREMENTS AND DECAY SCHEMES

In the following paragraphs, the coincidence experiments are discussed together with the development of the decay scheme. Table II presents a summary of the coincidence results. The letter A designates that the combination indicated was observed with certainty and that the interpretation is deemed to be reliable. The letter B indicates that coincidences were observed, but that some ambiguity or other element of uncertainty exists. The numbers refer to the associated paragraph in which experimental details are discussed.

TABLE II. Summary of β-γ and γ-γ coincidence measurements on $_{32}Ge^{77}$ (12 hr).

		Gamma rays (Mev)																	
		0.210	0.215	0.265	0.365	0.410	0.560	0.625	0.71	0.80	0.91	1.09	1.19	1.36	1.46	1.54	1.75	2.0	2.3
Beta	~1.3											B11							
	~1.5		B6	B6	B6	B6	A6												
	~2.1		B4	A4	A4	A4													
Gamma rays (Mev)	2.3																		
	2.0																		
	1.75		B8	B8	B8	B8													
	1.54																		
	1.46																		
	1.36		B7	A7	A7	A7		B7											
	1.19			A9															
	1.09																		
	0.91		B10	A10	B10	B10													
	0.80		B7	A7	A7	A7	A7												
	0.71																		
	0.625						A5												
	0.560		B5	A5	A5	A5													
	0.410		A?																
	0.365			A2															
	0.265	A3																	
	0.215																		

Referring to the decay scheme, Fig. 6, the energy levels up to and including the 625-kev state are established from the following evidence:

(1) From Fig. 4 (*a* and *d*), it is apparent that the 410-kev gamma ray is in coincidence with at least one of the gamma rays represented by the 210,215-kev peak (later shown, in paragraph 3, to be the 215-kev). The fact that the energy sum is equal within statistical limits to 625-kev suggests that these coincident radiations are adjacent in the cascade and that the 625-kev gamma ray represents the crossover transition.

(2) A similar argument to (1) holds for the 265- and 365-kev gamma rays which are also seen to be in coincidence from Fig. 4 (*b* and *c*).

The hypothesis that these two cascades, each totaling 625 kev, are in parallel is substantiated by the fact that no coincidences are observed between the 625-kev peak and any of these radiations, Fig. 4 (*a* and *d*). It is further apparent from energy considerations that if the two double cascades originate from the 625-kev level, no coincidences should be observed between the 410-kev gamma ray and either the 265- or 365-kev radiations. From Fig. 4 (*b*, *c*, and *d*) this is seen to be the case.

(3) It will now become evident why the peak referred to as 210,215 kev must be interpreted as being representative of two different gamma rays. If this peak represents only a single transition, the strong coincidences with the 265-kev peak seen in Fig. 4 (*a* and *b*) can only be accounted for if a third "coupling" transition of about 145 kev were present. There is no evidence for a transition of this energy with sufficient intensity to account for the observed coincidences. The coincidences which do appear in the spectra in the region of 150 kev may reasonably be attributed to scattering effects. The coincidences between the 265 and 210,215 peaks cannot be accounted for by scattering. Distributions similar to those shown in Fig. 4(*a*) and (*b*) were obtained when the probes were arranged with their axes at 90° and shielded from each other with a lead block. The possibility was therefore investigated that one of the two peaks represented two gamma rays. The ten-channel analyzer was set to define the 210,215-kev peak. Without changing any adjustments on the apparatus, coincidence distributions were obtained in immediate succession with the 265- and 410-kev peaks. The distribution in coincidence with the 410-kev peak, Fig. 5(*b*), is seen to be shifted upward in energy from the normal distribution, Fig. 5(*a*), and that in coincidence with the 265-kev peak, Fig. 5(*c*), is seen to be shifted downward. The difference in energy between the two peaks is about 5 kev. The experiment was repeated several times. Counting was continued long enough to insure that the observed shift was well outside that which would be possible due to statistical fluctuations. It could thus be concluded that the 210,215-kev peak in fact represents two different gamma rays.

This result obviates the apparent anomaly in the coincidence experiments. A similar experiment was done with the ten-channel analyzer covering the 265-kev peak. No such shift was observed between the coincidence distributions taken with the 210,215- and the 365-kev peaks.

The sequence of the 410–215-kev cascade is established as follows:

Recall that the 52-second metastable state in Ge^{77} decays by means of a beta ray of about 2.7 Mev to an excited state of As^{77}. The gamma ray associated with this transition is seen to be in the neighborhood of 210,215 kev. The pulse-height distribution associated with this gamma ray was determined during the course of the coincidence measurements just described, and it can be seen from Fig. 5(*d*) that this radiation is

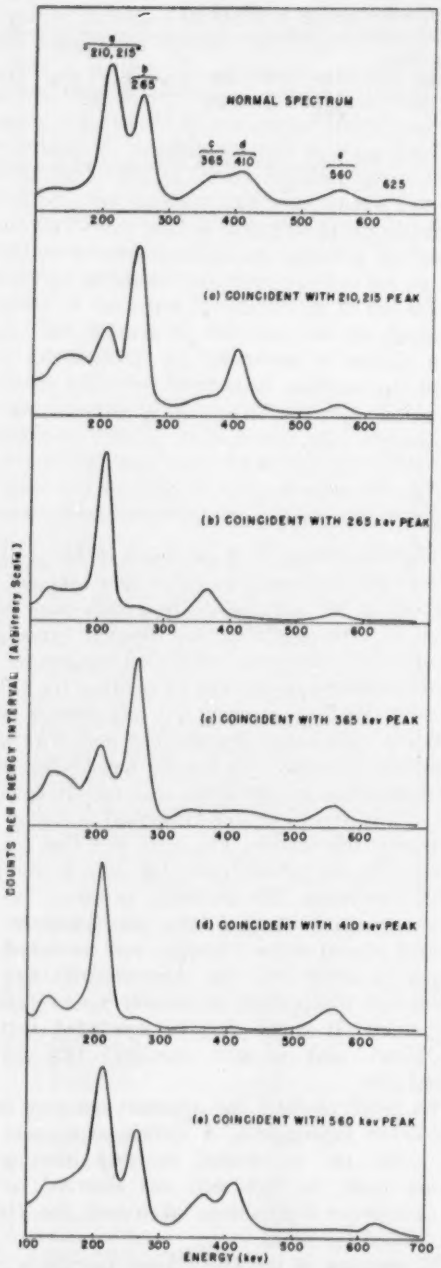
a 210, 215
b 265
NORMAL SPECTRUM
c 365
d 410
e 560
625
200 300 400 500 600
(a) COINCIDENT WITH 210, 215 PEAK
(b) COINCIDENT WITH 265 kev PEAK
(c) COINCIDENT WITH 365 kev PEAK
(d) COINCIDENT WITH 410 kev PEAK
(e) COINCIDENT WITH 560 kev PEAK
COUNTS PER ENERGY INTERVAL (Arbitrary Scale)
100 200 300 400 500 600 700
ENERGY (kev)

FIG. 4. Gamma-gamma coincidence pulse height distributions for $_{33}Ge^{77}$ (12 hr). The five coincidence distributions which are plotted correspond to the single-channel settings labeled as *a*, *b*, *c*, *d*, and *e* on the normal spectrum.

experimentally indistinguishable from that which is in coincidence with the 410-kev gamma ray. It is thus concluded that it is the 215-kev transition which follows beta decay of the 52-second state in Ge^{77}. Since it is the only gamma ray in coincidence with this beta ray, it must lead to the ground state of As^{77}. Thus, the 410-kev gamma ray must represent a transition between the 625-kev level and the 215-kev state.

The sequence of the 265–365-kev cascade (2) will now be considered. The 265-kev transition is placed at the bottom of the cascade since it is the only one of the five low-energy transitions seen to be in coincidence with the high energy gamma ray of 1.19 Mev. The arrangement also provides a reasonable explanation for the 210–265-kev coincidences if an energy level is placed at 475 kev.

(4) All of the foregoing arguments concerning the low-lying levels are consistent with the beta-gamma coincidence measurements. The half-thickness in aluminum for the beta rays in coincidence with each of the peaks, "210,215," 265, 365, and 410, was determined. In each case, in addition to a weak low-energy component, a value of about 120 mg/cm² was observed which corresponds to a beta transition energy of approximately 2.1 Mev. Taking into consideration the weak intensity of the higher-energy gamma rays, it may be concluded that a beta transition of approximately 2.1 Mev feeds the 625-kev state. A beta branch feeding the 475-kev level is required to explain the strong 210–265-kev coincidences. It is not surprising that these two branches are not resolved in the absorption experiments since they differ by only about 145 kev.

(5) Consider the level at 1.185 Mev (Fig. 6). The 560-kev gamma ray is seen to be in coincidence with those represented by all the other low-energy peaks including the one at 625 kev, Fig. 4(*a–e*). This suggests that the 560-kev transition feeds the 625-kev level. Notice that in the coincidence distribution taken with the 560-kev peak (Fig. 4*e*) the two peaks at "210,215" and 265 kev are lower in intensity relative to the 365- and 410-kev peaks than in the normal distribution. This effect may be attributed to the fact that only a portion of the "210,215" and 265-kev peaks are fed by the 560-kev gamma ray, the remainder following beta decay to the 475-kev level. As a result of these interpretations, the placement of the state at 1.185 Mev in the level scheme is justified.

(6) Beta-gamma coincidence measurements confirm this placement. The half-thickness in aluminum for the beta rays in coincidence with the 560-kev peak was found to be about 70 mg/cm², corresponding to a beta-transition energy of about 1.5 Mev. Coincidence between this beta branch and the lower energy gamma transitions may also account for the complex structure of the other absorption curves previously mentioned.

(7) The energy level at 2.0 Mev is established from the following: The slight shoulder apparent at about 800 kev in the normal distribution stood out definitely as a separated peak in the coincidence distribution whenever the single channel was set to cover any one of the low-energy peaks, including the 560-kev and 625-kev ones. Typical of this effect is the distribution shown in Fig. 7, which was obtained with the single

channel covering the 265-kev peak. These coincidences with all of these different peaks indicate not only the presence of a transition of ~790 kev, but that it must be placed above the 560-kev transition in the energy level scheme. If the 790–560 coincidences represent a two-step cascade, then there must be a level at about 2.0 Mev. This hypothesis is supported by the fact that a peak corresponding to a gamma ray of about 2.0 Mev is present in the normal spectrum. The gamma ray of 1.36 Mev is then readily interpreted as the transition from the 2.0-Mev state to the 625-kev level. The coincidence data substantiate this interpretation, for the 1.36-Mev radiation, while not in coincidence with the 560-kev gamma ray, is found to be in coincidence with all the low-energy peaks, including the one at 625 kev.

(8) The experimental energy difference between the two peaks at 2.3 and 1.75 Mev is consistent with interpreting the former as a transition to the ground state from a level at about 2.3 Mev and the latter as a transition to the 625-kev state. In fact, counting for several hours did provide evidence that the 1.75-Mev peak was in coincidence with the low-energy gamma rays.

(9) The state at 1.46 Mev is established on the basis of experiments which show that coincidences exist between the 265-kev gamma ray and the 1.19-Mev radiation represented by a small peak in the normal distribution. This peak was seen to stand out strongly only when the single channel was covering the 265-kev peak, Fig. 7, and essentially vanished when the single channel was accepting pulses from any of the other peaks. (The 1.19-Mev radiation might be interpreted as arising from a transition from the 1.185-Mev level

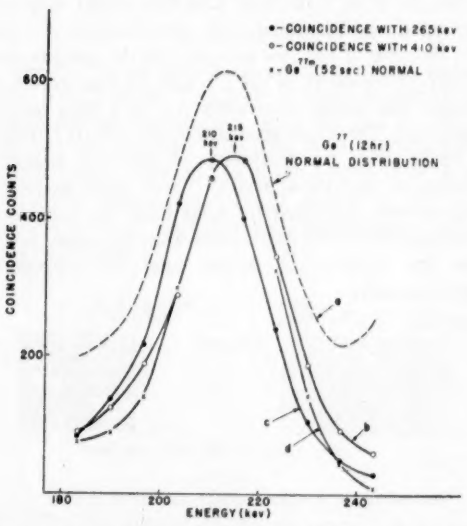

FIG. 5. Resolution of the 210- and 215-kev photopeaks. (*a*) Normal pulse-height distribution of $_{32}Ge^{77}$ (12 hr). (*b*) In coincidence with 410-kev photopeak. (*c*) In coincidence with the 265-kev photopeak. (*d*) Normal distribution of $_{32}Ge^{77m}$ (52 sec).

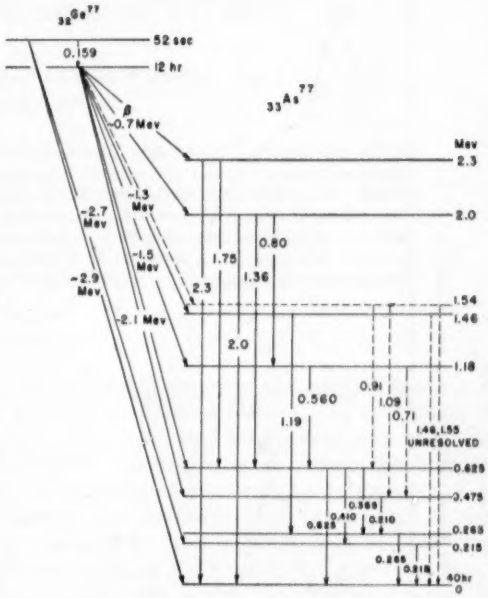

FIG. 6. Decay scheme of $_{32}Ge^{77}$.

to the ground state. This would necessitate a second 265-kev radiation above that level in order to explain the coincidences. The assignment indicated is preferred, although it is not unlikely that some branching to the ground state from the 1.185-Mev level is also represented in the 1.19-Mev peak.)

(10) The existence of the level at 1.54 Mev is deduced from experiments which indicate that the 910-kev peak represents a transition feeding the 625-kev level. The 910-kev peak was seen to be in coincidence with the four peaks, "210,215," 265 (see Fig. 7), 365, and 410, but not with the 560-kev peak. Because of its weak intensity, it is not clear whether coincidences also exist with the 625-kev peak as would be expected.

The rise in the normal spectrum in the neighborhood of 1.5 Mev may thus be interpreted as arising from transitions from either the 1.46-Mev or the 1.54-Mev level to the ground state, or a mixture of both.

(11) The foregoing discussion has disposed of all the gamma rays in the spectrum except two, the 710-kev and the 1.09-Mev radiations. They are included in the arrangement on the basis of their energy alone. The only gamma-gamma coincidences observed with the 710-kev peak seemed to be associated with other radiation of about the same energy (perhaps 790-kev); however, no clear result could be obtained because of the low intensity. All efforts to find coincidences between the 1.09-Mev peak and any of the others met with failure. An aluminum absorption curve of the beta rays in coincidence with the 1.09-Mev peak showed a half-value thickness of about 55 mg/cm². The corresponding beta-ray energy is about 1.3 Mev, but

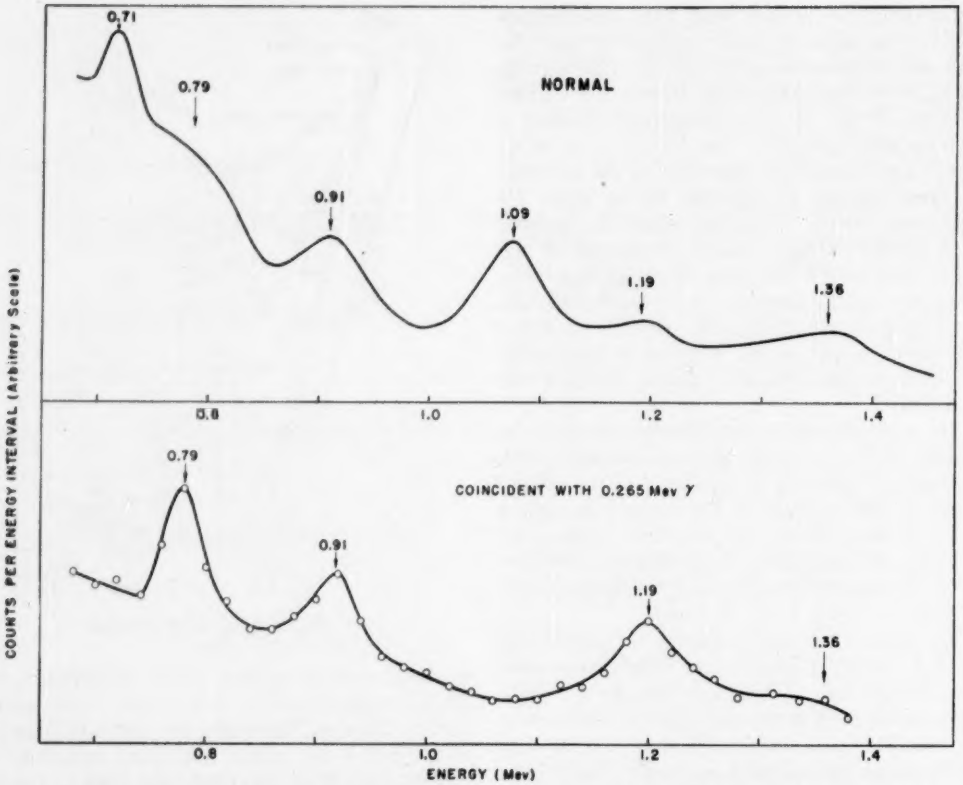

Fig. 7. Pulse-height distribution of high-energy gamma rays which are in coincidence with the 265-kev photopeak.

because of the low counting rates, rather wide limits of error must be allowed. If the 475-kev state is metastable with a lifetime long compared to the 1.6-microsecond resolving time of the coincidence circuit, the arrangement shown is a possible one and is consistent with the beta-gamma coincidence measurements.

Because of the weak intensity of the gamma rays above 600 kev, the beta-gamma coincidence measurements involving those peaks are not considered useful as evidence. The scheme proposed is not considered to be at variance with the measurements by Smith on the beta spectrum. As previously suggested, the two branches feeding the 475- and 625-kev levels would not be resolvable because of their small difference in energy and might appear as a single group in his beta spectrometer analysis. Likewise, the three components feeding the 1.18-, 1.46-, and 1.54-Mev states may also be grouped and identified with Smith's value of 1.379 Mev. Because of the low intensity of the gamma rays emitted during decay of the 2.0- and 2.3-Mev states, no attempt was made to resolve the beta rays feeding these levels. The single groups referred to as 0.710-Mev by Smith may be composed of the two branches required to feed these states. Those portions of the decay scheme indicated by solid lines are considered to be reasonably well established from the experiments, while the portions in dotted lines are considered suggestive only.

Gamma-Ray Absorption Coefficients at 6.13 Mev

RONALD S. PAUL
Hanford Atomic Products Operation, Richland, Washington*
(Received September 7, 1954)

Narrow-beam geometry attenuation measurements have been made with 6.13-Mev gamma rays which follow the beta decay of N^{16} using a NaI scintillation spectrometer detector. The measured absorption coefficients in cm^2/g are: 0.0244 (C), 0.0264 (Al), 0.0309 (Cu), 0.0359 (Sn), 0.0359 (Cd), 0.0436 (Pb), 0.0459 (U), 0.0284 (H_2O), 0.0350 (NaI). The statistical standard deviations range from 0.2 percent to 0.4 percent. These results are in good agreement with previous experimental work in those cases for which earlier data exist. "Experimental" pair-production cross sections are derived from the data and compared with the calculated values from the Born approximation to the Bethe-Heitler theory. A discrepancy of 7 to 8 percent is observed for high atomic number elements (Pb and U).

I. INTRODUCTION

EXPERIMENTAL gamma-ray absorption coefficients, with a statistical accuracy of ± 2 percent, have been reported by Colgate[1] for gamma rays of 6.13-Mev energy obtained from the $F^{19}(p,\alpha)O^{16*}\gamma O^{16}$ reaction. The narrow-beam geometry measurements reported here had been initiated prior to the publication of Colgate's work and were subsequently completed to provide an independent measurement with a statistical accuracy of ± 0.2 percent to ± 0.4 percent, to include several additional elements of interest, and to furnish some information needed for planning attenuation experiments in poor geometry with 6.1-Mev gamma rays. The reduced statistical uncertainties were realized by using a high specific activity source of nitrogen-16 produced by irradiating water in a high neutron flux, and by using, for the detector, a NaI scintillation spectrometer biased to accept only the N^{16} gamma rays. Results of these measurements are compared with those of Colgate and with theoretical predictions.

II. APPARATUS

The 6.13-Mev[2] gamma rays were obtained from the $O^{16}(n,p)N^{16}\beta O^{16*}\gamma O^{16}$ reaction in water passed through a high flux nuclear reactor. Since N^{16} has a 7.3-second half-life, the detector viewed a continuously flowing source. Water entered the central tube of a co-axial cylindrical source chamber as shown in Fig. 1. A flow-meter with electrical trip limits monitored the water flow rate.

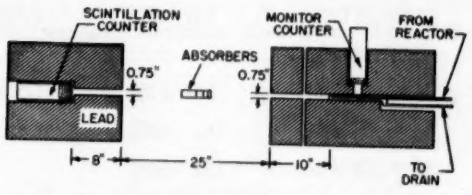

FIG. 1. Schematic diagram of counting geometry.

The collimated geometry arrangement shown in Fig. 1 was used for all measurements. The solid angles were made as small as possible consistent with maintaining reasonable counting rates to reduce the magnitude of the scattering corrections. Large amounts of lead shielding were required around the detector to reduce the background from other sources of high energy gamma radiation and to eliminate scattering into the detector from the room. The absorber samples were centered in the beam by Lucite holders. There was no detectable scattering into the detector by the sample supports.

The primary detector was a scintillation counter using a 2-in. diameter by 2-in. thick NaI(Tl) crystal mounted on a DuMont 6292 photomultiplier tube. This counter only had a resolution of 17 percent for the Cs^{137} 0.66-Mev photopeak but this was adequate to bias out lower energy gammas in the source. The electronic portion of the spectrometer consisted of a conventional *A*-1 linear amplifier, differential and integral discriminators, and scalers. Drifts in the gain of the spectrometer were negligible during the three to five hours required to complete a run with any one absorber material. As shown in the spectrum in Fig. 2, gamma rays of energies lower than 6.1 Mev were present in the source due to the $O^{18}(n,\gamma)O^{19}$ reaction, neutron activation of impurities in the water, and

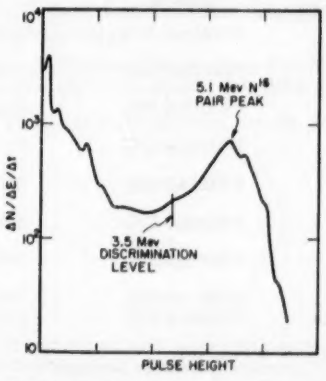

FIG. 2. Scintillation spectrum from N^{16} source.

* Operated for the U. S. Atomic Energy Commission by the General Electric Company.

[1] S. A. Colgate, Phys. Rev. **87**, 592 (1952).

[2] Millar, Bartholomew, and Kinsey, Phys. Rev. **81**, 150 (1951).

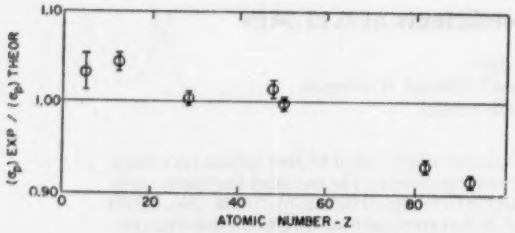

FIG. 3. Ratio of the "experimental" pair-production cross section to the theoretical cross section obtained from the Born approximation to the Bethe-Heitler theory.

annihilation quanta. Preliminary experiments established that these were not detectable and that an optimum count-to-background ratio was obtained for the 6.13-Mev gammas with an integral discriminator setting at 3.5 Mev. As discussed later a small theoretical correction was applied for the presence in the beam of the 7.1-Mev gamma which is present in about eight percent[2] of the O^{16*} decay events.

In the initial measurements, the beam intensity was monitored by a second scintillation spectrometer for variations in source strength which could result from reactor flux level changes or small water flow rate changes. It was found, however, that these changes were negligible during any one run and better statistical accuracy could be obtained by taking periodic zero absorber and background counts with the main detector.

The density of the absorbers was determined to better than 0.10 percent by weight and volume measurements. High purity materials were used and the purities were also checked spectroscopically. No corrections for impurities were required for any of the materials. The aluminum, copper, cadmium, and tin absorbers were 1.0 inch diameter cylinders of varying lengths. The lead and uranium cylinders were about 1.25 inches and the carbon (graphite) 1.4 inches in diameter. The water was contained in 1.2-inch diameter glass cells with thin parallel aluminum windows. Two sodium-iodide crystals of 1.5-inch diameter and 1.0- and 2.0-inch lengths were used. These were contained in thin polyethylene bags during the measurement. The handbook density of 3.667 g/cm³ was used for the sodium-iodide calculations.

III. EXPERIMENTAL PROCEDURE

Transmission ratios suitably corrected for background counts were obtained for a series of absorber thicknesses for each element. The background was determined by (*i*) diverting the water flow from the source chamber, and (*ii*) placing absorbers with transmissions of less than 10^{-6} in the beam. Both methods gave identical results within the counting statistics. The counting periods with the absorber in and out of the beam were chosen to give a standard deviation in the final value of the absorption coefficient of less than 0.5 percent. The background counting rate was about 2 percent of the unattenuated beam counting rate. In all cases true exponential absorption was observed over the range of attenuations measured.

IV. EXPERIMENTAL RESULTS

Two small theoretically calculated corrections were applied to the experimental data. The first (Δ_c) corrected for the small-angle Compton scattering received at the detector. This was determined by a method similar to that described by Davisson and Evans[3] who show that for small angles the amount of scattered radiation reaching the detector is independent of the photon energy and proportional to the solid angle of the scattering cone being considered. This procedure is valid in this experiment since the maximum scattering angles were from 2° to 3°. These Compton scattering corrections to the measured transmissions

TABLE I. Absorption measurements with 6.13-Mev gamma rays.

Absorber	τ_m (cm²/g)	τ_e (cm²/g)	$a\mu$ (cm²/atom) Corrected	$a\mu$ (cm²/atom) Experimental by Colgate (in units of 10^{-24} cm²/atom)	$a\mu$ (cm²/atom)[a] Theoretical
Carbon $Z=6$	0.0241±0.23%	0.0244±0.23%	0.487±0.23%	0.491±2%	0.4823
Aluminum $Z=13$	0.0262±0.20%	0.0264±0.20%	1.184±0.20%	1.17 ±2%	1.167
Copper $Z=29$	0.0307±0.19%	0.0309±0.19%	3.255±0.19%	3.27 ±2%	3.237
Cadmium $Z=48$	0.0359±0.32%	0.0359±0.32%	6.708±0.32%		
Tin $Z=50$	0.0359±0.16%	0.0359±0.17%	7.079±0.17%	7.07 ±2%	7.057
Lead $Z=82$	0.0436±0.43%	0.0436±0.43%	14.99 ±0.43%	15.1 ±2%	15.51
Uranium $Z=92$	0.0459±0.23%	0.0459±0.24%	18.14 ±0.24%	18.2 ±2%	
Water	0.0281±0.30%	0.0284±0.30%			
Sodium-Iodide	0.0348±0.41%	0.0350±0.41%			

[a] Values given directly or derived from data given by C. Davisson and R. D. Evans, Revs. Modern Phys. **24**, 79 (1952).

[3] C. M. Davisson and R. D. Evans, Revs. Modern Phys. **24**, 79 (1952).

TABLE II. Calculation of (σ_p)exp (in units of 10^{-24} cm²/atom).

Element	C(6)	Al(13)	Cu(29)	Cd(48)	Sn(50)	Pb(82)	U(92)
$_a\mu$ Experimental	0.487	1.184	3.255	6.708	7.079	14.99	18.14
$\sigma_{Compton}$	0.433	0.938	2.092	3.464	3.608	5.92	6.64
σ_{photo}			0.004	0.047	0.058	0.54	0.93
$\sigma_{pair\ electron\ field}$	0.003	0.007	0.016	0.026	0.027	0.04	0.05
(σ_{pair})exp	0.051	0.239	1.143	3.171	3.386	8.49	10.52
	±0.011	±0.002	±0.006	±0.022	±0.012	±0.06	±0.04
(σ_{pair})theor	0.0495	0.229	1.141	3.125	3.391	9.12	11.48

range from less than 0.1 percent to 0.2 percent for the largest absorber thickness with carbon. In evaluating the statistical accuracy of the final absorption coefficient, an uncertainty of ±20 percent was assigned to the small Compton corrections.

Bremsstrahlung below 3.5 Mev and annihilation quanta which are produced in the absorber were experimentally eliminated by biasing the detector at 3.5 Mev. Rayleigh scattering is negligible in this experiment.

A second small correction was calculated for the presence in the beam of the 7.10-Mev gamma from O^{16}. The ratio of the intensity of the 7.10-Mev gamma to the 6.13-Mev gamma (η_7/η_6) is given as 0.08 by Millar *et al.* The correction was determined as a factor f given by

$$f=e^{-\mu_6 X}\frac{\epsilon_6\eta_6+\epsilon_7\eta_7}{\epsilon_6\eta_6 e^{-\mu_6 X}+\epsilon_7\eta_7 e^{-\mu_7 X}},$$

where μ_6 and μ_7 are the theoretical[3] absorption coefficients for a particular material for 6.13 and 7.10 Mev, respectively, ϵ_6 and ϵ_7 are the respective detector efficiencies for the two energies, and X is absorber thickness. The values of f were all within the range from 9.985 to 1.013 and were assigned an uncertainty of ± 20 percent of $|1-f|$.

The final corrected transmission ratio, T_c, for a particular absorber thickness was determined from the measured transmission, T_m, as follows:

$$T_c=f(T_m-\Delta_c).$$

Values of the absorption coefficient τ in cm²/g were determined by weighted least squares fit of the T_m's and T_c's for each material to the equation $T=e^{-\tau X}$. The standard deviation associated with each as-measured coefficient τ_m and corrected coefficient τ_c were determined. τ_m, τ_c and their standard deviations are listed in Table I together with the atomic absorption coefficient

$$_a\mu(\text{cm}^2/\text{atom})=A\tau_c/N$$

where A is the atomic weight and N Avogradro's number.

Table I also lists the experimental values of $_a\mu$ determined by Colgate and those calculated theoretically by Davisson and Evans. The values from this measurement agree well within the statistical limits with those of Colgate. Disagreement with the theoretical values increases with increasing atomic number. This is expected since the pair cross section becomes a successively larger fraction of the total cross section with increasing Z and the Born approximation to the Bethe-Heitler theory of pair-production has been shown to be inadequate.[2,4,5]

An experimental pair-production cross section $[(\sigma_p)_{exp}]$ may be obtained by subtracting from the experimental $_a\mu$ calculated Compton, photoelectric and electronic pair-production cross sections as shown in Table II. The tabulated values as well as the theoretical Bethe-Heitler pair-production cross section $[(\sigma_p)_{theor}]$ are derived from reference 3. Figure 3 shows the ratio $(\sigma_p)_{exp}/(\sigma_p)_{theor}$ plotted *versus* atomic number. At 6.13 Mev the discrepancy is only appreciable for high Z where σ_p is more than half of $_a\mu$. The empirical correction to the Bethe-Heitler pair cross section as derived by Davies-Bethe-Maximon[6] for Pb yields a value of 8.95 barns which is in somewhat better agreement with the experimental value.

[4] Rosenblum, Shrader, and Warner, Phys. Rev. **88**, 612 (1952).
[5] D. R. Corson and A. O. Hanson, Ann. Revs. Nuclear Sci. **3**, 67 (1953).
[6] Davies, Bethe, and Maximon, Phys. Rev. **93**, 792 (1954).

Absorption Cross Section of Boron for Thermal Neutrons

G. VON DARDEL* AND N. G. SJÖSTRAND
Department of Physics, AB Atomenergi, Stockholm, Sweden
(Received July 29, 1954)

The thermal neutron absorption cross section of boron of different origin has been determined by comparing the decay of the neutron flux from a water solution of the sample with the flux decay from the same volume of distilled water. The ratio of the two decay curves is a pure exponential, independent of slowing down and of the presence of harmonic modes. After application of small corrections the decay constant of the ratio curve gives directly the absorption cross section. The result for the Argonne-Brookhaven standard boron is 764±3 barns as compared to 755±5, 749±4, and 771±5 barns obtained at Argonne, Brookhaven, and Harwell, respectively.

NEUTRON time-of-flight transmission measurements have shown that the capture cross section of boron for neutrons varies as $1/v$.[1] The constant of proportionality, stated as the cross section at the standard velocity 2200 m/sec, has been determined repeatedly,[1–6] but the spread of the results is much larger than is to be expected from the standard errors claimed by the authors. These discrepancies have been attributed to variations in the isotopic abundance,[7] impurities in the boron compounds, and the chemical analysis. A further source of error lies in the need to subtract the scattering cross section from the measured total cross section to obtain the capture cross section.[5,6]

In view of these discrepancies we have made a determination of the boron capture cross section by a new and independent method, which is simpler and probably capable of higher accuracy than the transmission method, and which is much less influenced by the scattering of the sample. In this method a burst of neutrons is produced in a homogeneous moderating material by a pulsed neutron source. The subsequent free decay of the neutron flux from the moderator is measured with BF_3-counters and a time analyzer. Two decay measurements are made, the moderator being in one case distilled water and in the other an equal volume of a dilute solution of a boron compound. The experimental arrangement is identical with the one used for a study of the neutron diffusion parameters of water.[8]

The boron content of the solution was determined by titration with NaOH after addition of mannite. The NaOH used was calibrated against a known amount of cp grade borax, which had been allowed to assume the normal crystal water content by recrystallization and subsequent storage for several days above a saturated solution of $Ca(NO_3)_2$ in a desiccator.

Figure 1 shows typical decay curves obtained with distilled water and a borax solution. The curves are corrected for counting losses amounting to less than 2 percent for the first channels after the end of the neutron burst. The initial parts of the decay curves are not exponential because of the presence during the first time intervals of non-slowed-down neutrons and of harmonic modes in the neutron distribution.[9]

The neutron absorption in the dissolved boron compound will give rise to a factor $\exp(-\Sigma n_i\sigma_i vl)$ in the expression for the decay of the neutron flux but will not otherwise influence the decay. $\Sigma n_i\sigma_i$ is the macroscopic absorption cross section of the dissolved compound per unit volume of the solution. For a $1/v$-absorber the validity of the above statement is quite general and does not depend on the common approximations of neutron physics, such as diffusion theory or the one-group model. If we take the ratio of the two decay curves of Fig. 1 measured with and without a dissolved boron salt, we will thus expect to get a pure exponential curve. This is indeed shown by the dotted curve of the diagram, which is an exponential even during the initial time intervals, where the individual curves are not. From the decay constant, $\Sigma n_i\sigma_i v$, of the exponential ratio curve, and the chemical analysis, we can calculate directly the absorption cross section. Minor corrections—a few tenths of one percent —have to be applied for the influence of the scattering cross section of the boron compound and for small differences of the volume and temperature of the liquid in the two measurements. Repeated measurements were made by the new method with different boron compounds, different concentrations, and different amounts of liquid. The results are shown in Table I.

The length of the neutron burst was always 40 μsec, and the channel width 10 μsec. The repetition time was 400 μsec, except for the measurements I-1 and I-2 where a shorter repetition time of 200 μsec was used in the runs with the boron solution. This was done in an

* Now at CERN, Laboratory Group, Geneva, Switzerland.
[1] Sutton, McDaniel, Anderson, and Lavatelli, Phys. Rev. **71**, 272 (1947).
[2] J. Rainwater and W. W. Havens, Jr., Phys. Rev. **70**, 136 (1946).
[3] Fermi, Marshall, and Marshall, Phys. Rev. **72**, 193 (1947).
[4] Hamermesh, Ringo, and Wexler, Phys. Rev. **90**, 603 (1953).
[5] Carter, Palevsky, Myers, and Hughes, Phys. Rev. **92**, 716 (1953).
[6] P. A. Egelstaff, Atomic Energy Research Establishment, Harwell, Report N/M 62, 1953 (unpublished).
[7] Thode, Macnamara, Lossing, and Collins, J. Am. Chem. Soc. **70**, 3008 (1948).
[8] G. von Dardel and N. G. Sjöstrand, Phys. Rev. **96**, 1245 (1954).
[9] G. von Dardel, Trans. Roy. Inst. Technol. Stockholm No. 75, (1954).

attempt to gain intensity. It was found, however, that the use of different repetition times influenced the shape of the neutron burst, so that the decay curves with different repetition time are not directly comparable. The results obtained in these measurements are therefore discarded in taking the mean, but they show that the result does not depend on the amount of the solution.

In order to investigate the influence of the scattering cross section on the results we also made measurements on strong solutions of the weakly absorbing substance $Na_2S_2O_3$. These measurements confirmed that the influence of the scattering of the solute was very small and could be calculated correctly from the scattering cross sections using diffusion theory, except for very concentrated solutions.

The statistical error of a typical measurement with a boron concentration of 1 g/l is 0.28 percent. The uncertainty of the various corrections is less than 0.1 percent. The random error in the chemical analysis as determined by repeated measurements of the same solution is 0.15 percent. The total random error is thus about 0.3 percent. In weaker solutions the error is somewhat larger than 0.3 percent as shown by the last column in Table I. The spread around the mean of different results for the same salt is in substantial agreement with the estimated random errors.

The major systematic uncertainty lies in the chemical analysis. Since good agreement was found when the same solution was analyzed by us and by Argonne and Harwell chemists, we estimate this systematic error to be as low as 0.3 percent.

The result 764±3 barns for salt II is somewhat higher than the values 749±4 barns obtained by Carter *et al.*[5] and 755±5 barns obtained by Hamermesh *et al.*,[4] using the same salt. On the other hand it is lower than the value 771±5 barns obtained for this salt from the measured cross section of the Harwell standard boron, 782±5 barn,[6] and the ratio 0.986 ±0.003 between the Harwell and Argonne boron[10] measured with a pile oscillator.

TABLE I. Experimental results.

Boron compound	No.	Volume of solution liters	Concentration of boron g/l	Cross section barns	Random error barns
I. Borax (cp grade, Kebo, Stockholm)	I-1	3.3	1	(770)	2.5
	I-2	2.5	1	(770)	2.5
	I-3	3.3	1	764	2.5
	I-4	2.5	0.5	761	6
		Weighted average		763	2.3
		Total standard error		±3	
II. Boric acid (Argonne[a] and Brookhaven[b] standard)	II-1	2.5	1	764	2.5
		Total standard error		±3	
III. Boric acid (cp grade, Coleman and Bell, Norwood, Ohio)	III-1	2.5	1	760	2.5
	III-2	2.5	1.5	759	2.4
	III-3	2.5	1	765	2.5
	III-4	2.5	0.5	748	6
	III-5	2.5	0.7	761	3.5
		Weighted average		760.5	1.3
		Total standard error		±3	

[a] See reference 4.
[b] See reference 5.

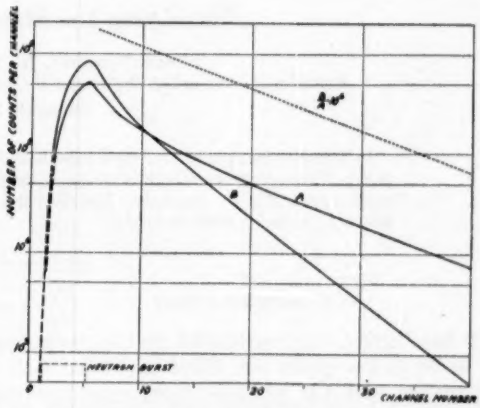

FIG. 1. Experimental decay curves for measurement I-3. Curve *A* was measured with distilled water, and curve *B* with borax solution. Measuring times were 2 and 4 hours respectively.

Salt I has been compared at Argonne[11] and Harwell[10] with salt II by means of a pile oscillator method, and the values 0.991±0.005 and 0.997±0.004 were obtained for the ratio between the boron cross section in salt I and II. The latter value is in excellent agreement with the ratio 0.999±0.004 of our experimental results.

The cross section of salt I has previously been measured by von Dardel and Waltner,[12] who obtained a value of 708±12 barns using a pulsed method in a large geometry. As discussed elsewhere[8] in connection with the neutron-proton cross section, we believe the discrepancy to be due to the possible presence in the large geometry experiment of a probably time-dependent neutron background, for which an accurate correction could not be applied.

A method very similar to ours was used independently by Scott, Thomson, and Wright[13] to determine the cross section of a California-mined boron. Their result, 744±20 barns, is in agreement with ours though of lower accuracy. In their treatment of the data it has to be assumed that the decay curves are pure exponentials, and the result would be influenced by the presence of harmonic modes and fast neutrons, which distort the decay curves. With the refinements described in the present article the lifetime method of measuring thermal neutron cross sections should compete favorably in accuracy with other methods, such as the pile oscillator or slow chopper.

The authors are grateful to Mrs A. Arnfelt for the chemical analysis, Mr. O. Nicolaysen for assistance with the measurements, and Mr. A. Rentze for the numerical calculations.

[10] D. Littler (private communication).
[11] G. R. Ringo and S. Wexler, Phys. Rev. **95**, 660 (A) (1954). and private communication.
[12] G. von Dardel and A. W. Waltner, Phys. Rev. **91**, 1284 (1953).
[13] Scott, Thomson, and Wright, Phys. Rev. **95**, 582 (1954).

Low-Lying 1− States in Even-Even Nuclei*

FRANK STEPHENS, JR., FRANK ASARO, AND I. PERLMAN
Radiation Laboratory and Department of Chemistry, University of California, Berkeley, California
(Received September 7, 1954)

In a limited isotopic region, there have been found low-lying states in even-even nuclei of spin 1, odd parity. Other energy levels in the vicinity are the well characterized 0+, 2+, and 4+ states of the even-even nuclear type. The 1− states were identified through α-γ angular correlation measurements supported by internal conversion coefficient data.

I. INTRODUCTION

IT has become well established that for even-even nuclei in the region well above the closed shell of 82 protons and 126 neutrons there exist low-lying energy levels with spin and parity assignments 0+, 2+, 4+, $\cdots$.[1] Such a sequence of levels is described as a *rotational band* because the spins, parities, and energy spacing conform with the expectations of rotational states according to the Bohr-Mottelson[2] unified collective and individual particle nuclear model. In all cases examined by study of the alpha-decay process the fundamental state is the 0+ ground state, and the energies of the 2+ and 4+ states follow a regular trend in their level spacings: narrower toward heavier nuclei and wider toward lighter nuclei.[2-4] For Th^{228} decay, as an example, the 2+ state is at 84 kev and the 4+ state at 253 kev.[5] Consistent with the parities and spins of these even spin states is the finding that they are joined by cascading $E2$ transitions.

In a rather confined region (around $Z=90$, $N=136$) a low-lying excited state appears which is not a member of this rotational sequence. The level is apparently 1− and was first recognized in Th^{228} decay (excited states of Ra^{224}).[6] Here there was found a state between the 2+ and 4+ states which decayed to the 2+ and 0+ (ground state) by $E1$ transitions. The $E1$ character of the radiation allows only a 1− assignment and furthermore the odd spin-odd parity combination is a conservation requirement in the alpha decay of an even-even nucleus.

There are now five cases in which the 1− state has been recognized, lying either between the 4+ and 2+ states or just above the 4+ state. The present paper is concerned with α-γ angular correlation measurements on three of these, the results of which are consistent with the 1− assignment, and incidentally, show the difference in correlation with the α-γ sequence involving the 2+ states. The three alpha emitters examined were Th^{228}, Th^{226}, and U^{230} which give information on the excited states of Ra^{224}, Ra^{222}, and Th^{226}, respectively.

II. EXPERIMENTAL

The gamma side of the angular correlation apparatus consisted of a commercial Harshaw NaI (Tl activated) crystal ($1\frac{1}{2}$ in. diameter by 1 in. thick) mounted on a Dumont 6292 photomultiplier tube and placed from two to four inches away from the sample. The output from the photomultiplier tube was amplified and shaped and then fed into a gated 50-channel pulse height analyzer.

Two different types of alpha detectors were used depending upon whether or not it was necessary to distinguish alpha groups. In the case of Th^{228}, where the daughter Ra^{224} grows in relatively slowly, it was possible to use a ZnS screen fastened to the end of an RCA 5819 photomultiplier tube, the output of which was amplified, shaped, and then used as a gate for the gamma-ray detector as it fed into the 50-channel pulse height analyzer. For Th^{226} and U^{230}, however, where the daughters grow in rapidly, it was necessary to have sufficient resolution of alpha energies to be able to separate the five alpha emitters in the family and to measure gamma-ray coincidences with each alpha emitter. This was accomplished by using a thin NaI crystal as a rough spectrometer in the following manner: The newly cleaved crystal ($\frac{1}{4}$ in. square$\times\frac{1}{32}$ in. thick) was fastened (in a drybox) onto a Dumont 6292 photomultiplier tube. The assembly was then mounted in a vacuum chamber, and samples introduced by means of an air lock. Silica gel was present in the vacuum chamber to absorb moisture and a liquid nitrogen trap was placed between the pump and the chamber, but even so the resolution decreased from an optimum of 3 percent (full width at half maximum) to about 5 percent over a period of two weeks. The output from the photomultiplier tube was amplified, shaped and fed into a single channel pulse height analyzer. Pulses of a particular height were selected and used to gate the 50-channel pulse height analyzer. The resolving time of the coincidence unit described was of the order of ten microseconds.

An example of the alpha spectrum so obtained for the U^{230} series is shown in Fig. 1. Each of these peaks is comprised almost entirely of the ground state transi-

* This work was performed under the auspices of the U. S. Atomic Energy Commission.
[1] F. Asaro and I. Perlman, Phys. Rev. **91**, 763 (1953).
[2] A. Bohr and B. Mottelson, Kgl. Danske Videnskab. Selskab, Mat.-fys. Medd. **27**, No. 16 (1953); A. Bohr, *Rotational State of Atomic Nuclei* (Ejnar Munksgaards, Copenhagen, 1954).
[3] F. Asaro and I. Perlman, Phys. Rev. **87**, 393 (1952).
[4] K. W. Ford, Phys. Rev. **90**, 29 (1953).
[5] Asaro, Stephens, and Perlman, Phys. Rev. **92**, 1495 (1953).

tion which in some cases is considerably removed from the low abundance-low energy group which is coincident with the gamma ray of interest. Nevertheless, with a knowledge of the gamma ray under consideration, the alpha energy gate could be set at the proper place to minimize conflicting coincidences.

The Th^{228} and the U^{230} family sources for the alpha-gamma coincidence measurements were prepared somewhat differently. The Th^{228} sample, separated from its decay products by a resin column technique,[5] was simply evaporated from aqueous solution as a $\frac{1}{4}$-in. diameter spot on a 6-mil thick aluminum plate. The low atomic number was employed for the backing since the gamma rays had to penetrate it to reach the detector.

The U^{230} source was one previously prepared for measuring its alpha spectrum.[6] The material had been vacuum sublimed onto a 2-mil platinum plate forming a band $\frac{1}{8}$ in.×1 in. Because of the appreciable attenuation of the gamma rays in traversing the platinum plate, differences in attenuation due to differences in thickness were minimized by rotating the plate with the gamma-ray detector. Both of these sources were considerably larger than desirable for precise angular correlation measurements.

III. RESULTS

U^{230} family gamma-ray spectrum.—Previous work,[6] using both chemical methods and recoil techniques to separate members of the decay family, identified the following gamma rays in the series:

U^{230}	Th^{226}	Ra^{222}	Ra^{222} (or daughters)
70 kev	109	330	609
160	~130		
230	~190		
	240		

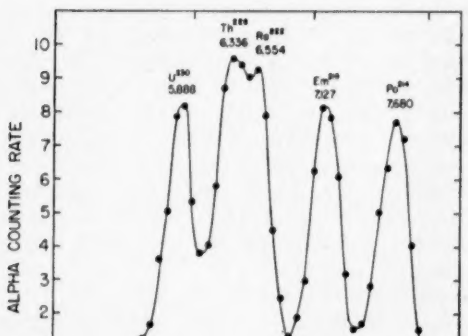

FIG. 1. Alpha-particle spectrum of U^{230} series taken with NaI crystal and pulse-height analyzer. (Ordinate scale is arbitrary.)

[6] Asaro, Slater, and Perlman (unpublished).

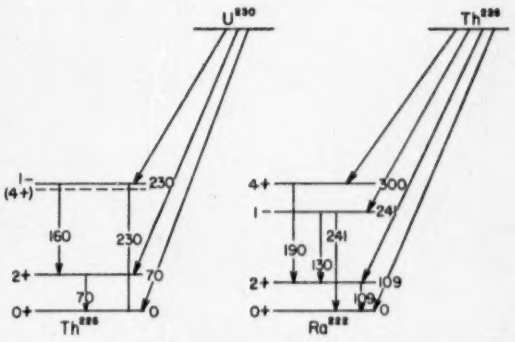

FIG. 2. Decay schemes of U^{230} and Th^{226}.

These assignments were confirmed with the apparatus described above by observing the gamma-ray spectrum as a function of the position of the gate set according to alpha-particle energy. For example, the 230-kev gamma ray of U^{230} decay and the 240-kev gamma ray of Th^{226} would not be resolved by the gamma-ray spectrometer operating as a single event instrument, but when the alpha-particle gate was set at about 5.66 Mev (U^{230} maximum energy minus 230 kev) the 230-kev gamma ray showed a maximum coincidence rate and when the gate was set at about 6.10 Mev (Th^{226} maximum energy minus 240 kev) the 240-kev gamma ray showed up. Since the 240-kev peak is four times as intense as the 230-kev peak, there was still some overlap when the gate was set at 5.66 Mev. It was estimated that roughly 15 percent of the 230-kev peak was due to 240-kev gamma rays. In addition to the above confirmation of assignments, the 609-kev gamma ray was proved to belong to Em^{218}, which assignment was suspected but not determinable from the earlier measurements.

The proposed decay schemes for U^{230} and Th^{226} are shown in Fig. 2. These are based on alpha and gamma spectra and gamma-gamma coincidence measurements made previously[6] and on the alpha-gamma angular correlations of the present study. It will be noted that the 230-kev state of U^{230} is shown as an unresolved doublet comprising the 1− and the 4+ states while in Th^{226} the 1− state is well separated from the others.

U^{230} series alpha-gamma angular correlations.—The angular correlations obtained by gating with the alpha particles of a particular energy and rotating the gamma ray detector, are shown in Figs. 3 and 4. In Fig. 3 the gate was set corresponding to 6.10 Mev which is the energy of Th^{226} α_{240},[7] and the gamma-ray peak at 240 kev shows a distribution with a minimum at 180° and maxima at 90° and 270°. The theoretical correlation function for the sequence $0+ \rightarrow^{\alpha} 1- \rightarrow^{\gamma} 0+$ is plotted as Fig. 5. It is seen that maxima and minima occur in the same positions, but the angular

[7] This nomenclature refers to the alpha group of Th^{226} which populates the 240-kev level of the daughter nucleus.

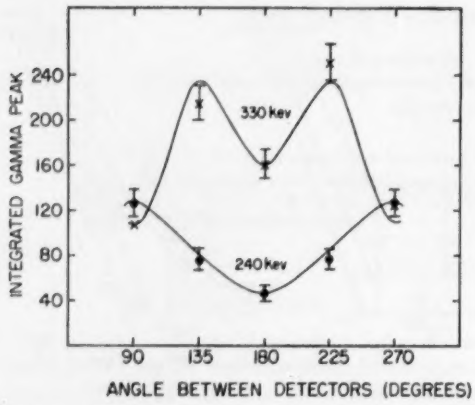

FIG. 3. α-γ angular correlations for 240-kev gamma ray of Th^{226} decay and 330-kev gamma ray of Ra^{222} decay.

anisotropy is not so pronounced for the experimental data. Two of the most important reasons for this are the large sample size and relatively high geometry, for which no corrections were made. Nevertheless this correlation may be taken as rather good support for the 1− assignment of the 240-kev state of Th^{226}, particularly since there are limitations in other possible assignments. From the alpha-particle spectrum of Th^{226} and the present coincidence measurements, it is fairly certain that the 240-kev gamma ray leads to the ground state of Ra^{222} and is therefore electric radiation. (The conservation of spin and parity demands that a gamma ray must be electric if it leads to the ground state of an even-even nucleus and arises from a level populated by alpha decay.) Assignment of $E3$ and higher multipolarities can be ruled out by consideration of lifetimes since in this case prompt coincidences were observed (few microseconds maximum delay) whereas the calculated lifetime for an $E3$ transition would be 10^6 fold longer. Therefore, we need consider only $E1$ or $E2$ assignments and it will be shown presently that the angular correlation expected if the radiation were $E2$ is quite different from that observed.

As seen in Fig. 3, a peak at 330 kev with different correlation has appeared. This comes from coincidence with α_{330} of Ra^{222} (6.23 Mev) which, because of the poor resolution of the alpha peaks, overlaps considerably the gating energy (6.10 Mev). Because of this lack of discrimination and the fact that the 330-kev gamma ray is more intense than the 240, the coincidence intensity of the 330-kev peak is likewise more intense. The angular correlation of the 330-kev gamma ray is consistent with that for a $0+ \rightarrow^{\alpha} 2+ \rightarrow^{\gamma} 0+$ sequence as would be expected for an alpha transition to the first excited state of an even-even nucleus.

The data in Fig. 4 were taken in the same manner except the alpha gate was set at 5.66 Mev which

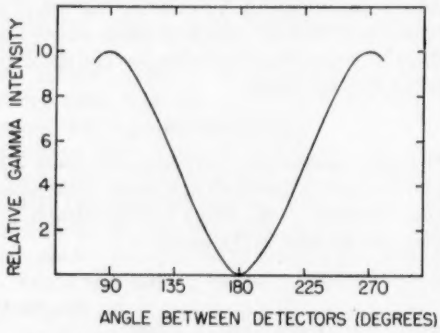

FIG. 5. Theoretical α-γ angular correlation for a $0+ \rightarrow 1- \rightarrow 0+$ sequence.

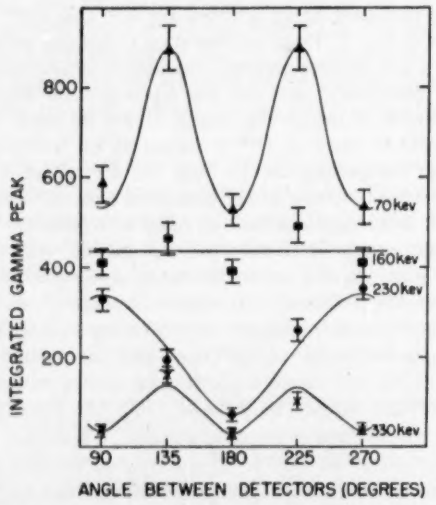

FIG. 4. α-γ angular correlations for the following gamma-ray transitions: 70, 160, and 230 kev from U^{230} decay; 330 kev from Ra^{222} decay.

corresponds to α_{230} of U^{230}. A different gamma spectrum appeared and included was the 230-kev gamma ray showing the $0+ \rightarrow^{\alpha} 1- \rightarrow^{\gamma} 0+$ correlation. The 160-kev peak involves the same energy level and its virtual absence of angular correlation is consistent with our supposition that the 230-kev level is a doublet of a 4+ and a 1− state and therefore the sequence measured is a mixture of $0+ \rightarrow 1- \rightarrow 2+$ and $0+ \rightarrow 4+ \rightarrow 2+$. Other evidence that the 230-kev level is actually a pair of close lying levels will not be reviewed here in detail. Briefly, part of the argument lies in the well-established systematic spacing of the 4+ state which, for U^{230} decay, should be at about 230 kev. Also, the abundance ratio of the 160-kev gamma ray to the 230-kev gamma ray appears to differ by a factor of two between the alpha decay of U^{230} and the beta decay of Ac^{226}.[8] If true, this can mean only that there are two levels populated to different degrees by the two modes of decay.

The abundant 70-kev transition of U^{230} decay shows

[8] J. Grover and G. T. Seaborg (unpublished).

up in Fig. 4 with the $0+ \rightarrow 2+ \rightarrow 0+$ correlation as expected, as does the 330-kev gamma ray of Ra^{222} decay appearing in low intensity.

Th^{228} α-γ angular correlations.—The decay scheme previously proposed[5] for Th^{228} is shown in Fig. 6. The 212-kev gamma ray was considered to be of principal interest and its angular correlation is shown in Fig. 7. The correlation is seen to be similar to that for the 230-kev transition of U^{230} and the 240-kev transition of Th^{228} indicating that all three involve the sequence $0+ \rightarrow^{\alpha} 1- \rightarrow^{\gamma} 0+$. The correlation for the 84-kev transition (not shown) behaved as expected for the type $0+ \rightarrow^{\alpha} 2+ \rightarrow^{\gamma} 0+$.

1− states in Th^{230} and U^{232} decay.—In addition to the three cases for which angular correlation studies were made in the present study, two others also apparently have the same type of decay scheme. In the decay of Th^{230} a 250-kev level has been recognized[9,10] which decays both to the ground state $(0+)$[11] and to the first even spin state $(2+)$.[12] The similarity of this decay

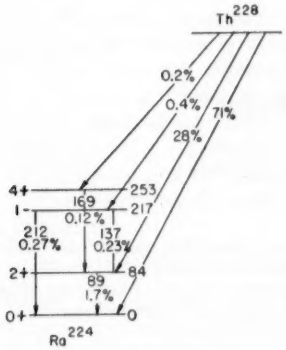

FIG. 6. Decay scheme for Th^{228}.

scheme and the proximity of this isotope to others having 1− states in the same energy range make it likely that this 250-kev level is a 1− state. In the decay of U^{232} a similar structure is seen from a level of 330 kev above the ground state.[13] Figure 8 shows a plot of the energy of these 1− states as a function of neutron number. A few other nuclei in this region are susceptible to this type of measurement and should be of interest in extending the picture based on these few cases.

IV. DISCUSSION

There is currently a considerable amount of speculation on the nature of the nuclear spectroscopic states in the heavy element region and this inevitably carries back to some nuclear model. It is not immediately

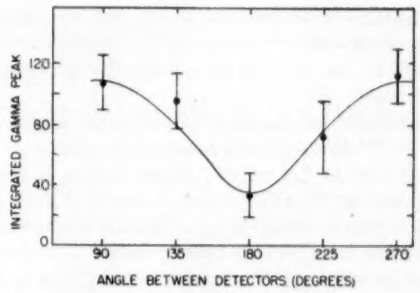

FIG. 7. α-γ angular correlation for 217-kev transition for Th^{228} decay.

obvious how the existence of low-lying 1− states fits as a predictable consequence into any of the pictures. A factor which must be considered in an explanation is that the appearance of these states at low enough energies to be discernible in the alpha-decay process apparently takes place only in a limited region. Although energy level density near the ground state becomes greater as one proceeds to heavier nuclei, the 1− state has apparently disappeared as indicated by careful studies of the alpha spectra of Pu^{238} [14] and Cm^{242}.[15] The failure to find 1− states for these heavier nuclei could stem from two reasons: Either the levels have become so high that the alpha population to these states is low beyond detection, or the levels are in a region in which the energy dependence is not the deterring factor but some selection process hinders the transitions. In this connection it should be mentioned that the population by alpha decay of the 1− states which have been observed are of the order of tenfold lower than would be expected from alpha-decay theory. Those transitions to the 4+ state in this region are similarly hindered.

If the 1− states are to be explained by some coupling of single-particle states, there is then implied close proximity of states of opposite parity. Other evidence that this is the case in the heavy element region may be taken from the identification of a number of low-lying

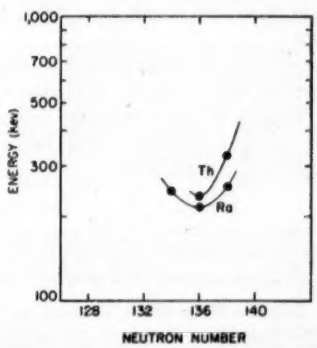

FIG. 8. Energy levels of 1− states in thorium and radium isotopes.

[9] Rosenblum, Valadares, Blandin-Vial, and Bernas, Compt. rend. **238**, 1496 (1954).
[10] G. Valladas and R. Bernas, Compt. rend. **236**, 2230 (1953).
[11] F. Rasetti and E. C. Booth, Phys. Rev. **91**, 315 (1953).
[12] Stephens, Asaro, and Perlman (unpublished).
[13] F. Asaro and I. Perlman (unpublished).
[14] F. Asaro and I. Perlman, Phys. Rev. **94**, 381 (1954).
[15] Asaro, Thompson, and Perlman, Phys. Rev. **92**, 694 (1953).

$E1$ transitions in odd-nucleon nuclei, as for example, in the decay of Am^{241} [16] and Am^{243} [17] where the states involved lie 60 and 75 kev respectively above the ground states.

Rasmussen[18] has discussed some of the implications of the Am^{241} decay scheme and his considerations may be applicable to the heavy element region in general. He pointed out that for protons in the 82–126 shell the only even parity orbital is $i_{13/2}$. The odd parity orbitals should have considerably lower j values and the only manner in which an $E1$ transition could arise is if j is not a good quantum number. His explanation is through the unified nuclear model involving strong coupling between the single particle and nuclear surface deformation which is a collective property. If strong coupling is assumed, the particle angular momentum vector j precesses rapidly around the symmetry axis of the spheroidal nucleus and the projection of j on the symmetry axis defines the spin. We then have a situation in which transitions between states of similar spin can involve large changes in the single particle wave function. Rasmussen suggests that such a situation may be responsible for the abnormally long lifetime for the 60-kev $E1$ transition. He also has found it necessary to employ this picture to explain features of β^- decay processes which would be anomalous on the basis of conventional selection rules.

The pertinence of this discussion to the problem at hand is that, at least in the heavy-element region, it may be necessary to look more deeply into the meaning of spectroscopic states than would appear just from spin assignments. Some of the implications of this idea have also been discussed in reference to the alpha-decay process.[18,19]

[16] Beling, Newton, and Rose, Phys. Rev. **87**, 670 (1952).
[17] F. Asaro and I. Perlman, Phys. Rev. **93**, 1423 (1954).
[18] J. O. Rasmussen, Jr., Arkiv Fysik **7**, 185 (1953).
[19] Perlman, Ghiorso, and Seaborg, Phys. Rev. **77**, 26 (1950).

PHYSICAL REVIEW VOLUME 96, NUMBER 6 DECEMBER 15, 1954

Capture-Positron Branching Ratios*

P. F. ZWEIFEL
Knolls Atomic Power Laboratory,† Schenectady, New York
(Received September 1, 1954)

Expressions are given for allowed and first-forbidden K and L capture probabilities, and rules are formulated for obtaining such expressions for capture of any order of forbiddenness from any orbit. The effect of screening on branching ratios is discussed, and a table for the rapid calculation of allowed branching ratios, including screening effects, is given. The results are then applied to the decays of Zn^{65}, Na^{22}, Sc^{44}, and V^{48}.

I. INTRODUCTION

IN attempting to classify a negatron decay as to order of forbiddenness and to gain information as to the form of lepton-nucleon interaction, one generally uses as evidence the shape of the spectrum, the logft value of the decay, and the spin and parity changes involved, the last either measured or obtained from shell-model considerations.[1]

In the case of radioactive nuclei which emit positrons, however, there is another piece of evidence available, namely the branching ratio between orbital electron capture and positron emission. The branching ratio (b.r.) is defined by the relation

$$\text{b.r.}=\lambda_e/\lambda_+, \tag{1}$$

where λ_e and λ_+ are, respectively, the probabilities per unit time of electron capture and positron emission.

The quantity λ_+ is given by the well-known relation for an nth forbidden decay,

$$\lambda_+=\frac{1}{2\pi^3}\sum_{x,y} g_x g_y \tfrac{1}{2}(1+\delta_{xy}) \times\int_1^{W_0} pW(W_0-W)^2 F_0(W,Z) C_{nxy}(W,Z)\,dW =\int_1^{W_0} N(W,Z)\,dW, \tag{2}$$

where the notation is the same as Greuling's[2] except that here we allow for the possibility of a linear combination of interactions—hence the presence of two indices, x and y. Greuling tabulates the C_{nxy} for pure interactions while Smith[3] and Pursey[4] give the interference terms which arise when more than one form of interaction is assumed to be present.

In calculating λ_+, numerical values for the Fermi

* Based, in part, on a thesis submitted to the Graduate School of Arts and Sciences, Duke University, in partial fulfillment of the requirements for the degree of Doctor of Philosophy.
† Operated for the U. S. Atomic Energy Commission by the General Electric Company.
[1] Mayer, Moskowski, and Nordheim, Revs. Modern Phys. **23**, 315 (1951); L. W. Nordheim, Revs. Modern Phys. **23**, 322 (1951).
[2] E. Greuling, Phys. Rev. **61**, 568 (1942).
[3] A. M. Smith, Phys. Rev. **82**, 955 (1951).
[4] D. L. Pursey, Phil. Mag. **42**, 1193 (1951). We adopt Pursey's notation rather than Smith's.

function $F_0(W,Z)$ were obtained from the tables of Dismuke *et al*,[5] while the radial function combinations appearing in C_{nxy} were taken from the tables prepared by Rose, Perry, and Dismuke.[6] The effect of screening by the orbital electrons is treated in the manner discussed in Sec. III. The integral in Eq. (2) was then performed numerically.

In Sec. II, expressions for λ_e are given. The screening effect also enters into the calculations of λ_e, although the discussions of Secs. III and V indicate that the screening correction is smaller for capture probabilities than for positron emission probabilities. The discussion of Sec. V concerns the decays of Zn^{65}, Na^{22}, Sc^{44}, and the 0.802 branch of the V^{48} decay. We conclude from the available evidence that the decays of Zn^{65} and Na^{22} are *l*-forbidden, the 0.802-Mev decay of V^{48} may be first-forbidden unique, and that further experiments should be performed on Sc^{44}, the last decay being allowed from all except the branching-ratio evidence.

Furthermore, it is concluded that unless the effect of screening on the positron spectrum is considered, fallacious results for the branching ratio may easily be obtained. In particular, the unscreened branching ratio of Zn^{65} is outside of experimental limits, and screening brings the theoretical branching ratio of Na^{22} into better agreement with experiment so that some conclusions previously reached by other authors as to the amount of Fierz interference present in this decay appear to be invalidated.

II. CAPTURE PROBABILITIES

The probability per unit time that a radioactive nucleus consisting of Z protons and $A-Z$ neutrons will decay via orbital electron capture into a nucleus consisting of $Z-1$ protons and $A-Z+1$ neutrons, with the accompanying emission of a neutrino, may be written in the form,

$$\lambda_c=\sum_{x,y}\lambda_c^{xy}\tfrac{1}{2}(1+\delta_{xy}). \tag{3}$$

The summation indices, x and y, take on five values corresponding to the five covariant forms of the nucleon-lepton interaction (i.e., S, V, T, A, or P). When x and y are equal, the term is said to be "pure," while terms for which $x\neq y$ are referred to as "interference" terms.

Expressions[7] for λ_e^x have been given by many authors including Nataf and Bouchez,[8] Marshak,[9] and DeGroot and Tolhoek.[10] None of these gives a complete treatment, although the Nataf and Bouchez paper, which quotes results for allowed and first-forbidden K capture, is the most nearly complete. These results are extended here to $L_{\rm I}$, $L_{\rm II}$, and $L_{\rm III}$ capture and to include "interference" terms. Also, rules are given for finding capture probabilities from all orbits for all orders of forbiddenness, although the usefulness of such formulas is questionable.

TABLE I. Radial function combinations for capture.

Orbit of captured electron:	K $(n=1,\kappa=-1)$	$L_{\rm I}$ $(n=2,\kappa=-1)$	$L_{\rm II}$ $(n=2,\kappa=+1)$	$L_{\rm III}$ $(n=2,\kappa=-2)$
L_0	g^2_{-1K}	g^2_{-1L}	f^2_{1L}	0
L_1	0	0	0	$\rho^{-2}g^2_{-2L}$
M_0	$\rho^{-2}f^2_{-1K}$	$\rho^{-2}f^2_{-1L}$	$\rho^{-2}g^2_{1L}$	0
N_0	$\rho^{-2}f_{-1K}g_{-1K}$	$\rho^{-2}f_{-1L}g_{-1L}$	$-\rho^{-2}f_{1L}g_{1L}$	0
P_0	g^2_{-1K}	g^2_{-1L}	$-f^2_{1L}$	0
P_1	0	0	0	$\rho^{-2}g^2_{-2L}$
Q_0	$-\rho^{-2}f^2_{-1K}$	$-\rho^{-2}f^2_{-1L}$	$\rho^{-2}g^2_{1L}$	0
R_0	$\rho^{-2}f_{-1K}g_{-1K}$	$\rho^{-2}f_{-1L}g_{-1L}$	$\rho^{-2}f_{1L}g_{1L}$	0

The calculation of the λ_e^{xy} are carried out in the same manner in which Konopinski and Uhlenbeck[11] and Greuling[2] calculated the probability of radioactive electron emission, except that a sum over discrete energy levels of the captured electron replaces the integration over a continuous energy spectrum. We write

$$\lambda_e^{xy}=\sum_{\kappa,n} g_x g_y\left(\frac{W_0+\epsilon_{n\kappa}}{2\pi}\right)^2 C_{n\kappa}^{xy} \tag{4}$$

where κ and n are the (Dirac) quantum numbers of the orbital electron, g_x and g_y measure the strength of the interaction as well as the amount of admixture, while $C_{n\kappa}^{xy}$ is the "capture correction factor." The quantity $\epsilon_{n\kappa}$ is the (screened) energy of the bound electron before capture.

The $C_{n\kappa}^{x}$ and $C_{n\kappa}^{xy}$ are identical with the $C_{n\beta}$ formulas (given by Konopinski and Uhlenbeck or Greuling) and the $C_n(x,y)$ formulas (given by Smith or Pursey) for positron emission, if the radial function combinations (L_0, M_0, P_0, Q_0, etc.), now functions of the indices n and κ, are redefined as in Table I.

Here the f's and g's are the radial functions given by Bethe.[12] The subscript numbers refer to the κ value, while the subscript letters give the principal quantum number n. The symbol ρ represents the nuclear radius.

Correction factors for higher orbits may be obtained simply by changing the definitions of the radial function combinations given above in such a manner that the subscripts give the quantum numbers of the orbit under consideration. Thus, for M_1 capture, L_0 becomes $g_{-1M}{}^2$, etc.

For second and higher-forbidden capture, the same fules for forming λ_e apply as do for allowed and first-forbidden capture. However, now other radial function combinations besides those given above will appear. In this instance the modified expressions applicable to

[5] Dismuke, Rose, Perry, and Bell, unclassified Oak Ridge National Laboratory Report ORNL-1222 (unpublished).

[6] Rose, Perry, and Dismuke, unclassified Oak Ridge National Laboratory Report ORNL-1459 (unpublished).

[7] For $x=y$, only one superscript will be retained.

[8] R. Nataf and R. Bouchez, J. phys. et radium **13**, 190 (1952).

[9] R. E. Marshak, Phys. Rev. **61**, 431 (1941).

[10] S. R. DeGroot and H. A. Tolhoek, Physica **16**, 456 (1950).

[11] E. J. Konopinski and G. E. Uhlenbeck, Phys. Rev. **60**, 308 (1941).

[12] H. A. Bethe, *Handbuch der Physik* (Springer, Berlin, 1933), second edition, Vol. 24, Part II, pp. 311 ff.

TABLE II. Allowed K to positron branching ratios.

W_0/mc^2 \ Z	16	29	49	84	92
1.28	93.11	711.3	10 070	5.066×10^5	1.620×10^6
1.44	17.29	112.7	1 317	5.000×10^4	1.528×10^5
1.60	5.654	33.78	354.2	1.148×10^4	3.335×10^4
1.76	2.468	13.94	136.2	3961	9.100×10^3
1.92	1.280	6.954	64.70	1741	4850
2.08	0.7449	3.933	35.27	895.8	2462
2.40	0.3070	1.605	13.67	320.6	870.6
2.88	0.1224	0.6005	4.883	107.1	286.4
3.84	0.03382	0.1605	1.256	26.23	70.76
4.80	0.01397	0.06517	0.5021	10.53	28.52
5.76	7.114×10^{-3}	0.03298	0.2517	5.356	14.63
6.72	4.111×10^{-3}	0.01896	0.1443	3.129	8.627
7.68	2.593×10^{-3}	0.01192	0.09062	2.000	5.564
8.64	1.739×10^{-3}	7.978×10^{-3}	0.06077	1.364	3.824
9.60	1.256×10^{-3}	5.633×10^{-3}	0.04278	0.9759	2.753
10.56	8.946×10^{-4}	4.119×10^{-3}	0.03138	0.7245	2.055
11.52	6.736×10^{-4}	3.086×10^{-3}	0.02340	0.5535	1.579
12.48	5.200×10^{-4}	2.382×10^{-3}	0.01825	0.4365	1.244

electron capture may be found from Rose's definitions of the radial function combinations[6] if

a. The normalization factor $(2p^2F_0)^{-1}$ is set equal to unity.

b. For capture from a given subshell (i.e., specified values of n and κ) only those radial functions with the appropriate κ value are retained. Then the n subscript is added. For example, Rose defines

$$L_2=\frac{1}{2p^2F_0\rho^4}(g_{-3}^2+f_3^2).$$

For electron capture, only those orbits for which $\kappa=\pm3$ will contribute to L_2, just as only those orbits for which $\kappa=\pm2$ can contribute to L_1.

It should be noted however that this does not imply that only such orbits contribute to second-forbidden K and L capture, inasmuch as radial function combinations with all subscripts up to and including n appear in the nth forbidden spectral correction factors.

III. SCREENING CORRECTIONS

The wave functions of both the bound electrons and the positrons are affected by the perturbation on their electrostatic potential energy of the (other) orbital electrons.

Reitz[13] has calculated the screening effect on allowed positron spectra by the use of a Thomas-Fermi-Dirac model of the atom. In order to extend these calculations to the forbidden spectra, the Thomas-Fermi-Dirac wave functions obtained by Reitz[14] were used to form the radial function combinations appearing in expressions for allowed and first-forbidden positron decay probabilities. In this way, it was found numerically that the first-forbidden positron spectra are screened by approximately the same factor as are the allowed spectra. That is, if $N(W,Z)dW$ and $N_{\text{Coul}}(W,Z)dW$ are the screened and Coulomb positron spectra respectively, then the equation,

$$N(W,Z)dW=N_{\text{Coul}}(W,Z)S(W,Z)dW, \qquad (5)$$

holds for both the allowed and first-forbidden positron spectra with the screening function $S(W,Z)$ being approximately the same for both cases. Good[15] and Huster[16] have discussed this point in some detail.

Thus, positron screening was taken into account by the use of Reitz's allowed screening factors, with intermediate values being obtained by graphical interpolation.

It is found that in the region of $Z\sim25$, the effect of screening on the K wave functions can be neglected, Bethe's formulas for hydrogen-like atoms giving values about one percent higher than Reitz's wave functions. Incidentally, Slater wave functions[17] are somewhat closer to the Reitz wave functions than are the Bethe wave functions.

For L electrons, on the other hand, the screening effect is much larger, and if L to positron branching ratios are of interest, even Slater wave functions are not adequate. However, in most cases when K capture is energetically possible, the L capture is a small fraction of total capture, so that the choice of wave functions is not of great importance.

IV. TABLE OF ALLOWED BRANCHING RATIOS

Table II gives allowed K to positron branching ratios as a function of W_0 and Z, where W_0 is the end-point energy of the positron spectrum and Z is the charge of the parent nucleus. Branching ratios for intermediate values of W_0 and Z may be obtained by graphical inter-

[13] J. R. Reitz, Phys. Rev. **77**, 19 (1950).
[14] J. R. Reitz, *Relativistic Electron Wave Functions for a Thomas-Fermi-Dirac Statistical Atom* (University of Chicago Press, Chicago, 1949).
[15] R. H. Good, Jr., Phys. Rev. **94**, 931 (1954).
[16] E. Huster, Z. Physik **136**, 303 (1953).
[17] J. C. Slater, Phys. Rev. **36**, 57 (1930).

polation, although the results should not be extrapolated beyond the Z-values given.

The effect of screening, both on the positron and capture decay probabilities, was taken into account by using Reitz's wave functions.

Allowed branching ratios for L-capture to positron emission may also be obtained readily if Table II is used in conjunction with the graph given by Rose and Jackson[18] plotting the ratio of allowed L capture to K capture as a function of Z.

V. COMPARISON WITH EXPERIMENT

a. Zn-65

The 0.325-Mev decay of Zn^{65} has been measured by Haynes and Perkins,[19] who find a Kurie plot linear down to 1.12 mc^2, if the experimental points are corrected for screening. Since the shell model[1] predicts this transition to be $f_{\frac{5}{2}} \rightarrow p_{\frac{1}{2}}$, ($\Delta J = 1$, "no") the allowed shape is no surprise. The high logft value of 7.34[20] is assumed to be caused by the fact that $\Delta l = 2$ (i.e., the transition is "l-forbidden").

Under the assumptions that it is valid to evaluate the lepton wave functions at the nuclear radius[21] and that second-order corrections[22] are unimportant, the K-positron branching ratio is the same for an l-forbidden decay as for an allowed decay.

The theoretical K-positron branching ratio for this decay is 28.9, which is in good agreement with the measured value of 28.0 ± 3.0.[19] If the effect of screening on the positron spectrum is ignored, the theoretical branching ratio for an allowed decay is 33, which is outside the experimental limits.

It is interesting to note that if the experimental points are corrected for screening before the Kurie plot is drawn, the end-point energy is found to be 0.330 Mev rather than the 0.325-Mev figure usually quoted in the literature.

b. Na-22

The 0.54-Mev decay of Na^{22} should be another $\Delta J = 1$, "no" allowed transition.[23] The theoretical allowed branching ratio ($L+K$) for such a decay is 0.111, which is in good agreement with recent measurements by Kreger and Cook[24] and Sherr and Miller[25] both of whom measure 11 percent. Our theoretical value is slightly lower than that given by the latter authors because of the effect of screening on the positron spectrum. Since Sherr and Miller failed to include this effect, their conclusions concerning the amount of Fierz interference present are largely invalidated, the discrepancy between the experimental and theoretical branching ratios which they used in their argument becoming much smaller when screening is included.

The high logft value of this decay (log$ft = 7.38$) indicates that this too is an l-forbidden transition.

c. Sc-44

The 1.463-Mev decay of Sc^{44} is presumably allowed and shows a linear Kurie plot with a logft value of 5.3.[23,26] Bruner and Langer, however, quote electron capture as being the same order of magnitude as positron emission for this transition. The theoretical allowed K to positron branching ratio for this isotope assuming an allowed transition may readily be calculated to be 0.062, in very bad agreement with experiment, suggesting the need of more work on this decay.

d. V-48

The 0.802-Mev decay of V^{48}, the route by which about 5 percent of the isotope decays, is presumably first-forbidden unique, at least according to the spin and parity assignments of Roggenkamp *et al.*, and the quoted logft value of 7.4.[27]

The theoretical K to positron branching ratio is 2.02, while if the decay were allowed the branching ratio would be only 0.534. Roggenkamp quotes the branching ratio only as >0.7, so that the branching-ratio evidence is not inconsistent with the conclusion that the decay is first-forbidden unique. An experiment designed to measure accurately this branching ratio would be of great value in determining firm spin and parity assignments for the nuclear levels involved in this decay.

VI. ACKNOWLEDGMENT

The author owes a great debt of gratitude to Professor Eugene Greuling who directed this research. Also, stimulating discussions were held with Professor Eugen Merzbacher during the early stages of the work.

[18] M. E. Rose and J. L. Jackson, Phys. Rev. **76**, 1540 (1949).
[19] S. K. Haynes and J. F. Perkins, Phys. Rev. **92**, 687 (1953).
[20] King, Dismuke, and Way, unclassified Oak Ridge National Laboratory Report ORNL-1450 (unpublished).
[21] M. E. Rose and R. K. Osborne, Phys. Rev. **93**, 1315 (1954).
[22] P. F. Zweifel, Phys. Rev. **95**, 112 (1954).
[23] P. M. Endt and J. C. Kluyver, Revs. Modern Phys. **26**, 99 (1954).
[24] W. E. Kreger and C. Sharp Cook, Bull. Am. Phys. Soc. **29**, No. 6, 19 (1954).
[25] R. Sherr and R. H. Miller, Phys. Rev. **93**, 1076 (1954).
[26] J. A. Bruner and L. M. Langer, Phys. Rev. **79**, 606 (1950).
[27] Roggenkamp, Pruett, and Wilkinson, Phys. Rev. **88**, 1262 (1952).

Berkelium and Californium Isotopes Produced in Neutron Irradiation of Plutonium

L. B. MAGNUSSON, M. H. STUDIER, P. R. FIELDS, C. M. STEVENS, J. F. MECH, A. M. FRIEDMAN, H. DIAMOND, AND J. R. HUIZENGA
Argonne National Laboratory, Lemont, Illinois

(Received September 1, 1954)

Californium isotopes of mass numbers 249, 250, 251, and 252 have been identified by mass spectrometric analyses of californium samples produced from neutron-irradiated plutonium. The half-lives of Bk^{249}, Cf^{249}, Cf^{250}, Cf^{252}, and Cf^{253} are 290±20 days, 470±100 years, 10.0±2.4 years, 2.2±0.2 years, and 18±3 days, respectively. The alpha-particle energies of the most prominent alpha peaks for Cf^{249}, Cf^{250}, and Cf^{252} are 5.81±0.03, 6.033 ±0.010, and 6.117±0.010 Mev, respectively. The plot of alpha-particle energies *vs* mass number for the isotopes of californium shows a break (i.e., the alpha energy of Cf^{252} is larger than the alpha energy of Cf^{250}) indicating an irregularity in the nuclear energy surface. The alpha spectra of Cf^{250} and Cf^{252} exhibit characteristic even-even nuclide fine structure peaks. The beta-particle energy of Bk^{249} is 80±20 kev. The spontaneous fission half-lives of Cf^{250} and Cf^{252} are $1.5\pm0.5\times10^4$ and 66±10 years, respectively. Lower limits of 2×10^8 and 5×10^6 years have been placed on the partial spontaneous fission half-lives of Bk^{249} and Cf^{249}. The pile (Materials Testing Reactor at Arco, Idaho) neutron capture cross sections of Bk^{249}, Cf^{250}, Cf^{251}, and Cf^{252} are 350, 1500, 3000, and 25 barns, respectively.

INTRODUCTION

THE preliminary identification of new isotopes of berkelium and californium formed by multiple order neutron capture reactions in the MTR (Materials Testing Reactor at Arco, Idaho) has been reported in a recent communication.[1] These isotopes were found in three plutonium samples, designated henceforth as I, II, and III, which had been subjected to integrated fluxes of 4.2×10^{21}, 1.14×10^{22}, and 1.40×10^{22} neutrons, respectively. Relatively large amounts of transcurium elements were created in the plutonium samples; e.g., about 3×10^{-4} microgram of californium was separated from sample II. The information obtained from measurements of re-irradiated berkelium and californium fractions will be included in this report.

EXPERIMENTAL

The actinide elements produced in neutron irradiation of plutonium were chemically separated from fission products and other impurities by procedures briefly indicated in other publications.[2-4] The transplutonium elements were separated by elution from a hot Dowex-50 cation resin column.[4,5] The nonvolatile solid content of the eluate fractions was reduced for the preparation of radioactive assay plates by organic solvent extractions. Gross amounts of solid impurity were eliminated by extraction of the actinide elements into tributyl phosphate from salted nitric acid solution.[6] Essentially weightless deposits of the actinide elements were formed by evaporating toluene solutions of the thenoyltrifluoroacetone (TTA) chelate complexes of the +3 ions. The chelates are extracted by contacting aqueous solutions of the ions at a *p*H of about 4 with 0.2*M* TTA in toluene.[7] Plates prepared by the TTA method proved to be excellent for alpha-particle pulse analysis since the energy degradation by sample self-absorption is negligible.

Alpha-particle energies were measured with the ionization chamber and twenty-channel pulse-height analyzer described elsewhere.[8] The known alpha-group energies of Cm^{242} (6.110 Mev) and Bi^{212} (6.047 Mev) were used as reference standards. Spontaneous fission counting was done with conventional ionization chambers and scaling circuits.[9]

Isotopic compositions of the californium samples were measured in a 12-in., 60° mass spectrometer with multiple filament surface ionization source.[10] Samples containing as little as 10^{-11} g of californium were successfully analyzed in the mass spectrometer.

The origins and irradiation histories of the various californium samples described in this article are as follows:

I, II, and III were isolated from the initial irradiated plutonium samples I, II, and III, respectively;

IIa was a small fraction of californium sample II which had been left with the berkelium fraction from plutonium sample II for five weeks before chemical separation;

TABLE I. Mass spectrometric analyses of three californium samples giving isotopic abundances in mole percent.

Cf Isotope	Sample II	Sample IIa	Sample IIb
$_{98}Cf^{249}$	4.3±0.5	28±7	< 7
$_{98}Cf^{250}$	49 ±6	34±8	<10
$_{98}Cf^{251}$	11 ±3	8±1	< 6
$_{98}Cf^{252}$	36 ±5	30±3	>77

[1] Diamond, Magnusson, Mech, Stevens, Friedman, Studier, Fields, and Huizenga, Phys. Rev. **94**, 1083 (1954).
[2] Studier, Fields, Sellers, Friedman, Mech, Diamond, Sedlet, and Huizenga, Phys. Rev. **93**, 1428 (1954).
[3] Stevens, Studier, Fields, Mech, Sellers, Friedman, Diamond, and Huizenga, Phys. Rev. **94**, 974 (1954).
[4] Studier, Fields, Diamond, Mech, Friedman, Sellers, Pyle, Stevens, Magnusson, and Huizenga, Phys. Rev. **93**, 1433 (1954).
[5] Fields, Studier, Mech, Diamond, Friedman, Magnusson, and Huizenga, Phys. Rev. **94**, 207 (1954).
[6] Peppard, Gray, and Markus, J. Am. Chem. Soc. **75**, 6063 (1953).
[7] L. B. Magnusson and M. L. Anderson (unpublished results).
[8] D. W. Engelkemeir and L. B. Magnusson, Rev. Sci. Instr. (to be published).
[9] A. H. Jaffey and A. Hirsch (unpublished results).
[10] M. G. Inghram and W. A. Chupka, Rev. Sci. Instr. **24**, 518 (1953).

IIb was a fraction (*ca* 3×10^4 alpha-dis/min) of californium sample II which was reirradiated in the MTR for six weeks (*ca* 10^{21} neutrons);

IIc was separated from reirradiated berkelium (*ca* 6×10^{19} neutrons) which had been isolated from plutonium sample II.

The final chemical purification produced a californium sample with an alpha-disintegration rate of about 2.3×10^5/minute from the neutron-irradiated plutonium sample II. An aliquot, 2.3×10^4 alpha disintegrations/minute, was analyzed in the mass spectrometer. Californium isotopes of mass numbers 249, 250, 251, and 252 were detected in mole percentages given in column 2 of Table I. A small quantity of the californium, about 9×10^3 alpha disintegrations/minute, was left with the berkelium chemical fraction during the initial actinide element separation (californium sample IIa). After a five-week growth period, californium sample IIa was chemically separated from the berkelium and analyzed in the mass spectrometer. The isotopic analysis of this sample is given in Column 3 of Table I. The Cf^{250}/Cf^{252}, Cf^{251}/Cf^{250}, and Cf^{251}/Cf^{252} mole ratios of samples II and IIa are constant within statistical error (Table II). The Cf^{249} in sample IIa has, however, been enhanced by a factor of about 9. These data are evidence for assigning to Cf^{249} the 5.81-Mev alpha particles observed to grow into a purified berkelium fraction and to elute chemically in the californium position.

TABLE II. Isotopic enrichment of californium-249 in sample IIa.

Californium isotope ratio	Sample II	Sample IIa	Sample IIa/ sample II
250/252	1.36±0.25	1.13±0.29	0.83±0.27
251/250	0.22±0.07	0.24±0.06	1.05±0.42
251/252	0.31±0.09	0.27±0.04	0.87±0.30
249/250	0.09±0.015	0.82±0.29	9.1 ±3.5
249/251	0.39±0.12	3.50±0.98	9.0 ±3.8
249/252	0.12±0.02	0.93±0.25	7.8 ±2.6

A portion of californium sample II containing approximately 3×10^4 alpha disintegrations/minute was reirradiated for six weeks (integrated flux 10^{21} neutrons) in the MTR. After irradiation this californium (sample IIb) was again chemically separated, and a major part of the sample was used for a mass spectrometric analysis. The quantity of this sample was much smaller than the quantities of the other californium samples examined in the mass spectrometer, therefore the results reported in column 4 of Table I are limits.

ALPHA-PARTICLE AND SPONTANEOUS FISSION INTENSITIES

Alpha-pulse analysis of californium sample II showed two prominent alpha groups of 6.03 and 6.12 Mev. The calibration of alpha-particle energies is presented in the next section of this paper. The 6.12-Mev alpha peak in californium sample II was 77±2 percent of the combined 6.03 and 6.12-Mev alpha peaks as shown in Fig. 1. Californium samples I and III contained 38±4 and 82±2 percent, respectively, of 6.12-Mev alpha particles. Californium sample II was reirradiated (integrated flux *ca* 10^{21} neutrons) for six weeks in the MTR. The alpha spectrum of the resulting californium sample (californium sample IIb) is shown in Fig. 1 and contains about 97±2 percent 6.12-Mev alpha particles.

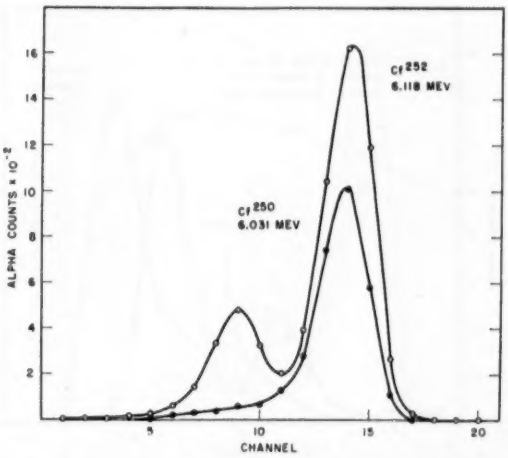

FIG. 1. Californium alpha spectra. Alpha counts per alpha-pulse analyzer channel *vs* channel number which is a linear function of energy. The open circles (○) and solid circles (●) represent the alpha-pulse analyses of californium samples II and IIb, respectively. The samples were deposited on 2-mil platinum by evaporating TTA-toluene solutions of californium. The alpha particles were collimated with a ½×1-inch copper ring.

The ratios of alpha disintegrations (6.03-plus 6.12-Mev) to spontaneous fission disintegrations for californium samples I, II, III, and IIb are 74±5, 39±1, 36 ±1, and 32±1, respectively. As the percentage of 6.12-Mev alpha particles increases, the alpha-to spontaneous fission disintegration ratios decrease, indicating that a major fraction of the spontaneous fission activity is associated with the isotope emitting the 6.12-Mev alpha particles, or other higher mass isotopes whose alpha particles were not detected.

A sample of berkelium-249, 3.6×10^4 beta disintegrations/minute, chemically separated from traces of californium impurity was irradiated in the "rabbit" of the MTR for 3.5 days. Prior to irradiation no spontaneous fission events were observed in this berkelium sample during one day of fission counting. The spontaneous fission counting rate is therefore less than 1.3×10^{-3} disintegration/minute (standard error), and the calculated californium alpha disintegrations/minute is less than 0.05. Approximately sixty californium alpha-disintegrations/minute were produced by the irradiation which were by activity greater than 98 percent 6.03-Mev alpha particles (californium sample IIc). The californium alpha disintegrations/minute to spontaneous fission disintegrations/minute ratio of this sample was 875±26.

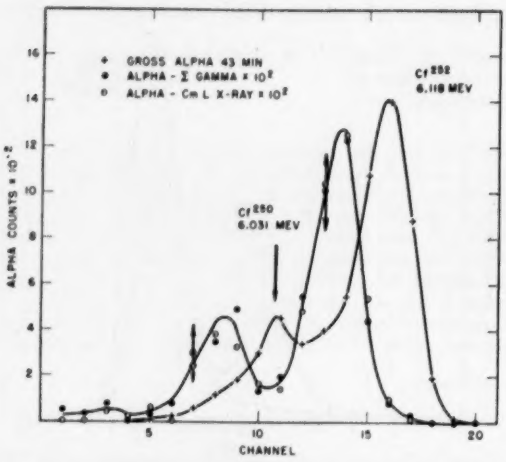

FIG. 2. Gamma-alpha coincidence spectra of Cf^{250} and Cf^{252}. The crosses (+) are the gross californium alpha counts. The solid circles (●) are the alpha-Σgamma (>10 kev) coincidence counts and the open circles (○) are the alpha—Cm *L* x-ray (14–23 kev) coincidence counts. The sample was deposited on 0.5-mil aluminum foil by evaporation of a tributyl phosphate solution. The alpha particles were collimated by covering the foil with 2-mil Lektromesh screen.

ALPHA- AND BETA-PARTICLE ENERGIES

The californium alpha-particle energies were calibrated by intercomparisons of samples II, IIa, IIb, and IIc and the 6.047-Mev and 6.110-Mev alpha-particle groups of Bi^{212} and Cm^{242}, respectively.

Pb^{212} recoil atoms from an emanating source of RdTh were caught on a sample of californium II deposited by evaporation and ignition of a drop of ammonium citrate solution from a column elution. The alpha particles were collimated by covering the platinum sample disk with 2-mil Lektromesh screen.[8] With this type collimator the 6.047-Mev alpha particle[11] of Bi^{212} can be used as an energy standard for ion pulse analysis since the conversion electron energy liberated in the deexcitation of the daughter Tl^{208} atom is not added to the alpha-particle ionization.[8] The intensity of the Bi^{212} alpha particles was adjusted by the length of recoil collection time to be several times greater than the lower intensity californium alpha particle (6.03 Mev). The position of the resultant pulse-analyzer peak was essentially governed by the 6.047-Mev Bi^{212} alpha-particles. The higher intensity californium alpha particle was found to be *ca* 60 kev more energetic than the 6.047-Mev Bi^{212} alpha particles. The energy separation of the prominent californium peaks was *ca* 80 kev (no Bi^{212} present). The californium alpha-particle energies obtained with this sample are known to be too small but are valuable supporting evidence for the energies measured with the Cm^{242} standard. The californium peak widths (full width at half the maximum height) in the ignited citrate sample were 50 kev, whereas the normal width is about 30 kev for a thin sample.

The alpha-particle energy of the californium (sample IIc) produced by neutron irradiation of berkelium was compared with the Cm^{242} 6.110-Mev alpha particle.[12] Both alpha emitters were mounted on pieces of 2-mil platinum by the TTA method. The platinum pieces were placed within a single collimating ring. Although both the californium and curium have branching decay to excited states, as will be shown in the next section only single ion pulse peaks appear for each of the two alpha-emitters. The peak energy is that for the alpha particle emitted in decay to the ground state. The californium alpha particle was found to be 77 kev less energetic than the Cm^{242} alpha particle. In other comparisons, the alpha-particle energy of sample IIc was identical with that of the lower energy alpha particle of samples II and IIa and less energetic than the higher energy alpha particle in samples II, IIa, and IIb by 84 kev. Relative to the Cm^{242} alpha-particle energy of 6.110 Mev, the energies of the californium alpha particles are 6.033 and 6.117 Mev. The uncertainty in the relative peak positions in the pulse spectra were estimated to be equivalent to less than 5 kev.

Californium sample IIa also contained a small alpha-particle peak at 5.81 Mev. A peak of this energy was observed to grow into a beta-emitting berkelium sample which had previously been separated from all detectable californium alpha activity. The 5.81-Mev peak appeared to be the only one present. The limit of detection of any other peak in the sample was estimated to be less than 5 percent of the 5.81-Mev peak intensity.

Absorption measurements showed the energy of the Bk^{249} beta particles to be 80 ± 20 kev. A Bk^{249} sample of 1.5×10^5 beta disintegrations/minute also contained an alpha-particle peak (*ca* 2 disintegrations/minute) at 5.40 ± 0.05 Mev. The alpha- to beta-branching ratio of Bk^{249} is therefore about 10^{-5}.

MASS ASSIGNMENTS OF THE 6.03- AND 6.12-MEV ALPHA-PARTICLE GROUPS

It has been shown (see Table I and reference 1) that californium-249 emits a prominent alpha group with energy of 5.81 Mev. The 6.03-Mev and 6.12-Mev alpha groups are assigned to Cf^{250} and Cf^{252}, respectively, from the following arguments.

(1) Californium produced by a short irradiation (3.5 days) of Bk^{249} showed an alpha activity consisting almost entirely (>98 percent) of 6.03-Mev particles.

(2) Since the 6.12/6.03-Mev alpha-activity ratio increased with the integrated neutron flux received by the plutonium, the 6.12-Mev activity is probably a higher order capture product than the 6.03-Mev activity.

(3) Re-irradiation of californium sample II for six weeks (californium sample IIb) depleted the 6.03-Mev

[11] A. Rytz, Compt. rend. **233**, 790 (1951).

[12] Asaro, Reynolds, and Perlman, Phys. Rev. **87**, 277 (1952).

activity relative to the 6.12-Mev activity. The mass spectrometric analysis of californium sample IIb also showed the mass 250 depleted relative to the 252.

(4) The alpha-particle spectrum of californium sample II was found to have characteristics to be expected for the decay of two even-even nuclides. Figure 2 shows the alpha-particle spectrum measured in coincidence with electromagnetic radiations from a sample collimated with Lektromesh screen. The spectrum in coincidence with radiation in the energy range of curium L x-rays (14 to 23 kev) was the same, within the statistical uncertainty, as that in coincidence with all radiations of energy greater than *ca* 10 kev. In a corollary measurement, no significant coincident rates were detected between alpha particles and electromagnetic radiation of energy greater than the curium L x-rays. The two alpha particles observed in the gross spectrum are not seen in the coincident spectrum. These alpha particles (6.033 and 6.117 Mev) must be emitted in decays to the ground states of two curium isotopes. The coincident spectrum also shows two alpha-particle peaks but with energies of *ca* 5.99 and 6.08 Mev. The ratio of the intensity of the 5.99-Mev particle to that of the 6.08-Mev particle is approximately the same as the intensity ratio of the 6.033-Mev and 6.117-Mev particles. The alpha particles coincident with L x-rays appear to be emitted in decays to the first excited states (40-45 kev) of the two curium isotopes. The 40–45 kev energies of the first excited states, which are deduced from the separations of the coincident and gross alpha-particle peaks, must be highly converted in the L shells of the curium isotopes. A first excited state energy of *ca* 40 kev and high conversion in the transition to ground appear to be universal properties of the known even-even nuclides with atomic number greater than 90.[13] The percentage of branching decay to the first excited state was measured by comparing the L x-ray—alpha-particle coincidence rates of californium sample II and a plutonium-238 sample under the same conditions. From the known branching of Pu^{238} (24 percent)[14] the branching in the decays of both californium isotopes was calculated to be about 10 percent, an unusually small percentage for the decay of even-even nuclides in this region.

The lack of evidence for alpha particles from Cf^{251} is not surprising. The mass of Cf^{251} is low relative to the masses of Cf^{250} and Cf^{252} in sample II and the odd neutron nuclide as a rule has a much longer half-life than the neighboring even-even nuclides. The resolution of the alpha-particle pulse analyzer is not high enough to detect very low intensity particles.

The mass assignments of Cf^{250} (6.03-Mev alpha particles) and Cf^{252} (6.12-Mev alpha particles) have important implications in that the plot of alpha-particle energies *vs* mass number for the isotopes of californium shows an irregularity in this region. Except for the large irregularities in the alpha energies near the closed shell $N=126$, the plots of alpha-particle energies *vs* mass number for other elements exhibit a monotonic decrease in alpha-particle energy with increasing mass.[15] Ghiorso, Thompson, Higgins, Harvey, and Seaborg[16] have used the break in the alpha energies of the californium isotopes to postulate a subshell at $N=152$.

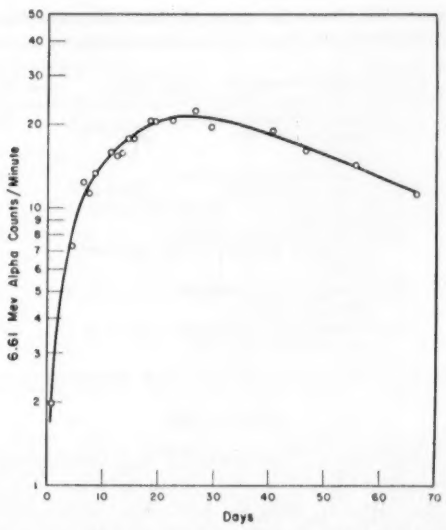

FIG. 3. Growth and decay of 6.61-Mev alpha particles in a chemically separated californium sample as a function of time.

$$Cf^{253} \xrightarrow{\beta^-} 99^{253} \xrightarrow{\alpha} \underset{6.61\ \text{Mev}}{\phantom{99^{253}}}.$$

Alpha particles of 6.61-Mev energy have been observed to grow into a chemically separated californium fraction (see Fig. 3). From the growth and decay of the 6.61-Mev alpha particles, a beta half-life of 18 ± 3 days has been calculated for the beta-emitting californium isotope. The mass of this isotope is greater than 252 since two mass spectrometer analyses of a californium sample separated by five weeks showed Cf^{251} to have a beta half-life much longer than 18 days or to be beta stable. The yield of the 18-day beta-emitting isotope was about one-hundredth that of Cf^{252} in californium sample II. Californium-254 would be predicted to be beta stable, and such a large yield of Cf^{255} is very unlikely. In addition, alpha-decay systematics favor mass 253 over 255 for the 6.61-Mev alpha particles of element 99. Thus the 18-day beta-emitting isotope of californium is almost certainly mass 253. An attempt to identify the Cf^{253} beta particles has not been successful owing to the large amount of spontaneous fission activity in the californium.

[13] F. Asaro and I. Perlman, Phys. Rev. **91**, 763 (1953).
[14] Hollander, Perlman, and Seaborg, Revs. Modern Phys. **25**, 469 (1953).
[15] Perlman, Ghiorso, and Seaborg, Phys. Rev. **77**, 26 (1950).
[16] Ghiorso, Thompson, Higgins, Harvey, and Seaborg, Phys. Rev. **95**, 293 (1954).

TABLE III. [Alpha disintegrations/minute]/[spontaneous fission disintegrations/minute] ratios for five californium samples.

Californium sample	$\frac{(6.03+6.12)\text{-Mev } \alpha \text{ dis/min}}{\text{spon. fission dis/min}}$	$\frac{6.12\text{-Mev } \alpha \text{ dis/min}}{(6.03+6.12)\text{-Mev } \alpha \text{ dis/min}}$	$\frac{6.12\text{-Mev } \alpha \text{ dis/min}}{\text{spon. fission dis/min}}$
I (from plutonium which received 4.2×10^{21} neutrons)	74+5	0.38±0.04	28±4
II (from plutonium which received 1.14×10^{22} neutrons)	39±1	0.77±0.02	30±1
III (from plutonium which received 1.40×10^{22} neutrons)	36±1	0.82±0.02	30±1
IIb (sample II re-irradiated with 10^{21} neutrons)	32±1	0.97±0.02	31±1
IIc (berkelium re-irradiated with 6×10^{19} neutrons)	875±26	0.013±0.004	

HALF-LIVES

The half-life of berkelium-249 has been measured by following the decay of its beta activity. The best half-life value is 290±20 days. The californium-249 half-life has been calculated from the growth of alpha activity (0.6 disintegration/minute per day) into a berkelium-249 sample of 1.5×10^5 beta disintegrations/minute. A berkelium-249 counting efficiency in a Bradley PC-10 counter of 56 percent from a calibration curve of beta energy *vs* counting efficiency[17] was used. The half-life of Cf^{249} from the above data is 470±100 years.

An aliquot of the californium sample II was followed for the decay of the spontaneous fission activity. The spontaneous fission activity decayed with a 2.2±0.2-yr half-life as shown in Fig. 4. Data from Table III (compare samples II and IIc) and Table I show that the fraction of spontaneous fission events due to Cf^{250} in the above sample is less than 1.3 percent [$<(0.23/875)/0.77/39)=0.013$]. The spontaneous fission half-life of Cf^{249} is long, and it is not expected that the odd-neutron nuclides, Cf^{251} and Cf^{253}, would contribute to the spontaneous fission activity. It is also improbable that higher even A californium isotopes (e.g., Cf^{254}) are contributing to the spontaneous fission activity. The integrated neutron flux received by californium samples I, II, III, and IIb varied by a factor of about three. The spontaneous fission activities (Cf^{250} spontaneous fission contribution negligible in each of those samples) of each of the above samples are directly proportional to their 6.12-Mev alpha activities (Cf^{252}). One would not expect this relation with neutron flux if higher order capture products (Cf^{254}, etc.) were making a measurable spontaneous fission contribution. From these considerations the decay of the spontaneous fission activity may be taken as a measure of the Cf^{252} half-life, although the main mode of decay of Cf^{252} is by alpha-particle emission. The direct measurement by pulse analysis of decay of the Cf^{252} alpha activity was not attempted during the relatively short time of these experiments.

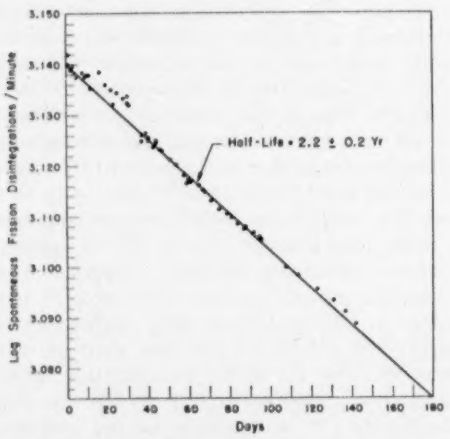

FIG. 4. Decay of Cf^{252}. The log of the spontaneous fission disintegrations/minute of californium sample II is plotted as a function of time.

[17] We are indebted to Kevin Flynn for the absolute beta-disintegration rate of this berkelium sample.

The half-life of Cf^{252} (6.12-Mev alphas) has also been determined relative to Cf^{249} from californium sample IIa with the aid of an alpha-pulse analysis and a mass spectrometric determination. Californium sample IIa was found to have 0.34±0.10 percent 5.81-Mev alpha activity. Employing the mass spectrometric data of Table I, a 470±100-yr half-life for Cf^{249}, and alpha-pulse analysis data showing the sample to be 77 percent by activity 6.12-Mev alpha particles one calculates a half-life for Cf^{252} of 2.2±1.0 years. Although the experimental uncertainty is large, this half-life value agrees with the previous value. The half-life of Cf^{250} is calculated from mass spectrometric and alpha-pulse analyses of californium sample II to be 4.56±1.00 times longer than that of Cf^{252}, or 10.0±2.4 years.

SPONTANEOUS FISSION HALF-LIVES

The Cf^{252} alpha-/spontaneous fission disintegration ratios from californium samples I, II, III, and IIb are

TABLE IV. Nuclear properties of some isotopes of berkelium and californium.

Isotope	Radiation	Half-life	Alpha-particle energies (Mev)	Spontaneous fission half-life (years)
$_{97}Bk^{249}$	β^-, α branching ratio $\beta^-/\alpha \approx 10^5$	290±20 days	5.40±0.05	$\geqslant 2\times10^8$
$_{97}Bk^{250}$	β^-	<12 hours		
$_{98}Cf^{249}$	α, α/s.f. $\geqslant 1.2\times10^4$	470±100 years	5.81±0.03	$\geqslant 5\times10^6$
$_{98}Cf^{250}$	α, spontaneous fission (s.f.)	10.0±2.4 years	6.033±0.010 (90%)	1.5±0.5×10⁴
	α/s.f. = 1460±350		5.99±0.01 (10%)	
$_{98}Cf^{251}$	(α)	...	...	...
$_{98}Cf^{252}$	α, spontaneous fission	2.2±0.2 years	6.117±0.010 (90%)	66±10
	α/s.f. = 30±1		6.08±0.01 (10%)	
$_{98}Cf^{253}$	β^-	18±3 days	...	...

28±4, 30±1, 30±1, and 31±1, respectively. The partial spontaneous fission half-life of Cf^{252} is calculated to be 66±10 years. The Cf^{250} alpha-/spontaneous fission disintegration ratio is subject to a greater error since a very small change in the calculated content of Cf^{252} in the sample changes the ratio considerably. Californium sample IIc contains 1.3±0.4 percent Cf^{252} (Fig. 5), and the gross californium alpha-to spontaneous fission disintegration ratio is 875±26. Making the correction for the contributions from Cf^{252}, one calculates that the alpha-to spontaneous fission disintegration ratio for Cf^{250} is 1460±350. This ratio and the alpha-decay half-life gives a partial spontaneous fission half-life for Cf^{250} of 1.5±0.5×10⁴ years.

A sample of Bk^{249} (1.5×10^5 beta disintegrations/minute) was fission counted for seven days following chemical separation of the berkelium (a small quantity of Cf^{249} grew in during this period), in which time four spontaneous fission events were recorded. Some or all of these fission events may have been background or Cf^{249} spontaneous fission. The partial half-life for spontaneous fission of Bk^{249} is therefore equal to, or greater than, 2×10^8 years.

Five alpha disintegrations/minute of Cf^{249} were fission counted for 10^4 minutes, in which time 4 spontaneous fission events were observed. The alpha-to spontaneous fission disintegration ratio is equal to or greater than 1.2×10^4. Employing an alpha-decay half-life of 470 years for Cf^{249} gives a lower limit to its spontaneous fission half-life of 5×10^6 years.

The measured spontaneous fission half-lives of Cf^{250} and Cf^{252} do not agree with values predicted for even-even nuclides from the plots of Seaborg[18] and Whitehouse and Galbraith.[19] These authors plotted the logarithms of the spontaneous fission half-lives of several even-even nuclides as a function of their Z^2/A values. Cf^{252} has a shorter spontaneous fission half-life than Cf^{250}, which supports the idea that the even-A isotopes of each even-Z element go through a maximum stability for spontaneous fission as A increases.[20,21]

The spontaneous fission decay rates of the heavy odd-nucleon isotopes are several factors of ten slower than corresponding even-even nuclides, in agreement with previously measured spontaneous fission half-lives of other odd-nucleon isotopes.

PILE NEUTRON CROSS SECTIONS

A sample of Bk^{249} with a disintegration rate of approximately 3.6×10^4/minute was irradiated for 3.5 days in the "rabbit" of the MTR. Cf^{250} with 60 alpha disintegrations/minute was produced. Assuming a flux of 2×10^{14} neutrons/cm²−sec, one calculates the pile neutron capture cross section of Bk^{249} to be 350 barns.

From the amount of Cf^{253} present in a sample of californium (containing isotopes of mass numbers 249,

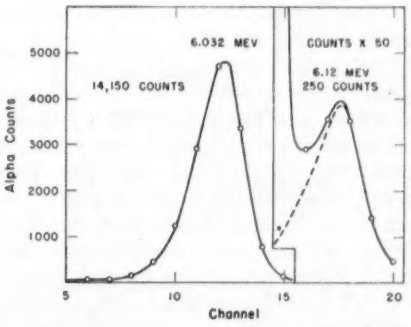

FIG. 5. Alpha-pulse analysis of californium sample IIc. This sample contains 1.3±0.4 percent 6.12-Mev alpha particles (Cf^{252}). The sample was deposited on 2-mil platinum by evaporating a TTA-toluene solution.

[18] G. T. Seaborg, Phys. Rev. **85**, 157 (1952).
[19] W. J. Whitehouse and W. Galbraith, Nature **169**, 494 (1952).
[20] J. R. Huizenga, Phys. Rev. **94**, 158 (1954).
[21] Fields, Studier, Magnusson, and Huizenga, Nature **174**, 265 (1954).

250, 251, and 252) irradiated for six weeks in the MTR, the pile neutron capture cross section of Cf^{252} was calculated to be 25 barns.

Crude calculations of the pile neutron capture cross sections of Cf^{250} and Cf^{251} from mass spectrometric data indicate that these values are about 1500 and 3000 barns, respectively.

A summary of the nuclear properties of the isotopes of berkelium and californium observed in these experiments is given in Table IV.

The experimental assistance given by J. E. Gindler and M. M. Petheram is gratefully acknowledged. We also wish to express our gratitude to W. M. Manning for his interest in this work.

PHYSICAL REVIEW VOLUME 96, NUMBER 6 DECEMBER 15, 1954

Decay of $_{22}Ti^{51}$ (5.8 min)

W. C. JORDAN, S. B. BURSON, AND J. M. LEBLANC
Argonne National Laboratory, Lemont, Illinois

(Received July 6, 1954)

The radiations from Ti^{51} have been studied with a scintillation coincidence spectrometer. Gamma rays of 0.32, 0.61, and 0.92 Mev are resolved. Their intensities are estimated to be in the ratio 100:1:5, respectively. The 0.32- and 0.61-Mev gamma rays are in coincidence. Two beta-ray components are resolved; one of approximately 2.3 Mev is in coincidence with the 0.32-Mev gamma ray, and one of 1.8 Mev is in coincidence with the 0.92-Mev radiation. No indication of a beta transition to the ground state of V^{51} is observed.

A SHORT-LIVED radioactivity induced in titanium by irradiation with deuterons and neutrons was first observed by Walke.[1] His tentative assignment to Ti^{51} has been confirmed.[2] A 72-day activity at first believed to be isomeric has been shown[3,4] to be due to contamination of the source. From a careful measurement,[5] the half-life of the short activity is now known to be 5.79±0.03 min. Gamma radiation of 0.32 Mev has been detected by several experimenters.[6–8] Bunker and Starner[8] have reported additional weak gamma rays of 0.60 and 0.915 Mev. They find that the 0.60-Mev radiation is in coincidence with the 0.32-Mev gamma ray and assume the 0.915-Mev gamma ray to be the cross-over transition. A marked disagreement exists between different measurements of the beta transition energies and hence of the total disintegration energy. Der Mateosian[9] found the beta spectrum to be complex, consisting of two components with energies of 1.85 and 2.1 Mev. He observed coincidences between the 1.85-Mev beta ray and the 0.32-Mev gamma ray. Other investigators[2,10] have also reported the maximum beta energy to be about 1.7 Mev. A disintegration energy of 1.7 Mev is much smaller than that expected from a consideration of the energy systematics of odd-mass beta emitters. Koester *et al.*[7] also find the beta spectrum to be complex but report the maximum beta energy to be 2.2 Mev. They conclude that this transition leads to the ground state.

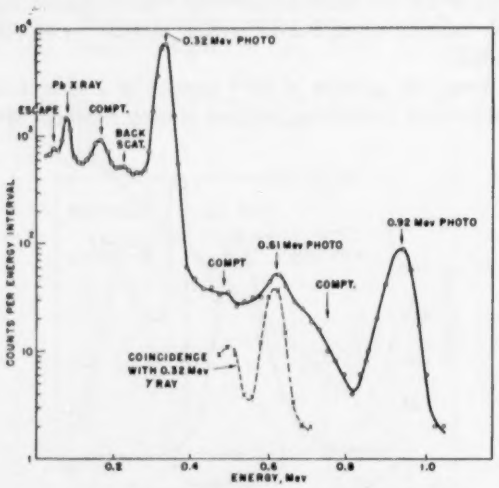

FIG. 1. NaI(Tl) pulse-height distribution of Ti^{51} (5.8 min).

We have undertaken an investigation of the decay of Ti^{51} using our ten-channel scintillation coincidence spectrometer. NaI (Tl) crystals ($2\frac{1}{4}$ in.×$2\frac{1}{4}$ in.×$2\frac{1}{8}$ in.) were used for the detection of gamma radiation, and an anthracene crystal was used for the detection of beta radiations. The anthracene is provided with a thin aluminum window (<0.001 in.). Sources were

[1] H. Walke, Phys. Rev. **52**, 777 (1937).
[2] Hammond, Kundu, and Pool, Phys. Rev. **90**, 157 (1953).
[3] E. der Mateosian and M. Goldhaber, Phys. Rev. **79**, 192 (1950); Miskel, der Mateosian, and Goldhaber, Phys. Rev. **79**, 193 (1950).
[4] W. Forsling and A. Ghosh, Arkiv Fysik **4**, 331 (1951).
[5] Sargent, Yaffe, and Gray, Can. J. Phys. **31**, 235 (1953).
[6] E. der Mateosian, Phys. Rev. **83**, 223 (1951).
[7] Koester, Maier-Leibnitz, Mayer-Kuckuk, Schmeiser, and Schulze-Pillot, Z. Physik **133**, 319 (1952).
[8] M. Bunker and J. Starner (private communication).
[9] E. der Mateosian (private communication).
[10] E. Segrè [unpublished data quoted by E. Segrè and A. Helmholtz, Revs. Modern Phys. **21**, 271 (1949)].

prepared by irradiation of TiO_2 (enriched in Ti^{50}) in the Argonne reactor (CP-3′).

The pulse-height distribution associated with Ti^{51} (5.8 min) is displayed in Fig. 1. The data for this curve were obtained with the source approximately one foot from the crystal and with a collimator ($\frac{3}{4}$-in. diameter hole through a 2-in. lead block) interposed. This increases the percentage of full-height pulses and virtually eliminates the possibility of "sum peaks" (simultaneous detection of coincident radiation). Analysis of the distribution confirms the presence of three gamma rays in the spectrum, the intense 0.32-Mev gamma ray and two weak radiations of 0.610±0.015 and 0.920±0.015 Mev. Taking into account the variation in detecting efficiency, the ratio of the intensities is estimated to be 100:1:5. Other peaks and structure in the pulse-height distribution are attributed to secondary processes.

The dashed curve in Fig. 1 shows the pulse-height distribution obtained in coincidence with the 0.32-Mev

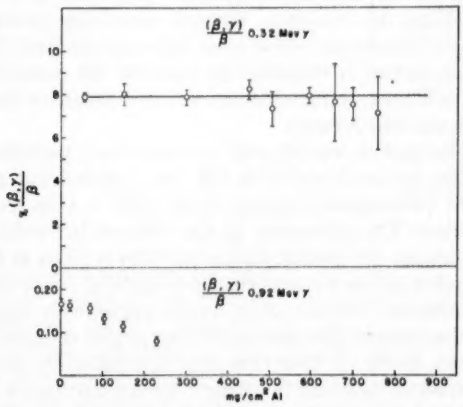

FIG. 2. Beta-gamma coincidences per beta of Ti^{51} (5.8 min).

gamma ray. It is clear that the 0.32- and 0.61-Mev transitions are in cascade. A search for 0.32−0.92 Mev coincidences yielded no counts above the random coincidence rate. The existence of an excited state at 0.92 Mev in V^{51} is thus confirmed. This state decays either directly to the ground state or to the 0.32-Mev level.

To determine the total disintegration energy, we measured the energy of the beta rays feeding the two excited states of V^{51}. The ten-channel analyzer was set to accept pulses from the 0.32-Mev photopeak and aluminum absorption carried out on the beta rays in coincidence with this distribution. From analysis of these data a half-value thickness of 135±10 mg/cm² corresponding to a beta transition energy of about 2.3 Mev was obtained. An absorption plot of the counting rate of the beta detector exhibits the same half-value thickness. The similarity implies that little if any beta branching to the ground state occurs. This

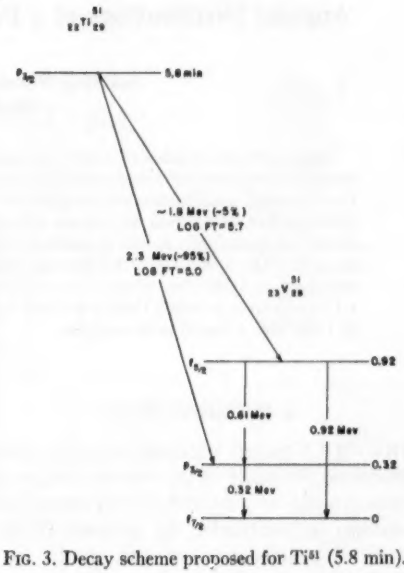

FIG. 3. Decay scheme proposed for Ti^{51} (5.8 min).

conclusion is substantiated by the plot of beta-gamma (0.32 Mev) coincidences per beta *vs* absorber thickness, which is seen to be flat as far as the data are meaningful (760 mg/cm²) (Fig. 2). From these data we estimate that the intensity of a ground state beta branch is less than 15 percent.

In the same manner as above, the beta component feeding the 0.92-Mev state is found to have a half-value thickness of about 95 mg/cm² corresponding to a beta transition energy of about 1.8 Mev. As would be expected, the plot of beta-gamma (0.92 Mev) coincidences per beta is seen to fall off with increasing absorber thickness (Fig. 2). Thus, as earlier reported, the beta spectrum is seen to be complex. However, both branches are shown to decay to excited states of V^{51}. Hence, the total decay energy is established by two independent measurements as 2.6±0.2 Mev.

The decay scheme which we propose is shown in Fig. 3. The spin of the ground state of V^{51} has been measured to be 7/2.[11,12] The orbital assignments indicated are those which would be expected from the single-particle shell model. The log *ft* values shown for the beta transitions are obtained assuming a five percent branch to the 0.92-Mev state, and indicate that both transitions are "allowed." This is consistent with the assignment of $p_{\frac{1}{2}}$ and $f_{\frac{5}{2}}$ to the excited states of V^{51} and of $p_{\frac{3}{2}}$ to the ground state of Ti^{51}. If the orbital assignment of $p_{\frac{3}{2}}$ to the ground state of Ti^{51} is correct, then a beta transition to the ground state of V^{51} would be "second forbidden."

We are indebted to Dr. M. G. Mayer, whose interest in Ti^{51} stimulated this investigation.

[11] Bleaney, Ingram, and Scovil, Proc. Phys. Soc. (London) **A64**, 601 (1951).

[12] Kikuchi, Sirvetz, and Cohen, Phys. Rev. **88**, 149 (1952); **92**, 109 (1953).

Angular Distributions of α Particles from the $Na^{23}(p,\alpha)Ne^{20}$ Reaction

P. H. STELSON
Oak Ridge National Laboratory, Oak Ridge, Tennessee
(Received August 9, 1954)

The angular distribution of α particles produced by the $Na^{23}(p,\alpha)Ne^{20}$ reaction and leading to the ground state of the residual Ne^{20} nucleus has been measured at six resonances occurring in the region $E_p=1$ to 2 Mev. The measured distributions are compared to the calculated angular distributions. In many cases the calculated angular distribution for a given type of compound state is not unique in that an unknown mixture of channel spins enters as well as possible admixtures of higher l values. The best assignments for the resonances at 1.137, 1.012, and 1.166 Mev are respectively 0^+, 3^-, and 2^+. A large anisotropy is observed for the resonance at 1.288 Mev which is not predicted by any simple assignment. It can, however, be fitted by a 1^- assignment in which there is a rather large admixture of f-wave to the p-wave protons. The resonance at 1.804 Mev is found to be complex.

I. INTRODUCTION

A PREVIOUS paper[1] (referred to as S.P. hereafter) described the study of the resonant states of Mg^{24} from measurements of the yield of γ rays and α particles when sodium is bombarded by protons. This paper reports on a continuation of this study in which angular distributions of α particles were measured at several resonances.

Since an angular distribution is governed by the combining of angular momentum vectors during the course of the reaction, one hopes to work back from the measured distribution to the discovery of the particular combination of vectors responsible for the distribution. In this way the total angular momentum and parity of the compound state can be assigned and, in addition, information is obtained on the mixing of channel spins and percentage admixture of higher orbital angular momenta.

In practice, the relatively large number of theoretically possible angular distributions and the limited accuracy of the experimental results make unique assignments difficult. For this reason it was thought that the angular distributions of the α particles produced by the $Na^{23}(p,\alpha)Ne^{20}$ reaction and leading to the ground state of the residual Ne^{20} nucleus (α_0 channel) would give the most clear-cut information. It was pointed out in S.P. that to decay by this channel the compound states must be of the type 0^+, 1^-, 2^+, 3^-, etc., and this restriction cuts down the number of possible distributions to be considered by a factor of two. Furthermore, for a given type of compound state one must consider, in general, an unknown mixture of channel spins and possible admixture of higher l values in both the entrance and exit channels, while for this case only the channel-spin of zero and one l value need be considered for the exit channel.

II. EXPERIMENTAL METHOD

Figure 1 is a schematic diagram of the apparatus used to measure the angular distributions. The proton beam from the electrostatic generator enters from the left. The beam is trimmed by two pairs of adjustable slits at right angles to each other. A diaphragm shields the reaction chamber by intercepting protons scattered by the slits. Two sylphon bellows allow movement of the chamber for alignment purposes. Alignment is facilitated by the two glass sections containing movable quartz viewers on which cross hairs are marked. The beam current is measured by catching the protons in the insulated, retractable cup which is biased to eliminate electron currents.

The type of counter used to detect the α particles is similar to that described in S.P., *viz.*, a cylindrical, gas-filled proportional counter fitted with a thin nickel window. The discussion of the method by which it singles out the ground state α particles is given in S.P. Detail *A* in Fig. 1 is a schematic diagram of the counter. Differential bias curves at several angles with respect to the forward direction and at two proton energies are shown in Fig. 2. It is seen that this relatively simple method of detecting the ground state α particles is not reliable at the forward angles due to the large pile-up of elastically scattered protons. The effect becomes more serious for low proton energies. For this reason the distributions could not be extended to the forward angles.

The counter window (diameter of 0.4 cm) was placed 7 cm from the target. The angular spread is 3° or the maximum Δx, where $x=\cos\theta_{c.m.}$ is 0.05 at 90°. With this angular resolution the attenuation coefficients for $P_2(x)$ and $P_4(x)$ differ from unity by a negligible amount (see Rose[2]). The angular spread caused by the finite size of the source is, on the average, about one-half as large as that due to the counter window.

The alignment of the counter with respect to the proton beam was carried out in the following manner. The center of the circle on which the counter swings was located by measuring the variation with angle position of the counting rate of α particles from a U^{233} source placed on the target support. The chamber was then moved to make the proton beam hit this point. A

[1] P. H. Stelson and W. M. Preston, Phys. Rev. **95**, 974 (1954).

[2] M. E. Rose, Phys. Rev. **91**, 610 (1953).

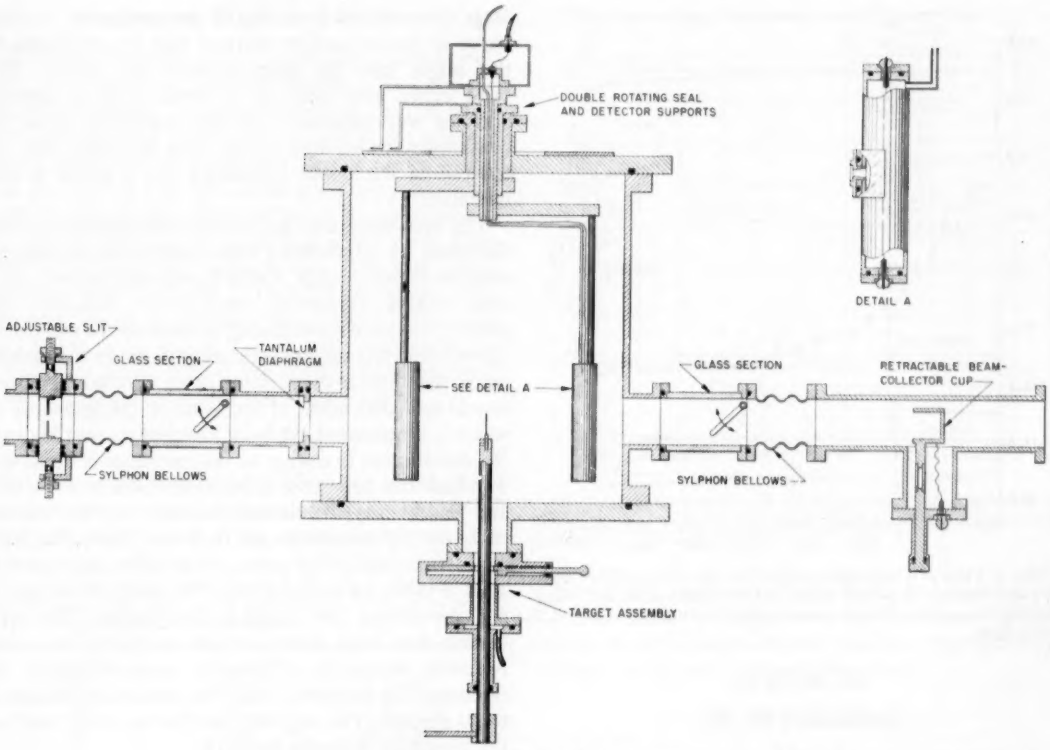

FIG. 1. Reaction chamber.

check on the alignment was made by counting protons elastically scattered from the target on both sides of the forward direction. It is judged that for the (p,α) angular distributions measurements the variation of the solid angle with angular position is not more than 3 percent.

Since we wished to investigate several fairly sharp resonances, it was thought that normalizing with respect to beam current would not be reliable because of the difficulty in maintaining a constant proton energy and constant target condition over long bombardment periods. Therefore, counts were collected in a second, stationary α particle counter and used to normalize the data. Changes in target condition and/or drifts in the proton energy were noted from the ratio of counts in the stationary counter to beam current collected.

Targets were prepared by vacuum evaporation of sodium iodide onto thin [25-mg/cm²] Formvar backings. By means of the valve arrangement shown in Fig. 1, a target could be admitted without disturbing the vacuum in the chamber. The proton beam at the target was a 3 mm square. Currents were limited to approximately $\frac{1}{10}$ μamp to keep the targets from burning up.

The angle ϕ between the plane of the target and the plane perpendicular to the beam is variable. For a fixed angle ϕ, the area of the source changes for different angular positions of the detector. A check on whether this might cause errors was made by keeping the counter in a fixed position and measuring the counting rate caused by elastically scattered protons for different values of ϕ. It was determined that for the angles of ϕ used in the angular distribution measurements the variation is less than one percent.

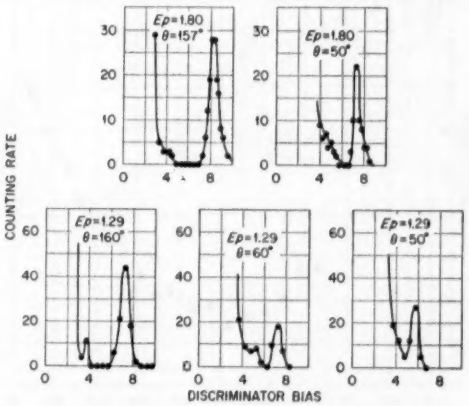

FIG. 2. Differential bias curves at several angles with respect to the forward direction and at two proton energies. The peak observed at high bias values is due to particles in the α_0 channel. The large rise at low bias is due to scattered protons. The weak intermediate peak observable in two of the curves is due to particles in the α_1 channel.

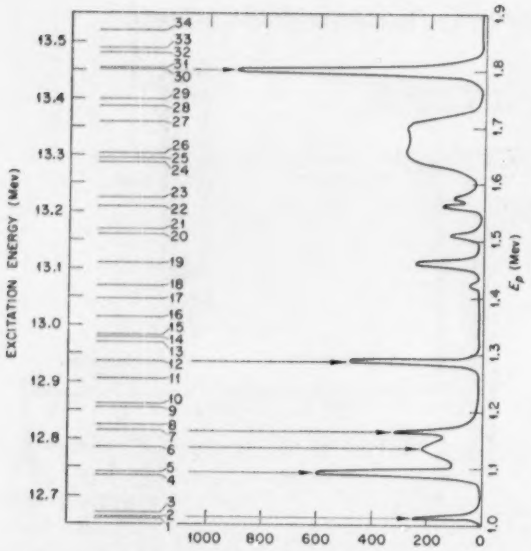

FIG. 3. Yield of α particles produced by the $Na^{23}(p,\alpha)Ne^{20}$ reaction and leading to ground state of Ne^{20} (taken from S.P.) and the positions of the virtual states of Mg^{24} for the region $E_p=1.0$ to 1.9 Mev.

III. RESULTS

Resonance No. 12

A yield curve of the α particles in the α_0 channel and an energy level diagram of the virtual states of Mg^{24} occurring in the region $E_p=1.0$ to 1.9 Mev is given in Fig. 3.[8] Resonance No. 12 ($E_p=1.288$ Mev) was thought to be especially suitable for study because it is well removed from neighboring resonances and has a large cross section for decay by the α_0 channel. A yield curve of the α particles showed that the thickness of the target used for measurements was 10 kev. The yield curve also indicated a small yield at proton energies well removed from the resonance. This flat continuum, which was found to be isotropic, may be the tail of the broad Resonance No. 6 which is also isotropic.

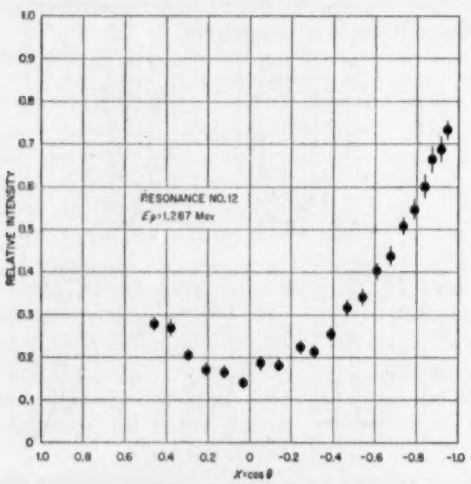

FIG. 4. Angular distribution of the ground state α particles at Resonance No. 12 ($E_p=1.288$ Mev). Data have been transformed to center-of-mass system.

[8] The numbers assigned to the resonances are those given in S.P.

The possibility that the angular distribution is being disturbed by interference from neighboring resonances must be borne in mind. A single, well-isolated resonance must exhibit symmetry about $x=0$. Although the yield at the more forward angles could not be measured, the existing data suggest symmetry about $x=0$. Furthermore, the angular distribution of an isolated resonance should be independent of the point on the resonance at which it is measured, while an interference should cause the distribution to change as the resonance is traversed. To check this point, the ratios of the yield at $x=-0.05$ and -0.94 were measured half-way up the leading edge, on the maximum and half-way down the back edge. No change in the ratios of the yields was observed. This is taken as evidence that the small continuum is not perturbing the angular distribution. The continuum has been subtracted in analyzing the data. At $x=0$, where the differential cross section of the resonance has its lowest value, the continuum amounted to 20 percent. The angular distribution at the peak of the resonance is shown in Fig. 4.

The data from several runs of the angular distribution on the maximum of the resonance were fitted by a least-squares analysis to the expression

$$B_0P_0(x)+B_2P_2(x)+B_4P_4(x), \qquad (1)$$

where the $P_i(x)$ are Legendre polynomials. The coefficient B_4 was found to be zero to within the expected errors. The ratio B_2/B_0 is listed in Table I. The assigned error is based on the statistical accuracy of the points and an estimate of the errors discussed in Part II.

Resonance No. 2

Resonance No. 2 ($E_p=1.012$ Mev) has a close neighbor on each side. However, the yield curve indicates that neither of these neighboring resonances decays by the α_0 channel and, hence, is not expected to distort the angular distribution of the ground state α particles. The angular distribution at the maximum of the resonance is shown in Fig. 5. The yield curve showed no measurable continuum in the region of this resonance. The ratios of the yields at $x=-0.05$ and -0.94 taken half-way up the leading edge, at the maximum, and half-way down the back edge showed no significant variation. The data were fitted to expression (1). The coefficient B_4 was not significantly different from zero. The ratio B_2/B_0 and its error are listed in Table I.

Resonances No. 30 and No. 31

Although the poorer resolution of the α-particle yield curve shows a strong, isolated resonance at 1.80 Mev, the high-resolution γ-ray yield curves reveal two resonances separated by 3 kev. Yet because of the selection rules operative in the α_0 channel there is a good chance that just one of the resonances is decaying by the α_0 channel. The angular distribution of the maximum of the peak is found to be symmetric about $x=0$. However, the ratios of the yields at $x=-0.05$ and -0.94, which are listed in Table I, varied well outside of the statistical errors at different points on the resonance. This is taken as evidence that both resonances are decaying by the α_0 channel. No further study was made of the resonance because of this complication.

Resonance No. 6

Resonance No. 6 ($E_p=1.137$ Mev) is a broad, fairly strong resonance which appeared with measurable intensity only in the yield of the ground state α particles.

TABLE I. Experimental values of B_2/B_0. E_p is given in Mev. The change in the ratio of the yield at $x=-0.94$ to -0.05 is listed for the resonance at 1.804 Mev.

Resonance number	E_p (Mev)	B_2/B_0
2	1.012	0.86±0.09
5	1.093	0.15±0.05
6	1.137	0.05±0.05
7	1.166	0.03±0.05
12	1.288	1.16±0.09
(30+31)?	1.804	
Half-way up leading edge:		$\frac{I(x=-0.94)}{I(x=-0.05)}=1.32\pm0.06$
At the peak:		$\frac{I(x=-0.94)}{I(x=-0.05)}=1.72\pm0.05$
Half-way down the back edge:		$\frac{I(x=-0.94)}{I(x=-0.05)}=1.78\pm0.11$

Although Resonances No. 5 and No. 7 are situated on the wings of No. 6, these are fairly sharp resonances and should not influence the angular distribution at the maximum. The distribution at the maximum is shown in Fig. 6. The least-squares fit to expression (1) gives a B_4 equal to zero. B_2/B_0 and its assigned error are listed in Table I.

Resonances No. 5 and No. 7

As previously mentioned, Resonances No. 5 ($E_p=1.093$ Mev) and No. 7 ($E_p=1.166$ Mev) are situated on the wings of the broad Resonance No. 6. A moderately thin target of 6-kev thickness was used to reduce the intensity of No. 6 at the positions of No. 5 and No. 7. With this target the contribution of No. 6 to the intensity at the maxima of No. 5 and No. 7 is estimated as roughly 20 percent. The angular distribution at the maximum of No. 7 is found to be isotropic; B_2/B_0 and its error are listed in Table I. No. 5 exhibits a definite, but weak anisotropy; B_2/B_0 and its error are listed in Table I. A check on the invariance of the angular distribution at different points on the resonance was not carried out for these resonances.

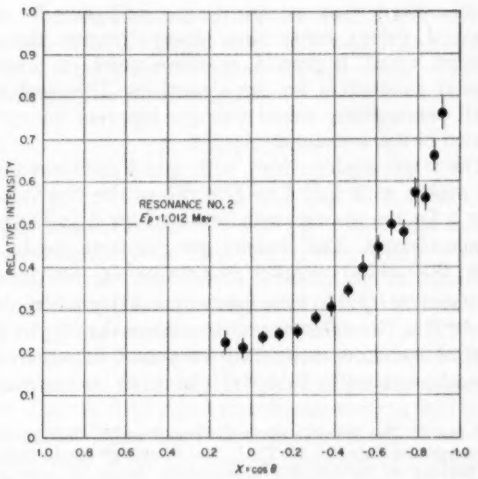

FIG. 5. Angular distribution of the ground state α particles at Resonance No. 2 ($E_p=1.012$ Mev). Data have been transformed to center-of-mass system.

IV. DISCUSSION

1. Theory

We use the theory and terminology of angular distributions given by Blatt and Biedenharn[4] to interpret the measured distributions. Compound states of the type 0^+, 1^-, 2^+, 3^-, and 4^+ are considered. It is thought

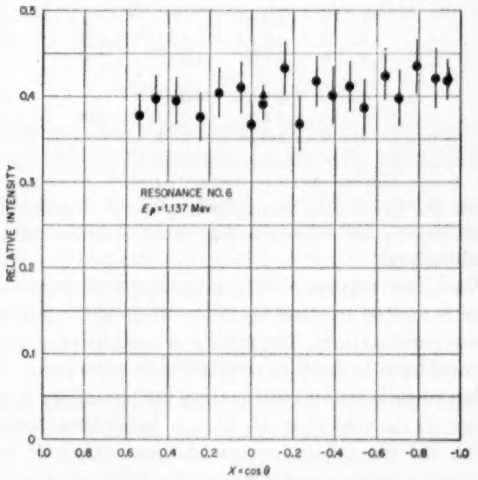

FIG. 6. Angular distribution of the ground state α particles at Resonance No. 6 ($E_p=1.137$ Mev). Data have been transformed to center-of-mass system.

[4] J. M. Blatt and L. C. Biedenharn, Revs. Modern Phys. 24, 258 (1952).

quite unlikely that we are dealing with any 5^- (or larger J value) states since decay through the α_0 channel would require 5 or more units of orbital angular momentum for the α particles. The resulting small penetrability would strongly suppress the cross section in the α_0 channel.

The target nucleus, Na^{23}, with spin $\frac{3}{2}$ combines with the proton with spin $\frac{1}{2}$ to give rise to the two values 1 or 2 for the channel spin (denoted by s) in the entrance channel. The channel spin, in turn, combines with the orbital angular momentum of the proton [denoted by $l(p)$] to form the compound state (denoted by J^{parity}). The different vector combinations by which each of the above-mentioned compound states can be formed are listed in Table II. Also listed are the coefficients B_2/B_0, B_4/B_0, etc., which give the angular distribution to be expected for each of these vector combinations.

TABLE II. The different vector combinations by which each of the compound states 0^+, 1^-, 2^+, 3^-, and 4^+ of Mg^{24} can be formed by protons on sodium and subsequently decay by α-particle emission to the ground state of Ne^{20} are listed. The entrance channel spin is s while l_p is the proton orbital angular momentum, l_α the α-particle orbital angular momentum, and s' the exit channel spin. Also listed are the coefficients B_2/B_0, B_4/B_0, etc., which give the angular distribution to be expected for each of these vector combinations.

s	l_p	Compound state	l_α	s'	B_2/B_0	B_4/B_0	B_6/B_0	B_8/B_0
		0^+						
2	2		0	0	0	0	0	0
		1^-						
1	1		1	0	−1.00	0	0	0
2	1		1	0	+0.20	0	0	0
2	3		1	0	+0.80	0	0	0
		2^+						
2	0		2	0	0	0	0	0
2	2		2	0	−0.51	+0.73	0	0
1	2		2	0	+0.71	−1.71	0	0
2	4		2	0	+1.02	+0.55	0	0
		3^-						
2	1		3	0	+0.80	0	0	0
2	3		3	0	+0.42	−0.82	+1.26	0
1	3		3	0	+1.00	+0.27	−2.27	0
		4^+						
2	2		4	0	+1.02	+0.55	0	0
2	4		4	0	+1.10	+0.73	−0.09	−2.74
1	4		4	0	+0.74	−0.72	−0.93	+1.75

Now, one expects that a given type of compound state is excited to some extent by each of the possible vector combinations. The mixing of combinations must be considered in order to compare with experiment. We assign to each vector combination the parameter $g_{s,l(p)}$ where $g_{s,l(p)}=\pm(\Gamma_{s,l(p)})^{\frac{1}{2}}$, $\Gamma_{s,l(p)}$ being the partial width for the particular combination $s,l(p)$. If two different orbital angular momenta, $l(p)$ and $l(p)+2$, can combine with one channel spin to form a given compound state, an interference of the $l(p)$ and $l(p)+2$ waves exists. Formula (5.9) of reference 3 is used to calculate the variation of the coefficients B_2/B_0, B_4/B_0, etc., for different values of the ratio

$$\delta=g_{s,l(p)+2}/|g_{s,l(p)}|+|g_{s,l(p)+2}|,$$

ranging from 1 to 0 to −1. The formula contains the phase difference $\xi_{l(p)+2}-\xi_{l(p)}$. For a single, isolated resonance the phase difference is given by

$$\xi_{l(p)+2}-\xi_{l(p)}=\left[\tan^{-1}\left(\frac{\eta}{l(p)+2}\right)+\tan^{-1}\left(\frac{\eta}{l(p)+1}\right)\right]-\left[\tan^{-1}\left(\frac{F_{l(p)+2}}{G_{l(p)+2}}\right)-\tan^{-1}\left(\frac{F_{l(p)}}{G_{l(p)}}\right)\right],$$

where $\eta=Z_1Z_2e^2/\hbar v$ and the Coulomb wave functions F and G are evaluated at the nuclear surface. The contribution of the terms involving F and G (second bracket) is almost negligible for the present situation so that the phase difference is insensitive to the value taken for the nuclear radius. The phase difference depends on the energy of the incident proton so that

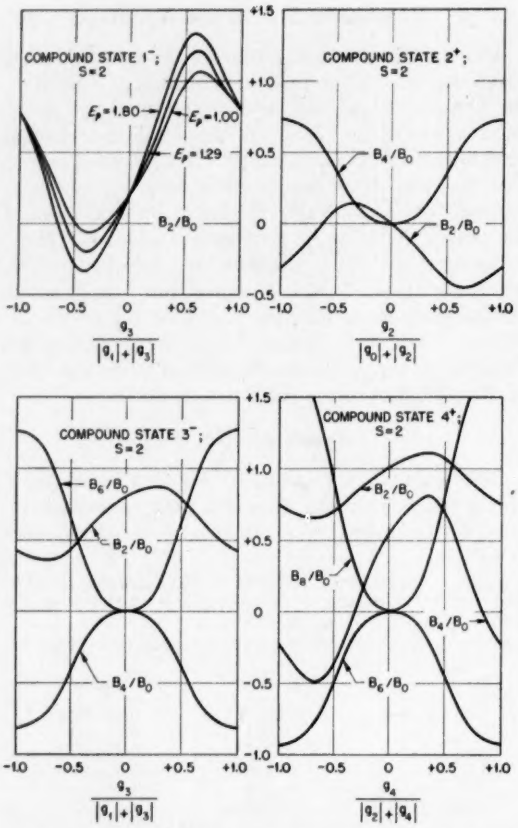

FIG. 7. Calculated curves showing the coherent interference resulting from mixtures of l_p values in a given channel spin s. The variation in B_2/B_0, B_4/B_0, etc., is shown as δ (defined in the text) varies from −1 to 0 to +1.

the strength of the interference changes somewhat at different resonances. These interference effects have been worked out for all the cases listed in Table II for $E_p=1.0$ Mev (Resonance No. 2) except the admixture of $l(p)=4$ for the 2^+ resonance. The interference effect for the 1^- state has also been calculated for $E_p=1.29$ Mev (Resonance No. 12) and $E_p=1.80$ Mev (Resonances No. 30 and No. 31) to illustrate the change with proton energy. The calculations are presented in Fig. 7 in the form of curves showing the variation of B_2/B_0, B_4/B, etc., as a function of δ.

It is seen that the interference may strongly affect the shape of the angular distribution. Perhaps the most striking case is the interference of p-wave and f-wave protons for $s=2$, compound state 1^-, which is given in the upper left-hand corner of the figure. An f-wave contribution of one percent to the intensity of the resonance ($\delta=\pm 0.10$) will change the B_2/B_0 ratio from $+0.20$ to $+0.05$ or $+0.35$ depending on the sign of δ.

Designating $T_{l(p)}$ as the penetration factor for protons of orbital angular momentum $l(p)$ through the Coulomb plus centrifugal barrier and $\gamma_{l(p)}^2$ as the reduced width for the formation of the compound state by $l(p)$ protons, we can express $|\delta|$ as

$$\frac{(\gamma_{l(p)+2}^2/\gamma_{l(p)}^2)^{\frac{1}{2}}(T_{l(p)+2}/T_{l(p)})^{\frac{1}{2}}}{1+(\gamma_{l(p)+2}^2/\gamma_{l(p)}^2)^{\frac{1}{2}}(T_{l(p)+2}/T_{l(p)})^{\frac{1}{2}}}.$$

The quantity $[T_{l(p)+2}/T_{l(p)}]^{\frac{1}{2}}$ varies with proton energy and with $l(p)$. For the resonances and $l(p)$ values here considered the value is of the order of 1/10 to 1/20.

Little is known about the values to expect for the quantity $[\gamma_{l(p)+2}^2/\gamma_{l(p)}^2]^{\frac{1}{2}}$. If the compound state were a simple, single particle state in which $l(p)$ is a good quantum number (quite unlikely at these high excitation energies) one would expect the values zero or infinity depending on whether the compound state is characterized by $l(p)$ or $l(p)+2$. On the other hand, if the compound state is sufficiently complicated one expects a statistical picture to prevail in which case $[\gamma_{l(p)+2}^2/\gamma_{l(p)}^2]^{\frac{1}{2}}$ is unity.

If $[\gamma_{l(p)+2}^2/\gamma_{l(p)}^2]^{\frac{1}{2}}$ is unity, the small values of 1/10 to 1/20 for $[T_{l(p)+2}/T_{l(p)}]^{\frac{1}{2}}$ limit the possible values of δ to a small region of approximately ± 0.10 about the zero point. If the statistical picture is correct, we should be able to fit the data with the restriction that $|\delta| \lesssim 0.10$. However, if larger values of δ are required we have a measure of the deviation from the strictly statistical model.

Finally, when both channel spins can contribute to the excitation of a given type of resonance, mixtures of these must also be considered. Since the two channels are incoherent this is considerably easier to work out than mixtures of $l(p)$ values. Mixtures are obtained by simply adding together different percentages of the angular distribution in each channel. When the minimum value of $l(p)$ differs by 2 units for the two channels, the contribution to angular distribution of the channel with the larger value is strongly suppressed since it is governed by the ratio $T_{l(p)+2}/T_{l(p)}$ which is of the order of 1/100 to 1/400.

2. Assignments

Resonance No. 6

The broad Resonance No. 6 has a measured B_2/B_0 value of 0.05 ± 0.05. This small value, which is consistent with isotropy, can be fitted by three alternative assignments: (1) a 0^+ assignment, which is isotropic, (2) a 2^+ assignment in which there is a reasonably small admixture of d-wave to the s-wave protons, or (3) a 1^- assignment in which there is a fortuitous combination of mixtures to give a distribution close to isotropic. The probability is small that the 1^- assignment is the correct one. While the angular distribution is equally well accounted for by either the 0^+ or the 2^+ assignment, the fact that this resonance shows a strong preference for decay by the α_0 channel favors the 0^+ state. A 2^+ state would be expected to show a strong decay by the α_1 and p_1 channels.[5]

Resonance No. 2

Resonance No. 2, with a measured value of 0.86 ± 0.09 for B_2/B_0 and a B_4/B_0 of zero, agrees well with a 3^- assignment. The value of $[T_3/T_1]^{\frac{1}{2}}$ is calculated to be 0.050. If $[\gamma_3^2/\gamma_1^2]^{\frac{1}{2}}$ is taken as unity, we have $\delta=\pm 0.050$, both of which give the value of approximately 0.80 for B_2/B_0 (see Fig. 7). The reaction goes by the $s=2$ channel since f-wave protons are required in the $s=1$ channel.

Two other assignments of 4^+ and 1^- are conceivable but require large values of the order of 10 for the quantity $[\gamma_{l(p)+2}^2/\gamma_{l(p)}^2]^{\frac{1}{2}}$.

Resonances No. 5 and No. 7

The fact that these resonances are not well isolated makes assignment somewhat tenuous. No assignment is given to No. 5 which showed a weak anisotropy. Resonance No. 7 is isotropic; hence the possibilities listed under No. 6 should also apply here. Of these, the 2^+ state is favored because, in contrast to No. 6, the resonance exhibits a strong decay by the α_1 channel and an observable decay by the p_1 channel.

Resonance No. 12

Resonance No. 12 has a B_2/B_0 of 1.16 ± 0.09 and no observable B_4 term. This large anistropy of a pure P_2 type is not given by any assignment in which δ is restricted to the small value it would have if $[\gamma_{l(p)+2}^2/\gamma_{l(p)}]^{\frac{1}{2}}=1$. An assignment of 1^- can be made

[5] The channels α_1 and p_1 are those, respectively, in which the compound state decays to the first excited states of Ne^{20} (1.63 Mev) and Na^{23} (0.44 Mev).

to give a sufficiently large, positive B_2/B_0 if we simultaneously require that $\delta \gtrsim +0.45$ and that the reaction goes mostly by the $s=2$ channel. The large value of δ demands the rather high value of 5 or greater for $[\gamma_8^2/\gamma_1^2]^{\frac{1}{2}}$. If this assignment is correct, we have an indication that $[\gamma_{l(p)+2}/\gamma_{l(p)}{}^2]^{\frac{1}{2}}$ may undergo large deviations from unity. It would be desirable to measure angular distributions of other reaction products at this resonance to corroborate or disprove this assignment.

The author wishes to thank Dr. Albert Simon for several discussions of the theory of angular distributions and the members of the High Voltage Group of the Oak Ridge National Laboratory for their interest and cooperation.

PHYSICAL REVIEW VOLUME 96, NUMBER 6 DECEMBER 15, 1954

Proton Polarization in (d,ϕ) Reactions*†

W. B. CHESTON
University of Minnesota, Minneapolis, Minnesota
(Received July 16, 1954)

The polarization of the proton produced in a (d,ϕ) reaction is calculated under the assumption that "stripping" is the primary mechanism operative. The model adopted for the polarization production consists in a proton-nucleus interaction potential of the spin-orbit type which has been successful in describing polarization effects in neutron scattering. The model is applied to the specific reaction $C^{13}(d,\phi)C^{12}$ for $E_d=3.29$ Mev.

I. INTRODUCTION

THE apparent usefulness of (d,ϕ) and (d,n) reactions as tools in nuclear spectroscopy stems from the now classic paper on these reactions by Butler.[1] The form of the differential cross section for such reactions predicted by the stripping theory is in surprisingly good agreement with the experimental results, especially if deuterons of not too low an energy are used as projectile particles. However, the results of experiments using deuterons of about 3 Mev exhibit features which the stripping theory has difficulty in explaining, even if the modifications[2] of the theory suggested subsequent to Butler's paper are taken into account. Particular reference is made here to the pronounced "resonances" observed in the excitation function and the form of the differential cross sections measured off and on resonance.[3] In brief summary, the resonance behavior of the excitation function is caused by a very pronounced change in magnitude of the forward-angle stripping peak whereas the back-angle yield is relatively constant over the range of energies including the resonances.

It has been suggested[4–6] that the nucleon produced as a product in the stripping reaction is polarized. The model sketched below for producing such polarization was chosen because of its apparent reasonableness in that such a model correctly describes the elastic scattering of polarized neutrons[7] in the medium-energy range. Since the stripping approximations are used throughout the polarization calculation, the extent of disagreement between the herein predicted polarization and the eventually forthcoming experimental results will indicate the extent to which the stripping assumptions are suspect at the deuteron energies considered below, namely, $E_d \sim 3$ Mev.

II. POLARIZATION CALCULATION

In the so-called "Born approximation" discussion[8] of stripping reactions, the final state nucleon is assumed to have no specifically nuclear interaction with the residual nucleus and no polarization of the proton results. In the calculation below, the assumption will be made that the final state nucleon is scattered in a spin-orbit potential superimposed upon the "clouded crystal ball" or complex central potential of Feshbach *et al.*[9] which adequately describes the elastic scattering of low-energy neutrons.[10] Strictly speaking, therefore, the model applies to (d,n) reactions; it will be applied to (d,ϕ) reactions as well, with justification supplied by the

* This work was supported in part by the joint program of the Office of Naval Research and the U. S. Atomic Energy Commission.

† The results of this calculation were first reported at the Minneapolis meeting of the American Physical Society, June, 1954.

[1] S. T. Butler, Proc. Roy. Soc. (London) **A208**, 559 (1951).

[2] See, for example, W. Tobocman and M. H. Kalos, Phys. Rev. **95**, 605(A) (1954).

[3] Van Patter, Simmons, Stratton, and Zipoy, Bull. Am. Phys. Soc. **29**, No. 5, 14 (1954).

[4] H. C. Newns, Proc. Phys. Soc. (London) **A401**, 477 (1953).

[5] J. Horowitz and A. Messiah, Phys. Rev. **92**, 1326 (1953).

[6] N. Francis and K. Watson, Phys. Rev. **93**, 313 (1954). The model used in the present discussion was suggested in this article.

[7] Darden, Fields, and Adair, Phys. Rev. **93**, 931 (1954).

[8] See, for example, P. Daitch and J. French, Phys. Rev. **87**, 900 (1952).

[9] Feshbach, Porter, and Weisskopf, Phys. Rev. **90**, 166 (1953).

[10] Note, however, that the depth of the well suggested by Feshbach *et al.* to explain the scattering data is too small by a factor ~ 2 to harmonize with the data on neutron bound states interpreted on the basis of the shell model. [See A. Bohr and B. Mottelson, Kgl. Danske Videnskab. Selskab, Mat.-fys. Medd. **27**, 159 (1953); R. K. Adair, Phys. Rev. **94**, 737 (1954).]

apparent charge independence of nuclear forces. The Coulomb distortion of the deuteron and proton waves is ignored; this should not change the order of magnitude of the results obtained. The additional restriction will be made to spin-zero target nuclei since it is for these targets that the Butler approximation should most nearly apply, i.e., that the nucleon absorbed by the target exists in a single, definite state of orbital angular momentum, at least for a time as long as the interaction period.

Since the final-state proton will scatter in a spin-orbit potential, it will be useful to express the wave function for the proton as a linear superposition of eigenfunctions of the $\mathbf{L}\cdot\mathbf{S}$ operator:

$$\Psi_p(\mu_p)=\sum_{L,M_L}\sum_{J,M_J} a(L,M_L) \times C_{L,\frac{1}{2}}(J,M_J;M_L,\mu_p)\Psi(J,L,M_J), \quad (1)$$

where the C-symbol is the Clebsch-Gordan coefficient in the notation of Blatt and Weisskopf.[11] The remaining undefined symbols in Eq. (1) have their usual meaning. If it is assumed that the residual nucleus may be represented as a neutron in a definite orbital angular momentum l about the target nucleus (spin zero) as a core, the state vector for the residual nucleus is:

$$\Psi_f(\mu_f)=\sum_{m,\mu_n} C_{l,\frac{1}{2}}(j_f,\mu_f;m,\mu_n)\Psi(l,m)\chi(\tfrac{1}{2},\mu_n)\Phi_0, \quad (2)$$

where $\Psi(l,m)$ = single-particle neutron orbital, $\chi(\frac{1}{2},\mu_n)$ = neutron spin function, and Φ_0 = target nucleus (final state core) wave function. It is convenient to make a partial wave expansion of the incident deuteron wave:

$$\Phi_d(\mu_d)=\sum_{L_d,M_d}\sum_{\mu_n',\mu_p'} b^*(L_d,M_d) \times\Phi(L_d,M_d)\chi(\tfrac{1}{2},\mu_n')\chi(\tfrac{1}{2},\mu_p') \times C_{1,\frac{1}{2}}(1,\mu_d;\mu_n',\mu_p'). \quad (3)$$

If one adopts the symbol T for the transition operator representing the stripping reaction, the matrix element for the reaction may be written as a linear combination of terms of the type:

$$\langle\Psi(J,L,M_J)\Psi(l,m)\chi(\tfrac{1}{2},\mu_n) \times|T|\Phi(L_d,M_d)\chi(\tfrac{1}{2},\mu_n')\chi(\tfrac{1}{2},\mu_p')\rangle. \quad (4)$$

The axis of quantization will be defined by the vector product between the incident deuteron wave vector ($\mathbf{K}$) and the final state proton wave vector ($\mathbf{k}$). With this designation of the quantization axis, the matrix element, Eq. (4), of the transition operator reduces to:

$$\langle\Psi(J,L,M_J)\Psi(l,m)\chi(\tfrac{1}{2},\mu_n)|T|\Phi(L_d,M_d)\chi(\tfrac{1}{2},\mu_n')\chi(\tfrac{1}{2},\mu_p')\rangle =C_{L,\frac{1}{2}}(J,M_J;M_L,\mu_p)\langle\Psi(J,L,M_L)\Psi(l,m) \times|T|\Phi(L_d,M_d)\rangle\delta(\mu_n,\mu_n')\delta(\mu_p,\mu_p'). \quad (5)$$

[11] J. M. Blatt and V. F. Weisskopf, *Theoretical Nuclear Physics* (John Wiley and Sons, Inc., New York, 1952).

In establishing the relation of Eq. (5), use has been made of the fact that with the quantization axis chosen, a nucleon produced in a definite state of spin orientation in the original stripping act will maintain this orientation after scattering in the spin-orbit potential. The stripping matrix element, $\mathfrak{M}(\mu_d\to\mu_f,\mu_p)$, may now be written via Eq. (5) and the properties of the Clebsch-Gordan coefficients:

$$\mathfrak{M}(\mu_d\to\mu_f,\mu_p) =\sum_{L_d,L,J,M_d,M_L} a(L,M_L)b^*(L_d,M_d) \times C_{L,\frac{1}{2}}{}^2(J,M_L+\mu_p;M_L,\mu_p) \times C_{l,\frac{1}{2}}(j_f,\mu_f;\mu_f-\mu_d+\mu_p,\mu_d-\mu_p) \times C_{\frac{1}{2},\frac{1}{2}}(1,\mu_d;\mu_d-\mu_p,\mu_p) \times\langle\Psi(J,L,M_L)\Psi(l,m)|T|\Phi(L_d,\mu_d)\rangle. \quad (6)$$

In the Born approximation treatment (neglect of proton-nucleus interaction) of the (d,p) stripping reaction, Gerjuoy[12] has shown that the reaction amplitude, f, for spinless nucleons takes the form:[13]

$$f=-\frac{2M}{\hbar^2}\frac{1}{4\pi}\int \exp(i\mathbf{k}\cdot\mathbf{r}_p)\Psi^*(\mathbf{r}_n) \times V^{np}(\mathbf{r}_n,\mathbf{r}_p)\Phi_d(\mathbf{r}_n,\mathbf{r}_p)d\mathbf{r}_n d\mathbf{r}_p, \quad (7)$$

where $\Psi(\mathbf{r}_n)$ = neutron wave function in the final (bound) state, and V^{np} = neutron-proton interaction potential. To take account of the nuclear scattering of the final (free) state proton, the usual replacement is made:

$$\exp(i\mathbf{k}\cdot\mathbf{r}_p)\chi(\tfrac{1}{2},\mu_p)\to\exp(i\mathbf{k}\cdot\mathbf{r}_p)\chi(\tfrac{1}{2},\mu_p) -\sum_{L,J} i^L[4\pi(2L+1)]^{\frac{1}{2}}C_{L,\frac{1}{2}}(J,\mu_p;0,\mu_p) \times h_L^{(1)}(kr_p)\beta(L,J)\mathfrak{Y}(L,J,M_J=\mu_p), \quad (8)$$

where $\mathfrak{Y}(L,J,M_J=\mu_p)$ = normalized eigenfunction of the total angular momentum, $h_L^{(1)}(kr_p)$ = spherical Hankel function of the first kind, and $\beta(L,J)\equiv\frac{1}{2}\eta(L,J)$, a complex number describing the distortion of the proton wave by the nuclear potential (see reference 11). To evaluate the reaction amplitude of Eq. (7) using the modification of Eq. (8), it is convenient to employ the "zero-range" $n-p$ interaction potential. The reaction amplitude conveniently separates into two parts, f^{Born} and f^{scat}, where f^{Born} is the reaction amplitude of Eq. (7) unmodified by the proton-nucleus interaction. Con-

[12] E. Gerjuoy, Phys. Rev. **91**, 645 (1953).

[13] This form of the scattering amplitude neglects the indistinguishability between the proton in the deuteron and a proton in the target nucleus during the interaction period. Antisymmetrization of the total wave function for the system with respect to the protons leads to an exchange amplitude in addition to the direct amplitude of Eq. (7). The neglect of the former with respect to the latter should be legitimate for the type of targets considered here. However, for odd-proton nuclei, the exchange amplitude may be comparable in magnitude to the direct amplitude (A. French and K. Case, private communication).

TABLE I. Proton polarization in ${}_6C^{12}(d,p){}_6C^{13}$ for $E_d=3.29$ Mev.

θ (in degrees)	P (in percent)
0	0
10	−22
20	−14
30	−17
40	−26

stants common to both parts of the reaction amplitude will be omitted since the only characteristics of importance in the polarization calculation are their relative magnitudes and phases.

To calculate f^{Born}, the assumption of stripping theory that $\Psi(\mathbf{r}_n)$ represents a single particle orbital of prescribed orbital angular momentum will be made: i.e.,

$$\Psi^*(\mathbf{r}_n)=\text{const}\sum_m h_l^{(1)}(i\mathfrak{l}r)Y_l^m(\theta_n,\phi_n),$$

where $\hbar^2\mathfrak{l}^2/2M=$ binding energy of absorbed neutron in residual nucleus, yielding

$$f_m^{\text{Born}}\sim 4\pi i^l Y_l^m(\theta_q)\int_{R_0}^{\infty} j_l(qr)h_l^{(1)}(i\mathfrak{l}r)r^2dr, \quad (9)$$

where $-\mathbf{q}=\mathbf{K}-\mathbf{k}=$ wave vector of recoil (residual) nucleus, and θ_q is the angle between $\mathbf{q}$ and $\mathbf{K}\times\mathbf{k}$.

The parameter R_0 appearing in Eq. (9) is the "stripping radius" corresponding to the smallest distance of separation of the target and deuteron for the stripping mechanism to be operative. The integral of Eq. (9) may be performed analytically:

$$\int_{R_0}^{\infty} j_l(qr)h_l^{(1)}(i\mathfrak{l}r)r^2dr\equiv B(R_0)$$
$$=(q^2+\mathfrak{l}^2)^{-1}\left\{\frac{d}{dR_0}[j_l(qR_0)R_0]h_l^{(1)}(i\mathfrak{l}R_0)R_0\right.$$
$$\left.-\frac{d}{dR_0}[h_l^{(1)}(i\mathfrak{l}R_0)R_0]j_l(qR_0)R_0\right\}. \quad (10)$$

In passing from the stationary to time-dependent perturbation description of the reaction process, the Born approximation to the matrix element of Eq. (6) becomes (with arbitrary normalization):

$$\mathfrak{M}^{\text{Born}}(\mu_d\to\mu_f,\mu_p)$$
$$=C_{l,\frac{1}{2}}(j_f,\mu_f;m,\mu_n)C_{\frac{1}{2},\frac{1}{2}}(1,\mu_d;\mu_n,\mu_p)$$
$$\times 4\pi i^l Y_l^m(\theta_q)B(R_0). \quad (11)$$

If it is assumed further that the incoming deuteron wave is distorted by a nonspin dependent potential, the elements of the T operator become (normalized with respect to $\mathfrak{M}^{\text{Born}}$ of Eq. (11)):

$$\langle\Psi(J,L,M_J)\Psi(l,m)|T|\Phi(L_d,M_d)\rangle$$
$$=(-1)^{M_L}\left[\frac{(2L+1)(2L_d+1)}{4\pi(2l+1)}\right]^{\frac{1}{2}}$$
$$\times C_{L,L_d}(l,0;0,0)C_{L,L_d}(l,-m;m_L,-m_L-m)$$
$$\times\int_{R_0}^{\infty}[j_L(kr)-\beta(L,J)h_L^{(1)}(kr)]$$
$$\times[j_{L_d}(Kr)-\beta(L_d)h_{L_d}^{(1)}(Kr)]h_l^{(1)}(i\mathfrak{l}r)r^2dr. \quad (12)$$

Evaluation of the integral appearing in the above expression is straightforward by numerical methods.

Finally, the degree of polarization, P, of the protons produced in the reaction is defined as:

$$P\equiv\frac{\sum_{\mu_d,\mu_f}\{|\mathfrak{M}(\mu_d\to\mu_f,\mu_p=+\frac{1}{2})|^2-|\mathfrak{M}(\mu_d\to\mu_f,\mu_p=-\frac{1}{2})|^2\}}{\sum_{\mu_d,\mu_f}\{|\mathfrak{M}(\mu_d\to\mu_f,\mu_p=+\frac{1}{2})|^2+|\mathfrak{M}(\mu_d\to\mu_f,\mu_p=-\frac{1}{2})|^2\}}. \quad (13)$$

III. APPLICATION TO THE REACTION ${}_6C^{12}(d,p){}_6C^{13}$

The above formalism has been applied to the reaction ${}_6C^{12}(d,p){}_6C^{13}$ for a deuteron bombarding energy of 3.29 Mev. The differential cross section for this reaction has been measured by Holmgren[14] who has found a pronounced stripping maximum in the angular distribution of the protons at approximately 20°. The angular distribution obtained is consistent with the assignment of $(\frac{1}{2},-)$ to the ground state of C^{13}.

The scattering potential experienced by the final state proton was taken to be:

$$V^p(\text{in Mev})=-19(1+0.05i)-2\mathbf{L}\cdot\mathbf{S}, \quad r\leq r_0$$
$$=0, \quad r>r_0,$$

where $r_0=1.45\times10^{-13}A^{\frac{1}{3}}$ cm. In addition, the $L_d=0$, 1 waves of the incoming deuteron were assumed distorted by a hard sphere potential whose radius was arbitrarily chosen to be R_0, the stripping radius (in this case $R_0=6.5\times10^{-13}$ cm). The results of such a calculation are contained in Table I.

ACKNOWLEDGMENTS

The author wishes to acknowledge many stimulating conversations with Professor C. L. Critchfield on general aspects of polarization problems.

[14] H. Holmgren, Ph.D. thesis, University of Minnesota, 1954 (unpublished).

Beta Spectrum of Radium E

E. A. PLASSMANN AND L. M. LANGER
*Physics Department, Indiana University, Bloomington, Indiana**
(Received August 5, 1954)

The beta spectrum of RaE has been remeasured with improved techniques. The distribution is fitted by a shape factor appropriate to a once forbidden transition with a spin change, $\Delta J=1$ involving interference between the S and T couplings. The experimental measurement is used to set limits on the ratio of the beta moments which are treated as parameters.

INTRODUCTION

THE RaE beta spectrum has had a long history of measurements and interpretations. It was the first spectrum definitely proved[1] to have a shape which deviates markedly from the "statistical" shape characteristic of the allowed beta transitions. The interpretation went through three main stages as the general knowledge of beta-decay phenomena and nuclear states broadened.

1

In the earliest stage, attempts were concentrated on making a "single" form of coupling law work for all beta radiation phenomena. Either the scalar (S), the vector (V), the tensor (T), the pseudovector (A), or the pseudoscalar (P) form of beta coupling was presumed to represent the complete interaction. Under this restriction, Konopinski and Uhlenbeck[2] were unable to fit the observed shape with any of the alternative predictions for *once* forbidden transitions. They did report that the expectations for *twice* forbidden transitions were sufficiently elastic to permit a fair fitting of the measurements within the accuracy then current.

The situation was changed by the subsequent advent of the shell model for nuclear states, in two main respects. The consequent classification of all known beta transitions showed that the comparative half-life of RaE, $ft=10^8$ sec, was about a factor 10^4 shorter than that characteristic of well authenticated *twice* forbidden transitions. Furthermore, the shell model predicted a change of parity in the RaE transition. This violates the selection rules for allowed and twice forbidden transitions and hence makes the classification of the RaE decay as a *once* forbidden (parity change) transition difficult to escape.

2

A second stage in the interpretations arrived when all the evidence in beta decay began to make it clear that the fundamental coupling law must consist of more than one component of the five: S, V, T, A, or P. The existence of S and T components is essential[3]; the *absence* of V and A components is also essential, but the existence of a P component is neither confirmed nor contradicting to the evidence in general.

Petschek and Marshak[4] tried all the possible linear combinations of the couplings in attempting to reproduce the observed RaE spectrum, on the basis that it is a once forbidden transition. They concluded that only a TP combination could work. The P component contributes only to once forbidden transitions with no spin change. Hence, it was supposed that RaE undergoes a $0-\!\!\rightarrow 0+$ transition. For such transitions, the S component of coupling is unable to contribute.

The Petschek-Marshak analysis provided practically the only evidence for the existence of a P component in the beta coupling law.

Konopinski and Langer[5] pointed out the essential feature which allowed Petschek and Marshak to reproduce the RaE spectrum shape. All normal once forbidden transitions with $\Delta J=0$ or 1 are expected and observed to yield very nearly statistical spectrum shapes. The strong deviations observed for RaE are possible only through nearly complete destructive interference between the radiations due to two components of coupling (T and P in the Petschek and Marshak analysis). The destructive interference should also prolong the comparative half-life and, indeed, RaE has an ft value about a factor $10^{2.5}$ greater than observed for other comparable (nearly doubly magic) once forbidden transitions.

3

The final stage of interpretation arrived when Smith[6] measured the spin of RaE and thus showed that it actually undergoes a $1-\!\!\rightarrow 0+$ transition.

Meanwhile, Yamada[7] showed that the Petschek-Marshak analysis was incomplete in an essential respect. It is usually found that it is highly accurate to neglect the radial variation of the electronic wave

* Assisted in part by the joint program of the Office of Naval Research and the U. S. Atomic Energy Commission, and a grant from the Frederick Gardner Cottrell Fund of the Research Corporation.

[1] L. M. Langer and M. D. Whitaker, Phys. Rev. **51**, 713 (1937); E. M. Lyman, Phys. Rev. **51**, 1 (1937).

[2] E. J. Konopinski and G. E. Uhlenbeck, Phys. Rev. **60**, 308 (1941).

[3] H. M. Mahoud and E. J. Konopinski, Phys. Rev. **88**, 1266 (1952).

[4] A. G. Petschek and R. E. Marshak, Phys. Rev. **85**, 698 (1952).

[5] E. J. Konopinski and L. M. Langer, Ann. Revs. Nuclear Sci. **2**, 261 (1953).

[6] K. F. Smith (private communication).

[7] M. Yamada, Progr. Theoret. Phys. (Japan) **10**, 252 (1953).

function across the nucleus. Two circumstances conspire to invalidate this assumption, in the special case of RaE. It is one of the most highly charged nuclei studied; the strong Coulomb attraction shortens the de Broglie wavelength of the electron. More important, the destructive interference between the component RaE radiations cancels the usually largest contributions and leaves small ones which are much more sensitive to this so-called[8] "finite de Broglie wavelength effect." Taking it into account, Yamada showed that Petschek and Marshak were wrong in their conclusion that the combination ST could not lead to the RaE spectrum shape.

Yamada was successful in reproducing the observed RaE shape on the basis that it undergoes a $1-\!\!\rightarrow 0+$ transition. Now the S component of the coupling contributes and a P component cannot, even if it exists. Hence, now it is the destructive interference between S and T contributions which accounts for the singular RaE spectrum shape in Yamada's interpretation. His result removes the evidence for the existence of P coupling. (There is also no evidence against its existence because theoretically it would elude giving observable effects in all cases known so far.)

At least two unsatisfactory features remain in Yamada's analysis which occasion the present remeasurement and refitting of the RaE spectrum.

First, there is a small discrepancy between the low-energy part (<175 kev) of the experimental spectrum and the theoretical spectrum arising from Yamada's analysis. The source of this discrepancy may be at least partially theoretical.

Yamada used electronic wave functions appropriate to a point charge nucleus; it has been shown[9] that the spread of the charge on the nucleus may sometimes have appreciable effects. However, Yamada's argument that this should not be important for RaE seems correct. The finite nuclear size affects mainly the large singular terms ($\sim aZ/R$) of the electronic wave functions and these are just the ones cancelled out by the destructive interference in the RaE radiation. The remaining "finite de Broglie wavelength" effects are determined by parts of the wave function farther from the center and less sensitive to redistribution of the point charge. A fully precise conclusion on this point must await numerical analysis by machine computation.

On the other hand, it is not impossible that the low-energy discrepancy is due to errors of measurement associated with the inherent difficulties encountered in attempting to obtain such low energy information in such a high-Z element. Also, the accuracy of the experimental data used by Yamada did not impose the more stringent limits on the theoretical fit which are required by the results of the present investigation. The experimental work reported here was meant to test these points, taking advantage of improved techniques developed since the earlier measurements.[10]

Perhaps the second reason for the present reinvestigation of RaE, is the more important. Early in his analysis, Yamada quite arbitrarily chose a special ratio for two of the three nuclear moments (matrix elements) responsible for the beta radiation. The successful conclusion of his work implies that the special assumption he thus employed is an essential one. As we shall see here, this is not at all the case. Yamada's special assumption was justified insofar as the interest was concentrated only on showing that by using it the RaE spectrum is at all explainable. However, the spectrum measurements should ultimately help in the evaluation of the moments possessed by the RaE transition for the radiation of beta particles. To this end, it is necessary to show what the necessary limits are that the experiments put on the values of the nuclear beta moments. As will be seen here, the correct values of the beta moments are probably somewhat different from those used by Yamada.

EXPERIMENTAL PROCEDURE AND RESULTS

The beta spectrum was measured by using the high-resolution, 40-cm radius of curvature, 180-degree shaped magnetic field spectrometer.[11]

An intense source of RaE was obtained by a carrier free separation from an equilibrium mixture of RaD, E, and F with the use of an anion exchange resin column.[12] The source thus produced was superior to those obtained by electroplating separation because of the increased yield. The RaE activity was deposited from a dilute nitric acid solution on a backing of 3 $\mu g/cm^2$ of zapon. The source was spread quite uniformly with the aid of insulin[13] covering an area of 0.5 cm by 2.5 cm and was then covered by a 1.5 $\mu g/cm^2$ layer of zapon. Grounding of the source was obtained by means of electron emission from an oxide-coated-filament assembly[14] mounted directly below the source in the spectrometer.

In order to maintain a counting efficiency which is independent of the incident electron energy over the entire RaE spectrum, the usual side window G-M tube whose sensitivity had a slight dependence on energy was replaced with a counter of unusual design. This is essentially an end window counter, the effective volume of which is confined between an aluminum covered mylar window of 0.9 mg/cm^2 total thickness and a loop of three mil stainless steel wire. The counter slit

[8] M. E. Rose and C. L. Perry, Phys. Rev. **90**, 479 (1953).
[9] M. E. Rose and D. K. Holmes, Phys. Rev. **83**, 190 (1951).

[10] A Flammersfeld, Z. Physik **112**, 727 (1939); G. J. Neary, Proc. Roy. Soc. (London) **A175**, 71 (1940); L. M. Langer, Phys. Rev. **75**, 328 (1949); R. Morrissey and C. S. Wu, Phys. Rev. **75**, 1288 (1949).
[11] L. M. Langer and C. S. Cook, Rev. Sci. Instr. **19**, 249 (1948).
[12] B. A. Raby and E. K. Hyde, U. S. Atomic Energy Commission Declassified Document AECD-3525, 1952 (unpublished); and University of California Radiation Laboratory Report UCRL-2069 (unpublished).
[13] L. M. Langer, Rev. Sci. Instr. **20**, 216 (1949).
[14] L. M. Langer and R. J. D. Moffat, Phys. Rev. **88**, 689 (1952).

was adjusted to 0.4 cm in width and 2.5 cm in height. A gas mixture of nine parts of argon to one part of ethylene was maintained at a constant pressure of 10 cm of Hg with the use of a Cartesian manostat.[15] These conditions yield a counting plateau of well over 100 volts at a threshold of 950 volts and with a slope of 1.5 percent rise per 100 volts.

Calibration for the spectrometer is in terms of the K-line from the 0.661-Mev[16] gamma ray of Cs^{137} and the magnetic field measurements were made by use of a continuously rotating coil arrangement.[17]

Figure 1 shows the conventional Fermi-Kurie plot of the data obtained with the source described above. A minimum of 10 000 counts were recorded for each experimental point below the energy corresponding to $W=2.8$ so that the statistical deviation of these points on the F-K plot is ± 0.5 percent.

These data were combined with similar results obtained with a much weaker source, which had been prepared from electrochemically separated RaE, and all the experimental points together with their statistical errors were plotted on a greatly expanded scale so that a best fitting curve could be drawn through them. Table I gives a tabulation of values $[N(p)/p^2F]^{\frac{1}{2}}$ read from this curve at convenient intervals of the electron momentum, p. In both Fig. 1 and Table I the Coulomb factor, F, has been corrected for screening.[18]

TABLE I. Beta spectrum of RaE.[a]

p	W	$N(p)$	$(N/p^2F)^{\frac{1}{2}}$
0.6	1.1662	0.5594	0.1676
0.7	1.2207	0.5939	0.1579
0.8	1.2806	0.6219	0.1496
0.9	1.3454	0.6395	0.1409
1.0	1.4142	0.6452	0.1327
1.1	1.4866	0.6413	0.1244
1.2	1.5621	0.6225	0.1162
1.3	1.6401	0.5990	0.1078
1.4	1.7205	0.5639	0.09950
1.5	1.8028	0.5243	0.09158
1.6	1.8868	0.4846	0.08410
1.7	1.9723	0.4390	0.07676
1.8	2.0591	0.3940	0.06961
1.9	2.1471	0.3435	0.06250
2.0	2.2361	0.2959	0.05590
2.1	2.3259	0.2464	0.04931
2.2	2.4166	0.2021	0.04318
2.3	2.5080	0.1616	0.03732
2.4	2.6000	0.1249	0.03178
2.5	2.6926	0.09205	0.02638
2.6	2.7857	0.06384	0.02133
2.7	2.8792	0.04034	0.01648
2.8	2.9732	0.02262	0.01200
2.9	3.0676	0.009950	0.00776
3.0	3.1623	0.002601	0.00386
3.05	3.2097	0.000862	0.00220
3.10	3.2573	0.000113	0.00079
3.134	3.2900	0	0

[a] p and W are the momentum and energy in relativistic units; N is the number of particles per unit momentum interval; F is the Coulomb factor and is corrected for screening. The estimates of error are: p less than 0.1%; N less than 1.0% for $p<2.7$.

DISCUSSION OF RESULTS

The experimental RaE spectrum represented by Fig. 1 and Table I differs slightly from the older results. Part of this difference may arise from the fact that some of the earlier measurements were made with separate low-energy and high-energy counters and the exact normalization of the data was therefore made somewhat uncertain by the possibilities of partial transmission through the grid supporting the low-energy counter window and the energy sensitive transmission through the mica window of the high-energy counter. The present results were obtained with a single thin window counter whose detection sensitivity was found to be independent of energy over the entire region of the RaE distribution.

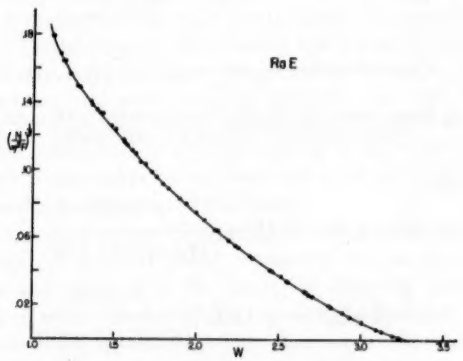

FIG. 1. Conventional Fermi-Kurie plot of the RaE beta spectrum.

The new measurements, if anything, *increase* the discrepancy between the experiments and Yamada's theoretical curve. The statistical accuracy of the present data demands a more exacting fit than the data used by Yamada. Therefore it was felt worthwhile to attempt a complete refitting in place of just taking over Yamada's final curve.

Moreover, as discussed further in the section on "Theoretical Interpretation", instead of presuming a value for the ratio of the matrix elements, as Yamada did, here *measured* limits are put on the ratio of the moments through the fitting procedure.

THEORETICAL INTERPRETATION

The beta spectrum for a once forbidden transition is described by an equation which gives the number of electrons $N(W)$ emitted in the energy range between W and $W+dW$, as

$$N(W)dW=(G^2/2\pi^3)F(Z,W)pW(W_0-W)^2C(W)dW, \quad (1)$$

where the energy W, and the momentum p of the electron are in relativistic units. W_0 is the end point

[15] L. M. Langer and R. D. Moffat, Phys. Rev. **80**, 651 (1950).
[16] L. M. Langer and R. D. Moffat, Phys. Rev. **78**, 74 (1950).
[17] L. M. Langer and R. F. Scott, Rev. Sci. Instr. **21**, 522 (1950).
[18] The screening correction was carried out using *Tables for the Analysis of Beta Spectra*, Applied Mathematics Series No. 13, National Bureau of Standards (U. S. Government Printing Office, Washington, D. C., 1952).

energy of the electron spectrum. G is the Fermi coupling constant. In (1), the "statistical shape", $\sim pW(W_0-W)^2$ is modified not only by the Coulomb factor, $F(Z,W)$, but also by the "shape factor" (or correction factor), $C(W)$. It is this shape factor which is of special interest. Its precise form depends on the particular nuclear moments (matrix elements) which are responsible for the beta radiation.

With the RaE transition having the character $1-\!\!\rightarrow 0+$, any P coupling which may exist will not contribute, and only S and T couplings need be considered. The relative strength of these are denoted by G_S and G_T; other beta decay evidence has shown these to be roughly equal. The S coupling acts on the nuclear moment $\int\beta\mathbf{r}$, in standard[2] notation, and the T coupling depends on $\int\beta\boldsymbol{\sigma}\times\mathbf{r}$ and $\int\beta\boldsymbol{\alpha}$. Only ratios of the moments affect the spectrum shape, and it is convenient to define:

$$\xi_1=i\frac{G_S}{G_T}\frac{\int\beta\mathbf{r}}{\int\beta\boldsymbol{\sigma}\times\mathbf{r}},\qquad \eta_1=\left(\frac{\alpha Z}{2R}\right)^{-1}\frac{\int\beta\boldsymbol{\alpha}}{\int\beta\boldsymbol{\sigma}\times\mathbf{r}}. \tag{2}$$

The factor $\alpha Z/R$ is the Coulomb energy in units of mc^2, at the nuclear radius R. The ξ_1 and η_1 are real numbers which depend on the details of the nuclear states. There is no satisfactory theory for calculating them and they should be regarded as nuclear properties to be determined by measurement. Here, they will be at least partially measured by being treated as parameters in the fitting of the theoretical shape factor to the observed spectrum. Yamada quite arbitrarily put $\xi_1=\frac{1}{2}$, before attempting the fitting. We find this unnecessary.

A shape factor appropriate to RaE will have terms proportional to ξ_1^2, due to the S coupling, others proportional to ξ_1 arising from interference between the S and T couplings, and further terms due to the T coupling alone. Precise expressions are most conveniently obtained from Konopinski and Uhlenbeck[2] and from Smith.[19] They are usually easily evaluated by recourse to the tables of Rose, Perry, and Dismuke.[20] However, these tables turn out to have an insufficient number of significant figures for cases like RaE.

RaE is peculiar because its spectrum deviates substantially from the statistical shape, i.e., $C(W)$ is observed to be heavily energy dependent, yet its Coulomb energy, $\alpha Z/R\approx 30$, far exceeds the kinetic energy $W_0-1\approx 2.3$. Normally, once forbidden spectra with $\Delta J\leq 1$ show a closely statistical shape (constant C) when $\alpha Z/R\gg W_0-1$. The large energy independent terms $\sim(\alpha Z/R)^2$ must be nearly cancelled from C in the case of RaE. One must presume the existence of ξ_1 and η_1 values which cause such cancellations, and these are to be understood as a destructive interference between contributions from the three moments involved.

For an accurate treatment of the cancellations we follow Yamada's procedure closely and define the presumably small difference ($x\ll\alpha Z/R$):

$$x=\frac{\alpha Z}{2R}\left(\eta_1-2\frac{1+\xi_1}{1+S}\right), \tag{3}$$

where $S=(1-\alpha^2Z^2)^{\frac{1}{2}}$. Our definition (3) coincides with Yamada's x only if we put $\xi_1=\frac{1}{2}$. Yet we lose none of the essential advantages asserted for his definition by Yamada. As did Yamada, we replace η_1 with x in the shape factor formulas. With our definition of x, we obtain:

$$C=x^2-\tfrac{2}{3}(1-\xi_1)qx-4x(1+\xi_1)\frac{p^2+\alpha^2Z^2}{(S+1)(2S+1)W}+\frac{q^2}{6}(1+2\xi_1^2)+\frac{4}{3}q(1-\xi_1^2)\frac{p^2+\alpha^2Z^2}{(S+1)(2S+1)W}+4(1+\xi_1)^2\frac{p^2+\alpha^2Z^2}{(S+1)^2(2S+1)^2}+\frac{(1-2\xi_1)^2}{1+S}L_1, \tag{4}$$

within an irrelevant constant multiplying factor. This reduces to Yamada's (13) if we put $\xi_1=\frac{1}{2}$. The

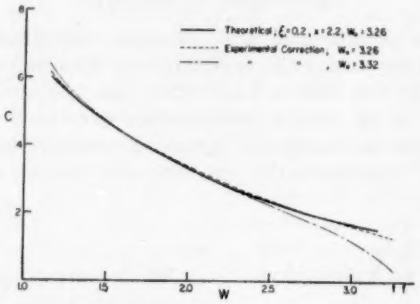

FIG. 3. Shape factors for the RaE spectrum for $\xi_1=0.2$, $x=2.2$. This is the best fit of theory to experiment.

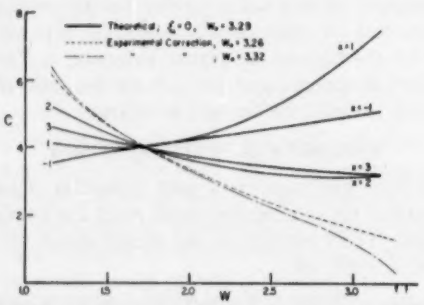

FIG. 2. Shape factors for the RaE spectrum for $\xi_1=0$. This corresponds to zero S coupling.

[19] A. M. Smith, Phys. Rev. 82, 955 (1951).

[20] Rose, Perry, and Dismuke, Oak Ridge National Laboratory Report ORNL-1459, 1953 (unpublished).

small quantity L_1 is adequately given by the tables of Rose *et al.*[20] The electron momentum is $p=(W^2-1)^{\frac{1}{2}}$ and q is the momentum of the neutrino.

Our procedure was to choose various values of ξ_1 and then find the scale factor and the value of x which make (4) coincide most closely with the experimental shape factor.

The experimental curves for C are obtained from the observed spectrum, $N(W)$, through the relation (1). This involves division by $(W_0-W)^2$ and hence the experimental C is very sensitive to the precise value of the maximum electron energy W_0 when W approaches W_0. Close inspection of the experimental points near $W=W_0$ only can set the limits $3.26<W_0$

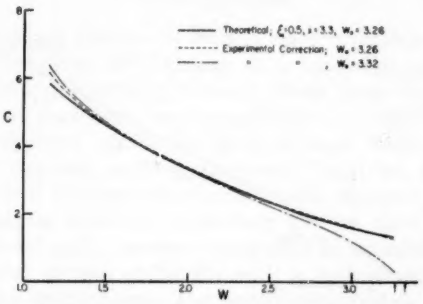

FIG. 4. Shape factors for the RaE spectrum for $\xi_1=0.5$. This is the value used by Yamada.

<3.32, because of the inevitably low intensity near the end point. We have then worked mainly with two experimental C curves corresponding to these limits. The choice of W_0 is not so critical for the theoretical C curves. It was found, however, that the value of $W_0=3.26$ leads to the best agreement between theory and experiment. For a case like RaE, where the ordinary F-K plot cannot be easily extrapolated, this is probably the best method of determining the maximum energy release. Since no theory provides for a shape factor concave downward near the end-point, the best value for the maximum energy can be set at $W_0=3.26\pm0.01$. This corresponds to a kinetic energy of $E_0=1.155$ Mev and is somewhat lower than the value of 1.17 Mev usually assigned to the RaE decay.

We tried values of ξ_1 ranging from $\xi_1=0$ to $\xi_1=2$. Only for $\xi_1\geq0.17$ could reasonable fits be obtained, for any value of x. The degree of disparity obtained for $\xi_1=0$ is shown in Fig. 2. Comparisons are also shown for $\xi_1=0.2$, $\xi_1=0.5$ (Yamada's value), and $\xi_1=1$ in Figs. 3, 4, and 5 respectively. All attempts with $\xi_1<0.17$ led to detailed discrepancies which we consider to exceed the experimental limits of error. In all cases, the curves are normalized at $W=1.72$ (or $p=1.4$).

The uncertainties are best discussed in relation to the conventional "linearized" plots of

$$[N(W)/pWFC]^{\frac{1}{2}}\sim W_0-W, \tag{5}$$

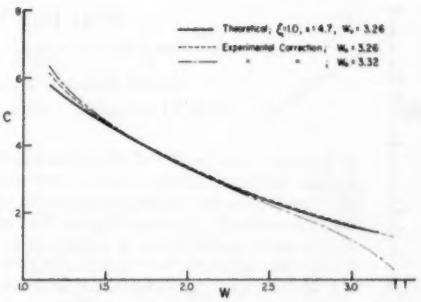

FIG. 5. Shape factors for the RaE spectrum for $\xi_1=1.0$.

where N is taken from the observed spectrum and C from (4) with the stated values of ξ_1 and x. Such plots are much less sensitive than those giving C directly, but represent the current accuracy of measurement (especially that of W_0) more appropriately.

The linearized plot in Fig. 6 shows that the fitting we achieved is as good as any obtained, so far, for any beta spectrum. The low energy discrepancy for $\xi_1=0.2$ and $x=2.2$ is much smaller than that obtained using Yamada's value of $\xi_1=0.5$, and $x=3.3$ as shown in Fig. 7. It may well be that this residual low energy discrepancy lies within the accuracy of even the present measurements. While attempting to find the best values for the parameters in the formula for C, it was noticed that ξ_1 could be chosen over a fairly wide range to obtain shape factors which were not too inconsistent with the experimental correction curve. It is perhaps worth noting that if ξ_1 is plotted against the corresponding value of x which yields the best fit, as is done in Fig. 8, it is found that an almost linear plot results.

Finally, we gave some consideration to what values of ξ_1 and $\eta_1(x)$ are consistent with the little which can be surmised theoretically. We restricted our consideration to predictions from the formulas given by Rose and Osborn.[21] This necessitates decisions about the probable orbital characters of the nuclear states.

The current ideas based on the shell model consider RaE and its daughter each to have two nucleons

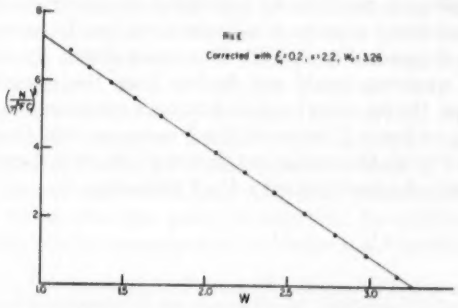

FIG. 6. Linearized plot of the RaE spectrum using the best fit values for the shape factor, C.

[21] M. E. Rose and R. K. Osborn, Phys. Rev. **93**, 1326 (1954).

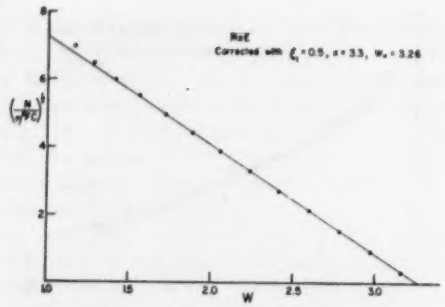

FIG. 7. Linearized plot of the RaE spectrum using Yamada's choice for $\xi_1=0.5$.

outside a doubly-closed shell of 82 protons and 126 neutrons. The daughter presumably has two $h_{9/2}$ protons outside closed shells. The parent has an $h_{9/2}$ proton with a neutron which may either be $g_{9/2}$ or $i_{11/2}$ to give a resultant spin $J'=1$. We applied Rose and Osborn formulas to both possibilities.

A two-nucleon state formed by j-j coupling has a degeneracy which prevents a definite conclusion unless it is removed on the basis of further assumptions. It may be removed by presuming the isotopic spin to be a good quantum number, an assumption which is hardly justifiable for as highly charged a nucleus as RaE. Nevertheless, it is of some interest to see just how much isotopic spin selection rules are violated. We obtain sets of values for the moments which are essentially the same irrespective of the choice $g_{9/2}$ or $i_{11/2}$ for the neutron.

The two proton daughter state must have isotopic spin, $I=1$, but the parent state may have $I'=0$ or 1. This has peculiar consequences. We find that the S coupling moment, $\int\beta\mathbf{r}$, nearly vanishes (exactly so for a $g_{9/2}$ neutron) if $I'=1$ whereas both the T coupling moments vanish (only nearly so for the $i_{11/2}$ neutron) if $I'=0$. Thus, we are led to the conclusion that, if the isotopic spin is a good quantum number for RaE, the S and T couplings cannot simultaneously contribute to its radiation. This is clearly wrong, since the nearly complete destructive interference between these two couplings is essential for explaining the spectrum. The unsuccessful attempt at a fit for $\xi_1=0$ (no S coupling) was shown in Fig. 2. With T coupling absent ($\xi_1\to\infty$), the spectrum would not deviate from the statistical shape. On the other hand, it may have some significance that as low a ξ_1 value as $\xi_1\approx\frac{1}{3}$ works so well (Fig. 3 and Fig. 6). One might say that the RaE state does not deviate far from having a $I'=1$ character.

A more consistent way of removing the degeneracy may be to assume that only the single transforming nucleon state is significant for the transition. We then find that $\xi_1^2=1/100$ for a $g_{9/2}\to h_{9/2}$ transition whereas $\xi_1^2=1$ if the transition is $i_{11/2}\to h_{9/2}$.

Discarding the absurd case in which the T coupling moments vanish, we find for η_1 the same result by either of the two methods for removing the degeneracy. This is

$$\eta_1=\Lambda, \tag{6}$$

which is a number expected to be between 1 and 3 by various investigators.[21–23] This result may have some significance, since it arises irrespective of rather extremely different assumptions.

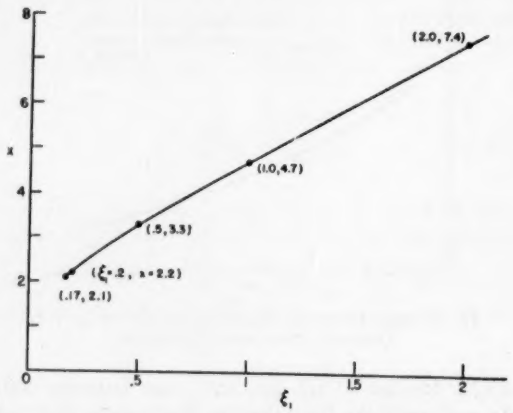

FIG. 8. Plot of values of ξ_1 and x that lead to reasonable fits to the experimental data.

The range of expected values of Λ easily covers the range of uncertainty in our experimental evaluations of ξ_1 and x. Values of these parameters which can be made to yield a reasonably fit of the RaE spectrum are shown in Fig. 8. As (ξ_1,x) range from (0.2, 2.2) to (1.0, 4.7),

$$\Lambda=\eta_1=1.5 \text{ to } 2.5,$$

according to (3).

The authors are greatly indebted to Professor E. J. Konopinski for detailed discussions on the theoretical aspects of the problem. They also wish to thank Mr. R. Johnson for helping with some preliminary measurements.

[22] T. Ahrens and E. Feenberg, Phys. Rev. 86, 64 (1951).
[23] D. L. Pursey, Phil. Mag. 42, 1193 (1951).

Disintegration of Ir^{192} and Ir^{194}

M. W. JOHNS AND S. V. NABLO
Department of Physics, McMaster University, Hamilton, Ontario
(Received May 14, 1954; revised manuscript received September 17, 1954)

The energies and intensities of 20 gamma rays of Ir^{192} and 16 gamma rays of Ir^{194} have been measured by studying their external conversion spectra with a high resolution beta-ray spectrometer. A Fermi analysis of the beta spectrum of Ir^{194} reveals four components with the following end-points and intensities: 2236 kev (70 percent), 1905 kev (16 percent), 975 kev (9 percent) and 430 kev (2.8 percent). The observed beta and gamma radiations are consistently accounted for in terms of transitions to the following levels of Pt^{194}: 0.0, 328.1, 621, 1265, 1477, 1665, 1794, 1802, 1836, 1946, and 2048 kev. The Ir^{194}—Pt^{194} energy difference is 2236 ± 10 kev. The Ir^{192} gamma-ray energies are classified in terms of levels at 0.0, 283, 485, 690, and 1064 kev in Os^{192} and 0.0, 316, 612, 784, 921, 1155, 1201, and 1359 kev in Pt^{192}. The results for Ir^{192} serve chiefly as confirmation of earlier investigations.

I. INTRODUCTION

THE n-γ reaction in iridium leads to 70-day Ir^{192} and 19-hr Ir^{194}. With an 18-hr irradiation period the initial Ir^{194} activity is about fifteen times that of Ir^{192} and conditions remain favorable for a study of the short-lived nuclide for about 80 hours thereafter.

Ir^{192} has been studied extensively[1–5] and the main features of its decay scheme are known. However, the information available concerning Ir^{194} is quite incomplete[1,2] and it seemed worthwhile to examine its beta and gamma radiations with a high resolution beta-ray spectrometer. The results presented in this paper show that there is a rich spectrum of weak gamma rays accompanying the decay of Ir^{194}. In order to study these radiations it was necessary to re-examine the complex background caused by the decay of the Ir^{192}. Our observations concerning the latter spectrum serve mainly to confirm the findings of other workers.

Since the decay of Au^{192} and Au^{194} leads to excited states of Pt^{192} and Pt^{194} respectively, the data available for these nuclides[6,7] are also pertinent to this study.

II. APPARATUS AND METHOD

Six sources of "spec-pure" iridium powder, sealed in quartz, were irradiated in the Brookhaven reactor and studied in a high resolution beta-ray spectrometer[8] by examining the external conversion spectrum produced in uranium and gold radiators of thicknesses ranging from one to fifty mg/cm^2. Photoelectron peaks from twenty gamma rays in Ir^{192} and sixteen in Ir^{194} were observed. The decay of each of the latter peaks was followed for at least forty hours and found to be consistent with a 19-hr half-life. Since none of the radiations which might be expected from the possible impurities were found, it is felt certain that all of these gamma rays do occur in the decay of Ir^{194}. A 3-curie Ir^{192} source was used to examine the weak high-energy spectrum of the lighter isotope.

Most of the measurements were made with uranium radiators of thickness 1.85, 10.3, and 20.1 mg/cm^2 and area 3.0×0.8 cm prepared according to the technique described by Dodson.[9] The spectrometer was adjusted to give a resolution of 0.65 percent in momentum (full width at half-maximum) on the thorium F line. The external conversion peaks with these radiators ranged from 0.8 to 2 percent in width, depending on the choice of radiator and the electron energy under study. These photoelectron peaks all possess a characteristic shape, marked by a steep, high-energy profile which rises from the base line to the peak in a momentum change of about 0.3 percent and a low-energy profile whose slope depends on both the electron energy and radiator thickness. In any region the peaks have a clearly defined shape and width; any marked change in this shape indicates the presence of an unresolved doublet.

The electron momentum was obtained by measuring the magnetic field strength corresponding to the point of inflection of the high-energy edge of the peak. This point was found to be quite independent of radiator thickness, providing the latter was great enough to give a peak wider than 1 percent, and it was also found to be relatively independent of the manner in which the underlying Compton distribution was drawn in. Measurements of the field were made with a flip coil and galvanometer, using the external conversion peak of the Co^{60} radiation at 1.3325 Mev[10] as a standard. Calibration runs were made on this line, the external conversion line of the Cs^{137} radiation[9] and the thorium F and X internal conversion lines.[8,11] For the internal conversion lines the peak position was used rather than the point of inflection. In addition, the very precise measurements of Muller *et al.*[3] provided

[1] *Nuclear Data*, National Bureau of Standards Circular No. 499 (U. S. Government Printing Office, Washington, D. C., 1950), p. 224.
[2] J. M. Cork *et al.*, Phys. Rev. **82**, 258 (1951).
[3] D. E. Muller *et al.*, Phys. Rev. **88**, 775 (1952).
[4] K. I. Roulston and R. W. Pringle, Phys. Rev. **87**, 930 (1952).
[5] Pringle, Turchinetz, and Taylor, Phys. Rev. **95**, 115 (1954).
[6] G. T. Ewan and A. L. Thompson, Trans. Roy. Soc. Can **47**, 126 (1953).
[7] Steffen, Huber, and Humbel, Helv. Phys. Acta **22**, 167 (1949).
[8] Johns, Waterman, and Cox, Can. J. Phys. **31**, 225 (1953).
[9] A. C. Graves and D. K. Froman, *Miscellaneous Physical and Chemical Techniques of the Los Alamos Project* (McGraw-Hill Book Company, New York, 1952), National Nuclear Energy Series, Plutonium Project Record, Vol. 3, Div. V.
[10] Lind, Brown, and DuMond, Phys. Rev. **76**, 591 (1949).
[11] W. Brown, Phys. Rev. **83**, 271 (1951).

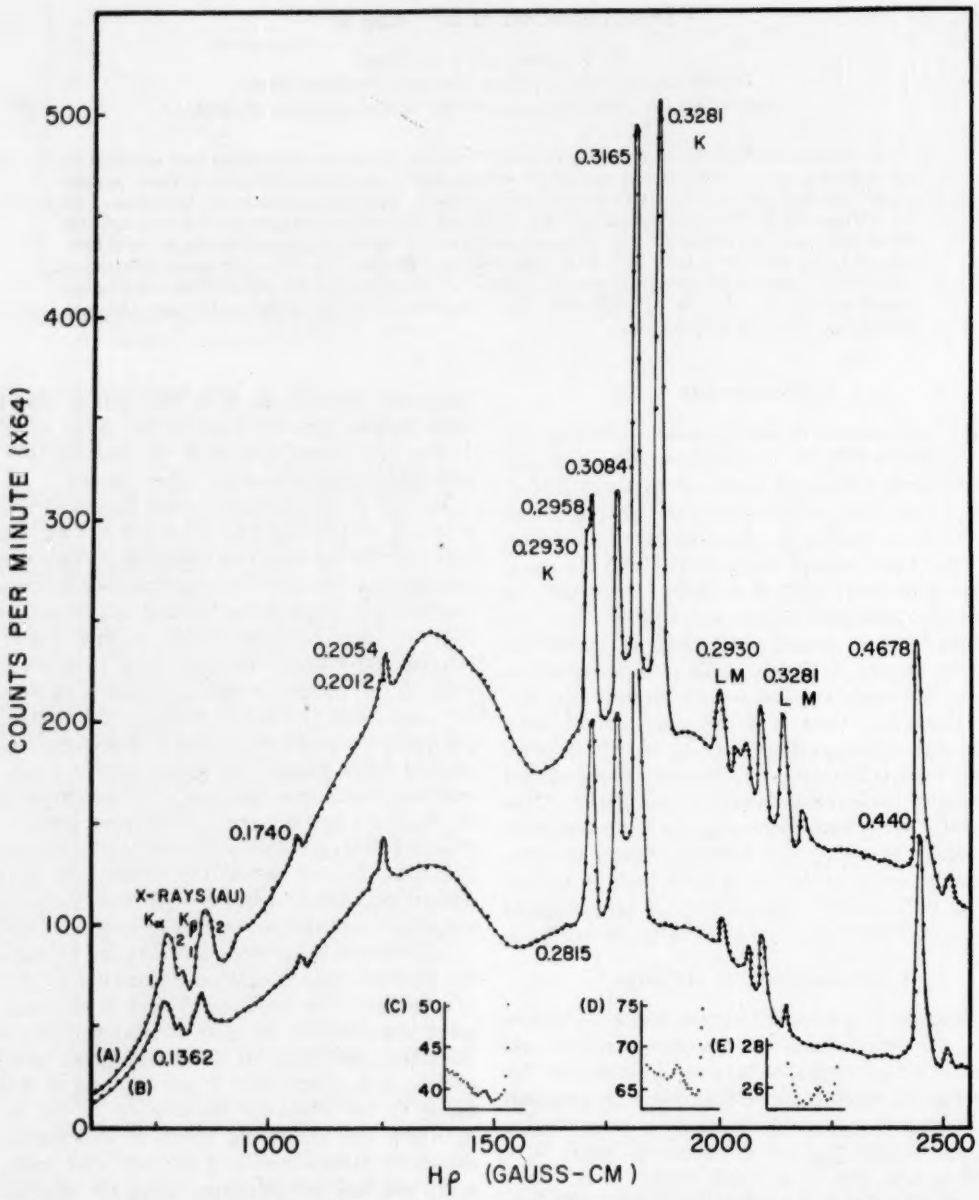

FIG. 1. The external conversion spectrum below 0.490 Mev. Curves *A* and *B* were obtained with a 1.2-mg/cm² Au radiator; *C*, *D*, and *E* with a 1.8 mg/cm² U radiator. *A* presents the total spectrum 12 hours after irradiation and *B* the Ir^{192} component 10 days later. *C* shows the weak 0.281-Mev *K* peak just below the 0.296-Mev *K* peak, *D* presents the 0.374-Mev *K* peak which falls just below the 0.296-Mev *L* peak and *E* shows the weak 0.440-Mev *K* peak between the 0.316-Mev *M* and the 0.467-Mev *K* peaks.

excellent internal standards up to 600 kev. These standards were used to draw a correction curve for any lack of linearity in the galvanometer scale. The corrections applied were never greater than 0.3 percent over the range of $H\rho$ from 500 to 9000. Peak positions were reproducible to 0.1 percent in any given run, but systematic errors of about twice this amount appeared over the fifteen months during which measurements were made.

The intensities were calculated using a modification of the formula given by Deutsch, Elliott, and Evans.[12] Following their argument, one can write:

$$N = K[n/p\beta^3\tau]\cdot[(Rp\beta^3/l)^2+k^2]^{\frac{1}{2}},$$

[12] Deutsch, Elliott, and Evans, Rev. Sci. Instr. 15, 178 (1944).

in which N is the intensity of the gamma ray, n the height of the photoelectron peak of momentum p, β is v/c, R the instrumental resolution, t the radiator thickness, τ the photoelectric cross section, and K a constant, depending on the source-radiator geometry and the instrumental transmission. The quantity k, which may be expected to vary slowly with energy, was evaluated semi-empirically using Bohr's theory and the data given by White and Millington.[13] It was found that gamma-ray intensities computed by this means were practically independent of the chemical composition or thickness of the radiator. Values for τ were obtained either directly or by extrapolation, from the data given by Davisson and Evans.[14] It is felt that in the region from 200 to 1800 kev, intensity measurements made in this way can be relied on to within 20 percent for well-defined peaks.

The iridium for preparation of beta sources was dissolved by a method suggested by Yaffe.[15] A quartz vial containing 1 mg of irradiated metal was placed in a porcelain crucible and crushed under ether to keep the active powder under control. The ether was allowed to evaporate, equal parts of potassium hydroxide and potassium nitrate were added and the mixture heated strongly until the iridium dissolved in the melt. The flux was allowed to cool and was then leached with concentrated hydrochloric acid. The iridium came out as a deep blue solution of iridium tetrahydroxide. To remove the large quantities of potassium salts and silica from the solution, the iridium was precipitated as

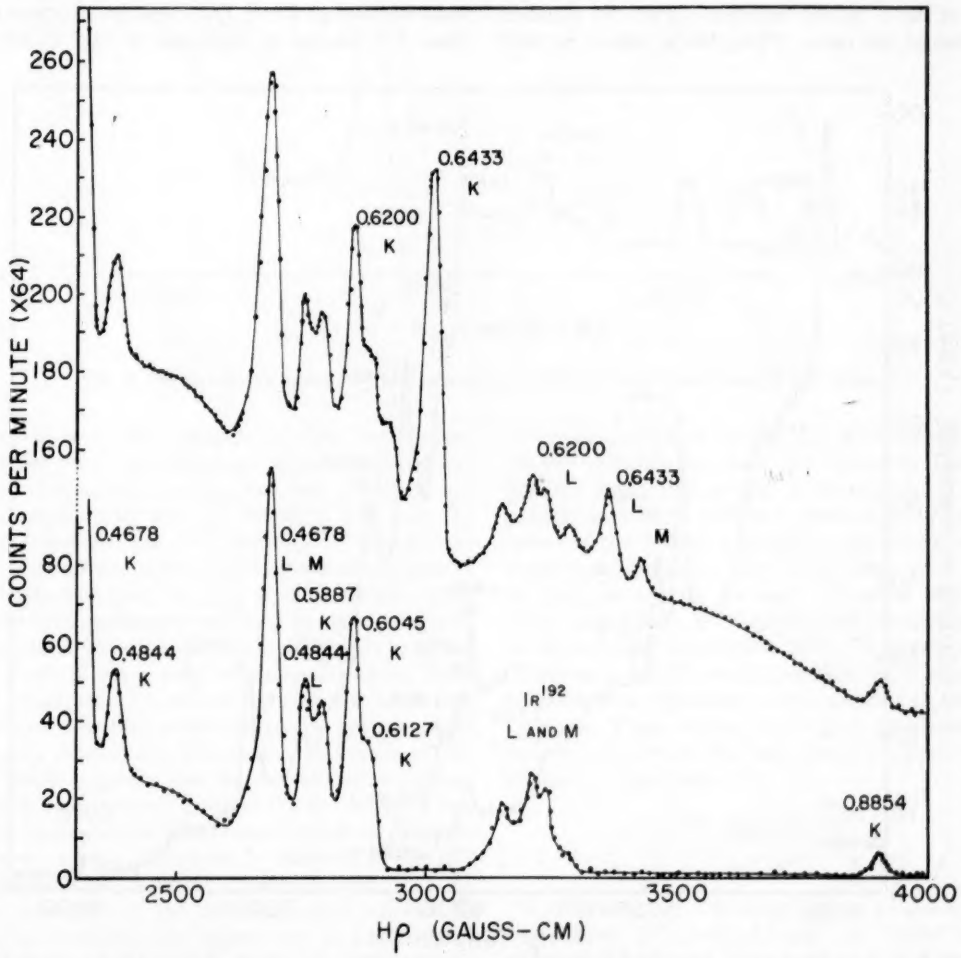

FIG. 2. The external conversion spectrum from 0.470 Mev to 0.900 Mev obtained with a 10-mg/cm² U radiator. The Ir^{194} peaks are identified on the upper curve, obtained about 12 hours after irradiation and the Ir^{192} peaks are shown on the lower curve, taken after the short-lived activity had disappeared.

[13] Rutherford, Chadwick, and Ellis, *Radiations from Radioactive Substances* (Cambridge University Press, London, 1930), p. 430.
[14] C. M. Davisson and R. D. Evans, Revs. Modern Phys. **24**, 79 (1952).
[15] L. Yaffe, McGill University, Montreal, P. Q. (private communication).

iridium thiocyanate by adding ammonium thiocyanate and then dissolved in ethyl acetate. The resulting solution when deposited on a thin film gave strong sources whose Fermi plots were well behaved to energies as low as 125 kev.

III. EXPERIMENTAL RESULTS

(a) Gamma-Ray Measurements

Composites of the external conversion spectra of both Ir^{192} and Ir^{194} from $H\rho = 500$ to 8000 are shown in Figs. 1 to 3. In addition, the weak high-energy spectrum of Ir^{192} obtained with the 3-curie source is shown in Fig. 4. The gamma-ray energies and intensities are presented in Tables I and II. The energies of most of the radiations were measured at least ten times and the limits of error quoted represent twice the standard deviation of the mean. These limits include at least 80 percent of the individual measurements. For each of the weak, high-energy radiations, the Compton contribution in the absence of the radiator was also observed as a check on the reality of the photoelectron peaks. The intensities are given as quanta per disintegration. These will be correct as relative values even if the decay scheme on which they are based proves to be incomplete.

(b) Beta Spectra

Three separate beta sources were analyzed. Since the irradiation periods were too short to give good Ir^{192} specific activity, no attempt was made to study the Ir^{192} beta spectrum in detail. Its end point was found to be 0.672 Mev in good agreement with Levy's value of 670 ± 13 kev.[16] The Fermi plot for one of the three Ir^{194} sources is presented in Fig. 5. All three

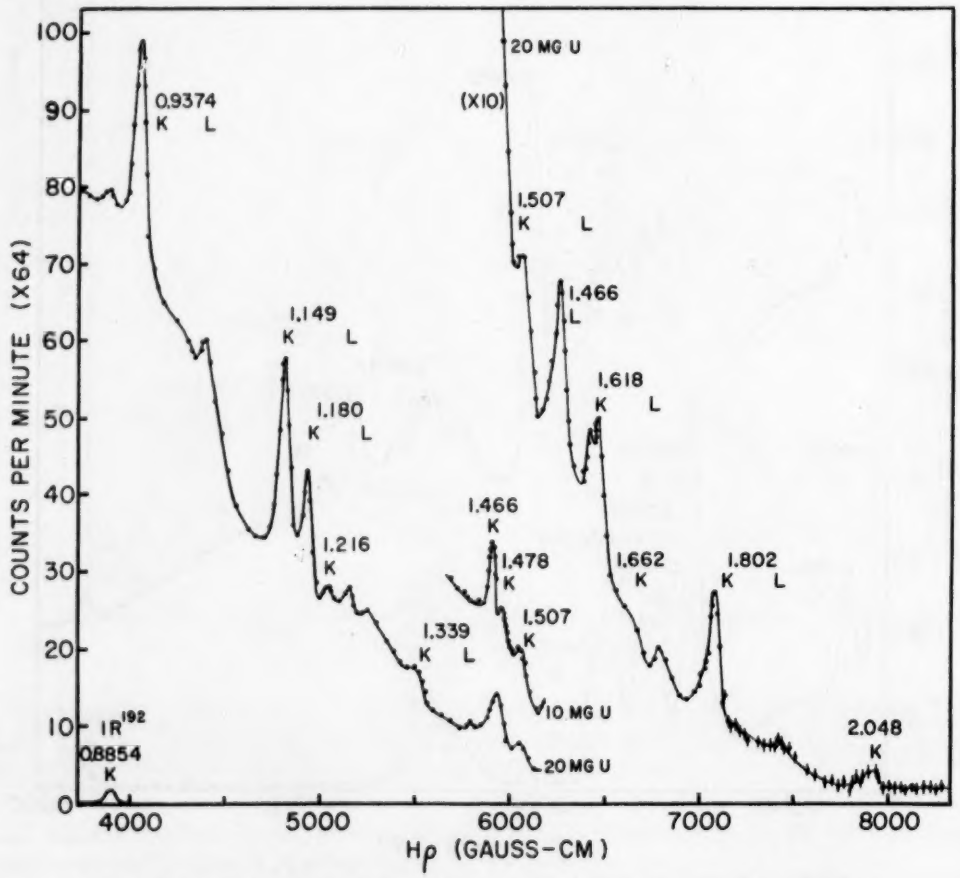

FIG. 3. The Ir^{194} high-energy external conversion spectrum obtained with a 20.1-mg/cm² U radiator. The insert shows the profile of the 1.466–1.478 Mev doublet observed with a 10-mg/cm² U radiator. This doublet is not resolved with a 20-mg/cm² radiator but the high-energy profile of the peak obtained does not seem to be steep enough for a normal peak of this height. The unresolved peak corresponds to an energy of 1.467 Mev.

[16] P. W. Levy, Phys. Rev. **72**, 352 (1947).

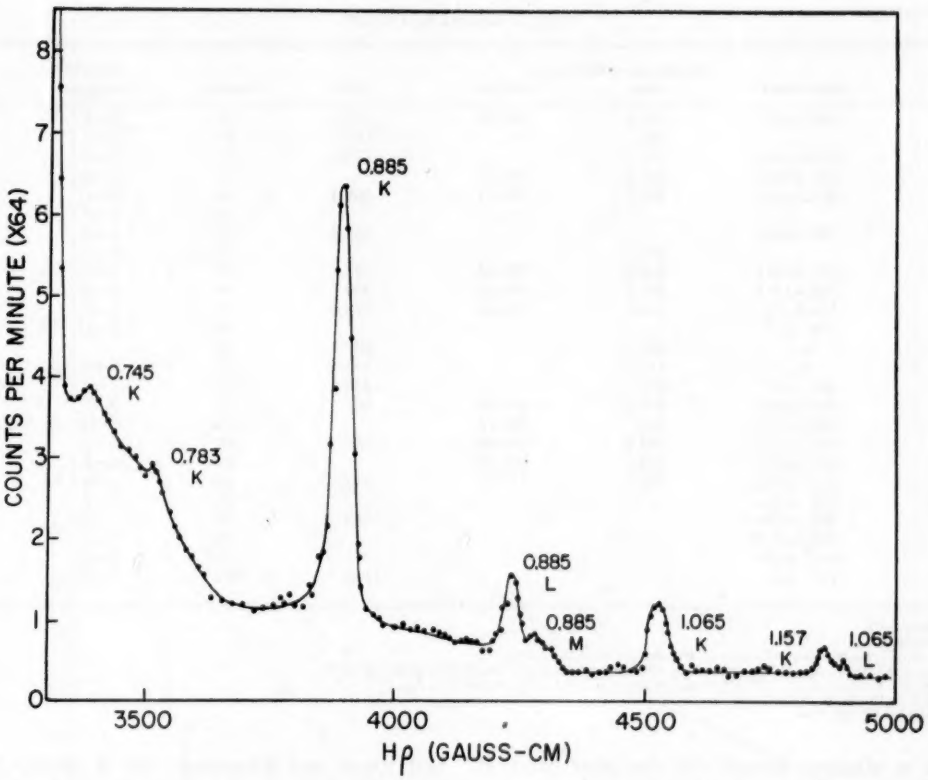

FIG. 4. The high-energy external conversion spectrum of Ir^{192} obtained with a 10-mg/cm² U radiator.

sources showed the presence of four well-defined components with the following end-point energies and relative intensities (average values): 2236±10 kev (66 percent); 1905 kev (15 percent); 975 kev (9.7 percent); and 430 kev (~8 percent). In drawing the Fermi plot, the end point of the high-energy component was determined from the data above 1900 kev, while the other end points were adjusted to correspond with that expected from the decay scheme already proposed on the basis of the gamma measurements alone. These slight adjustments ($\leq$10 kev) were made in order that the relative intensities of the beta groups might be more accurately determined. The relative intensities of the first three beta groups were found to be quite reproducible. The yield and end point of the low-energy group are much more uncertain because of the effects of source thickness and the difficulties in subtracting the Ir^{192} background with its strong conversion lines.

The intensities of the beta transitions can also be found by combining the gamma-ray intensities with the relative intensities of the 2236- and 1905-kev beta groups found from the Fermi analysis. The distortion of the gamma-ray intensities caused by ignoring the effect of internal conversion is negligible, except for the strong 293- and 328-kev radiations. Even for these the distortion is quite insensitive to the values of the total conversion coefficient chosen. The $E2$ character of the 328-kev radiation has been established by Mihelich[17] from its K/L ratio so that a value of 0.075 for its internal conversion coefficient seems appropriate. The nature of the 293-kev radiation is not known, but for these intensity calculations an arbitrary value of 0.2 has been chosen for its total conversion coefficient. Using these values, a straightforward calculation leads to the following intensities: 2236 (70 percent); 1905 (16 percent); 975 (9 percent); and 430 kev (2.8 percent). All other beta transitions should amount to less than 3 percent. These values are in good agreement with those obtained from the beta analysis, except for the low-energy component.

IV. DISCUSSION

(a) Ir^{193}

A comparison of the energy values obtained in this investigation with those of Cork[2] and Muller[3] for Ir^{192} and those of Ewan and Thompson[6] for Au^{192} is presented in Table I. Since Cork's energies were computed from the internal conversion spectrum, he was unable to decide whether the weaker lines were converted in the

[17] J. W. Mihelich (private communication), quoted by F. Scharff-Goldhaber, Phys. Rev. 90, 587 (1953).

TABLE I. Gamma rays of Ir^{192}.

Intensity	Gamma-ray energy (kev) Present work	Cork[a]	Muller[b]	Au^{192}[c]	Nucleus	Assignment Transition	ΔE(kev)
2.6	136.2±0.3	135.9	136.33	136.5	Pt	4→3	+0.2
		156		157.7	Pt	7→6	+1
0.8	174.0±0.4	173		173.4	Pt	3→2	−2
0.8	201.2±0.3	201.1	201.31		Os	*C*→*B*	+0.1
3.5	205.4±0.2	205.7	205.74	205.4	Os	*D*→*C*	+0.3
					Pt	7→5	−1
1.0	281.5±0.5			281.8	Pt	6→4	−1.5
		283			Os	*B*→*A*	+0.4
26	295.8±0.1	294.9	295.94	295.7	Pt	2→1	+0.2
28	308.4±0.1	307.7	308.45	308.1	Pt	4→2	0.0
77	316.5±0.1	316.1	316.46	316.0	Pt	1→*O*	0.0
0.5	374 ±2[d]				Os[f]	*E*→*D*	0
	e	400		401	Pt		
	e	415.1		415.5	Pt	6→3	+1.3
0.5	440 ±2	438		435.5	Pt	7→4	−2
57	467.8±0.1	467.4	467.98	467	Pt	3→1	+0.2
5.2	484.4±0.2	484	484.75		Os	*C*→*A*	+0.3
6.4	588.7±0.3	588.6	588.40	588	Pt	6→2	−0.3
10	604.5±0.3	603.7	604.53		Pt	4→1	−0.1
7.7	612.7±0.2	611.2	612.87	612	Pt	2→0	−0.2
0.05	745 ±3				Pt[f]	7→2	+1.5
0.05	783 ±2[g]			783	Pt	3→0	+1.5
0.9	885.4±1.0[g]				Pt[f]	6→1	−1.0
0.15	1065 ±2[g]				Os[f]	*E*→*A*	−1
0.08	1157 ±2			1158	Pt	5→0	−2

[a] See reference 2.
[b] See reference 3.
[c] Ewan and Thompson (see reference 6) and private communication.
[d] Falls on the *L* peaks of the 295–316 triplet when converted in Pt, Au, or Pb; observed in U.
[e] Falls on the *L* peaks of the 295–316 triplet when converted in U; not seen in Au.
[f] Assigned on the basis of energy alone.
[g] Obtained by Pringle *et al.*

osmium or platinum branch. On the other hand, all the Au^{192} data refer to transitions in platinum. By comparing the four columns it is nearly always possible to assign each gamma ray uniquely to one branch of the decay scheme, as shown in Table I.

Since Cork assigns the 205-kev radiation to osmium on the basis of its *K* and *L* internal conversion peaks and Ewan and Thompson find it clearly in Au^{192}, radiation of this energy must appear in both branches of the decay scheme, with the stronger probably belonging in osmium. The situation with respect to the much weaker 281-kev radiation is similar but not so clearly defined. Its presence in platinum is indicated by Ewan and Thompson, while Cork's value of 283 kev is based on internal conversion in osmium. Cork's corresponding energy for internal conversion in platinum would have been 288 kev; there is no other evidence for the existence of a 288-kev radiation, though admittedly it would be very difficult to detect by external conversion, since its *K* peak would fall on the low-energy edge of the strong 295-kev *K* peak. For four of the weakest lines the decision as to the branch in which they belong has been made purely from their position in the decay scheme. Confirmation for most of the weak, high-energy lines reported is found in the coincidence and scintillation spectrometer studies of Pringle *et al.*[4,5]

TABLE II. Gamma-rays of Ir^{194}.

Intensity	Gamma-ray Energy (kev)	Assignment	ΔE (kev)
5.1	293.0±0.3[a]	2→1	0.1
27	328.1±0.2[a]	1→0	0.0
<3	466[ab]	9→4	+3
1.7	620.0±1.0	2→0	+1.0
6.2	643.3±0.6	3→2	+0.7
2.9	937.4±0.4	3→1	−0.5
2.9	1149.2±0.6	4→1	−0.2
1.7	1180 ±1	7→2	+1
0.4	1216 ±1	8→2	−1
0.3	1339 ±2	5→1	−2
0.8	1466 ±1[a]	6→1	0
0.2	1478 ±1[c]	4→0	−1
		or	
		7→1	−4
0.3	1507 ±2	8→1	+1
0.3	1618 ±2	9→1	0
0.2	1662 ±3	5→0	+3
0.3	1802 ±2	7→0	0
0.05	2048 ±4[a]	10→0	0

[a] Observed by Steffen *et al.* (see reference 7) in the decay of Au^{194}.
[b] Falls underneath the strong 468-kev peak in Ir^{192}. The upper limit for its intensity is set by observing the decay of the Ir^{192} peak intensity.
[c] Appears as a partially resolved peak between the 1466- and 1507-kev peaks when studied with a 10-mg/cm² uranium radiator.

All but one of the radiations given in Table I can be accounted for as transitions between the energy levels shown in Fig. 6. In calculating these energy levels from the data, Muller's energy values have been used wherever possible. The last three columns of Table I show the assignment of each radiation and the difference between the expected value and that observed in this work. The scheme is essentially that suggested by Cork's group and extended by Pringle

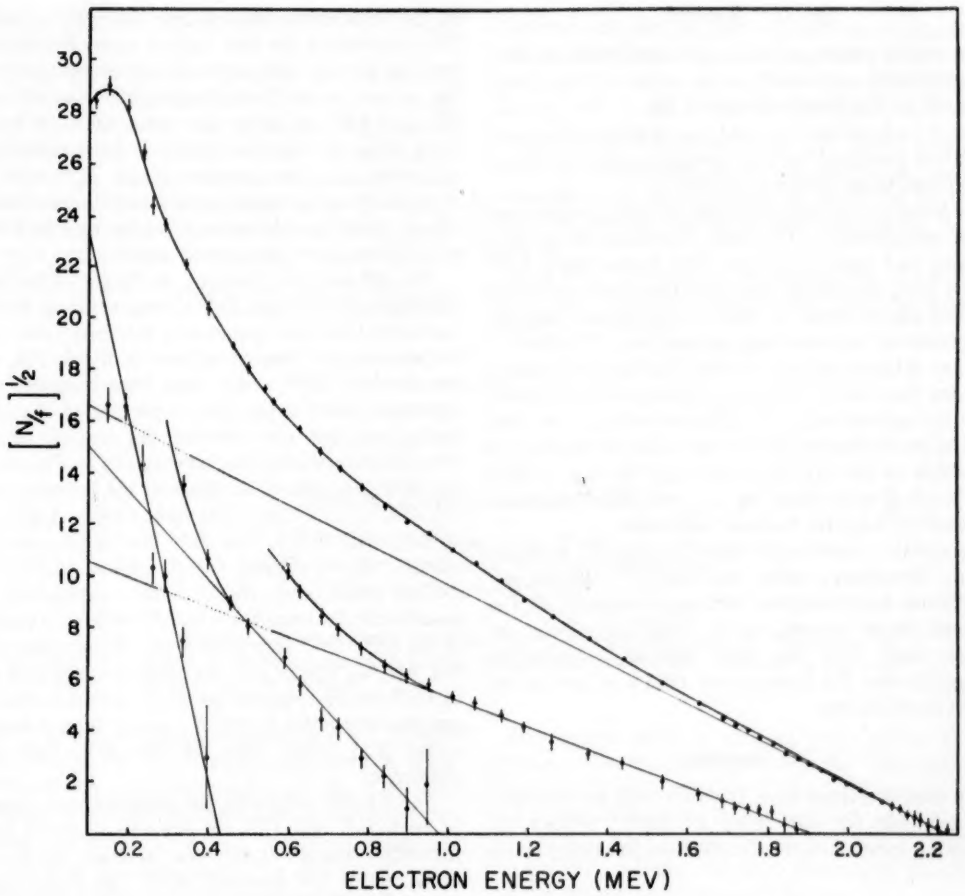

FIG. 5. Fermi plot of the beta spectrum of Ir^{194}.

and his colleagues. Slight modifications of the energies of the upper levels have been made necessary by the more accurate data presented here. The evidence for the 1156-kev level is based on two weak lines, while the 1359-kev level is based on four weak lines. The level at 1064 kev in osmium, suggested by Pringle, is rather insecurely established.

On the basis of the beta-ray end-point energy of 672 kev and Pringle's value of 1490±20 kev for the $Ir^{192}-Pt^{192}$ mass difference, it would appear that the highest-energy beta group feeds the 784-kev level and that no direct transitions from Ir^{192} pass to the three lowest-lying levels. Support for this view is given by the gamma-ray intensities, which indicate that very few beta rays can proceed to either the 316- or 612-kev levels. The gamma-ray intensity measurements also indicate that roughly 50 percent of the beta rays go to the 784-kev level, 35 percent to the 921-kev level, 8 percent to the 1200-kev level, and 1 percent to the 1359-kev level. K capture occurs in 6 percent of the disintegrations, with most of the transitions proceeding to the 485- and 690-kev levels. These estimates are admittedly rather rough, since the internal conversion coefficients of the gamma rays are not known.

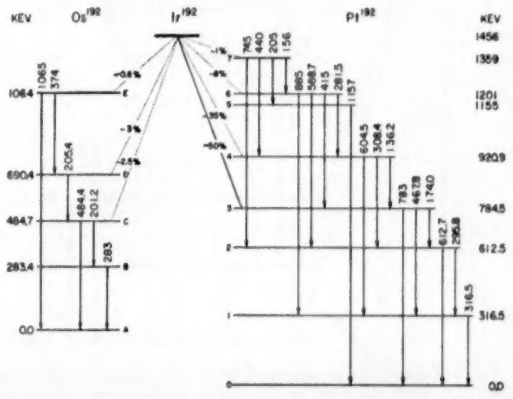

FIG. 6. Disintegration scheme of Ir^{192}.

(b) Ir^{194} Results

The results presented in Sec. III and Table II may be consistently accounted for in terms of the levels presented in the decay scheme of Fig. 7. The classification of each gamma ray and the agreement between the values predicted by this scheme and the observed measurements are shown in Table II.

The levels at 328, 621, and 1265 kev may be regarded as well established on the basis of evidence from both the beta and gamma spectra. The levels above 1265 kev are much less certain since the cross-over transitions expected are too weak to show on the strong Compton background of higher-energy gamma rays. The level at 1793 kev is based on only one line, the relatively strong 1466-kev line which Steffen and his co-workers[7] found to be in cascade with the 328-kev radiation in their study of Au^{194}. On the basis of our expected errors, it is impossible to identify this level with the one at 1802 kev, which is established by two well defined gamma rays and the doubtful 1478-kev radiation.

Coincidence experiments carried out by Ian Williams of this laboratory, using two NaI(Tl) gamma-ray scintillation spectrometers, offer good support for the proposed decay scheme up to 1265 kev above the ground state, but the more difficult experiments arranged to test the levels above 1265 kev have so far proven inconclusive.

(c) General

The data presented here, together with the information available for the decay of Au^{196} [7] provide an interesting comparison of the positions of energy levels in the three even-even isotopes, Pt^{192}, Pt^{194}, and Pt^{196}. The positions of the first excited states for these three nuclides are 316, 328, and 358 kev respectively above the ground states; the second excited states lie at 611, 621, and 688 kev above the same reference levels. In both cases the regular change in level position with increasing neutron number is in agreement with expectation and removes an anomaly in the literature[18] which states that the second excited state in Pt^{194} falls at 1.8 Mev above the ground state.

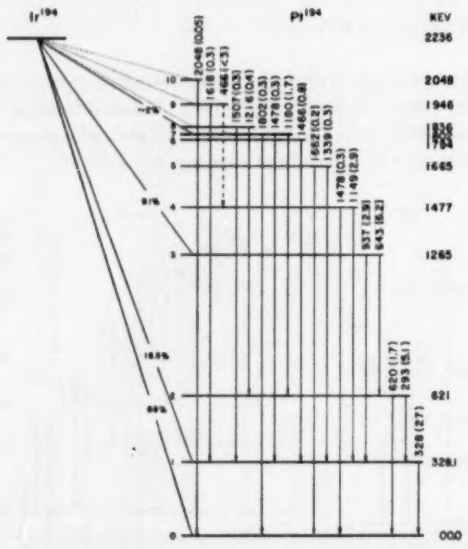

FIG. 7. Disintegration scheme of Ir^{194}. Beta transitions shown as solid lines were obtained in the Fermi analysis; the others are deduced from gamma-ray intensities.

The difference in intensity of the ground-state beta transitions of Ir^{192} and Ir^{194} is very striking. Using the measured beta- and gamma-ray intensities and making the assumption that transitions to the 0, 316, or 612 kev levels of Pt^{192} would have been observed if their intensities were larger than 1 percent of the 670-kev beta group, one can calculate the $\log(f_0 t)$ values for transitions to each of the levels given in Figs. 6 and 7. For Ir^{192} this calculation leads to the following values: (0)$>$11.2, (1)$>$11.0, (2)$>$10.4, (3)8.3 (4)8.2, (5)10, (6)8.0, and (7)7.9. For Ir^{194} the values are (0)8.3, (1)8.7, (2)$>$9, (3)7.8, (4)7.9, (5)8.3, (6)7.8, (7)7.3, (8)7.6, (9)6.7, and (10)6.9. Such a calculation is not possible for the transitions to Os^{192} without a knowledge of the $Ir^{192}-Os^{192}$ energy difference. If one assumes that the $\log(f_0 t)$ values for transitions to levels D and E in Os^{192} are also approximately 8, consideration of the gamma intensities in the K-capture branch leads to a value of 1.3 ± 0.2 Mev for the $Ir^{192}-Os^{192}$ energy difference.

The $\log(f_0 t)$ values for the observed beta transitions in both Ir^{192} and Ir^{194} are close to those of the first forbidden transitions for other odd-odd nuclei in this mass range; for example, Re^{186} has values ranging from 7.7 to 8.2, Re^{188} from 8.2 to 8.9,[19] and Au^{198} values of 7.4 and 7.6.

On the basis of these $\log(f_0 t)$ values and the observed pattern of gamma-ray intensities, it seems necessary to describe the Ir^{192} ground state as 4^- and the Ir^{194} ground state as 1^- or 2^-, with the former choice preferred since there was no evidence of departure from the allowed shape in the analysis of the 2.236-kev beta spectrum.

According to shell theory[20] the ground state of the Ir^{192} nucleus is described as a $(6h_{11/2})^{12}(4d_{3/2})^1$; $(7i_{13/2})^8(4p_{3/2})^1$ configuration. That of Ir^{194} should possess the same configuration with the addition of two neutrons to the $7i_{13/2}$ subshell. Such a configuration leads readily to the desired 1^- state for Ir^{194}, but it is not easy to see how a 4^- state for Ir^{192} can be achieved. However, the difference in stability between the $6h_{11/2}$ and $4d_{3/2}$ shells is very small and it may be that in Ir^{192} the odd proton is in the $6h_{11/2}$ shell. Support for

[18] Gertrude Scharff-Goldhaber, Phys. Rev. **90**, 587 (1953).
[19] C. C. McMullen, Ph.D. thesis, McMaster University, Hamilton (unpublished).
[20] P. F. A. Klinkenberg, Revs. Modern Phys. **24**, 63 (1952).

this view is provided by the existence of a 1.5 min isomer of Ir^{192}.[1]

It would be expected that the first excited state of each of the three nuclides Os^{192}, Pt^{192}, and Pt^{194} has spin 2 and even parity. Experimental evidence for this exists from the K/L ratio of the 328-kev line in Ir^{194}.[17] Moreover, angular correlation studies[21,22] indicate that some of the higher levels in the Ir^{194} decay scheme also have spin 2, but at the time these experiments were performed the complex nature of the spectrum was not realized, so that the interpretation of these experiments is open to question.

[21] C. E. Whittle and P. S. Jastram, Phys. Rev. **87**, 203 (1952).
[22] J. J. Krauschaar and M. Goldhaber, Phys. Rev. **89**, 1081 (1953).

ACKNOWLEDGMENTS

The authors are indebted to Dr. G. T. Ewan and Dr. A. L. Thompson for permission to use their unpublished data on the decay of Au^{194} and to Dr. L. Yaffe for advice concerning the preparation of beta sources.

This work is supported by grants from the National Research Council of Canada and from the Research Council of Ontario.

PHYSICAL REVIEW VOLUME 96, NUMBER 6 DECEMBER 15, 1954

Internal Conversion in Ne^{22}†

R. D. Leamer and G. W. Hinman
Carnegie Institute of Technology, Pittsburgh, Pennsylvania
(Received September 3, 1954)

The internal conversion coefficient of the 1.28-Mev γ ray in Ne^{22} has been measured to determine its multipole character. It has been found to be $E2$. The spin and parity assignments to the Ne^{22} excited state and the Na^{22} ground state are discussed.

THE internal conversion coefficient of the 1.28-Mev gamma ray of Ne^{22} has been measured in order to determine the spin and parity of the 1.28-Mev excited state. Two methods were used to find the total conversion coefficient. One way, the least accurate, was to compare the area under the conversion peak with the area under the continuous spectrum. The second way was to compare the conversion coefficient of the neon gamma ray with that[1] of the 1.33-Mev gamma ray of Ni^{60}.

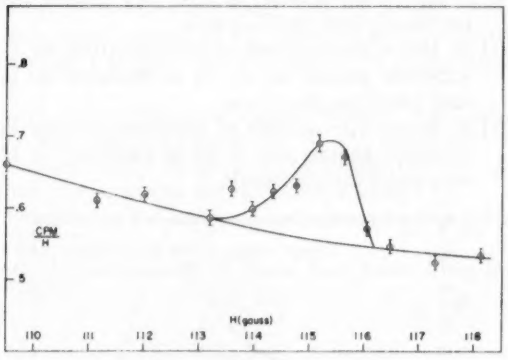

FIG. 1. Internal conversion peak of 1277-kev γ ray in Ne^{22}, source I.

The source used in method one (source I) was prepared from cyclotron produced Na^{22} obtained from Oak Ridge in the form of NaCl. The NaCl was deposited on a zapon film covered by a 0.1-mg/cm² layer of silver. The average thickness of the source was 4 mg/cm² but was not very uniform; the total source area was 10 cm² and the source strength one millicurie.

The data taken on the conversion peak are shown in Fig. 1. Actually several runs were made, but only the data with the best statistics are included in the plot. The curve drawn indicates a somewhat poorer resolution than is usual for the counter and baffle arrangement used. The line was broadened by the thick source. A

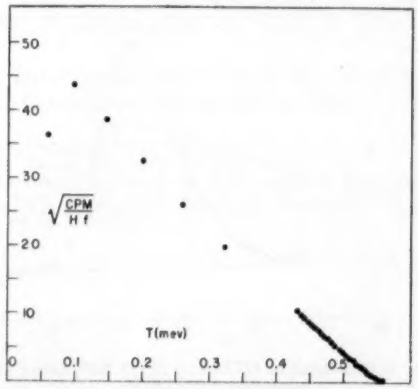

FIG. 2. Kurie plot of positrons from the decay of Na^{22}, source I, 4 mg/cm².

† This research was supported by the U. S. Army Office of Ordnance Research.
[1] C. Y. Fan, Phys. Rev. **87**, 252 (1952); Waggoner, Moon, and Roberts, Phys. Rev. **80**, 420 (1950).

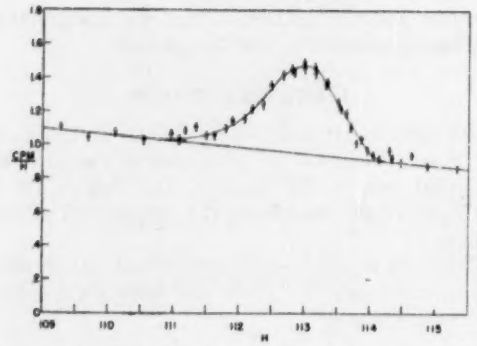

FIG. 3. Internal conversion peak of 1277-kev γ ray in Ne^{22}, source II; resolution, 1.22 percent. Open and closed circles indicate two different runs.

Kurie plot of the continuous positron spectrum is shown in Fig. 2. The number of low-energy positrons is too large because of the source thickness. Data taken on a thinner source showed a straight plot down to 170 kev. All deviations from straight Kurie plots are attributed to source thickness, for the spectrum is known to have an allowed shape.[2] For measurements of conversion coefficients a very thin source is not necessary, of course, for the area under the spectrum is the information desired.

By using the ratio of the area under the conversion peak to the area under the continuous spectrum, corrected for K capture, as the conversion coefficient, one obtains $\alpha_T=(0.85\pm0.20)\times10^{-5}$.

The second method for measuring the α_T is much more accurate. This work was done on a different source (source II) also obtained from Oak Ridge as NaCl. The NaCl was deposited in solution on a zapon film covered with an evaporated aluminum coat and a layer of insulin to increase uniformity. It was approximately 0.3 mg/cm² thick, 8 cm long, and 1.0 cm wide. The conversion peak and the photopeak of the 1.28-Mev gamma ray were measured several times and the areas under them calculated. Typical curves are shown in Figs. 3 and 4. The photoconverter used was lead 7.5 mg/cm² thick evaporated onto an aluminum plate.

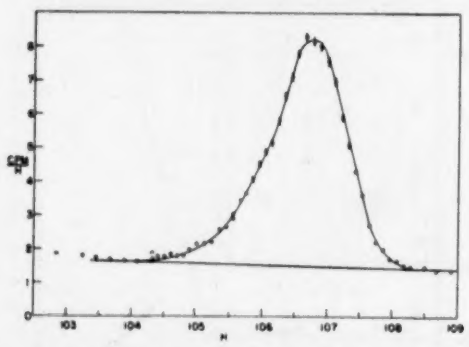

FIG. 4. Photopeak of 1277-kev γ ray of Ne^{22}, source II; resolution, 1.22 percent.

[2] Macklin, Lidofsky, and Wu, Phys. Rev. 78, 318 (1950).

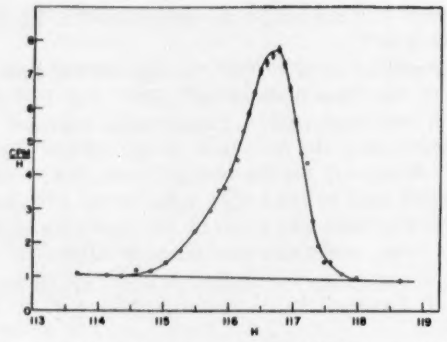

FIG. 5. Internal conversion peak of 1332-kev γ ray in Ni^{60}; resolution, 0.93 percent.

The conversion coefficient of the neon gamma ray was found by comparing its conversion and photopeak areas with those for the 1.33-Mev gamma ray of Ni^{60}, for which the α_T is known.[1] The cobalt source used in the comparison was similar in shape to the sodium source described above and was prepared in the same manner from a $CoCl_2$ source obtained from Oak Ridge. Its thickness was approximately 0.3 mg/cm². A typical conversion and photopeak for the nickel gamma ray are shown in Figs. 5 and 6.

In order to indicate how the α_T(1.28 Mev−Ne) was calculated, the following definitions are necessary:

N(1.28 Mev−Ne) = number of conversion electrons for the 1.28-Mev gamma ray of Ne as measured by the area under the conversion peak,

N(1.33 Mev−Ni) = number of conversion electrons for the 1.33-Mev gamma ray of Ni as measured by the area under the conversion peak,

I(1.28 Mev−Ne) = number of 1.28-Mev gamma rays per second from the Na source,

I(1.33 Mev−Ni) = number of 1.33-Mev gamma rays per second from the Co source,

P(1.28 Mev−Ne) = number of photoelectrons for the 1.28-Mev gamma ray of Ne as measured by the area under the photopeak,

P(1.33 Mev−Ni) = number of photoelectrons for the 1.33-Mev gamma ray of Ni as measured by the area under the photopeak,

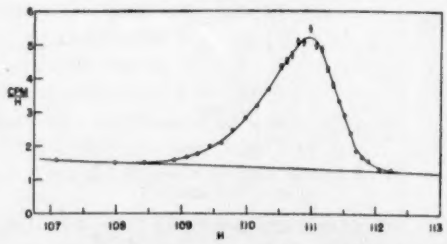

FIG. 6. Photopeak of 1332-kev γ ray of Ni^{60}; resolution, 1.14 percent.

$\sigma(1.28\ \text{Mev}-\text{Pb})$ = photoelectric cross section in lead at 1.28 Mev,
$\sigma(1.33\ \text{Mev}-\text{Pb})$ = photoelectric cross section in lead at 1.33 Mev.

The calculations then proceeded as follows, if one assumed, as was the case, that the source and instrument geometry were similar for the Co and Na:

$$\frac{N(1.28\ \text{Mev}-\text{Ne})}{N(1.33\ \text{Mev}-\text{Ni})}=\frac{\alpha_T(1.28\ \text{Mev}-\text{Ne})}{\alpha_T(1.33\ \text{Mev}-\text{Ni})}\frac{I(1.28\ \text{Mev}-\text{Ne})}{I(1.33\ \text{Mev}-\text{Ni})},$$

$$\frac{P(1.28\ \text{Mev}-\text{Ne})}{P(1.33\ \text{Mev}-\text{Ni})}=\frac{\sigma(1.28\ \text{Mev}-\text{Pb})}{\sigma(1.33\ \text{Mev}-\text{Pb})}\frac{I(1.28\ \text{Mev}-\text{Ne})}{I(1.33\ \text{Mev}-\text{Ni})}.$$

Eliminating the I's yields

$$\frac{\alpha_T(1.28\ \text{Mev}-\text{Ne})}{\alpha_T(1.33\ \text{Mev}-\text{Ni})}=\frac{N(1.28\ \text{Mev}-\text{Ne})}{N(1.33\ \text{Mev}-\text{Ni})}\times\frac{P(1.33\ \text{Mev}-\text{Ni})}{P(1.28\ \text{Mev}-\text{Ne})}\frac{\sigma(1.28\ \text{Mev}-\text{Pb})}{\sigma(1.33\ \text{Mev}-\text{Pb})}. \quad (1)$$

In order to find $\alpha_T(1.28\ \text{Mev}-\text{Ne})$ it is necessary to know the σ's and the conversion coefficient for the Ni gamma ray. Waggoner, Moon, and Roberts[1] give $\alpha_T(1.33\ \text{Mev}-\text{Ni})=(1.286\pm0.035)\times10^{-4}$ and Fan reports it to be $(1.24\pm0.12)\times10^{-4}$. An interpolation of the recent shielded K_1 and L_I coefficients of Rose *et al.*[3] gives a value $\alpha_T(1.33\ \text{Mev}-\text{Ni})=1.24\times10^{-4}$, but this value is possibly a few percent off because the coefficients for L_{II}, L_{III}, M_I, etc., could only be estimated (they were assumed to total 0.03 of the K-shell coefficient). After considering the measured and calculated values, $\alpha_T(1.33\ \text{Mev}-\text{Ni})$ was taken to be $(1.26\pm0.03)\times10^{-4}$.

The photoelectric cross sections required were taken from the paper of Davisson and Evans.[4] No correction was made for any variation in the angular distribution of the photoelectrons but this effect is small.

Substituting the measured and calculated quantities into the equation (1), $\alpha_T(1.28\ \text{Mev}-\text{Ne})=(6.74\pm0.67)\times10^{-6}$, where $\pm0.67\times10^{-6}$ indicates our estimate of twice the standard deviation of the result arising from all known errors.

TABLE I. Total shielded internal conversion coefficients for Ne^{22}.

Multipole order	Electric (α_T)	Magnetic (α_T)
1	3.32×10^{-6}	4.97×10^{-6}
2	6.59×10^{-6}	9.3×10^{-6}
3	12.2×10^{-6}	17.0×10^{-6}

The theoretical conversion coefficients, with which the experimental value is to be compared, have been calculated using the calculations of Rose as a base. It is known that for light elements and high-energy gamma rays the conversion coefficient depends approximately only upon the value of the initial state electron wave function at the origin.[5] This fact makes possible a correction to the α_K calculated by Rose, which neglects shielding, to take account of the shielding and also to include α_{LI}. The coefficients α_{LII}, α_{LIII} are neglected as the wave function at the origin is zero for p electrons. The calculation of α_{LI} is exactly the same as that for α_K except that the $2S$ wave function rather than the $1S$ is used. Thus,

$$\alpha_T(\text{shielded})=\alpha_K(\text{unshielded})\times\left[\left(\frac{\psi_{1S}(\text{shielded})}{\psi_{1S}(\text{unshielded})}\right)^2+\left(\frac{\psi_{2S}(\text{shielded})}{\psi_{1S}(\text{unshielded})}\right)^2\right].$$

Excellent values for ψ_{1S} and ψ_{2S} are available[6] for Ne. Using them, $\alpha_T(\text{shielded})=0.967\alpha_K(\text{unshielded})$. The values of $\alpha_T(\text{shielded})$ for various multipole orders of radiation are listed in Table I, from which it is clear that the radiation is $E2$. This makes the 1.28-Mev level of Ne^{22} a $2+$ state if the ground state is $0+$.

A considerable amount of information[7] has been gathered on the decay of Na^{22} which can be of assistance in classifying the Na^{22} ground state. The spin is known to be 3 and the parity is most probably plus although this makes the β^+ transition allowed and leaves the problem of understanding the large ft value ($\log ft=7.6$).

The authors would like to thank Mr. David Brower for help in taking part of the data on Na^{22}.

[3] Rose, Goertzel, and Swift (unpublished).
[4] C. M. Davisson and R. D. Evans, Revs. Modern Phys. **24**, 79 (1952).
[5] G. W. Hinman (to be published).
[6] F. W. Brown, Phys. Rev. **44**, 214 (1933).
[7] See review article by P. M. Endt and J. C. Kluyver, Revs. Modern Phys. **26**, 95 (1954). See also R. Sherr and R. H. Miller, Phys. Rev. **93**, 1076 (1954).

K-Electron Ejection in the Beta Decay of S^{35}*

WILLIAM RUBINSON AND J. J. HOWLAND, JR.†
Department of Chemistry, Brookhaven National Laboratory, Upton, New York

(Received September 3, 1954)

By means of proportional-counter pulse-height analysis, it is found that S^{35} sources emit K photons of chlorine with a probability of $2.47(\pm 0.6)\times 10^{-4}$ photon/beta (the indicated error being an extreme), equivalent to a probability for K-hole production of $2.3(\pm 0.7)\times 10^{-3}$ K hole/beta. The theory, which has about the same accuracy as the experiments, predicts 3.0×10^{-3} K hole/beta.

I. INTRODUCTION

IN continuation of experimental studies at this laboratory[1,2] on the transitions suffered by an extranuclear electron of an atom when the nucleus undergoes radioactive transformation, we have investigated the case of K-electron ejection in the beta decay of S^{35}.

The apparatus and the general procedure for such measurements are described at length in reference 1. By means of a proportional counter and pulse-height analyzer, one makes a pulse-height analysis of the photon spectrum emitted from a source at known geometry and of known radioactive disintegration rate, establishes that the photons under study are characteristic x-radiations of the daughter atom, and makes appropriate corrections on the observed rate of emission of these photons to obtain their total emission rate. This total emission rate is divided by the radioactive disintegration rate of the source to give the "photon yield," i.e., the probability, per decay, of emission of the x photon in question. Then the probability of electron ejection from the shell in question is the photon yield divided by the appropriate fluorescence yield.

In the case of beta emitters, the x-ray peaks are superposed on a relatively intense bremsstrahlung background which varies considerably with energy, so that special consideration must be given to background subtractions.

II. PREPARATION OF THE S^{35} SOURCES

Source strengths of about a millicurie are required for convenient photon counting rates. There are rather stringent requirements on the isotopic and chemical purity of the sources for two reasons:

(1) Absorption of Cl K photons in the source. If the S^{35} atoms are distributed uniformly through a disk of S^{32} atoms 200 $\mu g/cm^2$ thick, then, since the absorption coefficient of sulfur for Cl $K\alpha$ photons (2.63 kev) is[3] 1800 cm^2/g, some 25 percent of the Cl radiations will be absorbed in the source.

(2) Excitation of atoms in the source by beta particles. Any isotopic or chemical contaminant in a source is under beta bombardment, and so may be excited to x-ray emission. If the contaminant is sulfur or chlorine, the cross section for ejecting a K electron from a contaminant atom by an incident beta of 65-kev energy ($\sim$ the mean energy of a S^{35} beta) is about 1200 barns, as computed from a theoretical formula deduced by Bethe.[4] The corresponding total cross section for a disk of contaminant 200 $\mu g/cm^2$ thick is about 10^{-3} cm^2, i.e., the probability, per beta, of creating a K hole in some disk atom is $\sim 10^{-3}$. Since 10^{-3} is also the order of magnitude of the probability that a S^{35} decay results in a Cl^{35} with a K hole (see Sec VI below), the K x-ray spectrum from such a contaminated source consists of a superposition of Cl K x-rays from S^{35} decay and contaminant K x-rays from excitation by betas, the intensities of the two being approximately equal. Indeed, this is just what we have observed with a 5-mC S^{35} source containing 1000 S^{32} atoms per S^{35} atom, and 0.5 cm^2 in area.[5]

S^{35} sources of adequate strength and purity were prepared as follows: Mallinckrodt Reagent Grade KCl which, according to its label, contains less than 20 parts per million of sulfate, was recrystallized twice from doubly distilled water, and then volatilized in vacuum at 1050° (quartz tube). This treatment reduced the sulfate content by a factor of at least 30, as shown by the use of S^{35} tracer. The purified KCl was ground finely in a Pyrex mortar, and a 5-gram quantity of it, in an atmosphere of 5 cm of O_2, was sealed into a quartz ampoule provided with a breakseal.[6] Two such ampoules were made, one of which was irradiated for five days, and the other for ten days, at the center of the Brookhaven reactor. An irradiated ampoule was placed in a quartz tube on a vacuum line, and opened

* Research carried out under the auspices of the U. S. Atomic Energy Commission.

† Present address: University of California Radiation Laboratory, Livermore, California.

[1] W. Rubinson and W. Bernstein, Phys. Rev. **86**, 545 (1952).

[2] J. A. Miskel and M. L. Perlman, Phys. Rev. **94**, 1683 (1954).

[3] Interpolation of data tabulated in A. H. Compton and S. K. Allison, *X-rays in Theory and Experiment*" (D. Van Nostrand Company, Inc., New York, 1935).

[4] See N. F. Mott and H. S. W. Massey, *The Theory of Atomic Collisions* (The Clarendon Press, Oxford, 1949), second edition, p. 243.

[5] Before realizing the magnitude of this effect, we permitted quotation (references 14 and 16) of measurements that were high by a factor of 2.

[6] W. Koski and V. W. Cohen gave us the essentials of this recipe for extracting S^{35} from neutron-irradiated KCl.

in vacuo by means of a magnetic hammer sealed in quartz. The tube was then heated at about 1050° for several hours, under which treatment the KCl volatilizes out of the ampoule to deposit on a six-inch section of the tube immediately above the furnace, while the S^{35} compound of unknown composition (perhaps SO_2 or $SOCl_2$) diffuses through some three feet of glass tubing wound into a coil of three turns, and is finally caught in a U tube at liquid-air temperature. The U tube was then sealed off the vacuum line, and its invisible contents were taken up in 2 ml of $1N$ HNO_3 (prepared with doubly distilled water). This constituted a S^{35} stock solution containing about 20 mC, or about 10^{-8} mol, of S^{35} (about half the S^{35} initially in the irradiated KCl). When an aliquot of stock solution was evaporated to dryness to prepare a source, traces of impurity in the solvent sufficed to provide the necessary cations.

Stock solutions were assayed by evaporating 10λ of a 10^4 dilution on a backing of aluminized "Mylar" 700 $\mu g/cm^2$ thick, and counting in a 4π counter.[7]

A source was prepared by evaporating under a heat lamp a 100λ pipette-full (~1.5 mC of S^{35}) of the stock solution plus a pipette-full of $1N$ HNO_3 wash in a clean, polished polystyrene cup $\frac{3}{8}$ inch in diameter and $\frac{1}{8}$ inch deep.

III. EXPERIMENTAL ARRANGEMENT

This is shown schematically in Fig. 1. The source sits at the bottom of a well in a polystyrene block in a 3000-gauss magnetic field, where the radius of curvature of a maximum energy S^{35} beta (167 kev) is ~5 mm. The geometry for photon detection is defined by a hole of $\frac{1}{4}$-inch diameter in a diaphragm of $\frac{1}{32}$-inch thick aluminum located 1.70 inches above the source. The photons pass into the counter through an 18 mg/cm^2 Be window, in which about half the Cl K photons are absorbed. Since 70 percent of Cl K photons are absorbed in a 1.70-inch air path, the space between source and

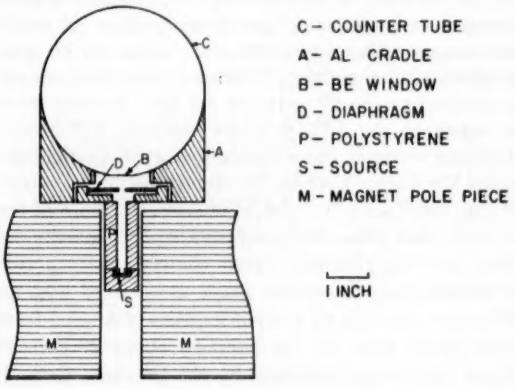

FIG. 1. Experimental arrangement.

[7] 4π counting of S^{35} on a 700 $\mu g/cm^2$ backing requires a 12 percent correction for absorption of betas in the backing, according to R. C. Hawkings of Chalk River (private communication).

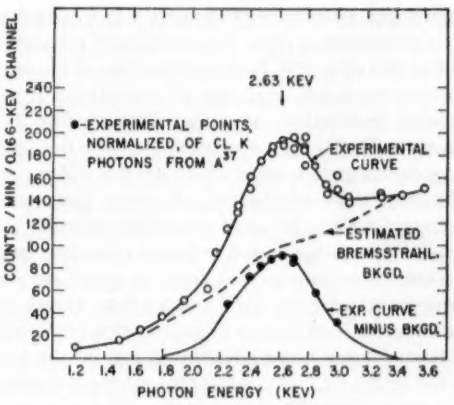

FIG. 2. Photons from S^{35}.

counter window was kept filled with helium. The counter gas for these experiments consisted of 9 parts of Kr and 1 part of CH_4 at a total pressure of 1 atmosphere. The counter pulses were amplified to about 30 volts, and a channel-width of 1.55 volts was used for the pulse-height analysis.

IV. PROOF THAT THE PHOTONS ARE K X-RAYS OF CHLORINE

One of our experimental curves, obtained with a S^{35} source of strength 3.9×10^9 dis/min, is shown in Fig. 2. The dotted line is an estimated bremsstrahlung background (see below). The difference peak obtained by subtracting the estimated bremsstrahlung background from the experimental curve coincides in energy with the Cl $K\alpha$ peak from an A^{37} (K-capture) source,[8] as shown in Fig. 2, where the counting rates observed with the A^{37} source, normalized to have the same peak-maximum rate as the difference peak, are entered as black circles. Now, the energy coordinate of the difference peak is very insensitive to the particular bremsstrahlung background one assumes, so long as the latter is not completely fantastic. For instance, by making extreme assumptions about the shape of the bremsstrahlung background one can vary the height of the difference peak by a factor of three without changing the energy coordinate by as much as one percent. This, together with the fact that the K x-ray energies of elements adjacent to Cl differ from the K x-ray energy of Cl by more than 10 percent, suffices to establish that the photons under study are Cl K photons.

The possibility that these photons arose from excitation under beta bombardment of Cl impurity in the source or source mount is eliminated by the following considerations.

In view of the method of source preparation, any chloride in the source would be accompanied by at least

[8] We are indebted to J. A. Miskel and M. L. Perlman who prepared the A^{37} for us by the method described in reference 2.

an equivalent amount of potassium, which would give rise to potassium x-rays. No significant intensity of the latter was observed. In the preparation of the second of our two stock solutions, the S^{35} was subjected to an additional distillation, at about 200°, before being taken up in HNO_3. The sources made from this second stock solution gave spectra which did not differ significantly from those of the first. A source prepared by deliberately adding 50 μg of potassium chloride to an aliquot of S^{35} stock solution before evaporation gave a potassium x-ray intensity at least as great as, and a chlorine x-ray intensity little greater than, the chlorine x-ray intensity from a clean S^{35} source. From the slightly increased chlorine x-ray intensity shown by the source with the added KCl we can infer that in the preparation of this source about 80 percent of the added chloride was fumed off (as HCl) by the HNO_3 of the S^{35} stock solution. By comparing the magnitude of the potassium x-ray intensity of this source with that from the clean sources we can estimate that the clean sources certainly contained less than 5 μg of potassium and therefore, in view of chloride fume-off, less than one microgram of chloride. By Bethe's theory (see reference 4) we compute that such a small quantity of chloride would make a completely negligible contribution to the observed chlorine photon intensity.

The possibility of chlorine in the polystyrene of the source mount is eliminated by the fact that no chlorine photons were observed when the S^{35} sources were replaced by an identically mounted source of C^{14} (as Li_2CO_3, 20 mg/cm^2 thick), which has a beta energy about the same as that of S^{35}.

Thus, all the Cl K photons from our S^{35} sources must be attributed to K holes in the Cl daughter atoms of S^{35} decay.

V. MEASUREMENT OF THE PHOTON YIELD

The computed intensity of Cl K photons depends very sensitively, of course, upon the estimate of bremsstrahlung background. Now, in the case of both internal[9] and external[10] bremsstrahlung the photon intensity per unit range of photon energy increases somewhat faster than the inverse of the photon energy. The mass absorption coefficients of polystyrene and the Be window increase exponentially as the photon energy decreases. For the photon energy range of concern here, in the neighborhood of 2.5 kev, both bremsstrahlung intensity and photon absorption increase very rapidly with decrease of photon energy, and it would be an exceedingly tedious task to make an accurate theoretical calculation of the resultant bremsstrahlung spectrum seen by the counter. We have made rough calculations of this kind which serve as a rough verification of our estimated bremsstrahlung spectrum, and have avoided an accurate computation by the following empirical approach.

The bremsstrahlung background must be such that on subtracting it from the experimental curve the resulting difference peak has the same shape as the clean Cl peak observed with an A^{37} source. This single consideration serves to fix the bremsstrahlung background with considerable accuracy, because the half-width and the symmetry of the difference peak are very sensitive to the shape and magnitude of the bremsstrahlung background assumed. Thus, to analyze an experimental curve one needs only to try different background curves until a Cl peak of correct shape is obtained. The agreement between a Cl peak obtained in this way and a clean Cl peak from A^{37} can be seen in Fig. 2.

The five sources used in our measurements, including those prepared from the same stock solution, gave experimental curves whose background intensities at energies above 2.8 kev differed as much as 30 percent, though the curves were essentially superposable at lower energies. We cannot explain this. However, with the method of estimating bremsstrahlung background described above, the Cl x-ray intensities obtained with the different sources were all in reasonable agreement (see Table I).

TABLE I. Photon yield in S^{35} decay.

Source	Date	Photon rate (photons/min)	Source strength dis/min	Photon yield
I-B	1 June 54	1.12×10^6	4.04×10^9	2.77×10^{-4}
I-A	3 June	0.93	3.98	2.34
I-D	8 June	1.23	4.37	2.81
II-A	31 May	0.79	3.90	2.03
II-A	3 June	0.815	3.81	2.14
II-B	14 June	0.96	3.49	2.75
				Mean $=2.47\times10^{-4}$

This method of subtracting the bremsstrahlung background may be compared to another in which the bremsstrahlung spectrum was taken to be that obtained with the thick C^{14} source mentioned above, normalized to the S^{35} curve at 3.4 kev. Account must be taken of the fact that the observed C^{14} bremsstrahlung curve is considerably distorted, particularly in the low energy portion, by absorption in the source. In the case of several of the S^{35} sources, the shape of the Cl x-ray peak obtained by subtracting this background from the experimental curve showed unacceptable deviations from the known shape as obtained with an A^{37} source, and the Cl x-ray intensities computed from these peaks were, on the average, about 20 percent higher than those obtained by the previous method. We consider the previous method to be much the more accurate of the two. However, the C^{14} bremsstrahlung curve was of considerable help in finding the correct background curve. It was the C^{14} curve that suggested

[9] See, e.g., J. K. Knipp and G. E. Uhlenbeck, Physica **3**, 425 (1936).

[10] W. Heitler, *The Quantum Theory of Radiation* (Oxford University Press, London, 1944), p. 166.

the bremsstrahlung hump in the neighborhood of the chlorine peak (see Fig. 2).

Table I shows the data and results of six runs with five different S^{35} sources made from two independently prepared and assayed S^{35} stock solutions. The geometry for photon detection, as defined by a $\frac{1}{4}$-inch diameter hole located 1.70 inches from an effectively point source, was 1.35×10^{-3}, and 0.517 of the Cl photons were absorbed in the Be window. Thus, the total photon rate was 1.43×10^{3} times the observed rate. Reproducibility of results with a single source can be seen from the two runs with source *II-A*, made on different days, which agree to better than 5 percent.

The mean photon yield computed from the six runs is: Cl K photons/beta $=2.47\times10^{-4}$. The standard deviation of a single measurement is 14 percent of the mean, so that the 99:1 probable error is about 25 percent of the mean. The spread of the results is 31.6 percent of the mean.

The measured[11] fluorescence yield of a Cl K hole is 0.108, with limits of error stated as 15–20 percent. Thus, the probability of K-hole production in S^{35} decay is: K holes/beta $=2.29\times10^{-3}$, with an extreme error of about 32 percent.

VI. COMPARISON WITH THEORY

The theory of the process involved here has been the subject of fairly extensive study,[12–17] and is well understood. In the act of β decay, the nuclear charge increases by one unit in a time that is short compared to the orbital periods of the bound electrons if (as is true of S^{35}) the orbital electron speed is very much smaller than the beta speed. In this case, the decay act is a "sudden" perturbation on the electronic eigenfunctions, so that the probability for transition of an electron from a given bound state of the parent atom to a given bound or continuum state of the daughter atom is, by standard theory, simply the square of the overlap integral of the eigenfunctions of the two states. Then the total probability of ejection of an electron from a given initial state can be obtained by computing the distribution of probability over all final states, and summing. But if, as is the case in our experiments, the distribution of ejected electrons over the final states is of no interest, the probability of creation of a hole in a shell is much more easily computed by way of the completeness theorem, as is done by both Levinger[14] and Schwartz,[15] whose results obtained with the use of non-relativistic hydrogenic wave functions are identical.[18] In this method one computes the probability, P_0, that an electron initially in, say, a $1s$ state of the parent atom remains a $1s$ electron of the daughter atom. Then the probability that the electron does *not* remain a $1s$ electron, i.e., the probability of K-hole creation, is $1-P_0$ minus the sum of the probabilities of transitions to otherwise allowed states that are excluded by the Pauli principle.

Taking account of the fact that the $2s$ and $3s$ states in Cl are occupied and of the existence of two $1s$ electrons in the initial state of S^{35}, we get from tables in the cited papers:

$$(K \text{ holes/beta})_{\text{theor}}=0.78/Z^2,$$

where Z is an effective nuclear charge appropriate to the hydrogenic wave functions used.

The theory does not distinguish between the nuclear charges of the parent and daughter nuclei. As the appropriate nuclear charge we choose $Z=16.2$, which is the mean nuclear charge of S and Cl, minus the shielding effect of 0.3 unit charge that K electrons have for each other. With this choice, the theoretical probability of K-hole creation in S^{35} decay is

$$(K \text{ holes/beta})_{\text{theor}}=2.97\times10^{-3},$$

about 30 percent higher than our experimental value, 2.29×10^{-3}. The agreement between experiment and theory is quite satisfactory since the experimental error is about 35 percent, and since the use of hydrogenic wave functions in the theory may be expected to introduce an error of about the same magnitude.

We point out that the probability of K-hole production in P^{32} decay (1.7-Mev maximum beta energy), which should be about the same as that in S^{35} decay, has been found by Renard[19] to be 4.23×10^{-3}, about 25 percent higher than the theoretical value computed in the above manner.

[11] A. Haas, Ann. Physik **16**, 473 (1933).
[12] E. L. Feinberg, J. Phys. (U.S.S.R.) **4**, 423 (1941).
[13] A. Migdal, J. Phys. (U.S.S.R.) **4**, 449 (1941).
[14] J. S. Levinger, Phys. Rev. **90**, 11 (1953).
[15] H. M. Schwartz, J. Chem. Phys. **21**, 45 (1953).
[16] H. Primakoff and F. T. Porter, Phys. Rev. **89**, 930 (1953).
[17] P. Benoist-Gueutal, Ann. phys. **8**, 593 (1953).

[18] We do not use the results that Levinger (reference 14) has obtained with Hartree functions, since he believes them to be in error.
[19] G.-A. Renard, Compt. rend. **238**, 1991 (1954).

Fission Yield of Gd^{159} and Tb^{161}

HENRY G. PETROW* AND GREGORY ROCCO
Tracerlab, Boston, Massachusetts
(Received August 26, 1954)

Normal uranium, irradiated with thermal neutrons, has been examined for the presence of Gd^{159} and Tb^{161}. Both isotopes were found and their fission yields measured. For purposes of calibration, the yields for Sm^{153} and Eu^{156} have also been determined. The chemical separations were made using a combination of ion exchange and extraction techniques.

RECENTLY, the formation of Gd^{159} (18 hr), and Tb^{161} (7.0 days) in uranium fission has been reported.[1] Similar work was proceeding independently in this laboratory at the time, and since no fission yields of gadolinium or terbium were published, their determination was undertaken.

Two 0.43-gram samples of U_3O_8, I-1, and I-2, were irradiated for 7 days in the Oak Ridge reactor at 50 percent maximum flux. Besides the gadolinium and terbium measurements, the fission yields of Sm^{153} (46.8 hours) and Eu^{156} (15.4 days) were also determined for calibration purposes. All values were calculated on the basis of a Mo^{99} thermal fission yield of 6.2 percent.[2] The values obtained are listed in Table I.

The chemical purification consisted, briefly, of the following steps:

To an aliquot containing at least 5×10^{14} fissions, 10 mg each of the four rare earths were added. Samarium and europium were extracted with sodium amalgam from an acetate-acetic acid buffer. The samarium and europium were then separated from each other, and from the 60 percent of the Np^{239} that was also extracted, on a 45-cm column of 200–400 mesh, ammonium form Dowex 50-X4, 0.9 cm^2 in area, and maintained at 80°C. The elutriant, 4.25 percent lactic acid, *p*H 3.42, was passed through the bed at 30 ml/hour. The terbium and gadolinium were separated from each other, as well as from yttrium and the other rare earths, on an identically operated column. The elution pattern for the four rare earths and yttrium is plotted in Fig. 1.

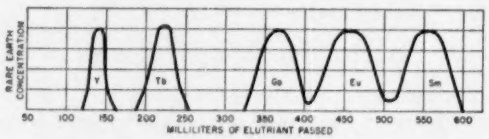

FIG. 1. The elution of rare earths from Dowex 50-X4 with 4.25 percent lactic acid, *p*H 3.42, at 80°C.

TABLE I. percent fission yields.

Isotope	I-1	I-2
Sm^{153}	1.3×10^{-1}	1.3×10^{-1}
Eu^{156}	1.2×10^{-2}	1.2×10^{-2}
Gd^{159}	1.1×10^{-3}	1.0×10^{-3}
Tb^{161}	7.4×10^{-5}	7.1×10^{-5}

In actual practice, of course, all five elements were not eluted from the same column.

All samples were counted on an aluminum end-window proportional-flow counter. The counting rates were corrected for self absorption, scattering, and for air and window losses. The instrument's geometry was assumed to be identical for all samples being counted since all mounts were of the same dimensions.

Finally, no allowances were made for the possible presence of gadolinium impurity in the uranium except that prior to the irradiation, reagent grade uranium was subjected to several purification steps designed to remove trace quantities of rare earths.

* Now at National Lead Company, Inc., Winchester, Massachusetts.

[1] E. C. Freiling and L. R. Bunney, J. Am. Chem. Soc. **76**, 1021 (1954).

[2] Finkle, Hoagland, Katcoff, and Sugarman, *Radio Chemical Studies: The Fission Products* (McGraw-Hill Book Company, Inc., New York, 1951), Paper No. 96, National Nuclear Energy Series, Plutonium Project Record, Vol. 9, Div. IV.

Excitation Functions for Nitrogen-Induced Nuclear Reactions in Carbon

H. L. REYNOLDS AND A. ZUCKER
Oak Ridge National Laboratory, Oak Ridge, Tennessee
(Received August 19, 1954)

The excitation functions for the reactions $C^{12}(N^{14},2p)Na^{24}$, $C^{12}(N^{14},\alpha)Na^{22}$, and $C^{12}(N^{14},2\alpha)F^{18}$ were measured with the external 29-Mev nitrogen beam of the 63-inch cyclotron. Thick-target yields as a function of energy were differentiated to obtain absolute cross sections from 16 to 29 Mev. A similarity to the excitation functions for reactions produced by protons on Mg^{25} is suggested.

A RECENT survey[1] of reactions produced by bombarding a number of light elements in the internal nitrogen beam of the 63-inch cyclotron at the Oak Ridge National Laboratory disclosed reactions such as $N^{14}(N^{14},N^{13})N^{15}$ in which only one nucleon is exchanged between participating nuclei. Another type of reaction, such as $C^{12}(N^{14},2p)Na^{24}$, was observed in which the major part of the nuclear matter fuses.

Since this survey was made the 63-inch cyclotron beam has been deflected and a program has been initiated to investigate the mechanism of heavy-particle reactions. At present, the reactions investigated are only those leading to radioactive nuclei. The nitrogen-induced reactions observed in carbon are $C^{12}(N^{14},\alpha)Na^{22}$, $C^{12}(N^{14},2p)Na^{24}$, and $C^{12}(N^{14},2\alpha)F^{18}$. The half-lives of the beta activities were used in identifying the nuclides. These reactions may be compared to proton-induced reactions on Mg^{25} to see if the nitrogen-induced reactions proceed through the compound nucleus Al^{26}.

EXPERIMENTAL METHOD

Bombardments were made in the following manner. Carbon buttons $\frac{1}{16}$-in. thick and $\frac{7}{8}$-in. in diameter were placed in a motor-driven 12-position target holder which was rotated rapidly through the deflected beam of nitrogen ions (Fig. 1). Nickel foils, increasing in thickness by 0.5-mg/cm^2 steps, were placed in front of these individual targets to reduce the effective energy of the beam. In this way a large part of the energy spectrum was covered in one run. The energy of the initial deflected beam was measured[2] by observing the energy of recoil protons from a gas target at zero degrees. From the initial energy and from the range-energy relations for nitrogen ions in nickel,[2] it was then possible to calculate the energy of nitrogen ions striking each carbon target.

The carbon targets, together with the absorbers in front of them, were placed in eleven positions of the target holder. One position was left open for monitoring; each time the wheel rotated a pulse of current passing through the open hole was collected in a Faraday cup placed above the wheel. The Faraday cup was in the 2000-oersted fringing magnetic field. A vibrating reed current integrator was used to record the total number of particles passing through the hole. The integrator was calibrated with a battery and vacuum resistor to about two percent. Electron loss for the triply charged nitrogen ions before collection in the Faraday cup was negligible at the pressure in the target assembly. When compared with the uncertainties due to absolute beta counting current measurement errors may thus be considered unimportant.

At the end of a run the targets were placed in an automatic sample changer and the beta particles were counted with an end-window Geiger counter. The Geiger counter was calibrated with P^{32} and RaE sources of known intensity, obtained from the National Bureau of Standards. The RaE source had a thick backing of silver; the P^{32} source was placed on a thin plastic backing. The saturation backscattering correction was measured for the P^{32} sample with both silver and carbon backings. The value for silver agreed with that given by Burtt,[3] and the value obtained for carbon was 1.18. Burtt has shown that the saturation backscattering correction is essentially independent of the maximum beta-particle energy if it is above 0.5 Mev. The P^{32} and RaE calibrations agreed to within 5 percent and gave a beta counting efficiency of 8.25 percent for the geometry used. Window and air-absorption corrections were applied by standard methods while self absorption in the targets was neglected because of the short range of nitrogen ions.

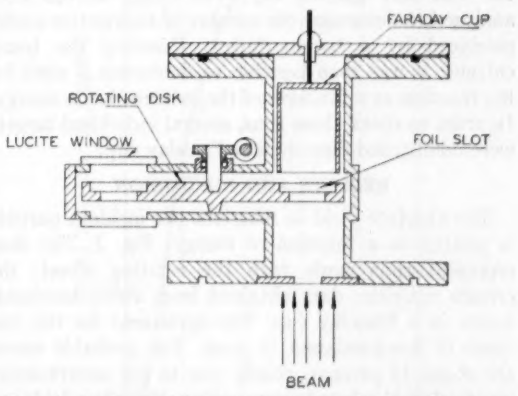

FIG. 1. Twelve-position rotating target holder. The beam emerges vertically from the cyclotron; the target holder rotates in the horizontal plane.

[1] Reynolds, Scott, and Zucker, Proc. Nat. Acad. Sci. **39**, 975 (1953).
[2] Reynolds, Scott, and Zucker, Phys. Rev. **95**, 671 (1954).
[3] B. P. Burtt, Nucleonics **5**, 28 (1949).

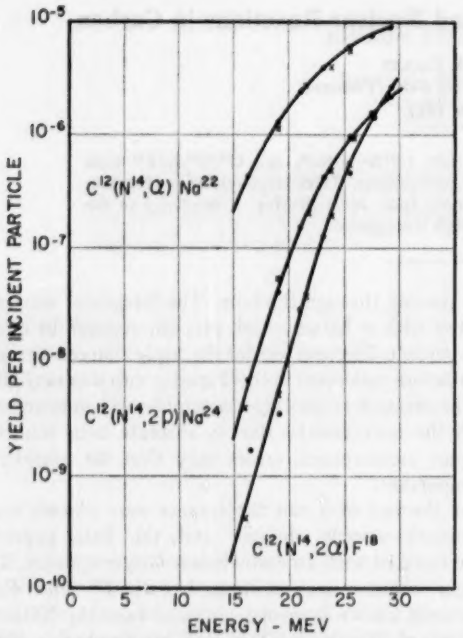

FIG. 2. Yield of nitrogen-induced reactions in carbon as a function of incident beam energy. The dots represent runs made with the rotating wheel; the crosses represent data obtained from direct bombardment in a Faraday cup.

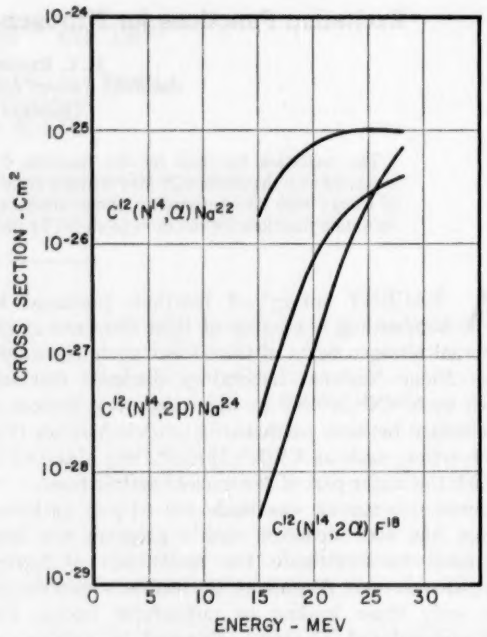

FIG. 3. Absolute cross sections for nitrogen-induced reactions in carbon as a function of nitrogen ion energy.

A correction for the K-capture branching in Na^{22} was applied.[4]

The activities observed in carbon were found to be due to F^{18}, Na^{24}, and Na^{22}, with half-lives of 112 minutes, 15 hours, and 2.6 years respectively. Chemical identification was not required since the few possible reaction products, after energy requirements were fulfilled, were widely separated in half-life. The decay curves were followed for several weeks until only the long-lived Na^{22} remained; it was identified by observing the 1.28-Mev gamma ray. The decay curves were analyzed to determine the number of radioactive nuclei produced by a bombardment. Knowing the beam current, it was then possible to determine a yield for the reaction as a function of the incident beam energy. In order to check these runs, several individual targets were bombarded directly in a Faraday cup.

RESULTS AND DISCUSSION

The absolute yield in reactions per incident particle is plotted as a function of energy, Fig. 2. The dots represent runs made with the rotating wheel; the crosses represent data obtained from direct bombardments in a Faraday cup. The agreement for the two types of bombardment is good. The probable errors are about 15 percent, chiefly due to the uncertainties involved in absolute beta counting. Relative yields are probably in error by less than 5 percent.

Smooth curves drawn through the points in Fig. 2 were differentiated to give the absolute cross sections as a function of energy, Fig. 3. Errors in the yield become very important when the slope of the yield curve is small. In this region the errors in the cross section are greatest because differentiation involves subtracting large numbers to get small differences. Subtraction of experimentally determined yields proved less reproducible than the differentiation of smoothly drawn yield curves. For the differentiation it is necessary to know the range of nitrogen ions in carbon. The range of nitrogen ions in aluminum was measured and it was found that this range can be computed from the range of nitrogen ions in nickel, by using the relative stopping power for protons[5] of equal velocities. From the relative stopping power for protons in carbon and nickel, the range of nitrogen ions in carbon was calculated.

The relative yield of F^{18} to Na^{24} produced in the bombardment of carbon varies rapidly with the energy of the nitrogen beam; at 26 Mev the relative yield changes by 30 percent for a 4 percent change in energy. Thus, a simple relative yield determination provides a good beam energy measurement if the initial energy spread is not large.

The excitation functions, Fig. 3, have an exponential rise, suggesting a barrier penetration at low energies. They exhibit marked similarities to proton-induced reactions in Mg^{25}. A detailed comparison of excitation functions for reactions produced by protons on Mg^{25} and nitrogen on carbon is made in the following paper.[6]

[4] R. H. Miller and R. Sherr, Phys. Rev. **93**, 1076 (1954).

[5] S. K. Allison and S. D. Warshaw, Revs. Modern Phys. **25**, 779 (1953).

[6] Cohen, Reynolds, and Zucker, following paper [Phys. Rev. **96**, 1617 (1954)].

Comparison of Nitrogen- and Proton-Induced Nuclear Reactions

B. L. COHEN, H. L. REYNOLDS, AND A. ZUCKER
Oak Ridge National Laboratory Oak Ridge, Tennessee
(Received August 19, 1954)

Excitation functions for $(p,2p)$, (p,α), and $(p,2\alpha)$ reactions on Mg^{25} were measured with the internal 22-Mev proton beam of the 86-inch cyclotron. The results are compared with the excitation functions obtained for the reactions produced by 29-Mev nitrogen ions on carbon in the 63-inch cyclotron. Both sets of reactions may proceed via the same compound nucleus, Al^{26}. After corrections for the barrier penetrations of the incident particles, the $(N,2p)$ and $(p,2p)$ results are quite comparable. The corrected (N,α) and $(N,2\alpha)$ cross sections are larger than those for the corresponding proton-induced reactions by factors of about two and four respectively, indicating that processes other than conventional compound nucleus formation are involved in these nitrogen-induced reactions. The shape of the excitation functions for the nitrogen-induced reactions indicates that the protons and alpha particles are emitted from nearly spherical nuclei with charge equal to that of the compound nucleus; direct interactions such as stripping are thus excluded.

IN order to study the nuclear reactions induced by energetic nitrogen ions on carbon reported in a preceding paper,[1] one can compare them with reactions induced by other particles forming the same compound nucleus, Al^{26}. Such a case is available in the bombardment of Mg^{25} with protons. The excitation functions involved, namely for (p,α), $(p,2\alpha)$, and $(p,2p)$, leading to Na^{22}, F^{18}, and Na^{24}, respectively, have been measured by Meadows and Holt[2] with 95-Mev protons, and the (p,α) excitation function has been measured by Batzel and Coleman[3] with 32-Mev protons. In each case, however, only a few points were obtained in the energy region below 30 Mev, and the accuracy is affected by straggling due to the energy degradation. Measurements of these cross sections were therefore undertaken with the 22-Mev protons in the internal beam of the 86-inch cyclotron at the Oak Ridge National Laboratory.

EXPERIMENTAL METHOD

The methods of measuring excitation functions and absolute cross sections have been described previously.[4] Natural magnesium metal foils approximately 25 mg/cm² thick were used as targets. The stopping power of magnesium relative to that of aluminum was measured, and no difference was found. In the beta counting of Na^{24} and F^{18} corrections for self absorption, backscattering, etc., were made by using the methods of Zumwalt.[5] The Na^{22} activity was counted on the 1.28-Mev gamma-ray peak with a scintillation spectrometer. The spectrometer efficiency relative to the beta counting efficiency of the Geiger counter was determined with a weightless Na^{22} source mounted on a thin backing. The Na^{24} and F^{18} activities were identified by their half lives and absorption characteristics. The Na^{22} activity was identified by its gamma-ray spectrum and by chemical means. However, since it was found that two weeks after the bombardment the Na^{22} activity was the only one of appreciable intensity for all incident proton energies, the chemical separations were not carried out routinely.

RESULTS

The excitation functions for the reactions $Mg^{25}(p,2p)Na^{24}$, $Mg^{25}(p,2\alpha)F^{18}$, and $Mg^{25}(p,\alpha)Na^{22}$ are shown in Figs. 1–3. The absolute cross sections were calculated by assuming that the activities are due to Mg^{25} only. In the first two reactions there is every indication that this is the case. For Na^{22}, however, the rise beginning at about 19 Mev is due to the $(p,\alpha n)$

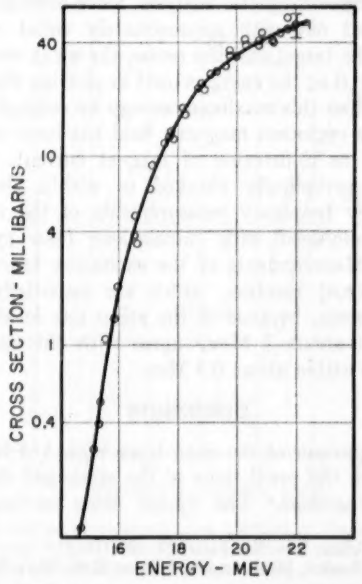

FIG. 1. Excitation function for $Mg^{25}(p,2p)Na^{24}$ as a function of incident beam energy.

[1] H. L. Reynolds and A. Zucker, preceding paper [Phys. Rev. **96**, 1615 (1954)].
[2] I. W. Meadows and R. B. Holt, Phys. Rev. **83**, 1257 (1951).
[3] R. E. Batzel and G. H. Coleman, Phys. Rev. **93**, 280 (1954).
[4] B. L. Cohen *et al.*, Phys. Rev. **94**, 620 (1954); G. H. McCormick and B. L. Cohen, Phys. Rev. **96**, 722 (1954).
[5] L. R. Zumwalt, U. S. Atomic Energy Commission Report MDDC-1346 (unpublished, 1947).

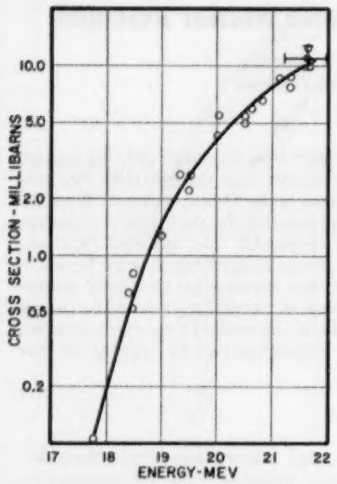

FIG. 2. Excitation function for $Mg^{25}(p,2\alpha)F^{18}$ as a function of incident beam energy.

reaction in Mg^{26} so that beyond that point this curve will not be used in the discussion to follow.

There is a serious discrepancy between the excitation function for $Mg^{25}(p,\alpha)Na^{22}$ and a similar measurement by Batzel and Coleman[5] whose excitation function, while similar in shape, is shifted to higher energy by approximately 3 Mev. It would be very difficult to explain this as being due to an error in the present measurements. The maximum energy of the cyclotron beam is limited by a probe placed at 180 degrees from the target so that the maximum orbit diameter, and thus the maximum energy on the target, is determined by 180 degree magnetic analysis. Since bombardments are carried out with approximately equal currents striking the target and the probe, the mean energy on the target (i.e., the energies used in plotting Figs. 1–3) is lower than this maximum energy by only about 0.3 Mev. The cyclotron magnetic field has been carefully measured as a function of magnet current, and its value is periodically checked to within about 0.2 percent by frequency measurements of the resonant system combined with calculations from cyclotron theory.[6] Measurements of the excitation function for the $Cu^{63}(p,n)$ reaction, which are essentially range measurements, because of the steep rise in the cross section at about 5 Mev,[7] agree with the calculated energy to within about 0.3 Mev.

DISCUSSION

A comparison of the data from Figs. 1–3 has been made with the predictions of the statistical theory of nuclear reactions.[8] The $(p,2p)$ cross sections were calculated by assuming the first proton to be emitted with the energy distribution for aluminum observed by Gugelot,[9] and by determining the total probabilities for emission of both the first and second protons (i.e., their probabilities relative to that of neutron or alpha emission) by the methods of Blatt and Weisskopf.[8] The (p,α) and $(p,2\alpha)$ cross sections were calculated by straightforward application of the formulas from Blatt and Weisskopf.[8]

In all cases the energy dependence of the experimental curves are in reasonable agreement with the theoretical predictions. The observed absolute values of the $(p,2p)$ cross sections are larger than the calculated values, by a factor of about three, but this discrepancy is perhaps understandable in view of the limitations of the theory for light elements. The maximum and the subsequent drop-off in the (p,α) excitation function are explained by the fact that proton emission following emission of alphas becomes energetically possible, so that the (p,α) reaction becomes a $(p,\alpha p)$ reaction. Theoretical calculations[4] indicate that the maximum should occur at about 15 Mev (quite independent of the nuclear temperatures assumed), which is in good agreement with the data from Fig. 3. The observed absolute values of the (p,α) cross section are smaller than the calculated values by a factor of three, but this again may be explained by the well known difficulties in the theory.

The $(p,2\alpha)$ cross section is at least ten times larger than predicted by statistical theory, but this is probably due to the fact that levels of very low excitation, for which the theory is inadequate, are of primary im-

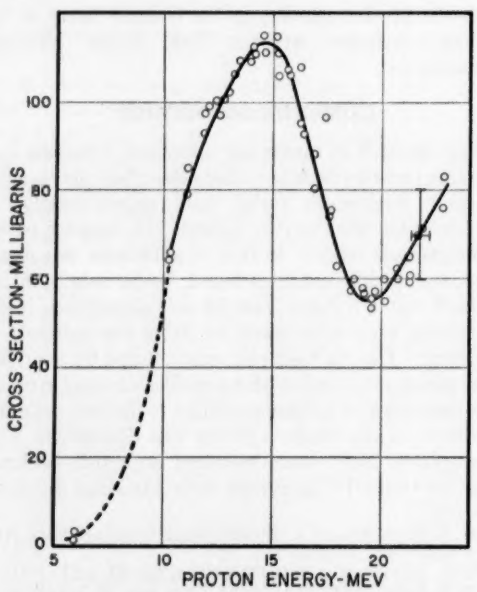

FIG. 3. Excitation function for $Mg^{25}(p,\alpha)Na^{22}$ as a function of incident beam energy.

[5] B. L. Cohen, Rev. Sci. Instr. **24**, 589 (1953).
[6] Blaser, Boehm, Marmier, and Peaslee, Helv. Phys. Acta **24**, 3 (1951).
[7] J. M. Blatt and V. F. Weisskopf, *Theoretical Nuclear Physics* (John Wiley and Sons, Inc., New York, 1952).
[8] P. C. Gugelot, Phys. Rev. **93**, 420 (1954).

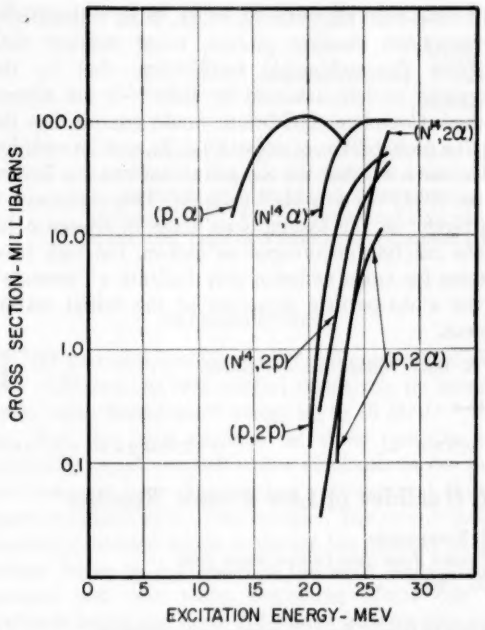

FIG. 4. Proton- and nitrogen-induced reaction cross sections as a function of the excitation energy of the compound nucleus.

portance in the calculation. From their very nature it seems natural to assume that $(p,2p)$, (p,α), and $(p,2\alpha)$ reactions are compound nucleus reactions, and there is nothing in these measurements to indicate that such is not the case.

The reactions produced by nitrogen on carbon may lead to the same compound nucleus, Al^{26}, as the above described reaction. The compound nucleus is excited to about the same degree for 22-Mev protons as for the 29-Mev nitrogen ions.[10] A comparison of excitation functions for proton- and nitrogen-induced reactions should indicate whether they proceed by the same mechanism. The proton- and nitrogen-induced reaction cross sections are given in Fig. 4 as a function of the excitation energy of the compound nucleus. Since the Coulomb barriers for these two sets of reactions are different, entrance barrier penetration considerations have been eliminated in the comparison by plotting the ratios of the observed cross sections to the theoretical total reaction cross sections. The resulting ratio is the probability of the decay of the compound nucleus through a given type of reaction. These ratios are plotted as a function of the excitation energy of the compound nucleus, Fig. 5. The theoretical total reaction cross section has been calculated in the usual manner by assuming a sticking probability of unity and by using the tables of penetrability given by Feshbach *et al.*[11]

It is apparent from Fig. 5 that the percentage of total cross sections for the reactions $(N,2p)$ and $(p,2p)$ are identical within the accuracy of the experiment. This strongly suggests that this nitrogen-induced reaction proceeds by a compound nucleus interaction. In the case of the reactions yielding one or two alpha particles, there is a similarity between the shapes of the corresponding excitation functions in Fig. 5. The energy dependence of the curves given in Fig. 5 should be determined primarily by exit Coulomb barrier penetration factors. The close correspondence between the shapes of these curves for the nitrogen- and proton-induced reactions thus indicates that the exit Coulomb barriers are essentially identical in the two cases. It therefore seems that some sort of compound nucleus is formed in the nitrogen-induced reaction. If the particles were emitted from C^{12} or N^{14} nuclei, or from a dumbbell-shaped structure consisting of these two in grazing contact, the exit Coulomb barriers would be much lower. For example, the barrier height in the 2α-emission reaction—the "knee" in the excitation function occurs at about this energy above the energetic threshold—is about 6 Mev higher for an Al^{26} nucleus than for a C^{12} or N^{14} nucleus. For the $2p$-emission

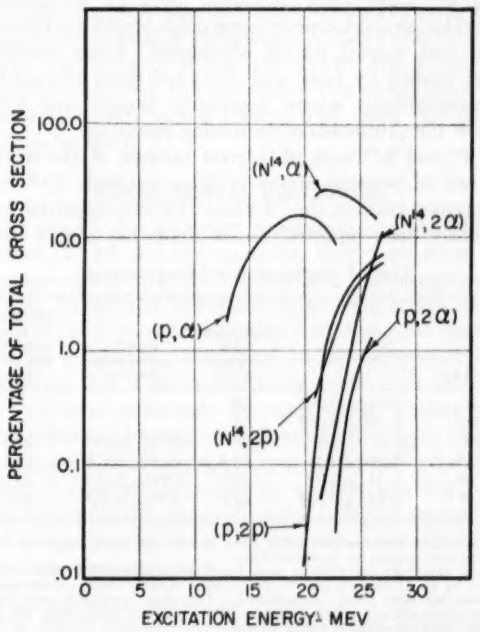

FIG. 5. Ratios of observed cross sections to theoretical total cross sections for proton- and nitrogen-induced reactions, plotted as a function of the excitation energy of the compound nucleus.

[10] Actually, the orbital angular momenta in the incident nitrogen ion beam are somewhat higher than in the proton case, so that some states of the compound nucleus with very large spin ($J \geqslant 6$) can be formed by the nitrogen ions but not by the protons. However, it is conventional to assume that the energy dependence of level densities at high excitation energies is independent of spin [e.g., reference 8, and S. N. Ghoshal, Phys. Rev. **80**, 939 (1950)], in which case the competition among the various modes of decay is not affected by spin.

[11] Feshbach, Shapiro, and Weisskopf, U. S. Atomic Energy Commission Report NYO-3077, 1953 (unpublished).

reaction the difference is about 4 Mev. In both cases the correspondence between the curves for the proton- and nitrogen-induced reactions in Fig. 5 is much too close to allow such a difference in exit barrier heights. It therefore seems that these nitrogen-induced reactions do not proceed by direct interactions of the "stripping"[12] or "buckshot"[13] type. It would seem rather that the particles are emitted from a conglomerate nucleus which has proceeded toward thermodynamic equilibrium, at least to the point of being nearly spherical in shape. Alpha and two-alpha emission is more probable, however, in the case of nitrogen reactions by a factor of two and four, respectively, which, in an undoubtedly oversimplified classical picture, could indicate that complete thermodynamic equilibrium—that is, the compound nucleus assumed by Bohr[14]—is not always reached. Complete equilibrium would require that the relative probabilities of decay by α, 2α, and $2p$ emission be the same whether the compound nucleus was formed by an N^{14}-C^{12} or a p-Mg^{25} collision. This statement is contingent on the assumptions made in reference 10. In the reaction of nitrogen on carbon, the high cross sections for alpha emission may indicate a "memory" of the alpha-particle structure of the initial carbon nucleus.

[12] J. R. Oppenheimer and M. Phillips, Phys. Rev. **48**, 500 (1935).
[13] Chackett, Fremlin, and Walker, Phil. Mag. **45**, 173 (1954).
[14] N. Bohr, Nature **137**, 344 (1936).

PHYSICAL REVIEW VOLUME 96, NUMBER 6 DECEMBER 15, 1954

Decay Characteristics of Some Short-Lived Nuclides of Low Atomic Number*

R. M. KLINE† AND D. J. ZAFFARANO
Institute for Atomic Research and Department of Physics, Iowa State College, Ames, Iowa
(Received August 20, 1954)

The short-lived activities in Cl^{34}, K^{38}, Ca^{39}, Li^8, He^6, and O^{15} formed by high-energy bremsstrahlung irradiation have been examined, and some improved values for the half-lives of these nuclides are reported.

THE half-lives of the isomeric states in Cl^{34} and K^{38}, as well as the half-lives of Ca^{39}, Li^8, He^6, and O^{15} have been measured with an anthracene scintillation spectrometer using pulse-height discrimination and special timing equipment. These nuclides were formed by (γ,n) and (γ,p) reactions induced by bremsstrahlung whose maximum energy was kept below the thresholds of competing reactions.

Cl^{34} and K^{38} were of interest because of the recent report[1] of isomeric states in these nuclides. Ca^{39} was of interest because the "ft value" for this transition has recently been reported[2] to be somewhat higher than the ft values for some of the other "mirror transitions." A comparison with previously observed values for Li^8, O^{15} and He^6 was of general interest.

TABLE I. Summary of half-lives measured.

Nuclide[a]	Half-life (sec)	Maximum beam energy (Mev)	Possible interfering reaction	Threshold for interfering reaction[b] (Mev)
Li^8	0.841±0.004	65	...	...
He^6	0.799±0.003	65	...	...
O^{15}	123.4 ±1.3	25	$O^{16}(\gamma,2n)O^{14}$	26.8
Ca^{39}	0.90 ±0.01	19.5	$Ca^{40}(\gamma,d)K^{38}$	17.6
Cl^{34}	1.53 ±0.02	22.0	$Cl^{35}(\gamma,2n)Cl^{33}$	23.8
K^{38}	0.935±0.025	22.0	$K^{39}(\gamma,2n)K^{37}$	24.0

[a] The first two nuclides listed were formed by (γ,p) reactions. The others were formed by (γ,n) reactions.
[b] All threshold calculations were based on semiempirical mass values given by N. Metropolis and G. Reitwiesner, Atomic Energy Commission Report NP-1980, 1950 (unpublished). The same thresholds calculated using semiempirical values given by W. H. Barkas, Phys. Rev. **55**, 691 (1939), give consistently higher values.

Since all the nuclides studied except O^{15} had half-lives of less than two seconds, a cyclic programming device which channeled the scintillation pulses into nine scalers in the time succession was used.[3] Bombardment and counting durations were adjustable and were controlled by a master clock operating cascaded stepping relays. The beam duration and counting periods were optimized for each measurement.

The essential results of this work are presented in Table I. In each case the accuracy is thought to be improved over previous measurements.

The authors would like to thank Dr. A. G. W. Cameron and Mr. Philip Phipps for valuable discussions and assistance.

* Work was performed in the Ames Laboratory of the U. S. Atomic Energy Commission.
† Now at Sperry Gyroscope Company, Great Neck, Long Island, New York.
[1] P. Stähelin, Helv. Phys. Acta **26**, 691 (1953).
[2] Hunt, Kline, and Zaffarano, Phys. Rev. **95**, 611(A) (1954).
[3] The detailed experimental equipment and procedure are described in Atomic Energy Commission Report ISC-510 (unpublished).

Comparison of H^3 and He^3 Production in High-Energy Deuteron-Deuteron Collisions*

CHARLES S. GODFREY
Radiation Laboratory, University of California, Berkeley, California
(Received August 30, 1954)

The relative production of H^3 and He^3 from deuteron-deuteron collisions at 190 Mev has been measured at 30° (center of mass). The method of detection required that the particles traverse a magnetic channel and a pulse-height counter telescope. The pulses were displayed on a fast cathode-ray oscilloscope and recorded photographically. A liquid deuterium target was employed. The comparison shows a ratio of H^3 to He^3 of 0.86 ± 0.14. These data support the hypothesis that charge symmetry of nuclear forces exists at high energy.

INTRODUCTION

THE production of H^3 and He^3 in deuteron-deuteron collisions has been studied extensively by investigators using deuterons of energy up to 10 Mev.[1-6] The fact that the cross sections for these particles are essentially equal (except where Coulomb forces predominate) has been considered as evidence that charge symmetry exists up to these energies. The term "charge symmetry" is used herein to denote the equality of *n-n* nuclear forces to *p-p* forces of the same angular momentum and spin state, neglecting effects due to Coulomb forces and mass differences between the particles. Many other data have been published which confirm this conclusion. Ajzenberg and Lauritsen[7] conclude from their studies of nuclear spectroscopy that charge symmetry of nuclear forces, insofar as it is manifested in low-lying energy states, can be regarded as an established fact. A study of the three-body stable nuclei[8] leads to the conclusion that the binding energies of H^3 and He^3 can be understood most simply under the assumption that charge symmetry exists for the ^1S state. Further evidence of charge symmetry can be inferred from low-energy scattering[9,10] data which indicate that the dineutron is probably just unbound and that the assumption of equal scattering lengths for *n-n* and *p-p* scattering in the ^1S state is not inconsistent with these data.

Evidence of charge symmetry at high energies, where many higher states, strong tensor forces and meson fields are expected to play important roles, is very meager. Yet all theoretical approaches to high-energy scattering assume its existence. The most conclusive evidence would of course be a comparison of high-energy *p-p* scattering with *n-n* scattering. Since targets of neutrons do not exist, however, one must turn to less direct methods. Evidence is available in a comparison of *n-d* and *p-d* scattering at the same energy. The width of available neutron spectrums, however, and the differences of experimental technique required to perform the experiments make a direct comparison of results difficult. A comparison of the results of Chamberlain and Stern[11] for *d-p* scattering and those of Powell[12] and Youtz[13] for *n-d* scattering shows discrepancies in shape and absolute value that make any conclusion suspect. Barkas and Wilson[14] have examined the ratio for the production of π^+ and π^- mesons at 90° when carbon is bombarded with 390-Mev alpha particles. The mesons, however, are relatively low in energy and are appreciably affected by the Coulomb barrier. They conclude that the data are not inconsistent with the assumption of charge symmetry. A direct comparison of the production of H^3 and He^3 in 190-Mev deuteron-deuteron collisions can be made. The assumption of charge symmetry would require that these two cross sections be equal.

EXPERIMENTAL PROCEDURE

To provide the necessary separation and identification of the H^3 and He^3 particles, they were made to pass through a magnetic channel and pulse-height detectors. In order to provide a direct comparison, both types of particles should have the same angular resolution, the same energy resolution, and the same multiple-scattering. For a given scattering angle, both H^3 and He^3 will have essentially the same energy (about one Mev difference because of their mass difference). Originating in the same target, however, and passing through identical amounts of intervening windows in going from target to detector, they will have different scattering and energy distributions. The general scheme of attack had three basic features:

* This work was performed under the auspices of the U. S. Atomic Energy Commission.

[1] Allred, Phillips, and Rosen, Phys. Rev. **82**, 782 (1951).
[2] Burrows, Gibson, and Rotblat, Proc. Roy. Soc. (London) **A209**, 489 (1951).
[3] Leiter, Rodgers, and Kruger, Phys. Rev. **78**, 663 (1950).
[4] G. Hunter and H. Richards, Phys. Rev. **76**, 1445 (1949).
[5] Erickson, Fowler, and Stovall, Phys. Rev. **76**, 1141 (1949).
[6] Blair, Freier, Lampi, Sleator, and Williams, Phys. Rev. **74**, 1599 (1948).
[7] F. Ajzenburg and T. Lauritsen, Revs. Modern Phys. **24**, 321 (1952).
[8] J. M. Blatt and V. F. Weisskopf, *Theoretical Nuclear Physics* (John Wiley and Sons, Inc., New York, 1952), p. 204.
[9] K. Watson and R. Stuart, Phys. Rev. **82**, 738 (1951).
[10] Allen, Almquist, Dewan, Pepper, and Sanders, Phys. Rev. **82**, 262 (1951).
[11] O. Chamberlain and M. Stern, Phys. Rev. **94**, 666 (1954).
[12] W. Powell, Physics Division Quarterly Report, University of California Radiation Laboratory Report UCRL-1191, March 20, 1951 (unpublished).
[13] B. Youtz, "Elastic and inelastic scattering of 90-Mev neutrons by deuterons," University of California Radiation Laboratory Report UCRL-2307, August 13, 1953 (unpublished).
[14] W. Barkas and H. Wilson, Phys. Rev. **89**, 758 (1953).

(1) The same magnetic channel (physically) was used for both particles. To detect He^3, the magnetic field intensity was reduced to half that used for H^3. This procedure had the advantage of insuring identical geometry for both particles.

(2) The energy spread of the H^3 was made to equal that of the He^3. Any loss of counting efficiency due to energy spread was thereby balanced out.

(3) The mean scattering angle of H^3 from the material in and near the target was made to approximate that of He^3. Multiple scattering was made to occur as near the target as possible. The path of the particles from the vicinity of the target to the vicinity of the detectors was evacuated to minimize multiple scattering errors along this path.

A pulse-height telescope behind the magnet provided pulses corresponding to specific ionization (dE/dx) and total energy (E). It may seem that the three parameters —$H\rho$, dE/dx, and E—overdetermine the separation problem. The separation of deuterons from tritons, however, is marginal under optimum conditions when only two parameters are used. It was felt that wider limits on the resolutions of both the magnetic channel and the pulse-height equipment could be allowed by the use of all three parameters.

The experimental arrangement for comparison of H^3 and He^3 is shown schematically in Fig. 1. The incident deuterons were collimated to a beam one inch in diameter and monitored with an ionization chamber. The

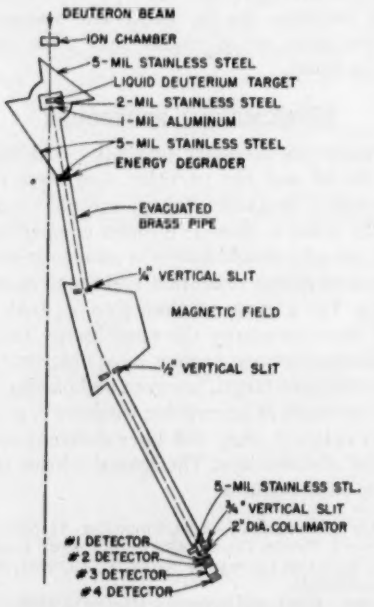

FIG. 1. Schematic diagram showing experimental arrangement for comparing production of H^3 and He^3 in deuteron-deuteron collisions.

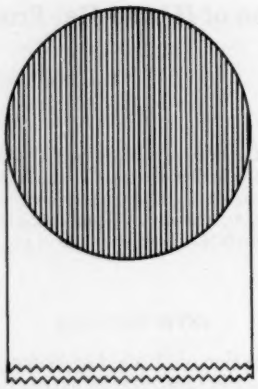

FIG. 2. Energy degraded for H^3.

energy of the deuteron beam has been measured as 192±2 Mev.[16]

In order to keep background counts at a minimum, a liquid-deuterium target was used. This target had a volume of deuterium 1½ inches in diameter and approximately ½ inch thick. The windows were 2-mil stainless steel. Blank runs were obtained by closing the valve leading to the top of the deuterium target. The evaporation from the surface of the liquid built up enough pressure to force the liquid deuterium out of the target into a reservoir. The blank runs, therefore, were not truly blank, since deuterium gas at approximately 21°K remained in the target. Since this experiment was a comparison of two cross sections, no error was introduced by this residual gas.

The magnet used was a pair-spectrometer magnet readily capable, with a three and one-half inch gap, of providing 14 kilogauss over a path length of 30 inches. The path traversed by the H^3 particles is shown in Fig. 1. The path traversed by the He^3 is identical except that the energy degrader is removed. The location of this path was determined by using the well-known current-carrying wire to trace the orbit of the desired particle through the magnetic field.

The procedure used was as follows. A wire was strung down the channel from the center of the target to the center of the detector. Tension was provided by a weight strung over a pulley. The calculated current for a H^3 of proper energy was applied through the wire. The magnetic field was adjusted so that the wire passed down the centers of the brass pipes. The collimating slits were all put in position so that the wire bisected them. The magnetic-field potentiometer reading was recorded. Next the calculated current for a He^3 of proper energy was applied to the wire. The magnetic field was then adjusted so that the wire again bisected the channel and collimating slits. The magnetic-field potentiometer reading was recorded. Thus a single physical channel was defined which could be adjusted

[16] A. L. Bloom and O. Chamberlain, Phys. Rev. 94, 659 (1954).

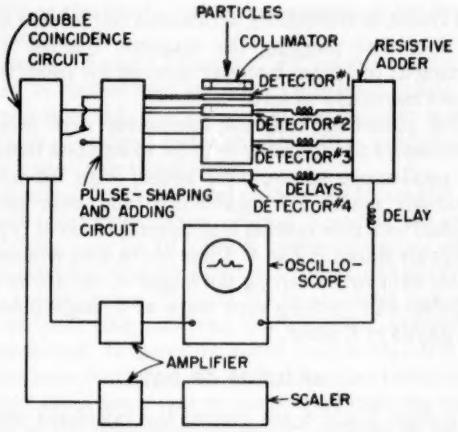

FIG. 3. Block diagram of electronics for comparing H^3 and He^3.

to accept either H^3 or He^3 of the proper energy by changing the magnetic field.

The energy degrader is shown in Fig. 2. It was placed in position as shown in Fig. 1 for H^3 and removed for He^3. It had a dual function: to provide the same spread in energy of the H^3 as for the He^3, and to provide the same multiple scattering for both H^3 and He^3. The principle of the degrader is obvious from Fig. 2. Particles go through different thicknesses of absorber and suffer various energy losses. Ideally, if the grooves were very close together, the energy losses would be quite random horizontally. Since the horizontal distance across the degrader to go from maximum attenuation to minimum attenuation is only $\frac{1}{16}$ inch, it was felt that the random ideal was approached. The depth of the grooves was calculated to equalize the H^3 energy spread to that of the He^3. The residual thickness of the degrader was calculated to equalize the multiple scattering of the mean H^3 to that of the He^3. Fortuitously, this also served to drop the mean energy of the H^3 to a value equal to that of He^3. In as much as the energy of the He^3's from the target was 163 ± 6 Mev, it is apparent that the effects of such an energetic particle would not be large, even without the use of the energy degrader.

The exact value of the magnetic field was later checked during the run by varying the magnetic field of the magnet over a range of values close to the calibrated value, and plotting the counting rate. A magnetic field was used corresponding to the peak of the counting rate. The value of the field thus determined was found to lie very close to the expected value.

The detectors used were liquid scintillators of the general type described by Garwin,[16] with one difference: in addition to a 5819 photomultiplier tube to give pulse height, each liquid cell was viewed by two 1P21 photomultiplier tubes. These latter tubes were used to drive a coincidence circuit.

Three pulse-height detectors were employed. The first detector served to measure dE/dx of the He^3. The second detector served to measure both E of the He^3 and dE/dx of the H^3. The third detector served to measure E of the H^3. The fourth detector was merely a liquid cell viewed by one 1P21 tube. Since the desired particles did not have sufficient energy to get into this detector, any particle making a pulse in this detector could be discarded.

By placing the detector telescope directly in the deuteron beam and by varying the amount of absorber between the beam and the detector, the detector telescope was calibrated for various energy deuterons. The pulses from these essentially monoenergetic deuterons were used to obtain resolution curves of the individual detectors. These data were obtained immediately after the H^3 data were obtained, without changing voltages or relative positions of the detectors. This procedure made it possible to use these resolution curves in differentiating between H^3's and deuterons.

A block diagram of the electronics is shown in Fig. 3. Double coincidences were made either between the first and second detector (for He^3) or between the second

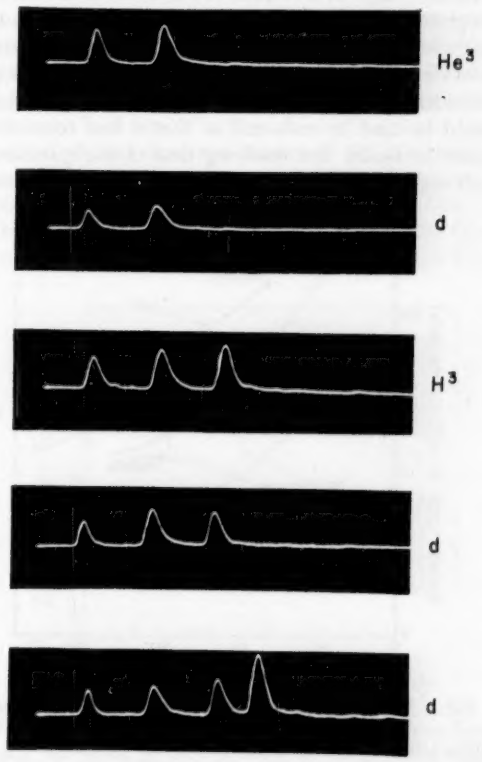

FIG. 4. Film traces of typical He^3, and H^3 and background pulses. First two during He^3 run; last three during H^3 run.

[16] R. L. Garwin, Rev. Sci. Instr. **23**, 755 (1952).

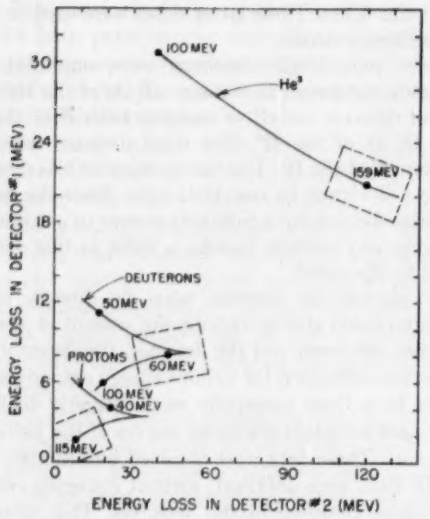

FIG. 5. Plot of calculated energy loss in first detector *vs* calculated energy loss in second detector for He^3 and other particles. Areas outlined indicate regions where pulses expected to lie.

and third detector (for H^3). The pulse-shaping and coincidence units were similar to those described by Frank.[17] Amplified outputs from the coincidence unit were used to trigger the sweep of the oscilloscope and to drive a scalar. The use of separate photomultipliers to provide coincidence pulses and pulse-height pulses was considered advantageous, so that optimum voltages could be used on each and so that a fast coincidence could be made. The resolving time of the coincidence unit was about three millimicroseconds. The success of this circuit in eliminating accidentals can be seen from the fact that plugging the magnetic channel when running at full beam intensity reduced the coincidence counts essentially to zero.

The pulse-height signals themselves were delayed with respect to each other in order to separate them on the oscilloscope screen, were added, were fed into a Tektronix model 517 oscilloscope, and were photographed on a slow moving film. Several traces of typical pulses are shown in Fig. 4. These traces were reduced to usable data by measuring the height of the dE/dx and E pulses and plotting each trace as a single point in the dE/dx *vs* E plane.

ANALYSIS OF DATA

In Figs. 5 and 6 are plotted the calculated energy losses of various particles traversing the detector system.[18] Figure 5, for example, shows that He^3's of various energies fall along a line. If the mechanism by which the energy loss of the particle is converted to pulse height were perfectly linear, these curves would also represent the pulse-height locus for He^3's of various energy (assuming the scales to be suitably chosen). Owing primarily to saturation effects in the detector for high values of specific ionization and to nonlinearity of the amplification system, one would not expect the actual pulse-height locus to have the same slope or position as the energy-loss curve. The over-all resolution of the detecting system, moreover, as manifested by the Landau-effect,[19] the statistical fluctuation in the number of photoelectrons released from the photocathode, and the optical resolution of the detector spreads the expected line out into a band. The

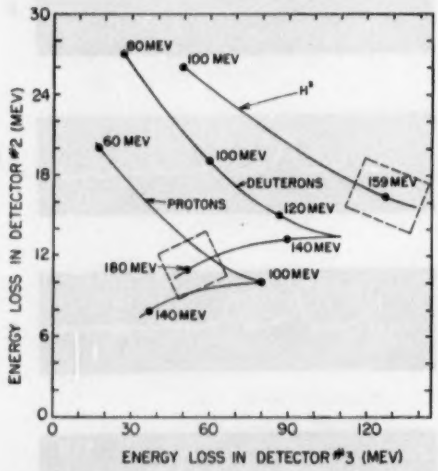

FIG. 6. Plot of calculated energy loss in second detector *vs* calculated energy loss in third detector for H^3 and other particles. Areas outlined indicate regions where pulses expected to lie.

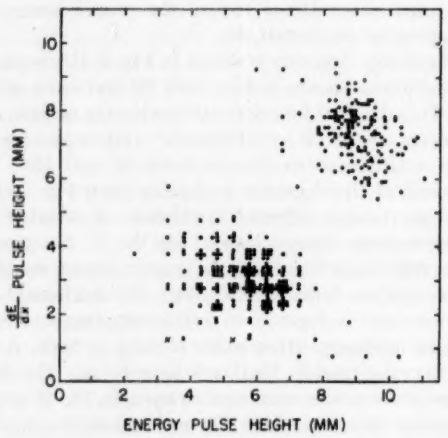

FIG. 7. Data for counting rate of He^3 using liquid deuterium target. Data obtained in 10 integrated beam units. Crosses represent particles making a pulse in the third detector.

[17] Frank, Bandtel, Madey, and Moyer, Phys. Rev. **94**, 1716 (1954).

[18] Aron, Hoffman, and Williams, University of California Radiation Laboratory Report AECU-663, Revised 1949 (unpublished).

[19] L. Landau, J. Phys. (U.S.S.R.) **8**, 201 (1944).

width of this band obtained is a measure of the over-all resolution.

In Figs. 5 and 6, therefore, the general regions outlined by dashed lines are where pulse-height pairs were expected to fall. The energies of the particles in these regions correspond to the energies of the particles that can come down the channel.

Figure 7 shows the total data collected for He^3 with liquid deuterium target. Figure 8 shows the corresponding data for H^3. (Blank target data is not shown but counting rates are listed in Table II.) The He^3 data are unambiguous. The He^3 fall in an island well separated from the expected slow-deuteron and proton background. It should be noted that several He^3 particles have the proper dE/dx, but have an energy pulse height lying below that to be expected from the resolution of the equipment. These are assumed to be He^3

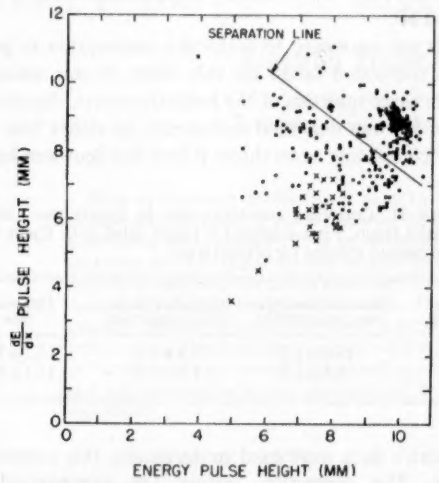

FIG. 8. Data for counting rate of H^3 using liquid deuterium target. Data obtained in 10 integrated beam units. Crosses represent particles making a pulse in the fourth detector.

particles that suffered an inelastic event in stopping in the energy detector. This argument is developed in the discussion of the H^3 data, where a calculation of this effect is required.

The H^3 data in Fig. 8 do not resemble the anticipated results. Instead of having two well-defined areas of H^3 and fast deuterons, they show that deuterons of lower energy than those anticipated are being detected. By a process of elimination, it was determined that these deuterons did come from the target and did come down the channel. With the collimation used, however, they could not come down the channel in a direct path. It was finally determined that they represented deuterons that had scattered off one edge of the collimating slit at the entrance to the magnet. A further check of the geometry showed that deuterons might reach the detectors by such a process with energies down to approximately 120 Mev.

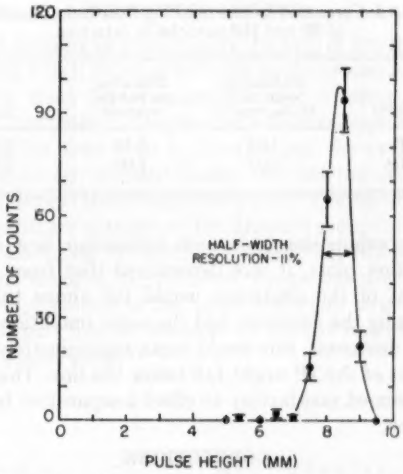

FIG. 9. Distribution in pulse height for 200 random deuterons of 130-Mev initial energy as measured by third detector.

In order to separate these deuterons from the H^3, the resolution of the second and third detectors for deuterons of various energy was first determined from the deuteron calibration data. Figure 9 shows a resolution function for detector No. 3 as determined by 200 random deuterons of 130 Mev. These resolution functions not only determine the width of the deuteron band, but locate accurately the center of the distribution on the dE/dx *vs* energy plot for each calibration energy. In Fig. 10 the locus of the center of these distributions is shown. (For the sake of illustration, there are also plotted the pulse heights of 160 random deuterons of various energies ranging from 110 Mev to 150 Mev.) A line was drawn parallel to this line and lying midway between the center of the deuteron distribution and the center of the triton distribution of Fig. 8.

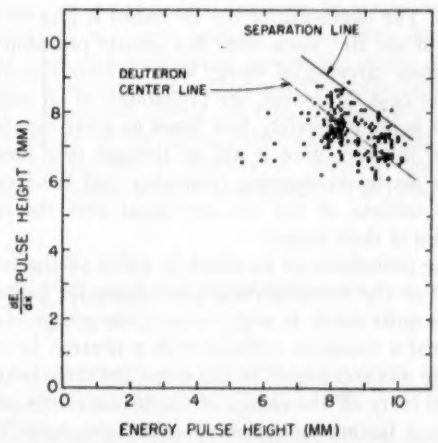

FIG. 10. 160 random traces made by deuterons of various energy. One curve shows locus of center of deuteron distribution. Other curve shows separation line between H^3 and deuterons.

TABLE I. Correction factors resulting from inelastic collisions of H^3 and He^3 particles in detectors.

Particle	Attenuation before or in dE/dx detector	Degrading in energy detector	Total
H^3	1.07	1.13	1.21
He^3	1.01	1.00	1.01

By superimposing this new separation line on the resolution plots, it was determined that from 2 to 3 percent of the deuterons would fall above this line. Assuming the detectors had the same resolution for H^3 as for deuterons, this would mean approximately 2 to 3 percent of the H^3 might fall below the line. This much was deemed satisfactory to effect a separation between the two.

CORRECTIONS

It was necessary at this point to introduce the only correction factors applied to the data. The H^3 and He^3 can suffer inelastic events in the detectors that affect their pulse heights. The most common event is a stripping off of one or two particles in a manner similar to the familiar deuteron stripping. In the event that such a process occurs before or in the dE/dx detector, the particle is very probably lost, since neither the dE/dx or the energy pulse is proper for a H^3 or He^3. Crandall[20] has measured the total inelastic cross section of high-energy He^3 particles for various elements. Assuming the probability of a nuclear event at high energy is the same for H^3 as for He^3, one can calculate the attenuation of H^3 and He^3 prior to entering the energy detector.

The effect of an inelastic event in the energy detector is impossible to predict rigorously. Since the resultant deuterons, neutrons, or protons from the stripping process will be less ionizing than the original particle, it is assumed that the energy pulse is degraded in all cases. The degrading of the H^3 pulses is greater than that of the He^3, since there is a greater probability of neutrons' carrying off energy with no ionization in the former case. Moreover, the probability of an inelastic event is approximately four times as great for the H^3 as for the He^3, since it will go through four times as much matter in stopping (assuming that the inelastic cross sections of the two are equal over the major portion of their range).

The probability of an event in which all the energy of H^3 or He^3 would become unavailable for ionization seems quite small. It might occur if the proton of a H^3 suffered a knock-on collision with a neutron in which charge was exchanged. In this event the three neutrons would carry off the energy of the H^3 with little probability of further ionization. It might also occur if the proton were stripped from the H^3 by a nucleus in such a manner that the resulting excited nucleus produced little or no ionization. The possibility of an event in which a He^3 would fail to produce a substantial amount of ionization is hard to conceive.

Since the degraded He^3 particles are still readily separable from the background, it is apparent that no correction need be applied to the He^3 from this source. It is reasonable to assume, however, that a considerable number of the particles in Fig. 8 that fall in the category of deuterons, are actually H^3, whose energy pulse has been degraded sufficiently to make them indistinguishable from deuterons. That this is a reasonable assumption can be further argued from the fact that the scattering of deuterons off the collimating slit can account only for detected deuterons of energies ranging down to about 120 Mev. It is felt that a majority of the particles in Fig. 8 whose dE/dx pulse was larger than about 8.5 on the ordinate scale were actually degraded H^3.

It is not necessary to make this assumption to get a rough correction factor for this effect. It was assumed that in three-quarters of the inelastic events, the energy of the H^3 was degraded sufficiently to either lose the count completely or to throw it into the deuteron band.

TABLE II. Corrected counting rates in counts per volt of integrated beam. First column for target filled with liquid deuterium. Second column for blank target.

Particle	Corrected deuterium rate (counts/volt)	Corrected blank rate (counts/volt)	Difference rate
H^3	15.6±1.3	2.4±1.1	13.2±1.7
He^3	16.5±1.3	1.2±0.7	15.3±1.5

Crandall's data were used to determine this correction factor. The correction factors are summarized in Table I.

RESULTS

The final counting rates are summarized in Table II.

The final ratio for the production of H^3 to He^3 at the center-of-mass scattering angle of 30 degrees is 0.86 ±0.14. The errors shown are the statistical deviations related to the number of counts constituting the original data. Within statistics, therefore, the production probabilities of He^3 and H^3 are equal. Although the correction factors are relatively small, they may introduce an uncertainty the order of 5 percent. An additional 5 percent uncertainty is estimated for possible differences in angular resolution and other systematic errors.

CONCLUSIONS

The existence of charge symmetry would require that the cross sections for the production of H^3 and He^3 be the same. Unfortunately, the inverse is not necessarily true. The cross sections might conceivably

[20] W. Crandall (private communication).

be equal at some specific angle in spite of an asymmetry in the nuclear forces. Moreover, the matter of degree must be considered. Since the cross sections cannot be calculated explicitly in terms of the n-n and p-p forces, it is not possible to say how much effect an asymmetry in the forces would have upon the cross sections. The following conclusion, however, seems justified. At low energy, charge symmetry is an established fact and the cross sections for the production of H^3 and He^3 from deuteron-deuteron collisions are equal (neglecting of course Coulomb and mass-difference effects). The fact that the cross sections are nearly equal at high energy supports the hypothesis of charge symmetry at high energy.

ACKNOWLEDGMENTS

It is a pleasure to acknowledge the help of Dr. Burton S. Moyer, which included not only guidance and advice, but also many late evenings at the cyclotron. The author is indebted to Drs. Kenneth Bandtel and Wilson J. Frank for their help in carrying out the cyclotron runs and to Dr. Richard Madey who led the development of the electronic equipment used. Thanks are due to the graduate students of Dr. Moyer's group for their help in executing the cyclotron runs. Paul Nikonenko has made much of the electronic equipment used. The successful operation of the liquid deuterium target is in no mean part due to the work of Roscoe Byrnes and Robert Mathewson.

PHYSICAL REVIEW VOLUME 96, NUMBER 6 DECEMBER 15, 1954

Electron Tridents between 0.1 and 10 Bev

M. M. Block,* D. T. King, and W. W. Wada
Nucleonics Division, Naval Research Laboratory, Washington, D. C.
(Received July 2, 1954)

Data on the direct production of pairs by fast electrons of the cosmic radiation have been collected in nuclear emulsions by a track-following method. Multiple-scattering measurements were made on the secondaries of 61 tridents with energies between 0.1 and 10 Bev; of these, 14 originated on arms of pairs. A mean free path of 134 ± 42 cm was deduced for the latter, corresponding to a cross section of $0.92\pm0.29\times10^{-25}$ cm². An appropriate statistical treatment for small numbers has been adopted, and a correction has been made for the inclusion of pseudo-tridents. The theoretical cross sections of Bhabha and Racah, which apparently disagree by a factor of about 2 in this energy region, have been shown to be consistent. The theoretical cross section averaged over the experimental energy distribution is 0.82×10^{-25} cm². The distributions in fractional energy transfer to the created pair and internal energy partition in the pair have been derived and are compared with our observations. It is concluded that trident theory is in agreement with this experiment.

I. INTRODUCTION

OBSERVATIONS of the direct creation of electron pairs arising from the interaction of fast charged particles with the Coulomb fields of nuclei have been extensively studied.[1–12] These phenomena, called tridents, consist of an incoming, or primary track of a relativistic charged particle, and three emergent tracks as shown by the photomicrograph in Fig. 1. Experiments made chiefly in photographic emulsions indicate that the great majority of tridents have electron primaries. In this text we refer to both electrons and positrons as electrons. In those instances where identification has been possible, it has been demonstrated that the secondaries are of electronic mass. Energy measurements have indicated that the primary energy is conserved among the three secondary tracks.

The theory of the direct pair creation process has been discussed by a number of authors, notably Bhabha,[13] Nishina *et al.*,[14] and Racah.[15] The cross sec-

FIG. 1. A photomosaic of a trident in a G5 emulsion. In this example, less than one percent of the primary energy is transferred to the directly created pair.

* On military leave of absence from Duke University, Durham, North Carolina.

[1] H. R. Crane and O. Halpern, Phys. Rev. **55**, 838 (1939).
[2] J. R. Feldmeier and G. B. Collins, Phys. Rev. **58**, 200 (1940).
[3] H. L. Bradt, Helv. Phys. Acta **17**, 59 (1944).
[4] K. Seigbahn and H. Slätis, Arkiv. Mat. Astron. Fysik **A34**, 6 (1947).
[5] C. F. Powell, Nuovo cimento, Suppl. **6**, 379 (1949).
[6] G. P. S. Occhialini, Nuovo cimento, Suppl. **6**, 413 (1949).
[7] Bradt, Kaplon, and Peters, Helv. Phys. Acta **23**, 24 (1950).
[8] Hooper, King, and Morrish, Phil. Mag. **42**, 304 (1951).
[9] Barkas, Deutsch, Gilbert, and Violet, Phys. Rev. **86**, 59 (1952).
[10] Hooper, King, and Morrish, Phil. Mag. **43**, 853 (1952); Can. J. Phys. **29**, 545 (1952).
[11] S. T. Goldsack and M. L. T. Kannangara, Phil. Mag. **44**, 811 (1953).
[12] J. E. Naugle and P. S. Freier, Phys. Rev. **92**, 1086 (1953).
[13] H. J. Bhabha, Proc. Roy. Soc. (London) **A152**, 559 (1935).
[14] Nishina, Tomonaga, and Kobayasi, Sci. Papers Inst. Phys. Chem. Research Tokyo **27**, 137 (1935).
[15] G. Racah, Nuovo cimento **14**, 93 (1937).

tion is predicted to increase slowly with primary energy, in qualitative agreement with experiment.[8] Theory shows that the cross section is $\sim 10^{-25}$ cm^2 for primary electron energies of several hundred Mev, the corresponding cross section for primary mesons being smaller by a factor of ~ 50. Bhabha, Nishina *et al.* and Ravenhall[16] have considered the effect of screening and have found it to be small up to ~ 1 Bev. However, the magnitude of the trident cross section given by Bhabha is about twice that given by Racah for the energies found in the cosmic radiation.

Experimental identification of a trident rests upon the observer's ability to distinguish between pair origins truly coincident with the primary track and those due to chance superposition. The latter arise chiefly from the materialization of bremsstrahlung photons indistinguishably close to the parent track. A recent study[17] has been made of 200 bremsstrahlung pairs found in this experiment. This work has established the magnitude of bremsstrahlung pair confusion, or pseudo-trident occurrence, and shows that for primary energies between 0.1 and 10 Bev this effect is not large. Calculations further indicate that for the high electron energies found in the cores of "jets," the proportion of pseudo-tridents among the tridents becomes markedly greater. An additional experimental factor encountered in "jet" observations is the difficulty in distinguishing the individual tracks due to the locally high track densities. We have therefore confined our study to a general cosmic ray exposure with events of energy below 10 Bev and of low track density, in order to minimize the possibility of misinterpretation.

In the present experiment the data have been collected by a track following method which allows a quantitative measure of the cross section. The number of tridents of primary energy between 0.1 and 10 Bev, initiated by particles originating in pairs, was compared with the total length of pair tracks within the same energy interval. The division of the primary energy among the three secondaries has also been examined. In the course of the present study a comparison has been made between the work of Bhabha and Racah in order to determine the basis of their numerical disagreement. It has been found that a more detailed application of Bhabha's method leads to a result in substantial agreement with that of Racah. A comparison between theory and experiment has been made.

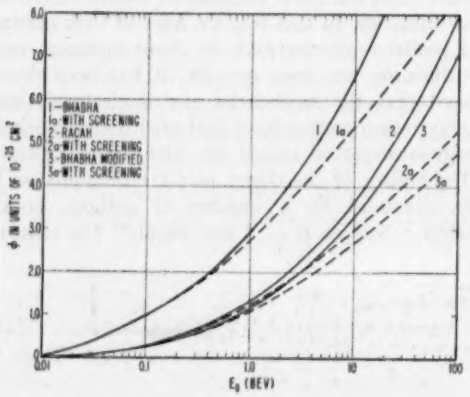

FIG. 2. The theoretical total cross section for the direct creation of a pair by a fast electron, as a function of primary energy.

[16] D. G. Ravenhall, Proc. Phys. Soc. (London) **A63**, 1177 (1950).

[17] D. T. King and M. M. Block, Phys. Rev. **95**, 648 (1954); M. M. Block and D. T. King, Phys. Rev. **95**, 171 (1954).

II. THEORY

A. Total Cross Section

According to Bhabha[18] the expression for the electron trident cross section ϕ is, neglecting screening,

$$\phi(E_0)=\frac{28}{27\pi}\left(\frac{r_0Z}{137}\right)^2\ln^3\left(\frac{kE_0}{mc^2}\right), \tag{1}$$

where E_0 is the energy of the primary electron which initiates the process, mc^2 the electron rest energy, r_0 the classical electron radius, and Z the atomic number of the target nucleus. k is a number of the order of unity. This expression is accurate only when the energy of the primary electron is extremely large in relation to its rest energy, so that terms of lower powers in $\ln(E_0/mc^2)$ can be neglected in comparison to the cubic term in (1). In order to study the behavior of the cross section at lower energies where this condition is no longer valid, we have attempted a more detailed integration of the differential cross section $d^2\phi$ which is given by Eq. (32) of Bhabha's paper,

$$d^2\phi(E_0,E_+,E_-)=\frac{8}{\pi}\left(\frac{r_0Z}{137}\right)^2\frac{E_+^2+E_-^2+\frac{2}{3}E_+E_-}{(E_++E_-)^4}$$
$$\times\ln\frac{kE_+E_-}{(E_++E_-)mc^2}\ln\frac{k'E_0}{E_++E_-}dE_+dE_-; \tag{2}$$

k and k' are again numbers of the order of unity, and E_+ and E_- are the energies of the created electrons. Following Bhabha, we introduce a new variable E_T, the total energy of the created pair, and perform the integration with respect to E_-. However, we depart from Bhabha's treatment in that we retain all terms, making approximations only after completing all integrations. We then obtain the modified differential cross section $d\phi_m$, which, after putting $k=k'=1$, becomes

$$d\phi_m(E_0,E_T)=\frac{56}{9\pi}\left(\frac{r_0Z}{137}\right)^2\frac{1}{E_T}\ln\frac{E_0}{E_T}$$
$$\times\left\{\ln\frac{E_T}{mc^2}-\frac{44}{21}+\frac{18}{7}\frac{mc^2}{E_T}+\frac{2}{7}\left(\frac{mc^2}{E_T}\right)^2-\frac{1}{3}\left(\frac{mc^2}{E_T}\right)^3\right.$$
$$\left.+\frac{9}{14}\left(\frac{mc^2}{E_T}\right)^4+\cdots\right\}dE_T. \tag{3}$$

In the derivation of (3), the terms in mc^2/E_T which, when integrated over E_T would contribute to lower powers of $\ln(E_0/mc^2)$ in the total cross section, have been preserved. This result is to be contrasted with the corresponding expression derived by Bhabha [(34) of his paper, when $k=k'=1$],

$$d\phi(E_0,E_T)=\frac{56}{9\pi}\left(\frac{r_0Z}{137}\right)^2\frac{1}{E_T}\ln\left(\frac{E_0}{E_T}\right)\ln\left(\frac{E_T}{mc^2}\right)dE_T. \quad (4)$$

Integrating (3) between the limits $2mc^2$ and $E_0-2mc^2\approx E_0$, we obtain the modified expression for the total cross section

$$\phi_m(E_0)=\frac{28}{27\pi}\left(\frac{r_0Z}{137}\right)^2\left\{\ln^3\left(\frac{E_0}{mc^2}\right)-\frac{44}{7}\ln^2\left(\frac{E_0}{mc^2}\right)+\left(\frac{54}{7}+\frac{88}{7}\ln 2-3\ln^2 2\right)\ln\left(\frac{E_0}{mc^2}\right)-\frac{54}{7}-\frac{54}{7}\ln 2-\frac{44}{7}\ln^2 2+2\ln^3 2+\cdots\right\}, \quad (5)$$

which is to be compared with (1). For energies of several hundred Mev, numerical evaluation of (5) shows that the terms in $\ln^2(E_0/mc^2)$, $\ln(E_0/mc^2)$ and the constant are not negligible in comparison to $\ln^3(E_0/mc^2)$ which is the only corresponding term in (1). In Fig. 2 we have plotted the Bhabha cross section (1) and the modified cross section (5), together with the corresponding cross section obtained by Racah.[15] The cross sections have been evaluated for photographic emulsions, with effective $Z=22.1$. Bhabha's original cross section is about twice as large as that found by Racah; the close agreement of our modified result (5) and that of Racah is satisfactory in view of the approximations involved in both treatments. There is thus a simpler theoretical basis against which experiment is to be compared.

Screening has been neglected in the above calculations. Ravenhall[16] has estimated the effects of screening in photographic plates, and concludes that the cross section is reduced by 6 percent for primary electron energies of 1 Bev, and by 18 percent for 10 Bev. Since the energies of the tridents found in this study are mainly in the vicinity of 500 Mev, the effect of screening is trivial, reducing the cross section by ~ 3 percent. The dashed curves in Fig. 2 take screening[13,14,16] into account.

In our experiment the energies of the primary electrons are distributed over a wide range. To achieve a meaningful comparison with theory it is necessary to average the theoretical cross section over the energy spectrum of the primary electrons. A power law of the form

$$dN(E_0)=\text{constant}\ E_0^{-1.6}dE_0 \quad (6)$$

has been assumed for the differential distribution in electron energy, derived from the experimentally determined π^0 meson spectrum.[18] The average cross section is then given by

$$\bar{\phi}=\int_{E_0(\min)}^{E_0(\max)}\phi(E_0)dN(E_0)\Big/\int_{E_0(\min)}^{E_0(\max)}dN(E_0), \quad (7)$$

where $E_0(\min)$ and $E_0(\max)$, the minimum and maximum primary electron energies of our experiment, are 0.1 Bev and 10 Bev, respectively. Using the modified Bhabha cross section $\phi_m(E_0)$ we obtain 0.82×10^{-25} cm^2 for $\bar{\phi}$. From Fig. 2, this corresponds to an average primary electron energy of $\sim$400 Mev. Assuming that screening reduces the cross section by 3 percent at this energy, we conclude that the average theoretical cross section for the tridents found in our study is 0.80×10^{-25} cm^2.

B. Energy Partition

In order to facilitate further comparison with experiment it is instructive to introduce new variables $R=E_T/E_0$ and $r=E_+/E_T$ into (2). R is the fractional transfer of primary energy to the trident pair, whereas r expresses the fraction of the trident pair energy carried off by the positron. The theory is completely symmetric in E_+ and E_- as seen in (2). In terms of R and r, (2) becomes

$$d^2\phi(E_0,R,r)=\frac{8}{\pi}\left(\frac{r_0Z}{137}\right)^2\left(1-\frac{4}{3}r+\frac{4}{3}r^2\right)\frac{1}{R}\ln\left(\frac{1}{R}\right)\times\ln\left(\frac{E_0Rr(1-r)}{mc^2}\right)dRdr. \quad (8)$$

When the dependence on r is integrated out of (8), we obtain

$$d\phi(E_0,R)=\frac{56}{9\pi}\left(\frac{r_0Z}{137}\right)^2\frac{1}{R}\ln\left(\frac{1}{R}\right)\left\{\ln\left(\frac{E_0R}{mc^2}\right)-\frac{44}{21}+\frac{18}{7}\frac{mc^2}{E_0R}+\frac{2}{7}\left(\frac{mc^2}{E_0R}\right)^2-\frac{1}{3}\left(\frac{mc^2}{E_0R}\right)^3+\frac{9}{14}\left(\frac{mc^2}{E_0R}\right)^4+\cdots\right\}dR. \quad (9)$$

This is the equivalent of (3) in terms of the new variables. Similarly, by integrating R out of (8), we find

$$d\phi(E_0,r)=\frac{4}{3\pi}\left(\frac{r_0Z}{137}\right)^2\left(1-\frac{4}{3}r+\frac{4}{3}r^2\right)\times\left[\ln^3\left(\frac{E_0}{mc^2}\right)+3\ln^2\frac{E_0}{mc^2}\ln[r(1-r)]-6\ln\frac{E_0}{mc^2}\{\tfrac{1}{2}\ln^2 r-\ln r\ln[r(1-r)]\}-2\ln^3 r+3\ln^2 r\ln[r(1-r)]\right]dr. \quad (10)$$

[15] Carlson, Hooper, and King, Phil. Mag. **41**, 701 (1950).

In Figs. 3 and 4 we have plotted $d\phi(E_0,R)/dR$ and $d\phi(E_0,r)/dr$, respectively, for several primary energies. It is instructive to compare the R-distribution with the corresponding distribution in the Bethe-Heitler theory[19] for bremsstrahlung, and the r-distribution with the corresponding distribution for energy partition in pair production. With increasing trident primary energy the similarity becomes marked. It is interesting to conjecture that this similarity is due, in the direct creation process, to the virtual photon exhibiting a behavior more and more like that of a real photon, with increasing primary energy.

Let us now consider $P(R,E_0)dR$, the probability distribution in fractional energy transfer, namely, the probability that R lie between R and $R+dR$ for a given E_0. This is given by the ratio of (9) to (5), i.e., $d\phi(E_0,R)/\phi(E_0)$. In order to enable a comparison with experiment where the primary energies range between 0.1 and 10 Bev, we average $P(R,E_0)$ over the energy distribution (6). Thus

$$\bar{P}(R)dR=\frac{\int_{E_0(\min)}^{E_0(\max)}P(R,E_0)dN(E_0)dR}{\int_{E_0(\min)}^{E_0(\max)}dN(E_0)}. \quad (11)$$

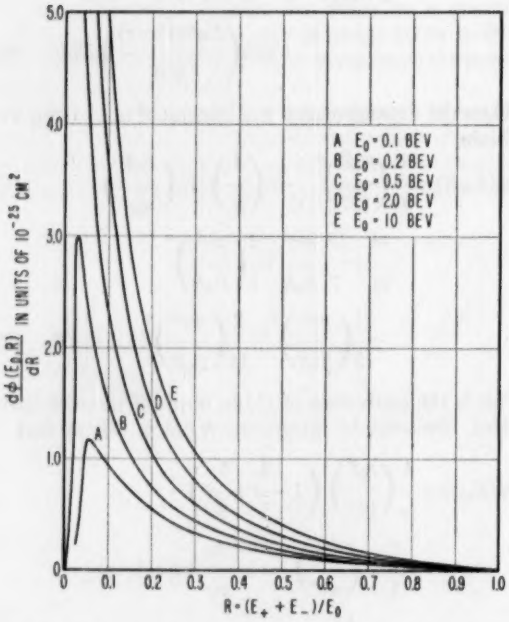

FIG. 3. The theoretical differential cross section $d\phi(E_0,R)/dR$ as a function of R, illustrating the fractional transfer of primary energy to the trident pair. E_0 is the primary energy and $R=E_{pair}/E_0$.

[19] W. Heitler, *Quantum Theory of Radiation* (Oxford Press, London, 1944).

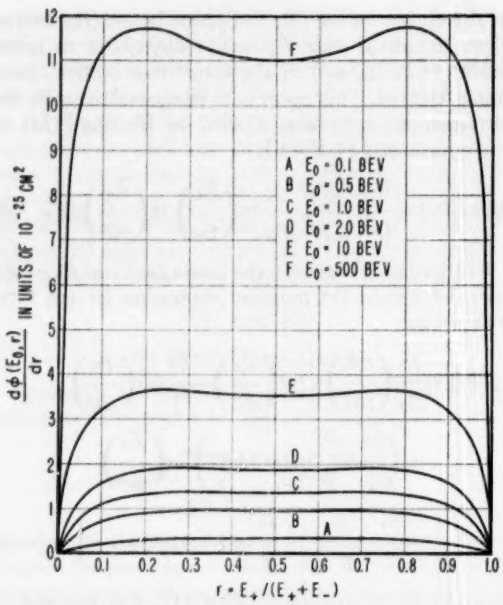

FIG. 4. The theoretical differential cross section $d\phi(E_0,r)/dr$ as a function of r, illustrating the internal energy partition within trident pairs. E_0 is the primary energy and $r=E_+/E_{pair}$.

In the same manner we obtain

$$\bar{P}(r)dr=\frac{\int_{E_0(\min)}^{E_0(\max)}P(r,E_0)dN(E_0)dr}{\int_{E_0(\min)}^{E_0(\max)}dN(E_0)}, \quad (12)$$

where $P(r,E_0)=d\phi(E_0,r)/\phi(E_0)$. We have plotted (11) and (12) as the smooth curves in Figs. 6 and 7, respectively.

III. EXPERIMENT

A. Exposure, Search Method, and Measurement

Twenty-six Ilford G5 nuclear emulsions 400 microns thick were exposed to the cosmic radiation at altitudes exceeding 95 000 feet and at geomagnetic latitude 55°N for a period of 6 hours. The plates employed in this study were arranged under differing amounts of Pb and C absorber, as several simultaneous experiments with energetic particles were being made. In such exposures a large number of tracks attributable to the soft component can be found.

An appropriate search procedure, track following, was employed in order to detect more efficiently those configurations consisting only of lightly ionizing tracks. In earlier experiments[8,10] on tridents the material was found by a systematic examination of the emulsion volume; this led to criticism[20] that tridents of highly unequal secondary energies tended to escape observa-

[20] G. Gottstein and K. Ott (private communication).

tion. With the present search method it is found that tridents of all types are relatively conspicuous. The examination is limited to those tracks which are inclined to the emulsion plane at angles less than $\sim 5°$, and which have grain densities less than three times the minimum. These criteria describe the long paths of charged particles which penetrate the emulsion with velocities exceeding about one-half that of light.[21] Our scan proceeds by following along such tracks using oil immersion objectives. The observer picks at random the first satisfactory track and follows it until it leaves the volume under examination. He then makes a small arbitrary displacement of the microscope stage, selects a second track and repeats the procedure. An area of 4×7 cm^2 of each plate is scanned in this manner. If a plate is examined by this method for a total time of ~ 40 hours, it can be shown that about 30 percent of the tracks are found more than once and approximately 20 percent of the material escapes detection altogether. Among the observations recorded were electron pairs, tridents, and electromagnetic cascade phenomena including bremsstrahlung pairs which have been discussed previously.[17] The quantum energies of the pairs were estimated from the opening angles. The energies of the secondary particles from tridents were measured by multiple scattering and in favorable circumstances the energy of the primary was similarly determined.

The measurement of electron energies by multiple scattering is complicated by the appreciable radiative losses which may occur along the necessary minimum length of track. An additional difficulty arises from the fact that great path lengths are required for even a rough energy measurement of the very energetic particles, so that the determinations for high energies are relatively uncertain. For very low energies there is a tendency for the particles to scatter out of the emulsion so that insufficient track length is available for measurement. Thus there is a considerable measurement bias at both high and low energies. Further it is well known that the determination of quantum energies from opening angles of pairs is at best a crude estimate. We conclude that the majority of energy measurements made in this work are subject to considerable error.

B. Cross-Section Determination

The total cross section is derived from the experimentally determined mean free path; for this purpose the number of tridents found is compared with the length of electron track examined. Since the emulsion is traversed by an admixture of fast protons, mesons and electrons, it is not generally possible to estimate the total track length of the electrons alone. However, it is possible to determine that length of electron track which originates from pairs formed in the emulsion. In order, therefore, to evaluate the electron trident cross section, only those tridents occurring on arms of pairs can be used. Out of 67 tridents found through our scanning procedure, only 14 occurred on pairs and could be employed for the cross section determination.

The quantum energies of the pairs found in our experiment ranged from several Mev to many Bev. Since ~ 90 percent of the tridents were found to have primary energy between 0.1 and 10 Bev, we have restricted our analysis to those pairs and the 61 tridents in this interval of energy. Our choice of 10 Bev as the upper limit is arbitrary; the evaluation of total track length from pairs is not greatly influenced by this selection since from the spectrum given by (6) the major intensity contribution is from lower energy electrons.

(*i*) *Total Track Length from Pairs*

A direct measurement of length and energy for all pair tracks would be unduly costly in time. We have therefore measured the track lengths in a sample of 3 out of the 26 plates. In order to exclude tracks due to electrons of energy less than 100 Mev, we have made two corrections. Firstly, the pairs with quantum energies estimated from opening angle to be less than 100 Mev were eliminated. Secondly, the contribution due to electrons of energies less than 100 Mev arising from pairs with quantum energies exceeding 100 Mev was subtracted. For the latter correction the distribution (6) and a random energy partition within the pairs was assumed. Details of the path length determination together with the estimated uncertainties are shown in Table I. The total length of pair tracks within the energy interval was found to be 1440 ± 490 cm. The indicated probable error includes both the uncertainty in correcting for the amount of electron track with energies less than 100 Mev and the error in extrapolation of the path length from the sample. The major source of error arises from the attempt to apply a sharp cutoff at 100 Mev where the spectral intensity is greatest.

(*ii*) *Correction for Pseudo-Tridents*

In the same energy interval and volume of emulsion in which the 61 tridents were found, a study of 200

TABLE I. Evaluation of mean free path for tridents formed on arms of pairs in the energy interval 0.1–10 Bev. The determination was confined to the track length from pairs created in the emulsion and to tridents formed on arms of such pairs.

Track length per plate from pairs with quantum energy $E_\gamma > 100$ Mev.	84.3 ± 13.3 cm
Calculated length correction factor (allows for the inclusion of electrons of energy less than 100 Mev originating in pairs with quantum energies exceeding 100 Mev; includes error in estimate of E_γ).	0.66 ± 0.20
Number of plates	26
Corrected track length	1440 ± 490 cm
Number of tridents on arms of pairs	14
Number corrected for pseudo-tridents	11.8
Maximum likelihood value of mean free path	134 ± 42 cm

[21] These characteristics were adopted because studies of meson emission were pursued concurrently.

bremsstrahlung pairs has been made in order to estimate the incidence of pseudo-tridents.[17] In this work the calculations on the proximity distribution of bremsstrahlung pairs indicated that ~6 percent of these phenomena are experimentally indistinguishable from tridents. In order to estimate the true number of tridents among the observations we apply a correction factor of $(1-0.06\times 200/61)=0.81$ to the number, 14, of tridents initiated by pair particles. Thus the appropriate number of tridents upon which to base the mean free path determination is $0.81\times 14=11.8$.

(iii) *Evaluation of Mean Free Path*

In experiments of this type the mean free path is conventionally taken to be $\bar{\lambda}$, the total path length divided by the number of events. However, if the total path length is finite, the true mean free path is in general somewhat larger than $\bar{\lambda}$ and approaches $\bar{\lambda}$ as the number of events increases. This effect is due to events occurring near the end of the total path where the available remaining path length may be smaller than the mean free path. The magnitude of this effect is evaluated by employing the statistical method of "maximum likelihood," as shown below.

We assume that all events are characterized by the same mean free path λ. A convenient model is to picture all of the scanned track laid end to end to form one continuous path of length Y, in which M events are observed. Let us measure the path lengths of the individual events from the beginning of the composite track and denote them by $y_1, y_2, y_3 \cdots y_M$, where $y_1 \leq y_2 \leq y_3 \leq \cdots \leq y_M \leq Y$. Define $x_j = y_j - y_{j-1}$, and $X_j = Y - y_{j-1}$, where $y_0 = 0$; x_j is the distance traveled to event j from the preceding event, and X_j is the amount of track length available in which event j can take place. The probability that event 1 occurs between the origin and Y (or in distance X_1) is unity. Similarly, the probability that event 2 occurs between y_1 and Y (or in distance X_2) is unity. In general, the probability that event j occurs in distance X_j is unity. Thus, the probability that event j occurs between x_j and x_j+dx_j is given by

$$P(\lambda,x_j)dx_j=\exp\{-x_j/\lambda\}(1-\exp\{-X_j/\lambda\})^{-1}dx_j/\lambda.$$

The compound simultaneous probability that all x_j lie in their corresponding dx_j is given by

$$G(\lambda,x_1,x_2,\cdots x_M)dx_1dx_2\cdots dx_M = \prod_{j=1}^{M} \exp\{-x_j/\lambda\}(1-\exp\{-X_j/\lambda\})^{-1}dx_j/\lambda.$$

Following Annis *et al.*,[22] we obtain λ_l, the "maximum likelihood" estimate of λ, by maximizing G, i.e., by solving the equation

$$\frac{\partial G}{\partial \lambda}(\lambda,x_1,x_2,\cdots x_M)\Big]_{\lambda=\lambda_l}=0 \quad \text{for} \quad \lambda_l.$$

In this fashion we obtain

$$\lambda_l \approx \lambda + M^{-1}\sum_{j=1}^{M} X_j(\exp\{X_j/\bar{\lambda}\}-1)^{-1}, \quad X_j \gg \bar{\lambda}. \quad (13)$$

Equation (13) is formally identical with Eq. (54) of Annis *et al.*, but arises from consideration of a different physical situation. In the same manner, a measure of the statistical uncertainty is given by

$$\epsilon(\lambda)\approx\lambda_l\left\{M-\sum_{j=1}^{M}\left(\frac{X_j}{\bar{\lambda}}\right)^2\left[1-\exp\left(-\frac{X_j}{\bar{\lambda}}\right)\right]^{-2}\times\exp\left(-\frac{X_j}{\bar{\lambda}}\right)\right\}^{-\frac{1}{2}}. \quad (14)$$

Since in our experiment we have no information regarding the individual values of the X_j's, but only know $\bar{\lambda}$ and M it is reasonable to assume that on the average, when $j=1$, $X_1=M\bar{\lambda}$; $j=2$, $X_2=(M-1)\bar{\lambda}$; $\cdots j=j$, $X_j=(M-j+1)\bar{\lambda}$. If for simplicity we put $i=M-j+1$, and subsitute in (13), we obtain

$$\lambda_l=\bar{\lambda}\{1+M^{-1}\sum_{i=1}^{M} i(e^i-1)^{-1}\},$$

which, for $M \gtrsim 8$, becomes

$$\lambda_l \approx \bar{\lambda}(1+1.18M^{-1}). \quad (15)$$

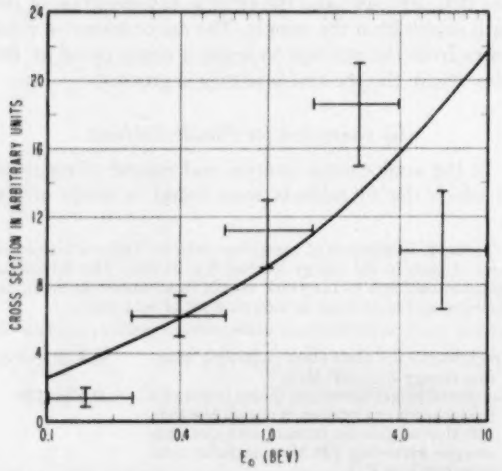

FIG. 5. Comparison of the experimental number of tridents per unit energy interval weighted by the primary electron spectrum, with the theoretical total cross section as a function of primary energy. The theoretical cross section, which includes screening, has been arbitrarily normalized to the experimental point at a primary energy of 0.4 Bev.

[22] Annis, Cheston, and Primakoff, Revs. Modern Phys. 25, 818 (1953).

Thus, as $M\to\infty$, λ_l approaches $\tilde{\lambda}$, as is expected. Similarly, from (14), the statistical uncertainty is given by

$$\epsilon(\lambda)=\lambda_l(M-2.39)^{-\frac{1}{2}}. \tag{16}$$

For our experiment, where M is 11.8, we obtain from (15) and (16), $\lambda_l=1.1\tilde{\lambda}$ and $\epsilon(\lambda)=0.33\lambda_l$. Thus we see that the mean free path is 10 percent greater than the usual determination and the associated statistical uncertainty is 14 percent greater than the uncertainty conventionally taken as $M^{-\frac{1}{2}}$ (standard deviation).

Consideration of the total path length from pairs (1440±490 cm), the corrected number of tridents (11.8) and the appropriate statistical error leads to a value of trident mean free path $\lambda_l=134\pm42$ cm for our experiment. This value of λ_l corresponds to a cross section of $0.93\pm0.29\times10^{-25}$ cm^2, where the number of atoms per cm^3 is taken to be 8.03×10^{22} for G5 emulsion and the uncertainties indicated are probable errors.

(iv) *Comparison with Theory*

The experimental result, $0.93\pm0.29\times10^{-25}$ cm^2, is to be compared with the theoretical prediction from Sec. II, 0.80×10^{-25} cm^2. The agreement is satisfactory. In order to investigate whether this agreement is fortuitous, we have attempted a test of the assumptions upon which the theoretical prediction is based. The theoretical cross section averaged from 0.1 to 10 Bev is compounded of the energy variations of both the trident cross section and the incident electron spectrum. A simultaneous check of the assumed forms of these variations, (5) and (6), is afforded by a comparison of the experimental excitation function with theory. All 61 tridents were employed; a plot of the relative yield with energy is given in Fig. 5. The experimental number of tridents per unit energy interval was divided by the spectrum (6) and compared to (5), modified by screening. The curve was arbitrarily normalized to the experimental value at 400 Mev. The indicated errors are standard deviations due to statistics. In view of the limited number of observations and the errors in energy determination, the prediction is consistent with experiment. It therefore appears justifiable to employ (5) and (6) in an evaluation of the averaged theoretical cross section.

C. Energy Division Among the Secondaries

It is not possible to identify the created pair among the three secondaries. Theory, however, suggests that a large majority of the pairs produced have energies less than one-half that of the primary electron. In Fig. 3, the plot of the differential cross section as a function of R, where $R=E_{\text{pair}}/E_{\text{primary}}$, illustrates this point. Following earlier experiments,[10] we employ the convention in which the two secondaries of lowest energy are taken to be the created particles. Under this assumption the largest attainable value of the quantity R is $\frac{2}{3}$. The energies of the outgoing particles have been

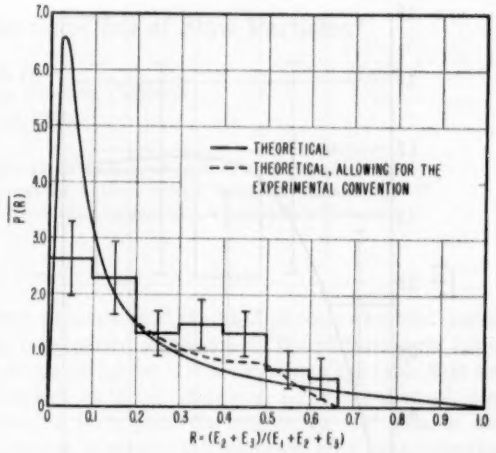

FIG. 6. Comparison of experimental R-distribution with the averaged theoretical probability for fractional transfer of primary energy to trident pairs. E_1, E_2, and E_3 are the energies of the secondaries with $E_1\geq E_2\geq E_3$.

measured by multiple scattering; for each trident R is determined as the ratio of the sum of the two lowest energies to the sum of all three. The experimental probability distribution in R is given as a histogram in Fig. 6. All 61 tridents found in the energy interval 0.1 to 10 Bev were used in this plot, and indicated uncertainties are standard deviations.

For comparison with experiment the quantity $\bar{P}(R)$ of (11) is shown in Fig. 6 as the solid curve. It has been modified to take account of the effects of our convention, on the assumption of random energy partition within the created pair. The modification results in a small redistribution of the area under $\bar{P}(R)$ for $R>\frac{1}{2}$ and a cutoff at $R=\frac{2}{3}$. The altered $\bar{P}(R)$ is the dashed curve in Fig. 6. The experimental results are not in marked disagreement with the theory. It appears, however, that the experimental values are higher than the theoretical for large values of R, but the significance of this conclusion is doubtful because of poor statistics and because distortion of the R-distribution may occur through systematic errors in energy measurement.

A previous determination[10] of the R-distribution was in poor agreement with theory; this may have been due to the search procedure by which the material was found, in which possibly there was a discrimination against low values of R. In the present experiment this disadvantage was probably minimized by scanning along tracks.

A similar study has been made of the experimental probability distribution in r. For this purpose, r was taken to be the ratio of the lowest secondary energy to the sum of the two lowest secondary energies. Figure 7 shows the experimental histogram compared with the theoretical averaged probability distribution $\bar{P}(r)$ of (12). We have examined the effects of our experimental convention upon the theoretical r-distribution and have

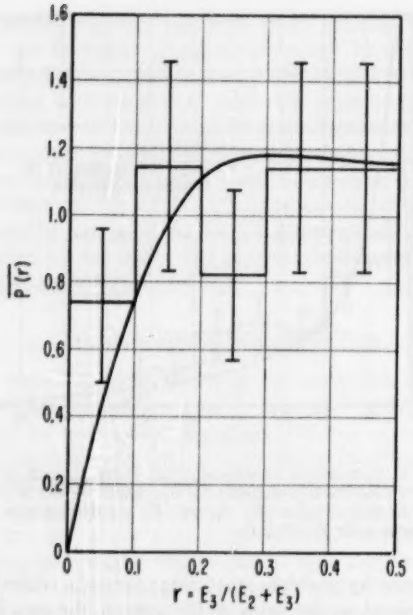

FIG. 7. Comparison of experimental r-distribution with the averaged theoretical probability for internal energy partition within trident pairs. E_2 and E_3 are the two lowest secondary energies with $E_2 \geq E_3$.

concluded that in this case the redistribution results in a sufficiently small change in the shape of $\bar{P}(r)$ that we have neglected it. The agreement between theory and experiment is again satisfactory.

IV. CONCLUSIONS

In the course of this text we have made the observations summarized as follows:

(a) a reconsideration of Bhabha's theory shows that it is consistent with Racah's prediction of total cross section;

(b) the experimentally determined total cross section in the energy interval between 0.1 and 10 Bev is consistent with the above predictions;

(c) the experimental variation of total cross section with energy for the same energy region is consistent with theory;

(d) the experimental distributions in both the fractional energy transfer to the trident pair and the energy partition within the pair are consistent with Bhabha's theory.

From the above evidence we conclude that the quantum electrodynamical description of direct pair production by fast electrons, as given by Bhabha, is a satisfactory representation of the trident process in the energy interval 0.1 to 10 Bev.

Freier and Naugle[23] have recently reported an experimental determination of electron trident mean free path which is in serious disagreement with theory. Their measurements, made in the core of a "jet," were of primary energy of the order of 100 Bev; the experimental m.f.p. was several times less than the theoretical value. As a result of these measurements it has been suggested that the theory of direct pair creation might break down at these energies. More recently, Koshiba and Kaplon[24] have presented somewhat similar results at energies $\sim$10 Bev. In a recent communication[17] we have estimated that rather large corrections might be appropriate to these experiments; consideration of the pseudo-trident contribution would lead to a significant increase in the value of the experimental mean free path. We are therefore of the opinion that there is no firm evidence at this time that theory is in serious disagreement with experiment.

ACKNOWLEDGMENTS

We are indebted to Dr. M. M. Shapiro for his continued interest and support of this work and to Dr. P. S. Freier, Dr. M. F. Kaplon, and their colleagues for interesting discussions. Mrs. N. T. Redfearn assisted in gathering much of the data and B. Stiller and F. O'Dell processed the emulsions.

[23] P. S. Freier and J. E. Naugle, Proceedings of the Duke University Cosmic Ray Conference, *I-22*, 1953 (unpublished).
[24] M. Koshiba and M. F. Kaplon, Phys. Rev. **95**, 647 (1954).

Čerenkov Radiation Detector for the Selection of Slow Particles*

CARL M. YORK, JR.†
California Institute of Technology, Pasadena, California
(Received August 2, 1954)

A cloud chamber in a magnetic field has been operated at an altitude of 1750 m. The chamber was triggered by a slow-particle selector which utilizes the properties of the Čerenkov radiation. An analysis of 1142 pictures is presented and one possible example of the nuclear capture of a K^- particle is discussed in detail.

SEVERAL authors[1,2] have described slow-particle selectors using a Čerenkov radiation detector as a means of imposing a restriction on the velocity of the particles traversing their apparatus. A device very similar to that described by Hyams[1] is shown in Fig. 1 and has been operated at Mt. Wilson (1750 m) for several months. In principle the cloud chamber is triggered by charged particles which trip the Geiger counters A, B, and C without emitting any Čerenkov radiation on traversing the Lucite block. This last restriction is obtained by using the amplified output pulses of the photomultiplier tube (RCA 5819) in anticoincidence with the Geiger counters. Because Čerenkov radiation is emitted only by particles traveling faster than the critical velocity for the dielectric material they traverse, fast particles will not trip the chamber. This critical velocity is $\beta \sim 0.66$ for Lucite.

The cloud chamber was operated in an average magnetic field of 3500 gauss and was held at constant temperature (± 0.1°C) by a surrounding thermostatted heat shield. All momentum and angle measurements were made and corrected in the manner described by Leighton *et al.*[3] A brief study of no-field curvatures of tracks in the chamber indicated that a reasonable value of the maximum detectable momentum for a 12-cm track in the chamber is 1.5 Bev/c. Table I gives an analysis of the 1142 pictures obtained during the total period of operation. The pictures were taken at a rate of 2.5 hr^{-1}. It is clear from the table that the Čerenkov detector allows a large number of fast particles to trigger the apparatus, but this is not surprising in view of the relatively poor light collection efficiency of the photomultiplier tube for the total volume of the Lucite block. The initial identification of particles was obtained either from momentum measurements and a visual estimate of the ionization or from the loss in momentum suffered by a particle traversing the ½-in. copper plate mounted in the center of the chamber. No pictures which could be interpreted as the decay in flight of an unstable particle were obtained.

TABLE I. An analysis of 1142 pictures triggered by the Čerenkov selector.

Type of event	Number
Single slow particles:	
Possible K particle	1
Protons	38
Mesons	51
Undetermined	10
Single fast particles:	519
Multiple events:	
Electron showers	146
Penetrating showers	8
Blanks	298
Slow electrons from top of chamber	71
Total	1142

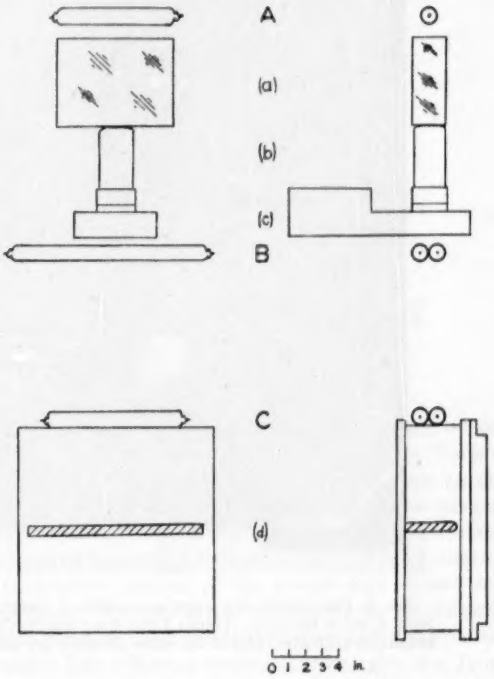

FIG. 1. Diagram of the apparatus. A, B, and C are Geiger counters; (a) is a Lucite block, (b) an RCA 5819 photomultiplier tube, (c) a preamplifier, and (d) the cloud chamber containing a ½-in. copper plate. A 2-in. layer of lead bricks mounted 18 in. above counter A, the mu metal and iron magnetic shields surrounding the photomultiplier (b), and the magnet yoke are not included in the figure.

* Supported by the joint program of the U. S. Atomic Energy Commission and the U. S. Office of Naval Research.
† Now at the University of Chicago, Chicago, Illinois.
[1] T. Duerden and B. Hyams, Phil. Mag. 43, 717 (1952); B. Hyams, Bagneres Conference Report, (unpublished, 1953).
[2] J. Keuffel and L. Mezzetti, Phys. Rev. 94, 797(A) (1954).
[3] Leighton, Wanlass, and Anderson, Phys. Rev. 89, 148 (1953).

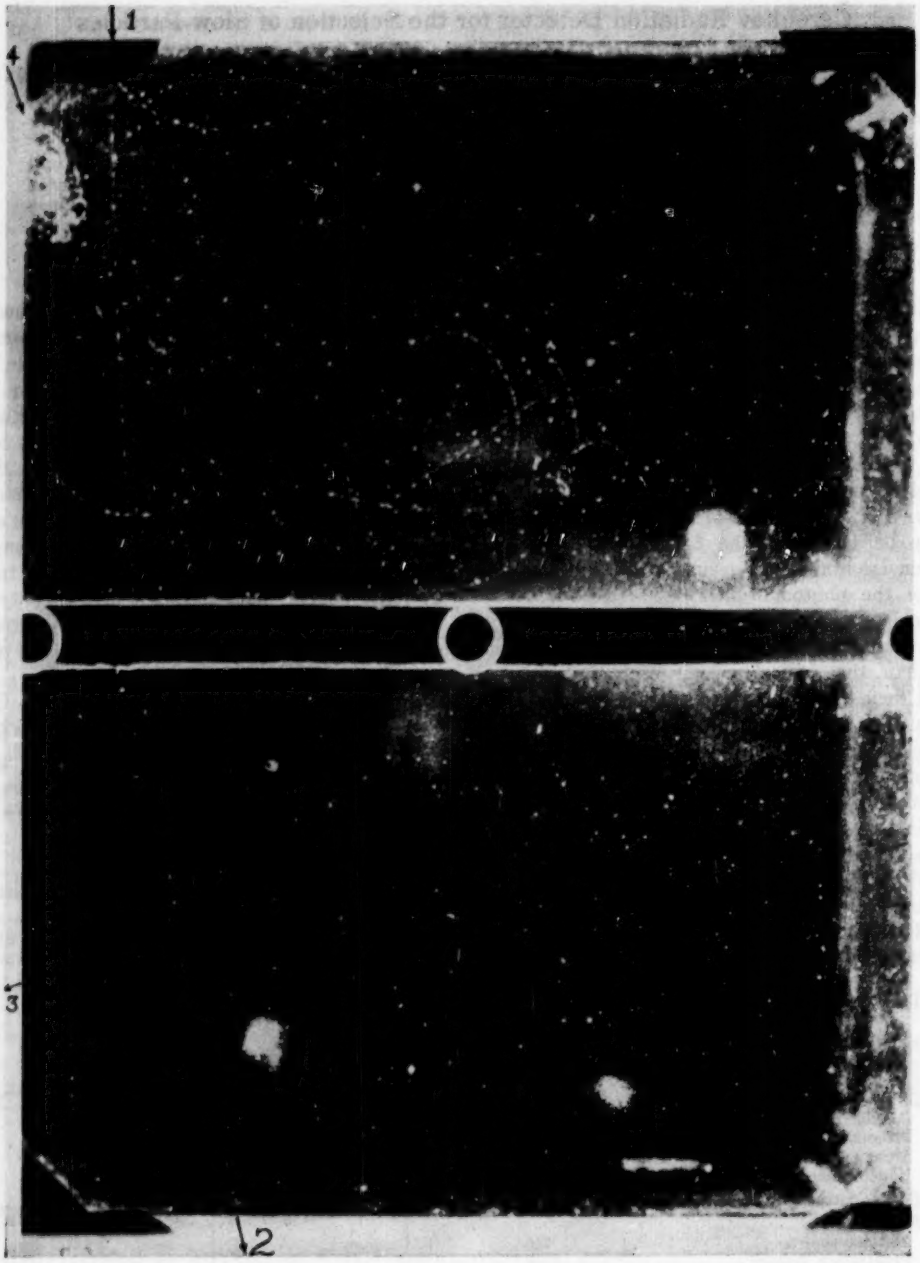

FIG. 2. Photograph of a negative particle, 1, entering the upper left-hand side of the chamber and giving rise to track 2 below the plate. Tracks 3 and 4 are electron tracks in the plane of the chamber used for comparison in the ionization estimates. (All of the other electrons are moving steeply forward or backward in the chamber.)

One event in which a negative particle apparently traverses the copper plate proved to be of considerable interest and is shown in Fig. 2. The measurements are: $P_1=230\pm37$ Mev/c, $I_1=5(\pm1)\times I_{\min}$; $P_2=116\pm12$ Mev/c, $I_2=3(\pm1)\times I_{\min}$; $P_3=9.3$ Mev/c; and $P_4=11$ Mev/c. The angle between tracks 1 and 2 is $5°\pm2°$. Tracks 3 and 4 are assumed to be electrons and have had their density on the film compared to that of tracks 1 and 2 by a photometric method to give the ionization values, I_1 and I_2 quoted above. Although this photometric method has not yet been developed in complete detail, it is considered to be less subjective

than the usual visual estimates and hence has been used in the analysis. If one accepts these values of the ionization, the masses of the particles are: M_1: 840–1440 m_e and M_2: 250–520 m_e where the range of values results from the combined uncertainty in the momenta and ionizations. The simplest explanation of this event is that a K^- particle comes to rest in the plate and causes the ejection of a light meson. If the K^- is assumed to have a mass of $\sim$1000 m_e, it should come to rest very near the center of the copper plate, and a light meson (π or μ) would lose about 15 Mev/c before emerging from the plate with a momentum of 116 Mev/c. Thus this event can be interpreted either as a K^--produced star which ejects a π meson of 51-Mev kinetic energy or as a K^- decay at rest with the emission of a light meson. The former possibility seems to be more likely because the stopping material has a high atomic number and similar events have been reported elsewhere.[4] However, it should be emphasized that both of these interpretations hinge on the ionization determinations. If ionization is ignored, the momentum change implies either that a particle of mass $\sim$600 m_e traversed the plate or that a lighter particle (π meson or electron) suffered an anomalously large momentum loss on traversal. The possibility that this event represents a positive π meson which goes upward and gives rise to a proton which in turn emerges from the plate in an upward direction is energetically acceptable, but considered highly unlikely in view of the ionization of track 1 and the geometry of the experiment. Thus the simplest and most consistent explanation of this event seems to be that a K^- particle stops in the plate and ejects a π^- meson from a nuclear interaction.

The author would like to express his thanks to Dr. R. B. Leighton who constructed the magnet and cloud chamber and to Mr. E. K. Bjørnerud for performing the ionization measurements referred to above. He would also like to express his appreciation to Professor C. D. Anderson for many stimulating and enlightening discussions.

[4] Lal, Pal, and Peters, Phys. Rev. **92**, 438 (1953); Hill, Salant, and Widgoff, Phys. Rev. **94**, 1794 (1954); Major, Macpherson, Parkash, and Rochester (private communication).

PHYSICAL REVIEW VOLUME 96, NUMBER 6 DECEMBER 15, 1954

Nuclear Fine Structure in the μ-Mesonic Atom*

BORIS A. JACOBSOHN
Department of Physics, University of Washington, Seattle, Washington

(Received August 23, 1954)

The $2p-1s$ transition of a μ-mesonic atom is split not only by the spin-orbit energy but also by the electric quadrupole interaction between meson and nucleus. If a high-Z nucleus has excited states at several hundred kilovolts or less this interaction can be expected to mix nuclear states, so that for example an even-even nucleus with ground state spin zero can produce a quadrupole fine structure. General formulas are given for the calculation of the line patterns; these are worked out for W, U^{238}, and Ta^{181}. The resulting fine structure is spread over a region of 300–500 kev. The details of the positions and intensities of the lines depend on the quadrupole moments of the excited nuclear states as well as on other parameters which can in principle be measured in other types of experiments; the effect therefore offers a method for investigating these excited moments. A certain fraction of the mesonic gamma rays can be followed by a nuclear radiation; this fraction can be as high as 0.50.

I. INTRODUCTION

THE μ-mesonic atom has proved to be a useful tool in the measurement of nuclear size.[1,2] The reasons for its utility as a probe for nuclear electromagnetic effects are well summarized by Wheeler,[3] who emphasizes the smallness of the Bohr orbits and the transparency of nuclear matter to μ mesons.

Atomic electrons are also commonly used as a tool in nuclear physics, the fine structure of their spectrum yielding values of magnetic dipole and electric quadrupole moments for the ground states of nuclei. There are certain striking differences, however, between an electronic- and a μ-mesonic atom which enable the spectrum of the latter to yield additional nuclear information. The most important of these, for our purposes, concerns the relative fineness of the atomic and nuclear level spacings. (All qualitative arguments in the following shall be made for nuclei at the heavy end of the periodic table.) The difference between the energies of a $2p$ and $1s$ μ meson is several Mev; if now the nucleus in question has low-lying levels with spacings $\sim$100 kev, the meson sees the nucleus not as a rigid structure in its ground state, but as a system in an almost degenerate mixture of several states. A fine structure is induced in the μ levels which depends on the nondiagonal as well

* A preliminary report on this work was given at the May, 1954 Washington meeting of the Americal Physical Society [Phys. Rev. **95**, 654 (1954)]. It has subsequently been called to the author's attention that a paper on the same subject by L. Wilets is to be published.

[1] V. L. Fitch and J. Rainwater, Phys. Rev. **92**, 789 (1953).
[2] L. N. Cooper and E. M. Henley, Phys. Rev. **92**, 801 (1953).
[3] J. A. Wheeler, Phys. Rev. **92**, 812 (1953).

as the diagonal matrix elements of the nonspherical electromagnetic interaction between μ and nucleus. Thus, an even-even nucleus which, since its ground state spin is zero, would look spherically symmetric to an atomic electron might appear to be a mixture of $I=0$ and $I=2$ to a μ meson in a low Bohr orbit. In the former case, no hyperfine structure would appear; in the latter it would.

Before we consider the conditions necessary for this effect to be appreciable, we should mention several other differences between mesonic and electronic atoms. First we recall the fact that, in low orbits, the μ spends an appreciable amount of time inside the nucleus. This fact, which has proved so useful in the measurement of nuclear size, shall prove for us to be somewhat of a nuisance. It makes the fine structure depend not only on gross properties of the nucleus, such as the quadrupole moment, but also on other things such as the distribution of the quadrupole-producing charge. At some future time, if experiments such as those outlined here should prove feasible, such dependence might prove advantageous; in the present calculation, it forces us to introduce a nuclear model midway in the formulas (Sec. II).

Another important difference is that, although magnetic dipole and electric quadrupole hyperfine structure effects are of approximately equal importance for electrons, the former will be completely negligible for a μ.[3] The ratio of quadrupole to dipole interaction energy is, in order of magnitude,

$$\frac{\langle e^2Q_N/r^3\rangle}{\langle \mu_N\mu_a/r^3\rangle}=\frac{e^2Q_N}{\mu_N\mu_a},$$

where μ_N and μ_a are the magnetic moments of the nucleus and the atomic particle, respectively. This ratio, which is ~ 1 in the electronic case, is instead ~ 100 for the meson if its magnetic moment is one mesonic magneton. We shall ignore all magnetic effects except for the meson spin-orbit interaction, which is comparable to the quadrupole energy. Moreover, although many arguments can be given in favor of omitting from consideration all electric interactions other than quadrupole, we shall bypass them by pointing out that in this calculation we shall be concerned with orbital μ's with $l=0$ and 1; these can produce at the most a quadrupole field at the nucleus. Since we shall restrict ourselves to nuclei which have low states all of the same parity, electric dipole effects shall also be ignored.[4]

We shall now estimate the amount of mixing of nuclear levels to be expected. This will be appreciable whenever the matrix elements of the quadrupole interaction are comparable to the separation of two nuclear levels a and b; i.e., if

$$1\lesssim\left\langle\frac{e^2}{r^3}\right\rangle_{2p}\frac{|(b|Q|a)|}{|E_a-E_b|}\sim\frac{e^2Z_{\rm eff}^3}{24a_\mu^3}\frac{|Q_a|}{\Delta E}$$
$$\sim(4\times10^{20}\ \text{kev/cm}^2)Z_{\rm eff}^3|Q_a|/\Delta E. \quad (1)$$

[Equation (1) makes use of the fact pointed out by Bohr and Mottelson[5] that many nuclei have large off-diagonal quadrupole matrix elements (collective transitions) comparable in size to the large ground state quadrupole moments.] Thus nuclei with fairly high Z and with excited states at about 100 kev can be expected to show this effect, provided that the quadrupole moments in the region of the periodic table under consideration are $>1\times10^{-24}$ cm^2. As BM has shown, the last two requirements are likely to be satisfied simultaneously in regions of the periodic table far from the magic numbers.

The formulas developed in the following sections include as a special case the static quadrupole effect considered by Wheeler;[3] his results are valid when ΔE is large enough to reverse the inequality (1).

II. GENERAL THEORY

The Hamiltonian to be used for the system of meson and nucleus is

$$H=H_N+H_\mu+H_S+H_{\mu N}. \quad (2)$$

H_N operates only on the nuclear coordinates and has eigenvalues E_1, E_2, $\cdots$, the experimentally known nuclear levels. H_μ depends on the meson coordinates and contains the spherically symmetric potential energy $V(r)$ arising from the nucleus in its ground state.[2] In the equation

$$H_S=g\left(\frac{h}{2Mc}\right)^2\frac{1}{r}\frac{dV}{dr}(\boldsymbol{\sigma}\cdot\mathbf{L}/\hbar), \quad (3)$$

M = meson mass and $g=-[2Mc/h|e|]\times$[meson magnetic moment]. Henceforth, we shall take $g=1$.

The last term in Eq. (2) contains all electric effects not already included in $V(r)$; we expand it and, as previously explained, keep only the electric quadrupole part. Thus

$$H_{\mu N}\to H_q=-e^2\textstyle\sum_P F(r,R_P)P_2(\cos\Theta_P)$$
$$=-e^2\textstyle\sum_P F(r,R_P)\mathbf{C}^{(2)}(\theta_P,\varphi_P)\cdot\mathbf{C}^{(2)}(\theta,\varphi), \quad (4)$$

$$F(r_1,r_2)=(r_<)^2/(r_>)^3. \quad (5)$$

All the notation used here for angular factors and matrix elements is taken from Racah.[6] The coordinates with subscripts P refer to the protons, those without subscripts to the meson.

[4] Even if low-lying states of opposite parity should be present, electric dipole effects would be small since (a) the meson would be in a state which mixes $2s$ and $2p$, introducing a large energy denominator [see J. A. Wheeler, Revs. Modern Phys. **21**, 133 (1949)], and (b) the nuclear dipole matrix elements are presumably not enhanced by collective effects.

[5] A. Bohr and B. R. Mottelson, Kgl. Danske Videnskab. Selskab, Mat.-fys. Medd **27**, No. 16 (1953). We shall continually refer to this paper as BM.

[6] G. Racah, Phys. Rev. **62**, 438 (1942).

To solve the Hamiltonian (2) for large Z and for small nuclear level spacing, we ignore all elements $(n'l'\cdots|H|nl\cdots)$ unless $n=n'$, and $l=l'$. This is fully justified if we wish to treat only the low orbits; for example, the nearest orbit connected to the $2p$ by H_q is the $3p$, which lies one or two Mev higher in energy. An immediate consequence of this approximation is that H_q has no effect for the $l=0$ orbits; the $1s$ group consists of pure nuclear states with energies

$$E=E_\mu(1s_{\frac{1}{2}})+E_N(I). \tag{6}$$

For the $2p$ orbit, we write down the matrix elements of expression (4) in a scheme in which the following are diagonal: H_N (with energy E_N and angular momentum I), j (total angular momentum of the meson), and J ($\mathbf{J}=\mathbf{I}+\mathbf{j}$). Equations (38) and (53) of reference[6] yield immediately

$$(I_1j_1J|H_q|I_2j_2J)=e^2(-1)^{I_1+\frac{1}{2}-J}(4/5)^{\frac{1}{2}}W(I_1j_1I_2j_2;J2)\times\langle(I_1\|\sum F(r,R_P)C^{(2)}(\theta_P,\varphi_P)\|I_2)\rangle_{2p}. \tag{7}$$

W is a Racah coefficient; extensive numerical tables of these have recently appeared.[7]

If the meson orbit were always outside of the nucleus, we could write $F(r,R_P)=R_P^2/r^3$. The double-barred symbol of Eq. (7) could then be factored into $\langle r^{-3}\rangle_{2p}$ $\times$ {a factor proportional to the nuclear quadrupole moment if $E_N(1)=E_N(2)$, or the quadrupole matrix element for $E_N(1)\neq E_N(2)$}. We utilize this fact to guide us in making some new definitions which separate out the factor which depends on the penetration of the meson into the nucleus.

First, for those cases in which $E_N(1)=E_N(2)$, $I_1=I_2=I$, we define the quadrupole moment of the nuclear state in the customary way:

$$Q(I)\equiv(I,+I|\sum R_P^2(3\cos^2\theta_P-1)|I,+I). \tag{8}$$

If we now define the "penetration function" $P(I,I;r)$ for $I\geqslant 1$ (the double-barred symbol is zero for $I<1$) by

$$Q(I)\frac{P(I,I;r)}{r^3}\equiv\left\{\frac{4I(2I-1)}{(I+1)(2I+1)(2I+3)}\right\}^{\frac{1}{2}}\times(I\|\sum F(r,R_P)C^{(2)}\|I), \tag{9}$$

it follows from the formulas of Racah[6] that $P(I,I;r)=1$ for all r larger than the nuclear radius R_0. For $r<R_0$, $P(I,I;r)$ is a form factor depending on the radial distribution of the quadrupole-producing charge; the model of a slightly ellipsoidal uniform charge distribution yields

$$P(I,I;r)=(r/R_0)^5 \quad \text{for} \quad r<R_0, \tag{10}$$

which has been used here in all numerical calculations.

Similarly one can separate the form factor for those matrix elements in Eq. (7) which are nondiagonal in the nuclear states. From the customary definition[5] for the reduced quadrupole transition probability,

$$B(I_1\to I_2;2)=e^2\textstyle\sum_{\mu,M_2}|(I_1M_1|\sum R_P^2Y_{2\mu}|I_2M_2)|^2, \tag{11}$$

the function $P(I_1,I_2;r)$ is defined by

$$\left\{\frac{4\pi}{5e^2}(2I_1+1)B(I_1\to I_2;2)\right\}^{\frac{1}{2}}\frac{P(I_1I_2;r)}{r^3}\equiv(I_1\|\sum F(r,R_P)C^{(2)}\|I_2), \tag{12}$$

for $E_2>E_1$. (The cases with $E_2<E_1$ need not be written down; the required matrix elements are most easily found from the Hermitian property of H_q.) With the phases of the nuclear wave functions chosen appropriately, it can easily be shown that $P(I_1I_2;r)=1$ for $r>R_0$. In the numerical calculations, the Bohr-Mottelson result for a collective transition has been used:

$$P(I_1I_2;r)=(r/R_0)^5 \quad \text{for} \quad r<R_0. \tag{10'}$$

All the formulas necessary for calculating the $2p$ energy levels and wave functions are contained in Eqs. (3), (7), (9), and (12). These are completely independent of any model of the nucleus, and correspondingly contain many unknown quantities. In principle, a precise measurement of the fine structure combined with other experiments which measure the $B(2)$'s and the ground state Q could be made to yield information about some of the form factors. However, since for all but the largest Z's a $2p$ meson does not spend a great fraction of its time inside the nucleus, the spectrum is not extremely sensitive to the penetration factors. This enables us to decrease the number of unknowns by inserting Eqs. (10) and (10') for the penetration factors (R_0 is here the electromagnetic nuclear radius). The results then depend only weakly on the nuclear model; for example, for $Z\sim 70$ the very extreme assumption that all the quadrupole-producing charge is concentrated at the center of the nucleus increases our estimate of $\langle P(r)/r^3\rangle_{2p}$ by a factor of only 1.6.

With this approximation, the positions and intensities (as we shall see in Sec. III) of the fine structure of the $2p-1s$ lines are completely determined in terms of the nuclear electromagnetic radius, the nuclear energy levels, and the nuclear quadrupole moments (static and dynamic). Some of these parameters are susceptible to measurement by other methods; a study of the effect here considered could then yield information about the remaining parameters, such as the quadrupole moments of certain excited nuclear states. For this reason, we prefer not to insert as yet definite predictions derived from a nuclear model for these parameters. They shall be left free so that the sensitivity of the spectrum to variations in the quadrupole moment of an excited state can be examined.

For those nuclei which follow the Bohr-Mottelson strong-coupling sequence of states ($I=0, 2, 4, \cdots$ for A even; $I=I_0, I_0+1, I_0+2, \cdots$ for A odd), it is convenient to introduce one more bit of notation.

[7] Simon, Van der Sluis, and Biedenharn, Oak Ridge National Laboratory Report, 1679, 1954 (unpublished).

TABLE I. The factors $f(I,I';I_0)$ of Eq. (14) where I_0 is the ground state spin, and equals zero for an even-even nucleus.

I'	$f(I,I';I_0)$
I	$\left\{\frac{1}{5}\frac{2I+1}{I(2I-1)(I+1)(2I+3)}\right\}^{\frac{1}{2}}[3I_0^2-I(I+1)]$
$I+1$	$\left\{\frac{3}{5}\frac{I_0^2[(I+1)^2-I_0^2]}{I(I+1)(I+2)}\right\}^{\frac{1}{2}}$
$I+2$	$\left\{\frac{3}{10}\frac{[(I+1)^2-I_0^2][(I+2)^2-I_0^2]}{(I+1)(I+2)(2I+3)}\right\}^{\frac{1}{2}}$

Instead of the quadrupole moments $Q(I)$, we define a set of numbers $Q_0(I,I)$:

$$Q(I)\equiv\frac{3I_0^2-I(I+1)}{(I+1)(2I+3)}Q_0(I,I), \tag{13}$$

where I_0 is the ground-state spin. $Q_0(I,I)$ has been chosen so that it would be independent of I and just equal to the BM intrinsic quadrupole moment Q_0 if the nucleus were correctly described by the strong coupling collective model and if all the quadrupole moment arose from the core. Similarly we define $Q_0(I_1,I_2)=Q_0(I_2,I_1)$ (we choose these to be positive) for $I_1\neq I_2$ by Eqs. (VII. 17, 18, and 19) of BM, inserting into these definitions $K=I_0$. Again these would all equal $|Q_0|$ if the transitions were the BM pure rotational ones.

The final expressions for the quadrupole matrix elements can be written as

$$(I_1j_1J|H_q|I_2j_2J)=e^2(-1)^{I_1+\frac{1}{2}-J}W(I_1j_1I_2j_2;J2)\times f(I_1I_2;I_0)Q_0(I_1,I_2)\langle P(r)/r^3\rangle_{2p}, \tag{14}$$

for $I_2\geq I_1$, where the factors $f(I_1I_2;I_0)$ are listed in Table I.

If we shift the zero of energy so that $H_S=0$ for a $p_{\frac{1}{2}}$ state, then the only nonvanishing matrix elements of the spin-orbit interaction are

$$(I\tfrac{1}{2}J|H_S|I\tfrac{1}{2}J)=\frac{3}{4}\left(\frac{\hbar}{Mc}\right)^2\left\langle\frac{1}{r}\frac{dV}{dr}\right\rangle_{2p}\equiv E_S. \tag{15}$$

In order to carry out the appropriate averages over the $2p$ meson wave function in (14) and (15) we have assumed a uniformly charged nucleus in H_μ. The averages were then carried out using nonrelativistic hydrogenic wave functions in which there was left a variation parameter (Z') chosen to minimize the $2p$ energy of H_μ. The value $R_0=r_0A^{\frac{1}{3}}$ with $r_0=1.1\times10^{-13}$ cm was used.[8]

III. INTENSITIES OF SPECTRAL LINES

The intensity of a given line arising from a meson transition $a\rightarrow b$ is proportional to the probability of excitation of a times the probability that a, if excited, decays into b. We shall first consider the latter question.

Consider a single state a (labeled by J, M, and an additional index ν) when the meson is in a p orbit. When the Hamiltonian discussed in the last section is diagonalized, its wave function is found to be

$$\psi(2p;\nu JM)=\sum_{jI}x(jI\nu J)\varphi(2p;jIJM),$$

and its energy is $E(\nu J)$. With the μ in a $1s$ orbit, the label ν can be replaced by I, and

$$\psi=\varphi(1s;IJM),$$

with energy $E_N(I)$. (We omit all contributions to the energies which are independent of I, J, and ν.) The probability of a mesonic transition with frequency $[E(\nu,J)-E_N(I)]$ from a single state $(2p;\nu JM)$ to the entire level $(1s;I)$ can straightforwardly be shown to be independent of M and proportional to

$$\sum_j|x(jI\nu J)|^2\equiv p(I\nu J). \tag{16}$$

Next must be considered the question of the excitation of the various $2p$ states. The meson arrives in one of these by falling from some higher state, utilizing some non-nuclear process such as radiative emission or the Auger effect. Since in the initial state the meson is far from the nucleus, the mixing of nuclear levels should be small. If we make the simplifying assumption that all states which populate the $2p$ level have the nucleus in the ground state I_0, then the relative population of a single state $(2p;\nu JM)$ can be shown to be $p(I_0\nu J)$, independent of the process by which the state was formed as long as the meson was initially unpolarized.

The frequencies and intensities of the spectral lines are thus given by

$$\hbar\omega=E(\nu J)-E_N(I)+\text{constant}; \tag{17}$$

$$\text{intensity}=(2J+1)p(I\nu J)p(I_0\nu J), \tag{18}$$

where $\sum_I p(I\nu J)=1$.

A simple consequence of Eq. (18) is that only nuclear states connected by H_q to the ground state (directly or indirectly) need be considered.

IV. NUCLEAR TRANSITIONS

Since the lifetimes for nuclear transitions are very long (10^{-8} or 10^{-9} sec for the nuclei considered here) compared to the meson lifetimes (10^{-18} sec for $2p-1s$), we can ignore spontaneous nuclear radiation until after the meson settles into the $1s$ orbit. If the nucleus is left in an excited state, it will then radiate with the same frequency it would have in the absence of the meson (we recall that a $1s$ meson produces only a spherically symmetric field at the nucleus), *except* that the process of meson K-capture may occur before the nuclear transition. The K-capture mean life has been measured to be ~5 to 10×10^{-8} second for heavy

[8] Hofstadter, Hahn, Knudsen, and McIntyre, Phys. Rev. 95, 512 (1954).

nuclei,[9] and should successfully compete with the nuclear decay for a nucleus such as U with an excited state at 44 kev. On the other hand, the rapid dependence of nuclear lifetime on energy ($\tau^{-1}\sim\omega^5Q_0^2$) enables one to predict that, for Ta (first excited state at 137 kev), K-capture in excited nuclear states will be small. In Secs. V and VI, the fraction of $2p-1s$ gamma rays which should be followed by nuclear gammas is calculated, ignoring the possible effect of K-capture in depleting the excited states.

V. EVEN-EVEN NUCLEI

In an even-even nucleus with low-lying states of even parity and $I=0$, 2, 4, only the ground and first excited states are involved in the fine structure. A $2p$ meson combines with the nuclear spins $I=0$ and 2 to give two levels with $J=\frac{1}{2}$ and three with $J=\frac{3}{2}$. Levels with higher J are not connected to the nuclear ground state and give no contribution to the spectrum [see Eq. (18)]. We introduce a parameter α with the dimensions

TABLE II. $(I'j'|H|Ij)$ for meson in $2p$ orbit; even-even nucleus with $I=0,2$.

J	(I,j)			
		$(0,\frac{1}{2})$		$(2,\frac{3}{2})$
$\frac{1}{2}$	$(0,\frac{1}{2})$	0		$-\sqrt{2}$
	$(2,\frac{3}{2})$	$-\sqrt{2}$		$\epsilon_N+\epsilon_S-\rho$
		$(0,\frac{3}{2})$	$(2,\frac{1}{2})$	$(2,\frac{3}{2})$
	$(0,\frac{3}{2})$	ϵ_S	1	1
$\frac{3}{2}$	$(2,\frac{1}{2})$	1	ϵ_N	$-\rho$
	$(2,\frac{3}{2})$	1	$-\rho$	$\epsilon_N+\epsilon_S$

of energy

$$\alpha=\frac{e^2}{10}Q_0(0,2)\left(\frac{P(r)}{r^3}\right)_{2p}, \tag{19}$$

and write

$$E_N(2)=\alpha\epsilon_N, \quad E_S=\alpha\epsilon_S, \quad \rho=Q_0(2,2)/Q_0(0,2). \tag{20}$$

If E_S were known from experiments on a "stiff" nucleus such as Pb, and E_N and $Q_0(0,2)$ from Coulomb excitation experiments or life-time studies, the fine structure pattern would depend on a single parameter not susceptible to measurement by other experiments: the quadrupole moment of the excited state (essentially ρ). The extreme BM strong-coupling model predicts $\rho=+1$ for a prolate, -1 for an oblate nuclear shape.

The H matrices to be diagonalized are presented in Table II. (H_μ has been omitted, since it gives no contribution to the fine structure.) The eigenvalues of these matrices are the energies $E(\nu J)$ [Eq. (17)] in units of α; the eigenfunctions yield the intensities of the spectral lines [Eq. (18)].

For $_{74}W^{even}$, the fine structure has been calculated

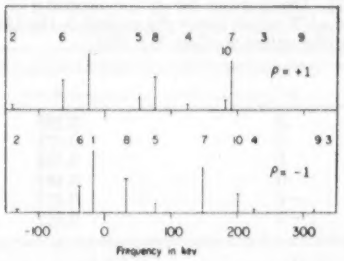

FIG. 1. $2p-1s$ fine structure for $_{74}W^{even}$ for two values of ρ [see Eq. (20)]. The quadrupole moment of the first excited state is $-2.0\rho\times10^{-24}$ cm^2. The numbers serve to indentify lines which go continuously into each other as ρ is varied. Even numbered lines (drawn with horizontal bars at their tops) leave the nucleus in the first excited state. If all quadrupole effects were absent, all lines would disappear except No. 1, which would have $\frac{1}{4}$ the total intensity at 0 kev, and No. 7, with $\frac{3}{4}$ of the intensity at 155 kev.

by using as parameters[10] $E_N=115$ kev, $E_S=155$ kev, and $Q_0(0,2)=7\times10^{-24}$ cm^2; the latter gives $\alpha=53$ kev. The Bohr-Mottelson value of ρ is $+1$, since neighboring odd-A nuclei have positive quadrupole moments. The positions and relative intensities of the spectral lines are presented in Fig. 1 for $\rho=+1$ and $\rho=-1$. In this as well as all other spectra, the zero of the abscissa has

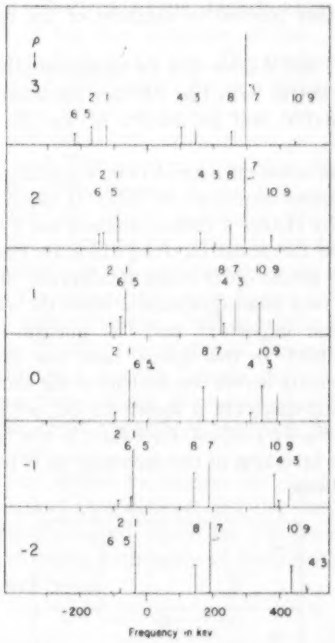

FIG. 2. Fine structure of the $2p-1s$ line for $_{92}U^{238}$ for several values of ρ. The quadrupole moment of the first excited state is $-2.9\rho\times10^{-24}$ cm^2. The lines are numbered as in Fig. 1. The arbitrary intensity units are the same throughout the diagram. If all quadrupole effects were absent, there would be one line at 0 kev, and a second with twice the intensity at 260 kev.

[9] Keuffel, Harrison, Godfrey, and Reynolds, Phys. Rev. **87**, 942 (1952).

[10] T. Huus and C. Zupancic, Kgl. Danske Videnskab. Selskab, Mat. fys. Medd. **28**, No. 1 (1953).

TABLE III. The fraction (ϵ) of the intensity of the $2p-1s$ transition in $_{92}U^{238}$ which leaves the nucleus in the 44-kev excited state for various values of ρ [see Eq. (20)].

ρ	ϵ
3	0.293
2	0.375
1	0.504
0	0.482
−1	0.413
−2	0.312

been chosen at the energy which a $2p_{\frac{1}{2}}-1s$ gamma ray would have if all quadrupole effects were absent. The height of each line is proportional to its intensity, and those with horizontal lines at their tops are followed by a nuclear gamma ray. The fraction of the intensity of the lines which leave the nucleus excited is 0.408 for $\rho=+1$ and 0.412 for $\rho=-1$.

A second even-even calculation has been carried through for $_{92}U^{238}$ to see the effect of changes in the parameters; in this case the sensitivity of the spectrum to variations in ρ has been examined more thoroughly. We have used[11] $E_S=260$ kev, $E_N=44$ kev, $Q_0(0,2)=10\times10^{-24}$ cm², and $\alpha=95$ kev. Figure 2 shows the spectrum for various values of ρ. The fractional intensities of the transitions to the excited nuclear state are listed in Table III, which shows that these fractions form a rather insensitive measure of the quadrupole moment.

Figures 1 and 2 show that an experimental resolution somewhat better than the 100 kev reported by Fitch and Rainwater[1] will be needed to see the complete structure.

Before we leave the even-A case, a special peculiarity of the matrices displayed in Table II should be mentioned. If by chance a certain nucleus has E_N equal to E_S, the first two states for $J=\frac{3}{2}$ which are listed are degenerate to zeroth order in the quadrupole effect. Then even for a very small quadrupole effect the off-diagonal elements are important and the nuclear states are strongly mixed. In this special case, one third of the $2p-1s$ intensity leaves the nucleus in the excited state. In Fig. 3 the spectrum is shown for (a), $\alpha\ll|E_N-E_S|$ and (b), $|E_N-E_S|\ll\alpha\ll(E_N+E_S)$; in the latter case, there is an inversion of the intensity ratio for the two groups of lines.

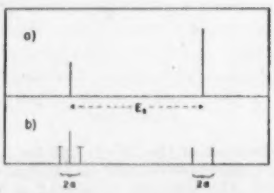

FIG. 3. (a) The $2p-1s$ fine structure for $\alpha\ll|E_N-E_S|$ (i.e., spin-orbit splitting only) and (b) the special case $|E_N-E_S|\ll\alpha\ll E_N+E_S$.

[11] N. P. Heydenburg and G. M. Temmer, Phys. Rev. **93**, 906 (1954); also G. M. Temmer (private communication).

The parameters for W roughly approximate the special case while those for U do not at all; this should be remembered when comparing the qualitative aspects of Figs. 1 and 2.

VI. ODD-A NUCLEI

The odd-A nuclei give patterns considerably more complicated than those considered above, since there is more than one excited state connected by quadrupole matrix elements to the ground state. We have worked out the formulas explicitly for the case of a nucleus with $I_0=7/2$, $I_1=9/2$, and $I_2=11/2$ (all parities equal), omitting any possible effects of higher nuclear states. An enumeration of the possible mixings in this case predicts a $2p-1s$ fine structure with 37 lines; although many of these can be expected to be extremely weak, the resultant pattern is considerably harder to resolve and to interpret than those shown in Figs. 1 and 2.

In this case, the fine structure depends on the six quantities $Q_0(I,I')$ (i.e., the quadrupole moments of the three states and the matrix elements connecting

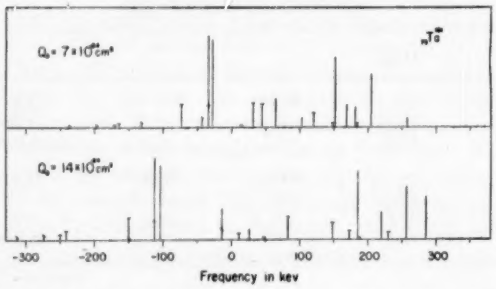

FIG. 4. The $2p-1s$ fine structure for $_{73}Ta^{181}$ for two values of Q_0 using the Bohr-Mottelson model ($\rho=+1$). The lines with horizontal tops leave the nucleus in the first excited state; those with slanting tops leave it in the second excited state.

them) in addition to the energies $E_N(9/2)$, $E_N(11/2)$, and E_S. We introduce the energy α just as in Eq. (19), substituting $Q_0(7/2,9/2)$ for the $Q_0(0,2)$ appearing there, and define $\rho(I,I')=Q_0(I,I')/Q_0(7/2,9/2)$. The energies and eigenfunctions can then be found by diagonalizing the matrices appearing in Table IV, where, however, to achieve the general case each matrix element of H_q must be multiplied by the ρ appropriate to the indices of that matrix element. For example,

$$(4,7/2,3/2|H|4,7/2,1/2)=-(28/45)^{\frac{1}{2}}\rho(7/2,7/2).$$

The solution has been carried out for $_{73}Ta^{181}$ by using the Bohr-Mottelson model of pure rotational states: $\rho(I,I')=+1$ for all I, I'. The parameters used were $E_S=151$ kev, $E(9/2)=137$ kev and $E(11/2)=300$ kev; the spectrum plotted in the upper part of Fig. 4 is for $Q_0=7\times10^{-24}$ cm², a value taken from Coulomb excitation cross sections;[10] that in the lower part of Fig. 4 is for $Q_0=14\times10^{-24}$ cm² (which agrees with the measured quadrupole moment of the ground state).

TABLE IV. $(I'j'|H|Ij)$ for meson in $2p$ orbit; odd-A nucleus with $I=7/2, 9/2, 11/2$. Every off-diagonal matrix element is the positive square root of the appropriate entry unless the entry is followed by an asterisk, in which case it is the negative square root.

J	(I,j)					
		(7/2,3/2)				
2	(7/2,3/2)	ϵ_S+1				
		(7/2,1/2)	(7/2,3/2)	(9/2,3/2)		
	(7/2,1/2)	0	4/3	2/3		
3	(7/2,3/2)		$\epsilon_S-1/3$	8/9*		
	(9/2,3/2)			$\epsilon(9/2)+\epsilon_S+1/3$		
		(7/2,1/2)	(7/2,3/2)	(9/2,1/2)	(9/2,3/2)	(11/2,3/2)
	(7/2,1/2)	0	28/45*	0	98/99*	64/165*
	(7/2,3/2)		$\epsilon_S-13/15$	56/45*	56/495*	112/825
4	(9/2,1/2)			$\epsilon(9/2)$	16/99	98/165
	(9/2,3/2)				$\epsilon(9/2)+\epsilon_S-5/33$	1568/1815*
	(11/2,3/2)					$\epsilon(11/2)+\epsilon_S+1/55$
		(7/2,3/2)	(9/2,1/2)	(9/2,3/2)	(11/2,1/2)	(11/2,3/2)
	(7/2,3/2)	$\epsilon_S+7/15$	392/1815	3136/5445	192/605	624/3025
	(9/2,1/2)		$\epsilon(9/2)$	32/363*	0	7938/7865*
5	(9/2,3/2)			$\epsilon(9/2)+\epsilon_S-10/33$	147/121*	588/7865*
	(11/2,1/2)				$\epsilon(11/2)$	4/7865
	(11/2,3/2)					$\epsilon(11/2)+\epsilon_S-7/715$

The corresponding values of α are 53 and 105 kev, respectively.

The lines with single horizontal bars over them leave the nucleus in its first excited (9/2) state; those with slanting bars leave it in the second excited (11/2) state. The fraction of the total intensity going to the 9/2 state is 0.241 for $Q_0=7$ barns and 0.235 for $Q_0=14$ barns; the corresponding fractions for the 11/2 state are 0.035 and 0.049.

Perturbation theory would predict a group of lines of intensity 1 near 0 kev and another group of intensity 2 near 150 kev, accompanied by a sprinkling of very weak lines shifted by 137 and 300 kev toward the low-frequency end of the spectrum. Figure 4 indicates that the groups spread apart as Q_0 increases and also spread considerably within themselves; moreover, the one to two intensity ratio is considerably changed even for $Q_0=7\times10^{-24}$ cm^2.

Free variation of all six parameters $Q_0(I,I')$ could be made to produce a large variety of spectral features, especially since it is possible to get approximate degeneracies of some of the diagonal elements in Table IV. There is little point in thus refining the calculations at this stage.

VII. SUMMARY

The electric quadrupole field of a $2p$ μ meson in a heavy atom can be expected to mix several of the lowest nuclear levels provided that (a) these are separated by $\sim$100 kev and (b) the quadrupole matrix elements connecting them are large. A large number of nuclei are known (from Coulomb excitation experiments) to satisfy both these conditions. $_{92}U^{238}$, the even isotopes of $_{74}W$, and $_{73}Ta^{181}$, have been singled out for a detailed calculation of the fine structure of the $2p-1s$ line resulting from this interaction. The spectrum in these cases is found to be spread out over a region of 300–500 kev in a way which is sensitive to the quadrupole moments and transition probabilities of the nuclear states involved. The interpretation of an experimental spectrum would be clearest in the case of an even-A nucleus. Here the single parameter which strongly influences the spectrum and which is not easily measureable in other types of experiments is the quadrupole moment of the first excited state. Figure 2 shows most clearly how this parameter would influence the pattern in one case. Finally, the mixing of the nuclear levels should result in a nuclear gamma ray following the $2p-1s$ transition (unless K-capture competes); this will happen 25–50 percent of the time in the cases considered here.

The author wishes to express his appreciation to Professor Robert Oppenheimer and the Faculty of the Institute for Advanced Study for the extension of a grant and of warm hospitality at the Institute, where this work was begun.

Integral Equations for Cascade Showers

JOHN M. BLATT
School of Physics, The University of Sydney, Sydney, Australia
(Received September 13, 1954)

Integral equations of a new type are derived for the lateral and angular distribution functions in a cascade shower. The moment recursion relations of Nordheim are direct consequences of these integral equations. The method of derivation has some intrinsic interest since it involves the formal device of the introduction of negative probabilities for events in which nothing happens. This formal device may have applications in other fields. No solutions of the integral equations derived here are given in this note.

1. INTRODUCTION

THE angular and lateral distribution of the particles in large air showers presents a difficult theoretical problem, which is so far only incompletely solved. The present note is intended to indicate a possible line of attack, not a solution.

Rather than restricting ourselves from the start to the (usually considered) electron-photon cascade initiated by a single electron or photon, we shall derive integral equations for a more general type of shower which we shall call a type A shower. Type A showers may contain any number of components (particles of different types) which are genetically related in any way. The crucial assumptions are: (1) Only one kind of particle (particles of type 1, say) suffers appreciable angular deviation in passing through the medium. (2) The production processes involved in the cascade do not lead to appreciable angular deviations between the directions of the primary and produced particles.

These conditions are satisfied to a good approximation in electron-photon cascades. Photons are deviated in direction only by Compton scattering, which is of negligible importance in air showers, and the production processes (pair creation and bremsstrahlung) involve angular deviations much smaller than the angular deviations due to Coulomb scattering of the electrons by the nuclei in the medium, for electrons of energies less than 10^{12} ev. Higher-energy electrons are on the average so close to the axis of the shower that their angular and lateral deviations are of little experimental importance.

These conditions are also satisfied in the multiple scattering of a single particle without cascade multiplication. Thus the equations we obtain will be equally applicable to this trivial kind of "cascade." Since the equations for multiple scattering are simple and well-known, the equations derived here can be tested on that example.

We shall consider the projected angular and lateral distributions, i.e., the distributions projected onto a plane containing the shower axis (the line defined by the direction of the initial particle of the shower). Furthermore, we are interested in the distribution functions for particles of "type 1" only, i.e., for those particles which themselves suffer angular deviations during flight. Since these are commonly charged particles which are most easily detected, this is a reasonable restriction.

The next restriction is apparently serious: we require that the particle starting the shower itself be of type 1. However, it is easily seen that a shower started by some other type of particle can be thought of as a superposition of showers generated by type 1 particles, as far as the angular and lateral development is concerned. We follow through the initial development of the cascade until the *first* particle of type 1 is created; this particle is still produced along the shower axis, and moving along it. Hence the solution of the angular or lateral problem for showers initiated by type 1 particles forms a Green's function for showers initiated by particles of other types. This point is developed in more detail in the accompanying note.[1]

We now define the conditional probability:

$Q(E_0,E,t;\theta)d\theta$ = probability of finding a particle at a projected angle with the shower axis between θ and $\theta+d\theta$, *given that* the shower was started by a particle of type 1 with energy E_0, and that the observed particle is of type 1, has energy E, and is observed at a depth t from the origin of the shower. (1.1)

It is understood that there may be any number of other particles in the shower at depth t, particles of various types, energies, and angles. On the other hand, for an infinitesimal angle interval $d\theta$, the probability of finding more than one particle within this interval is of order $(d\theta)^2$ and can be ignored.

We define a similar conditional probability for the projected lateral distribution:

$P(E_0,E,t;x)dx$ = probability of finding a particle at a projected distance from the shower axis between x and $x+dx$, *given that* the shower was started by a particle of type 1 with energy E_0, and that the observed particle is of type 1, has energy E, and is observed at a depth t from the origin of the shower. (1.2)

[1] B. Chartres and H. Messel, following paper [Phys. Rev. **96**, 1651 (1954)].

As a result of these definitions, we have the normalization conditions,

$$\int_{-\pi}^{+\pi} Q(E_0,E,t;\theta)d\theta=\int_{-\infty}^{\infty} P(E_0,E,t;x)dx=1. \quad (1.3)$$

If the cascade is predominantly forward, $Q(E_0,E,t;\theta)$ approaches zero rapidly for values of θ larger than some $\theta_{\max}(E)$, and the first integral in (1.3) may be extended formally to cover the range from $-\infty$ to $+\infty$. We shall use the "small angle approximation" throughout this paper. The methods developed here are *not* restricted to this approximation, however.

We shall also need the longitudinal distribution function for particles of type 1; for our purposes this is also best defined as a conditional probability:

$\pi(E_0,E,t)dE$ = probability of finding a particle of type 1 in the energy range E to $E+de$, *given that* the shower was started by a particle of type 1 with energy E_0, and that the point of observation is at a depth t from the origin of the shower. (1.4)

The distribution functions usually considered in cascade theory are given by

$$q(E_0,E,t,\theta)=\pi(E_0,E,t)Q(E_0,E,t;\theta), \quad (1.5)$$

and

$$p(E_0,E,t,x)=\pi(E_0,E,t)P(E_0,E,t;x). \quad (1.6)$$

These can also be defined by saying that $q(E_0,E,t,\theta)\times dEd\theta$ equals the average number of particles of type 1, with energies between E and $E+dE$ and angles between θ and $\theta+d\theta$, at depth t from the origin of the shower, given that the shower was started by a particle of type 1 with energy E_0.[2] A similar definition can be used for p.

2. REGENERATION POINT EQUATIONS FOR PARTICLES OF KNOWN HISTORY

Suppose we find a particle of type 1, energy E, and angle between θ and $\theta+d\theta$, at a depth t from the origin of the shower. We can then trace back the past history of this particle. This is shown schematically in Fig. 1. Just before reaching depth t, we have the same particle undergoing angular deflections. We then trace back to the point where this particle was produced, let us say by some particle not of type 1. The producing particle, as well as the particles not of type 1 from which it may have originated, are shown by dotted lines. According to our basic assumptions, the dotted lines are straight lines, i.e., these other particles are not deflected in passing through the medium, or in transforming into each other. At an even earlier depth, the ancestor of our particle is again a particle of type 1, indicated by the next solid line, and so on, until we reach the originating particle of the shower before the first cascade collision. We specify the "history" of the particle by stating, for each depth t', whether the ancestor at depth t' was a particle of type 1 or of some other type, and if the ancestor was of type 1, stating its energy $E'(t')$. We do *not* include statements about angles or positions in this "history."

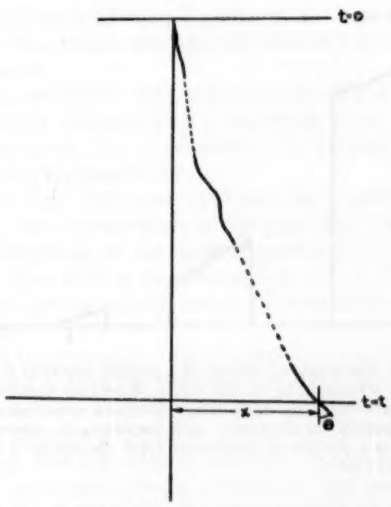

FIG. 1. The ancestry of a particle of type 1, observed at depth t and distance x from the shower axis, can be traced back as indicated schematically in this diagram. The dotted straight portions indicate ancestors of type other than 1, which by assumption do not suffer angular deviations.

The following convention will prove useful: for any value of t' at which the ancestor of our particle was a particle of some other type, we shall say that it can be treated as if it had been a particle of type 1 but energy $E'=0$. The reason why we can use this convention is simply that particles of zero energy (which never occur in the ancestry of a particle of finite energy E) can be assigned any scattering cross section whatever, and we shall assign scattering cross section 0 to particles of energy 0, formally. The advantage of this convention is that now the entire history of our particle is given by a single function $E'(t')$, whoe behavior is shown schematically in Fig. 2. $E'(0)=E_0$, then E' is a monotonically decreasing function of t' (due to collision loss) until we reach the point of the first cascade collision. From then on $E'=0$ until we reach the point in the shower at which the ancestry of our particle again consists of a particle of type 1, and so on. Finally, $E'(t)=E$.

The method of derivation used in this paper is based upon the approach of Nordheim;[3] that is, we

[2] The equations derived here hold for a homogeneous medium, i.e., the relevant cross sections and numbers of scattering centers per unit volume are independent of t. In a nonhomogeneous medium, the derivation goes through with minor changes, which consist mostly in specifying separately the depth of observation t_1 and the depth of the origin of the shower, t_0, not merely their difference $t=t_1-t_0$. We avoid this complication in order to keep the treatment as simple as possible and limited to essentials. The generalization to a nonhomogeneous medium is given in reference 1.

[3] L. W. Nordheim, Z. Physik **133**, 94 (1952).

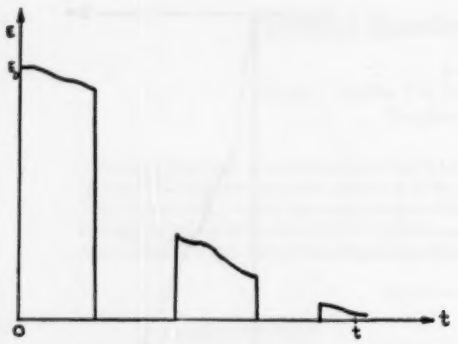

FIG. 2. The energetic history of a particle observed at depth t is shown schematically in this figure. Whenever the ancestor is itself a particle of type 1, its energy decreases monotonically (but not necessarily continuously) with increasing t; whenever the ancestor is a particle of some other type, the energy is formally set equal to zero.

first derive equations for particles of *given* energetic history, and then average over all possible energetic histories of the particles under consideration.

We shall need the probability for angular deviations (in projected angle) between α and $\alpha+d\alpha$ for particles of type 1 and energy E, when traversing an infinitesimal layer dt of the medium. Under the assumption of a homogeneous medium, this probability is independent of t (see reference 2). We define

$$\sigma(E,\alpha)d\alpha dt = \text{probability of a deviation in projected angle, of amount between } \alpha \text{ and } \alpha+d\alpha \text{ for a particle of type 1 and energy } E \text{ traversing a layer } dt \text{ of the medium.} \quad (2.1)$$

According to our previous convention, we define

$$\sigma(0,\alpha)=0. \quad (2.2)$$

We also introduce the total deviation probability,

$$\mu(E)=\int_{-\infty}^{\infty}\sigma(E,\alpha)d\alpha. \quad (2.3)$$

We should point out that the probability of a definite deviations in *projected* angle can be defined only in the small-angle approximation (otherwise this probability depends upon the projection angle in the other plane containing the shower axis); hence it is consistent to use infinite limits of integration in Eq. (2.3).

We shall now concentrate our attention on the *first* scattering collision in the history of our particle. Until this first scattering collision, all the ancestors of the particle were moving along the shower axis. We emphasize that we consider only scattering collisions, *not* collisions involved in the cascade process (since by our fundamental assumption (2) the latter collisions do not lead to angular deviations). We shall need the "survival probability,"

$$g(t)=\text{probability that no scattering collision occurred between } t=0 \text{ and } t=t. \quad (2.4)$$

In the special case $\mu(E)$ independent of E we have $g(t)=\exp(-\mu t)$; this special case is of no use to us because over part of the range 0 to t we had particles of type other than 1, for which $E=0$ (by convention) and $\mu(E)=0$ [by fundamental assumption (1)]. The generalization to arbitrary $\mu(E)$ is

$$g(t)=\exp\left\{-\int_0^t \mu[E'(t')]dt'\right\}. \quad (2.5)$$

We then determine the probability that the first collision occurred in the interval t', $t'+dt'$, and deviated the particle by an angle between α and $\alpha+d\alpha$. This probability is

$$g(t')\sigma[E'(t'),\alpha]d\alpha dt'.$$

By assumption we are looking at particles which make an angle θ with the shower axis at depth t. Hence they must have been deviated through an angle $\theta-\alpha$ in the remaining distance $t-t'$. The probability for this is $Q(E',E,t-t';\theta-\alpha)$. Hence we get a contribution to the final probability $Q(E_0,E,t;\theta)$ equal to

$$g(t')\sigma(E',\alpha)Q(E',E,t-t';\theta-\alpha)dt'd\alpha.$$

The occurrence of the first scattering collision at depth t', with a scattering angle α, is a unique event, and the various choices of t' and α are mutually exclusive. Hence the probabilities can be added up to yield a total probability. This total, however, is still not equal to $Q(E_0,E,t;\theta)$ because we have ignored the possibility that no scattering collision at all occurred in the range 0 to t. This latter possibility contributes an amount $g(t)\delta(\theta)$, where δ is Dirac's delta function. We thus get the regeneration point equation

$$Q(E_0,E,t;\theta)=\int_0^t dt'\int_{-\infty}^{\infty}d\alpha g(t')\sigma(E',\alpha)\times Q(E',E,t-t';\theta-\alpha)+g(t)\delta(\theta). \quad (2.6)$$

In this equation, we must replace E', wherever it occurs, by the (presumed known) value $E'(t')$ at the depth in question. We observe that the cascade history of the particle *before* the first scattering collision (at depths $t''<t'$) enters implicitly through the survival probability $g(t')$ [Eq. (2.5)].

We use entirely analogous arguments to obtain a regeneration point equation for the lateral distribution function $P(E_0,E,t;x)$. If the first scattering collision occurs at t' and deviates the particle through an angle α, the new "axis" is displaced with respect to the original one at depth t by the amount,

$$x_\alpha(t,t')=\alpha(t-t')+\text{terms of higher order in } \alpha. \quad (2.7)$$

In order that the particle be finally observed at a distance x from the old shower axis, the subsequent deflections (between t' and t) must shift it laterally, with respect to the new axis, by the amount $x-x_\alpha$.

Hence we obtain:

$$P(E_0,E,t;x)=\int_0^t dt'\int_{-\infty}^{\infty} d\alpha g(t')\sigma(E',\alpha)$$
$$\times P[E',E,t-t';x-\alpha(t-t')]+g(t)\delta(x). \quad (2.8)$$

We observe that Eq. (2.8) is an integral equation for the *lateral* distribution function alone; the angular distribution does not occur at all in this equation. This is characteristic for regeneration point equations. The more usual "forward" or "last-collision" equations are derived by considering what happens in the last interval of depth (from $t-dt$ to t) or what happened in the last collision. In either case it is impossible to get an equation for the lateral distribution which does not involve the angular distribution.

Equations (2.7) and (2.8) are *not* the conventional regeneration point equations for the shower. We have concentrated our attention on the first *scattering* collision, whereas the conventional regeneration point method considers the first collision of any kind, scattering or cascade. Conversely, Eqs. (2.7) and (2.8) apply only to particles of known history $E'(t')$, and cannot be used, in this form, for the actual cascade.

3. AN INVARIANCE PROPERTY OF REGENERATION POINT EQUATIONS

The various recursion relations for the moments of the angular and lateral distributions given in the literature[3,4] all have this in common: the lateral and angular moments of all orders can be obtained from a knowledge of the moments of the scattering cross section

$$\sigma_n=\int_{-\infty}^{\infty}\alpha^n\sigma(E,\alpha)d\alpha. \quad (3.1)$$

The remarkable feature of all the moment recursion relations is that *the zeroth moment, i.e., the total cross section $\sigma_0=\mu$, never enters into the recursion relations.* To the extent that the moments of the distribution function determine the function uniquely, the angular and lateral distribution of the particles in the cascade do not depend at all on the total cross section for angular deviations.

Let us try to understand this remarkable invariance. Two cross sections $\sigma(E,\alpha)$ and $\sigma'(E,\alpha)$ give the same final distributions provided all the moments agree, $\sigma_n=\sigma_n'$, except for the zeroth moment $\sigma_0\neq\sigma_0'$. Two functions all of whose moments agree except the zeroth moment differ by a multiple of the delta function, hence we conclude that

$$\sigma'(E,\alpha)=\sigma(E,\alpha)+k(E)\delta(\alpha). \quad (3.2)$$

Here $k(E)$ is an arbitrary function of E. Cross sections σ' and σ lead to the *same* final distribution functions for the cascade.

This is intuitively clear, also, since the term $k(E)\delta(\alpha)$ represents a probability of a scattering event though an angle $\alpha=0$, i.e., a probability of nothing at all happening, experimentally.

Hence Eqs. (2.6) and (2.8) are still correct if we replace σ by σ' everywhere in the equations [including in the definition of the survival probability $g(t)$, Eq. (2.5)]. Since $k(E)$ is an arbitrary function at our disposal, we get an infinite variety of regeneration point equations.

While the invariance under insertion of a probability of nothing happening was shown here for the special case of multiple scattering problems, this is of course a *general invariance property of all regeneration point equations, and last collision equations as well.* We can always introduce a formal probability (per unit path length) of nothing happening at all, and obtain a modified, but still correct, regeneration point equation. We shall use this invariance in the next section.

4. AVERAGING OVER PAST HISTORIES

Relation (2.6) is valid for particles of known history $E'(t')$. In order to obtain a result for the actual cascade, we must average over all possible past histories $E'(t')$, each weighted according to its probability of occurrence in this particular cascade. This is at first sight a hopeless task unless much more is known about the details of the cascade process than what we have assumed to be known. The survival probability $g(t)$ is particularly awkward to handle in such an average.

We now employ the invariance property pointed out in the preceding section to eliminate, formally, the survival probability $g(t)$ from the equations. To do this, we choose the arbitrary function $k(E)$ in Eq. (3.2) to be

$$k(E)=-\mu(E), \quad (4.1)$$

i.e., $k(E)$ is the negative of the total scattering cross section. Insertion in Eq. (3.2) gives the modified cross section,

$$\sigma'(E,\alpha)=\sigma(E,\alpha)-\mu(E)\delta(\alpha), \quad (4.2)$$

and hence the modified total cross section,

$$\mu'(E)=\int_{-\infty}^{\infty}\sigma'(E,\alpha)d\alpha=\mu(E)-\mu(E)=0. \quad (4.3)$$

The total cross section μ' vanishes as a result of the cancellation of the total probability of actual scattering events against the (assumed negative) probability of nothing happening at all. We emphasize that this negative probability of nothing happening is a purely formal device which is justified by the (physically immediate) invariance of the equations under the substitution (3.2) for all positive functions $k(E)$, and hence by analytic continuation also for negative functions $k(E)$.

[4] H. S. Green and H. Messel, Phys. Rev. **88**, 331 (1952); L. Landau, J. Phys. (U.S.S.R.) **3**, 237 (1940); L. Eyges and S. Fernbach, Phys. Rev. **82**, 23 (1951); L. Eyges, Phys. Rev. **74**, 1801 (1948).

Equation (2.5) shows that the modified survival probability $g'(t)=1$, identically, so that Eqs. (2.6) and (2.8) can be transformed into

$$Q(E_0,E,t;\theta)=\int_0^t dt'\int_{-\infty}^{\infty} d\alpha[\sigma(E',\alpha)-\mu(E')\delta(\alpha)]$$
$$\times Q(E',E,t-t';\theta-\alpha)+\delta(\theta), \quad (4.4)$$

$$P(E_0,E,t;x)=\int_0^t dt'\int_{-\infty}^{\infty} d\alpha[\sigma(E',\alpha)-\mu(E')\delta(\alpha)]$$
$$\times P[E',E,t-t';x-\alpha(t-t')]+\delta(x). \quad (4.5)$$

We now observe that we can carry out the averaging over past histories in a very direct fashion. Let us first keep E' fixed, and average over histories $E''(t'')$ in the range $t'<t''\leqslant t$. This averaging procedure affects only the term $Q(E',E,t-t';\theta-\alpha)$ in Eq. (4.4) [and the corresponding term in Eq. (4.5)], and it leads simply to the distribution function $Q(E',E,t-t';\theta-\alpha)$ for a *cascade* started by a particle of type 1, of energy E', and propagating through a layer of thickness $t-t'$. Next we average over past histories $E''(t'')$ in the range $0\leqslant t''<t'$. This average is particularly simple since according to the structure of Eq. (4.4) the history before the first "scattering" collision (at t') has no influence whatever. [In the original Eq. (2.6) the corresponding history did have an influence, since it affected the survival probability $g(t')$.]

Next we must average over all possible choices of E' at depth t'. We need the conditional probability $W(E_0,E,t;E',t')dE'$ of finding the ancestor of our particle at depth t' to be a particle of type 1 in the energy range E', $E'+dE'$, given that the initial particle is of type 1 with energy E_0 and the final particle is of type 1 with energy E at depth t. According to the definition of $\pi(E_0,E,t)$, formula (1.4), W is given by[5]

$$W(E_0,E,t;E',t')dE'=\frac{\pi(E_0,E',t')\pi(E',E,t-t')}{\pi(E_0,E,t)}dE'. \quad (4.6)$$

The integrand in Eq. (4.4) must be multiplied by this W, and we must integrate over all possible E' for a given t', i.e., over the range $E<E'<E_0$.

Finally we integrate over all possible t' as indicated in Eq. (4.4). No special weighting of different values of t' is necessary because we have arranged Eq. (4.4) in such a way that the formal survival probability $g'(t')$ is unity, hence the first formal scattering collision (which may be either an actual scattering collision or a scattering through an angle zero) is as likely to occur at one value of t' as at any other.

The result is an integral equation for the probability function $Q(E_0,E,t;\theta)$ for the *cascade*, i.e., if one takes into account all possible past histories $E'(t')$ of the particles under consideration.

$$Q(E_0,E,t;\theta)=\int_0^t dt'\int_E^{E_0} dE'\int_{-\infty}^{\infty} d\alpha W(E_0,E,t;E',t')$$
$$\times[\sigma(E',\alpha)-\mu(E')\delta(\alpha)]\times Q(E',E,t-t';\theta-\alpha)$$
$$+\delta(\theta). \quad (4.7)$$

This equation can be rewritten in terms of the more usual distribution function $q(E_0,E,t,\theta)$ given by Eq. (1.5). We multiply both sides of Eq. (4.7) by $\pi(E_0,E,t)$ to get

$$q(E_0,E,t,\theta)=\int_0^t dt'\int_E^{E_0} dE'\int_{-\infty}^{\infty} d\alpha\,\pi(E_0,E',t')$$
$$\times[\sigma(E',\alpha)-\mu(E')\delta(\alpha)]\,q(E',E,t-t',\theta-\alpha)$$
$$+\pi(E_0,E,t)\delta(\theta). \quad (4.8)$$

By an entirely analogous argument we obtain an integral equation for the lateral distribution function p, Eq. (1.6):

$$p(E_0,E,t,x)=\int_0^t dt'\int_E^{E_0} dE'\int_{-\infty}^{\infty} d\alpha\,\pi(E_0,E',t')$$
$$\times[\sigma(E',\alpha)-\mu(E')\delta(\alpha)]\,p[E',E,t-t',x-\alpha(t-t')]$$
$$+\pi(E_0,E,t)\delta(x). \quad (4.9)$$

Equations (4.8) and (4.9) are the main results of this note. We now point out some features of these equations. First of all, the equations have been derived without making any specific assumptions about the genetic relations in the cascade. The basic assumptions are merely that particles of type other than 1 are not scattered by the medium, and that no appreciable angular deviation occurs in the various production processes which give rise to the cascade. The details of the cascade process, including even the average numbers of particles of type other than 1 at various depths, are not needed in Eqs. (4.8) and (4.9). The only necessary knowledge about the cascade is the longitudinal distribution function $\pi(E_0,E,t)$, i.e., the *average* number of particles of type 1 and energy E at depth t in a cascade started by a particle of type 1 and energy E_0 at depth $t=0$.

[5] This formula was first given by Nordheim, reference 4, Eq. (13). The factor dt' in Nordheim's formula 13 is misleading, however, and should be dropped. We would also like to point out that this is the only point at our derivation where we make essential use of the fact that the shower was started by a particle of type 1, and that the observed particle, at depth t, is also of type 1. Suppose that the initial particle is of type i and the observed particle is of type j; we then need the conditional probability $W_{ij}(E_0,E,t;E',t')$ of finding a particle of type 1 (because these are the only particles that scatter) at depth t' with energy in E', $E'+dE'$; this is given by

$$W_{ij}(E_0,E,t;E',t')dE'=\frac{\pi_{i1}(E_0,E',t')\pi_{1j}(E',E,t-t')}{\pi_{ij}(E_0,E,t)}dE', \quad (4.6a)$$

where $\pi_{ij}(E_0,E,t)$ is the probability of finding a particle of type j and energy E at depth t in a shower started by a particle of type i and energy E_0. With this modification and suitable addition of subscripts to the functions Q and P we get Eq. (5.2) of reference 1; however, this method does not give in any direct way the more general equations in Eq. (3.10) of reference 1.

In particular, we can specialize to simple multiple scattering without cascade multiplication or energy loss by setting

$$\pi(E_0,E,t)=\delta(E_0-E)$$
(multiple scattering without energy loss). (4.10)

It is shown in the appendix that the equations of Scott and Snyder,[6] for example, are consistent with Eqs. (4.8) and (4.9) if Eq. (4.10) is substituted for $\pi(E_0,E,t)$. We also observe Eqs. (4.8) and (4.9) determine the respective distribution functions $q(t,\theta)$ and $p(t,x)$ *uniquely*.

To get multiple scattering with definite energy loss, we first determine the energy $E(t)$ at depth t and then set

$$\pi(E_0,E,t)=\delta[E-E(t)]$$
(multiple scattering with unique energy loss). (4.11)

If there is straggling in the energy loss, the function $\pi(E_0,E,t)$ must be determined from the longitudinal equations.

In cascade theory, the longitudinal distribution func-$\pi(E_0,E,t)$ is well-known for electron-photon cascades (or at least its Mellin transform is well-known). In cascade theory it has been customary until recently to use the Landau approximation of pure multiple scattering, i.e., to neglect single and plural scattering contributions. This amounts to an assumption about the scattering cross section $\sigma(E,\alpha)$, namely

$$\sigma(E,\alpha)=(E_s/2E)^2\delta''(\alpha), \tag{4.12}$$

where $E_s=21$ Mev is a characteristic energy for multiple scattering and the second derivative of the delta function has to be understood in the usual way, in terms of integrations by parts. The resulting equation for the angular distribution has been given in the literature[7] and has proved to be useful. The corresponding equation for the lateral distribution in the Landau approximation had been surmised from the Nordheim moment recursion relation[8] but had not been derived directly. It has not proved useful so far in cascade theory, since it is very difficult to obtain explicit solutions of that equation.

The derivation of Eqs. (4.8) and (4.9) given here has made use of the absolute minimum amount of information about the cascade, namely that information which eventually enters the final equations, i.e., the function $\pi(E_0,E,t)$. It is of course possible to derive these equations in other ways. One way, suggested by H. Messel, consists in writing down the conventional regeneration point (first collision) equations for the cascade in question, and afterwards using the (presumed known) solutions of the purely longitudinal problem to eliminate explicit reference to the cross sections involved in the cascade multiplication. This program is carried through in the accompanying paper.[1]

From integral equations such as Eqs. (4.8) and (4.9) it is usually possible to derive recursion relations for the moments of the distribution functions. This case is no exception. We define moments by

$$q_n(E_0,E,t)=\int_{-\infty}^{\infty}\theta^n q(E_0,E,t,\theta)d\theta, \tag{4.13}$$

$$p_n(E_0,E,t)=\int_{-\infty}^{\infty}x^n p(E_0,E,t,x)dx, \tag{4.14}$$

and observe that

$$q_0(E_0,E,t)=p_0(E_0,E,t)=\pi(E_0,E,t). \tag{4.15}$$

We multiply both sides of Eq. (4.8) by θ^n and integrate over all values of θ. We notice that odd powers of θ give zero by symmetry; we also write $\theta^n=(\theta-\alpha+\alpha)^n$ and use the binomial theorem; this gives

$$q_{2n}(E_0,E,t)=\sum_{k=1}^{n}\binom{2n}{2k}\int_0^t dt'\int_E^{E_0}dE'\pi(E_0,E',t')$$
$$\times\sigma_{2k}(E')q_{2n-2k}(E',E,t-t')+\delta_{n,0}\pi(E_0,E,t). \tag{4.16}$$

Here σ_{2k} is defined by Eq. (3.1), and $\delta_{n,0}$ equals 1 if $n=0$, and equals 0 otherwise. The Nordheim recursion relation for the angular distribution moments (reference 3) is a special case of Eq. (4.16) obtained by the substitution (4.12), i.e., $\sigma_2(E)=\frac{1}{2}(E_s/E)^2$ and all other moments of σ vanish.

An entirely similar derivation gives the lateral moment recursion relation,

$$p_{2n}(E_0,E,t)=\sum_{k=1}^{n}\binom{2n}{2k}\int_0^t dt'\int_E^{E_0}dE'\pi(E_0,E',t')$$
$$\times\sigma_{2k}(E')(t-t')^{2k}p_{2n-2k}(E',E,t-t')$$
$$+\delta_{n,0}\pi(E_0,E,t). \tag{4.17}$$

Again the Nordheim moment recursion relation is a special case of Eq. (4.17). It should be pointed out that these moment recursion relations can be obtained directly by an extension of Nordheim's derivation, without going via the integral equations (4.8) and (4.9), and hence also without the introduction of negative probabilities. This explicit generalization of Nordheim's proof has been performed by the author, but it is too complicated to warrant repeating here.

We notice that the recursion relations (4.16) and (4.17) determine all the moments q_{2n} and p_{2n} uniquely, starting only from the longitudinal distribution function π of particles of type 1. This is a way of seeing that the integral equations (4.8) and (4.9) determine the distribution functions uniquely. We conclude that *the*

[6] H. S. Snyder and W. T. Scott, Phys. Rev. **76**, 220 (1949).
[7] M. H. Kalos and J. M. Blatt, Australian J. Phys. (to be published).
[8] Osborne, Nordheim, and Blatt, Proceedings of the Echo Lake Conference on Cosmic Rays, 1949 (unpublished).

angular and lateral distribution functions of type 1 particles in a cascade satisfying our fundamental conditions of Sec. 1 are determined uniquely by the average longitudinal numbers $\pi(E_0,E,t)$ of type 1 particles and by the scattering probability $\sigma(E,\alpha)$, independently of the detailed nature of the cascade process. This is a rather surprising conclusion, since it is quite possible to obtain the same $\pi(E_0,E,t)$ from two fundamentally different cascades. Conversely, this theorem shows that one must be careful in interpreting experimental information on lateral and angular distributions unless the basic nature of the cascade process is well understood from other sources. This may be important to keep in mind when analyzing angular and lateral distribution data on the nucleon cascade inside a heavy nucleus or in the atmosphere.

5. CONCLUSION

Having derived these equations, we now consider possible applications. These fall into two classes: applications of the equations themselves, and applications of the tricks used in the derivation. As regards the equations themselves, we believe that a straightforward attack on the lateral distribution function, using Eq. (4.9) and standard analytic methods, is likely to fail. Equation (4.9) is a rather nasty equation, even in the Landau approximation (4.12), and our attempts to obtain explicit analytic solutions to it have not succeeded so far. However, we feel that a purely numerical attack on Eq. (4.9), using the Monte Carlo method and a fast digital computer, may perhaps be worth while.

The more interesting applications are in the direction of applying the tricks used in the derivation here to other stochastic processes. The introduction of negative probabilities for events in which nothing happens has enabled us to average over one set of stochastic variables while retaining probability statements about another set of stochastic variables, in spite of the fact that the two sets of variables (e.g., energy and angle) are genetically related to each other. There are surely many other fields of physics in which similar "partial probabilities" are desired, but have so far been found only indirectly by first solving the complete stochastic problem and *afterwards* averaging over the unwanted stochastic variables.

APPENDIX. MULTIPLE SCATTERING WITHOUT ENERGY LOSS

We wish to show that Eqs. (4.8) and (4.9) with the substitution (4.10) are correct for multiple scattering without energy loss. Putting Eq. (4.10) into Eq. (4.8), cancelling the common factor $\delta(E_0-E)$, and setting $t-t'=t''$ gives

$$q(t,\theta)=\int_0^t dt''\int_{-\infty}^{\infty} d\alpha[\sigma(\alpha)-\mu\delta(\alpha)] \times q(t'',\theta-\alpha)+\delta(\theta). \quad (A.1)$$

When we differentiate both sides with respect to t, we get directly the usual equation for multiple scattering [for example, Scott and Snyder, reference 6, Eq. (5); their Eq. (5) includes the lateral distribution, and must be integrated over their variable x to obtain the equivalent of Eq. (A.1); also the notation differs somewhat: their η is our θ, their z is proportional to our t, and their $p(\eta)$ is proportional to our $\sigma(\alpha)$].

The equivalence is harder to show for the lateral equation (4.9), since Scott and Snyder do not have such an equation at all. Inserting Eq. (4.10) into Eq. (4.9) gives, again setting $t''=t-t'$,

$$p(t,x)=\int_0^t dt''\int_{-\infty}^{\infty} d\alpha[\sigma(\alpha)-\mu\delta(\alpha)] \times p(t'',x-\alpha t'')+\delta(x). \quad (A.2)$$

We introduce a Fourier transform on x,

$$u(t,k)=\int_{-\infty}^{\infty} dx\,\exp(ikx)p(t,x), \quad (A\,3)$$

and the notation

$$S(k)=\int_{-\infty}^{\infty} d\alpha\,\exp(ik\alpha)\sigma(\alpha) \quad (A.4)$$

to get

$$u(t,k)=\int_0^t dt''\,[S(kt'')-\mu]\,u(t'',k)+1. \quad (A.5)$$

We differentiate with respect to t,

$$\partial u(t,k)/\partial t=[S(kt)-\mu]u(t,k), \quad (A.6)$$

and observe that Eq. (A.5) implies the initial condition $u(0,k)=1$. The solution can be written best in terms of the function

$$h(t)=\int_0^t [\mu-S(t')]dt', \quad (A.7)$$

and is

$$u(t,k)=\exp\left[\frac{h(0)-h(kt)}{k}\right]. \quad (A.8)$$

This is exactly the solution of Scott and Snyder, except for notation.

New Formulation of a General Three-Dimensional Cascade Theory

B. A. CHARTRES AND H. MESSEL
F. B. S. Falkiner Nuclear Research and Adolph Basser Computing Laboratories, School of Physics, The University of Sydney, Sydney, Australia*

(Received September 13, 1954)

A new simple and straightforward formulation of a general three-dimensional cascade is given. The resultant integral equations include those derived by Blatt as a special case. The equations have a number of interesting features which distinguish them from those commonly used in cascade theory. They also lead to a simple moment recursion relation which is valid for all energies and which includes various processes such as Compton effect and ionization loss. The paper greatly simplifies previous work on the subject.

1. INTRODUCTION

AN integral equation for the projected lateral distribution function of a cascade shower developing in a uniform medium has recently been obtained by Blatt.[1] This equation is unique in that the angular distribution does not appear in it; neither do the details of the cascade process, such as the bremsstrahlung and pair production cross sections. The only information necessary about the cascade is the average numbers; it is this which takes into account the details of the cascade process. As a consequence a moment recurrence formula can be written down for the lateral distribution which does not include the angular and mixed moments. It should be noted that in all previous work equations for the angular distribution could be written down which are independent of the lateral distribution, but not vice versa.

In his derivation Blatt makes the following assumptions: (1) Only one type of particle involved in the cascade suffers appreciable angular deviations. (2) The multiplicative processes involved in the cascade do not lead to appreciable angular deviations. In other words, the cascading process and the lateral spreading of the shower are due to different types of collisions.

In addition the following two assumptions, which are not necessary for the validity of the final equation, were made to simplify the argument: (*a*) The medium is of uniform composition. (*b*) The cascade is initiated by a particle of the type that suffers angular deflections. His derivation is presented in a general form without reference to the particular nature of the cascade involved, but *it should be noted that the stringent requirements of assumptions (1) and (2) effectively limit the application of Blatt's equation to the electron-photon cascade.*

It is the purpose of this paper to present an alternative, straightforward derivation which is so general in its application that it enables us to dispense completely with all four of the above-mentioned assumptions. This means that we have here a powerful method of tackling the general problem of the lateral spread of the mixed atmospheric cascade,[2,3] with electron-photon showers as a special case. In addition, the equations take into account such processes as the Compton effect, ionization loss, etc. This leads to simple moment recursion relation in which all these processes are taken into account in the average numbers. This vastly simplifies all previous work on the subject.

The general equations are derived using the so-called "first collision" or "regeneration point" method developed in recent work on cascade fluctuation theory.[4,5]

2. DEFINITIONS

Let $p_{i,j}(E_0,t_0;E,r,\theta,t)dEdrd\theta$ be the average number of particles of type $j(j=1, 2, \cdots, n)$ of energy in the range E to $E+dE$, at a distance from the shower axis in the range r to $r+dr$, and travelling in a direction making an angle θ to $\theta+d\theta$ to the shower axis at depth t in a cascade initiated at depth t_0 by a particle of type i of energy E_0 travelling along the shower axis. The fact that we allow the cascade to be initiated at depth t_0 makes allowance for the inhomogeneity of the atmosphere. Let $\pi_{i,j}(E_0,t_0;E,t)dE$ be the corresponding average number integrated over all θ and r. We assume that the $\pi_{i,j}$ are known functions; that is, we shall assume that the problem of the longitudinal development of *whatever cascade* (including ionization loss, etc.) is under consideration has been solved.

Let $x_{i,j}(E_0,t;E,\theta)dEd\theta$ be the probability that an i particle of energy E_0 suffers a collision at depth t from which arise any number of any type of secondary particles, but one of them is a j particle of energy E travelling in a direction at an angle θ to the primary i particle.

The probability $x_{i,j}$ is completely general and can include all known cascade phenomena. It may for instance include terms representing collisions which are not contributory to the development of the cascade, that is collisions producing only one secondary which can be identified with the primary. The effect of such

* Also supported by the Nuclear Research Foundation within the University of Sydney.

[1] J. M. Blatt, preceding paper [Phys. Rev. **96**, 1644 (1954)].

[2] H. Messel and R. B. Potts, Nuovo cimento **10**, 754 (1953).

[3] H. Messel and H. S. Green, Proc. Phys. Soc. (London) **A66**, 1009 (1953).

[4] L. Janossy, Proc. Phys. Soc. (London) **A63**, 241 (1950).

[5] H. Messel and R. B. Potts, Proc. Phys. Soc. (London) **A65**, 473 and 854 (1952).

a collision is to reduce the energy of the primary particle and/or deviate its direction of motion. There are two examples which are worth noting.

1. The angular deviations of electrons in an electron-photon cascade by Rutherford scattering. If the scattering cross section is taken as $\sigma_i(E,t;\theta)d\theta$ this can be included in our $x_{i,j}$ as

$$\delta_{i,j}\delta(E_0-E)\sigma_i(E,t;\theta). \tag{2.1}$$

2. The continuous loss of energy of a charged particle through ionization of the medium. If the energy lost is β units of energy per unit distance travelled, this effect can be included by incorporating the following term in $x_{i,j}(E_0,t_0;E,\theta)$:

$$\delta_{i,j}\delta(\theta)\operatorname*{Lim}_{\epsilon\to 0}\beta/\epsilon\cdot\delta(E_0-E-\epsilon). \tag{2.2}$$[6,7]

Define the cross section $w_{i,j}(E_0,t;E)dE$ by the equation,

$$w_{i,j}(E_0,t;E)=\int_{-\infty}^{\infty}x_{i,j}(E_0,t;E,\theta)d\theta. \tag{2.3}$$

Then $w_{i,j}$ is the analog of $x_{i,j}$ in the theory of the purely longitudinal development of the cascade.

Let $\alpha_i(E_0,t)$ be the total probability that an i particle of energy E_0 will suffer a collision of any type in travelling unit distance at depth t. Then in general,

$$\alpha_i(E_0,t)<\sum_{j=1}^{n}\int_0^{E_0}w_{i,j}(E_0,t;E)dE. \tag{2.4}$$

The right-hand side of (2.4) is the average number of secondary particles produced by an i particle of energy E_0 in travelling unit distance, while $\alpha_i(E_0,t)$ is the average number of collisions suffered by that particle in the same distance. Events of the type defined in (2.1) and (2.2) contribute equal amounts to both sides of (2.4).

The functions defined above can conveniently be grouped in the following matrices:

$$\begin{gathered}\mathbf{P}=(p_{i,j}),\quad \boldsymbol{\pi}=(\pi_{i,j}),\quad \mathbf{X}=(x_{i,j}),\quad \mathbf{W}=(w_{i,j}),\\ \mathbf{A}=(a_{i,j}),\quad \text{where}\quad a_{i,j}=\delta_{i,j}\alpha_i,\\ \mathbf{Y}(E_0,t;E,\theta)=\mathbf{X}(E_0,t;E,\theta)-\delta(E-E_0)\delta(\theta)\mathbf{A}(E_0,t),\\ \mathbf{V}(E_0,t;E)=\int_{-\infty}^{\infty}d\theta\mathbf{Y}(E_0,t;E,\theta)\\ =\mathbf{W}(E_0,t;E)-\delta(E-E_0)\mathbf{A}(E_0,t).\end{gathered} \tag{2.5}$$

We note that $\mathbf{P}$ and $\boldsymbol{\pi}$ satisfy the initial condition,

$$\begin{gathered}\mathbf{P}(E_0,t_0;E,r,\theta,t_0)=\delta(r)\delta(\theta)\delta(E_0-E)\mathbf{I},\\ \boldsymbol{\pi}(E_0,t_0;E,t_0)=\delta(E_0-E)\mathbf{I},\end{gathered} \tag{2.6}$$

where $\mathbf{I}$ is the unit matrix.

3. THE FIRST COLLISION EQUATION

Consider a cascade initiated by a particle of type i which is known to have the energy E_0 at depth t_0 in the medium. The probability $g_i(E_0,t')$ that this particle will reach a depth t' without suffering any type of collision, and therefore still having its original energy E_0, is given by

$$g_i(E_0,t')=\exp\left[-\int_{t_0}^{t'}\alpha_i(E_0,\tau)d\tau\right]. \tag{3.1}$$

A collision giving rise to a k particle of energy E' travelling at an angle θ' to the initiating particle may then occur. The probability of this is

$$x_{i,k}(E_0,t';E',\theta')dE'd\theta'dt'. \tag{3.2}$$

The cascade initiated by this secondary particle then has, for its distribution function at depth t,

$$P_{k,j}(E',t';E,r-\theta'(t-t'),\theta-\theta',t). \tag{3.3}$$

The contribution to the total cascade arising from the probability of this particular event occurring first is therefore given by the product of expressions (3.1), (3.2), and (3.3). By now summing over the contributions of all possible first collisions we should recover the distribution function of the total cascade. This procedure yields the "first collision integral equation":

$$\begin{aligned}&p_{i,j}(E_0,t_0;E,r,\theta,t)\\ &=\delta(E-E_0)\delta(r)\delta(\theta)\delta_{i,j}g_i(E_0,t)+\int_{t_0}^{t}dt'g_i(E_0,t')\\ &\quad\times\sum_{k=1}^{n}\int_E^{E_0}dE'\int_{-\infty}^{\infty}d\theta'x_{i,k}(E_0,t';E',\theta')\\ &\quad\times p_{k,j}(E',t';E,r-\theta'(t-t'),\theta-\theta',t).\end{aligned} \tag{3.4}$$

The first term on the right-hand side of (3.4) covers the possibility of no collision at all occurring. By using the matrix notation (2.5) the first collision equation becomes

$$\begin{aligned}&\mathbf{P}(E_0,t_0;E,r,\theta,t)\\ &=\delta(E_0-E)\delta(r)\delta(\theta)\exp\left[-\int_{t_0}^{t}\mathbf{A}(E_0,\tau)d\tau\right]\\ &\quad+\int_{t_0}^{t}dt'\exp\left[-\int_{t_0}^{t'}\mathbf{A}(E_0,\tau)d\tau\right]\\ &\quad\cdot\int_E^{E_0}dE'\int_{-\infty}^{\infty}d\theta'\mathbf{X}(E_0,t';E',\theta')\\ &\quad\times\mathbf{P}(E',t';E,r-\theta'(t-t'),\theta-\theta',t).\end{aligned} \tag{3.5}$$

[6] Ionization loss is usually treated as a continuous deterministic process (see reference 7) whereas a cross section like $x_{i,j}$ defines a statistical process with resultant fluctuations. By defining ionization loss as in (2.2) we are expressing a deterministic process as a limit of a statistical one.

[7] H. J. Bhabha and S. K. Chakrabarty, Proc. Roy. Soc. (London) **A181**, 267 (1943).

Differentiating Eq. (3.5) with respect to t_0 gives the first collision integro-differential equation,

$$\frac{\partial}{\partial t_0}\mathbf{P}(E_0,t_0;E,\mathbf{r},\theta,t)$$
$$=-\int_E^{E_0}dE'\int_{-\infty}^{\infty}d\theta'\mathbf{Y}(E_0,t_0;E',\theta')$$
$$\times\mathbf{P}(E',t_0;E,\mathbf{r}-\theta'(t-t_0),\theta-\theta',t). \quad (3.6)$$

Integrating the above equation through all $\mathbf{r}$ and θ yields the equivalent equation for the average numbers solution π,

$$\frac{\partial}{\partial t_0}\pi(E_0,t_0;E,t)+\int_E^{E_0}dE'\mathbf{V}(E_0,t_0;E')$$
$$\times\pi(E',t_0;E,t)=0. \quad (3.7)$$

Equation (3.6) can be put in a form closely resembling (3.7) by the addition to both sides of the expression

$$\int_E^{E_0}dE'\int_{-\infty}^{\infty}d\theta'\mathbf{Y}(E_0,t_0;E',\theta')\mathbf{P}(E',t_0;E,\mathbf{r},\theta,t), \quad (3.8)$$

which on the left-hand side is put in the form

$$\int_E^{E_0}dE'\mathbf{V}(E_0,t_0;E')\mathbf{P}(E',t_0;E,\mathbf{r},\theta,t), \quad (3.8a)$$

and on the right-hand side in the form

$$\int_E^{E_0}dE'\int_{-\infty}^{\infty}d\theta'\mathbf{V}(E_0,t_0;E')\delta(\theta')$$
$$\times\mathbf{P}(E',t_0;E,\mathbf{r}-\theta'(t-t_0),\theta-\theta',t). \quad (3.8b)$$

Equation (3.6) then reads

$$\frac{\partial}{\partial t_0}\mathbf{P}(E_0,t_0;E,\mathbf{r},\theta,t)$$
$$+\int_E^{E_0}dE'\mathbf{V}(E_0,t_0;E')\mathbf{P}(E',t_0;E,t)$$
$$=-\int_E^{E_0}dE'\int_{-\infty}^{\infty}d\theta'[\mathbf{Y}(E_0,t_0;E',\theta')$$
$$-\delta(\theta')\mathbf{V}(E_0,t_0;E')]$$
$$\times\mathbf{P}(E',t_0;E,\mathbf{r}-\theta'(t-t_0),\theta-\theta',t)$$
$$=-\int_E^{E_0}dE'\int_{-\infty}^{\infty}d\theta'[\mathbf{X}(E_0,t_0,E',\theta')$$
$$-\delta(\theta')\mathbf{W}(E_0,t_0;E')]$$
$$\times\mathbf{P}(E',t_0;E,\mathbf{r}-\theta'(t-t_0),\theta-\theta',t) \quad (3.9)$$

By treating the term on the right-hand side of (3.9) as a known inhomogeneity, a comparison of (3.9) and (3.7) yields the following general integral equation for $\mathbf{P}$:

$$\mathbf{P}(E_0,t_0;E,\mathbf{r},\theta,t)$$
$$=\delta(\theta)\delta(\mathbf{r})\pi(E_0,t_0;E,t)+\int_{t_0}^{t}dt'\int_E^{E_0}dE'$$
$$\times\int_E^{E'}dE''\int_{-\infty}^{\infty}d\theta'\pi(E_0,t_0;E',t')$$
$$\times[\mathbf{X}(E',t';E'',\theta')-\delta(\theta')\mathbf{W}(E',t';E'')]$$
$$\times\mathbf{P}(E'',t';E,\mathbf{r}-\theta'(t-t'),\theta-\theta',t). \quad (3.10)$$

4. MOMENT RECURRENCE RELATIONS

The integral equation (3.10) enables us to write down very simply the recurrence relations for the moments, angular, radial and mixed if desired, of the lateral distribution functions $\mathbf{P}$. We are interested in the nth radial moment defined by

$$\mathbf{R}_n(E_0,t_0;E,t)=\int_{-\infty}^{\infty}d\theta\int_{-\infty}^{\infty}r^n dr\mathbf{P}(E_0,t_0;E,\mathbf{r},\theta,t), \quad (4.1)$$

and the mth angular moment,

$$\mathbf{Q}_m(E_0,t_0;E,t)=\int_{-\infty}^{\infty}\theta^m d\theta\int_{-\infty}^{\infty}dr\mathbf{P}(E_0,t_0;E,\mathbf{r},\theta,t). \quad (4.2)$$

We obtain the solutions:

$$\mathbf{R}_n(E_0,t_0;E,t)$$
$$=\sum_{p=1}^{n}\binom{n}{p}\int_{t_0}^{t}dt'(t-t')^p\int_E^{E_0}dE'\int_E^{E'}dE''$$
$$\times\pi(E_0,t_0;E',t')\mathbf{X}_p(E',t';E'')\mathbf{R}_{n-p}(E'',t';E,t), \quad (4.3)$$

$$\mathbf{Q}_m(E_0,t_0;E,t)$$
$$=\sum_{q=1}^{m}\binom{m}{q}\int_{t_0}^{t}dt'\int_E^{E_0}dE'\int_E^{E'}dE''\pi(E_0,t_0;E',t')$$
$$\times\mathbf{X}_q(E',t';E'')\mathbf{Q}_{m-q}(E'',t';E,t), \quad (4.4)$$

where

$$\mathbf{X}_n(E,t;E')=\int_{-\infty}^{\infty}d\theta\theta^n\mathbf{X}(E,t;E',\theta). \quad (4.5)$$

5. ELECTRON-PHOTON SHOWERS

In the electron-photon cascade it is assumed that the multiplicative processes, *viz.*, bremsstrahlung, pair production and Compton scattering, do not contribute to the lateral spread of the shower. Hence their differential cross sections have the form,

$$x_{i,j}(E_0,t;E,\theta)=\delta(\theta)w_{i,j}(E_0,t,E)_{i,j=1,2}, \quad (5.1)$$

and will therefore not appear in Eq. (3.10). If expression (2.1) is used for the Coulomb scattering of the electrons Eq. (3.10) becomes

$$p_{i,j}(E_0,t_0;E,r,\theta,t)=\delta(\theta)\delta(r)\pi_{i,j}(E_0,t_0;E,t)$$
$$+\int_{t_0}^{t}dt'\int_{E}^{E_0}dE'\int_{-\infty}^{\infty}d\theta'\pi_{i,1}(E_0,t_0;E',t')$$
$$\times[\sigma_1(E',t';\theta')-\delta(\theta')\mu_1(E',t')]$$
$$\times p_{1,j}(E',t';E,r-\theta'(t-t'),\theta-\theta',t). \quad (5.2)$$

This is also a generalization of Blatt's equation[1] in that it also treats the case of an incident photon ($i=2$). It should be noted that for this case it yields an immediate solution for $p_{2,j}$ in terms of the equivalent expression for a primary electron.

It should be noted that $\pi_{i,1}$ may contain such processes as ionization loss, Compton effect, etc., and hence (5.2) is valid for any energy range for which we have the average numbers. It is obvious that this leads to a simple recursion relation for the moments which greatly simplifies previous work. See for instance Chartres and Messel.[8]

One of us (B.A.C.) wishes to thank Commonwealth Scientific and Industrial Research Organization for the grant of a studentship.

[8] B. A. Chartres and H. Messel, Proc. Phys. Soc. (London) **A67**, 158 (1954).

PHYSICAL REVIEW VOLUME 96, NUMBER 6 DECEMBER 15, 1954

Possible Triple-Scattering Experiments*

L. WOLFENSTEIN
Carnegie Institute of Technology, Pittsburgh, Pennsylvania
(Received September 7, 1954)

Triple-scattering experiments may be used to get additional information about the spin-dependence of the scattering matrix of the second scatterer. In general two new parameters describing the scattering may be determined by means of two distinct experiments, one in which the successive scattering planes are parallel and one in which the successive scattering planes are at right angles to each other. The relation between these parameters and the scattering matrix is given for the cases of protons scattered from a spin-zero target and of proton-proton scattering. For the former case the magnitude of the left-right asymmetry in the third scattering is calculated on the basis of a phenomenological model due to Fermi in the Born approximation. Further experimental possibilities for p-p scattering are discussed.

1. GENERAL FORMULATION

RECENT successful experiments[1] on the double scattering of high-energy protons make it of interest to note that further information may be obtained by means of triple-scattering experiments. Such experiments would be designed to determine how the second scatterer changes the direction and/or magnitude of the polarization of the proton; thus, the first scatterer serves simply as a polarizer and the final scatterer as an analyzer.

To describe the geometry of a triple-scattering experiment we first define for each scattering the unit vector $\mathbf{n}$,

$$\mathbf{n}=(\mathbf{k}\times\mathbf{k}')/|\mathbf{k}\times\mathbf{k}'|, \quad (1.1)$$

where $\mathbf{k}$ and $\mathbf{k}'$ are unit vectors in the incident and outgoing laboratory directions, respectively. The beam incident on the second scatterer is polarized along the direction $\mathbf{n}_1$. For a given scattering angle θ, the second scattering is completely defined by an azimuthal angle φ, here defined by

$$\cos\varphi=\mathbf{n}_1\cdot\mathbf{n}_2 \quad \sin\varphi=\mathbf{n}_1\times\mathbf{n}_2\cdot\mathbf{k}_2. \quad (1.2)$$

In the third scattering a left-right asymmetry is measured relative to a direction $\mathbf{n}_3$; since polarization along the direction of motion cannot be detected, two "settings" of the analyzer are sufficient; that is, two directions for $\mathbf{n}_3$. Therefore we need only consider the cases when $\mathbf{n}_3$ is parallel to $\mathbf{n}_2$ and when $\mathbf{n}_3$ is along the direction

$$\mathbf{s}=\mathbf{n}_2\times\mathbf{k}_2'. \quad (1.3)$$

Thus the third scattering may be chosen to determine either $\langle\boldsymbol{\sigma}\rangle_2\cdot\mathbf{n}_2$ or $\langle\boldsymbol{\sigma}\rangle_2\cdot\mathbf{s}$, where $\langle\boldsymbol{\sigma}\rangle_2$ is the expectation value of the spin vector after the second scattering; the corresponding asymmetries in triple scattering will be designated e_{3n} and e_{3s}.[2] The discussion throughout is nonrelativistic.

* Work supported in part by U. S. Atomic Energy Commission.
[1] Oxley, Cartwright, and Rouvina, Phys. Rev. **93**, 806 (1954); Chamberlain, Segrè, Tripp, Wiegand, and Ypsilantis, Phys. Rev. **93**, 1430 (1954); Marshall, Marshall, and Carvalho, Phys. Rev. **93**, 1431 (1954); J. M. Dickson and D. C. Salter, Nature **173**, 946 (1954); Kane, Stallwood, Sutton, Fields, and Fox, Phys. Rev. **95**, 1694 (1954).

[2] The asymmetry e_{3n} (or e_{3s}) is defined as $[I_3(+)-I_3(-)]/[I_3(+)+I_3(-)]$ where $I_3(\pm)$ refers to scattering such that $\mathbf{n}_3$ is parallel to $\pm\mathbf{n}_3$ (or $\pm\mathbf{s}$).

It may be shown[3] that $I_2\langle\boldsymbol{\sigma}\rangle_2$ depends at most linearly on $\langle\boldsymbol{\sigma}\rangle_1$, where I_2 is the differential scattering cross section of the second scatterer and $\langle\boldsymbol{\sigma}\rangle_1$ is the expectation value of the spin vector before the second scattering. Using this fact and noticing that $\langle\boldsymbol{\sigma}\rangle_2\cdot\mathbf{n}_2$ is a scalar while $\langle\boldsymbol{\sigma}\rangle_2\cdot\mathbf{s}$ is a pseudoscalar, we determine the most general dependence of these quantities on $\mathbf{k}_2$, $\mathbf{k}_2'$, and $\langle\boldsymbol{\sigma}\rangle_1$:

$$I_2\langle\boldsymbol{\sigma}\rangle_2\cdot\mathbf{n}_2=I_0(P_2+D\langle\boldsymbol{\sigma}\rangle_1\cdot\mathbf{n}_2) \tag{1.4a}$$

$$I_2\langle\boldsymbol{\sigma}\rangle_2\cdot\mathbf{s}=I_0[A\langle\boldsymbol{\sigma}\rangle_1\cdot\mathbf{k}_2+R\langle\boldsymbol{\sigma}\rangle_1\cdot(\mathbf{n}_2\times\mathbf{k}_2)]. \tag{1.4b}$$

Here P_2, D, A, and R are arbitrary functions of $\mathbf{k}_2\cdot\mathbf{k}_2'$, that is, of the scattering angle θ; for convenience we have factored out I_0, the differential cross section for an unpolarized beam, which is a function of θ alone.[4] If the beam entering the second scatterer is unpolarized it leaves with a polarization given by P_2, which is therefore just the familiar polarization function determined in double-scattering experiments. For later purposes we also write the expression for the undetectable component of $\langle\boldsymbol{\sigma}\rangle_2$:

$$I_2\langle\boldsymbol{\sigma}\rangle_2\cdot\mathbf{k}_2'=I_0[A'\langle\boldsymbol{\sigma}\rangle_1\cdot\mathbf{k}_2+R'\langle\boldsymbol{\sigma}\rangle_1\cdot(\mathbf{n}_2\times\mathbf{k}_2)]. \tag{1.4c}$$

In the appendix it is shown that only three of the four parameters A, R, A', and R' are independent at any angle θ.

Substituting $P_1\mathbf{n}_1$ for $\langle\boldsymbol{\sigma}\rangle_1$ and recalling that

$$I_2=I_0(1+P_1P_2\cos\varphi) \tag{1.5}$$

as is well known from discussions of double scattering, we find for the asymmetry in the triple-scattering experiments:

$$e_{3n}=P_3(P_2+DP_1\cos\varphi)/(1+P_1P_2\cos\varphi), \tag{1.6}$$

$$e_{3s}=P_3P_1R\sin\varphi/(1+P_1P_2\cos\varphi), \tag{1.7}$$

where P_3 characterizes the third scatterer. Since $\langle\boldsymbol{\sigma}\rangle_1$ must be perpendicular to the direction of motion, $\mathbf{k}_2$, after a single scattering, the function A cannot be determined in a triple-scattering experiment. (See Sec. 4.)

Thus there exist in general two new parameters D and R that may be determined from two distinct triple-scattering experiments. The first of these consists of measuring e_{3n} with φ equal to 0 or 180°; this means that all three scattering planes are parallel. For either value of φ, one can then determine D from Eq. (1.6), assuming P_3P_2, P_3P_1, and P_1P_2 have been determined from double-scattering experiments. Alternatively one can use both values of φ; assuming that the first scattering is to the left, one then has four possible scattered intensities LL, LR, RL, and RR, where LR is the intensity when second and third scatterings are to the left and right, respectively, etc. Using Eqs. (1.6) and (1.5) and noting that e_{3n} is defined relative to $\mathbf{n}_2$ we find that

$$D=\frac{LL+RL-LR-RR}{(LL+RL+LR+RR)P_3P_1}. \tag{1.8}$$

Use of this procedure eliminates the most obvious intrinsic experimental asymmetry in the combination of second and third scatterings and uses only one result (P_3P_1) from a double-scattering experiment.

The parameter D may be considered as giving the extent to which the second scattering depolarizes an initially polarized beam. This may be seen by looking at $\langle\boldsymbol{\sigma}\rangle_2$ for the case P_1 equals unity and $\cos\varphi$ equals ±1; from Eqs. (1.4) and (1.5) we find

$$\langle\boldsymbol{\sigma}\rangle_2=\mathbf{n}_2(P_2\pm D)/(1\pm P_2). \tag{1.9}$$

It follows that a necessary and sufficient condition that there be no depolarization of a beam initially completely polarized normal to the scattering plane is that D equals unity. Looking at Eq. (1.9) one notes that if D equals P_2^2, $\langle\boldsymbol{\sigma}\rangle_2$ has the same value as if the original beam were unpolarized; however, in general D may be less than this so that D may not represent a depolarization but actually a reversal of the initial spin. Equation (1.9) together with the condition $|\langle\boldsymbol{\sigma}\rangle_2|\leq1$ yield the following limits on D:

$$-1+2|P_2|\leq D\leq1. \tag{1.10}$$

The second triple scattering experiment consists of measuring e_{3s} with φ around $\pm90°$. This means that the successive scattering planes are at right angles. For either value of φ the parameter R is determined from Eq. (1.7) using the experimental value of P_1P_3. To maximize e_{3s} the second scattering actually should be somewhat to the low cross-section side of "up" or "down" rather than at $\varphi=90°$; from Eq. (1.7) this maximum is given by

$$\cos\varphi=-P_1P_2. \tag{1.11}$$

Considering once again the case P_1 equal to unity and setting φ equal to 90°, we find from Eqs. (1.4) and (1.5):

$$\langle\boldsymbol{\sigma}\rangle_2=P_2\mathbf{n}_2+R\mathbf{s}+R'\mathbf{k}_2'. \tag{1.12}$$

It follows from Eq. (1.12) that

$$|R|\leq(1-P_2^2)^{\frac{1}{2}}. \tag{1.13}$$

2. SPIN-ZERO TARGET

If the target has zero spin and the incident particle is completely polarized, the particle after scattering will still be represented by a pure wave function and so will still be completely polarized. From our previous discussion, therefore, D is equal to unity. We may also give a physical picture of the parameter R for the case $\varphi=90°$. From Eq. (1.12) we see that the original spin

[3] L. Wolfenstein and J. Ashkin, Phys. Rev. 85, 947 (1952). This reference will be referred to hereafter as A. Equation (5) of this reference shows in general the linear relation between the expectation value of operators before and after collision.

[4] We omit the subscript 2 on some of the scattering parameters (such as D, A, R, I_0, θ, φ) where this will cause no ambiguity. All the scattering parameters, of course, may depend on the energy.

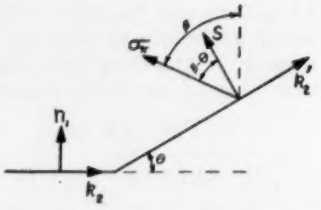

FIG. 1. Directions of vectors in the scattering plane for $\varphi=90°$.

vector $\mathbf{n}_1$ is bent out of the scattering plane so that its component along the normal $\mathbf{n}_2$ is P_2 and therefore since $\langle\boldsymbol{\sigma}\rangle_2$ must equal unity its projection in the plane has a magnitude $(1-P_2^2)^{\frac{1}{2}}$. The projected vector $\boldsymbol{\sigma}_\pi$ (Fig. 1) may be rotated by an angle β about the $\mathbf{n}_2$ axis from the direction $\mathbf{n}_1$. It follows that

$$R=(1-P_2^2)^{\frac{1}{2}}\cos(\Theta-\beta), \tag{2.1}$$

where Θ is the laboratory scattering angle.

The scattering amplitude may be written as a matrix M operating on the initial spinor. An arbitrary matrix may be written

$$M=g+\boldsymbol{\sigma}\cdot\mathbf{h}, \tag{2.2a}$$

and invariance arguments[5] restrict us to the form

$$M=g(\Theta)+\boldsymbol{\sigma}\cdot\mathbf{n}h(\Theta). \tag{2.2b}$$

In this notation the unpolarized differential cross section is clearly given by

$$I_0=|g|^2+|h|^2, \tag{2.3}$$

while the left-right asymmetry in the single scattering of a completely polarized beam is given by

$$P=2\,\mathrm{Re}(g^*h)/(|g|^2+|h|^2). \tag{2.4}$$

By applying Eq. (2.2b) to an arbitrary spinor, we find that β in Eq. (2.1) is given by

$$\begin{aligned}\sin\beta&=2\,\mathrm{Im}(g^*h)/I_0(1-P^2)^{\frac{1}{2}},\\ \cos\beta&=(|g|^2-|h|^2)/I_0(1-P^2)^{\frac{1}{2}}.\end{aligned} \tag{2.5}$$

A few general features of β as a function of the scattering angle may be predicted. The relatively large values of polarization P at certain angles show that the absolute values of g and h are of the same order of magnitude. Since h must contain a factor $\sin\Theta$, $g(\Theta)$ and $h(\Theta)$ should behave quite differently as functions of Θ, and so these two curves might be expected to cross somewhere near the angle of maximum polarization; at smaller angles $|g|$ is larger than $|h|$. If this is so, then it follows from Eq. (2.5) that β increases in absolute value as a function of Θ starting at 0 at 0° and passing through $\pm90°$ somewhere near the polarization maximum. For angles around the expected diffraction minimum, β might exhibit some large variations with Θ. Further predictions can be made by employing a model proposed by Fermi and others[6] consisting of a complex potential supplemented by a real spin-orbit coupling term. In the Born approximation one finds immediately:

$$\sin\beta=(B/B_a)\{P/(1-P^2)^{\frac{1}{2}}\}, \tag{2.6}$$

where B and B_a are proportional to the magnitudes of the real and imaginary parts of the central potential, and the result is independent of the form of the spin-orbit coupling chosen. Values of β and the asymmetry e_{3s} shown in Table I have been calculated by using Eqs. (1.7), (1.11), (2.1), and (2.6), the value of 27/16 for (B/B_a) and the values for $P_2(\theta)$ given by Fermi, and by assuming $P_1=P_3=0.65$. For comparison, values of e_{3n} from Eq. (1.6) (with $D=1$) obtained with the same value of φ are also shown.

Although at each angle Θ the measurements of I_0, P, and β are quite independent, the functions $I_0(\Theta)$, $P(\Theta)$, and $\beta(\Theta)$ must be interrelated. This is clear from the possibility of a phase-shift analysis of the scattering. In principle the $(2L+1)$ complex phase shifts should be determined by the $(2L+1)$ coefficients in $I_0(\theta)$, the $2L$ coefficients[7] in $P(\theta)$, when these are expanded in powers of $\cos\theta$, and the total absorption cross section (including inelastic scattering). In practice such a phase shift analysis is hopeless for these cases, where many partial waves are involved. Furthermore, as a matter of principle, if L is the maximum orbital angular momentum to be considered it is of doubtful validity to analyze terms in the expansion of $I_0(\theta)$ much beyond the first $(L+1)$ terms since there may be significant contributions to the remaining terms from the interference of partial waves beyond the Lth with low-order partial waves. Therefore it seems likely that determination of $\beta(\theta)$ would add significant information about the scattering.[8]

TABLE I. Asymmetry e_{3s} in triple scattering for $P_1=P_3=0.65$ as a function of scattering angle θ in the second scattering, obtained by using Fermi's theory. φ is chosen to maximize e_{3s}. For comparison, the value of e_{3n} for the same value of φ is shown. The value e_{3s}' is the value of e_{3s} predicted by Fermi's theory with a change in sign of the spin-orbit interaction.

θ	P_2	β	φ	e_{3s}	e_{3n}	e_{3s}'
5	0.4	47	105	0.25	0.16	0.21
10	0.51	90	109	0.06	0.21	−0.06
15	0.49	108	109	−0.02	0.20	−0.18
20	0.42	129	106	−0.11	0.17	−0.29
30	0.33	144	102	−0.14	0.13	−0.35

[5] L. Wolfenstein, Phys. Rev. **75**, 1664 (1949).

[6] E. Fermi, Nuovo cimento **11**, 407 (1954); W. Heckrotte and J. Lepore, Phys. Rev. **94**, 500 (1954); Snow, Sternheimer, and Yang, Phys. Rev. **94**, 1073 (1954); R. Sternheimer, Phys. Rev. **95**, 588 (1954). Dr. Sternheimer has kindly communicated to me a few calculations of β on the basis of the same model previously used to calculate P. These calculations seem to bear out the general remarks made above.

[7] Theorem 3(b) of reference 5. For this discussion results are expressed in terms of the c.m. angle θ rather than the lab angle Θ.

[8] This should be contrasted with the simpler case of protons of 1 to 4 Mev scattered from helium, C. L. Critchfield and D. C. Dodder, Phys. Rev. **76**, 602 (1949); M. Heusinkveld and G. Freier, Phys. Rev. **85**, 80 (1952). In this case the phase shifts are real and only s and p waves need be considered; then I_0 alone limited one to two possible sets of phase shifts and the measurement of P resolved this ambiguity.

Even if the complex phase shifts could be determined from $I_0(\theta)$ and $P(\theta)$ it is likely the determination would not be unique and measurements of $\beta(\theta)$ would help resolve ambiguities. The most common and most interesting ambiguity in analyses of this kind is the uncertainty as to the sign of the spin-orbit coupling. In the Born approximation the only effect of a change of sign of the spin-orbit interaction is to reverse the sign of h and thus change both the sign of P and of β. When many partial waves are involved in a phase-shift analysis, there should exist two very similar solutions obtained from each other by exchanging the phase shifts for $J=l+\frac{1}{2}$ and $J=l-\frac{1}{2}$, and these two will differ essentially only in the sign of P and of β. While no direct method seems to exist for determining the absolute value of the sign of P, [L. Marshall and J. Marshall have recently made a measurement of the sign of P (private communication)] it is clear from Eq. (2.1) that the triple scattering asymmetry e_{3s} depends on the sign of β. Such a measurement may thus give a key to the sign of the spin-orbit coupling. It must be noted however that for a given scattering angle Θ it is impossible to distinguish between a value β_1 and a value $(-\beta_1+2\Theta)$. In the last column of Table I values of e_{3s}' are given, which are the values predicted by Fermi's theory, with a reversal of the sign of the spin-orbit coupling.

3. PROTON-PROTON SCATTERING

The scattering in the case of proton scattering from a target with spin can again be described by a matrix of the form (2.2a), but in this case g and $\mathbf{h}$ are operators in the spin space of the target nucleus. The unpolarized differential cross section is now expressed

$$I_0=\mathrm{Tr}(gg^\dagger+\mathbf{h}\cdot\mathbf{h}^\dagger)/2(2s+1), \tag{3.1}$$

where s is the spin of the target and Tr stands for the trace of the matrix in the *composite* spin space of proton plus target. P can be calculated from M[9] and is given by

$$P=\frac{\mathrm{Tr}(g\mathbf{h}^\dagger+g^\dagger\mathbf{h})\cdot\mathbf{n}}{\mathrm{Tr}(gg^\dagger+\mathbf{h}\cdot\mathbf{h}^\dagger)}. \tag{3.2}$$

The expectation value of the spin after the second scattering[10] may be found from Eq. (5) of A:

$$\begin{aligned}I_2\langle\boldsymbol{\sigma}\rangle_2&=\{\mathrm{Tr}(M\boldsymbol{\sigma}\cdot\langle\boldsymbol{\sigma}\rangle_1 M^\dagger\boldsymbol{\sigma})+\mathrm{Tr}(MM^\dagger\boldsymbol{\sigma})\}/2(2s+1)\\&=\{\mathrm{Tr}[(gg^\dagger-\mathbf{h}\cdot\mathbf{h}^\dagger)\langle\boldsymbol{\sigma}\rangle_1\\&\quad+i(g^\dagger\mathbf{h}-g\mathbf{h}^\dagger)\times\langle\boldsymbol{\sigma}\rangle_1+\langle\boldsymbol{\sigma}\rangle_1\cdot\mathbf{h}\mathbf{h}^\dagger+\mathbf{h}\mathbf{h}^\dagger\cdot\langle\boldsymbol{\sigma}\rangle_1]\\&\quad+PI_0\mathbf{n}\}/2(2s+1).\end{aligned} \tag{3.3}$$

For the case of proton-proton scattering the most general form of M is given by Eq. (9) of A with $D=0$, and this may be rewritten in the form:

$$\begin{aligned}M=&BS+C(\boldsymbol{\sigma}+\boldsymbol{\sigma}_t)\cdot\mathbf{n}+\tfrac{1}{2}G(\boldsymbol{\sigma}\cdot\mathbf{K}\boldsymbol{\sigma}_t\cdot\mathbf{K}+\boldsymbol{\sigma}\cdot\mathbf{P}\boldsymbol{\sigma}_t\cdot\mathbf{P})T\\&+\tfrac{1}{2}H(\boldsymbol{\sigma}\cdot\mathbf{K}\boldsymbol{\sigma}_t\cdot\mathbf{K}-\boldsymbol{\sigma}\cdot\mathbf{P}\boldsymbol{\sigma}_t\cdot\mathbf{P})T+N\boldsymbol{\sigma}\cdot\mathbf{n}\boldsymbol{\sigma}_t\cdot\mathbf{n}T,\end{aligned} \tag{3.4}$$

where $\mathbf{K}$ and $\mathbf{P}$ are unit vectors in the directions $(\mathbf{p}'-\mathbf{p})$ and $(\mathbf{p}'+\mathbf{p})$, respectively, $\mathbf{p}'$ and $\mathbf{p}$ are outgoing and incident momenta in the c.m. system, and S and T are singlet and triplet projection operators, respectively. From parity considerations it follows that B and H are even functions of $\cos\theta$, G and N are odd functions, and C is an even function times $\sin\theta$. Comparing Eq. (3.4) with Eq. (2.2a) we find the operators g and $\mathbf{h}$ and then using Eqs. (3.1) through (3.3) we obtain

$$\begin{aligned}I_0=&\tfrac{1}{4}|B|^2+2|C|^2+\tfrac{1}{4}|G-N|^2\\&+\tfrac{1}{2}|N|^2+\tfrac{1}{2}|H|^2,\end{aligned} \tag{3.5a}$$

$$I_0P=2\,\mathrm{Re}(C^*N), \tag{3.5b}$$

$$I_0(1-D)=\tfrac{1}{4}|G-N-B|^2+|H|^2, \tag{3.5c}$$

$$\begin{aligned}I_0R=&\tfrac{1}{2}\,\mathrm{Re}[(G-N)^*(N+H)+B^*(N-H)]\\&\times\cos(\theta/2)+\mathrm{Im}[C^*(G-N+B)]\sin(\theta/2).\end{aligned} \tag{3.5d}$$

In finding the expression for R in terms of the c.m. angle θ we have used the fact that the vector $\mathbf{s}$ defined in the lab system by Eq. (1.3) becomes the vector $\mathbf{K}$ in the present case.

The value of D for $\theta=90°$ may be particularly revealing; there is then no interference term in D and the three possible terms B, C, and H give by themselves values of D of 0, 1, and -1, respectively. Experiments[11] suggest a value of D at 90° of about 0.7, from which it would follow that at least 70 percent of the 90° cross section is due to the C term and at most 15 percent is due to the H term; thus at most 30 percent of the 90° cross section could be caused by singlet scattering. Further information on the singlet scattering at 90° may be obtained from the value of R at 90° since this is determined completely by singlet-triplet interference: a nonzero value of R sets a lower limit on the singlet scattering. If we take the value of D at 90° as 0.7 the maximum possible absolute value of R is close to 0.5, and if this were the actual value of R it would fix the singlet scattering at about 30 percent. Of course there is no simple converse conclusion from a zero value of R. It may also be noted that $D(\theta)$ may contain odd terms as a function of $\cos\theta$ due to the contribution of singlet-triplet interference so that a measurement of the triple scattering asymmetry e_{3n} on both sides of 90° could yield information on the singlet scattering at other angles.

Once again we may ask the extent to which I, P, D, and R are independent as functions of the scattering angle θ. If we assume the phase shifts are real[12] and

[9] Equation (7a) of A. In some of the equations in the present paper the obvious generalization to a target of spin s is made. In place of the notation $\boldsymbol{\sigma}_1$ and $\boldsymbol{\sigma}_2$, in the present paper $\boldsymbol{\sigma}$ and $\boldsymbol{\sigma}_t$ are used.

[10] This result Eq. (3.3) is the same as Eq. (15) of reference 5, except that there the trace is omitted; it is essential to take the trace when the scattering depends on the target spin.

[11] Chamberlain, Segrè, Tripp, Wiegand, and Ypsilantis (private communication). More recent results suggest a value of D around 0.5. It must be emphasized that these are preliminary results and may be subject to large corrections.

[12] The imaginary part of the phase shifts can be estimated from the analysis of data on meson production.

ignore the mixing of different partial waves due to tensor forces there are then $2(L+1)$ real numbers to be determined where L is the maximum orbital angular momentum (assumed for convenience to be odd). Since $I(\theta)$ contains $(L+1)$ coefficients when expanded in powers of $\cos^2\theta$ and $P(\theta)$ contains L coefficients there remains a one-parameter family of phase shifts fitting this data.[13] Thus $D(\theta)$ or $R(\theta)$ could reduce these possibilities. Actually for the energies for which such a phase-shift analysis is most feasible, a study of Coulomb interference effects[14] may be a simpler method for reducing the possibilities. However, at higher energies where Coulomb interference is hard to measure and the number of partial waves increases the measurement of $D(\theta)$ and $R(\theta)$ should be of real value in determining the scattering matrix M.

4. FURTHER EXPERIMENTAL POSSIBILITIES

For the case of a spin-zero target the triple scattering experiment coupled with the previously-measured P and I_0 completely determines the scattering matrix [Eq. (2.2b)] except for the phase of the scattered amplitude, which we cannot expect to determine directly by any reasonable experiment. For proton-proton scattering, on the other hand Eq. (3.4) contains nine real parameters at each angle θ, whereas the experiments discussed here determine only four: I_0, P, D, and R. It may be of interest to inquire whether it would be possible to acquire any further information by successive scatterings without using a polarized target. The triple scattering experiments considered here are not the most general experiments of this type because they are restricted by the fact that the initial polarization and the part of the final polarization that is detected must be at right angles to the direction of motion. In general we might hope to determine all parameters relating the final polarization vector to the initial. As shown in the appendix there are five independent parameters of this type, which are conveniently chosen as P, D, R, A, and R' of Eq. (1.4). While A and R' might be determined from quadruple scattering experiments, a more practical mothod would be to use a magnetic field directed at right angles both to the path of the proton and the direction of its spin. Because of the anomalous moment of the proton, the proton spin precesses about this field with an angular frequency larger than that of the proton's motion. Such a magnet placed between the first and second scatterers would cause the proton to end up with a spin component along the direction of motion and so would allow a determination of the parameter A. If the magnet were placed between the second and third scatterers it would partially convert the undetectable $\mathbf{k}_2'$-component of spin to a component at right angles to the direction of motion and so allow the determination of R'.

Even these do not exhaust the possibilities without polarized targets. Additional information at any angle θ may be obtained by a suggested experiment on the polarization correlation of the scattered protons in $p-p$ scattering. Such an experiment involves analyzing in coincidence the polarization states of the scattered and recoil protons and would determine the expectation values of operators such as $(\boldsymbol{\sigma}\cdot\mathbf{n})(\boldsymbol{\sigma}_1\cdot\mathbf{n})$. This would be of interest even for the case in which the initial beam is unpolarized.

APPENDIX. TIME-REVERSAL ARGUMENTS

When we take the trace of the factors involving g and $\mathbf{h}$ in Eq. (3.3) these factors reduce to expressions which depend only on the vectors $\mathbf{p}$ and $\mathbf{p}'$. From rotation and reflection invariance it follows that the first term must reduce to form $f_1(\theta)\langle\boldsymbol{\sigma}\rangle_1$, the second term to $f_2(\theta)\mathbf{n}\langle\boldsymbol{\sigma}\rangle_1$, and the third term to

$$f_3(\theta)\langle\boldsymbol{\sigma}\rangle_1\cdot\mathbf{nn}+f_4(\theta)\langle\boldsymbol{\sigma}\rangle_1\cdot\mathbf{KK}+f_5(\theta)\langle\boldsymbol{\sigma}\rangle_1\cdot\mathbf{PP}+f_6(\theta)\langle\boldsymbol{\sigma}\rangle_1\cdot\mathbf{PK}+f_7(\theta)\langle\boldsymbol{\sigma}\rangle_1\cdot\mathbf{KP}. \quad (A.1)$$

The invariance of M under time-reversal requires that in Eq. (2.2a) the operator g be even and $\mathbf{h}$ be odd under time-reversal. Consequently the third term in Eq. (3.3) is even under time-reversal so that the last two terms in Eq. (A.1) must vanish by the arguments used in A. By combining $f_1(\theta)\langle\boldsymbol{\sigma}\rangle_1$ with the remaining terms in Eq. (A.1) we reduce Eq. (3.3) to the form

$$I_2\langle\boldsymbol{\sigma}\rangle_2=I_0(P\mathbf{n}+J\mathbf{n}\times\langle\boldsymbol{\sigma}\rangle_1+D\langle\boldsymbol{\sigma}\rangle_1\cdot\mathbf{nn}+X\langle\boldsymbol{\sigma}\rangle_1\cdot\mathbf{KK}+Y\langle\boldsymbol{\sigma}\rangle_1\cdot\mathbf{PP}). \quad (A.2)$$

Since the quantities A, R, A', and R' can be derived directly from Eq. (A.2) and (1.4) in terms of J, X, and Y it follows that only three of these four are independent.

A direct calculation also gives in Eq. (3.3) a term independent of $\langle\boldsymbol{\sigma}\rangle_1$ proportional to $\mathrm{Tr}(\mathbf{h}\times\mathbf{h}^\dagger)$; this same term with opposite sign occurs in the direct calculation of Eq. (3.2) from Eq. (7a) of A. Now rotation-reflection invariance tells us this term must be proportional to $\mathbf{n}$ since it is a pseudovector, but the term must be even under time inversion (since it involves $\mathbf{h}$ times itself). However $\mathbf{n}$ is odd. Therefore this term vanishes. Indeed it is just the vanishing of this term that guarantees the validity of Eq. (8) of A. This paragraph is essentially equivalent to Sec. 3 of A.

[13] A. Garren, Phys. Rev. **92**, 213, 1587 (1953), gives an example for s and p waves alone.

[14] R. M. Thaler and J. Bengston, Phys. Rev. **94**, 679 (1954); A. Garren, Phys. Rev. (to be published).

Nucleon-Antinucleon Scattering and Vacuum Polarization

KENNETH A. JOHNSON*
Harvard University, Cambridge, Massachusetts
(Received July 23, 1954)

The cross section for nucleon-antinucleon scattering is calculated by using the covariant form of the two-body equation in a simple approximation. The meson Green's function used is corrected for the first order radiative effects. The resulting S matrix is shown to be unitary. The cross section is nearly independent of the coupling constant. A graph is included.

IN the course of an examination of the vacuum polarization of the symmetrical pseudoscalar meson field, it was thought appropriate to calculate the cross section for the scattering of nucleons on antinucleons in an approximation where the polarization of the meson field plays an important role. Thus, we take the portion of the interaction operator which represents a single-quantum virtual annihilation of the nucleon-antinucleon pair.

In the notation of Karplus and Klein,[1] the two-body equation in the form appropriate to scattering problems, is

$$G^{-+}(12,34)=G^{-}(13)G^{+}(24)+G^{+}(24')G^{-}(13')I(3'4',1'2')G^{-+}(1'2',34). \quad (1)$$

The portion of the interaction operator which we retain is the point-interaction term which may be interpreted as a virtual, single-quantum annihilation:

$$I(3'4',1'2')G^{-+}(1'2',34)=-ig^2\gamma_5(\xi 3'3'')C(3''4)\mathcal{G}_+(\xi\xi')\times C^{-1}(2'4')\gamma_5(\xi'4'4'')G^{-}(4''3)G^{+}(2'4). \quad (2)$$

(We choose units such that $\hbar=c=1$ throughout.) We may note here that γ_5 contains implicitly the isotopic spin. We see that the integral equation (1) is solved when Eq. (2) is inserted. One may then simply calculate the S matrix from the two-body Green's function in the usual manner[2] which gives

$$(\lambda_1'p_1'\lambda_2'p_2'|S-1|\lambda_1p_1\lambda_2p_2)=ig^2(2\pi)^4\delta(p-p')\mathcal{G}_+(p^2)\times C_{12}C_{12}'(\bar{u}_{\lambda p1}\gamma_5 u_{\lambda p2}')(\bar{u}_{\lambda p2}\gamma_5 u_{\lambda p1}) \quad (3)$$

where $p=p_1+p_2$, $p'=p_1'+p_2'$; 1, 2 symbolize the initial coordinates of the nucleon and antinucleon, 1′, 2′, their respective final coordinates. The $u_{\lambda p}$ are the spinors as defined by Schwinger;[3] hence λ_2 and λ_2' are negative and the $u_{\lambda p}$ also implicitly include the isotopic state of the particle. Further,

$$C_{12}=\left(\frac{(d\mathbf{p}_1)}{(2\pi)^3}\frac{(d\mathbf{p}_2)}{(2\pi)^3}\frac{M^2}{p_{01}p_{02}}\right)^{\frac{1}{2}}, \quad p_0=(\mathbf{p}^2+M^2)^{\frac{1}{2}}, \quad (4)$$

is the normalization for the spinors. Finally $\mathcal{G}_+(k^2)$ is the meson Green's function given symbolically by:

$$\mathcal{G}_+(k^2)=\frac{1}{k^2+\mu^2+P(k^2)}, \quad (5)$$

where $P(k^2)$ is the vacuum polarization of the meson field. The approximate form of the S matrix thus obtained may be shown to be unitary if we can verify the identity

$$(i|(S-1)(S-1)^{\dagger}|i)=-2\,\mathrm{Re}(i|S-1|i), \quad (6)$$

where i symbolizes the initial state. The left side of this may be calculated by multiplying Eq. (3) by its conjugate and summing over the final states. This gives

$$(g^4/\pi)VT|\mathbf{p}|p_0|\mathcal{G}_+(-4p_0^2)|^2C_{12}^2|(\bar{u}_{\lambda p2}\gamma_5 u_{\lambda p1})|^2 \quad (7)$$

in the center-of-mass system, where $p=p_1+p_2=2ip_0=2i(\mathbf{p}^2+m^2)^{\frac{1}{2}}$ is the common momentum of the particles of equal mass. This is to be compared with the right side of Eq. (6),

$$-2\,\mathrm{Re}[i\mathcal{G}_+(-4p_0^2)]g^2VT|(\bar{u}_{\lambda p2}\gamma_5 u_{\lambda p1})|^2. \quad (8)$$

Equality of Eqs. (7) and (8) hinges upon

$$\mathrm{Im}\,P(-4p_0^2)=-1/(2\pi)g^2p_0|\mathbf{p}|. \quad (9)$$

One may establish Eq. (9) and complete the calculation of S by calculating the polarization P explicitly to the

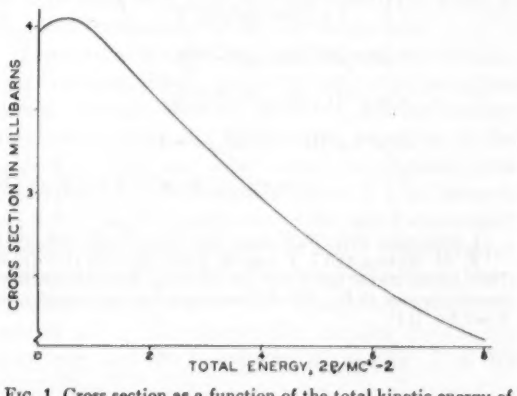

FIG. 1. Cross section as a function of the total kinetic energy of the incident particles in the center-of-mass system, $2p_0-2Mc^2=2(p^2c^2+M^2c^4)^{\frac{1}{2}}-2Mc^2$, for the $T_3=\pm1$ state. The abscissa gives the total kinetic energy in units of rest energy.

* Corning Glass Works Foundation Fellow at Harvard University 1953–1954.

[1] R. Karplus and A. Klein, Phys. Rev. **87**, 848 (1952).
[2] R. Karplus *et al.*, Phys. Rev. **90**, 1072 (1953).
[3] J. Schwinger, Phys. Rev. **92**, 1283 (1953).

lowest order. P is given to this order by[4]

$$(\xi|P|\xi')=-ig^2\,\mathrm{tr}(\gamma_5(\xi)G\gamma_5(\xi')G). \tag{10}$$

This expression can be easily cast into the symbolic form,

$$P(k^2)=4i\frac{g^2}{(2\pi)^4}\times\int(dp)\frac{p^2-\frac{1}{4}k^2+M^2}{[(p-\frac{1}{2}k)^2+M^2][(p+\frac{1}{2}k)^2+M^2]}, \tag{11}$$

where k is the meson momentum. The main effect of the polarization P is to alter the meson mass μ, and the strength of the coupling constant g^2. After these renormalizations have been carried out we are left with the finite portion of P which describes the nonlocal properties of the meson field:

$$P^{(1)}(k^2)=\frac{g^2}{4\pi^2}\left(\frac{2M}{k\mu}\right)^4k^2(k^2+\mu^2)^2\times\int_0^1dv\frac{v^2}{[v^2-(2M/k)^2-1][v^2+(2M/\mu)^2-1]^2}. \tag{12}$$

In deriving Eq. (12) from Eq. (11), use was made of the identity

$$\frac{1}{ab}=\int_{-1}^{+1}\tfrac{1}{2}dv\int_0^\infty-sds\times\exp\{-is[\tfrac{1}{2}(1-v)a+\tfrac{1}{2}(1+v)b]\}, \tag{13}$$

and the renormalization scheme as outlined by Karplus and Klein.[1] Explicit calculation of Eq. (12) yields[5]

$$\begin{aligned}P^{(1)}(k^2)=\frac{g^2}{4\pi}\frac{1}{2\pi}\Bigg\{&k^2\left[1+\left(\frac{2M}{k}\right)^2\right]^{\frac{1}{2}}\\&\times\left(\log\frac{1-[1+(2M/k)^2]^{\frac{1}{2}}}{1+[1+(2M/k)^2]^{\frac{1}{2}}}+\pi i\right)\\&+(k^2-\mu^2)[(2M/\mu)^2-1]^{\frac{1}{2}}\\&\times\tan^{-1}\{[(2M/\mu)^2-1]^{-\frac{1}{2}}\}\\&+(k^2+\mu^2)[1-[(2M/\mu)^2-1]^{-\frac{1}{2}}\\&\times\tan^{-1}\{[(2M/\mu)^2-1]^{-\frac{1}{2}}\}]\Bigg\}.\end{aligned} \tag{14}$$

One may now quickly establish the truth of Eq. (9), and hence the unitarity of the S matrix.

We can now calculate the cross section from Eq. (7) by dividing by the reaction volume VT, by the relative velocity of the particles in the center-of-mass system $2p/p_0$, and by the reciprocal of the density of particles in the initial state C_{12}^2. Thus

$$\sigma=\left(\frac{g^2}{4\pi}\right)^2\frac{\pi/2M^2}{|1-(\mu/2p_0)^2+[P^{(1)}(-4p_0^2)/-4p_0^2]|^2}. \tag{15}$$

Reduction of the spinor factors then yields

$$\sigma=\left(\frac{g^2}{4\pi}\right)^2\frac{\pi/2M^2}{|1-(\mu/2p_0)^2+[P^{(1)}(-4p_0^2)/(-4p_0^2)]|^2}\times\delta_{0i}\begin{Bmatrix}1\\2\end{Bmatrix}, \tag{16}$$

where $i=0$ for the singlet state, $i=1$ for the triplet state. The fact that $\sigma^2=0$ for the triplet state is a simple consequence of the null spin of the meson field, and the fact that the only interaction considered is the virtual annihilation of the pair of spin $\frac{1}{2}$ particles. The factor $\begin{Bmatrix}1\\2\end{Bmatrix}$ results from an evaluation of the isotopic spin operators, the upper term for the $T_3=\pm1$ state, the lower term for the $T_3=0$ state, where T is the isotopic spin of the pair. For calculational purposes we may neglect $(\mu/2M)^2$ compared to 1, and

$$\sigma\sim\left\{\frac{\pi}{2M^2}\Big/\left\{\left[\frac{4\pi}{g^2}+\frac{1}{2\pi}\left(\frac{|\mathbf{p}|}{p_0}\log\frac{p_0-|\mathbf{p}|}{p_0+|\mathbf{p}|}+2\right)\right]^2+\left(\frac{|\mathbf{p}|}{2p_0}\right)^2\right\}\right\}\delta_{0i}\begin{Bmatrix}1\\2\end{Bmatrix}. \tag{17}$$

We see that σ is nearly independent of $g^2/4\pi$ in the usual range of values. We have chosen $g^2/4\pi=10$ for the graph.

We have shown that, as in the work of Karplus, Kivelson, and Martin,[2] a unitary approximation to the S matrix may be achieved if one uses a Green's function, corrected for the radiative effects to the same order to which the interaction operator is taken. The damping gives a result nearly independent of the coupling constant.

The author would like to thank Professor R. Karplus for suggesting this problem, and for valuable discussions.

[4] J. Schwinger, Proc. Natl. Acad. Sci. U. S. **37**, 452, 455 (1951).
[5] K. M. Watson and J. V. Lepore, Phys. Rev. **76**, 1157 (1949). Their results do not agree with our Eq. (12). The error lies in the renormalization of Eq. (8) of Watson and Lepore's paper, which is our Eq. (11).

Fourth Order Corrections to Meson-Nucleon Scattering in Pseudoscalar Meson Theory*†

H. W. WYLD, JR.‡
Physics Department, The University of Chicago, Chicago, Illinois
(Received September 3, 1954)

The low-energy S- and P-wave phase shifts for meson-nucleon scattering in the relativistic pseudoscalar coupling theory are calculated in perturbation theory to fourth order in the coupling constant. A comparison is made of the complete relativistic theory and the nonrelativistic approximation to it, obtained by use of the Foldy-Wouthuysen transformation, via a comparison of the low-energy scattering predicted by both theories. It is concluded that the S-wave scattering is similar in the two theories but that the P-wave scattering is very different in the two theories in fourth order. An analysis of the sources of the differences between the two theories is made by calculating the fourth order scattering in a version of the relativistic theory in which all effects due to the production of pairs are eliminated.

An investigation is made of the nature and possible validity of the Tamm-Dancoff approximation. Two possible viewpoints with respect to this approximation are developed, and the extent to which the Tamm-Dancoff method is applicable to the pseudoscalar coupling theory according to these two points of view is determined, insofar as the low-energy calculations of this paper allow.

I. INTRODUCTION

IN recent years considerable experimental evidence has accumulated on the nature of the π meson and the character of its interaction with nucleons. The experiments indicate that the π meson is a pseudoscalar particle and that the interaction is, to a good approximation, charge independent. In addition to these simple facts, a large amount of detailed information on the nature of the interaction is now available.

A great deal of effort has gone into attempts to understand this meson nucleon interaction on the basis of meson theory. In this approach one starts with a free meson field ϕ_α and a free nucleon field ψ and then couples the two with an interaction term consistent with the pseudoscalar character of ϕ_α and the charge independence of the interaction. Two simple types of coupling have been suggested and extensively studied. In the pseudoscalar coupling theory the interaction term in the Lagrangian density is

$$\mathcal{L}_I = -ig\bar{\psi}\gamma_5\tau_\alpha\phi_\alpha\psi, \tag{1}$$

and in the pseudovector coupling theory the interaction term is

$$\mathcal{L}_I = -(ig/2m)\bar{\psi}\gamma_5\gamma_\mu\tau_\alpha(\partial\phi_\alpha/\partial x_\mu)\psi. \tag{2}$$

Here m is the nucleon mass, and g is the dimensionless coupling constant, the value of which determines the strength of the interaction. If the interactions are written as in Eqs. (1) and (2), then in a certain very approximate sense to be explained below, g in Eq. (1) can be taken to be equivalent to g in Eq. (2). The interaction (1) leads to a theory from which all divergences can be removed by renormalization, while Eq. (2) leads to a theory which is still divergent after renormalization. This has led some physicists to believe that the interaction (1) is much more likely to be correct than the interaction (2), although this point is still in dispute. In any event, with the help of the renormalization procedure calculations based on the interaction (1) can be performed in an unambiguous manner, at least in perturbation theory. On the other hand, if one wishes to go beyond the lowest order in perturbation theory in calculating with the interaction (2), one must introduce some sort of cutoff procedure in order to get finite results.

In order to simplify the mathematical problem of computing with these theories, use has frequently been made of the so-called static approximation, in which all effects of nucleon recoil and all effects due to pair production are eliminated at the outset, so that the nucleon is simply regarded as a source of the meson field. In the case of the pseudovector interaction (2) this leads to a Hamiltonian,

$$H = m + H_\phi + (g/2m)\boldsymbol{\sigma}\cdot\nabla\tau_\alpha\phi_\alpha(\mathbf{x}), \tag{3}$$

for a problem with only one nucleon at the point $\mathbf{x}$. H_ϕ is the Hamiltonian of the free meson field.

If one makes the static approximation to the pseudoscalar coupling theory, the entire interaction term goes to zero. One can, however, perform a series of unitary transformations on the Hamiltonian according to the method of Foldy and Wouthuysen[1] to eliminate from the Hamiltonian, to successive orders in $1/m$, terms in which the "large" components of the field ψ are coupled to the "small" components. The static approximation is then obtained by carrying out the Foldy-Wouthuysen transformation to order m^0 only. To get any interaction term at all for the pseudoscalar coupling theory, one must carry out the transformation to order $1/m$. Up

* A thesis presented in partial fulfillment of the requirements for the Ph.D. at The University of Chicago, Chicago, Illinois.

† Supported in part by a U. S. Atomic Energy Commission predoctoral fellowship and a grant from the U. S. Atomic Energy Commission.

‡ Present address Princeton University, Princeton, New Jersey.

[1] L. L. Foldy and S. A. Wouthuysen, Phys. Rev. **78**, 29 (1950); see also L. L. Foldy, Phys. Rev. **84**, 168 (1951) and G. Wentzel, Phys. Rev. **86**, 802 (1952).

to terms of order $1/m$ one finds

$$H=H_\phi+\int d^3x\psi^\dagger(\mathbf{x})\left(m-\frac{\nabla^2}{2m}\right)\psi(\mathbf{x})$$
$$+\frac{g}{2m}\int d^3x\psi^\dagger(\mathbf{x})\boldsymbol{\sigma}\cdot\nabla\tau_a\phi_a(\mathbf{x})\psi(\mathbf{x})$$
$$+\frac{g^2}{2m}\int d^3x\psi^\dagger(\mathbf{x})\phi_a{}^2(\mathbf{x})\psi(\mathbf{x}). \quad (4)$$

Here the "small" components of $\psi(\mathbf{x})$ have been dropped, so that $\psi(\mathbf{x})$ has two spin components. Examination of this Hamiltonian indicates that the unitary transformation has effectively made a non-relativistic approximation to the nucleon motion and at the same time approximated by the last term in Eq. (4) that part of the interaction in which one virtual pair is produced. The third term in Eq. (4) is essentially equivalent to the interaction term in Eq. (3). Note in particular that the coupling constants have been chosen in such a way that the coefficients of these two terms are the same. In this sense only g from Eq. (1) and g from Eq. (2) are equivalent. The Hamiltonian (4), as it stands, contains a nucleon recoil term. This term helps to make calculations based on Eq. (4) more convergent than they otherwise would be, but the recoil term does not provide enough convergence factors to make a theory based on Eq. (4) finite after renormalization. Furthermore, the cutoff factors provided by the recoil term in the Hamiltonian (4) are not like those provided by the relativistic theory. For these reasons we prefer to simplify Eq. (4) still further by ignoring the nucleon recoil term. This gives us a Hamiltonian,

$$H=m+H_\phi+\frac{g}{2m}\boldsymbol{\sigma}\cdot\nabla\tau_a\phi_a(\mathbf{x})+\frac{g^2}{2m}\phi_a{}^2(\mathbf{x}). \quad (5)$$

One must of course use a cutoff in calculating with either Eq. (3) or (5). The interaction term in Eq. (3) couples only P state mesons with the nucleon. The interaction term $(g^2/2m)\phi_a{}^2(\mathbf{x})$ in Eq. (5) couples only S state mesons with the nucleon.

One of the objectives of this paper is a comparison of the full relativistic pseudoscalar coupling theory, the interaction term of which is given in Eq. (1), and the approximation to the full relativistic theory embodied in Eq. (5). This comparison is made by calculating the low-energy meson nucleon scattering to fourth order in the coupling constant for the full relativistic theory and comparing with the calculations of the fourth order scattering for the Hamiltonian (3) already published by Blair and Chew.[2] The results of Blair and Chew to fourth order and the S state scattering to fourth order as given by the Hamiltonian (5) are reviewed in Sec. II. In Sec. III the scattering to fourth order predicted by the complete relativistic pseudoscalar coupling theory is given.

As will be seen, these two theories, while very similar in second order in g, are quite different in fourth order. In order to facilitate the analysis of the differences between the two theories, it will be convenient to develop some approximations to the full relativistic theory which are less drastic than the Hamiltonian (5). First we shall eliminate from the complete relativistic theory all pair production phenomena. This gives us a theory which is a relativistic generalization of the theory studied by Chew, i.e., the Hamiltonian (3). If we write the Hamiltonian of our theory as

$$H=H_0+H_I=H_\phi+H_\psi+H_I, \quad (6)$$

where H_ϕ and H_ψ are the Hamiltonians of the free meson field and the free nucleon field respectively, and H_I is the interaction Hamiltonian,

$$H_I=ig\int d^3x\bar{\psi}(\mathbf{x})\gamma_5\tau_a\phi_a(\mathbf{x})\psi(\mathbf{x}), \quad (7)$$

then our problem is

$$(E-H_0)\Psi=H_I\Psi. \quad (8)$$

Let $\Psi_{\mathbf{p}si}$ be a vector in Fock space[3] representing a single nucleon with momentum $\mathbf{p}$ in spin state s and isotopic spin state i. We introduce the wave function,

$$\Psi_{si}(\mathbf{p})=(\Psi_{\mathbf{p}si},\Psi). \quad (9)$$

Note that $\Psi_{si}(\mathbf{p})$ is still a state vector with respect to the meson occupation numbers. We now take the scalar product of Eq. (8) with $\Psi_{\mathbf{p}si}$. Ignoring completely the production of pairs, we get

$$(E-H_\phi-E_\mathbf{p})\Psi_{si}(\mathbf{p})$$
$$=\sum_{s'i'}\sum_{\mathbf{p}'}(\Psi_{\mathbf{p}si},H_I\Psi_{\mathbf{p}'s'i'})\Psi_{s'i'}(\mathbf{p}'), \quad (10)$$

where[4] $E_\mathbf{p}=(\mathbf{p}^2+m^2)^{\frac{1}{2}}$ and we use discrete normalization in momentum space. It is not difficult to work out the matrix element $(\Psi_{\mathbf{p}si},H_I\Psi_{\mathbf{p}'s'i'})$, and if this is done one gets, in matrix notation for the spin and isotopic spin indexes,

$$(E-E_\mathbf{p}-H_\phi)\Psi(\mathbf{p})=\frac{1}{V^{\frac{1}{2}}}\sum_{\mathbf{p}'}ig\gamma_5(\mathbf{p},\mathbf{p}')$$
$$\cdot\tau_a(a_{\mathbf{p}-\mathbf{p}',a}+a^\dagger{}_{\mathbf{p}'-\mathbf{p},a})\Psi(\mathbf{p}'). \quad (11)$$

Here V is the normalization volume and

$$\gamma_5(\mathbf{p},\mathbf{p}')=\frac{1}{(2\omega_{\mathbf{p}-\mathbf{p}'})^{\frac{1}{2}}}$$
$$\times\left\{\frac{(E_{\mathbf{p}'}+m)\boldsymbol{\sigma}\cdot\mathbf{p}-(E_\mathbf{p}+m)\boldsymbol{\sigma}\cdot\mathbf{p}'}{2[E_\mathbf{p}E_{\mathbf{p}'}(E_\mathbf{p}+m)(E_{\mathbf{p}'}+m)]^{\frac{1}{2}}}\right\}, \quad (12)$$

[2] J. S. Blair and G. F. Chew, Phys. Rev. **90**, 1065 (1953).

[3] V. Fock, Z. Physik **75**, 622 (1932).

[4] We use always units such that $\hbar=c=1$.

where $\omega_p=(\mathbf{p}^2+\mu^2)^{\frac{1}{2}}$, μ being the meson mass. Except for the factor $(2\omega_{p-p'})^{\frac{1}{2}}$, $\gamma_5(\mathbf{p},\mathbf{p}')$ is the matrix element of the Dirac matrix γ_5 between two positive energy nucleon states. $a_{p-p',\alpha}$ and $a^\dagger_{p'-p,\alpha}$ are destruction and creation operators for mesons. If we neglect recoil in Eq. (12), we find

$$\gamma_5(\mathbf{p},\mathbf{p}')\rightarrow\frac{1}{(2\omega_{p-p'})^{\frac{1}{2}}}\frac{\boldsymbol{\sigma}\cdot(\mathbf{p}-\mathbf{p}')}{2m}. \tag{13}$$

With this approximation for $\gamma_5(\mathbf{p},\mathbf{p}')$ Eq. (11) is identical with the corresponding Schrödinger equation derived from Eq. (3). Equation (11) is just the relativistic generalization of Chew's theory or the P state scattering part of the Hamiltonian (5).

We can also find a relativistic generalization of the S state scattering term in the Hamiltonian (5). To do this we take account only of the production of one pair at a time. We introduce in addition to $\Psi_{\mathbf{p}si}$ another vector in Fock space describing one nucleon and one pair. Let $\Psi_{\mathbf{p}'rj,\,\mathbf{p}''ql;\,\mathbf{p}'''lm}$ represent a state with two nucleons in states designated by $\mathbf{p}'rj$ and $\mathbf{p}''ql$ and an antinucleon in a state designated by $\mathbf{p}'''lm$. We now take the scalar product of Eq. (8) with $\Psi_{\mathbf{p}si}$ and $\Psi_{\mathbf{p}'rj,\,\mathbf{p}''ql;\,\mathbf{p}'''lm}$. Taking account only of the production of one pair at a time, we find

$$(E-H_\phi-E_p)\Psi_{si}(\mathbf{p})=\sum_{rql}\sum_{jlm}\sum_{\mathbf{p}',\mathbf{p}'',\mathbf{p}'''}\times(\Psi_{\mathbf{p}si},H_I\Psi_{\mathbf{p}'rj,\,\mathbf{p}''ql;\,\mathbf{p}'''lm})(\Psi_{\mathbf{p}'rj,\,\mathbf{p}''ql;\,\mathbf{p}'''lm},\Psi), \tag{14}$$

and

$$(E-H_\phi-E_{p'}-E_{p''}-E_{p'''})(\Psi_{\mathbf{p}'rj,\,\mathbf{p}''ql;\,\mathbf{p}'''lm},\Psi)=\sum_{s'i'}\sum_{\mathbf{p}^{iv}}(\Psi_{\mathbf{p}'rj,\,\mathbf{p}''ql;\,\mathbf{p}'''lm},H_I\Psi_{\mathbf{p}^{iv}s'i'})\Psi_{s'i'}(\mathbf{p}^{iv}). \tag{15}$$

Eliminating the one nucleon, one pair amplitude between Eqs. (14) and (15) we get

$$(E-E_p-H_\phi)\Psi_{si}(\mathbf{p})=\sum_{s'i'}\sum_{\mathbf{p}^{iv}}\langle\mathbf{p}si|H_I|\mathbf{p}^{iv}s'i'\rangle\Psi_{s'i'}(\mathbf{p}^{iv}), \tag{16}$$

where

$$\langle\mathbf{p}si|H_I|\mathbf{p}^{iv}s'i'\rangle=\sum_{r,q,t}\sum_{j,l,m}\sum_{\mathbf{p}',\mathbf{p}'',\mathbf{p}'''}(\Psi_{\mathbf{p}si},H_I\Psi_{\mathbf{p}'rj,\,\mathbf{p}''ql;\,\mathbf{p}'''lm})\cdot\frac{1}{E-E_{p'}-E_{p''}-E_{p'''}-H_\phi}\times(\Psi_{\mathbf{p}'rj,\,\mathbf{p}''ql;\,\mathbf{p}'''lm},H_I\Psi_{\mathbf{p}^{iv}s'i'}). \tag{17}$$

The matrix elements in Eq. (17) can be worked out without great difficulty. As it stands $\langle\mathbf{p}si|H_I|\mathbf{p}^{iv}s'i'\rangle$ contains terms which correspond to the formation of closed loops, in Feynman language. We drop these terms. Then Eq. (16) becomes, in matrix notation,

$$(E-E_p-H_\phi)\Psi(\mathbf{p})=\frac{1}{V^{\frac{1}{2}}}\sum_{\mathbf{p}'}\Bigg[\frac{1}{V^{\frac{1}{2}}}\sum_{\mathbf{p}''}ig\gamma_5'(\mathbf{p},\mathbf{p}')\times ig\gamma_5'(\mathbf{p}'',\mathbf{p}')\sum_{\alpha,\alpha'}(a_{\mathbf{p}''-\mathbf{p}',\alpha}+a^\dagger_{\mathbf{p}'-\mathbf{p}'',\alpha})\times\frac{\tau_{\alpha'}\tau_\alpha}{E-E_p-E_{p'}-E_{p''}-H_\phi}\times(a_{\mathbf{p}-\mathbf{p}'',\alpha'}+a^\dagger_{\mathbf{p}''-\mathbf{p},\alpha'})\Bigg]\Psi(\mathbf{p}'), \tag{18}$$

where

$$\gamma_5'(\mathbf{p},\mathbf{p}')=\frac{1}{(2\omega_{p-p'})^{\frac{1}{2}}}\times\left\{\frac{(E_p+m)(E_{p'}+m)+\boldsymbol{\sigma}\cdot\mathbf{p}\boldsymbol{\sigma}\cdot\mathbf{p}'}{2[E_pE_{p'}(E_p+m)(E_{p'}+m)]^{\frac{1}{2}}}\right\}. \tag{19}$$

Except for the factor $(2\omega_{p-p'})^{\frac{1}{2}}$, $\gamma_5'(\mathbf{p},\mathbf{p}')$ is the matrix element of the Dirac matrix γ_5 between a positive energy nucleon state and a negative energy nucleon state. If we drop all recoil terms in Eq. (19), we find

$$\gamma_5'(\mathbf{p},\mathbf{p}')\rightarrow 1/(2\omega_{p-p'})^{\frac{1}{2}}. \tag{20}$$

If, in addition, we make the crude approximation,

$$E-E_p-E_{p'}-E_{p''}-H_\phi\rightarrow -2m \tag{21}$$

in the energy denominator in Eq. (18), we obtain an equation which is precisely the same as what would be obtained from the Hamiltonian (5) if only the pair term in the interaction were kept. So the interaction term of Eq. (18) is just the relativistic generalization of the S state scattering part of the Hamiltonian (5). At this point it becomes apparent that the factors E_p, $E_{p'}$, etc., which appear in the denominators of $\gamma_5(\mathbf{p},\mathbf{p}')$ and $\gamma_5'(\mathbf{p},\mathbf{p}')$ provide the cutoff which makes calculations based on the interaction (1) finite after renormalization. Since E_p begins to become appreciably larger than m in the neighborhood of $|\mathbf{p}|=m$, the relativistic theory is cut off in the neighborhood of $|\mathbf{p}|=m$. Thus insofar as we wish to simulate the complete relativistic theory by the simplified Hamiltonian (5), we should use a cutoff of the order of m in calculating with Eq. (5). In Sec. IV of this paper the differences between the fourth order scattering in the complete relativistic theory and the fourth order scattering according to the Hamiltonian (5) will be analyzed with the help of Eqs. (11) and (18).

It is a well known fact that the coupling constant g of meson theory is sufficiently large so that perturbation theory, or the weak coupling approximation, cannot be used in calculations which are intended to be compared with experimental results. In view of this failure of perturbation theory, a new method of calculation known

as the Tamm-Dancoff (TD) approximation[5] has been seriously investigated recently. The nature of this approximation can be explained in various ways. Dancoff, for example, takes the following point of view. Let us write the true state vector of the meson-nucleon system as a superposition of vectors in Fock space referring to various numbers of particles in various free-particle momentum states. For the meson-nucleons scattering problem we can write

$$\Psi=\sum_{\mathbf{p},\iota} a_\iota(\mathbf{p})\Psi_{\mathbf{p}\iota}+\sum_{\mathbf{p},\mathbf{k},\iota,\alpha} b_{\iota;\alpha}(\mathbf{p};\mathbf{k})\Psi_{\mathbf{p}\iota;\mathbf{k}\alpha}$$
$$+\sum_{\mathbf{p},\mathbf{k}_1,\mathbf{k}_2,\iota,\alpha,\beta} c_{\iota;\alpha,\beta}(\mathbf{p};\mathbf{k}_1,\mathbf{k}_2)\Psi_{\mathbf{p}\iota;\mathbf{k}_1\alpha,\mathbf{k}_2\beta}+\cdots$$
$$+\sum_{\mathbf{p}_1,\mathbf{p}_2,\mathbf{p}_3,\iota,\kappa,\lambda} d_{\iota,\kappa;\lambda}(\mathbf{p}_1,\mathbf{p}_2;\mathbf{p}_3)\Psi_{\mathbf{p}_1\iota,\mathbf{p}_2\kappa;\mathbf{p}_3\lambda}$$
$$+\sum_{\mathbf{p}_1,\mathbf{p}_2,\mathbf{p}_3,\mathbf{k},\iota,\kappa,\lambda,\alpha} f_{\iota,\kappa;\lambda;\alpha}(\mathbf{p}_1,\mathbf{p}_2;\mathbf{p}_3;\mathbf{k})$$
$$\times\Psi_{\mathbf{p}_1\iota,\mathbf{p}_2\kappa;\mathbf{p}_3\lambda;\mathbf{k}\alpha}+\cdots. \quad (22)$$

Here $\Psi_{\mathbf{p}\iota}$ is a vector in Fock space describing a single nucleon in a momentum state $\mathbf{p}$ and spin and isotopic spin state ι; $\Psi_{\mathbf{p}\iota;\mathbf{k}\alpha}$ describes a nucleon in state $\mathbf{p}\iota$ and a meson in state $\mathbf{k}\alpha$; $\Psi_{\mathbf{p}_1\iota,\mathbf{p}_2\kappa;\mathbf{p}_3\lambda;\mathbf{k}\alpha}$ describes two nucleons in state $\mathbf{p}_1\iota$ and $\mathbf{p}_2\kappa$, an antinucleon in state $\mathbf{p}_3\lambda$, and a meson in state $\mathbf{k}\alpha$. The TD approximation consists of keeping in this expansion of Ψ only a certain set of the simpler terms, the terms kept depending to a certain extent on which processes one deems to be important. Once this approximation has been made, an attempt is made to solve to the remainder of the problem rigorously. The approximate expansion of Ψ is substituted into Schrödinger's equation, yielding a set of integral equations for the amplitudes $a_\iota(\mathbf{p})$ $b_{\iota;\alpha}(\mathbf{p};\mathbf{k})$, $\cdots$. For the scattering problem the amplitudes other than $b_{\iota;\alpha}(\mathbf{p};\mathbf{k})$ would be eliminated by substitution from the integral equations to yield an integral equation for $b_{\iota;\alpha}(\mathbf{p},\mathbf{k})$.

In the case of the scattering problem the amplitudes usually retained are those describing two, one, or no mesons. Amplitudes referring to states with three or more mesons are arbitrarily dropped. What is done with the pair terms depends to a large extent on which theory is used. For the static pseudovector coupling theory, Eq. (3), there are no pairs. If a relativistic but non-covariant approach, e.g., Eq. (22), is used, one might restrict oneself to terms obtainable from the one meson, one nucleon state by a single action of the interaction Hamiltonian (1). The TD approximation can also be written out in covariant Feynman notation. In this case one obtains equations of the form of the Bethe-Salpeter[6] equation. If this is done, all of the pair terms with the exception of the closed loops are taken care of by a one nucleon amplitude, since the one nucleon can go "backward in time."

Proceeding from a certain point of view, we have defined the TD approximation mathematically. Let us now see what physical significance we can attach to this point of view. Keeping only those terms involving two or fewer mesons in the field at a time will evidently be a good approximation if processes involving the emission of more than two virtual mesons are strongly inhibited. We have a qualitative reason for supposing that this might actually be the case. Terms associated with the emission of many virtual mesons will necessarily involve large energy denominators, which will tend to make the contributions from these terms smaller than the contributions from those terms involving the emission of only one or two virtual mesons. More physically, according to the Heisenberg uncertainty relation for time and energy, the system will spend only short periods of time in those states involving many virtual mesons.

Let us now consider the meson-nucleon scattering problem and compare the TD method with a straightforward perturbation theory approach. In Fig. 1 the second and fourth order Feynman diagrams for meson-nucleon scattering are enumerated. It is apparent that the approximation of keeping only terms referring to states with two or fewer mesons in the field will include both second order diagrams and all iterations and cross iterations of them, so that diagrams (*c*), (*d*), (*e*), (*f*) will be included. Diagrams (*g*), (*h*), (*i*), (*j*), however, will not be included, because they involve three mesons at a time in the field. Note that some of the energy

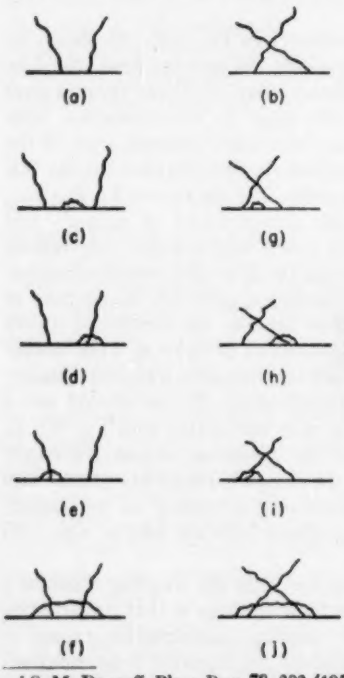

FIG. 1. Second- and fourth-order Feynman diagrams for meson nucleon scattering.

[5] S. M. Dancoff, Phys. Rev. **78**, 382 (1950); I. Tamm, J. Phys. (U.S.S.R.) **9**, 449 (1945); see also M. M. Levy, Phys. Rev. **88**, 72 (1952).

[6] E. E. Salpeter and H. A. Bethe, Phys. Rev. **84**, 1232 (1951).

denominators in diagrams (*c*), (*d*), (*e*), (*f*) may vanish for certain values of the momenta of the virtual mesons, whereas for diagrams (*g*), (*h*), (*i*), (*j*) the energy denominators are always at least as large as μ, the meson mass. One can hope to test the validity of the TD approximation according to the ideas we have developed simply by calculating the contributions to the fourth order scattering from diagrams (*g*), (*h*), (*i*), (*j*) and comparing with the contributions from diagrams (*c*), (*d*), (*e*), (*f*). If the contributions of diagrams (*g*), (*h*), (*i*), (*j*) should turn out to be small compared to the contributions of diagrams (*c*), (*d*), (*e*), (*f*), one would have some confidence in the validity of the TD method. Blair and Chew[2] have attempted to justify the use of the TD approximation for the static pseudovector coupling theory on the basis of the sort of argument outlined here. The results of the calculations of the fourth order scattering in the relativistic pseudoscalar coupling theory, given in Sec. III of this paper, show very definitely that this sort of argument cannot be used to justify the use of the TD method for the pseudoscalar coupling theory.

The TD method can also be considered from a somewhat different point of view. We shall explain this new point of view in terms of the relativistic TD or Bethe-Salpeter approximation. We consider only the meson nucleon scattering problem. The treatment of the meson-nucleon scattering problem in terms of covariant integral equations was first considered by Gell-Mann and Goldberger[7] and has recently been discussed in detail by Levy.[8] All conceivable Feynman diagrams for meson-nucleon scattering can be divided into two classes. In class one are all diagrams in which the incoming nucleon line appears completely bare of virtual or real mesons at some point in the middle of the diagram. Diagrams (*a*), (*c*), (*d*), (*e*), of Fig. 1 are diagrams of this class. In class two are all other scattering diagrams. All diagrams of class one are represented in the contribution,

$$S_1=ig\Gamma_b(P-k',P)\tau_\alpha S_F'(P)ig\Gamma_b(P,P-k)\tau_\beta, \quad (23)$$

to the S matrix. Here k, k' are the initial and final meson four-momenta, and P is the total four-momentum of the system. Γ_b is the modified vertex operator, and S_F' is the modified nucleon propagation function. Note that S_1 contributes to the scattering only for states in which both the isotopic spin and the angular momentum are 1/2. The second class of Feynman diagrams describing scattering can be generated by an integral equation of the form,

$$\psi_\alpha(k)=\phi_{\alpha i}(k)+D_F'(k^2)S_F'(P-k) \times\frac{1}{(2\pi)^4}\sum_\beta\int d^4qG_{\alpha\beta}(k,q)\psi_\beta(q). \quad (24)$$

[7] M. Gell-Mann and M. L. Goldberger (unpublished).
[8] M. M. Levy, Phys. Rev. **94**, 460 (1954).

$\phi_{\alpha i}(k)$ in Eq. (24) represents the incoming plane wave. D_F' is the modified meson propagation function. The kernel $G_{\alpha\beta}(k,q)$ contains a term for each Feynman diagram of class two which is not itself the iteration or cross iteration of simpler diagrams of class two. The iteration of simple scattering diagrams is taken care of by the integral Eq. (24) itself. In terms of the solution of Eq. (24), a matrix element of that part of the S matrix coming from diagrams of class two is given by

$$(S_2)_{fi}=\int d^4k'\bar{\phi}_{\alpha f}(k')i(\mu^2+k^2) \times[i\gamma\cdot(P-k')+m]\psi_\alpha(k'), \quad (25)$$

where $\phi_{\alpha f}(k')$ is the final plane wave state.

All of the diagrams contributing to $G_{\alpha\beta}(k,q)$ can be generated from irreducible scattering diagrams by substituting for the bare nucleon and meson lines and simple vertices the complete nucleon and meson self energy parts and the complete vertex parts. The same division of effects can of course be made in the terms of $G_{\alpha\beta}(k,q)$ themselves, so that the operators S_F', D_F' and Γ_b can be clearly separated out in $G_{\alpha\beta}(k,q)$. Renormalization of these equations is now an easy matter, at least symbolically. One simply replaces S_F', D_F', and Γ_b, wherever they occur in Eqs. (24) and (25), by the renormalized propagation functions and vertex operators and at the same time changes the coupling constant g to the renormalized coupling constant. The division of diagrams into two classes is necessary if the equations are to be renormalized in a simple fashion.

$G_{\alpha\beta}(k,q)$ is known only as a power series in g. To second order in g we have

$$G_{\alpha\beta}(k,q)=ig\gamma_b\tau_\beta\frac{1}{i\gamma\cdot(P-k-q)+m}ig\gamma_b\tau_\alpha, \quad (26)$$

corresponding to the second order diagram (*b*) of Fig. 1. The fourth order corrections to $G_{\alpha\beta}(k,q)$ are represented by the fourth order diagrams (*g*), (*h*), (*i*), (*j*). Now, Eq. (24) is a sort of Schrödinger equation in momentum space for the wave function $\psi_\alpha(k)$, and $G_{\alpha\beta}(k,q)$ is the potential energy of this Schrödinger equation. It is a complicated energy- and momentum-dependent potential energy, but still, in a formal way at least, it can be thought of as a potential energy. It is not difficult to see that the TD approximation essentially amounts to cutting off the power series development of $G_{\alpha\beta}(k,q)$ at some arbitrary power of g. This definition of the TD approximation is not quite identical with the definition previously given. But certainly the spirit of the two approximations is the same. From this point of view we see that the TD approximation will be a good approximation when the coupling constant is sufficiently small so that only the first term in Eq. (26) of the power series development of $G_{\alpha\beta}(k,q)$ need be kept. Weak-coupling theory will be a valid approximation when g is sufficiently smaller still so that the potential

$G_{\alpha\beta}(k,q)$ can be treated in Born approximation. A test of the validity of the TD approximation according to this point of view would be quite complicated. The fourth order potential would have to be calculated and compared with the second order potential in Eq. (26) for the whole range of the variables k and q, g being taken as whatever value was found necessary to fit the experimental data. To carry out this calculation completely would be an extremely laborious job. In this paper the fourth order scattering has been computed only for very low energies, where the S-wave phase shifts vary as the first power of the momentum and the P-wave phase shifts as the third power of the momentum. These calculations will enable us to compare the zero-energy matrix element of the fourth order potential with the zero-energy matrix element of the second order potential. This is done for Chew's theory in Sec. II and for the relativistic pseudoscalar coupling theory in Sec. III.

II. CHEW'S THEORY

Recently, Chew has investigated in great detail the predictions of a theory based on the Hamiltonian (3). We shall be interested in Chew's results for the scattering problem as an approximation to the P-wave scattering of the relativistic pseudoscalar coupling theory. It must be emphasized that Chew has never considered his theory as an approximation to the relativistic theory. He regards his theory as an independent nonrelativistic form of meson theory. For the sake of convenience, however, we shall often refer to Chew's theory as an approximation to the relativistic theory in this paper. Blair and Chew[2] have calculated the second and fourth order scattering with the Hamiltonian (3). They find for the phase shifts

$$\begin{aligned}\delta_{11}&=-4y(1-4\Delta_--2\Delta_+),\\ \delta_{13}=\delta_{31}&=-y(1-\Delta_-+\Delta_+),\\ \delta_{33}&=2y(1+2\Delta_-+\Delta_+),\end{aligned}\tag{27}$$

where

$$y=\frac{1}{6}\left(\frac{g^2}{4\pi}\right)\left(\frac{\mu}{m}\right)^2\left(\frac{k}{\mu}\right)^3,$$

$$\Delta_\pm=\frac{1}{6\pi}\left(\frac{g^2}{4\pi}\right)\left(\frac{\mu}{m}\right)\frac{1}{m}\int_0^K dq\frac{q^4}{\omega_q^3}\frac{1}{\omega_q\pm\mu}.\tag{28}$$

We shall always use the notation δ_{2I} for S-wave phase shifts and $\delta_{2I,2J}$ for P-wave phase shifts, I and J being the isotopic spin and angular momentum respectively. Here we have restricted ourselves to very low energies and expanded the phase shifts in powers of the momentum k, keeping only the lowest order term. K is the cutoff momentum. We indicated in the Introduction that we should take $K=m$ if we wish to regard the Hamiltonian (3) as an approximation to the P-state scattering part of the pseudoscalar coupling theory. Actually, the calculations of Sec. IV will indicate that the effective value of K is somewhat smaller than m. For future reference the contributions to the phase shifts from the various fourth order diagrams for the case $K=m$ have been evaluated numerically and are given in Table I.

The integral Δ_- comes from the TD diagrams (c), (d), (e), (f) in Fig. 1. Δ_+ comes from the diagrams which are ignored in the TD approximation, (g), (h), (i), (j). Because of the vanishing energy denominator in Δ_-, Δ_- is always larger than Δ_+. How much larger it is depends on the cutoff K. As K increases, the significance of the vanishing denominator in Δ_- decreases, and Δ_- approaches Δ_+. For $K=m$, $\mu/m=0.147$, we find

$$\Delta_+/\Delta_-=0.54,\quad K=m.\tag{29}$$

If the cutoff K is decreased, Δ_+/Δ_- decreases. For $K\approx\mu$ we find

$$\Delta_+/\Delta_-=0.11,\quad K=\mu.\tag{30}$$

Note also that to lowest order in μ/m for $K=m$,

$$\Delta_+=\Delta_-=\frac{1}{6\pi}\left(\frac{g^2}{4\pi}\right)\left(\frac{\mu}{m}\right).\tag{31}$$

Thus the difference between Δ_+ and Δ_- is a μ/m correction, a large one, however, according to Eq. (29). For small cutoff then, $K<m$, the TD approximation can be justified for the Hamiltonian (3) simply on the basis that the contribution of the TD terms to the fourth order scattering is considerably larger than the contribution of the terms ignored in the TD method. Precisely this argument has been used by Blair and Chew, who at the time their paper was written were investigating the Hamiltonian (3) with a small cutoff. For $K=m$ this sort of argument is considerably weaker as can be seen from Eq. (29).

Consider now the Hamiltonian (5), which is supposed to be a rough approximation to the complete relativistic pseudoscalar coupling theory. This Hamiltonian contains, in addition to the terms of the static pseudovector coupling theory, a new term, which gives rise to S-wave scattering. Examination of the diagrams involved shows that to fourth order in g the pair term in Eq. (5) contributes nothing to the P-state scattering, so that the P-state scattering due to the Hamiltonian (5) is identical with that in Chew's theory, as given in Eqs. (27) and Table I. The S wave scattering to fourth order with the Hamiltonian (5) turns out to be

$$\delta_1=\delta_3=-\left(\frac{g^2}{4\pi}\right)\left(\frac{\mu}{m}\right)\left(\frac{k}{\mu}\right)\times\left[1-\frac{1}{\pi}\frac{g^2}{4\pi}\left\{2\frac{K}{m}-\frac{4}{3}\frac{1}{m^2}\int_0^K\frac{q^4dq}{\omega_q^3}\right\}\right].\tag{32}$$

The first term in the curly bracket here comes from the pair term in Eq. (5). The last term is a charge renormalization term, which must be put in if the

TABLE I. Fourth order phase shifts in Chew's theory with $K=m$. The letters in the first column refer to the diagrams in Fig. 1.

	δ_{11} / $1/\pi(g^2/4\pi)^2(\mu/m)^3(k/\mu)^3$	δ_{31} / $1/\pi(g^2/4\pi)^2(\mu/m)^3(k/\mu)^3$	δ_{13} / $1/\pi(g^2/4\pi)^2(\mu/m)^3(k/\mu)^3$	δ_{33} / $1/\pi(g^2/4\pi)^2(\mu/m)^3(k/\mu)^3$
(c)	0.58			
$(d)=(e)$	−0.064			
(f)	0.0072	0.0288	0.0288	0.115
(g)	0.034	−0.068	−0.068	0.136
$(h)=(i)$	−0.0038	0.0076	0.0076	−0.0152
(j)	0.096	0.038	0.038	0.015

coupling constant g of Eq. (32) is to be the same as the coupling constant used by Chew in Eqs. (27). If we evaluate the integral only to lowest order in μ/m, we find for $K=m$,

$$\delta_1=\delta_3=-\left(\frac{g^2}{4\pi}\right)\left(\frac{\mu}{m}\right)\left(\frac{k}{\mu}\right)\left[1-\frac{4}{3\pi}\frac{g^2}{4\pi}\right]. \quad (33)$$

We can also test the TD method for Chew's theory according to point of view that the TD method represents an expansion of the potential energy in powers of g. To do this we simply find the ratio of the sum of the contributions of the diagrams (g), (h), (i), (j) of Fig. 1 to the contribution of diagram (b) in the formulas (27). The contribution of diagram (b) to δ_{11} is $y/2$, so we find for the ratios of the matrix elements of the fourth order potentials to the second order potentials the values,

$$\left(\frac{V_4}{V_2}\right)_{11}=16\Delta_+, \quad \left(\frac{V_4}{V_2}\right)_{13}=\left(\frac{V_4}{V_2}\right)_{31}=\Delta_+,$$

$$\left(\frac{V_4}{V_2}\right)_{33}=4\Delta_+. \quad (34)$$

Recent indications are that $g^2/4\pi$ is of the order of 10. Using this value we find $\Delta_+=0.043$ for $K=m$. With this value of Δ_+, Eq. (34) tells us that the fourth order potential is small compared to the second order potential for the states (13), (31), and (33). For the (11) state the fourth order potential is not very small compared to the second order potential.[9] Note that the figures given here are for zero energy only. As the energy increases Δ_+ increases according to the formula

$$\Delta_+(k)=\frac{1}{6\pi}\left(\frac{g^2}{4\pi}\right)\left(\frac{\omega_k}{m}\right)\frac{1}{m}\int_0^K \frac{q^4dq}{\omega_q^3}\frac{1}{\omega_q+\omega_k}. \quad (28a)$$

There is one more point worth mentioning in connection with the non-relativistic Hamiltonian (5). Examination of Eqs. (27), (31), and (33) shows that for S states the ratio of the fourth order contributions to the second order contributions is of order $g^2/4\pi$, while for P states it is of order $(g^2/4\pi)(\mu/m)$. This might lead one to hope that for P-wave scattering there is an effective coupling constant, i.e., that the expansion parameter of perturbation theory is effectively $(g^2/4\pi)(\mu/m)$ rather than $g^2/4\pi$. Actually this is not the case. The factor μ/m appears only once, in going from second order to fourth order. Except for certain special cases, the ratio of a sixth order contribution to a fourth order contribution is $g^2/4\pi$ rather than $(g^2/4\pi)(\mu/m)$. The situation is best described by saying that the second order contributions to the phase shifts are anomalously large by one power of m/μ. This has the interesting consequence that for very small μ/m perturbation theory would become valid at low energies, all of the radiative corrections becoming small compared to the contributions of diagrams (a) and (b). These remarks also have some bearing on our test of the validity of the TD method according to the idea that this method represents an expansion of the potential energy as a power series in g. The anomalous factor μ/m, which appears in the ratio of the fourth order scattering to the second order scattering, also appears in Δ_+, which determines the ratio of the fourth and second order potentials according to Eq. (34). This factor will not appear, however, in the ratio of the sixth order potential to the fourth order potential. So the rate of convergence of the potential series which one would estimate from Eq. (34) is entirely false. Note also that, according to Eq. (28a), the factor μ/m in Δ_+ disappears as the energy increases.

It is not difficult to show that for low energies the radiative corrections are smaller by one power of μ/m than the contributions of the diagrams (a) and (b) of Fig. 1. Consider first the set of diagrams which we called class one diagrams in the Introduction. The contribution of these diagrams to the transition or reaction matrices is given in Chew's theory by an equation of the same form as Eq. (23). For these diagrams our theorem follows directly from the general theory of renormalization developed by Chew for his theory.[10] Chew has renormalized the nucleon propagation functions and vertex operators in such a way that for zero-energy scattering the contributions from all the radiative corrections in Eq. (23) are smaller by one power

[9] It should be noted that if we were to count the sum of the contributions of diagrams (a) and (b) as the second order potential, we would get $(V_4/V_2)_{11}=-2\Delta_+$ instead of the value given in Eq. (34).

[10] G. F. Chew, Phys. Rev. 94, 1748 (1954).

of μ/m than the contribution of the irreducible diagram (a). Note, however, that, except for certain special cases, the higher order radiative corrections are not smaller by successive powers of $(g^2/4\pi)(\mu/m)$. The factor μ/m comes in only once in going from second order to fourth order. In considering the diagrams of class two, one cannot prove anything from the renormalization procedure alone. However, the dependence on m of the integral representing an arbitrary nth order radiative correction of class two can be ascertained simply by counting the powers of the integration variables in the numerator and denominator of the integrand and using the fact that the cutoff is of order m. One concludes in this way that for zero energy scattering all of the radiative corrections of class two are smaller by one power of μ/m than the contribution of the second order diagram (b) of Fig. 1. This happens simply because for the second order diagram the energy denominator has the value μ, while for the higher order diagrams the energy denominators depend on momenta which are integrated over up to a value of the order of m for cutoff $K=m$. For the S-wave scattering this is not the case, because the energy denominator for the second order scattering is $2m$, because of the formation of the pair.

III. THE RELATIVISTIC PSEUDOSCALAR COUPLING THEORY

In an attempt to understand something about the nature of the complete relativistic pseudoscalar coupling theory and the possible validity of the Tamm-Dancoff approximation as applied to it, the low-energy S- and P-wave phase shifts have been calculated rigorously to fourth order in this theory using the Feynman Dyson techniques[11] and the renormalization theory developed by Dyson, Ward,[12] *et al.* The interaction term in this theory is given by Eq. (1).

The phase shift for the state of total angular momentum J, parity $(-1)^{J\pm\frac{1}{2}}$, and isotopic spin I at momentum k in the center-of-mass system is given by the formula

$$\frac{\exp[2i\delta_{I,J,(-1)^{J\pm\frac{1}{2}}}(k)]-1}{2i}=\frac{\pi^2kE_k}{(2\pi)^4(E_k+\omega_k)}\int d\Omega_{\mathbf{k}}\int d\Omega_{\mathbf{k}'}$$
$$\times\phi^*_{I,n}\psi^*_{J,m,(-1)^{J\pm\frac{1}{2}}}(\mathbf{k}')\beta S\psi_{J,m,(-1)^{J\pm\frac{1}{2}}}(\mathbf{k})\phi_{I,n}. \quad (35)$$

Here $\phi_{I,n}$ is the isotopic spin function for total isotopic spin I and z component n; and the $\psi_{J,m,(-1)^{J\pm\frac{1}{2}}}$ are the normalized relativistic angular momentum functions for a spin 1/2 particle:

$$\psi_{J,m,(-1)^{J-\frac{1}{2}}}(\mathbf{k})$$
$$=\frac{-\boldsymbol{\alpha}\cdot\mathbf{k}+\beta m+E_k}{[2E_k(E_k+m)]^{\frac{1}{2}}}\left\{\left(\frac{J+m}{2J}\right)^{\frac{1}{2}}Y_{J-\frac{1}{2}}{}^{m-\frac{1}{2}}(\mathbf{k})\begin{pmatrix}1\\0\\0\\0\end{pmatrix}\right.$$
$$\left.+\left(\frac{J-m}{2J}\right)^{\frac{1}{2}}Y_{J-\frac{1}{2}}{}^{m+\frac{1}{2}}(\mathbf{k})\begin{pmatrix}0\\1\\0\\0\end{pmatrix}\right\},$$

$$\psi_{J,m,(-1)^{J+\frac{1}{2}}}(\mathbf{k})$$
$$=\frac{-\boldsymbol{\alpha}\cdot\mathbf{k}+\beta m+E_k}{[2E_k(E_k+m)]^{\frac{1}{2}}}\left\{\left[\frac{J+1-m}{2(J+1)}\right]^{\frac{1}{2}}Y_{J+\frac{1}{2}}{}^{m-\frac{1}{2}}(\mathbf{k})\begin{pmatrix}1\\0\\0\\0\end{pmatrix}\right.$$
$$\left.-\left[\frac{J+1+m}{2(J+1)}\right]^{\frac{1}{2}}Y_{J+\frac{1}{2}}{}^{m+\frac{1}{2}}(\mathbf{k})\begin{pmatrix}0\\1\\0\\0\end{pmatrix}\right\}. \quad (36)$$

These are eigenfunctions of J^2 and J_z and positive-energy eigenfunctions of the Dirac Hamiltonian,

$$H=-\boldsymbol{\alpha}\cdot\mathbf{k}+\beta m. \quad (37)$$

The minus sign comes in because we have regarded $\mathbf{k}$ as the meson momentum in the center-of-mass system. After integration over the angles of $\mathbf{k}$ and $\mathbf{k}'$ in Eq. (35) we set $|\mathbf{k}|=|\mathbf{k}'|=k$. S is the S matrix calculated according to the Feynman-Dyson methods with meson propagation function,

$$D_F(k^2)=1/i(\mu^2+k^2), \quad (38)$$

nucleon propagation function

$$S_F(p)=1/(i\boldsymbol{\gamma}\cdot p+m), \quad (39)$$

and interaction operator

$$ig\gamma_5\tau_\alpha. \quad (40)$$

In order to calculate diagrams (c) and (g) of Fig. 1, one must first find the renormalized nucleon propagation function to second order. This has been done by Brueckner, Gell-Mann, and Goldberger.[13] The result of their calculation is that to second order in g the renormalized propagation function is

$$S_{F_r}'(p)=\frac{1}{i\boldsymbol{\gamma}\cdot p+m}+\frac{1}{i\boldsymbol{\gamma}\cdot p+m}\Sigma_r(p)\frac{1}{i\boldsymbol{\gamma}\cdot p+m}, \quad (41)$$

[11] R. P. Feynman, Phys. Rev. **76**, 749 (1949) and **76**, 769 (1949); F. J. Dyson, Phys. Rev. **75**, 486 (1949) and **75**, 1736 (1949).

[12] F. J. Dyson, Phys. Rev. **75**, 1736 (1949); J. C. Ward, Phys. Rev. **84**, 897 (1951).

[13] Brueckner, Gell-Mann, and Goldberger, Phys. Rev. **90**, 476 (1953).

where

$$\Sigma_r(p)=\frac{3g^2}{16\pi^2}\int_0^1 dx\Big[\{(i\gamma\cdot p+m)(1-x)+mx\}\times\log\frac{p^2x(1-x)+m^2x+\mu^2(1-x)}{m^2x^2+\mu^2(1-x)}-(i\gamma\cdot p+m)\frac{2m^2x^2(1-x)}{m^2x^2+\mu^2(1-x)}\Big]. \quad (42)$$

In order to calculate diagrams (d), (e), (h), (i), one must renormalize the vertex operator to second order in g. This has been done in the following way: If p, p' are the nucleon four-momenta to the left and right of the vertex, the vertex operator has the form

$$\Gamma_5(p,p')=\gamma_5+Y_5(p,p'). \quad (43)$$

On grounds of covariance $Y_5(p,p')$ can be written in the form[14]

$$Y_5(p,p')=F(p^2,p'^2,p\cdot p')\gamma_5+G(p^2,p'^2,p\cdot p')i\gamma\cdot p\gamma_5+H(p^2,p'^2,p\cdot p')\gamma_5 i\gamma\cdot p'+K(p^2,p'^2,p\cdot p')i\gamma\cdot p\gamma_5 i\gamma\cdot p'. \quad (44)$$

We renormalize by taking

$$\Gamma_{5r}(p,p')=\gamma_5+Y_5(p,p')-Y_5(p,p')|_{p=p',\,i\gamma\cdot p=-m,\,i\gamma\cdot p'=-m}. \quad (45)$$

The symbol $Y_5(p,p')|_{p=p',\,i\gamma\cdot p=-m,\,i\gamma\cdot p'=-m}$ means

$$Y_5(p,p')|_{p=p',\,i\gamma\cdot p=-m,\,i\gamma\cdot p'=-m}=F(-m^2,-m^2,-m^2)\gamma_5+G(-m^2,-m^2,-m^2)(-m)\gamma_5+H(-m^2,-m^2,-m^2)\times\gamma_5(-m)+K(-m^2,-m^2,-m^2)(-m)\gamma_5(-m). \quad (46)$$

Note carefully that $i\gamma\cdot p$ is commuted through to the left of γ_5 and $i\gamma\cdot p'$ to the right of γ_5 before they are evaluated at $(-m)$.[15] By using this procedure the renormalized vertex operator given below was calculated:

$$\Gamma_{5r}(p,p')=\gamma_5+\frac{g^2}{16\pi^2}\gamma_5\int_0^1 dx\int_0^1 xdy\Big[\{\mu^2(1-x)+m^2(1+x)-i\gamma\cdot pi\gamma\cdot p'(1-x)+m(-i\gamma\cdot p+i\gamma\cdot p')\}\times\frac{1}{\Lambda(x,y)}-\frac{\mu^2(1-x)}{m^2x^2+\mu^2(1-x)}-2\log\frac{\Lambda(x,y)}{m^2x^2+\mu^2(1-x)}\Big], \quad (47)$$

where

$$\Lambda(x,y)=\mu^2(1-x)+m^2x+p^2xy(1-x)+p'^2x(1-x)(1-y)+(p-p')^2x^2y(1-y).$$

The renormalization procedure given by Eqs. (45) and (46) is not the only possible one. It was chosen for a definite reason. Brueckner, Gell-Mann, and Goldberger showed in their paper[15] that at low energies for $P_{\frac{1}{2}}$ states the second order correction in Eq. (41) is of order $(g^2/4\pi)(\mu/m)$ times the unmodified nucleon propagation function for terms of the form of Eq. (23). For $S_{\frac{1}{2}}$ states, on the other hand, the second order correction in Eq. (41) is of order $g^2/4\pi$ times the unmodified nucleon propagation function. For other states the scattering due to terms of the form of Eq. (23) vanishes. These statements can be generalized. It can be shown by an argument similar to that to be given below for the vertex operator that for $P_{\frac{1}{2}}$ states all of the radiative corrections in the complete renormalized nucleon propagation function are smaller by one power of μ/m than the unmodified propagation function for terms of the form of Eq. (23). The same situation obtains for the vertex operator with the form of renormalization defined by Eqs. (45) and (46). This is not difficult to see in general. Suppose we consider the vertex operator $\Gamma_{5r}(P,P-k)$ of Eq. (23). Then $P-k$ is a free nucleon momentum, so that $i\gamma\cdot(P-k)=-m$, $(P-k)^2=-m^2$. For scattering at zero energy, $P=[0,0,0,i(m+\mu)]$ in the center-of-mass system. At low energies Eq. (36) gives for the $S_{\frac{1}{2}}$ and $P_{\frac{1}{2}}$ wave functions:

$$\psi_{S\frac{1}{2}}(\mathbf{k})=\frac{1}{(4\pi)^{\frac{1}{2}}}\begin{pmatrix}1\\0\\0\\0\end{pmatrix},$$

$$\psi_{P\frac{1}{2}}(\mathbf{k})=\left(\frac{-\boldsymbol{\alpha}\cdot\mathbf{k}}{k}+\frac{k}{2m}\right)\frac{1}{(4\pi)^{\frac{1}{2}}}\begin{pmatrix}0\\0\\1\\0\end{pmatrix}. \quad (48)$$

For the part of the S matrix in Eq. (23) the term involving $\boldsymbol{\alpha}\cdot\mathbf{k}$ drops out on integration over the angles of $\mathbf{k}$ to get a phase shift. Using these facts, we get for the $P_{\frac{1}{2}}$ state

$$\Gamma_{5r}(P,P-k)\to\gamma_5+F(-(m+\mu)^2,-m^2,-m(m+\mu))\gamma_5+G(-(m+\mu)^2,-m^2,-m(m+\mu))(-(m+\mu))\gamma_5+H(-(m+\mu)^2,-m^2,-m(m+\mu))\gamma_5(-m)+K(-(m+\mu)^2,-m^2,-m(m+\mu))(-(m+\mu))\times\gamma_5(-m)-Y_5(p,p')|_{p=p',\,i\gamma\cdot p=-m,\,i\gamma\cdot p'=-m}, \quad (49)$$

where the last term is given by Eq. (46). If we expand Eq. (49) in powers of μ/m, it becomes apparent that

[14] The invariance of the theory with respect to charge conjugation implies that $F(p^2,p'^2,p\cdot p')=F(p'^2,p^2,p\cdot p)$, $K(p^2,p'^2,p\cdot p')=K(p'^2,p^2,p'\cdot p)$, $G(p^2,p'^2,p\cdot p')=H(p'^2,p^2,p'\cdot p)$. We will not need these relations for our purposes, however.

[15] This is the same renormalization prescription as used by N. Kroll and M. Ruderman, Phys. Rev. 93, 233 (1954).

the correction term to γ_5 is of order $(\mu/m)\gamma_5$. For the $S_{\frac{1}{2}}$ state $i\gamma\cdot P\to m+\mu$, instead of $-(m+\mu)$, and the correction term to γ_5 is of order γ_5. So the renormalization procedure defined by Eqs. (45) and (46) is a good one for $P_{\frac{1}{2}}$ states in the sense that it tends to make the radiative corrections small. Note that with the form of renormalization used here the whole term Eq. (23) reduces to lowest order in μ/m to just the second order contribution represented by diagram (*a*) of Fig. 1 for *P*-state scattering. This is exactly the same situation as we encountered in Chew's theory.

The phase shift calculations have been done only for very low energies. Only the lowest order terms in an expansion in powers of k have been kept, so that the *S*-wave phase shifts vary as k and the *P*-wave phase shifts as k^3. We shall signify the contributions of various diagrams by symbols such as $\delta_{11}(a)$. Here the (*a*) refers to diagram (*a*) in Fig. 1. Also we let $\alpha=\mu/m$, the ratio of the mass of the meson to the mass of the nucleon. The second order phase shifts for diagram (*a*) are

$$\delta_1(a)=-3\frac{g^2}{4\pi}\frac{\alpha}{(1+\alpha)(2+\alpha)}\left(\frac{k}{\mu}\right),$$
$$\delta_{11}(a)=-\frac{3}{4}\frac{g^2}{4\pi}\frac{\alpha^2}{1+\alpha}\left(\frac{k}{\mu}\right)^3. \tag{50}$$

All other phase shifts vanish for diagram (*a*). For diagram (*b*) we find

$$\delta_1(b)=\frac{g^2}{4\pi}\frac{\alpha}{(1+\alpha)(2-\alpha)}\left(\frac{k}{\mu}\right),$$
$$\delta_3(b)=-2\frac{g^2}{4\pi}\frac{\alpha}{(1+\alpha)(2-\alpha)}\left(\frac{k}{\mu}\right),$$
$$\delta_{11}(b)=\frac{1}{12}\frac{g^2}{4\pi}\frac{\alpha^2(4-3\alpha^2)}{(1+\alpha)(2-\alpha)^2}\left(\frac{k}{\mu}\right)^3,$$
$$\delta_{31}(b)=-\frac{1}{6}\frac{g^2}{4\pi}\frac{\alpha^2(4-3\alpha^2)}{(1+\alpha)(2-\alpha)^2}\left(\frac{k}{\mu}\right)^3, \tag{51}$$
$$\delta_{13}(b)=-\frac{2}{3}\frac{g^2}{4\pi}\frac{\alpha^2}{(1+\alpha)(2-\alpha)^2}\left(\frac{k}{\mu}\right)^3,$$
$$\delta_{33}(b)=\frac{4}{3}\frac{g^2}{4\pi}\frac{\alpha^2}{(1+\alpha)(2-\alpha)^2}\left(\frac{k}{\mu}\right)^3.$$

The fourth order phase shifts have been calculated analytically also, but the formulas are much too long to reproduce here. In Table II are given the lowest order terms in an expansion in powers of μ/m of the analytical formulas. In Table III the formulas in Table II have been evaluated numerically for $\alpha=0.147$. In Table IV the results of evaluating the complete analytical formulas for the phase shifts for $\alpha=0.147$ are tabu-

TABLE II. Lowest order terms in expansion in powers of μ/m of the fourth order phase shifts for the pseudoscalar coupling theory.

	δ_1 $1/\pi(g^2/4\pi)^2(\mu/m)(k/\mu)$	δ_3 $1/\pi(g^2/4\pi)^2(\mu/m)(k/\mu)$	δ_{11} $1/\pi(g^2/4\pi)^2(\mu/m)^2(k/\mu)^3$	δ_{31} $1/\pi(g^2/4\pi)^2(\mu/m)^2(k/\mu)^3$	δ_{13} $1/\pi(g^2/4\pi)^2(\mu/m)^2(k/\mu)^3$	δ_{33} $1/\pi(g^2/4\pi)^2(\mu/m)^2(k/\mu)^3$
(*c*)	$\frac{9}{8}$		$\frac{9}{32}$			
(*d*)=(*e*)	$-\frac{3}{4}$		$-\frac{\alpha}{16}\left(\log\frac{1}{\alpha}-\frac{1}{6}-\frac{\pi}{2}\right)$			
(*f*)	$\frac{1}{4}$	1	$\frac{1}{36}$	$\frac{1}{9}$	$\frac{1}{36}$	$\frac{1}{9}$
(*g*)	$\frac{3}{8}$	$\frac{3}{4}$	$\frac{1}{4}\left(\log\frac{1}{\alpha}-\frac{15}{8}\right)$	$-\frac{1}{2}\left(\log\frac{1}{\alpha}-\frac{15}{8}\right)$	$\frac{1}{4}\left(\log\frac{1}{\alpha}-3\right)$	$-\frac{1}{2}\left(\log\frac{1}{\alpha}-3\right)$
(*h*)=(*i*)	$\frac{1}{4}$	$-\frac{1}{2}$	$-\frac{1}{12}\left(\log\frac{1}{\alpha}-1\right)$	$\frac{1}{6}\left(\log\frac{1}{\alpha}-1\right)$	$-\frac{1}{12}\left(\log\frac{1}{\alpha}-\frac{5}{2}\right)$	$\frac{1}{6}\left(\log\frac{1}{\alpha}-\frac{5}{2}\right)$
(*j*)	$\frac{5}{4}$	$\frac{1}{2}$	$\frac{5}{12}\left(\log\frac{1}{\alpha}-\frac{1}{3}\right)$	$-\frac{1}{6}\left(\log\frac{1}{\alpha}-\frac{1}{3}\right)$	$-\frac{5}{12}\left(\log\frac{1}{\alpha}-\frac{11}{6}\right)$	$\frac{1}{6}\left(\log\frac{1}{\alpha}-\frac{11}{6}\right)$

TABLE III. The formulas of Table II evaluated numerically with $\alpha=0.147$.

	δ_1 / $1/\pi(g^2/4\pi)^2(\mu/m)(k/\mu)$	δ_0 / $1/\pi(g^2/4\pi)^2(\mu/m)(k/\mu)$	δ_{11} / $1/\pi(g^2/4\pi)^2(\mu/m)^3(k/\mu)^3$	δ_{01} / $1/\pi(g^2/4\pi)^2(\mu/m)^3(k/\mu)^3$	δ_{10} / $1/\pi(g^2/4\pi)^2(\mu/m)^3(k/\mu)^3$	δ_{00} / $1/\pi(g^2/4\pi)^2(\mu/m)^3(k/\mu)^3$
(c)	1.13		0.281			
(d)=(e)	−0.75		−0.0017			
(f)	0.25	1.00	0.028	0.111	0.028	0.111
(g)	−0.38	0.75	0.01	−0.02	−0.27	0.54
(h)=(i)	0.25	−0.50	−0.077	0.154	0.048	−0.096
(j)	1.25	0.50	−0.663	−0.265	−0.04	−0.014

TABLE IV. The rigorous fourth order phase shifts for the pseudoscalar coupling theory.

	δ_1 / $1/\pi(g^2/4\pi)^2(\mu/m)(k/\mu)$	δ_0 / $1/\pi(g^2/4\pi)^2(\mu/m)(k/\mu)$	δ_{11} / $1/\pi(g^2/4\pi)^2(\mu/m)^3(k/\mu)^3$	δ_{01} / $1/\pi(g^2/4\pi)^2(\mu/m)^3(k/\mu)^3$	δ_{10} / $1/\pi(g^2/4\pi)^2(\mu/m)^3(k/\mu)^3$	δ_{00} / $1/\pi(g^2/4\pi)^2(\mu/m)^3(k/\mu)^3$
(c)	1.36		0.230			
(d)=(e)	−0.83		−0.0078			
(f)	0.32	1.27	0.026	0.103	0.027	0.108
(g)	−0.17	0.33	0.202	−0.404	0.057	−0.114
(h)=(i)	0.15	−0.30	−0.112	0.224	−0.035	0.070
(j)	0.64	0.26	−0.731	−0.293	−0.317	−0.127

lated. Comparison of Tables III and IV indicates that for P states the approximation of expanding in powers of μ/m and keeping only the lowest order terms is a very bad approximation. Note that the phase shifts $\delta_{13}(g)$, $\delta_{33}(g)$, $\delta_{13}(h)=\delta_{13}(i)$, and $\delta_{33}(h)=\delta_{33}(i)$ actually change sign in going from Table III to Table IV. For the S states the agreement between Tables III and IV is considerably better. Observe that the phase shift $\delta_{11}(d)=\delta_{11}(e)$ shows a somewhat anomalous behavior in Table II, being smaller by one power of α than the other phase shifts. An analysis of the differences between the results of the relativistic theory given in Tables II, III, and IV and the results of Chew's theory will be given in Sec. IV.

Examination of Tables II, III, and IV reveals a number of interesting points with respect to the possible validity of the TD approximation applied to the relativistic theory. Table II shows that for P states the diagrams with three meson in the field at a time, i.e., the diagrams which are not included in the TD approximation, all contain to lowest order in α terms varying as $\log(1/\alpha)$. On the other hand, the TD diagrams have no logarithmic terms to lowest order in α. If α were very very small, the diagrams ignored by the TD approximation would make much larger contributions to the phase shifts than the diagrams retained. Of course $\alpha=0.147$ is not very small. Consider then Table IV, which gives the rigourous results of the pseudoscalar coupling theory with $\alpha=0.147$. Except for a few cases in the S-state scattering, the terms ignored by the TD approximation are as large as or larger than the corresponding terms kept. If one adds up the figures in the columns of Table IV to get the total fourth order contributions to the phase shifts, one finds

$$\begin{aligned}
\delta_1^{(4)}&=-\frac{1}{\pi}\left(\frac{g^2}{4\pi}\right)^2\left(\frac{\mu}{m}\right)\left(\frac{k}{\mu}\right)(0.02+0.77),\\
\delta_3^{(4)}&=-\frac{1}{\pi}\left(\frac{g^2}{4\pi}\right)^2\left(\frac{\mu}{m}\right)\left(\frac{k}{\mu}\right)(1.27-0.01),\\
\delta_{11}^{(4)}&=-\frac{1}{\pi}\left(\frac{g^2}{4\pi}\right)^2\left(\frac{\mu}{m}\right)^3\left(\frac{k}{\mu}\right)^3(0.240-0.753),\\
\delta_{31}^{(4)}&=-\frac{1}{\pi}\left(\frac{g^2}{4\pi}\right)^2\left(\frac{\mu}{m}\right)^3\left(\frac{k}{\mu}\right)^3(0.103-0.249),\\
\delta_{13}^{(4)}&=-\frac{1}{\pi}\left(\frac{g^2}{4\pi}\right)^2\left(\frac{\mu}{m}\right)^3\left(\frac{k}{\mu}\right)^3(0.027-0.330),\\
\delta_{33}^{(4)}&=-\frac{1}{\pi}\left(\frac{g^2}{4\pi}\right)^2\left(\frac{\mu}{m}\right)^3\left(\frac{k}{\mu}\right)^3(0.108-0.101).
\end{aligned}\tag{52}$$

In each case here the first number in parentheses gives the sum of the contributions from the TD diagrams, and the second number gives the sum of the contribution from the three meson diagrams.

It is quite apparent from Eqs. (52) that one cannot justify the use of the TD approximation in the pseudoscalar coupling theory by the sort of argument Chew has used to justify the TD method for the static pseudovector coupling theory with a small cutoff. Comparison of Tables I and IV and Eqs. (27) and (52) indicates that the three meson diagrams make a relatively much larger contribution to the fourth order phase shifts in the pseudoscalar coupling theory than in the static pseudovector coupling theory, even when a large cutoff $K=m$ is used in the latter.

It will be recalled that in Chew's theory the TD approximation could be regarded as a large μ/m approximation, i.e., an approximation which became better and better as $\mu/m=\mu/K$ increased. In order to ascertain whether or not this was also the case for the relativistic pseudoscalar coupling theory, the fourth order phase shifts were computed for the relativistic theory in the case $\alpha=\mu/m=1$. We find

$$\begin{aligned}
\delta_1^{(4)}&=-\frac{1}{\pi}\left(\frac{g^2}{4\pi}\right)^2\left(\frac{k}{\mu}\right)(-0.14+0.04),\\
\delta_3^{(4)}&=-\frac{1}{\pi}\left(\frac{g^2}{4\pi}\right)^2\left(\frac{k}{\mu}\right)(1.72-0.20),\\
\delta_{11}^{(4)}&=-\frac{1}{\pi}\left(\frac{g^2}{4\pi}\right)^2\left(\frac{k}{\mu}\right)^3(0.052-0.247),\\
\delta_{31}^{(4)}&=-\frac{1}{\pi}\left(\frac{g^2}{4\pi}\right)^2\left(\frac{k}{\mu}\right)^3(0.060-0.044),\\
\delta_{13}^{(4)}&=-\frac{1}{\pi}\left(\frac{g^2}{4\pi}\right)^2\left(\frac{k}{\mu}\right)^3(0.022-0.087),\\
\delta_{33}^{(4)}&=-\frac{1}{\pi}\left(\frac{g^2}{4\pi}\right)^2\left(\frac{k}{\mu}\right)^3(0.088+0.020),
\end{aligned}\tag{53}$$

where the same conventions are used as in Eq. (52). Comparison of Eqs. (52) and (53) indicates that increasing the value of α tends to make the three meson terms less important, although the effect is certainly not as pronounced as in Chew's theory.

The situation with respect to the validity of the TD method looks somewhat better if we examine this approximation from the point of view that it represents an expansion of the potential energy in powers of g. The ratios of the zero-energy matrix elements of the fourth and second order potentials can be easily calculated from Eqs. (50), (51), and (52), and we obtain,

for $g^2/4\pi=10$,

$$\begin{aligned}(V_4/V_2)_1&=5.2,\\(V_4/V_2)_3&=0.034,\\(V_4/V_2)_{11}&=-4.2,^{16}\\(V_4/V_2)_{31}&=0.73,\\(V_4/V_2)_{13}&=0.91,\\(V_4/V_2)_{33}&=-0.14.\end{aligned}\tag{54}$$

Comparison of these figures with Eqs. (34) indicates that the ratios (V_4/V_2) are larger for the relativistic theory than they are for Chew's theory. Even so, the figures given in Eqs. (54), taken by themselves, are rather encouraging for the prospects of the TD method for P-wave scattering, especially for the most important state (33). However, it should be recalled that in Chew's theory the ratios (V_4/V_2) were increasing functions of the energy, and this may well be the case for the relativistic theory also. Moreover, as we shall show below, the ratios of the sixth order potentials to the fourth order potentials must be expected to be larger than the ratios V_4/V_2 by one power of m/μ.

Comparison of Eqs. (50) and (51) with Table II indicates that for P states the ratio of the fourth order phase shifts to the second order phase shifts is of order $(g^2/4\pi)(\mu/m)$ except for the $\log(1/\alpha)$ terms. For S states this ratio is of order $g^2/4\pi$. The situation here is almost identical with that in the non-relativistic approximation to the pseudoscalar coupling theory discussed in Sec. II. We have already proved quite generally—see the discussion following Eq. (47)—that for all class one diagrams, represented in Eq. (23), the radiative corrections are smaller by one power of μ/m than the irreducible diagram (a) of Fig. 1. Actually, according to Table II, the second order correction to the vertex operator of diagrams (d) and (e) is a somewhat anomalous case in that it is smaller than the primitive vertex operator γ_5 by a factor $(\mu/m)^2$. It is not easy to see how to prove generally and rigorously a corresponding theorem for the diagrams of class two, although the fourth order results of Table II indicate that among the diagrams of class two the radiative corrections are smaller except for logarithmic factors by one power of μ/m than the contribution of the second order diagram (b) of Fig. 1. Just as for Chew's theory, comparison of the second and fourth order results might lead one to hope that the expansion parameter of perturbation theory is $(g^2/4\pi)(\mu/m)$ rather $g^2/4\pi$ for P states, i.e., that there is an effective coupling constant $(g^2/4\pi)(\mu/m)$. This point was checked by calculating the sixth-order iteration of diagram (b) of Fig. 1 to lowest order in μ/m for a $P_{\frac{1}{2}}$ state. The phase shift turned out to have the form

$$\delta=N(g^2/4\pi)^6\alpha^3(k/\mu)^3,$$

where N was a nonvanishing number independent of α. Comparison with Table II indicates that there is no effective coupling constant. It would seem that, just as for the non-relativistic theory, the second order diagrams make anomalously large contributions by one power of m/μ for P-wave scattering at low energies. These remarks have the same implications for our test of the TD method according to the idea that this method is an expansion of the potential in powers of g as they did in the case of Chew's theory. The ratios in Eq. (54) must be regarded as anomalously small by one power of μ/m, since they contain the factor μ/m which appears only in going from second order to fourth order.

Gell-Mann and Goldberger[17] have proved an interesting theorem in connection with the S-state scattering. They have shown that to lowest order in expansion in powers of μ/m the low-energy S-state scattering is isotopic spin independent to all orders in the coupling constant g. That this is true to fourth order can be seen from Eqs. (50), (51), and Table II. We find, to lowest order in μ/m,

$$\delta_1=\delta_3=-\left(\frac{g^2}{4\pi}\right)\left(\frac{\mu}{m}\right)\left(\frac{k}{\mu}\right)\left[1-\frac{5}{4\pi}\frac{g^2}{4\pi}\right].\tag{55}$$

The effect on this theorem to fourth order in g of the μ/m corrections can be determined from Eqs. (50), (51), and Table IV. We find including the μ/m corrections

$$\begin{aligned}\delta_1&=-\left(\frac{g^2}{4\pi}\right)\left(\frac{\mu}{m}\right)\left(\frac{k}{\mu}\right)\left[0.75-\frac{0.79}{\pi}\frac{g^2}{4\pi}\right],\\\delta_3&=-\left(\frac{g^2}{4\pi}\right)\left(\frac{\mu}{m}\right)\left(\frac{k}{\mu}\right)\left[0.94-\frac{1.26}{\pi}\frac{g^2}{4\pi}\right].\end{aligned}\tag{56}$$

The μ/m corrections lead to a slight isotopic spin dependence. However, to fourth order at least the μ/m corrections are not anomalously large. Compare, for example, the small μ/m corrections in going from Eq. (55) to Eq. (56) with the large μ/m corrections in going from the P wave scattering in Table III to the P wave scattering in Table IV. This would seem to indicate that the theorem of Gell-Mann and Goldberger is a meaningful theorem, which must be taken seriously even though it has been proved only to lowest order in μ/m. The indications are that the low-energy S-wave scattering is approximately isotopic-spin-independent. Gell-Mann and Goldberger's theorem is proved by balancing the contribution of a given diagram in which the incoming and outgoing meson lines are not crossed against the contribution of the corresponding diagram in which the external meson lines are crossed. Referring to Table II, we see that diagrams (c) and (g) taken together give an isotopic-spin-independent contribution, and similarly for diagrams (d) and (h), etc. If the TD approximation is used, this isotopic spin inde-

[16] If the sum of the contributions of diagrams (a) and (b) is used to determine the second order potential energy instead of just the contribution of diagram (b) alone, we find $(V_4/V_2)_{11}=0.53$, instead of the value given in Eq. (54).

[17] M. Gell-Mann and M. L. Goldberger (unpublished).

pendence of the theory will be destroyed. The total contribution of all the TD diagrams in Table II, for example, is not isotopic-spin-independent. Since the indications are that the pseudoscalar coupling theory gives an S-state scattering which is approximately isotopic-spin-independent, while on the other hand the TD approximation destroys this isotopic spin independence, there would seem to be very little justification for using this approximation to discuss the S-state scattering. Equations (52) and (54) also indicate that there is little hope for the TD approximation in the case of the S-wave scattering.

IV. INTERPRETATION OF RESULTS

Since the Hamiltonian (5) was derived, using the Foldy-Wouthuysen transformation, as an approximation to the Hamiltonian of the complete relativistic pseudoscalar coupling theory, we would expect *a priori* that the results of the calculations in Sec. II based on the Hamiltonian (5) should bear a close relationship to the results of the calculations in Sec. III based on the complete relativistic theory. It will be the purpose of this section to analyze, partially at least, the similarities and differences between these two sets of calculations. Some of the differences between these two theories arise from complicated effects of one sort or another which appear as higher order μ/m corrections in the calculations based on the relativistic theory. It is to be expected that many of these effects would not appear in the calculations based on the Hamiltonian (5), because this Hamiltonian was obtained by a Foldy-Wouthuysen transformation carried out only to order $1/m$. On the other hand, some higher order μ/m corrections, e.g., the difference between Δ_+ and Δ_-, are retained in the transformed Hamiltonian (5). We shall concentrate on trying to understand the differences between these two theories to lowest order in μ/m.

Consider first the S-wave scattering. The results of the relativistic theory are given in Eq. (55). The results of the non-relativistic theory are given in Eq. (33). Comparing Eq. (55) with Eq. (33), we see that to second order in g the phase shifts are identical and that in fourth order they differ only very slightly. Since the coefficient of the fourth order correction in Eq. (33) depends on the precise value of the cutoff, this was to be expected. The simplified Hamiltonian (5) evidently gives a pretty fair approximation to the S-wave scattering to fourth order in the relativistic theory. In the relativistic theory the only isotopic spin dependence arises from μ/m corrections. In the nonrelativistic theory the isotopic spin dependence can arise only from higher order terms in the Foldy-Wouthuysen transformation than those we have kept.

The similarity between the two theories does not extend to the P-wave scattering. Indeed, to second order in g the two theories agree according to Eqs. (27), (50), and (51). However, comparison of Tables II, III, IV with Table I indicates that there are drastic differences between the predictions of the two theories with respect to the fourth order P-wave scattering. The most obvious difference is the appearance of the $\log(1/\alpha)$ terms in Table II. According to Eq. (31) there are no logarithm terms in Chew's theory to lowest order in μ/m. Also, all of the P-wave phase shifts due to diagram (j) of Fig. 1. are negative in the relativistic theory, whereas they are positive in Chew's theory. According to Table II the $\log(1/\alpha)$ terms determine the signs of these phase shifts, so that if we can find the origion of these logarithmic terms, we will presumably understand the reason for the sign change in going from Chew's theory to the relativistic theory. Note that all of the logarithmic terms in Table II are independent of whether the state involved is $P_{\frac{1}{2}}$ or $P_{\frac{3}{2}}$ as long as the isotopic spin is the same. This suggests that the logarithmic terms come from a spin independent recoil effect.

In an attempt to understand some of these effects, some calculations were made with Eqs. (11) and (18) derived in the Introduction. It will be recalled that the interaction terms of Eqs. (11) and (18) are relativistic generalizations of the interaction terms $\boldsymbol{\sigma}\cdot\nabla\tau_\alpha\phi_\alpha$ and $\phi_\alpha^2/2m$ of the Hamiltonian (5). With the non-covariant approach of Eqs. (11) and (18) it is easier to separate the calculations into terms which have a simple physical significance than with the Feynman-Dyson methods used in Sec. III. The phase shift $\delta_{L,J,I}(k)$ at momentum k for the state with orbital angular momentum L, total angular momentum J, and isotopic spin I is related to an element of the reaction matrix K calculated from Eqs. (11) or (18) by the formula

$$\tan\delta_{L,J,I}(k)=\frac{-\pi k}{(2\pi)^3}\frac{E_k\omega_k}{E_k+\omega_k}\int d\Omega_{\mathbf{k}'}\int d\Omega_{\mathbf{k}} \times\phi^*_{I,n}\psi^*_{L,J,m}(\mathbf{k}')K\psi_{L,J,m}(\mathbf{k})\phi_{I,n}, \quad (57)$$

where the $\psi_{L,J,m}$ are non-relativistic angular momentum functions.

Consider first the relativistic generalization of Chew's theory, Eq. (11). Recall that this theory was derived from the complete relativistic theory with the single approximation that all terms involving the production of pairs were dropped. The S-wave scattering vanishes in this theory in the approximation that we keep only terms proportional to k in the S-wave phase shifts. The second order P-wave phase shifts agree to lowest order in μ/m with those given by the relativistic theory in Eqs. (50) and (51). The fourth order P-wave scattering has been calculated to lowest order in μ/m and is given in Table V. For comparison purposes the results of Chew's theory to lowest order in μ/m are also given in Table V. Table V should be compared with Tables II and III, which give the results of the complete relativistic theory, which includes the effects of pair production. It will be observed that the $\log(1/\alpha)$ terms

TABLE V. The top numbers in each row give the fourth order P-wave scattering calculated to lowest order in μ/m from Eq. (11). The bottom numbers in each row are the results of Chew's theory to lowest order in μ/m for cutoff $K=m$.

	δ_{11} / $1/\pi(g^2/4\pi)^3(\mu/m)^3(k/\mu)^3$	δ_{31} / $1/\pi(g^2/4\pi)^3(\mu/m)^3(k/\mu)^3$	δ_{13} / $1/\pi(g^2/4\pi)^3(\mu/m)^3(k/\mu)^3$	δ_{33} / $1/\pi(g^2/4\pi)^3(\mu/m)^3(k/\mu)^3$
(c)	0.422 0.563			
$(d)=(e)$	−0.030 −0.063			
(f)	0.0041 0.0069	0.0164 0.028	0.012 0.028	0.048 0.111
(g)	0.047 0.063	−0.094 −0.125	−0.094 −0.125	0.188 0.250
$(h)=(l)$	−0.0033 −0.0069	0.0067 0.014	0.0067 0.014	−0.0134 −0.028
(j)	0.073 0.174	0.029 0.070	0.033 0.070	0.013 0.028

have all disappeared in Table V. These terms are associated with pair production in the relativistic theory. Examination of Table V indicates that that part of the relativistic theory left when pair production phenomena are eliminated shows much the same behavior as Chew's theory except that the results of the calculations based on Eq. (11) seem to be smaller than the results of Chew's theory by a factor of the order of 2. As explained below, this factor of 2 arises from the differences in the cutoff procedures in the two theories. There has been some speculation recently, based on the results of a calculation of the S-wave scattering in the non-relativistic theory (5) by Wentzel,[18] that the terms in the relativistic theory involving pair production may be highly damped by higher order radiative corrections. If this should turn out to be true, the results of Table V would indicate that the relativistic theory and Chew's theory should show much the same behavior for the P-wave scattering calculated so as to include the radiative corrections. It must be emphasized, however, that the proposed damping of the effects of pair production can only be speculated at present, particularly in the case of P-wave scattering.

The vertex operator $\gamma_5(\mathbf{p},\mathbf{p}')$, Eq. (12), of this theory from which the pair effects have been eliminated does not in general have quite the same form as the vertex operator of Chew's theory. However, examination of the cases which arise in calculating the low-energy P-wave scattering in fourth order shows that for these cases the vertex operator $\gamma_5(\mathbf{p},\mathbf{p}')$ reduces approximately to an operator which does have the same form as Chew's vertex operator except for the presence of momentum-dependent cutoff factors. It is the differences between the cutoff procedures in the two cases which give rise to the almost constant ratio between the results of calculations based on Eq. (11) and the results of Chew's theory as given in Table V. If a cutoff smaller than m were used in calculating with Chew's theory, the results of his theory could be brought into closer agreement with the calculations based on Eq. (11). It is perhaps significant that Chew actually uses a cutoff somewhat smaller than m in fitting his theory to the experiments.[19]

The renormalization of the vertex operator and of the nucleon propagation function which was necessary in order to carry out the calculations reported in Table V was done in almost exactly the same way as Chew did the renormalization of his theory.[10] Only one difficulty arises. On writing out Chew's renormalization scheme for Eq. (11) it appears at first sight that the self-mass and the renormalization constants Z_1 and Z_2 depend on the momenta. On closer examination it is seen that these quantities are all given by divergent integrals, the most divergent parts of which are independent of the momenta. This is perhaps not very satisfactory, but it is probably the best that can be done in the way of renormalizing Eq. (11).

We have now come to the conclusion that the very large differences between the low-energy P-wave scattering in the relativistic pseudoscalar coupling theory and in Chew's theory arise from the intrusion of effects due to the production of pairs. This situation is to be contrasted with that in the non-relativistic theory based on the Hamiltonian (5). There the pair term did not enter at all in calculating the fourth-order P-wave scattering. For illustrative purposes we shall now report the results of some calculations with Eq. (18). It will be recalled that the interaction term of Eq. (18) is a relativistic generalization of the pair term $\phi_a^2/2m$ of the non-relativistic theory. In deriving Eq. (18) only the effects due to the production of one pair at a time were kept. No attempt was made to renormalize the calculations based on Eq. (18), so only the results for the finite diagrams will be reported in fourth order.

[18] G. Wentzel, Phys. Rev. 86, 802 (1952).

[19] G. F. Chew, Phys. Rev. 95, 285 (1954).

In second order the S-wave scattering calculated from Eq. (11) agrees to lowest order in μ/m with the S-wave scattering calculated in the complete relativistic theory, as given in Eqs. (50) and (51). The second order P-wave phase shifts are smaller by one power of μ/m than those calculated from Eq. (11). In fourth order, however, the pair-forming part of the interaction contributes to the P-wave scattering to the same order in μ/m as that part of the interaction in which no pairs are formed. In Table VI will be found the results of some fourth order phase shift calculations with Eq. (18) for the finite diagrams. These calculations have been done only to lowest order in μ/m. The integrals giving the contributions of diagram (l) in Fig. 2 were very complicated, and only the coefficients of the $\log(1/\alpha)$ terms were computed. A numerical term independent of α must be added to the $\log(1/\alpha)$ terms in Table VI in order to get the whole contribution to lowest order in μ/m for diagram (l). Diagrams (m) and (n) in Fig. 2 represent a cross-product term between the interaction terms of Eqs. (11) and (18). Comparison of Tables V and VI shows that terms involving the production of pairs make large contributions to the P-wave scattering in fourth order and cannot be neglected in a perturbation-theoretic calculation. Comparison of Tables VI and II shows that the coefficients of the $\log(1/\alpha)$ terms for diagram (l) in Table VI are the same as the coefficients of the $\log(1/\alpha)$ terms for diagram (j) in Table II. For the finite diagram (j) the $\log(1/\alpha)$ terms in the relativistic theory all come from that component of the relativistic Feynman diagram (j) which is represented by diagram (l) of Fig. 2.

If one writes down according to noncovariant methods like those used in Eqs. (11) and (18) all the various components which are collected together in the one relativistic Feynman diagram (j), one can locate all of the log $(1/\alpha)$ terms simply by investigating whether or not the integrals diverge as $\alpha \to 0$. An investigation of this sort indicates that one can get a $\log(1/\alpha)$ term only from that component of diagram (j) which is represented by diagram (l) of Fig. 2. Even in this term the $\log(1/\alpha)$ comes from a recoil effect. If the initial and final mesons have momenta $\mathbf{k}$, $\mathbf{k}'$ and the virtual meson has momentum $\mathbf{q}$ in diagram (l), the energy denominator after the emission of the virtual meson is

$$\frac{1}{E-E_{\mathbf{k}+\mathbf{k}'+\mathbf{q}}-\omega_{\mathbf{k}}-\omega_{\mathbf{k}'}-\omega_{\mathbf{q}}}=\frac{1}{E-E_{\mathbf{q}}-2\mu-\omega_{\mathbf{q}}}\times\left[1+\frac{\mathbf{k}\cdot\mathbf{k}'}{E_{\mathbf{q}}(E-E_{\mathbf{q}}-2\mu-\omega_{\mathbf{q}})}+\cdots\right]. \quad (58)$$

The term involving $\mathbf{k}\cdot\mathbf{k}'$ in Eq. (58) leads to the $\log(1/\alpha)$ terms in the phase shifts. In diagram (k) of Fig. 2, where the initial and final meson lines are not crossed, the $\mathbf{k}\cdot\mathbf{k}'$ term of Eq. (58) is absent, and hence there are no $\log(1/\alpha)$ terms. Examination of the details of the calculations shows that the virtual meson is emitted and absorbed as an S-wave meson in the case of this term which leads to the $\log(1/\alpha)$ terms in the phase shifts. Presumably the $\log(1/\alpha)$ terms which appear in the contributions from the fourth order diagrams which must be renormalized arise from recoil effects similar to those which caused the appearance of the $\log(1/\alpha)$ terms in the finite diagram.

As one final point, note the excellent agreement between the S-wave scattering terms as far as they have been calculated in Table VI and the corresponding terms in Table II. Apparently the contributions to the S-wave scattering of diagrams in which a second pair is produced before the first pair is annihilated are quite small. In other words, the contributions of the term $(\phi_a^2/2m)^2$, obtained when the Foldy-Wouthuysen transformation is carried out to order $1/m^2$, are negligibly small.

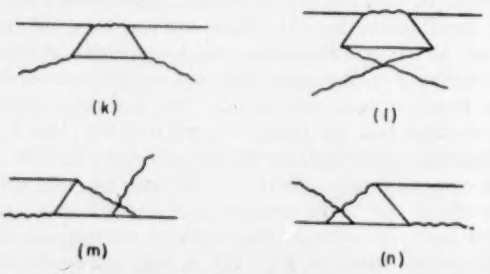

FIG. 2. Some scattering diagrams, the contributions of which are given in Table VI. In this figure a nucleon line going backward indicates the production of a pair.

V. CONCLUSIONS AND COMPARISON WITH EXPERIMENT

In this section we want to summarize our arguments and discuss the relation of our calculations to the experiments on meson-nucleon scattering. When the coupling constant $g^2/4\pi$ is as large as 10, the results of a perturbation theory calculation cannot be compared directly with experiment. However, we can speculate a little on what our fourth order results indicate about the nature of a more complete calculation and how the results of this more complete calculation might agree or disagree with the experiments.

We consider first the S-wave scattering. We have presented arguments in Sec. IV to the effect that the S-wave scattering in the complete relativistic pseudoscalar coupling theory is probably well approximated by the non-relativistic approximation to the relativistic theory obtained by performing the Foldy-Wouthuysen transformation to order $1/m$ only. In the non-relativistic theory the S-wave scattering arises from a pair term $\phi_a^2/2m$ in the Hamiltonian. A higher order term $(\phi_a^2/2m)^2$ in the Foldy-Wouthuysen transformed Hamiltonian seems to be negligible. The S-wave scattering in

the non-relativistic theory is isotopic-spin-independent. According to the arguments of Sec. III, this is probably approximately true for the relativistic theory also. Insofar as these arguments are valid, there is disagreement between the theory and the experiments for S-wave scattering. Experimentally, at low energies δ_1 is large and positive and δ_3 is very small and probably negative according to the latest analysis.[20] The phase shifts given by Wentzel's calculations[18] with the pair term including the damping have about the right magnitude, but the phase shifts are both negative and equal. Furthermore, the energy dependence predicted by Wentzel's calculations is in disagreement with the experiments. It is conceivable that some queer effect due to the μ/m corrections in higher-order processes, perhaps the meson-meson interaction, could lead to the observed isotopic spin dependence, but there is no indication of this to fourth order.

In any event the arguments given at the end of Sec. III make it appear unlikely that the TD approximation will be a useful one in discussing the S-wave scattering.

The situation for the P-wave scattering is somewhat more complicated. The calculations of Secs. II and III show that the nonrelativistic theory gives a very bad approximation to the P-wave scattering of the relativistic theory in fourth order. One might be inclined to infer from this that a rigorous calculation of the P-wave scattering in the relativistic theory to all orders in the coupling would show no relation to a corresponding calculation in Chew's theory. However, we have shown in Sec. IV that the differences between the relativistic theory and Chew's theory in fourth order arise from the pair effects which are present in the relativistic theory. With a suitably chosen cutoff, Chew's theory can be brought into quite good agreement with that part of the relativistic theory left when the production of pairs is eliminated. Now it may be, as we have mentioned before, that when the calculation is carried out to all orders in $g^2/4\pi$ the effects due to the production of pairs are highly damped. If this happens, Chew's theory may give a reasonably good description of the P-wave scattering in the relativistic theory.

As for the TD approximation, the calculations of Sec. III indicate that this method is of somewhat dubious validity as applied to the complete relativistic theory. On the other hand, if the pair effects are damped out by higher order processes, the relativistic theory is reduced essentially to Chew's theory, for which the TD method has a much greater chance of success. A TD calculation in the relativistic theory including pair effects might indeed show this damping of the pair effects if it exists.

Experimentally δ_{33} is large and positive and may go through 90° in the neighborhood of 200 Mev. The other

TABLE VI. Some phase shifts calculated according to Eqs. (11) and (18). The letters in the first column refer to the diagrams in Fig. 2.

	δ_1	δ_3	δ_{11}	δ_{31}	δ_{13}	δ_{33}
	$1/\pi(g^2/4\pi)^2(\mu/m)(k/\mu)$	$1/\pi(g^2/4\pi)^2(\mu/m)(k/\mu)$	$1/\pi(g^2/4\pi)^2(\mu/m)^4(k/m)^3$	$1/\pi(g^2/4\pi)^2(\mu/m)^4(k/\mu)^3$	$1/\pi(g^2/4\pi)^2(\mu/m)^4(k/\mu)^3$	$1/\pi(g^2/4\pi)^2(\mu/m)^4(k/\mu)^3$
(k)	0.24	0.96	0.010	0.040	0.0033	0.0132
(l)	1.20	0.48	$-\frac{5}{12}\log\frac{1}{\alpha}$	$-\frac{1}{6}\log\frac{1}{\alpha}$	$-\frac{5}{12}\log\frac{1}{\alpha}$	$-\frac{1}{6}\log\frac{1}{\alpha}$
$(m)=(n)$			0.0038	0.0142	0.0048	0.0192

[20] H. A. Bethe and F. de Hoffman, *Meson Fields* (Row, Peterson, and Company, Evanston, to be published), Vol. II.

P-wave phase shifts seem to be very small.[20] The fourth order phase shifts in Chew's theory give some indication that this sort of behavior might be predicted by a more complete calculation, the fourth order corrections reinforcing the second order phase shift for δ_{33} and detracting from it for δ_{11} and $\delta_{13}=\delta_{31}$. And, indeed, a TD calculation by Chew[19] has succeeded in reproducing the experimental phase shifts as far as they are known. The results of the calculations for the relativistic theory given in Eq. (52) are not nearly so encouraging. For the relativistic theory the fourth order correction to δ_{33} is very very small. If we invoke the damping of the pair effects again, the phase shifts in the relativistic theory will reduce essentially to those given by Chew's theory, and things will look more encouraging.

The chances both for the success of the TD method as applied to the pseudoscalar coupling theory and for the success of this theory in agreeing with experiment would be considerably improved if it could be unambiguously shown that the effects due to pair production are damped out by higher order radiative corrections. Unfortunately, this has not been done as yet.

I would like to thank Dr. M. Gell-Mann and Dr. M. L. Goldberger for suggesting to me some of the problems treated in this paper and for much help during the course of the investigation.

PHYSICAL REVIEW VOLUME 96, NUMBER 6 DECEMBER 15, 1954

Renormalization of a Neutral Vector Meson Interaction

R. J. N. PHILLIPS
Trinity College, Cambridge University, Cambridge, England
(Received September 7, 1954)

A proof is given that the vector interaction of neutral vector mesons and fermions can be renormalized, to replace a fallacious proof by Matthews. A new interaction representation, formally different from the usual one, is used. The basic idea, not a new one, is that the objectionable part of the interaction can be identified with a certain scalar meson interaction, known to be illusory.

1. INTRODUCTION

IN general, vector and pseudovector meson theories cannot be renormalized by present-day methods, because derivatives of the Δ function in the free-field commutation rules give rise to an unlimited number of primitive divergent graphs in S-matrix calculations.[1] One exception to this rule is the vector interaction of neutral vector mesons with fermions. Matthews[2] has given a fallacious proof for this, using the formulation in the interaction representation of Miyamoto[3] and Stückelberg.[4]

We prove renormalizability by transforming to a new interaction representation, formally different from the usual one. The proof is based essentially upon identifying the objectionable part of the interaction with a certain scalar meson interaction, which is known to be illusory, and to this extent our work is simply a refinement of that of Matthews.

The fallacy in Matthews' work lay in the mathematical tools he used. He had previously proposed[5] a generalization of the Tomonaga-Schwinger theory to the Schrödinger representation,

$$i\hbar\delta\Psi_\sigma[\sigma]/\delta\sigma(x)=H_\sigma(\sigma,x)\Psi_\sigma[\sigma] \tag{1.1}$$

starting from a generalized form of the Heisenberg field equations,

$$i\hbar\delta\phi(x)/\delta\sigma(x')=[\phi(x), H(x)']. \tag{1.2}$$

This generalization he assumed in his proof of renormalizability. However, it has been shown by the author (in an unpublished work) that Eq. (1.2) is not integrable in cases of physical interest, and that a direct transformation $U[\sigma]$ from the Heisenberg representation to this generalized Schrödinger representation cannot be found, since it would be defined by

$$i\hbar\delta U[\sigma]/\delta\sigma(x)=U[\sigma]H(x), \tag{1.3}$$

(in the Heisenberg representation) which is not integrable either. Nor can an analogous transformation be found from the interaction representation. Thus, even if such a generalized formulation can be made in the Schrödinger representation in a self-consistent way, it cannot be equivalent to the usual theory.

2. STUCKELBERG'S FORMULATION

Stückelberg[4] has shown how to express the Proca field $\phi_\mu(x)$, with rest mass $\hbar\kappa$, in terms of a vector field $A_\mu(x)$ and a scalar field $C(x)$, using the Lagrangian,

$$L=-\tfrac{1}{2}(A_{\mu\nu}A_{\mu\nu}+\kappa^2A_\mu A_\mu+C_\nu C_\nu+\kappa^2C^2)+L', \tag{2.1}$$

where L' describes any other fields, and their interactions with the A_μ and C fields. C and the four components A_μ are quantized in the usual way as inde-

[1] F. J. Dyson, Phys. Rev. **75**, 1736 (1949).
[2] P. T. Matthews, Phys. Rev. **76**, 1254 (1949).
[3] Y. Miyamoto, Progr. Theoret. Phys. **3**, 124 (1948).
[4] E. C. G. Stückelberg, Helv. Phys. Acta **11**, 299 (1938).
[5] P. T. Matthews, Phys. Rev. **75**, 1270 (1949).

pendent operators. ϕ_μ can now be expressed, in the Heisenberg representation, by

$$\phi_\mu(x)=A_\mu(x)+(1/\kappa)C_\mu(x), \tag{2.2}$$

if we also postulate two auxiliary conditions,

$$A_{\mu\mu}(x)+\kappa C(x)=0, \tag{2.3}$$

and its time-derivative,

$$[\int H(x')d^3x',\ A_{\mu\mu}(x)+\kappa C(x)]=0, \tag{2.4}$$

which are self-consistent. Of course, if the required Proca field interaction is such that $\phi_{\mu\mu}\neq 0$, Eqs. (2.3) and (2.4) are modified.

For vector interaction with fermions, the interaction Hamiltonian in a single-time interaction representation proves to be

$$H_1(x)=j_\mu(x)[A_\mu(x)+1/\kappa C_\mu(x)]+1/2\kappa^2[j_0(x)]^2, \tag{2.5}$$

where $j_\mu(x)=\frac{1}{2}ig[\bar{\psi}(x)\gamma_\mu\psi(x)-\bar{\psi}'(x)\gamma_\mu\psi'(x)]$ in the usual notation, g being a coupling constant. Miyamoto[3] considered a modification of the Stückelberg formalism, taking the auxiliary conditions (2.3) and (2.4) to be conditions on the Heisenberg state-vector Φ, and leaving C and the four components A_μ independent. He observed that if $j_0(x)$ in Eq. (2.5) is replaced by $j_\mu(x)n_\mu(x)$, where n_μ is the normal at x to a space-like surface σ, pointing to the future, the equation,

$$i\hbar\delta\Psi[\sigma]/\delta\sigma(x)=H_1(\sigma,x)\Psi[\sigma], \tag{2.6}$$

is integrable. Hence the theory can be stated in the Tomonaga-Schwinger formalism in the interaction representation.

It is not immediately obvious that the latter formulation is wholly equivalent to the canonical formulation in this case. For, when a transformation is made from the Heisenberg representation,

$$\Psi[\sigma]=V[\sigma]\Phi, \tag{2.7}$$

$$i\hbar\delta V[\sigma]/\delta\sigma(x)=V[\sigma]\mathfrak{H}(x), \tag{2.8}$$

where $\mathfrak{H}(x)$ contains field momenta, the transformed field variables are not simple point-functions in general, but depend on the orientation of the surface.[6] Miyamoto assumes no such surface-dependence in his interaction representation. However, since $A_\mu(x)$ and $C(x)$ prove to be surface-independent in this sense, and no use is made of the momentum conjugate to $C(x)$ or any other surface-dependent variables, the two formulations are in effect equivalent.

[6] F. J. Belinfante, Phys. Rev. **76**, 66 (1949).

3. QUASI-INTERACTION REPRESENTATION

We consider the transformation $W[\sigma]$ defined by the integrable equation,

$$i\hbar\delta W[\sigma]/\delta\sigma(x)=W[\sigma]A_\mu(x)j_\mu(x), \tag{3.1}$$

in the Heisenberg representation, and transform to a quasi-interaction representation (denoted by an asterisk),

$$\Psi^*[\sigma]=W[\sigma]\Phi, \tag{3.2}$$

$$i\hbar\delta\Psi^*[\sigma]/\delta\sigma(x)=A_\mu^*(x)j_\mu^*(x)\Psi^*[\sigma]. \tag{3.3}$$

It can easily be shown, by the methods of Schwinger[6,7] that this is effectively an interaction representation, for $A_\mu^*(x)$ obeys its free-field equations, and $\bar{\psi}^*(x)$, $\psi^*(x)$, $C^*(x)$ behave as if their free fields are coupled by a term $-(1/\kappa)j_\mu(x)C_\mu(x)$ in the Lagrangian. It is well known that the latter coupling is quite illusory,[8] and that a transformation $\Psi'=e^{iS}\Psi$ [where $S=(\hbar\kappa)^{-1}\int j_0(x)C(x)d^3x$], in the Schrödinger representation, removes the interaction altogether. Carrying out the corresponding transformation in the Heisenberg representation, we see that $\bar{\psi}^*(x)$, $\psi^*(x)$, $C^*(x)$ have free-field (anti-) commutation rules.

The S-matrix in this quasi-interaction representation closely resembles that for electrodynamics,[1] and can clearly be renormalized by the same methods. The primitive divergent graphs are the same in both cases, but the graphs corresponding to photon self-energy parts here lead to genuine divergences. Ward's[9] formal proof that photon-photon scattering graphs lead to no divergences can be applied to the corresponding graphs in this theory too. It is possible consistently to account for all divergences in terms of renormalization of the meson and fermion masses, and of the coupling constant, by means of Dyson's technique.[1] κ-renormalization must of course affect the C-field too, for consistency.

The auxiliary conditions on the state vector can be transformed to this new representation without causing further difficulties.

The methods of this section fail for charged mesons, and pseudovector mesons,[8] since the coupling terms which correspond to $-(1/\kappa)j_\mu(x)C_\mu(x)$ represent genuine interactions.

In conclusion, my thanks are due to Professor P. A. M. Dirac for stimulating discussions.

[7] J. Schwinger, Phys. Rev. **74**, 1439 (1948).

[8] F. J. Dyson, Phys. Rev. **73**, 929 (1948). Matthews has pointed out an error in this paper: there should be no residual $[j_0(x)]^2$ term after the transformation.

[9] J. C. Ward, Phys. Rev. **77**, 293 (1950).

Many-Parameter Wave Functions in the Independent-Particle Model

ERWIN H. KRONHEIMER
Department of Mathematics, Birkbeck College, London, England

(Received August 19, 1954)

It is shown that it is possible to introduce additional parameters into the single-particle wave functions used in estimating, by the Slater method, the lowest eigenvalue of a given Hamiltonian for an N-nucleon system, without altering the structure of the matrix elements. This is done by associating a different radial parameter with each shell of each N-particle wave function, subject to certain restrictions. The modification of the matrix elements is given.

1. INTRODUCTION

THERE are two well-known methods available of finding upper bounds, E_0, for the lowest eigenvalue, E, of the Hamiltonian, H, of an N-particle nucleus, when a particular two-body interaction is assumed.

In the variational method, we choose a plausible wave function, Ψ_V (antisymmetric[1] and normalized), containing a number of variable parameters, with respect to which we minimize the integral

$$\langle \Psi_V^* H \Psi_V \rangle, \tag{1}$$

the minimum value itself being taken as E_0. The introduction of further parameters into Ψ_V will generally yield a further decrease of E_0.

In the method due to Slater in atomic spectroscopy,[2] we begin by choosing an auxilliary Hamiltonian, H_A, representing the N nucleons moving independently in an "average" central field, $V_C = a^{-2}F(r/a)$ (where a is a constant length).[3] We classify the antisymmetric eigenfunctions, ψ, of H_A, by configurations and those "good" quantum numbers which will still be good for H, as well as by any further quantum numbers which we have reason to believe will be approximately good. We then set up the matrix of H with respect to k functions of this set, and find its lowest latent root, E_0. Adding further functions to the k already chosen can only cause E_0 to decrease.

How good an approximation E_0 is to E for a given value of k (which must usually be small), depends on the choice both of H_A and of the k functions, $\psi^{(1)}, \psi^{(2)}, \cdots, \psi^{(k)}$, used. The quantum numbers for these can largely be obtained from the transformation properties of H (and of Hamiltonians differing only slightly from H), as also (for good quantum numbers) from experimental data. The choice of configurations will be dictated by the ordering of the eigenvalues of H_A; i.e., $\langle \psi^* H_A \psi \rangle$. Here the assumption is that this order will be roughly maintained among the corresponding diagonal matrix elements of H, $\langle \psi^* H \psi \rangle$.

[1] In all N particles: the use of the isobaric-spin formalism is implied.

[2] J. C. Slater, Phys. Rev. **34**, 1293 (1929).

[3] This functional form of V_C is chosen in order that the eigenfunctions should (apart from a normalizing factor proportional to $a^{-\frac{1}{2}}$) depend on r and on a only through their ratio. The corresponding eigenvalues vary as a^{-2}.

The Slater technique can formally be regarded as a special type of variational method: Ψ_V is taken to be an arbitrary linear combination of the functions $\psi^{(h)}$ ($h=1, 2, \cdots, k$), and the k coefficients (related by a single normalizing condition, but otherwise independent) serve as variational parameters. If we introduce p arbitrary parameters into the ψ's themselves, the process of finding the minimum latent root of the H matrix remains equivalent to minimizing the expression (1)—but with respect, now, to all $\{(k-1)+p\}$ independent parameters—provided only that the orthogonality of the ψ's is unaffected by the additional parameters. This last requirement can be satisfied by introducing the parameters into the expression for H_A, without impairing the status of the ψ's as eigenfunctions of a single Hamiltonian; and the one constant a already included in the definition of H_A is generally treated as a variation-parameter in this way. But to complicate H_A beyond this makes it difficult to find its eigenfunctions; and we instead consider a method of introducing additional parameters *directly* into the ψ's.

2. MODIFIED WAVE FUNCTIONS

We have already seen how to introduce a common parameter, a, into all the functions: one possible modification would be to allot a different parameter, $a^{(1)}, a^{(2)}, \cdots, a^{(k)}$, to each of them. But we can go further.

Let us write the spatial eigenfunction with quantum numbers n, l, m of a single particle in the central field V_C as

$$R(nl; a)\Theta(lm)\Phi(m),$$

where R, Θ, Φ, depend respectively on the polar coordinates r, θ, φ, and are separately normalized to unity; R and Θ being real. Then the constant a will enter only into the radial wave function R, which alone depends on the form of V_C. The antisymmetric eigenfunction, ψ, of H_A, belonging to a configuration $\mathfrak{C}$, where

$$\mathfrak{C} \equiv (n_\alpha l_\alpha)^A (n_\beta l_\beta)^B \cdots (n_\gamma l_\gamma)^C, \quad (A+B+\cdots+C=N), \tag{2}$$

can then always be split into a finite sum of terms, each involving the coordinates r_1 to r_N, as well as the constant a, only in the factor

$$R_1(n_\lambda l_\lambda; a) R_2(n_\mu l_\mu; a) \cdots R_N(n_\xi l_\xi; a), \tag{3a}$$

where $\lambda, \mu, \cdots, \xi$ is some permutation of A α's, B β's, $\cdots$, and C γ's.

It is therefore possible to modify the radial wave functions, R, in each factor of the type (3a), without destroying any of the existing symmetry properties of ψ with respect to permutations and rotations, provided the same modification is made to all radial wave functions belonging to the same shell (i.e., having the same quantum numbers n and l); for those belonging to different shells are not significantly related. The modification which suggests itself is to associate with each shell in $\mathfrak{C}$ a different a: which we can label $a_\alpha, a_\beta, \cdots, a_\gamma$. Then (3a) is replaced by

$$R_1(n_\lambda l_\lambda; a_\lambda)R_2(n_\mu l_\mu; a_\mu)\cdots R_N(n_\xi l_\xi; a_\xi), \qquad (3b)$$

which is a product of A functions of the type $R(n_\alpha l_\alpha; a_\alpha)$ B of the type $R(n_\beta l_\beta; a_\beta)$, $\cdots$, and C of the type $R(n_\gamma l_\gamma; a_\gamma)$. We have now succeeded in introducing additional parameters into ψ without affecting its previous status as an eigenfunction (belonging to a given eigenvalue) of any operator independent of r—in particular, it is still antisymmetric; but it has ceased to be an eigenfunction of H_A.

If we apply the process to each of the k functions $\psi^{(k)}$, we can evidently associate a different set of parameters, $a_\alpha^{(k)}, a_\beta^{(k)}, \cdots, a_\gamma^{(k)}$, with each wave function. The different $\psi^{(k)}$ may belong to different configurations $\mathfrak{C}^{(k)}$ [characterized by a particular set of exponents—some of which may vanish[4]—$A^{(k)}$, $B^{(k)}$, $\cdots$, $C^{(k)}$, in (2)]; but this fact will no longer by itself suffice to ensure the orthogonality which we require of the modified $\psi^{(k)}$. The wave functions which cease to be orthogonal are those whose orthogonality as eigenfunctions of H_A depended exclusively on their configurations differing in a principal quantum number; i.e., on the vanishing of the integral

$$\langle R(nl; a)R(n'l'; a')\rangle, \qquad (4)$$

when $n' \neq n$, $l' = l$, and $a' = a$; for this fails to vanish when $a' \neq a$.

We now reduce the generality with which we can associate different parameters with different shells in each wave function by the following *stipulation:* If any two among all the shells, $n_\alpha l_\alpha, n_\beta l_\beta, \cdots, n_\gamma l_\gamma$, represented in the various configurations $\mathfrak{C}^{(k)}$, differ only in their principal quantum number, then the identical parameter shall be associated with both those shells wherever they occur, whether in the same or in different wave functions.

Therefore the integral (4), howsoever it arises, will vanish whenever it would originally have done so, i.e., when $n' \neq n$, $l' = l$. (5)

Hence, certainly, all previously orthogonal wave functions remain so; for either it is the coefficients of (3) which independently determine orthogonality—and these have not been altered—or the original orthogonality arose from the vanishing of integrals of the type (4), and (5) applies.

[4] If one of the shells, say $n_\gamma l_\gamma$, is not represented in the configuration of a particular function, say $\psi^{(k)}$, we need not, of course, define the corresponding parameter $a_\gamma^{(k)}$.

3. EFFECT ON CALCULATIONS

To show how the use of the modified wave functions affects the results in what we shall always call the "original" case of only the single constant a, we will assume that the reduction of the matrix elements to sums of radial integrals has, in this case, already been carried out. Methods of doing so—with a general two-body interaction—are well developed.[5]

We consider first a matrix element

$$\langle \psi^* F \psi' \rangle = N \langle \psi^* F_1 \psi' \rangle, \qquad (6)$$

where

$$F = \sum_{i=1}^{N} F_i, \quad F_i = f_i \Lambda_i,$$

f_i being an operator on the coordinate r_i, and Λ_i an operator on the other coordinates of the ith particle. ψ and ψ' are any members of the modified set $\psi^{(1)}, \psi^{(2)}, \cdots, \psi^{(k)}$; possibly both the same.

Expression (6) can be expanded as a finite sum of terms depending on the radial wave functions through a factor of the form

$$\langle R_1(n_\lambda l_\lambda; a_\lambda) f_1 R_1(n_\lambda' l_\lambda'; a_\lambda')\rangle \langle R_2(n_\mu l_\mu; a_\mu) R_2(n_\mu' l_\mu'; a_\mu')\rangle \times \cdots \langle R_N(n_\xi l_\xi; a_\xi) R_N(n_\xi' l_\xi'; a_\xi')\rangle. \qquad (7)$$

Here $n_\lambda l_\lambda, n_\mu l_\mu, \cdots, n_\xi l_\xi$ is some permutation of the elements of the configuration, $\mathfrak{C}$, of ψ (and similarly $n_\lambda' l_\lambda'$, etc., of $\mathfrak{C}'$); a_χ is the parameter associated in ψ with the shell determined by $n_\chi l_\chi$, and a_χ' the parameter in ψ' for the $n_\chi' l_\chi'$ shell. Note that (unless $\psi' \equiv \psi$) $n_\chi' l_\chi' \equiv n_\chi l_\chi$ does not necessarily imply $a_\chi' = a_\chi$.

The coefficient of (7) [in the expansion of (6)], which has its original value, must itself be a sum of terms, each containing a factor of the type

$$\langle \Theta_2(l_\mu m_\mu)\Phi_2^*(m_\mu)\Theta_2(l_\mu' m_\mu')\Phi_2(m_\mu')\rangle \times \cdots \langle \Theta_N(l_\xi m_\xi)\Phi_N^*(m_\xi)\Theta_N(l_\xi' m_\xi')\Phi_N(m_\xi')\rangle = \delta(l_\mu, l_\mu')\delta(m_\mu, m_\mu')\cdots\delta(l_\xi, l_\xi')\delta(m_\xi, m_\xi'),$$

so that the whole coefficient contains the factor $\delta(l_\mu, l_\mu')\cdots\delta(l_\xi, l_\xi')$. [$\delta(p,q) \equiv$ Kronecker δ_{pq}.] We may therefore, in (7), replace l_μ' by $l_\mu, \cdots, l_\xi'$ by l_ξ; from which it follows by (5), that we can multiply (7) by $\delta(n_\mu, n_\mu')\cdots\delta(n_\xi, n_\xi')$ and replace n_μ' by $n_\mu, \cdots, n_\xi'$ by n_ξ elsewhere in the expression.

Thus (7) can be written

$$\delta(n_\mu, n_\mu')\cdots\delta(n_\xi, n_\xi') \times \rho \cdot \langle R_1(n_\lambda l_\lambda; a_\lambda) f_1 R_1(n_\lambda' l_\lambda'; a_\lambda')\rangle, \qquad (7a)$$

where

$$\rho = \langle R_2(n_\mu l_\mu; a_\mu) R_2(n_\mu l_\mu; a_\mu')\rangle \cdots \times \langle R_N(n_\xi l_\xi; a_\xi) R_N(n_\xi l_\xi; a_\xi')\rangle;$$

[5] See, for instance, J. P. Elliott, Proc. Roy. Soc. (London) **A218**, 345 (1953).

and, for the original case, (7a) reduces to

$$\delta(n_\mu,n_\mu')\cdots\delta(n_\xi,n_\xi')\langle R_1(n_\lambda l_\lambda;a)f_1R_1(n_\lambda'l_\lambda';a)\rangle. \quad (7b)$$

Since (7b) vanishes identically only when (7a) does, the modified calculation can be deduced from the original one by replacing (7b) by (7a), without introducing any additional terms. (We are assuming that the original coefficient of every integral of the type $\langle R_1f_1R_1'\rangle$ in (7b) has been calculated, even though a particular integral might happen to be zero.) Dropping the unnecessary particle-suffices, we can formalize this into the following rule for the modified calculation:

In the original case, expand (6) as a sum of terms

$$\mathrm{A}\cdot\langle R(n_\lambda l_\lambda;a)fR(n_\lambda'l_\lambda';a)\rangle,$$

and replace each such term by

$$\mathrm{A}\cdot\rho\cdot\langle R(n_\lambda l_\lambda;a_\lambda)fR(n_\lambda'l_\lambda';a_\lambda')\rangle,$$

where

$$\rho=\langle R(n_\mu l_\mu;a_\mu)R(n_\mu l_\mu;a_\mu')\rangle\cdots\langle R(n_\xi l_\xi;a_\xi)R(n_\xi l_\xi;a_\xi')\rangle;$$

the values of $n_\mu l_\mu$, $\cdots$, $n_\xi l_\xi$ being determined by the requirement that $n_\lambda l_\lambda$, $n_\mu l_\mu$, $\cdots$, $n_\xi l_\xi$ should constitute a re-arrangement of $\mathfrak{C}$, and $n_\lambda'l_\lambda'$, $n_\mu l_\mu$, $\cdots$, $n_\xi l_\xi$ a re-arrangement of $\mathfrak{C}'$.[6]

By a precisely similar argument, we see that we can perform the modified calculation of a matrix element

$$\langle\psi^*G\psi'\rangle=\tfrac{1}{2}N(N-1)\langle\psi^*G_{12}\psi'\rangle, \quad (8)$$

where

$$G=\sum_{j>i=1}^{N}G_{ij}, \quad G_{ij}=g_{ij}\Gamma_{ij},$$

(g_{ij} being an operator on $\mathbf{r}_i$ and $\mathbf{r}_j$, and Γ_{ij} an operator on the other coordinates of the ith and jth particles) by the following rule:

In the original case, expand (8) as a sum of terms

$$\mathrm{B}\cdot\langle R_1(n_\lambda l_\lambda;a)R_2(n_\mu l_\mu;a)g_{12}R_1(n_\lambda'l_\lambda';a)R_2(n_\mu'l_\mu';a)\rangle,$$

and replace each such term by

$$\mathrm{B}\cdot\sigma\cdot\langle R_1(n_\lambda l_\lambda;a_\lambda)R_2(n_\mu l_\mu;a_\mu)g_{12}R_1(n_\lambda'l_\lambda';a_\lambda')R_2(n_\mu'l_\mu';a_\mu')\rangle, \quad (9)$$

where

$$\sigma=\langle R(n_\nu l_\nu;a_\nu)R(n_\nu l_\nu;a_\nu')\rangle\cdots\langle R(n_\xi l_\xi;a_\xi)R(n_\xi l_\xi;a_\xi')\rangle;$$

the values of $n_\nu l_\nu$, $\cdots$, $n_\xi l_\xi$ being determined by the requirement that, together with $n_\lambda l_\lambda$ and $n_\mu l_\mu$, they should form a re-arrangement of $\mathfrak{C}$, while, together with $n_\lambda'l_\lambda'$ and $n_\mu'l_\mu'$, they must form a re-arrangement of $\mathfrak{C}'$.[7]

Since H can always be expanded as a sum of operators of the type F and G, our two rules determine the calculation of its matrix with respect to the k modified wave functions.

[6] This double condition restricts the functions ψ', for which the matrix element (6) does not vanish, to those whose configurations differ in at most one state from ψ.

[7] This double condition restricts the functions ψ', for which the matrix element (8) does not vanish, to those whose configurations differ in at most two states from ψ.

4. SPHERICAL OSCILLATOR WAVE FUNCTIONS

As an illustration, we give the very simple form which the constituents of ρ and σ take when the auxilliary potential is that of a three-dimensional harmonic oscillator; i.e., $V_C=(\hbar^2/2Ma^2)(r/a)^2=\frac{1}{2}M\omega^2r^2$, where M denotes the nucleon-mass and $2\pi/\omega$ the period of the corresponding classical oscillator.

The energy of the single-particle eigenstate with quantum numbers n and l is[8] $(2n-l-\frac{1}{2})\hbar\omega$. The radial wave function of the *lowest* eigenstate with a given l, i.e., of the state (with energy $(l+\frac{3}{2})\hbar\omega$) for which $n=l+1$, is $K_l\cdot a^{-\frac{1}{2}}(r/a)^l\cdot\exp[-\frac{1}{2}(r/a)^2]$, where K_l, determined by the normalizing condition, depends only on l. In this case (with $n=l+1$), $\langle R(nl;a)R(nl;a')\rangle=\{2aa'/(a^2+a'^2)\}^{l+\frac{1}{2}}$, or $|\sin^{l+\frac{1}{2}}\kappa|$, where $a'/a=\tan\frac{1}{2}\kappa$.

Corresponding expressions for $n>l+1$ will not be required in practice, since the configurations of the k functions used will always include one in which any given value of l that is represented at all among them occurs in association with the lowest possible value of n, *viz.*, $l+1$; and if any other shell associates that l with some higher n, the identical-parameter stipulation comes into play.

A formula by which the rather complex integrals of the type occurring in (9) can be calculated in the present case is given elsewhere.[9]

5. CONCLUDING REMARKS

The effect of the modification is to add a "synthetic" mixture of states to the k originally chosen.

We can expand a radial wave function of given parameter in terms of all those, associated with the same orbital angular momentum, of any other parameter; i.e.,

$$R(n'l;a')=\sum_{n=l+1}^{\infty}c_nR(nl;a),$$

where the c_n do not depend on r.[10] It follows that the variation of the parameter of a particular shell $(n_\chi l_\chi)$, within a particular eigenstate of H_A, is important just in so far as—in building up the correct wave function—those eigenstates are important whose configurations associate l_χ with other principal quantum numbers than n_χ. The identical-parameter stipulation allows the parameter to vary just when such configurations as these are not represented among the eigenstates originally considered.

The author wishes to acknowledge gratefully the advice of Professor H. A. Jahn, and to thank the University of Southampton for a research award.

[8] We define n to be $(\bar{n}+l+1)$, as in atomic spectroscopy [rather than $(\bar{n}+1)$]; where $\bar{n}$ is the number of finite nodes of the function R for $r>0$.

[9] E. H. Kronheimer, Phys. Rev. **90**, 1003 (1953); Phys. Rev. **91**, 1580 (1953).

[10] They are, of course, the integrals (4) with $l'=l$.

Gravitation and Electromagnetism

SURAJ N. GUPTA
Department of Physics, Purdue University, Lafayette, Indiana
(Received May 10, 1954; revised manuscript received September 10, 1954)

Einstein's theory of gravitation is compared with Maxwell's theory of the electromagnetic field, and some common features of the two theories are pointed out. It is also shown that the well-known peculiarities of Einstein's theory are a necessary consequence of the fact that Einstein's field corresponds to particles of spin 2.

1. INTRODUCTION

ALTHOUGH Einstein's theory of the gravitational field is the most widely accepted theory of gravitation, it is rather disconcerting to note that Einstein's theory appears to be strikingly different from the present theories of the electromagnetic field and the meson fields. In fact, in the formulation of fundamental physical laws we always seek for harmony in nature, and we intuitively expect that there should be some uniformity in the description of various fields in nature. Therefore, Einstein himself and others[1] have tried to construct a unified theory of the gravitational and the electromagnetic fields, while some other authors[2] have tried to find a linear theory of the gravitational field in flat (Minkowskian) space analogous to other existing field theories. All such attempts, however, are still in a speculative stage.

The aim of the present paper is to compare Einstein's theory of the gravitational field with Maxwell's theory of the electromagnetic field, and to show that the two theories have many features in common. We shall also see that the main differences between the two theories can be attributed to the fact that while the Maxwell field corresponds to particles of spin 1, the Einstein field corresponds to particles of spin 2. This shows that Maxwell's theory of electromagnetism and Einstein's theory of gravitation provide us with a fairly uniform description of nature, and therefore there is no *philosophic* necessity for trying to alter any of these theories.

2. REMARKS ON EINSTEIN'S THEORY OF GRAVITATION

Einstein's gravitational field is described by the field equation

$$R^{\mu\nu}-\tfrac{1}{2}Rg^{\mu\nu}=-\tfrac{1}{2}\kappa^2T^{\mu\nu}, \tag{1}$$

where the symbols $g^{\mu\nu}$, $R^{\mu\nu}$ and R have the usual meaning, κ is a constant, and $T^{\mu\nu}$ is the energy-momentum tensor of the "matter" field, which includes everything except the gravitational field. We shall, however, express the gravitational field equation in a different form, which will be more suitable for the present purpose.

As is well known, the Lagrangian density for Einstein's gravitational field may be taken as

$$\mathfrak{L}=-\kappa^{-2}\mathfrak{g}^{\mu\nu}\left(\begin{Bmatrix}\alpha\\ \mu\beta\end{Bmatrix}\begin{Bmatrix}\beta\\ \nu\alpha\end{Bmatrix}-\begin{Bmatrix}\alpha\\ \mu\nu\end{Bmatrix}\begin{Bmatrix}\beta\\ \alpha\beta\end{Bmatrix}\right), \tag{2}$$

which gives for the canonical energy-momentum pseudotensor density of the gravitational field

$$\mathfrak{t}_\nu{}^\mu=\frac{\partial\mathfrak{L}}{\partial(\partial\mathfrak{g}^{\alpha\beta}/\partial x^\mu)}\frac{\partial\mathfrak{g}^{\alpha\beta}}{\partial x^\nu}-\delta_\nu{}^\mu\mathfrak{L}. \tag{3}$$

We can further obtain the symmetrical energy-momentum pseudotensor density of the gravitational field by Belinfante's method.[3] For this, we consider an infinitesimal linear transformation

$$\delta x^\mu=-\epsilon^{\mu\lambda}\delta\omega_{\lambda\nu}x^\nu \quad\text{with}\quad \delta\omega_{\lambda\nu}=-\delta\omega_{\nu\lambda}, \tag{4}$$

where $\epsilon^{\mu\nu}$ is a set of quantities given by

$$\epsilon^{\mu\nu}=\begin{bmatrix}-1&0&0&0\\0&-1&0&0\\0&0&-1&0\\0&0&0&+1\end{bmatrix}. \tag{5}$$

Then, the symmetrical energy-momentum pseudotensor density of the gravitational field will be

$$\theta^{\mu\nu}=\epsilon^{\mu\lambda}\mathfrak{t}_\lambda{}^\nu-\frac{1}{2}\frac{\partial}{\partial x^\rho}(\mathfrak{f}^{\mu\nu,\rho}+\mathfrak{f}^{\rho\mu,\nu}+\mathfrak{f}^{\rho\nu,\mu}), \tag{6}$$

where

$$\mathfrak{f}^{\mu\nu,\rho}\equiv-\frac{\delta\mathfrak{g}^{\alpha\beta}}{\delta\omega_{\mu\nu}}\frac{\partial\mathfrak{L}}{\partial(\partial\mathfrak{g}^{\alpha\beta}/\partial x^\rho)}=2\frac{\partial\mathfrak{L}}{\partial(\partial\mathfrak{g}^{\alpha\beta}/\partial x^\rho)}(\epsilon^{\alpha\mu}\mathfrak{g}^{\beta\nu}-\epsilon^{\alpha\nu}\mathfrak{g}^{\beta\mu}). \tag{7}$$

Adding the symmetrical energy-momentum tensor density of the matter field $\epsilon^{\mu\lambda}\mathfrak{T}_\lambda{}^\nu$ to (6), we obtain for the total energy-momentum pseudotensor density $\Theta^{\mu\nu}$ of the system

$$\Theta^{\mu\nu}=\epsilon^{\mu\lambda}(\mathfrak{T}_\lambda{}^\nu+\mathfrak{t}_\lambda{}^\nu)-\frac{1}{2}\frac{\partial}{\partial x^\rho}(\mathfrak{f}^{\mu\nu,\rho}+\mathfrak{f}^{\rho\mu,\nu}+\mathfrak{f}^{\rho\nu,\mu}). \tag{8}$$

[1] For an account of the unified field theories, see P. G. Bergmann, *Introduction to the Theory of Relativity* (Prentice-Hall, Inc., New York, 1942), and A. Einstein, *The Meaning of Relativity* (Princeton University Press, Princeton, 1950).

[2] F. J. Belinfante and J. C. Swihart, Phys. Rev. **90**, 357 (1953) and **91**, 500 (1953); G. D. Birkhoff, Proc. Natl. Acad. Sci. **29**, 231 (1943).

[3] F. J. Belinfante, Physica **6**, 887 (1939).

Substituting (7) in (8), we get after some simplification[4]

$$\frac{\partial^2}{\partial x^\alpha \partial x^\beta}(\mathfrak{g}^{\mu\nu}\epsilon^{\alpha\beta}-\mathfrak{g}^{\mu\alpha}\epsilon^{\nu\beta}+\mathfrak{g}^{\alpha\beta}\epsilon^{\mu\nu}-\mathfrak{g}^{\alpha\nu}\epsilon^{\mu\beta})=\kappa^2\Theta^{\mu\nu}, \quad (9)$$

which is an alternative form of Einstein's gravitational field equation. It is interesting to note that the left-hand side of (9) is linear in $\mathfrak{g}^{\mu\nu}$, which is due to the fact that all the nonlinear terms of the field equation are contained within the quantity $\Theta^{\mu\nu}$ on the right-hand side of (9).

Since neither $\epsilon^{\alpha\beta}$ nor $\Theta^{\mu\nu}$ transforms as a tensor under arbitrary coordinate transformations, the field Eq. (9) is not manifestly covariant. Nevertheless, Einstein's field equation can be expressed in the form (9) in any arbitrary frame of reference. Moreover, if we confine ourselves only to those frames of reference in which the coordinate condition

$$\partial\mathfrak{g}^{\mu\nu}/\partial x^\nu=0 \quad (10)$$

is satisfied, then (9) reduces to

$$\epsilon^{\alpha\beta}\partial^2\mathfrak{g}^{\mu\nu}/\partial x^\alpha\partial x^\beta=\kappa^2\Theta^{\mu\nu}. \quad (11)$$

Further, we can regard the flat space as the zeroth order approximation to the Riemannian space. It can then be shown[4] that the field quantities, occurring in Einstein's theory, can be expressed as infinite series in the flat space. Therefore, keeping Einstein's theory mathematically unchanged, we can pass over from the Riemannian space to the flat space. After passing over to the flat space, the general covariance of the theory is no longer apparent, but the theory still remains manifestly Lorentz covariant. In this way Einstein's theory can also be regarded as a theory of gravitation in flat space with a Lagrangian density containing an infinite number of terms.

3. COMPARISON OF EINSTEIN'S THEORY OF GRAVITATION AND MAXWELL'S THEORY OF ELECTROMAGNETISM

We shall now compare some aspects of Einstein's theory of the gravitational field and Maxwell's theory of the electromagnetic field, and show that the two theories have many features in common. In this section and the subsequent ones, we shall follow the usual simplified flat space notation, taking the space-time coordinates as x_1, x_2, x_3 and $x_4=ict$.

Field Equations

According to Maxwell and Lorentz, the electromagnetic field is described by the field equation

$$\Box^2 A_\mu=-(1/c)j_\mu, \quad (12)$$

with the supplementary condition

$$\partial A_\mu/\partial x_\mu=0, \quad (13)$$

where A_μ is the electromagnetic potential, and j_μ is the current four-vector. It is evident that (12) and (13) have a remarkable similarity to (11) and (10). In fact, the only difference between the two sets of equations is that in place of the four-vectors A_μ and j_μ in the electromagnetic field equations, we have the symmetrical quantities $\mathfrak{g}^{\mu\nu}$ and $\Theta^{\mu\nu}$ in the gravitational field equations.

Covariance

The field equation (12) is covariant not only under Lorentz transformations but also under all those gauge transformations which leave the supplementary condition (13) invariant. Similarly, the gravitational equation (11) is covariant not only under Lorentz transformation but also under all those general coordinate transformations which leave the coordinate condition (10) invariant. Thus, the two theories share the common property that they are both covariant under groups of transformations, which are more general than the Lorentz transformations. This property not only enhances the mathematical beauty of Maxwell's and Einstein's theories, but it is also very helpful in the investigation of the interaction of electromagnetic and gravitational fields with other fields.

Quantization

In the quantization of the electromagnetic field the supplementary condition gives rise to certain difficulties,[5] which can be overcome by using a generalized vector space with an indefinite metric.[6] When we try to quantize the gravitational field, similar difficulties appear, and they can again be overcome by means of an indefinite metric.[7] It is then found that the quantized gravitational field corresponds to gravitational quanta or gravitons of spin 2, while it is well known that the quantized electromagnetic field corresponds to photons of spin 1. However, on quantization the electromagnetic and the gravitational fields have several properties in common. Both of these fields correspond to neutral particles of integral spin and vanishing rest-mass, and both photons and gravitons have two states of polarization with their spin axes parallel or antiparallel to their directions of motion.

Although there are several interesting analogies between the electromagnetic and the gravitational fields, there are also some dissimilarities between the two fields, which will be discussed in the next section.

4. PECULIARITIES OF EINSTEIN'S GRAVITATIONAL FIELD

The most striking difference between the gravitational and the electromagnetic fields is that the gravitational field is nonlinear and its Lagrangian density in flat space

[4] For details see S. N. Gupta, Proc. Phys. Soc. (London) **A65**, 608 (1952).

[5] F. J. Belinfante, Phys. Rev. **76**, 226 (1949).

[6] S. N. Gupta, Proc. Phys. Soc. (London) **A63**, 681 (1950).

[7] S. N. Gupta, Proc. Phys. Soc. (London) **A65**, 161, 608 (1952).

consists of an infinite number of terms. We shall now show that these peculiarities of the gravitational field are a necessary consequence of the fact that the gravitational field corresponds to particles of spin 2.

If we assume that the gravitational field corresponds to neutral particles of zero rest-mass and spin 2, its field equation in the absence of interaction will be[8]

$$\Box^2 U_{\mu\nu}=0 \tag{14}$$

with the supplementary condition

$$\partial U_{\mu\nu}/\partial x_\mu=0, \tag{15}$$

where $U_{\mu\nu}$ is a real symmetrical tensor.

In the presence of interaction, the field equation (14) will be modified as

$$\Box^2 U_{\mu\nu}=\kappa\Theta_{\mu\nu}, \tag{16}$$

where κ is a constant, and $\Theta_{\mu\nu}$ is some symmetrical tensor. Then, differentiating (16) with respect to x_μ, and using (15), we get

$$\partial\Theta_{\mu\nu}/\partial x_\mu=0. \tag{17}$$

The only known physical quantity, which is described by a symmetrical tensor of vanishing divergence, is the total energy-momentum tensor of a closed system of fields. This suggests that the quantity $\Theta_{\mu\nu}$ in (16) should represent the total energy-momentum tensor due to the gravitational field as well as other fields. It should be noted that the gravitational radiation has not yet been experimentally observed. Therefore, from the experimental point of view it is conceivable to have a theory of gravitation in which the divergence of the non-gravitational energy-momentum tensor alone vanishes. However, it is mathematically impossible to construct such a theory in a consistent way, except in the trivial case when there is no interaction between the gravitational field and other fields.

Now, we can write the total energy-momentum tensor $\Theta_{\mu\nu}$ as

$$\Theta_{\mu\nu}=t_{\mu\nu}+T_{\mu\nu}, \tag{18}$$

where $t_{\mu\nu}$ is the energy-momentum tensor of the gravitational field, and $T_{\mu\nu}$ is the energy-momentum tensor of all other fields. Hence, in the absence of all other fields, a pure gravitational field of spin 2 will be described by the field equation

$$\Box^2 U_{\mu\nu}=\kappa t_{\mu\nu}. \tag{19}$$

According to the present ideas of the field theory, the field Eq. (19) must be derived from a Lagrangian density by means of a variational principle. We shall, therefore, try to find the required Lagrangian density for the pure gravitational field by successive approximations.

[8] M. Fierz and W. Pauli, Proc. Roy. Soc. (London) **A173**, 211 (1939).

Let us first choose the Lagrangian density as

$$L=-\tfrac{1}{2}\frac{\partial U_{\mu\nu}}{\partial x_\lambda}\frac{\partial U_{\mu\nu}}{\partial x_\lambda}, \tag{20}$$

which gives the field equation

$$\Box^2 U_{\mu\nu}=0 \tag{21}$$

and the energy-momentum tensor

$$t_{\mu\nu}=\frac{\partial U_{\lambda\rho}}{\partial x_\mu}\frac{\partial U_{\lambda\rho}}{\partial x_\nu}-\tfrac{1}{2}\delta_{\mu\nu}\frac{\partial U_{\lambda\rho}}{\partial x_\sigma}\frac{\partial U_{\lambda\rho}}{\partial x_\sigma}. \tag{22}$$

We now have to modify (20) in such a way that in the resulting equation the quantity (22) appears on the right-hand side of (21). For this it is evident that we must take a Lagrangian density of the form

$$L'=-\tfrac{1}{2}\frac{\partial U_{\mu\nu}}{\partial x_\lambda}\frac{\partial U_{\mu\nu}}{\partial x_\lambda}+f_3, \tag{23}$$

where f_3 consists of one or more terms such that each term is a product of *three* factors, each factor being either $U_{\mu\nu}$ or its derivative. However, then the energy-momentum tensor becomes

$$t_{\mu\nu}'=\left(\frac{\partial U_{\lambda\rho}}{\partial x_\mu}\frac{\partial U_{\lambda\rho}}{\partial x_\nu}-\tfrac{1}{2}\delta_{\mu\nu}\frac{\partial U_{\lambda\rho}}{\partial x_\sigma}\frac{\partial U_{\lambda\rho}}{\partial x_\sigma}\right)+g_3, \tag{24}$$

where g_3 also consists of one or more terms such that each term is a product of three factors, each factor being either $U_{\mu\nu}$ or its derivative. Again, we have to modify (23) in such a way that in the resulting field equation the quantity (24) appears on the right-hand side of (21). For this we must choose a Lagrangian density of the form

$$L''=-\tfrac{1}{2}\frac{\partial U_{\mu\nu}}{\partial x_\lambda}\frac{\partial U_{\mu\nu}}{\partial x_\lambda}+f_3+f_4, \tag{25}$$

where f_4 consists of one or more terms such that each term is a product of *four* factors, each factor being either $U_{\mu\nu}$ or its derivative. In this way it follows that in order to obtain the field equation (19) we shall have to introduce an infinite number of terms in the Lagrangian density.

Hence, not only do Maxwell's theory of the electromagnetic field and Einstein's theory of the gravitational field have many similarities, but the dissimilarities between these fields are a necessary consequence of the difference in their spins.

It is a pleasure to thank Professor K. Lark-Horovitz for his interest in this work, and Professor F. J. Belinfante for stimulating discussions. I am also indebted to Professor P. G. Bergmann for a very profitable correspondence.

Tensor Virial Equations*

EUGENE N. PARKER
Department of Physics, University of Utah, Salt Lake City, Utah
(Received January 15, 1954; revised manuscript received August 23, 1954)

The tensor virial equations for an aggregate of particles are developed. They are tensor equations of second rank, and on contraction yield the familiar virial equation. To illustrate their application, the diffusion of molecules through a gas is considered and a kinetic derivation of the Navier-Stokes equations is worked out. The latter may here be carried out in more general terms than is usual, the generalization leading to results that are of interest in turbulence theory. In anisotropic systems the use of the tensor in place of the scalar virial becomes imperative. An astrophysical example of this (anisotropic star cluster) is given in outline.

1. INTRODUCTION

THE use of the virial theorem in kinetic theory is well known. It seems to have escaped general attention that the usual virial equation is the contraction of a second-order tensor equation which is essentially the equation of motion of the moment-of-inertia tensor of an aggregate of particles. Lord Rayleigh,[1] who wrote down the off-diagonal terms of the tensor equations, remarked that they should have application to problems in viscosity. Moreover, one readily finds that the diagonal terms apply to anisotropic systems in the same way in which the usual scalar virial theorem applies to isotropic systems.

Consider a system of particles in a space with Cartesian coordinates x_i. A particle of mass m on which there is a net force F_j has the equation of motion[2]

$$F_j = m d^2x_j/dt^2. \tag{1}$$

We multiply by x_i and rearrange to obtain

$$\frac{d}{dt}\left(mx_i\frac{dx_j}{dt}\right) = m\frac{dx_i}{dt}\frac{dx_j}{dt} + x_iF_j. \tag{2}$$

Summing over all the particles in the system and defining the tensors

$$J_{ij}=\sum mx_i\frac{dx_j}{dt}, \quad 2T_{ij}=\sum m\frac{dx_i}{dt}\frac{dx_j}{dt}, \quad \Phi_{ij}=\sum x_iF_j, \tag{3}$$

we obtain the *tensor virial equation:*

$$dJ_{ij}/dt = 2T_{ij}+\Phi_{ij}. \tag{4}$$

To interpret T_{ij} and Φ_{ij} we note that the total kinetic energy, T, of the system is just the spur of T_{ij}. Accordingly we shall call T_{ij} the *kinetic tensor*. If F_i is expressible in terms of a potential energy V which is a homogeneous function of degree n of the x_i, then the spur of Φ_{ij} is

$$\Phi=\Phi_{ii}=-\sum x_i(\partial V/\partial x_i)=-nV, \tag{5}$$

by Euler's theorem. For electrostatic and gravitational interactions, $n=-1$. We shall call Φ_{ij} the *potential tensor*.

It is of interest to separate (4) into its symmetric and antisymmetric parts. The moment of inertia tensor I_{ij} of the system is the symmetric part of J_{ij}. Thus,

$$\frac{d}{dt}I_{ij}=\tfrac{1}{2}(J_{ij}+J_{ji})=\frac{d}{dt}\sum mx_ix_j. \tag{6}$$

We denote the antisymmetric part of J_{ij} by K_{ij} so that

$$2K_{ij}=J_{ij}-J_{ji}=\sum m(x_idx_j/dt-x_jdx_i/dt). \tag{7}$$

$2K_{ij}$ is obviously the angular momentum of the system. The kinetic tensor, T_{ij}, is clearly symmetrical. If, finally, we split the potential tensor, Φ_{ij}, into its symmetrical and antisymmetrical parts,

$$2M_{ij}=\Phi_{ij}+\Phi_{ji}, \quad 2N_{ij}=\Phi_{ij}-\Phi_{ji}, \tag{8}$$

Eq. (4) decomposes into the two equations:

$$d^2I_{ij}/dt^2=2T_{ij}+M_{ij}, \quad dK_{ij}/dt=N_{ij}. \tag{9}$$

The first equation is the equation of motion for the moment of inertia tensor; the second gives us the rate of change of the angular momentum. We shall concern ourselves primarily with the equation for I_{ij}; its contraction gives the familiar scalar virial equation.

2. DIFFUSION

Consider a space filled with a homogeneous distribution of particles. At time t_0 we mark every particle within the rectangle with sides $x_i=\pm a_i(t_0)$. We ask how these marked particles will spread out with time.

The tensor virial equations do not determine the form of the spatial distribution: If we assume a distribution described by certain characteristic lengths, then from (9) we can compute how these lengths vary with time. Thus our solution has the disadvantage of being an approximate one but the related advantage that the computation will be easy.

Let us characterize the distribution of the particles at time t by three moments, say $\frac{1}{2}a_i(t)$. At time t_0 the a_i represent the initial rectangular step functions; as time goes on, the step functions will spread out into

* This work was in part supported by the Office of Naval Research.

[1] Lord Rayleigh, Phil. Mag. **50**, 210 (1900). This reference was pointed out to us by Professor Chandrasekhar.

[2] We confine ourselves here to the Newtonian formalism. The Lagrangian generalization is straightforward.

Gaussians; $\frac{1}{2}a_i(t)$ will then approximately represent the standard deviation. The tensor virial equations reduce to

$$\frac{d}{dt}\left[a_i(t)\frac{d}{dt}a_j(t)\right]=0. \tag{10}$$

The solution of (10) is

$$a_i(t)=a_i(t_0)(t/t_0)^{\frac{1}{2}},\ da_i(t)/dt=a_i(t_0)/(2t_0)(t_0/t)^{\frac{1}{2}}. \tag{11}$$

To evaluate the integration constant t_0, we note that at time t_0 the expansion of the rectangular region of marked particles is brought about by only those particles within a distance L of each face, where L is the mean free path; of all the particles in the region, only a fraction $L/a_i(t)$ are contained in a slab of thickness L and normal to the i direction. Half of these particles are moving outward across the face with velocity $\langle v_i\rangle_{Av}$. Thus, $a_i(t)$ must at time $t=t_0$ increase at the rate,

$$da_i(t)/dt=\tfrac{1}{2}\langle v_i\rangle_{Av}L/a_i(t). \tag{12}$$

Comparing (12) with (11), we find that

$$t_0=[a_i(t_0)]^2/(L\langle v_i\rangle_{Av}), \tag{13}$$

and (11) becomes

$$a_i(t)=(L\langle v_i\rangle_{Av}t)^{\frac{1}{2}},\quad da_i(t)/dt=[L\langle v_i\rangle_{Av}/(4t)]^{\frac{1}{2}}. \tag{14}$$

3. MOTION OF A FLUID

Let us next use the tensor virial equation to derive the equation of motion of a *finite* region of fluid. We let the boundaries of the region move with the fluid. If y_i is the center of mass of the region, we set for each particle

$$x_i=y_i+\xi_i. \tag{15}$$

Defining w_i as the velocity of the center of mass, we write the velocity v_i of a particle as

$$v_i=w_i+u_i,\quad w_i=dy_i/dt,\quad u_i=d\xi_i/dt. \tag{16}$$

Obviously,

$$\sum m\xi_i=\sum mu_i=0. \tag{17}$$

We shall refer to u_i as the *local velocity field* and w_i as the *translocal field*; the local field is the portion of the velocity composed of fluctuations of smaller scale than the region. Finally, defining G_i as the average force on the region so that

$$G_i=mdw_i/dt, \tag{18}$$

we write

$$F_i=G_i+f_i. \tag{19}$$

With these definitions we may rewrite (3) as

$$\begin{gathered}J_{ij}=My_iw_j+\sum m\xi_iu_j,\quad 2T_{ij}=Mw_iw_j+\sum mu_iu_j,\\ \Phi_{ij}=y_i\sum G_j+\sum \xi_if_j,\end{gathered} \tag{20}$$

where M is the total mass of the region. After some rearranging of terms (4) may be rewritten as

$$M\frac{dw_j}{dt}=\sum G_j+\frac{1}{y_i}\left[\sum mu_iu_j+\sum \xi_if_j-\frac{d}{dt}\sum m\xi_iu_j\right]. \tag{21}$$

However, since for the center of mass

$$Mdw_j/dt=\sum G_j, \tag{22}$$

Eq. (21) reduces to

$$\frac{d}{dt}\sum m\xi_iu_j=\sum mu_iu_j+\sum \xi_if_j. \tag{23}$$

We see that *the tensor virial equation referred to the center of mass of a region is invariant with respect to translocal accelerations.*

Now f_i in the purely hydrodynamic case results only from collisional forces. Thus, it cancels out over the interior of the region where both members of each pair of colliding particles enter into the summation; only the collisions at the surface of the region contribute. It becomes convenient to introduce[3] the usual stress tensor σ_{ij} interpreted as the force per unit area in the i direction across an element of area normal to the j direction. We choose our signs so that σ_{ij} represents the force exerted by the matter on the positive side of the area on the matter on the negative side. This is the customary definition in elasticity[4] and electrodynamics. Remembering that all forces other than collisional are assumed to be zero, we may express $\sum \xi_if_j$ as the surface integral $\int dS_k\xi_i\sigma_{jk}$. Replacing the summation by a volume integral in the other terms of (23) and using Gauss's theorem, we obtain

$$\frac{d}{dt}\int dV\rho\xi_iu_j=\int dV\rho u_iu_j+\int dV\sigma_{ij}+\int dV\xi_i\frac{\partial}{\partial\xi_k}\sigma^{jk}, \tag{24}$$

where summation convention is used with respect to k.

Let us now introduce the assumption that

$$\int dV\rho u_iu_j\gg\frac{d}{dt}\int dV\rho\xi_iu_j. \tag{25}$$

---

[3] The introduction of a stress tensor and the associated processes and parameters such as integration, differentiation, pressure, viscosity, etc. require a limited form of continuity in our hitherto unrestricted system. Our notion of infinitesimal becomes that of the physical infinitesimal, *viz.*, that the smallest elements of volume dV which we consider must be sufficiently large so as to contain many particles. If n represents the number of particles in dV, then the fluctuation of n is of the order of $\sqrt{n}$. We must require that

$$\sqrt{n}\ll n$$

in order that our averaging process over dV have a smoothing effect. To be treated as an infinitesimal, dV, of course, must be of smaller scale than the phenomena in which we are interested. The alternative to these restrictions on dV is to consider an ensemble of systems, so that the average may be carried out over the given dV in all the member systems rather than just in a single system.

[4] A. Sommerfield, *The Mechanics of Deformable Bodies* (Academic Press, New York, 1950), p. 61.

Physically, this condition implies that the acceleration of the rate of distortion of the region is small over periods of time comparable to the time of local circulation, ξ_i/u_j. This requires that the local forces $\partial\sigma_{ik}/\partial\xi_k$ do not vary too rapidly over the region, in which case the last term of (24) is also small, and (24) reduces to

$$0=\int dV\rho u_i\ddot{u}_j+\int dV\sigma_{ij}. \tag{26}$$

This is satisfied if

$$\sigma_{ij}=-\rho u_i u_j, \tag{27}$$

and we see that σ_{ij} is the familiar Reynolds tensor.

It is of interest to note that if (26) were rigorously true, rather than only in the approximation of (25), then (24) would reduce to

$$\frac{d}{dt}\int dV\rho\xi_i u_j=\int dV\xi_i f_j. \tag{28}$$

Let us investigate under what circumstances this relation is valid.

The antisymmetric part of (28) is the angular momentum equation,

$$\frac{d}{dt}\int dV\rho(\xi_i u_j-\xi_j u_i)=\int dV(\xi_i f_j-\xi_j f_i),$$

and is rigorously true. The symmetric part, on the other hand is

$$\frac{d}{dt}\int dV\rho(\xi_i u_j+\xi_j u_i)=\int dV(\xi_i f_j+\xi_j f_i). \tag{29}$$

Assuming an incompressible flow, we may write (29) as

$$\int dV\rho\left(2u_i u_j+\xi_i\frac{du_j}{dt}+\xi_j\frac{du_i}{dt}\right)=\int dV(\xi_i f_j+\xi_j f_i).$$

Inasmuch as

$$\rho du_k/dt=f_k,$$

we may reduce the relation to

$$\int dV\rho u_i u_j=0, \tag{30}$$

which implies that u_i and u_j are uncorrelated over the region. In (32) we shall assume that u_i and u_j are correlated by an amount proportional to $\partial w_i/\partial y_i$ times the mean free path. Thus, (30) leads one to assume that this product be small, which is equivalent to (25).

Given that the hydrodynamic stresses are of the form (27), we return to (22) and write the equation of motion for the center of mass of the region as

$$\frac{dw_i}{dt}=-\frac{1}{M}\int dS_k\rho u_i u_k=-\frac{1}{M}\int dV\frac{\partial}{\partial\xi_k}(\rho u_i u_k). \tag{31}$$

To write (31) in the conventional form of hydrodynamics, we introduce the usual argument that u_i and $u_i(i\neq j)$ will be correlated only if there is translocal shearing present: If u_j transports a particle an average distance L_j across a velocity gradient $\partial w_i/\partial y_j$ without collision, the particle will have a velocity $-L_j\partial w_i/\partial y_j$ in the i direction relative to the general velocity field; L_j is essentially the mean free path, or mixing length. We construct the relation, for $\alpha\neq\beta$,

$$\langle\rho u_\alpha u_\beta\rangle\equiv\frac{1}{V}\int dV\rho u_\alpha u_\beta=-a\langle\rho u_\alpha L_\alpha\rangle\frac{\partial w_\beta}{\partial y_\alpha}-b\langle\rho u_\beta L_\beta\rangle\frac{\partial w_\alpha}{\partial y_\beta},$$

(where we indicate by Greek indices that we do not observe summation convention); a and b are numerical constants. More generally,

$$\langle\rho u_\alpha u_\beta\rangle=p(\alpha)\delta_{\alpha\beta}-a\mu(\alpha)\frac{\partial w_\beta}{\partial y_\alpha}-b\mu(\beta)\frac{\partial w_\alpha}{\partial y_\beta}, \tag{32}$$

where $\delta_{\alpha\beta}$ is the Kronecker delta and $\mu(\alpha)$ is the viscosity,

$$\mu(\alpha)=\langle\rho u_\alpha L_\alpha\rangle.$$

$p(\alpha)$ is taken to be the average over the region of the portion of $\rho u_\alpha u_\alpha$ which is independent of the translocal shear; $p(\alpha)$ is the pressure and is independent of α if the local velocity field is statistically isotropic.

Now,

$$\int dV\frac{\partial}{\partial\xi_k}(\rho u_i u_k)=V\frac{\partial}{\partial y_k}\langle\rho u_i u_k\rangle, \tag{33}$$

where V is the volume of the region. Thus (28) may be rewritten as

$$\langle\rho\rangle\frac{dw_\alpha}{dt}=-\frac{\partial}{\partial y_\alpha}p(\alpha)+a\frac{\partial}{\partial y_k}\mu(\alpha)\frac{\partial w_k}{\partial y_\alpha}+b\frac{\partial}{\partial y_k}\mu(k)\frac{\partial w_\alpha}{\partial y_k}, \tag{34}$$

where $\langle\rho\rangle=M/V$. (34) is the equation for the translocal field in the general case that the local velocity field is anisotropic.

Assuming isotropy so that $p(\alpha)$ and $\mu(\alpha)$ are independent of α, assuming that $\mu(\alpha)$ is independent of y_i, and assuming that an isotropic dilatation of the region produces no dissipation of energy, we obtain the familiar Navier-Stokes equations for a compressible fluid.

We note how the tensor virial equations with the assumption (24) lead quite naturally to the Reynolds stress tensor. Equation (31) indicates that the translocal velocity field depends only on the statistical properties of the local field. Introducing Prandtl's mixing length ideas, we find that the statistical properties of the local motions appear as an "eddy" viscosity, as was assumed by Heisenberg[8] in his theory of isotropic turbulence.

[8] W. Heisenberg, Z. Physik 124 628 (1948).

4. ISOLATED SYSTEMS

The tensor virial equation is of particular interest in problems involving an anisotropic isolated system of particles; for instance, an interstellar gas cloud or a cluster of stars. One postulates some definite spatial distribution for the system; the differential Eq. (9) can then be used to investigate how the scale of such a distribution varies with time.

Consider a star cluster, or another isolated dynamical system, in which the velocities of the individual stars are not statistically isotropic. In such a case one may assume that the particles are distributed uniformly throughout an ellipsoidal region of space. To compare the calculations with an observed system, one interprets the semi-axes of the ellipsoid as representing the scale of the system, say the distance from the center out to where the density has decreased by e. Choosing the coordinate axes along the axes of the ellipsoid, one computes the potential tensor to be[6]

$$\Phi_{\alpha\beta}=\begin{cases}0 & \text{if} \quad \alpha\neq\beta \\ -(3/10)GM^2(a_\alpha)^2N_\alpha & \text{if} \quad \alpha=\beta.\end{cases} \tag{35}$$

M is the total mass of the system; G is the gravitational constant; a_α is the semi-axis in the α direction. We arrange the axes so that $a_1\geqslant a_2\geqslant a_3$; the N_α are given by

$$\begin{aligned}N_1&=2[(a_1)^2-(a_3)^2]^{-\frac{1}{2}}k^{-2}[v-E(\omega,k)],\\ N_2&=2[(a_1)^2-(a_3)^2]^{-\frac{1}{2}}\left\{\frac{E(\omega,k)}{k^2(1-k^2)}\right.\\ &\qquad\left.-\frac{1}{(1-k^2)}\frac{\operatorname{sn}v\operatorname{cn}v}{dnv}-\frac{v}{k^2}\right\},\\ N_3&=2[(a_1)^2-(a_3)^2]^{-\frac{1}{2}}(1-k^2)^{-1}[\operatorname{sn}v\operatorname{dn}v/cnv-E(\omega,k)],\end{aligned} \tag{36}$$

where

$$\sin\omega=\operatorname{sn}v=[1-(a_3/a_1)^2]^{\frac{1}{2}},$$

$$\operatorname{cn}v=a_3/a_1, \quad \operatorname{dn}v=a_2/a_3, \tag{37}$$

and

$$k^2=[(a_1)^2-(a_2)^2]/[(a_1)^2-(a_3)^2], \quad v=F(\omega,k). \tag{38}$$

[6] W. D. MacMillan, *The Theory of the Potential* (McGraw-Hill Book Company, Inc., New York, 1930), p. 60.

$F(\omega,k)$ and $E(\omega,k)$ are Legrendre's elliptic integrals of the first and second kind, respectively.

If $\langle(u_\alpha)^2\rangle$ is the mean square velocity in the α direction, the kinetic tensor is given by

$$2T_{\alpha\beta}=\begin{cases}0 & \text{if} \quad \alpha\neq\beta \\ M\langle(u_\alpha)^2\rangle+(1/10)M(da_\alpha/dt)^2 & \text{if} \quad \alpha=\beta.\end{cases} \tag{39}$$

The complexity of the potential tensor prohibits our giving a general integration of (9). Even in the somewhat more simple case when $a_1=a_2$ this does not seem feasible. Thus, we investigate here only the equilibrium configuration. Setting $d^2I_{ij}/dt^2=0$ in (9), we obtain a relation for the mean velocities in terms of the anisotropy:

$$\langle(u_\alpha)^2\rangle=(3/10)GM(a_\alpha)^2N_\alpha. \tag{40}$$

Integration of (9) in the case of spherical symmetry is elementary, and we but briefly indicate the development. We use the scalar virial equation, the contraction of (9). For a homogeneous sphere it is readily shown that

$$\Phi_{ii}=-3GM/(5a), \quad I_{ii}=3Ma^2/10, \tag{41}$$

where a is the radius of the sphere. The radial oscillations contribute $(3/10)M(da/dt)^2$ to the kinetic energy. If the internal motions follow a polytrope law,

$$\langle u^2\rangle=\langle u^2\rangle_0(a/a_0)^{3(A-1)} \tag{42}$$

where A is the effective γ of the motions, then

$$2T_{ii}=\tfrac{3}{5}M(da/dt)^2+M\langle u^2\rangle_0(a_0/a)^{3(A-1)}. \tag{43}$$

Putting (41) and (43) into the scalar virial equation, we obtain the differential equation

$$\frac{d^2a}{dt^2}=\frac{5}{3}\langle u^2\rangle_0\frac{a_0^{3(A-1)}}{a^{3A-2}}-\frac{GM}{a^2}, \tag{44}$$

which is readily integrated to give da/dt and finally a as a function of time.

I should like to express my gratitude to Professor W. M. Elsasser for several valuable suggestions in the development of this work.

Tamm-Dancoff Methods and Nuclear Forces*†

BEHRAM KURŞUNOĞLU‡
Laboratory of Nuclear Studies, Cornell University, Ithaca, New York
(Received June 3, 1954)

It is shown that by the use of 3-dimensional Feynman diagrams an equal-time two-particle wave equation can be written down. The procedure is the same one as Bethe and Salpeter used in deriving the 4-dimensional two-body equation. In this way all the terms of the new Tamm-Dancoff method of Dyson, in the form of the Lévy-Klein expansion of the interaction function, can easily be recorded.

The connection between the Bethe-Salpeter and Dyson equations is discussed. The spurious energy denominators of the fourth order interaction, in the adiabatic limit, can be eliminated by including all the contributions to the fourth order term arising from the 4- and 5-particle amplitudes that are coupled back to the two-particle amplitudes. The potential derived in the adiabatic limit to the fourth order term of the interaction operator is the same as the Lévy-Klein potential derived from the old Tamm-Dancoff method.

The Appendix contains a discussion of the Bethe-Salpeter equation and a simple method of derivation of equal-time equations from the 4-dimensional theories.

I. INTRODUCTION

THE field-theoretical investigations of the nature of nuclear forces received great impetus as a result of Lévy's[1] extension of the Tamm-Dancoff method to include nucleon pair effects in the intermediate states and higher order meson-exchange processes. The theory as used by Lévy was not fully relativistic. This had the consequence that renormalization was, in effect, not possible within his formulation of the theory. Furthermore, the use of the non-interacting vacuum state, in the definition of the Tamm-Dancoff amplitudes, introduced additional difficulties connected with the vacuum self-energy. It has been pointed out by Gell-Mann and Low,[2] and more recently by Dyson,[3] that most of the difficulties encountered in the old Tamm-Dancoff method can be avoided by defining the amplitudes with respect to the interacting vacuum state.

The observation that no vacuum self-energy appears when the amplitudes are defined with respect to the interacting vacuum state was, essentially, the starting point of Dyson[4] in his formulation of the new Tamm-Dancoff method.

In Dyson's formulation of the new Tamm-Dancoff method, just as in the 4-dimensional Bethe-Salpeter formalism, the wave function contains positive as well as negative energy parts. Actually, the statement of "negative energy" in the Bethe-Salpeter formalism has quite a different meaning: it is the energy of the "pair" which is positive. In Dyson's equal-time formalism pairs are mixed with the negative energies, which is a consequence of dealing with the equal-time amplitudes right at the starting point of the theory.

In the adiabatic limit the weak-coupling forms of the new and old Tamm-Dancoff methods do not differ substantially; the adiabatic limit of the new Tamm-Dancoff method is understood to include the statement that all the components of the two-particle wave function not referring to positive energy states of the particles vanish. It is hard to justify such an approximation, but the rejection of those components of the wave function referring to negative energies seems to be a necessity. It is known that there are some difficulties involved in the use of the interacting vacuum state as a boundary condition, but with the aforementioned approximation the vacuum difficulty does not arise. The vanishing of ψ_{+-}, ψ_{-+}, and ψ_{--} components of the wave function is not meant to be connected with the fact that the vacuum should be the state of lowest energy. The cancellation of the so-called spurious divergences in the second and fourth order interactions takes place only in the adiabatic limit. In the nonadiabatic form of the interactions they are not cancelled.

In this paper we have extended Dyson's formulation of the new Tamm-Dancoff method to include higher order amplitudes. In principle, it corresponds to Lévy's method of including the effects of the higher order amplitudes on the lower ones, as applied to the new Tamm-Dancoff method. Theoretically one considers an infinite number of linear integral equations for all the particle amplitudes. The use of the infinite set of equations in the elimination of all the Tamm-Dancoff amplitudes, except the amplitude for the two-particle state, if carried to completion, leads to a linear integral equation for the two-particle wave function.

We have carried out this procedure to the fourth order in the coupling constant G by assuming that the amplitudes of all states involving 5 or more particles should vanish. In Sec. II the most general form of the two-nucleon equation is first written down from the analogies using the methods of Bethe-Salpeter[5] and Lévy-Klein[6] in the derivation of the 4-dimensional and

* Supported in part by the joint program of the Office of Naval Research and the U. S. Atomic Energy Commission.
† Read at the 1954 annual meeting of the American Physical Society in New York.
‡ Now at Department of Physics, University of Miami, Coral Gables, Florida.
[1] M. M. Lévy, Phys. Rev. **88**, 72 and 725 (1952).
[2] M. Gell-Mann and F. Low, Phys. Rev. **84**, 350 (1951).
[3] F. J. Dyson, Phys. Rev. **90**, 994 (1953).
[4] F. J. Dyson, Phys. Rev. **91**, 1543 (1953).
[5] E. E. Salpeter and H. A. Bethe, Phys. Rev. **84**, 1232 (1951).
[6] A. Klein, Phys. Rev. **90**, 1101 (1953).

the old Tamm-Dancoff equations, respectively. The relation between the Dyson and Bethe-Salpeter wave functions is discussed briefly. Section III contains a derivation of the fourth order interaction operator together with its adiabatic limit leading to the derivation of the fourth order potential. The Tamm-Dancoff equations are given in Appendix A, and in Appendix B, we give a simple method of derivation of the old Tamm-Dancoff equation for two nucleons from the Bethe-Salpeter formalism.

II. THE SECOND ORDER INTERACTION

In this section we discuss the most general form of a 3-dimensional covariant equation for two nucleons. For this purpose it is convenient to represent the kernel of the equation in terms of 3-dimensional Feynman diagrams. In such a diagram a nucleon line will represent (initial and final states included) both positive and negative energy states. A second order graph, e.g., can be considered as the sum of 4 sub-graphs consisting of minus and plus particle states. There will be a single time-co-ordinate for any number of nucleon lines. If one of the nucleons emits a meson to be absorbed by the other nucleon or by itself, then, in the intermediate state, the energy of the emitted or absorbed meson is to be added to the energy of that nucleon with which it later interacts. The resulting expression can assume both positive and negative signs, according as they are plus or minus particles, respectively. By using this prescription we can write down all the terms of the interaction operator in the form of an infinite series in powers of the coupling constant G. We have verified the above rule by actual calculation with the new Tamm-Dancoff equations given in the Appendix A.

The two-nucleon equation used in this paper can be written as

$$[H_a(\mathbf{p})+H_b(-\mathbf{p})-E]\psi(\mathbf{p}) = -\int I(\mathbf{p},\mathbf{p}';E)\psi(\mathbf{p}')d^3p', \quad \text{(II.1)}$$

where $H(p)=\boldsymbol{\alpha}\cdot\mathbf{p}+\beta M$, E is the total energy in the center-of-mass system, and $\psi(\mathbf{p})$ is the two-nucleon component of the Tamm-Dancoff wave functions. The word wave function is not used in the strict sense of a probability amplitude.

The first term $I_2(\mathbf{p},\mathbf{p}',E)$ of the interaction operator $I(\mathbf{p},\mathbf{p}';E)$, which was already given by Dyson, consists of the four diagrams shown in Fig. 1. The first diagram

FIG. 1. Three-dimensional Feynman diagrams contributing to the second-order interaction of two nucleons.

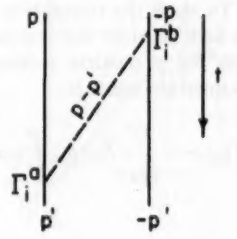

FIG. 2. Labels used in writing the matrix element for the first diagram of Fig. 1. The arrow indicates the time direction of the interaction.

(which is repeated with labels in Fig. 2) represents the matrix element:

$$\frac{G^2}{(2\pi)^3}\frac{1}{2\omega_{p-p'}}\Gamma_i^a[\eta_a(\mathbf{p})(E_p+\omega_{p-p'})+\eta_b(-\mathbf{p}')E_{p'}-E]^{-1}\Gamma_i^a,$$

where

$$\Gamma_i^a=(i\beta\gamma_5)_a\tau_i^a, \quad \eta_a(\mathbf{p})=H_a(p)/E_p.$$

This matrix element can easily be understood in terms of the prescription outlined at the beginning of this section.

We have not succeeded in deriving Eq. (II.1) from the Bethe-Salpeter equation. However, we shall now discuss its relation to the Bethe-Salpeter theory. In Dyson's theory, for a state Ψ of one proton and one neutron in interaction, we singled out the 3-dimensional two-particle wave function $\psi(\mathbf{p})$ satisfying Eq. (II.1). The function $\psi(\mathbf{p})$ is the lowest component of the Tamm-Dancoff wave functions. The 4-dimensional wave function $\chi(p_n)$ satisfies the Bethe-Salpeter equation. In Bethe-Salpeter theory one also defines an equal-time wave function $\varphi(\mathbf{p})$ by

$$\varphi(\mathbf{p})=\int\chi(\mathbf{p},p_0)dp_0. \quad \text{(II.2)}$$

If any relation exists between the Dyson and the Bethe-Salpeter theories it should be one that relates the functions $\psi(\mathbf{p})$ and $\varphi(\mathbf{p})$. Originally the function $\varphi(\mathbf{p})$ was not defined as a Tamm-Dancoff wave function, but it is reasonable to hope for the possibility of deriving the Bethe-Salpeter equation from a 4-dimensional formalism analogous to the Tamm-Dancoff method. In this case it is natural to expect a correlation between the functions $\psi(\mathbf{p})$ and $\varphi(\mathbf{p})$. We have been able to verify that $\psi(\mathbf{p})$ and $\varphi(\mathbf{p})$ satisfy the same equation if only one fermion's second order interaction is taken into account. In the fourth order we obtain different equations. For the two-particle case we do not know whether further transformations of the interaction and the equations would bring the two expressions into agreement. The similarity is, certainly, not apparent in the present form of Dyson's theory. The investigations were made for both one- and two-nucleon systems. Especially in the former case, the result may be considerably modified by renormalization which is not obvious for the 3-dimensional equation.

To show the connection between $\psi(\mathbf{p})$ and $\varphi(\mathbf{p})$, let us first consider the one-particle Bethe-Salpeter equation for a particle interacting with itself, which in momentum space is

$$\chi(p_\mu)=-\frac{G^2}{(2\pi)^4}S_F(p_\mu)\int\gamma_5\tau_\varphi S_F(p_\mu-p_\mu')\times\gamma_5\tau_i\Delta_F(p_\mu')d^4p'\chi(p_\mu)$$
$$=\frac{G^2}{(2\pi)^4}\frac{1}{H(\mathbf{p})-p_0}\int\Gamma_i\frac{1}{H(\mathbf{p}-\mathbf{p}')-p_0+p_0'}\times\Gamma_i\frac{d^4p'\chi(p_\mu)}{(\omega_{p'}-p_0')(\omega_{p'}+p_0')}. \quad \text{(II.3)}$$

Now, a one-particle, 4-dimensional wave function in momentum space can be defined by

$$\chi(p_\mu)=\chi(\mathbf{p})\delta(p_0-E), \quad \text{(II.4)}$$

where E is the energy of a proton of momentum $\mathbf{p}$, including self-energy. On substituting (II.4) in (II.3) and integrating both sides of the resulting equation with respect to p_0, we get

$$[H(\mathbf{p})-E]\chi(\mathbf{p})=\frac{G^2}{8\pi^3}\int\frac{d^3p'}{2\omega_{p'}}\times\Gamma_i[\eta(\mathbf{p}-\mathbf{p}')(E_{p-p'}+\omega_{p'})-E]^{-1}\Gamma_i\chi(\mathbf{p}). \quad \text{(II.5)}$$

This equation is identical with the one Dyson derived from his new Tamm-Dancoff method.

The two-particle Bethe-Salpeter wave function is not separable according to (II.4) and, therefore, the above method cannot be carried through. It is of interest, however, to record the result that can be obtained for the second order interaction. The Bethe-Salpeter equation for the one-meson interaction of two nucleons in the centimeter system is given by

$$\chi(p_\mu)=\frac{G^2}{(2\pi)^4}S_{Fa}(\tfrac{1}{2}K_\mu+p_\mu)S_{Fb}(\tfrac{1}{2}K_\mu-p_\mu)\beta_a\beta_b\Gamma_i^a\Gamma_i^b\times\int\Delta_F(p_\mu-p_\mu')\chi(p_\mu')d^4p'. \quad \text{(II.6)}$$

The integration of both sides of (II.6) over the relative energy variable p_0 can be effected in accordance with the hole theory (see Appendix B), giving the result

$$[H_a(\mathbf{p})+H_b(-\mathbf{p})-E]\varphi(\mathbf{p})=\frac{G^2}{8\pi^3}\int\frac{d^3p'dp_0'}{2\omega_{p-p'}}\{\Gamma_i^b[\eta_a(\mathbf{p})(E_p+\omega_{p-p'})-\tfrac{1}{2}E-p_0']^{-1}\Gamma_i^a+\Gamma_i^a[\eta_b(-\mathbf{p})(E_p+\omega_{p-p'})-\tfrac{1}{2}E+p_0']^{-1}\Gamma_i^b\}\chi(\mathbf{p}'p_0'). \quad \text{(II.7)}$$

It was not possible to find a suitable ansatz for the function $\chi(\mathbf{p}',p_0')$ on the right-hand side of the equation, so the integration over p_0' had to be left as it is. The comparison with Dyson's theory shows some similarities, but they disappear in the fourth order where some curious energy denominators of the form $(E_p+E_{p'}+\omega_{p-p'})^{-1}$ show up which are independent of p_0'. The energy denominators of that form also arose in the derivation[6] of the old Tamm-Dancoff two-nucleon equations[7] from the Bethe-Salpeter theory and were among the differences between the original Tamm-Dancoff method used by Lévy and the one derived from the Bethe-Salpeter equation. There is, however, one unexpected result that can be obtained from (II.7). If we use the ansatz (5) of Appendix A with the total energy E having a small negative imaginary part, in Eq. (II.7) we obtain, after the p_0' integration, Dyson's second order equation for two-nucleons. This is a mixture of hole and one-particle theories. It is not possible to derive a general conclusion from this result, but it certainly is not accidental.[8]

A complete correspondence, to the second order, between the positive energy parts of the wave functions $\psi(\mathbf{p})$ and $\varphi(\mathbf{p})$ can be established if we assume that (i) the p_0-dependence of the Bethe-Salpeter wave function has the form (see Appendix B)

$$\chi(\mathbf{p},p_0')=\frac{1}{2\pi i}[S_{Fa}(\tfrac{1}{2}K_\mu+p_\mu)\beta_a+S_{Fb}(\tfrac{1}{2}K_\mu-p_\mu)\beta_b]\Phi(\mathbf{p});$$

(ii) all components of the Dyson wave function vanish which do not refer to positive energy states.

Under these assumptions one easily obtains the relation

$$\psi_{++}(\mathbf{p})=\Phi_{++}(\mathbf{p}),$$

where the function $\psi_{++}(\mathbf{p})$ satisfies the old Tamm-Dancoff equation of second order. The approximation (ii) eliminates, to second order, the complications related to the vacuum being used as a boundary condition. For higher order terms of the interaction operator, the condition (ii) is not enough to eliminate the spurious energy denominators, but in the adiabatic limit to the interaction it is a sufficient condition. The last statement has been verified only for the fourth order interaction. A general method of elimination of the spurious denominators of the two-nucleon equation is not known; if this can be done consistently, then one expects to get the results of the old Tamm-Dancoff except for small deviations.

III. THE FOURTH ORDER INTERACTION

It has been observed by Bethe, on the basis of the perturbation theory, that the fourth order interaction

[7] A simpler derivation is given in Appendix A.

[8] We were not able to explain this curious result, but one thing is clear: it does not arise in the derivation of the old Tamm-Dancoff equation from the Bethe-Salpeter equation.

term needs to be included in the $ps-ps$ theory. There are, at present, no definite conclusions concerning the behavior of the whole series of interactions. The convergence of the adiabatic nuclear potential, without renormalization terms, has been discussed by Klein.[9] In the following we discuss the fourth order term in the interaction operator of Eq. (II.1). The aim of this investigation is to see in what way the qualitative features of the γ_5-interaction are altered in the fourth order, by a 3-dimensional covariant theory. The fourth order terms which are radiative corrections to the second order interactions will not be included. There exist about 30 of these corrections that may contribute significantly, even in the adiabatic limit. The 12 no-pair terms of the old Tamm-Dancoff method, with a different interpretation, constitute part of the interaction kernel. In the new Tamm-Dancoff method only 12 of the 24 one-pair terms of the old Tamm-Dancoff method appear and the 12 two-pair terms of the old method do not arise; this is a consequence of the use of the interacting vacuum state and the covariance of the theory. In this case the creation of three particles out of the vacuum, proceeding in the same time direction at a given vertex, is not allowed. This is the reason for the non-appearance of the aforementioned terms in the new Tamm-Dancoff method and precisely this has been verified by actual calculation. Altogether one is left with 24 interaction terms. A detailed discussion of these points for the one-particle case is given by Klein[9], and therefore they will not be elaborated in this paper.

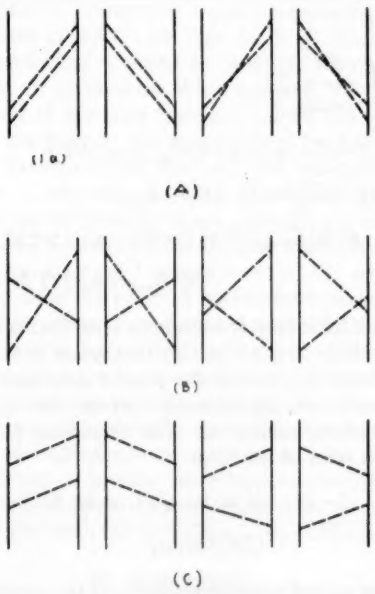

FIG. 3. The set (A) of fourth order diagrams contain the main spurious divergences in Dyson's new Tamm-Dancoff method. The sets (B) and (C) do not contain terms proportional to $(2M)^{-2}$. Because of the time ordering of the interaction, all the diagrams in the Tamm-Dancoff method can be divided into pairs. Of the above 12 interaction terms one need only calculate the 6 corresponding matrix elements. The remaining six can be obtained by a reflection of time. As an example, we give in Eq. (III.1) the matrix element that corresponds to the diagram labeled (1a).

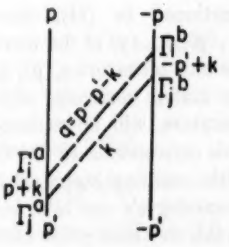

FIG. 4. Labels used in writing the matrix element [Eq. (III.1)] for diagram (1a) of Fig. 3.

First, we shall consider the 8 irreducible interactions and those that follow from the iteration of the second order interaction [Figs. 3 (A), (B), and (C)]. Of the set shown in Fig. 3(C) we shall include only those contributions arising from the pair processes in the intermediate states. The argument for the contribution from positive-energy intermediate states is the same as given by Klein.[6]

The prescription given in Sec. II is not complete for writing down the matrix elements corresponding to the set shown in Fig. 3 (C). It has to be amended for those interactions which contain one or two mesons in the intermediate states and also for those in which one of the nucleon lines is bent. In this case we can state the rules for writing down the interaction terms as follows:

(i) If the emission (absorption) of a meson is the earliest event in the diagram, then the latest absorbed (emitted) meson is either in the state Ψ or in the state Ψ_0 and is absorbed (emitted) by the second (first) nucleon in a positive (negative) energy state, respectively.

(ii) The energy of the remaining meson is to be added to that nucleon energy with which it interacts later. The sum can take both positive and negative signs. In the above, for convenience, we assume that the mesons are always emitted and absorbed by the first and second nucleon, respectively.

As an example we give the matrix element corresponding to the diagram (1a) of Fig. 3(A) (see also Fig. 4):

$$\left[\frac{G^2}{8\pi^3}\right]^2\int\frac{d^3k}{2\omega_k 2\omega_{p-p'-k}}\sum_{\pm}\Gamma_i^b[E-\eta_a(\mathbf{p})(E_p+\omega_q)$$
$$-\eta_b(-\mathbf{p}'-\mathbf{k})E_{p'+k}]^{-1}\Gamma_j^b[E-\eta_a(\mathbf{p})(E_p+\omega_q)$$
$$-\eta_b(-\mathbf{p}')E_{p'}\pm\omega_k]^{-1}\Gamma_i^a[E-\eta_b(-\mathbf{p}')E_{p'}$$
$$\pm(E_{p'+k}+\omega_k)]^{-1}\Lambda_{\mp}^a(\mathbf{p}'+\mathbf{k})\Gamma_j^a. \quad \text{(III.1)}$$

In calculating the adiabatic limit we shall assume, as

[9] A. Klein, Phys. Rev. 92, 1017 (1953).

mentioned in (II), that the components $\psi_{+-}(\mathbf{p})$, $\psi_{-+}(\mathbf{p})$, $\psi_{--}(\mathbf{p})$ of the wave function $\psi(\mathbf{p})$ vanish. Thus, the unit operators $\eta_a(\mathbf{p})$, $\eta_b(-\mathbf{p})$, $\eta_a(\mathbf{p}')$ and $\eta_b(-\mathbf{p}')$ in the matrix elements, with the appropriate projection operators, will be replaced by their $+1$ eigenvalues. This corresponds to the fact that the nucleons in the initial and final states are in positive energy states. The remaining η's can take both $+1$ and -1 eigenvalues. In this way each graph corresponds to 4 terms according as the two remaining η's in the interaction function take the values $+1$ or -1. In connection with the calculation of the matrix elements of the sets (A), (B), and (C) of Fig. 3 with respect to positive-energy free-particle Dirac wave functions, we use the relations

$$\eta(\mathbf{p})\Lambda_+(\mathbf{p})=\eta(\mathbf{p})[\tfrac{1}{2}+\tfrac{1}{2}\eta(\mathbf{p})]=\Lambda_+(\mathbf{p}),$$

$$\eta(\mathbf{p})\Lambda_-(\mathbf{p})=\eta(\mathbf{p})[\tfrac{1}{2}-\tfrac{1}{2}\eta(\mathbf{p})]=-\Lambda_-(\mathbf{p}),$$

and the identity

$$[\Lambda_+(\mathbf{p})+\Lambda_-(\mathbf{p})]_a[\Lambda_+(-\mathbf{q})+\Lambda_-(-\mathbf{q})]_b$$
$$=\Lambda_+{}^a(\mathbf{p})\Lambda_+{}^b(-\mathbf{q})+\Lambda_+{}^a(\mathbf{p})\Lambda_-{}^b(-\mathbf{q})$$
$$+\Lambda_-{}^a(\mathbf{p})\Lambda_+{}^b(-\mathbf{q})+\Lambda_-{}^a(\mathbf{p})\Lambda_-{}^b(-\mathbf{q})=1.$$

The matrix element of the integrand of (III.1) in the adiabatic limit is given by

$$\langle p,-p|I_4{}^{(1)}(\mathbf{p},\mathbf{p}',E)|\mathbf{p}-\mathbf{q}-\mathbf{k},-\mathbf{p}+\mathbf{q}+\mathbf{k}\rangle$$
$$=(3-2\boldsymbol{\tau}\cdot\boldsymbol{\tau}_b)\left\{\frac{1}{(2M)^2}\frac{1}{4\omega_k\omega_q(\omega_k-\omega_q)}+\frac{1}{(2M)^3}\left[\frac{(\boldsymbol{\sigma}\cdot\mathbf{q}\boldsymbol{\sigma}\cdot\mathbf{k})_b}{4\omega_k\omega_q{}^2(\omega_k-\omega_q)}-\frac{(\boldsymbol{\sigma}\cdot\mathbf{q}\boldsymbol{\sigma}\cdot\mathbf{k})_a}{4\omega_q\omega_k{}^2(\omega_k+\omega_q)}\right]\right.$$
$$\left.+\frac{1}{(2M)^4}\left[-\frac{(\boldsymbol{\sigma}\cdot\mathbf{q}\boldsymbol{\sigma}\cdot\mathbf{k})_a(\boldsymbol{\sigma}\cdot\mathbf{q}\boldsymbol{\sigma}\cdot\mathbf{k})_b}{4\omega_k{}^2\omega_q{}^2(\omega_k+\omega_q)}+\frac{(\boldsymbol{\sigma}\cdot\mathbf{q}\boldsymbol{\sigma}\cdot\mathbf{k})_a+(\boldsymbol{\sigma}\cdot\mathbf{q}\boldsymbol{\sigma}\cdot\mathbf{k})_b-[\boldsymbol{\sigma}\cdot\mathbf{p}\boldsymbol{\sigma}\cdot(\boldsymbol{\zeta}+\mathbf{k})]_a-[\boldsymbol{\sigma}\cdot\mathbf{p}\boldsymbol{\sigma}\cdot(\mathbf{q}+\mathbf{k})]_b}{4\omega_k\omega_q(\omega_k-\omega_q)}\right]\right\}, \quad \text{(III.2)}$$

where

$$\mathbf{q}=\mathbf{p}-\mathbf{p}'-\mathbf{k}.$$

The terms associated with $(2M)^{-5}$ and higher are neglected. The adiabatic limit includes also the approximation of replacing the terms $[2M-\omega_q]^{-1}$ and $[2M+\omega_k]^{-1}$ by $[2M]^{-1}$. This is equivalent to cutting off the high-energy contributions of the virtual mesons, so that the resulting potential is not valid for all r. The sets (B) and (C) do not contain terms proportional to $[2M]^{-3}$. The largest contributions come from the set (A).

Apart from the sets (A), (B), and (C), we also have to consider the coupling of the 4-fermion amplitudes back to the 2-fermion wave function $\psi(\mathbf{p})$. If one neglects 5-particle amplitudes of the new Tamm-Dancoff method, then there are only two more terms contributing to the fourth order potential. They are shown as the two upper diagrams [set (D)] of Fig. 5. The first diagram (1.3) in Fig. 5 represents the matrix element:

$$\left[\frac{G^2}{8\pi^3}\right]^2\int\frac{d^3k}{2\omega_k 2\omega_q}\sum_{\mp}$$
$$\pm\Gamma_i{}^b[E-E_p-\eta_b(-\mathbf{p}+\mathbf{k})E_{p-k}\pm\omega_k]^{-1}\Gamma_i{}^a$$
$$\times\Lambda_-{}^a(\mathbf{p}'+\mathbf{k})[E-E_p-E_{p'}-E_{p'+k}$$
$$-\eta_b(-\mathbf{p}+\mathbf{k})E_{p-k}]^{-1}\Gamma_j{}^a[E-E_{p'}-\eta_b(-\mathbf{p}+\mathbf{k})$$
$$\times(E_{p-k}+\omega_q)]^{-1}\Gamma_j{}^b. \quad \text{(III.3)}$$

In the adiabatic limit it contains a term that is infinite. This is similar to the situation that arises in the study of the terms (C), but in the present case such terms, when combined algebraically before the adiabatic limit is taken, cancel out. The remaining part contributes a term of the form

$$-\frac{(3-2\boldsymbol{\tau}_a\cdot\boldsymbol{\tau}_b)[(\boldsymbol{\sigma}\cdot\mathbf{k}\boldsymbol{\sigma}\cdot\mathbf{q})_b+(\boldsymbol{\sigma}\cdot\mathbf{q}\boldsymbol{\sigma}\cdot\mathbf{k})_a]}{(2M)^3 2\omega_k{}^2\omega_q{}^2},$$

where the second term corresponds to the contribution of the second diagram.

If we were to confine ourselves only to the 2-, 3-, and 4-particle amplitudes, then the above 14 diagrams are all that would need to be included. There are actually other contributions to the fourth order potential arising from the coupling of the five-particle amplitudes back to the 2-fermion wave function.[10]

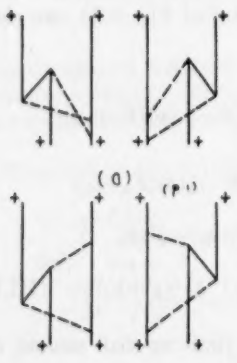

FIG. 5. These diagrams contain spurious interactions with signs opposite to those arising from the previous interactions. There are 8 more of these diagrams and they contribute in a manner similar to the ones shown here.

[10] This point was communicated to the author by A. Klein.

We also have to include interactions of the type that include 4 fermions and one meson in the intermediate states. The new Tamm-Dancoff equations in Appendix A do not include 5-particle amplitudes, but the method of writing down the matrix elements for any interaction term is now quite easy. The prescription given in Sec. II can be generalized in all cases.[11]

Two typical interactions involving 5 particles in the intermediate state are shown in the two lower diagrams of Fig. 5. There are altogether 10 diagrams of this type. We shall write down the matrix element corresponding to the first one as

$$\left[\frac{G^2}{8\pi^3}\right]^2\int\frac{d^3k}{2\omega_k 2\omega_q}\sum_{\mp}\pm\Gamma_i^b[E-E_p-\eta_b(-\mathbf{p}+\mathbf{k})E_{p-k}\pm\omega_k]^{-1}\Gamma_j^b\times[E-E_p-E_{p'}-\omega_q\pm\omega_k]^{-1}\Gamma_i^a\Lambda_-^a(\mathbf{p}'+\mathbf{k})\times[E-E_p-2E_{p'}-E_{p'+k}-\omega_q]^{-1}\Gamma_j^a. \quad \text{(III.4)}$$

Its contribution to the fourth order potential in the adiabatic limit is

$$-\frac{3-2\boldsymbol{\tau}_a\cdot\boldsymbol{\tau}_b}{(2M)^2}\left[\frac{1}{4\omega_k\omega_q(\omega_k+\omega_q)}+\frac{1}{4\omega_k\omega_q(\omega_k-\omega_q)}\right]-\frac{(\boldsymbol{\sigma}\cdot\mathbf{q}\boldsymbol{\sigma}\cdot\mathbf{k})_b(3-2\boldsymbol{\tau}_a\cdot\boldsymbol{\tau}_b)}{(2M)^3}\left[\frac{1}{4\omega_k^2\omega_q(\omega_k+\omega_q)}-\frac{1}{4\omega_k^2\omega_q(\omega_k-\omega_q)}\right]$$

$$+\frac{(3-2\boldsymbol{\tau}_a\cdot\boldsymbol{\tau}_b)}{(2M)^4}\left[\frac{[\boldsymbol{\sigma}\cdot\mathbf{p}\boldsymbol{\sigma}\cdot(\mathbf{q}+\mathbf{k})]_a+[\boldsymbol{\sigma}\cdot\mathbf{p}\boldsymbol{\sigma}\cdot(\mathbf{q}+\mathbf{k})]_b-(\boldsymbol{\sigma}\cdot\mathbf{q}\boldsymbol{\sigma}\cdot\mathbf{k})_a-(\boldsymbol{\sigma}\cdot\mathbf{q}\boldsymbol{\sigma}\cdot\mathbf{k})_b}{4\omega_k\omega_q(\omega_k+\omega_q)}\right.$$

$$\left.+\frac{[\boldsymbol{\sigma}\cdot\mathbf{p}\boldsymbol{\sigma}\cdot(\mathbf{q}+\mathbf{k})]_a+[\boldsymbol{\sigma}\cdot\mathbf{p}\boldsymbol{\sigma}\cdot(\mathbf{q}+\mathbf{k})]_b-(\boldsymbol{\sigma}\cdot\mathbf{q}\boldsymbol{\sigma}\cdot\mathbf{k})_a-(\boldsymbol{\sigma}\cdot\mathbf{q}\boldsymbol{\sigma}\cdot\mathbf{k})_b}{4\omega_k\omega_q(\omega_k-\omega_q)}\right]. \quad \text{(III.5)}$$

The number of interaction terms contributing to the fourth order potential are thus 24 in all. Each interaction consists of 4 terms so that one must include altogether 96 interactions. When summed, the spurious divergences of the type $(\omega_k-\omega_q)^{-1}$ cancel out and the result is the same as the one obtained by Klein from the old Tamm-Dancoff method. The one-pair terms also give a spin-orbit coupling term with the same coefficient as obtained by Klein from the old method. We note that the cancellation of the spurious divergence of the type $(\omega_k-\omega_q)^{-1}$ occurs only in the adiabatic limit adopted in this paper. A nonadiabatic cancellation of such interaction terms does not occur. In the sense of the adiabatic approximation the role of the interacting vacuum state in the definition of the new Tamm-Dancoff amplitudes is reduced to the one played by the non-interacting vacuum state. The last statement is, of course, verified only up to the fourth order interaction. However, it is quite reasonable to conclude that in the adiabatic limit the new Tamm-Dancoff method will not differ from the old one in higher orders.

IV. CONCLUSION

An attempt to study the entire series of interactions in the new Tamm-Dancoff method, even without renormalizations, would certainly be an ambitious enterprise. The inclusion of the renormalizations would make the whole problem next to impossible. In any case, the problem of renormalization in this theory is not well understood, and from this point of view the old Tamm-Dancoff method as derived from the Bethe-Salpeter equation is in a better situation.

It is very unlikely that in the near future we shall know much about the complete series. We are, therefore forced to base all our arguments on the fourth-order interaction which, of course, does not do justice to the theory. However, if we attribute a special place to the fourth order interaction, then our results show that the extreme nonrelativistic approximation to a relativistic theory does not lead to sensible results. If the Tamm-Dancoff method of approximation is to be maintained, then it is necessary to abandon the adiabatic approximation to the kernel of the equation. The same conclusion is implied by the work of Klein.[6]

An important problem is, now, the investigation of the nonadiabatic terms. It may well be that the nonadiabatic parts will contribute effectively near the core and change the sign of the interaction that was repulsive in the nonrelativistic region without the nonadiabatic terms. We have no reason for assuming that the nonadiabatic terms in a $ps-ps$ theory are small. This aspect of the problem is being investigated for the second order equation.

The author wishes to express his gratitude to Professor H. A. Bethe and to the Laboratory of Nuclear Studies for their kind hospitality. He would also like to thank Professor Bethe and Dr. A. Klein, Dr. R. H. Dalitz, Dr. E. Power, and Dr. S. S. Schweber for many stimulating discussions on this and related topics.

[11] More general rules of writing down the matrix elements for the one-particle case has also been discussed by A. Klein, Phys. Rev. **95**, 1061 (1954).

APPENDIX A

In this Appendix we give the coupled set of integral equations mentioned in the introduction to this paper, and we shall use the notation of Dyson.[4] The Schrödinger equation for the new Tamm-Dancoff amplitudes was derived by Dyson as

$$E(\Psi_0{}^*C(N)A(N')\Psi)=[\Pi(N)\Pi(N')]^{-\frac{1}{2}}(\Psi_0{}^*[C(N)A(N'),H_0+H']\Psi).$$

The new Tamm-Dancoff equations for a state Ψ representing two nucleons in interaction with, at most, four fermions at a given time can be obtained by calculating the commutators,

$$[b_p{}^u d_q{}^v,H'],\quad [b_{p-k}{}^w d_q{}^s a_k,H'],\quad [b_{p-k}{}^w d_q{}^s a_{-k}{}^*,H'],\quad [b_{p-k-s}{}^{w'} d_q{}^{v'} a_k a_s,H'],\quad [b_{p-k-s}{}^{w'} d_q{}^{v'} a_{-k}{}^* a_s,H'],$$
$$[b_{p-k-s}{}^{w'} d_q{}^{v'} a_{-k}{}^* a_{-s}{}^*,H'],\quad [N(b_{p-k}{}^u d_q{}^v d_s{}^{*w} d_{k+s}{}^z),H'],\quad [N(b_{p-k}{}^u b_s{}^{*w} b_{k+s}{}^z d_q{}^v,H'].$$

In the last commutator, N stands for the normal product of the 4 operators. We shall use the following definitions in arranging the various commutators according to the number of particles that take part in the interaction:

$$\sum u^*\gamma_5 u=0,\quad \sum_u \bar{u}u(\mathbf{p})\theta_u=\Lambda_+(\mathbf{p}),$$
$$\langle b_p{}^u b_q{}^{*v}\rangle_0=(1-\theta_u)\delta_{uv}\delta_{pq},\quad \langle b_p{}^u b_q{}^{*v}\rangle_0=\theta_u\delta_{uv}\delta_{pq},$$

where

$$\theta_u=\begin{cases}1 & \text{for proton states}\\ 0 & \text{for anti-proton states.}\end{cases}$$

The notation is the same as in Dyson's paper. We assume that all Tamm-Dancoff amplitudes which contain five or more particles vanish. In the actual case this assumption was not made in calculating the fourth order potential. Since our aim is to derive general rules for writing the matrix elements, there is no harm in the above assumption. In this case one obtains equations that involve the wave functions $\psi(\mathbf{p},\mathbf{q})$, $\psi^+(\mathbf{p}-\mathbf{k},\mathbf{q},\mathbf{k})$, $\psi^-(\mathbf{p}-\mathbf{k},\mathbf{q},\mathbf{k})$, $\psi^{++}(\mathbf{p}-\mathbf{k},\mathbf{q}-\mathbf{s},\mathbf{k},\mathbf{s})$, $\psi^{-+}(\mathbf{p}-\mathbf{k},\mathbf{q}-\mathbf{s},\mathbf{k},\mathbf{s})$, $\psi^{--}(\mathbf{p}-\mathbf{k},\mathbf{q}-\mathbf{s},\mathbf{k},\mathbf{s})$, $\phi^p(\mathbf{p}-\mathbf{k},-\mathbf{s},\mathbf{k}+\mathbf{s},\mathbf{q})$, $\phi^N(\mathbf{p}-\mathbf{k},\mathbf{q},-\mathbf{s},\mathbf{k}+\mathbf{s})$, for two and four fermions (in states Ψ or Ψ_0) and one and two mesons in the states Ψ and Ψ_0 as plus or minus particles. The four-fermion wave function is defined as

$$\phi^p(\mathbf{p}-\mathbf{k},-\mathbf{s},\mathbf{k}+\mathbf{s},\mathbf{q})=\sum_{uvzw^*}[\Psi_0{}^*N(b_{p-k}{}^u b_s{}^{*w} b_{k+s}{}^z d_q{}^v)\Psi]uvw^*z,$$
$$\phi^n(\mathbf{p}-\mathbf{k},\mathbf{q},-\mathbf{s},\mathbf{k}+\mathbf{s})=\sum_{uvzw^*}[\Psi_0{}^*N(b_{p-k}{}^u d_q{}^v d_s{}^{*w} d_{k+s}{}^z)\Psi]uvw^*z.$$

The integral equations satisfied by the first six wave functions are given by

$$[E-\eta_a(\mathbf{p})E_p-\eta_b(\mathbf{q})E_q]\psi(\mathbf{p},\mathbf{q})$$
$$=G\sum_s(2v\omega_s)^{-\frac{1}{2}}\{\gamma^a[\psi^+(\mathbf{p}-\mathbf{s},\mathbf{q},\mathbf{s})+\psi^-(\mathbf{p}-\mathbf{s},\mathbf{q},\mathbf{s})]\}+\{\gamma^b[\psi^+(\mathbf{p},\mathbf{q}-\mathbf{s},\mathbf{s})+\psi^-(\mathbf{p},\mathbf{q}-\mathbf{s},\mathbf{s})]\}. \tag{A.1}$$

$$[E-\eta_a(\mathbf{p}-\mathbf{k})E_{p-k}-\eta_b(\mathbf{q})E_q-\omega_k]\psi^+(\mathbf{p}-\mathbf{k},\mathbf{q},\mathbf{k})$$
$$=G(2v\omega_k)^{\frac{1}{2}}[\Lambda_+{}^a(\mathbf{p}-\mathbf{k})\gamma^a\psi(\mathbf{p},\mathbf{q})+\Lambda_+{}^b(\mathbf{q})\gamma^b\psi(\mathbf{p}-\mathbf{k},\mathbf{q}+\mathbf{k})]+G\sum_s(2v\omega_s)^{-\frac{1}{2}}[\gamma^a(\psi^{++}(\mathbf{p}-\mathbf{k}-\mathbf{s},\mathbf{q},\mathbf{s},\mathbf{k})$$
$$+\psi^{-+}(\mathbf{p}-\mathbf{k}-\mathbf{s},\mathbf{q},\mathbf{s},\mathbf{k}))+\gamma^b(\psi^{++}(\mathbf{p}-\mathbf{k},\mathbf{q}-\mathbf{s},\mathbf{s},\mathbf{k})+\psi^{-+}(\mathbf{p}-\mathbf{k},\mathbf{q}-\mathbf{s},\mathbf{s},\mathbf{k}))]$$
$$+G(2v\omega_k)^{-\frac{1}{2}}\sum_s[\gamma^a\phi^p(\mathbf{p}-\mathbf{k},-\mathbf{s},\mathbf{k}+\mathbf{s},\mathbf{q})+\gamma^b\phi^n(\mathbf{p}-\mathbf{k},\mathbf{q},-\mathbf{s},\mathbf{k}+\mathbf{s})], \tag{A.2}$$

$$[E-\eta_a(\mathbf{p}-\mathbf{k})E_{p-k}-\eta_b(\mathbf{q})E_q+\omega_k]\psi^-(\mathbf{p}-\mathbf{k},\mathbf{q},\mathbf{k})$$
$$=G(2v\omega_k)^{-\frac{1}{2}}[\Lambda_-{}^a(\mathbf{p}-\mathbf{k})\gamma^a(\mathbf{p},\mathbf{q})+\Lambda_-{}^b(\mathbf{q})\gamma^b\psi(\mathbf{p}-\mathbf{k},\mathbf{q}+\mathbf{k})]+G\sum_s(2v\omega_s)^{-\frac{1}{2}}[\gamma^a(\psi^{-+}(\mathbf{p}-\mathbf{k}-\mathbf{s},\mathbf{q},\mathbf{k},\mathbf{s})$$
$$+\psi^{--}(\mathbf{p}-\mathbf{k}-\mathbf{s},\mathbf{q},\mathbf{k},\mathbf{s}))+\gamma^b(\psi^{-+}(\mathbf{p}-\mathbf{k},\mathbf{q}-\mathbf{s},\mathbf{k},\mathbf{s})+\psi^{--}(\mathbf{p}-\mathbf{k},\mathbf{q}-\mathbf{s},\mathbf{k},\mathbf{s}))]$$
$$+G(2v\omega_k)^{-\frac{1}{2}}\sum_s[\gamma^a\phi^p(-\mathbf{s},\mathbf{k}+\mathbf{s},\mathbf{p}-\mathbf{k},\mathbf{q})+\gamma^b\phi^n(\mathbf{p}-\mathbf{k},-\mathbf{s},\mathbf{k}+\mathbf{s},\mathbf{q})], \tag{A.3}$$

$$[E-\eta_a(\mathbf{p}-\mathbf{k}-\mathbf{r})E_{p-k-r}-\eta_b(\mathbf{q})E_q-\omega_k-\omega_r]\psi^{++}(\mathbf{p}-\mathbf{k}-\mathbf{r},\mathbf{q},\mathbf{k},\mathbf{r})$$
$$=G(2v\omega_k)^{-\frac{1}{2}}[\Lambda_+{}^a(\mathbf{p}-\mathbf{k}-\mathbf{r})\gamma^a\psi^+(\mathbf{p}-\mathbf{r},\mathbf{q},\mathbf{r})+\Lambda_+{}^b(\mathbf{q})\gamma^b\psi^+(\mathbf{p}-\mathbf{k}-\mathbf{r},\mathbf{q}+\mathbf{k},\mathbf{r})]$$
$$+G(2v\omega_r)^{-\frac{1}{2}}[\Lambda_+{}^a(\mathbf{p}-\mathbf{k}-\mathbf{r})\gamma^a\psi^+(\mathbf{p}-\mathbf{k},\mathbf{q},\mathbf{k})+\Lambda_+{}^b(\mathbf{q})\gamma^b\psi^+(\mathbf{p}-\mathbf{k}-\mathbf{r},\mathbf{q}+\mathbf{r},\mathbf{k})], \tag{A.4}$$

$$[E-\eta_a(\mathbf{p}-\mathbf{k}-\mathbf{r})E_{p-k-r}-\eta_b(\mathbf{q})E_q-\omega_k+\omega_r]\psi^{-+}(\mathbf{p}-\mathbf{k}-\mathbf{r},\,\mathbf{q},\,\mathbf{r},\,\mathbf{k})$$
$$=G(2v\omega_k)^{-\frac{1}{2}}[\Lambda_+{}^a(\mathbf{p}-\mathbf{k}-\mathbf{r})\gamma^a\psi^-(\mathbf{p}-\mathbf{r},\,\mathbf{q},\,\mathbf{r})+\Lambda_+{}^b(\mathbf{q})\gamma^b\psi^-(\mathbf{p}-\mathbf{k}-\mathbf{r},\,\mathbf{q}+\mathbf{k},\,\mathbf{r})]$$
$$+G(2v\omega_r)^{-\frac{1}{2}}[\Lambda_-{}^a(\mathbf{p}-\mathbf{k}-\mathbf{r})\gamma^a\psi^+(\mathbf{p}-\mathbf{k},\,\mathbf{q},\,\mathbf{k})+\Lambda_-{}^b(\mathbf{q})\gamma^b\psi^+(\mathbf{p}-\mathbf{k}-\mathbf{r},\,\mathbf{q}+\mathbf{r},\,\mathbf{k})]. \quad \text{(A.5)}$$

$$[E-\eta_a(\mathbf{p}-\mathbf{k}-\mathbf{r})E_{p-k-r}-\eta_b(\mathbf{q})E_q+\omega_k+\omega_r]\psi^{--}(\mathbf{p}-\mathbf{k}-\mathbf{r},\,\mathbf{q},\,\mathbf{k},\,\mathbf{r})$$
$$=G(2v\omega_k)^{-\frac{1}{2}}[\Lambda_-{}^a(\mathbf{p}-\mathbf{k}-\mathbf{r})\gamma^a\psi^-(\mathbf{p}-\mathbf{r},\,\mathbf{q},\,\mathbf{r})+\Lambda_-{}^b(\mathbf{q})\gamma^b\psi^-(\mathbf{p}-\mathbf{k}-\mathbf{r},\,\mathbf{q}+\mathbf{k},\,\mathbf{r})]$$
$$+G(2v\omega_r)^{-\frac{1}{2}}[\Lambda_-{}^a(\mathbf{p}-\mathbf{k}-\mathbf{r})\gamma^a\psi^-(\mathbf{p}-\mathbf{k},\,\mathbf{q},\,\mathbf{k})+\Lambda_-{}^b(\mathbf{q})\gamma^b\psi^-(\mathbf{p}-\mathbf{k}-\mathbf{r},\,\mathbf{q}+\mathbf{r},\,\mathbf{k})]. \quad \text{(A.6)}$$

The equation for the wave function $\phi^p(\mathbf{p}-\mathbf{k},\,-\mathbf{s},\,\mathbf{k}+\mathbf{s},\,\mathbf{q})$ follows from a careful study of the commutator,

$$[N(b_{p-k}{}^u b_s{}^{*w} b_{k+s}{}^z d_q{}^v), H']$$
$$=+G(2v\omega_k)^{-\frac{1}{2}}(z^*\gamma^a w)(1-\theta_w)(a_k+a_{-k}{}^*)b_{p-k}{}^u d_q{}^v-G(2v\omega_k)^{-\frac{1}{2}}(z^*\gamma^a w)(1-\theta_s)(a_k+a_{-k}{}^*)b_{p-k}{}^u d_q{}^v$$
$$+G(2v\omega_{p-k-s})^{-\frac{1}{2}}(u^*\gamma^a w)\theta_w(a_{p-k-s}+a_{-p+k+s})b_{k+s}{}^z d_q{}^v-G(2v\omega_{p-k-s})^{-\frac{1}{2}}(u^*\gamma^a w)\theta_u(a_{p-k-s}+a_{-p+k+s}{}^*)b_{k+s}{}^z d_q{}^v.$$

There are only 8 possibilities for the signs of the energies along the proton line. It is easy to see that if u, w, and z represent positive or negative energy spinors simultaneously, the right-hand side of the above equation vanishes. Therefore the $\phi_{+++}{}^p$ and $\phi_{---}{}^p$ components of the wave function must vanish. The sum of the remaining six components of the wave function satisfies the equation

$$\phi^p(\mathbf{p}-\mathbf{k},\,-\mathbf{s},\,\mathbf{k}+\mathbf{s},\,\mathbf{q})=-G(2v\omega_k)^{-\frac{1}{2}}\Lambda_-{}^a(\mathbf{k}+\mathbf{s})\Lambda_-{}^a(\mathbf{s})[E+\eta_a(\mathbf{p}-\mathbf{k})E_{p-k}-E_s+E_{k+s}-\eta_b(\mathbf{q})E_q]^{-1}$$
$$\times\gamma^a(\psi^+(\mathbf{p}-\mathbf{k},\,\mathbf{q},\,\mathbf{k})+\psi^-(\mathbf{p}-\mathbf{k},\,\mathbf{q},\,\mathbf{k}))+G(2v\omega_k)^{-\frac{1}{2}}\Lambda_+{}^a(\mathbf{k}+\mathbf{s})\Lambda_+{}^a(\mathbf{s})[E+\eta_a(\mathbf{p}-\mathbf{k})E_{p-k}+E_s-E_{k+s}-\eta_b(\mathbf{q})E_q]$$
$$\times\gamma^a(\psi^+(\mathbf{p}-\mathbf{k},\,\mathbf{q},\,\mathbf{k})+\psi^-(\mathbf{p}-\mathbf{k},\,\mathbf{q},\,\mathbf{k}))-G(2v\omega_{p-k-s})^{-\frac{1}{2}}\Lambda_+{}^a(\mathbf{p}-\mathbf{k})\Lambda_+{}^a(\mathbf{s})[E+\eta_a(\mathbf{k}+\mathbf{s})E_{k+s}-E_{p-k}+E_s$$
$$-\eta_b(\mathbf{q})E_q]^{-1}\gamma^a(\psi^+(\mathbf{k}+\mathbf{s},\,\mathbf{q},\,\mathbf{p}-\mathbf{k}-\mathbf{s})+\psi^-(\mathbf{k}+\mathbf{s},\,\mathbf{q},\,\mathbf{p}-\mathbf{k}-\mathbf{s}))+G(2v\omega_{p-k-s})^{-\frac{1}{2}}\Lambda_-{}^a(\mathbf{p}-\mathbf{k})\Lambda_-{}^a(\mathbf{s})$$
$$\times[E+\eta_a(\mathbf{k}+\mathbf{s})E_{k+s}+E_{p-k}-E_s-\eta_b(\mathbf{q})E_q]^{-1}\gamma^a(\psi^+(\mathbf{k}+\mathbf{s},\,\mathbf{q},\,\mathbf{p}-\mathbf{k}-\mathbf{s})+\psi^-(\mathbf{k}+\mathbf{s},\,\mathbf{q},\,\mathbf{p}-\mathbf{k}-\mathbf{s}). \quad \text{(A.7)}$$

In a similar way the function $\phi^N(\mathbf{p}-\mathbf{k},\,\mathbf{q},\,-\mathbf{s},\,\mathbf{k}+\mathbf{s})$ satisfies the equation

$$\phi^n(\mathbf{p}-\mathbf{k},\,\mathbf{q},\,-\mathbf{s},\,\mathbf{k}+\mathbf{s})=G(2v\omega_k)^{-\frac{1}{2}}\Lambda_+{}^b(\mathbf{k}+\mathbf{s})\Lambda_+{}^b(\mathbf{s})[E-\eta_a(\mathbf{p}-\mathbf{k})E_{p-k}+E_s-E_{k+s}+\eta_b(\mathbf{q})E_q]^{-1}$$
$$\times\gamma^b(\psi^+(\mathbf{p}-\mathbf{k},\,\mathbf{q},\,\mathbf{k})+\psi^-)-G(2v\omega_k)^{-\frac{1}{2}}\Lambda_-{}^b(\mathbf{k}+\mathbf{s})\Lambda_-{}^b(\mathbf{s})[E-\eta_a(\mathbf{p}-\mathbf{k})E_{p-k}-E_s+E_{k+s}+\eta_b(\mathbf{q})E_q]^{-1}$$
$$\times\gamma^b(\psi^+(\mathbf{p}-\mathbf{k},\,\mathbf{q},\,\mathbf{k})+\psi^-(\mathbf{p}-\mathbf{k},\,\mathbf{q},\,\mathbf{k}))+G(2v\omega_{q-s})^{-\frac{1}{2}}\Lambda_-{}^b(\mathbf{q})\Lambda_-{}^b(\mathbf{s})[E-\eta_a(\mathbf{p}-\mathbf{k})E_{p-k}-E_s+E_q+\eta_b(\mathbf{k}+\mathbf{s})E_{k+s}]^{-1}$$
$$\times\gamma^b(\psi^+(\mathbf{p}-\mathbf{k},\,\mathbf{k}+\mathbf{s},\,\mathbf{q}-\mathbf{s})+\psi^-(\mathbf{p}-\mathbf{k},\,\mathbf{k}+\mathbf{s},\,\mathbf{q}-\mathbf{s}))-G(2v\omega_{q-s})^{-\frac{1}{2}}\Lambda_+{}^b(\mathbf{q})\Lambda_+{}^b(\mathbf{s})[E-\eta_a(\mathbf{p}-\mathbf{k})E_{p-k}+E_s$$
$$-E_q+\eta_b(\mathbf{k}+\mathbf{s})E_{k+s}]^{-1}(\psi^+(\mathbf{p}-\mathbf{k},\,\mathbf{k}+\mathbf{s},\,\mathbf{q}-\mathbf{s})+\psi^-). \quad \text{(A.8)}$$

We have, thus, completed the derivation of the new Tamm-Dancoff equations. In carrying out the first Born approximation to these equations the radiative correction terms can easily be recognized and dropped from the interaction. This leads to the sets (A), (B), and (D).

APPENDIX B

In connection with the elimination of spurious plane wave solutions of the Bethe-Salpeter (integro-differential) equation we can introduce a transformation of the two-body wave function $\chi(12)$:

$$\chi(12)=\frac{1}{2\pi i}\left[\int S_{Fa}(11')\beta_a\phi(1'2)d1'+\int S_{Fb}(22')\beta_b\phi(12')d2'\right] \quad \text{(B.1)}$$

where the physical meaning of the spinor function $\phi(12)$ is not directly obvious. A simple interpretation for the function $\phi(12)$ can, however, be found in some special cases.

Now, the momentum space transform of (B.1) in the center-of-mass system can be written as

$$\chi(p_\mu)=\frac{1}{2\pi i}\left[\frac{1}{H_a(\mathbf{p})-\frac{1}{2}E-p_0}+\frac{1}{H_b(-\mathbf{p})-\frac{1}{2}E+p_0}\right]\phi(p_\mu). \quad \text{(B.2)}$$

In general there are two cases of interest: (*a*) we substitute the expression (B.2) in the Bethe-Salpeter equation and obtain an equation for $\phi(p_\mu)$,

$$[H_a(\mathbf{p})+H_b(-\mathbf{p})-E]\phi(p_\mu)=-\frac{G^2}{(2\pi)^4}\Gamma_i^a\Gamma_i^b\int\Delta_F(p_\mu-p_\mu')\left[\frac{1}{H_a(\mathbf{p}')-\frac{1}{2}E-p_0'}+\frac{1}{H_b(-\mathbf{p}')-\frac{1}{2}E+p_0'}\right]\phi(p_\mu')d^4p'. \quad \text{(B.3)}$$

When the particles interact instantaneously ($p_0=p_0'$ in Δ_F), the kernel of (B.3) is independent of p_0 so that the function $\phi(p_\mu)$ does not depend on the relative energy variable p_0. Equation (B.3), after the p_0-integration on the right-hand side, reduces to

$$[H_a(\mathbf{p})+H_b(-\mathbf{p})-E]a(\mathbf{p})=\frac{G^2}{8\pi^3}\Gamma_i^a\Gamma_i^b\int\frac{d^3p'}{\omega_{p-p'}{}^2}\Lambda_-{}^{ab}(\mathbf{p}')a(\mathbf{p}'), \quad \text{(B.4)}$$

where $a(p)$ is the wave function of two instantaneously interacting nucleons and

$$\Lambda_-{}^{ab}(\mathbf{p})=\Lambda_+{}^a(\mathbf{p})\Lambda_+{}^b(-\mathbf{p})-\Lambda_-{}^a(\mathbf{p})\Lambda_-{}^b(-\mathbf{p}).$$

In the nonrelativistic limit, for the $a_{++}(p)$-components, the wave equation (B.4) reduces to the usual Yukawa form of the $ps-ps$ theory. Thus, in the above special case the physical meaning of $\phi(p_\mu)$ is clear.

(*b*) Let us now assume that the system first propagates as two free particles and then the interaction takes place in a time-ordered way. We use an equal-time wave function $\varphi(\mathbf{p})=\int\chi(\mathbf{p},p_0)dp_0$ and the ansatz of replacing $\phi(p_\mu)$ in (B.2) by a function $\phi(\mathbf{p})$ independent of p_0, *viz.*,

$$\chi(p_\mu)=\frac{1}{2\pi i}\left[\frac{1}{H_a(\mathbf{p})-\frac{1}{2}E-p_0}+\frac{1}{H_b(-\mathbf{p})-\frac{1}{2}E+p_0}\right]\phi(\mathbf{p}). \quad \text{(B.5)}$$

The function $\phi(\mathbf{p})$ will not describe the system in a fully relativistic way, since its ϕ_{+-} and ϕ_{-+} components will not appear in the resulting 3-dimensional equation. This can be seen by integrating both sides of (B.5) with respect to p_0,

$$\varphi(\mathbf{p})=\int\chi(p_\mu)dp_0=\phi_{++}(\mathbf{p})-\phi_{--}(\mathbf{p}) \quad \text{(B.6)}$$

so that

$$\varphi_{+-}(\mathbf{p})=\varphi_{-+}(\mathbf{p})=0.$$

This is one of the reasons that the definition (B.5) cannot be used as an ansatz in the Bethe-Salpeter equation to derive Dyson's equation.

In deriving an equal-time formalism from the Bethe-Salpeter equation the operation of integration over the relative energy variables must precede the use of the ansatz (B.5); namely, we must first integrate both sides of the Bethe-Salpeter equation with respect to p_0 to include the contributions from the free particle states. In this case the function $\phi_{++}(\mathbf{p})$ can be identified as a Tamm-Dancoff wave function.

We now proceed to the discussion of the 3-dimensional wave function $\phi_{++}(\mathbf{p})$. The Bethe-Salpeter equation for one-and-two meson interactions of two nucleons is

$$\chi(p_\mu)=-S_{Fa}(\tfrac{1}{2}K_\mu+p_\mu)S_{Fb}(\tfrac{1}{2}K_\mu-p_\mu)\beta_a\beta_b\int\beta_a\beta_b[I_2(p_\mu,p_\mu';K_\mu)+I_4(p_\mu,p_\mu';K_\mu)]\chi(p_\mu')d^4p', \quad \text{(B.7)}$$

where $I_2(p_\mu,p_\mu';K_\mu)$ and $I_4(p_\mu,p_\mu';K_\mu)$ represent the ladder and crossed diagrams given by

$$\beta_a\beta_bI_2(p_\mu,p_\mu';K_\mu)=\frac{G^2}{(2\pi^4)}\Gamma_i^a\Gamma_i^b\Delta_F(p_\mu-p_\mu'), \quad \text{(B.8)}$$

$$\beta_a\beta_bI_4(p_\mu,p_\mu';K_\mu)=\left[\frac{G^2}{(2\pi)^4}\right]^2\int\Delta_F(p_\mu-p_\mu'-k_\mu)\Delta_F(k_\mu)$$

$$\times\Gamma_i^a[H_a(\mathbf{p}'+\mathbf{k})-\tfrac{1}{2}E-p_0'-k_0]^{-1}\Gamma_j^a\Gamma_j^b[H_b(-\mathbf{p}+\mathbf{k})-\tfrac{1}{2}E+p_0-k_0]^{-1}\Gamma_i^bd^4k. \quad \text{(B.9)}$$

In order to derive an equation for $\phi_{++}(\mathbf{p})$ we replace $\chi(p_\mu)$ in (B.7) by the expressions

$$\chi_{++}(p_\mu)=\frac{1}{2\pi i}\frac{2A_p}{(A_p-p_0)(A_p+p_0)}\phi_{++}(\mathbf{p}), \quad A_p=E_p-\tfrac{1}{2}E, \tag{B.10}$$

leading to

$$\frac{1}{2\pi i}\frac{2A_p}{(A_p-p_0)(A_p+p_0)}\phi_{++}(\mathbf{p})=-\frac{\Lambda_+^a(\mathbf{p})\Lambda_+^b(-\mathbf{p})}{(A_p-p_0)(A_p+p_0)}\int\beta_a\beta_b[I_2(p_\mu,p_\mu';K_\mu)+I_4(p_\mu,p_\mu';K_\mu)]$$
$$\times\frac{2A_{p'}}{2\pi i(A_{p'}-p_0')(A_{p'}+p_0')}\phi_{++}(\mathbf{p}')d^3p'idP_0'. \tag{B.11}$$

Because the p_0-integration has to precede the use of the ansatz, the factors $(A_p-p_0)^{-1}$, $(A_p+p_0)^{-1}$ on both sides of the equation (B.11) will not be cancelled out. The 3-dimensional equation can, now, be obtained by integrating both sides of (B.11) with respect to p_0,

$$\phi_{++}(\mathbf{p})=-\Lambda_+^a(\mathbf{p})\Lambda_+^b(-\mathbf{p})\int\frac{2A_{p'}d^3p'}{2\pi i(A_p-p_0)(A_p+p_0)(A_{p'}-p_0')(A_{p'}+p_0')}$$
$$\times\beta_a\beta_b[I_2(p_\mu,p_\mu';K_\mu)+I_4(p_\mu,p_\mu';K_\mu)]\phi_{++}(\mathbf{p}')dp_0idp_0'. \tag{B.12}$$

In this equation the first term to be integrated with respect to p_0 and p_0' is

$$M_2=\frac{G^2}{(2\pi)^4}\frac{1}{2\pi}\Gamma_i^a\Gamma_i^b\int_{-\infty}^{\infty}\frac{2A_{p'}dp_0dp_0'}{(A_p-p_0)(A_p+p_0)(A_{p'}-p_0')(A_{p'}+p_0')(\omega_{p-p'}-p_0+p_0')(\omega_{p-p'}+p_0-p_0')}. \tag{B.13}$$

Usually one carries out the integration over p_0 in the complex plane of p_0 and the resulting expression can then be integrated over p_0' in the complex plane of p_0'. This is a long and tedious business. Actually, we can accomplish both integrations simultaneously if we note that, because of the small negative imaginary parts in A_p's and $\omega_{p-p'}$, the expression (B.13) can be written as

$$M_2=\frac{G^2}{(2\pi)^5}(i)^6\Gamma_i^a\Gamma_i^b\int_{-\infty}^{\infty}dp_0dp_0'\int_0^{\infty}d\alpha d\beta d\gamma d\delta d\mu d\nu 2A_{p'}\exp[-i\alpha(A_p-p_0)-i\beta(A_p+p_0)-i\gamma(A_{p'}-p_0')$$
$$-i\delta(A_{p'}+p_0')-i\mu(\omega_{p-p'}-p_0+p_0')-i\nu(\omega_{p-p'}+p_0-p_0')],$$
$$=\frac{G^2}{8\pi^3}(i)^6\Gamma_i^a\Gamma_i^b\int_0^{\infty}2A_{p'}d\alpha d\beta d\gamma d\delta d\mu d\nu\exp[-i(\alpha+\beta)A_p-i(\gamma+\delta)A_{p'}-i(\mu+\nu)\omega_{p-p'}]$$
$$\times\delta(\beta-\alpha+\mu-\nu)\delta(\gamma-\delta+\mu-\nu), \tag{B.14}$$

where α, β, γ, δ, μ, and ν are positive parameters. From the two δ-functions we have two linear algebraic equations,

$$\beta-\alpha+\mu-\nu=0, \quad \gamma-\delta+\mu-\nu=0. \tag{B.15}$$

The positive character of the parameters α, β, γ, δ, μ, and ν does not allow an arbitrary elimination of two of them from the integral in (B.14). Let

$$\beta-\alpha=\pm a, \quad \gamma-\delta=\pm b, \quad \mu-\nu=\pm c,$$

where a, b, and c are also positive. The signs for the set a, b, and c can be fixed by considering the 8 possible signs for the set a, b, and c. There are only two possible combinations that are consistent with the positive character of the 6 parameters, namely the combinations $(++-)$ and $(--+)$. The two solutions of (B.15) are, therefore,

$$\text{(i)}: \ \beta=\alpha+a, \quad \gamma=\delta+a, \quad \nu=\mu+a, \qquad \text{(ii)}: \ \alpha=\beta+a, \quad \delta=\gamma+a, \quad \mu=\nu+a. \tag{B.16}$$

Other solutions are thus excluded. By using the solutions (i) and (ii) in (B.14), we obtain the matrix elements

$$M_2=-2\frac{G^2}{8\pi^3}\Gamma_i^a\Gamma_i^b(i)^4\int_0^{\infty}2A_{p'}d\alpha'd\beta'd\gamma'd\delta'\exp[-i\alpha'(2A_p)-i\beta'(2A_{p'})-i\gamma'(2\omega_{p-p'})-i\delta'(A_p+A_{p'}+\omega_{p-p'})].$$

Hence

$$M_2=\frac{G^2}{8\pi^3}\Gamma_i{}^a\Gamma_i{}^b\frac{2}{(2E_p-E)(2\omega_{p-p'})(E-E_p-E_{p'}-\omega_{p-p'})}. \tag{B.17}$$

The second order equation is, therefore, given by

$$(E-2E_p)\phi_{++}(\mathbf{p})=\frac{G^2}{8\pi^3}\Lambda_+{}^a(\mathbf{p})\Lambda_+{}^b(-\mathbf{p})\Gamma_i{}^a\Gamma_i{}^b\int\frac{\phi_{++}(\mathbf{p}')d^3p'}{\omega_{p-p'}(E-E_p-E_{p'}-\omega_{p-p'})}. \tag{B.18}$$

For the fourth order case we use the Casimir projection operators in the second term of (B.11). We have altogether 4 terms to be integrated in the integrand of the second term, the first one of which is

$$M_4{}^{(1)}=\left[\frac{G^2}{(2\pi)^4}\right]^2\frac{1}{2\pi}\int 2A_{p'}O(\mathbf{p},\mathbf{p}';\mathbf{k})d^3kdp_0dp_0'dk_0$$
$$\times\frac{1}{(A_p-p_0)(A_p+p_0)(A_{p'}-p_0')(A_{p'}+p_0')(A_{p'+k}-p_0'-k_0)(A_{p-k}+p_0-k_0)}$$
$$\times\frac{1}{(\omega_k-k_0)(\omega_k+k_0)(\omega_{p-p'-k}-p_0+p_0'+k_0)(\omega_{p-p'-k}+p_0-p_0'-k_0)}, \tag{B.19}$$

where

$$O(\mathbf{p},\mathbf{p}';\mathbf{k})=\Lambda_+{}^a(\mathbf{p})\Lambda_+{}^b(-\mathbf{p})(\Gamma_i\Lambda_+(\mathbf{p}'+\mathbf{k})\Gamma_j)_a(\Gamma_j\Lambda_+(-\mathbf{p}+\mathbf{k})\Gamma_i)_b.$$

As before, the integrations over p_0, p_0', k_0 can be effected in accordance with the hole theory, so that (B.19) can be written as

$$M_4{}^{(1)}=\left[\frac{G^2}{(2\pi)^4}\right]^2\frac{(i)^{10}}{2\pi}\int 2A_{p'}O(\mathbf{p},\mathbf{p}';\mathbf{k})d^3kdp_0dp_0'dk_0\int_0^\infty d\alpha d\beta d\gamma d\delta d\epsilon d\lambda d\mu d\nu d\rho d\sigma\exp[-i\alpha(A_p-p_0)$$
$$-i\beta(A_p+p_0)-i\gamma(A_{p'}-p_0')-i\delta(A_{p'}+p_0')-i\epsilon(A_{p'+k}-p_0'-k_0)-i\lambda(A_{p-k}+p_0-k_0)-i\rho(\omega_k-k_0)$$
$$-i\sigma(\omega_k+k_0)-i\mu(\omega_{p-p'-k}+p_0-p_0'-k_0)-i\nu(\omega_{p-p'-k}+p_0'+k_0-p_0)]$$

or

$$M_4{}^{(1)}=\left[\frac{G^2}{8\pi^3}\right]^2(i)^{10}\int\int_0^\infty 2A_{p'}O(\mathbf{p},\mathbf{p}';\mathbf{k})d^3kd\alpha d\beta\cdots d\sigma\exp[-i(\alpha+\beta)A_p-i(\gamma+\delta)A_{p'}-i(\rho+\sigma)\omega_k$$
$$-i(\mu+\nu)\omega_{p-p'-k}-i\epsilon A_{p'+k}-i\lambda A_{p-k}]\delta(-\alpha+\beta+\lambda+\mu-\nu)\delta(-\gamma+\delta-\epsilon-\mu+\nu)$$
$$\times\delta(-\epsilon-\lambda-\mu+\nu-\rho+\sigma). \tag{B.20}$$

We have to eliminate 3 of the 10 parameters in the expression (B.20) by using the 3 linear algebraic equations for 10 unknowns,

$$\epsilon=(\delta-\gamma)+(\nu-\mu),\quad \lambda=(\alpha-\beta)+(\nu-\mu),\quad (\alpha-\beta)+(\delta-\gamma)+(\rho-\sigma)+(\nu-\mu)=0. \tag{B.21}$$

We put

$$\alpha-\beta=\pm a,\quad \delta-\gamma=\pm b,\quad \rho-\sigma=\pm c,\quad \nu-\mu=\pm d,$$

and then consider the 16 possible signs for the quantities a, b, c, and d. The only sets of signs consistent with the positive character of α, β, γ, δ, μ, ν, λ, ϵ, ρ, and σ are 6 in number and are given by the combinations $(++-+)$, $(++--)$, $(-+-+)$, $(--++)$, $(---+)$, and $(+--+)$, leading to the solutions:

(i)	(ii)	(iii)	(iv)	(v)	(vi)
$\alpha=\beta+a$,	$\alpha=\beta+\lambda+a$,	$\alpha=\beta+a$,	$\beta=\alpha+a$,	$\beta=\alpha+\epsilon+a$,	$\beta=\alpha+a$,
$\delta=\gamma+b$,	$\delta=\gamma+\epsilon+a$,	$\gamma=\delta+b$,	$\delta=\gamma+b$,	$\gamma=\delta+\lambda+a$,	$\gamma=\delta+b$,
$\sigma=\rho+a+b+c$,	$\sigma=\rho+\epsilon+\lambda+a$,	$\sigma=\rho+\epsilon+a$,	$\sigma=\rho+\lambda+b$,	$\rho=\sigma+a$,	$\sigma=\rho+c$,
$\nu=\mu+c$,	$\mu=\nu+a$;	$\nu=\mu+\epsilon+b$,	$\nu=\mu+\lambda+a$,	$\nu=\mu+\epsilon+\lambda+a$;	$\nu=\mu+a+b+c$,
$\epsilon=b+c$,		$\lambda=\epsilon+a+b$;	$\epsilon=\lambda+a+b$;		$\lambda=b+c$,
$\lambda=a+c$;					$\epsilon=a+c$.

On using these in (20), we obtain $M_4^{(1)}$ as a sum of 6 matrix elements:

$$M_4^{(1)}=\left[\frac{G^2}{8\pi^3}\right]^2\frac{1}{2E_p-E}\int\frac{O(\mathbf{p},\mathbf{p}',\mathbf{k})d^3k}{2\omega_k 2\omega_{p-p'-k}}$$
$$\times\Bigg[\frac{1}{(E_p+E_{p-k}+\omega_k-E)(E_{p'}+E_{p'+k}+\omega_k-E)(E_{p'+k}+E_{p-k}+\omega_k+\omega_{p-p'-k}-E)}$$
$$\times\frac{1}{(E_p+E_{p'}+\omega_{p-p'-k}+\omega_k-E)(E_p+E_{p-k}+\omega_k-E)(E_{p'}+E_{p'+k}+\omega_k-E)}$$
$$\times\frac{1}{(E_p+E_{p-k}+\omega_k-E)(E_{p'}+E_{p-k}+\omega_{p-p'-k}-E)(E_{p-k}+E_{p'+k}+\omega_k+\omega_{p-p'-k}-E)}$$
$$\times\frac{1}{(E_p+E_{p'+k}+\omega_{p-p'-k}-E)(E_{p'}+E_{p'+k}+\omega_k-E)(E_{p-k}+E_{p'+k}+\omega_{p-p'-k}+\omega_k-E)}$$
$$+\frac{1}{(E_p+E_{p'}+\omega_{p-p'-k}+\omega_k-E)(E_p+E_{p-k}+\omega_{p-p'-k}-E)(E_{p'}+E_{p-k}+\omega_{p-p'-k}-E)}$$
$$+\frac{1}{(E_p+E_{p'+k}+\omega_{p-p'+k}-E)(E_{p'}+E_{p-k}+\omega_{p-p'-k}-E)(E_{p-k}+E_{p'+k}+\omega_k+\omega_{p-p'-k}-E)}\Bigg]. \quad \text{(B.22)}$$

These are just the no-pair terms of the old Tamm-Dancoff method, so that each of the above solutions corresponds to a Feynman diagram.

The remaining 3 terms of the second term of (B.10) can be treated in the same manner, each giving 6 matrix elements. Altogether the crossed diagram corresponds to 24 Tamm-Dancoff diagrams. The method can be applied to the iterated ladder and the results will come out in the form of reducible and irreducible terms. Finally, we note that the above method of integration can be generalized to more complicated cases.

Letters to the Editor

PUBLICATION of brief reports of important discoveries in physics may be secured by addressing them to this department. The closing date for this department is five weeks prior to the date of issue. No proof will be sent to the authors. The Board of Editors does not hold itself responsible for the opinions expressed by the correspondents. Communications should not exceed 600 words in length and should be submitted in duplicate.

Environmental Effect on Atomic Hydrogen Hyperfine Structure in Acids*

HENRY ZELDES AND RALPH LIVINGSTON

Chemistry Division, Oak Ridge National Laboratory, Oak Ridge, Tennessee

(Received October 29, 1954)

PARAMAGNETIC resonance absorption lines of atomic hydrogen have been observed[1] in $HClO_4$, H_2SO_4, and H_3PO_4 after irradiation with Co^{60} gamma rays at 77°K. In the course of re-examining some samples showing very intense lines in these acids relatively weak satellite lines have been observed. Figure 1 shows the high-field atomic hydrogen line and these satellites for irradiated $HClO_4$ at a microwave frequency of about 23 050 Mc/sec. The main line can be readily power-saturated, causing the ratio of satellite to main line intensity to increase. The low-field hydrogen line as well as the pair of hydrogen lines in irradiated H_2SO_4 and H_3PO_4 show essentially similar satellites.

The spacing of satellite to main line is field-dependent, and within our present accuracy of measurement corresponds to the proton magnetic resonance frequency. For example, the high-field $HClO_4$ central line of Fig. 1 appeared at a measured field of 8482.8 gauss with the satellites spaced at ±12.9 gauss. At the microwave frequency of 23 050 Mc/sec this corresponds to a spacing in frequency units of ±35.1 Mc/sec and is, within our experimental error, the same as the proton magnetic resonance frequency at this field, 36.12 Mc/sec. The low-field hydrogen line appeared at 7980.6 gauss with ±11.95 gauss or ±34.5 Mc/sec separated satellites which compares favorably with the proton frequency of 33.98 Mc/sec for this field. The results for the other two acids were similar. Observations were also made with a spectrometer operating at a nominal frequency of 9000 Mc/sec. The satellites could just be revolved in the three acids, and in the one preliminary measurement made on the high-field line in H_2SO_4 appearing at 3428.8 gauss and 8945 Mc/sec the satellites were spaced at ±4.6 gauss or ±12 Mc/sec to be compared with a proton resonance frequency of 14.60 Mc/sec.

These lines seem to originate from the flipping of nearby proton spins in conjunction with the flipping of the electron spin as a consequence of a weak magnetic dipole-dipole coupling. Calculations made by George Trammell using this model gave a reasonable intensity ratio of center to satellite line for a reasonable distance to neighboring proton. The intensity ratio varies essentially as the inverse sixth power of the distance making an accurate calculation of the distance possible. The final value awaits the evaluation of several integrals. The observed intensity ratio in $HClO_4$ at low power levels is roughly 35:1 which gives a preliminary value for this distance of 1.8A. This ratio may represent a single proton at this value or more than one at greater distances. Although these results are highly preliminary, we are inclined to interpret the ratio as representing the effect of more than one proton distributed more or less randomly in the chemical sample at distances usually greater than 1.8 A. It should be pointed out that the satellite separation is strikingly insensitive to variation in this distance, and an averaging over a distribution of distances as well as over all angular orientations of a powdered sample does not give a smudging of the satellites.

FIG. 1. The high-field atomic hydrogen line in $HClO_4$ at 23 050 Mc/sec. and 8483 gauss with progressively increasing microwave power from top to bottom.

In addition to the saturation effect illustrated for $HClO_4$ in Fig. 1, H_2SO_4 and H_3PO_4 showed another interesting effect. The satellite on one side of the central line was always much weaker than on the other side. The weak-satellite side was always the trailing side for the direction of the magnetic field sweep in the field-modulated spectrometer. In other words, in these two acids the strength of the satellite depends on how recently a moderate amount of power has been applied to effect the main transition. We presume this means that the thermal relaxation time is longer than in $HClO_4$, and by varying the sweep rate we may vary the relative intensity of the trailing-side satellite.

These experiments, along with more detailed calculations on the satellite transition probabilities, are continuing and will be reported in greater detail later.

We are particularly grateful to George Trammell for his help.

* This work was performed for the U. S. Atomic Energy Commission.

[1] Livingston, Zeldes, and Taylor, Phys. Rev. **94**, 725 (1954).

Observation of Paramagnetic Resonances in Single Crystals of Barium Titanate

A. W. HORNIG AND E. T. JAYNES, *Department of Physics, Stanford University, Stanford California*

AND

H. E. WEAVER, *Varian Associates, Palo Alto, California*

(Received October 25, 1954)

PARAMAGNETIC resonances consisting of several components have been observed at microwave frequencies in single crystals of barium titanate,[1] which contain small amounts of iron. Figure 1 illustrates the nature of the observed lines obtained at room temperature from a single crystal polarized in a direction perpendicular to the plane of the crystal, and to the direction of the dc and rf magnetic fields. Approximate g values, at 9.5 kMc/sec and room temperature, of the four observable components were 3.52, 2.72, 2.41, 1.79. Preliminary measurements indicate a variation with temperature in both the amplitudes and positions of the quartet. These approximate measurements are summarized in graph form in Fig. 2. The structure of the resonance changes radically at the Curie temperature (~120°C) indicating the occurrence of the tetragonal-cubic phase transition. Finer details of the growth and decay of the paramagnetic resonances at the region of the Curie temperature (not shown in Fig. 2) suggest that the transition of any domain in the crystal is discontinuous but that the crystal as a whole does not change structure at one temperature. Such effects may be caused by crystal imperfections or the existence of a temperature gradient over the crystal. Quantitative measurements of the resulting signals at the Curie temperature were complicated by the lossy nature of the sample at microwave frequencies.

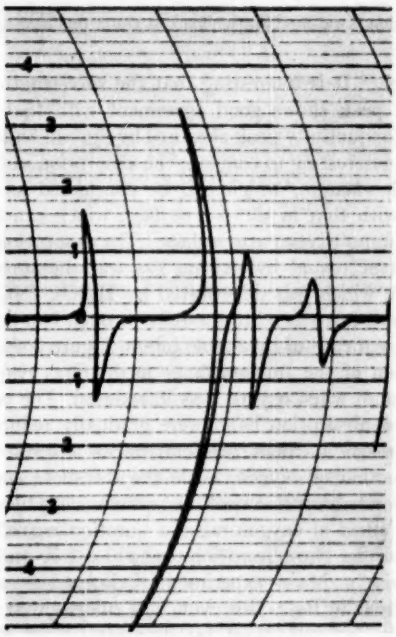

FIG. 1. The above reproduction illustrates typical signals obtained from $BaTiO_3$ crystals, in the ferroelectric state corresponding to room temperature, and polarized perpendicular to the direction of the dc magnetic field produced by the V-4007 Electromagnet and V-2200 Power Supply. The resonant frequency of the V-260 Klystron was set at 9.5 kMc/sec.

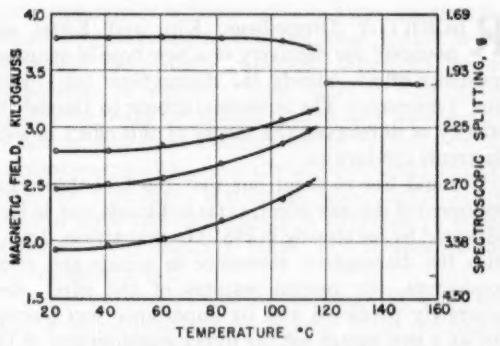

FIG. 2. Graphical representation of the change in the relative positions of the structure with temperature. A single detectable line at $g=2.0$ results from the cubic phase of barium titanate.

As the temperature is lowered below about 0°C, barium titanate crystals undergo a phase transition involving a change in direction of polarization resulting in orthorhombic symmetry. Signals observed below this transition temperature show a marked change from those obtained at room temperature. In particular, they consist of two principal lines easily resolved and located approximately symmetrically about a g value of two, and superimposed upon a background of unresolved information.

It is assumed that the small amount of iron (added to the pre-melt mixture in the form of Fe_2O_3) is acting as the source of the electron resonances, since other crystals of essentially pure $BaTiO_3$ do not yield a detectable electron resonance. The ferric ion, with a $^6S_{5/2}$ basic level, would be expected to give crystalline field splittings much smaller than those observed. It is believed therefore, that the electron resonances result from ferrous ions ($^5D_4$ basic level), probably located at the barium position in the lattice. Further experimental and theoretical work designed to identify the states involved is underway.

The authors wish to express their thanks to Professor G. Pake and Dr. H. R. Sands of Stanford University for helpful discussions.

[1] Supplied through the courtesy of Dr. S. O. Morgan at Bell Telephone Laboratories, Murray Hill, New Jersey.

Diamagnetic Resonance in Electronic Conductors

J. G. DORFMAN
Leningrad, Russia
(Received October 7, 1954)

RECENTLY Dresselhaus, Kip, and Kittel announced[1] the discovery of a new type of quantum resonance effect, namely the diamagnetic (or "cyclotron") resonance. The authors attribute to Dingle[2] the priority of developing the theory of this effect in solid electronic conductors.

I should like to point out that the first theoretical treatment of this new effect, as far as I know, was, in fact, advanced by me already in 1951.[3] In that article, dealing with the diamagnetic resonance in metals and semiconductors, the general features of the effect were accurately predicted and its importance was pointed out as a new means for the direct measurement of the effective mass of the carriers.

[1] Dresselhaus, Kip, and Kittel, Phys. Rev. **92**, 827 (1953).
[2] R. B. Dingle, Proc. Roy. Soc. (London) **A212**, 38 (1952).
[3] J. G. Dorfman, Doklady Akad. Nauk S.S.S.R. **81**, 765 (1951).

Ultraviolet Absorption in Barium Oxide Films

KOJI OKUMURA *
Research Laboratory of Nippon Electric Company, Kawasaki City, Japan
(Received October 25, 1954)

OPTICAL absorption in BaO films evaporated on quartz tubes from BaO coatings was measured in the wavelength region between 2100A and 3500A. The structure of the experimental tubes used in these measurements is illustrated in Fig. 1. The film was evaporated on one side of the quartz wall from the coating which was activated thermally beforehand for about one hour. Particular caution was taken for the evacuation of the tubes, so the measured absorption curves were almost stable.

Sproull and Tyler[1,2] reported the presence of two distinct absorption bands in BaO; the first one exists in the energy region between 3.8 ev and 4.8 ev, and the second one, of shorter wavelength, begins at 4.8 ev. The former with accompanying photoconduction was assumed by them to be exciton absorption, while the latter was ascribed to band-to-band excitation.

The results of the present measurements were similar to theirs; that is, the threshold energy of the first absorption is 3.95 ev and the second absorption threshold is 4.95 ev. However, precise plotting of the transmittance *versus* wavelength at intervals of 2A or 5A made it possible to distinguish two peaks in the first absorption band, existing at 4.1 ev and 4.4 ev respectively.[3] It is interesting that the wavelength of the former peak shows good agreement with that of the photoconductivity peak obtained by Sproull and Tyler.[2]

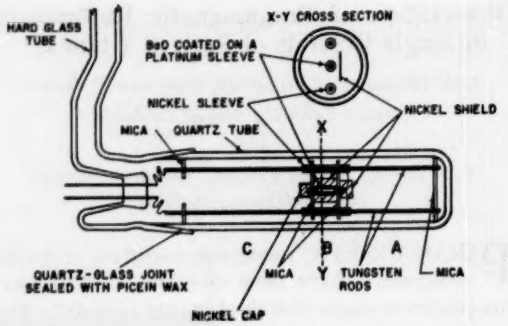

FIG. 1. The structure of the experimental tubes. The tube was evacuated to a pressure less than 1×10^{-6} mm Hg and baked by a gas flame for about one hour except for the wax joint, which was cooled by running water during the baking process; then getter was flashed in a getter chamber. The cathode mount is movable along the tungsten rods. The decomposition and activation of the cathode were carried out at position *A* and evaporation at position *B*. Position *C* was used for the blank in absorption measurements.

It is interesting to compare the absorption in the film in high vacuum, which can be considered as *n*-type BaO, with that in the *p*-type film, which can be produced in an oxygen atmosphere.[4] The absorption in the films deactivated by oxygen gas was measured. The oxygen, which was dehydrated by H_2SO_4, $CaCl_2$, and P_2O_5, was introduced to the tube through two liquid air traps by means of breakable joints. Figure 2 shows the variation of the transmittance in the films evaporated in vacuum when oxygen was introduced. The peaks of the first absorption band were gradually reduced and disappeared at room temperature as a result of the introduction of oxygen, while the threshold energy of the second absorption remained uninfluenced by oxygen.

The effect of oxygen raises a question regarding the origin of the two absorption peaks at 4.1 ev and 4.4 ev respectively. Many experiments indicate the existence of excitons in BaO. However, it is evident that the exciton is not influenced by deactivation of BaO by oxygen. Accordingly, as far as the effect of the oxygen is

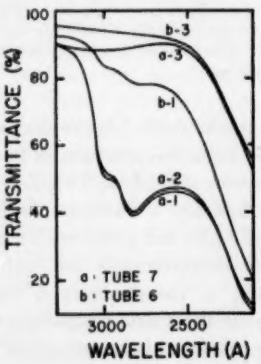

FIG. 2. Variation of the transmittance *versus* wavelength curves in two BaO films when oxygen was introduced at pressure of about 10 mm Hg: $a-1$ and $b-1$ show the curves measured in vacuum; $a-2$ shows the curve measured just after the introduction of oxygen; $a-3$ and $b-3$ show the curves measured after more than 10 hours in an oxygen atmosphere.

concerned, it is more reasonable to attribute these peaks to the electronic transition occurring at the donor energy levels than to the excitons. On the other hand, there are some reasons which make it difficult to consider that these peaks are a structure-sensitive property as was indicated by Sproull and Tyler; that is, large absorption constant and small temperature shift.

The author intends to continue this work. He wishes to express his gratitude to Dr. Y. Ishikawa, Research Laboratory of Nippon Electric Company, under whom this work was undertaken.

* Now in the Department of Physics, University of Missouri, Columbia, Missouri.

[1] W. W. Tyler and R. L. Sproull, Phys. Rev. **83**, 548 (1951); W. W. Tyler, Phys. Rev. **76**, 1887 (1949).

[2] R. L. Sproull and W. W. Tyler, in *Semiconducting Materials* (Butterworths Scientific Publications, London, 1951), p. 122.

[3] After this work was performed, the author received a communication from Dr. Sproull that R. J. Zollweg of Cornell University has found similar peaks in this region.

[4] Ishikawa, Sato, Okumura, and Sasaki, Phys. Rev. **84**, 371 (1951).

Mechanism for Photovoltaic and Photoconductivity Effects in Activated CdS Crystals

D. C. Reynolds, *Aeronautical Research Laboratory Wright Air Development Center, Air Research and Development Command, United States Air Force, Wright-Patterson Air Force Base, Ohio*

AND

S. J. Czyzak, *Physics Department, University of Detroit, Detroit, Michigan*

(Received September 17, 1954)

In previous papers,[1,2] experimental results with activated CdS crystals were reported that could be explained by the Brosser-Kallmann-Warminsky theory of conduction.

Brosser, Kallmann, and Warminsky[3] suggest two possible mechanisms which can explain conduction in activated crystals: (a) They propose that the holes formed by excitation are localized in the filled band and cannot migrate to the electrodes; as long as this is the case, electrons in the conduction band can be in thermal potential equilibrium with the electrodes. This permits a re-supply of electrons from the cathode. The conductivity then depends on the number of bound holes and on the length of time the holes are localized. (b) They apply the Riehl-Schön model. Here it is assumed that part of the excited electrons pass into a band which is somewhere between the conduction band and the filled band and in which the electrons can move freely. The electron density in this band is in thermal potential equilibrium with the electrodes and electrons remain in this band for a relatively long time. As long as there are sufficient electrons in this band, additional electrons can pass from the electrodes. During this period, metallic conduction is possible.

Recent investigation of the spectral response of the photovoltaic effect in activated CdS single crystals[2] shows a response in the red portion of the spectrum. Photoconductivity measurements as a function of wavelength show two peaks: one at the absorption cutoff and the other in the longer-wavelength region. When the photoconductivity is measured from short wavelengths toward long wavelengths and *vice versa*,[1] a shift in the position of the peaks is observed. When the photoconductivity is measured from short to long wavelengths, the peaks are shifted toward long wavelengths because of long-lived electrons in the impurity band; this also causes a tailing out in the long-wavelength region. When the experiment is reversed, photocurrent is not observed until sufficient energy is available to excite electrons to the impurity band; this diminishes the long-wavelength tail.

The energy separation of the bands in CdS would not give rise to the photovoltaic response in the red region mentioned above. The excitation of electrons in impurity levels below the conduction band by light of wavelengths in the red and near infrared could explain the spectral response by allowing a two-step process to the conduction band; however, this would not explain the photoconductivity.

These long lifetimes cannot be explained by the above-mentioned two-step excitation process unless we assume that the holes are fixed. If this were the case, the photovoltaic effect would not be observed. Therefore, to be consistent with both photovoltaic and photoconductivity effects, it appears that the intermediate energy level must be a band. This conforms to the Riehl-Schön model.

[1] Reynolds, Czyzak, Allen, and Reynolds (to be published).

[2] Reynolds, Leies, Antes, and Marburger, Phys. Rev. **96**, 533 (1954).

[3] Brosser, Kallmann, and Warminsky, Z. Naturforsch. **4A**, 631 (1949).

Electronic Susceptibility in Certain Alloys*

E. N. Adams, II, and R. Zitter

Chicago Midway Laboratories, Chicago, Illinois

(Received October 18, 1954)

In recent measurements of magnetic susceptibility *vs* composition in the $MgCu_2-MgZn_2$ system (Fig. 1), Klee and Witte[1] have discovered some interesting features in the dependence of susceptibility on electron concentration, and have analyzed the experimental results using the model of nearly free electrons moving in a weak cosine potential. In particular they attribute the two peaks on the left part of the experimental cuve of Fig. 1 to anomalies in the orbital magnetism of the valence electrons associated with the successive touching of the Fermi surface to the two kinds of faces of the

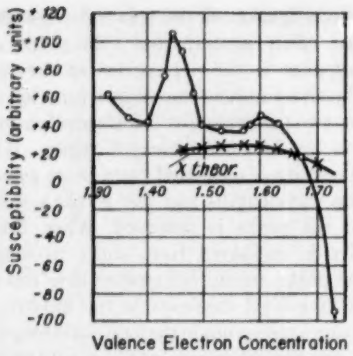

FIG. 1. Valence electron contribution to room-temperature magnetic susceptibility of $MgCu_2$–$MgZn_2$ system (after Fig. 5 of Klee and Witte). χ_{theor} represents the susceptibility of a free electron gas.

higher Brillouin zone of Fig. 2. The purpose of this note is to point out that if one takes such a treatment seriously, the experimental curve actually provides direct evidence of the strong effect of band-band interaction on the electron susceptibility.

For the simple model used by Klee and Witte, all contributions to the orbital susceptibility can be calculated to good accuracy.[2] It is not difficult to show that when the Fermi surface is near a single kind of zone face the nearly free electron model yields (for cubic symmetry):

$$\chi=\chi_0+\chi_1+\chi_3, \tag{1}$$

$$\chi_1=\tfrac{2}{3}N\chi_0\{1-[1-(1/s^2)]^{\frac{1}{2}}\} \qquad (s\leqslant -1) \tag{2a}$$

$$=\tfrac{2}{3}N\chi_0 \qquad (-1\leqslant s\leqslant 1), \tag{2b}$$

$$\chi_3=\tfrac{1}{2}N\chi_0\{s\sin^{-1}(1/s)-3+(5/3)[1-(1/s^2)]^{\frac{1}{2}} +\tfrac{2}{3}s^2(1-[1-(1/s^2)]^{\frac{1}{2}})\} \qquad (s\leqslant -1) \tag{3a}$$

$$=\tfrac{1}{2}N\chi_0\{-\tfrac{1}{2}\pi s-3+\tfrac{2}{3}s^2\} \qquad (-1\leqslant s\leqslant 1). \tag{3b}$$

Here χ_0 is the susceptibility of a free electron gas of the given electron concentration, N is the number of equivalent pairs of zone faces, χ_1 and χ_3 are defined in reference 2, $\chi_0+\chi_1$ gives the total electronic susceptibility in the Peierls[3] approximation, χ_3 is the contribution to χ from the band-band interaction, and s is a dimensionless parameter which measures the difference between the Fermi energy and the energy at the zone faces in units of half the minimum energy gap between bands. The Fermi surface touches the zone face for $s=-1$ and overlaps it for $s=+1$.

Figure 3 shows the behavior of the theoretical susceptibility as the Fermi surface is brought up to a zone face. Curve (1) shows the susceptibility $\chi_0+\chi_1$, curve (2) χ_3, and curve (3) the total susceptibility. It is evident from Fig. 1 that the experimental behavior is like that of curve (3) and not at all like that of curve (1), so the susceptibility contribution χ_3 is qualitatively very important.

Our formulas (2–4) indicate that in the very nearly free electron model the ratio of the peak susceptibility to the free electron susceptibility is independent of the width of the energy gap. Putting $N=12$ (for the large zone faces), we get for this ratio a value of 4.5, in excellent agreement with the height of the first observed peak. Similarly, with $N=4$ (for the small faces), we get a value 2.2 which agrees well with the height of the

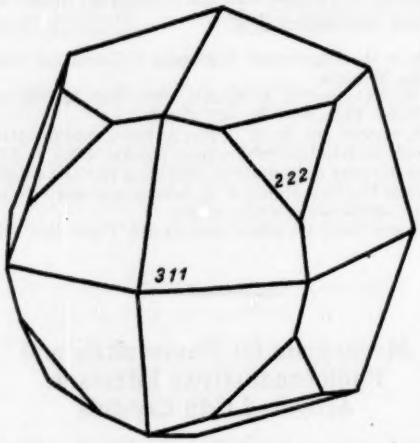

FIG. 2. Higher Brillouin zone formed from planes (3,1,1) and (2,2,2) (after Klee and Witte).

second peak, although actually our formulas would not be expected to apply to parts of the curve very much to the right of the first peak.

In view of the basic complexity of the susceptibility problem the quantitative success of our theory should

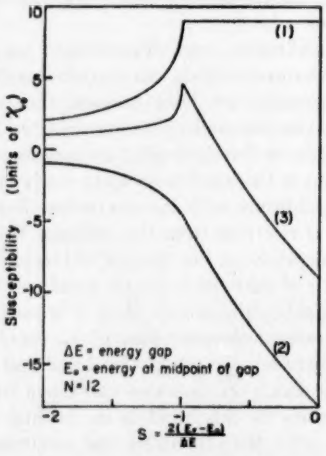

FIG. 3. Theoretical valence electron susceptibility calculated on nearly free electron model. The susceptibility is shown over a range of concentrations about that for which the Fermi surface touches a single zone face. s measures the deviation of the Fermi energy from the midpoint of the energy gap.

not be stressed unduly. Nevertheless, while maintaining strong reservations of judgement because of our very literal application of the nearly free electron model, we are inclined to view the results of Klee and Witte as providing an experimental demonstration of the great strength of band-band interaction in influencing the magnetic properties of electrons in metals.

* This research was supported in part by the United States Air Force.

[1] H. Klee and H. Witte, Z. Phys. Chem. **202**, 352 (1954).
[2] E. N. Adams, II, Phys. Rev. **89**, 633 (1953).
[3] R. Peierls, Z. Physik. **80**, 763 (1933).

Quantum Statistics of Closed and Open Systems

F. ANSBACHER AND P. T. LANDSBERG

Department of Natural Philosophy, University of Aberdeen, Scotland

(Received November 1, 1954)

THE exact mean occupation numbers for an ideal Fermi-Dirac or Bose-Einstein gas on the basis of a canonical ensemble are respectively given by[1,2]

$$n(N,j)=1\Big/\left\{\frac{Z_{N+1}}{Z_N}\frac{n(N+1,j)}{n(N,j)}\exp\eta(j)\pm 1\right\}$$

$$(\text{all } j, \text{ all } N,\ T>0). \quad (1)$$

$\eta(j)$ is the energy divided by nT of the jth quantum state and Z_N is the partition function if N particles are in the volume V. It has been shown[3,4] that these expressions go over into those which are obtained on the basis of a grand canonical ensemble under those limiting conditions for which

$$n(N+1,j)/n(N,j)\sim 1 \ (\text{all } j,\ T>0), \quad (2)$$

where $\sim$ denotes an equality for the limiting case. It has been pointed out[3,4] that condition (2) should hold if the system is infinitely large, but has a finite and nonzero volume density of particles (the "limit L"). The proof of this statement was made to depend on the inequalities

$$n(N+1,j)/n(N,j)>1 \ (\text{all } j, \text{ finite } N,\ T>0), \quad (3)$$

which hold for Fermi-Dirac[3] and Bose-Einstein[5] systems. But the argument employed was not rigorous.[6]

In fact, let

$$n(N+1,j)/n(N,j)=1+\alpha(N,j),$$

$$\alpha(N,j)>0 \ (\text{all } j, \text{ all } N); \quad (4)$$

then

$$\textstyle\sum_j \alpha(N,j)n(N,j)=1. \quad (5)$$

It is easy to see from (5) that $\alpha\leqslant 1/N$ for *some* (or possibly all) quantum states, so that (2) may hold as $N\to\infty$, whatever the volume V of the system, However, (5) does not ensure that (2) holds for *all* quantum states, though this now becomes a reasonable conjecture. The argument which was previously used fails now because the inequality $n(N+1,j)/n(N,j)$ $\sum_k n(N+1,k)/\sum_k n(N,k)$ does not necessarily hold for all states j.

We therefore consider it worth while to give an independent and rigorous argument which leads to (2) in the limit L. In the Fermi-Dirac case we use (3) and the result[2]

$$n(N+1,j)=(Z_N/Z_{N+1})[1-n(N,j)]\exp[-\eta(j)]. \quad (6)$$

Replacing first $n(N+1,j)$ by $n(N,j)$ on the left, and then $n(N,j)$ by $n(N+1,j)$ on the right, we find

$$\cdots>n(N+1,j)>\mu(N,j)>n(N,j)$$

$$>\mu(N-1,j)>\cdots, \quad (7)$$

where

$$\mu(N,j)\equiv 1/[1+(Z_{N+1}/Z_N)\exp\eta(j)]. \quad (8)$$

For all limiting processes for which $Z_{N+1}/Z_N\sim Z_N/Z_{N-1}$ we must have $n(N,j)\sim\mu(N,j)$. Comparison of (8) and (1) shows then that (2) holds.

In the Bose-Einstein case no relation of type (7) can be found which has equal generality, and one must proceed in a different way. The basic recurrence relation is in this case[5]

$$x_{N+1}a_{N+1}=a_N+1-(1/x_N), \quad (9)$$

where $x_N\equiv n(N,j)/n(N-1,j)$, $a_N\equiv(Z_N/Z_{N-1})\exp\eta(j)$. For all limiting processes for which $a_{N+1}\sim a_N$ ($\sim a$ say) and $x_{N+1}\sim x_N$ ($\sim x$ say), one finds that x must be a solution of $ax^2-(a+1)x+1\sim 0$, whence $x\sim 1$ or $1/a$. The last possibility is ruled out since $x_N>1$, $a_N>1$ for all j and finite N. Hence (2) must hold again in these cases. It remains to discuss the various limiting relations whose existence has been assumed in the above argument.

For Fermi-Dirac systems the relation Z_{N+1}/Z_N $\sim Z_N/Z_{N-1}$ is valid in the limit L (and possibly for other limiting processes). Let

$$P\equiv V^{-1}\textstyle\sum_j\mu(N,j), \quad Q\equiv V^{-1}\sum_j\mu(N-1,j),$$

$$\epsilon\equiv 1-\frac{Z_{N+1}/Z_N}{Z_N/Z_{N-1}}, \quad 0\leqslant\epsilon\leqslant 1,$$

$$c_j\equiv\frac{\epsilon(Z_N/Z_{N-1})\exp\eta(j)}{1+(Z_N/Z_{N-1})\exp\eta(j)}.$$

Then

$$VP=\textstyle\sum_j[1+(Z_N/Z_{N-1})\exp\eta(j)]^{-1}[1-c_j]^{-1},$$

and

$$\frac{1}{1-c_j}\geqslant 1+\frac{\epsilon Z_N/Z_{N-1}}{1+(1-\epsilon)Z_N/Z_{N-1}}.$$

Now by (7), $(N+1)/V>P>N/V>Q>(N-1)/V$, so that $Q=(N-\alpha)/V$, $0<\alpha<1$. These relations give rise to

$$\frac{N+1}{V}>Q+\left(\frac{N-\alpha}{V}\right)\frac{\epsilon Z_N/Z_{N-1}}{1+(1-\epsilon)Z_N/Z_{N-1}}$$

$$>Q>\frac{N-1}{V}. \quad (10)$$

It follows that in the limit L, $\epsilon Z_N/Z_{N-1}\to 0$. This proves our statement.

For Bose-Einstein systems, we use[5]

$$(1+1/N)(Z_{N+1}/Z_N)>Z_N/Z_{N-1}>Z_{N+1}/Z_N. \quad (11)$$

Thus for all limiting processes for which N tends to infinity $Z_{N+1}/Z_N\sim Z_N/Z_{N-1}$, and therefore relations $a_{N+1}\sim a_N$ hold.

To establish relations of the type $x_{N+1}\sim x_N$ for Bose-Einstein systems, one can use an argument of the type given in Sec. 4 of Fraser's paper. If M be a positive integer smaller than N, one first notes that

$$R(N,M)\equiv\sum_{r=M+1}^{\infty}a_N^{-r}-\sum_{r=M+1}^{N}\frac{Z_{N-r}}{Z_N}\exp(-r\eta_j)$$

$$<a_N^{-M}(a_N-1). \quad (12)$$

Hence

$$n(N,j)>b_M(1-a_N^{-M})/(a_N-1),$$

where $b_M\equiv(N-1)(N-2)\cdots(N-M+1)N^{-r+1}$. Since $x_{N+1}=(1/a_{N+1})\{1+[1/n(N,j)]\}$, it follows that

$$a_N/a_{N+1}<x_{N+1}<\frac{1}{a_{N+1}}\left[1+\frac{1}{b_M}\frac{a_N-1}{1-a_N^{-M}}\right]. \quad (13)$$

The first inequality follows immediately from (9). Let M go to infinity with N, but more slowly than $\sqrt{N}$, so that[6] $b_M\to 1$. It now follows from (13) that for all limiting processes for which $N\to\infty$, $x_{N+1}\to a_N/a_{N+1}$ whether $a_N\to 1$ or $a_N\to a>1$. By (11), $a_N/a_{N+1}=1+\gamma/N$ where $0<\gamma<1$. Hence relations $x_N\sim x_{N+1}$ hold for all limiting processes of this type, and, in particular, for the limit L. Fraser's restrictions on the nature of the single-particle energy spectrum are not required.

For $T=0$ the mean occupation numbers can be calculated exactly from (1) by evaluating $(Z_{N+1}/Z_N)\times\exp\eta(j)$ directly. The results agree with those obtained from the grand canonical ensemble.

[1] T. Sakai, Proc. Phys. Math. Soc. (Japan) **22**, 193 (1940).
[2] F. Ansbacher and W. Ehrenberg, Phil. Mag. **40**, 626 (1949).
[3] P. T. Landsberg, Proc. Cambridge Phil. Soc. **50**, 65 (1954).
[4] P. T. Landsberg, Phys. Rev. **93**, 1170 (1954).
[5] A. R. Fraser, Phil. Mag. **42**, 165 (1951).
[6] We are grateful to Dr. R. Nozawa of the Tokyo Institute of Technology for drawing our attention to this fact.

Use of *p-n* Junctions for Solar Energy Conversion

E. S. Rittner

Philips Laboratories, Irvington-on-Hudson, New York

(Received October 25, 1954)

THE recent discovery[1] that silicon *p-n* junction photovoltaic cells possess a nearly tenfold higher efficiency for solar energy conversion than photocells previously available has reawakened interest in this type of device. Cummerow[2] has presented a theory of the photovoltaic effect in a *p-n* junction cell with monochromatic radiation incident in a direction normal to the plane of the junction and has also made as estimate of the efficiency to be expected from the use of a silicon cell in solar energy conversion.[3] Similar calculations by the writer[4] lead to conclusions substantially identical to those arrived at by Cummerow with one exception. For maximum power conversion efficiency we propose the use of a semiconductor with an energy separation in the neighborhood of 1.5–1.6 ev in preference to Cummerow's choice of a "gap energy somewhere near the photon energy characteristic of the peak of the solar spectrum, i.e., 2 ev."

The basis for this conclusion may be found in Fig. 1 which shows a plot of conversion efficiency (neglecting surface reflection losses and ohmic losses within the cell, and assuming that the depth of the junction below the illuminated surface is small compared to a diffusion length) as a function of band separation for several values of donor and acceptor densities ($N_d=N_a=10^{15}$, 10^{17}, $10^{19}/\text{cm}^3$). The plot is based upon computations performed for germanium ($\Delta E=0.7$ ev), silicon (1.0 ev), aluminum antimonide (1.6 ev) and for a hypothetical substance with a band separation of 2.0 ev. The values taken for the diffusion constants and lifetimes in germanium and silicon are the same as those employed by Cummerow[2,3] and values equal to those of silicon have been assumed for the remaining substances. Fortunately

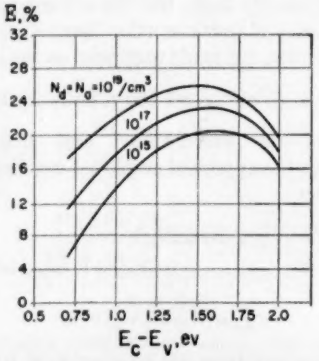

FIG. 1. Computed conversion efficiency *vs* band separation for several values of donor and acceptor density. Load resistance chosen for maximum power output.

the conversion efficiency is quite insensitive to the choice of numerical values of these parameters. The solar spectrum has been approximated by the distribution from a black body at a temperature of 5760°K with an integrated intensity at the earth's surface of 0.1 watt/cm^2.

Note that the conversion efficiency increases with the degree of doping because of an increase in the height of the potential barrier; that the band separation best matching the solar spectrum is, as noted above, 1.5–1.6 ev; and that the maximum obtainable efficiency (assuming that the saturation solubility of donors and acceptors is of the order of 10^{19}/cm^3) is roughly twenty five percent, corresponding to a power output of about 250 watts/meter^2 in full sunlight. A slight further increase in efficiency may be realized with the use of an optical collection system which increases the radiation intensity at the photocell surface. Note in addition that silicon is clearly a better choice for the present purpose than other materials that have been proposed[2,5,6] such as germanium and cadmium sulfide ($\Delta E = 2.4$ ev) but that silicon is in turn surpassed by aluminum antimonide. The superiority of AlSb over Si with respect to conversion efficiency would prevail even if the minority carrier lifetimes were lower by several orders of magnitude in the former material. The possibility of substantially improving the efficiency of experimental units over that heretofore realized[1] appears quite promising.

It is a pleasure to acknowledge several valuable discussions with Dr. F. K. du Pré and with T. R. Kohler.

[1] Chapin, Fuller, and Pearson, J. Appl. Phys. **25**, 676 (1954).
[2] R. L. Cummerow, Phys. Rev. **95**, 16 (1954).
[3] R. L. Cummerow, Phys. Rev. **95**, 561 (1954).
[4] E. S. Rittner, Technical Report No. 84, Philips Laboratories, September 1954 (unpublished).
[5] R. P. Ruth and J. W. Moyer, Phys. Rev. **95**, 562 (1954).
[6] D. C. Reynolds and G. M. Leies, Elec. Eng. **73**, 734 (1954).

Influence of the Geomagnetic Field on the Extensive Air Showers

P. Chaloupka

Czechoslovakian Academy of Science, Prague, Czechoslovakia

(Received September 14, 1954)

RECENTLY, Cocconi[1] published a paper on the influence of the geomagnetic field on the extensive air showers. According to this calculation the shape of the lateral spread of an extensive shower should not be circular, but elliptical, the main axis in the east-west direction being about twice as long as the other one.[2]

In July, 1954, we measured this effect on the top of Lomnický Štít (altitude 2634 m, 48° N geomagnetic latitude). We used two telescopes, each of which consisted of two trays of five argon-ethylene counters (two of them 40×500 mm, three of them 45×600 mm). The distance between these telescopes was 7 m. The separation of the trays of counters in the telescope was 800 mm. The telescopes were at the zenith angle of 45°, successively oriented towards east, west, north, and south; and fourfold coincidences were recorded. The results are as follows:

E: 45.2±2.9 coincidences per hour,
W: 50.1±2.6 coincidences per hour,
N: 38.3±2.3 coincidences per hour,
S: 38.5±2.3 coincidences per hour.

In view of the rather large statistical errors, we would not like to draw any conclusion about the precise value of the influence of the geomagnetic field on the extensive air showers, but it seems that our measurements prove the existence of such an effect. The measurements are being continued. A more complete paper, containing also a discussion of the results, will be published soon in the *Czechoslovakian Journal of Physics*.

[1] G. Cocconi, Phys. Rev. **93**, 646 (1954).
[2] See, however, the erratum by G. Cocconi, Phys. Rev. **95**, 1705 (1954).

Coulomb Interference Effects in Proton-Proton Scattering*

A. Garren†

Department of Physics, Carnegie Institute of Technology, Pittsburgh, Pennsylvania

(Received November 1, 1954)

COULOMB interference effects in proton-proton scattering should be useful in discriminating between different combinations of phase shifts which equally well describe the cross section and polarization arising from purely nuclear interactions.[1] Calculations have been made of these effects for 200 Mev on the assumption only that s and p waves enter into the interaction.

In order to include the Coulomb interaction, the Møller formula for relativistic electron-electron scattering has been generalized by adding a Pauli term to the interaction Hamiltonian, to account for the proton's anomalous magnetic moment $\mu_a = 1.793$. The Coulomb scattering matrix so obtained may conveniently be written, correct through terms of order $1/\theta$,

$$M_c = M_{c+} + M_{c-}, \quad M_{c-}{}^S(\theta,\phi) = (-1)^S M_{c+}(\pi-\theta,\pi-\phi),$$

$$M_{c+} = -\frac{\eta}{2k\sin^2(\theta/2)}\left[1 - i\nu\left(\frac{\boldsymbol{\sigma}_1+\boldsymbol{\sigma}_2}{2}\right)\cdot\mathbf{n}\sin\theta\right], \quad (1)$$

$$\nu = \frac{(\epsilon-1)}{(2\epsilon^2-1)}[(2\epsilon+1)+2\epsilon(\epsilon+1)\mu_a]. \quad (2)$$

Here S is the total spin, σ_1 and σ_2 are the Pauli spin matrices for particles 1 and 2, θ and ϕ are the c.m. scattering angles, k is the c.m. momentum/$\hbar$ of each proton, ϵ is the c.m. total energy of each particle/mc^2, $\eta=e^2/\hbar v$, with v the incident velocity in the laboratory system and $\mathbf{n}$ is the unit normal to the scattering plane $(\mathbf{n}=(\mathbf{k}_i\times\mathbf{k}_f)/|\mathbf{k}_i\times\mathbf{k}_f|)$.[2] In order to make M_e reduce to the exact nonrelativistic formula, M_{e+} as given by Eq. (1) was multiplied by the Coulomb phase factor $\exp[-2i\eta\times\ln\sin(\theta/2)]$ for the numerical computations.

The total scattering matrix is $M=M_e+M_N$, where M_N is the nuclear scattering matrix which can be expressed in terms of phase shifts in the manner of Ashkin and Wu,[3] except that each factor $[\exp(2i\delta_L{}^J)-1]$ has been multiplied by $\exp 2i(\eta_L-\eta_0)$, where $\eta_L=\arg\Gamma(1+L+i\eta)$. The scattering matrix M so expressed may be substituted into the formulas of Wolfenstein and Ashkin[4] for the unpolarized cross section $\sigma(\theta)$ and the polarization $P(\theta)$:

$$\sigma(\theta)=\tfrac{1}{4}\,\mathrm{Tr}MM^+,\quad \sigma(\theta)P(\theta)\mathbf{n}=\tfrac{1}{4}\,\mathrm{Tr}MM^+\boldsymbol{\sigma}_1, \qquad (3)$$

giving expressions for σ and P in terms of the phase shifts.

This has been done for the case where only s and p phase shifts are supposed to exist, yielding expressions for σ and P in terms of the following $\delta_L{}^J$; $\delta_0{}^0$, $\delta_1{}^0$, $\delta_1{}^1$, and $\delta_1{}^2$. Calculations reported previously[5] enable one to select, subject to the restriction to $L<2$, all phase shifts consistent with isotropy of the unpolarized cross section and any given values of σ and P in the angular region where Coulomb effects are negligible. For such angles experimental data gives $\sigma(\theta)=3.56$ mb/sterad, $P(45)^\circ=0.22$, at 213 Mev.[6-7] By the use of these values the possible $\delta_L{}^J$ are limited to values lying on a one-parameter curve with four branches, in the space of the four $\delta_L{}^J$. These branches differ from each other in the sign of $\delta_0{}^0$ and of the $\delta_1{}^J$. Thus, if a certain point on one branch is $\delta_0{}^0$, $\delta_1{}^J$ the corresponding points on the other branches are $\pm\delta_0{}^0$, $\pm\delta_1{}^J$ (all of the $\delta_1{}^J$ preserve the same sign relative to each other). For the present calculation the values of the phase shifts given in Table I of the previously published letter[5] (which are representative points on one of these branches corresponding to 200 Mev) have been revised to fit the lower value of $\sigma(\theta)$ quoted above.

Of all possible phase shifts so determined, seven sets were found which also give $\sigma(\theta)$ in accord with the small-angle measurements,[8-9] where Coulomb effects are important. These are given in Table I, along with values of the corresponding polarization at 15°, where the Coulomb interference effect is strongest.[10]

TABLE I. Phase shifts $\delta_L{}^J$ for 213 Mev chosen to fit the following data: $\sigma(\theta)=3.56$ mb/sterad independent of θ with no Coulomb interference, $\sigma(15^\circ)=1.02\sigma(90^\circ)$, $|P(45^\circ)|=0.22$. The last column gives the polarization at 15°.

Set	$\delta_0{}^0$	$\delta_1{}^0$	$\delta_1{}^1$	$\delta_1{}^2$	$P(15^\circ)$
a	29	48	−7	−7	−0.133
b	20	−13	25	−12	−0.106
c	0	−69	5	4	0.065
d	37	−37	6	10	0.103
e	−36	41	−6	−8	−0.120
f	−38	−31	4	12	0.112
g	−30	10	−16	17	0.132

It turns out that the spin-dependent term in the Coulomb scattering matrix, Eq. (1), plays a negligible role in the unpolarized cross section, while for the polarization it is of about the same importance as the spin-independent term.

Recent experiments at Harwell[11] at 133 Mev indicate that $P(\theta)$ does not vary as $\sin(2\theta)$ between 30° and 45° c.m. The Coulomb effects are not large enough at these angles to explain the divergence, so that there appears to be some contribution from other than s and p waves at this energy.

Further details about these and related calculations will be published later. The author wishes to thank Professor Lincoln Wolfenstein, who suggested looking into Coulomb interference effects, for his interest and valuable advice. He is also grateful for helpful discussions with Professors Gian-Carlo Wick and Julius Ashkin.

* This research was supported in part by the U. S. Atomic Energy Commission.

† To be submitted in partial fulfillment of the requirements for the degree of Doctor of Philosophy at Carnegie Institute of Technology.

[1] R. M. Thaler and J. Bengston, Phys. Rev. **94**, 679 (1954), have also considered Coulomb effects on the cross section.

[2] It is of interest to note that the anomalous moment part of Eq. (1) is energy-independent.

[3] Julius Ashkin and Ta-You Wu, Phys. Rev. **73**, 973 (1948).

[4] L. Wolfenstein and J. Ashkin, Phys. Rev. **85**, 947 (1952).

[5] A. Garren, Phys. Rev. **92**, 213 (1953); **92**, 1587 (1953).

[6] Chamberlain, Pettengill, Segrè, and Wiegand, Phys. Rev. **93** 1424 (1954).

[7] Oxley, Cartwright, and Rouvina, Phys. Rev. **93**, 806 (1954).

[8] O. A. Towler, Phys. Rev. **84**, 1262 (1951).

[9] Owen Chamberlain and John D. Garrison, Phys. Rev. **95**, 1349 (1954).

[10] If there were no Coulomb interference all of these sets of phase shifts would give $|P(15^\circ)|=0.11$.

[11] J. M. Dickson and D. C. Salter, Nature **173**, 946 (1954).

High-Energy Electron Pair Produced by 113-Mev Positive Pion*

JAY OREAR, † R. G. GLASSER, ‡ D. M. HASKIN, ‡ AND MARCEL SCHEIN ‡

University of Chicago, Chicago, Illinois

(Received October 15, 1954)

A HIGH energy pair of electrons has been found in a nuclear emulsion exposed to the 122-Mev positive pion beam of the University of Chicago synchrocyclotron.

During measurements on positive pion-proton scattering,[1] 600-micron Ilford G-5 plates were scanned for "possible hydrogen events," that is, all stars which in addition to the incident pion had a single black prong in the forward hemisphere. The average energy of the pions in the plate is 113±2 Mev. These "possible

hydrogen events" were examined under high magnification to determine whether one or more light tracks were also associated. One example of a pair of light tracks, assumed to be electrons, was found (Fig. 1).

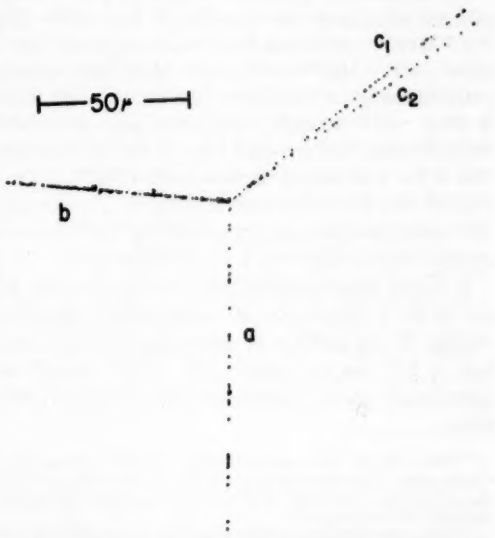

FIG. 1. Electron pair produced by 113-Mev positive pion: *a*, incident pion; *b*, proton of 75±10 Mev or other fragment of same ionization; c_1, c_2 electrons of 27±9 and 56±14 Mev, respectively.

The angle between the two electron tracks θ is 5.2 ±1.0° and the angle between the direction of the incident pion and the direction of the center of mass of the pair ϕ is 62±2°. The energies of the two electrons are 27±9 Mev and 56±14 Mev. These data are consistent with the earlier results obtained on the negative-pion-produced pairs[2] except for the angle ϕ, which is smaller than any of the angles reported earlier and which seemed in the earlier work to have an improbably sharp distribution centered around 115° in the laboratory system. Since this is the only case in the positive beam, the significance of the occurrence of such an angle is not clear.

In the area scanned for this experiment, there were $(1.56\pm0.05)\times10^5$ cm of pion track.[2] Since the mean free path for pions at very nearly the same energy[3] is 33.6±17 cm, approximately 4600 interactions must have occurred. Approximately one-eighth of these would be "possible hydrogen events" as described earlier. Thus one pair was found in about 600 stars examined.

There is no visible gap on this pair, and a gap would have been seen if it were as large as one micron.

It is suggested that this pair can be interpreted as the result of the charge-exchange scattering of a pion on a neutron in a nucleus of the emulsion:

$$\pi^+ + n \rightarrow \pi^0 + p, \qquad (1)$$

followed by the direct decay of the neutral pion, as predicted by Dalitz[4] and as observed by various authors:[5]

$$\pi^0 \rightarrow e^+ + e^- + \gamma. \qquad (2)$$

Process (1) is the charge-symmetric analog of the process which was used to explain the pairs in the negative pion beam:

$$\pi^- + p \rightarrow \pi^0 + n. \qquad (3)$$

Since there are approximately as many neutrons as protons in the emulsion the cross sections for (1) and (3) should be nearly the same, which is not inconsistent with the results reported here. The lack of a visible gap between the pair and the star is in agreement with the short lifetime reported earlier.

* Supported in part by the joint program of the Office of Naval Research and the U. S. Atomic Energy Commission.
† Institute for Nuclear Studies. Now at Department of Physics, Columbia University, New York, New York.
‡ Department of Physics.
[1] Jay Orear, Phys. Rev. **96**, 1417 (1954).
[2] Schein, Fainberg, Haskin, and Glasser, Phys. Rev. **91**, 973 (1953).
[3] Mann, Grandey, and Clark, Phys. Rev. **95**, 648 (1954).
[4] R. H. Dalitz, Proc. Phys. Soc. (London) **A64**, 667 (1951).
[5] Lindenfeld, Sachs, and Steinberger, Phys. Rev. **89**, 531 (1953); Daniel, Davies, Hulvey, and Perkins, Phil. Mag. **43**, 753 (1952); B. M. Anand, Proc. Roy. Soc. (London) **A220**, 183 (1953).

Long-Lived Radioactive Aluminum 26*

JAMES R. SIMANTON, ROBERT A. RIGHTMIRE, ALTON L. LONG, AND TRUMAN P. KOHMAN

Department of Chemistry, Carnegie Institute of Technology, Pittsburgh, Pennsylvania

(Received October 18, 1954)

THERE are experimental[1–5] and theoretical[6–9] indications of a state in Al^{26} lying below the 6-second positron-emitting 0^+ state. The ground state apparently[4,5] lies 4.0 Mev above that of Mg^{26} and is expected[6–9] to have a 5^+ configuration. If the Mg^{26} states at 1.83 and 2.97 Mev[10] both have 2+ configurations, Al^{26g} should decay predominantly by positron emission to the 1.83-Mev state with a half-life estimated[4,9] at 10^4–10^6 years, with smaller amounts of electron capture to both states.

We have sought radioactivity in aluminum carrier isolated from a target of commercial magnesium bombarded with 400 μa-hr of 15-Mev deuterons in the University of Pittsburgh cyclotron. After numerous NH_4OH precipitations at *p*H∼6, numerous NaOH precipitations of $Fe(OH)_3$, and two 8-hydroxyquinoline precipitations, the aluminum was weighed and counted as Al_2O_3 ("Al*x*"). It was then dissolved by a $Na_2B_4O_7$ fusion and put through a cycle consisting of: NH_4OH precipitation at *p*H∼6 with Zn hold-back carrier; CuS precipitation in dilute HCl; $BaSO_4$ precipitation

in dilute HCl; 8-hydroxyquinoline precipitation at pH$\sim$5 with Be and phosphate hold-back carriers; precipitation of $Fe(OH)_3$ in 0.1N NaOH; NH_4OH precipitation at pH$\sim$6; and ignition to Al_2O_3 ("Al_Y"). After weighing and counting it was put through the same cycle plus a LaF_3 precipitation in dilute HCl, and again weighted and counted ("Al_Z").

Beta activities were measured with a mica-window Geiger counter at a counting yield of 0.2 count/disintegration. Gamma activities were measured with a NaI(Tl) scintillation spectrometer, all pulses above $\sim$0.25 Mev being counted. The results are summarized in Table I. The constancy of the specific activity

TABLE I. Activity of successively purified aluminum samples.

Sample	Al_X	Al_Y	Al_Z
Wt. AL_2O_3(mg)	38.6	29.0	16.0
β activity[a] (counts/min)	26.4±1.2	19.7±1.3	10.3±1.4
γ activity[a] (counts/min)	14.5±1.5	>9.1±1.0[b]	4.5±1.2
Spec. β activity[a] (counts/min mg)	0.68±0.03	0.68±0.04	0.64±0.09
Spec. γ activity[a] (counts/min mg)	0.38±0.04	>0.31±0.03[b]	0.28±0.08

[a] Precision indices are standard deviations calculated from counting statistics only; true uncertainties are somewhat greater.
[b] γ activity low because bias was $\sim$0.33 Mev instead of $\sim$0.25 Mev.

through the variety of chamical separations indicates that the residual activity is definitely aluminum, and that sample Al_X was already essentially radiochemically pure.

Absorption measurements on Al_X indicated $\sim$1-Mev electrons; the weakness of the sample prevented an end-point determination. A low-resolution pulse analysis of the γ-activity present after the first 8-hydroxyquinoline precipitation ("Al_W") showed peaks at 0.5 and 1.9 Mev, a band from 0.1 to 0.3 Mev, and a band from 0.8 to 1.6 Mev which seemed to contain some unresolved peaks. Broad-channel measurements of the smaller and weaker Al_X showed the same distribution of pulses as in Al_W, indicating that the Al_W γ activity was essentially the same as that surviving the subsequent purifications. These observations are consistent with a dominant mode of disintegration of Al^{26g} by positron emission to the 1.83-Mev first excited state of Mg^{26}. The 0.5-Mev peak is presumably due to annihilation radiation, and the two bands principally to secondary effects. More definite characterization of the disintegration awaits the preparation of a more intense source.

The reactions responsible for Al^{26g} production are $Mg^{25}(d,n)$ and $Mg^{26}(d,2n)$. In the absence of (d,n) and $(d,2n)$ cross sections for comparable elements, we take the yield of each to be similar to that of $Mg^{24}(d,\alpha)Na^{22}$ in the same cyclotron. The latter is 0.28 millicurie per 150 μa-hr.[11] The specific β activity found indicates a total Al^{26g} activity of $\sim$600 disintegrations/minute in the 100 mg of Al carrier added to the target. Assuming that equal amounts of Al^{26m} and Al^{26g} were produced and considering the relative abundances of the Mg isotopes, the above yield corresponds to a half-life of $\sim 10^6$ years.

The occurrence of positrons in series with 1.83-Mev gammas eliminates the possibility[1] that $Al^{26g}-Mg^{26g}=2.5$ Mev. If, as follows from the most precise reaction data,[5] $Al^{26g}-Mg^{26g}=4.01\pm0.02$ Mev, the maximum positron energy is 1.16 Mev. The comparative lifetime is then $\sim 10^{14}$ seconds, consistent with second-order forbiddenness, which would result if the Al^{26g} configuration is 5+ and that of the first excited Mg^{26} level is 2+ (rather than 1+ as favored by others[12]). The slowness of the transition eliminates the possibility[9] that the second excited state of Mg^{26} has a 4+ configuration.

Hitherto, aluminum has been the only element without either a radioactive or stable isotope suitable for tracing. If the problem of producing sufficient quantities of Al^{26} can be solved, this nuclide should be of considerable value in chemistry, metallurgy, and related fields.

* This work has been supported by the U. S. Atomic Energy Commission. The cooperation of Professor Alexander J. Allen and the staff of the University of Pittsburgh Cyclotron Laboratory is gratefully acknowledged.

[1] Swann, Mandeville, and Whitehead, Phys. Rev. **79**, 598 (1950).
[2] Montalbetti, Katz, and Goldemberg, Phys. Rev. **91**, 659 (1953).
[3] Haslam, Roberts, and Robb, Can. J. Phys. **32**, 361 (1954).
[4] Kluyver, van der Leun, and Endt, Phys. Rev. **94**, 1795 (1954).
[5] C. P. Browne, Phys. Rev. **95**, 860 (1954).
[6] R. W. King and D. C. Peaslee, Phys. Rev. **90**, 1001 (1953).
[7] P. Stähelin, Helv. Phys. Acta **26**, 691 (1953).
[8] P. Stähelin, Phys. Rev. **92**, 1076 (1953).
[9] S. A. Moszkowski and D. C. Peaslee, Phys. Rev. **93**, 455 (1954).
[10] P. M. Endt and J. C. Kluyver, Revs. Modern Phys. **26**, 95 (1954).
[11] A. J. Allen (private communication from J. H. Gillette).
[12] J. E. May and B. P. Foster, Phys. Rev. **90**, 243 (1953).

Orbital Electron Excitation Associated with Electron Capture in A^{37}†

MAX WOLFSBERG

Chemistry Department, Brookhaven National Laboratory, Upton, Long Island, New York

(Received November 1, 1954)

RECENTLY, Miskel and Perlman[1] have analyzed in a proportional counter the pulse-height spectrum produced by the decay of A^{37}, which consists mainly of one peak, centered at 2.83 kev, the K binding energy of chlorine. They interpreted the processes giving rise to pulses in the region between 5.4 and 9.7 kev, after appropriately correcting the data, as K-electron excitation and ejection accompanying K capture. Thoeretical computations on such processes had previously been carried out by Primakoff and Porter.[2] It is the purpose of this note to investigate the

magnitudes of two other processes which might give rise to a significant number of events in the energy interval considered. The two processes to be considered are L-electron excitation associated with K-electron capture and K-electron excitation accompanying L capture. Since the sum of the K and L binding energies corresponds to about 3.00 kev,[3] only excitation of electrons to unbound states in the above two processes can give rise to events in the energy region considered.

Primakoff and Porter[2] considered that K capture would give rise to no L excitation since they felt that the K electron exerts complete shielding on the L electrons before capture. In using the Slater[4] recipe for formulating atomic wave functions, one does however take only a shielding constant of 0.85 for the effect of a K electron on an L electron.[5] Using this number for the K-shielding constant, one finds for the total probability of $2s$ and $2p$ excitation $0.27/Z_a^2$ compared to $0.25/Z_b^2$ found by Primakoff and Porter for K-electron excitation,[6] where Z_b is the charge of the parent nucleus and Z_a is the charge of the parent nucleus minus 4.15 (the effective charge on an $n=2$ electron shielded by two $1s$ electrons and seven other $n=2$ electrons). Only a fraction of these $0.27/Z_a^2$ events would give rise to observations in the energy region looked at by Miskel and Perlman. The form of the energy distribution spectra for the $2s$ and $2p$ electrons was computed in the manner of Primakoff and Porter and gave rise to the corresponding expressions already computed for the case of beta decay by Levinger[7] multiplied by 0.0225 (this being the change in the effective value of Z). One finds that processes in the energy region of interest occur with a probability of 9×10^{-6} per decay.

K-electron excitation accompanying L capture gives rise to the same type of matrix elements as in the corresponding case of K capture except that now the change effective Z is more properly taken as 1. The L- to K-capture ratio is taken as 0.087.[1] Using this number, one finds for the probability of this process per K capture (remembering that there are two K electrons) $0.174/Z^2$.[8] Using the ejection probability spectrum, one finds that this process gives rise to events in the energy region of interest with a probability of 5.1×10^{-6} per decay.[8]

The total added probability we have calculated here is then 6×10^{-6} which compares with the theoretical value[1] of 2.8×10^{-4} expected for K excitation in K capture. The total theoretical probability is then 3.4×10^{-4} while the experiment of Miskel and Perlman gave a result of 3.9×10^{-4}. The added probability here calculated will also tend to bring the theoretical pulse-height distribution into better agreement with the experimental one although this has not been analyzed in detail. I am much indebted to Dr. J. Miskel and Dr. M. L. Perlman for stimulating discussions.

† Research carried out under the auspices of the U. S. Atomic Energy Commission.

[1] J. A. Miskel and M. L. Perlman, Phys. Rev. **94**, 1683 (1954).

[2] H. Primakoff and F. T. Porter, Phys. Rev. **89**, 930 (1953).

[3] We used 200 kev for the L-binding energy in chlorine although we should have used 200 and 280 kev for L_I and $L_{II,III}$ binding energies respectively [B. Pontecorvo *et al.*, Phys. Rev. **75**, 982 (1949)]. This makes very little difference in the final results.

[4] J. C. Slater, Phys. Rev. **36**, 57 (1930).

[5] It must be admitted that this assertion has not been extensively tested.

[6] Both of these numbers need to be corrected due to the fact that other extra-nuclear electrons are present. Primakoff and Porter therefore add an extra multiplicative factor of uncertain magnitude. We shall discuss this correction in detail in a subsequent publication.

[7] J. S. Levinger, Phys. Rev. **90**, 11 (1953).

[8] This number would be correspondingly larger if the L-capture probability were found to be larger.

Errata

A New Titanium Nuclide: Ti^{44}, R. A. SHARP AND R. M. DIAMOND [Phys. Rev. **93**, 358 (1954)]. The value given for the half-life of Ti^{44}, 2.7 years, is too short. This value was obtained by a least-squares analysis of five months' decay data of a sample originally of an intensity of 122 counts/min in a Geiger counter. In this period, the sample decayed to 112 counts/min. Now, however, after fourteen months' total decay, the sample is still 112 counts/min. Apparently the original sample had about 10 counts/min of a shorter-lived contamination which decayed out and led to the erroneously short value given above. A lower limit to the true value can be obtained assuming that there has been decay to the extent of the possible counting errors. These correspond to about 2 percent decay in eight months or a half-life ≥ 23 years.

To prove that the activity remaining is indeed Ti^{44} scandium carrier was added to the sample and separated chemically as had been done in the original identification. The separated daughter activity was then counted with a scintillation counter by using a well-type NaI(Tl) crystal. The decay observed was the four-hour period of Sc^{44}, just as in the separations performed a year earlier on the same sample.

Low-Energy Gamma Radiation from the Bombardment of Carbon by Protons, H. H. WOODBURY, A. V. TOLLESTRUP, AND R. B. DAY [Phys. Rev. **93**, 1311 (1954)]. The value for δ on page 1314, second column, should read "$\delta=214\pm10°$" instead of "$\delta=2.4\pm10°$."

The Angular Correlation of Three Nuclear Radiations, G. R. SATCHLER [Phys. Rev. **94**, 1304 (1954)]. Delete $i^{l'-l}$ from the first line of Eq. (4b) and insert it in the third line. Replace Y_ν^{-m} in Eq. (5) by Y_λ^{-m}. In the first unnumbered equation of the right hand column of p. 1304, replace $(-)^{J_1+J_2-1}$ by $(-)^{J_1+J_2-L}$.

Centrifugal Distortion in Asymmetric Top Molecules. III. H_2O, D_2O, and HDO. D. W. POSENER AND M. W. P. STRANDBERG [Phys. Rev. **95**, 374 (1954)]. The following corrections should be made: p. 375—the left-hand side of first line of Eq. (4) should read $\sigma_{vv'}$; p. 376—the first line of Eq. (13) should read

$$R_0=\tfrac{1}{2}(a+c)J(J+1)+\tfrac{1}{2}(a-c)FJ(J+1) \\ -D_JJ^2(J+1)^2;$$

p. 379—the third word of line 17 (left-hand column) should be "methods"; p. 382—the expression in line 18 (left-hand column) should read

$$P=100\times[\nu^0(J_K)-\nu^t(J_K)]/\nu^D(J_K);$$

p. 384—in Table XVI, the value for κ should read -0.6841 ± 0.0002.

Low-Temperature Luminescence of Cadmium Sulphide, L. R. FURLONG [Phys. Rev. **95**, 1086 (1954)]. The phrase "together with the absence of photoconductivity[2]" in the first sentence of the third paragraph should be deleted. Reference 2 should be omitted.

Meson-Proton Scattering Phase Shift Analysis, H. A. BETHE AND F. DE HOFFMANN [Phys. Rev. **95**, 1100 (1954)]. Figure 2 inadvertently plotted the value of δ_1 at 40 Mev as 4.4°. The correct value, as given by our analysis, is $\delta_1=5.4°$.

Production of Charged Pions from Hydrogen and Carbon, A. H. ROSENFELD [Phys. Rev. **96**, 130 (1954)]. In Sec. II F, we stated that we used a cross section of (41 ± 3) mb at 400 Mev for the $C^{12}(p,pn)C^{11}$ monitoring reaction [Rosenfeld, Swanson, and Warshaw (to be published)]. Suspecting that this value was too high, we are currently repeating this experiment using the new Chicago external proton beam. Now we find about 34 mb. This cross section is probably the more correct one, in which case all our results must be reduced 17 percent. This change serves to eliminate most of the discrepancy discussed in Sec. VI.

Bound States and the Formal Theory of Scattering, M. N. HACK [Phys. Rev. **96**, 196 (1954)]. In reference 9, "See, e.g., Eq. (36a) of reference 8" should read "See, e.g., Eq. (36a) of this reference."

Results of a Phase Shift Calculation of High-Energy Electron Scattering, D. G. RAVENHALL AND D. R. YENNIE [Phys. Rev. **96**, 239 (1954)]. Figures 2 and 3 should be reversed.

Author Index to Volume 93

References with (A) are to abstracts of papers presented at meetings of the American Physical Society; references with (T) are to titles of invited papers; references with (L) are to Letters to the Editor; references with (E) are to Errata.

Abeles, B. (see Meiboom, S.)—1121(L)

Abell, D. F. and W. D. Knight. Saturation behavior of Gaussian magnetic resonance line—940(A)

Adair, R. K. (see Darden, S. E.)—931(A)

Adams, Raymond V. Decay of elementary particles—363(T)

—— (see Whetten, N. R.)—1356

Aden, A. L. (see Faire, A. C.)—650(A)

Aitken, A., H. Mahmoud, E. M. Henley, M. A. Ruderman, and K. M. Watson. Some possible relationships between π-meson nucleon scattering and π-meson production in nucleon-nucleon collisions—1349

Ajzenberg, F., W. Franzen, and J. G. Likely. Neutrons from proton bombardment of N^{14}—925(A)

Alger, R. S. Coloring and bleaching of alkali halide crystals containing *U* centers—953(A)

Allen, J. R. Specific ionization and energy loss of fast charged particle—353(L)

Allis, W. P. and D. J. Rose. Transition from free to ambipolar diffusion—84

Amin, M. R. Fast time analysis of burst pulse, Preonset streamer, and Trichel pulse point-to-plane coronas—649(A)

Andersen, E. (see McReynolds, A. W.)—195

Anderson, A. B. C. Jet-tone orifice number for orifices of small thickness-diameter ratio—946(A)

Anderson, J. D., C. A. McDonald, Jr., and R. F. Post. Triplet production in H_2 at 300 Mev by a total absorption method—948(A)

Anderson, J. M. and L. Goldstein. Phenomena associated with small temperature variations of electron gas in discharge plasmas around 300°K. I. Cross modulation—648(A)

—— (see Goldstein, L.)—648(A)

Anderson, K. (see Winckler, J. R.)—596

Anderson, P. W., F. R. Merritt, J. P. Remeika, and W. A. Yager. Magnetic resonance in αFe_2O_3—717

Andre, C. G. and J. R. Huizenga. Neutron binding energy in Bi^{210}—931(A)

——, **W. J. Ramler, E. G. Rauh, R. J. Thorn, and J. R. Huizenga.** Proton-induced reactions in Bi—925(A)

Ang, C. and C. Wert. Internal friction of alloys Au and Ni—922(A)

Arnold, J. S. (see Sherburne, R. K.)—946(A)

Arnold, James R. Energy levels in Lu^{176} and Hf^{176}—743

Arnold, W. R., J. A. Phillips, G. A. Sawyer, E. J. Stovall, Jr., and J. L. Tuck. Cross sections for reactions $D(d,p)T$, $D(d,n)He^3$, $T(d,n)He^4$, and $He^3(d,p)He^4$ below 120 kev—483

Arroe, Hack. Isotope shift in $_{58}$Ce II spectrum—94

—— Isotope shift in spectra of some elements of intermediate atomic number—933(T)

Asaro, Frank and I. Perlman. Decay properties of Am^{243} and possible rotational bands in α spectra of odd-even nuclei—1423(L)

Ashkin, J., J. P. Blaser, F. Feiner, J. Gorman, and M. O. Stern. Total cross sections of 135-Mev to 250-Mev negative pions in H—1129(L)

Atkins, K. R. and M. H. Edwards. Coefficient of expansion of liquid He II—1416(L)

Atterling, Hugo (see Slätis, Hilding)—646(L)

Aukerman, L. W. Photoinduced conductivity in solutions of anthracene in *n*-hexane—929(A)

Austern, N. (see Butler, S. T.)—355(L)

Azumi, K. and J. E. Goldman. Volume magnetostriction in Ni and Bethe-Slater interaction curve—630(L)

Backman, M. E. and H. L. Morrison. Measurements of Rittenger's number for glass and decomposed granite—953(A)

Baez, A. V. and M. Weissbluth. X-ray microscope mirror systems—942(A)

Ballam, J. and P. G. Lichtenstein. Interaction and production of cosmic-ray protons in C—851

Band, William. Low-temperature diamagnetism of electrons in cylinder—350(L)

Bandel, H. W. Current growth in formative time lag of sparks—944(A); 649(A)

Banta, H. E. (see Macklin, R. L.)—924(A)

Baranger, Elizabeth Urey. Scattering of high-energy electrons by heavy nuclei—1127(L)

—— (see Yennie, D. R.)—1128(L)

Barber, W. C. Specific ionization of high-energy electrons in H_2 and N_2—942(A)

Barbour, Ian G. Emulsion studies of cosmic-ray stars produced in metal foils—535

Barbour, J. P. (see Dolan, W. W.)—943(A)

Barden, S. E. Space-charge forces in strong-focusing synchrotrons—1378

Barnes, B. T. Physical processes in fluorescent lamps—359(T)

Barnes, C. A. (see Peterson, R. W.)—951(A)

Barnes, C. B. (see Heer, C. V.)—362(A)

Barnes, R. G. and W. V. Smith. Electric field gradients of atomic *p* electrons—95

Barnett, C. F. (see Stier, P. M.)—926(A)

Barschall, H. H. Interactions of fast neutrons with heavy nuclei—917(T)

—— (see Walt, M.)—1062

Bartholomew, G. A. and B. B. Kinsey. Neutron capture γ rays from Sc, V, Mn, Co, and Cu—1434(E)

—— (see Kinsey, B. B.)—1260

Barut, A. O. Mechanism of secondary electron emission—981

Batzel, R. E. and G. H. Coleman. Cross sections for formation of Na^{22} from Al and Mg bombarded with protons—280

Bayard, Robert T. and J. L. Yntema. Elastic scattering of 1-Mev electrons from Al and Au—1412(L)

Beard, David Breed. Interpretation of experiments on nuclear temperatures—950(A)

Bearden, J. A., M. D. Earle, J. M. Minkowski, and J. S. Thomson. Present status of atomic constants—629(L)

Becker, E. W., R. Misenta, and F. Schmeissner. Viscosity of gaseous He^3 and He^4 between 1.3° and 4.2°K—244(L)

Bedard, F. D. (see Gallagher, J. J.)—729

Beeninga, D. E. Opportunities for physics graduates in General Electric—360(T)

Beer, A. C., R. K. Willardson, and A. E. Middleton. Degeneracy in high-purity InSb—912(A)

—— (see Harman, R. K.)—912(A)

—— (see Willardson, R. K.)—912(A)

Belinfante, F. J. Positon theory without "holes"—935(A)

Bell, E. E. (see Burstein, E.)—65

Belser, Richard B. and Margaret C. Chester. Observation of diffusion effects occurring during artificial aging of dual layer bi-metal films—937(A)

—— **and Margaret C. Chester.** Electrical resistances of dual layer and simultaneously evaporated bi-metal films before and after artificial aging—930(A)
—— **and Walter H. Hicklin.** Effects of alloying actions of dual-layer bi-metal electrodes on frequencies of piezoelectric quartz resonators—937(A)
—— (see Raudebaugh, Robert J.)—930(A)
—— (see Woolf, William E.)—930(A)
Bengston, J. (see Thaler, R. M.)—643(L); 644(L)
Bennett, W. E., P. A. Roys, and B. J. Toppel. Low-energy yield of (α,n) reactions—924(A)
—— (see Bradford, C. E.)—921(A)
Berlincourt, D. A. Low-temperature coefficient ceramics—362(A)
Berlincourt, Ted G. and John K. Logan. Further correlation between magnetoresistance variations and de Haas-van Alphen effect—348(L)
Bernardini, Gilberto. Photomesons near production threshold—930(T)
Bernstein, Richard B. (see Cleveland, Forrest F.)—933(A)
Bernstein, Seymour (see Roberts, L. D.)—917(T)
—— (see Stanford, C. P.)—931(A)
Bernstein, W., S. S. Markowitz, and S. Katcoff. Radiations of 13.9-min Ce^{144} and 24.4-min Pr^{144}—1073
—— (see Markowitz, S. S.)—178
Bessey, William H. and Harold Weisbrod. Thermal conductivity of NaCl—923(A)
Bethe, H. A. and L. C. Maximon. Theory of bremsstrahlung and pair production. I. Differential cross section—768
—— (see Breit, G.)—888
—— (see Davies, Handel)—788
Bhatnagar, P. L. (see Krook, M.)—936(A)
Biedenharn, L. C. and J. M. Blatt. n-p scattering with spin-orbit coupling. II. Variational formulation and effective range theory—1387
—— **and J. M. Blatt.** Variation principle for eigenfunctions—230
—— (see Sack, S.)—321
Biondi, Manfred A. Diffusion cooling of electrons in ionized gases—1136
—— Doppler broadening of dissociative recombination lines—650(A)
Birnbaum, Milton. Precision determination of photoneutron thresholds—146
Blair, J. M. (see Hintz, N. M.)—924(A)
Blanchard, C. H. (see Spencer, L. V.)—114
Blaser, J. P. (see Ashkin, J.)—1129(L)
Blatt, J. M. (see Biedenharn, L. C.)—230; 1387
Blau, Henry H., Jr., John H. Shaw, and Dudley Williams. Study of pressure broadening in near infrared—360(A)
Blau, M. (see Caulton, M.)—919(A)
Blewitt, T. H., R. R. Coltman, Jr., and J. K. Redman. Structural defects in Cu and the electrical resistivity minimum—891(L)
Blizard, J. B. European and American productivity in basic science—364(A)
Bloch, Claude. Theory of nuclear level density—1094
Bloch, Felix. Recent developments in nuclear induction—944(T)
Bloembergen, N. and S. Wang. Relaxation effects in para- and ferromagnetic resonance—72
Bloom, Arnold and Dolan Mansir. Measurement of nuclear induction relaxation times in weak magnetic fields—941(A)
Bloom, David S. Specific heat of alloy $FeNi_3$ and of sigma phase FeCr—953(A)
——, **H. S. Gutowsky, D. W. McCall, and J. G. Powles.** Effect of molecular motion on intensity of pure quadrupole resonances—920(A)
—— **and R. E. Norberg.** Transient nuclear induction signals associated with pure quadrupole interactions—638(L)
Boato, G. Primeval cosmic abundance of deuterium—640(L)
Bodansky, D., A. M. Sachs, and J. Steinberger. Scattering of 65-Mev pions in H—918(A); 1367
Boehm, F. and C. S. Wu. Internal bremsstrahlung and ionization accompanying β decay—518
Boorse, H. A. (see Worley, R. D.)—45
Borowitz, Sidney and Bernard Friedman. Three-body scattering problems—251(L)
—— (see Boyet, Howard)—1225
Bortner, T. E. and G. S. Hurst. Ionization of pure gases and mixtures of gases by 5-Mev α particles—1236
Boyet, Howard and Sidney Borowitz. Variational calculation of elastic scattering of electrons by H atoms—1225
Brachman, Malcolm K. Generalized Fermi-Thomas theory—636(L)
—— (see Smaller, B.)—940(A)
Bradford, C. E., T. Kikuchi, and W. E. Bennett. Ion source for doubly charged He—921(A)
Bradley, Richard C. Sputtering of alkali atoms by inert gas ions of low energy—719
—— Sputtering of alkali metals by inert gas ions of low energy—652(A)
Bramley, Arthur. Wavelength of scattered radiation—246(L)
Branscomb, Lewis M. and Wade L. Fite. Photodetachment of H_2 negative ion—651(A)
Breen, R. J. and A. H. Weber. Neutron diffraction in vitreous silica—923(A)
Breit, G. and H. A. Bethe. Ingoing waves in final state of scattering problems—888
—— (see Sack, S.)—321
—— (see Thaler, R. M.)—644(L)
Brice, M. K. (see Cork, J. M.)—1059
Briggs, H. B., R. F. Cummings, H. J. Hrostowski, and M. Tanenbaum. Optical properties of some group III-group V compounds—912(A)
Brinkman, J. A. Effect of temperature gradients on diffusion in crystals—345(L)
Brockhouse, B. N., L. M. Corliss, and J. M. Hastings. Diffuse magnetic scattering of neutrons: zinc ferrite—923(A)
Brode, Robert B. Cosmic-ray transition phenomena due to electrons, photons, and mesons—947(A)
Brodie, Laird C. Hall effect in Bi at low temperatures—935(A)
Broecker, W. S. (see Grosse, A. V.)—250(L)
Brooks, R. A. (see Dunlap, W. C., Jr.)—911(A)
Brown, Fielding and David Park. Magnetic resonance phenomena in ferrites—381
Brown, Karl L. and Richard Wilson. Electrodisintegration of Cu^{65}, Zn^{64}, Ag^{109}, and Ta^{181}—443
Brown, R. J. S. (see Famularo, K. F.)—928(A)
Brown, S. LeRoy (see Lee, Chu Jui)—945(A)
Brown, Sanborn C. Microwave studies of electron diffusion in gases—943(T)
—— (see Looney, Duncan H.)—649(A); 965
Brown, W. B. (see Hendee, C. F.)—651(A)
Brown, W. W. Cosmic-ray nuclear interactions in gases—518
——, **J. Oeser, H. H. Staub, and C. G. Telschow.** Nuclear magnetic moments of Xe^{129} and Xe^{131}—904(L)
Brun, E., J. Oeser, H. H. Staub, and C. G. Telschow. Nuclear magnetic moments of K^{41}, Y^{89}, Ag^{107}, and Ag^{109}—172
Burch, D. S., R. C. Irick, and R. Geballe. Further studies of photon production in externally sustained discharges—650(A)
Burger, E. E. (see Cobine, J. D.)—653(A)

Burke, Bernard F., M. W. P. Strandberg, Victor W. Cohen, and Walter S. Koski. Nuclear magnetic moment of S^{33} by microwave spectroscopy—193
Burke, W. H., Jr., and W. G. Meinschein. Methane proportional counter method for C^{14} age determinations—915(A)
——, **J. R. Risser, and G. C. Phillips.** Angular distributions and excitation curves for $B^{10}(d,p)B^{11}$ and $B^{10}(d,n)$ and $B^{11}(d,n)$ reactions below 2-Mev bombarding energy—188
Burrus, Charles A. and Walter Gordy. Sub-millimeter wave spectroscopy—897(L)
—— (see Gordy, Walter)—419
Burson, S. B. (see LeBlanc, J. M.)—916(A); 1124(L)
Burstein, Elias. Anomalous optical absorption limit in InSb—632(L)
——, **J. W. Davisson, E. E. Bell, W. J. Turner, and H. G. Lipson.** Infrared photoconductivity due to neutral impurities in Ge—65
Butler, S. T. and N. Austern. Coulomb corrections in stripping—355(L)

Caird, R. S. and Allan C. G. Mitchell. Disintegration of Co^{60}—916(A)
Caldwell, David O., J. Reginald Richardson, and Herbert N. Royden. Proton-deuteron scattering at 20 Mev—942(A)
Cameron, A. G. W. Origin of anomalous abundances of elements in giant stars—932(A)
Cap, Ferdinand. New spinor theory of elementary particles—907(L)
Caretto, Albert A., Jr., and Edwin O. Wiig. New neutron-deficient isotope of Kr—175
Carlson, B. C. (see Rohrlich, F.)—38
Carmichael, H. and J. F. Steljes. Cosmic-ray ionization bursts in eight-inch sphere at sea level—913(A)
—— (see Steljes, J. F.)—913(A)
Carpenter, Robert and Dudley Williams. Proton line shapes in magnetic resonance spectra of NH_4 salts—360(A)
Carr, H. E. (see Donnally, B. L.)—111
Carroll, K. G. (see Fisher, R. M.)—921(A)
Cartwright, W. F. (see Oxley, C. L.)—806
Cashman, R. J. (see Soule, D. E.)—635(L)
Caulton, M., M. Blau, and J. E. Smith. Interactions of 500-Mev negative pions with emulsion nuclei—919(A)
Chamberlain, O. G., G. Pettengill, E. Segrè, and C. Wiegand. Cross sections for p-p scattering at 330 and 225 Mev—1424(L)
——, **E. Segrè, R. Tripp, C. Wiegand, and T. Ypsilantis.** Experiments with high-energy polarized protons—1430(L)
Charbonnier, Francis M. (see Miller, Charles E.)—590
Chasson, Robert L. Effects of atmosphere on penetrating cosmic radiation—1434(E)
Ch'en, Shang-Yi and William J. Parker. Shift and broadening of blue Cs doublet produced by A and He—946(A)
—— (see Takeo, Makoto)—420
Chester, G. V. Feynman's theory of liquid He—1412(L)
—— Quantum-mechanical partition function—606
Chester, Margaret C. (see Belser, Richard B.)—930(A); 937(A)
Cheston, W. (see Primakoff, H.)—908(L)
Chetham-Strode, A., Jr., and E. M. Kinderman. Half-life of Y^{90}—1029
Chew, Geoffrey F. One of Schwinger's variational principles for scattering—341
Chiarotti, G. and L. Giulotto. Proton relaxation in water—1241
Chilton, Arthur B., John N. Cooper, and James C. Harris. Stopping powers of various elements for protons of energies from 400 to 1050 kev—413
Chinowsky, William, A. Sachs, and J. Steinberger. Mass difference of neutral and negative π mesons—917(A)
—— **and Jack Steinberger.** Mass difference of neutral and negative π mesons—586
Choppin, Gregory R. (see Harvey, Bernard G.)—1129(L)
—— (see Thompson, S. G.)—908(L)
Clay, W. G. (see Hendricks, C. D., Jr.)—952(A)
Cleland, J. W. and J. H. Crawford, Jr. Radiation effects in InSb—894(L)
Clement, J. R. Apparent anomalies in low temperature heat capacities—1420(L)
Cleveland, Forrest F., Richard B. Bernstein, and Fred L. Voelz. Raman and infrared spectra of $C^{13}H_3I$—933(A)
—— (see Weber, Alfons)—933(A)
Cobine, J. D. and E. E. Burger. High-pressure arc anode phenomena—653(A)
Coburn, T. J., H. H. Nielsen, and Dudley Williams. New vacuum near-infrared spectrometer—360(A)
Cocconi, Giuseppe. Influence of earth's magnetic field on extensive air showers—646(L)
—— Nucleon-nucleus collisions at relativistic energies—1107
Cochran, L. W. (see Stanford, C. P.)—931(A)
Coensgen, F. H. Compton effect at 250 Mev—948(A)
Coester, F. Influence of extranuclear fields on angular correlations—1304
Cohen, Bernard L. and T. H. Handley. Experimental studies of (p,t) reactions—514
—— **and Rodger V. Neidigh.** Angular distributions of 22-Mev protons elastically scattered by various elements—282
Cohen, S. G. and A. Weinreb. Energy transfer from solvent to solute in liquid organic solutions under ultraviolet excitation—1117(L)
Cohen, Victor W., Noel R. Corngold, and Norman F. Ramsey. Experiment for measurement of magnetic moment of neutron—941(A)
—— (see Burke, Bernard F.)—193
—— (see Kikuchi, C.)—394
Cole, C. D. and S. Mrozowski. Forbidden lines in spectrum of Bi II—933(A)
Coleman, G. H. (see Batzel, R. E.)—280
Collins, R. J. and H. Y. Fan. Infrared lattice absorption bands in Ge, Si, and diamond—674
Coltman, R. R., Jr. (see Blewitt, T. H.)—891(L)
Condit, Richard I. Shock-wave valve—945(A)
Conger, R. L. and L. E. Schilberg. Photosensitive cell response to sinusoidally varying light flux—943(A)
Conwell, Esther M. Experimental evidence concerning degeneracy in Ge—1118(L)
—— (see Debye, P. P.)—693
Cool, R. L., L. Madansky, and O. Piccioni. Total cross section of pions at 1.5 Bev—249(L)
——, **L. Madansky, and O. Piccioni.** Total interaction cross section of negative pions at kinetic energies of 1.0 and 1.45 Bev—918(A)
——, **L. Madansky, and O. Piccioni.** Total interaction cross section of pions with protons and deuterons at 1.0 Bev—637(L)
Coomes, E. A. (see Haas, G. A.)—930(A); 1421(L)
—— (see Kruse, P. W.)—929(A)
Cooper, Duane H., David C. Oakley, and Robert L. Walker. 500-Mev pair spectrometer—950(A)
Cooper, John N. (see Chilton, Arthur B.)—413
—— (see Taylor, Warren E.)—1056
Copeland, Paul L. (see DeLany, B. Pearson)—926(A)
—— (see Kouba, J. T.)—926(A)
Corenzwit, E. (see Matthias, B. T.)—1415(L)
Cork, J. M., M. K. Brice, G. D. Hickman, and L. C. Schmid. Radiation from Sb^{122}—1059
—— (see LeBlanc, J. M.)—916(A); 1124(L)
Corliss, L. M., J. M. Hastings, and J. E. Goldman. Neutron diffraction study of anisotropy transition in α-Fe_2O_3—893(L)

—— (see Brockhouse, B. N.)—923(A)
Cornelius, R. C. (see Sargent, C. P.)—917(A)
Corngold, Noel R. (see Cohen, Victor W.)—941(A)
Cotts, R. M. and W. D. Knight. Nuclear resonance of Nb^{93} in $KNbO_3$—940(A)
Cox, Mason C., Jan J. van Loef, and D. A. Lind. γ rays from inelastic scattering of protons by Ne—925(A)
Crane, H. R. Method of eliminating cathode activation effects in G-M counter—921(A)
Crasemann, Bernd. Isomeric state of Ga^{66}—1034
Crawford, J. H., Jr. (see Cleland, J. W.)—894(L)
Creedon, John E. (see Udelson, Burton J.)—648(A)
Cronemeyer, D. C. (see Johnston, R. W.)—634(L)
Crouch, M. F. (see Diller, D. E.)—362(A)
Crussard, J., M. F. Kaplon, J. Klarmann, and J. H. Noon. Observation of new decay mode of heavy meson—253(L)
Culp, Richard and Bernard Hamermesh. Determination of energy of Sb-Be photoneutrons—1025
Cummings, R. F. (see Briggs, H. B.)—912(A)

Dabbs, J. W. T. and L. D. Roberts. Thermodynamic properties of $Mn(ND_4)_2(SO_4)_2 \cdot 6D_2O$ below 1°K—935(A)
Dalby, F. W., F. P. Dickey, and Dudley Williams. Infrared emission spectrum of CO in 2.4 μ region—361(A)
Dalitz, R. H. Angular correlations in τ-meson decay—914(A)
Daniels, R. D. and R. W. Hoffman. Formation of dislocation rings by vacancy migration—361(A)
Danielson, G. C. (see Gardner, W. R.)—46
Danner, H. (see Shirane, G.)—672
Darden, S. E., R. E. Fields, and R. K. Adair. Scattering of polarized neutrons from heavy nuclei—931(A)
—— (see Okazaki, A.)—461
Darken, L. S. (see Fisher, R. M.)—921(A)
Darnell, F. J. (see Howling, D. H.)—1416(L)
Das, T. P. and A. K. Saha. Mathematical analysis of Hahn spin-echo experiment—749
Daunt, J. G. (see De Vries, G.)—361(A); 631(L)
—— (see Heer, C. V.)—362(A)
Davidson, R. A. (see Hendricks, C. D., Jr.)—952(A)
Davies, Handel, H. A. Bethe, and L. C. Maximon. Theory of bremsstrahlung and pair production. II. Integral cross section for pair production—788
Davies, R. W. Connection between Smoluchowski equation and Kramers-Chandrasekhar equation—1169
Davis, Leverett, Jr. Fermi's theory of origin of cosmic rays—947(A)
Davis, R. E. and Colman Goldberg. New galvanomagnetic effect. II. Experiments with Ge—913(A)
Davis, Robert H. (see Divatia, Ajay S.)—926(A)
Davis, Sumner P. Nuclear spins and band spectra of Se isotopes—159
Davis, William R. (see Miller, Charles E.)—590
Davisson, J. W. (see Burstein, E.)—65
Dawson, Maynard and George Finn. Capacity measurements on point contact Ge diodes—913(A)
Day, R. B. (see Woodbury, H. H.)—1311
DeBenedetti, S. (see Stearns, M. B.)—1123(L)
deBretteville, A., Jr., and E. D. Harris. Threshold field *vs* temperature slope for paraelectric-ferroelectric change in $BaTiO_3$—934(A)
Debye, P. P. and E. M. Conwell. Electrical properties of *n*-type Ge—693
de Carvalho, H. G. (see Marshall, J.)—1431(L)
Dehmelt, H. G., H. G. Robinson, and Walter Gordy. Nuclear quadrupole resonance of Hg^{201}—480; 920(A)
De Juren, James A. and Hyman Rosenwasser. Pulse height measurements of recoils from $B^{10}(n,\alpha)Li^7$—831
de Klerk, D., R. P. Hudson, and J. R. Pellam. Second sound propagation below 1°K—28
DeLany, B. Pearson and Paul L. Copeland. Use of pinhole for producing glow to arc transitions—926(A)
de Launay, Jules. Isotope effect in superconductivity—661
Delbecq, C. J., J. E. Robinson, and P. H. Yuster. Iodide impurity absorption in KBr and NaBr—262
Demichelis, F. and R. Malvano. Angular correlation of cascade γ rays from decay of $_{84}Po^{214}$—526
Deser, Stanley. Radiative effects in meson-nucleon scattering—612
de-Shalit, A. (see Gillon, L. P.)—124
—— (see Mihelich, J. W.)—135
Deutsch, Martin (see Kendall, H. W.)—932(A)
de Vries, G. and J. G. Daunt. Specific heat of 96 percent He^3 below 1°K—631(L)
—— **and J. G. Daunt.** Specific heat of 96 percent liquid He^3 between 1.3°K and 2.3°K—361(A)
Dexter, D. L. *F*-center wave functions in alkali halides—244(L)
—— X-ray coloration of alkali halides—985
Dexter, R. N. (see Lax, Benjamin)—1418(L)
Diamond, H. (see Studier, M. H.)—1428(L)
Diamond, R. M. (see Sharp, R. A.)—358(L)
Dicke, R. H. Coherence in spontaneous radiation processes—99
Dickey, F. P., R. V. Zumstein, and Dudley Williams. Atomic spectra in infrared and electrodeless discharge source—361(A)
—— (see Dalby, F. W.)—361(A)
Dienes, G. J. (see Vineyard, G. H.)—265
Diller, D. E. and M. F. Crouch. Branching ratio of $Be^9(\alpha,n)C^{12*}$—362(A)
Dillon, John A., Jr., and H. E. Farnsworth. Improved radiotracer technique for study of gaseous adsorption on metals—364(A)
Ditzenberger, J. A. (see Fuller, C. S.)—1182
Divatia, Ajay S., Robert H. Davis, and R. G. Herb. Evapor-ion pump—926(A)
Diven, B. C. (see Martin, H. C.)—199
Dolan, W. W., W. P. Dyke, J. K. Trolan, and J. P. Barbour. Effect of temperature on field emission—943(A)
Donnally, B. L. and H. E. Carr. Metastable negative ions—111
Douglas, R. A. (see Galonsky, A.)—928(A)
—— (see Goldberg, E.)—799
Dresden, M. Speculations on behavior of positrons in superconductors—1413(L)
Dresselhaus, G. (see Kip, A. F.)—952(A)
Dudley, John M. (see Kenney, Robert W.)—951(A)
Dudziak, Walter F. and Ryokichi Sagane. Dependence of relative low-energy π^+ production cross section on atomic and neutron numbers—948(A)
—— (see Sagane, Ryokichi)—948(A)
Duffendack, C. S. and C. F. Hendee. X-ray absorption processes in proportional counter gases—653(A)
Duller, N. M. and W. D. Walker. High-energy meson production—284
DuMond, Jesse W. M. (see Felt, Gaelen L.)—1434(E)
Dunlap, W. C., Jr., D. E. McMillan, and R. A. Brooks. Conduction properties of *p*-type Ge between 25°C and 925°C—911(A)
Dyke, W. P. (see Dolan, W. W.)—943(A)
Dzimianski, J. W. (see Jones, T. B.)—654(A)

Earle, M. D. (see Bearden, J. A.)—629(L)
Ebel, A. A. and Clark Goodman. Inelastic scattering of neutrons by In^{115} and Au^{197}—197
Eby, F. S., R. D. Hill, and W. K. Jentschke. Angular distribution of protons from $Zn^{66}(d,p)Zn^{67}$—925(A)
Edwards, M. H. (see Atkins, K. R.)—1416(L)

Efremov, N. New method of calculation of effective ionic radii of lanthanides—934(A)
—— Numerical regularities in periodic system of ions—945(A)
Eggleston, R. R. (see Meechan, C. J.)—953(A)
Eisberg, R. M. and G. Igo. Inelastic scattering of 31-Mev protons from heavy elements—1039
Eisenstein, Albert S. X-ray-induced photostimulated conductivity in MgO—1017
Elder, S. A., J. Kolb, and W. L. Nyborg. Physical factors involved in sonic irradiation of liquids—364(A)
Elliot, J. O., W. I. McGarry, and W. R. Faust. Energy spectrum of neutrons from Po-Be—1348
Elliott, J. Is electroluminescence practical light source?—360(T)
Elliott, L. G., R. L. Graham, J. Walker, and J. L. Wolfson. Spins and parities of energy levels in Pb^{208}—356(L)
Elsken, R. H. and T. M. Shaw. Quantitative measurement of magnetic absorption utilizing null-balance system—943(A)
Emigh, C. R. and L. R. Megill. Long-lived phosphorescent components of Tl-activated NaI—1190
English, W. N. Thermal microstructure in ocean—945(A)
Epstein, A. and H. Fritzsche. Electrical resistivity of pure Te at the melting point and in liquid state—922(A)
Epstein, Saul T. Deriving Schrödinger's equation—364(A)
Ergen, William Krasny. Kinetics of circulating-fuel nuclear reactor—920(A)
Erickson, R. A. and L. D. Roberts. Measurement and calculation of liquid He vapor pressure-temperature scale from 1° to 4.2°K—957
Ernst, H. (see Hayward, R. W.)—916(A)
Evans, G. E. (see Stier, P. M.)—926(A)

Fairbank, Henry A. (see King, J. C.)—21
Faire, A. C., O. T. Fundingsland, and A. L. Aden. Measurement of dissociative recombination in N_2—650(A)
Falkoff, D. L. Impedance concept in nuclear scattering—364(A)
Famularo, K. F., R. J. S. Brown, H. D. Holmgren, and T. F. Stratton. Differential cross sections for elastic scattering of protons by He^3—928(A)
Fan, H. Y. Effect of traps on carrier injection in semiconductors—1434(E)
—— (see Collins, R. J.)—674
—— (see Kaiser, W.)—911(A); 977
—— (see Navon, D.)—911(A)
Fankuchen, Isador. New applications of x-ray diffraction—359(T)
Fano, U. Inelastic collisions in Molière theory of multiple scattering—117
—— Stokes parameter technique for treatment of polarization in quantum mechanics—121
— (see Spencer, L. V.)—1172
Farnsworth, H. E. (see Dillon, John A., Jr.)—364(A)
Farwell, George W. and Harvey E. Wegner. Elastic scattering of intermediate-energy α particles by Au—356(L)
Faust, W. R. (see Elliot, J. O.)—1348
Feher, G. and T. W. Griswold. Electron-spin resonance absorption in bulk and dispersed Li and Na—952(A)
Feiner, F. (see Ashkin, J.)—1129(L)
Feld, B. T. (see Wattenberg, A.)—915(A)
Feldman, David. Interaction between two nucleons at low energies—935(A)
Feldmann, W. L. (see Tanenbaum, M.)—912(A)
Felt, Gaelen L., John N. Harris, and Jesse W. M. DuMond. Precision measurement at 24 500 volts of conversion constant λV—1434(E)
Ferguson, A. J. (see Gove, H. E.)—928(A)
Ferigle, Salvador M. (see Weber, Alfons)—933(A)
Fermi, Enrico. Multiple production of pions in nucleon-nucleon collisions at cosmotron energies—1434(E)
—— Pion-hydrogen scattering—917(T)
Fields, P. R. (see Studier, M. H.)—1428(L); 1433(L)
Fields, R. F. (see Darden, S. E.)—931(A)
Fine, S. Proportional counter "escape" peak resolution and fine structure—653(A)
Finn, George (see Dawson, Maynard)—913(A)
Firor, J., F. Jory, and S. B. Treiman. Solar magnetic moment and diurnal variation in cosmic-ray intensity—551
Fisher, L. H. (see Lessin, I.)—649(A)
—— (see Mayer, Alex)—649(A)
Fisher, R. M., L. S. Darken, and K. G. Carroll. Accelerated growth of Sn whiskers—921(A)
Fite, Wade L. (see Branscomb, Lewis M.)—651(A)
Foldy, Leslie L. Elementary particles and Lamb-Retherford line shift—880
—— Operators and observables in isotopic spin space—1395
Foley, H. M., R. M. Sternheimer, and D. Tycko. Nuclear quadrupole coupling in polar molecules—734
Foote, H. L., Jr. (see Sailor, V. L.)—1292
Forro, M. End-point energy determination of β emitters—915(A)
Forsbergh, P. W., Jr. Effect of two-dimensional pressure on Curie point of $BaTiO_3$—686
Foster, B. P., G. S. Stanford, and L. L. Lee, Jr. γ rays from Ne^{20}—1069
Fowler, W. A. (see Mozer, F.)—829
—— (see Peterson, R. W.)—951(A)
Fowler, W. B., R. P. Shutt, A. M. Thorndike, and W. L. Whittemore. Production of heavy unstable particles by negative pions—861
Francis, N. C. and K. M. Watson. Theory of deuteron stripping reactions—313
Franck, Kurt. Prismatic light control—360(T)
Frank, R. M. and J. L. Gammel. Inelastic scattering of protons and neutrons by deuterons—463
Frankel, Sherman (see Goldberg, Norman)—1425(L)
Franzen, W. (see Ajzenberg, F.)—925(A)
Fraser, J. S. and J. C. D. Milton. Distribution of prompt neutron emission probability for fission fragments of U^{235}—818
Frauenfelder, H., J. S. Lawson, Jr., and W. Jentschke. Magnetic moment of first excited state of Pb^{206}—1126(L)
Freier, G. and H. Holmgren. Interaction between D^2 and He^3 in neighborhood of 18.6-Mev level of Li^{5*}—825
Friedland, Stephen S. (see Katzenstein, Henry S.)—363(A)
—— (see Lane, George H.)—363(A)
—— (see Ogushwitz, Howard)—363(A)
Friedman, A. M. (see Studier, M. H.)—1428(L); 1433(L)
Friedman, Bernard (see Borowitz, Sidney)—251(L)
Fritzsche, H. (see Epstein, A.)—922(A)
Frizzell, C. 701 calculator—359(T)
Fry, W. F. Inelastic scattering of 220-Mev π^- mesons in emulsions—845
—— **and George R. White.** Negative π-μ meson decays in photographic emulsion—1427(L)
Frye, Glenn M., Jr. Charged particles from interaction of 14-Mev neutrons with Li^6 and Li^7—1086
Fuller, C. S., J. D. Struthers, J. A. Ditzenberger, and K. B. Wolfstirn. Diffusivity and solubility of Cu in Ge—1182
Fulton, Thomas and Robert Karplus. Bound state corrections in two-body systems—1109
—— **and Paul C. Martin.** Radiative corrections in positronium—903(L)
Fundingsland, O. T. (see Faire, A. C.)—650(A)

Gallagher, J. J., F. D. Bedard, and C. M. Johnson. Microwave spectrum of $N^{14}O^{16}$—729
Galonsky, A. I., R. Douglas, W. Haeberli, M. McEllistrem, and H. T. Richards. Elastic scattering of deuterons by He—928(A)
—— (see Goldberg, E.)—799
Galt, J. K., W. A. Yager, and F. R. Merritt. Temperature dependence of ferromagnetic resonance line width in nickel iron ferrite: new loss mechanism—1119(L)
Gammel, J. L. (see Frank, R. M.)—463
Gardner, W. R. and G. C. Danielson. Electrical resistivity and Hall coefficient of sodium tungsten bronze—46
Garrison, Gerald R. (see Miller, Charles E.)—590
Garstens, M. A. Paramagnetic resonance in gases at low fields—1228
Gasiorowicz, S. Production of positive mesons in heavy nuclei—843
Geballe, R. (see Burch, D. S.)—650(A)
Gellman, H. (see McManus, H.)—924(A)
Gell-Mann, Murray. Theoretical speculations about new unstable particles—930(T)
Gerjuoy, E. (see Stein, S.)—934(A)
Ghiorso, Albert, G. Bernard Rossi, Bernard G. Harvey, and Stanley G. Thompson. Reactions of U^{235} with cyclotron-produced nitrogen ions—257(L)
—— (see Harvey, Bernard G.)—1129(L)
—— (see Thompson, S. G.)—908(L)
Ghosh, S. N. Charge transfer in upper atmosphere—650(A)
Gilbert, F. C. Range distribution of α particles following decays of Li^8 and B^8—499
Gillon, L. P., K. Gopalakrishnan, A. de-Shalit, and J. W. Mihelich. Nuclear spectroscopy of neutron-deficient Hg isotopes—124
Giulotto, L. (see Chiarotti, G.)—1241
Glass, Neel W. and J. Reginald Richardson. Radiations from Sc^{46}, Cl^{38}, P^{32}, and Al^{24}—942(A)
Goertzel, G. (see Spruch, Larry)—642(L)
Goldberg, Arthur E. (see Mitchell, George R.)—1421(L)
Goldberg, Colman. New galvanomagnetic effect. I. Theory—913(A)
—— (see Davis, R. E.)—913(A)
Goldberg, E., W. Haeberli, A. I. Galonsky, and R. A. Douglas. Elastic scattering of α particles by Ne—799
Goldberg, Norman and Sherman Frankel. *K*-conversion electron-γ angular correlation measurements in Te^{123} and Te^{125}—1425(L)
Goldemberg, J. Photon monochromator for bremsstrahlung radiation—1426(L)
Goldhaber, Gerson (see Homa, George)—554
Goldman, J. E. (see Azumi, K.)—630(L)
—— (see Corliss, L. M.)—893(L)
Goldsmith, G. J. Photoconductivity of single crystals of anthracene—929(A)
Goldstein, L. and J. M. Anderson. Phenomena associated with small temperature variations of electron gas in discharge plasmas around 300°K. II. Afterglow quenching—648(A)
—— (see Anderson, J. M.)—648(A)
Gomer, Robert. Chemisorption of O_2 on W—926(A)
Good, R. H., Jr. Hamiltonian mechanics of fields—239
Goodman, Clark (see Ebel, A. A.)—197
—— (see Kiehn, Robert M.)—177
—— (see McClelland, C. L.)—904(L)
Goodrich, Max and Wilbur B. Payne. Inner bremsstrahlung from P^{32}—916(A)
Gopalakrishnan, K. (see Gillon, L. P.)—124
Gordy, Walter and Charles A. Burrus. Spectrum of DBr in 1-mm wave region—419
—— (see Burrus, Charles A.)—897(L)
—— (see Dehmelt, H. G.)—480; 920(A)
—— (see Hill, Robert M.)—1019
—— (see King, William C.)—407
Gorman, J. (see Ashkin, J.)—1129(L)
Gould, Lawrence. Microwave measurement of velocity dependence of collision cross section of slow electrons in He—648(A)
Gove, H. E., A. J. Ferguson, and J. T. Sample. Elastic scattering of protons by N_2—928(A)
Graham, R. L. (see Elliott, L. G.)—356(L)
Graham, Walter J. and Arthur J. Ruhlig. Calculated values of parameters of noble gas discharges—647(A)
Green, Louis C., Margaret N. Lewis, Marjorie M. Mulder, Cynthia W. Wyeth, and John W. Woll, Jr. Correlation energies and angular components of wave functions of ground states of H^-, He I, and Li II—757
——, **Marjorie M. Mulder, Margaret N. Lewis, and John W. Woll, Jr.** Discussion of analytic and Hartree-Fock wave functions for $1s^2$ configurations from H^- to C V—757
Greenstadt, John. Variational formulas in evaporation theory—1140
Gregg, E. C. (see Tucker, B. L.)—362(A)
Griffel, M., R. E. Skochdopole, and F. H. Spedding. Heat capacity of gadolinium from 15 to 355°K—657
Griswold, T. W. (see Feher, G.)—952(A)
Groetzinger, G. (see Wiener, B.)—922(A)
Gross, E. P. Solution of Boltzmann equation for Maxwellian molecules—347(L)
—— **and M. Krook.** Kinetic approach to collision processes in gases—936(A)
—— (see Krook, M.)—936(A)
Grosse, A. V., A. D. Kirshenbaum, J. Laurence Kulp, and W. S. Broecker. Natural tritium content of atmospheric hydrogen—250(L)
Grossweiner, L. I. and M. S. Matheson. Luminescent centers in x-ray excited fluorescence of ice—929(A)
Grove, G. R. and L. N. Russell. Thin lens β-ray spectrometer—361(A)
Gugelot, P. C. Level densities of nuclei from inelastic scattering of 18-Mev protons—425
Guth, Eugene. Nuclear magnetism study of polymers—944(T)
Gutowsky, H. S. (see Bloom, Myer)—920(A)
—— (see McGarvey, B. R.)—940(A)
—— (see Williams, G. A.)—1428(L)
Gyorgy, E. M. and G. G. Harvey. Spectroscopy of solid state: some of transition elements—365

Haas, G. A. and E. A. Coomes. Effect on periodic Schottky deviations resulting from SrO layer deposited on clean Mo—930(A)
—— **and E. A. Coomes.** Temperature dependence of periodic deviations from Schottky line—1421(L)
Haeberli, W. (see Galonsky, A.)—928(A)
—— (see Goldberg, E.)—799
Hagstrum, Homer D. Reflection of ions as ions or as metastable atoms at metal surface—652(A)
Hahn, Erwin L. Free nuclear induction experiments involving pure nuclear electric quadrupole interactions—944(T)
—— **and B. Herzog.** Anisotropic relaxation of quadrupole spin echoes—639(L)
Halpern, J. (see Nathans, R.)—437
Halsted, R. E. and L. R. Koller. Electroluminescence in thin films of ZnS: Mn—349(L); 929(A)
Hamermesh, Bernard (see Culp, Richard)—1025
Hamermesh, Morton and James Monahan. Non-single scattering of electrons at oblique incidence—963
Hamilton, Joseph G. (see Rossi, G. Bernard)—256(L)
Handley, Thomas H. and Elmer L. Olson. New radioactive nuclides of rare earths—524

—— (see Cohen, B. L.)—514
Hardy, George F. and John K. Hulm. Superconductivity of some transition metal compounds—1004
Harlow, Francis H. and Boris A. Jacobsohn. Nucleon isobars in intermediate coupling—333
Harman, T. C., R. K. Willardson, and A. C. Beer. Temperature dependence of transverse magnetoresistance effect in InSb—912(A)
Harris, E. D. (see deBretteville, A., Jr.)—934(A)
Harris, James C. (see Chilton, Arthur B.)—413
Harris, John N. (see Felt, Gaelen L.)—1434(E)
Harrison, Don E., Jr. Statistical mechanics of cathode sputtering—652(A)
Harrison, Sol E. Conductivity and Hall effect of ZnO at low temperatures—52
Hartzler, A. J. and R. T. Siegel. n-p scattering at 395 Mev —928(A)
—— (see Siegel, R. J.)—928(A)
Harvey, Bernard G., Stanley G. Thompson, Albert Ghiorso, and Gregory R. Choppin. Further production of transcurium nuclides by neutron irradiation—1129(L)
—— (see Ghiorso, Albert)—257(L)
—— (see Thompson, S. G.)—908(L)
Harvey, G. G. (see Gyorgy, E. M.)—365
Hastings, J. M. (see Brockhouse, B. N.)—923(A)
—— (see Corliss, L. M.)—893(L)
Haugsnes, J. (see Roberts, James H.)—920(A)
Havas, Peter. Classical theory of particles interacting with electromagnetic and mesonic fields—882
—— Multipole singularities of classical scalar and pseudoscalar meson fields—1400
Haxby, R. O. (see Voss, J. R.)—918(A)
Hayden, R. J. (see Wasserburg, G. J.)—645(L)
Hayward, Evans and John Hubbell. Albedo of various materials for 1-Mev photons—955
Hayward, R. W., D. D. Hoppes, and H. Ernst. Disintegration of 10-yr Ba^{133}—916(A)
Hazen, W. E., R. W. Williams, and C. A. Randall, Jr. Structure of air showers—578
Heer, C. V., C. B. Barnes, and J. G. Daunt. Operational data for magnetic refrigerator for maintaining temperatures below 1°K—362(A)
Heller, J. and H. Keller. Direct integration of neutron transport equation—932(A)
Hemstreet, H. W. (see Reynolds, J. M.)—247(L)
Hendee, C. F. and W. B. Brown. Time-resolved spectroscopy of N_2 and H_2—651(A)
—— (see Duffendack, C. S.)—653(A)
Henderson, Joseph E. Recent developments in field emission—943(T)
—— (see Miller, Charles E.)—590
Hendrick, Roy W., Jr. Measurements of reflection of 8A x-rays by mirror surfaces—942(A)
Hendricks, C. D., Jr., M. E. Van Valkenburg, W. G. Clay, and R. A. Davidson. Ionization by ultra-speed pellets—952(A)
Henley, E. M. (see Aitken, A.)—1349
Henry, Warren E. Strong-field induced paramagnetic anomaly in $NiSiF_6 \cdot 6H_2O$—935(A)
Herb, R. G. (see Divatia, Ajay S.)—926(A)
Herman, Frank. Calculation of energy band structures of diamond and Ge crystals by method of orthogonalized plane waves—1214
Herring, Conyers. Correlation of electronic band structure with properties of Si and Ge—943(T)
Hershberger, W. D. (see Hurd, F. Kenneth)—373; 919(A)
Herwig, Lloyd O., G. H. Miller, and N. G. Utterback. Characteristics of gridded parallel-plate ionization chambers—926(A)
—— (see Miller, Glenn H.)—932(A)
Herzog, B. (see Hahn, E. L.)—639(L)
Heydenburg, N. P. and G. M. Temmer. Coulomb excitation of heavy and medium heavy nuclei by α particles—906(L)
—— (see Temmer, G. M.)—351(L)
Hickam, W. M. Ionization probability curves near threshold for Hg, Cd, and Zn—652(A)
Hicklin, Walter H. (see Belser, Richard B.)—937(A)
Hickman, G. D. (see Cork, J. M.)—1059
Hildebrand, Roger H. Measurement of fraction of $n+p \rightarrow \pi^0$ events in which deuteron is formed—918(A)
Hill, David L. Nuclear Coulomb excitation by heavy particles—923(A)
Hill, R. D. (see Eby, F. S.)—925(A)
Hill, Robert M. and Walter Gordy. Zeeman effect and line breadth studies of microwave lines of O_2—1019
—— (see Mizushima, Masataka)—745
Hintermann, K. Angle of divergence of pairs produced by photons—898(L)
Hintz, N. M., J. M. Blair, and D. M. Van Patter. γ radiation from excited state of Li^8—924(A)
Hochman, R. (see Kuczynski, G. C.)—952(A)
Hoffman, R. W. (see Daniels, R. D.)—361(A)
Holcomb, D. F. and R. E. Norberg. Effects of imperfections and of electron interactions on magnetic resonance in alkali metals—919(A)
Hollander, Jack M. (see Rossi, G. Bernard)—256(L)
Holmgren, H. D. (see Famularo, K. F.)—928(A)
—— (see Freier, G.)—825
Holstein, T. (see Stein, S.)—934(A)
Holton, Gerald. Are we achieving our aims in general education?—363(T)
Homa, George, Gerson Goldhaber, and Leon M. Lederman. Scattering of 151 and 188-Mev positive pions by protons—554
Honig, A., M. Mandel, M. L. Stitch, and C. H. Townes. Pure rotational spectra of alkali halides—953(A)
Hope, J. (see Jahn, H. A.)—318
Hoppes, D. D. (see Hayward, R. W.)—916(A)
Horn, F. Hubbard (see Taft, E. A.)—64
Hornbostel, J. and E. O. Salant. Artificially-produced negative heavy meson—902(L)
Horton, G. K. and G. E. Tauber. Electrical conductivity of graphite—911(A)
Howling, D. H., F. J. Darnell, and E. Mendoza. Temperature measurement below 1°K—1416(L)
Hrostowski, H. J. (see Briggs, H. B.)—912(A)
Hubbell, John (see Hayward, Evans)—955
Huber, Elsa L. Velocity of spread of burst pulses in air with coaxial cylindrical geometry—950(A)
Hudson, A. M. and F. X. Roser. Uniformity of pulse heights from a large-area photomultiplier—941(A)
Hudson, G. E. and D. H. Potts. Class of solutions of Maxwell's equations—936(A)
Hudson, R. P. (see de Klerk, D.)—28
Hughes, D. J. (see Kato, W. Y.)—931(A)
Huizenga, John R. (see Andre, C. G.)—925(A); 931(A)
—— (see Studier, M. H.)—1428(L); 1433(L)
Hulm, John K. (see Hardy, George F.)—1004
Hunter, L. P. Transistor physics—359(T)
Huntington, H. B. Creation of displacements in radiation damage—1414(L)
Hurd, F. Kenneth, Mendel Sachs, and W. D. Hershberger. Paramagnetic resonance absorption of Mn^{++} in single crystals of $CaCO_3$—373; 919(A)
Hurst, G. S. (see Bortner, T. E.)—1236
Huxford, W. S. Time constants of self-sustained Townsend discharges—652(A)

Igo, G. (see Eisberg, R. M.)—1039
Ilakovac, K. and P. B. Moon. Resonant scattering of recoil-broadening γ rays—254(L)
Irick, R. C. (see Burch, D. S.)—650(A)
Ito, Takashi, Yukito Tanabe, and Masataka Mizushima. Line width of rotational spectra of some symmetric top molecules due to nuclear quadrupole moments—1242

Jacobs, I. S. Effect of pressure on F-center absorption in alkali halides—993
Jacobsohn, Boris A. (see Harlow, Francis H.)—333
Jahn, H. A. and J. Hope. Symmetry properties of Wigner $9j$ symbol—318
Jakobson, M. J. and F. H. Schmidt. Characteristics of proposed double-mode cyclotron—303
James, Ralph A. Excitation functions of proton-induced reactions of Nb^{93}—288
Janes, G. Sargent and William L. Kraushaar. Photoproduction of π^+ mesons from H and C—900(L)
Jastram, P. S. Elastic scattering of positive and negative electrons from nuclei—928(T)
Jeffries, C. D. (see Sogo, P. B.)—174
Jeffries, Carson. Recent measurements of nuclear moments—944(T)
Jentschke, W. K. (see Eby, F. S.)—925(A)
—— (see Eby, F. S.)—925(A)
—— (see Frauenfelder, H.)—1126(L)
—— (see Kreger, W. E.)—837
Johnson, C. H. and C. C. Trail. Yields near threshold for (p,n) reactions in intermediate nuclei—924(A)
Johnson, C. M. (see Gallagher, J. J.)—729
Johnson, J. B. and K. G. McKay. Secondary electron emission from Ge—668
Johnson, J. L. and H. M. Jones. Nuclear cross sections at low energies—1286
Johnson, M. H. and E. Teller. Classical theory of heavy nuclei—947(A)
—— **and E. Teller.** Proton distribution in heavy nuclei—357(L)
—— (see Teller, E.)—947(A)
Johnston, D. F. Hall constant of graphite—1420(L)
Johnston, R. W. and D. C. Cronemeyer. Infrared absorption of NiO—634(L)
Jones, H. M. (see Johnson, J. L.)—1286
Jones, Shannon. Physical characteristics of phosphors for fluorescent lamps—360(T)
Jones, T. B. and J. W. Dzimianski. Equation for V-I curve of high current A arc—654(A)
Jones, William B. (see Rossi, G. Bernard)—256(L)
Jordan, W. C. (see LeBlanc, J. M.)—1124(L)
Jory, F. (see Firor, J.)—551
Julian, A. (see Wattenberg, A.)—915(A)
Jungerman, J. and H. Steiner. Photofission produced by 335-Mev bremsstrahlung—949(A)

Kaiser, W. and H. Y. Fan. Infrared absorption, photoconductivity, and impurity states in Ge—911(A); 977
Kaplon, M. F., G. W. Racette, and D. M. Ritson. Light elements of the primary cosmic radiation—interpretation—914(A)
——, **W. D. Walker, and M. Koshiba.** Neutral-to-charge ratio in high-energy interactions—1424(L)
—— (see Crussard, J.)—253(L)
—— (see Racette, G. W.)—914(A)
Karash, W. J. Critical effects of electric fields in fluorescent lamp starting and their use in new lamp design—360(T)
Karplus, Robert (see Fulton, Thomas)—1109
Katcoff, S. (see Bernstein, W.)—1073
—— (see Markowitz, S. S.)—178
Kato, W. Y., D. J. Hughes, and J. S. Levin. Determination of scattering resonance parameters from total cross section—931(A)
Katz, Robert (see Lee, Milford R.)—155
Katzenstein, Henry S. and Stephen S. Friedland. Time-of-flight mass spectrometer—363(A)
—— (see Lane, George H.)—363(A)
Kaufman, Sheldon and W. F. Libby. Natural distribution of tritium—1337
Keck, J., R. M. Littauer, G. K. O'Neill, A. M. Perry, and W. M. Woodward. Photodisintegration of deuteron by 180-Mev and 260-Mev γ rays—827
Keister, G. L. and F. H. Schmidt. Second-forbidden β spectra of Co^{60} and Sc^{46}—140
Keller, H. (see Heller, J.)—932(A)
Kendall, H. W. and Martin Deutsch. Annihilation of positrons in flight—932(A)
Kenney, Robert W., John M. Dudley, and Charles A. McDonald, Jr. Absolute photon attenuation cross section for non-pair processes in Be at 300 Mev—951(A)
—— (see McDonald, C. A., Jr.)—951(A)
Kent, D. W. (see Rothman, M. A.)—1434(E)
Kenty, Carl. New method for exciting metallic spectra by active N_2. Excitation of Xe—651(A)
Kiehn, Robert M. and Clark Goodman. Neutron inelastic scattering—177
Kierstead, Henry A. (see McDonell, William R.)—247(L)
Kikuchi, C. Dielectric absorption of liquid crystalline biaxial molecules—934(A)
—— **and V. W. Cohen.** Paramagnetic resonance absorption of carbazyl and hydrazyl—394
Kikuchi, T. (see Bradford, C. E.)—921(A)
Kinderman, E. M. (see Chetham-Strode, A., Jr.)—1029
Kling, D. T., N. Seeman, and M. M. Shapiro. $K^{\pm}$ mesons from "fundamental" nuclear collisions—914(A)
—— (see Shapiro, M. M.)—914(A)
—— (see Wada, W. W.)—914(A)
King, J. C. and Henry A. Fairbank. Second sound in He^3–He^4 mixtures below 1°K—21
King, William C. and Walter Gordy. 1–2 mm wave spectroscopy. IV. Experimental methods and results for OCS, CH_3F, and H_2O—407
Kingston, R. H. Water vapor and "channel" effect in n-p-n junction transistors—346(L)
Kinsey, B. B. and G. A. Bartholomew. Dipole and quadrupole transition probabilities in neutron-capture γ radiation—1260
—— (see Bartholomew, G. A.)—1434(E)
Kip, A. F., G. Dresselhaus, and C. Kittel. Cyclotron resonance in Ge crystals—952(A)
Kirby, H. W. and Murrell L. Salutsky. Half-life of La^{140}—1051
Kirshenbaum, A. D. (see Grosse, A. V.)—250(L)
Kittel, C. (see Kip, A. F.)—952(A)
Klarmann, J. (see Crussard, J.)—253(L)
Knight, W. D. Nuclear magnetic resonance phenomena in metals and alloys—944(T)
—— (see Abell, D. F.)—940(A)
—— (see Cotts, R. M.)—940(A)
Koehler, W. F. Aging of evaporated Ag films—953(A)
Kohman, Truman P. (see Waldron, Esther C.)—254(L)
Kolb, J. (See Elder, S. A.)—364(A)
Koller, L. R. (see Halsted, R. E.)—349(L); 929(A)
Konopinski, E. J. Universal Fermi interaction—936(T)
Koshiba, M. (see Kaplon, M. F.)—1424(L)
Koski, Walter S. (see Burke, Bernard F.)—193
Kouba, J. T. and P. L. Copeland. Stability of low-pressure Hg arcs with positive conducting rod—926(A)
Kovacs, J. S. Angular correlation of mesons produced in inelastic meson-nucleon collisions—252(L)

Kraus, Alfred A., Jr. γ radiation from proton bombardment of Li^7—1308
Kraushaar, William L. and Lawrence J. Marks. Meson production in high-energy nucleon-nucleon collisions—326
—— (see Janes, G. Sargent)—900(L)
Kraybill, H. L. Altitude and angular dependence of cosmic-ray air showers—1362
—— Density of extensive air showers at airplane altitudes—1360
—— (see Whetten, N. R.)—1356
Kreger, W. E., W. Jentschke, and P. G. Kruger. Elastic scattering of protons by He at 5.78 Mev—837
—— **and L. McIsaac.** NaI counting response for γ rays—943(A)
Kroll, Norman M. and Malvin A. Ruderman. Theorem on photomeson production near threshold and suppression of pairs in pseudoscalar meson theory—233
Krone, R. W. (see Teener, J. W.)—1035
Krook, M., P. L. Bhatnagar, and E. P. Gross. Kinetic approach to collision processes in gases—936(A)
—— (see Gross, E. P.)—936(A)
Krueger, Helmut. Mechanical properties of ceramic $BaTiO_3$—362(A)
Kruger, P. G. (see Kreger, W. E.)—837
Krumhansl, J. A. Theoretical calculations of *F*-center energy levels—245(L)
Kruse, P. W. and E. A. Coomes. Study of SrO on Mo by use of field emission microscope—929(A)
Kuczynski, G. C. Strain sensitivity of AuCu and $AuCu_3$ alloys—922(A)
—— **and R. Hochman.** Kinetics of ordering in AuCu alloys—952(A)
Kulp, J. Laurence (see Grosse, A. V.)—250(L)
Kusch, P. Observations of double and triple quantum transitions—1022

Landon, H. H. Doppler effect in slow neutron resonance of Rh—931(A)
—— **and V. L. Sailor.** Slow neutron resonances in Cs, Pd, and Au—1030
—— (see Sailor, V. L.)—1292
Landsberg, P. T. Quantum statistics of closed and open systems—1170
Lane, George H., Henry S. Katzenstein, and Stephen S. Friedland. Mass spectrometry of low vapor-pressure molecules—363(A)
Lane, R. O. and D. J. Zaffarano. Transmission of 0–50 kev electrons by thin films with applications to β spectra—916(A)
Langer, L. M. and J. W. Starner. Triple γ-ray cascade in Sb^{124}—245(L)
Lauritsen, C. C. (see Mozer, F.)—829
—— (see Peterson, R. W.)—951(A)
Lawson, A. W. and Lothar Meyer. Light scattering in liquid He—259
Lawson, J. S., Jr. (see Frauenfelder, H.)—1126(L)
Lax, Benjamin, H. J. Zeiger, R. N. Dexter, and E. S. Rosenblum. Directional properties of cyclotron resonance in Ge—1418(L)
Lazarus, David. Effect of screening on solute diffusion in metals—973
LeBlanc, J. M., J. M. Cork, S. B. Burson, and W. C. Jordan. Decay of V^{52}—1124(L)
——, **J. M. Cork, and S. B. Burson.** γ spectra of Cd^{117} and In^{117}—916(A)
LeClaire, A. D. Predicted effects of temperature gradients on diffusion in crystals—344(L)
Lederman, Leon M. (see Homa, George)—554
—— (see Sargent, C. P.)—917(A)
Lee, Chu Jui and S. LeRoy Brown. Response currents in coupled circuits by Laplace transformation and mechanical harmonic synthesizer—945(A)
Lee, L. L., Jr. (see Foster, B. P.)—1069
Lee, Milford R. and Robert Katz. Radioactivity of Sm^{153} and Eu^{155}—155
Leinhardt, T. E. (see Reynolds, J. M.)—247(L)
Leipuner, L. (see Stearns, M. B.)—1123(L)
Leivo, W. and R. Smoluchowski. γ-ray coloring of 400-Mev proton-irradiated KCl—1415(L)
Leonard, Stanley L. Production of charged pions at 180° to beam by 340-Mev protons on C—1380
—— **and Donald H. Stork.** Total cross section for positive pions in H—568; 1435(E)
Lessin, I. and L. H. Fisher. Formative time lags of uniform field breakdown in H_2—649(A)
Letaw, Harry, Jr., Lawrence M. Slifkin, and William M. Portnoy. Self-diffusion in Ge—892(L)
Levin, J. S. (see Kato, W. Y.)—931(A)
Levinger, J. S. Harmonic mean energy of nuclear photoeffect—932(A)
Levy, Henri A., S. W. Peterson, and S. H. Simonsen. Neutron diffraction study of ferroelectric modification of KH_2PO_4—1120(L)
Lewis, Margaret N. (see Green, Louis C.)—757; 757
Liao, T. W. Impulse corona and breakdown of a point-plane gap—650(A)
Libby, W. F. (see Kaufman, Sheldon)—1337
Lichtenstein, Philip G. Differential range spectrum of cosmic-ray mesons at sea level—858
—— (see Ballman, J.)—851
Likely, J. G. (see Ajzenberg, F.)—925(A)
Lind, D. A. (see Cox, Mason C.)—925(A)
Lindenbaum, S. J. and Luke C. L. Yuan. Energy spectrum of negative pions produced in Be by 2.3-Bev protons—917(A)
—— (see Yuan, Luke C. L.)—917(A); 1431(L)
Lindener, Arthur (see Robson, J. W.)—362(A)
Lindstrom, G. (see Meyerhof, W. E.)—949(A)
Linlor, W. I. and B. Ragent. Neutron total cross section for Bi and U between 45 and 130 Mev—951(A)
—— (see Ragent, B.)—951(A)
Linsley, John. Čerenkov counter-cloud chamber measurement of multiply charged primary cosmic rays—899(L)
Lipson, H. G. (see Burstein, E.)—65
Littauer, R. M. (see Keck, J.)—827
Loeb, Leonard B. Hitherto unrecognized aspects of breakdown streamers—649(A)
Loferski, Joseph J. Infrared optical properties of single crystals of Te—707
Logan, John K. (see Berlincourt, Ted G.)—348(L)
Looney, Duncan H. and Sanborn C. Brown. Excitation of plasma oscillations—649(A); 965
Lord, J. J. (see Orear, Jay)—575
Lukesh, Joseph S. Structure of vitreous silica—264
Lynch, F. J. New fluorescence photometer—926(A)
Lyon, W. S. and J. J. Manning. Radioactive Si^{31}—501

Mackin, R. J., Jr., W. B. Mims, and W. R. Mills. γ radiation from $C^{12} + D^2$—950(A)
Macklin, R. L. and H. E. Banta. $Li^7(d,t)Li^6$—924(A)
Madansky, L. (see Cool, R. L.)—249(L); 637(L); 918(A)
Maeder, D. and A. H. Wapstra. New isomer in Pb—1433(L)
Magnusson, L. B. (see Studier, M. H.)—1428(L)
Mahmoud, H. (see Aitken, A.)—1349
Malvano, R. (see Demichelis, F.)—526
Mandel, M. (see Honig, A.)—953(A)
Mandeville, C. E. (see Rothman, M. A.)—796; 1434(E)
Manning, J. J. (see Lyon, W. S.)—501

Manring, Edward, Yu Ting, and Dudley Williams. Nuclear quadrupole transition in single crystal of $NaClO_3$—360(A)
Mansir, Dolan (see Bloom, Arnold)—941(A)
Margolis, B. Inelastic scattering of neutrons near thresholds—204
Mark, Hans (see McClelland, C. L.)—904(L)
Markowitz, S. S., W. Bernstein, and S. Katcoff. New 3.0-min Ce fission product and its 5.95-hr Pr daughter—178
—— (see Bernstein, W.)—1073
Marks, Lawrence J. (see Kraushaar, William L.)—326
Marshall, J., L. Marshall, and H. G. de Carvalho. Polarization by p-p collision at 310 Mev—1431(L)
——, **L. Marshall, and V. A. Nedzel.** p-p elastic scattering and pion production at 419 Mev—927(A)
—— (see Marshall, L.)—927(A)
—— (see Nedzel, V. A.)—927(A)
Marshall, L., V. A. Nedzel, and J. Marshall. Search for polarization of protons from 450-Mev synchrocyclotron—927(A)
—— (see Marshall, J.)—927(A); 1431(L)
—— (see Nedzel, V. A.)—927(A)
Martin, H. C. Cross sections for $O^{16}(n,p)N^{16}$ from 12 to 18 Mev—498
——, **B. C. Diven, and R. F. Taschek.** Cross sections for production of In^{115m} and Au^{197m} by inelastic scattering of neutrons—199
Martin, Paul C. (see Fulton, Thomas)—903(L)
Matheson, M. S. (see Grossweiner, L. I.)—929(A)
Matossi, Frank (see Nudelman, Sol)—929(A)
Matthias, B. T., E. Corenzwit, and C. E. Miller. Superconducting compounds—1415(L)
Maunsell, C. D. Absorption cross sections for photoionizing radiations in low-pressure gases—943(A)
Maximon, L. C. (see Bethe, H. A.)—768
—— (see Davies, Handel)—788
Mayer, Alex and L. H. Fisher. Buildup times of glow discharges in air—649(A)
McCall, D. W. (see Bloom, Myer)—920(A)
—— (see Williams, G. A.)—1428(L)
McClelland, C. L., Hans Mark, and Clark Goodman. Electric excitation of low-lying levels in separated W isotopes—904(L)
McCoubrey, A. O. Band fluorescence of Hg vapor—1249
McDonald, Charles A., Jr., R. W. Kenney, and R. F. Post. Monitor for high-energy photons—951(A)
—— (see Anderson, J. D.)—948(A)
—— (see Kenney, Robert W.)—951(A)
McDonell, William R. and Henry A. Kierstead. Expansion of Cu bombarded by 21-Mev deuterons—247(L)
McEllistrem, M. (see Galonsky, A.)—928(A)
McGarry, W. I. (see Elliot, J. O.)—1348
McGarvey, B. R. and H. S. Gutowsky. Temperature dependence of the nuclear resonance shift in metals—940(A)
McGowan, F. K. Angular correlations of γ rays in Ta^{181}—471
—— Measurement of K-shell internal conversion coefficients with coincidence scintillation spectrometer—163
McGuire, Thomas R. Microwave resonance absorption in Ni ferrite-aluminate—682
McIsaac, L. (see Kreger, W. E.)—943(A)
McKay, K. G. (see Johnson, J. B.)—668
McKay, R. E. Science day program for high-school students in Ohio—360(T)
McManus, H., W. T. Sharp, and H. Gellman. Nuclear interactions of high-energy nucleons—924(A)
McMillan, D. E. (see Dunlap, W. C., Jr.)—911(A)
McReynolds, A. W. and E. Andersen. Thermal neutron resonance of Sm—195
Mech, J. F. (see Studier, M. H.)—1428(L); 1433(L)
Medicus, G. Electron current saturation in a ball-of-fire diode—649(A)
Meechan, C. J. and R. R. Eggleston. Formation energy of vacancies in Cu—953(A)
Megill, L. R. (see Emigh, C. R.)—1190
Meiboom, S. and B. Abeles. Theory of galvanomagnetic effects in N-Ge—1121(L)
Meinschein, W. G. (see Burke, W. H., Jr.)—915(A)
Mendoza, E. (see Howling, D. H.)—1416(L)
Merritt, F. R. (see Anderson, P. W.)—717
—— (see Galt, J. K.)—1119(L)
Meshkov, Sydney. d^3 and d^4 configurations of V—270
Meyer, Lothar. Thickness of He film—655
—— (see Lawson, A. W.)—259
Meyer, Robert A. Influence of deuteron bombardment and strain hardening on mild steel—953(A)
Meyerhof, W. E. and G. Lindstrom. Decay of Cl^{38}—949(A)
Michel, L. and A. Wightman. μ-meson decay, β radioactivity, and universal Fermi interaction—354(L)
Michel, M. C. and D. H. Templeton. Mass assignments by isotope separation—1422(L)
Middleton, A. E. (see Beer, A. C.)—912(A)
—— (see Willardson, R. K.)—912(A)
Mihelich, J. W. and A. de-Shalit. Irregularities in nuclear level spacings of Hg, Au, and Pt—135
—— (see Gillon, L. P.)—124
Milford, F. J. Odd-nucleon-plus-liquid-drop model of heavy odd nuclei—1297
Miller, C. G. and N. L. Sanders. Motion of arc cathode spot in magnetic field—654(A)
Miller, Charles E., Joseph E. Henderson, David S. Potter, Jay Todd, Jr., Wayne M. Sandstrom, Gerald R. Garrison, William R. Davis, and Francis M. Charbonnier. Zenith angle dependence of cosmic-ray protons—590
—— (see Matthias, B. T.)—1415(L)
Miller, Frank N. Improved high-intensity short-duration light source—945(A)
Miller, Glenn H. and Lloyd O. Herwig. Ionization yields for fission fragments—932(A)
—— (see Herwig, L. O.)—926(A)
Miller, R. H. (see Sherr, R.)—1076
Mills, W. R. (see Mackin, R. J., Jr.)—950(A)
Milne, Edmund A. Energy levels in N^{14} from scattering of protons by C^{13}—762
Milton, J. C. D. (see Fraser, J. S.)—818
Mims, W. B. (see Mackin, R. J., Jr.)—950(A)
Minkowski, J. M. (see Bearden, J. A.)—629(L)
Misenta, R. (see Becker, E. W.)—244(L)
Mitchell, Allan C. G. (see Caird, Robert S.)—916(A)
Mitchell, George R. and Arthur E. Goldberg. Further evidence for energy gap of PbS—1421(L)
Mittleman, M. H. Higher-order potential effects in radiative correction to scattering of slow electrons—453
Mizushima, Masataka and Robert M. Hill. Microwave spectrum of O_3—745
—— (see Ito, Takashi)—1242
Molière, G. Spread of soft component of cosmic radiation—636(L)
Monahan, James (see Hamermesh, Morton)—963
Moon, P. B. (see Ilakovac, K.)—254(L)
Morin, F. J. Electrical properties of α-Fe_2O_3—1195
—— Electrical properties of NiO—1199
—— Lattice-scattering mobility in Ge—62
—— (see Pearson, G. L.)—666
Morinaga, H. and D. J. Zaffarano. Radioactive isotope separation by nuclear recoil—1422(L)
Morrison, G. L. and G. J. Plain. Limiting range of Reynolds' number in determining flow permeability—945(A)
Morrison, H. L. (see Backman, M. E.)—953(A)

Moszkowski, S. A. and D. C. Peaslee. Isotopic spin and odd-odd $N = Z$ nuclei—941(A); 455
—— **and C. H. Townes.** Tendency for positive nuclear quadrupole moments—306
Motz, Henry T. Slow neutron capture γ rays from Ti—925(A)
Motz, Lloyd. Nonconservation of rest mass and Dirac equation—901(L)
Mozer, F., W. A. Fowler, and C. C. Lauritsen. Inelastic scattering of protons by Li^7—829
Mrozowski, S. Forbidden line in spectrum of Pr—933(A)
—— "Magnetic scanning" method for investigating hfs and isotope shift—641(L)
—— (see Cole, C. D.)—933(A)
Muether, H. R. (see Palevsky, H.)—920(A)
Mulder, Marjorie M. (see Green, Louis C.)—757; 757
Müller, Ralph H. Interaction of β particles with matter—891(L)
Murakawa, Kiyoshi. Hfs in spectra of Sb, Sm, Hg, and Cd—1232

Nachtrieb, N. H. Effect of pressure on self-diffusion of Na—926(T)
Nagle, D. E. Scattering of negative pions by deuterium—918(A)
Nathans, R. and J. Halpern. Systematics of photoneutron reactions—437
Navon, D. and H. Y. Fan. Low-temperature recombination and trapping in Ge—911(A)
Neamtan, S. M. Čerenkov effect and dielectric constant—932(A)
Nedzel, V. A., J. Marshall, and L. Marshall. p-p differential elastic scattering cross sections at 144, 271, and 429 Mev—927(A)
—— (see Marshall, J.)—927(A)
—— (see Marshall, L.)—927(A)
Neidigh, Rodger V. (see Cohen, Bernard L.)—282
Nicolet, Marcel. Origin of emission of oxygen green line in airglow—633(L)
Nielsen, H. H. (see Coburn, T. J.)—360(A)
Nigam, B. P. V_0^1 particle as high angular state of meson-nucleon system—914(A)
Nijgh, G. J. (see van Lieshout, R.)—255(L)
Noel, E. B. Physics problems in high-pressure Hg-vapor light sources—360(T)
Noon, J. H. (see Crussard, J.)—253(L)
Norberg, R. E. (see Bloom, M.)—638(L)
—— (see Holcomb, D. F.)—919(A)
Nordsieck, A. Reduction of integral in theory of bremsstrahlung—785
Novey, T. B. Influence of electric quadrupole interaction on angular correlation—916(T)
Nudelman, Sol and Frank Matossi. Electroluminescence with nonsinusoidal electric fields—929(A)
Nussbaum, R. H. (see van Lieshout, R.)—255(L)
Nyborg, W. L. (see Elder, S. A.)—364(A)

Oakley, David C., R. L. Walker, J. G. Teasdale, and J. I. Vette. Photoproduction of neutral pions at high energies—949(A)
—— (see Cooper, Duane H.)—950(A)
Oberly, John J. Photoelectric Hall effect in Ge single crystals—911(A)
Odian, A. (see Wattenberg, A.)—915(A)
Oeser, J. (see Brun, E.)—172; 904(L)
O'Friel, Z. (see Sturcken, E. F.)—1053
Ogushwitz, Howard and Stephen S. Friedland. Improved chronotron for time-of-flight measurements—363(A)
Okazaki, A., S. E. Darden, and R. B. Walton. Total cross sections of rare earths for fast neutrons—461
O'Kelley, G. D. (see Olsen, J. L.)—1125(L)
Olsen, J. L. and G. D. O'Kelley. β-ray spectrum of Mg^{28}—1125(L)
Olsen, L. O. G.E.-Case fellowship program for high-school physics teachers—360(T)
Olson, Elmer L. (see Handley, Thomas H.)—524
O'Neill, G. K. (see Keck, J.)—827
Orear, Jay. Signs of phase shifts in pion-proton scattering—918(A)
——, **J. J. Lord, and A. B. Weaver.** Scattering of 45-Mev positive pions by H—575
Ortel, William C. G. Neutron production by cosmic rays—561
Osborn, R. K. (see Rose, M. E.)—1315; 1326
Osborne, L. S. (see Wattenberg, A.)—915(A)
Oxley, C. L. Double scattering of protons at high energies—928(T)
——, **W. F. Cartwright, and J. Rouvina.** Double scattering of high-energy protons—806
Ozarow, Vernon. Electrical properties of Ge crystals containing compensated impurities—371

Pack, J. L. (see Phelps, A. V.)—652(A)
Packard, Martin and Russell Varian. Free nuclear induction in earth's magnetic field—941(A)
Pake, G. E. Paramagnetic relaxation in free radical solutions exhibiting hfs—944(T)
Palevsky, H., H. R. Muether, and A. Stolovy. Scintillation detector for Brookhaven fast chopper—920(A)
Palfrey, T. R. (see Voss, J. R.)—918(A)
Panofsky, Wolfgang K. H. Achromatic translation system for high-energy beams—949(A)
Park, David (see Brown, Fielding)—381
Parker, James H., Jr. Electron ejection by slow positive ions incident on flashed and gas-covered metallic surfaces—652(A); 1148
Parker, William J. (see Ch'en, Shang-Yi)—946(A)
Patrick, Lyle. Antiferromagnetism of Mn—370
—— Change of ferromagnetic Curie points with hydrostatic pressure—384
Pavlovic, A. (see Shirane, G.)—672
Payne, Wilbur B. (see Goodrich, Max)—916(A)
Pearson, G. L., W. T. Read, Jr., and F. J. Morin. Dislocations in plastically-deformed Ge—666
—— (see Tanenbaum, M.)—912(A)
Peaslee, D. C. (see Moszkowski, S. A.)—455; 941(A)
Pellam, J. R. (see de Klerk, D.)—28
Pepinsky, R. (see Shirane, G.)—672
Perlman, I. (see Asaro, Frank)—1423(L)
Perry, A. M. (see Keck, J.)—827
Peter, Brother Simon. Nuclear resonance of P^{31} in CS_2 solutions—940(A)
Peterson, R. W., C. A. Barnes, W. A. Fowler, and C. C. Lauritsen. Inelastic scattering of protons by F^{19}—951(A)
Peterson, S. W. (see Levy, Henri A.)—1120(L)
Pettengill, G. (see Chamberlain, O.)—1424(L)
Phelps, A. V. and J. L. Pack. Improved optical absorption technique for study of metastable atoms—652(A)
Phillips, G. C. (see Burke, W. H.)—188
Phillips, J. A. (see Arnold, W. R.)—483
Piccioni, O. (see Cool, R. L.)—249(L); 637(L); 918(A)
Placzek, G. Incoherent neutron scattering by polycrystals—895(L)
—— **and L. Van Hove.** Crystal dynamics and inelastic scattering of neutrons—1207
Plain, G. J. (see Morrison, H. L.)—945(A)
Polkinghorne, J. C. Identity for S matrix for finite time interval—228

Pond, T. A. Annihilation of positrons in condensed materials—478
Poritsky, A. Spectroscopy in manufacture of W—360(T)
Portnoy, William M. (see Letaw, Harry, Jr.)—892(L)
Post, R. F. (see Anderson, J. D.)—948(A)
—— (see McDonald, C. A., Jr.)—951(A)
Potter, David S. (see Miller, Charles E.)—590
Potter, Roy F. Cross sections for charge transfer collisions of low-energy ions in N_2 and O_2—650(A)
Potts, D. H. (see Hudson, G. E.)—936(A)
Pound, R. V. Recent results in nuclear magnetism—944(T)
Powles, J. G. (see Bloom, Myer)—920(A)
Pratt, William W. Angular distribution of protons from $B^{10}(d,p)B^{11}$—816
Preston, R. S. (see Whetten, N. R.)—1356
Price, Glenn A. Energy spectra and angular distributions of photoneutrons from heavy nuclei—1279
Primakoff, H. and W. Cheston. "V dinucleons"—908(L)
Prince, M. B. Drift mobilities in semiconductors. II. Si—1204
Proctor, D. G. and T. A. Romanowski. Study of α-particle pulse heights from organic scintillators—362(A)
Pyle, G. (see Studier, M. H.)—1428(L)

Racette, G. W., M. F. Kaplon, and D. M. Ritson. Light elements of the cosmic radiation—experimental—914(A)
—— (see Kaplon, M. F.)—914(A)
Ragent, B. and W. I. Linlor. Total neutron cross sections for C, Fe, Sb, and Ta from 35 to 180 Mev—951(A)
—— (see Linlor, W. I.)—951(A)
Ramler, W. J. (see Andre, C. G.)—925(A)
Ramsey, Norman F. Nuclear interactions in molecules—944(T)
—— (see Cohen, Victor W.)—941(A)
Randall, C. A., Jr. (see Hazen, W. E.)—578
Rappaport, P. Electron-voltaic effect in p-n junctions induced by β-particle bombardment—246(L)
Rasmussen, John O., Jr. (see Slätis, Hilding)—646(L)
Raudebaugh, Robert J. and Richard B. Belser. Metallographic studies of dual layer and simultaneously evaporated bimetal films after artificial aging by heating—930(A)
Rauh, E. G. (see Andre, C. G.)—925(A)
Ravenhall, D. G., D. R. Yennie, and R. N. Wilson. Phase-shift calculation of high-energy electron scattering by nuclei—949(A)
—— (see Yennie, D. R.)—948(A); 1128(L)
Read, W. T., Jr. (see Pearson, G. L.)—666
Reagan, Daryl. Photospallation yields of N^{17}—947(A)
Redman, J. K. (see Blewitt, T. H.)—891(L)
Remeika, J. P. (see Anderson, P. W.)—717
Reynolds, Charles A. "Closed" fountain effect in liquid He II—363(A); 1118(L)
Reynolds, J. M., T. E. Leinhardt, and H. W. Hemstreet. Hall effect in Bi at 1.4°K—247(L)
Rhodes, J. Elmer, Jr. Thermal energy in almost normal modes—1
Rice, O. K. Nature of higher-order phase transitions with application to liquid He—1161
Richards, H. T. (see Galonsky, A.)—928(A)
Richardson, J. Reginald (see Caldwell, David O.)—942(A)
—— (see Glass, Neel W.)—942(A)
Rinehart, M. C. (see Sargent, C. P.)—917(A)
Risser, J. R. (see Burke, W. H.)—188
Ritson, D. M. (see Kaplon, M. F.)—914(A)
—— (see Racette, G. W.)—914(A)
Roberts, James H., J. Haugsnes, and D. E. Wood. Loading of nuclear emulsions with Li gloss specks—920(A)
—— (see Weddell, James B.)—924(A)
Roberts, L. D. and Seymour Bernstein. Capture of polarized neutrons by polarized Mn^{55} and Sm^{149} nuclei; (a) Production of nuclear polarization. (b) Observation of effects due to nuclear polarization—917(T)
—— (see Dabbs, J. W. T.)—935(A)
—— (see Erickson, R. A.)—957
Roberts, T. R. and S. G. Sydoriak. Specific heat of liquid He^3—1418(L)
Robinson, H. G. (see Dehmelt, H. G.)—480; 920(A)
Robinson, J. E. (see Delbecq, C. J.)—262
Robinson, W. J. Mixture of central, tensor, and two-particle spin-orbit interactions for N^{14} and D^2—1296
Robson, A. E. and A. von Engel. Origin of retrograde motion of arc cathode spots—1121(L)
Robson, J. W., R. L. Stearns, and Arthur Lindener. Energy loss and scattering of 0.624-Mev electrons—362(A)
Rogers, K. (see Sargent, C. P.)—917(A)
Rogers, T. F. Absolute intensity of water vapor absorption at microwave frequencies—248(L)
Rohrlich, Fritz and B. C. Carlson. Positron-electron differences in energy loss and multiple scattering—38
—— (see Warner, Charles, III)—406
Romanowski, T. A. (see Proctor, D. G.)—362(A)
Roos, Charles E. New method for measuring Auger transitions—401
Rose, D. J. (see Allis, W. P.)—84
Rose, M. E. Mixed γ-mixed γ angular correlation—477
—— **and R. K. Osborn.** Nuclear matrix elements in β decay—1326
—— **and R. K. Osborn.** Pseudoscalar interaction in β decay—1315
Rosen, Arthur Z. Proton intensities at sea level and 9000 feet—280
Rosenblum, E. S. (see Lax, Benjamin)—1418(L)
Rosendorff, S., R. Stahl, and G. Yekutieli. Double star connected by heavy meson—901(L)
Rosenstock, Herbert B. Quantization of nonlinear field theory—331
Rosenwasser, Hyman (see De Juren, James A.)—831
Roser, F. X. (see Hudson, A. M.)—941(A)
Ross, S. W., E. Tochilin, and B. W. Shumway. Measurements of cyclotron neutron and γ fields for animal irradiation studies—945(A)
Rossi, G. Bernard, William B. Jones, Jack M. Hollander, and Joseph G. Hamilton. Acceleration of nitrogen 14 (+6) ions in 60-inch cyclotron—256(L)
—— (see Ghiorso, Albert)—257(L)
M. A. Rothman, D. W. Kent, and C. E. Mandeville. Scattering of fast neutrons by Fe, Pb, and Cr—1434(E)
—— **and C. E. Mandeville.** γ rays excited by inelastic scattering of neutrons in Pb, Bi, Fe, Ni, and Cr—796
Rothstein, J. Analogies between lattice defects and current carriers in semiconductors—912(A)
Rouvina, J. (see Oxley, C. L.)—806
Royden, Herbert N. (see Caldwell, David O.)—942(A)
Roys, P. A. (see Bennett, W. E.)—924(A)
Ruderman, Malvin A. (see Aitken, A.)—1349
—— (see Kroll, Norman M.)—233
Ruhlig, Arthur J. (see Graham, Walter J.)—647(A)
Russell, F. N. (see Grove, G. R.)—361(A)
Russell, Leonard N. (see Taylor, Warren E.)—1056

Sachs, A. M. (see Bodansky, D.)—918(A); 1367
—— (see Chinowsky, W.)—917(A)
Sachs, Mendel (see Hurd, F. Kenneth)—373; 919(A)
Sack, S., L. C. Biedenharn, and G. Breit. Elastic scattering of protons by α particles—321

Sagane, Ryokichi and Walter F. Dudziak. Relative low-energy pion production cross sections by photons on H—948(A)
—— (see Dudziak, Walter F.)—948(A)
Saha, A. K. (see Das, T. P.)—749
Sailor, V. L., H. H. Landon, and H. L. Foote, Jr. Slow neutron resonances in Eu—1292
—— (see Landon, H. H.)—1030
Salant, E. O. (see Hornbostel, J.)—902(L)
Salkowitz, E. I. (see Weertman, J.)—922(A)
Salutsky, Murrell L. (see Kirby, H. W.)—1051
Sample, J. T. (see Gove, H. E.)—928(A)
Sanders, N. L. (see Miller, C. G.)—654(A)
Sandstrom, Wayne M. (see Miller, Charles E.)—590
Sargent, C. P., M. C. Rinehart, R. C. Cornelius, L. M. Lederman, and K. Rogers. Internal conversion of mesic γ rays—917(A)
Savitt, Jacob. Velocity attenuation of explosive-produced air shocks—927(A)
Sawyer, G. A. (see Arnold, W. R.)—483
Schardt, A. W. and Joan P. Welker. Decay scheme of Se^{75} and Ge^{75}—916(A)
Schein, Marcel. Reports on the cosmic-ray conferences held in July, 1953, at Bagnères-de-Bigorre. (b) Conference on fundamental particles—930(T)
Schiff, L. I. Interpretation of electron scattering experiments —1434(E)
Schilberg, L. E. (see Conger, R. L.)—943(A)
Schild, A. New modification of classical electromagnetic theory—936(A)
Schmeissner, F. (see Becker, E. W.)—244(L)
Schmid, L. C. (see Cork, J. M.)—1059
Schmidt, F. H. (see Jakobson, M. J.)—303
—— (see Keister, G. L.)—140
Schneider, E. E. Hfs in paramagnetic resonance of x-rayed LiF—919(A)
Schultz, Virginia A. (see Waldron, Esther C.)—254(L)
Schulz, L. G. Reflectivity of Ag in near infrared—922(A)
Schwinger, Julian. Theory of quantized fields. V—615
Seagondollar, L. W. (see Teener, J. W.)—1035
Sears, G. W. Hg whiskers—921(A)
Sedlet, J. (see Studier, M. H.)—1433(L)
Seeman, N. (see King, D. T.)—914(A)
—— (see Shapiro, M. M.)—914(A)
Segrè, Emilio (see Chamberlain, O.)—1424(L); 1430(L)
Seidl, F. G. P. Recent measurements of lowest neutron scattering resonance in Co—931(A)
Sellers, P. A. (see Studier, M. H.)—1428(L); 1433(L)
Shapiro, M. M., D. T. King, and N. Seeman. Charged particles intermediate in mass between protons and deuterons—914(A)
—— (see King, D. T.)—914(A)
Shapiro, Philip. Angular distribution of protons from $Na^{23}(d,p)Na^{24}$—290
Sharp, R. A. and R. M. Diamond. New Ti nuclide: Ti^{44}—358(L)
Sharp, W. T. (see McManus, H.)—924(A)
Shaw, John H. (see Blau, Henry H., Jr.)—360(A)
Shaw, T. M. (see Elsken, R. H.)—943(A)
—— (see Windle, J. J.)—952(A)
Sherburne, R. K. and J. S. Arnold. New observations of hydrocarbon flame growth—946(A)
Sherman, Christopher. Nuclear induction with separate regions of excitation and detection—1429(L)
Sherman, Noah. Atmospheric temperature effect for μ mesons observed at depth of 846 m.w.e.—277
Sherr, R. and R. H. Miller. Electron capture in decay of Na^{22}—1076
Sherrill, F. A. (see Wittels, M.)—1117(L)
Shirane, G., H. Danner, A. Pavlovic, and R. Pepinsky. Phase transitions in ferroelectric $KNbO_3$—672
Shockley, W. Predicted effects of temperature gradients on diffusion in crystals—345(L)
Shumway, B. W. (see Ross, S. W.)—945(A)
Shutt, R. P. (see Fowler, W. B.)—861
Siegel, R. T. and A. J. Hartzler. Neutron-proton scattering at 395 Mev—928(A)
—— (see Hartzler, A. J.)—928(A)
Simon, Albert. Theory of polarized particles and γ rays in nuclear reactions—1435(E)
—— **and T. A. Welton.** Production of polarized particles in nuclear reactions—1435(E)
Simonsen, S. H. (see Levy, Henri A.)—1120(L)
Simpson, J. A. Reports on the cosmic-ray conferences held in July, 1953, at Bagnères-de-Bigorre. (a) Conference on intensity-time variations—930(T)
Sinclair, Rolf M. γ radiation from certain nuclear reactions —1082
Singer, L. S. Magnetic resonance in some Cr^{++} complexes —919(A)
Skochdopole, R. E. (see Griffel, M.)—657
Skolnik, M. I. Rf noise from low-current, atmospheric-pressure arc discharges in air—648(A)
Slätis, Hilding, John O. Rasmussen, Jr., and Hugo Atterling. β decay of Np^{239}—646(L)
Slichter, C. P. Polarization of nuclear spins in metals by Overhauser method—920(T)
Slifkin, Lawrence M. (see Letaw, Harry, Jr.)—892(L)
—— (see Sonder, E.)—970
Smaller, B., E. Yasaitis, and M. Brachman. Paramagnetic resonance of Mn^{++} at radiofrequencies—940(A)
Smith, Alan W. Thermal conductivity of graphite—952(A)
Smith, Charles G. Orderly subdivision of Hg arc cathode spot—653(A)
Smith, J. E. (see Carlton, M.)—919(A)
Smith, R. E. Glass absorption factors in light bulbs—360(T)
Smith, R. W. Radiation from CdS crystals generated by dc electric fields—347(L)
Smith, Robert D. and Dudley Williams. Total emission of HCl and CO in region of their fundamentals—361(A)
Smith, W. V. (see Barnes, R. G.)—95
Smoluchowski, R. Influence of pressure on Curie temperature of Fe and Ni—392
—— (see Leivo, W.)—1415(L)
Sogo, P. B. and C. D. Jeffries. Magnetic moments of Ag^{107} and Ag^{109} and hfs anomaly—174
Sonder, E., L. Slifkin, and C. T. Tomizuka. Diffusion of Sb in Ag—970
Soule, D. E. and R. J. Cashman. Bulk photoconductivity in PbS—635(L)
Spedding, F. H. (see Griffel, M.)—657
Spencer, L. V. and C. H. Blanchard. Multiple scattering of relativistic electrons—114
—— **and U. Fano.** Energy spectrum resulting from electron slowing-down—1172
Spruch, Larry and G. Goertzel. Internal Compton effect in Ba^{137}—642(L)
Stahl, R. (see Rosendorff, S.)—901(L)
Stanford, C. P., T. E. Stephenson, F. W. Cochran, and S. Bernstein. Polarization of neutrons—931(A)
Stanford, G. S. (see Foster, B. P.)—1069
Starner, J. W. (see Langer, L. M.)—253(L)
Staub, H. H. (see Brun, E.)—172; 904(L)
Stearns, M. (see Stearns, M. B.)—1123(L)
Stearns, M. B., S. DeBenedetti, M. Stearns, and L. Leipuner. Relative intensities of π and μ meson x-rays of K and L series in low Z elements—1123(L)
Stearns, R. L. (see Robson, J. W.)—362(A)

Steeb, E. S. Problems in evaluating radiant energy from light sources—360(T)
Steenberg, N. R. Nuclear alignment at low temperatures—678
Steffen, R. M. Influence of extra-nuclear fields on angular correlation of nuclear radiation—916(T)
Stehn, J. R. Nuclear energy surface and isotopic mass values—932(A)
Stein, S., E. Gerjuoy, and T. Holstein. Rotational excitation of homonuclear molecules—934(A)
Steinberger, Jack (see Bodansky, D.)—918(A); 1367
—— (see Chinowsky, William)—586; 917(A)
Steiner, H. (see Jungerman, J.)—949(A)
Steljes, J. F. and H. Carmichael. Influence of Pb shielding on ionization bursts at sea level—913(A)
—— (see Carmichael, H.)—913(A)
Stelson, P. H. Angular distribution of α particles from $Na^{23}(p,\alpha)Ne^{20}$—925(A)
Stephenson, T. E. (see Stanford, T. E.)—931(A)
Stern, M. O. (see Ashkin, J.)—1129(L)
Sternglass, Ernest J. Energy distribution of secondary electrons from solids—929(A)
Sternheimer, R. M. Density effect for ionization loss at low energies—351(L)
—— Energy loss of fast charged particle by Čerenkov radiation—1434(E)
—— Kinematic criterion for meson production in fundamental particle collisions—642(L)
—— (see Foley, H. M.)—734
Stevens, C. M. (see Studier, M. H.)—1428(L); 1433(L)
Stier, P. M., C. F. Barnett, and G. E. Evans. Charge states of ion beams in various gases—926(A)
Stitch, M. L. (see Honig, A.)—953(A)
St. John, Robert and J. G. Winans. Retrograde motion of cathode spot in transverse magnetic fields—653(A)
Stolovy, A. (see Palevsky, H.)—920(A)
Stork, Donald Harvey. Interaction of pions with complex nuclei—868
—— (see Leonard, Stanley L.)—568; 1435(E)
Stovall, E. J., Jr. (see Arnold, W. R.)—483
Strandberg, M. W. P. (see Burke, Bernard F.)—193
Stratton, T. F. (see Famularo, K. F.)—928(A)
Struthers, J. D. (see Fuller, C. S.)—1182
Studier, M. H., P. R. Fields, H. Diamond, J. F. Mech, A. M. Friedman, P. A. Sellers, G. Pyle, C. M. Stevens, L. B. Magnusson, and J. R. Huizenga. Elements 99 and 100 from pile-irradiated plutonium—1428
——, **P. R. Fields, P. H. Sellers, A. M. Friedman, C. M. Stevens, J. E. Mech, H. Diamond, J. Sedlet, and J. R. Huizenga.** Pu^{244} from pile-irradiated Pu—1433(L)
Sturcken, E. F., Z. O'Friel, and A. H. Weber. Internal conversion coefficients of Nb^{95}, Zn^{65}, and Sc^{46}—1053
Sueoka, Seiichi. Matrix elements of spin-orbit interaction in d^5d configuration—302
Sunyar, A. W. Decay of Ho^{166}—1345
—— Short-lived metastable states of W^{188}—1122(L)
Swann, W. F. G. Alfvén's theory of effect of magnetic storms on cosmic-ray intensity—905(L)
Sydoriak, S. G. (see Roberts, T. R.)—1418(L)

Taft, E. A. and F. Hubbard Horn. Au as donor in Si—64
Takeda, Gyo. High-energy protons in nuclear interaction of 220-Mev π^- mesons in nuclear emulsions—848
Takeo, Makoto and Shang-Yi Ch'en. Theory of fine structure pressure broadening of spectral lines—420
Tamor, S. Scattering of many-particle systems—227
Tanabe, Yukito (see Ito, Takashi)—1242
Tanaka, Katsumi. Čerenkov radiation—459
Tanaka, Yoshio and Murray Zelikoff. Continuous emission spectra of Kr and Xe in vacuum uv region—933(A)
Tanenbaum, M., G. L. Pearson, and W. L. Feldmann. Magnetoresistance in InSb and GaSb single crystals—912(A)
—— (see Briggs, H. B.)—912(A)
Tannenwald, L. M. Asymptotic spherical shock decay—946(A)
—— (see Martin, H. C.)—199
Tauber, G. E. and Ta-You Wu. Energies of excited states of nuclei—434
—— **and Ta-You Wu.** *p*- and *d*-shell nuclei in intermediate coupling—295
—— (see Horton, G. K.)—911(A)
Taylor, Warren E., Leonard N. Russell, and John N. Cooper. Resonance capture of protons by Mg^{25}—1056
Tchen, Chan-Mou. Transport processes as foundations of Heisenberg and Obukhoff theories of turbulence—4
Teasdale, J. G. (see Oakley, D. C.)—949(A)
Teener, J. W., L. W. Seagondollar, and R. W. Krone. γ rays from proton bombardment of Na—1035
Telegdi, Valentine L. (see Thirion, Jacques)—950(A)
Teller, E. and M. H. Johnson. Classical theory of heavy nuclei—947(A)
—— (see Johnson, M. H.)—357(L); 947(A)
Telschow, C. G. (see Brun, E.)—172; 904(L)
Temmer, G. M. and N. P. Heydenburg. Coulomb excitation of heavy and medium heavy nuclei by α particles—351(L)
—— (see Heydenburg, N. P.)—906(L)
Templeton, D. H. (see Michel, M. C.)—1422(L)
Thaler, R. M. and J. Bengston. Phase shift analysis of high-energy nucleon-nucleon scattering—643(L)
——, **J. Bengston, and G. Breit.** Effect of $^3P_2$–$^3F_2$ coupling on nucleon-nucleon scattering—644(L)
Thayer, R. N. Physics and physicists in Ohio industry—electric lamps—359(T)
Thirion, Jacques and Valentine L. Telegdi. Lifetime measurements for first excited states of O^{17} and B^{10} from recoil studies—950(A)
Thompson, R. W. Evidence for existence of V_4 particle—930(T)
Thompson, Stanley G., A. Ghiorso, B. G. Harvey, and G. R. Choppin. Transcurium isotopes produced in neutron irradiation of Pu—908(L)
—— (see Ghiorso, Albert)—257(L)
—— (see Harvey, Bernard G.)—1129(L)
Thomson, J. S. (see Bearden, J. A.)—629(L)
Thorn, R. J. (see Andre, C. G.)—925(A)
Thorndike, A. M. (see Fowler, W. B.)—861
Ting, Yu (see Manring, Edward)—360(A)
Tochilin, E. (see Ross, S. W.)—945(A)
Todd, Jay, Jr. (see Miller, Charles E.)—590
Tollestrup, A. V. and W. A. Wentzel. Monitor for high-energy electron or γ-ray beams—950(A)
—— (see Woodbury, H. H.)—1311
Tomizuka, C. T. Diffusion of Cd, In, and Sn in single crystals of Ag—922(A)
—— (see Sonder, E.)—970
Toppel, B. J. (see Bennett, W. E.)—924(A)
Townes, C. H. (see Honig, A.)—953(A)
—— (see Moszkowski, S. A.)—306
Trail, C. C. (see Johnson, C. H.)—924(A)
Treiman, S. B. Cosmic radiation in trapped orbits of solar magnetic dipole field—544
—— (see Firor, J.)—551
Tripp, R. (see Chamberlain, O.)—1430(L)
Trolan, J. K. (see Dolan, W. W.)—943(A)
Tuck, J. L. (see Arnold, W. R.)—483
Tucker, B. L. and E. C. Gregg. Resonances in $Li^7(\gamma,p)He^6$ cross section and high-energy limit of bremsstrahlung spectra—362(A)

Turner, W. J. (see Burstein, E.)—65
Tweet, Arthur G. Small angle x-ray scattering from liquid He I and liquid He II—15
Tycko, D. (see Foley, H. M.)—734

Udelson, Burton J. and John E. Creedon. Microwave measurements of properties of a dc H_3 discharge—648(A)
Utterback, N. G. (see Herwig, L. O.)—926(A)

Vachaspati. Elastic scattering of electrons by Coulomb field of nuclei using Born approximations—502
Van Hove, Leon. Temperature variation of magnetic inelastic scattering of slow neutrons—268
—— (see Placzek, G.)—1207
van Lieshout, R., R. H. Nussbaum, G. J. Nijgh, and A. H. Wapstra. Decay of Cu^{60} and nuclear levels in Ni^{60}—255(L)
van Loef, Jan J. (see Cox, Mason C.)—925(A)
Van Patter, D. M. (see Hintz, N. M.)—924(A)
Van Valkenburg, M. E. (see Hendricks, C. D., Jr.)—952(A)
Varian, Russell (see Packard, Martin)—941(A)
Varney, Robert N. Liberation of electrons by positive ion impact on cathode of pulsed Townsend discharge tube—1156
Vette, J. I. (see Oakley, D. C.)—949(A)
Vineyard, G. H. and G. J. Dienes. Theory of defect concentration in crystals—265
Voelker, W. H. Angular distribution of Compton scattered γ rays—362(A)
Voelz, Fred L. (see Cleveland, Forrest F.)—933(A)
Volkoff, G. M. Quadrupole splitting of nuclear magnetic resonance lines in single crystals—944(T)
von Engel, A. (see Robson, A. E.)—1121(L)
von Krzywoblocki, M. Z. Application of solutions of Boltzmann equation to turbulence—927(A)
Voss, J. R., T. R. Palfrey, and R. O. Haxby. Photoproduction of low-energy charged π mesons—918(A)

Wada, W. W. and D. T. King. Cross section for trident production by electrons of cosmic radiation—914(A)
Wainfan, N., W. C. Walker, and G. L. Weissler. Photoionization in atmospheric gases—651(A)
—— (see Walker, W. C.)—651(A)
Wakely, P. G. Binding energy calculation on He^4 with single-particle wave functions—1434(E)
Waldron, Esther C., Virginia A. Schultz, and Truman P. Kohman. Natural α activity of Nd—254(L)
Walker, J. (see Elliott, L. G.)—356(L)
Walker, R. (see Whetten, N. R.)—1356
Walker, Robert L. (see Cooper, Duane H.)—950(A)
—— (see Oakley, D. C.)—949(A)
Walker, W. C., N. Wainfan, and G. L. Weissler. Photoelectric yields of some metals in vacuum uv—651(A)
—— (see Wainfan, N.)—651(A)
Walker, W. D. (see Duller, N. M.)—284
—— (see Kaplon, M. F.)—1424(L)
Wallace, Robert. High-frequency performance of junction tetrode transistors—363(T)
Walt, M. and H. H. Barschall. Scattering of 1-Mev neutrons by intermediate and heavy elements—1062
Walton, R. B. (see Okazaki, A.)—461
Wang, S. (see Bloembergen, N.)—72
Wangsness, Roald K. Magnetic resonance in ferrimagnetics—68
Wapstra, A. H. (see Maeder, D.)—1433(L)
—— (see van Lieshout, R.)—255(L)
Warner, Charles, III, and Fritz Rohrlich. Energy loss and straggling of electrons—406
Warren, Roger W. Refined electron beam probe studies in glow discharges—943(A)
Wasserburg, G. J. and R. J. Hayden. Branching ratio of K^{40}—645(L)
Watson, K. M. (see Aitken, A.)—1349
—— (see Francis, N. C.)—313
Wattenberg, A., B. T. Feld, A. Julian, A. Odian, and L. S. Osborne. Search for production of μ-meson pairs by 340-Mev bremsstrahlung—915(A)
Weaver, A. B. (see Orear, Jay)—575
Weber, A. H. (see Breen, R. J.)—923(A)
—— (see Sturcken, E. F.)—1053
Weber, Alfons, Forrest F. Cleveland, and Salvador M. Ferigle. Raman and infrared spectra of dimethyltriacetylene—933(A)
Weddell, James B. and James H. Roberts. Angular distribution of $Li^8(n,\alpha)H^5$ for fast neutrons—924(A)
Weertman, J. and E. I. Salkowitz. Internal friction of dilute alloys of Pb—922(A)
Wegner, Harvey E. (see Farwell, George W.)—356(L)
Wehner, Gottfried K. Sputtering by ion bombardment—momentum transfer problem—653(A)
—— Threshold energies for sputtering and sound velocity in metals—633(L)
Weinreb, A. (see Cohen, S. G.)—1117(L)
Weisbrod, Harold (see Bessey, William H.)—923(A)
Weissbluth, M. (see Baez, A. V.)—942(A)
Weissler, G. L. (see Wainfan, N.)—651(A)
—— (see Walker, W. C.)—651(A)
Welker, Joan P. (see Schardt, A. W.)—916(A)
Welton, T. A. (see Simon, A.)—1435(E)
Wentzel, W. A. (see Tollestrup, A. V.)—950(A)
Wert, C. (see Ang, C.)—922(A)
Westerkamp, J. F. Variation of *l*-type doubling constant in HCN—716
Westermark, Torbjörn. Energy loss of charged relativistic particles and periodicity of elements—400
—— Influence of chemical state on stopping of fast charged particles—835
Wexler, S. Average charge of recoil atoms from several nuclear transitions—182
Weymouth, John. Simple bent-crystal x-ray spectrograph for senior experiment—359(T)
Whetten, N. R., R. S. Preston, R. V. Adams, R. Walker, and H. L. Kraybill. Cloud-chamber investigation of nuclear interactions of cosmic rays—1356
White, George R. (see Fry, W. F.)—1427(L)
Whittemore, W. L. (see Fowler, W. B.)—861
Wiegand, Clyde (see Chamberlain, O.)—1424(L); 1430(L)
Wiener, B. and G. Groetzinger. Variation of magnetoresistivity and resistivity of AuCu during annealing from cold-worked and thermally-disordered states—922(A)
Wightman, A. (see Michel, L.)—354(L)
Wiig, Edwin O. (see Caretto, Albert A., Jr.)—175
Wiles, Donald R. Search for $p_{1/2}$ isomeric state in Tc^{101} and identification of energy levels—181
Willardson, R. K., A. C. Beer, and A. E. Middleton. Magnetic field dependence of Hall coefficient in InSb—912(A)
—— (see Beer, A. C.)—912(A)
—— (see Harman, T. C.)—912(A)
Williams, Dudley (see Blau, Henry H., Jr.)—360(A)
—— (see Carpenter, Robert)—360(A)
—— (see Coburn, T. J.)—360(A)
—— (see Dalby, F. W.)—361(A)
—— (see Dickey, F. P.)—361(A)
—— (see Manring, Edward)—360(A)
—— (see Smith, Robert D.)—361(A)
—— (see Wolfe, Peter N.)—360(A)

Williams, G. A., D. W. McCall, and H. S. Gutowsky. Nuclear spin of Si^{29}—1428(L)
Williams, R. W. (see Hazen, W. E.)—578
Willig, F. J. Fast jet actuated shock tubes—946(A)
Wilson, R. N. Second Born approximation to the scattering of fast electrons and positrons by nuclei—949(A)
—— (see Ravenhall, D. G.)—949(A)
—— (see Yennie, D. R.)—948(A)
Wilson, Richard (see Brown, Karl L.)—443
Winans, J. G. (see St. John, Robert)—653(A)
Winckler, J. R. and K. Anderson. Geomagnetic and albedo studies with Čerenkov detector at 40° geomagnetic latitude—596
Windle, J. J. and T. M. Shaw. Slotted resonant cavity for dielectric measurements—952(A)
Winsberg, Lester. Interaction of μ^- mesons with I^{127}—937(A)
—— Pure negative muon beam—915(A)
Wittels, M. and F. A. Sherrill. Radiation damage in SiO_2 structures—1117(L)
Witten, Louis. Generalization of Yang and Lee's theory of condensation—1131
Wolfe, Peter N. and Dudley Williams. Microwave spectrum of O_2—360(A)
Wolfson, J. L. (see Elliott, L. G.)—356(L)
Wolfstirn, K. B. (see Fuller, C. S.)—1182
Woll, John W., Jr. (see Green, Louis C.)—757; 757
Wood, D. E. (see Roberts, James H.)—920(A)
Woodbury, H. H., A. V. Tollestrup, and R. B. Day. Low-energy γ radiation from bombardment of C by protons—1311
Woodruff, Truman O. OPW method for calculating energy eigenvalues extended to crystals of compounds—947(A)
Woodward, Ervin C., Jr. Isotope displacement in λ4415A Cd II—948(A)
—— Nuclear spins of Mo^{95} and Mo^{97}—954(A)
Woodward, W. M. (see Keck, J.)—827
Woolf, William E. and Richard B. Belser. X-ray diffraction studies of dual layer and simultaneously evaporated bimetal films after artificial aging by heating—930(A)
Worley, R. D., M. W. Zemansky, and H. A. Boorse. Vapor pressure curve of He between 4.2°K and 4.8°K—45
Wu, C. S. (see Boehm, F.)—518
Wu, Ta-You (see Tauber, G. E.)—295; 434
Wyeth, Cynthia W. (see Green, Louis C.)—757

Yager, W. A. (see Anderson, P. W.)—717
—— (see Galt, J. K.)—1119(L)
Yalow, Rosalyn. Use of radioactive I in the study of thyroid function—359(T)
Yasaitis, E. (see Smaller, B.)—940(A)
Yekutieli, G. (see Rosendorff, S.)—901(L)
Yennie, D. R., D. G. Ravenhall, and E. Baranger. Sign of phase shift in elastic scattering of electrons—1128(L)
——, **R. N. Wilson, and D. G. Ravenhall.** Phase-shift calculation of high-energy electron scattering by nuclei—948(A)
—— (see Ravenhall, D. G.)—949(A)
Yntema, J. L. (see Bayard, Robert T.)—1412(L)
Yokota, Ryosuke. Color centers in alkali silicate glasses—896(L)
Young, D. R. Dielectric constant measurements of $BaTiO_3$—359(T)
Ypsilantis, T. (see Chamberlain, O.)—1430(L)
Yuan, Luke C. L. Meson-nucleon interaction experiments at Brookhaven cosmotron—363(T)
—— **and S. J. Lindenbaum.** Energy spectrum of negative pions produced in Be by 2.3-Bev protons—1431(L)
—— **and S. J. Lindenbaum.** Total interaction cross section of hydrogen for positive and negative 200–700 Mev pions—917(A)
—— (see Lindenbaum, S. J.)—917(A)
Yuster, P. H. (see Delbecq, C. J.)—262

Zaffarano, D. J. (see Lane, R. O.)—916(A)
—— (see Morinaga, H.)—1422(L)
Zeiger, H. J. (see Lax, Benjamin)—1418(L)
Zelikoff, Murray (see Tanaka, Yoshio)—933(A)
Zemansky, M. W. (see Worley, R. D.)—45
Zumstein, R. V. (see Dickey, F. P.)—361(A)
Zweifel, Paul F. Positron-capture branching ratios—915(A)
Zwicky, F. Atmospheric disturbances and stellar scintillations—946(A)

Author Index to Volume 94

References with (A) are to abstracts of papers presented at meetings of the American Physical Society; references with (T) designate title only. References with (L) are to Letters to the Editor. References with (E) are to Errata.

Aamodt, L. C., P. C. Fletcher, G. Silvey, and C. H. Townes. Spin and quadrupole moment of Se^{75}—789(A)
Abraham, Bernard M. (see Osborne, Darrell W.)—202(L)
Adair, Robert K. Nuclear potential well depth—737(L)
Adams, R. K. (see Fields, R. E.)—389
Ajzenberg, Fay and Wolfgang Franzen. Neutrons from proton bombardment of N^{14}—409
Albrecht, H. O. and C. E. Mandeville. Luminescence of BeO—776(A)
Albrecht, H. O. (see Mandeville, C. E.)—494(L)
Aldrich, R. (see Marvin, Robert S.)—1413(A)
Alford, W. L. (see Newman, E.)—748(A)
Alford, W. Parker and Donald R. Hamilton. Recoil spectrum in β decay of Ne^{19}—779(A)
Alfvén, Hannes. Magnetic storm effect on cosmic radiation—1182(L)
Allen, Harry C., Jr., and Earle K. Plyler. Infrared spectrum of hydrogen sulfide in 5100 cm^{-1} region—1423(A)
—— (see Risser, J. R.)—810(A)
Allen, James (see Coulter, George A.)—782(A)
Allison, B. A. (see Scherrer, V. E.)—791(A)
Alvarez, Luis W. (see Gow, J. D.)—365
Ament, W. S. and G. T. Rado. Electromagnetic effects of spin wave resonance—1411(A)
Ander, Paul (see Mesrobian, Robert B.)—1413(A)
Anderson, C. D. (see van Lint, V. A.)—1732
Anderson, G. W., P. S. Freier, and J. E. Naugle. Time and directional study of primary heavy nuclei—1317
—— (see Freier, P. S.)—677
Anderson, James L. "Dressed" particles in quantum field theory—745(A)
—— Green's-functions in quantum electrodynamics—703
Anderson, W. A. and J. T. Arnold. Line-narrowing experiment—497(L)
Andrew, J. F. and S. Mrozowski. Photoresponse of aromatic films—1438(A)
Andrews, R. D. Measure of orientation in polystyrene monofilaments by means of double refraction—1412(T)
Annis, Martin, Homer C. Wilkins, and John D. Miller. Nuclear interaction of fast μ mesons—1038
Anthony, R. L. (see Baldwin, F. P.)—1425(A)
Argence, E. (see Rawer, K.)—253
Arné, L. A. (see Smith, R. L.)—1407(A)
Arnold, Charles W. and F. A. Matsen. Infrared spectra of C_2D_4O—804(A)
Arnold, J. T. (see Anderson, W. A.)—497(L)
Arnowitt, R. and S. Deser. Virtual states of two-meson systems—798(A)
—— **and S. Gasiorowicz.** Effect of negative energy components in two-nucleon system—746(A); 1057
Arrott, A. Method for measuring magnetization and susceptibility at low temperatures—781(A)
—— (see Goldman, J. E.)—782(A)
Asaro, Frank and I. Perlman. α- and γ-ray spectra of Pu^{238}—381
Aschner, J. F. Self-diffusion in KCl—771(A)
Ashkin, Arthur, Lorne A. Page, and W. M. Woodward. Electron-electron and positron-electron scattering measurements—357
Askey, C. M. (see Palmatier, E. D.)—766(A)
Augustyniak, W. (see McReynolds, A. W.)—1417(A)
Auth, W. J., W. S. Emmerich, and J. D. Kurbatov. Nuclear spectra of Ce^{144} and Pr^{144}—794(A)
—— (see Emmerich, W. S.)—110
Auverman, Harry J. and Arthur E. Lockenvitz. Mechanical electric computer for solving polynomial equations—811(A)
Azuma, Toshio. β-ray spectrum of Ag^{110}—638
Azumi, K. and J. E. Goldman. Volume magnetostriction in Ni and its alloys—781(A)

Babiskin, J. (see Steele, M. C.)—1394(L)
Badar, L. J. and V. P. Jacobsmeyer. Electrical characteristics of polycrystalline boron—808(A)
Bagchi, S. N. (see Hosemann, R.)—71
Bair, J. K. (see Willard, H. B.)—786(A)
Baker, E. (see Friedlander, G.)—727(L); 775(A)
Baldwin, F. P., J. Ivory, and R. L. Anthony. Experimental investigation of statistical theory of rubber elasticity——1425(A)
Ballantine, David S. (see Mesrobian, Robert B.)—1413(A)
Bandtel, Kenneth C. (see Frank, Wilson J.)—1716
Banister, J. R., S. Legvold, and F. H. Spedding. Structure of Gd, Dy, and Er at low temperatures—1140
Panta, H. E. and R. L. Macklin. Search for $Li^7(n,l)$ reaction—807(A)
Barber, W. A., P. Debye, and B. H. Eckstein. Field-induced diffraction method for molecular weight determinations—1412(A)
Bardeen, John. Surface barrier effects in semiconductors—1419(T)
—— Theory of boundary effects of super-conductors—554
Barnes, C. A. (see Peterson, R. W.)—1075(L)
—— (see Thirion, J.)—1076(L)
Barnes, J. M. Multiple diffraction patterns in glass produced by ultrasonic waves of high intensity—1434(A)
Barnes, R. G., P. J. Bray, and N. F. Ramsey. Variations of hydrogen rotational magnetic moments with rotational quantum number and with isotopic mass—893
Barrett, Paul H. K-meson and hyperon decays—1328
Bartholomew, G. A. (see Gove, H. E.)—749(A)
—— (see Paul, E. B.)—749(A)
Battey, J. F. and R. M. Baum. Energy of high-lying acceptor level in Cu-doped Ge—1393(L)
Bauer, Ernest and Ta-You Wu. Cooling of gas by radiation—1424(A)
Baum, R. M. (see Battey, J. F.)—1393(L)
Bay, Z., V. P. Henri, and F. McLernon. Upper limits for lifetimes of Ni^{60}—780(A)
Bayard, Robert T. and J. L. Yntema. Elastic scattering of electrons from nuclei—757(A)
Beard, D. B. Level densities in heavy nuclei of 10- to 20-Mev excitation—738(L)
Becker, J. H. (see Blunt, R. F.)—1431(A)
Becker, Milton. Growth of long-lifetime Ge crystals—1420(A)
Becker, R. L. (see Fields, R. E.)—389
Becker, Stewart and Melvin Eisner. Paramagnetic resonance absorption in diphenyl picryl hydrazyl at low values of splitting field—811(A)
Beer, A. C. (see Harman, T. C.)—1065(L)
Beers, Yardley (see Sterzer, Fred)—1410(A)
Beghian, L. E. (see Eliot, E. A.)—144
Beguin, Gilbert and Kasimir Fajans. Influence of charge distribution on repulsive forces and internuclear distances between ions—1434(A)
Belinfante, F. J. Avoiding perturbation methods in quantum electrodynamics, meson theory, etc.—745(A)
Bell, P. R. (see Sheline, Raymond K.)—1642
Bemski, G., W. A. Nierenberg, and H. B. Silsbee. Spin-orbit interaction in RbF and CsF—767(A)

Benedek, G. B. (see Paul, W.)—1415(A)
Benedict, W. S. and Shirleigh Silverman. Line shapes in infrared—752(A)
Bengston, J. (see Thaler, R. M.)—679; 683
Bennett, W. E. Spallation studies of Bi—997
Bennett, Willard H. Mapping particle paths in earth's magnetic field—796(A)
Beresovski, T. (see Cuykendall, T. R.)—1421(A)
Berger, J. M. Deuteron photodisintegration at intermediate energies—1698
Bergmann, Peter G. Restrictions on invariant transformation groups in Lagrangian and Hamiltonian formalisms—788(A)
Beringer, Robert, E. B. Rawson, and Allan F. Henry. Microwave resonance in NO: λ doubling and hfs—343
Berkowitz, A. E. Effect on diffusion measurements of some β-ray absorption phenomena—1407(A)
——, **F. E. Jaumot, Jr., and F. C. Nix.** Diffusion of Co^{60} in some Ni-Al alloys containing excess vacancies—1407(A)
—— (see Franklin, A. D.)—1432(A)
Berlincourt, Ted G. de Haas-van Alphen effect in Cd—1172
Bernardini, G. and E. L. Goldwasser. Photoproduction of π^+ mesons from H near threshold—729(L)
—— (see Goldwasser, E. L.)—755(A)
Bernstein, Eugene. Production of *L*-shell x-rays by protons—774(A)
Bernstein, Ira B. and T. Holstein. Electron energy distributions in stationary discharges—1475
Bernstein, Seymour, L. D. Roberts, C. P. Stanford, J. W. T. Dabbs, and T. E. Stephenson. Interaction of polarized neutrons with polarized Mn^{56} nuclei—1243
—— (see Sherwood, J. E.)—791(A)
—— (see Stanford, C. P.)—374
—— (see Wilkinson, M. K.)—772(A)
Bestul, A. B. Energy requirements of mechanical shear degradation in concentrated polymer solutions—1425(A)
Betchov, R. Triple correlations in isotropic turbulence—783(A)
Beyen, Werner J. (see Mitchell, Dean L.)—1430(A)
Bhatnagar, P. L., E. P. Gross, and M. Krook. Model for collision processes in gases. I. Small amplitude processes in charged and neutral one-component systems—511
Bichsel, H. and R. F. Mozley. Range of protons in Be, Al, Cu, Ag, and Au—764(A)
Bickford, L. R., Jr., J. Pappis, and J. L. Stull. Permeability and magnetostriction of cation-substituted magnetite—1433(A)
Biedenharn, L. C. (see Gluckstern, R. L.)—768(A)
—— (see Hull, M. H., Jr.)—768(A)
—— (see Major, J. K.)—779(A)
Bilpuch, E. G. (see Block, R. C.)—774(A)
Binder, D. and W. J. Sturm. Equivalence of x-ray lattice parameter and density changes in neutron-irradiated LiF—760(A)
Binnie, W. P. and A. M. Liebschutz. Elastic constants of Si before and after neutron bombardment from x-ray diffuse scattering—1410(A)
Biondi, Manfred A. and Lorne M. Chanin. Mobilities of atomic and molecular ions in noble gases—910
Bird, G. R. and C. H. Townes. S bonds and quadrupole moments of O, S, and Se isotopes—1203
Birks, J. B. Energy transfer in organic phosphors—1567
—— **and F. D. Brooks.** Scintillation response of anthracene to soft x-rays—1800(L)
Biswas, N. N. and M. S. Sinha. Mean lives of positive and negative μ mesons—1400(L)
Biswas, S. N. Solutions of Heitler's integral equation by iteration method—1767
Bittner, J. W., R. G. Herb, R. D. Moffat, and J. A. Weinman. Doubly ionized He ion source—769(A)
—— (see Haberle, W.)—769(A)
Bjerregaard, Jørgen H. and Torben Huus. Coulomb excitation by means of bombardment with various particles—204(L)
Blackman, V. H. and D. K. Weimer. Reflection of shock waves from blunt wedge—508
Blair, J. M. (see Holmgren, H. D.)—748(A)
Blatt, J. M. (see Kalos, M. H.)—762(A)
Bleil, D. F. and A. R. Butz. Magnetostriction in nickel ferrite-aluminates and nickel ferrite-gallates—1440(A)
Blewett, J. P. Design of 25-Bev proton synchrotron for European organization for nuclear research—792(T)
Bloch, F. Line-narrowing by macroscopic motion—496(L)
Block, R. C., J. H. Gibbons, E. G. Bilpuch, and D. F. Herring. Total neutron cross sections in kev region: As, Zr, Nb, La, Ce, Pr, and Au—774(A)
Bloembergen, N. Nuclear magnetic relaxation in semiconductors—1411(A)
—— Nuclear magnetic resonance and structure of metals and alloys—1416(T)
Bloom, Arnold L. and Owen Chamberlain. Scattering of 190-Mev deuterons on protons—659
Bloom, M. "Slow beats" in nuclear quadrupole induction—1396(L)
Bludman, Sidney A. Reaction $p+d \rightarrow \pi^+ + t$—1722
Blunt, R. F., H. P. R. Frederikse, and J. H. Becker. Optical absorption of AlSb—1431(A)
Bockelman, C. K. and J. J. Jung. Energies of excited states of Be^{10}—748(A)
Bode, Donald E. and Henry Levinstein. Effect of oxygen on PbTe films—1430(A)
Bode, Donald E. (see Mitchell, Dean L.)—1430(A)
Boley, F. I. Short-lived isomeric states of Ag^{110} and In^{114}—1078(L)
Bolsterli, Mark. Photon splitting in nuclear electrostatic field—367
Bonfiglioli, G., A. Ferro, G. Montalenti, and G. Rosa. Behavior of ferromagnetic domains under stress—316
Bonner, T. W. and C. F. Cook. Neutron thresholds in $Li^7(d,n)Be^8$ and $Be^9(d,n)B^{10}$—807(A)
—— (see Cook, C. F.)—651; 807(A)
—— (see Marion, J. B.)—807(A)
—— (see McCrary, J. H.)—808(A)
—— (see Taylor, H. L.)—807(A)
Boorse, H. A. Recent studies of heat capacities of superconducting elements—771(T)
Boorse, H. A. (see Smith, B.)—772(A)
Bothe, W. and H. Kraemer. Shower structure in higher shower maxima—1402(L)
Bowen, D. B. and H. Hori. Change of resistivity of Cu with elastic strain—1422(A)
—— (see Dixon, C. E.)—1418(A)
Boyer, R. F. Physical properties of polymeric glasses—1425(T)
Bozorth, R. M. and R. C. Sherwood. Magnetostriction of Co—1439(A)
—— (see Nesbitt, E. A.)—1440(A)
Braams, C. M. Energy levels in Ca^{41} from $Ca^{40}(d,p)Ca^{41}$ reaction—763(A)
Bradshaw, B. C. and R. A. Shuttleworth. Mechanism of adsorption. I. Theory—753(A)
—— (see Shuttleworth, R. A.)—753(A)
Bransden, B. H. Rearrangement collisions—726(L)
Brattain, W. H. and C. G. B. Garrett. Electrical properties of interface between Ge single crystal and electrolyte—750(A)
Bray, P. J. Self-quenching superregenerative rf spectrometers—767(A)
—— (see Barnes, R. G.)—893
Brebrick, R. F. and W. W. Scanlon. Interdiffusion in PbS crystals—1430(A)
—— (see Scanlon, W. W.)—1430(A)
Breit, G. Longitudinal and transverse stability in linear accelerator systems—768(A)
—— (see Thaler, R. M.)—683

Brentano, J. C. M. and Colman Goldberg. Electrical conductance of pressed powders, in particular of ZnO—56
—— **and J. D. Richards.** Evaporated multiple layers with semiconductor properties—1427(A)
Brice, M. K. (see Cork, J. M.)—1218
Bridgman, P. W. Effects of pressure on twelve rare-earth metals—759(T)
Brockhouse, B. N. Antiferromagnetism in CuO—781(A)
Brockman, Karl W., Jr. p-α scattering at 17.5 Mev—785(A)
Broder, J. D. (see Wolff, G.)—753(A)
Brolley, J. E., Jr., and W. C. Dickinson. Angular distribution of fragments from neutron-induced fission—640
Brooks, F. D. (see Birks, J. B.)—1800(L)
Brooks, Harvey. Theory of g factor and spin-lattice relaxation time in alkali metals—1411(A)
—— (see Paul, William)—1128; 1415(A)
Broudy, R. and H. Levinstein. High-frequency resistance of photoconducting films—290
—— **and H. Levinstein.** High-frequency resistance of thin films—285
Brown, Douglas E. (see Hobbs, Lindsey M.)—1412(A)
Brown, Edmond. Electronic energy bands in crystals—1434(A)
Brown, H. (see Ruderman, M. A.)—746(A)
Brown, Sanborn (see Weinstein, Roy)—758(A)
Browne, C. P. (see Zimmerman, S. F., Jr.)—749(A)
Brueckner, K. A. and J. S. Kovacs. Effect of deuteron formation on multiple meson production—726(L)
Brysk, Henry. β-decay interaction—1794(L)
Buchdahl, Rolf and Lawrence E. Nielsen. Multiple dispersion regions in rigid polymeric systems—1414(A)
Bueche, F. Mechanics of molecular motion in bulk polymers—1425(T)
Bulliard, Hubert H. Photomagnetoelectric effect in Ge and Si—1564
Bunker, M. E., J. P. Mize, and J. W. Starner. Disintegration of Y^{91}—1694
Burch, D. E., J. N. Howard, and Dudley Williams. Effect of foreign gas broadening on total absorption by 6.3μ band of water vapor—1424(A)
Burns, F. P. Kinetics of ordering and disordering process in Cu_3Au—1429(A)
Burson, S. B., W. C. Jordan, and J. M. LeBlanc. Decay of $_{65}Tb^{160}$ (71 days)—103
—— (see LeBlanc, J. M.)—1436(A)
Burstein, Elias. Anomalous optical absorption limit in InSb—1431(A)
——, **B. W. Henvis, and N. Sclar.** Infrared properties of p-type Ge—750(A)
Butz, A. R. (see Bleil, D. F.)—1440(A)

Cadenhead, C. P. (see Little, R. N., Jr.)—807(A)
Caird, Robert S. and Allan C. G. Mitchell. Disintegration of Co^{55} and I^{130}—412
—— **and Allan C. G. Mitchell.** Disintegration of I^{130}—780(A)
Caldwell, David O. and J. Reginald Richardson. Mean excitation potentials—79
Caldwell, R. S. and H. Y. Fan. Infrared absorption of Te—1427(A)
Calhoun, B. A. Magnetic and electric properties of magnetite at low temperatures—1577
Callen, Earl. Configuration interaction applied to hydrogen molecule—1423(A)
Callen, Herbert B. (see Kriessman, C. J.)—781(A); 837
Campbell, R. C., J. D. Korsmeyer, and D. C. Ralph. Neutron yields from d-d reaction in various target materials—791(A)
Carlson, B. C. (see Gerhart, J. B.)—917
Carlson, R. R., E. H. Geer, and E. B. Nelson. Scintillation counter study of γ rays from proton capture in Na—1311
Carr, H. Y. and E. M. Purcell. Effects of diffusion on free precession in nuclear magnetic resonance experiments—630
Carter, R. S. (see Palevsky, H.)—1088(L)
Case, K. M. Nonrelativistic limit of half-integral-spin wave equations—1442(A)
—— Two extensions of Foldy-Wouthuysen transformation—786(A)
—— (see Mendlowitz, H.)—1436(A)
Castle, J. G., Jr. Paramagnetic resonance absorption in carbons—1410(A)
Caswell, R. S., R. F. Gabbard, W. P. Doering, and D. W. Padgett. Attenuation of 14.1-Mev neutrons in water—786(A)
Chaberski, A. (see Mrozowski, S.)—1427(A)
Chamberlain, Owen and James W. Easley. Small angle neutron-proton scattering at 90 Mev—208(L)
——, **G. W. Farwell, and E. Segrè.** $_{94}Pu^{240}$ and its spontaneous fission—156
—— **and Martin O. Stern.** Elastic scattering of 190-Mev deuterons by protons—666
—— (see Bloom, Arnold L.)—659
—— (see Clark, David D.)—785(A)
Chanin, Lorne M. (see Biondi, Manfred A.)—910
Charlesby, A. Effect of high-energy radiation on polymers—1412(T)
Charpie, R. A. (see Cohen, B. L.)—620
—— (see Cohen, B. L.)—953
Chase, D. M. and F. Rohrlich. Elastic scattering of protons by nuclei—81
Chen, F. F., C. P. Leavitt, and A. M. Shapiro. Attenuation of 870-Mev protons by various elements—784(A)
Chester, G. V. Theory of liquid He—246
Chew, Geoffrey F. Method of approximation for meson-nucleon problem when interaction is fixed and extended—1755
—— Renormalization of meson theory with fixed extended source—1748
Choppin, G. R., S. G. Thompson, A. Ghiorso, and B. G. Harvey. Nuclear properties of some isotopes of Cf, elements 99 and 100—1080(L)
—— (see Ghiorso, S. G.)—1081(L)
Christian, R. (see Lee, T. D.)—1760
Christian, Russell H. and Robert G. Shreffler. Hugoniot of gases by shock wave measurements—783(A)
Christy, R. F. Low excited states of F^{19}. IV. Angular distributions—1077(L)
—— (see Sherr, R.)—1076(L)
Chuoke, Robert L. Electron interactions in metals—808(A)
Church, E. L. and J. E. Monahan. Internal conversion in L and M sub-shells—762(A)
Claassen, H. H. (see Nielsen, J. Rud)—805(A)
Clark, A. F. (see Grandey, R. A.)—766(A)
Clark, David D. and Owen Chamberlain. Elastic scattering of 340-Mev protons by deuterons—785(A)
Clarke, Edward N. Electron traps on Ge surfaces produced by heating in oxygen—1420(A)
Clarkson, Henry Neal and Arthur E. Lockenvitz. Accurate determination of tidal variations of gravity—811(A)
Class, C. M. Coulomb excitation of nuclei—809(T)
——, **C. F. Cook, and J. T. Eisinger.** Coulomb excitation of heavy nuclei—747(A); 809(A)
—— (see Cohen, L.)—419
—— (see Dudley, J. D.)—807(A)
—— (see Eisinger, J. T.)—735(L)
Clauser, Francis H. Design of diffusers to avoid turbulent boundary layer separation—783(A)
Cleland, J. W. and J. H. Crawford, Jr. Radiation effects in InSb—1410(A)
—— (see Stevens, D. K.)—1409(A)
Clendenin, W. W. Gyromagnetic ratio in hfs of doublet states—1590
Cocconi, Giuseppe. Influence of earth magnetic field on extensive air showers—796(A)

—— Strange particles and multiple meson production—741(L)
Cochran, L. W. (see Stanford, C. P.)—374
Cohen, Bernard L. K^{41}—117
—— Angular distribution of products from 22-Mev proton reactions—803(T)
—— Diffraction scattering of 22-Mev protons—773(T)
——, **R. A. Charpie, T. H. Handley, and E. L. Olson.** Mn^{57}—953
——, **W. H. Jones, G. H. McCormick, and B. L. Ferrell.** Angular distributions of fission fragments from 22-Mev proton-induced Th fission—625; 758(A)
——, **E. Newman, R. A. Charpie, and T. H. Handley.** (p,pn) and $(p,\alpha n)$ excitation functions—620
Cohen, E. Richard (see DuMond, Jesse W. M.)—1790(L)
Cohen, L., S. S. Hanna, and C. M. Class. Angular correlations in $Be^9(d,p\gamma)Be^{10}$ and $Be^9(d,\alpha\gamma)Li^7$—419
Cohen, M. H. and F. Keffer. Dipolar ferromagnetism in cubic lattices—1412(A)
Coles, D. K. (see Gunther-Mohr, G. R.)—1184
Collins, G. B. Cosmotron as research tool—745(T)
Collins, R. L. and J. Rud Nielsen. Vibrational spectra of $H_3C\text{-}SiF_3$—805(A)
Collins, T. L., Walter H. Johnson, Jr., and Alfred O. Nier. Atomic masses in intermediate region—398
Conway, John G. and Ralph D. McLaughlin. Nuclear spin of Am^{242} and isotope shift in Am spectrum—498(L)
Conwell, Esther M. Electrical properties of p-type Ge—1416(A)
—— High-field effects in Ge—1068(L)
Cook, C. F. and T. W. Bonner. Neutron thresholds from $Cu^{65}(p,n)Zn^{65}$, $Cu^{63}(p,n)Zn^{63}$, and $Li^7(p,n)Be^7$—807(A)
—— **and T. W. Bonner.** Scattering of fast neutrons in light nuclei—651
—— (see Bonner, T. W.)—807(A)
—— (see Class, C. M.)—747(A); 809(A)
—— (see Eisinger, J. T.)—735(L)
—— (see Marion, J. B.)—807(A)
Cooke, Claude E. Study of electrokinetic relations using sinusoidal pressure and voltage—812(A)
Cooley, William C. (see Van Horn, David D.)—1418(A)
Coon, J. B. and J. K. Ward. Application of Franck-Condon principle to bent XY_2 molecule—805(A)
Coon, J. H. and R. W. Davis. Elastic scattering of 14-Mev neutrons—785(A)
Cooper, Daniel I., David H. Frisch, and Robert L. Zimmerman. p-p scattering near interference minimum—1209
Cooper, H. G., J. S. Koehler, and J. W. Marx. Resistivity changes in Cu, Ag, and Au produced by deuteron irradiation near 10°K—496(L)
Cooper, J. N. (see Green, D. W.)—764(A)
—— (see Smith, J. A.)—749(A)
Coor, T. (see Hill, D. A.)—791(A)
—— (see Snow, G. A.)—791(A)
Corben, H. C. Lamb shift in mesic atoms—787(A)
Corenzwit, E. (see Matthias, B. T.)—1069(L)
Cork, Bruce and Walter Hartsough. p-p scattering at 9.7 Mev—1300
Cork, J. M., M. K. Brice, L. C. Schmid, G. D. Hickman, and H. Nine. Neutron capture in separated isotopes of Pt—1218
—— (see LeBlanc, J. M.)—1436(A)
Corliss, L. (see Weiss, R. J.)—1420(A)
Cormack, A. M. Interference of Rayleigh and nuclear Thomson scattering—1397(L)
Corrsin, Stanley. Measure of area of homogeneous random surface in space—783(A)
—— (see Kistler, Alan)—783(A)
Corson, D. R. (see Davis, H. L.)—756(A)
Cotter, T. P. Structure of detonation in some liquid explosives —765(T)
Coulter, George A. and James Allen. Diffraction of step shoc— through double slits—782(A)
Courant, E. D. Interaction of high-energy pions with nucleisk 1081(L)
—— Particle orbits in alternating gradient synchrotron—792(T)
Courant, H. γ rays associated with S-particle decay—797(A)
Cowan, Alvin E. and Arthur E. Lockenvitz. Time rate of change for transformation of monoclinic Se into hexagonal—809(A)
Cowan, C. L., Jr., and F. Reines. Status of experiment to detect free neutrino—751(T)
Cowan, E. W. Properties of new V particles—796(T)
—— V-decay event with heavy negative secondary, and identification of secondary V-decay event in cascade—161
—— (see van Lint, V. A.)—1732
Cowen, J. A. and R. D. Spence. Ferromagnetic resonance relaxation times in single crystals of Ni and Fe—1411(A)
Cranberg, L. (see Henkel, R. L.)—141
Crane, H. R. Design of precision experiment on gyromagnetic ratio of free electron—1426(T)
—— Initiation of discharge in CO_2-filled GM counter by negative ions—1437(A)
—— (see Louisell, W. H.)—7
Crane, W. W. T. (see Higgins, G. H.)—735(L)
Crawford, J. H. Nucleon bombardment of semiconductors—803(T)
Crawford, J. H., Jr., and D. K. Stevens. Effective mass and degeneracy of carriers in Ge from diamagnetic behavior—1415(A)
—— (see Cleland, J. W.)—1410(A)
—— (see Stevens, D. K.)—1409(A)
Crittenden, E. C., Jr., and H. Dieckamp. Change of elastic constants of Cu on annealing after plastic deformation at 78°K—1421(A)
—— (see Dieckamp, H.)—1418(A)
Crownfield, Frederic R., Jr., and Peter Havas. Classical equations of motion of point particles in neutral meson fields—471
Crussard, J., W. D. Walker, and M. Koshiba. π^--p interactions at 1.5 Bev—736(L)
—— (see Hill, R. D.)—797(A)
Curtis, J. P. Absorption coefficients of air and nitrogen for extreme uv—908
Cuykendall, T. R., T. Beresovski, and H. S. Sack. Internal friction in single metal crystals at audiofrequencies—1421(A)
—— (see Sack, H. S.)—1414(A)

Dabbs, J. W. T. (see Bernstein, S.)—1243
Dailey, B. P. (see Kraitchman, J.)—788(A)
—— (see Solimene, N.)—789(A)
Daitch, P. B. (see Gluckstern, R. L.)—768(A)
—— (see Hull, M. H., Jr.)—768(A)
Dalby, F. W., H. H. Nielsen, and F. P. Dickey. Absorption spectra of water vapor in 2.7μ and 6.0μ regions—1423(A)
Dalitz, R. H. Decay of τ mesons of known charge—1046
D'Altroy, F. A. and H. Y. Fan. Microwave transmission in p-type Ge—1415(A)
Damask, A. C. and A. S. Nowick. Internal friction associated with precipitation in Al-Ag alloy—1421(A)
Danforth, W. E. (see Goldwater, D. L.)—754(A)
Danos, M. Čerenkov radiation from extended electron beams —758(A)
Darden, Sperry (see Nereson, Norris)—1678
Darrow, K. K. American Physical Society at Columbia University—776(T)
Dash, Jay Gregory. Critical and supercritical flow of liquid helium II—771(T); 772(A)

—— Superfluidity and dissipative processes in liquid He II—825
—— Superfluid dynamics of liquid He II—1091
Date, Muneyuki (see Okamura, Tosihiko)—314
Daunt, J. G. (see Gordon, W. L.)—771(A)
Davis, H. L. and D. R. Corson. Elastic production of π^0 photomesons from deuterium—756(A)
Davis, Marguerite. Range measurement of low voltage electrons—243
Davis, R. C. (see Sheline, Raymond K.)—1642
Davis, R. E. (see Goldberg, Colman)—1121
Davis, R. W. (see Coon, J. H.)—785(A)
Davisson, J. W. Electrical breakdown paths in nonpolar crystals—1437(A)
Daw, Harold. Generalized absorption coefficients of water vapor—1424(A)
Dayton, I. E. and P. C. Gugelot. Elastic scattering of 18.5-Mev protons by nuclei—785(A)
Deal, W. E., Jr. Shock Hugoniot of air—811(A)
DeBenedetti, S. and R. T. Siegel. 3-photon annihilation of positrons and electrons—955
——, **M. B. Stearns, M. Stearns, and H. J. Richings.** Spectroscopy of π- and μ-meson x-rays—766(A)
—— (see Stearns, M.)—766(A)
—— (see Sugarman, R.)—796(A)
deBretteville, A. P., Jr. Threshold field and free energy for antiferroelectric-ferroelectric phase transition in $PbZrO_3$—1125
—— **and E. D. Harris.** Heat of transition of $BaTiO_3$ at Curie point—1408(A)
Debye, P., P. P. Debye, and B. H. Eckstein. Dielectric high-frequency method for molecular weight determinations—1412(A)
—— (see Barber, W. A.)—1412(A)
Debye, P. P. and T. Kohane. Hall mobility of electrons and holes in Si—724(L)
—— (see Debye, P.)—1412(A)
de Carvalho, H. G., E. Heiberg, J. Marshall, and L. Marshall. Polarization by p-p collision at 439 Mev—1796(L)
de Groot, S. R. and P. Mazur. Extension of Onsager's theory of reciprocal relations. I—218
—— (see Mazur, P.)—224
Dekker, A. J. Energy and temperature dependence of secondary emission of MgO—1179
DeMarco, J. J. (see Weiss, R. J.)—1420(A)
Denney, J. M. Experimental evidence for melted regions in metal crystals resulting from particle bombardment—1417(A)
De-Saussure, G. and L. S. Osborne. Elastic photoproduction of π^0 in He—756(A)
Deser, S. and W. E. Thirring. Low-energy limits of meson processes—746(A)
——, **W. E. Thirring, and M. L. Goldberger.** Low-energy limits and renormalization in meson theory—711
—— (see Arnowitt, R.)—798(A)
de-Shalit, A. (see Schwartz, C.)—1257
Detwiler, D. P. Conductivity, Hall effect, and rectification of GaSb—1431(A)
Deutsch, Martin (see Weinstein, Roy)—758(A)
DeWire, J. W. (see Wolfe, B.)—756(A)
Dexter, D. L. Tunneling of electrons in alkali halides—771(A)
Diamond, H., L. B. Magnusson, J. F. Mech, C. M. Stevens, A. M. Friedman, M. H. Studier, P. R. Fields, and J. R. Huizenga. Identification of Cf isotopes 249, 250, 251, and 252 from pile-irradiated Pu—1083(L)
—— (see Fields, P. R.)—209(L)
—— (see Stevens, C. M.)—974
Dibeler, Vernon H. and Fred L. Mohler. Mass spectra of deuteroethylenes—754(A)
Dick, J. (see Sakai, M.)—779(A)
Dickey, F. P. (see Dalby, F. W.)—1423(A)
—— (see France, W. L.)—1423(A)
Dickinson, W. C. (see Brolley, J. E., Jr.)—640
DiDonato, A. R., A. A. MacLeod, and A. C. Webber. Creep and relaxation of plastics—770(A)
—— (see MacLeod, A. A.)—769(A)
Dieckamp, H. and E. C. Crittenden, Jr. Shear modulus of irradiated Cu—1418(A)
—— (see Crittenden, E. C., Jr.)—1421(A)
Dienes, G. J. (see Levy, Paul W.)—1409(A)
—— (see Mesrobian, Robert B.)—1413(A)
—— (see Rosenblatt, D. B.)—1417(A)
Dillon, J. A., Jr., and H. E. Farnsworth. Adsorption of CO_2 on Ni single crystal faces using radiotracer technique—753(A)
Dixon, C. E. and D. B. Bowen. Radiation ordering by cyclotron particles—1418(A)
Doering, W. P. (see Caswell, R. S.)—786(A)
Dolecek, R. L. Latent heat of transition of superconducting Pb—540
Domenicali, C. A. and F. A. Otter. Thermoelectric power and resistivity of dilute Cu-Si, Ni-Si, and Fe-Si alloys—1421(A)
Donahoe, F. J. (see Steijn, R. P.)—1432(A)
Dorfman, Leon M. and B. A. Hemmer. Ion-yield of tritium-oxygen reaction—754(A)
Dosanjh, Darshan (see Kovásznay, Leslie S. G.)—784(A)
Douglas, R. A. (see Jones, K. W.)—947
Dousmanis, G. C. Microwave spectrum of free OD radical—789(A)
Douthett, E. M. and D. H. Templeton. Ranges of fragments from high-energy fission of U—128
—— (see Templeton, D. H.)—759(A)
Dreicer, H. (see Strandberg, M. W. P.)—1393(L)
Dresden, M. and Martin Gutzwiller. Renormalization questions in curved spaces—745(A)
Dresner, Joseph. Spectral energy distribution of 2-Mev x-rays—751(A)
Dropkin, J. J. (see Watson, W. R.)—777(A)
Drost-Hansen, W. and E. J. Workman. Theory of volume rectification in ice—770(A)
—— (see Workman, E. J.)—770(A); 1073(L)
Drougard, M. E. and D. R. Young. Domain clamping effect in $BaTiO_3$ single crystals—1408(A); 1561
Drummond, W. E. and C. S. Gardner. Point-source kernel for diffusion with small-angle scattering—1491
Dudley, J. D. and C. M. Class. $N^{14}(n,2n)N^{13}$ cross-section measurement with 14-Mev neutrons—807(A)
Dudziak, Walter F. π^+ production cross sections from deuterium—756(A)
—— (see Sagane, Ryokichi)—755(A)
Duerig, William H. Rate of production of color centers in KCl and KBr by x-rays at 78°K—65
Duff, Russell E. and H. T. Knight. Observations of Taylor instability in gases—784(A)
—— (see Knight, Herbert T.)—784(A)
Duffield, Robert B. and Nathan Sugarman. Disintegration of heavy elements by 2.2-Bev protons—776(A)
—— (see Gindler, James)—759(A)
Duller, N. M., W. D. Walker, J. W. Graham, and J. R. Risser. Sea-level zenith-angle dependence of high-energy μ mesons—810(A)
DuMond, Jesse W. M. and E. Richard Cohen. Variety of our sources of information on Avogadro's number and other constants—1790(L)
Dunlap, W. C., Jr. Diffusion of impurities in Ge—1531
—— Properties of Zn-, Cu-, and Pt-doped Ge—1419(A)
—— (see Leifer, H. N.)—1431(A)
Dunnington, F. G., C. L. Hemenway, and J. D. Rough. Determination of h/e by new method—592
Dvorak, Henry R. (see Wills, James E.)—810(A)

Easley, James W. (see Chamberlain, Owen)—208(L)
Eatherly, W. P. Radiation damage effects on electronic properties of graphite—1432(T)
Eck, T. G. (see Kusch, P.)—1799(L)
Eckerman, J. (see Schwartz, R. N.)—1441(A)
Eckstein, B. H. (see Barber, W. A.)—1412(A)
—— (see Debye, P.)—1412(A)
Efremov, N. New method of approximate calculation of atomic radii—753(A)
—— Role of principal quantum number (n) in calculations of radii for ions with high (4, 5, 6, 7) valence—1424(A)
—— Role of Rydberg constant in calculation of ionic radii—813(A)
Eggleston, R. R. (see Meechan, C. J.)—1406(A)
Eisberg, R. M. Energy spectra of nucleons evaporated from compound nucleus—739(L)
—— (see Palevsky, H.)—1088(L)
Eisele, J. A. and F. Keffer. Effects of anisotropy on thermodynamic properties of antiferromagnets—1440(A)
Eisenstein, Albert S. X-ray induced luminescence in MgO—776(A)
Eisinger, J. T., C. F. Cook, and C. M. Class. Electric excitation of Ta—735(L)
—— (see Class, C. M.)—747(A); 809(A)
—— (see Gossett, C. R.)—807(A)
Eisner, Melvin (see Becker, Stewart)—811(A)
—— (see Mitchell, R. W.)—811(A)
Ekstein, H. Unitarity of U operator—1063
—— **and J. Kelly.** Rapid remagnetization of thin Mo permalloy strips—1440(A)
Elcock, E. W. Molecular field treatment of magnetic ordering transitions—1070(L)
Eliot, E. A., D. Hicks, L. E. Beghian, and H. Halban. Inelastic scattering of neutrons—144
Elliott, J. F., S. Legvold, and F. H. Spedding. Magnetic properties of Dy metal—1143
——, **S. Legvold, and F. H. Spedding.** Magnetic susceptibility of Nd metal—50
Elliott, L. G., R. L. Graham, J. Walker, and J. L. Wolfson. Energy levels of Pb^{208}—795(A)
Elliott, R. J. Resistance anomalies in some rare earth metals—564
El-Sabban, M. Z. and J. Rud Nielsen. Vibrational spectra of cyclobutforene—805(A)
Elsasser, Walter M. Magnetohydrodynamics of earth and sun—1440(T)
Emmerich, W. S., W. J. Auth, and J. D. Kurbatov. Nuclear spectra of Ce^{144} and Pr^{144}—110
——, **S. E. Singer, and J. D. Kurbatov.** Radiative electron capture of Fe^{55}, A^{37}, and Ni^{59}—113
—— (see Auth, W. J.)—794(A)
—— (see Singer, S. E.)—779(A)
Endt, P. M. (see Kluyver, J. C.)—1795(L)
Enge, Harald A. Spins of lowest states of K^{40}, P^{32}, and Al^{28} nuclei—730(L)
Engelbrecht, Alfred (see Lotspeich, J. F.)—789(A)
Engelkemeir, D. and L. B. Magnusson. Existence of 3.7×10^{-8}-sec metastable state in Pa^{233}—1395(L)
Enright, Dorothy (see Talley, Robert M.)—1431(A)
Epstein, A. and H. Fritzsche. Hall effect and thermoelectric power of pure Te at melting point and in liquid state—1426(A)
Ewald, A. W. Effect of impurities on conductivity of gray tin—1428(A)
Ewing, R. and J. C. Lee. Proton magnetic resonance in compounds having several liquid crystal phases—1411(A)

Fader, W. J. and A. Sperduto. Energy levels, from reaction $B^{10}(\alpha,p)C^{13}$—748(A)
Fagen, E., J. Goff, and N. Pearlman. Thermal conductivity and thermoelectric power of Ge at low temperatures—1415(A)
Fairhall, A. W., I. Halpern, and E. J. Winhold. Angular anisotropy of specific Th photofission fragments—733(L)
Fajans, Kasimir (see Beguin, Gilbert)—1434(A)
—— (see Caldwell, R. S.)—1427(A)
Fan, H. Y. (see D'Altroy, F. A.)—1415(A)
—— (see Kaiser, W.)—1431(A)
Farnsworth, H. E. (see Dillon, J. A., Jr.)—753(A)
—— (see Wallis, G.)—777(A)
Farquhar, R. M. (see Shillibeer, H. A.)—1793(L)
Farwell, G. W., J. E. Roberts, and A. C. Wahl. Half-lives of Pu^{240} and Pu^{238}—363
—— (see Chamberlain, O.)—156
Faust, W. R. (see Scherrer, V. E.)—791(A)
Feld, B. T., R. D. Godbole, A. Odian, F. Scherb, P. C. Stein, and A. Wattenberg. High-energy photoproton production by 325-Mev bremsstrahlung radiation—1000
Fermi, Enrico. Physics at Columbia University: genesis of nuclear-energy project—776(T)
—— What can we learn with high-energy accelerators?—773(T)
Ferrell, B. L. (see Cohen, B. L.)—625; 758(A)
Ferrell, R. A. (see Schulten, R.)—739(L)
Ferro, A. (see Bonfiglioli, G.)—316
Ferry, John D., Malcolm L. Williams, and Donald M. Stern. Slow relaxation mechanisms in concentrated polymer solutions—1413(A)
—— (see Williams, Malcolm L.)—1413(A)
Feshbach, Herman. Relativistic wave equations—786(A)
Feynman, R. P. Atomic theory of two-fluid model of liquid He—262
—— **and G. Speisman.** p-n mass difference—500(L)
Fields, P. R., M. H. Studier, J. F. Mech, H. Diamond, A. M. Friedman, L. B. Magnusson, and J. R. Huizenga. Additional properties of isotopes of elements 99 and 100—209(L)
—— (see Diamond, H.)—1083(L)
—— (see Stevens, C. M.)—974
Fields, R. E., R. L. Becker, and R. K. Adams. Measurement of n-p cross section at 1.0 and 2.5 Mev—389
Fine, M. E. and Nancy T. Kenney. Moduli and internal friction of magnetite as affected by low temperature transformation—1573
Fink, Richard W. and Edwin O. Wiig. Reactions of Cs with 240-Mev protons—1357
Fireman, E. L. and D. Schwarzer. Measurement of T concentration in natural waters by diffusion cloud chamber—385
Firor, John W. Cosmic radiation intensity-time variations and their origin. IV. Increases associated with solar flares—1017
——, **W. H. Fonger, and J. A. Simpson.** Cosmic radiation intensity-time variations and their origin. V. Daily variation of intensity—1031
Fisher, L. H. (see Menes, M.)—1
Fiske, Milan D. Effect of hydrostatic pressure on superconducting transition of Sn and Tl—495(L)
Fivel, Daniel I. and Gilbert N. Plass. Radiation flux in planetary atmosphere—752(A)
Fleeman, Jerome. $\beta\rightarrow\alpha$ transformation in Sn—1422(A)
Fletcher, P. C. (see Aamodt, L. C.)—789(A)
Fletcher, R. C., W. A. Yager, G. L. Pearson, A. N. Holden, W. T. Read, and F. R. Merritt. Spin resonance of donors in Si—1392(L)
Folen, V. J., F. C. Nix, and F. E. Jaumot, Jr. Ferromagnetic properties and order-disorder in Fe-Pd alloys—1432(A)
Foley, H. M. (see Sessler, A. M.)—761(A)
Fonger, W. H. (see Firor, J. W.)—1031
Foote, H. L., Jr. Te resonance scattering—790(A)

Ford, Kenneth W. and David L. Hill. Non-uniform nuclear charge distributions and measurements of nuclear electrical radius—1630
—— (see Hill, David L.)—1617; 787(A)
Forster, H. K. and N. Zuber. Bubble dynamics in superheated liquid—754(A)
Foster, B. P., G. S. Stanford, and L. L. Lee. γ rays from Ne^{22} 804(A)
Fowler, C. M., H. W. Kruse, V. Keshishian, R. J. Klotz, and G. P. Mellor. Energy levels in W^{182}—1082(L)
Fowler, Charles A., Jr., and Edward M. Fryer. Magnetic domains by longitudinal Kerr effect—52
Fowler, E. C., H. L. Kraybill, R. M. Walker, and R. S. Preston. Interaction with A and Pb of neutrons with energies up to 2.3 Bev—791(A)
Fowler, W. A. (see Peterson, R. W.)—1075(L)
Fox, David. Production of antiprotons in p-p collisions—499(L)
Fox, T. G. Effect of structural variables on specific volume and glass temperature—1425(T)
France, W. L. and F. P. Dickey. 2.7μ bands of CO_2—1423(A)
Frank, P. J. (see Gutowsky, H. S.)—1067(L)
Frank, Wilson J., Kenneth C. Bandtel, Richard Madey, and Burton J. Moyer. Angular distribution and yield of process $p+d \rightarrow t+\pi^+$—1716
Franklin, A. D., A. E. Berkowitz, and E. Klokholm. Ferromagnetism and order in Fe-Pt alloys near Fe_3Pt—1432(A)
Franzen, Wolfgang (see Ajzenberg, Fay)—409
Fraser, J. S. and J. C. D. Milton. Rates of decay of observed anisotropies in Am^{241} α-γ and Cd^{111} γ-γ angular correlations—795(A)
Fraser, P. A. (see Nicholls, R. W.)—1423(A)
Frazer, B. C., Marilyn McKeown, and Ray Pepinsky. Neutron diffraction studies of Rochelle-salt single crystals—1435(A)
Frederikse, H. P. R. (see Blunt, R. F.)—1431(A)
Freidman, M. B. (see Ludloff, J. F.)— 763(T)
Freier, P. S., G. W. Anderson, and J. E. Naugle. Decay of heavy nuclear fragment—677
—— (see Anderson, G. W.)—1317
Freistadt, Hans. Quantized interaction of relativistic fields—746(A)
Frenzen, P. (see Fultz, D.)—1471
Frerichs, Rudolf. Dielectric changes in crystal-phosphor condensers irradiated with x-rays—1408(A)
Fried, Burton D. and R. J. Riddell, Jr. Meson-nucleon scattering. II—746(A)
—— (see Riddell, R. J., Jr.)—1736; 745(A)
Friedlander, G., E. Baker, J. Hudis, J. M. Miller, and R. Wolfgang. Radioactive products from interaction of 2.2-Bev protons with Cu—775(A)
——, **J. M. Miller, R. Wolfgang, J. Hudis, and E. Baker.** Nuclear reactions of Cu with 2.2-Bev protons—727(L)
—— (see Hudis, J.)—775(A)
—— (see Wolfgang, R.)—775(A)
Friedman, A. M. (see Diamond, H.)—1083(L)
—— (see Fields, P. R.)—209(L)
—— (see Stevens, C. M.)—974
Friedman, Abraham S. and Lester Haar. General method for high-speed machine computation of ideal gas thermal properties. Isotopic water molecules—1423(A)
Frisch, David H. (see Cooper, Daniel I.)—1209
Fritzsche, H. Hall effect and resistivity of Ge at low temperatures—1415(A)
—— (see Epstein A.)—1426(A)
Frost, Albert D. (see Mingins, Charles R.)—770(A)
Fryer, Edward M. (see Fowler, Charles A., Jr.)—52
Fuller, C. S. (see Severiens, J. C.)—750(A)
Fuller, E. G. and Evans Hayward. Elastic scattering of photons—732(L)
Fultz, D., Y. Nakagawa, and P. Frenzen. Instance in thermal convection of Eddington's "overstability"—1471
Furst, Milton and Hartmut Kallmann. Energy transfer by means of collision in liquid organic solutions under high energy and uv excitations—503

Gabbard, R. F. (see Caswell, R. S.)—786(A)
Garber, M. and D. E. Mapother. Effect of hydrostatic pressure on superconducting transition of Sn—1065(L)
Gardner, C. S. (see Drummond, W. E.)—1491
Gardner, J. W. Effect of knock-on electrons on ionization loss—746(A)
Garrett, C. G. B. (see Brattain, W. H.)—750(A)
Garrison, Gerald R. (see Miller, Charles E.)—167
Gasiorowicz, S. (see Arnowitt, R.)—746(A); 1057
Gates, Halbert. Determination of ratio of photo-elastic constants of glasses by means of ultrasonic waves—1434(A)
Geballe, T. H. and G. W. Hull. Seebeck effect in Ge—1134
Geer, E. H. (see Carlson, R. R.)—1311
Gehatia, Matatiahu. Low even configurations of Hf II—618
Gellman, H. (see Sharp, W. T.)—762(A)
Geltman, S. Interpretation of ionic mobilities in N_2—1072(L)
George, Waller (see McLean, E. A.)—761(A); 1428(A)
Gerhart, J. B., B. C. Carlson, and R. Sherr. Annihilation of positrons in flight—917
Gerjuoy, E. and David S. Saxon. Application of variational methods to intermediate and high-energy scattering—478
—— **and David S. Saxon.** Variational principles for acoustic field—1445
Ghiorso, A., S. G. Thompson, G. R. Choppin, and B. G. Harvey. New isotopes of Am, Bk, and Cf—1081(L)
—— (see Choppin, G. R.)—1080(L)
Gibbons, J. H. Improved apparatus for high resolution neutron cross-section measurements—773(A)
—— (see Block, R. C.)—774(A)
Gibbs, Julian H. Electric polarization of charged particles in square potential wells—292
Gilbert, Richard S. (see Hicks, Harry G.)—371
Gilmer, T. E. (see Patterson, J. R.)—774(A)
Gindler, James and Robert B. Duffield. Photofission cross sections—759(A)
Ginzbarg, Arthur S. and William L. Roever. Transmission of pulses through elastic plate—812(A)
Givens, M. Parker (see Woodruff, Robert W.)—752(A)
Glasser, R. G. (see Sprague, A. D.)—994
Glassgold, Alfred E. Elastic scattering of high-energy electrons by nuclei—757(A)
Glauber, R. J. Scattering by lattices of deformable atoms—751(A)
—— (see Zemach, A. C.)—790(A)
Glendenin, L. E. (see Keller, R. N.)—969
Glicksman, Maurice. Scattering of 217-Mev negative pions by hydrogen—1335
Gluckstern, R. L., P. B. Daitch, L. C. Biedenharn, and M. H. Hull, Jr. Continuous parameter approximation in linear accelerator with independently excited cavities—768(A)
—— (see Feld, B. T.)—1000
—— (see Hull, M. H., Jr.)—768(A)
Godfrey, T. N. K. Negative μ-meson capture in carbon—756(A)
Goertzel, G. (see Spruch, Larry)—1671
Goff, J. (see Fagen, E.)—1415(A)
Gold, R. (see Lidofsky, L.)—780(A)
Goldberg, Colman and R. E. Davis. New galvanomagnetic effect—1121
—— (see Brentano, J. C. M.)—56
Goldberger, M. L. (see Deser, S.)—711
Goldburg, W. I. and R. M. Williamson. Energy dependence of Coulomb excitation of Ta and Au—747(A)

Goldman, J. E. and A. Arrott. Magnetic susceptibility of Ni-Cu and Ni-Cr alloys—782(A)
—— (see Azumi, K.)—781(A)
Goldwasser, E. L. and G. Bernardini. Photoproduction of π^+ mesons near threshold—755(A)
—— (see Bernardini, G.)—729(L)
—— (see Nicolai, V. O.)—755(A)
Goldwater, D. L. and W. E. Danforth. Electrolysis of sintered ThO—754(A)
Good, R. H., Jr. Effect of atomic electron screening on shape of forbidden β spectra—931
Good, W. E. (see Gunther-Mohr, G. R.)—1184
Good, W. M., W. E. Kunz, and C. D. Moak. He^3+He^3 reactions—87
Goodman, Clark (see McClelland, C. L.)—1437(A)
Goodman, P. Concentration dependence of mechanical shear degradation—1425(A)
Goodrich, Max. Recent scintillation-spectrometer measurements at Louisiana State University—803(T)
—— **and Wilbur B. Payne.** Internal bremsstrahlung from P^{32}—405
Gordon, W. L., C. H. Shaw, and J. G. Daunt. Structure of liquid He by x-ray scattering—771(A)
Gordy, Walter. Mm and sub-mm wave spectroscopy—803(T)
Gossett, C. R., G. C. Phillips, and J. T. Eisinger. Nuclear energy levels by absolute magnetic analysis of inelastically scattered protons—807(A)
Gossick, B. R. Transient response of p-n junction rectifiers—1427(A)
Gove, H. E., E. B. Paul, G. A. Bartholomew, and A. E. Litherland. Angular distribution of γ rays from $Al^{27}(p,\gamma)Si^{28}$—749(A)
—— (see Paul, E. B.)—749(A)
Gow, J. D. and Luis W. Alvarez. Ne^{18}—365
Graham, J. W. (see Duller, N. M.)—810(A)
Graham, R. L. and J. Walker. Disintegration of Sm^{153}—794(A)
—— (see Elliott, L. G.)—795(A)
Graham, Walter J. and Arthur J. Ruhlig. Calculated values of parameters of noble gas discharges—25
Grandey, R. A. and A. F. Clark. Elastic scattering of 160-Mev pions in emulsions—766(A)
Grannemann, W. W., C. W. Horton, and R. B. Watson. Diffraction of electromagnetic waves by metallic wedge of acute dihedral angle—812(A)
—— (see Horton, C. W.)—812(A)
Green, D. W., J. N. Cooper, and J. C. Harris. Stopping power of several elements for protons—764(A)
Green, Melville. Boltzmann equation from statistical mechanical point of view—792(A)
Grimsal, E. G. (see Levinger, J. S.)—772(A)
Grodzins, L. Scattering of 2.7-Mev positrons by Au and Al foils—758(A)
Gross, B. Theory of thermodielectric effect—1545
Gross, E. P. Shape of collision-broadened spectral lines—1424(A)
—— **and M. Krook.** Propagation of waves in ionized gases—778(A)
—— (see Bhatnagar, P. L.)—511
Gugelot, P. C. (see Dayton, I. E.)—785(A)
Gummel, Hermann and Melvin Lax. Thermal ionization of trapped electrons—1419(A)
Günther, Marian. Relativistic configuration space formulation of multi-electron problem. II—1347
Gunther-Mohr, G. R., C. H. Townes, and J. H. Van Vleck. Hfs in spectrum of $N^{14}H_3$. II. Theoretical discussion—1191
——, **R. L. White, A. L. Schawlow, W. E. Good, and D. K. Coles.** Hfs in spectrum of $N^{14}H_3$. I. Experimental results—1184
Gurnee, E. F. Theory of orientation and double refraction in polymers—1412(T)
Gutowsky, H. S. and P. J. Frank. Electron spin resonance in metals at low fields—1067(L)
Gutzwiller, Martin (see Dresden, M.)—745(A)

Haar, Lester (see Friedman, Abraham S.)—1423(A)
Haberle, W., J. W. Bittner, and R. D. Moffat. Elastic scattering of α particles by carbon—769(A)
Haber-Schaim, U., Y. Yeivin, and G. Yekutieli. Production of K mesons—184
Hagstrum, H. D. Theory concerning secondary electrons ejected from metals by ions—749(T)
Hahn, B. (see McIntyre, J. A.)—1084(L)
Hahn, T. M. (see Rayburn, L. A.)—1641
Halban, H. (see Eliot, E. A.)—144
Haldar, B. C. and Edwin O. Wiig. New neutron-deficient isotope of Ag—1713
Halpern, I. (see Fairhall, A. W.)—733(L)
Halpern, J. (see Weinstock, E. V.)—1651
Halpern, Otto. Magnetic quenching of positronium decay—904
Halpin, A. T. (see Watson, W. R.)—777(A)
Hamilton, Donald R. (see Alford, W. Parker)—779(A)
Hammel, Edward F. (see Kilpatrick, John E.)—1103
Hammerle, W. G. Theory of viscoelastic behavior—1425(T)
Handley, Thomas H. Neutron-deficient activities of Ho—945
—— **and Elmer L. Olson.** Yb^{167}—968
—— (see Cohen, B. L.)—620; 953
Hanna, S. S. (see Cohen, L.)—419
Hans, H. S. (see Rothman, M. A.)—791(A)
Hanson, A. O. (see Schriever, Barbara Dwight)—763(A)
—— (see Scott, M. B.)—763(A)
Harman, T. C., R. K. Willardson, and A. C. Beer. Hall coefficient in Ge—1065(L)
Harris, E. D. (see deBretteville, A.)—1408(A)
Harris, J. C. (see Green, D. W.)—764(A)
—— (see Smith, J. A.)—749(A)
Hartley, R. V. L. Corrected theory of relativity and its classical interpretation—792(A)
Hartmann, N. (see Sheer, C.)—769(A)
Hartsough, Walter (see Cork, Bruce)—1300
Harvey, B. G. (see Choppin, G. R.)—1080(L)
—— (see Ghiorso, S. G.)—1081(L)
Haskin, D. M. (see Sprague, A. D.)—994
Hastings, J. (see Weiss, R. J.)—1420(A)
Hatalkar, M. M. Theory of elementary particles in general relativity—1472
Havas, Peter (see Crownfield, Frederic R., Jr.)—471
Havens, W. W., Jr. (see Melkonian, E.)—790(A)
Haxby, R. O. (see Murray, P. C.)—764(A)
Hayes, W. D. Pseudo-transonic similitude and first-order wave structure—763(T)
Haynes, J. R. and J. A. Hornbeck. Decay in photoconductivity associated with hole traps in n-type Si—1438(A)
—— (see Hornbeck, J. A.)—1437(A)
Hayward, Evans (see Fuller, E. G.)—732(L)
Heaps, C. W. Electrical properties of molybdenite—809(A)
Heckrotte, Warren. Polarization of elastically scattered nucleons from nuclei in Born approximation—1797(L)
—— **and Joseph V. Lepore.** Polarization of elastically scattered nucleons from nuclei—500(L)
—— (see Schecter, Larry)—1086(L)
Hedgran, Arne and Sölve Hultberg. Angular distribution of photoelectrons from γ radiation of 0.4 and 1.3 Mev—498(L)
Heiberg, E. (see de Carvalho, H. G.)—1796(L)
Heidemann, E. A. (see Leitner, A.)—1441(A)
Heinz, Otto. Range and specific ionization for high-energy protons in nuclear emulsions—1728
Heller, Wilfried. Analysis of reduced viscosity equations—1426(A)

Hellund, E. J. and Katsumi Tanaka. Quantized space-time—192
Hemenway, C. L. (see Dunnington, F. G.)—592
Hemmer, B. A. (see Dorfman, M.)—754(A)
Hempstead, C. F. (see Parratt, L. G.)—1593
Henderson, Joseph E. (see Miller, Charles E.)—167
Henkel, R. L., L. Cranberg, G. A. Jarvis, R. Nobles, and J. E. Perry. Total neutron cross section for U from 20 kev to 20 Mev—141
Henri, V. P. (see Bay, Z.)—780(A)
Henry, Allan F. (see Beringer, Robert)—343
Henry, Warren E. Antiferromagnetic *H-T* boundaries and apparent molecular fields for $MnCl_2 \cdot 4H_2O$ and $MnBr_2 \cdot 4H_2O$—1146
—— High-field non-Brillouin moments for cobalt sulfate heptahydrate—781(A)
—— Magnetization of $CuK_2(SO_4)_2 \cdot 6H_2O$ at liquid He temperatures and in strong magnetic fields—1433(A)
Hensley, E. B. Conduction mechanism in oxide-coated cathodes—790(T)
Henvis, B. W. (see Burstein, E.)—750(A)
Herb, R. G. (see Bittner, J. W.)—769(A)
Hereford, F. L. Photoelectron production by polarized γ rays—806(T)
—— (see McMaster, W. H.)—757(A)
Herman, R. C., S. Silverman, and R. F. Wallis. Vibration-rotation line intensities of diatomic molecules—752(A)
Herring, D. F. (see Block, R. C.)—774(A)
Hersh, S. P. and D. J. Montgomery. Static electrification of filaments: dependence of charge transferred on normal force and velocity—1413(A)
Herwig, Lloyd O. and Glenn H. Miller. α-particle ionization yields in gridded chamber—1183
Hesketh, R. V. and E. E. Schneider. Restoration of F and V_1 centers following low-temperature bleaching—494(L)
Heybey, W. H. Theoretical determination of shock distances in ideal and real gases—1441(A)
Heydenburg, N. P. and G. M. Temmer. γ rays from inelastic scattering of α particles by Li and F—748(A)
—— **and G. M. Temmer.** γ rays from Li^7, F^{19}, Ne^{22}, and Na^{22} produced by α-particle bombardment of Li and F—1252
—— (see Temmer, G. M.)—1399(L); 747(A)
Hickman, G. D. (see Cork, J. M.)—1218
Hicks, D. (see Eliot, E. A.)—144
Hicks, Harry G. and Richard S. Gilbert. New isotope of Pd, 1.5-minute Pd^{113}—371
Hiedemann, E. A. (see Leitner, A.)—1441(A)
Higgins, G. H. and W. W. T. Crane. Thermal neutron fission cross section of Am^{242m}—735(L)
Hildebrandt, Alvin F. Narrow gap electromagnet for high-resolution nuclear resonance spectrometry—811(A)
Hill, D. A., T. Coor, W. F. Hornyak, L. W. Smith, and G. A. Snow. Experiments with neutrons from the Cosmotron. I—791(A)
—— (see Snow, G. A.)—791(A)
Hill, David L. and Kenneth W. Ford. μ-mesonic x-rays and shape of nuclear charge distribution—1617
—— **and Kenneth W. Ford.** Nuclear charge distribution—787(A)
—— (see Ford, Kenneth W.)—1630
Hill, R. D., E. O. Salant, and M. Widgoff. K-particle production by protons of 2.2 and 3.0 Bev—1794(L)
——, **E. O. Salant, M. Widgoff, L. S. Osborne, A. Pevsner, D. M. Ritson, J. Crussard, and W. D. Walker.** Unstable heavy particles from Cosmotron—797(A)
Hobbs, Lindsey M., Douglas E. Brown, and David W. Pletcher. Effects of Co^{60} γ radiation on formation and degradation of polymers—1412(A)
Hoch, Michael and Herrick L. Johnston. Germanium-oxygen system—749(A)
Hoff, E. A. W. Dynamic properties of high polymers—1425(T)
Hoffman, J. D. Rotation of chain molecules in crystals—1425(T)
Hoffman, R. W. and N. S. Rasor. Annealing kinetics of lattice imperfections using evaporated metal films—1406(A)
Hofstadter, Robert. Nuclear determinations from electron scattering—773(T)
—— (see McIntyre, J. A.)—1084(L)
Holden, A. N. (see Fletcher, R. C.)—1392(L)
—— (see Kunz, F. W.)—1417(A)
Holmes, John R. and Leon Pape. Pressure shift in He λ5875—902
Holmgren, H. D., J. M. Blair, B. E. Simmons, and R. V. Stuart. Differential cross sections for $C^{13}(d,t)C^{12}$ reaction—748(A)
Holstein, T. (see Bernstein, Ira B.)—1475
Honnold, V. R., F. McCaffrey, and B. A. Mrowca. Measurement of nuclear induction relaxation times in polymers—1414(A)
Hori, H. (see Bowen, D. B.)—1422(A)
Hornbeck, J. A. and J. R. Haynes. Decay in photo-conductivity associated with deep electron traps in p-type Si—1437(A)
—— (see Haynes, J. R.)—1438(A)
Hornig, D. F. Characteristics of shock fronts in liquids and gases—765(T)
Hornyak, W. F. (see Hill, D. A.)—791(A)
—— (see Snow, G. A.)—791(A)
Horton, C. W. and W. W. Grannemann. Diffraction measurements at 1.25 cm—812(A)
—— (see Grannemann, W. W.)—812(A)
Horton, G. K. and E. Phibbs. Perturbation theory with Sommerfeld-Maue wave function—1402(L)
Hosemann, R. and S. N. Bagchi. Diffraction effects of crystals with deformation faults—71
Houston, W. V. Variation method applied to wave functions in crystals—808(A)
Howard, J. N. (see Burch, D. E.)—1424(A)
Hoyer, W. A. Compressibility of liquid cholesterol benzoate at isotropic-anisotropic transition—812(A)
Hudis, J., R. Wolfgang, N. Sugarman, and G. Friedlander. Reactions of Al with 2.2-Bev protons—775(A)
—— (see Friedlander, G.)—727(L); 775(A)
Hudspeth, Emmett L. (see Rickard, James A.)—806(A)
—— (see Spearman, K. R.)—806(A)
Hughes, D. J. Statistical factors in radiation widths of nuclear energy levels—740(L)
—— (see Palevsky, H.)—1088(L)
Hughes, D. S. Thermodynamic properties of solids deduced from high-pressure measurements—803(T)
Hughes, Vernon W. and Werner B. Teutsch. Relativistic contributions to magnetic shielding of nuclei in atoms—761(A)
Huizenga, John R. Spontaneous fission systematics—158
—— (see Diamond, H.)—1083(L)
—— (see Fields, P. R.)—209(L)
—— (see Stevens, C. M.)—974
Hull, G. W. (see Geballe, T. H.)—1134
Hull, M. H., Jr., L. C. Biedenharn, P. B. Daitch, and R. L. Gluckstern. Stability of linear accelerator with independently excited cavities—768(A)
—— (see Gluckstern, R. L.)—768(A)
Hulm, John K. Superconductivity of pure metallic Re—1390(L)
Hultberg, Sölve (see Hedgran, Arne)—498(L)
Hunter, L. P. Graphical representation of semiconductor Hall effect—1426(A); 1157
Hurlbut, F. C. Molecular beam investigation of scattering of molecules from surfaces—754(A)

Huus, Torben (see Bjerregaard, Jørgen H.)—204(L)
—— (see Zupančič, Črtomir)—205(L)
Hyde, Earl K. Radiations of AcK—1221

Ingersoll, L. R. and D. H. Liebenberg. Faraday effect in gases—754(A)
Innes, Frederick R. Spin-other-orbit interaction in theory of complex spectra—761(A)
Ishiguro, Eiichi and Shoichiro Koide. Magnetic properties of H_2 molecules—350
Ivey, D. G. and A. Kwei. Stress-temperature-time studies through second-order transition region—1414(A)
Ivory, J. (see Baldwin, F. P.)—1425(A)

Jaccarino, Vincent, J. G. King, R. A. Satten, and H. H. Stroke. Hfs of I^{127}. Nuclear magnetic octupole moment—1798(L)
—— (see King, John Gordon)—1610
Jacobsen, E. H. Elastic spectrum of Cu from temperature scattering of x-rays—1420(A)
Jacobsmeyer, V. P. (see Badar, L. J.)—808(A)
James, Hubert M. (see Lehman, Guy W.)—1428(A)
Jarmain, W. R. (see Nicholls, R. W.)—1423(A)
Jarvis, G. A. (see Henkel, R. L.)—141
Jaumot, F. E., Jr., and A. Sawatzky. Order-disorder and cold-work phenomena in Cu-Pd alloys—1429(A)
—— (see Berkowitz, A. E.)—1407(A)
—— (see Folen, V. J.)—1432(A)
—— (see Smith, R. L.)—1407(A)
—— (see Sutcliffe, C. H.)—1429(A); 1429(A)
Javan, Ali (see Lotspeich, J. F.)—789(A)
Jenkins, T. L., D. Luckey, and R. R. Wilson. Photomeson production from hydrogen—755(A)
Jensen, E. N. (see Nichols, R. T.)—369
Jesse, William P. and John Sadauskis. α-particle ionization in noble gases and formation of metastable atoms—764(A)
Johnson E. J. and W. G. Spitzer. Optical properties of Ge in far infrared—1415(A)
Johnson, Noah R. (see Sheline, Raymond K.)—1642
Johnson, Peter D. Optical properties of MgO in vacuum uv—845
Johnson, V. A. Resistivity, thermoelectric power, and Hall effect in semiconductor with hexagonal structure—1427(A)
Johnson, Walter H., Jr. (see Collins, T. L.)—398
Johnston, Herrick L. (see Hoch, Michael)—749(A)
Johnston, R. W. and D. H. Tomboulian. Absorption spectrum of Be in neighborhood of K edge—1585
Jona, F., G. Shirane, and R. Pepinsky. Measurements of ferroelectric transition in single crystals of $Cd_2Nb_2O_7$—1408(A)
Jones, E. A. W. (see Shillibeer, H. A.)—1793(L)
Jones, H. Soft x-ray emission bands in metals—1072(L)
Jones, K. W., R. A. Douglas, M. T. McEllistrem, and H. T. Richards. Comparison of nuclear and γ-ray energy scales—947
Jones, L. W. and K. M. Terwilliger. Electromechanical analog for study of strong-focusing orbits—1436(A)
Jones, Royce J. (see Livingston, Robert S.)—1436(A)
Jones, W. H. (see Cohen, B. L.)—625; 758(A)
Jordan, W. C. (see Burson, S. B.)—103
Joyner, W. T. (p,γ) coincidence measurements utilizing proton time-of-flight—774(A)
Joynson, R. E. Elastic spectrum of Zn from temperature scattering of x-rays—851
Jung, J. J. (see Bockelman, C. K.)—748(A)

Kaenzig, Werner. Properties of very small ferroelectric particles—1408(T)
Kaiser, H. F. Microtron resonators—768(A)
Kaiser, W. and H. Y. Fan. Infrared properties of InSb—1431(A)
Kallmann, Hartmut (see Furst, Milton)—503
Kalos, M. H. and J. M. Blatt .Phenomenological n-p interaction—762(A)
Kane, Evan O. Thermionic emission and semiconduction in single crystals of BaO—1439(A)
Känzig, Werner (see Ueta, Masayasu)—1390(L)
Kao, L. P. and E. Katz. Magnetoresistance—1433(A)
Karplus, R. (see Luttinger, J. M.)—782(A)
Kasnitz, Harold L. and Kurt Sitte. Structure and composition of air shower cores—977
Katcoff, Seymour (see McKeown, Michael)—965
Katz, E. Theory of photographic intermittence effect at low light intensities—1441(A)
—— (see Kao, L. P.)—1433(A)
—— (see Schamp, H. W., Jr.)—828
Kauzman, W. D. Nature of liquid and glassy states—1425(T)
Keating, D. T. Diffraction studies of possible ordering in α brass—1429(A)
Keck, P. H. (see Wolff, G.)—753(A)
Keffer, F. (see Cohen, M. H.)—1412(A)
—— (see Eisele, J. A.)—1440(A)
Keller, R. N., E. P. Steinberg, and L. E. Glendenin. Yields of fission products from U^{238} irradiated with fission spectrum neutrons—969
Keller, William E. (see Kilpatrick, John E.)—1103
Kelly, John, James Ray, and Richard A. Ogg, Jr. Nuclear magnetic resonance spectra of boranes and derivatives—767(A)
—— (see Ekstein, H.)—1440(A)
Kenney, Nancy T. (see Fine, M. E.)—1573
Kerst, D. W. (see Scott, M. B.)—763(A)
Keshishian, V. (see Fowler, C. M.)—1082(L)
Kessler, John O. and Leon M. Lederman. Interactions of negative pions in C and Pb—689
Keuffel, J. W. and L. Mezzetti. Search for K particles using Čerenkov counters—797(A)
Keyes, R. J. and T. G. Maple. Variation of recombination velocity of Ge surfaces with ambient gases—1416(A)
Keyes, R. J. (see Stevenson, D. T.)—1416(A)
Keyes, Robert W. Diffusion of lattice defects in temperature gradient—1389(L)
Kies, J. A. and H. L. Smith. Methods for determining the energy for fracture propagation in plates—760(A)
—— (see Smith, H. L.)—760(A)
Kilpatrick, John E., William E. Keller, Edward F. Hammel, and Nicholas Metropolis. Second virial coefficients of He^3 and He^4—1103
Kim, Y. B. Energy distribution of neutral mesons produced in cosmic-ray stars—797(A)
King, John Gordon and Vincent Jaccarino. Hfs and nuclear moments of stable Br isotopes—1610
—— (see Jaccarino, V.)—1798(L)
King, R. W. and D. C. Peaslee. First forbidden matrix element in β decay—1284
—— **and D. C. Peaslee.** Spin of RaE—795(A)
Kingston, R. H. "Channels" in n-p-n junction transistors: new results and proposed model—1146(A)
Kington, J. D. (see Willard, H. B.)—786(A)
Kinoshita, Toichiro. Effect of Coulomb . . .—1331
—— V particles and γ decay of neutral pion—1384
—— **and Yoichiro Nambu.** Collective description of many-particle . . .—598
Kip, A. F. Electron spin resonance in semiconductors and metals—1416(T)
Kirby, H. W. and Murrell L. Salutsky. Half-life of La^{140}—1801(E)
Kistler, Alan, Vivian O'Brien, and Stanley Corrsin. Isotropic temperature fluctuations in isotropic turbulence—783(A)
Kittel, Charles. Solid-state cyclotron—768(T)
Klein, Abraham. Configuration space methods for construction of potentials—195

—— Single-time formalisms from covariant equations—1052
Klein, Ralph. Surface migration of C on W—1407(A)
Klick, Clifford C. Search for *F*-center luminescence—1541
—— Search for luminescent emission from *F* center—1438(A)
Klokholm, E. (see Franklin, A. D.)—1432(A)
Klontz, E. (see Pepper, R.)—1410(A)
Klotz, R. J. (see Fowler, C. M.)—1082(L)
Kluyver, J. C., C. van der Leun, and P. M. Endt. Ground state of Al^{26}—1795(L)
Knight, Herbert T. and Russell E. Duff. Precision measurement of detonation and strong shock velocity in gases—784(A)
—— (see Duff, R. E.)—784(A)
Knight, W. D. Nuclear resonance in ferroelectric crystals—1408(T)
Knowles, J. W. New method for measuring short γ-ray lifetimes—795(A)
Koehler, J. S. Pauli principle scattering and resistivity minimum—1071(L)
—— (see Cooper, H. G.)—496(L)
—— (see Sosin, A.)—1422(A)
Koehler, W. C. and E. O. Wollan. Paramagnetic scattering of neutrons by rare earth oxides—1801(E)
Kofsky, Irving L. (see Sitte, Kurt)—988
Kohane, T. (see Debye, P. P.)—724(L)
Kohn, W. Bombardment damage of Ge crystals by fast electrons—1409(A)
—— **and N. Rostoker.** Solution of Schrödinger equation in periodic lattices with application to metallic Li—1111
—— (see Lakin, W.)—787(A)
Koide, Shoichiro (see Ishiguro, Eiichi)—350
Konopinski, E. J. Possible relation between pseudoscalar β coupling and nuclear spin-orbit coupling—492
Korringa, J. Electron resonance in *F* centers—1388(L)
—— Orientation of nuclei by saturation of paramagnetic resonance—1388(L)
Korsmeyer, J. D. (see Campbell, R. C.)—791(A)
Koshiba, M. (see Crussard, J.)—736(L)
Koster, G. F. and J. C. Slater. Wave functions for impurity levels—1392(L)
—— (see Slater, J. C.)—1498
Kovacs, J. S. (see Brueckner, K. A.)—726(L)
Kovásznay, Leslie S. G. and Darshan Dosanjh. Shock tube experiments on grid flow—784(A)
Kraemer, H. (see Bothe, W.)—1402(L)
Kraitchman, J. and B. P. Dailey. Microwave spectrum of ethyl fluoride—788(A)
Kraus, Alfred A., Jr. γ rays from $N^{15}(p,\alpha\gamma)C^{12}$ and $N^{15}(p,\gamma)O^{16}$—975
Kraus, Olen. Solutions of Helmholtz and Schrödinger equations in sphero-conal coordinates—1442(A)
Kraybill, H. L. (see Fowler, E. C.)—791(A)
Kriessman, C. J. and Herbert B. Callen. Magnetic susceptibility of transition elements—781(A); 837
Krimm, S. Infrared spectrum of polyethylene—1426(A)
Kroll, N. M. Survey of quantum electrodynamics—747(T)
Krook, M. (see Bhatnagar, P. L.)—511
—— (see Gross, E. P.)—778(A)
Kruse, H. W. (see Fowler, C. M.)—1082(L)
Kruse, U. E., J. M. Teem, and N. F. Ramsey. Proton-proton scattering from 40 to 95 Mev—1795(L)
Kuczynski, G. C. Effect of elastic strain on electrical resistance of metals—61
Kunz, F. W. and A. N. Holden. Effect of short-time moderate-flux neutron irradiation on mechanical properties of some metals—1417(A)
Kunz, W. E. (see Good, W. M.)—87
Kurbatov, J. D. (see Auth, W. J.)—794(A)
—— (see Emmerich, W. S.)—110; 113
—— (see Murray, B. B.)—780(A)
—— (see Sakai, M.)—779(A)
—— (see Singer, S. E.)—779(A)
Kurnick, S. W., A. J. Strauss, and R. N. Zitter. Photoconductivity and photoelectromagnetic effects in InSb—1791(L)
Kursunoğlu, Behram. Interaction between two nucleons—746(A)
Kusch, P. and T. G. Eck. Hfs of In^{115}. Evidence of nuclear octupole moment—1799(L)
Kwei, A. (see Ivey, D. G.)—1414(A)

Lafferty, D. L. (see Rayburn, L. A.)—1641
Lakin, W. and W. Kohn. Distortion of nucleus in μ-mesic atoms—787(A)
Landauer, Rolf. Bound states in dislocations—1386(L)
Lander, J. J. Chemical observations on non-stoichiometric ZnO and interpretation of its conductivity—803(T)
Landon, H. H. Doppler effect in slow neutron resonance in Rh—1215
Landsberg, Peter T. Basic principles of quantum statistical mechanics—1442(A)
—— Continuous spectrum approximation in quantum statistics—469
Lane, R. O. and D. J. Zaffarano. Transmission of 0–40 kev electrons by thin films with application to β-ray spectroscopy—959
Lark-Horovitz, K. Nucleon bombardment of semiconductors—1432(T)
—— (see Pepper, R.)—1410(A)
Lauritsen, C. C. (see Peterson, R. W.)—1075(L)
—— (see Thirion, J.)—1076(L)
Lax, Melvin. Localized perturbations—1391(L)
—— **and R. Toupin.** Lattice of partly permanent dipoles—780(A)
—— (see Gummel, Hermann)—1419(A)
—— (see Toupin, R.)—781(A)
Lazarus, D. Solute diffusion in metals—1407(A)
Leaderman, Herbert and M. Wales. Steady-state elastic shear compliance and molecular weight distribution in polyisobutylene—1414(A)
Leavitt, C. P. (see Chen, F. F.)—784(A)
LeBlanc, J. M., J. M. Cork, and S. B. Burson. Activities of Zn^{71}—1436(A)
—— (see Burson, S. B.)—103
Leder, Lewis B. and L. Marton. Energy losses of electrons in passage through thin films—777(A)
—— (see Marton, L.)—203(L); 778(A)
Lederman, Leon M. Meson reactions in hydrogen—745(T)
—— (see Kessler, John O.)—689
Lee, J. C. (see Ewing, R.)—1411(A)
Lee, L. L. (see Foster, B. P.)—804(A)
Lee, T. D. and R. Christian. Intermediate coupling method for meson-nucleon scattering—1760
Legvold, S. (see Banister, J. R.)—1140
—— (see Elliott, J. F.)—50; 1143
Lehman, Guy W. and Hubert M. James. Interaction of impurities and mobile carriers in semiconductors—1428(A)
Lehnert, Bo. Magneto-hydrodynamic waves in liquid Na—815
Lehovec, Kurt. Electric breakdown of crystals in high-temperature region—770(A)
—— Theory of thermionic emission.—1439(A)
Leifer, H. N. and W. C. Dunlap. Properties of *p*-type GaSb between 15°K and 925°K—1431(A)
Leighton, R. B. (see van Lint, V. A.)—1732
Leipuner, L. (see Stearns, M.)—766(A)
Leitner, A. and E. A. Hiedemann. Symmetric modes of tapered reed—1441(A)
Leivo, W. and R. Smoluchowski. Color centers in KCl crystals produced by high-energy protons—771(A)
—— (see Smith, W. J.)—1435(A)

Leonard, B. P., Jr. (see Little, R. N., Jr.)—807(A)
Lepore, Joseph V., Maurice Neuman, and Richard N. Stuart. High-energy events—788(A)
—— **and Richard N. Stuart.** Nuclear events at high energies—1724
—— (see Heckrotte, Warren)—500(L)
Levinger, J. S. and E. G. Grimsal. Low-temperature oscillatory Hall effect—772(A)
Levinstein, Henry (see Bode, Donald E.)—1430(A)
—— (see Broudy, R.)—285; 290
—— (see Silverman, Searl J.)—871; 1430(A)
Levinthal, Cyrus. Structure and function in molecular biophysics—1426(T)
Levy, Harris B. and I. Perlman. Long-lived isomer of RaE (Bi^{210})—152
Lévy, Maurice M. Covariant treatment of meson-nucleon scattering—460
Levy, Paul W. and G. J. Dienes. Irradiation-induced optical absorption in Al_2O_3—1409(A)
Lewis, J. A. (see Mason, W. P.)—1439(A)
Li, C. W. (see Sherr, R.)—1076(L)
Li, Yin-Yuan and R. Smoluchowski. Diffraction of x-rays by lattice imperfections—751(A)
—— **and R. Smoluchowski.** Fourier analysis of x-rays small-angle scattering—1435(A)
—— **and R. Smoluchowski.** Theory of x-ray small-angle scattering—866
—— (see Robinson, W. H.)—1435(A)
Lide, David R., Jr. Microwave spectrum of methyl amine—788(A)
Lidiard, A. B. Ionic conductivity of impure polar crystals—29
Lidofsky, L., R. Gold, and C. S. Wu. Radiations of 18-min Br^{80}—780(A)
Liebenberg, D. H. (see Ingersoll, L. R.)—754(A)
Lieberman, D. S., M. S. Wechsler, and T. A. Read. Cubic to orthorhombic diffusionless phase change—experimental and theoretical studies of AuCd—760(A)
—— (see Read, T. A.)—759(A)
—— (see Wechsler, M. S.)—759(A)
Liebschutz, A. M. (see Binnie, W. P.)—1410(A)
Lindenbaum, J. Seymour (see Pevsner, Aihud)—765(A)
—— (see Williams, Ross)—765(A)
Lindner, M. and R. N. Osborne. Some studies of products of high-energy fission process—1323
Lindsay, Robert. Field-dependent magnetic susceptibility of MnSe—808(A)
Lindsley, John. Flux of primary cosmic-ray α particles—796(A)
Litherland, A. E. (see Gove, H. E.)—749(A)
—— (see Paul, E. B.)—749(A)
Little, R. N., Jr., C. P. Cadenhead, B. P. Leonard, Jr., J. T. Prud'homme, L. D. Vincent, and J. E. Wills. Angular distribution of $D(d,n)$ neutrons scattered from C, Al, S, Fe, Cd, Cu, W, and Pb—807(A)
Livingston, M. S. Design study for 15-Bev accelerator by Cambridge design study group—792(A)
Livingston, Ralph, Henry Zeldes, and Ellison H. Taylor. Atomic hydrogen hfs in irradiated acids—725(L)
Livingston, Robert S. and Royce J. Jones. Design features of high-current cyclotron—1436(A)
Lloyd, J. P. and G. E. Pake. Spin relaxation in free radical solutions exhibiting hfs—579
Lockenvitz, Arthur E. (see Auverman, Harry J.)—811(A)
—— (see Clarkson, Henry Neal)—811(A)
—— (see Cowan, Alvin E.)—809(A)
Loeb, Leonard B. Some aspects of breakdown streamers—227
Loebner, E. E. 2-phase graphitization—1435(A)
Logan, John K. Low-temperature magnetoresistance of Au in fields up to 50 kilogauss—1433(A)
Lomont, J. S. Time reversal *vs* Boltzmann equation—792(A)
Longini, R. L. (see McKelvey, J. P.)—750(A)
Lönsjö, O. (see Taylor, H. L.)—807(A)
Lotspeich, J. F., Ali Javan, and Alfred Engelbrecht. Microwave spectrum of ReO_3F—789(A)
Louisell, W. H., R. W. Pidd, and H. R. Crane. Experimental measurement of gyromagnetic ratio of free electron—7
Love, Temple and Fred Maienschein. γ-ray spectrum of Po-B source—795(A)
—— (see Maienschein, Fred)—778(A)
Lovell, L. C. (see Vogel, F. L.)—1791(L)
Löwdin, Per-Olov. Studies of atomic self-consistent fields. II. Interpolation problems—1600
Lu, Daniel C. and M. L. Wiedenbeck. Summation of γ-ray energies with single-crystal spectrometer—501(L)
Luckey, D. (see Jenkins, T. L.)—755(A)
Luckey, P. D. Production of charged mesons by γ rays on H and D—755(T)
Ludloff, J. F. and M. B. Freidman. Aerodynamics of blasts: Diffraction of blast around finite corners—763(T)
Lummis, F. L. (see Petritz, R. L.)—1430(A)
Luttinger, J. M. and R. Karplus. Hall effect in ferromagnetics—782(A); 1434(T)

MacGregor, M. H. and M. L. Wiedenbeck. Third forbidden β spectrum of Rb^{87}—138
MacKay, J. (see Pepper, R.)—1410(A)
Mackin, R. J., Jr. γ rays and internal pairs from Be^9+H^1—648
Macklin, R. L. (see Banta, H. E.)—807(A)
MacLeod, A. A., A. R. DiDonato, and A. C. Webber. Viscoelasticity in complex static stress systems—769(A)
—— (see DiDonato, A. R.)—770(A)
Madansky, L. and F. Rasetti. Radiative electron capture in Fe^{55}—407
Madey, Richard (see Frank, Wilson J.)—1716
Magnusson, L. B. (see Diamond, H.)—1083(L)
—— (see Engelkemeir, D.)—1395(L)
—— (see Fields, P. R.)—209(L)
Maienschein, Fred and Temple Love. γ-ray spectrum of Bulk Shielding Reactor—778(A)
—— (see Love, Temple)—795(A)
Maita, J. P. (see Morin, F. J.)—1525
Major, J. K. and L. C. Biedenharn. Sargent diagram and ft values for electron capture transitions—779(A)
Mandeville, C. E. and H. O. Albrecht. Luminescence of BeO—494(L)
—— **and Jagdish Varma.** Disintegration of Mo^{99}—780(A)
—— (see Albrecht, H. O.)—776(A)
—— (see Rothman, M. A.)—791(A)
—— (see Varma, Jagdish)—91
Maple, T. G. (see Keyes, R. J.)—1416(A)
Mapother, D. E. (see Garber, M.)—1065(L)
Marcus, Paul M. Theory of temperature waves—771(A)
Marion, J. B. LiI(Eu) crystals as neutron detectors—808(A)
——, **C. F. Cook, and T. W. Bonner.** Neutrons from proton bombardment of Be^9 and H^3—807(A)
Mark, Hans. Inelastic scattering of charged particles in electric excitation processes—1436(A)
Markham, Jordan J. Multiphonon transitions in F center—1395(L)
Marshak, H. Total neutron cross sections in kev region: Cu, Cu^{63}, Cu^{65}, and Ga—774(A)
Marshall, J. (see de Carvalho, H. G.)—1796(L)
Marshall, J. F. (see Shatas, R. A.)—757(A)
Marshall, L. (see de Carvalho, H. G.)—1796(L)
Martin, Don S., Jr. (see Schupp, Fritz D.)—80
Martin, R. L. Phase shift analysis of scattering of negative pions by H—765(A)
Marton, L. and Lewis B. Leder. Energy loss of electrons in passage through thin films—203(L)

—— **and Lewis B. Leder.** Penetration of medium fast electrons into photographic emulsions—778(A)
—— (see Leder, Lewis B.)—777(A)
Marvin, Robert S. Introductory remarks—1425(T)
——, **H. S. Sack, and R. Aldrich.** Calculation of dynamic bulk modulus of polyisobutylene—1413(A)
Marx, J. W. (see Cooper, H. G.)—496(L)
Mason, W. P. and J. A. Lewis. Equations for magneto-striction and anisotropic energy for hexagonal crystal of class $D_{6h}(6/m, 2/m, 2/m)$—1439(A)
Matarrese, L. M. and J. W. Stout. Magnetic anisotropy of NiF_2—1792(L)
Matheson, Max S. (see Smaller, Bernard)—202(L)
Matossi, Frank. Interpretation of electroluminescence effects in excited phosphor—1151
Matsen, F. A. (see Arnold, Charles W.)—804(A)
—— (see Miller, J. M.)—804(A)
—— (see Streetman, J. R.)—805(A)
Matthews, P. T. and Abdus Salam. Renormalization—185
Matthias, B. T. and E. Corenzwit. Superconducting alloys—1069(L)
Maxwell, Louis R. and Stanley J. Pickart. Magnetization in nickel ferrite indates—1433(A)
Mayburg, Sumner. Interstitial Ge in heat-treated Ge—750(A)
Mazur, P. and S. R. de Groot. Extension of Onsager's theory of reciprocal relations. II—224
—— (see de Groot, S. R.)—218
McCaffrey, F. (see Honnold, V. R.)—1414(A)
McClelland, C. L. and Clark Goodman. Electric excitation of Pt—1437(A)
McClure, G. W. Distribution of specific ionization of primary cosmic rays at $\lambda = 10°$N—796(A)
—— Search for anomalous positively-charged particles from P^{32}—1637
McCormick, G. H. (see Cohen, B. L.)—625; 758(A)
McCrary, J. H., H. L. Taylor, and T. W. Bonner. Fast neutron counter with energy resolution—808(A)
McEllistrem, M. T. (see Jones, K. W.)—947
McGinnis, C. L. Disintegration of In^{117}—780(A)
McGowan, F. K. (see Sheline, Raymond K.)—1642
McIntyre, J. A., B. Hahn, and R. Hofstadter. Inelastic scattering of 190-Mev electrons in Be—1084(L)
McKay, K. G. Avalanche breakdown in Si—877; 1437(T)
McKelvey, J. P. and R. L. Longini. Volume and surface recombination rates in Ge—750(A)
McKeown, Marilyn (see Frazer, B. C.)—1435(A)
McKeown, Michael and Seymour Katcoff. Radiations of 53-min I^{134} and 86-sec I^{136}—965
—— (see McReynolds, A. W.)—1417(A)
—— (see Mihelich, J. W.)—794(A)
McLaughlin, Ralph D. (see Conway, John G.)—498(L)
McLean, E. A. and Waller George. Nucleation of fracture origins—761(A)
—— **and Waller George.** Size effects found in nucleation of fracture origins—1428(A)
McLernon, F. (see Bay, Z.)—780(A)
McMaster, W. H. and F. L. Hereford. Angular distribution of photoelectrons—757(A)
McReynolds, A. W., W. Augustyniak, M. McKeown, and D. B. Rosenblatt. Neutron irradiation effects at low temperature—Cu and Al—1417(A)
—— (see Riste, T.)—1433(A)
Mech, J. F. (see Diamond, H.)—1083(L)
—— (see Fields, P. R.)—209(L)
—— (see Stevens, C. M.)—974
Meechan, C. J. and R. R. Eggleston. Formation energy of vacancies in Au—1406(A)
Meem, J. L. Measurement of energy released per fission in Bulk Shielding Reactor—759(A)
Meers, J. T. (see Palmatier, E. D.)—766(A)
Melchor, J. L. and A. A. Petrauskas. Ultrasonic properties of Hycar OS-10 and Paracril 35—1414(A)
Melkonian, E. and W. W. Havens, Jr. Calculation of effect of finite resolution on neutron transmission near resonance—790(A)
Mellor, G. P. (see Fowler, C. M.)—1082(L)
Melnick, Donald A. Photoconduction of ZnO semiconductor: oxygen adsorption process—1438(A)
Mendlowitz, H. and K. M. Case. Double scattering of electrons with magnetic perturbation—1436(A)
Menes, M. and L. H. Fisher. Positive point-to-plane corona studies in air—1
Merritt, F. R. (see Fletcher, R. C.)—1392(L)
Meshkov, Sydney. d^3 and d^4 configurations of V—761(A)
—— **and C. W. Ufford.** Complete Bacher and Goudsmit method—75
—— (see Ufford, C. W.)—761(A)
Mesrobian, Robert B., Paul Ander, David S. Ballantine, and G. J. Dienes. γ-ray polymerization of acrylamide in solid state—1413(A)
Metropolis, Nicholas (see Kilpatrick, John E.)—1103
Metzger, F. R. and W. B. Todd. Resonance fluorescence with nuclei: Hg^{198}—794(A)
Meyer, D. I. and F. H. Schmidt. Precise momentum measurement of F line of Th B—927
Mezzetti, L. (see Keuffel, J. W.)—797(A)
Mifsud, J. F. Absorption of ultrasonic waves in liquids under pressure—812(A)
Mihelich, J. W., Gertrude Scharff-Goldhaber, and Michael McKeown. Decay scheme of 5.5-hr isomer of Hf^{180m}—794(A)
—— (see Tomlinson, E. P.)—794(A)
Miller, Charles E., Joseph E. Henderson, Gerald R. Garrison, David S. Potter, Wayne M. Sandstrom, and Jay Todd, Jr. Cosmic-ray protons at 3.4 km—167
Miller, Glenn H. (see Herwig, Lloyd O.)—1183
Miller, J. M. and F. A. Matsen. Molecular wave-functions in e-notation—804(A)
—— (see Friedlander, G.)—727(L); 775(A)
Miller, John D. (see Annis, Martin)—1038
Miller, S. C., Jr. Normalization of WKB-type approximation—1345
Millett, Walter E. Decay of positrons in superconducting Pb—809(A)
Milton, J. C. D. (see Fraser, J. S.)—795(A)
Mingins, Charles R., Robert W. Perry, and Albert D. Frost. Effects of stepped surfaces on motional parameters of piezoelectric filter plates—770(A)
Minton, George H. Lifetime for annihilation of positrons in Al and Pb—758(A)
Miskel, J. A. and M. L. Perlman. Double vacancies in K shell associated with K-electron capture in A^{37}—1683
Mitchell, A. C. G. Recent advances in nuclear spectroscopy—803(T)
Mitchell, Allan C. G. (see Caird, Robert S.)—412
—— (see Caird, R. S.)—780(A)
Mitchell, Dean L., Werner J. Beyen, and Donald E. Bode. Current oscillations in photoconductive films of PbTe—1430(A)
Mitchell, R. W. and Melvin Eisner. Nuclear resonance absorption in weak, homogeneous fields—811(A)
Mittelman, Phillip S. Decay scheme of Zr^{95}—99
Mize, J. P. (see Bunker, M. E.)—1694
Mizushima, Masataka. Theory of hfs of NO molecule—569; 789(A)
Moak, C. D. (see Good, W. M.)—87
Mobley, R. C. (see Patterson, J. R.)—774(A)
Moffat, R. D. (see Bittner, J. W.)—769(A)
—— (see Haberle, W.)—769(A)
Mohler, Fred L. (see Dibeler, Vernon H.)—754(A)

Monahan, J. E. (see Church, E. L.)—762(A)
Montalenti, G. (see Bonfiglioli, G.)—316
Montgomery, D. J. (see Hersh, S. P.)—1413(A)
Moran, Norma B. (see Nielsen, J. Rud)—805(A)
Morgan, I. L. (see Spearman, K. R.)—806(A)
Morin, F. J. and J. P. Maita. Conductivity and Hall effect in intrinsic range of Ge—1525
—— (see Pearson, G. L.)—750(A)
Morrison, Philip, Stanislaw Olbert, and Bruno Rossi. Origin of cosmic rays—440
H. E. Moses. Determination of perturbation from scattering operator—1442(A)
Moyer, Burton J. (see Frank, Wilson J.)—1716
Mozley, R. F. (see Bichsel, H.)—764(A)
Mrowca, B. A. (see Honnold, V. R.)—1414(A)
Mrozowski, S. and A. Chaberski. Hall effect and magnetoresistivity in carbons—1427(A)
—— (see Andrew, J. F.)—1438(A)
Murray, B. B. and J. D. Kurbatov. Disintegration of As^{74}—780(A)
Murray, P. C., R. I. Scace, R. O. Haxby, and T. R. Palfrey, Jr. Photoprotons from 300-Mev bremsstrahlung—764(A)

Nagamatsu, H. T. Recent galcit hypersonic experimental investigations—763(T)
Nakagawa, Y. (see Fultz, D.)—1471
Nambu, Yoichiro (see Kinoshita, Toichiro)—598
Nanda, V. S. Heat of mixing of He^3 and He^4 solutions—241
Naugle, J. E. (see Anderson, G. W.)—1317
—— (see Freier, P. S.)—677
Naumann, R. A. 10.5-day isotope of Pt—794(A)
—— (see Tomlinson, E. P.)—794(A)
Neamtan, S. M. Quantum mechanical definition of refractive index—327
Nedzel, V. Alexander. Total cross sections for 410-Mev neutrons—174
Neighbours, John R. and Charles S. Smith. Elastic constants of Cu alloys—1421(A)
Nelson, E. B. (see Carlson, R. R.)—1311
Nereson, Norris. Survey of average total neutron cross sections in 3–12 Mev region—806(T)
—— **and Sperry Darden.** Average neutron total cross sections in 3- to 12-Mev region—1678
Nesbitt, E. A., H. J. Williams, and R. M. Bozorth. Factors determining permanent magnet properties of single crystals of Fe_2NiAl—1440(A)
Neufeld, Jacob. Bohr's theory of energy losses of moving charged particles—792(A)
—— (see Snyder, W. S.)—760(A)
Neuman, Maurice (see Lepore, Joseph V.)—788(A)
Newman, E. and W. L. Alford. Angular distribution of α particles from (p,α) reactions—748(A)
—— (see Cohen, B. L.)—620
Newman, Roger. Photoconductivity in Au-doped Si—1530
—— Photoconductivity in Au-Ge alloys—278
—— **and W. W. Tyler.** Photoconduction in Fe-, Co-, and Ni-doped Ge—1419(A)
—— (see Tyler, W. W.)—1419(A)
Newson, Henry W. and Robert H. Rohrer. Shell effects in highly excited nuclei—654
——, **R. M. Williamson, A. L. Toller, and P. F. Nichols.** Total neutron cross sections in kev region: Se, Br, Y, I, and Cs—774(A)
—— (see Patterson, J. R.)—774(A)
Newton, Roger G. Applications of mass operator in quantum electrodynamics—1773
—— Radiative corrections to electron scattering—788(A)
Nicholls, R. W., P. A. Fraser, R. G. Turner, and W. R. Jarmain. Intensities, electronic transition moments, and vibrational transition probabilities of diatomic molecules—1423(A)
Nichols, M. H. Growth and surface properties of Ta crystals—309
Nichols, P. F. (see Newson, H. W.)—774(A)
Nichols, R. T. and E. N. Jensen. Radioisotope P^{32}—369
Nicolai, V. O. and E. L. Goldwasser. Photodisintegration of He above meson threshold—755(A)
Nielsen, H. H. (see Dalby, F. W.)—1423(A)
Nielsen, J. Rud, H. H. Claassen, and Norma B. Moran. Infrared and Raman spectra of fluorinated ethanes. VIII. CF_3CF_2H—805(A)
—— (see Collins, R. L.)—805(A)
—— (see El-Sabban, M. Z.)—805(A)
Nielsen, John P. Origin of recrystallization nuclei—1428(A)
Nielsen, Lawrence E. Effect of crystallinity on dynamic mechanical properties of polyethylenes—1414(A)
—— (see Buchdahl, Rolf)—1414(A)
Nier, Alfred O. (see Collins, T. L.)—398
Nierenberg, W. A. (see Bemski, G.)—767(A)
Nine, H. (see Cork, J. M.)—1218
Nix, F. C. (see Berkowitz, A. E.)—1407(A)
—— (see Folen, V. J.)—1407(A); 1432(A)
Nobles, R. (see Henkel, R. L.)—141
Noland, James A. Optical absorption of single-crystal $SrTiO_3$—724(L)
Nolle, A. W. Effect of hydrostatic pressure in two-state model of compressional relaxation in liquids—812(A)
Norberg, R. E. Nuclear magnetic resonance in alkali metals—1416(T)
Nowick, A. S. Interpretation of recovery phenomena in cold-worked metals—760(A)
—— (see Damask, A. C.)—1421(A)
Noyes, H. P. and A. E. Woodruff. Phenomenology of pion-nucleon S waves—1401(L)
Nozick, Seymour. Writing speed and tonal range of dark trace tubes—778(A)
Nussbaum, Allen. Electrical properties of pure Te and Te-Se alloys—337

O'Brien, Vivian (see Kistler, Alan)—783(A)
Odian, A. (see Feld, B. T.)—1000
Ogg, Richard A., Jr. Nuclear magnetic resonance as criterion of chemical bonding—767(A)
—— (see Kelly, John)—767(A)
Okamura, Tosihiko and Muneyuki Date. Paramagnetic resonance of Cu complex salts—314
Olbert, Stanislaw (see Morrison, Philip)—440
Olson, Elmer L. (see Cohen, B. L.)—953
—— (see Handley, Thomas H.)—968
Ord-Smith, R. J. Symmetry relations of 12-j symbol—1227
Oriani, R. A. Thermodynamics of ordering alloys, II. Ordered and disordered solid solutions of Au and Cu system—760(A)
Orvis, A. L. and M. M. D. Williams. Coincidences in scintillation counter—810(A)
Osborne, Darrell W., Bernard M. Abraham, and Bernard Weinstock. Heat capacity and entropy of liquid He^3 from 0.42°K to 1.06°K—202(L)
Osborne, L. S. (see De-Saussure, G.)—756(A)
—— (see Hill, R. D.)—797(A)
Osborne, R. N. (see Lindner, M.)—1323
Oser, A. W., Jr. (see Peacock, C. L.)—372; 804(A)
Otter, F. A. (see Domenicali, C. A.)—1421(A)
Overhauser, Albert W. Polarization of nuclei in metals by magnetic resonance—768(T)
—— Stored energy in irradiated Cu—1432(T)
—— Stored energy measurements in irradiated Cu—1551

Padgett, D. W. (see Caswell, R. S.)—786(A)
Page, Lorne A. (see Ashkin, Arthur)—357
Pai, Shih I. Stability of vortex sheet in inviscid compressible fluid—782(A)

Pake, G. E. (see Lloyd, J. P.)—579
Palevsky, H., R. S. Carter, R. M. Eisberg, and D. J. Hughes. Neutron absorption cross section of U^{235} at 2200 m/sec—1088(L)
Palfrey, T. R., Jr. (see Murray, P. C.)—764(A) 257; 1801(E)
Palmatier, E. D., J. T. Meers, and C. M. Askey. Density effect for ionization energy losses in gases—766(A)
Pandya, S. P. Classical scattering of mesons—1037
Pape, Leon (see Holmes, John R.)—902
Pappis, J. (see Bickford, L. R., Jr.)—1433(A)
Parker, E. N. Tensor virial equations—1441(A)
Parkinson, W. C. Recent experimental results from stripping reactions—1436(T)
Parratt, L. G. and C. F. Hempstead. Anomalous dispersion and scattering of x-rays—1593
Parzen, Philip. Energy equation for sinusoidal solutions of Maxwell's equations with electron beams—793(A)
Patterson, J. R., H. W. Newson, R. C. Mobley, and T. E. Gilmer. Total neutron cross sections in kev region: Li, F, Cl, Sc, Rb, Mo, Ag, and Ta—774(A)
Paul, E. B., H. E. Gove, G. A. Bartholomew, and A. E. Litherland. Partial widths for reactions $Al^{27}(p,\gamma)Si^{28}$ and $Al^{27}(p,p')Al^{27}$—749(A)
—— (see Gove, H. E.)—749(A)
Paul, William, G. B. Benedek, and H. Brooks. Pressure dependence of Hall effect in Ge—1415(A)
—— **and Harvey Brooks.** Pressure dependence of resistivity of Ge—1128
Payne, Wilbur B. (see Goodrich, Max)—405
Peacock, C. L., A. W. Oser, and J. F. Quin. Disintegration of La^{140}—804(A)
——, **J. F. Quin, and A. W. Oser, Jr.** Radiations of La^{140}—372
Pearlman, N. (see Fagen, E.)—1415(A)
Pearlstein, Edgar. Change of electrical conductivity of alkali halides upon irradiation with 350-Mev protons—1409(A)
Pearson, G. L., W. T. Read, Jr., and F. J. Morin. Electrical properties of dislocations in plastically deformed Ge—750(A)
—— (see Fletcher, R. C.)—1392(L)
Peaslee, D. C. Pion production ratios—1085(L)
—— (see King, R. W.)—795(A); 1284
Pegram, G. B. Physics at Columbia University: early years—776(T)
Penning, J. R. and F. H. Schmidt. β spectra of O^{14}—779(A)
Pepinsky, Ray. X-ray and neutron diffraction investigations on ferroelectric crystal transitions—1408(T)
—— (see Frazer, B. C.)—1435(A)
—— (see Jona, F.)—1408(A)
—— (see Vand, V.)—1435(A)
Pepper, R., E. Klontz, K. Lark-Horovitz, and J. MacKay. Hall and resistivity measurements during electron bombardment of Ge and In-Sb—1410(A)
Percus, Jerome K. and George J. Yevick. New approach to classical and quantum theory of many interacting particles. II—787(A)
—— (see Yevick, George J.)—787(A)
Perlman, I. Nuclear spectroscopic states deduced from α decay—803(T)
—— (see Asaro, Frank)—381
—— (see Levy, Harris B.)—152
Perlman, M. L. (see Miskel, J. A.)—1683
Perry, J. E. (see Henkel, R. L.)—141
Perry, Leo F. (see Venable, Douglas)—784(A)
Perry, Robert W. (see Mingins, Charles R.)—770(A)
Peterson, R. W., C. A. Barnes, W. A. Fowler, and C. C. Lauritsen. Low excited states of F^{19}. I. Proton inelastic scattering—1075(L)
Petrauskas, A. A. (see Melchor, J. L.)—1414(A)
Petritz, R. L., W. W. Scanlon, and F. L. Lummis. Mobility and mean free path of electrons and holes in PbS crystals—1430(A)
Pevsner, Aihud, James Rainwater, Ross Williams, and Seymour J. Lindenbaum. Elastic scattering of 80-Mev π mesons on Al—765(A)
—— (see Hill, R. D.)—797(A)
—— (see Williams, Ross)—765(A)
Phibbs, E. (see Horton, G. K.)—1402(L)
Philipp, H. R. Photoelectric emission from BaO—777(A)
Phillips, G. C. (see Gossett, C. R.)—807(A)
—— (see Reich, C. W.)—804(A)
—— (see Russell, J., Jr.)—804(A)
—— (see Windham, Pat M.)—803(A)
Phillips, J. A. Equilibrium charge-exchange ratios for low-energy protons—806(T)
Pickart, Stanley J. (see Maxwell, Louis R.)—1433(A)
Picus, Gerald S. Film flow in liquid He II at low level differences—1459
Pidd, R. W. (see Louisell, W. H.)—7
Pinnick, H. T. Magnetic susceptibility of carbons and polycrystalline graphites—319
Piper, William W. and Ferd E. Williams. Theory of electroluminescence of ZnS crystals—777(A)
Placzek, G. Scattering of neutrons by systems of heavy nuclei—1801(E)
Plaskett, J. S. Peculiarity of electron density near impurity in metal and its effect on x-ray spectra—1420(A)
Plass, Gilbert N. (see Fivel, Daniel I.)—752(A)
Pletcher, David W. (see Hobbs, Lindsey M.)—1412(A)
Plint, C. A., R. M. B. Small, and H. L. Welsh. Density effects in Raman spectrum of ammonia—805(A)
Plyler, Earle K. (see Allen, Harry C., Jr.)—1423(A)
Pomerantz, M. A. (see Shatas, R. A.)—757(A)
Pomerantz, W. A. Cosmic radiation at very high altitudes near geomagnetic equator—796(A)
Pond, T. A. Annihilation of positrons in condensed materials—758(A)
Potter, David S. (see Miller, Chares E.)—167
Powell, W. M. Neutron-proton scattering cross sections at high energies—786(T)
Power, E. A. Nonadiabatic corrections to scalar theory—1442(A)
Pratt, William W. Some (d,p) reactions in Ni and statistical theory of nuclear reactions—1086(L)
Preston, R. S. (see Fowler, E. C.)—791(A)
Price, P. J. Density fluctuations at low temperatures—257; 1801(E)
Prud'homme, J. T. (see Little, R. N., Jr.)—807(A)
Purcell, E. M. (see Carr, H. Y.)—630

Quin, J. F. (see Peacock, C. L.)—372
—— (see Peacock, C. L.)—804(A)

Rabi, I. I. Physics at Columbia University: recent years—776(T)
Rado, G. T. and J. R. Weertman. Exchange interactions in spin wave resonance—1411(A)
—— **and J. R. Weertman.** Observation of exchange interaction effects in ferromagnetics by spin wave resonance—1386(L)
—— (see Ament, W. S.)—1411(A)
Rainwater, James. Nuclear size from mesonic atoms—773(T)
—— (see Pevsner, Aihud)—765(A)
—— (see Williams, Ross)—765(A)
Ralph, D. C. (see Campbell, R. C.)—791(A)
Ramsey, N. F. Rotational reorientation spectra of molecular hydrogen and deuterium—751(T)
—— (see Barnes, R. G.)—893
—— (see Kruse, U. E.)—1795(L)
Randall, H. M. Early days of infrared spectroscopy at University of Michigan—1426(T)

Rank, D. H., J. N. Shearer, and T. A. Wiggins. Precision determination of velocity of light derived from band spectrum method. II—575
Rappaport, P. Minority carrier lifetime in semiconductors as sensitive indicator of radiation damage—1409(A)
Rasetti, F. (see Madansky, L.)—407
Rasor, N. S. (see Hoffman, R. W.)—1406(A)
Rawer, K. and E. Argence. Origin of ionospheric *E* layer—253
Rawson, E. B. (see Beringer, Robert)—343
Ray, James (see Kelly, John)—767(A)
Rayburn, L. A., D. L. Lafferty, and T. M. Hahn. Energy levels of Cu from inelastic neutron scattering—1641
Read, T. A., M. S. Wechsler, and D. S. Lieberman. Experimental studies of diffusionless cubic—tetragonal phase changes—759(A)
—— (see Lieberman, D. S.)—760(A)
—— (see Wechsler, M. S.)—759(A)
Read, W. T. (see Fletcher, R. C.)—1392(L)
—— (see Pearson, G. L.)—750(A)
—— (see Vogel, F. L.)—1791(L)
Redfield, Alfred G. Electronic Hall effect in alkali halides—537
—— Electronic Hall effect in diamond—526
Reich, C. W., J. Russell, and G. C. Phillips. Differential pumping system for gas targets—804(A)
—— (see Russell, J., Jr.)—804(A)
Reiffel, L. Pressure effects in phosphorescence—856
Reines, F. (see Cowan, C. L., Jr.)—751(T)
Reitz, R. A. (see Whalin, E. A.)—752(A)
Reynolds, George T. and S. B. Treiman. Kinematics of Λ^0 production—207(L); 797(A)
Reynolds, H. L. (see Scott, D. W.)—810(A)
—— (see Zucker, A.)—748(A)
Reynolds, J. M. Periodic Hall effect at low temperatures—803(T)
Ribe, F. L. and J. D. Seagrave. Pickup reactions $B^{10}(n,d)Be^9$ for 14-Mev neutrons—934
Richards, H. T. (see Jones, K. W.)—947
Richards, J. D. (see Brentano, J. C. M.)—1427(A)
Richardson, J. Reginald (see Caldwell, David O.)—79
Richings, H. J. (see DeBenedetti, S.)—766(A)
Rickard, James A. and Emmett L. Hudspeth. Excitation function and *Q* value for $C^{14}(d,p)C^{15}$—806(A)
Riddell, R. J., Jr., and Burton D. Fried. Meson-nucleon scattering. I—745(A); 1736
—— (see Fried, Burton D.)—746(A)
Risser, J. R. and H. C. Allen, Jr. NaI γ-ray spectrometry techniques applied to outlining of brain tumors—810(A)
—— (see Duller, N. M.)—810(A)
—— (see Thompson, L. C.)—941
Riste, T. and A. W. McReynolds. Magnetic neutron diffraction in Fe_3O_4—1433(A)
Ritland, H. N. Relation between refractive index and density in glass—1434(A)
Ritson, D. M. (see Hill, R. D.)—797(A)
Rittner, Edmund S. Extension of theory of junction transistor—1161
—— Review of interface compound formation in oxide cathodes—790(T)
Roberts, A. and J. Tinlot. Angular distribution of π^--proton charge exchange scattering at 40 Mev. I. Apparatus—766(A)
—— (see Tinlot, J.)—766(A)
Roberts, J. E. (see Farwell, G. W.)—363
Roberts, L. D. (see Bernstein, S.)—1243
—— (see Wilkinson, M. K.)—772(A)
Robinson, W. H., Yin-Yuan Li, and R. Smoluchowski. Small-angle scattering of x-rays by irradiated diamond—1435(A)
Rodeback, G. W. Imperfections in Cu in terms of electrical resistivity and thermoelectric power—1406(A)
Roesch, William C. Age-diffusion theory for β-ray problems—779(A)
Roever, William L. (see Ginzbarg, Arthur S.)—812(A)
Rohrer, Robert H. (see Newson, Henry W.)—654
Rohrlich, F. (see Chase. D. M.)—81
Rollier, Mario A. and Einar Saeland. Half-life and β decay of long-lived Nb^{94}—1079(L)
Rollwitz, William L. Analysis of phase detectors for display of nuclear magnetic resonance signals—810(A)
Rorden, H. C. (see Wegel, R. L.)—782(A)
Rorschach, H. E., Jr. (see Swim, R. T.)—809(A)
Rosa, G. (see Bonfiglioli, G.)—316
Rosenblatt, D. B., R. Smoluchowski, and G. J. Dienes. Radiation-induced changes in electrical resistivity of α brass—1417(A)
—— (see McReynolds, A. W.)—1417(A)
Ross, Donald. Unnecessary, restrictive concept in turbulent boundary layer theory—783(A)
Ross, Marc. Connection between pion photoproduction and scattering phase shifts—454
Rossi, Bruno (see Morrison, Philip)—440
Rostoker, N. (see Kohn, W.)—1111
Rothman, M. A., H. S. Hans, and C. E. Mandeville. γ rays excited by inelastic scattering of fast neutrons in Bi, Ni, and Cu—791(A)
Rothstein, Jerome. Application of bimolecular kinetics to relaxation of order below Curie point—1429(A)
—— Application of group theory to statistical mechanics—792(A)
Rough, J. D. (see Dunnington, F. G.)—592
Ruderman, M. A. and H. Brown. Classical theory of high-energy processes—746(A)
Ruhlig, Arthur J. (see Graham, Walter J.)—25
Rumsey, V. H. Reaction concept in electromagnetic theory—1483
Russell, J., Jr., C. W. Reich, and G. C. Phillips. Large volume scattering chamber for angular distribution experiments—804(A)
—— (see Reich, C. W.)—804(A)
Russell, R. D. (see Shillibeer, H. A.)—1793(L)
Russell, R. K. Vibrational analysis of 3400–4000A absorption spectrum of SO_2—805(A)
Rustad, B. M. Electron-neutrino angular-correlation coefficient in decay of He^6—751(T)

Sack, H. S., T. R. Cuykendall, and T. J. Woods. Elastic and dielectric losses of some high polymers near and below second-order transition temperature—1414(A)
—— (see Cuykendall, T. R.)—1421(A)
—— (see Marvin, Robert S.)—1413(A)
Sadauskis, John (see Jesse, William P.)—764(A)
Saeland, Einar (see Rollier, Mario A.)—1079(L)
Sagalyn, Paul L. Hfs of $3P_{3/2}$ state of Na^{23}—885
Sagane, Ryokichi and Walter F. Dudziak. π^+/π^- ratios at low energies from complex nuclei—755(A)
Sakai, M., J. Dick, and J. D. Kurbatov. Disintegration of Co^{58}—779(A)
Salam, Abdus (see Matthews, P. T)—185
Salant, E. O. (see Hill, R. D.)—1794(L); 797(A)
Salkovitz, Edward I. and Paul L. Smith. X-ray study of prismatic punching in TlCl—770(A)
Salter, L. Simon melting equation and effective intermolecular potential—1434(A)
Salutsky, Murrell L. (see Kirby, H. W.)—1801(E)
Sampson, J. B. (see Tucker, C. W., Jr.)—1418(A)
Samuels, Arthur (see Turkevich, Anthony)—364
Sandstrom, Wayne M. (see Miller, Charles E.)—167
Saraf, Babulal. Inner bremsstrahlung in Cs^{131}—642; 793(A)
Satchler, G. R. Angular correlation of 3 nuclear radiations—1304

Satten, R. A. (see Jaccarino, V.)—1798(L)
Sawatzky, A. (see Jaumot, F. E., Jr.)—1429(A)
Saxon, David S. (see Gerjuoy, E.)—1445; 478
Scace, R. I. (see Murray, P. C.)—764(A)
Scanlon, W. W. and R. F. Brebrick. Preparation of PbS crystals of controlled electrical properties—1430(A)
—— (see Brebrick, R. F.)—1430(A)
—— (see Petritz, R. L.)—1430(A)
Schamp, H. W., Jr., and E. Katz. Self-diffusion and ionic conductivity in NaBr—828
Scharff-Goldhaber, Gertrude (see Mihelich, J. W.)—794(A)
Schawlow, A. L. (see Gunther-Mohr, G. R.)—1184
Schecter, Larry and Warren Heckrotte. Correction to deuteron stripping cross sections—1086(L)
Schein, Marcel (see Sprague, A. D.)—994
Schensted, Craige. Electromagnetic scattering by paraboloid of revolution—793(A)
Scherb, F. (see Feld, B. T.)—1000
Scherrer, V. E., B. A. Allison, and W. R. Faust. γ-γ coincidences from interaction of 3.1-Mev neutrons with various materials—791(A)
Schiessler, R. W. (see Webb, W.)—753(A)
Schindler, A. I. Hall effect of Pd-Ag alloy system—1422(A)
Schmid, L. C. (see Cork, J. M.)—1218
Schmidt, F. H. (see Meyer, D. I.)—927
—— (see Penning, J. R.)—779(A)
Schneider, E. E. Microwave resonance in color centers—768(T)
—— (see Hesketh, R. V.)—494(L)
Schrieffer, J. Robert. Effective carrier mobility in surface well—1420(A)
Schriever, Barbara Dwight, E. A. Whalin, and A. O. Hanson. Photodisintegration of deuterium by 60-280 Mev x-rays—763(A)
Schulten, R. and R. A. Ferrell. Nuclear shell model *ft* values for intermediate coupling—739(L)
Schulz, L. G. Effective mass of conduction electrons in Ag, Au, and Cu—1422(A)
Schupp, Fritz D. and Don S. Martin, Jr. $Mg^{24}(\gamma,3p3n)F^{18}$ reaction induced by 70-Mev bremsstrahlung—80
Schwartz, C. Ground states of odd-odd nuclei—95
—— **and A. de-Shalit.** Many-particle configurations in central field—1257
Schwartz, Robert M. 3-dimensional calculation of vibrational relaxation times in gases—793(A)
—— **and J. Eckerman.** Real gas effects by measurement of shock detachment distance—1441(A)
Schwarzer, D. (see Fireman, E. L.)—385
Schweber, S. S. Covariant formulation of Tamm-Dancoff method—1089(L)
Schwinger, Julian. Theory of quantized fields—1362
Sclar, N. (see Burstein, E.)—750(A)
Scott, D. W., H. L. Reynolds, and A. Zucker. Range and charge of energetic nitrogen ions in Ni—810(A)
Scott, M. B., A. O. Hanson, and D. W. Kerst. Electrodisintegration of Cu^{63}—763(A)
Seagrave, J. D. (see Ribe, F. L.)—934
Secrest, E. L. (see Smith, D. M.)—806(A)
Segrè, Emilio and Clyde Weigand. Energy spectrum of spontaneous fission fragments—157
—— (see Chamberlain, O.)—156
Seitz, Frederick. Nature of lattice defects in metals—1406(A)
—— Theory of radiation damage—1432(T)
Sellers, P. A., C. M. Stevens, and M. H. Studier. Half-life of U^{232}—952
—— (see Stevens, C. M.)—974
Serber, R. L. Interpretation of high-energy experiments—745(T)
Sessler, A. M. and H. M. Foley. Interaction current contribution to hfs of tritium—761(A)
Severiens, J. C. and C. S. Fuller. Mobility of impurity ions in Ge and Si—750(A)
Shapiro, A. M. (see Chen, F. F.)—784(A)
Sharp, W. T., H. Gellman, and G. E. Tauber Intermediate coupling in B^{10}—762(A)
Shatas, R. A., J. F. Marshall, and M. A. Pomerantz. Energy distribution of secondary electrons produced by 1.3-Mev primary electrons—757(A)
Shaw, C. H. (see Gordon, W. L.)—771(A)
—— (see Spielberg, N.)—752(A)
Shearer, J. N. (see Rank, D. H.)—575
Sheer, C., A. Zinn, and N. Hartmann. Variable Hg delay line equipment for measurement of short half-lives—769(A)
Sheline, Raymond K., Noah R. Johnson, P. R. Bell, R. C. Davis, and F. K. McGowan. Study of isobaric triplet Mg^{28}-Al^{28}-Si^{28}—1642
—— **and Joseph R. Wilkinson.** Nuclide V^{52}—729(L)
Sherr, R., C. W. Li, and R. F. Christy. Low excited states of F^{19}. III. Coulomb excitation by α particles—1076(L)
—— (see Gerhart, J. B.)—917
Sherwood, J. E., T. E. Stephenson, C. P. Stanford, and Seymour Bernstein. Stern-Gerlach experiment on polarized neutrons—791(A)
Sherwood, R. C. (see Bozorth, R. M.)—1439(A)
Shillibeer, H. A., R. D. Russell, R. M. Farquhar, and E. A. W. Jones. Radiogenic A measurements—1793(L)
Shirane, R. (see Jona, F.)—1408(A)
Shockley, W. (see van Roosbroeck, W.)—1558
Shreffler, Robert G. (see Christian, Russell H.)—783(A)
Shull, C. G. and M. K. Wilkinson. Small-angle neutron scattering by Fe at high temperatures—1439(A)
—— (see Wilkinson, M. K.)—1439(A); 772(A)
Shutt, R. P. Heavy unstable particles and multiple meson production observed in cloud chamber at cosmotron—745(T)
Shuttleworth, R. A. and B. C. Bradshaw. Mechanism of adsorption. II. Application—753(A)
—— (see Bradshaw, B. C.)—753(A)
Siegel, R. T. (see DeBenedetti, S.)—955
Silsbee, H. B. (see Bemski, G.)—767(A)
Silver, E. G. and R. W. Waniek. Use of wires embedded in nuclear emulsions to investigate reactions induced by high-energy neutrons—769(A)
Silverman, A. (see Wolfe, B.)—756(A)
Silverman, Searl J. and H. Levinstein. Electrical properties of single crystals and thin films of PbSe and PbTe—871
—— **and Henry Levinstein.** Electrical properties of single crystals and thin films of PbTe—1430(A)
Silverman, Shirleigh (see Benedict, W. S.)—752(A)
—— (see Herman, R. C.)—752(A)
Silvey, G. (see Aamodt, L. C.)—789(A)
Simmons, B. E. (see Holmgren, H. D.)—748(A)
Simon, A. and T. A. Welton. Polarization from isolated resonances—943
Simpson, J. A. Cosmic radiation intensity-time variations and their origin. III. The origin of 27-day variations—426
—— (see Firor, J. W.)—1031
Singer, S. E., W. S. Emmerich, and J. D. Kurbatov. Radiative electron capture in Fe^{55}, A^{37}, and Ni^{63}—779(A)
—— (see Emmerich, W. S.)—113
Singwi, K. S. and B. M. Udgaonkar. Polaron self-energy and Bloch-Nordsieck method—38
Sinha, M. S. (see Biswas, N. N.)—1400(L)
Sitte, Kurt, Don L. Stierwalt, and Irving L. Kofsky. Development of air showers in atmosphere—988
—— (see Kasnitz, Harold L.)—977
Skinner, Selby M. Contact potential, work function, and surface states—1428(A)
Slater, J. C. and G. F. Koster. Simplified LCAO method for periodic potential problem—1498

—— (see Koster, G. F.)—1392(L)
Slifkin, L. (see Tomizuka, C. T.)—1406(A)
Small, R. M. B. (see Plint, C. A.)—805(A)
Smaller, Bernard, Max S. Matheson, and Edward L. Yasaitis. Paramagnetic resonance in irradiated ice—202(L)
Smart, J. Samuel. Cation distributions in mixed ferrites—847
Smiley, E. F. Measurements of vibrational relaxation times in Cl_2 and Cl_2-He mixtures—1441(A)
Smith, Alan W. and John Turkevich. Effect of neutron bombardment on ZnS phosphor—857
—— Effect of radiation damage on thermal conductivity of graphite—1417(A)
Smith, B. and H. A. Boorse. Role of substrate and surface finish in He II film transport—772(A)
Smith, Charles S. Piezoresistance effect in Ge and Si—42
—— (see Neighbours, John R.)—1421(A)
Smith, Cyril Stanley. Properties of plutonium metal—1068(L)
Smith, D. M. and E. L. Secrest. Variation wave function for Na—806(A)
Smith, George F. Thermionic and surface properties of W crystals—295
Smith, H. L. and J. A. Kies. Energy to create fracture surfaces in glass—760(A)
—— (see Kies, J. A.)—760(A)
Smith, J. A., J. N. Cooper, and J. C. Harris. γ-ray energies from Al^{27} and S^{32}—749(A)
Smith, J. F. Electrostatic energy calculations for sodium tungsten bronze (Na_xWO_3)—1407(A)
Smith, L. W. (see Hill, D. A.)—791(A)
—— (see Snow, G. A.)—791(A)
Smith, Paul L. (see Salkovitz, Edward I.)—770(A)
Smith, R. L., F. E. Jaumot, Jr., and L. A. Arné, Jr. Comparison of diffusion techniques employing radioisotopes—1407(A)
Smith, Robert S. Dielectric constants of powders at uhf—1438(A)
Smith, W. J., W. J. Leivo, and R. Smoluchowski. Interferometric study of surface of x-ray and proton irradiated KCl crystals—1435(A)
Smoluchowski, R. Influence of nuclear radiation on electrical conductivity of alkali halides—1409(A)
—— Radiation effects in ionic and valence crystals—1432(T)
—— (see Leivo, W.)—771(A)
—— (see Li, Yin-Yuan)—1435(A); 751(A); 866
—— (see Robinson, W. H.)—1435(A)
—— (see Rosenblatt, D. B.)—1417(A)
—— (see Smith, W. J.)—1435(A)
Snow, G. A., T. Coor, D. A. Hill, W. F. Hornyak, and L. W. Smith. Experiments with neutrons from Cosmotron. II—791(A)
——, **R. M. Sternheimer, and C. N. Yang.** Polarization of nucleons elastically scattered from nuclei—1073(L)
—— (see Hill, D. A.)—791(A)
Snowdon, S. C. and W. D. Whitehead. Angular distribution of neutrons scattered from Cd, Sn, and Bi—786(A); 1267
Snyder, W. S. and Jacob Neufeld. Disordering of solids by heavy corpuscular radiation—760(A)
Solimene, N. and B. P. Dailey. Microwave spectrum of 1,1 difluoroethane—789(A)
Solmitz, Frank T. Coulomb effects in pion-proton scattering at relativistic energies—1799(L)
Sosin, A. and J. S. Koehler. Electrical resistivity of cold-worked Al single crystals—1422(A)
Soules, J. A. (see Spielberg, N.)—752(A)
Spearman, K. R., E. L. Hudspeth, and I. L. Morgan. γ-ray spectrum of C^{13} and γ rays from proton bombardment of C^{14}—806(A)
Spedding, F. H. (see Banister, J. R.)—1140
—— (see Elliott, J. F.)—50; 1143
Speisman, G. (see Feynman, R. P.)—500(L)
Spence, R. D. (see Cowen, J. A.)—1411(A)
—— (see Tahsin, Salah)—1442(A)
Spencer, J. W. (see Webb, W.)—753(A)
Sperduto, A. (see Fader, W. J.)—748(A)
Spetner, L. M. Errors in power spectra due to finite sample—778(A)
Spielberg, N., Shaw, C. H., and J. A. Soules. *L*-emission spectrum of Zr(40)—752(A)
Spiess, Fred Noel. α-emitting isomer: Po^{211}—1292
Spitzer, W. G. (see Johnson, E. J.)—1415(A)
Sprague, A. D., D. M. Haskin, R. G. Glasser, and Marcel Schein. Analysis of 405-Mev proton and 222-Mev negative pion stars—994
Sproull, R. L. Review of electronic processes in BaO crystals—790(T)
Spruch, Larry and G. Goertzel. Magnetic internal Compton coefficients in Born approximation—1671
Spry, W. Charge exchange scattering of negative pions at 42, 30, and 20 Mev in hydrogen—766(A)
Squire, C. F. Effect of pressure on superconductivity—803(T)
—— Solid state at low temperatures: survey of 1953 International Congress on Low Temperature-Physics—1426(T)
St. John, Robert M. and J. G. Winans. Motion of arc cathode spot in magnetic field—1097
Standing, K. G. Angular distribution of deuterons from N^{14}-$(p,d)N^{13}$—731(L)
Stanford, C. P., T. E. Stephenson, L. W. Cochran, and S. Bernstein. Neutron polarization—374
—— (see Bernstein, S.)—1243
—— (see Sherwood, J. E.)—791(A)
Stanford, G. S. (see Foster, B. P.)—804(A)
Starner, J. W. (see Bunker, M. E.)—1694
M. Stearns, M. B. Stearns, S. DeBenedetti, and L. Leipuner. Yields of π- and μ-meson x-rays in low Z materials—766(A)
—— (see DeBenedetti, S.)—766(A)
Stearns, M. B. (see DeBenedetti, S.)—766(A)
—— (see Stearns, M.)—766(A)
Steele, M. C. and J. Babiskin. Magneto-thermoelectric behavior of Bi at liquid He temperatures—1394(L)
Steijn, R. P. and F. J. Donahoe. Resistance studies of phase transformations in Fe-Pt alloys near composition Fe_3Pt—1432(A)
Stein, P. C. (see Feld, B. T.)—1000
Steinberg, E. P. (see Keller, R. N.)—969
Stephenson, T. E. (see Bernstein, S.)—1243
—— (see Sherwood, J. E.)—791(A)
—— (see Stanford, C. P.)—374
Stern, Donald M. (see Ferry, John D.)—1413(A)
Stern, Frank. Spin waves in antiferromagnetic face-centered cubic lattices—1412(A)
Stern, Martin O. (see Chamberlain, Owen)—666
Sternheimer, R. M. (see Snow, G. A.)—1073(L)
Sterzer, Fred and Yardley Beers. Pure quadrupole spectrum of methyl iodide vapor—1410(A)
Stevens, C. M., M. H. Studier, P. R. Fields, J. F. Mech, P. A. Sellers, A. M. Friedman, H. Diamond, and J. R. Huizenga. Cm isotopes 246 and 247 from pile-irradiated plutonium—974
—— (see Diamond, H.)—1083(L)
—— (see Sellers, P. A.)—952
Stevens, D. K., J. W. Cleland, and J. H. Crawford, Jr. Magnetic susceptibility of fast-neutron-bombarded Ge—1409(A)
—— (see Crawford, J. H., Jr.)—1415(A)
Stevenson, D. T. and R. J. Keyes. Measurement of lifetimes and diffusion constants in Ge—1416(A)
Stewart, J. W. and C. A. Swenson. Compressibilities of solid H_2 and D_2 at 4.2°K—772(A)
—— **and C. A. Swenson.** Compression to 10 000 atmos of solid hydrogen and deuterium at 4.2°K—1069(L)
Stierwalt, Don L. (see Sitte, Kurt)—988

Stout, J. W. (see Matarrese, L. M.)—1792(L)
Strandberg, M. W. P. and H. Dreicer. Doppler line width reduction—1393(L)
Strauch, K. and F. Titus. Scattering of 96-Mev protons from light nuclei. II. Angular distribution—785(A)
—— (see Titus, F.)—785(A)
Strauss, A. J. (see Kurnick, S. W.)—1791(L)
Streetman, J. R. and F. A. Matsen. United atom-separated atom treatment of H_2^+—805(A)
Stroke, H. H. (see Jaccarino, V.)—1798(L)
Stuart, R. V. (see Holmgren, H. D.)—748(A)
Stuart, Richard N. (see Lepore, Joseph V.)—1724; 788(A)
Studier, M. H. (see Diamond, H.)—1083(L)
—— (see Fields, P. R.)—209(L)
—— (see Sellers, P. A.)—952
—— (see Stevens, C. M.)—974
Stull, J. L. (see Bickford, L. R., Jr.)—1433(A)
Stump, Robert (see Talley, Harry)—809(A)
Sturm, W. J. (see Binder, D.)—760(A)
Sueoka, Seiichi. Decay of χ meson—1397(L)
Sugarman, Nathan and Anthony Turkevich. Production of Ga, Ge, and As nuclides by 2.2-Bev protons on Cu—775(A)
—— (see Duffield, Robert B.)—776(A)
—— (see Hudis, J.)—775(A)
—— (see Turkevich, Anthony)—728(L)
Sugarman, R. and S. DeBenedetti. Time structure of extensive air showers—796(A)
Suita, T. Dielectric properties of colored KCl crystals—1497
Suits, G. H. Metal-insulator-metal junction—1427(A)
Sutcliffe, C. H. and F. E. Jaumot, Jr. Long-range order in Cu-Au alloys of nonstoichiometric compositions—1429(A)
—— **and F. E. Jaumot, Jr.** Nature of order-disorder transformation in Cu-Au alloys of nonstoichiometric compositions—1429(A)
Sutherland, G. B. B. M. Infrared analysis of structure of large molecules—1426(T)
Swann, C. P. Initial performance of large Bartol Van de Graaff—768(A)
Swenson, C. A. (see Stewart, J. W.)—772(A); 1069(L)
Swim, R. T. and H. E. Rorschach, Jr. Flow of He II under hydrostatic pressure head—809(A)

Tahsin, Salah and R. D. Spence. Propagation of sound pulse in medium with complex elastic modulus—1442(A)
Takeda, G. and K. M. Watson. Polarization of fast protons scattered by nuclei—1087(L)
Talley, Harry and Robert Stump. Lifetime of positrons in superconductors—809(A)
Talley, Robert M. and Dorothy Enright. Optical and electrical measurements on InAs—1431(A)
Tamor, S. Polarization of high-energy protons scattered by complex nuclei—1087(L)
Tanaka, Katsumi (see Hellund, E. J.)—192
Taub, A. H. General relativistic variational principle for perfect fluids—1468
Tauber, G. E. and Ta-You Wu. Magnetic moment of K^{40} in intermediate coupling—762(A); 1307
—— (see Sharp, W. T.)—762(A)
Taylor, Ellison H. (see Livingston, Ralph)—725(L)
Taylor, H. L., O. Lönsjö, and T. W. Bonner. Nonelastic scattering of fast neutrons—807(A)
—— (see McCrary, J. H.)—808(A)
Taylor, T. B. Interpretation of measurements of total cross sections for nuclear scattering of high-energy neutrons—785(A)
Tchen, C. M. 1-dimensional walk with correlation by saturation for description of diffusion phenomena—1442(A)
Teem, J. M. (see Kruse, U. E.)—1795(L)
Temmer, G. M. and N. P. Heydenburg. Coulomb excitation of heavy and medium nuclei by α particles—747(A)
—— **and N. P. Heydenburg.** Rotational nuclear energy levels from Coulomb excitation—1399(L)
—— (see Heydenburg, N. P.)—748(A); 1252
Templeton, Charles C. Thickness of films left on capillary wall during displacement of one fluid by another—812(A)
Templeton, D. H. and E. M. Douthett. Measurement of fission fragment ranges in Al—759(A)
—— (see Douthett, E. M.)—128
Terwilliger, K. M. (see Jones, L. W.)—1436(A)
Teutsch, Werner B. (see Hughes, Vernon W.)—761(A)
Thaler, R. M. and J. Bengston. Phase shift analysis of high-energy nucleon-nucleon scattering experiments—679
——, **J. Bengston, and G. Breit.** Intermediate state coupling and interpretation of high-energy nucleon-nucleon scattering—683
Thirion, J., C. A. Barnes, and C. C. Lauritsen. Low excited states of F^{19}. II. Lifetime measurements—1076(L)
Thirring, W. E. (see Deser, S.)—711; 746(A)
Thompson, L. C. and J. R. Risser. γ rays from inelastic scattering of 14-Mev neutrons in C^{12} and O^{16}—941
Thompson, S. G. (see Choppin, G. R.)—1080(L)
—— (see Ghiorso, A.)—1081(L)
Thorn, R. N. Production of proton pairs—501(L)
Thulin, Sigvard. Decay scheme of Xe^{135}—734(L)
Tinlot, J. and A. Roberts. Angular distribution of π^--proton charge exchange scattering at 40 Mev. II. Analysis of results—766(A)
—— (see Roberts, A.)—766(A)
Titterton, E. W. Low-lying states of Be^8—206(L)
Titus, F. and K. Strauch. Scattering of 96-Mev protons from light nuclei. I. Energy distribution—785(A)
—— (see Strauch, K.)—785(A)
Tobocman, W. Theory of deuteron stripping—762(A)
—— Theory of the (d,p) reaction—1655
Todd, Jay, Jr. (see Miller, Charles E.)—167
Todd, W. B. (see Metzger, F. R.)—794(A)
Toller, A. L. (see Newson, H. W.)—774(A)
Tomboulian, D. H. (see Johnston, R. W.)—1585
Tomizuka, C. T. and L. Slifkin. Diffusion in Ag single crystals—1406(A)
Tomlinson, E. P., R. A. Naumann, and J. W. Mihelich. Decay of Pt^{191}—794(A)
Toupin, R. and M. Lax. Critical temperature and susceptibility of dipole lattices—781(A)
—— (see Lax, M.)—780(A)
Townes, C. H. Nuclear size from x-ray fine structure—773(T)
—— (see Aamodt, L. C.)—789(A)
—— (see Bird, G. R.)—1203
—— (see Gunther-Mohr, G. R.)—1191
—— (see Wang, T. C.)—767(A)
Treiman, S. B. Solar magnetic moment and cosmic-ray effects associated with solar flares—1029
—— (see Reynolds, George T.)—207(L); 797(A)
Truby, Frank K. (see Workman, E. J.)—1073(L)
Trumble, R. E., Jr. $(\alpha$-$n)$ reactions in Be^9, B^{11}, and C^{13}—748(A)
Tucker, C. W., Jr., and J. B. Sampson. Interstitial content of radiation-damaged metals from precision x-ray lattice parameter measurements—1418(A)
Turkevich, Anthony. Estimation of beam intensity and cross sections at Cosmotron from gross radioactivity in Cu—775(A)
—— **and Arthur Samuels.** Evidence for Si^{32}, long-lived β emitter—364
—— **and Nathan Sugarman.** Ga, Ge, and As nuclides produced in bombardment of Cu with 2.2-Bev protons—728(L)
—— (see Sugarman, Nathan)—775(A)
Turkevich, John (see Smith, Alan W.)—857
Turner, R. G. (see Nicholls, R. W.)—1423(A)

Tweet, Arthur G. Small angle x-ray scattering from liquid He I and liquid He II—1801(E)
Tyler, W. W., H. H. Woodbury, and R. Newman. Properties of Ge doped with Fe or Co—1419(A)
—— (see Newman, R.)—1419(A)

Uberoi, M. S. Effect of wind-tunnel contraction on free stream turbulence—763(T)
Udgaonkar, B. M. (see Singwi, K. S.)—38
Uehling, Edwin A. (see Young, J. A., Jr.)—544
Ueta, Masayasu and Werner Känzig. Effect of plastic flow upon color centers in alkali halide crystals—1390(L)
Ufford, C. W. and S. Meshkov. Complete Bacher and Goudsmit method—761(A)
—— (see Meshkov, Sydney)—75

Vallarta, M. S. Diurnal variation of cosmic radiation—806(T)
van der Leun, C. (see Kluyver, J. C.)—1795(L)
Van der Ziel, A. Noise mechanisms in oxide-coated cathodes—790(T)
Van Horn, David D. and William C. Cooley. Dimensional changes of α brass on dezincification and lattice strain in Cu introduced by vacancies—1418(A)
van Krzywoblocki, M. Z. New approach to theory of turbulence in gases—783(A)
van Lint, V. A. J., C. D. Anderson, E. W. Cowan, R. B. Leighton, and C. M. York, Jr. Cloud-chamber observations of some unusual neutral V particles having light secondaries —1732
van Roosbroeck, W. and W. Shockley. Photo-radiative recombination of electrons and holes in Ge—1558
Van Vleck, J. H. (see Gunther-Mohr, G. R.)—1191
Vand, V. and R. Pepinsky. Evaluation of statistical approach to phase determination in x-ray analysis—1435(A)
Varma, Jagdish. Nuclear energy levels of Tl^{203}—795(A); 1688
—— **and C. E. Mandeville.** Disintegration of Mo^{93}—91
—— (see Mandeville, C. E.)—780(A)
Venable, Douglas and Leo F. Perry. Statistical uncertainties in radiographic determination of gas densities—784(A)
Vilain, J. H. and Robert W. Williams. μ-meson decay spectrum —1011
—— (see Williams, Robert W.)—757(A)
Villars, F. and V. F. Weisskopf. Scattering of electromagnetic waves by turbulent atmospheric fluctuations—232
Vincent, L. D. (see Little, R. N., Jr.)—807(A)
Vineyard, G. H. Small-angle scattering—751(T)
Vogel, F. L., W. T. Read, and L. C. Lovell. Recombination of holes and electrons at lineage boundaries in Ge—1791(L)
Vogt, Erich and Gregory H. Wannier. Quantum mechanics of scattering by a r^{-4} attractive potential—793(A)
Volkov, A. B. Modified shell model of odd-even nuclei—1664
von Dardel, G. F. Interaction of neutrons with moderating materials—1272

Wahl, A. C. (see Farwell, G. W.)—363
Wales, M. (see Leaderman, Herbert)—1414(A)
Walker, J. (see Elliott, L. G.)—795(A)
—— (see Graham, R. L.)—794(A)
Walker, R. M. (see Fowler, E. C.)—791(A)
Walker, W. D. (see Crussard, J.)—736(L)
—— (see Duller, N. M.)—810(A)
—— (see Hill, R. D.)—797(A)
Wall, C. N. Metaphysics of physics teacher—773(T)
Wall, N. S. Deuteron-induced reaction studies—763(A)
Wallenmeyer, W. Study of cloud-chamber distortions—768(A)
Wallis, G. and H. E. Farnsworth. Effect of strain on work function of polycrystalline Ag—777(A)
Wallis, R. F. (see Herman, R. C.)—752(A)
Walsh, J. M. Metal equation of state from shock-wave studies —765(T)
Wang, T. C. and C. H. Townes. Ratios of quadrupole coupling constants of isotopes and their variation with temperature —767(A)
Waniek, R. W. (see Silver, E. G.)—769(A)
Wannier, Gregory H. (see Vogt, Erich)—793(A)
Ward, J. K. (see Coon, J. B.)—805(A)
Warekois, E. P. X-ray measurements of cold-worked α brass—1421(A)
Watson, K. M. (see Takeda, G.)—1087(L)
Watson, R. B. (see Grannemann, W. W.)—812(A)
Watson, W. R., J. J. Dropkin, and A. T. Halpin. Electroluminescence in ZnS single crystals—777(A)
Wattenberg, A. (see Feld, B. T.)—1000
Way, Katharine and Marion Wood. β-decay energy systematics—119
Webb, W., J. W. Spencer, and R. W. Schiessler. Effect of structure and molecular weight on viscosity of higher hydrocarbons at high pressures—753(A)
Webber, A. C. (see DiDonato, A. R.)—770(A)
—— (see MacLeod, A. A.)—769(A)
Weber, J. Quantum theory of damped electrical oscillator and noise. II—211
—— Quantum theory of radiation resistance—793(A)
—— Vacuum fluctuation noise—215
Wechsler, M. S., D. S. Lieberman, and T. A. Read. Theory of crystal geometry of cubic—tetragonal phase changes—759(A)
—— (see Lieberman, D. S.)—760(A)
—— (see Read, T. A.)—759(A)
Weertman, J. R. (see Rado, G. T.)—1411(A); 1386(L)
Wegel, R. L. and H. C. Rorden. Structure of vibration pattern of transverse waves in slow circular jets—782(A)
Weimer, D. K. (see Blackman, V. H.)—508
Weinman, J. A. (see Bittner, J. W.)—769(A)
Weinstein, Roy, Martin Deutsch, and Sanborn Brown. Fine structure of positronium—758(A)
Weinstock, Bernard (see Osborne, Darrell W.)—202(L)
Weinstock, E. V. and J. Halpern. Systematics of photoproton reactions—1651
Weiss, R. J., J. J. DeMarco, G. Weremchuk, J. Hastings, and L. Corliss. Anisotropic Debye-Waller factors in cubic crystals—1420(A)
Weisskopf, V. F. (see Villars, F.)—232
Weller, Charles E. Improved spark counter for detecting α radiation—810(A)
Welsh, H. L. (see Plint, C. A.)—805(A)
Welton, T. A. (see Simon, A.)—943
Weremchuk, G. (see Weiss, R. J.)—1420(A)
Wert, C. (see Wruck, D.)—1417(A)
Westervelt, D. R. R', colloidal, and Z bands in KCl—1438(A)
Whalin, E. A. and R. A. Reitz. Liquefied gas x-ray target—752(A)
—— (see Schriever, Barbara Dwight)—763(A)
Whaling, Ward. Energy loss of protons and deuterons in gases—806(T)
Wheeler, J. A. Fields and particles—773(T)
White, M. G. Summary of other accelerator studies in progress—792(T)
White, Robert L. Hfs in DCC, Cl, DCN, and HCN due to deuteron quadrupole coupling and field asymmetries—789(A)
—— (see Gunther-Mohr, G. R.)—1184
Whitehead, W. D. (see Snowdon, S. C.)—786(A); 1267
Wick, G. C. Scattering of neutrons by systems containing light nuclei—1228
Widgoff, M. (see Hill, R. D.)—1794(L); 797(A)
Wiedenbeck, M. L. (see Lu, Daniel C.)—501(L)
—— (see MacGregor, M. H.)—138

—— (see Segrè, Emilio)—157
Wiggins, T. A. (see Rank, D. H.)—575
Wigner, Eugene P. Application of Rayleigh-Schrödinger perturbation theory to hydrogen atom—77
—— Problem of multiple scattering—17
Wiig, Edwin O. (see Fink, Richard W.)—1357
—— (see Haldar, B. C.)—1713
Wilkins, Homer C. (see Annis, Martin)—1038
Wilkinson, Joseph R. (see Sheline, Raymond K.)—729(L)
Wilkinson, M. K. and C. G. Shull. Neutron diffraction observations on Fe at high temperatures—1439(A)
——, **C. G. Shull, L. D. Roberts, and S. Bernstein.** Neutron diffraction investigations on superconducting elements—772(A)
—— (see Shull, C. G.)—1439(A)
Willard, H. B., J. K. Bair, and J. D. Kington. Angular distributions of 0.2–1.5 Mev neutrons elastically scattered by light nuclei—786(A)
Willardson, R. K. (see Harman, T. C.)—1065(L)
Williams, Dudley. Recent developments in rf spectroscopy—803(T)
—— (see Burch, D. E.)—1424(A)
Williams, Ferd E. (see Piper, William W.)—777(A)
Williams, H. J. (see Nesbitt, E. A.)—1440(A)
Williams, M. M. D. (see Orvis, A. L.)—810(A)
Williams, Malcolm L. and John D. Ferry. Dynamic mechanical properties of polyvinyl acetate—1413(A)
—— (see Ferry, John D.)—1413(A)
Williams, Robert W. and J. H. Vilain. Spectrum of electrons from μ-meson decay—757(A)
—— (see Vilain, J. H.)—1011
Williams, Ross, Aihud Pevsner, James Rainwater, and Seymour J. Lindenbaum. Elastic scattering of positive and negative pions in Li—765(A)
—— (see Pevsner, Aihud)—765(A)
Williamson, R. M. (see Goldburg, W. I.)—747(A)
—— (see Newson, H. W.)—774(A)
Willig, F. J. Applications of high explosives and high-speed photography to physical research problems—765(T)
Wills, James E. and Henry R. Dvorak. Analyzing magnet for 100-kv modified Cockcroft-Walton accelerator—810(A)
—— (see Little, R. N., Jr.)—807(A)
Wilson, R. R. (see Jenkins, T. L.); 755(A)
Winans, J. G. (see St. John, Robert M.)—1097
Windham, Pat M. and G. C. Phillips. Angular correlation apparatus for $Li^7(p,\gamma_1\alpha)He^4$—803(A)
Winhold, E. J. (see Fairhall, A. W.)—733(L)
Winkler, Stanley. Nonuniform microwave transmission lines and solutions of Riccati equations—778(A)
Winston, Harvey. Studies on localized orbitals—328
Witmer, Enos E. Nuclear masses as integral or rational multiples of electron mass—764(A)
Wolfe, B., J. W. DeWire, and A. Silverman. Elastic photoproduction of neutral mesons from deuterium—756(A)
Wolfenstein, L. Possible angular correlations involving V particles—786(A)
Wolff, G. Triboluminescence in crystals—777(A)
——, **P. H. Keck, and J. D. Broder.** Preparation and properties of III–V compounds—753(A)
Wolff, P. A. Theory of energy distribution of secondary electrons—749(T)
Wolfgang, R. and G. Friedlander. Momentum transfer in high-energy nuclear interactions in Al—775(A)
—— (see Friedlander, G.)—727(L); 775(A)
—— (see Hudis, J.)—775(A)
Wolfson, J. L. (see Elliott, L. G.)—795(A)
Wollan, E. O. (see Koehler, W. C.)—1801(E)
Wood, John G. Bubble tracks in hydrogen-filled Glaser chamber—731(L)
Wood, Marion (see Way, Katharine)—119
Wood, R. E. Activation measurements in Eu with monoenergetic neutrons—794(A)
Woodbury, H. H. (see Tyler, W. W.)—1419(A)
Woodruff, A. E. (see Noyes, H. P.)—1401(L)
Woodruff, Robert W. and M. Parker Givens. Soft x-ray absorption of Te—752(A)
Woods, T. J. (see Sack, H. S.)—1414(A)
Woodward, W. M. (see Ashkin, Arthur)—357
Workman, E. J. and W. Drost-Hansen. Electrical conduction and dielectric properties of ice—770(A)
——, **Frank K. Truby, and W. Drost-Hansen.** Electrical conduction in halide-contaminated ice—1073(L)
—— (see Drost-Hansen, W.)—770(A)
Wruck, D. and C. Wert. Crystal structure as factor in radiation damage—1417(A)
Wu, C. S. (see Lidofsky, L.)—780(A)
Wu, Ta-You. Theory of directed valence—1424(A)
—— (see Bauer, Ernest)—1424(A)
—— (see Tauber, G. E.)—762(A); 1307

Yager, W. A. (see Fletcher, R. C.)—1392(L)
Yang, C. N. (see Snow, G. A.)—1073(L)
Yasaitis, Edward L. (see Smaller, Bernard)—202(L)
Yeivin, Y. (see Haber-Schaim, U.)—184
Yekutieli, G. (see Haber-Schaim, U.)—184
Yevick, George J. and Jerome K. Percus. New approach to classical and quantum theory of many interacting particles. I—787(A)
—— (see Percus, Jerome K.)—787(A)
Yntema, J. L. (see Bayard, Robert T.)—757(A)
York, C. M., Jr. (see van Lint, B. A.)—1732
Young, D. R. (see Drougard, M. E.)—1408(A); 1561
Young, J. A., Jr., and Edwin A. Uehling. Tensor formulation of ferromagnetic resonance—544

Zacharias, J. R. Precision measurements with molecular beams—751(T)
Zaffarano, D. J. (see Lane, R. O.)—959
Zeldes, Henry (see Livingston, Ralph)—725(L)
Zemach, A. C. and R. J. Glauber. Neutron scattering by rotators—790(A)
Zimmerman, Robert L. (see Cooper, Daniel I.)—1209
Zimmerman, S. F., Jr., and C. P. Browne. Energy levels of Al^{27}—749(A)
Zinn, A. (see Sheer, C.)—769(A)
Zitter, R. N. (see Kurnick, S. W.)—1791(L)
Zuber, N. (see Forster, H. K.)—754(A)
Zucker, A. and H. L. Reynolds. Excitation functions for nitrogen-induced nuclear reactions in C—748(A)
—— (see Scott, D. W.)—810(A)
Zumino, Bruno. Collision matrix for Dirac particles—747(A)
Zupančič, Črtomir and Torben Huus. Emission of δ- and x-rays from targets bombarded by accelerated ions—205(L)

Author Index to Volume 95

References with (A) are to abstracts of papers presented at meetings of the American Physical Society; references with (T) designate title only. References with (L) are to Letters to the Editor. References with (E) are to Errata.

Aarons, M. W., M. Pobereskin, J. E. Gates, and E. B. Dale. Distribution of mass transported from collector into Ge crystal by forming process—1345(L)

Abeles, B. and S. Meiboom. Theory of galvanomagnetic effects in Ge—31

Abrahams, Elihu. Electron-electron scattering in alkali metals—839(L)

Abrahams, I. C. Color television (with demonstrations)—309(T)

Acton, Forman S. (see Herman, Frank)—371

Ajzenberg, Fay and Wolfgang Franzen. Neutrons from proton bombardment of B^{10}—1531

——, **W. Franzen, and J. G. Likely.** Neutrons from proton bombardment of B^{10}—641(A)

Akers, Lawrence K. and Ernest A. Jones. Vibrational spectra of pentafluorides of Sb, As, and Br—300(A)

Albert, R. D., M. L. Yeater, and E. R. Gaerttner. Neutron capture measurements with G. E. betatron velocity selector—644(A)

Albrecht, H. O. (see Mandeville, C. E.)—598(A)

Alburger, D. E. Experimental and theoretical studies of levels in Pb^{208}—632(T)

—— **and M. H. L. Pryce.** Energy levels in Pb^{208} from decay of Bi^{208}—1482

Alei, E. Felix (see Fermi, E.)—1581

Alei, E. P. (see de Hoffmann, F.)—1586

Alexander, B. H. (see Levitas, A.)—846(L)

Alford, W. Parker and Donald R. Hamilton. Recoil spectrum in β decay of Ne^{19}—1351(L)

Allen, Lew, Jr., and A. O. Hanson. Photodistintegration of deuterium by 95-Mev bremsstrahlung—629(A)

Allen, Robert C. Sphere measurements of neutron inelastic collision cross sections—637(A)

Allison, B. A. (see Scherrer, V. E.)—637(A)

—— (see Shapiro, P.)—751

Altshuler, Edward E. (see Sampson, John L.)—298(A); 617(A)

Altshuler, Saul and J. F. Carlson. Time-dependent variational principle—546

Ambler, E. and R. P. Hudson. Measurements on chromium potassium alum below 1°K—1143

——, **R. P. Hudson, and G. M. Temmer.** Anisotropic γ radiation from aligned Ce^{141} nuclei—625(A)

Anderson, C. D. (see van Lint, V. A. J.)—295(L)

Anderson, W. S. (see Sakai, M.)—101

Andrews, David H. Automatic electrostatic field plotter—633(A)

Ard, W. B. (see Fairbank, William M.)—566(L)

Arnowitt, Richard and S. Gasiorowicz. Approximate equations for meson-nucleon systems—618(A)

—— **and S. Gasiorowicz.** Covariant approximation scheme for Green's functions of coupled fields—538

Arons, Arnold. Amherst program: Experience with calculus-physics course required of all students—297(T)

Aschenbrenner, F. A. Particle selection technique used at M.I.T. cyclotron—600(A)

Ashkin, J. (see Blaser, J.)—624(A)

Aström, Björn (see Atterling, Hugo)—585(L)

Atkinson, W. R., R. G. Fowler, and W. R. Holden. Magneto-hydrodynamic flows in H and He—634(A)

Atterling, Hugo, Wilhelm Forsling, Lennart W. Holm, Lars Melander, and Björn Aström. Element 100 produced by means of cyclotron-accelerated oxygen ions—585(L)

Austern, N. and S. T. Butler. Coulomb effects in deuteron stripping—605(A)

Austin, Pauline M. Quantitative measurements of radar echoes from precipitation—297(A)

Autler, S. H. and W. F. Roat. Light decay from electroluminescent phosphors—599(A)

Axel, P. and J. D. Fox. Implications of photonuclear effect in Zr^{90}—613(A)

Babiskin, J. and M. C. Steele. Magnetic dependence of thermoelectric power of Bi at low temperatures—602(A)

Baer, W. Migration areas of Po-Be neutrons in H_2O-Zr mixtures—660(A)

Bair, Joe K. (see Willard, Harvey B.)—1359(L)

Baker, C. P. (see Draper, J. E.)—644(A)

Baker, E. (see Hudis, J.)—612(A)

Baker, N. and O. Bergmann. Decay scheme of τ meson—174

Balazs, N. L. General properties of solutions in Dirac's new electrodynamics—305(A)

—— Resolution of four-dimensional vector fields and tensor fields—305(A)

Baldwin, G. C., F. R. Elder, and W. F. Westendorp. Betatron orbit stability as function of n—600(A)

Balestrini, Silvio J. Mass-spectrometric study of deuteron-induced reactions in iodine—1502

Bandel, H. W. Measurement of current during formative time lag of sparks in uniform fields in air—1117

Bandtel, Kenneth C., Wilson J. Frank, Richard Madey, and Burton J. Moyer. Comparison of reactions $H^3(H^1, \pi^+)H^3$ and $H^2(H^1,\pi^0)He^3$ as test of charge independence—639(A)

Banta, H. E. (see Macklin, R. L.)—302(A)

Bardeen, J. (see Hall, L. H.)—559(L)

Baril, Alnert, Jr. Photolysis of para-diazo-N, N-dimethylaniline ZnCl dihydrate—306(A)

Barnett, C. F., P. M. Stier, and G. E. Evans. Relative secondary electron emission for ions and atoms—307(A)

—— (see Stier, P. M.)—303(A)

Barrett, C. S. (see Cohen, M. H.)—1094(L)

Barrett, P., G. Cocconi, Y. Eisenberg, and K. Greisen. Atmospheric temperature effect for mesons far underground—1573

——, **G. Cocconi, Y. Eisenberg, and K. Greisen.** Diurnal variations of intensity of cosmic rays far underground—1571

Bartholomew, G. A., F. Brown, H. E. Gove, A. E. Litherland, and E. B. Paul. Resonances in proton bombardment of C^{14}—649(A)

—— (see Gove, H. E.)—650(A)

Bartnoff, Shepard. Drop size distribution and visibility in clouds and rain—615(A)

—— (see Fish, Joseph K.)—297(A)

Barton, M. Q. and J. H. Smith. Proton-neutron coincidences in high-energy photodistintegration of Li—573(L)

—— (see Yamagata, T.)—574(L)

Bashkin, Stanley. $Li^7(d,p)Li^8$ yield curve—640(A); 1012

Baumann, N. P., F. W. Prosser, Jr., and R. W. Krone. γ-ray resonances in proton bombardment of Na^{23}—650(A)

Bazorgan, G. A., J. W. Irvine, Jr., and C. D. Coryell. Preparation and half-life of Cr^{55}—781

Beams, J. W. and J. B. Breazeale. Methods of spinning rotors at low temperatures—601(A)

Beard, C. I. (see Massey, J. T.)—622(A)

Beard, George and M. L. Wiedenbeck. Natural radioactivity of Sm^{147}—1246
Becker, R. A. (see Brown, H. N.)—626(A)
Bedo, D. E. and D. H. Tomboulian. L-absorption spectrum of Si and SiO_2—621(A)
Beeman, W. W. and R. H. Neynaber. Equipment for measurement of very small x-ray scattering cross sections—617(A)
Beer, A. C. (see Harman, T. C.)—596(A); 699
—— (see Willardson, R. K.)—597(A)
Béique, R. (see Lorrain, Paul)—599(A)
Belinfante, F. J. and J. C. Swihart. Quantized linear theory of gravitation. I—630(A)
—— (see Swihart, J. C.)—630(A)
Beljers, H. G., L. van der Kint, and J. S. van Wieringen. Overhauser effect in free radical—1683(L)
Bell, P. R. Recent advances in scintillation spectrometry—299(T)
—— (see Lazar, N. H.)—612(A)
Bell, R. E. Measurement of (p,xn) cross sections in Bi—651(A)
Belmont, E. and J. M. Miller. Reactions of 370-Mev protons with Co—1554
Belser, Richard B. and Margaret C. Chester. Structures and resistivities of sputtered films of Pt metals before and after aging by heating—307(A)
—— (see Brown, John L.)—308(A)
—— (see Chester, Margaret C.)—307(A)
Bender, R. S. (see Levine, S. H.)—640(A)
Bennett, A. Measurements of distribution of velocities in K molecular beams—608(A)
Bennett, W. E. (see Sugihara, T. T.)—298(A)
Bennett, W. H. and E. O. Hulburt. Theory of aurora based on magnetic self-focusing of solar ion streams—315
Bent, R. D., R. W. Bonner, and R. F. Sippel. Energy levels in C^{14} and N^{14}—649(A)
Bergmann, O. (see Baker, N.)—174
—— (see Green, H. S.)—516
Bergmann, Peter G. Quantum theory of gravitation—631(A)
Bergström, I. (see Passell, T. O.)—999
Beringer, R. and Mark A. Heald. Electron spin magnetic moment in atomic hydrogen—1474
Berkowitz, A. E., F. E. Jaumot, Jr., and F. C. Nix. Diffusion of Co^{60} in Ni-Al alloys containing excess vacancies—1185
Berlincourt, Ted G. and M. C. Steele. De Haas-van Alphen effect in Zn at liquid O_2 temperatures—603(A)
—— **and M. C. Steele.** Temperature-dependent de Haas-van Alphen parameters in Zn—1421
Berman, A. S. (see Lassettre, E. N.)—635(A)
Berman, R. and C. A. Swenson. Absolute temperature scale between 4.2° and 5.2°K—311
Bernardini, G. and E. L. Goldwasser. Photopion S wave near threshold and pion-nucleon coupling constant—857(L)
Bernstein, E. M. and H. W. Lewis. L-shell ionization by protons of 1.5- to 4.25-Mev energy—83
Bernstein, J. and A. Klein. Exchange current effects in deuteron—655(A)
Bernstein, S. (see Roberts, L. D.)—105
—— (see Stanford, C. P.)—302(A)
Bernstein, W., J. Weiss, and J. B. H. Kuper. Oxidation yield of ferrous sulfate dosimeter by x-rays—609(A)
Bersohn, R. Double bond character of C—Cl bond—614(A)
Bethe, H. A. and F. de Hoffmann. Meson-proton scattering phase shift analysis—1100(L)
—— (see de Hoffman, F.)—1586
—— (see Dyson, F. J.)—1644
—— (see Nelkin, M. S.)—618(A)
Bhatia, A. B. Minimum in electrical resistance of metals at low temperatures—914
Bhattacherjee, S. K., B. Waldman, and W. C. Miller. Energy determination of Cs^{137} K conversion electrons—404
Biedenharn, L. C., R. L. Gluckstern, and M. H. Hull, Jr. Coulomb wave functions for large values of parameter n—656(A)
Bird, George R. Saturation in microwave spectrum of methyl chloride—1686(L)
Birkhoff, R. D. (see Blackstock, A. W.)—303(A)
—— (see Hungerford, E. T.)—6
Birks, J. B. Temperature dependence of organic scintillation materials—277(L)
Birman, Joseph. Calculation of electrostatic lattice potentials, including ionic overlap—618(A)
Birnbaum, G. and A. A. Maryott. Microwave absorption in compressed gases—622(A)
Birnbaum, W., W. E. Crandall, G. P. Millburn, and R. V. Pyle. Excitation function for $C^{13}(d;\ p,2n)C^{13}$, $C^{13}(He^3;\ 2p,2n)C^{13}$, and $C^{13}(\alpha;\ 2p,3n)C^{13}$—649(A)
—— (see Crandall, W. E.)—620(A)
—— (see Millburn, G. P.)—620(A); 1268
Bitter, Francis (see Waymouth, John F.)—941
Bjørnerud, E. K. (see York, Carl M., Jr.)—159
Blackstock, A. W., R. D. Birkhoff, and M. Slater. Discrete electron energy losses in thin foils—303(A)
Blair, J. M. (see Holmgren, H. D.)—1544
Blair, J. S. Theory of elastic scattering of α particles by heavy nuclei—605(A); 1218
Blakewood, C. H. (see Dyba, R. V.)—1365
Blaser, J., J. Ashkin, F. Feiner, J. Gorman, and M. O. Stern. Total cross sections for scattering of positive pions by hydrogen—624(A)
Blatt, F. J. Properties of thin metallic films—13
—— (see Hall, L. H.)—559(L)
Blevins, Gilbert (see Jache, Albert)—299(A)
Bloch, Ingram (see Hsieh, Yu-Chang)—305(A)
Block, M. M. and D. T. King. Contributions of bremsstrahlung conversion in trident experiments—171
—— **and D. T. King.** Pairs formed by bremsstrahlung of great energy. II. Theoretical separation distribution—648(A)
—— (see King, D. T.)—648(A)
Bloembergen, N. and R. V. Pound. Radiation damping in magnetic resonance experiments—8
Bludman, Sidney A. Classical radiation from moving charges—654(A)
—— **and P. B. Daitch.** Validity of Born-Oppenheimer approximation—823
Blume, M. (see Treiman, S. B.)—646(A)
Boag, J. and B. Zendle. Scattered radiation contribution to depth dose data for 35- and 90-Mev synchrotron x-rays—608(A)
Boehm, F., P. Marmier, and J. W. M. DuMond. γ transitions in W^{180}—864(L)
Bok, Bart J. Radio studies of clouds in Milky Way—297(T)
Bollinger, L. M., R. R. Palmer, and D. A. Dahlberg. Total neutron cross sections of Bi and Mn—645(A)
—— (see Dahlberg, D. A.)—645(A)
Bolsterli, M. and E. Feenberg. Superallowed transitions in $4n$-type nuclides—612(A)
Bonner, R. W. (see Bent, R. D.)—649(A)
Bonner, T. W. (see Cook, C. F.)—639(A)
Borowitz, Sidney. Perturbation calculation of elastic exchange scattering of electrons by H atoms—656(A)
Bortner, T. E. and G. S. Hurst. Ionization of pure gases and mixtures of gases by 5-Mev α particles—609(A)
—— **and G. S. Hurst.** w value in electron volts for 5-Mev α particles in gases and gas mixtures—303(A)

Box, Harold C. and G. Stanley Klaiber. γ-ray spectrum of Ac^{225}—1247
Boyd, G. E. Tc activities at mass 97—113
Bozorth, R. M. (see McSkimin, H. J.)—616(A)
Braams, C. M. (d,p) reactions of Ca^{43} and Ca^{44}—650(A)
Braden, C. H., E. T. Patronis, Jr., and L. D. Wyly. Decay of Hg^{195}—627(A)
——, L. D. Wyly, and E. T. Patronis, Jr. Activities produced in Au by proton bombardment—758
Bradner, Hugh and Robert Donaldson. Asymmetry in neutron production by bombardment targets with 285-Mev polarized protons—1701(L)
—— and R. E. Donaldson. Search for polarization in charge exchange scattering—663(A)
Brattain, W. H. (see Garrett, C. G. B.)—1091(L)
Bray, P. J. Method for detection of pure quadrupole resonances—606(A)
Breazeale, J. B. (see Beams, J. W.)—601(A)
Brentano, J. C. M. and J. D. Richards. Evaporated multiple layers with semiconductor properties—841(L)
Breton, A. (see Lorrain, Paul)—599(A)
Bridge, H. S., H. Courant, B. Dayton, H. C. DeStaebler, Jr., B. Rossi, and D. Willard. Recent results on S particles—662(A)
——, H. Courant, H. DeStaebler, Jr., and B. Rossi. Possible example of annihilation of heavy particle—1101(L)
—— (see DeStaebler, H. C., Jr.)—662(A)
Brisbout, Françoise A. (see Parsons, R. W.)—193
Brody, Selma B. Aging of crushed Si and Ge powders—298(A)
Broida, H. P. and J. R. Pellam. Phosphorescence of atoms and molecules of solid N_2 at 4.2°K—845(L)
Brolley, J. E., Jr., W. C. Dickinson, and R. L. Henkel. Angular distribution of U^{235} fragments from neutron-induced fission as function of incident neutron energy—651(A)
Brown, Fielding and Charles L. Gravel. Domain rotation in sintered Ni ferrite—652(A)
—— (see Bartholomew, G. A.)—649(A)
Brown, H. A. and J. M. Luttinger. Calculation of ferromagnetic and antiferromagnetic Curie temperatures—652(A)
Brown, H. N., F. B. Smith, and R. A. Becker. Radiations from Ho^{164}—626(A)
Brown, John L. and Richard B. Belser. Electron microscope and diffraction traversing technique for examination of bimetal films—308(A)
Brown, L. Carlton and Dudley Williams. Magnetic resonance spectra of beryl crystals—1110(L)
Brown, Sanborn C. (see Champion, K. S. W.)—634(A)
—— (see Gould, Lawrence)—897
—— (see Reder, Fritz H.)—885
Browne, Cornelius P. Energy levels of Al^{26}—860(L)
—— (see Buechner, W. W.)—609(A)
Broyles, A. A. W.K.B. approximation through turning point—656(A)
Brueckner, K., C. Levinson, and H. Mahmoud. Two-body forces and nuclear saturation. I. Method—655(A)
—— (see Levinson, C.)—655(A)
Brysk, Henry (see Goldman, David T.)—305(A)
Buechner, W. W., C. P. Browne, H. Enge, M. Mazari, and C. D. Buntschuh. Magnetic spectrograph for nuclear disintegration studies—609(A)
Bunker, M. E., J. W. Starner, and J. P. Mize. Disintegration of Ga^{70}—612(A)
—— (see Mize, J. P.)—627(A)
Buntschuh, C. D. (see Buechner, W. W.)—609(A)
Burford, A. O., J. F. Perkins, and S. K. Haynes. Intensities of radiations from Hf^{175}—303(A)
Burgess, James H. Magnetic resonance enhancement in multilevel system—608(A)
Burgus, Warren H., George A. Cowan, J. W. Hadley, Wilmot Hess, Theodore Shull, M. L. Stevenson, and H. F. York. Cross sections for reactions $Ti^{48}(d,2n)V^{46}$; $Cr^{50}(d,2n)Mn^{52}$; and $Fe^{56}(d,2n)Co^{56}$—750
Burgwald, G. M. (see Reiffel, L.)—1294
Burkhardt, J. L. and E. J. Winhold. $In^{115}(\gamma,\gamma')In^{115m}$ cross section—629(A)
Burrus, Charles A., Albert Jache, and Walter Gordy. Mm wave spectrum of phosphine—299(A)
——, Albert Jache, and Walter Gordy. 1–2 mm wave spectroscopy. V. PH_3 and PD_3—706
Burson, S. B., W. C. Jordan, and J. M. LeBlanc. Isomeric states in $_{32}Ge^{75}$ and $_{32}Ge^{77}$—613(A)
—— (see LeBlanc, J. M.)—627(A)
Burwell, J. R. (see Kim, Y. B.)—661(A)
—— (see Thompson, R. W.)—661(A); 1576
Butler, S. T. (see Austern, N.)—605(A)

Callaway, Joseph. Approximate correlation potential—656(A)
—— (see Herman, Frank)—371
Camac, M. (see McGuire, A. D.)—625(A)
Cameron, A. G. W. (see Katz, L.)—464
Campbell, E. C. (see Stelson, P. H.)—301(A)
Campbell, J. G. Resonance absorption of γ radiation by O^{16} nuclei—1357(L)
Cap, Ferdinand. Nonlinear meson theory of nuclear forces—287(L)
Cap, C. (see Rohrer, R. H.)—302(A)
Caren, R. P. and C. E. Nielsen. Vapor expansion chamber using ammonia and water. II—601(A)
Cargill, W. H. (see Rohrer, R. H.)—308(A)
Carlson, B. C. (see Talmi, I.)—606(A)
Carlson, J. F. (see Altshuler, Saul)—546
Carlson, R. R. and E. B. Nelson. Capture γ rays from 315-kev proton bombardment of Be^9—641(A)
—— (see Nelson, E. B.)—650(A)
Carroll, Thomas J. Air-guided propagation of short radio waves around earth bulge—623(A)
Carter, R. S. and J. A. Harvey. Parameters of neutron resonances in Cs, In, Sn, and Pr—645(A)
—— (see Pilcher, V. E.)—645(A)
Carver, T. R. (see Schumacher, R. T.)—1089(L)
Case, K. M. Some generalizations of Foldy-Wouthuysen transformation—1323
Castle, J. G., Jr. Paramagnetic resonance absorption in soft carbon—846(L)
Chamberlain, Owen, Robert Donaldson, Emilio Segrè, Robert Tripp, Clyde Wiegand, and Thomas Ypsilantis. Experiments on nucleon-nucleon scattering with 312-Mev polarized protons—850(L)
—— and John D. Garrison. p-p scattering experiments at 170 and 260 Mev—1349(L)
——, G. Pettengill, E. Segrè, and C. Wiegand. Small-angle p-p cross sections and polarization at 300 Mev—1348(L)
——, Emilio Segrè, Robert Tripp, Clyde Wiegand, and Thomas Ypsilantis. Mechanism of proton polarization in high-energy collisions—1105(L)
——, Emilio Segrè, Robert Tripp, Clyde Wiegand, and Thomas Ypsilantis. Polarization of high-energy deuterons—1104(L)
—— and Martin O. Stern. Elastic scattering of 190-Mev deuterons by protons—1705(E)
Champion, K. S. W. and S. C. Brown. Phenomena of plasma resonance—634(A)

Chang, W. Y. Sea level mesons stopped in thin Pb and Al foils. I. Possible emission of charged nuclear particles and related events—1282; II. Low-energy (1–5 Mev) γ-rays —1288
Chase, C. E. and Melvin A. Herlin. Ultrasonic measurements in magnetically cooled He—565(L)
Chase, D. M. Equations of motion of charged test particles in general relativity—243
Chaudhury, N. K. (see Ganguly, S. C.)—1148
Chen, F. F. (see Shapiro, A. M.)—663(A)
Chester, Margaret C. (see Belser, Richard B.)—307(A)
—— **and Richard B. Belser.** Solder-shear tests to metal films deposited on glass substrates by evaporation and sputtering—308(A)
—— (see Belser, Richard B.)—307(A)
Chester, P. F. and J. S. Dugdale. Melting curves of deuterium and hydrogen—278(L)
Cheston, W. B. Compton scattering—247
Chew, Geoffrey F. Comparison of cut-off meson theory with experiment—1669
—— Improved calculation of p-wave pion-nucleon scattering phase shifts in cut-off theory—285(L)
Chinowsky, W. and J. Steinberger. Absorption of negative pions in deuterium: Parity of pion—1561
—— **and Jack Steinberger.** Parity of pion—623(A)
—— (see Steinberger, Jack)—623(A)
Choppin, G. R. (see Harvey, B. G.)—581(L)
Christian, Schuyler M. (see Johnson, Everett R.)—560(L)
Church, E. L. and M. Goldhaber. Low-energy transitions in Gd and related rare-earth activities—626(A)
Clark, Arnold F. (see Kao, S. K.)—662(A)
—— (see Mann, Leonard A.)—648(A)
Clarke, Edward N. Oxygen and surface energy-level structure on Ge—284(L)
Class, C. M. (see Eisinger, J.)—628(A)
—— (see Hanna, S. S.)—110
Cleland, J. W. and J. H. Crawford, Jr. Neutron irradiation of InSb—1177
Clement, J. R. Effect of temperature scales on low-temperature calorimetric data—601(A)
—— (see Overton, W. C., Jr.)—602(A)
Clifford, Joseph M. and R. B. Sawyer. Analysis of Forbes bar method for measuring thermal conductivity of metals —665(A)
Cocconi, Giuseppe. Influence of earth's magnetic field on extensive air showers—1705(E)
—— (see Barrett, P.)—1571, 1573
Cochran, Lewis W. (see Stone, W. G.)—304(A)
Codrington, R. S., J. D. Olds, and H. C. Torrey. Paramagnetic resonance in organic free radicals at low fields —607(A)
Coester, F. Hyperquantization of Feynman amplitudes—631(A); 1318
Cohen, B. L., D. J. Coombe, and B. L. Ferrell. Recent progress in fission fragment angular distribution measurements—303(A)
——, **G. H. McCormick, T. H. Handley, and E. Newman.** $(p,2n)$, $(p,2p)$, (p,t), (p,He^3) and (p,f) cross sections and excitation functions—639(A)
—— (see Handley, T. H.)—611(A)
Cohen, David, Burton J. Moyer, Harlan Shaw, and Charles Waddell. Proton bremsstrahlung and high-energy γ emission from C—664(A)
Cohen, M. H. Decomposition of scalar product of 2 symmetric tensors—674
—— **and C. S. Barrett.** Interaction of electrons with grain boundaries—1094(L)
Cohen, Marshall H. Electromagnetic scattering by dielectric bodies—657(A)
Cohen, V. W. and D. A. Gilbert. Nuclear spin and hfs interaction of 3.1-hr Cs^{134} isomer—569(L)
Cohn, H. O. (see Kim, Y. B.)—661(A)
—— (see Thompson, R. W.)—661(A)
Colli, L. Uv photons in decay of metastable A atoms—892
Collier, Robert J. Direct l-doublet transition of HCN in 10-cm wavelength region—1201
Collins, T. L., T. T. Scolman, and A. O. Nier. Precision double-focusing mass spectrometer—615(A)
Collinson, J. A. and W. W. Watson. Spectroscopic isotope shift in Hf I and Hf II—621(A)
Cook, C. F., T. W. Bonner, and J. B. Marion. Neutron thresholds from (d,n) and (p,n) reactions—639(A)
—— (see Eisinger, J.)—628(A)
Coombe, D. J. (see Cohen, B. L.)—303(A)
Cooper, Daniel I. (see Zimmerman, Robert L.)—662(A)
Cooper, John N. (see Green, D. W.)—610(A)
—— (see Russell, Leonard N.)—99
Cooper, Leon N. and James Rainwater. Theory of multiple Coulomb scattering from extended nuclei—1107(L)
Corenzwit, E. (see Matthias, B. T.)—1435
Cork, J. M. (see LeBlanc, J. M.)—627(A)
Cormack, A. M. Heat generation in earth by solar neutrinos —580(L)
Coryell, Charles D. (see Bazorgan, G. A.)—781
—— (see Richter, Harold G.)—1550
—— (see Sugihara, T. T.)—298(A)
Courant, H. (see Bridge, H. S.)—662(A); 1101(L)
—— (see DeStaebler, H. C., Jr.)—662(A)
Cowan, D. A. (see Winnemore, B. J.)—301(A)
Cowan, George A. (see Burgus, Warren H.)—750
Cox, John, W. J. Orville Thomas, and Walter Gordy. Centrifugal distortion in methyl halides—299(A)
Cox, S. A. (see Goldburg, W. I.)—628(A)
Crandall, W. E., W. Birnbaum, L. Schecter, and G. P. Millburn. Nuclear radii and transparencies from inelastic cross-section measurements. II. Interpretation—620(A)
—— (see Birnbaum, W.)—649(A)
—— (see Millburn, G. P.)—620(A); 1268
—— (see Schecter, L.)—659(A)
Crane, W. W. T. and G. M. Iddings. New isotope protactinium-237—1702(L)
Crawford, F. S., Jr., and M. L. Stevenson. Reaction $p+p\rightarrow\pi^{+}+d$ with polarized protons—1112(L)
Crawford, J. H., Jr. (see Cleland, J. W.)—1177
Croft, G. T., W. F. Love, and F. C. Nix. De Haas-van Alphen effect in Sn and Sn-Sb alloys—1403
Cronemeyer, Donald C. Recombination center density measurements in Ge—309(T)
Cross, W. G. and T. A. Eastwood. γ radiation from the decay of UX_2 (Pa^{234})—628(A)
Crussard, J., M. F. Kaplon, J. Klarmann, and J. H. Noon. Heavy unstable particles in stripped emulsions—584(L)
——, **W. D. Walker, and M. Koshiba.** π^{-} interactions at 1.5 Bev. II—624(A)
—— (see Kaplon, M. F.)—660(A)
—— (see Noon, J. H.)—1103(L)
—— (see Walker, W. D.)—624(A); 852(L)
Culler, Vaughn and R. W. Waniek. Total cross sections for high-energy neutrons—585(L)
—— (see Hillman, Peter)—462
—— (see Waniek, R. W.)—659(A)
Cummerow, Robert L. Photovoltaic effect in p-n junctions —16
—— Use of Si p-n junctions for converting solar energy to electrical energy—561(L)
Cunnell, F. A. and E. E. Schneider. Ionic conductivity and x-ray coloration of alkali halides—598(A)
Cure, J. W. and G. S. Hurst. Neutron scattering—302(A)

Curtis, C. D. (see Winnemore, B. J.)—301(A)
Cutkosky, R. E. Internal bremsstrahlung—1222
—— Solutions of Bethe-Salpeter equation—653(A)

Dabbs, J. W. T. and L. D. Roberts. Method for brute force polarization of H nuclei—307(A)
—— **and L. D. Roberts.** Polarization of Mn^{56} nuclei; cryogenic aspects—970
—— (see Roberts, L. D.)—105; 307(A)
Daggett, E. H. and G. R. Grove. γ-ray spectrum of Po^{209}—627(A)
Dahlberg, D. A. and L. M. Bollinger. Analyses of neutron resonances in Zn isotopes—645(A)
—— (see Bollinger, L. M.)—645(A)
Daitch, P. B. (see Bludman, S.)—823
Dale, E. B. (see Aarons, M. W.)—1345(L)
Dalitz, R. H. Sachs exchange moment—799
Damon, P. E. and R. R. Edwards. Absolute intensities of γ rays and x-rays of RaD—1698(L)
Davies, R. W. Energy spectrum of turbulence for entire range—912
Davis, Charles F., Jr., and M. W. P. Strandberg. Paramagnetic resonance absorption in ammonium chrome alum—607(A)
Davis, L., Jr., G. A. deMars, L. G. Rubin, and W. D. Straub. Some electrical properties of several Si-Ge alloys—597(A)
Dawson, J. M. and Z. I. Slawsky. Effect of intermolecular forces on rapid expansion of gas from initial condition of very high density and temperature—614(A)
Day, E. A. (see Johnston, L. H.)—599(A)
Day, Robert B. and Torben Huus. γ radiation from B^{10} bombarded by protons—1003
Dayton, B. (see Bridge, H. S.)—662(A)
Dayton, Irving E. Elastic scattering of 18-Mev protons by Al, Fe, Ni, and Cu—754
DeBenedetti, S. (see Stearns, M. B.)—625(A); 1353(L)
de Boisblanc, D. R. and K. A. McCollom. MTR time-of-flight instrumentation—609(A)
Deeds, W. E. Vibrational analysis of polypeptide chains—300(A)
de Hoffmann, F., N. Metropolis, E. P. Alei, and H. A. Bethe. Pion-hydrogen phase shift analysis between 120 and 217 Mev—1586
—— (see Bethe, H. A.)—1100(L)
DeLuca, Lloyd B. Self-diffusion coefficient of nitrogen—306(A)
deMars, G. A. (see Davis, L., Jr.)—597(A)
Dempsey, E. and D. ter Haar. Statistics of face-centered cubic ferromagnet—651(A)
De Pangher, J. n-p scattering at 300 Mev—578(L)
der Mateosian, E. Applications of "internal source" scintillation spectrometer—646(A)
—— **and C. S. Wu.** β spectrum of I^{130} and its decay scheme—458
—— (see Muehlhause, C. O.)—598(A)
DeStaebler, Herbert, Jr. Nuclear absorption of negative K particles—1110(L)
——, **H. S. Bridge, H. Courant, and B. Rossi.** Unusual cosmic-ray event—662(A)
—— (see Bridge, H. S.)—662(A); 1101(L)
Dettman, J. W. and A. Schild. Conservation theorems in modified electrodynamics—631(A); 1057
Deverall, G. V., K. W. Meissner, and G. J. Zissis. Precision wavelength and isotopic shift measurements of Ge arc lines—1463
Devlin, G. E. (see Schawlow, A. L.)—1344(L)
DeWire, J. W. (see Edwards, D. A.)—629(A)
Dexter, R. N., H. J. Zeiger, and Benjamin Lax. Anisotropy of cyclotron resonance of holes in Ge—557(L)
——, **H. J. Zeiger, Benjamin Lax, and E. S. Rosenblum.** Anisotropy of cyclotron resonance in Ge. Part II. Experiment—597(A)
—— (see Lax, Benjamin)—597(A)
Diamond, R. M. New isotopes of Nb: Nb^{90} and Nb^{90m}—410
Dick, J. L. (see Sakai, M.)—101
Dickinson, W. C. (see Brolley, J. E., Jr.)—651(A)
Dillinger, J. R. (see Knudsen, W. C.)—279(L)
Dillon, J. A., Jr. (see Sheridan, W. F.)—635(A)
Dolan, W. W. and W. P. Dyke. Temperature-and-field emission of electrons from metals—327
Domenicali, C. A. and F. A. Otter. Thermoelectric power and electron scattering in metal alloys—1134
Donaghy, Charles F. and Clark Goodman. Determination of thickness of Li targets from position of geometric peak—298(A)
Donahoe, F. J. and F. C. Nix. Temperature and field dependence of de Haas-van Alphen effect—1395
Donaldson, Robert E. (see Bradner, H.)—663(A); 1701(L)
—— (see Chamberlain, Owen)—850(L)
Dondes, S. (see Harteck, P.)—320
Dorain, Paul B. (see Thacher, H. C., Jr.)—615(A)
Dorfman, Leon M. Absorption of tritium β particles in hydrogen and other gases—393
Drachman, R. J. and D. C. Peaslee. Isotopic spin factors in nuclear reactions—605(A)
Draper, J. E. and C. P. Baker. Self-indication measurement of σ_{t_0} for 5.2-ev neutron resonance in Ag—644(A)
Dratz, A. F. (see Rohrer, R. H.)—308(A)
Dresden, M. Estimate of lifetime of positrons in superconductors—603(A)
Dresselhaus, G., A. F. Kip, and C. Kittel. Spin-orbit interaction and effective masses of holes in Ge—568(L)
Drisko, R. M. Angular dependence of annihilation quanta from magnetic substates of triplet positronium—611(A)
Dropkin, J. J. and S. Orgel. Ac photoconductivity in phosphors—597(A)
Drougard, M. E. and D. R. Young. Dielectric constant behavior of single-domain single crystals of $BaTiO_3$ in vicinity of Curie point—1152
Dudziak, Walter F. Charged pion production from C by protons—866(L)
—— (see Sagane, Ryokichi)—863(L)
Duffield, Robert B. (see Huizenga, J. R.)—1009
—— (see Sugarman, Nathan)—1704(L)
Dugdale, J. S. (see Chester, P. F.)—278(L)
DuMond, Jesse W. M. (see Boehm, F.)—864(L)
—— (see Snelgrove, Philip)—1203
Dunlap, W. C., Jr. (see Leifer, H. N.)—51
Dyba, R. V., C. T. Lane, and C. H. Blakewood. Film flow and bulk formation of He II in capillaries—1365
Dyke, W. P. (see Dolan, W. W.)—327
Dyson, F. J., M. Ross, E. E. Salpeter, S. S. Schweber, M. K. Sundaresan, W. M. Visscher, and H. A. Bethe. Meson-nucleon scattering in Tamm-Dancoff approximation—1644

Eastwood, T. A. (see Cross, W. G.)—628(A)
Edwards, D. A., B. Wolfe, A. Silverman, and J. W. DeWire. Angular distributions of photodeuterons—629(A)
Edwards, R. R. (see Damon, P. E.)—1698(L)
Efremov, N. Role of principal quantum number (n) in calculation of radii of ions with low (1^+,2^+,3^+,4^+) valence—614(A)
Eggler, C. and C. M. Huddleston. Gaseous scintillation counter—600(A)
Eisberg, R. M., H. Palevsky, M. E. Rickey, and T. I. Taylor. Total cross section of O_2 for cold neutrons—659(A)

—— (see Palevsky, H.)—659(A)
Eisenberg, Y. Interaction of heavy primaries in Pb—647(A)
—— (see Barrett, P.)—1571; 1573
Eisinger, J., C. F. Cook, and C. M. Class. Electric excitation of Au—628(A)
Elbek, B., K. O. Nielsen, and O. B. Nielsen. Determination of maximum β energy in decay of P^{30}—96
Elder, F. R. (see Baldwin, G. C.)—600(A)
El-Hussaini, Jassim (see Snelgrove, Philip)—1203
Ellis, R. A., Jr., M. B. Gottlieb, and J. A. Van Allen. Low-momentum end of spectrum of heavy primary cosmic rays—304(A)
Elsasser, Walter M. Dimensional relations in magnetohydrodynamics—1
Enatsu, Hiroshi, Hiroichi Hasegawa, and Pong Yul Pac. Theory of unstable heavy particles—263
Endt, P. M., J. C. Kluyver, and C. van der Leun. γ rays from $Si^{29}(p,\gamma)P^{30}$—580(L)
Enge, H. (see Buechner, W. W.)—609(A)
Engel, Olive G. Some aspects of dynamics of waterdrop collisions with solids—615(A)
Engler, A. and U. Haber-Schaim. Primary cosmic-ray spectrum deduced from analysis of jets—1700(L)
Ennis, Malcolm E. and Arthur Hemmendinger. Small-angle cross sections for scattering of protons by tritons —772
Enright, Dorothy P. (see Talley, Robert M.)—1092(L)
Eriksen, Erik (see Foldy, Leslie L.)—1048
Evans, G. E. (see Barnett, C. F.)—307(A)
—— (see Stier, P. M.)—303(A)

Fafarman, A. and M. H. Shamos. Cosmic-ray μ-meson low-energy differential range spectrum—648(A)
Fairbank, Henry A. and J. Wilks. Thermal conductivity of liquid He below 1.0°K—277(L)
Fairbank, William M., W. B. Ard, and G. K. Walters. Fermi-Dirac degeneracy in liquid He^3 below 1°K—566(L)
Falkoff, D. L. Random pulses and electron-spin line widths in metals—607(A)
Fan, H. Y., W. Kaiser, E. E. Klontz, K. Lark-Horowitz, and R. R. Pepper. Energy levels and photoconductivity in electron-bombarded Ge—1087(L)
Fang, P. H. Variance properties of general field operator —631(A)
Fano, U. Ionizing collisions of very fast particles and dipole strength of optical transitions—1198
Farney, G. K. (see Givin, H. H.)—302(A); 641(A)
Farwell, George W. and Harvey E. Wegner. Elastic scattering of intermediate-energy α particles by heavy nuclei —664(A); 1212
Faust, W. R. (see Scherrer, V. E.)—637(A)
—— (see Shapiro, P.)—751
Feenberg, E. (see Bolsterli, M.)—612(A)
Feeny, Harold (see Trambarulo, Ralph)—622(A)
Feher, G. and A. F. Kip. Electron spin resonance in Be —1343(L)
Feiner, F. (see Blaser, J.)—624(A)
Feingold, A. M. (see Lyons, D. H.)—606(A)
Feldman, G. Antiproton production—1697(L)
Ferguson, G. A., J. Halpern, R. Nathans, and P. F. Yergin. Photoneutron cross sections in He, N, O, F, Ne, and A—659(A); 776
Fermi, E., N. Metropolis, and E. Felix Alei. Phase shift analysis of scattering of negative pions by hydrogen— 1581
Ferrell, B. L. (see Cohen, B. L.)—303(A)
Fields, P. R. (see Friedman, A. M.)—1501
Fields, T. H., J. G. Fox, J. A. Kane, R. A. Stallwood, and R. B. Sutton. π^+ production in H by 437-Mev protons—638(A)
—— (see Kane, J. A.)—662(A); 1694(L)
Fine, S. (see Hendee, C. F.)—281(L)
Finkelstein, R. J. and S. A. Moszkowski. Mesonic corrections to β-decay coupling constants—1695(L)
Finlay-Freundlich, E. Red-shifts in spectra of celestial bodies—654(A)
Firor, J. W., J. A. Simpson, and S. B. Treiman. Production of cosmic radiation at sun—1015
Fischer, David and Gerson Goldhaber. Small angle p-p scattering at 330 Mev—1350(L)
Fischer, G. E. Scattering of 10-Mev protons on Mg and C —664(A)
Fischer, Vera Kistiakowsky. Disintegration of Pm^{150}— 626(A)
Fish, Joseph K. and Shepard Bartnoff. Study of drop-size frequency distribution in clouds and rain—297(A)
Fisher, L. H. Buildup processes in sparks and positive corona—620(T)
Fitch, V. (see Koslov, S.)—291(L); 625(A)
Fitzpatrick, P. M. (see Howard, R. A.)—661(A)
Fleming, J. R. (see Hourd, R. F.)—647(A)
Fletcher, R. C., W. A. Yager, G. L. Pearson, and F. R. Merritt. Hyperfine splitting in spin resonance of Group V donors in Si—844(L)
Fletcher, William H. and W. E. Shuler. Infrared spectrum of allene-d_2—300(A)
Flood, W. F., Jr. (see Hrostowski, H. J.)—1683(L)
Fluharty, R. G. MTR fast chopper—609(A)
Foldy, Leslie L. and Erik Eriksen. Physical consequences of vacuum polarization—1048
Foley, H. M. (see Sucher, J.)—966
Foner, Simon. Measuring magnetic properties of ferromagnetic materials by means of Hall effect—652(A)
Ford, Kenneth W. Nuclear deformation and moment of inertia of nuclear rotational states—1250
Forsling, Wilhelm (see Atterling, Hugo)—585(L)
Fowler, Charles A., Jr., and Edward M. Fryer. Magnetic domains in CO by longitudinal Kerr effect—564(L); 652(A)
Fowler, J. L. (see Johnson, C. H.)—637(A)
Fowler, R. G. (see Atkinson, W. R.)—634(A)
Fowler, W. B., R. P. Shutt, A. M. Thorndike, and W. L. Whittemore. Meson production in n-p collisions at Cosmotron energies—1026
Fox, J. D. (see Axel, P.)—613(A)
Fox, J. G. (see Fields, T. H.)—638(A)
—— (see Kane, J. A.)—662(A); 1694
Frank, Wilson J. (see Bandtel, Kenneth C.)—639(A)
Frankel, Sherman (see Golden, Robert K.)—613(A)
Franzen, Wolfgang (see Ajzenberg, F.)—641(A); 1531
Fraser, J. S. (see Milton, J. C. D.)—628(A)
Frenkiel, F. N. Theory of turbulent diffusion—658(T)
Fried, Burton D. Phase shifts for high-energy nucleon-nucleon scattering—851(L); 1706(E)
Friedlander, G. (see Hudis, J.)—612(A)
—— (see Sugarman, Nathan)—1704(L)
Friedman, A. M., A. L. Harkness, P. R. Fields, M. H. Studier, and J. R. Huizenga. α half-lives of Cm^{244}, Cm^{246}, and Cm^{248}—1501
Friedman, A. S. (see Haar, Lester)—614(A)
Frisch, David H. 2-body forces and nuclear stability— 865(L)
—— (see Pugh, G. E.)—590(L); 611(A)
—— (see Storrs, C. L.)—1252
—— (see Zimmerman, Robert L.)—662(A)
Frisch, Harry L. and Joel L. Lebowitz. Simplified model of stationary nonequilibrium process—643(A)
Fryer, Edward M. (see Fowler, Charles A., Jr.)—564(L); 652(A)
Fuchs, L. (see Primak, W.)—22

Fujino, Takuzo (see Ishiguro, Masakazu)—1347(L)
Fuller, E. G. (see Hayward, Evans)—1106(L)
Fulton, Thomas and Paul C. Martin. Two-body system in quantum electrodynamics. Energy levels of positronium—811
Fung, Si-Chang and Anthony Turkevich. Radiochemical evidence for the $Cu^{65}(p,pn^{+})Ni^{65}$ reaction—176
Furlong, L. R. Low-temperature luminescence of CdS—1086(L)
Furuichi, Jiro (see Mitsui, Toshio)—558(L)
Fuson, Nelson, Marie-Louise Josien, and Essie M. Shelton. Infrared spectroscopic study of influence of molecular structure upon $\nu(NH)$, $\nu(CO)$, and $\nu(CH_3)$ in benzopyrroles and their analogs—300(A)

Gaerttner, E. R. (see Albert, R. D.)—644(A)
Gaffney, John and W. C. Overton, Jr. Temperature variations of elastic constants of Cu single crystals from 4.2°K to 300°K—602(A)
Ganguly, S. C. and N. K. Chaudhury. Anisotropy of fluorescence of some organic crystals—1148
Garber, M. and D. E. Mapother. Effect of pressure on superconducting transition of Sn—603(A)
Garlick, G. F. J. (see Halperin, A.)—1098(L)
Garrett, C. and G. N. Whyte. Build-up measurements on Co^{60} γ radiation in Fe and Pb—889
Garrett, C. G. B. and W. H. Brattain. Self-powered semiconductor amplifier—1091(L)
Garrison, John D. (see Chamberlain, Owen)—1349(L)
Gasiorowicz, S. (see Arnowitt, Richard)—538; 618(A)
Gates, J. E. (see Aarons, M. W.)—1345(L)
Geballe, T. H. and F. J. Morin. Ionization energies of groups III and V elements in Ge—1085(L)
—— (see Matthias, B. T.)—1435
Geer, E. H. (see Nelson, E. B.)—650(A)
Geiger, K. W. and D. C. Rose. Neutron multiplicity from spontaneous fission of U—646(A)
Geller, K., J. Halpern, and Paul F. Yergin. Photoneutron angular distribution—659(A)
Geller, S. (see Matthias, B. T.)—1435
Gell-Mann, M., M. L. Goldberger, and W. E. Thirring. Use of causality conditions in quantum theory—1612
—— **and F. E. Low.** Quantum electrodynamics at small distances—1300
—— (see Goldberger, M. L.)—654(A)
Gerardo, H. (see Toms, M. E.)—629(A)
Gerhart, J. B. O^{14} decay and Fermi coupling constant in β decay—288(L)
Ghiorso, A., S. G. Thompson, G. H. Higgins, B. G. Harvey, and G. T. Seaborg. Evidence for subshell at $N = 152$—293(L)
—— (see Harvey, B. G.)—581(L)
—— (see Hulet, E. K.)—1703(L)
Ghosh, S. N. (see Sheridan, W. F.)—635(A)
Gibbons, J. H. and H. W. Newson. Total neutron cross sections in kev region: Tl^{203} and Tl^{205}—644(A)
—— (see Newson, H. W.)—640(A)
—— (see Rohrer, R. H.)—302(A)
Gibson, G. and P. Stehle. Interference effects in annihilation process—657(A)
Gilbert, D. A. (see Cohen, V. W.)—569(L)
Gilmore, P. (see Lorrain, Paul)—599(A)
Gilvarry, J. J. Relativistic Thomas-Fermi atom model—71
Gindler, J. E. (see Huizenga, J. R.)—1009
Girard, P. E. (see Lorrain, Paul)—599(A)
Givin, H. H., G. K. Farney, T. M. Hahn, and B. D. Kern. Angular distribution of 12-Mev and 16-Mev γ rays from proton bombardment of boron—641(A)
——, **G. K. Farney, B. D. Kern, and T. M. Hahn.** Angular distribution of 12-Mev γ rays from reaction $B^{11}(p,\gamma)C^{12}$—302(A)
Glasser, R. G. (see Schein, Marcel)—855(L)
Glauber, R. J. and P. C. Martin. Radiative capture of orbital electrons—572(L)
—— (see Zemach, A. C.)—605(A)
Glendenin, L. E. (see Steinberg, E. P.)—431; 867(L)
Glicksman, Maurice. Scattering of 187-Mev negative pions by hydrogen—1045
Gluckstern, R. L. (see Biedenharn, L. C.)—656(A)
Gold, R. (see Koerts, L.)—612(A)
Goldberger, M. L., M. Gell-Mann, and W. E. Thirring. General conditions on scattering matrix—654(A)
—— (see Gell-Mann, M.)—1612
Goldburg, W. I., S. A. Cox, and R. M. Williamson. Coulomb excitation of Au—628(A)
—— **and R. M. Williamson.** Coulomb excitation of Ta, W, and Au—767
Goldemberg, J. and L. Katz. Fine structure in neutron yield curves from (γ,n) reactions in Li^{7}, C^{13}, O^{16}, and F^{19}—471
—— (see Spicer, B. M.)—629(A)
Golden, Robert K. and Sherman Frankel. K-conversion electron—γ angular correlation in Sn^{117}—613(A)
Goldhaber, Gerson (see Fischer, David)—1350(L)
Goldhaber, M. (see Church, E. L.)—626(A)
—— (see Sunyar, A. W.)—570(L)
Goldman, David T. and Henry Brysk. Spatial distribution of energy dissipation by bremsstrahlung spectrum—305(A)
Goldman, J. E. (see Urquhart, H. M. A.)—653(A)
Goldschmidt-Clermont, Y. (see Osborne, L. S.)—637(A)
Goldstein, J. H. (see Slayton, George R.)—299(A)
Goldstein, Louis. Theory of liquid He^{3}–He^{4} mixtures—869
Goldwasser, E. L., L. J. Koester, Jr., and F. E. Mills. Elastic photoproduction of π^{0} mesons from He—1692(L)
—— (see Bernardini, G.)—857(L)
Gomez, R. (see Pugh, G. E.)—590(L); 611(A)
Good, W. M. (see Kunz, W. E.)—640(A)
—— (see Moak, C. D.)—641(A)
Goodenough, John B. Theory of domain creation and coercive force in polycrystalline ferromagnetics—917
—— (see Loeb, A. L.)—616(A)
Goodman, Clark (see Donaghy, Charles F.)—298(A)
—— (see Guernsey, Janet B.)—297(A); 636(A)
—— (see Kiehn, Robert M.)—636(A); 989
—— (see Mark, Hans)—628(A)
Goodman, L. S. and S. Wexler. Nuclear spin and magnetic moment of 3.1-hr Cs^{134m}—570(L)
Gordon, Carroll K. Electrical conductivity of S—306(A)
Gordon, J. P., H. J. Zeiger, and C. H. Townes. Molecular microwave oscillator and new hfs in microwave spectrum of NH_3—282(L)
Gordy, Walter (see Burrus, Charles A.)—299(A); 706
—— (see Cox, John)—299(A)
—— (see Jache, Albert)—299(A)
Gorman, J. (see Blaser, J.)—624(A)
Gottlieb, M. B. (see Ellis, R. A., Jr.)—304(A)
Gould, Lawrence and Sanborn C. Brown. Microwave determination of probability of collision of electrons in He—897
Gourary, B. S. and R. W. Hart. Spherical model of antiferromagnet—652(A); 676
Gove, H. E., E. B. Paul, A. E. Litherland, and G. A. Bartholomew. Some spin assignments and partial width measurements of resonances in S^{33} from reaction $P^{31}(p,\gamma)S^{32}$—650(A)
—— (see Bartholomew, G. A.)—649(A)
Grandey, Ray A. (see Mann, Leonard A.)—648(A)

Gravel, Charles L. (see Brown, Fielding)—652(A)
Graves, Ernest D. and H. C. Thomas. Proportional counter for Auger electrons—304(A)
Green, Alex E. S. Coulomb radius constant from nuclear masses—1006
Green, C. D. and D. Ter Haar. Statistical aspects of second law of thermodynamics—643(A)
Green, D. W., J. N. Cooper, and J. C. Harris. Stopping powers of metals for low-energy protons—610(A)
Green, F. L. and J. A. Martin. High-intensity beam of low-energy protons in ORNL 86-inch cyclotron—304(A)
Green, H. S. Integral equations of quantized field theory—548
—— **and O. Bergmann.** Core structure in soft component showers—516
Greenberg, J. Mayo. High-energy electron scattering—619(A)
Greenberg, L. H., J. G. V. Taylor, and R. N. H. Haslam. Yield of α particles from photonuclear reactions at 23-Mev bremsstrahlung—1540
Greenblatt, M. H. Time delay in secondary emission—633(A)
Greisen, K. (see Barrett, P.)—1571; 1573
Griffith, Gordon L. De-excitation γ rays from inelastic scattering of neutrons—636(A)
Grove, G. R. (see Daggett, E. H.)—627(A)
Guernsey, Janet B. and Clark Goodman. Low-lying states in nuclei from $(n,n'\gamma)$ interactions—297(A)
—— **and Clark Goodman.** Neutron inelastic scattering in Ta and I—636(A)
Gupta, Suraj N. Electromagnetic interaction of particles of spin $\frac{1}{2}$—630(A)
—— Fierz-Pauli theory of particles of spin 3/2—1334
Gursky, H. (see Winnemore, B. J.)—301(A)
Guss, Donald, Lawrence Killion, and F. T. Porter. β spectra of Re^{186} and Re^{188}—627(A)
Gutowsky, H. S. Structural determinations by nuclear magnetism—596(T)

Haar, Lester and A. S. Friedman. General method for high-speed machine computation of ideal gas thermal properties. Diatomic free radicals of isotopic hydrides—614(A)
Haber-Schaim, U. (see Engler, A.)—1700(L)
Hadley, J. W. (see Burgus, Warren H.)—750
Hafner, Everett Mark. Refinement of uniform model—604(A)
—— (see Roberts, A.)—663(A); 1099(L)
Hahn, B. (see Hofstadter, R.)—512
Hahn, T. M. (see Givin, H. H.)—302(A); 641(A)
—— (see Lafferty, D. L.)—637(A)
—— (see Rayburn, L. A.)—301(A); 637(A)
Halbert, M. L. (see McGuire, A. D.)—625(A)
Hall, Harold H. Analysis of proton-proton scattering at 9.7 Mev—424
Hall, L. H., J. Bardeen, and F. J. Blatt. Infrared absorption spectrum of Ge—559(L)
Hall, T., M. Siegel, L. M. Sharpe, and D. Pressman. Production of I^{124} by deuteron bombardment of Te—1208
Halperin, A. and G. F. J. Garlick. Low-temperature bleaching and restoration of color centers—1098(L)
Halpern, I. (see Sugihara, T. T.)—630(A)
Halpern, J., R. Nathans, and P. F. Yergin. $A^{40}(\gamma,n)$ threshold and mass of A^{39}—1529
—— (see Ferguson, G. A.)—659(A); 776
—— (see Geller, K.)—659(A)
—— (see Weinstock, E. V.)—630(A)
Hamermesh, Bernard (see Recksiedler, Arthur)—650(A)
Hamilton, Donald R. (see Alford, W. Parker)—1351(L)
Hamlin, D. (see Merritt, J.)—638(A)
Handley, T. H. and B. L. Cohen. New isotope identification program on Oak Ridge 86-inch cyclotron—611(A)
—— (see Cohen, B. L.)—639(A)
Hanna, S. S., E. C. LaVier, and C. M. Class. β-α correlation in decay of Li^8—110
—— (see Shafroth, S. M.)—86; 641(A)
Hanson, A. O. (see Allen, Lew, Jr.)—629(A)
—— (see Yamagata, T.)—574(L)
Hanson, H. P. and J. R. Knight. K-absorption edge studies of compounds—621(A)
Hanson, W. B. and J. R. Pellam. Second sound attenuation in liquid He II—321; 604(A)
Hardy, W. A. and G. Silvey. Microwave spectrum of TeCS and masses of stable Te isotopes—385
Harkness, A. L. (see Friedman, A. M.)—1501
Harman, T. C., R. K. Willardson, and A. C. Beer. Analysis of magnetoresistance and Hall coefficient in p-type InSb and p-type Ge—699
——, **R. K. Willardson, and A. C. Beer.** Comparison of Hall and magnetoresistance phenomena in InSb with those in Ge—596(A)
—— (see Willardson, R. K.)—597(A)
Harris, D. R. and A. L. Hodson. Production of V^{48} particles in Cu—661(A)
Harris, J. (see Green, D. W.)—610(A)
Hart, Edward W. Electronic energy of ordered alloys—666(A)
Hart, Robert W. (see Gourary, Barry S.)—652(A); 676
Harteck, P. and S. Dondes. Origin of N_2O in atmosphere—320
Hartman, P. L. (see Tomboulian, D. H.)—600(A)
Hartzler, A. J. and R. T. Siegel. 400-Mev n-p scattering—185
——, **R. T. Siegel, and W. Opitz.** Small-angle n-p scattering at 400 Mev—591(L)
Harvey, B. G., H. P. Robinson, S. G. Thompson, A. Ghiorso, and G. R. Choppin. Some pile neutron cross sections of isotopes of americium, berkelium, californium, and element 99—581(L)
—— (see Ghiorso, A.)—293(L)
Harvey, J. A., C. E. Porter, and D. J. Hughes. Variation of $\overline{\Gamma}_n^0/\overline{D}$ ratio with atomic weight—645(A)
—— (see Carter, R. S.)—645(A)
Hasegawa, Hirochi (see Enatsu, Hiroshi)—263
Haskin, D. M. (see Schein, Marcel)—855(L)
Haslam, R. N. H. (see Greenberg, L. H.)—1540
—— (see Katz, L.)—464
Hayden, R. J. (see Steinberg, E. P.)—867(L)
Haynes, Sherwood K. (see Burford, A. O.)—303(A)
—— (see Meneely, George R.)—308(A)
Hayward, Evans and E. G. Fuller. Nuclear elastic scattering of photons—1106(L)
Heald, Mark A. (see Beringer, R.)—1474
Hebb, Elizabeth (see Mitchell, Allan C. G.)—727
Heckrotte, Warren. Nuclear cross sections and size of nucleus—619(A); 1279
—— **and Joseph V. Lepore.** Polarization of nucleons elastically scattered from nuclei—1109(L)
Heinz, O. Range and specific ionization for high-energy protons in nuclear emulsions—610(A)
Hellens, R. L. (see Jennings, B.)—636(A)
Hemmendinger, Arthur (see Ennis, Malcolm E.)—772
Hendee, C. F. and S. Fine. Moseley's law applied to proportional counter resolution of adjacent elements—281(L)
Henkel, John H. Equation of state and thermal dependence of elastic coefficients of crystalline argon—617(A)
Henkel, R. L. (see Brolley, J. E., Jr.)—651(A)

Hennig, G. R. Thermal neutron capture cross section of C^{13}—92
——, **B. Smaller, and E. L. Yasaitis.** Paramagnetic resonance absorption in graphite—1088(L)
Henry, Warren E. Low-temperature magnetization of two Ce salts—603(A)
—— Strong field induced paramagnetic anomaly in $NiSiF_6 \cdot 6H_2O$—1449
Herber, R. H. (see Sugihara, T. T.)—298(A)
Hereford, Frank L. Annihilation of positrons in liquid He—1097(L)
—— (see McMaster, William H.)—723
Herlin, Melvin A. (see Chase, C. E.)—565(L)
Herman, Frank. Speculations on energy band structure of Ge-Si alloys—847(L)
——, **Joseph Callaway, and Forman S. Acton.** Comparison of various approximate exchange potentials—371
Herman, R. C., L. L. Mador, R. F. Wallis, and M. C. Williams. X-ray production of *F* centers in NaCl and LiF—598(A)
Herr, W., H. Hintenberger, and H. Voshage. Half-life of rhenium—1691(L)
—— (see Hintenberger, H.)—1690(L)
Herring, Conyers. Role of low-energy phonons in thermal conduction—954
Herwig, Lloyd O. and Glenn H. Miller. Relative ionization yields for fission fragments in various gases—413
Hesketh, R. V. and E. E. Schneider. Shape of *F* band—837(L)
—— **and E. E. Schneider.** Thermal restoration of color centers at low temperature—598(A)
Hess, Wilmot (see Burgus, Warren H.)—750
Heydenburg, N. P. and G. M. Temmer. Coulomb excitation of energy levels in Rh and Ag—861(L)
—— **and G. M. Temmer.** Coulomb excitation *vs* compound nucleus formation in the lighter elements—629(A)
Hibi, Tadatosi and Kazuo Ishikawa. Spectral dependence of thermionic emission with activation from (Ba–Sr)O cathodes over 0.6–3.5 ev region—1183
Hickam, W. M. Ionization probability curves near threshold for Zn, Cd, and Hg—703
Hidalgo, John U., Sr. Measurements of solvent volume changes in sugar factory using radioactive tracer technic—306(A)
Higgins, G. H. (see Ghiorso, A.)—293(L)
Hill, R. D., E. O. Salant, and M. Widgoff. τ meson produced by 3.0-Bev protons—1699(L)
Hillman, Peter, Vaughn Culler, and N. F. Ramsey. Polarization in high-energy *p-n-n* double scattering—462
Hinnov, Einar and Hedwig Kohn. Intensity measurements of resonance lines in flame source—301(A)
—— (see Kohn, Hedwig)—301(A)
Hintenberger, H., W. Herr, and H. Voshage. Radiogenic Os from Re-containing molybdenite—1690(L)
—— (see Herr, W.)—1691(L)
Hodson, A. L. (see Harris, D. R.)—661(A)
Hoffman, H. E. (see Howard, R. A.)—661(A)
Hofstadter, R., B. Hahn, A. W. Knudsen, and J. A. McIntyre. High-energy electron scattering and nuclear structure determinations. II—512
Holden, W. R. (see Atkinson, W. R.)—634(A)
Holm, D. M. (see Terrell, J.)—650(A)
Holm, Lennart W. (see Atterling, Hugo)—585(L)
Holmes, John R. and Leon Pape. Pressure shift in He λ5875—621(A)
Holmgren, H. D., J. M. Blair, B. E. Simmons, T. F. Stratton, and R. V. Stuart. Differential cross sections for $C^{13}(d,p)C^{14}$ and $C^{13}(d,t)C^{12}$—1544
Honig, A. and A. F. Kip. Electron spin resonance of impurity level in silicon—1686(L)
Hood, H. P. (see Sands, R. H.)—607(A)
Hopper, V. D. (see Parsons, R. W.)—193
Hopson, J. E. and C. E. Nielsen. Vapor expansion chamber using pure water. I—601(A)
—— (see Nielsen, C. E.)—601(A)
Horrocks, D. L. and A. F. Voigt. Half-life of Tl^{204}—1205
Horsley, R. J. (see Katz, L.)—464
Horton, G. K. and E. Phibbs. Effect of nuclear charge on internally produced pairs—604(A)
Hourd, R. F., J. R. Fleming, and J. J. Lord. Flux of primary heavy nuclei at equator—647(A)
Howard, R. A., P. M. Fitzpatrick, H. E. Hoffman, and J. S. Urban. Decay of heavy neutral particle—661(A)
Howland, P. R. and W. E. Kreger. γ-ray absorption coefficients for NaI, Cu, Ta, and W—407
Hoyle, Fred. Observational tests in cosmology—309(T)
Hrostowski, H. J., G. H. Wheatley, and W. F. Flood, Jr. Anomalous optical behavior in InSb and InAs—1683(L)
Hsieh, Yu-Chang and Ingram Bloch. Normal coordinates in nuclear photoeffect—305(A)
Huddleston, C. M. (see Eggler, C.)—600(A)
Hudis, J., E. Baker, and G. Friedlander. Production of Be^7 in high-energy reactions—612(A)
Hudson, R. P. and C. K. McLane. Magnetic and thermal properties of chromic methylamine alum below 1°K—932
—— (see Ambler, E.)—625(A); 1143
Huebner, W. F. (see Phelps, John)—441
Huggett, R. W. (see Thompson, R. W.)—661(A); 1576
Hughes, D. J. (see Harvey, J. A.)—645(A)
—— (see Levin, J. S.)—645(A)
—— (see Seidl, F. G. P.)—476
Hughes, Raymond H. Isotope shift in Li I spectrum—621(A)
Hughes, Vernon W. (see Marder, S.)—611(A)
—— (see Teutsch, Werner B.)—1461
—— (see Weinreich, Gabriel)—1451
Huizenga, J. R., J. E. Gindler, and R. B. Duffield. Relative photofission yields of several fissionable materials—1009
—— (see Friedman, A. M.)—1501
Hulburt, E. O. (see Bennett, W. H.)—315
Hulet, E. K., S. G. Thompson, and A. Ghiorso. Isotopes of curium, berkelium, and californium—1703(L)
Hull, M. H., Jr. (see Biedenharn, L. C.)—656(A)
Hungerford, E. T. and R. D. Birkhoff. Electron straggling in thin foils—6
Hunt, W. A., R. M. Kline, and D. J. Zaffarano. β endpoint energies and half-lives for some mirror transitions—611(A)
Hurley, J. P. and P. S. Jastram. γ ray studies of Re^{188}—627(A)
Hurst, G. S. (see Bortner, T. E.)—303(A); 609(A)
—— (see Cure, J. W.)—302(A)
Hurwitz, H., Jr. (see Zweifel, P. F.)—660(A)
Hutchinson, Franklin (see Phelps, John)—441
Hutchison, Clyde A., Jr., and W. Burton Lewis. Paramagnetic resonance absorption in sodium plutonyl acetate—1096(L)
Huus, Torben (see Day, Robert B.)—1003
Hyde, Earl K. (see Mathur, Hirdaya B.)—708

Iddings, G. M. (see Crane, W. W. T.)—1702(L)
Igo, G. and M. S. Wertheim. Isotope shift in x-ray spectra of heavy elements—1097(L)
Inghram, M. G. (see Steinberg, E. P.)—867(L)
—— (see Malm, R.)—641(A); 993
Inoki, M., T. Yasaki, and Y. Matsukawa. Mass measurements of slow cosmic-ray mesons—1565
Irvine, J. W., Jr. (see Bazorgan, G. A.)—781

Ise, J. (see Schecter, L.)—659(A)
Ishiguro, Masakazu, Fujio Oda, and Takuzo Fujino. Plastic flow and low-frequency dispersion in alkali halide crystal—1347(L)
Ishikawa, Kazuo (see Hibi, Tadatosi)—1183

Jaccarino, Vincent (see King, John Gordon)—1706(E)
Jache, Albert, Gilbert Blevins, and Walter Gordy. Mm wave spectrum of arsine—299(A)
—— (see Burrus, Charles A.)—299(A); 706
Jackson, J. David. Schematic calculation of (p,xn) cross sections of heavy elements—651(A)
Jackson, J. L. Equations of motion of coupled ordered and dissipative systems—642(A)
Jacobs, Donald H. and Milton E. Pugh. JAINCOMP-C and -D digital computers—616(A)
Jacobsohn, B. A. Nuclear rotational levels and μ-mesonic atom—654(A)
Jakobson, M. and J. H. Manley. Phase properties of deflected ion beam from fixed-frequency cyclotron—600(A)
Jan, J.-P. and J. S. Koehler. Small angle x-ray scattering from cold-worked Al-Ag and Al-Zn alloys—665(A)
Jancovici, B. G. Coulomb energy and nuclear radius—389; 619(A)
—— **and I. Talmi.** Tensor forces and β decay of C^{14} and O^{14}—289(L)
Jansen, L. and Z. I. Slawsky. Deviations from additivity of intermolecular field at high densities—614(A)
Jastram, P. S. (see Hurley, J. P.)—627(A)
Jaumot, F. E., Jr. (see Berkowitz, A. E.)—1185
Jen, C. K. (see Massey, J. T.)—622(A)
Jenkins, T. L., D. Luckey, T. R. Palfrey, and R. R. Wilson. Photoproduction of charged π mesons from hydrogen and deuterium—179
Jennings, B., J. B. Weddell, and R. L. Hellens. Inelastic scattering of 4.3-Mev neutrons by Fe^{56}—636(A)
Jensen, E. N. (see Pohm, A. V.)—1523
Jentschke, W. (see Robinson, W. H.)—1412
Johnson, C. H. and J. L. Fowler. Differential cross section for elastic scattering of neutrons from N—637(A)
—— (see Trail, Carroll C.)—640(A); 1363(L)
Johnson, Everett R. and Schuyler M. Christian. Properties of Ge-Si alloys—560(L)
Johnson, F. S., J. D. Purcell, and R. Tousey. Extension of extreme uv solar spectrum—621(A)
Johnson, Peter D. and Ferd E. Williams. Effect of pressure on optical absorption of activator in luminescent solid—598(A)
—— **and Ferd E. Williams.** Effect of pressure on optical absorption of activator system in KCl: Tl—69
Johnson, T. H. AEC research programs and policies—299(T)
Johnston, L. H., E. A. Day, and J. H. Williams. Proposed design of 50-Mev proton linear accelerator—599(A)
Jones, D. R. Production of neutrons by negative μ mesons by complex nuclei—624(A)
Jones, Ernest A. (see Akers, Lawrence K.)—300(A)
—— (see Lovell, R. J.)—300(A)
Jones, Harry. Electronic wave functions in metals in relation to nuclear magnetic resonance—606(T)
Jordan, W. C. (see Burson, S. B.)—613(A)
Josien, Marie-Louise. Application of infrared spectroscopy to study of molecular interactions in solutions—299(T)
—— (see Fuson, Nelson)—300(A)

Kaiser, H. F. Microtron maximum particle energy—667(A)
—— Microtrons (electron cyclotrons for X and K band operation)—600(A)
—— Recent progress in microtron research—632(T)
Kaiser, W. (see Fan, H. Y.)—1087(L)
Kalos, M. (see Tobocman, W.)—605(A)
Kammer, E. W. Effect of small strains on electrical resistance of U wire—307(A)
Kanda, Eizo (see Sugawara, Tadashi)—1355(L)
Kanda, Teinosuke (see Sugawara, Tadashi)—1355(L)
Kane, J. A., R. A. Stallwood, R. B. Sutton, T. H. Fields, and J. G. Fox. External proton beam of Carnegie synchrocyclotron—662(A)
——, **R. A. Stallwood, R. B. Sutton, T. H. Fields, and J. G. Fox.** Polarization in p-p scattering at 415 Mev—1694(L)
—— (see Fields, T. H.)—638(A)
Kao, S. K. and A. F. Clark. p-p scattering in nuclear emulsions—662(A)
Kaplon, M. F., J. Crussard, J. Klarmann, and J. Noon. Observations on unstable particles in photographic emulsion—660(A)
—— (see Crussard, J.)—584(L)
—— (see Koshiba, M.)—647(A)
—— (see Noon, J. H.)—647(A); 1103(L)
Karle, I. L. Electron-diffraction studies of internal motion in molecules—633(T)
Karp, Samuel N. (see Shmoys, Jerry)—656(A)
Karplus, Robert. Hall effect in ferromagnetics—297(T)
—— **and J. M. Luttinger.** Hall effect in ferromagnetics—1154
Karzmark, C. J. (see Kim, Y. B.)—661(A)
—— (see Thompson, R. W.)—661(A); 1576
Kasper, J. S. (see Wilson, V. C.)—1408
Kato, Susumu (see Shinoda, Gunji)—840(L)
Kato, W. Y. (see Seidl, F. G. P.)—476
Katz, L., R. N. H. Haslam, R. J. Horsley, A. G. W. Cameron, and R. Montalbetti. Fine structure in $C^{13}(\gamma,n)C^{12}$ and $O^{16}(\gamma,n)O^{15}$ activation curves—464
—— (see Goldemberg, J.)—471
Keller, J. M. and E. Koenigsberg. Electronic quadrupole-quadrupole interactions in Ce metal—665(A)
Kelly, W. H. (see Lu, D. C.)—121; 1533
Kennedy, J. M. and W. T. Sharp. γ radiation from reactions induced by polarized particles—440
Kent, D. C. (see Levinger, J. S.)—418
Kereiakes, J. G. and A. T. Krebs. Use of scintillation counters in studies on luminous efficiency of biological materials—308(A)
Kern, B. D. (see Givin, H. H.)—302(A); 641(A)
—— (see Lamarsh, J. R.)—307(A)
Kerner, Edward H. Periodic impurities in periodic lattice—687
Kerr, Robert J. (see Meneely, George R.)—308(A)
Keuffel, J. W. (see Mezzetti, L.)—858(L)
Kiehn, Robert M. and Clark Goodman. Neutron inelastic scattering—636(A); 989
Killion, Lawrence (see Guss, Donald)—627(A)
Kim, Y. B., J. R. Burwell, H. O. Cohn, C. J. Karzmark, and R. W. Thompson. Magnetic cloud-chamber observation of V particles. I. Charged V particles—661(A)
King, Allen L. Rheological problem—298(A)
King, D. T. and M. M. Block. Pairs formed by bremsstrahlung of great energy. I. Experimental—648(A)
—— (see Block, M. M.)—171; 648(A)
King, Jean I. F. Potential theory formulation of radiant heat transfer—298(A)
King, John Gordon and Vincent Jaccarino. Hfs and nuclear moments of stable Br isotopes—1706(E)
Kington, Joe D. (see Willard, Harvey B.)—1359(L)
Kip, A. F. (see Dresselhaus, G.)—568(L)
—— (see Feher, G.)—1343(L)
—— (see Honig, A.)—1686(L)
Kirkwood, Robert L. Gravitational field equations—1051

Kittel, C. Statistical mechanics and Overhauser nuclear polarization effect—589(L)
—— (see Dresselhaus, G.)—568(L)
Klaiber, G. Stanley (see Box, Harold C.)—1247
Klarmann, J. (see Crussard, J.)—584(L)
—— (see Kaplon, M. F.)—660(A)
Klein, Abraham. Dyson's new Tamm-Dancoff method—654(A)
—— New Tamm-Dancoff formalism—1676
—— Suppression of pair coupling in nuclear forces—1061
—— Suppression of pair effects in nuclear forces—667(A)
—— (see Bernstein, J.)—655(A)
Klein, Martin J. and Paul H. E. Meijer. Principle of minimum entropy production—642(A)
Kleinman, D. A. (see Ryder, E. J.)—1342(L)
Kline, R. M. (see Hunt, W. A.)—611(A)
Klontz, E. E. (see Fan, H. Y.)—1087(L)
Kluyver, J. C. (see Endt, P. M.)—580(L)
Knight, J. R. (see Hanson, H. P.)—621(A)
Knowles, C. Harry and R. T. Lagemann. Some thermodynamic constants of liquid HF—306(A)
Knudsen, A. W. (see Hofstadter, R..)—512
Knudsen, W. C. and J. R. Dillinger. Experimental evidence for structure in He II film—279(L)
Koehler, J. S. (see Jan, J.-P.)—665(A)
Koehler, W. C. and E. O. Wollan. Neutron magnetic diffraction studies of La, Ca manganites—653(A)
—— **and E. O. Wollan.** Search for antiferromagnetism in V_3Si, Cr_3Si, and Mo_3Si—280(L)
Koenigsberg, E. (see Keller, J. M.)—665(A)
Koerts, Leo. Ground state of Re^{185}—1358(L)
——, **A. Schwarzschild, R. Gold, and C. S. Wu.** β spectrum of K^{40}—612(A)
Koester, L. J., Jr. (see Goldwasser, E. L.)—1692(L)
Kohn, Hedwig and Einar Hinnov. Photoelectric measurement of reversal temperature—301(A)
—— (see Hinnov, Einar)—301(A)
Kojima, S., K. Tsukada, S. Ogawa, and A. Shimauchi. New absorption lines of crystals in submicrowave region—1705(E)
Kooi, Clarence. Hall effect in ferromagnetics—843(L)
Korff, Serge A. Effect of melting of polar ice on length of day—296(L)
Kortright, J. M. (see Yearian, H. J.)—653(A)
Koshiba, M. and M. F. Kaplon. Observations on high-energy soft cascade—647(A)
—— (see Crussard, J.)—624(A)
—— (see Walker, W. D.)—624(A); 852(L)
Koslov, S., V. Fitch, and J. Rainwater. Experimental study of μ^--meson mass and vacuum polarization in mesonic atoms—291(L)
——, **V. Fitch, and J. Rainwater.** Mass of μ^- meson from mesonic x-rays—625(A)
Koster, G. F. Theory of scattering in solids—1436
—— **and J. C. Slater.** Wave functions for impurity levels—1167
Krasnow, M. E. (see Lassettre, E. N.)—635(A)
Kraushaar, J. J., J. W. Mihelich, and A. W. Sunyar. Directional correlation of γ rays of A^{38}—456
Krebs, A. T. (see Kereiakes, J. G.)—308(A)
Kreger, W. E. (see Howland, P. R.)—407
Krohn, V. E. and S. Raboy. Decay scheme of Pb^{203m}—1354(L)
—— **and S. Raboy.** Magnetic moment of first-excited state of Pb^{204}—608(A)
—— (see Raboy, S.)—1689(L)
Krone, R. W. (see Baumann, N. P.)—650(A)
Kruse, U. E. and J. M. Teem. p-p cross section at 95 Mev—662(A)
—— (see J. M. Teem)—664(A)
Kunz, W. E., C. D. Moak, and W. M. Good. $Li^7(He^3,p)Be^9$ reaction—640(A)
—— (see Moak, C. D.)—641(A)
Kuper, J. B. H. (see Bernstein, W.)—609(A)
Kurbatov, J. D. (see Sakai, M.)—101

Lackner, Henry (see Trambarulo, Ralph)—622(A)
Lafferty, D. L., L. A. Rayburn, and T. M. Hahn. γ-ray spectrum from inelastic scattering of fast neutrons in Fe—637(A)
—— (see Rayburn, L. A.)—301(A); 637(A)
Lagemann, R. T. (see Knowles, C. Harry)—306(A)
Lamarsh, J. R. and B. D. Kern. Metastable magnetic states—307(A)
Landsberg, P. T. Statistical mechanics of temperature-dependent energy levels—643(A)
Lane, C. T. (see Dyba, R. V.)—1365
Langenheim, R. H. (see Yearian, H. J.)—653(A)
Laporte, Otto. Interaction of shock waves—658(T)
Lark-Horowitz, K. (see Fan, H. Y.)—1087(L)
Lassettre, E. N., A. S. Berman, S. Silverman, and M. E. Krasnow. Electron spectrometer for study of inelastic collision cross sections—635(A)
LaVier, E. C. (see Hanna, S. S.)—110
Lawson, J. R. and M. B. Towns. Molecular association in perfluoroalkyl carboxylic acids—300(A)
Lax, Benjamin, H. J. Zeiger, and R. N. Dexter. Anisotropy of cyclotron resonance in Ge. I. Theory—597(A)
—— (see Dexter, R. N.)—557(L); 597(A)
Lax, Melvin. Infrared absorption in semiconductors—309(T)
—— **and Joel L. Lebowitz.** Vibration spectra of crystal lattices—617(A)
Lazar, N. H. Decay of Sb^{124}—292(L)
—— **and P. R. Bell.** γ radiation from K^{40}—612(A)
Leavitt, C. P. (see Shapiro, A. M.)—663(A)
LeBlanc, J. M., J. M. Cork, and S. B. Burson. Decay of Pt^{189}—627(A)
—— (see Burson, S. B.)—613(A)
Lebowitz, Joel L. (see Frisch, Harry L.)—643(A)
—— (see Lax, Melvin)—617
Leder, Lewis B. and L. Marton. Characteristic energy loss of electrons—634(A)
—— **and L. Marton.** Effect of chemical combination on characteristic energy loss of electrons—1345(L)
Lee, T. D. Some special examples in renormalizable field theory—1329
Lehner, J. and G. M. Wing. Solution of transport equation for case of slab geometry—642(A)
Leifer, H. N. and W. C. Dunlap, Jr. Some properties of p-type GaSb between 15°K and 925°K—51
Leighton, R. B. (see van Lint, V. A. J.)—295(L)
—— (see York, Carl M., Jr.)—159
Leipuner, L. (see Stearns, M. B.)—625(A); 1353(L)
Leiss, J. E. and C. S. Robinson. Photoproduction of π^+ mesons from hydrogen—638(A)
—— (see Penfold, A. S.)—637(A)
—— (see Robinson, C. S.)—638(A)
Lemonick, Aaron and Francis M. Pipkin. Spins and hyperfine splittings of Ag^{111} and Cu^{64}—1356(L)
Lepore, Joseph V. (see Heckrotte, Warren)—1109(L)
Lesk, I. A. Survey of Ge and Si devices—309(T)
Levin, J. S. and D. J. Hughes. Measurements of neutron resonance parameters in U, Th, Hg, and Au—645(A)
—— (see Seidl, F. G. P.)—476
Levine, S. H., R. S. Bender, J. N. McGruer, and W. F. Vogelsang. Reaction particles from 14.5-Mev deuteron bombardment of Li^7 and Li^6—640(A)

Levinger, J. S. and D. C. Kent. Independent particle model and nuclear photoeffect—418
Levinson, C., K. Brueckner, and H. Mahmoud. Two-body forces and nuclear saturation. II. Results—655(A)
—— (see Brueckner, K.)—655(A)
Levinson, John. Generator of linearly varying current for electromagnet—651(A)
Levinthal, Cyrus. Molecular structure and biological control mechanism—606(T)
Levitas, A., C. C. Wang, and B. H. Alexander. Energy gap of Ge-Si alloys—846(L)
Lewis, H. W. (see Bernstein, E. M.)—83
—— (see Schawlow, A. L.)—1344(L)
Lewis, W. Burton (see Hutchison, Clyde A., Jr.)—1096(L)
Lewis, W. E. (see Pohm, A. V.)—1523
Libby, W. F. (see Suttle, A. D., Jr.)—866(L)
Likely, J. G. (see Ajzenberg, F.)—641(A)
Lindenbaum, S. J. and Luke C. L. Yuan. Production of positive and negative pions in Be by 1.0 and 2.3-Bev protons—638(A)
Lindqvist, Torsten and Allan C. G. Mitchell. Disintegration of K^{43}—444; 612(A)
—— **and Allan C. G. Mitchell.** Nuclear levels in Ca^{43}—1535
Lindsay, John C. and A. V. Masket. High-speed transient dynamic analysis—665(A)
Linsley, John. Čerenkov counter measurement of fast multiply charged cosmic rays—647(A)
Litherland, A. E. (see Bartholomew, G. A.)—649(A)
—— (see Gove, H. E.)—650(A)
Loeb, A. L. and J. B. Goodenough. Influence of covalence on ion ordering and distortion in spinels—616(A)
Loeb, L. B. Some fundamental processes of gaseous electronics—620(T)
Loeliger, H. R. and L. R. Sarles. Magnetic moment of Os^{189}—291(L)
Lokanathan, S., J. Steinberger, and H. B. Wolfe. High-energy electrons in the capture of μ^- mesons by complex nuclei—624(A)
Lord, J. J. (see Fleming, J. R.)—647(A)
—— (see Orear, Jay)—624(A)
Lorrain, Paul, R. Béique, P. Gilmore, P. E. Girard, A. Breton, and P. Piché. Pressurized 500-kv high-frequency Cockroft-Walton accelerator—599(A)
Love, W. F. (see Croft, G. T.)—1403
—— (see Passaglia, E.)—666(A)
Lovell, R. J. and E. A. Jones. Potential constants for carbonyl fluoride—300(A)
Low, F. E. (see Gell-Mann, M.)—1300
Lu, D. C., W. H. Kelly, and M. L. Wiedenbeck. Decay schemes of Cd^{114} and Te^{125}—121
——, **W. H. Kelly, and M. L. Wiedenbeck.** γ-ray spectra following β-decay of Br^{80}, Sb^{124}, and I^{131}—1533
Luckey, D. (see Jenkins, T. L.)—179
Luckey, G. W. Formation of photographic latent image in Ag halides—309(T)
Lutes, O. S. (see Maxwell, E.)—333
Luttinger, J. M. (see Brown, H. A.)—652(A)
—— (see Karplus, Robert)—1154
Lyon, W. S. and J. E. Strain. Decay of Rb^{86}—1500
Lyons, D. H. and A. M. Feingold. Level structure of Li^8—606(A)
Lyons, Harold. Recent determinations of velocity of light—633(T)

Macdonald, J. Ross and John E. Robinson. Ac Hall and magnetoresistive effects in photoconducting alkali halides—44
Mackin, R. J. (see Mills, W. R., Jr.)—1206
Macklin, R. L. and H. E. Banta. $Li^6(d,t)$ reaction—302(A)
Madey, Richard (see Bandtel, Kenneth C.)—639(A)
Mador, L. L. (see Herman, R. C.)—598(A)
Magnuson, D. W. Molar polarization, dipole moment, and nonideality of trichloroheptafluorobutane vapor—301(A)
Mahmoud, H. (see Brueckner, K.)—655(A)
—— (see Levinson, C.)—655(A)
Malenka, Bertram J. Polarization in high-energy elastic nucleon-nucleus scattering—522
—— Polarization in scattering by nuclei at high energies—620(A)
Malm, R. and D. R. Inglis. Conservation of isobaric spin in reaction $Be^9(p,\alpha)Li^6$—993
—— **and D. R. Inglis.** Magnetic analysis indicating charge symmetry in reaction $Be^9(p,\alpha)Li^6$—641(A)
Malmberg, P. R. (see Sun, K. H.)—600(A)
Mandeville, C. E. and H. O. Albrecht. Phosphorescence of and energy storage in some uv-emitting phosphors—598(A)
Manley, J. H. (see Jakobson, M.)—600(A)
Mann, D. E. and Earle K. Plyler. Vibrational spectrum of fluorotrichloroethylene—622(A)
Mann, Leonard A., Ray A. Grandey, and Arnold F. Clark. Cross sections for meson-induced stars in Ilford G5 nuclear emulsions—648(A)
Mapother, D. E. (see Garber, M.)—603(A)
—— (see Mould, R. E.)—604(A)
Marcus, Jules A. (see Plumb, Harmon H.)—602(A)
Marder, S., V. W. Hughes, and C. S. Wu. Effect of angular dependence of annihilation radiation of orthopositronium in magnetic field—611(A)
Marion, J. B. (see Cook, C. F.)—639(A)
Mark, Hans, Clyde McClelland, and Clark Goodman. Electric excitation of Mn^{55} with protons—628(A)
Marmier, P. (see Boehm, F.)—864(L)
Marquez, Luis. Disintegration of Rh^{102}—67
Marshall, J. F., R. A. Shatas, and M. A. Pomerantz. Target-thickness dependence of δ-ray emission produced by 1.3-Mev electrons—634(A)
—— (see Pomerantz, M. A.)—633(A)
Marshall, John. Polarization of high-energy protons—644(T)
——, **L. Marshall, D. Nagle, and W. Skolnik.** Scattering of 314-Mev polarized protons by deuterium—1020
—— (see Nagle, D.)—663(A)
Marshall, L. (see Marshall, J.)—1020
—— (see Nagle, D.)—663(A)
Martin, J. A. (see Green, F. L.)—304(A)
Martin, P. C. (see Fulton, Thomas)—811
—— (see Glauber, R. J.)—572(L)
Martin, Ronald L. Phase shift analysis of scattering of negative pions on H—1606
Marton, L. Survey of characteristic energy losses of electrons—620(T)
——, **Tommy F. McCraw, and J. Arol Simpson.** Electron scattering in solids at 20 kev—634(A)
—— (see Leder, Lewis B.)—634(A); 1345(L)
Maryott, A. A. (see Birnbaum, G.)—622(A)
Masket, A. V. Interior value problems—305(A)
—— (see Lindsay, John C.)—665(A)
Massey, J. T., C. I. Beard, and C. K. Jen. Microwave spectral series of deuterated hydrogen peroxide—622(A)
Masuda, Yoshika (see Sugawara, Tadashi)—1355(L)
Mathur, Hirdaya B. and Earl K. Hyde. Spectrometer studies of radiation of neutron-deficient isotopes of Cs and of $E3$ isomers, Xe^{127m} and Xe^{129m}—708
Matsukawa, Y. (see Inoki, M.)—1565
Matthias, B. T. Superconducting compounds—633(T)

——, **T. H. Geballe, S. Geller, and E. Corenzwit.** Superconductivity of Nb_3Sn—1435
—— (see Schawlow, A. L.)—1344(L)
Maxwell, E. and O. S. Lutes. Threshold field properties of some superconductors—333
Mayburg, Sumner. Precipitation of impurities at dislocations in heat-treated Si—838(L)
—— Vacancies and interstitials in heat-treated Ge—38
Mayo, E. E. Generalization of theorem by Pappus—305(A)
Mazari, M. (see Buechner, W. W.)—609(A)
McCarthy, John T. Mass differences for isobars capable of double-β decay—447
McClelland, Clyde (see Mark, Hans)—628(A)
McClure, J. W. Axial ratios in hexagonal metals—665(A)
McCollom, K. A. (see de Boisblanc, D. R.)—609(A)
McCormick, G. H. (see Cohen, B. L.)—639(A)
McCormick, Philip T. Theoretical energy and angular distributions of bremsstrahlung electrons—657(A)
McCraw, Tommy F. (see Marton, L.)—634(A)
McGruer, J. N. (see Levine, S. H.)—640(A)
McGuire, A. D., M. Camac, M. L. Halbert, and J. B. Platt. X-rays from π mesonic atoms—625(A)
McIntyre, J. A. (see Hofstadter, R.)—512
McKeown, Michael (see Muehlhause, C. O.)—598(A)
—— (see Scharff-Goldhaber, Gertrude)—613(A)
McLane, C. K. (see Hudson, R. P.)—932
McMaster, William H. and Frank L. Hereford. Angular distribution of photoelectrons produced by 0.4–0.8 Mev polarized photons—723
McReynolds, A. W. and T. Riste. Magnetic neutron diffraction from Fe_3O_4—1161
McSkimin, H. J., A. J. Williams, and R. M. Bozorth. Elastic constants of Co and of CoZn ferrite crystals—616(A)
Meiboom, S. (see Abeles, B.)—31
Meijer, Paul H. E. Calculation of wavefunctions in symmetrical crystalline field—1443
—— (see Klein, Martin J.)—642(A)
Meissner, K. W. (see Deverall, G. V.)—1463
Melander, Lars (see Atterling, Hugo)—585(L)
Melton, Charles E. Measurements of ionization produced by 5-Mev α particles in argon mixtures—303(A)
Melvin, M. Avramy. Law of impact for generally shaped bodies—615(A)
Meneely, George R., Robert J. Kerr, Jesse E. Hoffman, and Sherwood K. Haynes. Rotating-sphere solid-angle scanner for γ rays—308(A)
Meneghetti, David and S. S. Sidhu. Neutron diffraction study of Cu-Mn system—666(A)
Mercer, C. F. (see Williams, Jack H.)—306(A)
Merritt, F. R. (see Fletcher, R. C.)—844(L)
Merritt, J. and D. Hamlin. Yield of π^+ mesons by 335-Mev protons as function of atomic number—638(A)
Merz, Walter J. Domain formation and domain wall motions in ferroelectric $BaTiO_3$ single crystals—690
Metropolis, N. (see de Hoffmann, F.)—1586
—— (see Fermi, E.)—1581
Metzger, F. R. and W. B. Todd. Nuclear resonance fluorescence in Hg^{198} and lifetime of 411-kev excited state of Hg^{198}—853(L)
—— **and W. B. Todd.** Resonance fluorescence with nuclei: Tl^{205}—627(A)
—— (see Swann, C. P.)—636(A)
Meyerott, R. E. Approximate Hartree type wave functions and matrix elements for K and L shells of atoms and ions—12
Mezzetti, L. and J. W. Keuffel. Decay curve of K particles—858(L)
Michel, M. C. (see Passell, T. O.)—999
Mihelich, J. W. Disintegration of Ta^{182}—626(A)
——, **A. W. Schardt, and E. Segrè.** Energy levels in Po^{210}—1508
—— (see Kraushaar, J. J.)—456
—— (see Sunyar, A. W.)—570(L)
Millburn, G. P., W. Birnbaum, W. E. Crandall, and L. Schecter. Nuclear radii and transparencies from inelastic cross-section measurements. I. Method—620(A)
——, **W. Birnbaum, W. E. Crandall, and L. Schecter.** Nuclear radii from inelastic cross-section measurements—1268
—— (see Birnbaum, W.)—649(A)
—— (see Crandall, W. E.)—620(A)
—— (see Schecter, L.)—659(A)
Miller, D. W., V. K. Rasmussen, and M. B. Sampson. Energy levels of C^{13} by inelastic α scattering—649(A)
Miller, Glenn H. (see Herwig, Lloyd O.)—413
Miller, J. M. (see Belmont, E.)—1554
—— (see Sugarman, Nathan)—1704(L)
Miller, R. C. High-energy, large-angle distribution of pair electrons produced by bremsstrahlung—796
Miller, W. C. (see Bhattacherjee, S. K.)—404
—— (see Noyes, J. C.)—396
Mills, F. E. (see Goldwasser, E. L.)—1692(L)
Mills, R. (see Yang, C. N.)—631(A)
Mills, W. R., Jr., and R. J. Mackin, Jr. Observations on 4.43-Mev γ-rays from C^{12}—1206
Milton, J. C. D. and J. S. Fraser. α-γ angular correlation in decay of Ra^{224}, Ra^{226}, and Pu^{239}—628(A)
Mingins, Charles R. (see Sampson, John L.)—617(A)
Miskel, J. A. and M. L. Perlman. Double vacancies in K shell associated with K-electron capture in A^{37}—612(A)
Mitchell, Allan C. G. and Elizabeth Hebb. Disintegration of Ba^{140}—727
—— (see Lindqvist, Torsten)—444, 612(A); 1535
Mitra, A. N. Modified nucleon propagators—1697(L)
Mitsui, Toshio and Jiro Furuichi. Kinetic properties of domains in Rochelle salt—558(L)
Mize, J. P., J. W. Starner, and M. E. Bunker. Radiations of Ir^{192m}—627(A)
—— (see Bunker, M. E.)—612(A)
Moak, C. D., W. M. Good, and W. E. Kunz. Be^9+He^4 reactions—641(A)
—— (see Kunz, W. E.)—640(A)
Montalbetti, R. (see Katz, L.)—464
Morin, F. J. (see Geballe, T. H.)—1085(L)
Morrison, P. Solar-connected variations of cosmic rays—646(A)
Moser, Paul (see Trambarulo, Ralph)—622(A)
Moses, H. E. Canonical transformation for electron-positron field coupled to time-independent electromagnetic field. II—237
Moszkowski, Steven A. Energy levels in spheroidal well—604(A)
—— (see Finkelstein, R. J.)—1695(L)
Mould, R. E. and D. E. Mapother. Superconductivity of precipitation hardening Al alloy—604(A)
Moyer, Burton J. (see Bandtel, Kenneth C.)—639(A)
—— (see Cohen, David)—664(A)
—— (see Wilcox, J. M.)—664(A)
Moyer, James W. (see Ruth, Ralph P.)—562(L)
Muckenthaler, F. (see Neiler, J. H.)—640(A)
Muehlhause, C. O., E. der Mateosian, and Michael McKeown. Effects of preparation and temperature on response of NaI phosphors—598(A)
Murray, R. B. Specific heat of $MnCl_2$ at temperatures of liquid He—307(A)
Muschlitz, E. E., Jr. Scattering of H^- ions in range 20–400 ev—635(A)

Myers, H., A. Odian, P. C. Stein, and A. Wattenberg. Neutrons in coincidence with high-energy photoprotons—576(L)

Nagle, D., J. Marshall, L. Marshall, and W. Skolnik. Polarization of 310-Mev protons by deuterium—663(A)
—— (see Marshall, J.)—1020
Nathans, R. (see Ferguson, G. A.)—659(A); 776
—— (see Halpern, J.)—1529
Neaves, A. and D. ter Haar. Thermal conductivity of semiconductors—596(A)
Neiler, J. H., F. Muckenthaler, and James Schenck. Fast neutron scintillation spectra of $Li^6(n,\alpha)H^3$ reaction in LiI(Eu)—640(A)
Nelkin, M. S. and H. A. Bethe. Meson production in meson-proton scattering—618(A)
Nelson, E. B., E. H. Geer, and R. R. Carlson. Scintillation counter study of γ rays from proton capture in Na—650(A)
—— (see Carlson, R. R.)—641(A)
Neufeld, Jacob. Bohr's theory of energy losses of moving charged particles—1128
Newkirk, J. B. Growth of CdI_2 crystals—616(A)
Newman, E. (see Cohen, B. L.)—639(A)
Newson, H. W. and J. H. Gibbons. Resonance near $Li^7(p,n)$ threshold—640(A)
—— (see Gibbons, J. H.)—644(A)
—— (see Rohrer, R. H.)—302(A)
Newson, Henry. Shell effects in highly excited nuclei—299(T)
Neynaber, R. H. (see Beeman, W. W.)—617(A)
Nickell, William E. Yield and angular distribution of protons from $Li^6(d,p)Li^7$—426
Nicklas, J. P. Isotope shift in neutral C—1469
Nielsen, Alvin H. Infrared spectrum of σ_3 for $B^{10}F_3$ and $B^{11}F_3$—300(A)
Nielsen, C. E. and J. E. Hopson. Vapor expansion chamber using pure gases at low temperatures. III—601(A)
—— (see Caren, R. P.)—601(A)
—— (see Hopson, J. E.)—601(A)
Nielsen, K. O. (see Elbek, B.)—96
Nielsen, O. B. (see Elbek, B.)—96
Nier, A. O. (see Collins, T. L.)—615(A)
Nix, F. C. (see Berkowitz, A. E.)—1185
—— (see Croft, G. T.)—1403
—— (see Donahoe, F. J.)—1395
Noon, J. H. and M. F. Kaplon. Fragmentation of heavy primary nuclei into light elements—647(A)
——, **M. F. Kaplon, and J. Crussard.** Anomalous event observed in photographic emulsion—1103(L)
—— (see Crussard, J.)—584(L)
—— (see Kaplon, M. F.)—660(A)
Noyes, H. P. Pion-nucleon S phase shifts at low energy—619(A)
Noyes, J. C., J. E. Van Hoomissen, W. C. Miller, and B. Waldman. Photodisintegration thresholds of D_2O and Be—396
Nyborg, Wesley L. Self-maintained oscillations in fluid flow—297(T)

Oda, Fujio (see Ishiguro, Masakazu)—1347(L)
Odian, A. (see Myers, H.)—576(L)
Ogawa, S. (see Kojima, S.)—1705(E)
O'Kelley, G. D. (see Olsen, J. L.)—1539
Olds, J. D. (see Codrington, R. S.)—607(A)
Olsen, J. L. and G. D. O'Kelley. Decay of Cs^{136}—1539
O'Neill, Gerard K. Time-of-flight measurements of inelastic neutron scattering—635(A)
—— Time-of-flight measurements on inelastic scattering of 14.8-Mev neutrons—1235
Opitz, W. (see Hartzler, A. J.)—591(L)
Orear, Jay, C. H. Tsao, J. J. Lord, and A. B. Weaver. Scattering of 145-Mev π^+ by H in emulsion—624(A)
Orgel, S. (see Dropkin, J. J.)—597(A)
Osborne, L. S., Y. Goldschmidt-Clermont, and G. Parker. Photoproduction of π^+ mesons near threshold—637(A)
Otter, F. A. (see Domenicali, C. A.)—1134
Overton, W. C., Jr., and J. R. Clement. Correlation techniques for testing Born-von Kármán theory of specific heats—602(A)
—— (see Gaffney, John)—602(A)
Owen, Henry R. (see Schaeffer, Oliver A.)—615(A)

Pac, Pong Yul (see Enatsu, Hiroshi)—263
Packard, M. E. Chemical applications of nuclear magnetic resonance—596(T)
Palevsky, H. and R. M. Eisberg. Magnetic scattering of cold neutrons by gaseous oxygen—659(A)
—— (see Eisberg, R. M.)—659(A)
—— (see Seidl, F. G. P.)—476
Palfrey, T. R. (see Jenkins, T. J.)—179
Palma, M. B., M. U. Palma, and D. Palumbo. Paramagnetic resonance absorption of $VOSO_4 \cdot 5H_2O$—608(A)
Palma, M. U. (see Palma, M. B.)—608(A)
Palmer, R. R. (see Bollinger, L. M.)—645(A)
Palumbo, D. (see Palma, M. B.)—608(A)
Pape, Leon (see Holmes, John R.)—621(A)
Park, David. Ferrimagnetic resonance in sintered masses—652(A)
Parker, G. (see Osborne, L. S.)—637(A)
Parker, Vincent E. (see Snyder, Conway W.)—635(A)
Parratt, L. G. Solid surface studies by total reflection of x-rays—617(A)
—— Surface studies of solids by total reflection of x-rays—359
Parsons, R. W., Françoise A. Brisbout, and V. D. Hopper. Meson showers and high-energy interactions in light and heavy nuclei—193
Passaglia, E. and W. F. Love. Resistivity of ordered and disordered Cu-Au alloys at low temperatures—666(A)
Passell, T. O., M. C. Michel, and I. Bergström. Decay of odd-odd isomer Tl^{198m}—999
Patronis, E. T., Jr. (see Braden, C. H.)—627(A); 758
Patterson, Reid. (p,n) reactions on As, Y, Nb, and Rh—303(A)
Paul, E. B. (see Bartholomew, G. A.)—649(A)
—— (see Gove, H. E.)—650(A)
Pearson, G. L. (see Fletcher, R. C.)—844(L)
Peaslee, D. C. Coulomb energies of light nuclei—717
—— Pion production ratios. II—1580
—— Supermultiplet evidence from isotopic spin spacing—605(A)
—— (see Drachman, R. J.)—605(A)
Pecjak, F. A. (see Sun, K. H.)—600(A)
Peck, R. A., Jr. Rf Cockroft-Walton generator for neutron production—599(A)
Pellam, J. R. (see Broida, H. P.)—845(L)
—— (see Hanson, W. B.)—321; 604(A)
Penfold, A. S. and J. E. Leiss. Determination of photo cross sections from bremsstrahlung activation curves—637(A)
—— (see Spicer, B. M.)—629(A)
Pepper, R. R. (see Fan, H. Y.)—1087(L)
Percus, Jerome K. and George J. Yevick. Domain of action of collective coordinates in new approach to many-body problem—642(A)
—— (see Yevick, George J.)—642(A)
Perkins, J. F. (see Burford, A. O.)—303(A)
Perlman, M. L. and Joan P. Welker. Disintegration of I^{126}—133; 613(A)

—— (see Miskel, J. A.)—612(A)
Perry, Robert W. (see Sampson, John L.)—298(A)
Peter, Martin and M. W. P. Strandberg. Microwave spectrum of OCS—622(A)
Pettengill, G. (see Chamberlain, O.)—1348(L)
Pfann, W. G. and W. Van Roosbroeck. Radioactive and photoelectric p-n junction power sources—597(A)
Phelps, John, W. F. Huebner, and Franklin Hutchinson. Stopping power of organic foils for 6-Mev alphas—441
Phibbs, E. (see Horton, G. K.)—604(A)
Piché, P. (see Lorrain, Paul)—599(A)
Pilcher, V. E., R. S. Carter, and A. Stolovy. Neutron resonances in Ho, Tm, and Lu—645(A)
Pines, David. Electron interaction in solids—620(T)
—— Paramagnetic and diamagnetic susceptibility of conduction electrons—1090(L)
Pipkin, Francis M. (see Lemonick, Aaron)—1356(L)
Platt, J. B. (see McGuire, A. D.)—625(A)
Pleasonton, Frances (see Snell, Arthur H.)—304(A)
Plumb, Harmon H. and Jules A. Marcus. Thermal conductivity of Ga single crystals at low temperatures—602(A)
Plyler, Earle K. (see Mann, D. E.)—622(A)
Pobereskin, M. (see Aarons, M. W.)—1345(L)
Pohm, A. V., W. E. Lewis, J. H. Talboy, Jr., and E. N. Jensen. β spectra of Pr^{142}, Tm^{170}, and Rb^{86}—1523
Pomerantz, Martin A. Cosmic radiation at very high altitudes near geomagnetic equator—531
—— Primary α particles near geomagnetic equator—1691(L)
——, **J. F. Marshall, and R. A. Shatas.** Forward-backward ratio of secondary emission produced by 1.3-Mev electrons—633(A)
—— (see Marshall, J. F.)—634(A)
Porter, C. E. (see Harvey, J. A.)—645(A)
Porter, F. T. (see Guss, Donald)—627(A)
Posener, D. W. and M. W. P. Strandberg. Centrifugal distortion in asymmetric top molecules. III. H_2O, D_2O, and HDO—374
Pound, R. V. (see Bloembergen, N.)—8
Pratt, William W. Energy and angular distribution of protons from deuteron bombardment of Ni—1517
Pressman, D. (see Hall, T.)—1208
Preston, W. M. (see Stelson, P. H.)—974
Price, P. J. Electronic thermal conduction in semiconductors—596(A)
Primak, William. The metamict state—837(L)
—— **and L. Fuchs.** Electrical conductivities of natural graphite crystals—22
Pringle, R. W., W. Turchinetz, and H. W. Taylor. Further study of decay scheme of Ir^{192}—115
Prosser, F. W. (see Baumann, N. P.)—650(A)
Pruett, C. H. and R. G. Wilkinson. Disintegration of Ce^{140}—625(A)
Pryce, M. H. L. (see Alburger, D. E.)—1482
Pugh, G. E., D. H. Frisch, and R. Gomez. Nuclear scattering of γ rays below meson threshold—590(L)
——, **D. H. Frisch, and R. Gomez.** Scattering of x-rays by nuclei—611(A)
Pugh, Milton E. (see Jacobs, Donald H.)—616(A)
Pulvari, C. F. Propagation of displacement in solid, having crystalline structure with bistable states—617(A)
Purcell, J. D. (see Johnson, F. S.)—621(A)
Pyle, R. V. (see Birnbaum, W.)—649(A)

Quimby, S. L. Temperature variation of mean Debye temperature of Cu_3Au, 20°C to 450°C—916

Raboy, S. and V. E. Krohn. Gyromagnetic ratio of 10^{-9}-second Ta^{181m}—1689(L)
—— (see Krohn, V.)—608(A); 1354(L)
Rainwater, James (see Cooper, Leon N.)—1107(L)
—— (see Koslov, S.)—291(L); 625(A)
Ramsey, N. F. Molecular-beam studies of molecules—596(T)
—— (see Hillman, Peter)—462
Rankin, Bayard. Simplifying approximation for determining cascade shower distributions—657(A)
Rao, K. Narahari. Near uv absorption spectrum of 1,2,4-trifluorobenzene—299(A)
Rasmussen, V. K. (see Miller, D. W.)—649(A)
Ravenhall, D. G. (see Yennie, D. R.)—500
Rayburn, L. A., D. L. Lafferty, and T. M. Hahn. γ rays produced by inelastic scattering of d-D neutrons in Cu, Al, and Mg—637(A)
——, **D. L. Lafferty, and T. M. Hahn.** Inelastic scattering of d-D neutrons by Fe and Cu—301(A)
—— (see Lafferty, D. L.)—637(A)
Rayne, John. Specific heats of metals below one degree absolute—1428
Recksiedler, Arthur and Bernard Hamermesh. Capture γ-ray studies using scintillation coincidence spectrometer—650(A)
Reder, Fritz H. and Sanborn C. Brown. Energy distribution function of electrons in pure He—885
Rediker, Robert H. Ionization chamber measurements at 10,600 feet of absorption of N component in carbon and hydrocarbon—526
Redlich, Martin G. Interactions between some two-nucleon configurations—448
—— **and Eugene P. Wigner.** β-decay matrix element for deformed core model—122
Reier, Melvin and Morris H. Shamos. Neutron-capture γ-ray spectra—636(A)
Reiffel, L. and G. M. Burgwald. Low-energy events—1294
Reynolds, H. L., D. W. Scott, and A. Zucker. Range and charge of energetic nitrogen ions in Ni—671
—— **and A. Zucker.** Equilibrium charge distribution of stripped 26-Mev N ions—1353(L)
—— **and A. Zucker.** Excitation function for reaction $Be^9(N^{14})F^{18}He^6$—302(A)
Reynolds, J. B. and K. G. Standing. Angular distribution of deuterons from (p,d) reactions in light nuclei—639(A)
Ribe, F. L. and J. D. Seagrave. Pickup reactions $B^{10}(n,d)Be^9$ for 14-Mev neutrons—649(A)
Richards, J. D. (see Brentano, J. C. M.)—841(L)
Richter, Harold G. and Charles D. Coryell. Low-energy photofission yields for U^{235}—1550
Rickey, M. E. (see Eisberg, R. M.)—659(A)
Ringo, G. R. and S. Wexler. Standards for thermal neutron capture measurements—660(A)
Riste, T. (see McReynolds, A. W.)—1161
Roat, W. F. (see Autler, S. H.)—599(A)
Roberts, A., J. Tinlot, and E. M. Hafner. Polarization in n-p scattering at 100–200 Mev—1099(L)
——, **J. Tinlot, and E. M. Hafner.** Polarization of 170-Mev neutrons—663(A)
—— (see Tinlot, J.)—137
Roberts, James H. (see Weddell, James B.)—117
Roberts, L. D., S. Bernstein, J. W. T. Dabbs, and C. P. Stanford. Capture of polarized neutrons by polarized Sm^{149} nuclei—105
—— **and J. W. T. Dabbs.** Approximate partition function for certain iron group salts at low temperatures—307(A)
—— (see Dabbs, J. W. T.)—307(A); 970
Robinson, C. S. and J. E. Leiss. Photoproduction of π^+ mesons from H near threshold—638(A)
—— (see Leiss, J. E.)—638(A)
Robinson, H. P. (see Harvey, B. G.)—581(L)
Robinson, John E. (see Macdonald, J. Ross)—44

Robinson, W. H. and W. Jentschke. Response of anthracene scintillation crystals to mono-energetic soft x-rays—1412
Rogers, F. T., Jr. General relations in fluid convection theory. I. Similarity theory for flow onset—305(A)
Rogers, T. F. Microwave and far infrared atmospheric water-vapor absorption—622(A)
Rogosa, G. L. (see Schwarz, G.)—950
Rohrer, R. H., W. H. Cargill, and A. F. Dratz. Applications of NaI γ-ray spectrometer to blood volume determinations—308(A)
——, **H. W. Newson, J. H. Gibbons, and P. Cap.** Activation of Al and Se^{80} by p-neutron capture in kev region—302(A)
Rohrlich, F. Pair production and bremsstrahlung in field of electron—657(A)
Rose, D. C. (see Geiger, K. W.)—646(A)
Rosenblum, E. S. (see Dexter, R. N.)—597(A)
Rosenfeld, Arthur H. Pion production by 440-Mev protons incident upon H and C—638(A)
—— (see Warshaw, S. D.)—649(A)
Rosenstock, Herbert B. Counting lattice frequencies—617(A)
Rosenthal, Jenny E. New technique for solving three-dimensional electron optics potential problems with axial symmetry—633(A)
Ross, A. W. and D. ter Haar. Volume changes in substitutional alloys—665(A)
Ross, I. M. (see Ryder, E. J.)—1342(L)
Ross, Marc H. Meson-meson effects in meson-nucleon scattering—619(A)
—— Meson-meson interaction in meson scattering—1687(L)
—— (see Dyson, F. J.)—1644
Rossi, B. (see Bridge, H. S.)—662(A); 1101(L)
—— (see DeStaebler, H. C., Jr.)—662(A)
Rothstein, Jerome. Can well-informed heat engine (WHE) have free will?—643(A)
—— Possible macroscopic effects of single lattice defects—370
Roys, P. A., K. Shure, and J. J. Taylor. Penetration of 6-Mev γ rays in water—911
—— (see Shure, K.)—610(A)
Ruark, Arthur E. Electrodynamic equations symmetrical in respect to charges and poles; with remarks on monopoles—305(A)
—— Properties of hypothetical atoms composed of magnetic poles—632(A)
Rubin, L. G. (see Davis, L., Jr.)—597(A)
Rubin, Robert J. Excluded-volume problem—642(T)
—— Quantum-mechanical molecular distribution functions in one-dimensional fluid composed of hard spheres—643(A)
Rumsey, V. H. Reaction concept in electromagnetic theory—1705(E)
Rushworth, F. A. Nuclear magnetic resonance in some solid hydrocarbons—608(A)
Russell, Leonard N., Warren E. Taylor, and John N. Cooper. γ radiation from Mg^{26} under proton bombardment—99
Russell, Paul N. Nonmetallic ferromagnetic materials—309(T)
Ruth, Ralph P. and James W. Moyer. Power efficiency for photovoltaic effect in Ge-grown junction—562(L)
Ryder, E. J., I. M. Ross, and D. A. Kleinman. Electron multiplication in Ge at low temperature—1342(L)

Sachs, R. G. Structure of nucleon. II. Pion-nucleon scattering—1065
Sagane, Ryokichi. Positrons from decay of μ mesons—660(T)
——, **Walter F. Dudziak, and James Vedder.** Positron spectrum from decay of μ meson—863(L)
Sakai, M., J. L. Dick, W. S. Anderson, and J. D. Kurbatov. Decay scheme of Co^{58}—101
Salant, E. O. (see Hill, R. D.)—1699(L)
Salpeter, E. E. (see Dyson, F. J.)—1644
Salzman, Freda F. and James N. Snyder. Numerical calculation of 3/2−3/2 pion-nucleon reaction matrix and phase shifts—286(L)
Salzman, G. and A. H. Taub. Born-type rigid motion in relativity—1659
Sampson, John L., Edward E. Altshuler, and Charles R. Mingins. Granular structure of $BaTiO_3$ ceramic—617(A)
——, **Edward E. Altshuler, and Robert W. Perry.** Replication of $BaTiO_3$ ceramic surfaces for electron microscopy—298(A)
Sampson, M. B. (see Miller, D. W.)—649(A)
Sands, Matthew, J. G. Teasdale, and Robert L. Walker. Negative-to-positive ratio of photomesons from deuterium—592(L)
Sands, R. H., J. Townsend, and H. P. Hood. Paramagnetic resonances in glasses—607(A)
Saraf, Babulal. Inner bremsstrahlung in A^{37} and Ge^{71}—612(A)
—— Inner bremsstrahlung in electron capture process—Ge^{71}—97
Sarles, L. R. (see Loeliger, H. R.)—291(L)
Sawamoto, K. (see Yamaka, E.)—848(L)
Sawyer, R. B. (see Clifford, Joseph M.)—665(A)
Saxon, David S. (see Woods, Roger D.)—577(L)
Schaeffer, Oliver A. and Henry R. Owen. Electron impact studies of isotopic O_2 and CO_2 molecules—615(A)
Schardt, A. W. (see Mihelich, J. W.)—1508
Scharff, Morris F. Moments of Na^{23}—1114(L)
—— Regularity in magnetic moments of odd nuclei—1112(L)
Scharff-Goldhaber, Gertrude and Michael McKeown. New isomers in Br and Cl—613(A)
Schawlow, A. L., B. T. Matthias, H. W. Lewis, and G. E. Devlin. Structure of intermediate state in superconductors—1344(L)
Schecter, L., W. E. Crandall, G. P. Millburn, and J. Ise. Cross section for producing high-energy neutrons from C targets bombarded by protons, deuterons, and He^4 particles—659(A)
—— (see Crandall, W. E.)—620(A)
—— (see Millburn, G. P.)—620(A); 1268
Schein, Marcel, D. M. Haskin, and R. G. Glasser. Narrow shower of pure photons at 100 000 feet—855(L)
Schenck, James (see Neiler, J. H.)—640(A)
Scherrer, V. E., B. A. Allison, and W. R. Faust. γ radiation from interaction of 3.1-Mev neutrons—637(A)
—— (see Shapiro, P.)—751
Schild, A. (see Dettman, J. W.)—631(A); 1057
Schluter, Robert A. Neutral pion-deuteron production in high-energy n-p collisions—639(A)
—— (see Wright, S. C.)—639(A)
Schmitt, Roman A. and Nathan Sugarman. U photofission yields—1260
Schneider, E. E. (see Cunnell, F. A.)—598(A)
—— (see Hesketh, R. V.)—598(A); 837(L)
Schumacher, R. T., T. R. Carver, and C. P. Slichter. Measurement of spin paramagnetism of conduction electrons—1089(L)
Schwarz, G. and G. L. Rogosa. Transmission of x-rays through calcite in Laue diffraction—950
Schwarzschild, A. (see Koerts, L.)—612(A)
Schweber, S. S. (see Dyson, F. J.)—1644
Schweitzer, W. G., Jr. (see Zahn, C. T.)—633(A)
Scolman, T. T. (see Collins, T. L.)—615(A)
Scott, D. W. (see Reynolds, H. L.)—671

Scott, F. R., D. B. Thomson, and W. Wright. Thermal neutron capture cross sections of hydrogen, B, and Ag—582(L)
Seaborg, G. T. (see Ghiorso, A.)—293(L)
Seagrave, J. D. (see Ribe, F. L.)—649(A)
Seeger, R. J. AEC research policies of National Science Foundation—299(T)
—— Role of physics in engineering education—309(T)
Segall, Benjamin. Nuclear shapes at half-filled shells—605(A)
Segrè, Emilio (see Chamberlain, Owen)—850(L); 1348(L); 1104(L); 1105(L)
—— (see Mihelich, J. W.)—1508
Seidl, F. G. P., D. J. Hughes, H. Palevsky, J. S. Levin, W. Y. Kato, and N. G. Sjöstrand. "Fast chopper" time-of-flight measurement of neutron resonances—476
Seliger, H. H. Transmission of monoenergetic positrons and electrons—610(A)
Selove, W. Pickup deuterons produced from 95-Mev protons—663(A)
Senitzky, I. R. Harmonic oscillator wave functions—1115
—— Quantum effects in interaction between electrons and high-frequency fields. I—904
Shaforth, S. M. and S. S. Hanna. Decay scheme and γ-γ correlations in B^{10}—86
—— **and S. S. Hanna.** γ-γ correlation in $Be^9(d,n)B^{10*}(\gamma)B^{10}$—641(A)
Shamos, Morris H. (see Fafarman, A.)—648(A)
—— (see Reier, Melvin)—636(A)
Shapiro, A. M., C. P. Leavitt, and F. F. Chen. Total p-p cross section above 400 Mev—663(A)
Shapiro, I. I. and J. M. Teem. Interpretation of scattering of high-energy nucleons by complex nuclei—619(A)
Shapiro, Maurice M. Recent results from study of cosmic rays with nuclear emulsions—299(T)
Shapiro, P., V. E. Scherrer, B. A. Allison, and W. R. Faust. n-γ coincidences produced by inelastic scattering of neutrons—751
Sharp, W. T. (see Kennedy, J. M.)—440
Sharpe, L. M. (see Hall, T.)—1208
Shatas, R. A. (see Marshall, J. F.)—634(A)
—— (see Pomerantz, M. A.)—633(A)
Shaw, C. H. (see Soules, Jack)—621(A)
Shaw, Harlan (see Cohen, David)—664(A)
Shelton, Essie M. (see Fuson, Nelson)—300(A)
Sheridan, Walter F. Rf mass spectrometer as rocket-borne instrument for atmospheric composition studies—298(A)
——, **J. A. Dillon, Jr., and S. N. Ghosh.** Experimental determination of charge transfer cross sections—635(A)
Shibuya, Motoichi. Magnetoresistance effect in cubic semiconductors with spheroidal energy surfaces—1385
Shimauchi, A. (see Kojima, S.)—1705(E)
Shinoda, Gunji, Tatsuro Suzuki, and Susumu Kato. Two types of band emission curves of Cu in soft x-ray region—840(L)
Shmoys, Jerry and Samuel N. Karp. Calculation of potential from transit time—656(A)
Shuler, W. E. (see Fletcher, William H.)—300(A)
Shull, Theodore (see Burgus, Warren H.)—750
Shure, K., P. A. Roys, and J. J. Taylor. Penetration of 6-Mev γ rays in Pb and Fe—610(A)
—— (see Roys, P. A.)—911
Shutt, R. P. (see Fowler, W. B.)—1026
Sidhu, S. S. (see Meneghetti, David)—666(A)
Siegel, M. (see Hall, T.)—1208
Siegel, R. T. (see Hartzler, A. J.)—185; 591(L)
Silver, E. G. and R. W. Waniek. Interactions of high-energy neutrons in Mo—586(L)
Silverman, A. (see Edwards, D. A.)—629(A)
Silverman, S. (see Lassettre, E. N.)—635(A)
Silvey, G. (see Hardy, W. A.)—385
Simmons, B. E. (see Holmgren, H. D.)—1544
Simmons, J. W. (see Slayton, George R.)—299(A)
Simon, Albert. High-speed computation of angular momentum functions—657(A)
Simpson, Arol (see Marton, L.)—634(A)
Simpson, J. A. (see Firor, J. W.)—1015
Simpson, O. D. Measurement of time jitter in BF_3 counters—600(A)
Singer, S. F. Storm decrease of cosmic radiation at pole—647(A)
Sippel, R. F. (see Bent, R. D.)—649(A)
Sjöstrand, N. G. (see Seidl, F. G. P.)—476
Skolnik, W. (see Marshall, J.)—1020
—— (see Nagle, D.)—663(A)
Sladek, Ronald J. Thermal conductivity of In-Tl alloys at liquid He temperatures—603(A)
Slater, J. C. (see Koster, G. F.)—1167
Slater, M. (see Blackstock, A. W.)—303(A)
Slawsky, Z. I. (see Dawson, J. M.)—614(A)
—— (see Jansen, L.)—614(A)
Slayton, George R., J. W. Simmons, and J. H. Goldstein. Microwave spectrum and dipole moment of vinylene carbonate—299(A)
Slichter, C. P. (see Schumacher, R. T.)—1089(L)
Smaller, B. (see Hennig, G. R.)—1088(L)
Smith, Alan W. Low-temperature thermal conductivity of Canadian natural graphite—1095(L)
—— (see Brown, H. N.)—626(A)
Smith, J. F. Electrostatic energy calculations for (Na_2WO_3)—1369
Smith, J. H. Nuclear scattering of high-energy electrons—271
—— (see Barton, M. Q.)—573(L)
—— (see Yamagata, T.)—574(L)
Smith, J. R. Scattering of 14.1-Mev neutrons in He, H, and N—730
Smith, Lyle. Research with Cosmotron—299(T)
Snelgrove, Philip, Jassim El-Hussaini, and Jesse W. M. DuMond. Corrected values of W K-series x-ray wavelengths with 2-meter curved crystal diffraction spectrometer—1203
Snell, Arthur H. and Frances Pleasonton. Magnetic spectrometer for recoil spectrometry—304(A)
Snyder, Conway W. and Vincent E. Parker. System for measuring flight times of fast neutrons—635(A)
Snyder, James N. (see Salzman, Freda F.)—286(L)
Solbrig, A. W., Jr. Effects of certain 3-body nuclear interactions in H^3 and He^3—831
Solt, I. H., Jr., and M. W. P. Strandberg. Conduction electron spin resonance absorption in Na—607(A)
Soules, Jack and C. H. Shaw. X-ray absorption in solid argon—621(A)
Spear, Vincent. New technique for visualizing thyroid outline using I^{131} and scintillation counter—308(A)
Spencer, L. V. Calculations on penetration of high-energy electrons—610(A)
Spicer, B. M., A. S. Penfold, and J. Goldemberg. Fine structure of $O^{16}(\gamma,n)O^{15}$ activation curve—629(A)
Spohr, D. A. and R. T. Webber. Electrical and thermal conductivity of Mg and Mg alloy at low temperatures—602(A)
Spry, W. J. Total cross section for charge exchange scattering of π^- mesons by H at 42, 30, and 20 Mev—1295
Squire, Charles F. Velocity of sound in superconducting Sn—1126
Stahl, R. H. n-p scattering at 91 Mev—664(A)
Stallwood, R. A. (see Fields, T. H.)—638(A)
—— (see Kane, J. A.)—662(A); 1694(L)
Standing, K. G. (see Reynolds, J. B.)—639(A)

Stanford, C. P., T. E. Stephenson, and S. Bernstein. Demonstration of neutron spin from Bloch-Alvarez-type experiment—302(A)
—— (see Roberts, L. D.)—105
Starner, J. W. (see Bunker, M. E.)—612(A)
—— (see Mize, J. P.)—627(A)
Stearns, M., M. B. Stearns, S. DeBenedetti, and L. Leipuner. Limits on π^--meson mass from mesonic x-rays —1353(L)
—— (see Stearns, M. B.)—625(A)
Stearns, M. B., M. Stearns, L. Leipuner, and S. DeBenedetti. Energy measurements of meson x-rays—625(A)
—— (see Stearns, M.)—1353(L)
Steele, M. C. (see Babiskin, J.)—602(A)
—— (see Berlincourt, Ted G.)—603(A); 1421
Steenberg, N. R. Reorientation of aligned nuclei—605(A); 982
Steffen, Rolf M. Mixed $E1+M2$ γ transition in Nd^{144}—614(A)
Stehle, P. (see Gibson, G.)—657(A)
Stein, Irving. Completed quantum theory—632(A)
Stein, P. C. (see Myers, H.)—576(L)
Steinberg, E. P. and L. E. Glendenin. Radiochemical investigation of spontaneous fission of Cm^{242}—431
——, **L. E. Glendenin, M. G. Inghram, and R. J. Hayden.** Fine structure in U^{233} fission—867(L)
Steinberger, Jack and William Chinowsky. Charge exchange scattering of stopped π^- mesons in deuterium—623(A)
—— (see Chinowsky, William—623(A); 1561
—— (see Lokanathan, S.)—624(A)
Stelson, P. H. and E. C. Campbell. Cross section for excitation of Pb^{207m} by inelastic neutron scattering—301(A)
—— **and W. M. Preston.** Resonant states of Mg^{24} excited by protons on Na—974
Stephens, William E. (see Toms, M. Elaine)—629(A); 1209
Stephenson, T. E. (see Stanford, C. P.)—302(A)
Stern, A. W. Invariance and isotopic spin—632(A)
Stern, Martin O. (see Blaser, J.)—624(A)
—— (see Chamberlain, Owen)—1705(E)
Sternglass, E. J. Energy expenditure per ion pair in solids —609(A)
Sternheimer, R. M. Effect of atomic core on nuclear quadrupole coupling—736
—— Electronic polarizabilities of ions from Hartree-Fock wave functions—655(A)
—— Polarization of nucleons elastically scattered from nuclei —587(L)
Stevenson, M. L. (see Burgus, Warren H.)—750
—— (see Crawford, F. S., Jr.)—1112(L)
Stier, P. M., C. F. Barnett, and G. E. Evans. Electron capture and loss cross sections for protons—303(A)
—— (see Barnett, C. F.)—307(A)
Stix, Thomas H. Primary heavy nuclei—782
St. John, Robert M. and J. G. Winans. Motion of arc cathode spot in a magnetic field—634(A)
Stolovy, A. (see Pilcher, V. E.)—645(A)
Stone, W. G. and Lewis W. Cochran. Energy per ion pair for recoil atoms in methane—304(A)
Storrs, C. L. and D. H. Frisch. Scattering of 1.32-Mev neutrons by protons—1252
Strain, J. E. (see Lyon, W. S.)—1500
Straley, Joseph W. Intensity of infrared absorption bands in methylene chloride—300(A)
Strandberg, M. W. P. and M. Tinkham. Effects of deviation of O_2 from Hund (b)—623(A)
—— (see Davis, Charles F., Jr.)—607(A)
—— (see Peter, Martin)—622(A)
—— (see Posener, D. W.)—374
—— (see Solt, I. H., Jr.)—607(A)
—— (see Tinkham, M.)—622(A)
Stratton, T. F. (see Holmgren, H. D.)—1544
Straub, W. D. (see Davis, L., Jr.)—597(A)
Strauch, K. and W. F. Titus. Scattering of 96-Mev protons from light nuclei—854(L)
Straumanis, M. E. Remark concerning absolute value of Avogadro's number—566(L)
Stuart, R. V. (see Holmgren, H. D.)—1544
Studier, M. H. (see Friedman, A. M.)—1501
Sucher, J. and H. M. Foley. Relativistic and magnetic spin interactions in He-like atoms—966
Sugarman, Nathan, Robert B. Duffield, G. Friedlander, and J. M. Miller. Disintegration of bismuth by 2.2-Bev protons—1704(L)
—— (see Schmitt, Roman A.)—1260
Sugawara, Tadashi, Yoshika Masuda, Teinosuke Kanda, and Eizo Kanda. Nuclear magnetic resonance in solid hydrogen with various *ortho* concentrations—1355(L)
Sugihara, T. T. and I. Halpern. Energy dependence of some photonuclear reactions—630(A)
——, **R. H. Herber, W. E. Bennett, and C. D. Coryell.** Absence of K capture in decay scheme of Pb^{205}—298(A)
Sun, K. H., P. R. Malmberg, and F. A. Pecjak. Scintillation detector for thermal and epithermal neutrons—600(A)
Sundaresan, M. K. (see Dyson, F. J.)—1644
Sunyar, A. W. Lifetime measurements of fast $E2$ transitions in even-even nuclei—626(A)
——, **J. W. Mihelich, and M. Goldhaber.** Decay of Cs^{134m} (3.1 hr)—570(L)
—— (see Kraushaar, J. J.)—456
Suttle, A. D., Jr., and W. F. Libby. Natural radioactivity of Re—866(L)
Sutton, R. B. (see Fields, T. H.)—638(A)
—— (see Kane, J. A.)—662(A); 1694(L)
Suzuki, Tatsuro (see Shinoda, Gunji)—840(L)
Swann, C. P. and F. R. Metzger. Inelastic scattering of neutrons by Ba^{137} and Hg^{199}—636(A)
Swann, W. F. G. Acquirement of cosmic-ray energies by betatron action—646(A)
Swanson, R. A. (see Warshaw, S. D.)—649(A)
Swenson, C. A. (see Berman, R.)—311
Swetnick, Martin Jay. Cosmic-ray neutrons in water at altitude of 10 600 feet—793
Swihart, J. C. and F. J. Belinfante. Quantized linear theory of gravitation. II—630(A)
—— (see Belinfante, F. J.)—630(A)

Takeda, Gyo. Application of intermediate coupling theory to scattering of pseudoscalar mesons by a nucleon—1078
Talboy, J. H., Jr. (see Pohm, A. V.)—1523
Talley, Robert M. and Dorothy P. Enright. Photovoltaic effect in InAs—1092(L)
Talmi, I. and B. C. Carlson. Pairing effects in Coulomb energies of mirror nuclei—606(A)
—— (see Jancovici, B.)—289(L)
Tamor, S. Polarization effects in high-energy proton-deuteron scattering—620(A)
Taub, A. H. (see Salzman, G.)—1659
Tauc, J. Theory of thermoelectric power in semiconductors —1394
Taylor, H. W. (see Pringle, R. W.)—115
Taylor, J. C. Tamm-Dancoff method—1313
Taylor, J. G. V. (see Greenberg, L. H.)—1540
Taylor, J. J. (see Roys, P. A.)—911
—— (see Shure, K.)—610(A)
Taylor, T. I. (see Eisberg, R. M.)—659(A)
Taylor, Warren E. (see Russell, Leonard N.)—99
Taylor, William J. Lattice distortion and x-ray diffraction intensities in dilute solid solutions—666(A)

Teasdale, J. G. (see Sands, Matthew)—592(L)
Teem, J. M. and U. E. Kruse. Elastic proton-deuteron scattering at 95 Mev—664(A)
—— (Kruse, U. E.)—662(A)
—— (see Shapiro, I. I.)—619(A)
Teller, Edward. Classical field theory of nuclei—632(T)
Temmer, G. M. Coulomb excitation of nuclear energy levels by α particles—628(T)
—— (see Ambler, E.)—625(A)
—— (see Heydenburg, N. P.)—629(A); 861(L)
ter Haar, D. Atomic theory of λ transition in liquid He—633(T)
—— Atomic theory of liquid He—604(A)
—— λ transition of liquid He—895
—— (see Dempsey, E.)—651(A)
—— (see Green, C. D.)—643(A)
—— (see Neaves, A.)—596(A)
—— (see Ross, A. W.)—665(A)
Terrell, J. and D. M. Holm. Excitation function for $Fe^{56}(n,p)Mn^{56}$—650(A)
Teutsch, Werner B. and Vernon W. Hughes. Hfs of He^3 in metastable triplet state—1461
Thacher, H. C., Jr., and Paul B. Dorain. Dielectric constant of dioctyl phthalate smoke—615(A)
Thirring, W. E. Classical limit of pseudoscalar coupling—653(A)
—— (see Gell-Mann, M.)—1612
—— (see Goldberger, M. L.)—654(A)
Thomas, H. C. (see Graves, Ernest D.)—304(A)
Thomas, W. J. Orville (see Cox, John)—299(A)
Thompson, R. W., J. R. Burwell, H. O. Cohn, R. W. Huggett, and C. J. Karzmark. Magnetic cloud chamber observations of V-particles. II. Status of work on θ^0 meson—661(A)
——, **J. R. Burwell, R. W. Huggett, and C. J. Karzmark.** Evidence for double production of V^0 particles—1576
—— (see Kim, Y. B.)—661(A)
Thompson, S. G. (see Ghiorso, A.)—293(L)
—— (see Harvey, B. G.)—581(L)
—— (see Hulet, E. K.)—1703(L)
Thomson, D. B. (see Scott, F. R.)—582(L)
Thorndike, A. M. (see Fowler, W. B.)—1026
Ting, Yu and Dudley Williams. Intensities of Zeeman components of quadrupole transitions in $NaClO_3$—607(A)
Tinkham, M. and M. W. P. Strandberg. Selection rules in the microwave magnetic resonance spectrum of O_2—622(A)
—— (see Strandberg, M. W. P.)—623(A)
Tinlot, John. Polarization in neutron-proton collisions—644(T)
—— **and A. Roberts.** Angular distribution of charge-exchange scattering of 40-Mev π^- mesons by hydrogen—137
—— (see Roberts, A.)—663(A); 1099(L)
Tittman, Jay. Neutron moderation in SiO_2—660(A)
Titus, W. F. (see Strauch, K.)—854(L)
Tobias, Cornelius. Radiation and dynamics of cell division—606(T)
Tobocman, W. and M. Kalos. Numerical calculation of stripping angular distribution—605(A)
Todd, W. B. (see Metzger, F. R.)—627(A); 853(L)
Tomboulian, D. H. and P. L. Hartman. Spectral distribution curves of far uv radiation from Cornell synchrotron—600(A)
—— (see Bedo, D. E.)—621(A)
Toms, M. Elaine, H. Gerardo, and W. E. Stephens. Photoprotons from Co—629(A)
—— **and William E. Stephens.** Photoprotons from Co—1209
Torrey, H. C. (see Codrington, R. S.)—607(A)
Tousey, R. (see Johnson, F. S.)—621(A)
Townes, C. H. Recent applications of microwave spectroscopy to study of molecules—596(T)
—— (see Gordon, J. P.)—282(L)
Towns, M. B. (see Lawson, J. R.)—300(A)
Townsend, J. (see Sands, R. H.)—607(A)
Trail, Carroll C. and C. H. Johnson. Energy levels in Be^9 from $Li^7(d,n)Be^9$—1363(L)
—— **and C. H. Johnson.** Proton recoil telescope for observing neutron spectra—640(A)
Trainor, L. E. H. Phenomenological many-body exchange forces—801
Trambarulo, Ralph, Henry Lackner, Paul Moser, and Harold Feeny. Pressure broadening of cyanogen bromide in microwave region—622(A)
Trammell, G. T. Electron scattering from nuclei—619(A)
Treanor, Charles E. Isotope shift in neutral O—1472
Treiman, S. B. Radiative decay of θ^0 particle—1360(L)
—— **and M. Blume.** Galactic rf radiation and cosmic-ray electrons—646(A)
—— (see Firor, J. W.)—1015
Trilling, G. H. (see van Lint, V. A. J.)—295(L)
Tripp, Robert (see Chamberlain, Owen)—850(L); 1104(L); 1105(L)
Tsao, C. H. (see Orear, Jay)—624(A)
Tsukada, K. (see Kojima, S.)—1705(E)
Turchinetz, W. (see Pringle, R. W.)—115
Turkevich, Anthony (see Fung, Si-Chang)—176
Turner, C. M. Ionization loading of electrostatic generators—599(A)

Underwood, Newton and G. F. Zindler, Jr. Small current dc amplifier—304(A)
Urban, J. S. (see Howard, R. A.)—661(A)
Urquhart, H. M. A. and J. E. Goldman. Magnetostrictive effects in α-Fe_2O_3—653(A)

Van Allen, J. A. (see Ellis, R. A., Jr.)—304(A)
van der Kint, L. (see Beljers, H. G.)—1683(L)
van der Leun, C. (see Endt, P. M.)—580(L)
Van Hoomissen, J. E. (see Noyes, J. C.)—396
Van Hove, Léon. Correlations in space and time and Born approximation scattering in systems of interacting particles—249
—— Time-dependent correlations between spins and neutron scattering in ferromagnetic crystals—1374
van Lint, V. A. J., G. H. Trilling, R. B. Leighton, and C. D. Anderson. Q value of A^6 decay—295(L)
Van Roosbroeck, W. (see Pfann, W. G.)—597(A)
van Wieringen, J. S. (see Beljers, H. G.)—1683(L)
Varma, Jagdish. Radiations from Cd^{113} (43-days)—613(A)
Vasileff, H. D. Thermal ionization of impurities in polar crystals—618(A)
Vedder, James (see Sagane, Ryokichi)—863(L)
Visscher, W. M. (see Dyson, F. J.)—1644
Vogelsang, W. F. (see Levine, S. H.)—640(A)
Vogt, Erich and Gregory H. Wannier. Scattering of ions by polarization forces—1190
Voigt, A. F. (see Horrocks, D. L.)—1205
Voshage, H. (see Hintenberger, H.)—1691(L)
Voyvodic, L. Charged heavy mesons from nuclear collisions—661(A)

Wacker, Paul F. SCF treatment of unclosed shells, operators containing spin, and radial correlation—656(A)
Wada, W. Internal pair production in radiative absorption of π^- mesons by H atoms—618(A)
Waddell, Charles (see Cohen, David)—664(A)
Wahl, John S. Energy distribution of fragments from fission of U^{235}, U^{238}, and Pu^{239} by fast neutrons—126

Waldman, B. (see Bhattacherjee, S. K.)—404
—— (see Noyes, J. C.)—396
Walker, Robert L. (see Sands, Matthew)—592(L)
Walker, W. D., J. Crussard, and M. Koshiba. π^--p collisions at 1.5 Bev. I—624(A)
——, **J. Crussard, and M. Koshiba.** π-meson production in π-nucleon collisions at 1.5 Bev—852(L)
—— (see Crussard, J.)—624(A)
Wallis, R. F. (see Herman, R. C.)—598(A)
Walters, G. K. (see Fairbank, William M.)—566(L)
Wang, C. C. (see Levitas, A.)—846(L)
Wangsness, Roald K. Susceptibility tensor and Faraday effect in ferrimagnetics—339
Waniek, R. W. and Vaughn Culler. Total cross sections for high-energy neutrons—659(A)
—— (see Culler, Vaughn)—585(L)
—— (see Silver, E. G.)—586(L)
Wannier, Gregory H. (see Vogt, Erich)—1190
Warshaw, S. D., R. A. Swanson, and A. H. Rosenfeld. Cross sections for reactions $C^{12}(p,pn)(n,2n)C^{11}$—649(A)
Watanabe, Hiroshi. Energy losses of electrons passing through MgO foil—1684(L)
Watanabe, Satosi. Superselection rule regarding spinor particle numbers—631(A)
Watson, Kenneth M. Some general relations between photoproduction and scattering of π mesons—228
Watson, W. W. (see Collinson, J. A.)—621(A)
Wattenberg, A. (see Myers, H.)—576(L)
Waymouth, John F. and Francis Bitter. Experiments on electroluminescence—941
Weaver, A. B. (see Orear, Jay)—624(A)
Webber, R. T. (see Spohr, D. A.)—602(A)
Weber, J. Quantum theory of damped electrical oscillator and noise. II. Radiation resistance—1706(E)
Weddell, James B. and James H. Roberts. Angular distribution of $Li^6(n,\alpha)H^3$—117
—— (see Jennings, B.)—636(A)
Wegner, Harvey E. (see Farwell, George W.)—664(A); 1212
Weinreich, Gabriel and Vernon W. Hughes. Hfs of He^3 in metastable triplet state—1451
Weinstock, E. V. and J. Halpern. Systematics of photoproton yields—630(A)
Weiss, J. (see Bernstein, W.)—609(A)
Welker, Joan P. (see Perlman, Morris L.)—133; 613(A)
Welton, T. A. Formulation of quantum electrodynamics in Minkowski space—632(A)
—— Theory of nuclear reactions with radioactive product—302(A)
Wertheim, M. S. (see Igo, G.)—1097(L)
Westendorp, W. F. (see Baldwin, G. C.)—600(A)
Wexler, S. (see Goodman, L. S.)—570(L)
—— (see Ringo, G. R.)—660(A)
Whalin, E. A., Jr. Photodisintegration of deuterium by 165-Mev x-rays—1362(L)
Wheatley, G. H. (see Hrostowski, H. J.)—1683(L)
White, M. G. (see Yntema, J. L.)—1226
Whittemore, W. L. (see Fowler, W. B.)—1026
Whyte, G. N. (see Garrett, C.)—889
Wick, G. C. Properties of Bethe-Salpeter wave functions—653(A)
Widgoff, M. (see Hill, R. D.)—1699(L)
Wiedenbeck, M. L. (see Beard, George)—1246
—— (see Lu, D. C.)—121; 1533
Wiegand, Clyde. High-energy experiments on polarization of protons—644(T)
—— (see Chamberlain, Owen)—850(L); 1348(L); 1104(L); 1105(L)
Wigner, Eugene P. (see Redlich, Martin G.)—122
Wilcox, J. M. and B. J. Moyer. Nuclear internal momentum distributions—664(A)
Wilkinson, R. G. (see Pruett, C. H.)—625(A)
Wilks, J. (see Fairbank, Henry A.)—277(L)
Willard, D. Momentum of S-particle secondaries—661(A)
—— (see Bridge, H. S.)—662(A)
Willard, Harvey B. Elastic scattering angular distributions and polarization of fast neutrons—299(T)
——, **Joe K. Bair, and Joe D. Kington.** Polarization of fast neutrons from nuclear reactions—1359(L)
Willardson, R. K., T. C. Harman, and A. C. Beer. Application of three-carrier model to Hall effect in Ge—597(A)
—— (see Harman, T. C.)—596(A); 699
Williams, A. J. (see McSkimin, H. J.)—616(A)
Williams, Dudley (see Brown, L. Carlton)—1110(L)
—— (see Ting, Yu)—607(A)
Williams, Ferd E. (see Johnson, Peter D.)—69; 598(A)
Williams, Jack H. and C. F. Mercer. Seismology in southeast—306(A)
—— (see Johnston, L. H.)—599(A)
Williams, M. C. (see Herman, R. C.)—598(A)
Williams, Robert W. Nuclear size and cross sections at cosmic-ray energies—647(A)
Williamson, R. M. (see Goldburg, W. I.)—628(A); 767
Wilson, R. N. (see Yennie, D. R.)—500
Wilson, R. R. (see Jenkins, T. L.)—179
Wilson, V. C. and J. S. Kasper. Neutron diffraction studies of NiZn ferrite—1408
Winans, J. C. (see St. John, Robert M.)—634(A)
Wing, G. M. (see Lehner, J.)—642(A)
Winhold, E. J. (see Burkhardt, J. L.)—629(A)
Winnemore, B. J., H. Gursky, D. A. Cowan, and C. D. Curtis. Further study of Po-Be neutron spectrum—301(A)
Winsberg, Lester. Interaction of negative muons with iodine—205
—— Interaction of negative pions with iodine—198
Witmer, Enos E. Formula for nuclear masses in terms of electron mass involving only rational numbers for light nuclei—610(A)
—— Nuclear masses as rational multiples of electron mass—667(A)
Wolfe, B. (see Edwards, D. A.)—629(A)
Wolfe, H. B. (see Lokanathan, S.)—624(A)
Wolfenstein, Lincoln. Theoretical considerations about polarization experiments—644(T)
Wolff, P. A. Theory of electron multiplication in Si and Ge—1415
—— Theory of secondary electron cascade in metals—56
Wollan, E. O. (see Koehler, W. C.)—280(L); 653(A)
Wong, Calvin. β decay of F^{17} and C^{11}—765
—— β decay of F^{20}—761
Wood, R. E. Eu activation studies with monochromatic neutrons—453
—— Resonance scattering of Ag and Au—644(A)
Woods, Roger D. and David S. Saxon. Diffuse surface optical model for nucleon-nuclei scattering—577(L)
Wright, S. C. and R. A. Schluter. Negative pion production in n-p collisions—639(A)
Wright, W. (see Scott, F. R.)—582(L)
Wu, C. S. (see der Mateosian, E.)—458
—— (see Koerts, L.)—612(A)
—— (see Marder, S.)—611(A)
Wyly, L. D. (see Braden, C. H.)—627(A); 758

Yager, W. A. (see Fletcher, R. C.)—844(L)
Yagoda, Herman. Ratio of π^-/π^+ meson production in cosmic-ray disintegrations of emulsion nuclei—648(A)
Yamagata, T., M. Q. Barton, A. O. Hanson, and J. H. Smith. Photodisintegration of deuterium by 265-Mev bremsstrahlung—574(L)

Yamaguchi, Yoriko and Yoshio Yamaguchi. Factorable neutron-proton interaction—654(A)
—— (see Yamaguchi, Yoshio)—1635
Yamaguchi, Yoshio. 2-nucleon problem when potential is nonlocal but separable. I—1628
—— **and Yoriko Yamaguchi.** 2-nucleon problem when potential is nonlocal but separable. II—1635
—— (see Yamaguchi, Yoriko)—654(A)
Yamaka, E. and K. Sawamoto. Electrical conductivity of MgO single crystals—848(L)
Yang, C. N. and R. Mills. Isotopic spin conservation and generalized gauge invariance—631(A)
Yasaitis, E. L. (see Hennig, G. R.)—1088(L)
Yasaki, T. (see Inoki, M.)—1565
Yearian, H. J., J. M. Kortright, and R. H. Langenheim. Lattice parameters of $FeFe_{(2-x)}Cr_xO_4$ spinel system—653(A)
Yeater, M. L. (see Albert, R. D.)—644(A)
Yennie, D. R., D. G. Ravenhall, and R. N. Wilson. Phase shift calculation of high-energy electron scattering—500
Yergin, Paul F. (see Ferguson, G. A.)—659(A); 776
—— (see Geller, K.)—659(A)
—— (see Halpern, J.)—1529
Yevick, George J. and Jerome K. Percus. Dynamical behavior of collective coordinates in new approach to many-body problem—642(A)
—— (see Percus, Jerome K.)—642(A)
Yntema, J. L. and M. G. White. Scattering of protons by H near 18 Mev—1226
Yokota, Ryosuke. Color centers in alkali silicate and borate glasses—1145
York, Carl M., Jr., R. B. Leighton, and E. K. Bjørnerud. Cloud-chamber study of charged V particles—159
York, H. F. (see Burgus, Warren H.)—750
Young, D. R. (see Drougard, M. E.)—1152
Ypsilantis, Thomas (see Chamberlain, Owen)—850(L); 1104(L); 1105(L)
Yuan, Luke C. L. (see Lindenbaum, S. J.)—638(A)

Zaffarano, D. J. (see Hunt, W. A.)—611(A)
Zahn, C. T. and Schweitzer, W. G., Jr. Excitation and separation of pure high-order modes in large high-Q cavities—633(A)
Zeiger, H. J. (see Dexter, R. N.)—557(L); 597(A)
—— (see Gordon, J. P.)—282(L)
—— (see Lax, Benjamin)—597(A)
Zemach, A. C. and R. J. Glauber. Spin correlations in neutron scattering by gases—605(A)
Zendle, B. (see Boag, J.)—608(A)
Zimmerman, Robert L., David H. Frisch, and Daniel I. Cooper. p-p scattering near interference minimum—662(A)
Zindler, G. F., Jr. (see Underwood, Newton)—304(A)
Zirkle, R. E. Effects of irradiating small fractions of individual dividing cells—606(T)
Zissis, G. J. (see Deverall, G. V.)—1463
Zucker, A. (see Reynolds, H. L.)—302(A); 671; 1353(L)
Zweifel, Paul F. Second-order corrections to β spectra—112
—— **and H. Hurwitz, Jr.** Slowing-down of neutrons in hydrogenous moderators—660(A)

THE PHYSICAL REVIEW

A journal of experimental and theoretical physics established by E. L. Nichols in 1893

VOLUME 96

Second Series

OCTOBER 1–DECEMBER 15, 1954

Published for the

AMERICAN PHYSICAL SOCIETY

by the

AMERICAN INSTITUTE OF PHYSICS

Incorporated

THE PHYSICAL REVIEW

A journal of experimental and theoretical physics established by E. L. Nichols in 1893

Published by the American Institute of Physics for the

AMERICAN PHYSICAL SOCIETY

Officers

President

H. A. BETHE
Cornell University
Ithaca, New York

Vice-President

R. T. BIRGE
University of California,
Berkeley, California

Secretary

K. K. DARROW
Bell Telephone Laboratories
Office:
Columbia University
New York 27, New York

Treasurer

G. B. PEGRAM
Columbia University
New York 27, New York

Local Secretary for the Pacific Coast

J. KAPLAN
University of California at Los Angeles
Los Angeles, California

Managing Editor

S. A. GOUDSMIT
Brookhaven National Laboratory
Upton, Long Island
New York

BOARD OF EDITORS

Editor

S. A. GOUDSMIT

Assistant Editor

S. PASTERNACK

Associate Editors

1952–1954	*1953–1955*	*1954–1956*
W. P. ALLIS	W. A. FOWLER	P. G. BERGMANN
F. G. BRICKWEDDE	KENNETH GREISEN	GREGORY BREIT
W. B. FRETTER	CHARLES KITTEL	F. J. DYSON
CONYERS HERRING	R. E. MARSHAK	P. KUSCH
H. W. LEVERENZ	W. K. H. PANOFSKY	R. SMOLUCHOWSKI
ARNOLD NORDSIECK	V. F. WEISSKOPF	J. C. STREET

Manuscripts for publication should be submitted to S. A. GOUDSMIT, Brookhaven National Laboratory, Upton, Long Island, New York. The authors' institutions are requested to pay a publication charge of $15 per page which, if honored, entitles them to 100 free reprints. Instructions will be sent with galley proofs.

Proof and all correspondence concerning papers in the process of publication should be addressed to the Publication Manager, American Institute of Physics, 57 East 55 Street, New York 22, New York.

Subscription Price

United States and Canada $30.00
Elsewhere $32.00

Back Numbers [1]

Yearly back number rate when complete year is available:
Prior to 1949: **$25.00**
Thereafter: **$33.00**
Single copies: **$3.00** each, prior to July, 1929;
$1.50 each, July, 1929–December, 1941;
$3.00 each, January, 1942–December, 1946;
$1.50 each, thereafter.
General index, 1893–1920: **$4.00.**
1921–1950: Paper binding, **$10** (Members); **$14** (Nonmembers)
Cloth binding, **$12** (Members); **$16** (Nonmembers)

Subscriptions, renewals, and orders for back numbers should be addressed to the American Institute of Physics, 57 East 55 Street, New York 22, New York.

Changes of address in the case of members of the American Physical Society should be addressed to the Treasurer; in the case of other subscribers to the American Institute of Physics.

[1] For Series 1 inquire of Physics Department, Cornell University, Ithaca, New York.

The Physical Review is published semi-monthly at Prince and Lemon Streets, Lancaster, Pennsylvania.

Entered as second-class matter March 6, 1947, at the Post Office at Lancaster, Pennsylvania, under the Act of March 3, 1879.

Acceptance for mailing at special rate of postage provided for in paragraph (d-2), section 34.40, P. L. & R. of 1948, authorized January 27, 1933.

Author Index to Volume 96

References with (A) are to abstracts of papers presented at meeting of the American Physical Society; references with (T) designate title only. References with (L) are to Letters to the Editor. References with (E) are to Errata.

Abe, Hidetaro (see Ôno, Kazuo)—38
Abramowitz, Milton and H. A. Antosiewicz. Coulomb wave functions in transition region—75
—— **and Philip Rabinowitz.** Evaluation of Coulomb wave functions along transition line—77
Adair, Robert K. Resonances in $Li^7(p,n)Be^7$—709
——, **S. E. Darden, and R. E. Fields.** Scattering of polarized neutrons from heavy nuclei—503
Adams, E. N., II. Elastoresistance in p-type Ge and Si—803(L)
—— **and R. Zitter.** Electronic susceptibility in certain alloys—1705(L)
Ahearn, A. J. Uv transmission and α bombardment conduction inhomogeneities in diamond—828(A)
Ahnlund, Katarina. Magnetic analysis of $O^{17}(d,p)O^{18}$ reaction—999
—— (see Mileikowsky, Curt)—996
Alder, K. and A. Winther. Theory of Coulomb excitation—237(L)
Alderman, J. O. (see Bretscher, M. M.)—103
Alexander, T. (see Erdman, K. L.)—858(A)
Allen, G. (see Barile, S.)—673
Allen, K. W., E. Almqvist, J. T. Dewan, and T. P. Pepper. Disintegration of Li^6 and Li^7 by 0.24-Mev tritons—684
Allen, R. G., T. E. Stephenson, C. P. Stanford, and S. Bernstein. Slow neutron cross sections of Au, Ag, In, Ni, and NiO—1297
Allen, William A., Joe M. Mapes, and Wesley G. Wilson. Critical angle associated with high speed impact of sphere on thin plate—844(A)
Allis, W. P. Microwave discharges—831(T)
Allison, B. A. (see Scherrer, V. E.)—386
Allison, H. W. and George E. Moore. Diffusion of W in Ni—840(A)
Almqvist, E. (see Allen, K. W.)—684
Ambler, E. and R. P. Hudson. Critical field phenomena in isotropic paramagnetic crystal—907
Anderson, A. B. C. Metastable jet-tone states of jets from sharp-edged, circular, pipe-like orifices—847(A)
Anderson, D. E. (see Peterson, R. W.)—840(A)
Anderson, K. A. Cosmic-ray studies with Čerenkov detector at $\lambda = 10°$ and 55°—829(A)
Andrew, A., M. R. Jeppson, R. L. Mather, and H. P. Yockey. Creep of Al under cyclotron irradiation—843(A)
Angello, Stephen J. and Theodore E. Ebert. New minority carrier phenomenon in Ge—221(L)
Ansbacher, F. and P. T. Landsberg. Quantum statistics of closed and open systems—1707(L)
Antes, L. L. (see Reynolds, D. C.)—533(L)
Antosiewicz, H. A. (see Abramowitz, Milton)—75
Apker, L. Photoelectric emission and electronic energy structure of some amorphous semiconductors—827(T)
—— (see Taft, E.)—827(A); 1496
Ard, W. B. (see Fairbank, W. M.)—846(A)
Arnold, W. H., J. Ballam, H. Gursky, A. L. Hodson, R. Ronald Rau, George T. Reynolds, and S. B. Treiman. Unstable cosmic-ray particles observed in double cloud-chamber arrangement—853(A)
—— (see Hodson, A. L.)—1089
Artman, J. O. and J. P. Gordon. Absorption of microwaves by O_2 in mm wavelength region—1237
Asaro, Frank. (see Stephens, Frank, Jr.)—1568
Ashkin, J., J. P. Blaser, F. Feiner, J. G. Gorman, and M. O. Stern. Total cross sections for negative and positive pions in hydrogen and deuterium—1104
Ashley, J. E. (see Koontz, P. G.)—862(A)

Babiskin, J. and M. C. Steele. Oscillatory thermal conductivity of Bi in magnetic fields at liquid He temperatures—822(A)
Backman, M. E. and H. L. Morrison. Rittinger's number for several minerals—844(A)
Bailey, V. A. Reflection of waves by inhomogeneous medium—865
Bair, J. K. (see Johnson, C. H.)—985
Baker, T. E., Jr., N. C. Blais, C. L. Hemenway, V. Rojansky, M. S. Webster, and M. S. Werman. Search for departures of cosmic rays from Poisson's law at low counting rates. I—828(A)
Balagna, J. P. (see Browne, C. I.)—827(A)
Balzs, W., J. Dempsey, and E. F. Rexer. Oxide impregnated Ni matrix cathode—840(A)
Ballam, J. (see Arnold, W. H.)—853(A)
—— (see Hodson, A. L.)—1089
Ballou, N. E. (see Freiling, E. C.)—102
Balser, Martin (see Silverman, Richard A.)—560
Band, William. Critical flow rate and zero entropy of He superfluid—843(A)
Banister, J. R. and C. D. Broyles. Response of pressure gauges to dust-laden shock waves—847(A)
—— (see Merritt, M. L.)—848(A)
Barile, S., R. Webeler, and G. Allen. Range and straggling of low-energy α particles in cloud chamber—673
Barkas, Walter H. and George Hahn. Emulsion tables—859(A)
—— (see Heckman, Harry H.)—858(A)
Barnes, C. A., W. A. Fowler, C. C. Lauritsen, and R. W. Peterson. Inelastic proton scattering cross section of F^{19}—851(A)
Barnett, C. F. (see Stier, P. M.)—973
Baroody, E. M. Inelastic scattering of medium-fast electrons in alkali metals—837(A)
Barschall, H. H. and J. L. Powell. Energy distribution of nuclear reaction products—713
—— (see Okazaki, A.)—836(A)
Bartholomew, G. A., F. Brown, H. E. Gove, A. K. Litherland, and E. B. Paul. Resonances in proton bombardment of C^{14}—1154(L)
—— (see Gove, H. E.)—825(A)
—— (see Litherland, A. E.)—825(A)
Basson, J. K. Direct quantitative observation of three-photon annihilation of positron-negatron pair—691
Baumann, K. (see Deser, S.)—774
Bean, C. P. (see Roberts, B. W.)—1494
Beaty, E. and R. Varney. Drift velocities of A ions in A at various temperatures—831(A)
Becker, J. H. (see Blunt, R. F.)—578
—— (see Breckenridge, R. G.)—571
Becker, R. L. (see Okazaki, A.)—836(A)
Becker, Robert A. (see Brown, Hugh N.)—1372
Bedford, R. E. and A. M. Crooker. Spectra of As—845(A)
Beer, A. C. (see Willardson, R. K.)—1512
Belinfante, Frederik J. Direct proof of covariance of Gupta's indefinite metric in quantum electrodynamics—780
Bell, S. and S. A. Schaaf. Free molecule flow of non-uniform gas—848(A)

Bender, R. S. Deuteron reaction studies with Pittsburgh cyclotron—849(T)
Benedict, F. D. (see Daitch, P. B.)—1449(L)
Benenson, R. E., M. B. Shurman, and W. Haeberli. Gas-recoil fast neutron spectrometer—836(A)
Bennett, Willard H. Model of solar proton streams—824(A)
Beringer, Robert (see Heald, Mark A.)—645
Berman, Arthur I. and Karl L. Brown. Absolute cross section *versus* energy of $Cu^{63}(\gamma,n)$ and $Cu^{63}(\gamma,2n)$ reactions—83
Bernstein, Seymour (see Allen, R. G.)—1297
—— (see Sherwood, J. E.)—1546
—— (see Stanford, C. P.)—983
Bernstein, W. (see Finston, H. L.)—71
Bethe, H. A. and F. de Hoffmann. Meson-proton scattering phase shift analysis—1714(E)
Binder, D. and W. J. Sturm. Equivalence of x-ray lattice parameter and density changes in neutron-irradiated LiF—1519
Biondi, Manfred A. Atomic collision processes in ionized gases—831(T)
—— Optical and infrared absorption of Cu at 4.2°K—534(L)
—— (see Chanin, Lorne M.)—831(A)
Bitter, F., S. P. Davis, B. Richter, and J. E. R. Young. Optical studies of radioactive Hg—1531
Bittner, J. W. and R. D. Moffat. Elastic scattering of α particles by C—374
Blair, J. M., N. M. Hintz, and D. M. Van Patter. Radiative capture of deuterons by He^3—1023
Blais, N. C. (see Baker, T. E., Jr.)—828(A)
Blakney, R. M. and D. L. Dexter. Effect of dislocations on optical absorption edge in nonmetals—227(L)
Blaser, J. P. (see Ashkin, J.)—1104
Blatt, John M. Integral equations for cascade showers—1644
—— **and S. T. Butler.** Superfluidity of boson gas—1149(L)
Blau, M. and Martin Caulton. Inelastic scattering of 500-Mev negative pions in emulsion nuclei—150
Blewett, J. P. Recent developments in design of high-energy synchrotrons—823(T)
Bloch, Ingram and Yü-Chang Hsieh. Properties of nuclear normal modes—382
—— **and Yü-Chang Hsieh.** Spin-orbit interactions in many-body nuclear shell theory—855(A)
Block, M. M., D. T. King, and W. W. Wada. Direct creation of electron pairs by electrons of great energy. III. Internal energy distributions—853(A)
——, **D. T. King, and W. W. Wada.** Electron tridents between 0.1 and 10 Bev—1627
—— (see King, D. T.)—852(A)
—— (see Wada, W.)—852(A)
Blood, H. L. and W. G. Proctor. Nuclear electric quadrupole interactions of B^{11} in kernite—861(A)
Bloom, Myer (see Muller, B. H.)—861(A)
Blunt, R. F., H. P. R. Frederikse, J. H. Becker, and W. R. Hosler. Electrical and optical properties of intermetallic compounds. III. AlSb—578
——, **W. R. Hosler, and H. P. R. Frederikse.** Electrical and optical properties of intermetallic compounds. II. GaSb—576
—— (see Breckenridge, R. G.)—571
Bockelman, C. K. (see Jung, J. J.)—1353
—— (see Sperduto, A.)—1316
Bode, Donald E. and Henry Levinstein. Effect of oxygen on electrical properties of PbTe films—259
Bohl, Leland. Light elements in cosmic rays—834(T)
Bohm, D. and J. P. Vigier. Model of causal interpretation of quantum theory in terms of fluid with irregular fluctuations—208
Bohm, H. V. (see Dunlap, W. C., Jr.)—822(A)
Bömmel, H. E. Ultrasonic attenuation in superconducting lead—220(L)
Bonner, T. W. and C. F. Cook. Excited states in B^{10} and Be^8—122
Borowitz, Sidney. Perturbation calculation of the elastic scattering of electrons by H atoms—1523
Bortner, T. E. (see Melton, C. E.)—643
Bowen, Theodore. Ionization energy loss of mesons in NaI scintillation crystal—754(A)
Bozorth, R. M. Magnetostriction and crystal anisotropy of single crystals of hexagonal Co—311
Brachman, Malcolm K. Space-time representation in wave mechanics: Illustration of method—516
Bragg, J. K. (see Crowe, R. W.)—10
Braun, E. A., A. Many, and A. E. Simchen. Color centers in chrome alum crystals—1505
Braunstein, R. (see Trischka, J. W.)—968
Brebrick, Robert F. and Wayne W. Scanlon. Electrical properties and solid-vapor equilibrium of PbS—598
Breckenridge, R. G., R. F. Blunt, W. R. Hosler, H. P. R. Frederikse, J. H. Becker, and W. Oshinsky. Electrical and optical properties of intermetallic compounds. I. InSb—571
Breed, Henry E. and J. Mayo Greenberg. Investigations of intensity anomalies in electron diffraction from crystals—823(A)
Breit, G. and P. B. Daitch. Correspondence between semiclassical and quantum treatments of Coulomb excitation—1447(L)
—— **and J. B. Ehrman.** Formula for polarization in nucleon-nucleon scattering—805(L)
——, **J. B. Ehrman, A. M. Saperstein, and M. H. Hull, Jr.** Phase shifts for nucleon-nucleon scattering at 280 Mev—807(L)
—— (see Daitch, P. B.)—1449(L)
Bretscher, M. M., J. O. Alderman, A. Elwyn, and F. B. Shull. Angular distributions of protons from $Na^{23}(d,p)Na^{24}$ and $Ti^{47,48}(d,p)Ti^{48,49}$—103
—— (see Shull, F. B.)—826(A)
Brice, M. K. (see Cork, J. M.)—1295
Bridge, H. S. Results with S particles—834(T)
Brogren, Gösta. Relation between the width of an x-ray line and resolving power of double-crystal spectrometer—589
Brook, M. and J. Kaplan. Dissociation energy of NO and N_2—1540
Brown, F. (see Bartholomew, G. A.)—1154(L)
Brown, Hugh N. and Robert A. Becker. Radiations from Ho^{164}—1372
Brown, Karl L. (see Berman, Arthur I.)—83
Brown, R. J. S., K. F. Famularo, H. D. Holmgren, D. Rankin, and T. F. Stratton. Elastic scattering of deuterons by He^3—80
Brown, W. L., R. C. Fletcher, and K. A. Wright. Traps produced by electron bombardment of Ge at low temperatures—834(A)
—— (see Fletcher, R. C.)—833(A)
—— (see Shulman, R. G.)—833(A)
Browne, C. I., D. C. Hoffman, H. L. Smith, M. E. Bunker, J. P. Mize, J. W. Starner, R. L. Moore, and J. P. Balagna. Radiations of Pa^{230}—827(A)
Browne, C. P., S. F. Zimmerman, and W. W. Buechner. Energy levels of Al^{27}—725
—— (see Sperduto, A.)—1316
Broyles, C. D. (see Banister, J. R.)—847(A)
Brueckner, K. A. Nuclear saturation and two-body forces. II. Tensor forces—508
Brysk, Henry. Spatial distribution of energy dissipation by high-energy x-rays—419

Bube, Richard H. Crystal imperfections in photoconductivity—827(T)
—— (see Jenny, Dietrich A.)—1190
Buechner, W. W. (see Browne, C. P.)—725
—— (see Sperduto, A.)—1316
Buehler, E. (see Fuller, C. S.)—833(A)
Bunker, M. E. (see Browne, C. I.)—827(A)
—— (see Mize, J. P.)—444
Bunney, L. R. (see Freiling, E. C.)—102
Burson, S. B., W. C. Jordan, and J. M. LeBlanc. Decay of $_{32}Ge^{75m}$ (49 sec), $_{32}Ge^{77m}$ (52 sec), and $_{32}Ge^{77}$ (12 hr)—1555
—— (see Jordan, W. C.)—1582
Burstein, E., J. W. Davisson, and N. Sclar. Low-frequency dielectric loss peaks in KCl containing divalent cation impurities—819(A)
Burwell, J. R. (see Kim, Y. B.)—229(L)
Bushkovitch, A. V. (see Liuima, F. A.)—434
Butler, J. (see Hird, B.)—702
Butler, S. T. (see Blatt, J. M.)—1149(L)
Byram, E. T., T. A. Chubb, and H. Friedman. Solar x-ray emission—860(A)

Cabrera, N., M. M. Levine, and J. S. Plaskett. Hollow dislocations and etch pits—1153(L)
Calcamuggio, G. L. (see Haller, W.)—1454(A)
Callaway, Joseph. Mach's principle and unified field theory—778
Capps, R. H. and R. G. Sachs. Scattering of γ rays by nucleons—540(L)
Carlson, B. C. and I. Talmi. Pairing effects in Coulomb energies and radii of mirror nuclei—436
Carlson, C. R. (see Matheson, W. E.)—826(A)
Carlson, R. R. (see Nelson, E. B.)—825(A)
Carroll, Paul E. Contact electrification in metal-metal system. II. Results for Hg-steel—820(A)
Carter, R. S., J. A. Harvey, D. J. Hughes, and V. E. Pilcher. Ratio of $\bar{\Gamma}_n^0/\bar{D}$ for slow neutron resonances—113
Cashman, Robert J. (see Jensen, Harald C.)—798(L)
Caulton, Martin (see Blau, M.)—150
Cegelski, W. M., A. T. Goble, C. L. Hemenway, K. Reinitz, V. Rojansky, and F. A. Rushworth. Search for departures of cosmic rays from Poisson's law at low counting rates. II—828(A)
Chaloupka, P. Influence of geomagnetic field on extensive air showers—1709(L)
Chamberlain, O., E. Segrè, R. Tripp, C. Wiegand, and T. Ypsilantis. Polarization of high-energy protons in elastic scattering on He and C—807(L)
Chang, C. H. and B. A. Jacobsohn. Elimination of pair interaction in pseudoscalar meson theory—856(A)
Chanin, Lorne M. and Manfred A. Biondi. Mobilities of various ions in noble gases—831(A)
Chapman, Seville. Corona discharge current from aircraft—831(A)
Charles, G. W., D. J. Hunt, G. Pish, and D. L. Timma. Preliminary description and analysis of spectrum of Po—838(A)
Chartres, B. A. and H. Messel. New formulation of general three-dimensional cascade theory—1651
Chasson, Robert L. Cosmic-ray intensity fluctuations at sea level—1116
Cheston, W. B. Proton polarization in (d,p) reactions—1590
—— Various comments on deuteron-induced reactions—830(T)
—— (see Naugle, J. E.)—1383
Chih, Chung Ying. n-p scattering at 90 Mev—856(A)
Chou, C. N. Studies of penetrating and cascade showers of cosmic rays with plastic scintillators at elevation of 11 500 feet—830(A)
Christensen, H. Surface "channel" detection method for semiconductors—827(A)
Christy, R. F. Rotational levels in W^{180}—858(A)
—— **and W. A. Fowler.** Hole configurations in light nuclei—851(A)
—— (see Sherr, R.)—1258
Chubb, T. A. (see Byram, E. T.)—860(A)
Chupp, E. L. Long-term studies of neutron and ionizing cosmic-ray intensities—853(A)
Cialella, Carment. (see Miller, William)—1344
Clark, K. C. and L. Kanal. Detection of Hg vapor by resonance ionization—860(A)
Class, C. M. (see Cook, C. F.)—658
Clendenin, William W. (see Rickard, James A.)—1272
Coester, F., Morton Hamermesh, and Katsumi Tanaka. Limiting processes in formal theory of scattering—1142
Cohen, B. L., H. L. Reynolds, and A. Zucker. Comparison of nitrogen- and proton-induced nuclear reactions—1617
—— (see McCormick, G. H.)—722
Cohen, David, Burton J. Moyer, Harlan Shaw, and Charles Waddell. Emission of high-energy γ line from C^{12}—714
—— (see Waddell, Charles)—858(A)
Cohen, M. H. Nuclear quadrupole spectra in solids—1278
Cohen, René. Easily reproducible thermal neutron density standard—850(A)
—— (see Thirion, Jacques)—850(A)
Colladay, G. S. Energy parameters of two-dimensional graphite—846(A)
Colli, Laura and Ugo Facchini. Secondary electron emission by photoelectric action and ion bombardment at cathode in corona breakdown of A—1
Collie, C. H. (see Hird, B.)—702
Collins, T. L. Probable age of earth—824(T)
—— (see Giese, Clayton F.)—823(A)
—— (see Quisenberry, K. S.)—823(A)
Collinson, J. A. Isotope shift in Hf I—949
Conway, John G. and Ralph D. McLaughlin. Nuclear spin of Np^{239}—541(L)
Cook, C. F., C. M. Class, and J. T. Eisinger. Electric excitation of Au^{197}—658
—— (see Bonner, T. W.)—122
Cook, C. J. "Zipper" scattering chamber—835(A)
Cook, C. Sharp and W. E. Kreger. γ radiation following decay of Pr^{144}—855(A)
—— (see Kreger, W. E.)—854(A)
—— (see Kreger, W. E.)—1279
Coomes, E. A. Surface-barrier determination by periodic deviations from Schottky effect—819(T)
Copeland, Paul L. (see Schwartz, Manuel)—1466
Corak, W. S., B. B. Goodman, C. B. Satterthwaite, and A. Wexler. Exponential temperature dependence of electronic specific heat of superconducting V—1442(L)
Corben, H. C. (see Mickelwait, A. B.)—1145
Cork, Bruce and Walter Hartsough. Elastic scattering of 9.7-Mev protons by α particles—859(A)
—— **and Walter Hartsough.** Elastic scattering of 9.7-Mev protons by He^4—1267
Cork, J. M., M. K. Brice, and L. C. Schmid. Energies of radiations from Ce^{144} and Pr^{144}—1295
Cormack, A. M. Resonance scattering of γ rays by nuclei—716
Coryell, Charles D. (see Wiles, Donald R.)—696
Cotts, R. M. and W. D. Knight. Nuclear resonance of Nb^{93} in $KNbO_3$—1285
Cowan, C. L., Jr., F. Reines, and F. B. Harrison. Upper limit on neutrino magnetic moment—1294
—— (see Harrison, F. B.)—1159(L)
—— (see Reines, F.)—1157(L)
Cowan, E. W. V-particles with neutral secondaries—848(T)

Craig, D. S., W. G. Cross, and R. G. Jarvis. γ rays from (p,γ) reactions in B^{11} and Mg^{24}—825(A)
Crooker, A. M. and E. B. Dorling. Dependence of signal-to-noise ratio in photoconductive PbSe layers on temperature of black-body source—846(A)
—— (see Bedford, R. E.)—845(A)
—— (see Nodwell, R. A.)—845(A)
Cross, W. G. (see Craig, D. S.)—825(A)
Crowe, Kenneth M. and Robert H. Phillips. Precision measurement of negative pion mass from its radiative absorption in hydrogen—470
—— (see Phillips, Robert H.)—484
Crowe, R. W., J. K. Bragg, and Virginia G. Thomas. Space-charge formation and Townsend mechanism of spark breakdown in gases—10
Curran, S. C. (see Moljk, A.)—395
Cutkosky, R. E. Solutions of Bethe-Salpeter equation—1135
Cutler, Melvin. Flow of electrons and holes through surface barrier region in point contact rectification—255
Czyzak, S. J. (see Reynolds, D. C.)—1705(L)

Daitch, P. B., J. P. Lazarus, M. H. Hull, Jr., F. D. Benedict, and G. Breit. Validity of semiclassical treatment of Coulomb excitation—1449(L)
—— (see Breit, G.)—1447(L)
Daly, Jr., R. T. and J. H. Holloway. Nuclear magnetic octupole moments of stable Ga isotopes—539(L)
Damon, R. W. and R. W. Redington. Electrical and optical properties of InSe—1498
Danielson, R. E., P. S. Freier, J. S. Naugle, and E. P. Ney. Flux and azimuthal asymmetry of primary cosmic-ray nuclei at equator—829(A)
Darden, S. E., W. Haeberli, and R. B. Walton. Small angle scattering of 1-Mev neutrons by intermediate and heavy nuclei—836(A)
—— (see Adair, R. K.)—503
Dash, W. C. Oxidation of thin films of Ge and Si—822(A)
Daunt, J. G. (see Gordon, W. L.)—1444(L)
Dauphinee, T. M. Semiautomatic apparatus for thermocouple comparison and calibration—843(A)
Davis, Leverett, Jr. Anisotropy of high-energy cosmic rays —743
—— Sidereal time variations in cosmic-ray intensities produced by Fermi's acceleration mechanism—853(A)
Davis, R. E. and Colman Goldberg. Magnetoresistance and planar Hall effects in n-type Ge—833(A)
Davis, S. P. (see Bitter, F.)—1531
Davisson, J. W. (see Burstein, E.)—819(A)
Day, R. B. (see Woodbury, H. H.)—1713(E)
Dayton, I. E. (see Schrank, G.)—1156(L)
Dean, C. Zeeman splitting of nuclear quadrupole resonances —1053
DeBenedetti, S. (see Stearns, M. B.)—804(L)
de Carvalho, Hervasio G. Total cross sections of light elements for 208-Mev and 315-Mev protons—398
——, **J. Marshall, and L. Marshall.** Polarization of protons by scattering from Be—1081
de Hoffman, F. (see Bethe, H. A.)—1714(E)
Dekker, A. J. Escape mechanism for secondary electrons—837(T)
Dempsey, J. (see Balas, W.)—840(A)
Dennison, David M. Energy levels of O^{16} nucleus—378
DePangher, John. Radiative capture of 300-Mev neutrons in H—859(A)
Desai, U. D. (see Sarabhai, V.)—469
Deser, S. Adiabatic theorems in field theory—843(A)
——, **M. L. Goldberger, K. Baumann, and W. Thirring.** Energy level displacements in π-mesonic atoms—774
Dewan, J. T. (see Allen, K. W.)—684
Dexter, D. L. Shapes of absorption and emission lines of impurities in solids—615
—— (see Blakney, R. M.)—227(L)
Dexter, R. N. and Benjamin Lax. Effective masses of holes in Si—223(L)
——, **Benjamin Lax, A. F. Kip, and G. Dresselhaus.** Effective masses of electrons in Si—222(L)
Diamond, H. (see Magnusson, L. B.)—1576
Diamond, R. M. (see Sharp, R. A.)—1713(E)
Dicke, R. H. (see Wittke, J. P.)—530(L)
Ditzenberger, J. A. (see Fuller, C. S.)—833(A)
Dolecek, R. L. Adiabatic magnetization of superconducting sphere—25
Dorfman, J. G. Diamagnetic resonance in electronic conductors—1704(L)
Dorling, E. B. (see Crooker, A. M.)—846(A)
Dresselhaus, G. (see Dexter, R. N.)—222(L)
Dugdale, J. S. and D. K. C. MacDonald. Vibrational anharmonicity and lattice thermal properties—57
DuMond, J. W. M. (see Murray, J. J.)—858(A)
Dunlap, W. C., Jr. Properties of Zn-, Cu-, and Pt-doped Ge—40
——, **H. V. Bohm, and H. P. Mahon, Jr.** Diffusion of impurities in Si—822(A)
Dunn, Eldon L. and Howard R. Kelly. Displacement effect of three-dimensional boundary layer of moderate thickness—847(A)

Ebert, Theodore E. (see Angelio, Stephen J.)—221(L)
Eby, F. S. Angular distribution of protons from (d,p) reactions on Be^9, N^{14}, and Zn^{68}—1355
—— **and W. K. Jentschke.** Fluorescent response of NaI(Tl) to nuclear radiations—911
Ehrman, J. B. (see Breit, G.)—805(L); 807(L)
Eichelberger, J. F., K. C. Jordan, S. R. Orr, and J. R. Parks. Calorimetric determination of half-life of Po^{210}—719
Eilenberg, S. L. (see Orear, Jay)—174
Eisele, J. A. and F. Keffer. Effects of anisotropy on thermodynamic properties of antiferromagnets—929
Eisenberg, Y. Interaction of heavy primary cosmic rays in Pb—1378
—— Possible existence of new hyperon—541(L)
Eisinger, J. T. (see Cook, C. F.)—658
Elliott, J. P. and A. M. Lane. Evidence for two-body spin-orbit forces in nuclei—1160(L)
Elliott, R. J. Effect of spin-orbit coupling on magnetic resonance in some semiconductors—266
—— Spin-orbit coupling in band theory—character tables for some 'double' space groups—280
Elvey, C. T. Morphology of auroral displays in Alaska—860 (T)
Elwyn, A. (see Bretscher, M. M.)—103
Engelbrecht, A. (see Javan, Ali)—649
Erdman, K. L., J. B. Warren, D. B. James, and T. Alexander. γ rays from Li^6+p—858(A)
—— (see Warren, J. B.)—857(A)
Etzel, H. W. and F. E. Geiger, Jr. K band in additively colored KCl—225(L)
Evans, G. E. (see Stier, P. M.)—973
Evans, J. E. Contour diagrams of thermal neutron absorption cross sections—849(A)
—— (see Joki, E. G.)—849(A)

Facchini, Ugo (see Colli, Laura)—1
Fafarman, A. and M. H. Shamos. Low-energy differential range spectrum of cosmic-ray μ mesons—1096
Fairbank, W. M., W. B. Ard, and G. K. Walters. Fermi-Dirac degeneracy in liquid He^3 below 1°K—846(A)
Famularo, K. F. (see Brown, R. J. S.)—80
—— (see Simmons, B. E.)—826(A)

—— (see Stratton, T. F.)—825(A)
Fan, C. Y. Excitation of air glow by electronic impact—860 (A)
Fano, U. Note on the quantum theory of irreversible processes—869
Farmer, Donald J. and J. F. Streib. One-quantum annihilation of positrons—855(A)
—— (see Kochendorfer, D. B.)—855(A)
Farney, G. K. (see Givin, H. H.)—1337
Farvis, W. E. J. (see Pringle, D. H.)—536(L)
Faust, W. R. (see Scherrer, V. E.)—386
Fechter, H. R. (see Tautfest, G. W.)—35
Feiner, F. (see Ashkin, J.)—1104
Feld, B. T., A. Julian, A. C. Odian, L. S. Osborne and A. Wattenberg. Search for the production of μ-meson pairs by a 345-Mev synchrotron beam—1386
Feldman, Charles. Thin films of $BaTiO_3$—819(A)
Ferrari, F. and C. Villi. Non-uniform charge distributions and μ-meson capture—1159(L)
Feshbach, H., C. E. Porter, and V. F. Weisskopf. Model for nuclear reactions with neutrons—448
Field, L. M. Post-war developments in amplifiers involving energy-exchange processes between electron beams and microwave electric fields—823(T)
Fields, P. R. (see Magnusson, L. B.)—1576
Fields, R. E. (see Adair, R. K.)—503
Fields, T. H., J. G. Fox, J. A. Kane, R. A. Stallwood, and R. B. Sutton. Reaction $p+p \rightarrow \pi^+ + d$ with polarized protons—812(L)
Fine, M. E. and N. T. Kenney. Low-temperature acoustic relaxation in Ni–Fe ferrites—1487
Fink, Richard W. and Edwin O. Wiig. Reactions of Cs with protons at 40, 80, 100, 150, and 240 Mev—185
Finston, H. L. and W. Bernstein. Decay scheme of I^{180}—71
Fischer, Gerhard E. Scattering of 10-Mev protons on carbon and magnesium—704
Fischer, Vera Kistiakowsky. Decay of Pm^{150}—1549
Fisher, L. H. Mechanism of electric spark—860(T)
Fiske, Milan D. Effects of elastic dilatation and shear on superconducting transition of Sn—821(A)
—— (see Schmitt, R. W.)—1445(L)
Fleming, John R. and J. J. Lord. Grain density and ionization loss in nuclear track emulsions—852(A)
—— (see Hoard, R. F.)—854(A)
Fletcher, R. C., W. L. Brown, and K. A. Wright. Absence of bombardment annealing in electron bombardment of Ge—833(A)
—— (see Brown, W. L.)—834(A)
—— (see Shulman, R. G.)—833(A)
Foglesong, G. M. and D. G. Foxwell. Magnetic analysis of $Co^{60}(d,p)Co^{60}$ reaction—1001
Foley, H. M. (see Sessler, A. M.)—366
Foote, Jr., H. L. (see Sailor, V. L.)—1014
Forman, R. Measurement and theoretical study of conductivity and Hall effect in oxide cathodes—839(A); 1479
Forster, H. H. and A. Oswald. β spectrum of C^{14}—1030
Fowler, C. M. (see Keshishian, V.)—1050
Fowler, W. A. (see Barnes, C. A.)—851(A)
—— (see Christy, R. F.)—851(A)
—— (see Peterson, R. W.)—1250
—— (see Webb, T. S.)—851(A)
Fox, David and Otto Schnepp. Exciton bands in crystalline benzene—1196
Fox, J. G. (see Fields, T. H.)—812(L)
Fox, R. E. (see Hickam, W. M.)—63
Foxwell, D. G. (see Foglesong, G. M.)—1001
Fraser, J. S. (see Milton, J. C. D.)—1508
Frederikse, H. P. R. (see Blunt, R. F.)—576; 578
—— (see Breckenridge, R. G.)—571
Freemantle, R. G., D. J. Prowse, A. Hossain, and J. Rotblat. Scattering of 9.5-Mev protons by Ne and A—1270
——, **D. J. Prowse, and J. Rotblat.** Scattering of 9.5-Mev protons by N—1268
Freier, Phyllis. High-energy nuclear and electromagnetic interactions—834(T)
—— (see Danielson, R. E.)—829(A)
—— (see Naugle, J. E.)—829(A)
—— (see Ney, E. P.)—829(A)
Freiling, E. C., L. R. Bunney, and N. E. Ballou. Identification of Gd and Tb radioisotopes as fission products of U^{235}—102
Freistadt, Hans. Classical field theory in Hamilton-Jacobi formalism—821(A)
Frenkiel, F. N. Turbulence and atmospheric pollution—857 (T)
Fretter, W. B. Identification of heavy mesons—848(T)
—— **and E. W. Friesen.** Cascade decay of negative hyperon —853(A)
Friedlander, G. (see Wolfgang, R. L.)—190
Friedman, A. M. (see Magnusson, L. B.)—1576
Friedman, H. (see Byram, E. T.)—860(A)
Friesen, E. W. (see Fretter, W. B.)—853(A)
Fry, W. F. and M. S. Swami. Energetic disintegration of heavy nuclear fragment—809(L)
—— **and M. S. Swami.** K mesons and charged hyperon produced by 3-Bev protons in emulsions—235(L)
Fuller, C. S., J. A. Ditzenberger, N. B. Hannay, and E. Buehler. Resistivity changes in Si induced by heat treatment—833(A)
—— **and J. C. Severiens.** Mobility of impurity ions in Ge and Si—21
Fuller, Everett G. Photodisintegration of He—1306
Furlong, L. R. Low-temperature luminescence of CdS—1714 (E)
Furst, Milton and Hartmut Kallmann. Excitation energy and energy transfer by collision in fluorescent solutions—902

Gallagher, C. J. and A. G. Tweet. Plastic deformation of Au-doped Ge—834(A)
Galonsky, A. and M. T. McEllistrem. Energy levels of Li^6—826(A)
Galt, John K. Motion of individual ferromagnetic domain walls—857(T)
Garren, A. Coulomb interference effects in p-p scattering —1709(L)
Garstens, M. A., L. S. Singer, and A. H. Ryan. Magnetic resonance absorption of diphenyl-picryl hydrazyl—53
Geballe, Ronald (see Reeves, M. L.)—862(A)
Geballe, T. H. and G. W. Hull. Seebeck effect in single crystal Si—846(A)
—— (see Hull, G. W.)—846(A)
Geiger, F. E., Jr. (see Etzel, H. W.)—225(L)
Gell-Mann, M. and M. L. Goldberger. Scattering of low-energy photons by particles of spin $\frac{1}{2}$—1433
Gerhart, J. B. (see Naumann, R. A.)—1452(L)
Ghosh, S. N., Walter Gordy, and D. G. Hill. Paramagnetic resonance in U salts—36
Gibbons, Martin D. (see Stout, Virgil L.)—819(A)
Giese, Clayton F. and T. L. Collins. Mass doublet measurements using modulated magnetic field—823(A)
Gilbert, W. S. and J. H. Pepper. Some experimental facilities and techniques used at Berkeley 60-in. cyclotron for irradiation effect studies—862(A)
Giles, Peter C. (see Heckman, Harry H.)—858(A)
Gilvarry, J. J. Solution of temperature-perturbed Thomas-Fermi equation—944

—— Thermodynamics of Thomas-Fermi atom at low temperature—934
Givin, H. H., G. K. Farney, T. M. Hahn, and B. D. Kern. Angular distribution of 12- and 16-Mev γ rays from proton bombardment of thin B target—1337
Glasser, R. G. Mass measurement by multiple Coulomb scattering on stopped particles—835(A)
—— (see Orear, Jay)—1710(L)
—— (see Schein, Marcel)—829(A)
—— (see Sprague, A. D.)—830(A)
Glazer, H. and H. Reiss. Thomas-Fermi calculation of C—H bond moment in methane—838(A)
Gliessman, J. R. (see Hung, C. S.)—1226
Goble, A. T. (see Cegelski, W. M.)—828(A)
Godfrey, Charles S. Comparison of H^3 and He^3 production in high-energy deuteron-deuteron collisions—1621
—— Production of tritons in high-energy deuteron-deuteron collisions—493
Goldberg, Colman (see Davis, R. E.)—833(A)
Goldberger, M. L. (see Deser, S.)—774
—— (see Gell-Mann, M.)—1433
Goldhaber, M. (see Mihelich, J. W.)—1450(L)
—— (see Reines, F.)—1157(L)
Goldstein, Louis. Theory of liquid He^3—1455
Good, W. M. (see Moak, C. D.)—1363
Goodman, B. Long-life luminescence and diffusion in MgO—824(A)
Goodman, B. B. (see Corak, W. S.)—1442(L)
Gordon, J. P. (see Artman, J. O.)—1237
Gordon, W. L., C. H. Shaw, and J. G. Daunt. X-ray diffraction patterns from liquid He—1444(L)
Gordy, Walter (see Ghosh, S. N.)—36
Gorman, J. G. (see Ashkin, J.)—1104
Gove, H. E., G. A. Bartholomew, E. B. Paul, and A. E. Litherland. Reaction $C^{14}(p,\gamma)N^{15}$ above (p,n) threshold—825(A)
—— (see Bartholomew, G. A.)—1154(L)
—— (see Litherland, A. E.)—825(A)
Grebenkemper, C. J. High-frequency resistance of Sn and In in normal and superconducting state—1197
—— Superconductivity of V at 24 000 Mc/sec—316
Green, David and J. Reginald Richardson. Radiations from some odd-odd N=Z nuclei—858(A)
Green, Louis C., Marjorie M. Mulder, Paul C. Milner, Margaret N. Lewis, John W. Woll, Jr., Eleanor K. Kolchin, and David Mace. Analysis of 3-parameter wave function of Hylleraas for He I ground state in terms of central field wave functions—319
Greenberg, J. Mayo. Comparison of several approximations to scattering of high-energy electrons—820(A)
—— (see Breed, Henry E.)—823(A)
Greenspan, Martin. Experiments on sound propagation in rarefied gases—857(T)
Grimes, D. M. and D. W. Martin. Reversible susceptibility of ferromagnetics—889
Groetzinger, Gerhart, David Kahn, and Philip Schwed. New criterion for superconductivity in metals—887
Gugelot, P. C. Elastic scattering of protons by medium and heavy nuclei—849(T)
—— (see Schrank, G.)—1156(L)
Guldner, W. G. (see Wooten, L. A.)—840(A)
Gupta, Suraj N. Gravitation and electromagnetism—1683
—— Multiple photon production in electron-positron annihilation—1453(L)
Gursky, H. (see Arnold, W. H.)—853(A)

Hack, M. N. Bound states and formal theory of scattering—196; 1714(E)
Haeberli, W. (see Benenson, R. E.)—836(A)
—— (see Darden, S. E.)—836(A)
Hagedorn, F. B. (see Webb, T. S.)—851(A)
Hagstrum, Homer D. Auger ejection of electrons from W by noble gas ions—325
—— Theory of Auger ejection of electrons frpm metals by ions—336
Hahn, George (see Barkas, Walter H.)—859(A)
Hahn, T. M. (see Givin, H. H.)—1337
—— (see Lafferty, D. L.)—381
Hall, J. G. Transition through contact region—847(A)
Haller, W. and G. L. Calcamuggio. New method for high-precision studies of rate processes—1454(A)
Hamermesh, Bernard (see Recksiedler, Arthur L.)—109
Hamermesh, Morton (see Coester, F.)—1142
Handley, Thomas H. and Elmer L. Olson. Neutron-deficient activities of Pr—1003
Hannam, H. J. Influence of tube structure and tube operating conditions upon flicker noise—837(A)
Hannay, N. B., J. R. Haynes, and R. G. Shulman. Interaction of traps and heat treatments in Si—833(A)
—— (see Fuller, C. S.)—833(A)
—— (see Morin, F. J.)—833(A)
Hanson, Howard G. Quenching of NaI fluorescence by various gases and vapors—832(A)
Harman, T. C. (see Willardson, R. K.)—1512
Harris, D. R. (see Hodson, A. L.)—1089
Harrison, F. B., C. L. Cowan, Jr., and F. Reines. Electron spectrum from μ-meson decay—1159(L)
—— (see Cowan, Jr., C. L.)—1294
Hartsough, Walter (see Cork, Bruce)—859(A); 1267
Hartzler, A. J. (see Siegel, R. T.)—859(A)
Harvey, J. A. (see Carter, R. S.)—113
Haskin, D. M. (see Orear, Jay)—1710(L)
—— (see Schein, Marcel)—829(A)
—— (see Sprague, A. D.)—830(A)
Hawkins, W. B. Alignment of Na atoms—532(L)
Haxby, R. O. (see Matheson, W. E.)—826(A)
—— (see Voss, J. R.)—830(A)
Haynes, J. R. (see Hannay, N. B.)—833(A)
Hays, Earl E. Time-of-flight mass spectrometer—1454(A)
Heald, Mark A. and Robert Beringer. Hfs of N—645
Heckman, Harry H., Peter C. Giles, and Walter H. Barkas. High-energy γ ray studies with nuclear track emulsions—858(A)
Heiberg, S. A. Reaction $B^{11}(n,\alpha)Li^8$—856(A)
—— (see James, D. B.)—856(A)
Heineman, R. E. Electron density distribution near large air shower axes at sea level—161
Helfer, H. L. Finley-Freundlich red-shift hypothesis—224(L)
Hemenway, C. L. (see Baker, T. E., Jr.)—828(A)
—— (see Cegelski, W. M.)—828(A)
Hempstead, C. F. (see Parratt, L. G.)—820(A)
Hemstreet, H. W. (see Reynolds, J. M.)—1203
Henry, I. George (see Peterson, Vincent)—850(A)
Herb, R. G. Recent progress in electrostatic-generator techniques—838(T)
Herbst, Roland F. Nuclear forces and β-decay matrix elements—372
Herman, R. C. (see Mador, I. L.)—617
Herring, Conyers. Theory of thermoelectric power of semiconductors—1163
Hess, W. N. and B. J. Moyer. Production of deuterons in high-energy nuclear bombardment of nuclei—859(A)
Heydenburg, N. P. (see Temmer, G. M.)—426
Hickam, W. M., R. E. Fox, and T. Kjeldaas, Jr. Probability curves near threshold for formation of He^+, Ne^{++}, A^{++}, Kr^{++}, and Xe^{++} by electron impact—63
Hill, D. G. (see Ghosh, S. N.)—36
Hill, F. K. Boundary layer problems in hypersonic flow—852(T)

Hillman, Peter, R. H. Stahl, and N. F. Ramsey. Total cross sections of liquefied gases for high-energy neutrons—115
Hiltner, W. A. Galactic magnetic fields—824(T)
Hinman, G. W. (see Leamer, R. D.)—1607
Hinteregger, Hans E. Photoelectric emission in extreme uv—538(L)
Hintz, Norton M. (see Blair, J. M.)—1023
—— (see Johnston, Lawrence H.)—835(A)
Hird, B., C. H. Collie, J. Butler, and C. Whitehead. γ rays from $C^{13}(p,\gamma)N^{14}$ and $Na^{23}(p,\gamma)Mg^{24}$ reactions—702
Hoard, R. F., J. R. Fleming, and J. J. Lord. Identification of primary cosmic-ray heavy nuclei—854(A)
Hobson, J. P., J. C. Hubbs, W. A. Nierenberg, and H. B. Silsbee. Spin, magnetic moment, and hfs of Rb^{81}—1450(L)
Hoch, Michael, Anthony J. Lamantia, and Herrick L. Johnston. Reaction between BaO and C and BaO and Si—839(A)
Hodson, A. L., J. Ballam, W. H. Arnold, D. R. Harris, R. Ronald Rau, George T. Reynolds, and S. B. Treiman. Cloud-chamber evidence for charged counterpart of θ^0 particle—1089
—— (see Arnold, W. H.)—853(A)
Hoff, R. W. and S. G. Thompson. Orbital electron capture in heaviest elements—1350
Hoffman, D. C. (see Browne, C. I.)—827(A)
Hofstadter, R., R. McAllister, and E. Wiener. Electron scattering in H and He—854(A)
—— (see McIntyre, J. A.)—854(A)
Holladay, W. G. and R. G. Sachs. Neutron-proton mass difference—810(L)
Hollander, J. M. (see Kalkstein, M. I.)—730
Holloway, J. H. (see Daly, R. T., Jr.)—539(L)
Holmgren, H. D. (see Brown, R. J. S.)—80
—— (see Stratton, T. F.)—825(A)
Holstein, T. Optical and infrared volume absorptivity of metals—535(L)
Honig, A. Polarization of As nuclei in Si semiconductor—234(L)
——, **C. H. Townes, M. L. Stitch, and M. Mandel.** Microwave spectra of alkali halides—629
Hornig, A. W., E. T. Jaynes, and H. E. Weaver. Observation of paramagnetic resonances in single crystals of $BaTiO_3$—1703(L)
Horton, G. K. and E. Phibbs. Effect of nuclear charge on internally produced pairs—1066
Horwitz, Nahmin. α-particles in primary cosmic rays—834(T)
Hoskins, Raymond and George Wiener. Ferromagnetic resonance in Fe-Ni alloys—1153(L)
Hosler, W. R. (see Blunt, R. F.)—576; 578
—— (see Breckenridge, R. G.)—571
Hossain, A. (see Freemantle, R. G.)—1268
Howard, B. T., H. F. Ivey, and W. Lehmann. Voltage dependence of electroluminescent brightness—799(L)
Howell, Erle, Jr. (see Neddermeyer, S. H.)—853(A)
Howland, J. J., Jr. (see Rubinson, William)—1610
Hsieh, Yü-Chang (see Bloch, Ingram)—382; 855(A)
Hubbs, J. C. (see Hobson, J. P.)—1450(L)
Hudson, R. P. (see Ambler, E.)—907
Hudspeth, Emmett L. (see Rickard, James A.)—1272
Hugenholtz, N. M. Variational principle in quantum mechanics—1158(L)
Huggett, R. W. (see Kim, Y. B.)—229(L)
Hughes, D. J. (see Carter, R. S.)—113
Huizenga, J. R. and C. M. Stevens. New long-lived isotopes of Pb—548(L)
—— (see Magnusson, L. B.)—1576
—— (see Studier, M. H.)—545(L)
Hull, G. W. and T. H. Geballe. Thermal conductivity of single crystalline Si—846(A)
—— (see Geballe, T. H.)—846(A)
Hull, M. H., Jr. and A. M. Saperstein. Formula for polarization in p-p scattering for P and F waves—806(L)
—— (see Breit, G.)—807(L)
—— (see Daitch, P. B.)—1449(L)
Hung, C. S. and J. R. Gliessman. Resistivity and Hall effect of Ge at low temperatures—1226
Hunt, D. J. (see Charles, G. W.)—838(A)
Hurst, G. S. (see Melton, C. E.)—643
Hutchison, Dwight A. Natural abundance of Li isotopes—1018
Hyde, Earl K. (see Mathur, Hirdaya B.)—126
Hyman, Morton A. Correlation function in Burgers' model of turbulence—821(A)

Ivey, H. F. (see Howard, B. T.)—799(L)

Jackson, J. L. and M. C. Yovits. Properties of quantum statistical impedance—15
Jacobsohn, Boris A. Nuclear fine structure in the μ-mesonic atom—1637
—— (see Chang, C. H.)—856(A)
Jahn, H. A. Direct evaluation of fractional parentage coefficients using Young operators. General theory and $\langle 4|2,2\rangle$ coefficients—989
James, D. B., W. Kubelka, and S. A. Heiberg. Pulse amplitude distribution in BF_3 counter irradiated with 4.87-Mev neutrons—856(A)
—— (see Erdman, K. L.)—858(A)
—— (see Warren, J. B.)—857(A)
Jarvis, R. G. (see Craig, D. S.)—825(A)
Jauch, J. M. S-operator in quantum electrodynamics—830(T)
Javan, Ali and A. Engelbrecht. Microwave absorption spectra of MnO_3F and ReO_3Cl—649
Jaynes, E. T. (see Hornig, A. W.)—1703(L)
Jen, C. K. and N. W. Lord. Color-center magnetic resonances in LiF—1150(L)
Jenny, Dietrich A. and Richard H. Bube. Semiconducting CdTe—1190
Jensen, Harald C. and Robert J. Cashman. Distribution of trapping levels in CdSe—798(L)
Jentschke, W. K., A. C. Juveland, and G. H. Kinsey. α-emitting isomer Po^{211}—231(L)
—— (see Eby, F. S.)—911
—— (see Zimmerman, E. J.)—1322
Jeppson, M. R. (see Andrew, A.)—843(A)
Johansson, Sven A. E. Decay of UX_1, UX_2, and UZ—1075
Johns, M. W. and S. V. Nablo. Disintegration of Ir^{188} and Ir^{194}—1599
Johnson, C. H., H. B. Willard, and J. K. Bair. Total cross section of Li^6 for neutrons—985
Johnson, C. M. P. (see Jones, G. A.)—547(L)
Johnson, Kenneth A. Nucleon-antinucleon scattering and vacuum polarization—1659
Johnston, Herrick L. (see Hoch, Michael)—839(A)
Johnston, Lawrence H., Norton M. Hintz, and Harry J. Schulte. Measurement of phase noise in pre-excited oscillator system—835(A)
—— (see Tucker, Edmund B.)—835(A)
Joki, E. G. and J. E. Evans. Hf and Zr total cross-section measurements—849(A)
Jones, G. A., W. R. Phillips, C. M. P. Johnson, and D. H. Wilkinson. Some properties of nuclei of mass 19—547(L)
Jordan, K. C. (see Eichelberger, J. F.)—719
Jordan, W. C., S. B. Burson, and J. M. LeBlanc. Decay of $_{22}Ti^{51}$ (5.8 min)—1582

—— (see Burson, S. B.)—1555
Jorgensen, Theodore, Jr. Comparison of proton energy loss by integral and differential experiments—835(A)
Joshi, M. C. and B. V. Thosar. γ-ray energies in decay of Cs^{134}—1022
Jossem, E. L. and L. G. Parratt. Electron energy levels in ionic crystals—834(A)
Julian, A. (see Feld, B. T.)—1386
Jung, J. J. and C. K. Bockelman. Energy levels of Be^{10}—1353
Juveland, A. C. (see Jentschke, W.)—231(L)

Kahn, David (see Groetzinger, Gerhart)—887
Kalkstein, M. I. and J. M. Hollander. New chain Ba^{139}—Cs^{139}—730
Kallmann, Hartmut (see Furst, Milton)—902
Kambe, K. and J. H. Van Vleck. g factors of ^3P terms of atomic O—845(A)
—— **and J. H. Van Vleck.** Improved theory of Zeeman effect of atomic O—66
Kanal, L. (see Clark, K. C.)—860(A)
Kane, J. A. (see Fields, T. H.)—812(L)
Kaplan, J. (see Brook, M.)—1540
Kaplan, Jerome I. Rf-induced transitions of nuclear spins at electronic resonance frequency—238(L)
Kaplon, M. F., J. H. Noon, and G. W. Racette. Abundance of Li, Be, and B in primary cosmic radiation—1408
Keck, J. C., A. V. Tollestrup, and W. R. Smythe, II. High-energy photodisintegration of deuteron—850(A)
—— (see Tollestrup, A. V.)—850(A)
Keepin, G. R. (see Koontz, P. G.)—862(A)
Keesom, P. H. and N. Pearlman. Atomic heat of Bi between 1° and 4°K—897
Keffer, Frederic. Relaxation processes in ferromagnetic resonance—857(T)
—— (see Eisele, J. A.)—929
Keister, Glenn L. Internal conversion coefficients in decay of Mn^{52}, Co^{60}, and Sc^{46}—855(A)
Keller, Joseph B. Electrohydrodynamics. I. Equilibrium of charged gas in container—843(A)
Kelly, Howard R. Incompressible laminar boundary layer on spinning cylinder at small angles of attack—847(A)
—— (see Dunn, Eldon L.)—847(A)
Kenney, N. T. (see Fine, M. E.)—1487
Kerman, R. O. (see Zimmerman, E. J.)—1322
Kern, B. D. (see Givin, H. H.)—1337
Kerr, Eugene C. Orthobaric densities of He^3, 1.3°K to 3.2°K—551
Keshishian, V., H. W. Kruse, R. J. Klotz, and C. M. Fowler. Energy levels in $_{66}Dy^{160}$—1050
Kikuchi, Ryoichi. λ Transition of liquid He—563
Kim, Y. B., J. R. Burwell, R. W. Huggett, and R. W. Thompson. Magnetic cloud chamber study of V^s events—229(L)
King, D. T., W. Wada, and M. M. Block. Direct creation of electron pairs by electrons of great energy. I. Experimental observations—852(A)
—— (see Block, M. M.)—853(A); 1627
—— (see Wada, W.)—852(A)
Kinoshita, Toichiro. Families of spinor fields—199
Kinsey, G. H. (see Jentschke, W.)—231(L)
Kip, A. F. (see Dexter, R. N.)—222(L)
Kittel, C. and A. H. Mitchell. Theory of donor and acceptor states in Si and Ge—1488
—— (see Ruderman, M. A.)—99
Kjeldaas, T., Jr. (see Hickam, W. M.)—63
Klein, Martin J. and Paul H. E. Meijer. Principle of minimum entropy production—250
Kline, R. M. and D. J. Zaffarano. Decay characteristics of some short-lived nuclides of low atomic number—1620
Klotz, R. J. (see Keshishian, V.)—1050
Knight, W. D. Temperature dependence of nuclear resonance in metals—861(A)
—— (see Cotts, R. M.)—1285
—— (see Teeters, D. R.)—861(A)
Kochendorfer, D. B. and Donald J. Farmer. Decay of Rh^{102}—855(A)
Kofoed-Hansen, O. Neutrino recoil spectrometer. Investigation of A^{37}—1045
Kohman, Truman P. (see Simanton, James R.)—1711(L)
Kohn, W. Interaction of conduction electrons and nuclear magnetic moments in metallic Li—590
—— **and J. M. Luttinger.** Quantum theory of cyclotron resonance in semiconductors—529(L)
—— (see Luttinger, J. M.)—802(L)
Koide, Shoichiro (see Ôno, Kazuo)—38
Kolchin, Eleanor K. (see Green, Louis C.)—319
Koontz, P. G., G. R. Keepin, and J. E. Ashley. ZnS(Ag) phosphor mixtures for neutron detection—862(A)
Koster, G. F. and J. C. Slater. Simplified impurity calculation—1208
Kovacs, Julius S. Final-state interaction in multiple production of mesons in nucleon-nucleon collisions—1454(A)
Krafft, Joseph M. Effect of surface friction on high-speed penetration—822(A)
Krasnow, M. E. (see Lassettre, E. N.)—832(A)
Kreger, W. E. K-capture to positron ratio for Na^{22}—1554
—— **and C. Sharp Cook.** γ radiation from Ce^{144} and Pr^{144}—855(A); 1279
—— **and C. Sharp Cook.** K-capture/positron ratio of Na^{22}—855(A); 1279
—— (see Cook, C. Sharp)—855(A)
Kroll, Norman M. (see Wichmann, Eyvind)—232(L)
Kronheimer, Erwin H. Multi-parameter nuclear wave functions in central-field approximation—1680
Kruger, P. Gerald (see Zimmerman, E. J.)—1322
Krumbein, A. D. (see Wiser, Herbert L.)—831(A)
Krumhansl, J. A., Jr. Elementary processes in semiconductor emitters—839(T)
Kruse, H. W. (see Keshishian, V.)—1050
Kubelka, W. (see James, D. B.)—856(A)
Kunz, W. E. (see Moak, C. D.)—1363
Kuper, A., H. Letaw, Jr., L. Slifkin, E. Sonder, and C. T. Tomizuka. Self-diffusion in Cu—1224
Kurbatov, J. D. (see Sakai, M.)—826(A); 862(A)
Kurşunoğlu, Behram. Tamm-Dancoff methods and nuclear forces—1690

Lafferty, D. L., L. A. Rayburn, and T. M. Hahn. Inelastic neutron scattering in Fe—381
Lagergren, C. Robert. Applications of rapid sweeping to single-focusing mass spectrometer—823(A)
Lamantia, Anthony J. (see Hoch, Michael)—839(A)
Landauer, Joseph K. Elastic moduli of Sn at superconducting transition—296
Landon, H. H. (see Sailor, V. L.)—1014
Landsberg, P. T. Method of transition probabilities in quantum mechanics and quantum statistics—1420
—— (see Ansbacher, F.)—1707(L)
Lane, A. M. (see Elliott, J. P.)—1160(L)
Langer, L. M. (see Plassmann, E. A.)—1593
Lasser, Marvin E. and Henry Levinstein. Optical properties of PbTe—47
Lassettre, E. N., M. E. Krasnow, and S. Silverman. Excitation by electron impact of optically forbidden transition $1^1S \rightarrow 2^1S$ in He—832(A)
Laurie, K. A. (see Warren, J. B.)—857(A)
Lauritsen, C. C. (see Barnes, C. A.)—851(A)
—— (see Peterson, R. W.)—1250
—— (see Webb, T. S.)—851(A)

Lawrence, Samuel C., Jr. Electromagnetic radiations from hydrocarbon flames—860(A)
Lawrence, W. (see Nelson, E. B.)—825(A)
Lax, Benjamin (see Dexter, R. N.)—222(L); 223(L)
Lax, Melvin and Joel L. Lebowitz. Moment singularity analysis of vibration spectra—594
Lazarus, J. P. (see Daitch, P. B.)—1449(L)
Leachman, R. B. and H. W. Schmitt. Fine structure in velocity distributions of slowed fission fragments—1366
Leamer, R. D. and G. W. Hinman. Internal conversion in Ne^{20}—1607
LeBlanc, J. M. (see Burson, S. B.)—1555
—— (see Jordan, W. C.)—1582
Lebowitz, Joel L. (see Lax, Melvin)—594
Leder, L. B. Low-energy-loss interaction of electrons with solids—823(T)
Legvold, Sam (see Rossing, Thomas)—839(A)
Lehmann, W. (see Howard, B. T.)—799(L)
Lehovec, Kurt. Theory of electric breakdown in high-temperature region and its relation to thermionic emission—921
Leies, G. (see Reynolds, D. C.)—533(L)
Leinhardt, T. E. (see Reynolds, J. M.)—1203
Leipuner, L. (see Stearns, M. B.)—804(L)
Letaw, H., Jr. (see Kuper, A.)—1224
Levengood, W. C. Study of moisture condensation patterns on glass and crystalline surfaces—1454(A)
Levine, M. M. (see Cabrera, N.)—1153(L)
Levinstein, Henry (see Bode, Donald E.)—259
—— (see Lasser, Marvin E.)—47
Lewis, Margaret N. (see Green, Louis C.)—319
Li, C. W. and R. Sherr. Inelastic scattering of α particles by Li—389
—— (see Sherr, R.)—1258
Lindemann, W. W. Influence of different activating agents on flicker noise in oxide-coated cathodes—837(A)
Ling, Daniel S., Jr. Expansion of wave packets—216
Linsley, John. Heavy cosmic-ray nuclei—829(A)
Litherland, A. E., E. B. Paul, G. A. Bartholomew, and H. E. Gove. Neutrons from reaction $C^{14}(p,n)N^{14}$—825(A)
—— (see Bartholomew, G. A.)—1154(L)
—— (see Gove, H. E.)—825(A)
Liuima, F. A., A. V. Bushkovitch, and A. G. Rouse. Pressure broadening of OCS in foreign gas mixture—434
Livingston, Ralph (see Zeldes, Henry)—1702(L)
Lofgren, E. J. Preliminary operation of bevatron—838(T)
Logan, R. A. and M. Schwartz. Thermal effects on lifetime of minority carriers in Ge—46
Long, Alton L. (see Simanton, James R.)—1711(L)
Lord, J. J. (see Fleming, John R.)—852(A)
—— (see Hoard, R. F.)—854(A)
—— (see Orear, Jay)—174
Lord, N. W. (see Jen, C. K.)—1150(L)
Low, F. E. Scattering of light of very low frequency by systems of spin $\frac{1}{2}$—1428
Lowen, R. W. Phase-shift analysis of elastic scattering of protons by He^3—826(A)
Lu, D. C. (see Slattery, R. E.)—465
Luttinger, J. M. and W. Kohn. Hyperfine splitting of donor states in Si—802(L)
—— (see Kohn, W.)—529(L)
Luyten, W. J. White dwarfs and degenerate stars—824(T)

MacDonald, D. K. C. (see Dugdale, J. S.)—57
MacDonald, William M., III, and John M. Richardson. Approximate variational principle in quantum statistics—18
Mace, David (see Green, Louis C.)—319
Mador, I. L., R. F. Wallis, M. C. Williams, and R. C. Herman. Production and bleaching of color centers in x-rayed alkali halide crystals—617
Magnusson, L. B., M. H. Studier, P. R. Fields, C. M. Stevens, J. F. Mech, A. M. Friedman, H. Diamond, and J. R. Huizenga. Bk and Cf isotopes produced in neutron irradiation of Pu—1576
Mahon, H. P. (see Dunlap, W. C., Jr.)—822(A)
Maita, J. P. (see Morin, F. J.)—28; 833(A)
Mandel, M. (see Honig, A.)—629
Mann, K. C. Nuclear spectroscopy—857(T)
Manring, Edward R. (see Ting, Yu)—408
Many, A. (see Braun, E. A.)—1505
Mapes, Joe M. (see Allen, William A.)—844(A)
Mapleton, Robert A. Cross-section theorem—415
Mapother, D. E. (see Mould, R. E.)—797(L)
Mara, R. T., G. B. B. M. Sutherland, and H. V. Tyrell. Infrared spectrum of $BaTiO_3$—801(L)
Marburger, R. E. (see Reynolds, D. C.)—533(L)
Marinace, John C. Electrical properties of natural crystals of iron pyrite—593
Marmier, P. E. (see Murray, J. J.)—858(A)
Marshall, J. (see de Carvalho, H. G.)—1081
Marshall, J. F. (see Shatas, R. A.)—1199
Marshall, L. (see de Carvalho, H. G.)—1081
Martin, A. E. (see Swalin, R. A.)—840(A)
Martin, D. W. (see Grimes, D. M.)—889
Mason, W. P. Derivation of magnetostriction and anisotropic energies for hexagonal, tetragonal, and orthorhombic crystals—302
Mather, R. L. (see Andrew, A.)—843(A)
Matheson, W. E., C. R. Carlson, F. S. Mathews, R. O. Haxby, and R. M. Whaley. Cloud-chamber investigation of high-energy photonuclear reactions—826(A)
Mathews, F. S. (see Matheson, W. E.)—826(A)
Mathur, Hirdaya B. and Earl K. Hyde. Spectrometer studies of radiations of some neutron-deficient isotopes of Xe and I—126
Matland, C. G. (see McCoubrey, A. O.)—832(A)
Mawardi, O. K. Turbulent boundary layer noise—857(T)
Maxwell, J. G. (see Silvidi, A. A.)—1454(A)
Maxwell, Louis R. and Stanley J. Pickart. Magnetic and crystalline behavior of certain oxide systems with spinel and perovskite structures—1501
McAllister, R. (see Hofstadter, R.)—854(A)
McClure, G. W. Composition of primary cosmic radiation at $\lambda=10°$N—1391
McCormick, G. H. and B. L. Cohen. Fission and total reaction cross sections for 22-Mev protons on Th^{232}, U^{235}, and U^{238}—722
McCoubrey, A. O. and C. G. Matland. Diffusion of metastable Hg molecules—832(A)
McEllistrem, M. T. (see Galonsky, A.)—826(A)
McIntyre, J. A. and R. Hofstadter. Electron scattering from H, deuterium, and C at 190 Mev—854(A)
McKeown, M. (see Mihelich, J. W.)—1450(L)
McLaughlin, Ralph D. (see Conway, John G.)—541(L)
Mech, J. F. (see Magnusson, L. B.)—1576
Meijer, Paul H. E. (see Klein, Martin J.)—250
Meinel, A. B. Particle-induced laboratory auroral phenomena—860(T)
Melton, C. E., G. S. Hurst, and T. E. Bortner. Ionization produced by 5-Mev α particles in A mixtures—643
Merritt, M. L. and J. R. Banister. Two-fluid flow with application to dust-laden air—848(A)
Merz, W. J. Domains and their formation in $BaTiO_3$ single crystals—819(T)
Meservey, Edward. Neutron-capture cross sections by capture-γ counting—1006
Messel, H. (see Chartres, B. A.)—1651
Meyer, Peter and J. A. Simpson. Changes in amplitude of cosmic-ray 27-day intensity variation with solar activity—1085

Mickelwait, A. B. and H. C. Corben. Vacuum polarization in mesonic atoms—1145
Mihelich, J. W., M. McKeown, and M. Goldhaber. *E*3 isomer in Ir^{193}—1450(L)
Mileikowsky, Curt and Katarina Ahnlund. Proton groups from reaction $O^{18}(d,p)O^{19}$—996
Miller, L. G. (see Smith, G. L.)—849(A)
Miller, William, J. W. Motz, and Carmen Cialella. Thick target bremsstrahlung spectra for 1.00-, 1.25-, and 1.40-Mev electrons—1344
—— (see Motz, J. W.)—544(L)
Mills, R. L. (see Yang, C. N.)—191
Milner, Paul C. (see Green, Louis C.)—319
Milton, J. C. D. and J. S. Fraser. Response of NaI(Tl), KI(Tl), and stilbene to fission fragments—1508
Mitchell, A. H. (see Kittel, C.)—1488
Mitchell, T. P. (see Plesset, M. S.)—848(A)
Mize, J. P., M. E. Bunker, and J. W. Starner. Radiations from Ir^{189m}—444
—— (see Browne, C. I.)—827(A)
Moak, C. D., W. M. Good, and W. E. Kunz. Charged particles from the bombardment of Li^7 by He^3—1363
Moffat, R. D. (see Bittner, J. W.)—374
Moljk, A. and S. C. Curran. β spectra of C^{14} and S^{35}—395
Monchick, Louis and Howard Reiss. Evaporation of small drops at low pressures—839(A)
Moore, George E., L. A. Wooten, and James Morrison. Excess Ba content of emitting oxide-coated cathodes—840(A)
—— (see Allison, H. W.)—840(A)
—— (see Wooten, L. A.)—840(A)
Moore, Richard L. Spins of excited states of some odd-*A* nuclei according to collective model—858(A)
—— (see Browne, C. I.)—827(A)
Morin, F. J. and J. P. Maita. Electrical properties of Si containing As and B—28
——, **J. P. Maita, R. G. Shulman, and N. B. Hannay.** Impurity levels in Si—833(A)
Morrison, H. L. (see Backman, M. E.)—844(A)
Morrison, James (see Moore, George E.)—840(A)
Moses, H. E. Application of variational principles to scattering problems—519
Motz, J. W. and William Miller. Differential cross-section measurements for 1-Mev bremsstrahlung—544(L)
—— (see Miller, William)—1344
Mould, R. E. and D. E. Mapother. Effect of precipitation hardening on superconducting transition of Al alloy—797(L)
Moyer, B. J. (see Hess, W. N.)—859(A)
—— (see Squire, R. K.)—856(A)
—— (see Waddell, Charles)—858(A)
—— (see Cohen, David)—714
Mulder, Marjorie M. (see Green, Louis C.)—319
Muller, B. H. and Myer Bloom. Nuclear spin lattice relaxation in supercooled menthol—861(A)
Müller, Erwin W. Work functions of W single-crystal planes—837(A)
Murakawa, Kiyoshi. Hfs of spectra of Nd and Gd—1543
Murray, B. (see Sakai, M.)—826(A); 862(A)
Murray, F. J. Order-disorder problem for cubic lattice—822(A)
Murray, J. J., P. Snelgrove, P. E. Marmier, and J. W. M. DuMond. Decay of Ta^{180}—858(A)

Nablo, S. V. (see Johns, M. W.)—1599
Naugle, J. E., P. S. Freier, and E. P. Ney. Example of unstable nuclear fragment being emitted from heavy-meson induced star—829(A)
——, **H. P. Ney, P. S. Freier, and W. B. Cheston.** Interaction of negative heavy meson—1383
—— (see Ney, E. P.)—829(A)
Naugle, J. S. (see Danielson, R. E.)—829(A)
Naumann, Robert A. Identification of Pt^{188}—90
—— **and J. B. Gerhart.** 5.6-second Ir^{191m} following Os^{191} decay—1452(L)
Neddermeyer, S. H. and Erle Howell, Jr. Electromagnetic events of high-energy particles at sea level—853(A)
Nelson, E. B., W. Lawrence, and R. R. Carlson. γ rays from proton capture in Li^7 and F^{19}—825(A)
Nergaard, L. S. Experiments bearing on mobile-donor hypothesis in oxide cathodes—839(T)
Neufeld, Jacob. Electron capture and loss by moving ions in dense media—1470
Newman, Roger. Optical studies of injected carriers. III. Infrared absorption in Ge at low temperatures—1188
—— **and W. W. Tyler.** Properties of Ge doped with Fe. II. Photoconductivity—882
Newton, J. O. γ radiation from reactions $Na^{23}+p$—241(L)
Newton, Roger G. Radiative effects in constant field—523
Ney, E. P., John Naugle, and Phyllis Freier. Densitometric measurement of emulsion tracks—829(A)
—— (see Danielson, R. E.)—829(A)
—— (see Naugle, J. E.)—829(A)
Ney, H. P. (see Naugle, J. E.)—1383
Nierenberg, W. A. (see Hobson, J. P.)—1450(L)
Nodvick, John S. and David S. Saxon. Suppression of coherent radiation by electrons in synchrotron—180
Nodwell, R. A. and A. M. Crooker. Spectra of indium—845(A)
Noon, J. H. (see Kaplon, M. F.)—1408
Novey, T. B. α-γ directional correlation measurements with liquid film sources—547(L)
Nussbaum, Allen. Computation of mobility ratio in pure *p*-type semiconductors—828(A)

Odian, A. C. (see Feld, B. T.)—1386
Okazaki, A., R. L. Becker, and H. H. Barschall. Scattering of polarized neutrons from heavy nuclei—836(A)
Okumura, Koji. Uv absorption in BaO films—1704(L)
Olbert, Stanislaw. Production spectra of cosmic-ray mesons in atmosphere—1400
Olson, Elmer L. (see Handley, Thomas H.)—1003
Ôno, Kazuo, Shoichiro Koide, Hisao Sekiyama, and Hidetaro Abe. Paramagnetic resonance in chromous sulfate pentahydrates—38
Opitz, W. (see Siegel, R. T.)—859(A)
Orear, Jay. Low-energy behavior of phase shifts in pion-proton scattering—176
—— Measurement of Coulomb interference in 113-Mev π^+-p scattering—1417
——, **R. G. Glasser, D. M. Haskin, and Marcel Schein.** High-energy electron pair produced by 113-Mev positive pion—1710(L)
——, **William Slater, J. J. Lord, S. L. Eilenberg, and A. B. Weaver.** Elastic scattering of 26-Mev negative pions by H in emulsion—174
Orr, S. R. (see Eichelberger, J. F.)—719
Osborne, L. S. (see Feld, B. T.)—1386
Osher, J. E. (see Squire, R. K.)—856(A)
Oshinsky, W. (see Breckenridge, R. G.)—571
Oswald, A. (see Forster, H. H.)—1030

Palfrey, T. R. (see Voss, J. R.)—830(A)
Parker, Eugene N. Tensor virial equations—1686
Parks, J. R. (see Eichelberger, J. F.)—719
Parratt, L. G. and C. F. Hempstead. Universal curves for dispersion and scattering of x-rays—820(A)
—— (see Jossem, E. L.)—834(A)
Parzen, G. and T. Wainwright. Relativistic Coulomb scattering of electrons and positrons—188

Paskin, Arthur. Contact electrification effects in metal-metal system. I. General theory—819(A)
Paul, E. B. (see Bartholomew, G. A.)—1154(L)
—— (see Gove, H. E.)—825(A)
—— (see Litherland, A. E.)—825(A)
Paul, Ronald S. γ-ray absorption coefficients at 6.13 Mev—1563
Pearlman, N. (see Keesom, P. H.)—897
Pearson, John and John S. Rinehart. Application of engravement method to study of particle velocity distribution in explosively loaded cylinders—844(A)
Pepper, J. H. (see Gilbert, W. S.)—862(A)
Pepper, T. P. (see Allen, K. W.)—684
Percus, J. K. Quantization of multiple frequency linear systems—1147
Peria, W. T. Optical absorption spectra of stoichiometric single crystals of MgO—824(A)
Perlman, I. (see Stephens, Frank, Jr.)—1568
Peterson, R. W., D. E. Anderson, and W. G. Shepherd. Applications of radioactive tracer techniques to study of thermionic emission of oxide-coated cathodes—840(A)
Peterson, R. W., W. A. Fowler, and C. C. Lauritsen. Fluorine-plus-proton reactions—1250
—— (see Barnes, C. A.)—851(A)
Peterson, Vincent. Photostar production up to 500 Mev—850(A)
—— **and I. George Henry.** Photoproduction of mesons from H near threshold—850(A)
Petrow, Henry G. and Gregory Rocco. Fission yield of Gd^{159} and Tb^{161}—1614
Phelps, A. V. Absorption studies of He metastable molecule—832(A)
Phibbs, E. (see Horton, G. K.)—1066
Philipp, H. R. Photoelectric emission from BaO—827(A)
Phillips, R. J. N. Renormalization of a neutral vector meson interaction—1678
Phillips, Robert H. and Kenneth M. Crowe. Indirect measurement of n-n interaction—484
—— (see Crowe, Kenneth M.)—470
Phillips, W. R. (see Jones, G. A.)—547(L)
Pickart, Stanley J. (see Maxwell, Louis R.)—1501
Pidd, R. W. Determination of nuclear radii by electron scattering—821(T)
Pilcher, V. E. (see Carter, R. S.)—113
Pinnick, H. T. Magnetic susceptibility of residual bisulfate compounds of C—832(A)
Pish, G. (see Charles, G. W.)—838(A)
Plaskett, J. S. (see Cabrera, N.)—1153(L)
Plassmann, E. A. and L. M. Langer. β spectrum of RaE—1594
Plesset, M. S. and T. P. Mitchell. Stability of spherical shape of vapor cavity in liquid—848(A)
Pomerantz, M. A. (see Shatas, R. A.)—1199
Porter, Charles E. Neutron cross sections of light nuclei—836(A)
—— (see Feshbach, H.)—448
Posener, D. W. and M. W. P. Strandberg. Centrifugal distortion in asymmetric top molecules. III. H_2O, D_2O, and HDO—1714(E)
Powell, J. L. (see Barschall, H. H.)—713
Preston, M. A. and J. Shapiro. Calculations on charge independence with repulsive core potentials—813(L)
Pringle, D. H. and W. E. J. Farvis. Electron groups in He negative glow—536(L)
Proctor, W. G. (see Blood, H. L.)—861(A)
Prowse, D. J. (see Freemantle, R. G.)—1268; 1270
Pruett, C. H. and R. G. Wilkinson. Disintegration of Ce^{139}—1340
Quisenberry, K. S., T. T. Scolman, and T. L. Collins. Stabilization of potentials in precision double-focusing mass spectrometer—823(A)
Rabinowitz, Philip (see Abramowitz, Milton)—77
Racette, G. W. (see Kaplon, M. F.)—1408
Ramsey, N. F. Recent cyclotron experiments at Harvard University—838(T)
—— (see Hillman, Peter)—115
—— (see Stahl, R. H.)—1310
Rankin, D. (see Brown, R. J. S.)—80
Rasmussen, V. K., John R. Rees, M. B. Sampson, and N. S. Wall. Search for 15-Mev γ radiation from $N^{14}+d$ and $Be^9+\alpha$—812(L)
Rau, R. Ronald (see Arnold, W. H.)—853(A)
—— (see Hodson, A. L.)—1089
Ravenhall, D. G. and D. R. Yennie. Results of phase shift calculation of high-energy electron scattering—239(L); 1714(E)
Rayburn, L. A. (see Lafferty, D. L.)—381
Recksiedler, Arthur L. and Bernard Hamermesh. Two-step cascades in Cl^{36} and Cd^{114} neutron-capture γ-ray spectra—109
Reddie, J. S. (see Roesch, W. C.)—854(A)
Redington, R. W. (see Damon, R. W.)—1498
Rees, John R. (see Rasmussen, V. K.)—812(L)
Reeves, M. L. and Ronald Geballe. Dc prebreakdown currents in gases of high dielectric strength—862(A)
Reid, A. T. Age-dependent branching stochastic processes in cascade theory—751
Reines, F., C. L. Cowan, Jr., and M. Goldhaber. Conservation of number of nucleons—1157(L)
—— (see Cowan, C. L., Jr.)—1294
—— (see Harrison, F. B.)—1159(L)
Reinitz, K. (see Cegelski, W. M.)—828(A)
Reiss, Howard (see Glazer, H.)—838(A)
—— (see Saltsburg, Howard)—838(A)
Rexer, E. F. (see Balas, W.)—840(A)
Reynolds, D. C. and S. J. Czyzak. Mechanism for photovoltaic and photoconductivity effects in activated CdS crystals—1705(L)
——, **G. Leies, L. L. Antes, and R. E. Marburger.** Photovoltaic effect in CdS—533(L)
Reynolds, George T. (see Arnold, W. H.)—853(A)
—— (see Hodson, A. L.)—1089
Reynolds, H. L. and A. Zucker. Excitation functions for N-induced nuclear reactions in C—1615
—— **and A. Zucker.** Range of N ions in emulsion—393
—— (see Cohen, B. L.)—1617
Reynolds, J. M., H. W. Hemstreet, T. E. Leinhardt, and D. D. Triantos. Hall effect in Bi—1203
—— **and D. D. Triantos.** Temperature dependence of periodic Hall effect in Bi—822(A)
Rice, O. K. Heat and entropy of mixing of He^3 and He^4 on the basis of the two-fluid theory of He^4—1464
—— Shape of coexistence curve of two-phase systems near critical point—838(A)
—— Statistical mechanics of He II near 1°K—1460
Richardson, John M. (see MacDonald, William M., III)—18
Richardson, J. Reginald (see Green, David)—858(A)
Richter, B. (see Bitter, F.)—1531
Rickard, James A., Emmett L. Hudspeth, and William W. Clendenin. Excitation curve for $C^{14}(d,p)C^{15}$ and properties of C^{15}—1272
Riess, Howard (see Monchick, Louis)—839(A)
Rightmire, Robert A. (see Simanton, James R.)—1711(L)
Rinehart, John S. (see Pearson, John)—844(A)
Rittner, E. S. Use of p-n junctions for solar energy conversion—1708(L)

Roberts, B. W. and C. P. Bean. Large magnetic Kerr rotation in BiMn alloy—1494
Rocco, Gregory (see Petrow, Henry G.)—1614
Roe, G. M. and R. H. Stark. Numerical solution of diffusion equation in cylindrical geometrics—820(A)
Roesch, W. C. and J. S. Reddie. Geiger-Mueller counter tube age characteristics—854(A)
Rohrlich, F. Formal and methodological aspects of present quantum electrodynamics—830(T)
Rojansky, V. (see Baker, T. E., Jr.)—828(A)
—— (see Cegelski, W. M.)—828(A)
Rosen, Philip. Entropy of radiation—555
Rosenfeld, A. H. Production of charged pions from H and C—130; 1714(E)
—— Production of pions in nucleon-nucleon collisions at cyclotron energies—139
Rossing, Thomas and Sam Legvold. Excitation of molecular vibrations in halogen-substituted methanes—839(A)
Rotblat, J. (see Freemantle, R. G.)—1268; 1270
Rouse, A. G. (see Liuima, F. A.)—434
Rowen, J. H. and W. von Aulock. Measurement of complex tensor permeability of ferrites—1151(L)
Royden, Virginia. Measurement of spin and gyromagnetic ratio of C^{13} by collapse of spin-spin splitting—543(L)
Rubinow, S. I. Generalized variational principle for scattering amplitude—218
Rubinson, William and J. J. Howland, Jr. K-electron ejection in the β decay of S^{35}—1610
Ruderman, M. A. and C. Kittel. Indirect exchange coupling of nuclear magnetic moments by conduction electrons —99
Rudnick, I. Attenuation of very high amplitude sound waves —857(T)
Rushworth, F. A. (see Cegelski, W. M.)—828(A)
Ryan, A. H. (see Garstens, M. A.)—53

Sachs, R. G. (see Capps, R. H.)—540(L)
—— (see Holladay, W. G.)—810(L)
Sailor, V. L., H. H. Landon, and H. L. Foote, Jr. Neutron resonances in rare earth elements—1014
Sakai, M., B. Murray, and J. D. Kurbatov. Comparative study of γ spectrum of I^{131} with scintillation and thick lens spectrometer—826(A)
——, **B. Murray, and J. D. Kurbatov.** Disintegration of As^{76}—862(A)
Saltsburg, Howard and Howard Reiss. Kinetics of phase transitions for systems undergoing association: Monomer-dimer equilibrium—838(A)
Sampson, M. B. (see Rasmussen, V. K.)—812(L)
Sands, M., J. G. Teasdale, and R. L. Walker. Photoproduction of charged mesons from deuterium—849(A)
Saperstein, A. M. (see Breit, G.)—807(L)
—— (see Hull, M. H., Jr.)—806(L)
Sarabhai, V., U. D. Desai, and D. Venkatesan. Cycle of world-wide changes in daily variation of meson intensity —469
Satchler, G. R. Angular correlation of three nuclear radiations—1713(E)
Satterthwaite, C. B. (see Corak, W. S.)—1442(L)
Saxon, David S. (see Nodvick, John S.)—180
Scanlon, Wayne W. (see Brebrick, Robert F.)—598
Schaaf, S. A. (see Bell, S.)—848(A)
Schafroth, M. R. Superconductivity of charged boson gas —1149(L)
—— Theory of superconductivity—1442(L)
Schein, Marcel, D. M. Haskin, and R. G. Glasser. Nuclear collisions at extreme relativistic energies—829(A)
—— (see Orear, Jay)—1710(L)
—— (see Sprague, A. D.)—830(A)
Schellenbaum, Ralph and Jay Todd, Jr. Path of triple point for spherical shocks above a rigid plane—848(A)
——(see Todd, Jay, Jr.)—847(A)
Scherrer, V. E., B. A. Allison, and W. R. Faust. γ radiation from interaction of 3.2-Mev neutrons with various materials—386
Schiff, L. I. Nuclear multipole transitions in inelastic electron scattering—765
Schlegel, Richard. Relativistic statistical mechanics of ideal gas—820(A)
Schluter, R. A. Neutral pion-deuteron production in 400-Mev n-p collisions—734
Schmid, L. C. (see Cork, J. M.)—1295
Schmidt, F. H. Investigations with University of Washington cyclotron—849(T)
Schmitt, H. W. (see Leachman, R. B.)—1366
Schmitt, R. W. Electrical resistivity minimum reported in Cu-Zn alloys—1446(L)
—— **and M. D. Fiske.** Electrical resistivity minimum and structural defects in Cu—1445(L)
Schnepp, Otto (see Fox, David)—1196
Schrank, G., P. C. Gugelot, and I. E. Dayton. Direct interaction in $Fe^{56}(p,p')Fe^{56}$—1156(L)
Schulte, Harry J. (see Johnston, Lawrence H.)—835(A)
Schuman, R. P. Production of Nb^{93m} by pile irradiation of Nb—121
Schwartz, Manuel and Paul L. Copeland. Secondary emission by positive ion bombardment—1466
——. (see Logan, R. A.)—46
Schwed, Philip (see Groetzinger, Gerhart)—887
Sclar, N. (see Burstein, E.)—819(A)
Scolman, T. T. (see Quisenberry, K. S.)—823(A)
Seagrave, John D. Elastic and inelastic scattering of 14-Mev neutrons by deuterons—855(A)
Seaton, N. T. Absolute differential range spectrum of low-energy cosmic-ray μ mesons—853(A)
Segrè, E. (see Chamberlain, O.)—807(L)
Sekiyama, Hisao (see Ôno, Kazuo)—38
Sengupta, S. Nuclear electric quadrupole moment of Na^{23} —235(L)
Serin, B. Structure of intermediate state of superconductors —228(L)
Sessler, A. M. Mesonic corrections to quadrupole moment of deuteron—793
—— **and H. M. Foley.** Statistical atom with angular momentum—366
Severiens, J. C. (see Fuller, C. S.)—21
Shamos, M. H. (see Fafarman, A.)—1096
Shapiro, J. (see Preston, M. A.)—813(L)
Sharp, R. A. and R. M. Diamond. New Ti nuclide: Ti^{44} —1713(E)
Shatas, R. A., J. F. Marshall, and M. A. Pomerantz. Emission of energetic secondary electrons produced by 1.3-Mev electron bombardment—1199
Shaw, C. H. (see Gordon, W. L.)—1444(L)
Shaw, Harlan, (see Cohen, David)—714
—— (see Waddell, Charles)—858(A)
Shepherd, W. G. (see Peterson, R. W.)—840(A)
Sherman, F. S. Low density wind tunnel study of shock-wave structure and relaxation phenomena in gases—852 (T)
Sherr, R., C. W. Li, and R. F. Christy. Coulomb excitation of F^{19} by α particles—1258
—— (see Li, C. W.)—389
Sherwood, J. E., T. E. Stephenson, and Seymour Bernstein. Stern-Gerlach experiment on polarized neutrons—1546
Shrader, Ross E. Excitation of ZnO phosphors by low-energy electrons—824(A)

Shull, F. B. and M. M. Bretscher. Angular distributions in (d,p) reactions with Ti^{47} and Ti^{48}—826(A)
—— (see Bretscher, M. M.)—103
Shulman, R. G., W. L. Brown, and R. C. Fletcher. Hole trapping due to lattice defects in Ge—833(A)
—— (see Hannay, N. B.)—833(A)
—— (see Morin, F. J.)—833(A)
Shurman, M. B. (see Benenson, R. E.)—836(A)
Siegel, R. T., A. J. Hartzler, and W. Opitz. Small-angle n-p scattering at 400 Mev—859(A)
Siegert, A. J. F. Theory of condensation—243
Silsbee, H. B. (see Hobson, J. P.)—1450(L)
Silverman, Richard A. and Martin Balser. Statistics of electromagnetic radiation scattered by turbulent medium—560
Silverman, S. (see Lassettre, E. N.)—832(A)
Silvidi, A. A. and J. G. Maxwell. β spectrum of Bi^{210} using diffusion cloud chamber—1454(A)
Simanton, James R., Robert A. Rightmire, Alton L. Long, and Truman P. Kohman. Long-lived radioactive Al^{26}—1711(L)
Simchen, A. E. (see Braun, E. A.)—1505
Simmons, B. E., D. M. Van Patter, K. F. Famularo, and R. V. Stuart. Coulomb excitation of Nd—826(A)
—— (see Van Patter, D. M.)—825(A)
Simpson, J. A. (see Meyer, Peter)—1085
Singer, L. S. (see Garstens, M. A.)—53
Singer, Sidney (see Zimmerman, E. J.)—1322
Sjöstrand, N. G. (see von Dardel, G.)—1245; 1567
Slater, J. C. (see Koster, G. F.)—1208
Slater, William (see Orear, Jay)—174
Slattery, R. E., D. C. Lu, and M. L. Wiedenbeck. Long-lived radioactivity of Eu^{153} and Eu^{154}—465
Slifkin, L. (see Kuper, A.)—1224
—— (see Tomizuka, C. T.)—610
Smith, F. Graham. Galactic and extra-galactic sources of radio waves—824(T)
Smith, G. L. and L. G. Miller. MTR crystal spectrometer data printing system—849(A)
Smith, H. L. (see Browne, C. I.)—827(A)
Smith, Lyle W. Research with cosmotron—838(T)
Smythe, W. R., II (see Keck, J. C.)—850(A)
—— (see Tollestrup, A. V.)—850(A)
Snelgrove, P. (see Murray, J. J.)—858(A)
Snyder, James, N. Determination of α-α scattering phase shifts—1333
Sonder, E. (see Kuper, A.)—1224
Speck, D. R. (see Woodward, E. C.)—529(L)
Sperduto, A., W. W. Buechner, C. K. Bockelman, and C. P. Browne. (d,p) reactions from C, N, and O—1316
Spicer, W. E. Luminescence from NaCl—824(A)
Sprague, A. D., D. M. Haskin, R. G. Glasser, and Marcel Schein. Comparison of proton and meson produced stars of comparable excitation energy—830(A)
Squire, C. F. (see Thompson, J. C.)—287
Squire, R. K., B. J. Moyer, and J. E. Osher. Čerenkov counter for electron detection—856(A)
Stadler, Henry L. Absorption of positive pions by deuterium at 76 and 94 Mev—496
Stahl, R. H. and N. F. Ramsey. n-p scattering at 91 Mev—1310
—— (see Hillman, Peter)—115
Stallwood, R. A. (see Fields, T. H.)—812(L)
Standil, S. Bursts in NaI(Tl) near sea level—777
Stanford, C. P., T. E. Stephenson, and Seymour Bernstein. Neutron spin from magnetic resonance experiment—983
—— (see Allen, R. G.)—1297
Stark, R. H. (see Roe, G. M.)—820(A)
Starner, J. W. (see Browne, C. I.)—827(A)
—— (see Mize, J. P.)—444
Stearns, M. (see Stearns, M. B.)—804(L)
Stearns, M. B., M. Stearns, S. DeBenedetti, and L. Leipuner. Energies of π^--mesonic x-ray K lines—804(L)
Steele, M. C. (see Babiskin, J.)—822(A)
Stein, Robert P. Back diffusion of electrons to plane emitting surface—862(A)
Stelson, P. H. Angular distributions of α-particles from the $Na^{23}(p,\alpha)Ne^{20}$ reaction—1584
Stephens, Frank, Jr., Frank Asaro, and I. Perlman. Low-lying 1− states in even-even nuclei—1568
Stephenson, T. E. (see Allen, R. G.)—1297
—— (see Sherwood, J. E.)—1546
—— (see Stanford, C. P.)—983
Stern, M. O. (see Ashkin, J.)—1104
Sternheimer, R. M. Electronic polarizabilities of ions from the Hartree-Fock wave functions—951
Stevens, C. M. (see Huizenga, J. R.)—548(L)
—— (see Magnusson, L. B.)—1576
Stevens, K. W. H. Electronic-lattice interaction in paramagnetic crystals—857(T)
Stevenson, J. R. Electronic structure of MgO—839(A)
Stewart, R. W. Hot-wire measurements of turbulence in ocean—847(A)
Stier, P. M., C. F. Barnett, and G. E. Evans. Charge states of heavy-ion beams passing through gases—973
Stitch, M. L. (see Honig, A.)—629
Stout, Virgil L. and Martin D. Gibbons. Gettering of vacuum vessel by Ti metal—819(A)
Strandberg, M. W. P. (see Posener, D. W.)—1714(E)
Stratton, T. F., K. F. Famularo, H. D. Holmgren, and R. V. Stuart. Excited state of O^{19}—825(A)
—— (see Brown, R. J. S.)—80
—— (see Van Patter, D. M.)—825(A)
Streib, J. F. (see Farmer, Donald J.)—855(A)
Stuart, R. V. (see Simmons, B. E.)—826(A)
—— (see Stratton, T. F.)—825(A)
Stubbins, Warren Fenton. Beam escape from synchrocyclotrons—856(A)
Studier, M. H. and J. R. Huizenga. Correlation of spontaneous fission half-lives—545(L)
—— (see Magnusson, L. B.)—1576
Stump, Robert and Harry E. Talley. Lifetime of positrons in superconducting Pb and Sn—904
Sturm, W. J. (see Binder, D.)—1519
Sutherland, G. B. B. M. (see Mara, R. T.)—801(L)
Sutton, R. B. (see Fields, T. H.)—812(L)
Suzuki, Tomizo (see Takayama, Kazuo)—531(L)
Swalin, R. A. and A. E. Martin. Solute diffusion in Ni—840(A)
Swami, M. S. (see Fry, W. F.)—235(L); 809(L)
Swan, P. Solution of many-body scattering problems by Fredholm's equation—1144
Swann, W. F. G. Acquirement of cosmic-ray energies by electromagnetic induction in galaxies—240(L)

Taft, E. and L. Apker. Fermi level in amorphous Sb films—1496
—— **and L. Apker.** Fermi level in semiconducting amorphous Sb films—827(A)
Takayama, Kazuo, Tomizo Suzuki, and Tadaichi Yabumoto. Hall effect in positive column—531(L)
Talley, Harry E. (see Stump, Robert)—904
Talmi, I. (see Carlson, B. C.)—436
Tanaka, Katsumi (see Coester, F.)—1142
Tannenwald, P. E. Microwave properties of Mn-ferrite single crystal—846(A)
Tautfest, G. W. and H. R. Fechter. Secondary electron yield from Al by high-energy primary electrons—35

Taylor, J. C. Calculation of potentials from new Tamm-Dancoff equation—1438
Teasdale, J. G. (see Sands, M.)—849(A)
Teeters, D. R. and W. D. Knight. Nuclear magnetic resonance in CuAl alloys—861(A)
Temmer, G. M. and N. P. Heydenburg. Coulomb excitation process in lighter odd-mass nuclei—426
Tessman, Jack R. Magnetic anisotropy at 0°K—1192
Thirion, Jacques, René Cohen, and Ward Whaling. Magnetic analysis of $O^{18}(d,p)O^{19}$ and $N^{15}(d,p)N^{16}$ reactions—850(A)
Thirring, W. (see Deser, S.)—774
Thomas, Virginia G. (see Crowe, R. W.)—10
Thompson, J. C. and C. F. Squire. Magnetization of Sn at superconducting transition—287
Thompson, L. C. γ radiation from deuterons on several light nuclei—369
Thompson, R. W. Recent results on V-particles—848(T)
—— (see Kim, Y. B.)—229(L)
Thompson, S. G. (see Hoff, R. W.)—1350
Thornton, W. A. Light output of luminescent plastics—292
Thosar, B. V. (see Joshi, M. C.)—1022
Timma, D. L. (see Charles, G. W.)—838(A)
Ting, Yu, Edward R. Manring, and Dudley Williams. Zeeman effects in Cl nuclear quadrupole resonance in $NaClO_3$—403
Todd, Jay, Jr., and Ralph Schellenbaum. Shape of shock wave derived from spherical shock wave incident on concave wedge—847(A)
—— (see Schellenbaum, Ralph)—848(A)
Tollestrup, A. V., J. C. Keck, and W. R. Smythe, II. High-energy photodisintegration of deuteron—850(A)
—— (see Keck, J. C.)—850(A)
—— (see Woodbury, H. H.)—1713(E)
Tomizuka, C. T. and L. Slifkin. Diffusion of Cd, In, and Sn in single crystals of Ag—610
—— (see Kuper, A.)—1224
Torrey, H. C. Nuclear spin relaxation by translational diffusion. II. Diffusion in b.c.c. lattice—690
Tove, P. A. (see Tyrén, H.)—773
Townes, C. H. (see Honig, A.)—629
Treiman, S. B. (see Arnold, W. H.)—853(A)
—— (see Hodson, A. L.)—1089
Triantos, D. D. (see Reynolds, J. M.)—822(A); 1203
Tripp, R. (see Chamberlain, O.)—807(L)
Trischka, J. W. and R. Braunstein. Rotational spectra of RbCl by molecular beam electric resonance method—968
Tucker, Edmund B., Lawrence H. Johnston, and Donald E. Young. 200-Mc phase detector—835(A)
Tweet, A. G. Grain-boundary conduction in Au-doped Ge—828(A)
—— (see Gallagher, C. J.)—834(A)
Tyler, W. W. Injection breakdown in Fe-doped Ge diodes—226(L)
—— **and H. H. Woodbury.** Properties of Ge doped with Fe. I. Electrical conductivity—874
—— (see Newman, R.)—882
Tyrell, H. V. (see Mara, R. T.)—801(L)
Tyrén, H. and P. A. Tove. Short-lived radionuclides produced by synchrocyclotron—773

Uehling, Edwin A. Relative contributions of K-shell and other electrons to stopping power of light and heavy elements—861(A)

Vaidya, P. C. Spherically symmetric solutions in nonsymmetrical field theories. II—5
van der Ziel, A. Noise mechanisms in oxide-coated cathodes—837(A)
Van Patter, D. M., B. E. Simmons, T. F. Stratton, and D. M. Zipoy. Angular distribution of $O^{18}(d,p)O^{17}$—825(A)
—— (see Blair, J. M.)—1023
—— (see Simmons, B. E.)—826(A)
Van Vleck, J. H. Some dilemmas in electron spin relaxation—857(T)
—— (see Kambe, K.)—66; 845(A)
Varney, R. N. Drift velocities and mobilities—831(T)
—— (see Beaty, E.)—831(A)
Vasileff, H. D. Thermal ionization of impurities in polar crystals. I. Formal theory—603
Venkatesan, D. (see Sarabhai, V.)—469
Vigier, J. P. (see Bohm, D.)—208
Villi, C. (see Ferrari, F.)—1159(L)
Vineyard, George N. Multiple scattering of neutrons—93
Visscher, William M. Self-energy effects on meson-nucleon scattering according to Tamm-Dancoff method—788
von Aulock, W. (see Rowen, J. H.)—1151(L)
von Dardel, G. and N. G. Sjöstrand. Absorption cross section of B for thermal neutrons—1566
—— **and N. G. Sjöstrand.** Diffusion parameters of thermal neutrons in water—1245
Voss, J. R., T. R. Palfrey, and R. O. Haxby. Coulomb effect on photoproduction of low-energy charged mesons—830(A)

Wada, W., M. M. Block, and D. T. King. Direct creation of electron pairs by electrons of great energy. II. Theoretical considerations—852(A)
—— (see Block, M. M.)—853(A); 1627
—— (see King, D. T.)—852(A)
Waddell, Charles, Harlan Shaw, David Cohen, and B. J. Moyer. 15.2-Mev γ emission from C^{13}—858(A)
—— (see Cohen, David)—714
Wainwright, T. (see Parzen, G.)—188
Wagner, Genevieve D. and Edwin O. Wiig. Reactions of cobalt with protons at 60, 100, 170, and 240 Mev—1100
Walker, R. L. (see Sands, M.)—849(A)
Wall, N. S. Neutron binding energies from (d,p) Q values—664
—— Proton angular distributions from deuteron bombardment of Bi^{209}, Pb^{207}, and Y^{89}—670
—— (see Rasmussen, V. K.)—812(L)
Wallis, R. F. (see Mador, I. L.)—617
Walters, G. K. (see Fairbank, W. M.)—846(A)
Walton, R. B. (see Darden, S. E.)—836(A)
Wannier, Gregory H. Corrected values for charge transfer cross section in noble gases—831(A)
Ward, J. K. Ground-state potential constants of ClO_2—845(A)
Wargo, Peter. Methods of preparing thin film MgO secondary emission surfaces on Ag-Mg alloys—837(A)
Warren, J. B., K. A. Laurie, D. B. James, and K. L. Erdman. γ radiation from proton bombardment of O—857(A)
Warren, J. B. (see Erdman, K. L.)—858(A)
Waterman, H. Nuclear magnetic resonance in kernite—862(A)
Wattenberg, A. (see Feld, B. T.)—1386
Weaver, A. B. (see Orear, Jay)—174
Weaver, H. E. (see Hornig, A. W.)—1703(L)
Webb, T. S., F. B. Hagedorn, W. A. Fowler, and C. C. Lauritsen. Elastic scattering of protons by F^{19}—851(A)
Webber, D. S. Polarized infrared absorption spectrum of gypsum—846(A)
Webeler, R. (see Barile, S.)—673
Weber, J. Vacuum fluctuation noise and dissipation—556
Webster, M. S. (see Baker, T. E., Jr.)—828(A)

Wegener, P. P. Review of experimental methods in hypersonic research—852(T)
Wehner, G. K. Recent results in sputtering by ion bombardment—819(T)
Weigl, John W. Action spectra for photoconductivity of dye films—834(A)
Weisskopf, V. F. (see Feshbach, H.)—448
Weisz, R. S. Magnetic anisotropy constants of ferromagnetic spinels—800(L)
Werman, M. S. (see Baker, T. E., Jr.)—828(A)
Wessel, Walter. Simple interpretation of Wehner's sputtering law—819(A)
West, Harry I., Jr. Low-energy pair production cross sections in scintillators—835(A)
Westervelt, D. R. Reversibility of additive coloring reaction in KCl—844(A)
Wetherill, George W. Variations in isotopic abundances of Ne and A extracted from radioactive minerals—679
Wexler, A. (see Corak, W. S.)—1442(L)
Whaley, R. M. (see Matheson, W. E.)—826(A)
Whaling, Ward (see Thirion, Jacques)—850(A)
White, Robert L. Magnetic interactions in $^2\Sigma$ molecules—845(A)
White, William C. Ablation from ultra-speed pellets—844(A)
Whitehead, C. (see Hird, B.)—702
Whyburn, William M. Oscillation and stability in certain nonlinear systems—843(A)
Wichmann, Eyvind and Norman M. Kroll. Vacuum polarization in strong Coulomb field—232(L)
Wick, G. C. Properties of Bethe-Salpeter wave functions—1124
Widom, B. Virial expansion of ideal Bose-Einstein gas—820(A)
—— Virial series of ideal Bose-Einstein gas—16
Wiedenbeck, M. L. (see Slattery, R. E.)—465
Wiegand, C. (see Chamberlain, O.)—807(L)
Wiener, E. (see Hofstadter, R.)—854(A)
Wiener, George (see Hoskins, Raymond)—1153(L)
Wiig, Edwin O. (see Fink, Richard W.)—185
—— (see Wagner, Genevieve D.)—1100
Wiles, Donald R. and Charles D. Coryell. Fission yield fine structure in mass region 99–106—696
Wilkinson, D. H. (see Jones, G. A.)—547(L)
Wilkinson, R. G. (see Pruett, C. H.)—1340
Willard, H. B. (see Johnson, C. H.)—985
Willardson, R. K., T. C. Harman, and A. C. Beer. Transverse Hall and magnetoresistance effects in p-type Ge—1512
Williams, Dudley (see Ting, Yu)—408
Williams, M. C. (see Mador, I. L.)—617
Wilson, Wesley G. (see Allen, William A.)—844(A)
Winslow, George H. α-decay theory with surface well potential—1032
Winther, A. (see Alder, K.)—237(L)
Wiser, Herbert L. and A. D. Krumbein. Mechanism of termination of Geiger-plateau region—831(A)
Wittke, J. P. and R. H. Dicke. Redetermination of hyperfine splitting in ground state of atomic H—530(L)
Wolfenstein, L. Possible triple scattering experiments—1654
Wolfgang, R. L. and G. Friedlander. Excitation function of $C^{12}(p,pn)C^{11}$ reaction in Bev region—190
Wolfsberg, Max. Orbital electron excitation associated with electron capture in A^{37}—1712(L)
Woll, John W., Jr. (see Green, Louis C.)—319
Woodbury, H. H., A. V. Tollestrup, and R. B. Day. Low-energy γ radiation from bombardment of C by protons—1713(E)
—— (see Tyler, W. W.)—874
Woodward, E. C. and D. R. Speck. Isotope shift in λ4415 Cd II—529(L)
Wooten, L. A., George E. Moore, and W. G. Guldner. Measurement of excess Ba in emitting oxide-coated cathodes—840(A)
—— (see Moore, George E.)—840(A)
Wright, G. T. Scintillation response of phosphors at low particle energies—569
Wright, K. A. (see Brown, W. L.)—834(A)
—— (see Fletcher, R. C.)—833(A)
Wyld, H. W., Jr. Fourth order corrections to meson-nucleon scattering in pseudoscalar meson theory—1661

Yabumoto, Tadaichi (see Takayama, Kazuo)—531(L)
Yamaka, Eiso. Afterglow of MgO single crystals—293
Yang, C. N. Experimental findings at Brookhaven National Laboratory—848(T)
—— **and R. L. Mills.** Conservation of isotopic spin and isotopic gauge invariance—191
Yennie, D. R. (see Ravenhall, D. G.)—239(L); 1714(E)
Yockey, H. P. (see Andrew, A.)—843(A)
York, Carl M., Jr. Čerenkov radiation detector for the selection of slow particles—1635
Young, Donald E. (see Tucker, Edmund B.)—835(A)
Young, J. E. R. (see Bitter, F.)—1531
Yovits, M. C. (see Jackson, J. L.)—15
Ypsilantis, T. (see Chamberlain, O.)—807(L)

Zaffarano, D. J. Nuclear radii from β transition-energies between mirror pairs—821(T)
—— (see Kline, R. M.)—1620
Zeldes, Henry and Ralph Livingston. Environmental effect on atomic H hfs in acids—1702(L)
Zener, C. Classical theory of temperature dependence of magnetic anisotropy energy—1335
Zimmerman, E. J., R. O. Kerman, Sidney Singer, P. Gerald Kruger, and W. Jentschke. Proton-proton scattering at 5.77 Mev—1322
Zimmerman, S. F. (see Browne, C. P.)—725
Zipoy, D. M. (see Van Patter, D. M.)—825(A)
Zitter, R. (see Adams, E. N., II)—1705(L)
Zucker, Alexander. Cross-section measurements with 29-Mev N ions—849(T)
—— (see Cohen, B. L.)—1617
—— (see Reynolds, H. L.)—393; 1615
Zumino, B. Evaluation of collision matrix for Dirac particles in external potential—202
Zweifel, P. F. Capture-positron branching ratios—1572

Analytic Subject Index to Volume 96

References with (A) are to abstracts of papers presented at meetings of the American Physical Society; references with (L) are to Letters to the Editor; references with (E) are to Errata. Items are listed under the following categories.

Acoustics
Astrophysics
Atomic and Molecular Beams
Atomic Mass and Abundance
Atomic Structure and Spectra
Biophysics
Chemical Effects and Properties
Constants, Standards, Units
Cosmic Radiation
Crystalline State
Dielectrics and Dielectric Properties
Diffraction
Diffusion
Elasticity and Plasticity
Electrical Conductivity and Resistance
Electrical Discharges
Electrical Properties
Electromagnetic Theory and Electrodynamics
Electrons and Positrons
Elementary Particle Interactions
Errata
Field Theory
Films, Properties
Fluid Dynamics
Gamma Rays
Gases
Geophysics
Helium, Liquid
Imperfections in Solids
Ionization
Ions
Ions and Electrons, Mobility
Liquids
Luminescence
Magnetic Properties
Magnetic Resonance
Mathematical Methods
Mechanics
Mesons and Hyperons
Methods and Instruments
Microwaves
Miscellaneous
Molecular Aggregates
Molecular Structure and Spectra
Neutrino
Noise
Nuclear Fission
Nuclear Moments and Spin
Nuclear Photoeffects
Nuclear Reactions, General
Nuclear Reactions Induced by α Particles and He^4
Nuclear Reactions Induced by Deuterons and Tritons
Nuclear Reactions Induced by Mesons
Nuclear Reactions Induced by Neutrons
Nuclear Reactions Induced by Protons
Nuclear Spectra
Nuclear Structure Theory
Optical Properties
Proceedings of the American Physical Society
Quantum Electrodynamics
Quantum Mechanics
Radiation
Radioactivity
Range and Energy Loss of Particles
Relativity and Gravitation
Scattering, General
Scattering of α Particles
Scattering of Deuterons
Scattering of Electrons and Positrons
Scattering of Mesons
Scattering of Neutrons
Scattering of Protons
Semiconductors
Spectra, General
Statistical Mechanics and Thermodynamics
Superconductivity
Thermal Properties
X-Rays

Absorption of Radiation (see **Radiation**)

Acoustics

Adsorption (see **Gases**)

Aerodynamics (see **Fluid Dynamics**)

Afterglow (see **Electrical Discharges**)

Alloys (see **Crystalline State**)

Annihilation (see **Electrons and Positrons**)

Antiferroelectric Phenomena (see **Dielectrics and Dielectric Properties**)

Antiferromagnetism (see **Magnetic Properties**)

Arcs (see **Electrical Discharges**)

Astrophysics

Acquirement of cosmic-ray energies by electromagnetic induction in galaxies, W. F. G. Swann—240(L)

Anisotropy of high-energy cosmic rays, Leverett Davis, Jr.—743

Finley-Freundlich red-shift hypothesis, H. L. Helfer—224(L)

Model of solar proton streams, Willard H. Bennett—824(A)

Sidereal time variations in cosmic-ray intensities produced by Fermi's acceleration mechanism, Leverett Davis, Jr.—853(A)

Solar x-ray emission, E. T. Byram, T. A. Chubb, and H. Friedman—860(A)

Atmosphere (see **Geophysics**)

Atomic and Molecular Beams

Rb^{85} spin, magnetic moment, and hfs, J. P. Hobson, J. C. Hubbs, W. A. Nierenberg, and H. B. Silsbee—1450(L)

Rotational spectra of RbCl by molecular beam electric resonance method, J. W. Trischka and R. Braunstein—968

Stern-Gerlach experiment on polarized neutrons, J. E. Sherwood, T. E. Stephenson, and Seymour Bernstein—1546

Atomic Mass and Abundance

Applications of rapid sweeping to single-focusing mass spectrometer, C. Robert Lagergren—823(A)

Mass doublet measurements using modulated magnetic field, Clayton F. Giese—823(A)

Microwave spectra of alkali halides, A. Honig, C. H. Townes, M. L. Stitch, and M. Mandel—629

Natural abundance of Li isotopes, Dwight A. Hutchison—1018

Stabilization of potentials in precision double-focusing mass spectrometer, K. S. Quisenberry, T. T. Scolman, and T. L. Collins—823(A)

Variations in isotopic abundances on Ne and A extracted from radioactive minerals, George W. Wetherill—679

Atomic Structure and Spectra

Analysis of 3-parameter wave function of Hylleraas for He I ground state in terms of central field wave functions, Louis C. Green, Marjorie M. Mulder, Paul C. Milner, Margaret N. Lewis, John W. Woll, Jr., Eleanor K. Kolchin, and David Mace—319

As spectra, R. E. Bedford and A. M. Crooker—845(A)

Direct quantitative observation of three-photon annihilation of positron-negatron pair, J. K. Basson—691

Electronic polarizabilities of ions from the Hartree-Fock wave functions, R. M. Sternheimer—951

Energies of π^--mesonic x-ray K lines, M. B. Stearns, M. Stearns, S. DeBenedetti, and L. Leipuner—804(L)

Energy level displacements in pi-mesonic atoms, S. Deser, M. L. Goldberger, K. Baumann, and W. Thirring—774

Environmental effect on atomic H hfs in acids, Henry Zeldes and Ralpl. Livingston—1702(L)

Excitation by electron impact of optically forbidden transition $1^1S \rightarrow 2^1S$ in He, E. N. Lassettre, M. E. Krasnow, and S. Silverman—832(A)
g factors of ^3P terms of atomic oxygen, K. Kambe and J. H. Van Vleck—845(A)
Hf I isotope shift, J. A. Collinson—949
Hfs of nitrogen, Mark A. Heald and Robert Beringer—645
Hyperfine splitting in ground state of atomic hydrogen, J. P. Wittke and R. H. Dicke—530(L)
Improved theory of Zeeman effect of atomic oxygen, K. Kambe and J. H. Van Vleck—66
Indium spectra, R. A. Nodwell and A. M. Crooker—845(A)
Isotope shift in λ4415 Cd II, E. C. Woodward and D. R. Speck—529(L)
Nd and Gd hfs, Kiyoshi Murakawa—1543
Np^{239} nuclear spin, John G. Conway and Ralph D. McLaughlin—541(L)
Nuclear fine structure in μ-mesonic atom, Boris A. Jacobsohn—1637
Nuclear magnetic octupole moments of stable Ga isotopes, R. T. Daly, Jr., and J. H. Holloway—539(L)
Optical studies of radioactive Hg, F. Bitter, S. P. Davis, B. Richter, and F. E. R. Young—1531
Po spectrum, G. W. Charles, D. J. Hunt, G. Pish, and D. L. Timma—838(A)
Solution of temperature-perturbed Thomas-Fermi equation, J. J. Gilvarry—944
Statistical atom with angular momentum, A. M. Sessler and H. M. Foley—366
Thermodynamics of Thomas-Fermi atom at low temperature, J. J. Gilvarry—934
Vacuum polarization in mesonic atoms, A. B. Mickelwait and H. C. Corben—1145

Aurora (see **Astrophysics; Geophysics**)

Barkhausen Effect (see **Magnetic Properties**)
Biophysics
Boson Theory (see **Field Theory**)
Bremsstrahlung (see **Radiation**)
Broadening of Spectral Lines (see **Atomic Structure and Spectra; Molecular Structure and Spectra; Spectra, General**)

Capture Cross Sections (see **Electrons and Positrons; Nuclear Reactions; Radiation**)
Čerenkov Effect (see **Radiation**)
Chemical Effects and Properties
Method for high precision studies of rate processes, W. Haller and G. L. Calcamuggio—1454(A)
Reaction between BaO and C and BaO and Si, Michael Hoch, Anthony J. Lamantia, and Herrick L. Johnston—839(A)
Chemical Reactions (see **Chemical Effects and Properties**)
Chemiluminescence (see **Luminescence**)
Cold Emission (see **Electrical Properties**)
Colloids (see **Chemical Effects and Properties; Molecular Aggregates**)
Compton Effect (see **Radiation**)
Conductivity, Electrical (see **Electrical Conductivity and Resistance**)
Conductivity, Thermal (see **Thermal Properties**)
Constants, Standards, Units
Easily reproducible thermal neutron density standard, René Cohen—850(A)
Cosmic Radiation (see also **Mesons and Hyperons**)
Absolute differential range spectrum of low-energy cosmic-ray μ mesons, N. T. Seaton—853(A)
Abundance of Li, Be, and B in primary radiation, M. F. Kaplon, J. H. Noon, and G. W. Racette—1408
Acquirement of cosmic-ray energies by electromagnetic induction in galaxies, W. F. G. Swann—240(L)
Age-dependent branching stochastic processes in cascade theory, A. T. Reid—751
Anisotropy of high-energy cosmic rays, Leverett Davis, Jr.—743
Bursts in NaI(Tl) near sea level, S. Standil—777
Čerenkov radiation detector for the selection of slow particles, Carl M. York, Jr.—1635
Changes in amplitude of 27-day intensity variation with solar activity, Peter Meyer and J. A. Simpson—1085
Composition of primary radiation at λ=10° N, G. W. McClure—1391
Cosmic-ray intensity fluctuations at sea level, Robert L. Chasson—1116
Cosmic-ray studies with Čerenkov detector at λ=10° and 55°, K. A. Anderson—829(A)
Cycle of world-wide changes in daily variation of meson intensity, V. Sarabhai, U. D. Desai, and D. Venkatesan—469
Direct creation of electron pairs by electrons of great energy. I. Experimental observations, D. T. King, W. Wada, and M. M. Block—852(A); II. Theoretical considerations, W. Wada, M. M. Block, and D. T. King—852(A); III. Internal energy distributions, M. M. Block, D. T. King, and W. Wada—853(A)
Electromagnetic events of high-energy particles at sea level, S. H. Neddermeyer and Erle Howell, Jr.—853(A)
Electron density distribution near large air shower axes at sea level, R. E. Heineman—161
Electron tridents between 0.1 and 10 Bev, M. M. Block, D. T. King, and W. W. Wada—1627
Flux and azimuthal asymmetry of primary cosmic-ray nuclei at equator, R. E. Danielson, P. S. Freier, J. S. Naugle, and E. P. Ney—829(A)
Heavy cosmic-ray nuclei, John Linsley—829(A)
Identification of primary cosmic-ray heavy nuclei, R. F. Hoard, J. R. Fleming, and J. J. Lord—854(A)
Influence of geomagnetic field on extensive air showers, P. Chaloupka—1709(L)
Integral equations for cascade showers, John M. Blatt—1644
Interaction of heavy primary cosmic rays in Pb, Y. Eisenberg—1378
Long-term studies of neutron and ionizing cosmic-ray intensities, E. L. Chupp—853(A)
Low-energy differential range spectrum of cosmic-ray μ mesons, A. Fafarman and M. H. Shamos—1096
New formulation of general three-dimensional cascade theory, B. A. Chartres and H. Messel—1651
Nuclear collisions at extreme relativistic energies, Marcel Schein, D. M. Haskin, and R. G. Glasser—829(A)
Production spectra of cosmic-ray mesons in atmosphere, Stanislaw Olbert—1400
Search for departures of cosmic rays from Poisson's law at low counting rates. I, T. E. Baker, Jr., N. C. Blais, C. L. Hemenway, V. Rojansky, M. S. Webster, and M. S. Werman—828(A); II, W. M. Cegelski, A. T. Goble, C. L. Hemenway, K. Reinitz, V. Rojansky, and F. A. Rushworth—828(A)
Sidereal time variations in cosmic-ray intensities produced by Fermi's acceleration mechanism, Leverett Davis, Jr.—853(A)
Studies of penetrating and cascade showers with plastic scintillators at elevation of 11 500 feet, C. N. Chou—830(A)
Unstable cosmic-ray particles observed in double cloud-chamber arrangement, W. H. Arnold, J. Ballam, H. Gursky, A. L. Hodson, R. Ronald Rau, George T. Reynolds, and S. B. Treiman—853(A)

Cosmology (see **Astrophysics; Relativity and Gravitation**)
Critical Potentials (see **Atomic Structure and Spectra; Molecular Structure and Spectra**)
Cross Section (see **Electrons and Positrons; Nuclear Reactions; Radiation; Scattering**)
Crystal Counters (see **Methods and Instruments**)
Crystalline State (see also **Electrical Properties; Imperfections in Solids; Magnetic Properties; Semiconductors; etc.**)
Atomic heat of Bi between 1° and 4°K, P. H. Keesom and N. Pearlman—897
Color centers in chrome alum crystals, E. A. Braun, A. Many, and A. E. Simchen—1505
Derivation of magnetostriction and anisotropic energies for hexagonal, tetragonal, and orthorhombic crystals, W. P. Mason—302
Diffusion of Cd, In, and Sn in single crystals of Ag, C. T. Tomizuka and L. Slifkin—610
Effect of dislocations on optical absorption edge in nonmetals, R. M. Blakney and D. L. Dexter—227(L)
Effect of precipitation hardening on superconducting transition of Al alloy, R. E. Mould and D. E. Mapother—797(L)
Effects of anisotropy on thermodynamic properties of antiferromagnets, J. A. Eisele and F. Keffer—929
Electron energy levels in ionic crystals, E. L. Jossem and L. G. Parratt—834(A)
Energy parameters of two-dimensional graphite, G. S. Colladay—846(A)
Equivalence of x-ray lattice parameter and density changes in neutron-irradiated LiF, D. Binder and W. J. Sturm—1519
Exciton bands in crystalline benzene, David Fox and Otto Schnepp—1196
Fermi level in amorphous Sb films, E. Taft and L. Apker—1496
Hollow dislocations and etch pits, N. Cabrera, M. M. Levine, and J. S. Plaskett—1153(L)
Intensity anomalies in electron diffraction from crystals, Henry E. Breed and J. Mayo Greenberg—823(A)
K band in additively colored KCl, H. W. Etzel and F. E. Geiger, Jr.—225(L)
Magnetic and crystalline behavior of certain oxide systems with spinel and perovskite structures, Louis R. Maxwell and Stanley J. Pickart—1501
Magnetostriction and crystal anisotropy of single crystals of hexagonal Co, R. M. Bozorth—311
Moisture condensation patterns on glass and crystalline surfaces, W. C. Levengood—1454(A)
Moment singularity analysis of vibration spectra, Melvin Lax and Joel L. Lebowitz—594
Optical and infrared absorption of Cu at 4.2°K, Manfred A. Biondi—534(L)
Optical and infrared volume absorptivity of metals, T. Holstein—535(L)
Production and bleaching of color centers in x-rayed alkali halide crystals, I. L. Mador, R. F. Wallis, M. C. Williams, and R. C. Herman—617
Relation between the width of an x-ray line and resolving power of double-crystal spectrometer, Gosta Brogren—589
Reversibility of additive coloring reaction in KCl, D. R. Westervelt—844(A)
Rittinger's number for several minerals, M. E. Backman and H. L. Morrison—844(A)
Shapes of absorption and emission lines of impurities in solids, D. L. Dexter—615
Simplified impurity calculation, G. F. Koster and J. C. Slater—1208
Spin-orbit coupling in band theory-character tables for some 'double' space groups, R. J. Elliott—280
Theory of effect of spin-orbit coupling on magnetic resonance in some semiconductors, R. J. Elliott—266
Thermal ionization of impurities in polar crystals. I. Formal theory, H. D. Vasileff—603
Vibrational anharmonicity and lattice thermal properties, J. S. Dugdale and D. K. C. MacDonald—57

Diamagnetism (see **Magnetic Properties**)
Dielectrics and Dielectric Properties
Dc prebreakdown currents in gases of high dielectric strength, M. L. Reeves and Ronald Geballe—862(A)
Infrared spectrum of $BaTiO_3$, R. T. Mara, G. B. B. M. Sutherland, and H. V. Tyrell—801(L)
Low-frequency dielectric loss peaks in KCl containing divalent cation impurities, E. Burstein, J. W. Davisson, and N. Sclar—819(A)
Thin films of $BaTiO_3$, Charles Feldman—819(A)
Diffraction (see also **Scattering**)
Intensity anomalies in electron diffraction from crystals, Henry E. Breed and J. Mayo Greenberg—823(A)
X-ray diffraction patterns from liquid He, W. L. Gordon, C. H. Shaw, and J. G. Daunt—1444(L)
Diffusion
Back diffusion of electrons to plane emitting surface, Robert P. Stein—862(A)
Diffusion of Cd, In, and Sn in single crystals of Ag, C. T. Tomizuka and L. Slifkin—610
Diffusion of impurities in Si, W. C. Dunlap, Jr., H. V. Bohm, and H. P. Mahon, Jr.—822(A)
Diffusion of metastable Hg molecules, A. O. McCoubrey and C. G. Matland—832(A)
Diffusion of W in Ni, H. W. Allison and George E. Moore—840(A)
Diffusion parameters of thermal neutrons in water, G. von Dardel and N. G. Sjöstrand—1245
Long-life luminescence and diffusion in MgO, B. Goodman—824(A)
Nuclear spin relaxation by translational diffusion. II. Diffusion in b.c.c. lattice, H. C. Torrey—690
Numerical solution of diffusion equation in cylindrical geometrics, G. M. Roe and R. H. Stark—820(A)
Self-diffusion in Cu, A. Kuper, H. Letaw, Jr., L. Slifkin, E. Sonder, and C. T. Tomizuka—1224
Solute diffusion in Ni, R. A. Swalin and A. E. Martin—840(A)
Discharge of Electricity in Gases (see **Electrical Discharges**)
Disintegration and Excitation of Nucleus (see **Nuclear Reactions**)
Dynamics (see **Mechanics**)

Elasticity and Plasticity
Ablation from ultra-speed pellets, William C. White—844(A)
Application of engravement method to study of particle velocity distribution in explosively loaded cylinders, John Pearson and John S. Rinehart—844(A)
Creep of Al under cyclotron irradiation, A. Andrew, M. R. Jeppson, R. L. Mather, and H. P. Yockey—843(A)
Critical angle associated with high-speed impact of sphere on thin plate, William A. Allen, Joe M. Mapes, and Wesley G. Wilson—844(A)
Effects of elastic dilatation and shear on superconducting transition of Sn, Milan D. Fiske—821(A)
Elastic moduli of Sn at superconducting transition, Joseph K. Landauer—296

Low-temperature acoustic relaxation in Ni-Fe ferrites, M. E. Fine and N. T. Kenney—1487
Rittinger's number for several minerals, M. E. Backman and H. L. Morrison—844(A)
Electrical Breakdown (see **Dielectrics and Dielectric Properties; Electrical Discharges**)
Electrical Conductivity and Resistance (see also **Semiconductors; Superconductors**)
Action spectra for photoconductivity of dye films, John W. Weigl—834(A)
Afterglow of MgO single crystals, Eiso Yamaka—293
Conductivity and Hall effect in oxide cathode, R. Forman—839(A)
Dependence of signal-to-noise ratio in photoconductive PbSe layers on temperature of blackbody source, A. M. Crooker, and E. B. Dorling—846(A)
Electrical and optical properties of InSe, R. W. Damon and R. W. Redington—1498
Electrical and optical properties of intermetallic compounds. I. InSb, R. G. Breckenridge, R. F. Blunt, W. R. Hosler, H. P. R. Frederikse, J. H. Becker, and W. Oshinsky—571; II. GaSb, R. F. Blunt, W. R. Hosler, and H. P. R. Frederikse—576; III. AlSb, R. F. Blunt, H. P. R. Frederikse, J. H. Becker, and W. R. Hosler—578
Electrical conductivity and Hall effect in oxide cathodes, R. Forman—1479
Electrical properties and solid-vapor equilibrium of PbS, Robert F. Brebrick and Wayne W. Scanlon—598
Electrical properties of natural crystals of iron pyrite, John C. Marinace—593
Electrical resistivity minimum and structural defects in Cu, R. W. Schmitt and M. D. Fiske—1445(L)
Electrical resistivity minimum reported in Cu-Zn alloys, R. W. Schmitt—1446(L)
Hall effect in Bi, J. M. Reynolds, H. W. Hemstreet, T. E. Leinhardt, and D. D. Triantos—1203
Hall effect in positive column, Kazuo Takayama, Tomizo Suzuki, and Tadaichi Yabumoto—531(L)
High-frequency resistance of Sn and In in normal and superconducting state, C. J. Grebenkemper—1197
Mechanism for photovoltaic and photoconductivity effects in activated CdS crystals, D. C. Reynolds and S. J. Czyzak—1705(L)
Properties of quantum statistical impedance, J. L. Jackson and M. C. Yovits—15
Temperature dependence of periodic Hall effect in Bi, J. M. Reynolds and D. D. Triantos—822(A)
Electrical Discharges
Absorption studies of He metastable molecule, A. V. Phelps—832(A)
Corona discharge current from aircraft, Seville Chapman—831(A)
Corrected values for charge transfer cross section in noble gases, Gregory H. Wannier—831(A)
Dc prebreakdown currents in gases of high dielectric strength, M. L. Reeves and Ronald Geballe—862(A)
Diffusion of metastable Hg molecules, A. O. McCoubrey and C. G. Matland—832(A)
Drift velocities of A ions in A at various temperatures, E. Beaty and R. Varney—831(A)
Electron groups in He negative glow, D. H. Pringle and W. E. J. Farvis—536(L)
Excitation of air glow by electronic impact, C. Y. Fan—860(A)
Hall effect in positive column, Kazuo Takayama, Tomizo Suzuki, and Tadaichi Yabumoto—531(L)
Mechanism of termination of Geiger-plateau region, Herbert L. Wiser and A. D. Krumbein—831(A)
Mobilities of various ions in noble gases, Lorne M. Chanin and Manfred A. Biondi—831(A)
Secondary electron emission by photoelectric action and ion bombardment at cathode in corona breakdown of argon, Laura Colli and Ugo Facchini—1
Space-charge formation and Townsend mechanism of spark breakdown in gases, R. W. Crowe, J. K. Bragg, and Virginia G. Thomas—10
Electrical Properties (see also **Dielectrics and Dielectric Properties; Electrical Conductivity and Resistance; Semiconductors; Superconductors**)
Applications of radioactive tracer techniques to study of thermionic emission of oxide-coated cathodes, R. W. Peterson, D. E. Anderson, and W. G. Shepherd—840(A)
Auger ejection of electrons from W by noble gas ions, Homer D. Hagstrum—325
Back diffusion of electrons to plane emitting surface, Robert P. Stein—862(A)
Contact electrification effects in metal-metal system. I. General theory, Arthur Paskin—819(A); II. Results for Hg-steel, Paul E. Carroll—820(A)
Effect of oxygen on electrical properties of PbTe films, Donald E. Bode and Henry Levinstein—259
Electronic polarizabilities of ions from the Hartree-Fock wave functions, R. M. Sternheimer—951
Electronic structure of MgO, J. R. Stevenson—839(A)
Emission of energetic secondary electrons produced by 1.3-Mev electron bombardment, R. A. Shatas, J. F. Marshall, and M. A. Pomerantz—1199
Excess Ba in emitting oxide-coated cathodes, L. A. Wooten, George E. Moore, and W. G. Guldner—840(A); George E. Moore, L. A. Wooten, and James Morrison—840(A)
Inelastic scattering of medium-fast electrons in alkali metals, E. M. Baroody—837(A)
Interpretation of Wehner's sputtering law, Walter Wessel—819(A)
Mechanism for photovoltaic and photoconductivity effects in activated CdS crystals, D. C. Reynolds and S. J. Czyzak—1705(L)
Methods of preparing thin-film MgO secondary emission surfaces on Ag-Mg alloys, Peter Wargo—837(A)
Oxide-impregnated Ni matrix cathode, W. Balas, J. Dempsey, and E. F. Rexer—840(A)
Photoelectric emission from BaO, H. R. Philipp—827(A)
Photoelectric emission in extreme uv, Hans E. Hinteregger—538(L)
Photovoltaic effect in CdS, D. C. Reynolds, G. Leies, L. L. Antes, and R. E. Marburger—533(L)
Reaction between BaO and C and BaO and Si, Michael Hoch, Anthony J. Lamantia, and Herrick L. Johnston—839(A)
Secondary electron yield from Al by high-energy primary electrons, G. W. Tautfest and H. R. Fechter—35
Secondary emission by positive ion bombardment, Manuel Schwartz and Paul L. Copeland—1466
Seebeck effect in single crystal Si, T. H. Geballe and G. W. Hull—846(A)
Theory of Auger ejection of electrons from metals by ions, Homer D. Hagstrum—336
Theory of electric breakdown in high-temperature region and its relation to thermionic emission, Kurt Lehovec—921
Theory of thermoelectric power of semiconductors, Conyers Herring—1163
Work functions of W single-crystal planes, Erwin W. Muller—837(A)
Electrodynamics (see **Electromagnetic Theory and Electrodynamics**)
Electrolysis (see **Chemical Effects and Properties**)

Electromagnetic Theory and Electrodynamics
Gravitation and electromagnetism, Suraj N. Gupta—1683
Radiative effects in constant field, Roger G. Newton—523
Reflection of waves by inhomogeneous medium, V. A. Bailey—865
Suppression of coherent radiation by electrons in synchrotron, John S. Nodvick and David S. Saxon—180
Vacuum fluctuation noise and dissipation, J. Weber—556
Electron Diffraction (see **Diffraction; Scattering of Electrons and Positrons**)
Electron Optics (see **Electromagnetic Theory and Electrodynamics**)
Electronic Tubes (see **Methods and Instruments**)
Electrons and Positrons (see also **Electromagnetic Theory and Electrodynamics; Elementary Particle Interactions; Scattering of Electrons and Positrons**)
Direct creation of electron pairs by electrons of great energy. I. Experimental observations, D. T. King, W. Wada, and M. M. Block—852(A); II. Theoretical considerations, W. Wada, M. M. Block, and D. T. King—852(A); III. Internal energy distributions, M. M. Block, D. T. King, and W. Wada—853(A)
Direct quantitative observation of three-photon annihilation of positron-negatron pair, J. K. Basson—691
Effect of nuclear charge on internally produced pairs, G. K. Horton and E. Phibbs—1066
Electron tridents between 0.1 and 10 Bev, M. M. Block, D. T. King, and W. W. Wada—1627
Lifetime of positrons in superconducting Pb and Sn, Robert Stump and Harry E. Talley—904
Low-energy pair production cross sections in scintillators, Harry I. West, Jr.—835(A)
Multiple photon production in electron-positron annihilation, Suraj N. Gupta—1453(L)
One-quantum annihilation of positrons, Donald J. Farmer and J. F. Streib—855(A)
Electrons, Mobility (see **Ions and Electrons, Mobility**)
Electrons, Scattering of (see **Scattering of Electrons and Positrons**)
Electrons, Secondary (see **Electrical Properties**)
Electrons, Thermionic (see **Electrical Properties**)
Electro-Optical Effects (see **Optical Properties**)
Electrostriction (see **Dielectrics and Dielectric Properties**)
Elementary Particle Interactions
Absorption of positive ions by deuterium at 76 and 94 Mev, Henry L. Stadler—496
Charge independence with repulsive core potentials, M. A. Preston and J. Shapiro—813(L)
Conservation of number of nucleons, F. Reines, C. L. Cowan, Jr., and M. Goldhaber—1157(L)
Coulomb interference effects in p-p scattering, A. Garren—1709(L)
Diffusion parameters of thermal neutrons in water, G. von Dardel and N. G. Sjöstrand—1245
Elastic scattering of 26-Mev negative pions by H in emulsion, Jay Orear, William Slater, J. J. Lord, S. L. Eilenberg, and A. B. Weaver—174
Final-state interaction in multiple production of mesons in nucleon-nucleon collisions, Julius S. Kovacs—1454(A)
Formula for polarization in nucleon-nucleon scattering, G. Breit and J. B. Ehrman—805(L)
Fourth-order corrections to meson-nucleon scattering in pseudoscalar meson theory, H. W. Wyld, Jr.—1661
High-energy photodisintegration of deuteron, J. C. Keck, A. V. Tollestrup, and W. R. Smythe, II—850(A); A. V. Tollestrup, J. C. Keck, and W. R. Smythe, II—850(A)
Indirect measurement of n-n interaction, Robert H. Phillips and Kenneth M. Crowe—484
Low-energy behavior of phase shifts in pion-proton scattering, Jay Orear—176
Meson-proton scattering phase shift analysis, H. A. Bethe and F. de Hoffmann—1714(E)
Mesonic corrections to quadrupole moment of deuteron, A. M. Sessler—793
Multiple photon production in electron-positron annihilation, Suraj N. Gupta—1453(L)
Negative pion mass from its radiative absorption in hydrogen, Kenneth M. Crowe and Robert H. Phillips—470
Neutral pion-deuteron production in 400-Mev n-p collisions, R. A. Schluter—734
n-p scattering at 90 Mev, Chung Ying Chih—856(A)
n-p scattering at 91 Mev, R. H. Stahl and N. F. Ramsey—1310
Nuclear forces and β-decay matrix elements, Roland F. Herbst—372
Nuclear saturation and two-body forces. II. Tensor forces, K. A. Brueckner—508
Nucleon-antinucleon scattering and vacuum polarization, Kenneth A. Johnson—1659
Phase shifts for nucleon-nucleon scattering at 280 Mev, G. Breit, J. B. Ehrman, A. M. Saperstein, and M. H. Hull, Jr.—807(L)
Photoproduction of charged mesons from deuterium, M. Sands, J. G. Teasdale, and R. L. Walker—849(A)
Photoproduction of mesons from H near threshold, Vincent Peterson and I. George Henry—850(A)
Polarization in p-p scattering for P and F waves, M. H. Hull, Jr., and A. M. Saperstein—806(L)
p-p scattering at 5.77 Mev, E. J. Zimmerman, R. O. Kerman, Sidney Singer, Gerald Kruger, and W. Jentschke—1322
Production of charged pions from hydrogen and carbon, A. H. Rosenfeld—130; 1714(E)
Production of pions in nucleon-nucleon collisions at cyclotron energies, A. H. Rosenfeld—139
Radiative capture of 300-Mev neutrons in hydrogen, John DePangher—859(A)
Reaction $p+p \rightarrow \pi^+ + d$ with polarized protons, T. H. Fields, J. G. Fox, J. A. Kane, R. A. Stallwood, and R. B. Sutton—812(L)
Self-energy effects on meson-nucleon scattering according to Tamm-Dancoff method, William M. Visscher—788
Small-angle n-p scattering at 400 Mev, R. T. Siegel, A. J. Hartzler, and W. Opitz—859(A)
Tamm-Dancoff methods and nuclear forces, Behram Kurşunoğlu—1690
Total cross sections for negative and positive pions in hydrogen and deuterium, J. Ashkin, J. P. Blaser, F. Feiner, J. G. Gorman, and M. O. Stern—1104
Total cross sections of light elements for 208-Mev and 315-Mev protons, Hervasio G. de Carvalho—398
Elements (see **Atomic Mass and Abundance**)
Energy Loss of Particles (see **Range and Energy Loss**)
Energy States of Atoms (see **Atomic Structure and Spectra**)
Energy States of Molecules (see **Molecular Structure and Spectra**)
Energy States of Nucleus (see **Nuclear Reactions; Nuclear Spectra; Nuclear Structure Theory**)
Equations of State (see **Chemical Effects and Properties**)
Errata
Angular correlation of three nuclear radiations, G. R. Satchler—1713(E)
Bound states and formal theory of scattering, M. N. Hack—1714(E)
Centrifugal distortion in asymmetric top molecules. III. H_2O, D_2O, and HDO, D. W. Posener and M. W. P. Strandberg—1714(E)

Low-energy γ radiation from bombardment of C by protons, H. H. Woodbury, A. V. Tollestrup, and R. B. Day—1713(E)
Low-temperature luminescence of CdS, L. R. Furlong—1714(E)
Meson-proton scattering phase shift analysis, H. A. Bethe and F. de Hoffmann—1714(E)
Phase shift calculation of high-energy electron scattering, D. G. Ravenhall and D. R. Yennie—1714(E)
Production of charged pions from hydrogen and carbon, A. H. Rosenfeld—1714(E)
Ti^{44}, new Ti nuclide, R. A. Sharp and R. M. Diamond—1713(E)
Errors of Measurement (see **Methods and Instruments**)
Evaporation (see **Liquids**)
Excitation of Atoms (see **Atomic Structure and Spectra**)
Excitation of Molecules (see **Molecular Structure and Spectra**)
Excitation of Nucleus (see **Nuclear Reactions; Nuclear Spectra; Nuclear Structure Theory**)
Explosion Phenomena (see **Fluid Dynamics**)

Faraday Effect (see **Optical Properties**)
Ferroelectric Phenomena (see **Dielectrics and Dielectric Properties**)
Ferromagnetism (see **Magnetic Properties**)
Field Emission (see **Electrical Properties**)
Field Theory (see also **Quantum Electrodynamics; Relativity and Gravitation**)
Adiabatic theorems in field theory, S. Deser—843(A)
Calculation of potentials from new Tamm-Dancoff equation, J. C. Taylor—1438
Classical field theory in Hamilton-Jacobi formalism, Hans Freistadt—821(A)
Conservation of isotopic spin and isotopic gauge invariance, C. N. Yang and R. L. Mills—191
Elimination of pair interaction in pseudoscalar meson theory, C. H. Chang and B. A. Jacobsohn—856(A)
Families of spinor fields, Toichiro Kinoshita—199
Fourth-order corrections to meson-nucleon scattering in pseudoscalar meson theory, H. W. Wyld, Jr.—1661
Gravitation and electromagnetism, Suraj N. Gupta—1683
Mach's principle and unified field theory, Joseph Callaway—778
Mesonic corrections to quadrupole moment of deuteron, A. M. Sessler—793
n-p mass difference, W. G. Holladay and R. G. Sachs—810(L)
Nucleon-antinucleon scattering and vacuum polarization, Kenneth A. Johnson—1659
Properties of Bethe-Salpeter wave functions, G. C. Wick—1124
Renormalization of a neutral vector meson interaction, R. J. N. Phillips—1678
Solutions of Bethe-Salpeter equation, R. E. Cutkosky—1135
Spherically symmetric solutions in nonsymmetrical field theories. II, P. C. Vaidya—5
Tamm-Dancoff methods and nuclear forces, Behram Kurşunoğlu—1690
Vacuum polarization in mesonic atoms, A. B. Mickelwait and H. C. Corben—1145
Variational principle in quantum mechanics, N. M. Hugenholtz—1158(L)
Films, Properties
Action spectra for photoconductivity of dye films, John W. Weigl—834(A)
Effect of oxygen on electrical properties of PbTe films, Donald E. Bode and Henry Levinstein—259
Fermi level in amorphous Sb films, E. Taft and L. Apker—1496
Fermi level in semiconducting amorphous Sb films, E. Taft and L. Apker—827(A)
Interpretation of Wehner's sputtering law, Walter Wessel—819(A)
Oxidation of thin films of Ge and Si, W. C. Dash—822(A)
Thin films of $BaTiO_3$, Charles Feldman—819(A)
Uv absorption in BaO films, Koji Okumura—1704(L)
Fine Structure (see **Atomic Structure and Spectra**)
Fission of Nucleus (see **Nuclear Fission**)
Fluctuation Phenomena (see **Noise**)
Fluid Dynamics
Corona discharge current from aircraft, Seville Chapman—831(A)
Correlation function in Burgers' model of turbulence, Morton A. Hyman—821(A)
Displacement effect of three-dimensional boundary layer of moderate thickness, Eldon L. Dunn and Howard R. Kelly—847(A)
Electrohydrodynamics. I. Equilibrium of charged gas in container, Joseph B. Keller—843(A)
Free molecule flow of nonuniform gas, S. Bell and S. A. Schaaf—848(A)
Hot-wire measurements of turbulence in ocean, R. W. Stewart—847(A)
Incompressible laminar boundary layer on spinning cylinder at small angles of attack, Howard R. Kelly—847(A)
Metastable jet-tone states of jets from sharp-edged, circular, pipe-like orifices, A. B. C. Anderson—847(A)
Path of triple point for spherical shocks above a rigid plane, Ralph Schellenbaum and Jay Todd, Jr.—848(A)
Response of pressure gauges to dust-laden shock waves, J. R. Banister and C. D. Broyles—847(A)
Shape of shock wave derived from spherical shock wave incident on concave wedge, Jay Todd, Jr., and Ralph Schellenbaum—847(A)
Stability of spherical shape of vapor cavity in liquid, M. S. Plesset and T. P. Mitchell—848(A)
Statistics of electromagnetic radiation scattered by turbulent medium, Richard A. Silverman and Martin Balser—560
Transition through contact region, J. G. Hall—847(A)
Two-fluid flow with application to dust-laden air, M. L. Merritt and J. R. Banister—848(A)
Fluorescence (see **Luminescence**)
Friction (see **Mechanics**)

Galvanomagnetic Effect (see **Magnetic Properties**)
Gamma Rays (see also **Nuclear Reactions; Nuclear Spectra; Range and Energy Loss**)
γ-ray absorption coefficients at 6.13 Mev, Ronald S. Paul—1563
High-energy γ-ray studies with nuclear track emulsions, Harry H. Heckman, Peter C. Giles, and Walter H. Barkas—858(A)
Scattering of γ rays by nucleons, R. H. Capps and R. G. Sachs—540(L)
Gases
Electrohydrodynamics. I. Equilibrium of charged gas in container, Joseph B. Keller—843(A)
Free molecule flow of nonuniform gas, S. Bell and S. A. Schaaf—848(A)
Geophysics
Excitation of air glow by electronic impact, C. Y. Fan—860(A)
Hot-wire measurements of turbulence in ocean, R. W. Stewart—847(A)

Geophysics (Continued)
Model of solar proton streams, Willard H. Bennett—824(A)
Variations in isotopic abundances of Ne and A extracted from radioactive minerals, George W. Wetherill—679
Glasses (see **Molecular Aggregates**)
Gravitation (see **Relativity and Gravitation**)
Gyromagnetization (see **Magnetic Properties**)

Hall Effect (see **Electrical Conductivity and Resistance; Semiconductors**)
Heat Capacity (see **Thermal Properties**)
Heat Conduction (see **Thermal Properties**)
Heat of Dissociation and Formation (see **Molecular Structure and Spectra**)
Heat of Fusion (see **Thermal Properties**)
Heat of Vaporization (see **Thermal Properties**)
Helium, Liquid
Critical flow rate and zero entropy of He superfluid, William Band—843(A)
Fermi-Dirac degeneracy in liquid He^3 below 1°K, W. M. Fairbank, W. B. Ard, and G. K. Walters—846(A)
Heat and entropy of mixing of He^3 and He^4 on the basis of two-fluid theory of He^4, O. K. Rice—1464
λ transition of liquid He, Ryoichi Kikuchi—563
Orthobaric densities of He^3, 1.3°K to 3.2°K, Eugene C. Kerr—551
Statistical mechanics of He II near 1°K, O. K. Rice—1460
Superfluidity of boson gas, J. M. Blatt and S. T. Butler—1149(L)
Theory of liquid He^3, Louis Goldstein—1455
X-ray diffraction patterns from liquid He, W. L. Gordon, C. H. Shaw, and J. G. Daunt—1444(L)
High-Voltage Tubes and Machines (see **Methods and Instruments**)
Hydrodynamics (see **Fluid Dynamics**)
Hyperfine Structure (see **Atomic Structure and Spectra; Molecular Structure and Spectra; Nuclear Moments and Spin**)
Hyperons (see **Mesons and Hyperons**)

Imperfections in Solids (see also **Crystalline States; Electrical Conductivity and Resistance; Luminescence; Semiconductors**)
Afterglow of MgO single crystals, Eiso Yamaka—293
Color-center magnetic resonances in LiF, C. K. Jen and N. W. Lord—1150(L)
Color centers in chrome alum crystals, E. A. Braun, A. Many, and A. E. Simchen—1505
Creep of Al under cyclotron irradiation, A. Andrew, M. R. Jeppson, R. L. Mather, and H. P. Yockey—843(A)
Distribution of trapping levels in CdSe, Harald C. Jensen and Robert J. Cashman—798(L)
Effect of dislocations on optical absorption edge in nonmetals, R. M. Blakney and D. L. Dexter—227(L)
Effect of precipitation hardening on superconducting transition of Al alloy, R. E. Mould and D. E. Mapother—797(L)
Electrical resistivity minimum and structural defects in Cu, R. W. Schmitt and M. D. Fiske—1445(L)
Electrical resistivity minimum reported in Cu-Zn alloys, R. W. Schmitt—1446(L)
Equivalence of x-ray lattice parameter and density changes in neutron-irradiated LiF, D. Binder and W. J. Sturm—1519
Hollow dislocations and etch pits, N. Cabrera, M. M. Levine, and J. S. Plaskett—1153(L)
K band in additively colored KCl, H. W. Etzel and F. E. Geiger—225(L)
Long-life luminescence and diffusion in MgO, B. Goodman—824(A)
Low-frequency dielectric loss peaks in KCl containing divalent cation impurities, E. Burstein, J. W. Davisson, and N. Sclar—819(A)
Optical absorption spectra of stoichiometric single crystals of MgO, W. T. Peria—824(A)
Production and bleaching of color centers in x-rayed alkali halide crystals, I. L. Mador, R. F. Wallis, M. C. Williams, and R. C. Herman—617
Reversibility of additive coloring reaction in KCl, D. R. Westervelt—844(A)
Uv absorption in BaO films, Koji Okumura—1704(L)
Uv transmission and α bombardment conduction inhomogeneities in diamond, A. J. Ahearn—828(A)
Inelastic Scattering (see **Nuclear Reactions; Scattering**)
Instruments (see **Methods and Instruments**)
Internal Conversion (see **Nuclear Spectra**)
Ionization (see also **Electrical Discharges; Range and Energy Loss**
Dc prebreakdown currents in gases of high dielectric strength, M. L. Reeves and Ronald Geballe—862(A)
Ionization energy loss of mesons in NaI scintillation crystal, Theodore Bowen—754(A)
Ionization produced by 5-Mev α particles in A mixtures, C. E. Melton, T. E. Bortner, and G. S. Hurst—643
Probability curves near threshold for formation of He^+, Ne^{++}, A^{++}, Kr^{++}, and Xe^{++} by electron impact, W. M. Hickam, R. E. Fox, and T. Kjeldaas, Jr.—63
Ionization Potentials of Atoms (see **Atomic Structure and Spectra**)
Ionization Potentials of Molecules (see **Molecular Structure and Spectra**)
Ionosphere (see **Geophysics**)
Ions (see also **Electrical Discharges**)
Auger ejection of electrons from W by noble gas ions, Homer D. Hagstrum—325
Charge states of heavy-ion beams passing through gases, P. M. Stier, C. F. Barnett, and G. E. Evans—973
Electron capture and loss by moving ions in dense media, Jacob Neufeld—1470
Electronic polarizabilities of ions from the Hartree-Fock wave functions, R. M. Sternheimer—951
Interpretation of Wehner's sputtering law, Walter Wessel—819(A)
Secondary emission by positive ion bombardment, Manuel Schwartz and Paul L. Copeland—1466
Theory of Auger ejection of electrons from metals by ions, Homer D. Hagstrum—336
Ions and Electrons, Mobility (see also **Electrical Discharges; Semiconductors**)
Mobilities of various ions in noble gases, Lorne M. Chanin and Manfred A. Biondi—831(A)
Mobility of impurity ions in Ge and Si, C. S. Fuller and J. C. Severiens—21
Mobility ratio in pure *p*-type semiconductors, Allen Nussbaum—828(A)
Isobars (see **Atomic Mass and Abundance**)
Isomers, Molecular (see **Molecular Structure and Spectra**)
Isomers, Nuclear (see **Nuclear Spectra**)
Isotopes (see **Atomic Mass and Abundance; Radioactivity**)

Kerr Effect (see **Optical Properties**)
Kinetic Theory of Gases (see **Gases; Statistical Mechanics and Thermodynamics**)

Liquid Helium (see **Helium, Liquid**)
Liquids
Evaporation of small drops at low pressures, Louis Monchick and Howard Reiss—839(A)

Luminescence
Afterglow of MgO single crystals, Eiso Yamaka—293
Distribution of trapping levels in CdSe, Harald C. Jensen and Robert J. Cashman—798(L)
Excitation energy and energy transfer by collision in fluorescent solutions, Milton Furst and Hartmut Kallmann—902
Excitation of ZnO phosphors by low-energy electrons, Ross E. Shrader—824(A)
Fluorescent response of NaI(Tl) to nuclear radiations, F. S. Eby and W. K. Jentschke—911
Light output of luminescent plastics, W. A. Thornton—292
Long-life luminescence and diffusion in MgO, B. Goodman —824(A)
Low-temperature luminescence of CdS, L. R. Furlong—1714(E)
Luminescence from NaCl, W. E. Spicer—824(A)
Quenching of NaI fluorescence by various gases and vapors, Howard G. Hanson—832(A)
Response of NaI(Tl), KI(Tl), and stilbene to fission fragments, J. C. D. Milton and J. S. Fraser—1508
Scintillation response of phosphors at low particle energies, G. T. Wright—569
Thermal ionization of impurities in polar crystals. I. Formal theory, H. D. Vasileff—603
Voltage dependence of electroluminescent brightness, B. T. Howard, H. F. Ivey, and W. Lehmann—799(L)
ZnS(Ag) phosphor mixtures for neutron detection, P. G. Koontz, G. R. Keepin, and J. E. Ashley—862(A)

Magnetic Fields (see **Electromagnetic Theory and Electrodynamics**)
Magnetic Properties
Adiabatic magnetization of superconducting sphere, R. L. Dolecek—25
Classical theory of temperature dependence of magnetic anisotropy energy, C. Zener—1335
Critical field phenomena in isotropic paramagnetic crystal, E. Ambler and R. P. Hudson—907
Derivation of magnetostriction and anisotropic energies for hexagonal, tetragonal, and orthorhombic crystals, W. P. Mason—302
Effects of anisotropy on thermodynamic properties of antiferromagnets, J. A. Eisele and F. Keffer—929
Electronic susceptibility in certain alloys, E. N. Adams, II, and R. Zitter—1705(L)
Ferromagnetic resonance in Fe-Ni alloys, Raymond Hoskins and George Wiener—1153(L)
Large magnetic Kerr rotation in BiMn alloy, B. W. Roberts and C. P. Bean—1494
Low-temperature acoustic relaxation in Ni-Fe ferrites, M. E. Fine and N. T. Kenney—1487
Magnetic and crystalline behavior of certain oxide systems with spinel and perovskite structures, Louis R. Maxwell and Stanley J. Pickart—1501
Magnetic anisotropy at 0°K, Jack R. Tessman—1192
Magnetic anisotropy constants of ferromagnetic spinels, R. S. Weisz—800(L)
Magnetic resonance absorption of diphenyl-picryl hydrazyl, M. A. Garstens, L. S. Singer, and A. H. Ryan—53
Magnetic susceptibility of residual bisulfate compounds of carbon, H. T. Pinnick—832(A)
Magnetization of Sn at superconducting transition, J. C. Thompson and C. F. Squire—287
Magnetostriction and crystal anisotropy of single crystals of hexagonal Co, R. M. Bozorth—311
Measurement of complex tensor permeability of ferrites, J. H. Rowen and W. von Aulock—1151(L)
Microwave properties of Mn-ferrite single crystal, P. E. Tannenwald—846(A)
Oscillatory thermal conductivity of Bi in magnetic fields at liquid He temperatures, J. Babiskin and M. C. Steele —822(A)
Reversible susceptibility of ferromagnetics, D. M. Grimes and D. W. Martin—889
Magnetic Resonance (see also **Nuclear Moments and Spin**)
Color-center magnetic resonances in LiF, C. K. Jen and N. W. Lord—1150(L)
Diamagnetic resonance in electronic conductors, J. G. Dorfman—1704(L)
Effect of spin-orbit coupling on magnetic resonance in some semiconductors, R. J. Elliott—266
Environmental effect on atomic H hfs in acids, Henry Zeldes and Ralph Livingston—1702(L)
Ferromagnetic resonance in Fe-Ni alloys, Raymond Hoskins and George Wiener—1153(L)
Hfs of nitrogen, Mark A. Heald and Robert Beringer—645
Hyperfine splitting of donor states in Si, J. M. Luttinger and W. Kohn—802(L)
Indirect exchange coupling of nuclear magnetic moments by conduction electrons, M. A. Ruderman and C. Kittel —99
Interaction of conduction electrons and nuclear magnetic moments in metallic Li, W. Kohn—590
Measurement of complex tensor permeability of ferrites, J. H. Rowen and W. von Aulock—1151(L)
Microwave properties of Mn-ferrite single crystal, P. E. Tannenwald—846(A)
Neutron spin from magnetic resonance experiment, C. P. Stanford, T. E. Stephenson, and Seymour Bernstein—983
Nuclear electric quadrupole interactions of B^{11} in kernite, H. L. Blood and W. G. Proctor—861(A)
Nuclear magnetic resonance in kernite, H. Waterman—862(A)
Nuclear quadrupole spectra in solids, M. H. Cohen—1278
Nuclear resonance of Nb^{93} in $KNbO_3$, R. M. Cotts and W. D. Knight—1285
Nuclear spin lattice relaxation in supercooled menthol, B. H. Muller and Myer Bloom—861(A)
Nuclear spin relaxation by translational diffusion. II. Diffusion in b.c.c. lattice, H. C. Torrey—690
Paramagnetic resonance in chromous sulfate pentahydrates, Kazuo Ono, Shoichiro Koide, Hisao Sekiyama, and Hidetaro Abe—38
Paramagnetic resonance in U salts, S. N. Ghosh, Walter Gordy, and D. G. Hill—36
Paramagnetic resonances in single crystals of $BaTiO_3$, A. W. Hornig, E. T. Jaynes, and H. E. Weaver—1703(L)
Polarization of As nuclei in Si semiconductor, A. Honig, —234(L)
Quantum theory of cyclotron resonance in semiconductors, W. Kohn and J. M. Luttinger—529(L)
Rb^{81} spin, magnetic moment, and hfs, J. P. Hobson, J. C. Hubbs, W. A. Nierenberg, and H. B. Silsbee—1450(L)
Rf-induced transitions of nuclear spins at electronic resonance frequency, Jerome I. Kaplan—238(L)
Rotational spectra of RbCl by molecular beam electric resonance method, J. W. Trischka and R. Braunstein —968
Spin and gyromagnetic ratio of C^{13} by collapse of spin-spin splitting, Virginia Royden—543(L)
Temperature dependence of nuclear resonance in metals, W. D. Knight—861(A)
Zeeman effects in Cl nuclear quadrupole resonance in $NaClO_3$, Yu Ting, Edward R. Manring, and Dudley Williams—408

Magnetic Resonance (Continued)
Zeeman splitting of nuclear quadrupole resonances, C. Dean—1053
Magneto-Optical Effects (see **Optical Properties**)
Magnetoresistance (see **Electrical Conductivity and Resistance; Semiconductors**)
Magnetostriction (see **Magnetic Properties**)
Mass Defects (see **Atomic Mass and Abundance**)
Mass Spectroscopy (see **Atomic Mass and Abundance; Methods and Instruments**)
Mathematical Methods
Age-dependent branching stochastic processes in cascade theory, A. T. Reid—751
Coulomb wave functions in transition region, Milton Abramowitz and H. A. Antosiewicz—75
Determination of α-α scattering phase shifts, James N. Snyder—1333
Evaluation of Coulomb wave functions along transition line, Milton Abramowitz and Philip Rabinowitz—77
Reflection of waves by inhomogeneous medium, V. A. Bailey—865
Solution of many-body scattering problems by Fredholm's equation, P. Swan—1144
Measurements (see **Methods and Instruments**)
Mechanics
Ablation from ultra-speed pellets, William C. White—844(A)
Application of engravement method to study of particle velocity distribution in explosively loaded cylinders, John Pearson and John S. Rinehart—844(A)
Critical angle associated with high-speed impact of sphere on thin plate, William A. Allen, Joe M. Mapes, and Wesley G. Wilson—844(A)
Effect of surface friction on high-speed penetration, Joseph M. Krafft—822(A)
Oscillation and stability in certain nonlinear systems, William M. Whyburn—843(A)
Mechanics, Quantum—Atomic Structure and Spectra (see **Atomic Structure and Spectra**)
Mechanics, Quantum—General (see **Quantum Mechanics**)
Mechanics, Quantum—Molecular Structure and Spectra (see **Molecular Structure and Spectra**)
Mechanics, Quantum—Nuclear (see **Nuclear Structure Theory**)
Mechanics, Quantum—of Solid Bodies (see **Crystalline State**)
Mechanics, Statistical (see **Statistical Mechanics and Thermodynamics**)
Meson Field Theory (see **Field Theory**)
Mesons and Hyperons (see also **Cosmic Radiation; Elementary Particle Interactions; Nuclear Reactions Induced by Mesons; Scattering of Mesons**)
Absolute differential range spectrum of low-energy cosmic-ray μ mesons, N. T. Seaton—853(A)
Cascade decay of negative hyperon, W. B. Fretter and E. W. Friesen—853(A)
Čerenkov radiation detector for the selection of slow particles, Carl M. York, Jr.—1635
Cloud-chamber evidence for charged counterpart of θ^0 particle, A. L. Hodson, J. Ballam, W. H. Arnold, D. R. Harris, R. Ronald Rau, George T. Reynolds, and S. B. Treiman—1089
Coulomb effect on photoproduction of low-energy charged mesons, J. R. Voss, T. R. Palfrey, and R. O. Haxby—830(A)
Cycle of world-wide changes in daily variation of meson intensity, V. Sarabhai, U. D. Desai, and D. Venkatesan—469
Electron spectrum from μ-meson decay, F. B. Harrison, C. L. Cowan, Jr., and F. Reines—1159(L)
Energetic disintegration of heavy nuclear fragment, W. F. Fry and M. S. Swami—809(L)
Energies of π^--mesonic x-ray K lines, M. B. Stearns, M. Stearns, S. DeBenedetti, and L. Leipuner—804(L)
Energy level displacements in pi-mesonic atoms, S. Deser, M. L. Goldberger, K. Baumann, and W. Thirring—774
Final-state interaction in multiple production of mesons in nucleon-nucleon collisions, Julius S. Kovacs—1454(A)
Fourth order corrections to meson-nucleon scattering in pseudoscalar meson theory, H. W. Wyld, Jr.—1661
High-energy electron pair produced by 113-Mev positive pion, Jay Orear, R. G. Glasser, D. M. Haskin, and Marcel Schein—1710(L)
Interaction of negative heavy meson, J. E. Naugle, H. P. Ney, P. S. Freier, and W. B. Cheston—1383
Ionization energy loss of mesons in NaI scintillation crystal, Theodore Bowen—754(A)
K mesons and charged hyperon produced by 3-Bev protons in emulsions, W. F. Fry and M. S. Swami—235(L)
Low-energy differential range spectrum of cosmic-ray μ mesons, A. Fafarman and M. H. Shamos—1096
Magnetic cloud-chamber study of V^s events, Y. B. Kim, J. R. Burwell, R. W. Huggett, and R. W. Thompson—229(L)
Negative pion mass from its radiative absorption in hydrogen, Kenneth M. Crowe and Robert H. Phillips—470
Neutral pion-deuteron production in 400-Mev n-p collisions, R. A. Schluter—734
Nonuniform charge distributions and μ-meson capture, F. Ferrari and C. Villi—1159(L)
Nuclear collisions at extreme relativistic energies, Marcel Schein, D. M. Haskin, and R. G. Glasser—829(A)
Nuclear fine structure in μ-mesonic atom, Boris A. Jacobsohn—1637
Photoproduction of charged mesons from deuterium, M. Sands, J. G. Teasdale, and R. L. Walker—849(A)
Photoproduction of mesons from H near threshold, Vincent Peterson and I. George Henry—850(A)
Possible existence of new hyperon, Y. Eisenberg—541(L)
Production of charged pions from hydrogen and carbon, A. H. Rosenfeld—130; 1714(E)
Production of pions in nucleon-nucleon collisions at cyclotron energies, A. H. Rosenfeld—139
Production spectra of cosmic-ray mesons in atmosphere, Stanislaw Olbert—1400
Reaction $p+p \rightarrow \pi^+ + d$ with polarized protons, T. H. Fields, J. G. Fox, J. A. Kane, R. A. Stallwood, and R. B. Sutton—812(L)
Search for production of μ-meson pairs by 345-Mev synchrotron beam, B. T. Feld, A. Julian, A. C. Odian, L. S. Osborne, and A. Wattenberg—1386
Unstable cosmic-ray particles observed in double cloud-chamber arrangement, W. H. Arnold, J. Ballam, H. Gursky, A. L. Hodson, R. Ronald Rau, George T. Reynolds, and S. B. Treiman—853(A)
Unstable nuclear fragment emitted from heavy-meson induced star, I. E. Naugle, P. S. Freier, and E. P. Ney—829(A)
Vacuum polarization in mesonic atoms, A. B. Mickelwait and H. C. Corben—1145
Metals (see **Crystalline State**)
Metastable Atoms (see **Atomic Structure and Spectra**)
Metastable Molecules (see **Molecular Structure and Spectra**)
Meteorology (see **Geophysics**)
Methods and Instruments
Applications of rapid sweeping to single-focusing mass spectrometer, C. Robert Lagergren—823(A)

Beam escape from synchrocyclotrons, Warren Fenton Stubbins—856(A)
Čerenkov counter for electron detection, R. K. Squire, B. J. Moyer, and J. E. Osher—856(A)
Čerenkov radiation detector for the selection of slow particles, Carl M. York, Jr.—1635
Densitometric measurement of emulsion tracks, E. P. Ney, John Naugle, Phyllis Freier—829(A)
Detection of Hg vapor by resonance ionization, K. C. Clark and L. Kanal—860(A)
Easily reproducible thermal neutron density standard, René Cohen—850(A)
Emulsion tables, Walter H. Barkas and George Hahn—859(A)
Experimental facilities and techniques used at Berkeley 60-in. cyclotron for irradiation effect studies, W. S. Gilbert and J. H. Pepper—862(A)
Gas-recoil fast neutron spectrometer, R. E. Benenson, M. B. Shurman, and W. Haeberli—836(A)
Geiger-Mueller counter tube age characteristics, W. C. Roesch and J. S. Reddie—854(A)
Gettering of vacuum vessel by Ti metal, Virgil L. Stout and Martin D. Gibbons—819(A)
Grain density and ionization loss in nuclear track emulsions, John R. Fleming and J. J. Lord—852(A)
High-energy γ-ray studies with nuclear track emulsion, Harry H. Heckman, Peter Giles, and Walter H. Barkas—858(A)
Mass doublet measurements using modulated magnetic field, Clayton F. Giese and T. L. Collins—823(A)
Mass measurement by multiple Coulomb scattering on stopped particles, R. G. Glasser—835(A)
Method for high-precision studies of rate processes, W. Haller and G. L. Calcamuggio—1454(A)
Methods of preparing thin film MgO secondary emission surfaces on Ag-Mg alloys, Peter Wargo—837(A)
MTR crystal spectrometer data printing system, G. L. Smith and L. G. Miller—849(A)
Neutrino recoil spectrometer. Investigation of A^m, O. Kofoed-Hansen—1045
Relation between width of x-ray line and resolving power of double-crystal spectrometer, Gosta Brogren—589
Response of NaI(Tl), KI(Tl), and stilbene to fission fragments, J. C. D. Milton and J. S. Fraser—1508
Scintillation response of phosphors at low particle energies, G. T. Wright—569
Semiautomatic apparatus for thermocouple comparison and calibration, T. M. Dauphinee—843(A)
Stabilization of potentials in precision double-focusing mass spectrometer, K. S. Quisenberry, T. T. Scolman, and T. L. Collins—823(A)
Suppression of coherent radiation by electrons in synchrotron, John S. Nodvick and David S. Saxon—180
Surface "channel" detection method for semiconductors, H. Christensen—827(A)
Time-of-flight mass spectrometer, Earl E. Hays—1454(A)
200-Mc phase detector, Edmund B. Tucker, Lawrence H. Johnston, and Donald E. Young—835(A)
"Zipper" scattering chamber, C. J. Cook—835(A)
ZnS(Ag) phosphor mixtures for neutron detection, P. G. Koontz, G. R. Keepin, and J. E. Ashley—862(A)

Microwaves (see also **Atomic Structure and Spectra; Magnetic Resonance; Molecular Structure and Spectra; Nuclear Moments and Spin**)
Microwave properties of Mn-ferrite single crystal, P. E. Tannenwald—846(A)
Phase noise in pre-excited oscillator system, Lawrence Johnston, Norton M. Hintz, and Harry J. Schulte—835(A)
200-Mc phase detector, Edmund B. Tucker, Lawrence H. Johnston, and Donald E. Young—835(A)

Miscellaneous

Mobility of Ions and Electrons (see **Ions and Electrons, Mobility**)

Molecular Aggregates
Moisture condensation patterns on glass and crystalline surfaces, W. C. Levengood—1454(A)

Molecular Beams (see **Atomic and Molecular Beams**)

Molecular Structure and Spectra
Absorption of microwaves by O_3 in mm wavelength region, J. O. Artman and J. P. Gordon—1237
Absorption studies of He metastable molecule, A. V. Phelps—832(A)
Centrifugal distortion in asymmetric top molecules. III. H_2O, D_2O, and HDO, D. W. Posener and M. W. P. Strandberg—1714(E)
Diffusion of metastable Hg molecules, A. O. McCoubrey and C. G. Matland—832(A)
Dissociation energy of NO and N_2, M. Brook and J. Kaplan—1540
Electromagnetic radiations from hydrocarbon flames, Samuel C. Lawrence, Jr.—860(A)
Excitation of air glow by electronic impact, C. Y. Fan—860(A)
Excitation of molecular vibrations in halogen-substituted methanes, Thomas Rossing and Sam Legvold—839(A)
Ground-state potential constants of ClO_3, J. K. Ward—845(A)
Magnetic interactions in $^2\Sigma$ molecules, Robert L. White—845(A)
Microwave absorption spectra of MnO_3F and ReO_3Cl, Ali Javan and A. Engelbrecht—649
Microwave spectra of alkali halides, A. Honig, C. H. Townes, M. L. Stitch, and M. Mandel—629
Polarized infrared absorption spectrum of gypsum, D. S. Webber—846(A)
Pressure broadening of OCS in foreign gas mixture, F. A. Liuima, A. V. Bushkovitch, and A. G. Rouse—434
Rotational spectra of RbCl by molecular beam electric resonance method, J. W. Trischka and R. Braunstein—968
Thomas-Fermi calculation of C—H bond moment in methane, H. Glazer and H. Reiss—838(A)

Moments, Nuclear (see **Nuclear Moments and Spin**)

Moments of Molecules (see **Molecular Structure and Spectra**)

Neutrino (see also **Nuclear Spectra; Radioactivity**)

Neutron Diffraction (see **Diffraction; Scattering of Neutrons**)

Neutrons (see **Elementary Particle Interactions**)

Noise
Dependence of signal-to-noise ratio in photoconductive PbSe layers on temperature of blackbody source, A. M. Crooker and E. B. Dorling—846(A)
Influence of different activating agents on flicker noise in oxide-coated cathodes, W. W. Lindemann—837(A)
Influence of tube structure and tube operating conditions upon flicker noise, H. J. Hannam—837(A)
Noise mechanisms in oxide-coated cathodes, A. van der Ziel—837(A)
Phase noise in pre-excited oscillator system, Lawrence H. Johnston, Norton M. Hintz, and Harry J. Schulte—835(A)
Vacuum fluctuation noise and dissipation, J. Weber—556

Nuclear Fission
Bk and Cf isotopes produced in neutron irradiation of Pu, L. B. Magnusson, M. H. Studier, P. R. Fields, C. M. Stevens, J. F. Mech, A. M. Friedman, H. Diamond, and J. R. Huizenga—1576
Correlation of spontaneous fission half-lives, M. H. Studier and J. R. Huizenga—545(L)

Nuclear Fission (Continued)
Fine structure in velocity distributions of slowed fission fragments, R. B. Leachman and H. W. Schmitt—1366
Fission and total reaction cross sections for 22-Mev protons on Th^{232}, U^{235}, and U^{238}, G. H. McCormick and B. L. Cohen—722
Fission yield fine structure in mass region 99–106, Donald R. Wiles and Charles D. Coryell—696
Fission yield of Gd^{159} and Tb^{161}, Henry G. Petrow and Gregory Rocco—1614
Gd and Tb radioisotopes as fission products of U^{235}, E. C. Freiling, L. R. Bunney, and N. E. Ballou—102
Response of NaI(Tl), KI(Tl), and stilbene to fission fragments, J. C. D. Milton and J. S. Fraser—1508
Nuclear Forces (see **Elementary Particle Interactions; Field Theory; Nuclear Structure Theory**)
Nuclear Induction (see **Magnetic Resonance; Nuclear Moments and Spin**)
Nuclear Isomers (see **Nuclear Spectra; Radioactivity**)
Nuclear Moments and Spin
Alignment of Na atoms, W. B. Hawkins—532(L)
Hfs of nitrogen, Mark A. Heald and Robert Beringer—645
Hyperfine splitting in ground state of atomic hydrogen, J. P. Wittke and R. H. Dicke—530(L)
Hyperfine splitting of donor states in Si, J. M. Luttinger and W. Kohn—802(L)
Indirect exchange coupling of nuclear magnetic moments by conduction electrons, M. A. Ruderman and C. Kittel—99
Interaction of conduction electrons and nuclear magnetic moments in metallic lithium, W. Kohn—590
Isotope shift in λ4415 Cd II, E. C. Woodward and D. R. Speck—529(L)
Microwave absorption spectra of MnO_3F and ReO_3Cl, Ali Javan and A. Engelbrecht—649
Na^{23} electric quadrupole moment, S. Sengupta—235(L)
Nd and Gd hfs, Kiyoshi Murakawa—1543
Neutron spin from magnetic resonance experiment, C. P. Stanford, T. E. Stephenson, and Seymour Bernstein—983
Np^{239} nuclear spin, John G. Conway and Ralph D. McLaughlin—541(L)
Nuclear electric quadrupole interactions of B^{11} in kernite, H. L. Blood and W. G. Proctor—861(A)
Nuclear fine structure in the μ-mesonic atom, Boris A. Jacobsohn—1637
Nuclear magnetic octupole moments of stable Ga isotopes, R. T. Daly, Jr., and J. H. Holloway—539(L)
Nuclear quadrupole spectra in solids, M. H. Cohen—1278
Nuclear resonance of Nb^{93} in $KNbO_3$, R. M. Cotts and W. D. Knight—1285
Nuclear spin relaxation by translational diffusion. II. Diffusion in b.c.c. lattice, H. C. Torrey—690
Optical studies of radioactive Hg, F. Bitter, S. P. Davis, B. Richter, and J. E. R. Young—1531
Polarization of As nuclei in Si semiconductor, A. Honig—234(L)
Rb^{81} spin, magnetic moment, and hfs, J. P. Hobson, J. C. Hubbs, W. A. Nierenberg, and H. B. Silsbee—1450(L)
Rf-induced transitions of nuclear spins at electronic resonance frequency, Jerome I. Kaplan—238(L)
Rotational spectra of RbCl by molecular beam electric resonance method, J. W. Trischka and R. Braunstein—968
Spin and gyromagnetic ratio of C^{13} by collapse of spin-spin splitting, Virginia Royden—543(L)
Spins of excited states of some odd A nuclei according to collective model, Richard L. Moore—858(A)
Stern-Gerlach experiment on polarized neutrons, J. E. Sherwood, T. E. Stephenson, and Seymour Bernstein—1546
Zeeman effects in Cl nuclear quadrupole resonance in $NaClO_3$, Yu Ting, Edward R. Manring, and Dudley Williams—408
Zeeman splitting of nuclear quadrupole resonances, C. Dean—1053
Nuclear Photoeffects
Absolute cross section *versus* energy of $Cu^{63}(\gamma,n)$ and $Cu^{63}(\gamma,2n)$ reactions, Arthur I. Berman and Karl L. Brown—83
Cloud-chamber investigation of high-energy photonuclear reactions, W. E. Matheson, C. R. Carlson, F. S. Mathews, R. O. Haxby, and R. M. Whaley—826(A)
Coulomb effect on photoproduction of low-energy charged mesons, J. R. Voss, T. R. Palfrey, and R. O. Haxby—830(A)
High-energy γ-ray studies with nuclear track emulsions, Harry H. Heckman, Peter C. Giles, and Walter H. Barkas—858(A)
High-energy photodisintegration of deuteron, J. C. Keck, A. V. Tollestrup, and W. R. Smythe, II—850(A); A. V. Tollestrup, J. C. Keck, and W. R. Smythe, II—850(A)
Photodisintegration of He, Everett G. Fuller—1306
Photoproduction of charged mesons from deuterium, M. Sands, J. G. Teasdale, and R. L. Walker—849(A)
Photoproduction of mesons from H near threshold, Vincent Peterson and I. George Henry—850(A)
Photostar production up to 500 Mev, Vincent Peterson—850(A)
Nuclear Reactions, General (see also **Elementary Particle Interactions; Scattering**)
Comparison of nitrogen- and proton-induced nuclear reactions, B. L. Cohen, H. L. Reynolds, and A. Zucker—1817
Correspondence between semiclassical and quantum treatments of Coulomb excitation, G. Breit and P. B. Daitch—1447(L)
Coulomb excitation, K. Alder and A. Winther—237(L)
Energy distribution of nuclear reaction products, H. H. Barschall and J. L. Powell—713
Excitation functions for nitrogen-induced nuclear reactions in carbon, H. L. Reynolds and A. Zucker—1615
Interaction of heavy primary cosmic rays in Pb, Y. Eisenberg—1378
Nuclear collisions at extreme relativistic energies, Marcel Schein, D. M. Haskin, and R. G. Glasser—829(A)
Nuclear multipole transitions in inelastic electron scattering, L. I. Schiff—765
Validity of semiclassical treatment of Coulomb excitation, P. B. Daitch, J. P. Lazarus, M. H. Hull, Jr., F. D. Benedict, and G. Breit—1449(L)
Nuclear Reactions Induced by α Particles and He^3 (see also **Scattering of α Particles**)
Charged particles from the bombardment of Li^7 by He^3, C. D. Moak, W. M. Good, and W. E. Kunz—1363
Coulomb excitation of F^{19} by α particles, R. Sherr, C. W. Li, and R. F. Christy—1258
Coulomb excitation process in lighter odd-mass nuclei, G. M. Temmer and N. P. Heydenburg—426
Inelastic scattering of α particles by Li, C. W. Li and R. Sherr—389
Properties of nuclei of mass 19, G. A. Jones, W. R. Phillips, C. M. P. Johnson, and D. H. Wilkinson—547(L)
Search for 15-Mev γ radiation from $N^{14}+d$ and $Be^9+\alpha$, V. K. Rasmussen, John R. Rees, M. B. Sampson, and N. S. Wall—812(L)

Nuclear Reactions Induced by Deuterons and Tritons (see also **Scattering of Deuterons**)
Angular distributions in (d,p) reactions with Ti^{47} and Ti^{48}, F. B. Shull and M. M. Bretscher—826(A)
Angular distributions of protons from $Na^{23}(d,p)Na^{24}$ and $Ti^{47,48}(d,p)Ti^{48,49}$, M. M. Bretscher, J. O. Alderman, A. Elwyn, and F. B. Shull—103
B^{10} and Be^{8} excited states, T. W. Bonner and C. F. Cook —122
Be^{10} energy levels, J. J. Jung and C. K. Bockelman—1353
$Co^{59}(d,p)Co^{60}$ magnetic analysis, G. M. Foglesong and D. G. Foxwell—1001
Disintegration of Li^{6} and Li^{7} by 0.24-Mev tritons, K. W. Allen, E. Almqvist, J. T. Dewan, and T. P. Pepper—684
(d,p) reactions from C, N, and O, A. Sperduto, W. W. Buechner, C. K. Bockelman, and C. P. Browne—1316
Excitation curve for $C^{14}(d,p)C^{15}$ and properties of C^{15}, James A. Rickard, Emmett L. Hudspeth, and William W. Clendenin—1272
γ radiation from deuterons on several light nuclei, L. C. Thompson—369
H^{3} and He^{3} production in high-energy deuteron-deuteron collisions, Charles S. Godfrey—1621
Magnetic analysis of $O^{18}(d,p)O^{19}$ and $N^{15}(d,p)N^{16}$ reactions, Jacques Thirion, Rene Cohen, and Ward Whaling —850(A)
Neutron binding energies from (d,p) Q values, N. S. Wall—664
$O^{16}(d,p)O^{17}$ angular distribution, D. M. Van Patter, B. E. Simmons, T. F. Stratton, and D. M. Zipoy—825(A)
$O^{17}(d,p)O^{18}$ magnetic analysis, Katarina Ahnlund—999
$O^{18}(d,p)O^{19}$ proton groups, Curt Mileikowsky and Katarina Ahnlund—996
O^{19} excited state, T. F. Stratton, K. F. Famularo, H. D. Holmgren, and R. V. Stuart—825(A)
Production of tritons in high-energy deuteron-deuteron collisions, C. S. Godfrey—493
Proton angular distributions from deuteron bombardment of Bi^{209}, Pb^{207}, and Y^{89}, N. S. Wall—670
Proton polarization in (d,p) reactions, W. B. Cheston—1590
Radiative capture of deuterons by He^{3}, J. M. Blair, N. M. Hintz, and D. M. Van Patter—1023
Search for 15-Mev γ radiation from $N^{14}+d$ and $Be^{9}+\alpha$, V. K. Rasmussen, John R. Rees, M. B. Sampson, and N. S. Wall—812(L)

Nuclear Reactions Induced by Mesons (see also **Elementary Particle Interactions; Mesons; Scattering of Mesons**)
Absorption of positive pions by deuterium at 76 and 94 Mev, Henry L. Stadler—496
Comparison of proton- and meson-produced stars of comparable excitation energy, A. D. Sprague, D. M. Haskin, R. G. Glasser, and Marcel Schein—830(A)
Inelastic scattering of 500-Mev negative pions in emulsion nuclei, M. Blau and Martin Caulton—150
Interaction of negative heavy meson, J. E. Naugle, H. P. Ney, P. S. Freier, and W. B. Cheston—1383
Negative pion mass from its radiative absorption in hydrogen, Kenneth M. Crowe and Robert H. Phillips—470
Nonuniform charge distributions and μ-meson capture, F. Ferrari and C. Villi—1159(L)
Possible existence of new hyperon, Y. Eisenberg—541(L)
Total cross sections for negative and positive pions in hydrogen and deuterium, J. Ashkin, J. P. Blaser, F. Feiner, J. G. Gorman, and M. O. Stern—1104
Unstable nuclear fragment emitted from heavy-meson induced star, J. E. Naugle, P. S. Freier, and E. P. Ney —829(A)

Nuclear Reactions Induced by Neutrons (see also **Elementary Particle Interactions; Scattering of Neutrons**)
Absorption cross section of B for thermal neutrons, G. von Dardel and N. G. Sjöstrand—1566
Angular distribution of protons from (d,p) reactions on Be^{9}, N^{14}, and Zn^{68}, F. S. Eby—1355
$B^{11}(n,\alpha)Li^{8}$ reaction, S. A. Heiberg—856(A)
Bk and Cf isotopes produced in neutron irradiation of Pu, L. B. Magnusson, M. H. Studier, P. R. Fields, C. M. Stevens, J. F. Mech, A. M. Friedman, H. Diamond, and J. R. Huizenga—1576
Contour diagrams of thermal neutron absorption cross sections, J. E. Evans—849(A)
Diffusion parameters of thermal neutrons in water, G. von Dardel and N. G. Sjöstrand—1245
Elastic and inelastic scattering of 14-Mev neutrons by deuterons, John D. Seagrave—855(A)
Final-state interaction in multiple production of mesons in nucleon-nucleon collisions, Julius S. Kovacs—1454(A)
γ radiation from interaction of 3.2-Mev neutrons with various materials, V. E. Scherrer, B. A. Allison, and W. R. Faust—386
Hf and Zr total cross-section measurements, E. G. Joki and J. E. Evans—849(A)
Indirect measurement of n-n interaction, Robert H. Phillips and Kenneth M. Crowe—484
Inelastic neutron scattering in Fe, D. L. Lafferty, L. A. Rayburn, and T. M. Hahn—381
Li^{6} total cross section for neutrons, C. H. Johnson, H. B. Willard, and J. K. Bair—985
Model for nuclear reactions with neutrons, H. Feshbach, C. E. Porter, and V. F. Weisskopf—448
Nb^{93m} production by pile irradiation of Nb, R. P. Schuman—121
Neutral pion-deuteron production in 400-Mev n-p collisions, R. A. Schluter—734
Neutron-capture cross sections by capture-γ counting, Edward Meservey—1006
Neutron cross sections of light nuclei, Charles E. Porter —836(A)
Neutron resonances in rare earth elements, V. L. Sailor, H. H. Landon, and H. L. Foote, Jr.—1014
Production of deuterons in high-energy nuclear bombardment of nuclei, W. N. Hess and B. J. Moyer—859(A)
Production of pions in nucleon-nucleon collisions at cyclotron energies, A. H. Rosenfeld—139
Pulse amplitude distribution in BF_3 counter irradiated with 4.87-Mev neutrons, D. B. James, W. Kubelka, and S. A. Heiberg—856(A)
Radiative capture of 300-Mev neutrons in hydrogen, John DePangher—859(A)
Ratio of Γ_n^0/D for slow-neutron resonances, R. S. Carter, J. A. Harvey, D. J. Hughes, and V. E. Pilcher—113
Slow neutron cross sections of Au, Ag, In, Ni, and Ni oxide, R. G. Allen, T. E. Stephenson, C. P. Stanford, and S. Bernstein—1297
Total cross sections of liquefied gases for high-energy neutrons, Peter Hillman, R. H. Stahl, and N. F. Ramsey —115

Nuclear Reactions Induced by Protons (see also **Elementary Particle Interactions; Scattering of Protons**)
Angular distribution of 12- and 16-Mev γ rays from proton bombardment of thin B target, H. H. Givin, G. K. Farney, T. M. Hahn, and B. D. Kern—1337
Angular distributions of α particles from the $Na^{23}(p,\alpha)Ne^{20}$ reaction, P. H. Stelson—1584
$C^{14}(p,\gamma)N^{15}$ reaction above (p,n) threshold, H. E. Gove, G. A. Bartholomew, E. B. Paul, and A. E. Litherland —825(A)

Nuclear Reactions Induced by Protons (Continued)
Comparison of nitrogen- and proton-induced nuclear reactions, B. L. Cohen, H. L. Reynolds, and A. Zucker—1617
Comparison of proton- and meson-produced stars of comparable excitation energy, A. D. Sprague, D. M. Haskin, R. G. Glasser, and Marcel Schein—830(A)
Conservation of number of nucleons, F. Reines, C. L. Cowan, Jr., and M. Goldhaber—1157(L)
Coulomb excitation of Nd, B. E. Simmons, D. M. Van Patter, K. F. Famularo, and R. V. Stuart—826(A)
Cs reactions with protons at 40, 80, 100, 150, and 240 Mev, Richard W. Fink and Edwin O. Wiig—185
Direct interaction in $Fe^{56}(p,p')Fe^{56}$, G. Schrank, P. C. Gugelot, and I. E. Dayton—1156(L)
Electric excitation of Au^{197}, C. F. Cook, C. M. Class, and J. T. Eisinger—658
Emission of high-energy γ line from C^{12}, David Cohen, Charles Waddell, Harlan Shaw, and Burton J. Meyer —714
Energy levels of Al^{27}, C. P. Browne, S. F. Zimmerman, and W. W. Buechner—725
Excitation function of $C^{13}(p,pn)C^{13}$ reaction in Bev region, R. L. Wolfgang and G. Friedlander—190
15.2-Mev γ emission from C^{12}, Charles Waddell, Harlan Shaw, David Cohen, and B. J. Moyer—858(A)
Fission and total reaction cross sections for 22-Mev protons on Th^{232}, U^{235}, and U^{238}, G. H. McCormick and B. L. Cohen—722
Fluorine-plus-proton reactions, R. W. Peterson, W. A. Fowler, and C. C. Lauritsen—1250
γ radiation from bombardment of C by protons, H. H. Woodbury, A. V. Tollestrup, and R. B. Day—1713(E)
γ radiation from proton bombardment of oxygen, J. B. Warren, K. A. Laurie, D. B. James, and K. L. Erdman —857(A)
γ radiation from reactions $Na^{23}+p$, J. O. Newton—241(L)
γ rays from $C^{13}(p,\gamma)N^{14}$ and $Na^{23}(p,\gamma)Mg^{24}$ reactions, B. Hird, C. H. Collie, J. Butler, and C. Whitehead—702
γ rays from Li^6+p, K. L. Erdman, J. B. Warren, D. B. James, and T. Alexander—858(A)
γ rays from (p,γ) reactions in B^{11} and Mg^{24}, D. S. Craig, W. G. Cross, and R. G. Jarvis—825(A)
γ rays from proton capture in Li^7 and F^{19}, E. B. Nelson, W. Lawrence, and R. R. Carlson—825(A)
Inelastic proton scattering cross section of F^{19}, C. A. Barnes, W. A. Fowler, C. C. Lauritsen, and R. W. Peterson—851(A)
K mesons and charged hyperon produced by 3-Bev protons in emulsions, W. F. Fry and M. S. Swami—235(L)
Neutrons from reaction $C^{14}(p,n)N^{14}$, A. E. Litherland, E. B. Paul, G. A. Bartholomew, and H. E. Gove—825(A)
Production of charged pions from hydrogen and carbon, A. H. Rosenfeld—130; 1714(E)
Production of deuterons in high-energy nuclear bombardment of nuclei, W. N. Hess and B. J. Moyer—859(A)
Production of pions in nucleon-nucleon collisions at cyclotron energies, A. H. Rosenfeld—139
Reaction $p+p\rightarrow\pi^++d$ with polarized protons, T. H. Fields, J. G. Fox, J. A. Kane, R. A. Stallwood, and R. B. Sutton—812(L)
Reactions of cobalt with protons at 60, 100, 170, and 240 Mev, Genevieve D. Wagner and Edwin O. Wiig—1100
Resonances in $Li^7(p,n)Be^7$, Robert K. Adair—709
Resonances in proton bombardment of C^{14}, G. A. Bartholomew, F. Brown, H. E. Gove, A. K. Litherland, and E. B. Paul—1154(L)
Scattering of 9.5-Mev protons by nitrogen, R. G. Freemantle, D. J. Prowse, and J. Rotblat—1268
Scattering of 9.5 protons by neon and argon, R. G. Freemantle, D. J. Prowse, A. Hossain, and J. Rotblat—1270
Scattering of 10-Mev protons on C and Mg, Gerhard E. Fischer—704
Short-lived radionuclides produced by synchrocyclotron, H. Tyrén and P. A. Tove—773
Total cross sections of light elements for 208-Mev and 315-Mev protons, Hervasio G. de Carvalho—398
Nuclear Scattering (see **Scattering**)
Nuclear Spectra (see also **Nuclear Reactions**; **Radioactivity**)
α-γ directional correlation measurements with liquid film sources, T. B. Novey—547(L)
Angular correlation of three nuclear radiations, G. R. Satchler—1713(E)
As^{76} disintegration, M. Sakai, B. Murray, and J. D. Kurbatov—862(A)
B^{10} and Be^9 excited states, T. W. Bonner and C. F. Cook —122
Be^{10} energy levels, J. J. Jung and C. K. Bockelman—1353
Bi^{210} β spectrum using diffusion cloud chamber, A. A. Silvidi and J. G. Maxwell—1454(A)
Bk and Cf isotopes produced in neutron irradiation of Pu, L. B. Magnusson, M. H. Studier, P. R. Fields, C. M. Stevens, J. F. Mech, A. M. Friedman, H. Diamond, and J. R. Huizenga—1576
C^{14} and S^{35} β spectra, A. Moljk and S. C. Curran—395
C^{14} β spectrum, H. H. Forster and A. Oswald—1030
Capture-positron branching ratios, P. F. Zweifel—1572
Ce^{139} disintegration, C. H. Pruett and R. G. Wilkinson—1340
Ce^{144} and Pr^{144} γ radiation, W. E. Kreger and C. Sharp Cook—1279
Ce^{144} and Pr^{144} γ-radiation energies, J. M. Cork, M. K. Brice, and L. C. Schmid—1295
Coulomb excitation, K. Alder and A. Winther—237(L)
Coulomb excitation of F^{19} by α particles, R. Sherr, C. W. Li, and R. F. Christy—1258
Coulomb excitation of Nd, B. E. Simmons, D. M. Van Patter, K. F. Famularo, and R. V. Stuart—826(A)
Coulomb excitation process in lighter odd-mass nuclei, G. M. Temmer and N. P. Heydenburg—426
Cs^{134} decay γ-ray energies, M. C. Joshi and B. V. Thosar —1022
Decay characteristics of some short-lived nuclides of low atomic number, R. M. Kline and D. J. Zaffarano—1620
Direct evaluation of fractional parentage coefficients using Young operators. General theory and $\langle 4|2,2\rangle$ coefficients, H. A. Jahn—989
Dy^{160} energy levels, V. Keshishian, H. W. Kruse, R. J. Klotz, and C. M. Fowler—1050
Emission of high-energy γ line from C^{12}, David Cohen, Charles Waddell, Harlan Shaw, and Burton J. Meyer —714
Eu^{152} and Eu^{154} long-lived radioactivity, R. E. Slattery, D. C. Lu, and M. L. Wiedenbeck—465
15.2-Mev γ emission from C^{12}, Charles Waddell, Harlan Shaw, David Cohen, and B. J. Moyer—858(A)
Fluorine-plus-proton reactions, R. W. Peterson, W. A. Fowler, and C. C. Lauritsen—1250
γ radiation from bombardment of C by protons, H. H. Woodbury, A. V. Tollestrup, and R. B. Day—1713(E)
Ge^{75m} (49 sec), Ge^{77m} (52 sec), and Ge^{77} (12 hr) decay, S. B. Burson, W. C. Jordan, and J. M. LeBlanc—1555
Ho^{164} radiations, Hugh N. Brown and Robert A. Becker —1372
I^{131} γ spectrum studies with scintillation and thick lens spectrometer, M. Sakai, B. Murray, and J. D. Kurbatov —862(A)
I^{132} decay scheme, H. L. Finston and W. Bernstein—71

Internal conversion coefficients in decay of Mn^{52}, Co^{60}, and Sc^{46}, Glen L. Keister—855(A)
Ir^{191} E3 isomer, J. W. Mihelich, M. McKeown, and M. Goldhaber—1450(L)
Ir^{191m} (5 sec) following Os^{191} decay, R. A. Naumann and J. B. Gerhart—1452(L)
Ir^{192} and Ir^{194} disintegration, M. W. Johns and S. V. Nablo—1599
Ir^{193m} radiations, J. P. Mize, M. E. Bunker, and J. W. Starner—444
Li^6 energy levels, A. Galonsky and M. T. McEllistrem—826(A)
Low-lying l states in even-even nuclei, Frank Stephens, Jr., Frank Asaro, and I. Perlman—1568
Na^{22} K-capture/positron ratio, W. E. Kreger and C. Sharp Cook—854(A); W. E. Kreger—1554
Nb^{93m} production by pile irradiation of Nb, R. P. Shuman—121
Ne^{22} internal conversion, R. D. Leamer and G. W. Hinman—1607
Neutrino recoil spectrometer. Investigation of A^{37}, O. Kofoed-Hansen—1045
Nuclear forces and β-decay matrix elements, Roland F. Herbst—372
O^{16} energy levels, David M. Dennison—378
Orbital electron capture in heaviest elements, R. W. Hoff and S. G. Thompson—1350
Orbital electron excitation associated with electron capture in A^{37}, Max Wolfsberg—1712(L)
Pa^{232} radiations, C. I. Browne, D. C. Hoffman, H. L. Smith, M. E. Bunker, J. P. Mize, J. W. Starner, R. L. Moore, and J. P. Balagna—827(A)
Pb long-lived isotopes, J. R. Huizenga and C. M. Stevens—548(L)
Pm^{150} decay, Vera Kistiakowsky Fischer—1549
Po^{211} α-emitting isomer, W. A. Jentschke, A. C. Juveland, and G. H. Kinsey—231(L)
Pr neutron-deficient activities, Thomas H. Handley and Elmer L. Olson—1003
Pr^{144} decay γ radiation, C. Sharp Cook and W. E. Kreger—855(A)
Properties of nuclei of mass 19, G. A. Jones, W. R. Phillips, C. M. P. Johnson, and D. H. Wilkinson—547(L)
Pt^{188} identification, Robert A. Naumann—90
Radiations from some odd-odd $N=Z$ nuclei, David Green and J. Reginald Richardson—858(A)
Radiations of neutron-deficient isotopes of xenon and iodine, Hirdaya B. Mathur and Earl K. Hyde—126
RaE β spectrum, E. A. Plassmann and L. M. Langer—1593
Resonance scattering of γ rays by nuclei, A. M. Cormack—716
Rh^{109} decay, D. B. Kochendorfer and Donald J. Farmer—855(A)
S^{35} β decay, K-electron ejection, William Rubinson and J. J. Howland—1610
Ta^{180} decay, J. J. Murray, P. Snelgrove, P. E. Marmier, and J. W. M. DuMond—858(A)
Ti^{44}, new Ti nuclide, R. A. Sharp and R. M. Diamond—1713(E)
Ti^{51} (5.8 min) decay, W. C. Jordan, S. B. Burson, and J. M. LeBlanc—1582
Two-step cascades in Cl^{36} and Cd^{114} neutron-capture γ-ray spectra, Arthur L. Recksiedler and Bernard Hamermesh—109
UX_1, UX_2, and UZ decay, Sven A. E. Johansson—1075
W^{188} rotational levels, R. F. Christy—858(A)

Nuclear Structure Theory (see also **Nuclear Reactions; Nuclear Spectra**)
α-decay theory with surface well potential, George H. Winslow—1032
Energy levels of O^{16} nucleus, David M. Dennison—378
Evidence for two-body spin-orbit forces in nuclei, J. P. Elliott and A. M. Lane—1160(L)
Hole configurations in light nuclei, R. F. Christy and W. A. Fowler—851(A)
Mesonic corrections to quadrupole moment of deuteron, A. M. Sessler—793
Model for nuclear reactions with neutrons, H. Feshbach, C. E. Porter, and V. F. Weisskopf—448
Multi-parameter nuclear wave functions in central-field approximation, Erwin H. Kronheimer—1680
Na^{23} electric quadrupole moment, S. Sengupta—235(L)
Neutron cross sections of light nuclei, Charles E. Porter—836(A)
Nonuniform charge distributions and μ-meson capture, F. Ferrari and C. Villi—1159(L)
n-p mass difference, W. G. Holladay and R. G. Sachs—810(L)
Nuclear forces and β-decay matrix elements, Roland F. Herbst—372
Nuclear normal modes, Ingram Bloch and Yü-Chang Hsieh—382
Nuclear saturation and two-body forces. II. Tensor forces, K. A. Brueckner—508
Pairing effects in Coulomb energies and radii of mirror nuclei, B. C. Carlson and I. Talmi—436
Resonances in $Li^7(p,n)Be^7$, Robert K. Adair—709
Spin-orbit interactions in many-body nuclear shell theory, Ingram Bloch and Yü-Chang Hsieh—855(A)
Spins of excited states of some odd-A nuclei according to collective model, Richard L. Moore—858(A)
W^{185} rotational levels, R. F. Christy—858(A)

Optical Instruments (see **Methods and Instruments**)
Optical Properties (see also **Luminescence**)
Action spectra for photoconductivity of dye films, John W. Weigl—834(A)
Afterglow of MgO single crystals, Eiso Yamaka—293
Color centers in chrome alum crystals, E. A. Braun, A. Many, and A. E. Simchen—1505
Distribution of trapping levels in CdSe, Harald C. Jensen and Robert J. Cashman—798(L)
Effect of dislocations on optical absorption edge in nonmetals, R. M. Blakney and D. L. Dexter—227(L)
Electrical and optical properties of InSe, R. W. Damon and R. W. Redington—1498
Electrical and optical properties of intermetallic compounds. I. InSb, R. G. Breckenridge, R. F. Blunt, W. R. Hosler, H. P. R. Frederikse, J. H. Becker, and W. Oshinsky—571; II. GaSb, R. F. Blunt, W. R. Hosler, and H. P. R. Frederikse—576; III. AlSb, R. F. Blunt, H. P. R. Frederikse, J. H. Becker, and W. R. Hosler—578
Electronic structure of MgO, J. R. Stevenson—839(A)
Exciton bands in crystalline benzene, David Fox and Otto Schnepp—1196
Infrared spectrum of $BaTiO_3$, R. T. Mara, G. B. B. M. Sutherland, and H. V. Tyrell—801(L)
K band in additively colored KCl, H. W. Etzel and F. E. Geiger, Jr.—225(L)
Large magnetic Kerr rotation in BiMn alloy, B. W. Roberts and C. P. Bean—1494
Optical absorption spectra of stoichiometric single crystals of MgO, W. T. Peria—824(A)
Optical and infrared absorption of Cu at 4.2°K, Manfred A. Biondi—534(L)

Optical Properties (Continued)
Optical and infrared volume absorptivity of metals, T. Holstein—535(L)
Optical studies of injected carriers. III. Infrared absorption in Ge at low temperatures, Roger Newman—1188
PbTe optical properties, Marvin E. Lasser and Henry Levinstein—47
Production and bleaching of color centers in x-rayed alkali halide crystals, I. L. Mador, R. F. Wallis, M. C. Williams, and R. C. Herman—617
Properties of Ge doped with Fe. I. Electrical conductivity, W. W. Tyler and H. H. Woodbury—874
Reversibility of additive coloring reaction in KCl, D. R. Westervelt—844(A)
Shapes of absorption and emission lines of impurities in solids, D. L. Dexter—615
Uv absorption in BaO films, Koji Okumura—1704(L)
Uv transmission and α-bombardment conduction inhomogeneities in diamond, A. J. Ahearn—828(A)

Pair Production (see **Electrons and Positrons**)
Phosphors and Phosphorescence (see **Luminescence**)
Photoconductivity (see **Electrical Conductivity and Resistance**)
Photodisintegration (see **Nuclear Photoeffects**)
Photoelasticity (see **Elasticity and Plasticity**)
Photoelectric Effect (see **Electrical Properties**)
Photography and Photographic Emulsions (see **Methods and Instruments; Range and Energy Loss**)
Photometry (see **Methods and Instruments**)
Photons (see **Radiation**)
Photovoltaic Effect (see **Electrical Properties; Semiconductors**)
Piezoelectric Effect (see **Dielectrics and Dielectric Properties**)
Plasticity (see **Elasticity and Plasticity**)
Polarization, Electrical (see **Dielectrics and Dielectric Properties**)
Polymers (see **Molecular Aggregates**)
Positrons (see **Electrons and Positrons**)
Probability (see **Mathematical Methods**)
Proceedings of the American Physical Society
Spring Meeting of the Ohio Section at Ohio University, Athens, Ohio, April 16–17, 1954—814
Minneapolis meeting at Minneapolis, Minnesota, June 28–30, 1954 [Bull. Am. Phys. Soc. **29**, No. 5 (1954)]—817
Pacific Northwest Meeting at University of Washington, Seattle, Washington, July 7–10, 1954 [Bull. Am. Phys. Soc. **29**, No. 6 (1954)]—842
Fall Meeting of the Ohio Section at University of Toledo, Toledo, Ohio, October 8–9, 1954—1454
Protons (see **Elementary Particle Interactions**)

Quantum Electrodynamics (see also **Field Theory**)
Calculation of potentials from new Tamm-Dancoff equation, J. C. Taylor—1438
Direct proof of covariance of Gupta's indefinite metric in quantum electrodynamics, Frederik J. Belinfante—780
Evaluation of collision matrix for Dirac particles in external potential, B. Zumino—202
Multiple photon production in electron-positron annihilation, Suraj N. Gupta—1453(L)
n-p mass difference, W. G. Holladay and R. G. Sachs—810(L)
Nucleon-antinucleon scattering and vacuum polarization, Kenneth A. Johnson—1659
Properties of Bethe-Salpeter wave functions, G. C. Wick—1124
Radiative effects in constant field, Roger G. Newton—523
Scattering of light of very low frequency by systems of spin $\frac{1}{2}$, F. E. Low—1428
Scattering of low-energy photons by particles of spin $\frac{1}{2}$, M. Gell-Mann and M. L. Goldberger—1433
Solutions of Bethe-Salpeter equation, R. E. Cutkosky—1135
Tamm-Dancoff methods and nuclear forces, Behram Kurşunoğlu—1690
Vacuum polarization in mesonic atoms, A. B. Mickelwait and H. C. Corben—1145
Vacuum polarization in strong Coulomb field, Eyvind Wichmann and Norman M. Kroll—232(L)

Quantum Mechanics
Approximate variational principle in quantum statistics, William M. MacDonald, III, and John M. Richardson—18
Bound states and formal theory of scattering, M. N. Hack—196; 1714(E)
Coulomb wave functions in transition region, Milton Abramowitz and H. A. Antosiewicz—75
Evaluation of Coulomb wave functions along transition line, Milton Abramowitz and Philip Rabinowitz—77
Expansion of wave packets, Daniel S. Ling, Jr.—216
Method of transition probabilities in quantum mechanics and quantum statistics, P. T. Landsberg—1420
Model of causal interpretation of quantum theory in terms of fluid with irregular fluctuations, D. Bohm and J. P. Vigier—208
Quantization of multiple frequency linear systems, J. K. Percus—1147
Quantum theory of irreversible processes, U. Fano—869
Solution of temperature-perturbed Thomas-Fermi equation, J. J. Gilvarry—944
Space-time representation in wave mechanics: Illustration of method, Malcolm K. Brachman—516
Thermodynamics of Thomas-Fermi atom at low temperature, J. J. Gilvarry—934
Variational principle in quantum mechanics, N. M. Hugenholtz—1158(L)

Quenching of Radiation (see **Radiation**)

Radar (see **Methods and Instruments; Radiation**)
Radiation (see also **Gamma Rays; Range and Energy Loss; X-Rays**)
Alignment of Na atoms, W. B. Hawkins—532(L)
Detection of Hg vapor by resonance ionization, K. C. Clark and L. Kanal—860(A)
Differential cross-section measurements for 1-Mev bremsstrahlung, J. W. Motz and William Miller—544(L)
Entropy of radiation, Philip Rosen—555
High-energy γ-ray studies with nuclear track emulsions, Harry H. Heckman, Peter C. Giles, and Walter H. Barkas—858(A)
Optical studies of radioactive Hg, F. Bitter, S. P. Davis, B. Richter, and J. E. R. Young—1531
Resonance scattering of γ rays by nuclei, A. M. Cormack—716
Scattering of γ rays by nucleons, R. H. Capps and R. G. Sachs—540(L)
Scattering of light of very low frequency by systems of spin $\frac{1}{2}$, F. E. Low—1428
Scattering of low-energy photons by particles of spin $\frac{1}{2}$, M. Gell-Mann and M. L. Goldberger—1433
Statistics of electromagnetic radiation scattered by turbulent medium, Richard A. Silverman and Martin Balser—560
Suppression of coherent radiation by electrons in synchrotron, John S. Nodvick and David S. Saxon—180
Thick target bremsstrahlung spectra for 1.00-, 1.25-, and

140-Mev electrons, William Miller, J. W. Motz, and Carmen Cialella—1344
Radio Waves (see **Radiation**)
Radioactivity (see also **Nuclear Spectra**)
α-decay theory with surface well potential, George H. Winslow—1032
α-γ directional correlation measurements with liquid film sources, T. B. Novey—547(L)
Ba^{136}—Cs^{136} chain, M. I. Kalkstein and J. M. Hollander—730
Bk and Cf isotopes produced in neutron irradiation of Pu, L. B. Magnusson, M. H. Studier, P. R. Fields, C. M. Stevens, J. F. Mech, A. M. Friedman, H. Diamond, and J. R. Huizenga—1576
Correlation of spontaneous fission half-lives, M. H. Studier and J. R. Huizenga—545(L)
Long-lived radioactive Al^{26}, James R. Simanton, Robert A. Rightmire, Alton L. Long, and Truman P. Kohman—1711(L)
Orbital electron capture in heaviest elements, R. W. Hoff and S. G. Thompson—1350
Pb long-lived isotopes, J. R. Huizenga and C. M. Stevens—548(L)
Po^{210} half-life, calorimetric determination, J. F. Eichelberger, K. C. Jordan, S. R. Orr, and J. R. Parks—719
Pr neutron-deficient activities, Thomas H. Handley and Elmer L. Olson—1003
Pt^{188} identification, Robert A. Naumann—90
RaE β spectrum, E. A. Plassmann and L. M. Langer—1593
Short-lived radionuclides produced by synchrocyclotron, H. Tyrén and P. A. Tove—773
Ti^{44}, new Ti nuclide, R. A. Sharp and R. M. Diamond—1713(E)
UX_1, UX_2, and UZ decay, Sven A. E. Johansson—1075
Raman Spectra (see **Molecular Structure and Spectra**)
Range and Energy Loss of Particles (see also **Scattering**)
Charge states of heavy-ion beams passing through gases, P. M. Stier, C. F. Barnett, and G. E. Evans—973
Electron capture and loss by moving ions in dense media, Jacob Neufeld—1470
Emulsion tables, Walter H. Barkas and George Hahn—859(A)
γ-ray absorption coefficients at 6.13 Mev, Ronald S. Paul—1563
Grain density and ionization loss in nuclear track emulsions, John R. Fleming and J. J. Lord—852(A)
Ionization energy loss of mesons in NaI scintillation crystal, Theodore Bowen—754(A)
Ionization produced by 5-Mev α particles in A mixtures, C. E. Melton, T. E. Bortner, and G. S. Hurst—643
Low-energy differential range spectrum of cosmic-ray μ mesons, A. Fafarman and M. H. Shamos—1096
Mass measurement by multiple Coulomb scattering on stopped particles, R. G. Glasser—835(A)
Proton energy loss by integral and differential experiments, Theodore Jorgensen, Jr.—835(A)
Range and straggling of low-energy α particles in cloud chamber, S. Barile, R. Webeler, and G. Allen—673
Range of nitrogen ions in emulsion, H. L. Reynolds and A. Zucker—393
Relative contributions of K-shell and other electrons to stopping power of light and heavy elements, Edwin A. Uehling—861(A)
Spatial distribution of energy dissipation by high-energy x-rays, Henry Brysk—419
Recombination (see **Molecular Structure and Spectra**)
Rectifiers (see **Electrical Conductivity and Resistance; Semiconductors**)
Relativity and Gravitation
Gravitation and electromagnetism, Suraj N. Gupta—1683
Mach's principle and unified field theory, Joseph Callaway—778
Spherically symmetric solutions in nonsymmetrical field theories. II, P. C. Vaidya—5
Resistance, Electrical (see **Electrical Conductivity and Resistance**)
Resonance Radiation (see **Radiation**)
Scattering, General (see also **Diffraction; Elementary Particle Interactions; Nuclear Reactions; Range and Energy Loss of Particles**)
Application of variational principles to scattering problems, H. E. Moses—519
Bound states and formal theory of scattering, M. N. Hack 196; 1714(E)
Cross-section theorem, Robert A. Mapleton—415
Expansion of wave packets, Daniel S. Ling, Jr.—216
Formula for polarization in nucleon-nucleon scattering, G. Breit and J. B. Ehrman—805(L)
Generalized variational principle for scattering amplitude, S. I. Rubinow—218
Limiting processes in formal theory of scattering, F. Coester, Morton Hamermesh, and Katsumi Tanaka—1142
Mass measurement by multiple Coulomb scattering on stopped particles, R. G. Glasser—835(A)
Nucleon-antinucleon scattering and vacuum polarization, Kenneth A. Johnson—1659
Phase shifts for nucleon-nucleon scattering at 280 Mev, G. Breit, J. B. Ehrman, A. M. Saperstein, and M. H. Hull, Jr.—807(L)
Possible triple scattering experiments, L. Wolfenstein—1654
Scattering of light of very low frequency by systems of spin $\frac{1}{2}$, F. E. Low—1428
Scattering of low-energy photons by particles of spin $\frac{1}{2}$, M. Gell-Mann and M. L. Goldberger—1433
Solution of many-body scattering problems by Fredholm's equation, P. Swan—1144
Scattering of α Particles (see also **Nuclear Reactions Induced by α Particles and He^3**)
α-α scattering phase shifts, James N. Snyder—1333
Elastic scattering of α particles by carbon, J. W. Bittner and R. D. Moffat—374
Inelastic scattering of α particles by Li, C. W. Li and R. Sherr—389
Scattering of Atoms and Molecules (see **Atomic and Molecular Beams**)
Scattering of Deuterons (see also **Nuclear Reactions Induced by Deuterons and Tritons**)
Elastic scattering of deuterons by He^3, R. J. S. Brown, K. F. Famularo, H. D. Holmgren, D. Rankin, and T. F. Stratton—80
Li^6 energy levels, A. Galonsky and M. T. McEllistrem—826(A)
Scattering of Electrons and Positrons (see also **Electrons and Positrons**)
Back diffusion of electrons to plane emitting surface, Robert P. Stein—862(A)
Comparison of several approximations to scattering of high-energy electrons, J. Mayo Greenberg—820(A)
Cross-section theorem, Robert A. Mapleton—415
Electron scattering from H, deuterium, and C at 190 Mev, J. A. McIntyre and R. Hofstadter—854(A)
Electron scattering in H and He, R. Hofstadter, R. McAllister, and E. Wiener—854(A)
Inelastic scattering of medium-fast electrons in alkali metals, E. M. Baroody—837(A)

Scattering of Electrons and Positrons (Continued)
Nuclear multipole transitions in inelastic electron scattering, L. I. Schiff—765
Perturbation calculation of elastic scattering of electrons by H atoms, Sidney Borowitz—1523
Phase shift calculation of high-energy electron scattering, D. G. Ravenhall and D. R. Yennie—239(L); 1714(E)
Relativistic Coulomb scattering of electrons and positrons, G. Parzen and T. Wainwright—188
Thick target bremsstrahlung spectra for 1.00-, 1.25-, and 140-Mev electrons, William Miller, J. W. Motz, and Carmen Cialella—1344
Scattering of Mesons (see also **Mesons; Nuclear Reactions Induced by Mesons**)
Elastic scattering of 26-Mev negative pions by H in emulsion, Jay Orear, William Slater, J. J. Lord, and S. L. Eilenberg—174
Inelastic scattering of 500-Mev negative pions in emulsion nuclei, M. Blau and Martin Caulton—150
Low-energy behavior of phase shifts in pion-proton scattering, Jay Orear—176
Measurement of Coulomb interference in 113-Mev π^+-p scattering, Jay Orear—1417
Meson-proton scattering phase shift analysis, H. A. Bethe and F. de Hoffman—1714(E)
Self-energy effects on meson-nucleon scattering according to Tamm-Dancoff method, William M. Visscher—788
Total cross sections for negative and positive pions in hydrogen and deuterium, J. Ashkin, J. P. Blaser, F. Feiner, J. G. Gorman, and M. O. Stern—1104
Scattering of Neutrons (see also **Nuclear Reactions Induced by Neutrons**)
Charge independence with repulsive core potentials, M. A. Preston and J. Shapiro—813(L)
Diffusion parameters of thermal neutrons in water, G. von Dardel and N. G. Sjöstrand—1245
Elastic and inelastic scattering of 14-Mev neutrons by deuterons, John D. Seagrave—855(A)
Inelastic neutron scattering in Fe, D. L. Lafferty, L. A. Rayburn, and T. M. Hahn—381
Multiple scattering of neutrons, George N. Vineyard—93
n-p scattering at 90 Mev, Chung Ying Chih—856(A)
n-p scattering at 91 Mev, R. H. Stahl and N. F. Ramsey—1310
Ratio of $\overline{\Gamma}_n^0/\overline{D}$ for slow neutron resonances, R. S. Carter, J. A. Harvey, D. J. Hughes, and V. E. Pilcher—113
Scattering of polarized neutrons from heavy nuclei, A. Okazaki, R. L. Becker, and H. H. Barschall—836(A); R. K. Adair, S. E. Darden, and R. E. Fields—503
Small-angle n-p scattering at 400 Mev, R. T. Siegel, A. J. Hartzler, and W. Opitz—859(A)
Small-angle scattering of 1-Mev neutrons by intermediate and heavy nuclei, S. E. Darden, W. Haeberli, and R. B. Walton—836(A)
Scattering of Protons (see also **Nuclear Reactions Induced by Protons**)
Charge independence with repulsive core potentials, M. A. Preston and J. Shapiro—813(L)
Coulomb interference effects in p-p scattering, A. Garren—1709(L)
Direct interaction in $Fe^{56}(p,p')Fe^{56}$, G. Schrank, P. C. Gugelot, and I. E. Dayton—1156(L)
Elastic scattering of 9.7-Mev protons by He^4, Bruce Cork and Walter Hartsough—859(A); 1267
Elastic scattering of protons by F^{19}, T. S. Webb, F. B. Hagedorn, W. A. Fowler, and C. C. Lauritsen—851(A)
Electric excitation of Au^{197}, C. F. Cook, C. M. Class, and J. T. Eisinger—658
Energy levels of Al^{27}, C. P. Browne, S. F. Zimmerman, and W. W. Buechner—725
Formula for polarization in nucleon-nucleon scattering, G. Breit and J. B. Ehrman—805(L)
Inelastic proton scattering cross section of F^{19}, C. A Barnes, W. A. Fowler, C. C. Lauritsen, and R. W. Peterson—851(A)
Phase-shift analysis of elastic scattering of protons by He^4, R. W. Lowen—826(A)
Phase shifts for nucleon-nucleon scattering at 280 Mev, G. Breit, J. B. Ehrman, A. M. Saperstein, and M. H. Hull, Jr.—807(L)
Polarization in p-p scattering for P and F waves, M. H. Hull, Jr., and A. M. Saperstein—806(L)
Polarization of high-energy protons in elastic scattering on helium and carbon, O. Chamberlain, E. Segrè, R. Tripp, C. Wiegand, and T. Ypsilantis—807(L)
Polarization of protons by scattering from Be, H. G. de Carvalho, J. Marshall, and L. Marshall—1081
Possible triple scattering experiments, L. Wolfenstein—1654
p-p scattering at 5.77 Mev, E. J. Zimmerman, R. O. Kerman, Sidney Singer, P. Gerald Kruger, and W. Jentschke—1322
Scattering of 9.5-Mev protons by neon and argon, R. G. Freemantle, D. J. Prowse, A. Hossain, and J. Rotblat—1270
Scattering of 9.5-Mev protons by nitrogen, R. G. Freemantle, D. J. Prowse, and J. Rotblat—1268
Scattering of 10-Mev protons on C and Mg, Gerhard E. Fischer—704
Scattering of Radiation (see **Gamma Rays; Radiation; X-Rays**)
Scintillation Counters (see **Methods and Instruments**)
Secondary Emission (see **Electrical Properties**)
Semiconductors
Absence of bombardment annealing in electron bombardment of Ge, R. C. Fletcher, W. L. Brown, and K. A. Wright—833(A)
Afterglow of MgO crystals, Eiso Yamaka—293
Conductivity and Hall effect in oxide cathode, R. Forman—839(A)
Dependence of signal-to-noise ratio in photoconductive PbSe layers on temperature of black-body source, A. M. Crooker and E. B. Dorling—846(A)
Diffusion of impurities in Si, W. C. Dunlap, Jr., H. V. Bohm, and H. P. Mahon, Jr.—822(A)
Effect of oxygen on electrical properties of PbTe films, Donald E. Bode and Henry Levinstein—259
Effect of spin-orbit coupling on magnetic resonance in some semiconductors, R. J. Elliott—266
Effective masses of electrons in Si, R. N. Dexter, Benjamin Lax, A. F. Kip, and G. Dresselhaus—222(L)
Effective masses of holes in Si, R. N. Dexter and Benjamin Lax—223(L)
Elastoresistance in p-type Ge and Si, E. N. Adams—803(L)
Electrical and optical properties of InSe, R. W. Damon and R. W. Redington—1498
Electrical and optical properties of intermetallic compounds. I. InSb, R. G. Breckenridge, R. F. Blunt, W. R. Hosler, H. P. R. Frederikse, J. H. Becker, and W. Oshinsky—571; II. GaSb, R. F. Blunt, W. R. Hosler, and H. P. R. Frederikse—576; III. AlSb, R. F. Blunt, H. P. R. Frederikse, J. H. Becker, and W. R. Hosler—578
Electrical conductivity and Hall effect in oxide cathodes, R. Forman—1479
Electrical properties and solid-vapor equilibrium of PbS, Robert F. Brebrick and Wayne W. Scanlon—598
Electrical properties of natural crystals of iron pyrite, John C. Marinace—593

Electrical properties of Si containing As and boron, F. J. Morin and J. P. Maita—28
Electronic structure of MgO, J. R. Stevenson—839(A)
Fermi level in amorphous Sb films, E. Taft and L. Apker —1496
Fermi level in semiconducting amorphous Sb films, E. Taft and L. Apker—827(A)
Flow of electrons and holes through surface barrier region in point contact rectification, Melvin Cutler—255
Grain-boundary conduction in Au-doped Ge, A. G. Tweet —828(A)
Hole trapping due to lattice defects in Ge, R. G. Shulman, W. L. Brown, and R. C. Fletcher—833(A)
Hyperfine splitting of donor states in Si, J. M. Luttinger and W. Kohn—802(L)
Impurity levels in Si, F. J. Morin, J. P. Maita, R. G. Shulman, and N. B. Hannay—833(A)
Injection breakdown in Fe-doped Ge diodes, W. W. Tyler —226(L)
Interaction of traps and heat treatments in Si, N. B. Hannay, J. R. Haynes, and R. G. Shulman—833(A)
Magnetic susceptibility of residual bisulfate compounds of carbon, H. T. Pinnick—832(A)
Magnetoresistance and planar Hall effects in *n*-type Ge, R. E. Davis and Colman Goldberg—833(A)
Mobility of impurity ions in Ge and Si, C. S. Fuller and J. C. Severiens—21
Mobility ratio in pure *p*-type semiconductors, Allen Nussbaum—828(A)
New minority carrier phenomenon in Ge, Stephen J. Angello and Theodore E. Ebert—221(L)
Optical studies of injected carriers. III. Infrared absorption in Ge at low temperatures, Roger Newman—1188
Oxidation of thin films of Ge and Si, W. C. Dash—822(A)
Photoconductivity of Ge doped with Fe, R. Newman and W. W. Tyler—882
Plastic deformation of Au-doped Ge, C. J. Gallagher and A. G. Tweet—834(A)
Properties of Ge doped with Fe. I. Electrical conductivity, W. W. Tyler and H. H. Woodbury—874
Properties of Zn-, Cu-, and Pt-doped Ge, W. C. Dunlap, Jr.—40
Quantum theory of cyclotron resonance in semiconductors, W. Kohn and J. M. Luttinger—529(L)
Resistivity and Hall effect of Ge at low temperatures, C. S. Hung and J. R. Gliessman—1226
Resistivity changes in Si induced by heat treatment, C. S. Fuller, J. A. Ditzenberger, N. B. Hannay, and E. Buehler—833(A)
Seebeck effect in single crystal Si, T. H. Geballe and G. W. Hull—846(A)
Semiconducting CdTe, Dietrich A. Jenny and Richard H. Bube—1190
Surface "channel" detection method for semiconductors, H. Christensen—827(A)
Theory of donor and acceptor states in Si and Ge, C. Kittel and A. H. Mitchell—1488
Theory of thermoelectric power of semiconductors, Conyers Herring—1163
Thermal conductivity of single crystalline Si, G. W. Hull and T. H. Geballe—846(A)
Thermal effects on lifetime of minority carriers in Ge, R. A. Logan and M. Schwartz—46
Transverse Hall and magnetoresistance effects in *p*-type Ge, R. K. Willardson, T. C. Harman, and A. C. Beer—1512
Traps produced by electron bombardment of Ge at low temperatures, W. L. Brown, R. C. Fletcher, and K. A. Wright—834(A)
Use of *p-n* junctions for solar energy conversion, E. S. Rittner—1708(L)
Uv absorption in BaO films, Koji Okumura—1704(L)

Shock Waves (see **Fluid Dynamics**)
Solid State (see **Crystalline State**)
Solutions (see **Liquids**)
Sound (see **Acoustics**)
Spallation (see **Nuclear Reactions**)
Spark Discharge (see **Electrical Discharges**)
Specific Heat (see **Thermal Properties**)
Spectra, Atomic (see **Atomic Structure and Spectra**)
Spectra, General
Electromagnetic radiations from hydrocarbon flames, Samuel C. Lawrence, Jr.—860(A)
Infrared spectrum of $BaTiO_3$, R. T. Mara, G. B. B. M. Sutherland, and H. V. Tyrell—801(L)
Spectra, Molecular (see **Molecular Structure and Spectra**)
Spectra, Nuclear (see **Nuclear Spectra**)
Spectroscopy Technique (see **Methods and Instruments**)
Spinor Fields (see **Field Theory**)
Standards (see **Constants, Standards, Units**)
Stark Effect (see **Atomic Structure and Spectra**)
Statistical Mechanics and Thermodynamics
Approximate variational principle in quantum statistics, William M. MacDonald, III, and John M. Richardson —18
Critical flow rate and zero entropy of He superfluid, William Band—843(A)
Effects of anisotropy on thermodynamic properties of antiferromagnets, J. A. Eisele and F. Keffer—929
Entropy of radiation, Philip Rosen—555
Heat and entropy of mixing of He^3 and He^4 on the basis of the two-fluid theory of He^4, O. K. Rice—1464
Kinetics of phase transitions for systems undergoing association: Monomer-dimer equilibrium, Howard Saltsburg and Howard Reiss—838(A)
Method of transition probabilities in quantum mechanics and quantum statistics, P. T. Landsberg—1420
Principle of minimum entropy production, Martin J. Klein and Paul H. E. Meijer—250
Properties of quantum statistical impedance, J. L. Jackson and M. C. Yovits—15
Quantum statistics of closed and open systems, F. Ansbacher and P. T. Landsberg—1707(L)
Quantum theory of irreversible processes, U. Fano—869
Relativistic statistical mechanics of ideal gas, Richard Schlegel—820(A)
Shape of coexistence curve of two-phase systems near critical point, O. K. Rice—838(A)
Solution of temperature-perturbed Thomas-Fermi equation, J. J. Gilvarry—944
Statistical mechanics of He II near 1°K, O. K. Rice—1460
Superconductivity of charged boson gas, M. R. Schafroth —1149(L)
Superfluidity of boson gas, J. M. Blatt and S. T. Butler—1149(L)
Tensor virial equations, Eugene N. Parker—1686
Theory of condensation, A. J. F. Siegert—243
Thermodynamics of Thomas-Fermi atom at low temperature, J. J. Gilvarry—934
Virial expansion of ideal Bose-Einstein gas, B. Widom—820(A)
Virial series of ideal Bose-Einstein gas, B. Widom—16

Statistical Methods (see **Mathematical Methods**)
Superconductivity
Adiabatic magnetization of superconducting sphere, R. L. Dolecek—25

Superconductivity (Continued)
Effect of precipitation hardening on superconducting transition of Al alloy, R. E. Mould and D. E. Mapother—797(L)
Effects of elastic dilatation and shear on superconducting transition of Sn, Milan D. Fiske—821(A)
Elastic moduli of Sn at superconducting transition, Joseph K. Landauer—296
Exponential temperature dependence of electronic specific heat of superconducting vanadium, W. S. Corak, B. B. Goodman, C. B. Satterthwaite, and A. Wexler—1442(L)
High-frequency resistance of Sn and In in normal and superconducting state, C. J. Grebenkemper—1197
Lifetime of positrons in superconducting Pb and Sn, Robert Stump and Harry E. Talley—904
Magnetization of Sn at superconducting transition, J. C. Thompson and C. F. Squire—287
New criterion for superconductivity in metals, Gerhart Groetzinger, David Kahn, and Philip Schwed—887
Structure of intermediate state of superconductors, B. Serin—228(L)
Superconductivity of charged boson gas, M. R. Schafroth—1149(L)
Superconductivity of V at 24 000 Mc/sec, C. J. Grebenkemper—316
Theory of superconductivity, M. R. Schafroth—1442(L)
Ultrasonic attenuation in superconducting lead, H. E. Bömmel—220(L)
Supersonics (see **Fluid Dynamics**)

Thermal Conductivity (see **Thermal Properties**)
Thermal Diffusion (see **Diffusion**)
Thermal Expansion (see **Thermal Properties**)
Thermal Properties
Atomic heat of Bi between 1° and 4° K, P. H. Keesom and N. Pearlman—897
Exponential temperature dependence of electronic specific heat of superconducting vanadium, W. S. Corak, B. B. Goodman, C. B. Satterthwaite, and A. Wexler—1442(L)
Oscillatory thermal conductivity of Bi in magnetic fields at liquid He temperatures, J. Babiskin and M. C. Steele—822(A)
Thermal conductivity of single crystalline Si, G. W. Hull and T. H. Geballe—846(A)
Vibrational anharmonicity and lattice thermal properties, J. S. Dugdale and D. K. C. MacDonald—57
Thermal Radiation (see **Radiation**)
Thermionic Emission (see **Electrical Properties**)
Thermodynamics (see **Statistical Mechanics and Thermodynamics**)
Thermoelectric Effect (see **Electrical Properties; Semiconductors**)
Thermoluminescence (see **Luminescence**)
Thermomagnetic Effect (see **Magnetic Properties**)
Total Cross Sections (see **Electrons and Positrons; Nuclear Reactions**)
Transmutation (see **Nuclear Reactions**)

Uncertainty Principle (see **Quantum Mechanics**)
Units (see **Constants, Standards, Units**)

Vacuum Tubes (see **Methods and Instruments**)
Van der Waals Forces (see **Molecular Structure and Spectra**)
Viscosity (see **Liquids**)

Wave Mechanics (see **Quantum Mechanics**)
Work Function (see **Electrical Properties**)

X-Rays
Electron energy levels in ionic crystals, E. L. Jossem and L. G. Parratt—834(A)
Energies of π^--mesonic x-ray K lines, M. B. Stearns, M. Stearns, S. DeBenedetti, and L. Leipuner—804(L)
Relation between the width of an x-ray line and resolving power of double-crystal spectrometer, Gösta Brogren—589
Solar x-ray emission, E. T. Byram, T. A. Chubb, and H. Friedman—860(A)
Spatial distribution of energy dissipation by high-energy x-rays, Henry Brysk—419
Universal curves for dispersion and scattering of x-rays, L. G. Parratt and C. F. Hempstead—820(A)
X-ray diffraction patterns from liquid He, W. L. Gordon, C. H. Shaw, and J. G. Daunt—1444(L)

CONTENTS

THE PHYSICAL REVIEW — Second Series, Volume 95, No. 6 — DECEMBER 15, 1954

On the Theory of Liquid He³ — Louis Goldstein 1455
Statistical Mechanics of Helium II near $T=0$ — O. K. Rice 1460
Heat and Entropy of Mixing of He^3 and He^4 on the Basis of the Two-Fluid Theory of He^4 — O. K. Rice 1465
Secondary Emission by Positive Ion Bombardment — Mischel Schwartz and Paul L. Copeland 1469
Electron Capture and Loss by Moving Ions in Matter — Jacob Neufeld 1470
Measurements and Theoretical Study of Townsend Coefficients and Hall Effect in Ozide Cathodes — R. Forman 1479
Low-Temperature Acoustic Relaxation in Solid Rare Gases — M. E. Fine and N. T. Kenney 1487
Theory of Donor and Acceptor States in Silicon and Germanium — C. Kittel and A. H. Mitchell 1488
Large Magnetic Kerr Rotation in Ferromagnetics — B. W. Roberts and C. P. Bean 1494
Fermi Level in Amorphous Antimony Films — R. Taft and L. Apker 1496
Residual and Optical Properties of Surface Silicates — R. W. Damon and R. W. Redington 1498
Magnetic and Crystalline Behavior of Certain Oxide Systems with Related and Perovskite Structures — Louis R. Maxwell and Stanley J. Pickart 1501
Color Centers in Chrome Alum Crystals — E. A. Braun, A. Many, and A. E. Simches 1505
Recovery of NaI(Tl), KI(Tl), and CsI(Tl) Crystal Phosphors Progressively Damaged by Fast Neutrons — J. C. D. Milton and J. S. Fraser 1508
Transverse Hall and Magnetoresistance Effects in p-Type Germanium — R. W. Williardson, T. C. Harman, and A. C. Beer 1512
Experiments on X-Ray Lattice Parameter and Density Changes in Neutron-Irradiated LiF — D. Binder and W. J. Sturm 1519
Perturbation Calculation of the Elastic Scattering of Electrons by Hydrogen Atoms — Sidney Borowitz 1524
Optical Studies of Radioactive Mercury — F. Bitter, E. P. Davis, B. Richter, and J. E. R. Young 1531
Dissociation Energy of NO and N_2 — M. Brook and J. Kaplan 1540
Hyperfine Structure of the Spectra of Ni and Ni — Kiyoshi Murakawa 1543
Stern-Gerlach Experiment on Polarized Protons — J. E. Sherwood, T. E. Stephenson, and Seymour Bernstein 1546
Decay of Fe^{52} — Vera Kistiakowsky Fischer 1549
K Capture to Positron Ratio for Na^{22} — W. E. Kreger 1554
Decay of $_{33}As^{74m}$ (49 sec), $_{32}Ge^{77m}$ (53 sec), and $_{33}As^{77}$ (12 hr) — S. B. Burson, W. C. Jordan, and J. M. LeBlanc 1555
Gamma-Ray Absorption Coefficients at 0.13 Mev — Ronald S. Paul 1558
Absorption Cross Section of Boron for Thermal Neutrons — G. von Dardel and N. G. Sjöstrand 1566
Low-Lying I = States in Even-Even Nuclei — Frank Stephens, Jr., Frank Asaro, and I. Perlman 1568
Capture-Positron Branching Ratios — P. F. Zweifel 1572
Berkelium and Californium Isotopes Produced in Heavier Irradiations of Plutonium — L. B. Magnusson, M. H. Studier, P. R. Fields, C. M. Stevens, J. F. Mech, A. M. Friedman, H. Diamond, and J. R. Huizenga 1576
Decay of $_{81}Tl^{200}$ (4.8 min) — W. C. Jordan, S. B. Burson, and J. M. LeBlanc 1582
Angular Distributions of α Particles from the $He^{3}(\phi,\alpha)He^{2}$ Reaction — P. H. Stelson 1584
Proton Polarization in (d,p) Reactions — W. B. Cheston 1590
Beta Spectrum of Radium B — E. A. Plassmann and L. M. Langer 1593
Disintegration of Ir^{192} and Ir^{194} — M. W. Johns and S. V. Nablo 1599
Internal Conversion in Ho^{65} — R. D. Leamer and G. W. Hinman 1607
K-Electron Ejection in the Beta Decay of Ni^{63} — William Rubinson and J. J. Howland, Jr. 1610
Fission Yield of Gd^{160} and Tb^{160} — Henry G. Petrow and Gregory Rocco 1614
Excitation Functions for Nitrogen-Induced Nuclear Reactions in Carbon — H. L. Reynolds and A. Zucker 1615
Comparison of Nitrogen- and Proton-Induced Nuclear Reactions — E. L. Cohen, H. L. Reynolds, and A. Zucker 1617
Decay Characteristics of Some Short-Lived Fissions of Low Atomic Number — R. M. Kline and D. J. Zaffarano 1620
Comparison of H^3 and He^3 Production in High-Energy Deuteron-Deuteron Collisions — Charles S. Godfrey 1621
Electron Tritons between 0.1 and 10 Mev — M. M. Block, D. T. King, and W. W. Wada 1627
Cerenkov Radiation Detector for the Detection of Slow Particles — Carl M. York, Jr. 1635
Nuclear Fine Structure in the p-Meson Atom — Boris A. Jacobsohn 1637
Integral Equations for Cascade Showers — John M. Blatt 1644
New Formulation of a General Three-Dimensional Cascade Theory — B. A. Chartres and H. Messel 1651
Possible Triple-Scattering Experiments — L. Wolfenstein 1656
Nucleon-Antinucleon Scattering and Yamaguchi Potentials — Kenneth A. Johnson 1659
Fourth Order Corrections to Meson-Nucleon Scattering in Pseudoscalar Meson Theory — H. W. Wyld, Jr. 1661
Renormalization of a Neutral Vector Meson Interaction — R. J. N. Phillips 1678
Many-Parameter Wave Functions in the Independent-Particle Model — Erwin H. Kronheimer 1680
Gravitation and Electromagnetism — Suraj N. Gupta 1683
Tensor Virial Equations — Eugene N. Parker 1686
Tamm-Dancoff Methods and Nuclear Forces — Behram Kurşunoğlu 1690

(continued on cover three)

LANCASTER PRESS, INC., LANCASTER, PA.